MMM 2023

HYATT REGENCY DALLAS

OCTOBER 30 - NOVEMBER 3

ABSTRACTS BOOK

Photo by CleanPix for Visit Dallas

IEEE MAGNETICS

Jointly sponsored by AIP Publishing LLC and the IEEE Magnetics Society

AIP Publishing

Session TU
TUTORIAL: MACHINE LEARNING IN MAGNETISM

Cindi Dennis, Chair
National Institute of Standards and Technology, Gaithersburg, MD, United States

INVITED PAPERS

TU-01. Basic Introduction to Machine Learning in a Physical Context. *S. Vock*[1] *1. Federal Institute for Occupational Safety and Health, Dresden, Germany*

Real-world modelling is a fundamental concern in physics. The use of self-learning methods, machine learning (ML), is the method of choice when dealing with large data sets, inverse problems, complex feature spaces and more. However, models are abstractions of the real world and thus implicitly subject to uncertainty. The applicability of ML in physics requires a basic understanding of the limitations of the applied ML-model, i.e. its trustworthiness and more precisely its dependability. This tutorial aims to provide an introduction to ML, assuming no prior knowledge beyond basic scientific understanding. An overview of ML tasks, models and data types relevant to applications in magnetism is given. A hands-on part will introduce the basic concept of a ML-based data evaluation approach using open-source software and data sets. The audience is asked to bring their laptops and follow along. The last part of the tutorial will cover the topic of ML dependability. The basic elements of dependability assessment of ML models will be introduced with a special focus on robustness.

TU-02. Machine Learning for Application-Specific Materials Search. *S. Sayed*[1] *1. University of California, Berkeley, Berkeley, CA, United States*

In recent years, significant efforts have been observed in reevaluating existing materials in the context of emerging spintronic phenomena—however, quantitatively ranking these materials for specific applications has proven to be a time-intensive task using traditional theoretical and experimental approaches. This presentation discusses a novel approach that leverages text-based machine learning to expedite such materials search process [1], [2]. In this approach, a computer program acquires knowledge about materials science, physics, and engineering from published scientific articles, enabling the identification of non-trivial results by deciphering patterns concealed within extensive text datasets. This method can be useful in the ongoing search for materials with large spin-orbit torque (SOT) [1], which are of great current interest for highly efficient magnetoresistive random access memory (MRAM) applications. The machine-learning-based method identified many known SOT materials and accurately ranked them according to their SOT strengths. Moreover, it successfully predicted the potential of a few materials to exhibit exceptionally large SOT, which has not been discussed in the literature. Specifically, the machine-learning-based prediction concerning a specific silicide exhibits quantitative agreement with recent experimental measurements outside the training dataset.

[1] S. Sayed et al. Pre-print: https://doi.org/10.21203/rs.3.rs-1718292/v1 (2022). [2] V. Tshitoyan et al. Nature 571, 95–98 (2019).

TU-03. Future Method for Estimating Parameters in Magnetic Films. *K. Tanabe*[1] *1. Toyota Technological Institute, Nagoya, Japan*

Estimating material parameters in fabricated materials is a crucial experiment in the field of materials science. Some parameters are difficult or time-consuming to estimate. In the fields of magnetism and spintronics, parameters such as the Dzyaloshinskii–Moriya exchange constant and the exchange stiffness constant are good examples of this. If these parameters could be easily and quickly estimated, our research field would grow rapidly. Here, we present a new method for estimating parameters in magnetic films from a magnetic domain image using machine learning. A magnetic structure is well-known to be deeply related to magnetic parameters. Although a complicated magnetic structure, which often appears in an as-grown magnetic film, is considered random by human eyes, it is influenced by magnetic energies such as magneto-static energy, magnetic exchange energy, and magneto-anisotropic energy. Thus, the characteristics of such parameters are probably hidden in the random magnetic structure. Such a relationship suggests that parameters can be estimated from a magnetic domain image by using pattern recognition. We collected a huge number of datasets of magnetic parameters and magnetic domain images made by micromagnetic simulation and/or taken by magnetic microscopes. Most of the datasets were used as training data for the convolution neural network, which is a famous technique in machine learning for pattern recognition, and the rest was used as test data. We succeeded in the estimation of the parameters from the magnetic image using machine learning[1]. This result may relieve future researchers from the difficulty of measuring parameters. In this tutorial talk, I want to take about from fundamentals of the convolution neural network technique as well as our experimental results[1-2].

TU-04. Application of Bayesian Optimization and Regression Analysis to Ferromagnetic Materials Development. *A.R. Will-Cole*[1] *1. Northeastern University, Boston, MA, United States*

Bayesian optimization (BO) is a well-developed machine learning (ML) field for black-box function optimization. In BO, a surrogate predictive model, here a Gaussian process, is used to approximate the black-box function. The estimated mean and uncertainty of the surrogate model are paired with an acquisition function to decide where to sample next. In this tutorial we will review the fundamentals of BO and present a case study of BO applied to magnetic material optimization. In this study, we applied this technique to known ferromagnetic thin-film materials such as ferromagnetic $(Fe_{100-y}Ga_y)_{1-x}B_x$ ($x = 0–21$ and $y = 9–17$) and $(Fe_{100-y}Ga_y)_{1-x}C_x$ ($x = 1–26$ and $y = 2–18$) to demonstrate optimization of structure–property relationships, specifically the dopant concentration or stoichiometry effect on magnetostriction and ferromagnetic resonance linewidth. Our results demonstrated that BO can be deployed to optimize structure–property relationships in FeGaB and FeGaC thin films. We have shown through simulation that using BO methods to guide experiments reduced the number of samples required to statistically determine the maximum or minimum by 50% compared to traditional methods. Our results suggest that BO can be used to save time and resources to optimize ferromagnetic films. This method is transferrable to other ferromagnetic material structure–property relationships, providing an accessible implementation of ML to magnetic materials development.

Session AA
FRONTIER TOPICS IN ANTIFERROMAGNETISM: ALTERMAGNETISM AND TOPOLOGY

Michelle E Jamer, Co-Chair
U.S. Naval Academy, Annapolis, MD, United States
Badih Assaf, Co-Chair
University of Notre Dame, Notre Dame, IN, United States

INVITED PAPERS

AA-01. Altermagnetism in 3- and 2-D: simple symmetry constraints and functionalization. I. Mazin[1] and *L. Šmejkal*[2] *1. Physics & Astronomy, George Mason University, Fairfax, VA, United States; 2. Johannes Gutenberg-Universität Mainz, Mainz, Germany*

Since many years, the canonical classification of ordered magnets included noncollinear (with many further subdivisions) and two collinear types: antiferromagnets (AF), which have net magnetization zero by symmetry, and ferro/ferrimagnets (FM), which do not have this property. The two have distinctly different micro- and macroscopic properties. It was supposed, for instance, that only FM can exhibit spin-splitting of the electronic bands in absence of spin-orbit coupling AND lack of inversion symmetry, have anomalous Hall effect (i.e., Hall effect driven by variation of the Berry phase), magnetooptical effects, suppressed Andreev scattering in contact with a singlet superconductor etc. A surprisingly recent development (~2019) is that this classification is incomplete: there are collinear magnets that would belong to AF by this classification, but show all characteristics of FM, *except the net spin polarization*! They were recently dubbed "altermagnets", AM. Incidentally, what has also not been fully appreciated was that there are also materials that have strictly zero net magnetization, but enforced not by symmetry, but by the Luttinger's theorem, and therefore truly belonging to the FM class ("Luttinger-compensated ferrimagnets"). In this talk I will present the new classification and explain, in specific examples, what are the symmetry conditions for AM, why these are a truly new class deserving a new name, and how their unusual properties appear. In the second part of the talk I will discuss single-layer *non-AM* antiferromagnets, and show how the can be *functionalized* to be AM by targeted symmetry lowering, with specific examples of $MnP(S,Se)_3$ and FeSe, and will discuss novel properties compared to 3D AM

[1] A Punch line: altermagnetism. Igor Mazin and The PRX Editors. Phys. Rev. X 12, 040002 (2022) [2] Igor Mazin and Libor Šmejkal, Altermagnetismin 2D, to be published. [2] Andriy Smolyanyuk, Olivia Taiwo, Libor Šmejkal and Igor I. Mazin, A tool to check whether a compensated collinear magnetic material is antiferro- or altermagnetic. https://github.com/amchecker/amcheck

AA-02. D-wave Magnetism in Spintronics: the Emergence of Altermagnetism. *J. Sinova*[1,2] *1. Institute of Physics, Johannes Gutenberg University Mainz, Mainz, Germany; 2. Department of Physics and Astronomy, Texas A&M University, College Station, TX, United States*

Antiferromagnetic spintronics has been a very active research area of condensed matter in recent years. As we have learned how to manipulate collinear antiferromagnets actively and their emergent topology by means of new types of spin-orbit torques, a key problem remained: the inefficiency of relativistic mechanism. The necessity of relativistic effects to manipulate and detect Néel order arises from the spin degeneracy of collinear antiferromagnets in the non-relativistic limit – or at least it was thought. The discovery of d-wave magnetic order in momentum space motivated a closer look at the symmetry classification of collinear magnetic systems. This has emerged as the third basic collinear magnetic ordered phase of altermagnetism, which goes beyond ferromagnets and antiferromagnets. Altermagnets exhibit an unconventional spin-polarized d/g/i-wave band structure in reciprocal space, originating from the local sublattice anisotropies in direct space. This gives properties unique to altermagnets (e.g., the spin-splitter effect), while also having ferromagnetic (e.g., polarized currents) and antiferromagnetic (e.g., THz spin dynamics and zero net magnetization) characteristics useful for spintronics device functionalities. I will cover the basic introductory view to altermagnetism and its consequences to spintronics in this talk.

[1] Libor Šmejkal, Jairo Sinova and Tomas Jungwirth, Phys. Rev. X 12, 031042 (2022) [2] Libor Šmejkal, Jairo Sinova and Tomas Jungwirth, Phys. Rev. X 12, 040501 (2022) [3] Zexin Feng, et al, Nature electronics 5, 735-743 (2022) [4] Libor Šmejkal, et al, Phys. Rev. X 12, 011028 (2022) [5] Rafael González-Hernández, et al, Phys. Rev. Lett. 126, 127701 (2021) [6] Libor Šmejkal, Rafael González-Hernández, T. Jungwirth and J. Sinova, Sci. Adv. 6, 23 (2020)

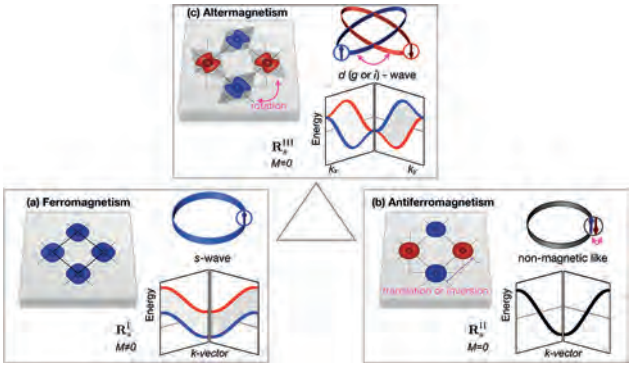

AA-03. Andreev Reflection in Altermagnets. *C. Sun*[1], A. Brataas[1] and J. Linder[1] *1. Center for Quantum Spintronics, Department of Physics, Norwegian University of Science and Technology, Trondheim, Norway*

Recent works have predicted materials featuring bands with a large spin-splitting distinct from ferromagnetic and relativistically spin-orbit coupled systems. Materials displaying this property are known as altermagnets and feature a spin-polarized band structure reminiscent of a *d*-wave superconducting order parameter. We here consider the contact between an altermagnet and a superconductor and determine how the altermagnetism affects the fundamental process of Andreev reflection. We show that the resulting charge conductance depends strongly on the interfacial orientation of the altermagnet relative to the superconductor, displaying features similar to normal metals or ferromagnets. The zero-bias conductance peaks present at the interface in the *d*-wave case are robust toward the presence of an altermagnetic interaction. Moreover, the spin conductance depends strongly on the orientation of the altermagnet relative the interface. These results show how the anisotropic altermagnetic state can be probed by conductance spectroscopy and how it offers voltage control over charge and spin currents that are modulated due to superconductivity.

C. Sun, A. Brataas, & J. Linder (2023). *arXiv preprint arXiv:2303.14236*.

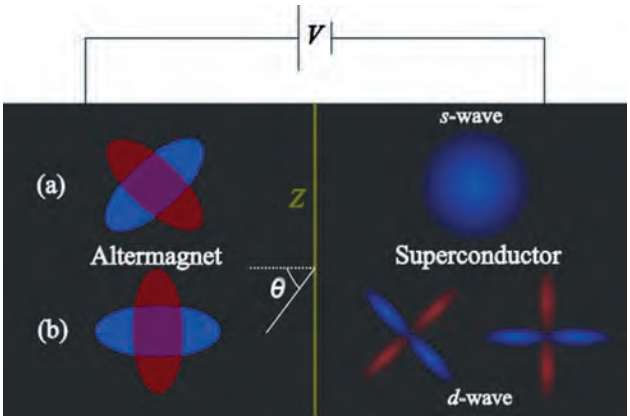

Fig. 1 Andreev reflection is probed in a bilayer consisting of an altermagnet (AM) and a superconductor (SC). The order parameter in the SC can have a *s*-wave or *d*-wave symmetry, including different nodal orientations of the *d*-wave case. Different interface orientations are also considered, effectively rotating the spin-resolved Fermi surface in the AM for majority (blue ellipse) and minority (red ellipse) spin carriers. A voltage *V* is applied to the system and the differential conductance provides information about the Andreev reflection.

AA-04. Quantum Geometric Detection and Control of a Layered Antiferromagnet. *Q. Ma[1] 1. Physics, Boston College, Chestnut Hill, MA, United States*

Close to massive objects, the geometry of space-time warps, causing the trajectory of light to bend and giving rise to phenomena like black holes and gravitational waves. Similarly, in the quantum world of electrons, there exists a geometric structure formed by their quantum wave functions. This quantum geometry, studied through quantum metric and Berry curvature, significantly impacts the behavior of electrons in unique ways [1]. In this talk, I will discuss how the interaction between quantum geometry and electromagnetic fields or waves can be utilized to detect and control a layered antiferromagnet MnBi2Te4 [2,3].

[1]Nature Materials 20, 1601 (2021) [2]Science DOI: 10.1126/science.adf150 (2023) [3]In preparation

AA-05. Anomalous Hall Effect in Unconventional Compensated Magnets. *D. Kriegner[1,2] 1. Institute of Physics AVCR, Prague, Czechia; 2. Technical University Dresden, Dresden, Germany*

Recently the classification of magnetically order material was revisited and the application of spin symmetry groups allowed the identification of three distinct classes of collinear magnets [1]. In addition to ferromagnets and antiferromagnets a third class of magnets named altermagnets was introduced. These altermagnets are classified by a compensated magnetic structure, however, show anisotropic spin split band structure. In my talk I will show how altermagnetic materials can be identified and discuss detection of odd in magnetic field effects like the anomalous Hall effect and X-ray circular magnetic dichroism [2]. In particular the anomalous Hall effect was so far used as experimental fingerprint of altermagnetismn in collinear compensated magnets like RuO_2 [3, 4], MnTe [5], and Mn_5Si_3 thin films [6, 7]. It can resemble the typical hysteretic transversal resistivity loops found in ferromagnets, however, in absence of any detectable magnetization and with strong anisotropy which is linked to the symmetry of the material (Fig. 1).

1. L. Šmejkal, J. Sinova, and T. Jungwirth, Phys. Rev. X 12, 031042 (2022) 2. A. Hariki, T. Yamaguchi, D. Kriegner, et al., arXiv:2305.03588 [cond-mat.mtrl-sci] (2023) 3. Z. Feng, X. Zhou, L. Šmejkal, *et al. Nat Electron* 5, 735–743 (2022) 4. T. Tschirner, R. D. Gonzalez Betancourt, T. Kotte, et al, submitted (2023) 5. R. D. Gonzalez Betancourt, J. Zubáč, R. J. Gonzalez-Hernandez, et al., Phys. Rev. Lett. 130, 036702 (2023) 6. H. Reichlová, R. Lopes Seeger, R. González-Hernández, et al. arXiv:2012.15651 [cond-mat.mes-hall] (2020) 7. I. Kounta, H. Reichlova, D. Kriegner, et al. Phys. Rev. Materials 7, 024416 (2023)

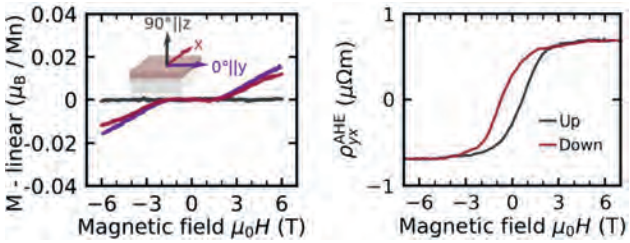

(left) Absence of spontaneous magnetization in SQUID magnetormetry investigations in various crystal directions. (right) Spontaneous anomalous Hall effect measured in c-axis oriented MnTe epitaxial thin films at T = 150 K.

Session AB
NEUROMORPHIC COMPUTING I

Joseph S. Friedman, Co-Chair
The University of Texas at Dallas, Richardson, TX, United States
Jayasimha Atulasimha, Co-Chair
Virginia Commonwealth University, Richmond, VA, United States

INVITED PAPER

AB-01. Spin-Hall nano-oscillators based on ferrimagnetic insulator-transition metal heterostructures. *H. Ren*[1,2], X. Zheng[3,4], S. Channa[5], G. Wu[1], D.A. O'Mahoney[6], Y. Suzuki[3,4] and A.D. Kent[1] *1. Center for Quantum Phenomena, Department of Physics, New York University, New York, NY, United States; 2. Design Department, TDK Headway Technologies Inc., Milpitas, CA, United States; 3. Department of Applied Physics, Stanford University, Stanford, CA, United States; 4. Geballe Laboratory for Advanced Materials, Stanford University, Stanford, CA, United States; 5. Department of Physics, Stanford University, Stanford, CA, United States; 6. Department of Materials Science and Engineering, Stanford University, Stanford, CA, United States*

Spin-Hall nano-oscillators (SHNO) are one of the potential devices to achieve current controlled GHz frequency signals in nanoscale devices for neuromorphic computing, magnonics, and creating Ising systems[1–3]. However, traditional SHNOs have high auto-oscillation threshold currents and those based on magnetic tunnel junctions require a complex etching process. Besides, it is challenging to couple the oscillators to form a connected network for these applications. Here we demonstrate SHNOs based on ferrimagnetic insulator-transition metal heterostructures, specifically epitaxial lithium aluminum ferrite thin films[4] with interfaces to permalloy and platinum. First, we showed that by depositing and patterning only Pt on unpatterned $Li_{0.5}Al_{0.5}Fe_2O_4$ (LFO) thin films, we can observe clear auto oscillations signals associated with the spin-Hall effect in Pt. We observed current polarity dependent spectral signals in Pt/LFO samples, showing that that the spin-orbit torques, not the spin Seebeck effect, are the origin of this auto oscillation signals. Further, we demonstrate a new type of hybrid SHNO based on a permalloy ferromagnetic-metal nanowire and again unpatterned low-damping ferrimagnetic insulator thin films of lithium aluminum ferrite (Pt/Py/$Li_{0.5}Al_{1.0}Fe_{1.5}O_4$ (LAFO))[5]. We associate the improved characteristics (*e.g.*, a lower threshold current and higher output power) of such hybrid SHNO with the simultaneous excitation of both magnetic layers. We further find that the presence of the ferrimagnetic insulator enhances the auto-oscillation amplitude of spin-wave edge modes, consistent with our micromagnetic modeling. Meanwhile, the localization of auto-oscillations reduces the threshold current and makes the edge mode the dominant power emission source rather than the bulk mode. Further, by varying the composition and thickness of the ferrimagnetic insulator layer, we successfully fabricated hybrid SHNOs with better performance (i.e., higher output power and quality factor) by replacing LAFO with LFO. This hybrid SHNO expands spintronic applications by providing improved oscillator characteristics and new means of coupling multiple SHNOs for neuromorphic computing and advancing magnonics. Acknowledgements This research was supported by the Quantum Materials for Energy Efficient Neuromorphic Computing (Q-MEEN-C), an Energy Frontier Research Center funded by the U.S. Department of Energy (DOE), Office of Science, Basic Energy Sciences (BES), under Award DE-SC0019273. Work at Stanford is supported under DOE BES DE-SC0008505.

[1] V.E. Demidov, S. Urazhdin, A. Zholud, A. V. Sadovnikov, and S.O. Demokritov, Appl. Phys. Lett. 105, 172410 (2014). [2] A. Khitun, M. Bao, and K.L. Wang, J. Phys. D. Appl. Phys. 43, 264005 (2010). [3] J. Grollier, D. Querlioz, K.Y. Camsari, K. Everschor-Sitte, S. Fukami, and M.D. Stiles, Nat. Electron. 3, 360 (2020). [4] X.Y. Zheng, S. Channa, L.J. Riddiford, J.J. Wisser, K. Mahalingam, C.T. Bowers, M.E. McConney, A.T. N'Diaye, A. Vailionis, E. Cogulu, H. Ren, Z. Galazka, A.D. Kent, and Y. Suzuki, Under Rev. (2022). [5] H. Ren, X.Y. Zheng, D.A.O. Mahoney, Y. Suzuki, S. Channa, G. Wu, and A.D. Kent, Nat. Commun. 14, 1406 (2023).

CONTRIBUTED PAPERS

AB-02. Artificial Spin Ice Dynamics Probed by Tunnel Magnetoresistance. *C. Sullivan*[1], H. Chen[2], B. Fang[3], X. Zhang[3] and S. Majetich[2] *1. Materials Science and Engineering, Carnegie Mellon University, Pittsburgh, PA, United States; 2. Physics, Carnegie Mellon University, Pittsburgh, PA, United States; 3. Materials Science and Engineering, King Abdullah University of Science and Technology, Thuwal, Saudi Arabia*

Magnetic tunnel junctions (MTJs) with a superparamagnetic free layer and artificial spin ice (ASI) nanodot arrays have been of interest for low power probabilistic computing applications [1][2]. Here, we combine the two systems by fabricating an ASI lattice of magnetostatically coupled nanodots on an MTJ free layer and investigate the dynamics through tunnel magnetoresistance (TMR). The array is a square lattice of 60 nm circular dots patterned on the free layer of a CoFeB/MgO/CoFeB MTJ, using a stack composition and methods described previously [3]. Conductive atomic force microscopy was used to make direct contact with the top electrode of a dot and TMR was measured as a function of magnetic field and time. TMR as a function of field revealed two state telegraphing with alternating preferred easy axis directions, as shown in Figure 1. The preferential axes of the array revealed a conventional ASI ground state following spin ice rules [4]. With a field varying along x, type 1 dots did not telegraph but had loops consistent with a magnetization along y [5]. Type 2 dots displayed a zero-field telegraphing square loop with a broadened telegraphing region compared to isolated dots [5]. By measuring TMR as a function of time for individual type 2 dots, different spin configurations were observed. Figure 2 shows time dependent TMR observes bursts of rapid telegraphing due to magnetic frustration interspersed with periods of relative stability. Autocorrelation analysis [3] revealed complex behavior in an array with at least three timescales, correlating with three energy landscapes. Previous Mumax3 simulations for a chain of dots showed energy landscapes dependent on nearest neighbor spin orientations [6]. Spin configurations in arrays are further investigated through Mumax3 simulations and experiments measuring the controlled dynamics for an assembly with magnetically stable, switchable dots surrounding a central superparamagnetic dot.

[1] M. Bapna and S. A. Majetich, Appl. Phys. Lett. 111, 243107 (2017) [2] W. A. Borders, A. Z. Pervaiz, S. Fukami, Nature 573, 390 (2019) [3] B. Parks, A. Abdelgawad, T. Wong, R. F. L. Evans, and S. A. Majetich, Phys. Rev. Applied 13, 014063 (2020) [4] R. F. Wang, C. Nisoli, R. S. Freitas, Nature 439, 303 (2006) [5] H. Chen, B. Parks, Q. Zhang, B. Fang, X. Zhang, and S.A. Majetich. Appl. Phys. Lett. 120, 21, 212401 (2022) [6] H. Chen, S. Y. Jeon, and S. A. Majetich, J. Phys. D: Appl. Phys. 55, 265002 (2022)

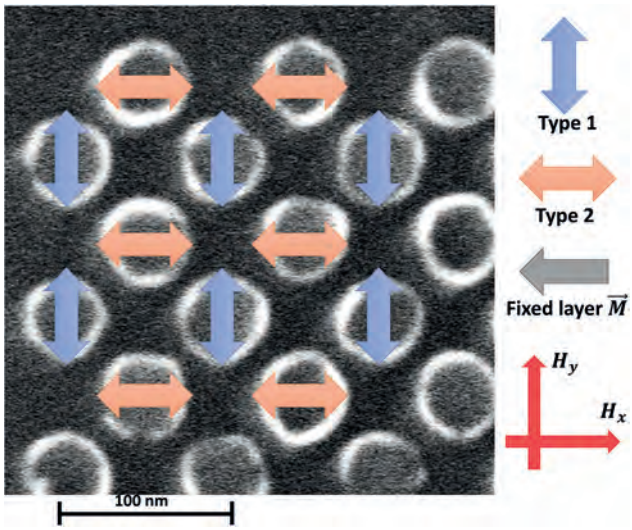

Fig1. Scanning electron microscope image of the patterned array superimposed with arrows indicating preferred magnetization.

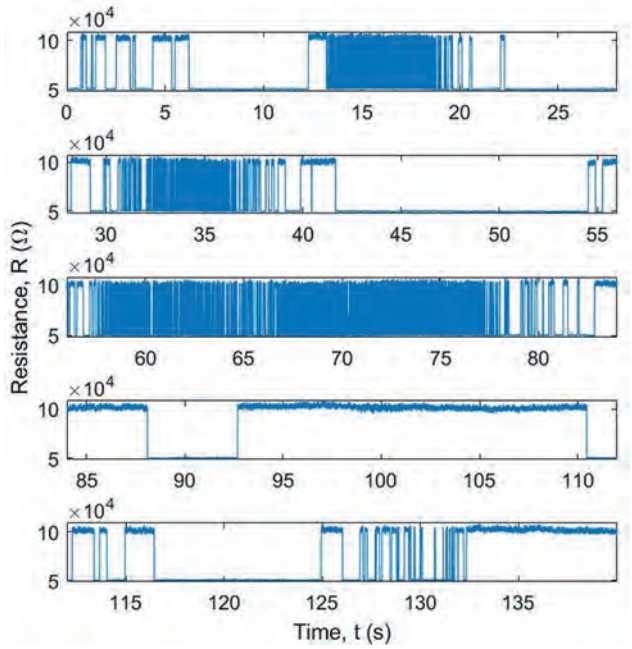

Fig.2 Resistance time profile for a single type 2 dot in the ASI array at a field of H_x=8 Oe to cancel the synthetic antiferromagnet field.

AB-03. Pattern recognition by a single spin torque oscillator with time multiplexing. *Y. Imai*[1] and T. Taniguchi[2] *1. The University of Tokyo, Bunkyo-ku, Japan; 2. National Institute of Advanced Industrial Science and Technology (AIST), Tsukuba, Japan*

Pattern recognition with coupled-oscillator networks has attracted considerable attention from both fundamental and practical perspectives, and various numerical demonstrations of this concept have been proposed [1,2,3]. A critical issue in the previous works is that any inhomogeneities in the oscillators are unavoidable, which lead to a failure of the recognition task without additional training [3]. To solve this issue, pattern recognition realized by a single spin torque oscillator (STO) has been recently investigated [4]. In this work, we develop a theoretical model of pattern recognition by a single STO [5]. Instead of using multiple (N) oscillators, we apply a time-multiplexing method to a single STO that divides the oscillator output into N pieces, thereby avoiding inhomogeneity. In the first iteration, the oscillator phases are saturated to values corresponding to colors of a pattern to be recognized by magnetic field represented by a linear combination of coupling strengths following the Hebbian rule and the time-multiplexed states without the magnetic field prepared in advance. In the second iteration, the coupling strengths are determined by the Hebbian rule for patterns in a memory, and combined with the time-multiplexed states in the first iteration to form the magnetic field. Then, the phases of the oscillators saturate to new values, which correspond to colors of the pattern in the memory that resembles most the pattern to be recognized (see Fig. 1). Figure 2 shows the change of the colors corresponding to the phases in the recognition task of the 60-pixel pattern from 3 memorized patterns shown in Fig. 1. In addition, the theoretical analysis shows the origin of the pattern recognition is the forced synchronization to the magnetic field. Our proposal will be a solution against the issue preventing an experimental realization of the pattern recognition by coupled-oscillator networks. This work was supported by JSPS KAKENHI Grant Number JP23KJ0331.

[1] P. Maffezzoni et al., IEEE Transactions on Circuits Syst. I: Regul. Pap. 62, 1591–1598 (2015). [2] K. Kudo and T. Morie, Appl. Phys. Express 10, 043001 (2017). [3] N. Prasad et al., Neuromorph. Comput. Eng. 2, 034003 (2022). [4] S. Tsunegi et al., The 83rd Japan Society of Applied Physics Autumn Meeting, 2022. [5] Y. Imai and T. Taniguchi, submitted.

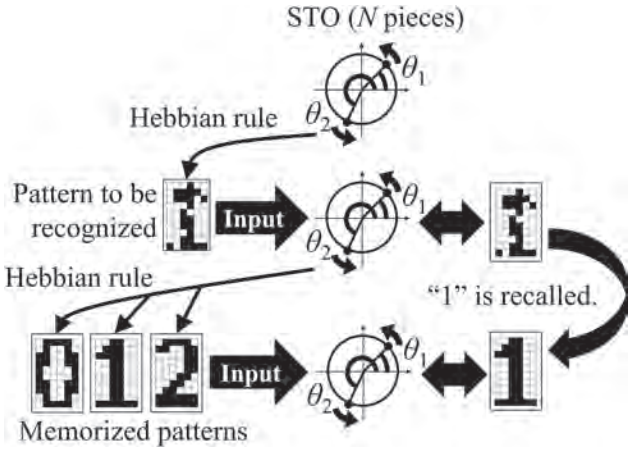

Fig. 1: Schematic illustration of pattern recognition by a single oscillator with time-multiplexing.

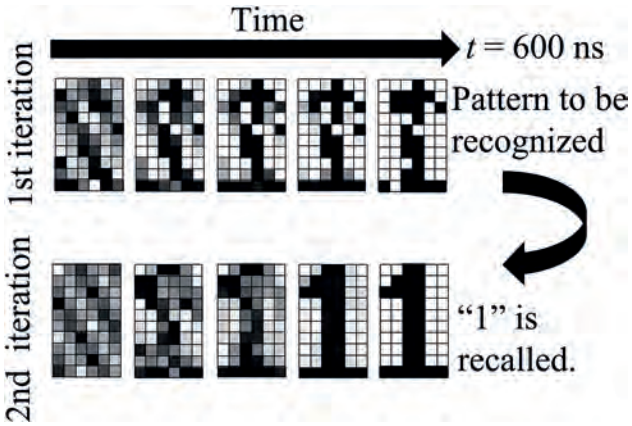

Fig. 2: The change of the colors corresponding to the phases in the recognition task.

AB-04. Experimental Demonstration of Unsupervised Online Learning with Stochastic STT-MTJ Switching. *P. Zhou*[1], A.J. Edwards[1], F. Mancoff[2], S. Aggarwal[2] and J.S. Friedman[1] *1. Department of Electrical and Computer Engineering, The University of Texas at Dallas, Richardson, TX, United States; 2. Everspin Technologies, Inc., Chandler, AZ, United States*

One of the primary hardware costs incurred by artificially-intelligent neural networks is due to vector-matrix multiplication (VMM), which is generally performed with floating-point binary numbers and computed exactly with cumbersome multiplication computations which scale with the number of entries in the matrix. Non-volatile analog resistive memory devices appear to naturally mimic the behavior of neurobiological synapses, and can be used to perform VMM by taking advantage of Ohm's and Kirchhoff's laws to efficiently perform these calculations in terms of voltage and current. Most research in this area has focused on crossbars composed of memristors and phase change memory (PCM). However, these devices suffer from several major challenges, including imprecise writing, weights drifting over time, limited endurance, etc. Spin-transfer torque magnetic tunnel junctions (STT-MTJs) resolves these issues, as it provides a stable non-volatile binary state. To provide analog behavior for neuromorphic learning, Querlioz *et al.* showed that the stochastic switching of STT-MJs can emulate analog synaptic behavior in a neuromorphic system. STT-MTJs therefore provides the best of both worlds – stable binary memory that enables reliable inference alongside analog stochastic switching that can be used for learning. We present the first experimental demonstration of unsupervised online learning with stochastic STT-MTJ switching. Eight MTJs are connected in a 4x2 neuromorphic structure through a probe station (Fig. 1a), with switches turned on and off to perform learning and inference (Fig. 1b). The experimental results (Fig. 2) show that the network is successfully able to learn from a training dataset comprising two distinct 2x2 pixel images, with stochastic STT-MTJ switching causing the network to learn to differentially recognize the two input images.

[1] A. F. Vincent, J. Larroque, N. Locatelli, N. Ben Romdhane, O. Bichler, C. Gamrat, W. S. Zhao, J.-O. Klein, S. Galdin-Retailleau, and D. Querlioz, "Spin-transfer torque magnetic memory as a stochastic memristive synapse for neuromorphic systems," IEEE Trans Biomed Circuits Syst, vol. 9, no. 2, pp. 166–174, 2015. [2] P. Zhou, J. A. Smith, L. Deremo, S. K. Heinrich-Barna, and J. S. Friedman, "Synchronous unsupervised stdp learning with stochastic stt-mram switching," arXiv:2112.05707, 2021. [3] P. Zhou, A. J. Edwards, F. B. Mancoff, D. Houssameddine, S. Aggarwal, and J. S. Friedman, "Experimental demonstration of neuromorphic network with stt mtj synapses," arXiv:2112.04749, 2021.

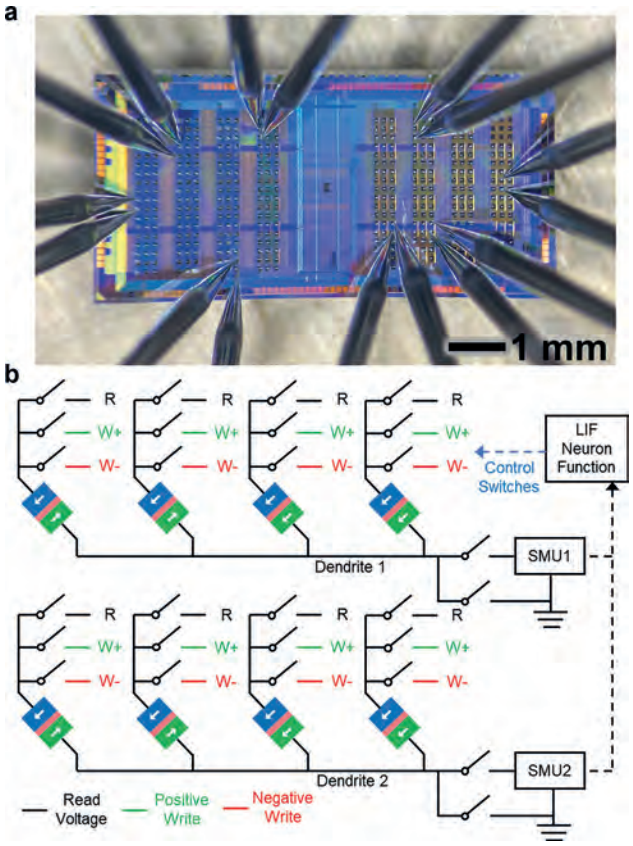

Fig. 1. (a) Photograph of the probe station with 16 probes connected to eight MTJs. (b) Schematic of the unsupervised online learning experiment configuration.

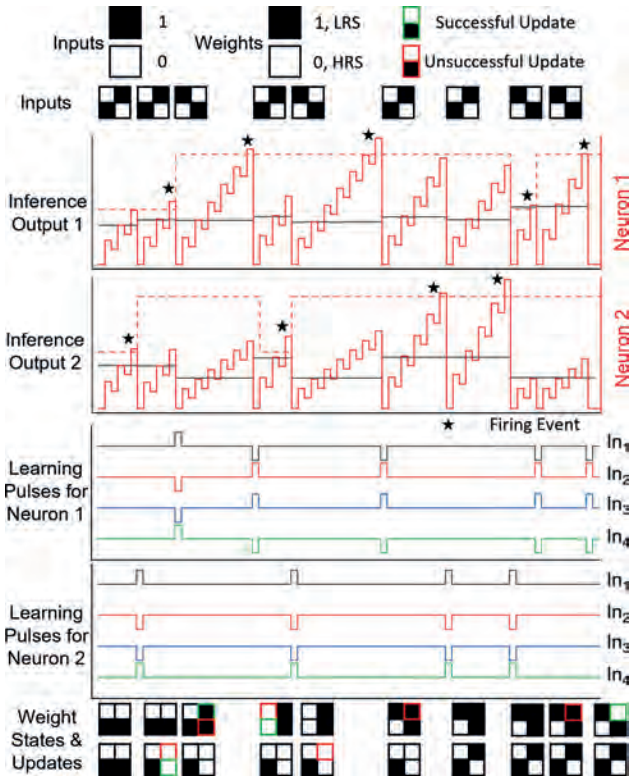

Fig. 2. The waveforms of the normalized SMU inference outputs and the unsupervised online learning signals, along with the inputs and weight states.

AB-05. Domain Wall – Magnetic Tunnel Junction Integrate-and-Fire Neuron with Auto-Reset. *C. Cui*[1], J. Kwon[1] and J.C. Incorvia[1]
1. Electrical and Computer Engineering, The University of Texas at Austin, Austin, TX, United States

The integrate-and-fire (IF) neuron model is a simple, yet realistic neuron model widely employed in spiking neural networks (SNNs)[1]. In this model, a neuron integrates input currents and builds up its membrane potential; once it reaches the firing threshold, the neuron outputs a current pulse to the downstream circuit. The three terminal domain wall-magnetic tunnel junction (3T DW-MTJ) nanodevice is a compact and power-efficient implementation of the IF model, using DW motion in the racetrack to emulate the integration process and the MTJ to read the output current[2]. Previous work using a single DW requires resetting the device using a current pulse or magnetic field after firing. Here, we present the experimental demonstration of a novel DW-MTJ IF neuron with potential auto-reset capability, utilizing the unidirectional motions of two, instead of one single DW. The designed device (Fig. 1(a)) consists of a "write" MTJ (MTJ_W) and a "read" MTJ (MTJ_R) sharing the DW racetrack free layer, confirmed by their similar coercivity (Fig.1(b)). Using spin-transfer torque, a single domain is locally injected into the racetrack under MTJ_W (Fig. 2(a)). Then, 50 ns voltage pulses of increasing amplitudes are applied between IN and CLK to drive the two DWs towards MTJ_R, and the resistances of both MTJs are measured (Fig. 2(b)). Under bias field $H_z = 30$ Oe, the R_P to R_{AP} switching of MTJ_W is first observed, followed by the R_{AP} to R_P switching of MTJ_R. In contrast, under no bias field $H_z = 0$ Oe, the R_{AP} to R_P switching of MTJ_R is first observed, followed by the R_P to R_{AP} switching of MTJ_W. The details of the switching of MTJ_W and MTJ_R are due to the field-dependent motion of two DWs (Fig. 2(c)), with the positive H_z assisting the motion of up-down DW and inhibiting the down-up DW. A control experiment without domain injection is performed where no switching of either MTJ is observed (blue square), ruling out random domain nucleation from racetrack edges. These results show electrical control and detection of two DWs in the DW-MTJ, endowing the device with the potential of implementing an IF neuron with auto-reset i.e., switching MTJ_R AP-P with the first DW and then P-AP with the second DW.

[1]A.N.Burkitt, A review of the integrate-and-fire neuron model: I. Homogeneous synaptic input. *Biological cybernetics*, *95*, pp.1-19. (2006) [2]N.Hassan, X. Hu, L. Jiang-Wei et al., *Journal of Applied Physics*, *124*(15), p.152127. (2018)

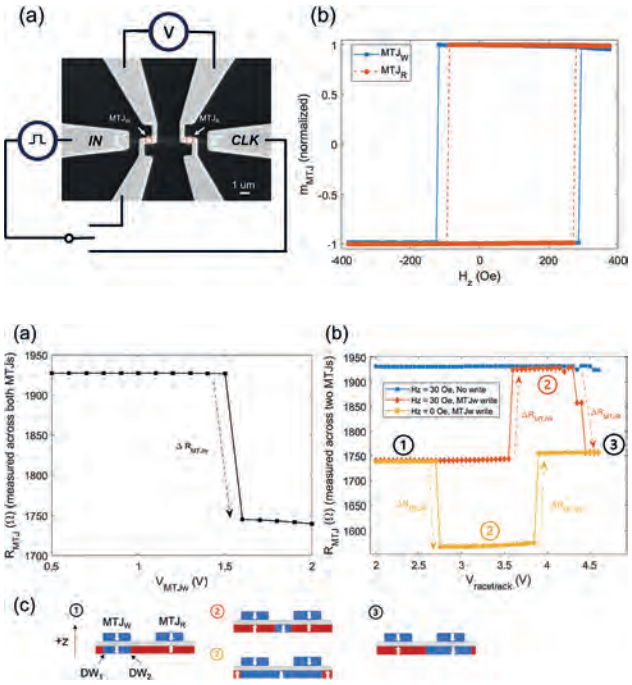

AB-06. Stochastic Domain Wall-Magnetic Tunnel Junction Artificial Neurons in Spiking Neural Networks for Enhanced Noise Resilience. *S. Liu*[1], T. Leonard[1], H. Jin[1] and J.C. Incorvia[1] *1. Department of Electrical and Computer Engineering, The University of Texas at Austin, Austin, TX, United States*

Artificial neural networks are powerful tools for data intensive classification and regression, but the memory wall in von Neumann architectures prevents efficient processing [1]. Spiking neural networks (SNNs) provide additional opportunities for energy efficient neuromorphic computing due to the encoding of information in both amplitude, frequency, and spatial characteristics of spikes [2]. Performing neural network training and inference on edge platforms requires current computing hardware to not only be more energy efficient, but more noise resilient as well. Here, we propose using the domain wall-magnetic tunnel junction (DW-MTJ) device platform as artificial spiking neurons for noise resilient spiking neural networks [3]. Previous work has shown through simulation that DW-MTJ devices can be operated as leaky integrate-and-fire (LIF) neurons [4], and through experiment that domain wall nucleation and notch depinning is a stochastic process [5]. We fabricate DW-MTJ devices with an offset MTJ (Fig. 1a) and perform device switching statistics to obtain switching probability as a function of write voltage (Fig. 1b), with an average energy dissipation of 44.9 pJ/spike. Along with data collected on multi-weight DW-MTJ devices, the statistics are used to simulate SNNs in Norse, showing that using binary stochastic neurons does not result in a significant loss of accuracy compared to the multiweight synapses, while resulting in a greatly enhanced noise-resilience in SNN inference (Fig. 2a-c). The results indicate that stochastic DW-MTJ artificial neurons are well-suited for neural network accelerators on the edge due to their noise resilience, energy dissipation, and radiation hardness of MTJs.

A. Sebastian, M. le Gallo, R. Khaddam-Aljameh, and E. Eleftheriou, (2020). Memory devices and applications for in-memory computing. *Nature Nanotechnology*, *15*(7), 529–544. K. Roy, A. Jaiswal, and P. Panda, (2019). Towards spike-based machine intelligence with neuromorphic computing. *Nature*, *575*(7784), 607–617. T. Leonard*, S. Liu*, H. Jin, and J. A. C. Incorvia, (2023). Stochastic Domain Wall-Magnetic Tunnel Junction Artificial Neurons for Noise-Resilient Spiking Neural Networks. *Applied Physics Letters,* accepted. W. H. Brigner, N. Hassan, X. Hu, C. H. Bennett, F. Garcia-Sanchez, C. Cui, A. Velasquez, M. J. Marinella, J. A. C. Incorvia, and J. S. Friedman, (2022). Domain Wall Leaky Integrate-and-Fire Neurons With Shape-Based Configurable Activation Functions. *IEEE Transactions on Electron Devices*, *69*(5), 2353–2359. M. Alamdar, T. Leonard, C. Cui, B. P. Rimal, L. Xue, O. G. Akinola, T. Patrick Xiao, J. S. Friedman, C. H. Bennett, M. J. Marinella, and J. A. C. Incorvia, (2021). Domain wall-magnetic tunnel junction spin-orbit torque devices and circuits for in-memory computing. *Applied Physics Letters*, *118*(11).

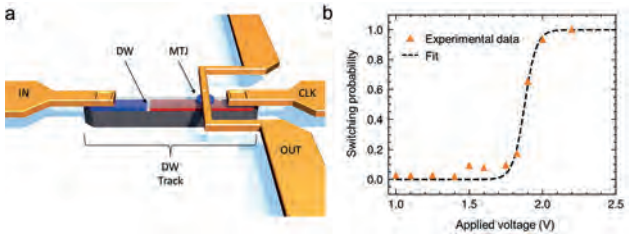

a) Diagram of stochastic DW-MTJ artificial neuron. b) Switching probability as a function of applied voltage, with a sigmoidal fit applied to the data.

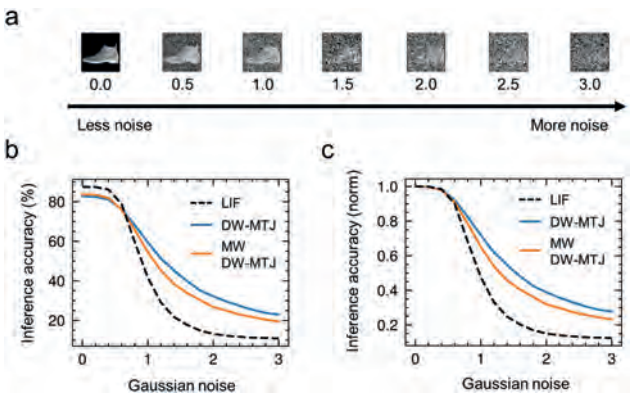

Performance of SNN trained on pristine data for inference on Fashion-MNIST (a) images with varying amounts of noise in terms of (b) raw inference accuracy and (c) inference accuracy normalized to maximum performance.

AB-07. A Leaky-Integrate-and-Fire spiking neuron by a Spin-Orbit Torque device. *R.I. Salinas*[1] and C. Lai[1] *1. Materials Science and Engineering, National Tsing Hua University, Hsinchu, Taiwan*

Neuromorphic computing, a promising approach to solve the von Neumann bottleneck, mimics the dynamics of the brain, where neurons and synapses play crucial roles in learning and memorization processes. However, the implementation of spiking neural networks (SNNs)— the third generation of artificial neural networks (ANNs)—is still under investigation due to significant energy consumption concerns. The Leaky-Integrate-and-Fire (LIF) neuron model leverages the spatio-temporal characteristics of brain information processing with low power consumption [1]. Spintronics devices use spin-orbit torques (SOT) to achieve current-driven magnetization switching, and due to their non-volatile characteristics, require a reset pulse to return the magnetization to its initial state for use in ANNs. In our study, we employ the IrMn/CoFeB/MgO stack to accomplish LIF switching without the need for a reset pulse current. The schematic diagram for the device setup is shown in Fig. 1. The IrMn layer is used as the spin current source as well as the antiferromagnetic (AFM) pinning layer. We leverage the exchange spring effect to achieve potentiation and depression behavior, essential for the development of low-power SNN, as depicted in Fig. 2. The exchange coupling between the IrMn bulk order and its interfacial spins facilitates the retraction of the domain wall (DW) to its initial state following the application of a pulse current. This retraction occurs because the pinned interfacial spins act as a node of the exchange spring, oriented perpendicular to the interface. The amplitude of the external field (Hx) allows for the adjustment of the retraction velocity of the DW, exhibiting what is referred to as depression behavior in SNN. Low (high) Hx leads to a slow (fast) retraction of the DW, characterized as long- and short-term depression, respectively. These findings underscore the critical role of AFM materials in the development of functional spintronic SNN.

1. Ismael Salinas R, Chen P-C, Yang C-Y, et al. Materials Research Letters. 2022;11(5):305-326.

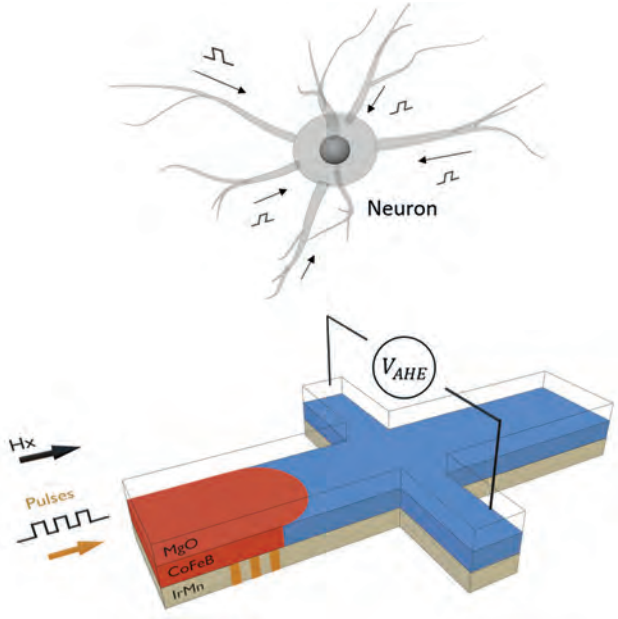

Fig.1: Spintronic LIF spiking neuron. Device stack of IrMn (5 nm)/CoFeB (1 nm)/MgO (1.5 nm) is patterned in a Hall bar structure.

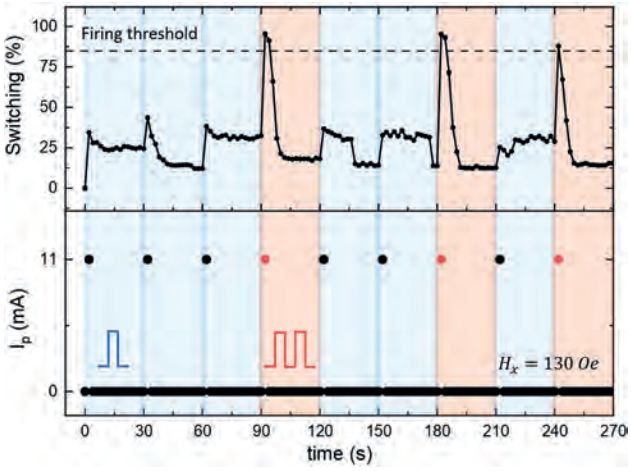

Fig. 2: Experimental demonstration of LIF switching. Pulse ampllitude (I_p) of 11 mA, pulse width of 10 µs, and delay between pulses of 10 µs.

AB-08. Multilayer spintronic devices as a synapse and neuron for neuromorphic computing. *A.H. Lone*[1], X. Zou[1], G. Maciel Garcia[1], G. Setti[1] and H. Fariborzi[1] *1. Computer, Electrical and Mathematical Sciences and Engineering Division, King Abdullah University of Science and Technology, Jeddah, Saudi Arabia*

Spintronic devices have shown promise for energy-efficient storage and neuromorphic computing [1][2][3]. In this abstract, we present the experimental and micromagnetic realization of a multilayer heterostructure spintronic device for memory and neuromorphic computing applications (see Fig. 1(a-c). We observe the discrete resistance behavior in the device as shown in Fig. 2(a-b). This behavior is attributed to the magnetic domain wall pinning/depinning and gradual switching of different magnetic layers. The anisotropy and saturation magnetization increase at lower temperatures and thermal effects [4] are reduced thus discrete switching behavior starts dominating at low temperatures. The discrete resistance states across the range of temperatures open a possible application as multistate memory devices for cryogenic electronics. The discrete resistance behavior is also observed in the micromagnetic simulations of similar crossbars of different widths. The evolution of resistance states with current pulses providing spin transfer torque and spin-orbit torque is also explored in both experiments and simulations. Considering the multi-resistance states behavior of the device, we propose its applications as a synaptic device for neuromorphic computing. We map these resistance states as the weights of a neural network architecture. Furthermore, the device also acts as a leaky integrate and fire neuron when stressed by spin-orbit torque and spin transfer torque pulses as shown in Fig. 2(b). We have trained and tested the network implemented with these devices on the MNIST data set using a supervised learning algorithm and spiking neural network. The system shows an accuracy of up to 90% (see Fig. 2(c)), which is comparable to the majority of the beyond CMOS synaptic devices.

[1] Grollier, J., Querlioz, D., Camsari, K.Y. *et al.* Neuromorphic spintronics. *Nat Electron* 3, 360–370 (2020). https://doi.org/10.1038/s41928-019-0360-9. [2] Fert, A., Reyren, N. & Cros, V. Magnetic skyrmions: Advances in physics and potential applications. *Nat. Rev. Mater.* 2, (2017). [3] A. H. Lone and H. Fariborzi, "Skyrmion-magnetic tunnel junction synapse with long -term and short-plasticity for neuromorphic computing," IEEE Transactions on Electron Devices, vol. 70, Jan - 2023. [4] O. Boulle et. al, "Non-adiabatic spin transfer torque in high anisotropy magnetic nanowires with narrow domain walls," PRL, 10.1103/PhysRevLett.101.216601

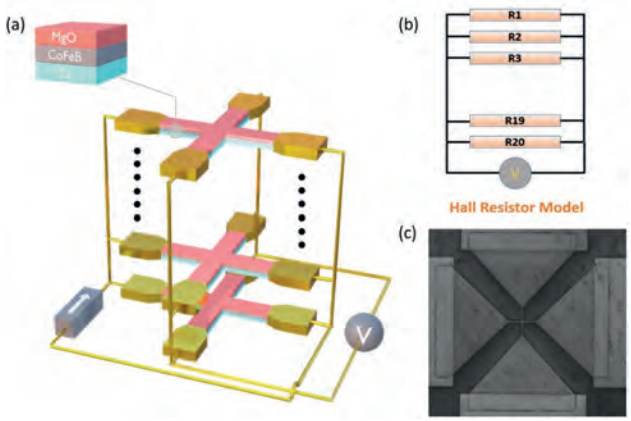

Fig. 1(a) Domain wall crossbar devices. (b) Equivalent resistor model (c) SEM Image

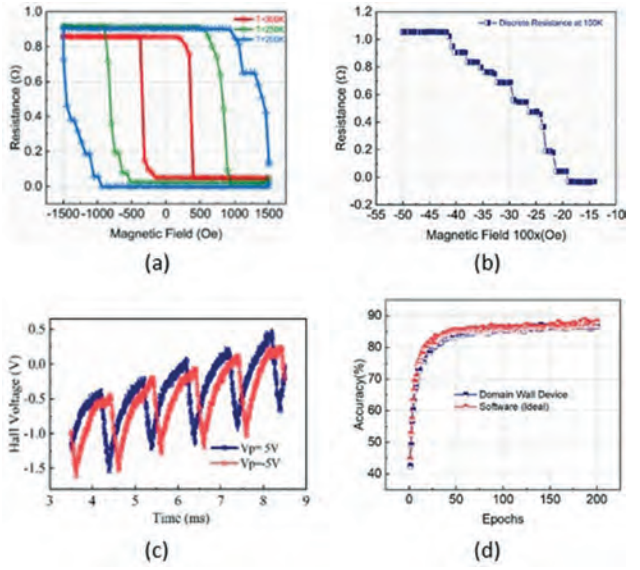

Fig. 2(a) Temperature-dependent discrete resistance. (b) Discrete resistance as a function of magnetic field (c) multi-layer spintronic leaky LIF neuron (d) MNIST data classification of the neural network -based on these devices

AB-09. Withdrawn

AB-10. Experimental demonstration of a heavy-metal-ferromagnetic-metal-multilayer-based, bulk-spin-orbit-torque-driven domain-wall synapse device for neuromorphic crossbar arrays. *R.S. Yadav*[1], P. Gupta[1], A. Sadashiva[2], P.K. Muduli[1] and D. Bhowmik[2] *1. Department of Physics, Indian Institute of Technology Delhi, New Delhi, India; 2. Indian Institute of Technology Bombay, Department of Electrical Engineering, Mumbai, India*

Spin orbit torque (SOT) driven domain-wall devices are attractive as non-volatile synapses in neuromorphic crossbar arrays [1-4]. But most SOT synapse devices are based on heavy metal/ ferromagnet/ oxide structures [1-3]. Due to the interfacial origin of the SOT in them, they exhibit a trade-off between thermal stability and programming current density [5]. Here, we experimentally demonstrate synaptic behavior in a heavy metal (Pt)/ ferromagnetic metal (Co) multilayer device (no oxide layer), which eliminates this trade-off since it works based on bulk SOT instead [5,6]. Fig. 1b shows an image of the Hall bar device fabricated from our sputtered multilayer stack (Fig. 1a), with increasing Pt layer thickness from bottom to top. Anomalous Hall resistance R_{AHE} (ratio of measured voltage to read current) vs field plot of Fig. 1c confirms perpendicular magnetic anisotropy (PMA), and Fig. 1d shows current-driven switching due to SOT [5]. Fig. 1e shows experimentally obtained synaptic characteristics: positive pulses of different current densities cause long-term potentiation (LTP)/ increase of synaptic weight (proportional to R_{AHE}), while negative pulses cause long-term depression (LTD)/ weight decrease. In Fig. 2a, we obtain non-linearity factors (α_P, α_D) [7] for LTP/ LTD plots of Fig. 1e. In Fig. 2b, we obtain bit resolution of weights stored in the device [3]. Next, we model on-chip learning of a crossbar array, for MNIST data set of handwritten digits, using experimentally obtained LTP/LTD of Fig. 1e/2a [3]. In Fig. 2c, with 2 devices per synapse unit in differential configuration [8], we use LTP characteristic under 3.17 x 10^7 A/cm^2 current (α_P = 2.46) and obtain good training (test accuracy > 60 %) for 2 synapse units/ 4 devices per synapse cell. In Fig. 2d, we use normal synapse configuration (1 device per synapse unit), LTP under 3.24 x 10^7 A/cm^2 current (α_P = 5.33), and LTD under -3.17 x 10^7 A/cm^2 current (α_D = -4.41). Now, we obtain good training for 3 synapse units/ 3 devices per cell.

1. D. Kumar *et al.,* Ultralow Energy Domain Wall Device for Spin-Based Neuromorphic Computing, ACS Nano 17 (7), 6261-6274 (2023) 2. S. Zhang *et al.*, A Spin–Orbit-Torque Memristive Device, Adv. Electron Mater. 1800782 (2019) 3. R. S. Yadav et al, Demonstration of Synaptic Behavior in a Heavy-Metal-Ferromagnetic-Metal-Oxide-Heterostructure-Based Spintronic Device for On-Chip Learning in Crossbar-Array-Based Neural Networks, ACS Appl. Electron. Mater. 5 (1), 484-497 (2023) 4. T. Leonard *et al.* Shape-Dependent Multi-Weight Magnetic Artificial Synapses for Neuromorphic Computing, Adv. Electron Mater. 2200563 (2022) 5. K. Zhang *et al,* Efficient and controllable magnetization switching induced by intermixing-enhanced bulk spin–orbit torque in ferromagnetic multilayers, Appl. Phys. Rev. 9, 011407 (2022) 6. X. Xie *et al,* Controllable field-free switching of perpendicular magnetization through bulk spin-orbit torque in symmetry-broken ferromagnetic films, Nature Comm. 12, 2473 (2021) 7. P. Y. Chen *et al,* NeuroSim: A circuit-level macro model for benchmarking neuro-inspired architectures in online learning, *IEEE Trans. CAD*, 37 (12), 3067--3080 (2018) 8. M. Suri *et al,* Phase change memory as synapse for ultra-dense neuromorphic systems: Application to complex visual pattern extraction, Proceedings of IEEE International Electron Devices Meeting (IEDM), 4.4.1-4.4.4 (2011)

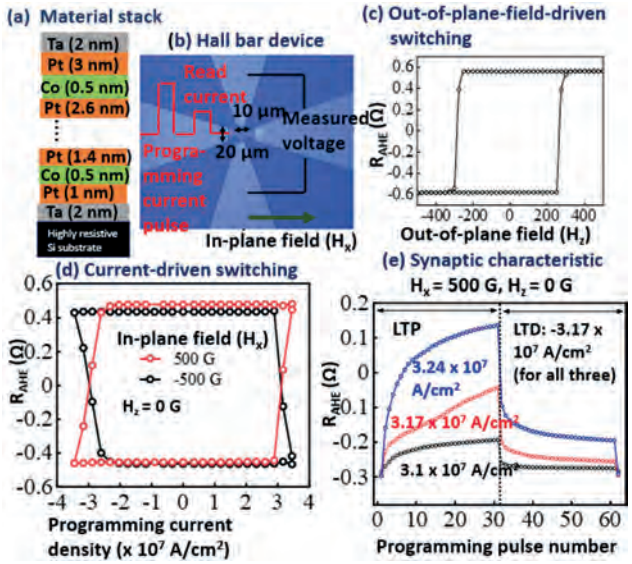

Fig. 1. Bulk SOT device and its experimentally obtained switching and synaptic characteristics

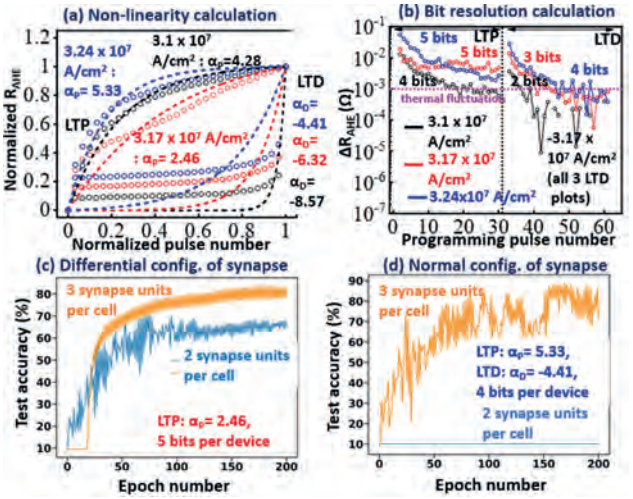

Fig. 2 a,b: Experimentally obtained synapse parameters, c,d: modeling of crossbar array using them and related training performance

AB-11. Validation of the Néel-Arrhenius law in nanomagnetic tunnel junctions. *S. Kanai*[1,2], M. Elyasi[3,4], G. Bauer[5,6], H. Ohno[7,8] and S. Fukami[9,10] *1. JST-PRESTO, Kawasaki, Japan; 2. Division for the Establishment of Frontier Sciences of Organization for Advanced Studies, Tohou University, Sendai, Japan; 3. Center for Science and Innovation in Spintronics, Tohoku University, Sendai, Japan; 4. WPI-Advanced Institute for Materials Research, Tohoku University, Sendai, Japan; 5. Institute for Materials Research, Tohoku University, Sendai, Japan; 6. Kavli Institute for Theoretical Sciences, University of Chinese Academy of Sciences, Beijing, China; 7. Laboratory for Nanoelectronics and Spintronics, Research Institute of Electrical Communication, Tohoku University, Sendai, Japan; 8. Center for Innovative Integrated Electronic Systems, Tohoku University, Sendai, Japan; 9. Graduate School of Engineering, Tohoku University, Sendai, Japan; 10. Inamori Research Institute for Science, Sendai, Japan*

Probabilistic computing with stochastic magnetic tunnel junctions (s-MTJs) has attracted significant attention [1,2]. The relaxation time τ of a thermally agitated state is often described by a *generalized* Arrhenius law, *viz.*, $\tau = \tau_0 \exp(E/k_BT)^n$ [τ_0: attempt time, E: energy barrier, k_BT: thermal energy, and n: stretching exponent]. $n = 1$ is called Néel-Arrhenius law for ferromagnets [3], but thermally activated phenomena with $n \neq 1$ are often observed in nature. In a previous meeting [4], we reported τ_0 for a single s-MTJ assuming $n = 1$. n can sometimes be deduced by an Arrhenius plot (τ *vs.* T), but this does not work for magnetic systems with a T-dependent E. Here we validate the Néel-Arrhenius law by a "constant-temperature" Arrhenius plot for several s-MTJs, determine their τ_0, and interpret results in terms of a non-uniform spin dynamics [5]. We prepare 10 CoFeB/MgO-based, in-plane easy-axis, ellipse-shaped s-MTJs with different perpendicular anisotropy fields H_K^{eff} that show stochastic behavior with $\tau \leq \sim 100$ s. We determine E at room temperature by measuring τ as a function of in-plane hard-axis magnetic fields. Figure 1(a) shows τ *vs.* E/k_BT, *i.e.*, the constant-temperature Arrhenius plot. The stretched exponential function $\tau = \tau_0 \exp(E/k_BT)^n$ with $n = 1.0$ fits the experimental results well. τ_0 (5 ~ 11 ns) is one-order-of-magnitude larger than expected from the macrospin model (0.2 ~ 0.5 ns). A theoretical model that includes four-magnon scattering explains this discrepancy in terms of the Suhl decay of the Kittel mode into spin waves that suppress the magnetization reversal [Fig. 1(b)]. We acknowledge contributions to this work by K. Hayakawa, K. Kobayashi, W. Borders, J. Igarashi, and B. Jinnai, as well as financial support by the JST-CREST JPMJCR19K3, the JST-PRESTO JPMJPR21B2, JST-AdCORP JPMJKB2305, JSPS-Kakenhi 19H05622 and 21K13847, the Shimadzu Research Foundation, the Takano Research Foundation, and Cooperative Research Projects of RIEC.

[1] K.Y. Camsari *et al*., Phys. Rev. X 7, 031014 (2017). [2] W.A. Borders *et al*., Nature 573, 390 (2019). [3] L. Néel Ann. Geophys. 5, 99 (1949). [4] K. Hayakawa *et al*., Joint MMM-Intermag 2022, GOK-11 (January 2022). [5] S. Kanai *et al*., *submitted* (2023). [6] S. Kanai *et al*., Phys. Rev. B 103, 094423 (2021). [7] K. Hayakawa *et al*., Phys. Rev. Lett. 126, 117202 (2021).

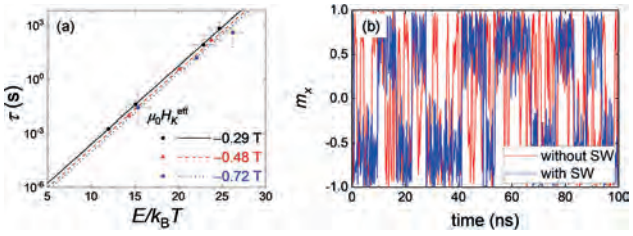

Figure 1 (a) Constant (room) temperature Arrhenius plot (b) Simulated magnetization dynamics with and without spin wave excitation induced by the Suhl instability.

Session AC
MICROSCOPY & CHARACTERIZATION I: SCANNING PROBES AND MATERIALS

Max Birch, Chair

RIKEN Center for Emergent Matter Science, Tokyo, Japan

INVITED PAPER

AC-01. Magnetic Force Microscopy – a quantitative Method for probing Magnetic Textures and their Dynamics on the Nanoscale.

V. Neu[1] 1. IFW Dresden, Dresden, Germany

Magnetic force microscopy (MFM) has established its place as an extremely valuable method for the investigation of static magnetic microstructures on the nanometer scale [1]. Beyond being a purely qualitative imaging technique, quantitative MFM has the capability to locally measure the stray fields and to provide quantitative input data for a reconstruction of the underlying magnetization structure [2, 3]. However, being a mechanical scanning technique, imaging of dynamic magnetic processes appears out of reach. Here, we will report on a new approach to image and analyze periodic nanoscale domain wall oscillations down to sub 100 nm oscillation amplitudes at kHz frequencies. The method is based on a quantitative assessment of the time-averaged MFM phase shift signal and its description by the locally varying dwell time function of an oscillating domain wall (DW) [4]. It is applied to the 180° Néel domain wall forming in micron-sized patterned permalloy rectangles. Figure 1 displays the phase shift signal across the oscillating Néel wall in standard lift-mode with the slow-scan axis (y-direction) disabled. The DW is excited sinusoidally at 1 kHz. Within the acquisition time of a pixel, the DW performs several periods of motion and the MFM tip senses a signal proportional to the averaged dwell time, the DW is present at the tip position. Due to the position dependent DW velocity, this interaction time between tip and DW is also position dependent and the return points of the DW are imaged as two darker vertical lines. The magenta line displays the scan profile averaged over several scan lines. The experimental profiles for static and dynamic domain walls excited at 1 kHz are plotted in Figure 2 as dotted lines. The dynamic profiles are fully described by a convolution of the static profile with the dwell-time function of a sinusoidal motion with one free parameter – the amplitude of the DW oscillation. This allowed for a detailed quantification of amplitude vs excitation field, frequency, and structure size of the permally rectangles, well below the resolution limit of optical magnetic microscopy. We understand the excited DW behavior as a forced damped harmonic oscillator with the restoring force being influenced by the geometry, thickness and anisotropy of the $Ni_{81}Fe_{19}$ structure. The new approach offers new possibilities for the analysis of DW motion at elevated frequencies in various branches of nanomagnetism.

[1] O. Kazakova, R. Puttock, C. Barton, H. Corte-León, M. Jaafar, V. Neu, and A. Asenjo, Journal of Applied Physics 125, 060901 (2019). [2] S.Guo, M. Henschel, D. Wolf, D. Pohl, A. Lubk, T. Blon, V. Neu, K. Leistner, Nano Letters 22, 4006 (2022). [3] N. Freitag, C. F. Reiche, V. Neu, P. Devi, U. Burkhardt, C. Felser, D. Wolf, A. Lubk, B. Büchner, and T. Mühl, Communications Physics, 6, 11 (2023). [4] B. Singh, R. Ravishankar, J.A. Otálora, I Soldatov, R. Schäfer, D. Karnaushenko, V. Neu, O.G. Schmidt, Nanoscale 14, 13667 (2022).

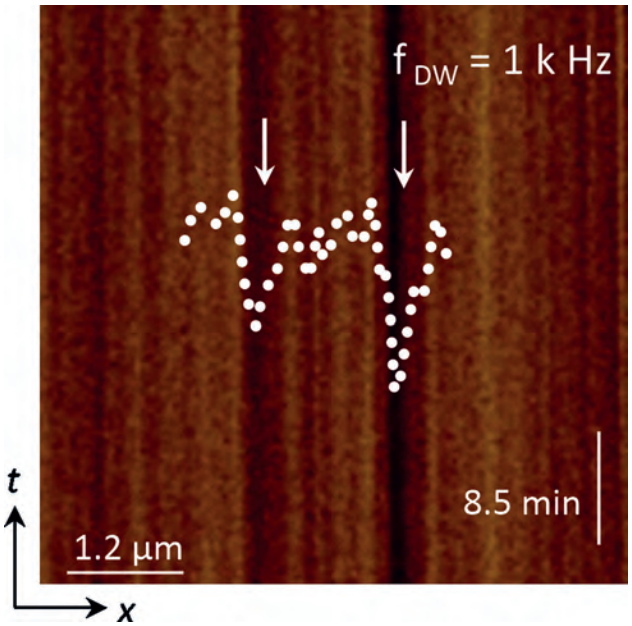

Fig.1: MFM phase shift signal of a 180° Neél wall in a rectangular Py structure oscillating at 1 kHz.

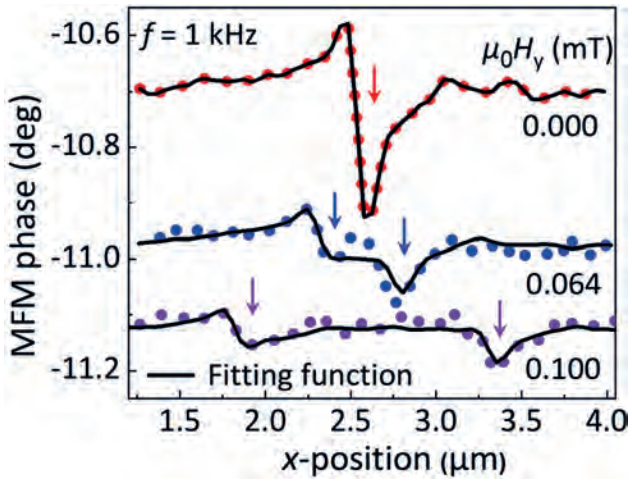

Fig. 2: MFM profiles across the non-excited DW ($\mu_0 H_y = 0$, red dots) and oscillating DWs (at 1 kHz) excited with two different field amplitudes ($\mu_0 H_y = 0.064$ and 0.10 mT) at a frequency of 1 kHz. The solid lines are fits to the experimental data applying the dwell-time function concept.

CONTRIBUTED PAPERS

AC-02. Depth Profiling for Embedded Metallic Nanostructures using Conductive Atomic Force Microscopy. A.K. Toh[1] and *V. Ng*[1]
1. Electrical and Computer Engineering, National University of Singapore, Singapore

Conductive-AFM (CAFM) [1] has been widely used to study dielectric and nanocomposite films [2-3]. The electrical potential between tip and sample allows electron transport through oxide samples by quantum tunnelling [4], enabling CAFM to perform sub-surface imaging of conductive nanostructures embedded in insulating matrices. This work will demonstrate depth profiling using CAFM on (i) patterned Py nanostructures at defined locations embedded in Al_2O_3 and (ii) granular films (GFs) with randomly dispersed Co nanoparticles (NPs) in HfO_2 matrix [5]. Fig 1 show topography and current images of the Py/Al_2O_3 /Py/Al_2O_3 sample with Py structures misaligned intentionally for both layers. Bias was varied between the probe and sample bottom electrode. The bright conducting regions at 6 V (fig 1b) match the fainter bottom layer features in the topography (fig 1a green outline) well, whereas the darker (lower current) regions match the top layer features (blue outline). This implies that current signals from the bottom structures were first detected at low bias. As the bias was increased to 8 V (fig 1c), all Py nanostructures were seen to contribute to the current signals. CAFM imaging was observed to be sensitive to the applied bias magnitude between the substrate and surface. Fig 2 show CAFM images of Co-HfO_2 GFs from sequentially sputtered Co and HfO_2 bilayers [5]. The thicker samples with more bilayers display faint contrast in the darker background, suggesting that the depth of the NPs within the GF can be observed, attributed to tunnelling electrons experiencing a thicker tunnel barrier for Co NPs deeper within the GF. A phenomenological model is developed to further investigate the above counter-intuitive observation of bottom Py structures appearing first at low bias, and the perceived depth of imaged Co NPs in GFs. This model, based on thermionic emission, Fowler-Nordheim and direct tunnelling, will be used to explain our experimental findings and understand the distribution of NPs in GFs [6-8].

[1] F. Hui and M. Lanza, "Scanning probe microscopy for advanced nanoelectronics," *Nat. Electron.,* vol. 2, no. 6, pp. 221-229, (2019), doi: 10.1038/s41928-019-0264-8. [2] A. Ranjan, S. J. O'Shea, M. Bosman, N. Raghavan, and K. L. Pey, "Localized probing of dielectric breakdown in multilayer hexagonal boron nitride," *ACS Appl. Mater. Interfaces,* vol. 12, no. 49, pp. 55000-55010, (2020), doi: 10.1021/acsami.0c17107. [3] J. Snikeris and V. Gerbreders, "Effects of electron beam irradiation on a Ag/AsS2 bilayer using conductive atomic force microscopy," *Thin Solid Films,* vol. 731, p. 7, (2021), doi: 10.1016/j.tsf.2021.138747. [4] W. Frammelsberger, G. Benstetter, J. Kiely, and R. Stamp, "C-AFM-based thickness determination of thin and ultra-thin SiO_2 films by use of different conductive-coated probe tips," *Appl. Surf. Sci.,* vol. 253, no. 7, pp. 3615-3626, (2007), doi: 10.1016/j.apsusc.2006.07.070. [5] M. Chadha and V. Ng, "Sequential sputtered Co-HfO_2 granular films," *J. Magn. Magn. Mater.,* vol. 426, pp. 302-309, (2017), doi: 10.1016/j.jmmm.2016.11.094. [6] F. C. Chiu, "A review on conduction mechanisms in dielectric films," *Adv. Mater. Sci. Eng.,* p. 18, (2014), doi: 10.1155/2014/578168. [7] M. Lenzlinger and E. H. Snow, "Fowler Nordheim tunneling into thermally grown SiO_2", *J. Appl. Phys.,* vol. 40, no. 1, pp. 278-283, (1969), doi: 10.1063/1.1657043. [8] A. K. J. Toh and V. Ng, "Tomographic imaging using conductive atomic force microscopy," *Mater. Charact.,* vol. 186, p. 9, (2022), doi: 10.1016/j.matchar.2022.111783.

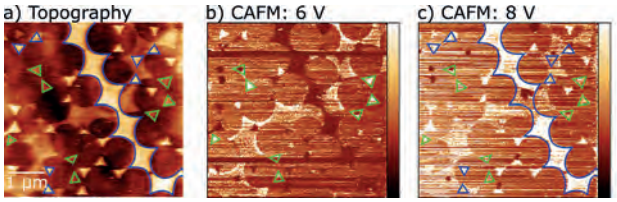

Fig 1: (a) AFM and CAFM images at (b) 6 V, (c) 8 V of Py/Al_2O_3/Py/Al_2O_3 nanostructures. Blue (green) outlines indicate top (bottom) layer.

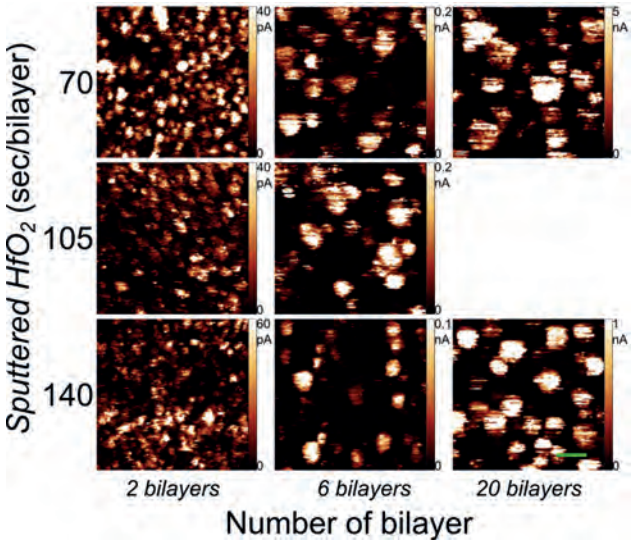

Fig 2: CAFM images of Co-HfO_2 granular films with varying deposition conditions.

AC-03. Evaluation of Martensite transformation temperatures using magnetometry. *N.J. Jones*[1], P.K. Lambert[2], J.H. Yoo[1], S.M. Na[1] and C.R. Fisher[3] *1. Physical Metallurgy and Fire Performance Branch, Naval Surface Warfare Center, Carderock Division, Bethesda, MD, United States; 2. Applied Physics Laboratory, Johns Hopkins University, Laurel, MD, United States; 3. Welding, Processing, and NDE Branch, Naval Surface Warfare Center, Carderock Division, Bethesda, MD, United States*

Martensite start and finish temperatures are two critical parameters needed to define the processing variables for steels. Accurately defining the martensite transformation range is critical for choosing quenching temperatures and subsequent annealing parameters to form the desired phases needed to achieve target mechanical properties and grain size. While these temperatures are normally measured using dilatometry samples, the austenite-to-martensite phase transformation also possesses a magnetic phase change, changing from the paramagnetic austenite phase to the ferromagnetic martensite phase. Magnetization measurements have been used herein as a method to determine these structural phase transformation temperatures. Eight compositions of steel having published martensite start temperatures ranging from -130 °C to +30 °C were synthesized *via* vacuum arc melting. After a high-temperature homogenization heat treatment, samples were extracted and room-temperature magnetic hysteresis loops were measured, followed by a magnetization versus temperature curve to cryogenic temperatures (-188 °C) at a constant applied field. An additional room temperature magnetic hysteresis loop was measured following the temperature cycling. Samples showed pronounced increases in magnetization as temperature decreased due to the irreversible martensitic transformation, and eventually magnetization plateaued below the sample's martensite finish temperature. In addition to the measured martensite start and finish temperatures and general characterization of the samples, the choice of applied magnetic field strength will be discussed, to ensure that the transformation is being appropriately characterized. It was determined that low applied magnetic fields

(H < 1 kOe) were not appropriate for resolving these structural changes. Despite variations due to sample geometry and applied magnetic field strength, the martensite start temperature was measured within 2 °C.

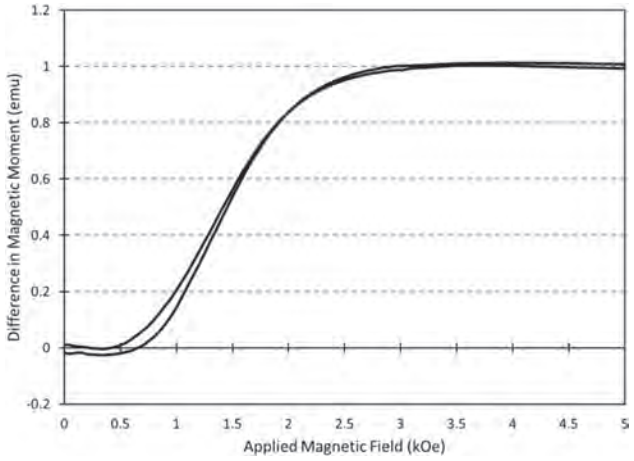

Fig 1. Difference in magnetic moment between room temperature hysteresis loops of a steel measured before and after cryogenic cycling.

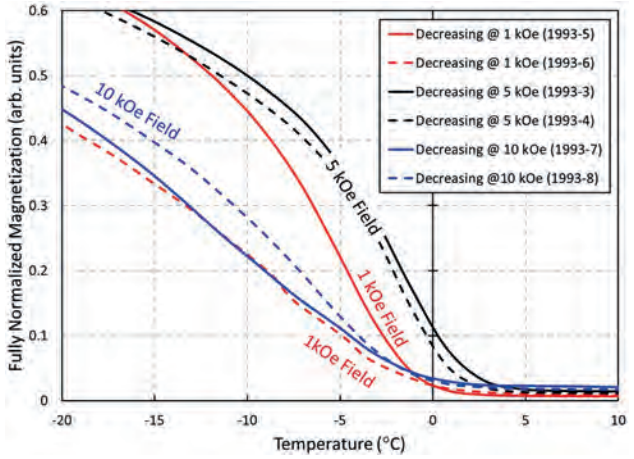

Fig 2. Fully normalized magnetization vs. temperature curves measured at various applied field strengths for samples of the same steel composition.

AC-04. Discussing the Universality Law in Magnetically Detected Residual Stresses in Steels. *T.V. Damatopoulou*[1], S. Angelopoulos[1], X. Vourna[1], A. Ktena[2] and E. Hristoforou[1] *1. Laboratory of Electronic Sensors, National TU of Athens, Athens, Greece; 2. National and Kapodistrian University of Athens, Athens, Greece*

In this paper, the universality law of the dependence of residual stresses on magnetic properties is revisited and discussed. Residual stresses are generated in a steel coupon by autogenous welding, using TIG, Plasma and RF induction welding process. The residual stress components are determined by XRD Bragg Brentano set-up and neutron diffraction for surface and bulk measurements respectively. The residual stresses are in a full agreement with magnetic permeability measurements. Therefore, the Magnetic Stress Calibration (MASC) curve for each type of steel can be determined. These MASC curves are different for different types of steel. However, it has been found that the normalization of the stress and permeability axes with the corresponding yield point and the maximum amplitude of permeability respectively, results in collapsing all MASCs in one sigmoid response. Due to this observation, the detection of stresses in an unknown type of steel can be realized by determining the stress-strain curve of this unknown type of steel. During measurement, magnetic permeability is detected in parallel for the yield point. Thus, the actual MASC for the unknown type of steel is provided. Finally, the explanation of the universality law is attempted due to the magnetoelastic theory.

Hristoforou, E., Vourna, P., Ktena, A., Svec, P., On the Universality of the Dependence of Magnetic Parameters on Residual Stresses in Steels, IEEE Transactions on Magnetics 52(5),7362189, 2016

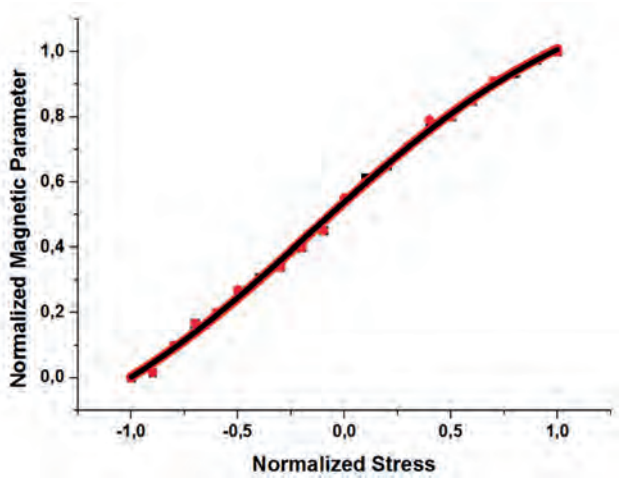

All different MASCs collapse in a single sigmoid response after normalization of the X- axis (residual stresses) with the yield point of each different steel and normalization of the Y- axis (differential magnetic permeability or Barkhausen noise) with the corresponding maximum amplitude.

INVITED PAPER

AC-05. Nitrogen-Vacancy Microscopy of Antiferromagnetic Domains in Undoped and Boron Doped Cr_2O_3 Thin Films. A. Erickson[1], A. Mahmood[2], S. Shah[2], R. Timalsina[1], I. Fescenko[3], C. Binek[2] and *A. Laraoui[1,2] 1. Department of Mechanical & Materials Engineering, University of Nebraska-Lincoln, Lincoln, NE, United States; 2. Department of Physics and Astronomy and the Nebraska Center for Materials and Nanoscience, University of Nebraska-Lincoln, Lincoln, NE, United States; 3. Laser Centre, University of Latvia, Riga, Latvia*

Diamond nitrogen vacancy (NV)-based magnetometry has become an alternative tool to study nanoscale magnetic phenomena with a unique combination of spatial resolution and magnetic sensitivity, opening up new frontiers in condensed physics matter research [1-3]. In this study, we use NV-scanning probe microscopy (NV-SPM, Fig.1a) to probe antiferromagnetic (AFM) domains in thin undoped chromia (Cr_2O_3) and boron (B) doped Cr_2O_3 films (thickness = 50 – 200 nm) grown by pulsed laser deposition on Al_2O_3 and V_2O_3 substrates. The AFM magnetoelectric sesquioxide Cr_2O_3 is an archetypical oxide that allows voltage-control of the Néel vector in the presence of an applied magnetic field (H) [4]. B doping increases Néel temperature (T_N) from 307 K to 400 K and permits realizing voltage controlled Néel vector rotation at zero H [4], a promising finding to AFM spintronics. B doping is believed to result in 90° rotation of the Néel vector into a new stable state vs 180° switching in undoped films [5]. Studying B-Cr_2O_3 in device structures remains unexplored, and it is not clear how the voltage control reversibly switches the Néel vector from in-plane to out-of-plane. In contrast with previous measurements of noncollinear AFMs, where the NV measured stray field (B_{NV}) emerges from an overall ferrimagnetic moment due to the canting of the spins, in Cr_2O_3 NV microscopy probes B_{NV} resulting from single layers of uncompensated spins on the surface and interface with the substrate (Fig.1). The acquired B_{NV} image confirms the presence of homogeneously magnetized domains, as signaled by areas of positive or negative B_{NV} with sharp domain walls (zeros in B_{NV}). By using

a reverse propagation protocol [1], we measured the magnetization profile, which shows well-defined magnetized nano-domains, with typical domain sizes > 300 nm in undoped (Fig.1b) [6] and ~40-300 nm (Fig.1c) in B- Cr_2O_3 films [7] respectively. We performed field cooling, i.e., cooling from above to below T_N in the presence of a magnetic field H (± 0.4 T), on nanostructured AFM domain walls (DWs) which resulted in the selection of one of the two 180° DWs in undoped Cr_2O_3 films (Figs. 2a, 2b, 2c). Lifting of such a degeneracy is achievable with a magnetic field alone due to the Zeeman energy of a weak parasitic magnetic moment in undoped Cr_2O_3 films that originates from defects and the imbalance of the boundary magnetization of opposing interfaces [6]. We studied the effect of voltage applied along micro-structured Pt Hall bars deposited on B-Cr_2O_3/V_2O_3 structures. As expected from anomalous Hall effect (AHE) measurements [5], the AFM domains in B-Cr_2O_3 films are controlled with voltage at zero H, emphasized by the change of the AFM domains' texture before (Fig. 3.d) and after applying -11 V (Fig. 3.e) [7]. Finally, we discuss ongoing measurements of the effect of temperature (295-400 K) on AFM domains, the dynamic AFM domain-wall evolution, and voltage-induced Néel vector rotation in B-Cr_2O_3 films and devices. Acknowledgement: This work is supported by the NSF/EPSCoR RII Track-1: Emergent Quantum Materials and Technologies, Award OIA-2044049. The research was performed in part in the Nebraska Nanoscale Facility: National Nanotechnology Coordinated Infrastructure and the Nebraska Center for Materials and Nanoscience (and/or NERCF), which are supported by NSF under Award ECCS: 2025298, and the Nebraska Research Initiative.

[1] F. Casola, T. van der Sar, and A. Yacoby. Nature Review Materials 3, 17088 (2018). [2] A. Laraoui, and K. Ambal, Applied Physics Letters 121, 060502 (2022). [3] S. Lamichhane, K. A. McElveen, A. Erickson, et al., ACS Nano 17 (9), 8694-8704 (2023). [4] N. Wu, X. He, A. L. Wysocki, et al., Physical Review Letters, 087202 (2011). [5] A. Mahmood, W. Echtenkamp, M. Street, et al., Nature Communications 12, 1674 (2021). [6] A. Erickson, S. Q. A. Shah, A. Mahmood, et al., RSC Advances 13, 178-185 (2023). [7] A. Erickson, A. Mahmood, S. Q. A. Shah, et al., under preparation (2023).

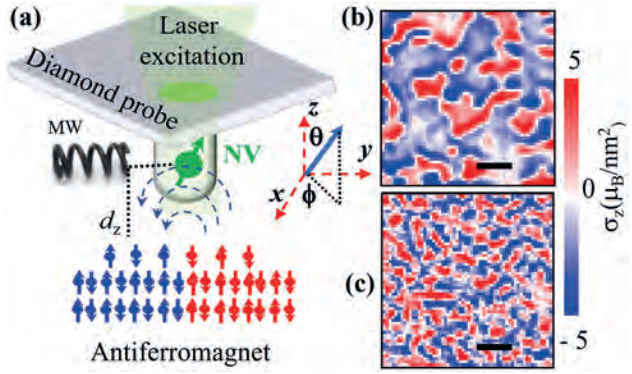

Fig.1: (a) Schematic of NV-SPM for probing spin textures in antiferromagnets. Extracted moment density profile from 200-nm thick undoped (b) and B doped (c) Cr_2O_3 films. The scale bar in (b) and (c) is 1 µm.

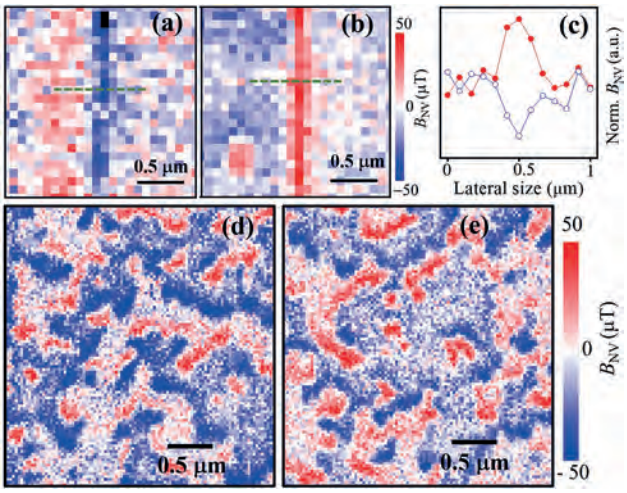

Fig.2: B_{NV} map for –0.4 T (a) and +0.4 T (b) field cooled AFM states in 200-nm thick undoped Cr_2O_3 film showing a magnetic field reversible edge DW. (c) Transverse cut of the B_{NV} maps in (a) and (b) showing the spatial profile of the edge DW. (d) B_{NV} map for 0 V (d) and -11 V (e) voltage-controlled AFM domains in 200-nm thick B-Cr_2O_3/V_2O_3 structures.

CONTRIBUTED PAPERS

AC-06. Accelerating scanning rates for cw-ODMR NV magnetometry and increasing sensitivity using pulsed protocols. B. Josteinsson[1], *G. Puebla Hellmann*[1], A. Morales[1], J. Rhensius[1] and S. Josephy[1] *1. QZabre Ltd, Zurich, Switzerland*

Nitrogen vacancy centers in a diamond can be used as quantum sensors to measure magnetic and electric fields with high sensitivity and accuracy. Single NVs enable high spatial resolution down to less than 30 nm with a theoretical sensitivity approaching 1 uT/sqrt(Hz), using continuous wave ODMR. This high sensitivity gives the possibility to measure e.g. weak stray fields of antiferromagnetic materials, with other applications in measuring skyrmions, 2D magnets, spin waves and current distributions. High sensitivity directly translates into increased scanning rates. We show that the combination of custom designed optics, optimized tip shapes and advanced signal processing is able to produce high quality, fully quantitative megapixel images at rates exceeding 200 pixels/s. In applications where the field strength is very weak and even higher sensitivity than what is attainable with cw-ODMR is desired, pulsed protocols can be used. Pulsed protocols give an increase in sensitivity by almost an order of magnitude, at the cost of higher setup complexity. We show how two such protocols, pulsed ODMR and gradiometry, compare when measuring samples with uT and sub uT magnetic fields. Other pulse protocols e.g. Ramsey, Rabi and Relaxation/T1 give the option of going beyond traditional magnetometry, where NVs can be used to map microwave fields in both space and time, with applications in e.g. RF systems-on-chip or ion traps for quantum computing.

AC-07. Magnetic Imaging of Individual Nanoparticles Using Nitrogen-Vacancy Microscopy. *S. Lamichhane*[1], K. McElveen[2], A. Erickson[3], I. Fescenko[4], S. Sun[2], R. Timalsina[3], Y. Guo[2], S. Liou[1], R. Lai[2] and A. Laraoui[3] *1. Department of Physics & Astronomy, University of Nebraska-Lincoln, Lincoln, NE, United States; 2. Department of Chemistry, University of Nebraska-Lincoln, Lincoln, NE, United States; 3. Department of Mechanical & Materials Engineering, University of Nebraska-Lincoln, Lincoln, NE, United States; 4. Laser center, University of Latvia, Riga, Latvia*

The nitrogen vacancy (NV) center in diamond is a spin-1 defect that offers an exceptionally quantum sensitive platform for detecting weak magnetic fields at the nanoscale [1-3]. In this work we report recent results on studying the magnetic properties of individual $[Fe(Htrz)_2(trz)](BF_4)$ (Fe triazole) spin crossover (SCO) nanorods and nanoparticle clusters (size: 20 nm to 1 μm) by using NV magnetometry [4]. The Fe-triazole SCO molecules exhibit thermal, electrical, and optical switching between high spin (HS) and low spin (LS) states [5]. Previous studies on Fe-triazole SCO systems were primarily conducted on a bulk scale, making it difficult to study their individual magnetic behavior due to their weak magnetic signal [6]. The magnetic field patterns produced by the Fe-triazole nanoparticles/nanorods are imaged by NV microscopy as a function of applied magnetic field (up to 350 mT) and correlated with scanning electron microscopy and Raman spectroscopy to determine the size of the nanoparticles/nanorods and to confirm their respective spin states. We found that most of the 300 nm and 1 μm nanorods display paramagnetic behavior, with magnetic field patterns well defined by a magnetostatic model using a volume susceptibility $\chi \sim 1.58 \times 10^{-4}$, that may be explained by the formation of Fe(III) at the nanorods' surface [7]. NV measurements on Fe-triazole 20-nm nanoparticle clusters revealed both diamagnetic and paramagnetic behavior of the LS state at 295 K [4]. We finally discuss ongoing experiments using NV magnetometry to investigate the magnetic behavior of individual hematite (Fe_2O_3) and magnetite (Fe_3O_4) nanoparticles with the goal of distinguishing between Fe(II) and Fe(III) spins. By studying these magnetic nanoparticles (size: 10 – 50 nm), we can gain insights into their magnetic behavior at the nanoscale, which can have implications for various applications such as magnetic data storage and biomedical imaging. Acknowledgement: This work is supported by the National Science Foundation/EPSCoR RII Track-1: Emergent Quantum Materials and Technologies, Award OIA-2044049.

[1] F. Casola, T. van der Sar, and A. Yacoby. Nature Review Materials 3, 17088 (2018). [2] A. Laraoui, and K. Ambal, Applied Physics Letters 121, 060502 (2022). [3] I. Fescenko, A. Laraoui, J. Smits, et al., Phys. Rev. Appl. 11, 034029 (2019). [4] S. Lamichhane, K. A. McElveen, A. Erickson, et al., ACS Nano 17 (9), 8694-8704 (2023). [5] J. Kroeber, J-P. Audiere, R. Claude, et al., Chem. Mater. 6, 1404–1412 (1994). [6] T. Boonprab, S. J. Lee, S.G. Telfer, et al., Angew. Chem. Int. Ed. 52, 1185–1188 (2013). [7] A. A. Blanco, D. J. Adams, J. D. Azoulay, et al., Molecules 27, 4 (2022).

AC-08. Determining the Sign of the Dzyaloshinskii-Moriya Interaction at the Magnetron Sputtered Ir|Co Interface. *M.C. de Jong*[1], M.J. Meijer[1], B. Koopmans[1] and R. Lavrijsen[1] *1. Department of Applied Physics, Eindhoven University of Technology, Eindhoven, Netherlands*

Chiral domain walls (DW) and skyrmions have gained enormous interest in recent years because of their possible applications in nanoelectronics. A strong Dzyaloshinskii-Moriya interaction (DMI) is essential for their stability. This is commonly achieved by sandwiching an ultrathin magnetic layer between two heavy metals (HM) with an opposite DMI strength D, such that the DMI contributions add up and produce a large net DMI [1]. The prevailing material combination for this additive DMI is Pt|Co|Ir, as an opposite DMI sign is predicted for these interfaces [2]. However, in sputtered multilayers it is not clear whether such an additive DMI occurs, because the DMI of sputtered Ir|Co is often reported to be the same as that of Pt|Co, *e.g.* Refs [3,4]. A second Co interface is always present however, making interpretation of a single interface DMI ambiguous. Measurements on epitaxially grown single Pt|Co and Ir|Co interfaces do show an opposite sign [5,6]. This suggests that interface quality might have a strong effect on the DMI of the Ir|Co interface. Using Secondary Electron Microscopy with Polarization Analysis (SEMPA) we analyze the magnetization inside the DWs of Pt|Co and Ir|Co grown using D.C. magnetron sputtering, and subsequently demagnetized and imaged *in-situ*. This allows us to study as-grown, single HM|Co interfaces and thus unambiguously attribute our observations to those interfaces. Two SEMPA measurements are shown in Fig. 1(a,b), where we show the magnetization texture in Pt|Co and Ir|Co, respectively. Analysis of the data reveals counter-clockwise Néel walls in Pt|Co [Fig. 2(a), $D>0$] and clockwise in Ir|Co [Fig. 2(b), $D<0$]. This demonstrates that an additive DMI can be achieved in sputtered systems. We are currently investigating the effect of growth parameters, and hence interface quality, on the DW structure and will report our findings in this talk.

[1] C. Moreau-Luchaire, C. Moutafis, N. Reyren, *et al.* Nature Nanotechnology 11, p. 444-448 (2016) [2] A. Belabbes, G. Bihlmayer, F. Bechstedt, *et al.* Physical Review Letters 117, 247202 (2016) [3] F. Ajejas, V. Krizáková, D. de Souza Chaves, *et al.* Applied Physics Letters 111, 202402 (2017) [4] Y. Ishikuro, M. Kawaguchi, N. Kato, *et al.* Physical Review B 99, 134421 (2019) [5] E. Corredor, S. Kuhrau, F. Kloodt-Twesten, *et al.* Physical Review B 96, 060410(R) (2017) [6] F. Kloodt-Twesten, S. Kuhrau, H. Oepen, *et al.*, Physical Review B 100, 100402(R) (2018)

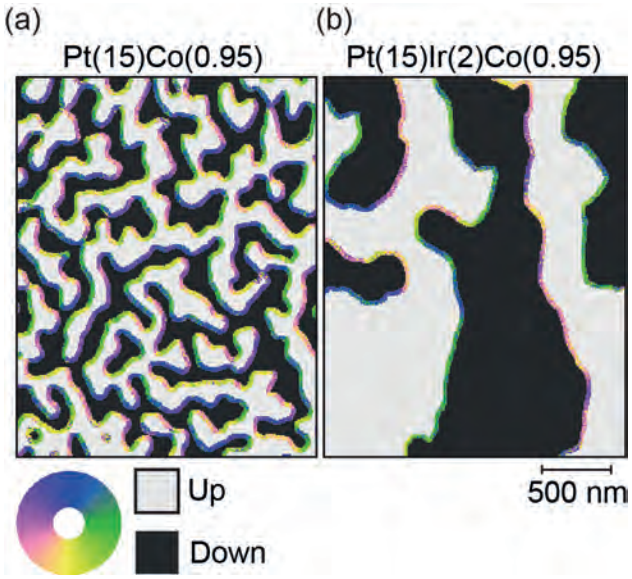

Fig. 1: SEMPA measurements on (a) Ta(4)Pt(15)Co(0.95) and (b) Ta(4)Pt(4)Ir(2)Co(0.95) (thicknesses in nm). White (black) represent the up (down) domains and the colorwheel gives the in-plane orientation of the magnetization in the DWs.

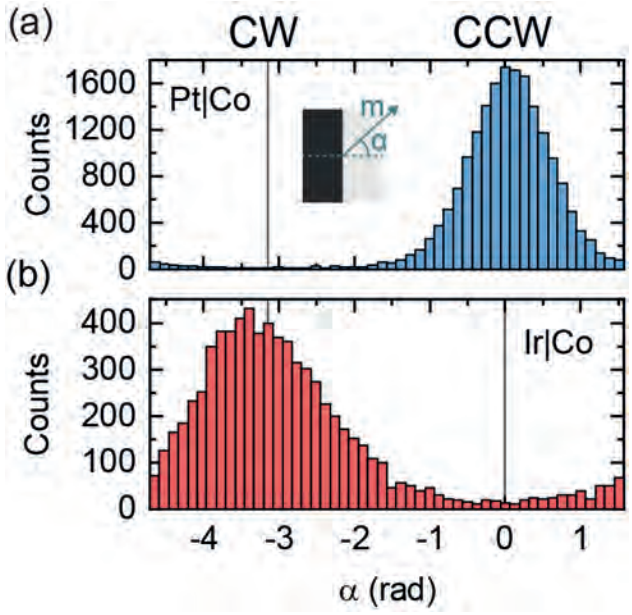

Fig. 2: Histograms of the measured angles α between the DW normal and magnetization (*m*) for (a) Pt|Co and (b) Ir|Co.

Session AD
MAGNETIZATION DYNAMICS I: MICROMAGNETICS AND MODELING

Anna S Semisalova, Co-Chair
University of Duisburg-Essen, Duisburg, Germany
Michael Tanksalvala, Co-Chair
NIST, Boulder, CO, United States

CONTRIBUTED PAPERS

AD-01. Solving periodic micromagnetic problems using finite element method. *F. Ai*[1,2] and V. Lomakin[1,2] *1. Electrical and Computer Engineering, University of California, San Diego, La Jolla, CA, United States; 2. Center for Memory and Recording Research, University of California, San Diego, La Jolla, CA, United States*

Periodic problems often arise in micromagnetic modeling, e.g., when considering an infinite space, film, or wire as well as dispersion diagrams of periodically modulated structures. Finite element method-based solvers typically require calculating the static magnetic periodic scalar potential (PSP), which, in principle, can be done via static scalar periodic Green's function (PGF). However, the scalar PGF diverges even for the 1D periodicity case. Here, we present an efficient technique for computing the PSP via a convolution with the PGF in 1D, 2D, and 3D periodicity cases. We represent the PGF as the near-zone term over a small number of nearby periodic images and far-zone term over the rest of the infinite periodic sum. PSP for the near-zone term is evaluated via a modified non-uniform Fast Fourier Transform method [1]. For the far-zone PSP term, we prove that while the infinite PGF sum diverges, the corresponding PSP converges for the micromagnetic case of zero total magnetic charge. We use a rapidly convergent spectral representation combined with interpolations for the infinite sum [2]. The accuracy can be controlled by a proper selection of the number of the near-zone images, interpolation order, and the interpolation grid density. Figure 1a illustrates the error control for the case of 1D periodicity. Figure 1b shows the computational time versus the number of randomly distributed charges in the periodic unit cell. Similar results are obtained for 2D and 3D periodicity cases and the technique can account for phase shifts needed for periodic dispersion diagrams.

[1] Y. Brick, V. Lomakin and A. Boag, IEEE Transactions on Antennas and Propagation, vol. 62, no. 8, pp. 4314-4324 (2014) [2] S. Li, D. A. Van Orden, and V. Lomakin, IEEE Transactions on Antennas and Propagation, vol. 58, no. 12, pp. 4005–4014 (2010)

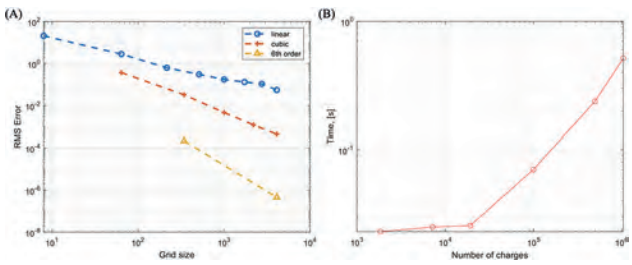

Fig. 1. Illustration of the error and performance for the 1D periodicity case. (A) Error comparison for 1st, 3rd, and 6th order interpolation with varying sparse grid sizes, considering the subtraction of only 0th and 1st near-zone images. (B) Computational time as a number of charges; the results were obtained on an AMD R9-5950X CPU.

AD-02. Vision for Unified Micromagnetic Modelling (UMM). *H. Fangohr*[1,2], M. Lang[1,2], S. Holt[1], S. Pathak[1], K. Zulfiqar[1,3] and M. Beg[4] *1. Computational Science, Max Planck Institute for the Structure and Dynamics of Matter (MPSD), Hamburg, Germany; 2. Engineering and Physical Sciences, University of Southampton, Southampton, United Kingdom; 3. Physics, University of Hamburg, Hamburg, Germany; 4. Imperial College, London, United Kingdom*

There is a growing number of micromagnetic simulation packages available, including OOMMF, mumax[3], Boris, magnum.np, Magpar, Nmag, Finmag and others. A scientist or engineer who wants to use one of them, needs to learn how to express the micromagnetic problem of interest in a "language" such as configuration file, script or GUI-clicks that the simulation software understands. This language varies from software to software. If the researchers needs to use another package - perhaps to run the same study on a GPU instead of a CPU - they need to learn a new language to re-express their (unchanged) micromagnetic problem for the next software. We discuss the vision of providing a unified micromagnetic modelling (UMM) interface with which researchers can express the micromagnetic problem once (top third in figure), and from which multiple simulation packages can be instructed automatically to carry out the actual numerical problem solving (middle third in figure). This can be thought of as a compiler that takes a micromagnetic problem description as source and translates the problem description into configuration files for a simulation package (such as mumax[3], OOMMF or others) of the users choice. The advantage of such an approach are: (i) As scientists do not need to familiarize themselves with multiple simulation configuration languages, they can more easily use multiple simulation packages. (ii) Being able to easily change the micromagnetic simulator makes it possible to (a) switch from a tool optimized for GPU usage to a CPU-based tool (if, for example, no GPU is present); (b) compare the results computed with different simulation packages; (c) make use of complementary features of the different simulation packages. With recent updates of Ubermag [1,2], we present a prototype of such a framework. Ubermag provides a unified interface (expressed in Python) from which micromagnetic problems can be solved using OOMMF and mumax[3]. After the simulation has finished, the results are made available to the researcher for analysis within the Python ecosystem of scientific libraries. We discuss the current state of capabilities and possible future developments. We also discuss challenges associated with the proposed approach.

[1] Marijan Beg, Martin Lang, Hans Fangohr, *Ubermag: Towards more effective micromagnetic workflows,* IEEE Transactions on Magnetics 58, 7300205 (2021), http://ubermag.github.io/ [2] Marijan Beg, Ryan A. Pepper, Hans Fangohr, *User interfaces for computational science: a domain specific language for OOMMF embedded in Python,* AIP Advances 7, 056025 (2017)

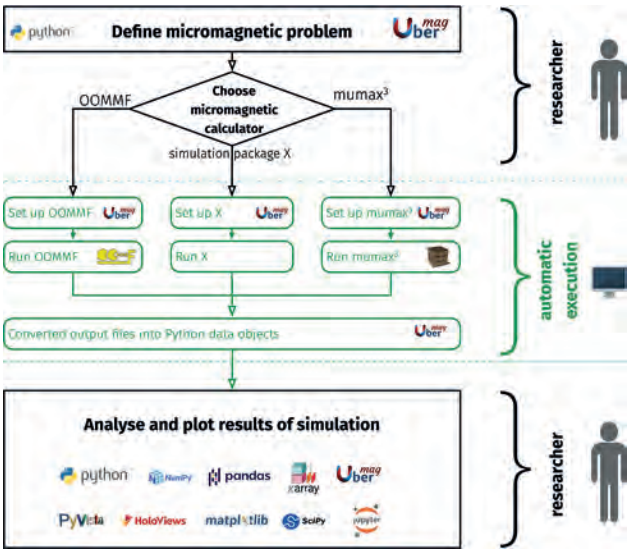

AD-03. Molecular Field Coefficient Modeling of Temperature-Dependent Ferrimagnetism in a Complex Oxide. *M. Gross*[1], T. Su[1], J.J. Bauer[1] and C.A. Ross[1] *1. MIT, Cambridge, MA, United States*

The temperature-dependence of the magnetic moment of a magnetically ordered material is fundamental to all aspects of its technological applications. In ferrimagnetic materials with multiple sublattices, the magnetization can vary nonmonotonically with temperature and can pass through zero at a magnetization compensation temperature T_{comp}. The net angular momentum can also reach zero at the angular momentum compensation temperature T_A, which differs from T_{comp} if the sublattices have different Lande g-factors. Recent studies reveal fast magnetization dynamics near T_A [1]. It is therefore useful to predict the temperature-dependent magnetic moment and angular momentum of a material with known site occupancy, or conversely to use the magnetization vs. temperature to identify the cation site occupancy. In this work we designed a Python computer code that models the magnetism of rare-earth iron garnets ($RE_3Fe_5O_{12}$, REIG) using a molecular field coefficient (MFC) approach. Following Dionne [2], the program calculates both the exchange interactions and the magnetic moment of each sublattice to determine the magnetization and angular momentum as a function of temperature. The model accounts for site occupancy on each sublattice including the effects of non-magnetic and magnetic substitutions, vacancies, Fe^{2+}, and deviations from the ideal RE:Fe stoichiometry by considering their effects on the net magnetization and the sublattice exchange coupling. Using data of Tb-rich terbium iron garnet thin films with Tb:Fe = 0.86 from Rosenberg et al. [3], we show that the model is consistent with the excess Tb accommodated in octahedral sites (which contain $Fe_{1.52}Tb_{0.48}$) and vacancies (V) in the tetrahedral sites (which contain $Fe_{2.53}V_{0.47}$), giving an excellent match to the measured magnetization, T_{comp}, and Curie temperature, as well as to XPS, XMCD and elementally resolved TEM data. This work provides accurate magnetic modeling of REIGs of a variety of compositions allowing for design and analysis of ferrimagnets with useful properties.

[1] Liang *et al.*, *Phys Rev B*, 104 174421 (2021); Weißenhofer and Nowak, *Phys Rev B*, 107 064423 (2023). [2] Dionne, *J Appl Phys*. 41, 4874 (1970); *Lincoln Laboratory Technical Report*, 534 (1979). [3] Rosenberg *et al.*, *Small*, doi: 10.1002/smll.202300824 (2023)

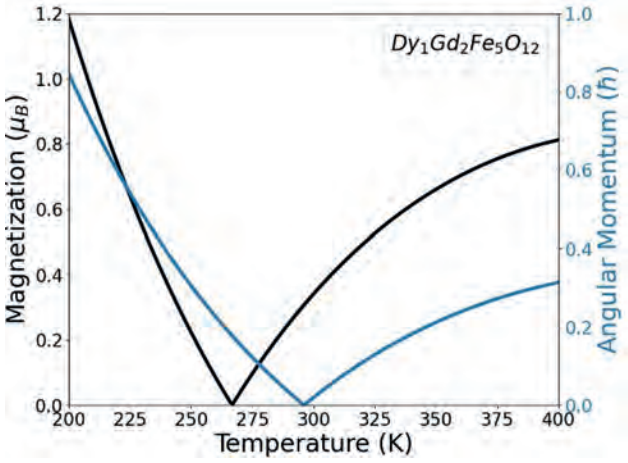

Model prediction of magnetization and angular momentum of $Dy_1Gd_2Fe_5O_{12}$ versus temperature.

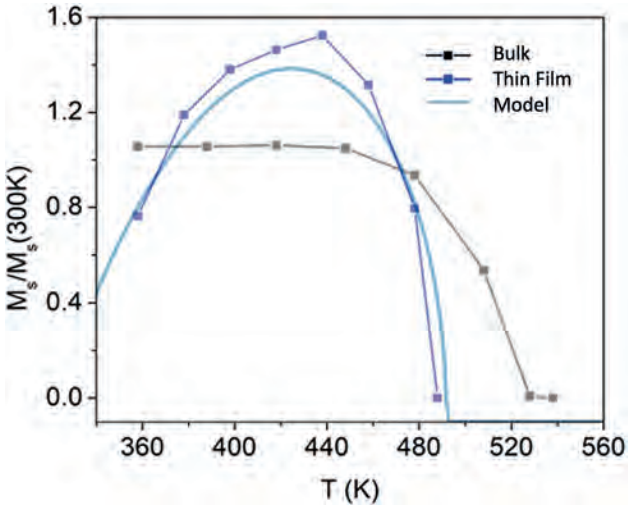

Magnetization of $Tb_3(Fe_{1.52}Tb_{0.48})(Fe_{2.53}V_{0.47})O_{12}$ from model with experimental data from [3].

AD-04. Generalized Drift Diffusion Model for Micromagnetics: Unifying Interface and Bulk Spin Transfer Torques, Spin Hall effect, and Anomalous Hall Effect. *X. Wang*[1] and V. Lomakin[1] *1. ECE, UCSD, San Diego, CA, United States*

Micromagnetic modeling of spin polarized current effects is important for a set of applications. Drift diffusion like models, such as Valet-Fert [1] and drift diffusion models [1, 2], have an appeal due to their ability to describe complex spin behaviors. The Valet-Fert model describes interfacial spin transfer torque via magnetoelectronic circuit theory with parameters that can be obtained experimentally. However, the model assumes the spin is aligned with the ferromagnetic layer. Drift diffusion model allows handling torques in cases of continuously varying magnetization, such as domain wall motion. However, it assumes that the spin accumulation is continuous at ferromagnetic – nonmagnetic interface, and it does not describe the interface torques. Additionally, its parameters are not directly linked to experimental results. Here, we show that the Valet-Fert and drift diffusion models can be unified, which allows using the Valet-Fert related experimental material parameters in the drift diffusion model as well as include interfacial and bulk torques in ferromagnetic layers via two more parameters describing the absorption of traverse spin accumulation. We also include spin accumulation generated by the spin hall effect and anomalous hall effect for non-magnetic and ferromagnetic layers [3, 4]. The unified model was implemented as a finite element solver

and coupled with the FastMag micromagnetic solver [5]. Fig. 1 shows the solution verification for a 5-layer structure. Numerical study of spin torque and spin Hall effects in various structures will be shown.

[1] T. Valet and A. Fert, Theory of the perpendicular magnetoresistance in magnetic multilayers, Phys. Rev. B 48, 7099, Sep 1993. [2] S. Zhang, P. M. Levy, and A. Fert, Mechanisms of Spin-Polarized Current-Driven Magnetization Switching, Phys. Rev. Lett. 88, 236601, May 2002. [3] M. Dyakonov, Magnetoresistance due to edge spin accumulation, Phys. Rev. Lett. 99, 126601 (2007). [4] V. P. Amin, Junwen Li, M. D. Stiles, and P. M. Haney, Intrinsic spin currents in ferromagnets, Phys. Rev. B 99, 220405(R), June 2019. [5] R. Chang, S. Li, M. Lubarda, B. Livshitz, and V. Lomakin, "FastMag: Fast micromagnetic simulator for complex magnetic structures," Journal of Applied Physics, vol. 109, p. 07D358, 2011.

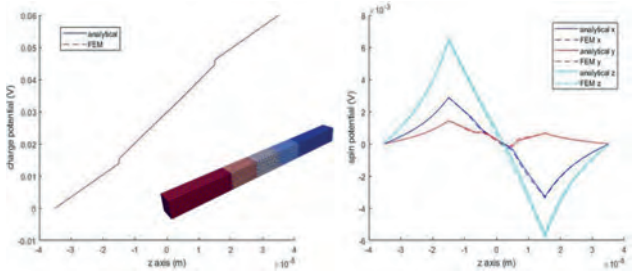

Figure 1: Comparison between analytical and FEM solution of the unified model. Inset in (a) shows the considered 5-layer structure with three magnetic layers separated by two non-magnetic layers. (a) Charge potential vs. z and (b) spin potential for the numerical and analytical solutions showing good agreement.

AD-05. Spatial Metrics for Physical Reservoir Computing: Insights from Skyrmion Reservoir Audio Classification. *R. Msiska*[1,2], J. Love[1], J. Mulkers[2], J. Leliaert[2] and K. Everschor-Sitte[1] *1. Faculty of Physics and Center for Nanointegration Duisburg-Essen (CENIDE), University of Duisburg-Essen, Duisburg, Germany; 2. Department of Solid State Sciences, Ghent University, Ghent, Belgium*

Physical reservoir computing (PRC) is a computational framework that exploits the inherent dynamics of a physical system, called a reservoir, to perform complex tasks such as pattern recognition and time-series prediction. In PRC, input signals are fed into the reservoir, whose internal dynamics transform the input signal into a higher-dimensional representation that can be read out using simple methods such as linear regression. In this study, we introduce spatially resolved metrics [1] to locally analyze memory and nonlinearity, two key quantities in PRC. Both our metrics can be calculated in parallel from a small dataset. To test our metrics, we propose a multi-channel skyrmion PRC made up of a magnetic thin-film hosting an array of magnetic skymions. By introducing grain inhomogeneity variations (Fig. 1a), a complex energy landscape is created, forming distinct pinning sites. Consequently, the magnetic film's local energetic minimum state transforms into an irregular configuration of skyrmions (Fig. 1b). We apply our metrics to analyze the skyrmion reservoir using a discrete-time random input signal. Fig. 1d) and e) visualize examples from this analysis. We observe a trade-off between memory and nonlinearity, both spatially and globally. Utilizing our metrics, we optimize a skyrmion reservoir for classification via an audio recognition benchmark of isolated spoken digits. In this process, audio signals are transformed into voltage signals then introduced as inputs into the reservoir. Outputs states are then used to create a linear classification model, which can correctly identify spoken digits with an overall accuracy of 97.4% [2] — Among the best ever report for physical reservoir computers! Fig. 2 illustrates the whole procedure.

[1] J. Love, J. Mulkers, R. Msiska, G. Bourianoff, J. Leliaert, and K. Everschor-Sitte, arXiv:2108.01512v2 (2022) [2] R. Msiska, J. Love, J. Mulkers, J. Leliaert, and K. Everschor-Sitte, Advanced Intelligent Systems, p. 2200388 (2023)

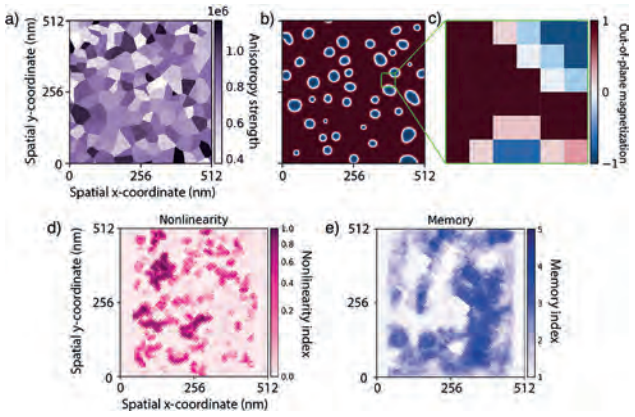

Magnetic thin film depicting: (a) the distribution of grain inhomogeneity, (b) the out-of-plane magnetization state, (c) example of a readout cell, and sample visualizations of the spatial metrics for nonlinearity (d) and memory capacity (e).

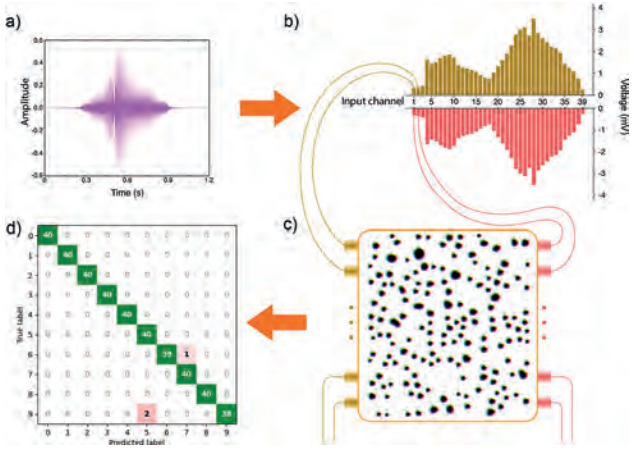

Audio recognition with a skyrmion reservoir. (a) Audio waveforms are converted to (b) voltage signals which in turn are used as inputs for (c) a multi-input skyrmion reservoir. (d) Reservoir output is trained to classify the audio sample.

AD-06. Reduced Order Model for Hard Magnetic Films. *H.A. Moustafa*[1], W. Rigaut[2], Y. Hong[2], T. Devillers[2], N. Dempsey[2], T. Schrefl[1,3] and H. Oezelt[1] *1. Department for Integrated Sensor Systems, University of Continuing Education Krems, Wiener Neustadt, Austria; 2. Institute Néel, Université Grenoble Aples, CNRS, Grenoble INP, Grenoble, France; 3. Christian Doppler Laboratory for Magnet Design through Physics Informed Machine Learning, Department for Integrated Sensor Systems, University of Continuing Education Krems, Wiener Neustadt, Austria*

In the quest for rare earth-lean permanent magnets for green technologies, microstructural optimization is a promising strategy to increase coercivity while reducing content of critical elements. While micromagnetic simulations are a vital tool, measurements of magnetic systems are required to tune the model and validate simulation results. Hard magnetic films can serve as model systems to study microstructural properties for bulk magnets[1]. Combinatorial synthesis and high-throughput analysis of films can be used to relate microstructure to hysteresis properties. While grain sizes can be several μm, the computational effort limits systems computed by micromagnetics to 1μm. Hence, to investigate large multigrain systems, a reduced order model (ROM) was developed [2]. The ROM is based on the assumption that magnetization reversal of the grains always start at their surface and switch the entire grain in a single step. Therefore, the magnetic configuration is represented by one magnetic moment per grain and the grains' switching fields are evaluated only at locations close to their

surface using the embedded Stoner-Wohlfarth model[3]. Good agreement was achieved (Fig. 1) while reducing the required computational resources thereby enabling the simulation of huge multigrain systems not accessible through classical micromagnetics. The ROM was used to investigate how the thickness of a non-magnetic grain boundary affects the coercivity. Similar to structures in measurements of $Nd_2Fe_{14}B$ films, 10 random variations of synthetical microstructures with columnar grains were generated by Neper [4]. A grain boundary was introduced with thicknesses 1 – 20nm at the expense of the grains' volume. Results show an increasing coercivity with growing boundary thickness (Fig. 2). A possible explanation is the reduced influence of the stray field with increasing distance between grains. This research was funded in whole or in part by the Austrian Science Fund (FWF) I 6159-N and the French National Research Agency ANR-22-CE91-0008.

[1] K. Hono and H. Sepehri-Amin, Scripta Mater., vol. 67, no. 6, pp. 530–535 (2012) [2] A. Kovacs et al., Front. Mater., vol. 9, p. 1094055 (2023) [3] R. Wood, IEEE Trans. Magn., vol. 45, no. 1, pp. 100–103 (2009) [4] R. Quey, P. R. Dawson, and F. Barbe, Comput Methods Appl Mech Eng, vol. 200, no. 17–20, pp. 1729–1745 (2011)

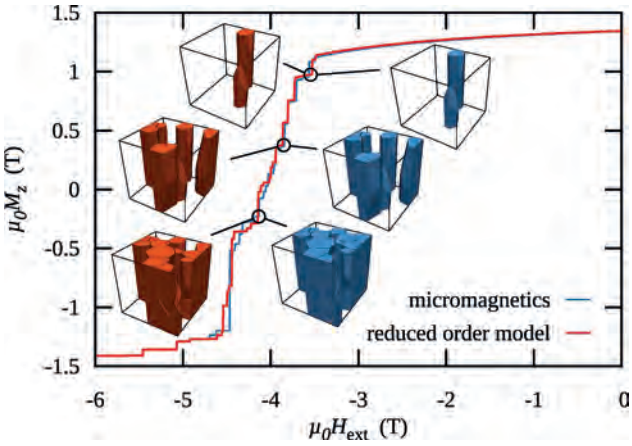

Fig.1: Comparison of demagnetization curves computed by classical micromagnetism and the reduced order model.

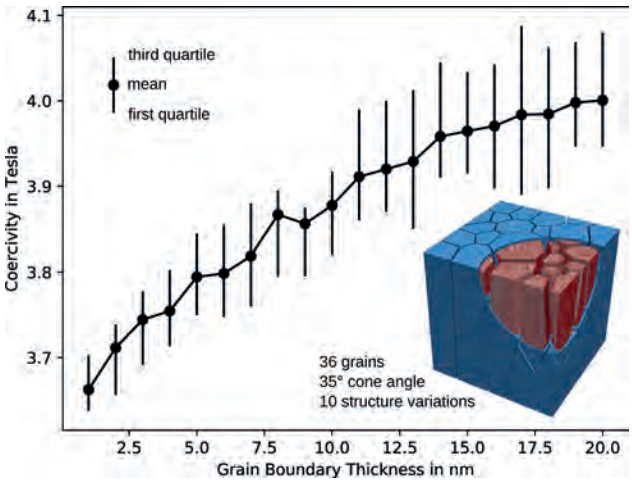

Fig. 2: The coercivity of granular systems increases with growing grain boundary thickness.

AD-07. Field-assisted spin-orbit-torque-driven dynamics in monodomain Mn_3Sn with perpendicular magnetic anisotropy. *A. Shukla*[1], S. Qian[1] and S. Rakheja[1] *1. Electrical and Computer Engineering, University of Illinois at Urbana-Champaign, Urbana, IL, United States*

Mn_3Sn generates large magneto-transport signatures such as anomalous Hall effect [1]. Recent experiments have shown that thin films of Mn_3Sn grown on an MgO (110)[001] substrate exhibit perpendicular magnetic anisotropy (PMA), owing to uniaxial tensile strain [2]. The perpendicular magnetic order (octupole) can be manipulated by the spin-orbit torque (SOT), in the presence of symmetry breaking magnetic fields [2]. Practical spintronic applications using Mn_3Sn, therefore, require clear understanding of the SOT-driven dynamics. Previous work investigated this current-driven dynamics numerically [2]; however, the dependence of the dynamics on the material properties, and the inputs is missing. We consider a spin-Hall (SHE) setup (Fig. 1(a)), where a magnetic field, H_0, is applied perpendicular to the initial magnetization state of Mn_3Sn (m_{oct}). Charge current, J_c, leads to the generation of a spin current, J_s, with spin polarization, n_p, perpendicular to the Kagome plane of Mn_3Sn. Firstly, numerical simulations from coupled LLG equations [3] reveal that there are two critical current densities, viz. J_s^{th1} and J_s^{th2}, associated with the octupole dynamics. If $J_s < J_s^{th1}$ the octupole stays in the initial well, whereas if $J_s^{th1} < J_s < J_s^{th2}$ the octupole switches to the other well. Finally, if $J_s^{th2} < J_s$ the octupole exhibits chiral rotation (Fig. 1(b)). Our perturbative analysis [4] shows that an increase in H_0 disturbs the symmetry of the system, reduces the barrier between the two stable states along itself (Fig. 2(a)), and hence reduces (increases) J_s^{th1} (J_s^{th2}). We obtain analytic expressions for J_s^{th1} and J_s^{th2} and find them to vary linearly with H_0 (Fig. 1(b)). We also obtain simplified models for the stationary states as a function of J_s and find them to match very well to numerical results (Fig. 2(b)). Our results should aid in understanding the SOT-driven dynamics in Mn_3Sn.

[1] X. Wang, H. Yan, X. Zhou, et al. Materials Today Physics (2022): 100878 [2] T. Higo, K. Kondou, T. Nomoto, et al. Nature 607.7919 (2022): 474-479. [3] A. Shukla, and S. Rakheja. Physical Review Applied 17.3 (2022): 034037. [4] J. Liu, and L. Balents. Physical review letters 119.8 (2017): 087202.

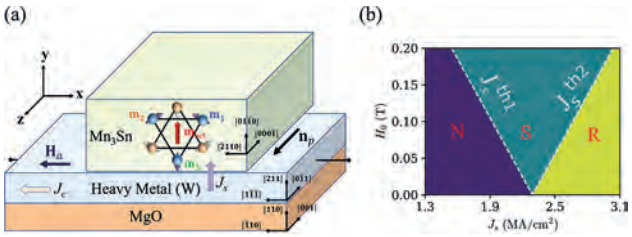

(a) SHE device setup to manipulate m_{oct} when $H_0 \neq 0$. (b) Final state of m_{oct} as a function of H_0 and J_s. N: No switching, S: Switching, R: Rotation. White dashed lines are the analytic expressions of threshold current.

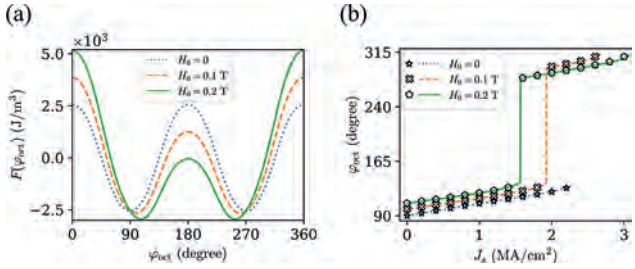

(a) Energy landscape, (b) Steady state solutions for different H_0. Numerical (symbol) and analytic (line) results match well.

AD-08. Withdrawn

AD-09. Nodal Finite-Difference Micromagnetics. *C. Abert*[1], R. Allayarov[1], F. Bruckner[1], S. Koraltan[1], S. Pathak[2], H. Fangohr[2] and D. Suess[1]
1. University of Vienna, Vienna, Austria; 2. Max Planck Institute for the Structure and Dynamics of Matter, Hamburg, Germany

Finite-difference micromagnetics is a long established numerical approach for the efficient solution of the Landau-Lifshitz-Gilbert equation. Its success is mostly based on the FFT accelerated demagnetization-field computation which leads to superior performance compared to many other numerical schemes. This convolution based method requires a regular cuboidal grid and assumes a constant magnetization in each simulation cell. While this discretization is reasonable for single-phase magnets, it is not well suited for the description of material interfaces. According to micromagnetic theory the magnetization is assumed to be continuous across material interfaces, while material properties exhibit discontinuities. Here, we propose a discretization scheme, with cell-based constant material parameters and node-based continuous magnetization for the fast and accurate description of multi-phase magnets. We use a product-space-based nodal basis for the discretization of the magnetization and apply a weak form with mass lumping for the computation of local effective field contributions such as the exchange field and the anisotropy field [2]. Due to the regularity of the mesh this strategy leads to constant element matrices and therefore allows for a trivial implementation of matrix free methods. For the demagnetization field we apply the FFT accelerated convolution method known from standard finite-difference micromagnetics. In this talk, we present the discretization formalism along with an implementation using the Tensor library PyTorch [1] that shows superior performance both with regard to accuracy as well as computational speed compared to established CPU and GPU finite-difference codes.

[1] Paszke, Adam, et al. "Pytorch: An imperative style, high-performance deep learning library." *Advances in neural information processing systems* 32 (2019). [2] Abert, Claas. "Micromagnetics and spintronics: models and numerical methods." *The European Physical Journal B* 92 (2019): 1-45.

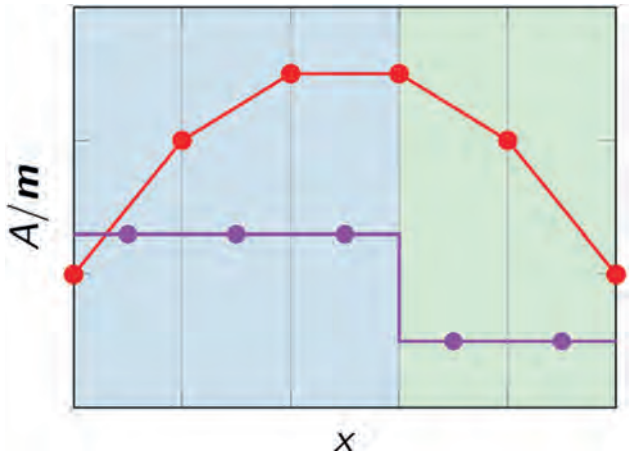

Discretization scheme for magnetization (red) and material parameters (purple) using nodal finite differences.

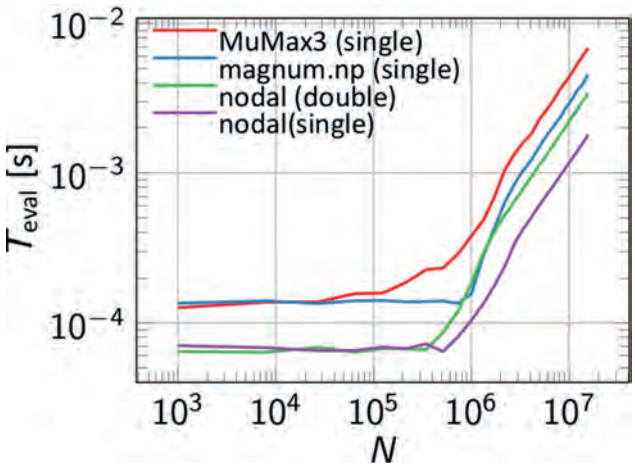

Computation time for the exchange-field evaluation on a cubic mesh with N cells computed on a Nvidia A100 Tensor Core GPU

INVITED PAPER

AD-10. Machine Learning Approaches for Magnetic Nanoparticles Applications in Biomedicine. *M. Coisson*[1], G. Barrera[1], F. Celegato[1], P. Allia[1] and P. Tiberto[1] *1. INRIM, Torino, Italy*

Machine learning (ML) is emerging as a valuable tool for building models of large datasets of highly interdependent, highly non-linearly coupled data. Magnetic systems, because of their intrinsic non linearity and complex interplay among many different quantities, are particularly suitable for being analysed with such approaches, provided large and coherent datasets are available to feed the machine learning model. In this work, we present two examples of machine learning approaches applied to magnetic nanoparticles of interest in biomedicine. With the first approach [1], we exploit datasets of magnetic nanoparticles (MNP) properties built through numerical simulations. The simulated MNPs and the environment in which they are supposed to operate can represent different scenarios of interest for biomedical applications, such as magnetic hyperthermia or heat-induced drug release. Input quantities, such as MNPs diameter, magnetic anisotropy, magnetic saturation, mutual interactions, space distribution, or operating conditions such as temperature, applied field maximum intensity (vertex value) and frequency are used to numerically calculate the MNPs response through a two-wells numerical model, and output values as coercivity, remanence, loop area are extracted and used to build the dataset. Finally, a ML model exploits the simulated dataset to predict the behaviour of the MNPs in conditions or for values of their properties that were not originally present in the dataset, but that may turn out to be valuable in biomedical applications. The second approach addresses the Magnetic Particles Imaging (MPI) technique, where magnetic nanoparticles with typical diameters in the 10-20 nm range are driven in correspondence of tumour masses and are triggered with a static magnetic field gradient to form a sensitive region that is excited to produce a measurable signal by an external, low-intensity ac electromagnetic field. By scanning with a suitable device (an antenna) over the patient's body, maps of the magnetic response of the magnetic nanoparticles can be obtained, which can be used to identify the cancer masses and characterise some of their properties. With respect to other imaging diagnostic techniques, MPI does not use ionising radiation or intense magnetic fields, and is therefore attracting much attention. The solution of the direct problem, i.e. the calculation within the sensitive region of the real and imaginary parts maps given the initial nanoparticles distribution and their magnetisation vs. field curve, is time consuming but can be solved numerically to build a large dataset, whereas the inverse problem, i.e. the calculation of the nanoparticles distribution from the real and imaginary parts maps, is not trivial and may be severely affected by incomplete or inaccurate knowledge of the physical

properties of the nanoparticles. Nonetheless, it is the inverse problem that is mostly relevant for diagnostic applications. We approach its solution with a machine learning model based on convolutional neural networks that reconstructs the magnetic nanoparticles distribution from their simulated third-harmonics susceptibility data. Both examples provide an insight on the power and versatility of ML approaches in investigating complex, highly nonlinear problems typical of magnetic systems, such as those involving magnetic nanoparticles, in the field of biomedical applications.

[1] M. Coïsson, G. Barrera, F. Celegato, P. Allia, P. Tiberto, "Specific loss power of magnetic nanoparticles: a machine learning approach", Appl. Phys. Lett. Materials 10 (2022) 081108, doi 10.1063/5.0099498

CONTRIBUTED PAPERS

AD-11. Parallel-In-Time Integration of the LLG With the Parallel Full Approximation Scheme in Time and Space. *R. Kraft*[1], S. Koraltan[2,3], D. Suess[1,2] and C. Abert[1,2] *1. Research Platform MMM Mathematics-Magnetism-Materials, University of Vienna, Vienna, Austria; 2. Physics of Functional Materials, University of Vienna, Vienna, Austria; 3. Vienna Doctoral School in Physics, University of Vienna, Vienna, Austria*

Speeding up computationally expensive problems, such as simulations of large micromagnetic systems, requires efficient use of parallel computing infrastructure. While parallelism across space is commonly exploited in micromagnetics, this strategy is only effective down to a minimum number of degrees of freedom per core. First attempts to additionally parallelize the solution of partial differential equations in the temporal domain date back almost 60 years, but many specialized algorithms for the so-called parallel-in-time integration have only been developed recently [1]. This work investigates the Parallel Full Approximation Scheme in Space and Time (PFASST) [2] as a space- and time-parallel solver for the Landau-Lifshitz-Gilbert equation (LLG). Said scheme is based on Spectral Deferred Correction (SDC) [3] methods, which on their own already provide an interesting class of timestepping methods for solving the LLG, especially at higher accuracies. Prototyping was done with the pySDC [4] python library, but this work uses a custom SDC/PFASST implementation developed as an extension to the magnum.pi [5] micromagnetic simulation software package. Figures 1 and 2 show the performance of the algorithm when simulating a 1000×1000×20 nm rectangular domain without an external field for 20 ns, starting from the initial state m = (0,0,1), with material parameters similar to permalloy and on an airbox mesh with 264264 elements in total. All results meet the same accuracy target in the form of a relative residual tolerance at every timestep. Computing up to 8 timesteps in parallel, an additional speedup of up to 3.2 over purely space-parallel simulations was achieved, where even higher speedups are expected with further optimization of the code.

[1] M. J. Gander, Contributions in Mathematical and Computational Sciences, Vol. 9, p.69–113 (2015) [2] M. Emmett and M. Minion, Communications in Applied Mathematics and Computational Science, Vol. 7(1), p.105–132 (2012) [3] A. Dutt, L. Greengard and V. Rokhlin, BIT Numerical Mathematics, Vol. 40, p.241–266 (2000) [4] R. Speck, ACM Transactions on Mathematical Software, Vol. 45(3), p.35:1–35:23 (2019) [5] C. Abert, L. Exl, F. Bruckner, A. Drews and D. Suess, Journal of Magnetism and Magnetic Materials, Vol. 345, p.29-35 (2013)

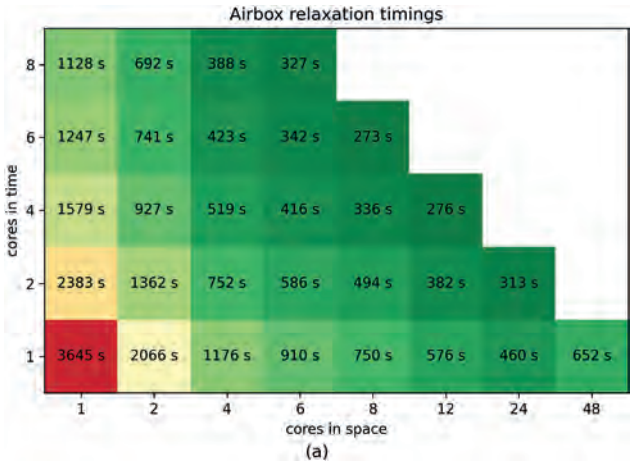

Simulating the relaxation process of a rectangular mesh in parallel (timings).

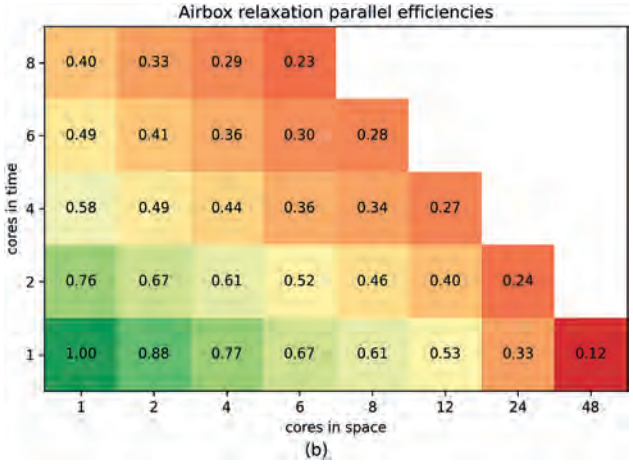

Simulating the relaxation process of a rectangular mesh in parallel (parallel efficiencies, where parallel efficiency is understood as achieved speedup divided by number of threads).

AD-12. Hybrid A-phi - correction method for solving eddy current problem with micromagnetics. *J. Duan*[1] and V. Lomakin[1] *1. University of California, San Diego, San Diego, CA, United States*

Magnetization dynamics is described by the Landau–Lifshitz–Gilbert (LLG) equation, which states that the dynamics of the magnetization is related to the torque related to various physical interactions, including a component due to the magnetic field. As the operating frequency and device size increase, the magnetostatic approximation for the magnetic field is no longer valid, and electrodynamic effects, such as eddy currents, must be accounted for. The dynamic magnetic field must be obtained via Maxwell's equations. Several methods have been introduced to solve Maxwell's equations for eddy current problems, including solving the phi-A-phi/phi-T-phi formulation derived from Maxwell equation using finite element method (FEM), and by evaluating an integral equation with proper boundary conditions [1-3]. One of the downsides of using typical FEM is the need in a large airbox region to properly account for the decaying magnetic field outside the conducting domain. Such an airbox increases the numerical problem size, thus reducing the performance and increasing the memory requirements, and also may introduce numerical errors. Here, we present a two-step approach, which allows truncating the computational domain to an arbitrary small airbox or not have an airbox at all. In the first step of this approach, we calculate the magnetic field assuming corresponding magnetic scalar potential to be zero on the outer boundary of the computational domain. In the second

step, we correct this solution by calculating the static field generated by the effective surface magnetic charges on the outer boundary obtained based on the domain truncation in the first step. We implement the approach in a FEM code with a combination of edge and nodal elements and coupled with the FastMag micromagnetic solver [4]. Fig. 1 shows the total and correcting eddy field for a case of no airbox. Fig. 2 shows the accuracy of the results.

1. S. Couture, X. Wang, A. Goncharov, and V. Lomakin, "A coupled micromagnetic-Maxwell equations solver based on the finite element method," J. Magn. Magn. Mater., vol. 493, p. 165672, Jan. 2020 2. [1] R. Chang, V. Lomakin, and E. Michielssen, "Coupling electromagnetics with micromagnetics," in Proceedings of the 2012 IEEE International Symposium on Antennas and Propagation, Jul. 2012 3. O. Bíró, G. Koczka, and K. Preis, "Finite element solution of nonlinear eddy current problems with periodic excitation and its industrial applications," Appl. Numer. Math., vol. 79, pp. 3–17, May 2014 4. R. Chang, S. Li, M. V. Lubarda, B. Livshitz, and V. Lomakin, "FastMag: Fast micromagnetic simulator for complex magnetic structures (invited)," J. Appl. Phys., vol. 109, no. 7, p. 07D358, Apr. 2011

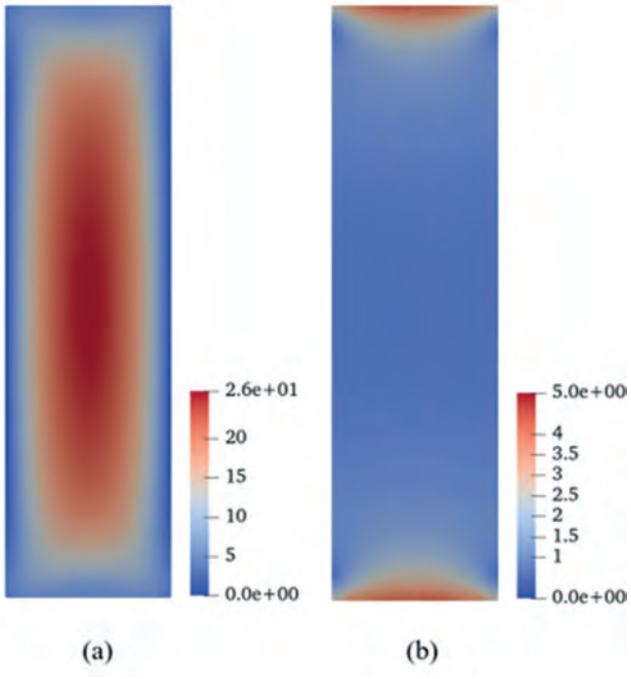

Fig.1 (a) Total eddy field; (b) correction eddy field in the second step of the method.

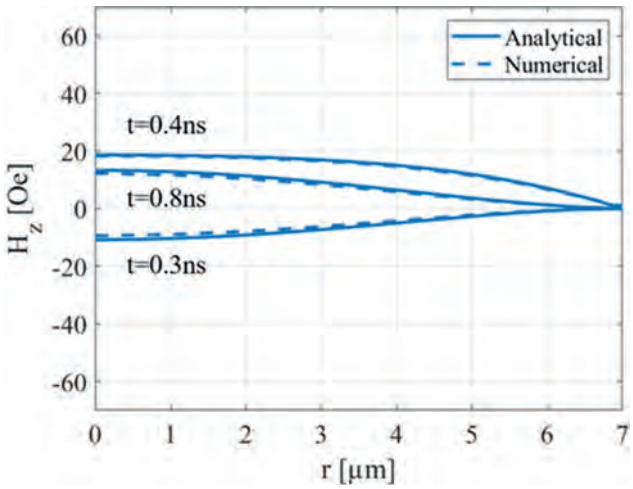

Fig.2 Axial component Hz of the eddy field for the numerical and analytical solutions from a fully couple micromagnetic solver at different time steps.

Session AE
COMPLEX OXIDES (BULK, FILMS AND HETEROSTRUCTURES)

Geoffrey Beach, Co-Chair
Massachusetts Institute of Technology, Cambridge, MA, United States
Vipul Chaturvedi, Co-Chair
University of Minnesota, Minneapolis, MN, United States

CONTRIBUTED PAPERS

AE-01. Significant Reduction of Dead Layers and Magnetic Anisotropy Change in a Transferred $La_{2/3}Sr_{1/3}MnO_3$ Thin Film on a Si Substrate.

T. Arai[1], S. Kaneta-Takada[1], L. Anh[1,2], M. Kobayashi[1,2], M. Onodera[3], K. Kinoshita[3], R. Moriya[3], T. Machida[3], M. Tanaka[1,2] and S. Ohya[1,2]
1. Department of Electrical Engineering and Information Systems, The University of Tokyo, Tokyo, Japan; 2. Center for Spintronics Research Network, The University of Tokyo, Tokyo, Japan; 3. Institute of Industrial Science, The University of Tokyo, Tokyo, Japan

$La_{1-x}Sr_xMnO_3$ is a promising material for spintronics applications due to its half-metallic nature [1], as evidenced by the recent demonstration of a large spin-valve ratio of up to 140 % in a $La_{2/3}Sr_{1/3}MnO_3$ (LSMO)-based lateral spin-MOSFET device [2]. However, a serious problem of so-called dead layers, where magnetization and conductivity significantly degrade at the interfaces between $La_{1-x}Sr_xMnO_3$ and other perovskite oxides, has been an obstacle to potential applications. The origins of dead layers are considered to be strain and bonding effects with other substrates. A candidate for resolving these effects is the epitaxial lift-off of a $La_{1-x}Sr_xMnO_3$ thin film from a substrate by using water-soluble $Sr_4Al_2O_7$ (SAO) as a buffer layer [3]. Here, we demonstrate a significant reduction of dead layers and magnetic anisotropy change in a 30-unit-cell-thick LSMO thin film released from a $SrTiO_3$ (STO) substrate by dissolving an SAO buffer layer and subsequently transferred onto a Si substrate. The saturation magnetization increased from 2.0 μ_B/Mn (T_C = 312 K) for the as-grown LSMO/SAO/STO sample (Fig. 1) to 4.0 μ_B/Mn (T_C = 323 K) for the transferred LSMO/Si sample (Fig. 2), where T_C represents the Curie temperature. We attribute this enhancement to the reduction in the strain and bonding effects due to the substrate. Moreover, we found that the anisotropy changed after the transfer by comparing the magnetization loops for different magnetic-field directions. These results will contribute to potential applications of released LSMO thin films for spintronics devices. This work is supported by Grants-in-Aid for Scientific Research of the Ministry of Education, Culture, Sports, Science and Technology, JST CREST, JST ERATO, and Spintronics Research Network of Japan.

[1] J. -H. Park et al., *Nature* 392, 794 (1988). [2] T. Endo et al., *Adv. Mater.* 35, 2300110 (2023). [3] D. Lu et al., *Nat. Mater.* 15, 1255 (2016).

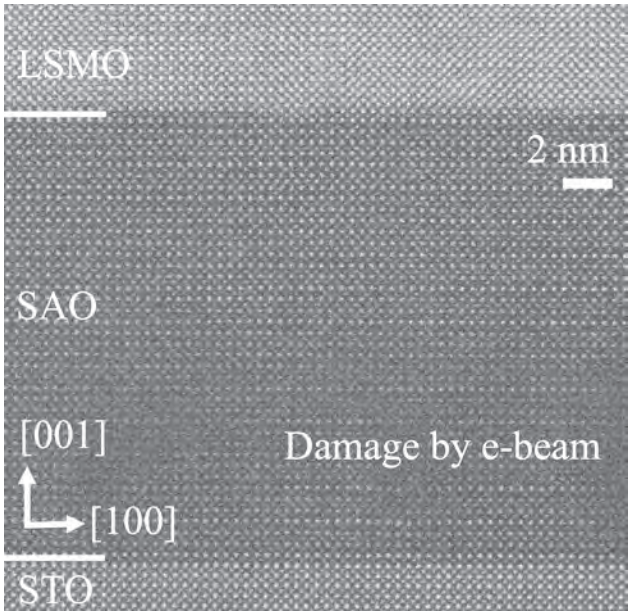

Fig. 1 Scanning transmission electron-microscopy image of the LSMO/SAO/STO sample.

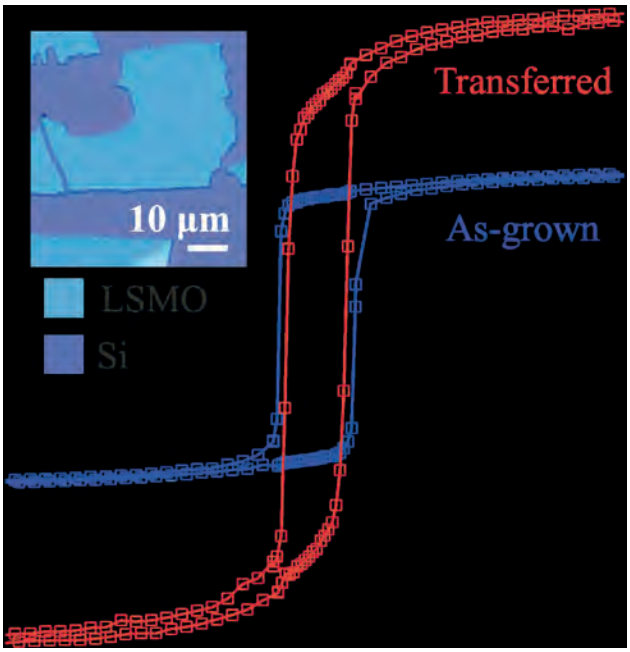

Fig. 2 Magnetization loops of the transferred (red) and the as-grown (blue) LSMO thin films with a magnetic field applied along the in-plane [110] direction at 5 K. The inset shows a microscope image of an LSMO membrane transferred onto a Si substrate.

AE-02. Vertically Aligned Nanocomposites and Exchange Coupling of Multiferroic $LuFeO_3$ and Magnetic $Co_xFe_{3-x}O_4$ Thin Films. *E. Cho*[1] and C.A. Ross[1] *1. Massachusetts Institute of Technology, Cambridge, MA, United States*

Nanocomposite thin films composed of two or more ferroic materials are particularly attractive for the development of energy-efficient, high-speed memory and logic devices. Such heterostructures provide a platform to incorporate multiple functionalities and utilize the interaction at the interface between different phases to enable magnetoelectric switching. For example, we showed voltage-controlled magnetic properties of a $Sr(Co,Fe)O_{3-\delta}$-Co_3O_4 nanocomposite by ionic liquid gating [1]. Here, we investigated vertically aligned nanocomposite thin films grown using pulsed laser deposition (PLD), consisting of pillars of spinel $Co_xFe_{3-x}O_4$ and/or rocksalt CoO embedded in a matrix of perovskite $LuFeO_3$, which is a canted antiferromagnet with concurrent ferroelectricity depending on cation stoichiometry [2]. PLD yielded two-phase (perovskite, spinel) or three-phase (perovskite, spinel, rocksalt) epitaxial nanocomposites on $SrTiO_3$, depending on the combination of targets and on the deposition temperature and oxygen pressure. Alternating ablation from $Lu_{1.4}FeO_{3+\delta}$ and $CoFe_2O_4$ targets resulted in $Co_{1.3}Fe_{1.7}O_4$ pillars in a Fe-rich $LuFeO_3$ matrix (Fig. 1a), whereas $Lu_{0.6}FeO_{3-\delta}$ and Co_3O_4 targets produced CoO and Fe_3O_4 pillars embedded in Fe-rich $LuFeO_3$ (Fig. 1b). The structure and chemistry of the films are characterized in detail via x-ray diffraction (XRD) and atomically resolved scanning transmission electron microscopy. Magnetization-magnetic field (M-H) hysteresis revealed the correlation between magnetic properties and growth conditions. For instance, $Lu_{0.8}FeO_{3-\delta}$-$Co_{1.3}Fe_{1.7}O_4$ films with ~37% $Co_{1.3}Fe_{1.7}O_4$ pillars of ~15 nm diameter had a saturation magnetization of 100 kA/m and coercivity of 450 Oe. By cooling the composites from 360 °C in a field of 10 kOe, an exchange coupling between antiferromagnetic $Lu_{0.8}FeO_{3-\delta}$ and ferrimagnetic $Co_{1.3}Fe_{1.7}O_4$ was established with an exchange bias of 110 Oe at room temperature (Fig. 2). The magnetoelectric coupling in these two- and three-phase epitaxial nanocomposite thin films of $LuFeO_3$, $Co_xFe_{3-x}O_4$ and CoO will be described.

[1] E. Cho, A. Kumar and C. A. Ross, ACS Appl. Nano Mater., Vol. 5, p.14646 (2022) [2] E. Cho, K. Klyukin and C. A. Ross, Adv. Electron. Mater., p.2300059 (2023)

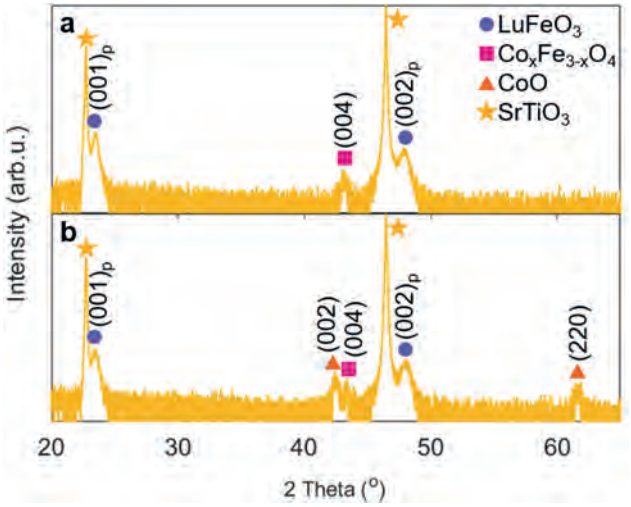

Fig. 1. XRD of films produced by (a) $Lu_{1.4}FeO_{3+\delta}$ and $CoFe_2O_4$ and (b) $Lu_{0.6}FeO_{3-\delta}$ and Co_3O_4 targets.

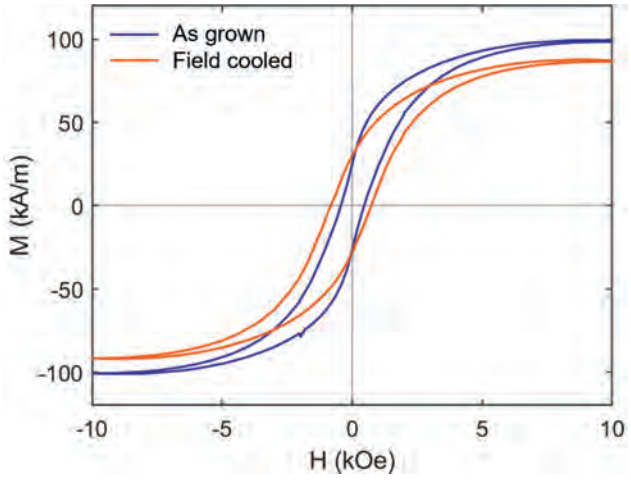

Fig. 2. M-H of $Lu_{0.8}FeO_{3-\delta}$-$Co_{1.3}Fe_{1.7}O_4$ film measured at 300 K.

AE-03. Scattering-Dependent Transport of $SrRuO_3$ Films: From Weyl Fermion Transport to Hump-Like Hall Effect Anomaly.
S. Kaneta-Takada[2,1], Y. Wakabayashi[2], Y. Krockenberger[2], H. Irie[2], S. Ohya[1,3], M. Tanaka[1,3], Y. Taniyasu[2] and H. Yamamoto[2] *1. Department of Electrical Engineering and Information Systems, The University of Tokyo, Bunkyo, Japan; 2. NTT Basic Research Laboratories, Atsugi, Japan; 3. Center for Spintronics Research Network (CSRN), The University of Tokyo, Bunkyo, Japan*

The ferromagnetic perovskite $SrRuO_3$ has attracted interest after observations of Weyl fermions and hump-like Hall effect anomaly, the so-called topological Hall effect (THE). The existence of Weyl fermions has been confirmed from the quantum transport [1,2]. In contrast, the origins of the hump-like Hall effect anomaly are still controversial, such as skyrmion-driven THE and multi-channel anomalous Hall effect (AHE). In this study, we performed magnetotransport measurements in stoichiometric $SrRuO_3$ and Ru-deficient $SrRu_{0.7}O_3$ films with various thicknesses (t) at different temperatures (T) to comprehensively understand the above magnetotransport properties [3]. We grew epitaxial stoichiometric $SrRuO_3$ and Ru-deficient $SrRu_{0.7}O_3$ films with various t (= 2–60 nm) on (001) $SrTiO_3$ substrates by machine-learning-assisted

molecular beam epitaxy. We performed magnetotransport measurements on the Hall bar devices at various T and estimated the residual resistivity ratio (RRR) and the Curie temperature T_C. The quantum transport of the Weyl fermion appears in the $SrRuO_3$ films with $t \geq 10$ nm (inset of Fig. 1), and the hump-like Hall effect anomaly appears in the $SrRu_{0.7}O_3$ films with $t \leq 5$ nm (inset of Fig. 2). To investigate the origin of the AHE, we examined the scaling law incorporating the intrinsic Karplus-Luttinger and extrinsic side-jump mechanisms between the anomalous Hall resistivity and longitudinal resistivity. While this scaling law can be applied broadly to most of the films regardless of stoichiometry, film thickness, and T, we found it not the case for those exhibiting the anomaly. Accordingly, we conclude that this anomaly does not have a topological origin. We also provide defect- and T-dependent transport diagrams for $SrRuO_3$ and $SrRu_{0.7}O_3$ (Figs. 1 and 2). These results serve as a guideline for the development of $SrRu_{1-x}O_3$-based spintronic and topological electronic devices.

[1] K. Takiguchi, Y. K. Wakabayashi *et al*., Nat. Commun. 11, 4969 (2020). [2] S. Kaneta-Takada, Y. K. Wakabayashi *et al*., npj Quantum Mater. 7, 102 (2022). [3] S. Kaneta-Takada, Y. K. Wakabayashi *et al*., Phys. Rev. Mater. 7, 054406 (2023).

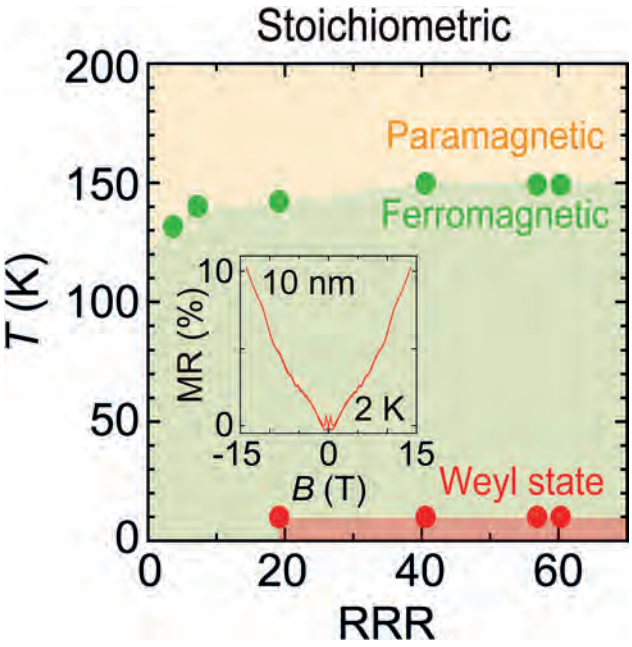

RRR and T dependence of the transport phenomena in the $SrRuO_3$ films. Here, red and green plots are the highest T where the quantum transport of the Weyl fermion appears and T_C.

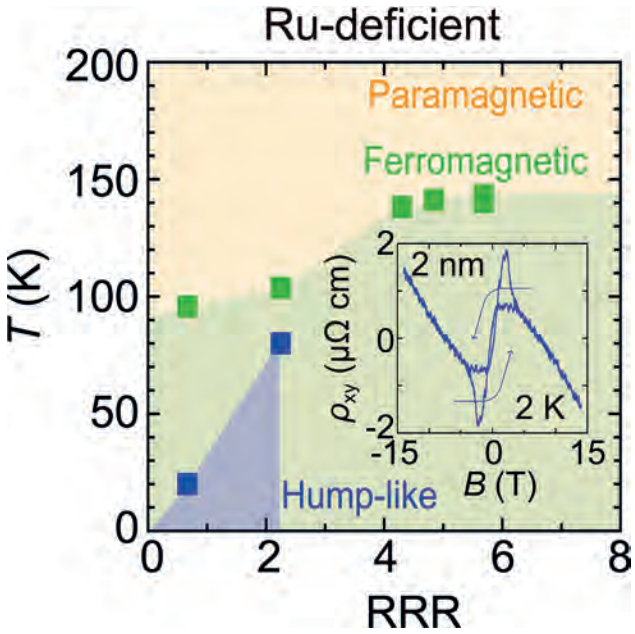

RRR and T dependence of the transport phenomena in the $SrRu_{0.7}O_3$ films. Here, the blue plot is the highest T where the hump-like Hall effect anomaly appears.

AE-04. Spin-flop Coupling at $La_{0.5}Sr_{0.5}FeO_3/La_{0.7}Sr_{0.3}MnO_3$ Interfaces.

I. Nihal[1], D.Y. Sasaki[1], M. Feng[1], C. Klewe[2], P. Shafer[3], A. Scholl[2] and Y. Takamura[1] *1. Materials Science and Engineering, University of California, Davis, Davis, CA, United States; 2. Advanced Light Source, Lawrence Berkeley National Laboratory, Berkeley, CA, United States; 3. Brookhaven National Laboratory, Upton, NY, United States*

Antiferromagnetic (AFM) spintronics has several advantages like high storage capacity and faster processing speed, but difficulties in controlling AFM moments impede its application. Spin-flop coupling is a promising interfacial phenomenon which can allow manipulation of AFM moments with modest applied magnetic field values and is characterized by perpendicular coupling between ferromagnetic (FM) and AFM moments. AFM $La_{1-x}Sr_xFeO_3$ (x=0 and 0.3) / FM $La_{0.7}Sr_{0.3}MnO_3$ (LSMO) heterostructures remain one of the few perovskite oxide systems where spin-flop coupling has been demonstrated. Previous studies showed that robust spin-flop coupling observed in 6 unit cells (u.c.) $La_{0.7}Sr_{0.3}FeO_3$ / 6 u.c. LSMO superlattices vanished once the layer thicknesses reached 18 u.c., as the magnetocrystalline anisotropy energy of the AFM layer overcame the spin-flop coupling strength [1]. In this study, epitaxial $La_{0.5}Sr_{0.5}FeO_3$ (LSFO) / LSMO bilayers with similar thickness of LSMO (~85 u.c.) and LSFO thicknesses varying from 10 to 50 u.c. were deposited on (001)-oriented $(LaAlO_3)_{0.3}(SrAl_{0.5}Ta_{0.5}O_3)_{0.7}$ substrates to investigate the relationship between Sr-doping, magnetocrystalline anisotropy, and the critical thickness for spin-flop coupling. Soft X-ray absorption magnetic spectroscopy was performed to probe the exchange interactions between the FM Mn moments and the AFM Fe moments. X-ray magnetic linear dichroism (XMLD) measurements demonstrated that the spin-flop coupling strength decreased with increasing LSFO layer thickness, persisting at a thickness of 50 u.c. (~20 nm), surpassing the $La_{0.7}Sr_{0.3}FeO_3$ / LSMO system (Fig.1). Also, photoemission electron microscopy imaged the domain-by-domain correlation between the FM and AFM domains consistent with the perpendicular orientation dictated by spin-flop coupling. As LSFO/LSMO system allows to control AFM moments through spin-flop coupling over a greater LSFO thickness, it is desirable for AFM spin transport measurements.

[1] Y. Takamura, F. Yang, N. Kemik, E. Arenholz, M. D. Biegalski, and H. M. Christen, "Competing interactions in ferromagnetic/antiferromagnetic perovskite superlattices," *Phys Rev B*, vol. 80, no. 18, p. 180417, Nov. 2009, doi: 10.1103/PhysRevB.80.180417.

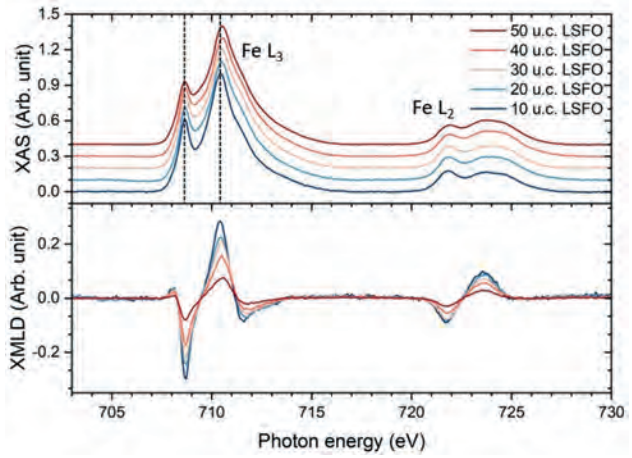

Fig.1. X-ray absorption spectra (XAS) and XMLD signals obtained from five bilayers with similar LSMO, but varying LSFO thicknesses. The Fe L_3 peak shifts with increasing LSFO thickness, implying increased concentration of Fe^{4+} ions in the Fe^{3+}/Fe^{4+} mixed valency.

AE-05. Garnet-perovskite epitaxial nanocomposite films templated by single-crystalline perovskite nanosheets. *K. Hayashi*[1,2], L. Nurdiwijayanto[2], R. Ma[2], T. Sasaki[2], T. Taniguchi[2] and C.A. Ross[1] *1. Department of Materials Science and Engineering, MIT, Cambridge, MA, United States; 2. Research Center for Materials Nanoarchitectonics, National Institute for Materials Science (NIMS), Tsukuba, Japan*

Epitaxial nanocomposites of perovskites and spinels have been widely studied, readily forming magnetic spinel pillars within a perovskite matrix due to the compatibility between the lattices of the two phases [1]. However, synthesis of nanocomposites incorporating garnets has been challenging due to lattice mismatch and the extensive solubility of cations in the garnet and perovskite lattice [2-4]. We have shown that ferrimagnetic iron garnets ($A_3Fe_5O_{12}$: A = Y, Bi, or rare earth) grow well on a $Gd_3Ga_5O_{12}$ (GGG) substrate but instead form a Fe-rich perovskites (Fe-rich $AFeO_3$) when grown on a perovskite substrate [3,4]. By partially covering a GGG substrate with single-crystalline $Ca_2Nb_3O_{10}$ (CNO) nanosheets, and then depositing a film with composition $Bi_3Fe_5O_{12}$ (BIG), we demonstrate here that a garnet-perovskite nanocomposite can be grown consisting of BIG and Fe-rich $BiFeO_3$ (BFO). Dimethyl sulfoxide containing CNO and graphene oxide (GO) nanosheets was spin-coated onto a GGG substrate to make a hybrid monolayer film of CNO and GO. The sample was treated with an oxygen plasma to remove the GO, exposing the GGG underneath, without disturbing the CNO. Then a film with composition of BIG was deposited onto the CNO-coated GGG by pulsed laser deposition at 520°C substrate temperature. Figure 1 shows a cross-sectional STEM image of the nanocomposite near the CNO/GGG substrate interface. In the garnet region, continuous lattice fringes are observed traversing the GGG substrate and the epitaxial film of single crystal BIG, while in the perovskite region, the CNO templates the growth of Fe-rich BFO with (001) orientation parallel to the substrate. The Faraday rotation of the nanocomposite and a single-phase BIG film on GGG fabricated simultaneously with the nanocomposite are shown in Fig. 2. The nanocomposite has a lower saturation field for the out-of-plane loop indicating that the magnetic anisotropy depends on the microstructure. Since the film thickness of both samples is 122 nm and the width of the BIG regions of the nanocomposite is on the order of micrometers, the origin of this difference is not due to shape anisotropy but likely represents a change in strain state between the nanocomposite and the homogeneous film.

[1] O. J. Lee, S. Misra, and J. L. MacManus-Driscoll, APL Mater 9, 030904 (2021). [2] G. Dong, Z. Zhou, and M. Liu, ACS Appl. Mater. Interfaces 9, 30733 (2017). [3] S. Ning, A. Kumar, and C. A. Ross, Nat. Commun. 12, 4298 (2021). [4] T. Su, S. Ning and C. A. Ross, Phys. Rev. Mater. 5, 094403 (2021).

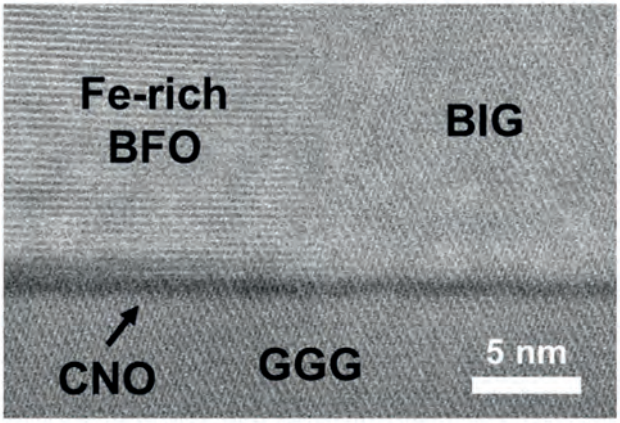

Fig. 1; Cross-sectional STEM image of the BIG and Fe-rich BFO nanocomposite film.

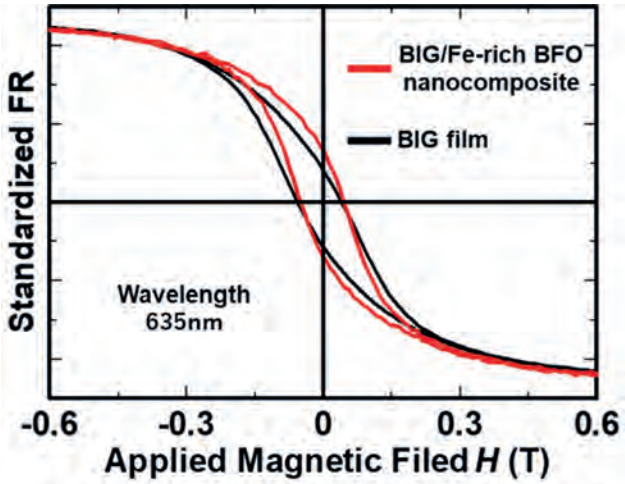

Fig. 2; Standardized Faraday rotation loops at 635 nm for the nanocomposite and BIG films.

AE-06. Tuning In-plane Magnetic Anisotropy and Exchange Bias in Epitaxial Complex Oxide Heterostructures. *M. Feng*[1], N. Ahlm[1], D.Y. Sasaki[1], I. Chiu[2], A. N'Diaye[3], P. Shafer[4], C. Klewe[3], A. Mehta[5] and Y. Takamura[1] *1. Materials Science and Engineering, University of California, Davis, Davis, CA, United States; 2. Chemical Engineering, University of California, Davis, Davis, CA, United States; 3. Advanced Light Source, Lawrence Berkeley National Laboratory, Berkeley, CA, United States; 4. Brookhaven National Laboratory, Upton, NY, United States; 5. Linear Coherent Light Source, SLAC National Accelerator Laboratory, Menlo Park, CA, United States*

Exchange coupling that occurs at interfaces between ferromagnetic perovskite oxide layers have the potential to play a key role in next generation spintronic and magnetic memory devices. In this study, we present a new approach to tune the magnetic easy axis of $La_{2/3}Sr_{1/3}MnO_3$ (LSMO) from its bulk magnetocrystalline anisotropy (MA) to interfacial MA by changing the thickness of the $La_{2/3}Sr_{1/3}CoO_3$ (LSCO) layer in LSCO/LSMO bilayers deposited on $(110)_o$-orientated $NdGaO_3$ (NGO) substrates. The LSMO layer had a fixed thickness of 6 nm and LSCO thicknesses (t_{LSCO}) varied from 1-10 nm. Despite the small difference (~0.2%) in lattice mismatch between the two in-plane directions, $[001]_o$ and $[1\text{-}10]_o$, a pronounced in-plane MA was observed, which dramatically modified the exchange bias (EB) behavior. Soft x-ray magnetic circular dichroism hysteresis loops revealed that for $t_{LSCO} \leq 4$ nm, the easy axes for both LSCO and LSMO layers were along

the $[001]_o$ direction. Furthermore, the LSCO layer was characterized by magnetically active Co^{2+} ions that strongly coupled to the LSMO layer, and no EB effect was observed. In contrast, along the $[1\text{-}10]_o$ direction, the LSCO and LSMO layers displayed a small difference in their coercivity values, and a small EB shift was found. As t_{LSCO} increased above 4 nm, the easy axis for the LSCO layer remained along the $[100]_o$ direction, but it gradually rotated to the $[1\text{-}10]_o$ direction for the LSMO layer, resulting in a large negative EB shift. With direct correlation to the in-plane anisotropy, Mn *L*-edge soft x-ray linear dichroism spectra highlighted the differing electron occupancy along the two in-plane directions with increasing t_{LSCO}. Therefore, we provide a way to control MA and EB by tuning the interfacial exchange coupling between two ferromagnetic layers, which can contribute to the potential needs of spintronic devices.

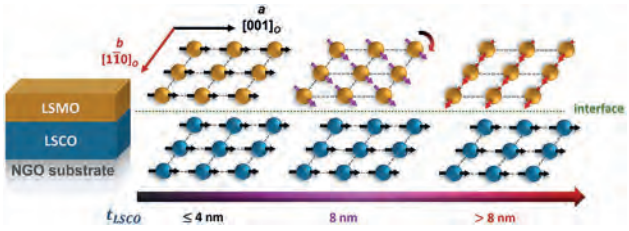

Fig. 1. LSCO thickness (t_{LSCO}) - dependent in-plane magnetocrystalline anisotropy in LSCO/LSMO bilayers on NGO substrates. The Mn and Co ions are colored in yellow and blue, respectively.

INVITED PAPER

AE-07. Voltage-Controlled Magnetism Driven by Electrical Triggering of a Metal-Insulator Transition. *P. Salev*[1], D.Y. Sasaki[2], L. Fratino[3,4], I. Volvach[5], E. Kisiel[6], A. Frano[6], V. Lomakin[5], M. Rozenberg[4], Y. Takamura[2] and I.K. Schuller[6] *1. Department of Physics & Astronomy, University of Denver, Denver, CO, United States; 2. Department of Materials Science and Engineering, University of California Davis, Davis, CA, United States; 3. Laboratoire de Physique Theorique et Modelisation, CY Cergy Paris Universite, Cergy-Pontoise, France; 4. CNRS Laboratoire de Physique des Solides, Universite Paris-Saclay, Orsay, France; 5. Center for Memory and Recording Research, University of California San Diego, La Jolla, CA, United States; 6. Department of Physics, University of California San Diego, La Jolla, CA, United States*

Naturally occurring phase separation often has a prominent impact on magnetic and magnetotransport properties in strongly correlated electronic systems, such as rare-earth manganites. This talk will present examples of how the volatile resistive switching in metal-insulator transition (MIT) materials, a phenomenon where applied voltage drives a large resistance change, enables creating and tuning artificial phase separation by electrical means. The MIT switching commonly occurs by the formation of characteristic local spatial patterns, e.g., longitudinal conducting filaments or transverse insulating barriers, which effectively results in the injection of a different electronic and magnetic phase into the otherwise homogeneous material. In a model system $(La,Sr)MnO_3$, an above threshold voltage triggers the intrinsic MIT due to the electrothermal effects and produces a phase-separated configuration in which a paramagnetic insulating barrier splits the ferromagnetic metallic matrix [1]. While magneto-optical studies showed that magnetic phase regions are well delineated, microdiffraction experiments revealed an inhomogeneous strain development throughout the entire device, suggesting that the applied voltage induces a highly nonuniform temperature profile. Electrical control of the electronic, magnetic, thermal and structural nonuniformities allows tuning of the magnetic properties in the MIT switching devices. *In-operando* magneto-optical and transport measurements revealed voltage-triggered easy-plane to uniaxial magnetic anisotropy switching [2] and multiple magnetoresistance anomalies including a large increase in magnitude and a sign flip of anisotropic and colossal magnetoresistance. This work demonstrates a unique approach to achieve voltage-controlled magnetism and introduces MIT switching materials as a nonlinear electrical platform to explore magneto-thermal phenomena. This work was supported by the U.S. Department of Energy (DOE), Office of Science, Basic Energy Sciences (BES), Materials Sciences and Engineering Division under Award No. DE-FG02-87ER45332.

[1] P. Salev, L. Fratino, D. Sasaki, *et. al.*, Nat. Commun. 12, 5499 (2021).
[2] P. Salev, I. Volvach, D. Sasaki, *et. al.*, Phys. Rev. B 107, 054415 (2023).

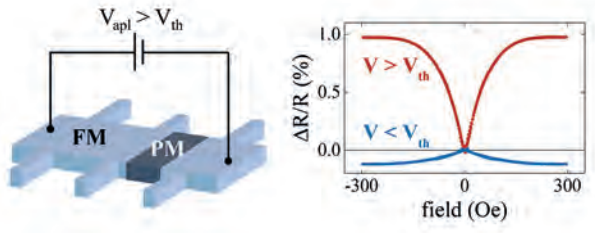

CONTRIBUTED PAPERS

AE-08. On the Low-temperature Local Magnetic Disorder, Orbital Degeneracy and Exchange Interactions in Highly Frustrated Spinels $(ZnCu)[Fe_{1-x}Mn_x]_2O_4$. *S.K. Jena*[1] and S. Thota[1] *1. Department of Physics, Indian Institute of Technology Guwahati, Guwahati, India*

Magnetic materials stabilizing in spinel oxide(AB_2O_4) structures are conversant systems that can accommodate diverse range of cations which interact among themselves via various exchange paths[1]. Site specific substitution in spinels leads to controllable lattice as well as magnetic orderings manifested over a wide range of temperatures which are favorable for multiferroic applications[2,3]. One such spinel is $ZnFe_2O_4$(ZFO) in which the corner-shared-tetrahedra geometry of *B* sublattice engenders high magnetic frustration(MF) leading to intricate magnetic phenomena: spin-ice/liquid/glass states[4]. Additionally, bulk $ZnMn_2O_4$(ZMO) shows greater MF factor $f(=|\theta|/T_N) \sim 14.2$ than ZFO(~12) with antiferromagnetic Néel temperature T_N=64K, and exhibits sporadic 2D spin-correlations[4,5]. Here, we present study on the magnetic properties of intermediate compositions of bulk ZFO and ZMO, diluted(20%) with Cu^{2+} on *A*-site in order to enhance the Jahn-Teller activity driven orbital degeneracy and exchange coupling(J_{AB}). Fig.1(a) and (b) shows the temperature dependency of magnetization in $(Zn_{0.8}Cu_{0.2})[Fe_{1-x}Mn_x]_2O_4$ for x=0.75 and 1, tetragonal($I4_1/amd$) systems, respectively. For x=0.75, the zero-field-cooled(ZFC) and field-cooled(FC) curves exhibit bifurcation(T_{irr}~38K) with lowering of temperature signifying huge anisotropy below the local maximum(T_D). However in x=1, strong spin-orbit coupling enhances the ferromagnetic interaction and lifts T_{irr} above T_D. An associated heat capacity relation($C_p \sim \partial(\chi T)/\partial T$) reveals that the ferri- to para-magnetic ordering temperature(T_{FiM}) is shifted to slightly higher Kelvins in x=1 than that of pristine ZMO, while T_{FiM} increased significantly to 145K with increasing the Fe content. However, coexistence of different short-range orders (more pronounced at lower applied field(H)), persists in the range 7-24K across T_G in x=1. Additional analysis based on the heat-capacity, dynamic susceptibility and varying H measurements on the series of systems ($0 \le x \le 1$) reveals exotic magnetic phases results from the dilute magnetic interaction in the percolation limit of x.

[1] R. Saha, S. Ghara and A. Sundaresan, *Phys. Rev. B* 94, 014428 (2016)
[2] S. K. Jena, D. C. Joshi and S. Thota, *J. Appl. Phys.* 128, 073908 (2020)
[3] C. De, R. Bag and A. Sundaresan, *Phys. Rev. B* 103, 094406 (2021) [4] K. Kamazawa, Y. Tsunoda and K. Kohn, *Phys. Rev. B* 68, 024412 (2003)
[5] N. R. Kumar, R. Karthik and R. K. Selvan, *J. Phys.: Condens. Matter* 32, 245802 (2020)

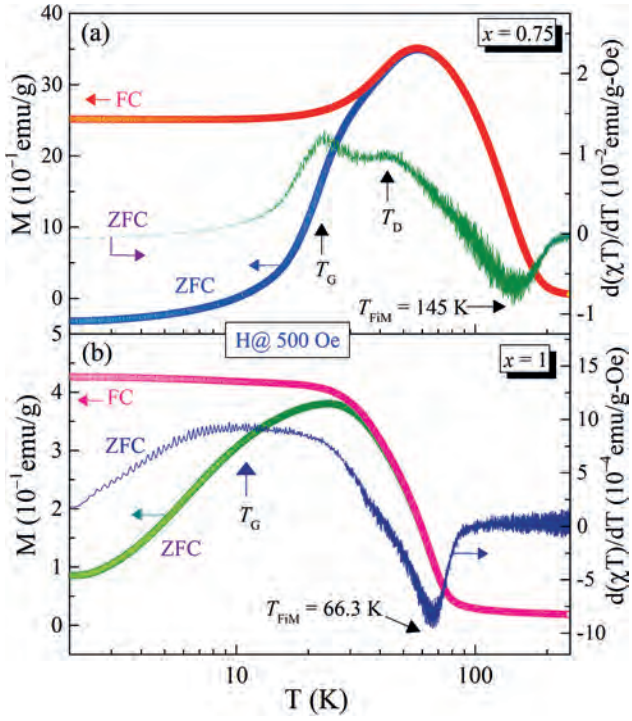

Fig. 1: Temperature dependence of magnetization on the LHS and $\partial(\chi T)/\partial T$ on RHS for (a)x=0.75 and (b)x=1, in $(Zn_{0.8}Cu_{0.2})[Fe_{1-x}Mn_x]_2O_4$.

AE-09. Fully Spin Polarized Ultrathin $La_{0.8}Sr_{0.2}MnO_3$ Films.
F. Stramaglia[1], G. Panchal[1], F. Nolting[1] and *C.A. Vaz*[1] *1. Swiss Light Source, Paul Scherrer Institut, Villigen PSI, Switzerland*

We report the observation of fully magnetically polarized ultrathin $La_{0.8}Sr_{0.2}MnO_3$ films by using 12 unit cells thick $LaMnO_3$ and 15 unit cells thick $La_{0.45}Sr_{0.55}MnO_3$ buffer layers grown epitaxially on $SrTiO_3$(001) substrates by oxide molecular beam epitaxy. Specifically, we show that $La_{0.8}Sr_{0.2}MnO_3$ films grown on $LaMnO_3$ have bulk-like magnetic moments starting from a single unit cell thickness, while for the $La_{0.45}Sr_{0.55}MnO_3$ buffer layer, the $La_{0.8}Sr_{0.2}MnO_3$ transitions from an antiferromagnetic state to a fully spin polarized ferromagnetic state at 4 unit cells. The magnetic results are confirmed by x-ray magnetic circular dichroism. Linear dichroic measurements carried out for the $La_{0.8}Sr_{0.2}MnO_3/La_{0.45}Sr_{0.55}MnO_3$ series show the presence of an orbital reorganization at the transition from the antiferromagnetic to ferromagnetic state corresponding to a change from a preferred in-plane orbital occupancy, characteristic of the A-type antiferromagnetic state of $La_{0.45}Sr_{0.55}MnO_3$, to preferentially out of plane. We interpret our findings in terms of the different electronic charge distribution between the adjacent layers, confined to the unit cell in the case of insulating $LaMnO_3$ and extended to a few unit cells in the case of conducting $La_{0.45}Sr_{0.55}MnO_3$.

AE-10. Magnetism and magnetotransport behavior of $SrRuO_3$/ $La_{0.35}Pr_{0.25}Ca_{0.4}MnO_3$ heterostructures. *K. Alka*[1,2], P.K. Siwach[1,2], P. Manral[3], V.K. Malik[3], G.D. Varma[3] and H.K. Singh[1,2] *1. Electrical and Electronics Division, CSIR-National Physical Laboratory, New Delhi, India; 2. Academy of Scientific and Innovative Research (AcSIR), Ghaziabad, India; 3. Department of Physics, IIT Roorkee, Roorkee, India*

Magnetism and magnetotransport behaviour in heterostructures composed of a phase separated (PS) manganite and 'Fermi liquid' is an interesting proposition.[1-4] In the present study we report extrinsic control of intrinsic PS behaviour of $La_{0.35}Pr_{0.25}Ca_{0.4}MnO_3$ (LPCMO) thin films through the variation in the thickness of the $SrRuO_3$ (SRO) overlayers. The individual SRO (6nm-36nm) and LPCMO (~40nm) films and the SRO/LPCMO heterostructures were grown on (001) oriented $LaAlO_3$ (LAO) substrates by RF magnetron sputtering of 2-inch targets. All the films were deposited at ~850°C and in-situ annealed. The films thickness was estimated by XRR, and the optimized growth rate was ~6nm/minute. The HRXRD reveals the high crystalline quality of the films and the interfaces. The magnetic behaviour of the pure LPCMO and the two heterostructures having 12nm (SRO12/LPC) and 36nm (SRO36/LPC) SRO overlayers are presented in Fig. 1. The M-T and M-H data (Fig. 1) shows that as compared with the LPCMO film, the two heterostructures have (i) smaller Curie temperature (T_C), (ii) appreciably lower magnetic moment, (iii) notably smaller remanence and saturation moment, and (iv) reduced glass phase fraction. The coercivity of the LPCMO film is H_C~660Oe, which first decreases to H_C~550Oe and then increases to H_C~720Oe. The magnetotransport measurements (Fig. 2) bring out that in heterostructures (i) the insulating PM state of LPCMO first transforms into a semiconducting and then into a metallic state, (ii) IMT is lowered, and (iii) ρ-T hysteresis is reduced. In heterostructures the magnetoresistance is also reduced and directly correlates with the SRO layer thickness. Our study brings out that the intrinsic PS in manganites can be extrinsically controlled and increase in the SRO thickness is equivalent to intrinsic enhancement of the FM phase.

1. Y. Tokura, *Rep. Prog. Phys.* 69 797 (2006) 2. G.Koster, L. Klein, Wolter Siemons, et al., Rev. Mod. Phys. 84 253 (2012) 3. S. Singh, P. Kumar, P. K. Siwach, et al., Appl. Phys. Lett. 104 212403 (2014) 4. S. Chauhan, S. Kumari, P.K. Siwach, et al. Physica E 128 114573 (2021)

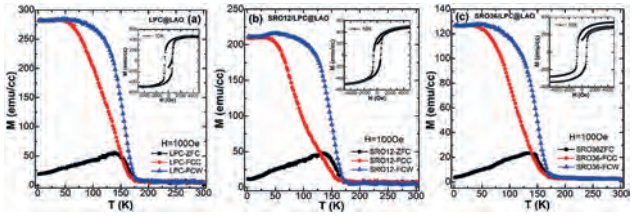

Fig. 1: The temperature dependent ZFC, FCC and FCW magnetization (M-T) of pure LPCMO film and SRO12/LPC and SRO36/LPC heterostructures measured at H=100 Oe employing a commercial SQUID magnetometer. The inset shows the M-H loop measured at T=10K.

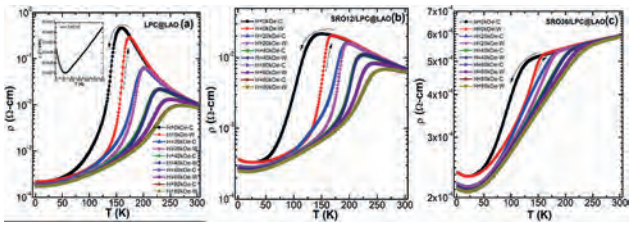

Fig. 2: The temperature dependent resistivity at different magnetic fields measured in cooling (C) and warming (W) cycles.

AE-11. Evidence of insulating ferromagnetic state in polycrystalline $Pr_{0.58}Ca_{0.42}MnO_3$. *A.K. Singh*[1,2], S. Chauhan[3], P.K. Siwach[1,2] and H.K. Singh[1,2] *1. Electrical and electronics metrology division, CSIR-National Physical Laboratory, Dr. K. S. Krishnan Marg, New Delhi-110012, India, New Delhi, India; 2. Academy of Scientific and Innovative Research (AcSIR), Ghaziabad-201002, India, Ghaziabad, India; 3. Department of Physics, SSJDW Government P.G. College, Rakikhet, Uttarakhand-263645, India, Ranikhet, India*

The $Pr_{1-x}Ca_xMnO_3$ family has been recognized as a robust charge and orbital ordered (CO/OO) antiferromagnetic insulator (AFI).[1,2] However, there have been sporadic reports regarding the occurrence of a metallic-ferromagnetic (M-FM) phase.[3,4] Despite more than three decades of research the nature of ground states this family unclear. In the present work, we investigate $Pr_{0.58}Ca_{0.42}MnO_3$ polycrystalline thin films deposited on (100)

oriented $SrLaAlO_4$ (SLAO, lattice constant a=b=0.3756nm, c= 1.263nm) substrates by nebulized spray pyrolysis. The films were deposited at ~200°C and annealed at ~1000°C for 2-4 hrs in air. The XRD data shows the films are textured but polycrystalline having a pseudo cubic lattice constant of a_{sc}=0.383nm, which is nearly the same as that of the bulk. The surface microstructure is found to be homogeneous with submicrometric grain size. The temperature and magnetic field dependent magnetization (M-T&M-H) and resistivity measurements show that (Fig. 1) (i) the CO is quenched, (ii) a clustered magnetic state exists at $T<T_{irr}$~202K, and (iii) a FM type ordering appears around T_C~206K (inset of Fig. 1). The occurrence of FM state is also supported by large magnetic moment in the lower temperature region (~280 emu/cc at 10K) and a well-formed M-H loop (data not shown here). The insulating nature of the FM state is demonstrated by the temperature dependent resistivity measured during cooling and warming cycles (Fig. 1 inset). The FM nature of the magnetic state was further confirmed by ZFC-M-T measurements at different magnetic fields (Fig. 1). The large increase in the magnetic moment with the increase in the applied magnetic field, especially in the lower temperature regime is evidence of the occurrence of ferromagnetism in place of an otherwise CO-AFI ground state. The observed phenomena have been explained in terms of the oxygen vacancy induced quenched disorder and supports our earlier findings.[4,5]

1. Y. Tokura, *Rep. Prog. Phys.* 69, 797 (2006) 2. C. L. Lu, S. Dong, K. F. Wang, et al., Appl. Phys. Lett. 91, 032502 (2007) 3. S. S. Rao, K. N. Anuradha, S. Sarangi, et al., Appl. Phys. Lett. 87, 182503 (2005) 4. V. Agarwal, R. Prasad, M. P. Singh, et al., *Appl. Phys. Lett.* 96, 052512 (2010) 5. V. Agarwal, P.K. Siwach, V.P.S. Awana et al., *Mater. Res. Express* 1 046117 (2014)

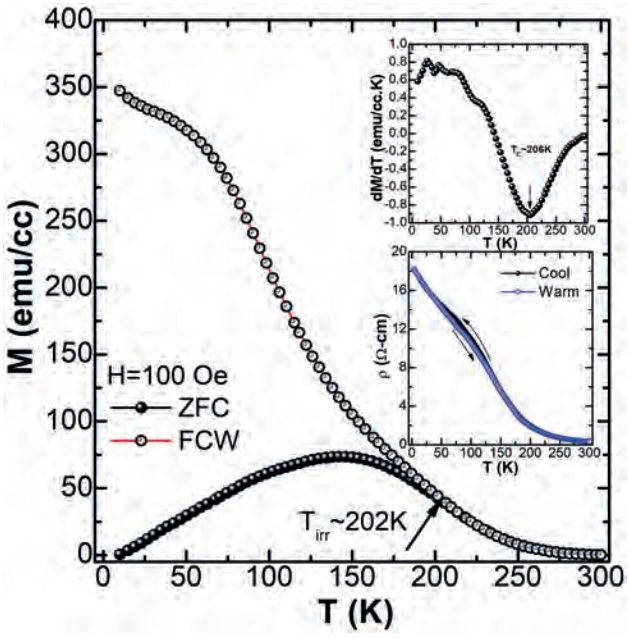

Fig. 1: The ZFC-FCW M-T measured at H=100 Oe. The upper inset shows dM-dT of the ZFC curve. The lower inset shows the resistivity measured during cooling and warming cycles.

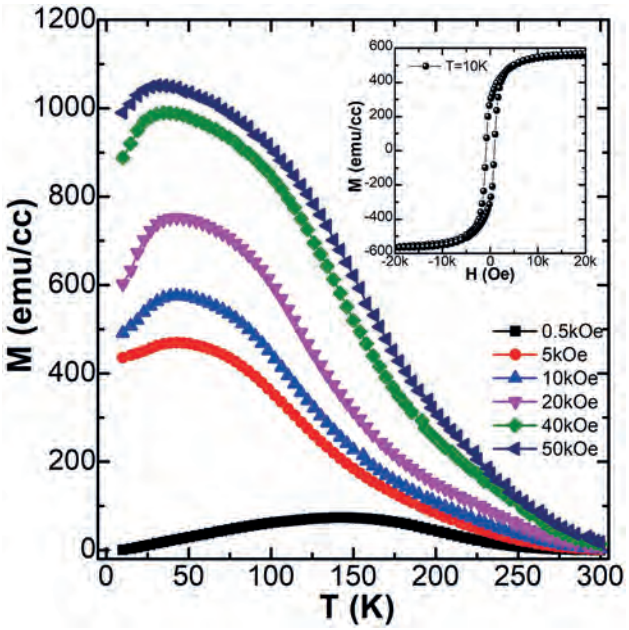

Fig. 2: The ZFC-FCW M-T measured at different magnetic fields. The inset shows the M-H loop measured at 10K.

AE-12. Imprinted atomic displacements drive spin-orbital order in a vanadate perovskite. *P. Radhakrishnan*[1,2], K.S. Rabinovich[1], A.V. Boris[1], K. Fuersich[1], M. Minola[1], G. Christiani[1], G. Logvenov[1], B. Keimer[1] and E. Benckiser[1] *1. Max Planck Institute for Solid State Research, Stuttgart, Germany; 2. Center for Quantum Phenomena, Department of Physics, New York University, New York, NY, United States*

Perovskites with the generic composition ABO_3 exhibit an enormous variety of quantum states such as magnetism, orbital order, ferroelectricity and superconductivity. Their flexible and comparatively simple structure allows for facile chemical substitution and cube-on-cube combination of different compounds in atomically sharp epitaxial heterostructures. However, already in the bulk, the diverse physical properties of perovskites and their anisotropy are determined by small deviations from the ideal perovskite structure, which are difficult to control. Here we show that directional imprinting of atomic displacements in the antiferromagnetic Mott insulator YVO_3 is achieved by depositing epitaxial films on different facets of an isostructural substrate. These facets were chosen such that other control parameters, including strain and polarity mismatch with the overlayer, remain unchanged. We use polarized Raman scattering and spectral ellipsometry to detect signatures of staggered orbital and magnetic order, and demonstrate distinct spin-orbital ordering patterns on different facets. These observations can be attributed to the influence of specific octahedral rotation and cation displacement patterns, which are imprinted by the substrate facet, on the covalency of the bonds and the superexchange interactions in YVO_3. Our results show that substrate-induced templating of lattice distortion patterns constitutes a unique mechanism for tuning the magnetic and electronic properties of quantum materials.

[1] Y. Ren, T. T. M. Palstra, D. I. Khomskii, A. A. Nugroho, A. A. Menovsky, Phys. Rev. Lett 87, 245501 (2001).

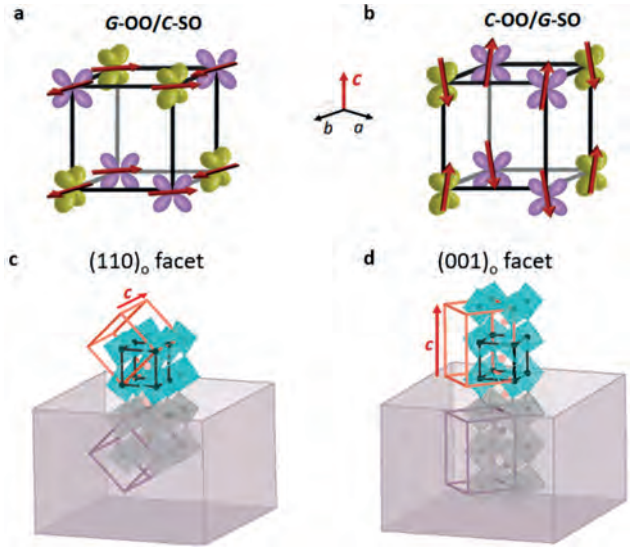

Spin-orbital phases of bulk RVO_3, epitaxial conditions that favor each phase. (a, b) *G*-OO/*C*-SO and *C*-OO/*G*-SO spin-orbital phases of bulk RVO_3 (adapted from Ref. [1]). The *xz* and *yz* orbitals are shown in yellow and purple and arrows indicate the spin at each site. (c, d) Compressive epitaxial strain provided by the substrate in $(110)_o$ and $(001)_o$ orientations, stabilizes the *G*-OO and *C*-OO phases, respectively in the YVO_3 thin films. The blue and grey octahedra represent the film and substrate, respectively and the orthorhombic and pseudocubic unit cells of the film are shown in orange and black, respectively. The film orthorhombic unit cell aligns with that of the substrate, shown in maroon.

AE-13. Mapping Three-dimensional Atomic Order in Rare-Earth Iron Garnets. *A. Kaczmarek*[1], Y. Song[1], A. Penn[2], G. Beach[1] and C.A. Ross[1]
1. Materials Science and Engineering, Massachusetts Institute of Technology, Cambridge, MA, United States; 2. MIT.nano, Massachusetts Institute of Technology, Cambridge, MA, United States

Engineered anisotropy in garnet films with perpendicular magnetization (PMA) enabled progress in spintronic and switching studies.[1,2] In magnonics, specific anisotropy landscapes and interface symmetry can enable more applications of rare earth iron garnets (REIGs).[3,4] We investigate the anisotropy of RE ion ordering on inequivalent surface sites during film growth, which was studied by liquid phase epitaxy in the 1960s, but has recently been revisited with pulsed laser deposition (PLD).[5,6] We consider a europium thulium iron garnet ($Eu_{1.5}Tm_{1.5}Fe_5O_{12}$) 78 nm film grown by PLD on (110) gadolinium gallium garnet. For this growth direction, it is predicted that the 24 dodecahedral (c) sites in the unit cell split into 3 types of non-equivalent orientations (Fig. 1) which will be occupied preferentially by Tm or Eu, leading to a 3D RE cation arrangement of lower symmetry than the parent unit cell. Magnetometry and magnetoresistance measurements yield a large anisotropy of ~80 kJ/m^3 attributed to cation ordering, dominating other contributions to anisotropy (from strain, etc.). Cation order is quantified by atomic resolution scanning transmission electron microscopy (STEM) in high angle annular dark field (HAADF) and energy-dispersive spectroscopy (EDS) modes. EDS reveals ordering of Eu and Tm (Fig. 2), with preference for Eu in α sites and Tm in β and γ sites. Further atom column fitting in HAADF confirms this ordering and suggests the presence and site-preference of Fe antisite defects within γ sites and stronger preference of Tm for β sites. Deviation of the RE:Fe ratio from the ideal 3:5, measured by atom probe tomography, supports the existence of antisite defects due to excess Fe ions. This work shows that atomic engineering of materials creates new means to control their magnetic properties and gives us hope that these phenomena may be observable for cations in other types of complex magnetic or multiferroic oxides.

1. Caretta, L. *et al. Nat Commun* 11, 1090 (2020). 2. Avci, C. O. *et al. Nature Mater* 16, 309–314 (2017). 3. Kajiwara, Y. *et al. Nature* 464, 262–266 (2010). 4. Liu, L. *et al. Nat. Nanotechnol.* 16, 277–282 (2021). 5. Callen, H. *Materials Research Bulletin* 6, 931–938 (1971). 6. Rosenberg, E. R. *et al. Advanced Electronic Materials* n/a, 2100452.

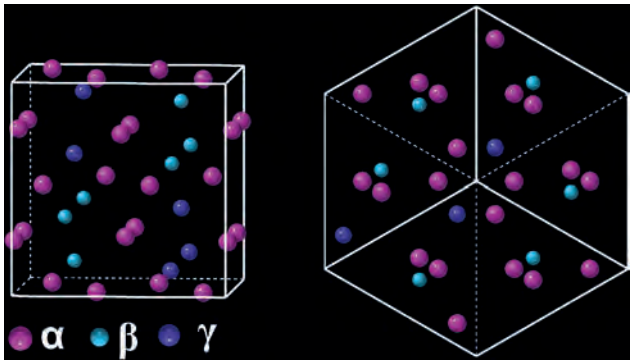

Fig. 1. Perspective and (111) projection views of the c site types for (110) growth.

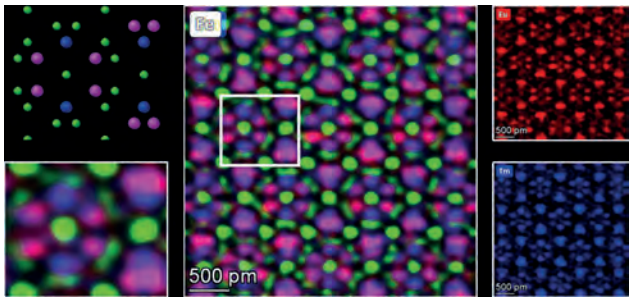

Fig. 2. STEM EDS of the (111) zone axis of $Eu_{1.5}Tm_{1.5}Fe_5O_{12}$ with inset of predicted cation order. Eu is represented by pink balls, and Tm is represented by blue balls (Fe is green).

Session AF
FUNDAMENTAL PROPERTIES I: 2D AND TOPOLOGICAL MATERIALS

Jiahao Han, Chair
Tohoku University, Sendai, Japan

INVITED PAPERS

AF-01. New Research Trends in Two-Dimensional van der Waals Magnetism. *M. Phan*[1] *1. University of South Florida, Tampa, FL, United States*

Two-dimensional (2D) van der Waals (vdW) magnets are being tapped as the primary components of a new generation of computing devices based on spintronics. In addition to their miniaturization, these 2D magnets enable faster processing speeds, lower energy consumption, and even increased storage capacity. To fully exploit their applications, these materials should not require cryogenic temperatures or other special protections to function. It is particularly important to control their atomic-level magnetism at room temperature, at which most of our devices operate [1-3]. In this talk, I will discuss emergent phenomena, opportunities, and challenges in the research of 2D vdW magnets. I will show how to manipulate 2D magnetism with light at room temperature [4] and exploit this to boost "spin to charge" conversion via the spin Seebeck effect (SSE), leading to the establishment of a new field named Opto-Spin-Caloritronics [5]. Finally, I show solid evidence for the existence of a magnetic quantum critical point in the vdW itinerant ferromagnet Fe_3GeTe_2 [6].

[1] M. Bonilla, M.H. Phan, *et al.*, Strong Room Temperature Ferromagnetism in VSe_2 Monolayers on van der Waals substrates, *Nature Nanotechnology* 13, 289 (2018) [2] F. Zhang, M.H. Phan, *et al.*, Monolayer Vanadium-doped Tungsten Disulfide: An Emerging Room-Temperature Diluted Magnetic Semiconductor, *Advanced Science* 7, 2001174 (2020) [3] Y.T.H. Pham, M.H. Phan, *et al.*, Tunable Ferromagnetism and Thermally Induced Spin Flip in Vanadium-doped Tungsten Diselenide Monolayers at Room Temperature, *Advanced Materials* 32, 2003607 (2020) [4] V.O. Jimenez, M.H. Phan, *et al.*, Light-controlled room temperature ferromagnetism in vanadium-doped tungsten disulfide semiconducting monolayers, *Advanced Electronic Materials* 7, 2100030 (2021) [5] M.H. Phan, *et al.*, A Perspective on Two-dimensional van der Waals Opto-Spin-Caloritronics, *Applied Physics Letters* 119, 250501 (2021) [6] N.T. Dang, M.H. Phan, *et al.,* High pressure – driven magnetic disorder and structural transformation in Fe_3GeTe_2: Emergence of a magnetic quantum critical point, *Advanced Science* 2206842 (2023)

AF-02. Magnetism in Quantum Flatland: Novel Excitons and Moiré Physics from First Principles. *T. Cao*[1] *1. University of Washington, Seattle, WA, United States*

The discovery of van der Waals (vdW) magnets has created opportunities for investigating new quantum properties and spintronic applications which are absent in conventional bulk magnets. This talk will show our recent theoretical and computational studies of tunable magnetism of vdW magnets, as well as a new type of magnet-based moiré heterostructure. In the first part, we show that the magnetism in a layered vdW magnetic semiconductors, CrSBr, is highly tunable by strain, pressure, chemical doping, and interfacing with other vdW materials. This allows for investigation of the coupling between optically excited states and the underlying magnetic order. In the second part, we propose a new moiré system consisting of transition metal dichalcogenide (TMD) layered with vdW magnets, where the lattice constants of the two materials are significantly different. By first-principles calculations, we demonstrate that the magnet can strongly couple the otherwise degenerate Kramers' valleys of TMD, resulting in valley pseudospin textures that depend on the magnetization, stacking geometry, and external field. We further construct a continuum model to describe the moiré potential and moiré topology. Finally, we connect our theoretical discoveries to experimental results and explore potential applications.

AF-03. Moiré magnetism in twisted double bilayer CrI_3. *L. Zhao*[1] *1. University of Michigan, Ann Arbor, MI, United States*

Moiré superlattice emerges from the interference between two mismatched atomic lattices, and it has led to tremendous success in designing and tailoring the electronic states in two-dimensional (2D) homo- and heterostructures. Yet, the power of moiré superlattice in controlling the spin degree of freedom and thus modifying the magnetic states is much less explored. Only very recently after the development of 2D magnet research, there have been a few experimental attempts in realizing moiré magnetism in twisted 2D magnet homo-structures. In this talk, I will show our recent effort in studying magnetic phases in twisted double bilayer chromium triiodide (CrI_3) and progressive steps towards realizing moiré magnetism. Noting that bilayer CrI_3 is a layered antiferromagnet and that any homogeneous stacking of two bilayers necessarily produces zero magnetization, we have revealed, in twisted double bilayer CrI_3, an unexpected net magnetization showing up at intermediate twist angles and its accompanied noncollinear spin textures. I will show the optical spectroscopy signatures of this twist-induced magnetic phase, then discuss its dependence on twist angle, external magnetic field, and temperature, and finally comment on its spin wave excitations.

1. H. Xie et al Nature Physics, 18, 30 (2022) 2. H. Xie et al Nature Physics, doi: 10.1038/s41567-023-02061-z (2023)

CONTRIBUTED PAPERS

AF-04. Electronic structure and magnetic properties of chiral molecular adsorbed two-dimensional 1T-$MnSe_2$ Monolayers. *W. Mi*[1] *1. Department of Applied Physics, Tianjin University, Tianjin, China*

Chirality opens up the possibility to manipulate electron spin without external magnetic field, thus preserving the time-reversal symmetry and allowing the local electronic control of spins to enable new spintronic device designs for quantum information science.[1] Although chiral induced optical and transport properties are observed and studied in chiral molecules[2], the interface properties between chiral organic molecules and two-dimensional ferromagnetic materials have not been systematically reported. In this work, the electronic structure and magnetic properties of *R*,*S*-MBA/1T-$MnSe_2$ interfaces are investigated comprehensively using first-principles calculations. It is found that MBA molecules tend to interact with 1T-$MnSe_2$ surface by the NH_3 group. The spin polarization of the *R*,*S*-MBA/1T-$MnSe_2$ interfaces is close to 100%. Both 1T-$MnSe_2$ monolayer and *R*,*S*-MBA/1T-$MnSe_2$

interfaces exhibit perpendicular magnetic anisotropy, which is mainly contributed by the matrix element differences between the p_x and p_y orbits of Se atoms. This work was supported by the National Natural Science Foundation of China (52271185).

[1] Q. Qian, H. Y. Ren, J. Y. Zhou, Z. Wan, J. X. Zhou, X. X. Yan, J. Cai, P. Q. Wang, B. L. Li, Z. Sofer, B. Li, X. D. Duan, X. Q. Pan, Y. Huang and X. F. Duan, Nature 606, 902-908 (2022). [2] Z. Y. Bian, K. Kato, T. Ogoshi, Z. Cui, B. S. Sa, Y. Tsutsui, S. Seki and M. Suda, Adv. Sci. 9, 2201063 (2022).

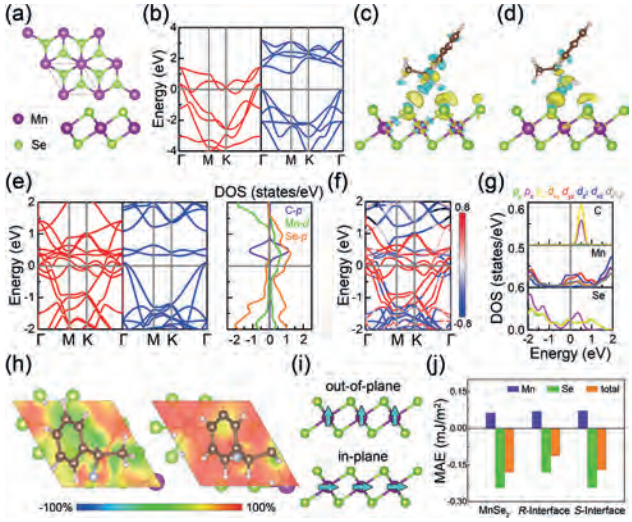

Fig. 1. (a) Atomic structure and (b) band structure of $MnSe_2$. (c-d) Difference charge density of *R*,*S*-MBA/$MnSe_2$ interfaces. Electronic structures (e) without and (f-g) with spin orbit coupling of *R*,*S*-MBA/$MnSe_2$ interfaces. (h) Space spin polarizability of *R*,*S*-MBA/$MnSe_2$ interfaces. (i) Side view of $MnSe_2$ monolayer, where the blue arrows indicate the two opposite spin configurations. (j) Total and atomic-layer-resolved magnetic anisotropy energy.

AF-05. Magnetic anisotropy probed by magnetic torque in a van der Waals antiferromagnetic $CrPS_4$. *J. Seo*[1], S. Lim[1], H. Shin[1], J. Kim[1], K. Jeong[1], J. Hong[1], K. Moon[1], M. Kim[1], N. Lee[1] and Y. Choi[1] *1. Physics, Yonsei University, Seoul, The Republic of Korea*

Exploration of van der Waals (vdW) antiferromagnets greatly enriched our understanding of intrinsic magnetism in the 2D limit. However, there is a limitation to identifying detailed spin states for highly anisotropic magnetism due to the experimental difficulty. In this work, we have revealed intricate spin states formed by rotating magnetic fields in van der Waals antiferromagnetic $CrPS_4$, utilizing combined magnetic torque measurements and spin model calculations. $CrPS_4$ exhibits an A-type antiferromagnetic order along the magnetically easy *c*-axis below $T_N = 38$ K. Our model calculations with uniaxial anisotropy determined magneto-crystalline anisotropy energy and visualized the spin configurations, closely connected to the evolution of magnetic torques through spin-flop transition. Our approach proposed in this work provides useful guidance for the analysis of distinctive magnetic characteristics in $CrPS_4$, which can be extended to other vdW antiferromagnetic materials.

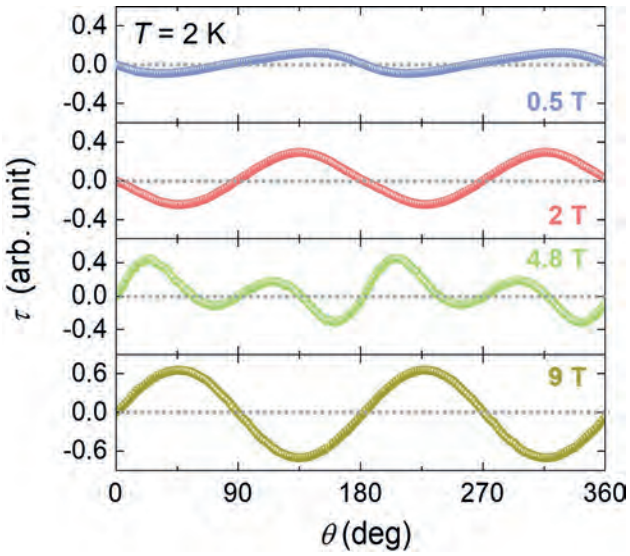

Angle-dependence of the magnetic torque per unit volume, $\tau = M \times H$, measured at $T = 2$ K and $H = 0.5$, 2, 4.8 and 9 T.

AF-06. Magnetic properities of newly discovered $Ir_3Ga_{2.4}Si_{4.6}$ single crystals. *B.K. Rai*[1], A.B. Bretaña[1] and B.S. Conner[1] *1. Savannah River National Laboratory, Aiken, SC, United States*

Compounds of the cubic Ir_3Ge_7 crystal structure type have recently garnered interest from a topological behavior perspective. For example, the electronic band structure calculations of $RhIn_{3.4}Ge_{3.6}$ single crystals reveal that this compound displays a complex Dirac-like electronic structure relatively close to the Fermi level [1]. In this talk, I will present the physical properties of newly discovered Ir3Ga2.4Si4.6 single crystals. $Ir_3Ga_{2.4}Si_{4.6}$ crystallizes in the cubic Ir_3Ge_7 structure type with space group Im-3m. Furthermore, it exhibits magnetic anomalies at low temperature. The presentation discusses physical properties of $Ir_3Ga_{2.4}Si_{4.6}$ assessed using magnetization, specific heat, and ac susceptibility data. The discovery of such new materials offers an opportunity to explore new physical phenomena.

1) Savvidou, Aikaterini Flessa, Judith K. Clark, Hua Wang, Kaya Wei, Eun Sang Choi, Shirin Mozaffari, Xiaofeng Qian, Michael Shatruk, and Luis Balicas. “Complex Dirac-like Electronic Structure in Atomic Site-Ordered Rh3In3. 4Ge3. 6.” *Chemistry of Materials* 33, no. 4 (2021): 1218-1227.

AF-07. Temperature-Induced Magnetostructural Coupling of Weyl Fermions in Co_2MnGa. *N. Schulz*[1], A. Chanda[1], G. Pantano[1], N. Alzahrani[1], E. Clements[2], M.A. McGuire[2], D. Arena[1], A. Markou[3,4], J.D. Gayles[1], C. Felser[4], M. Phan[1] and H. Srikanth[1] *1. Physics, University of South Florida, Tampa, FL, United States; 2. Oak Ridge National Laboratory, Oak Ridge, TN, United States; 3. University of Ioannina, Ioannina, Greece; 4. Max Planck Institute for Chemical Physics of Solids, Dresden, Germany*

Weyl semimetals have gained intense interest recently due to their exotic electronic properties, which give rise to giant anomalous Hall and Nernst responses, the chiral anomaly, etc. These effects are driven by the nontrivial topology of the electronic band structure, arising due to the existence of Weyl fermions[1]. Furthermore, Heusler compounds have been utilized to realize a broad range of unique physical phenomena including topological insulators, topological superconductivity, magnetic shape memory, etc[2]. Here, we demonstrate the effect of a temperature dependent magnetostructural change in the form of a tetragonal distortion in the Heusler ferromagnetic Weyl semimetal Co_2MnGa, as identified via temperature dependent X-ray diffraction measurements. These films were grown in a BESTEC UHV magnetron sputtering system on single crystal MgO(001) substrates. Non-monotonic changes in the magnetization and anisotropy as function

of temperature are observed through magnetometry and transverse susceptibility measurements[3]. These results are independently confirmed via temperature dependent magnetic force microscopy measurements, where a similar nonlinear temperature dependence of the average domain width and phase deviation are observed. DFT results indicate that the changes in the magnetic properties of Co_2MnGa are highly nonlinear for small perturbations in the *c/a* lattice constant ratio. Furthermore, it is shown that there exists a connection between the lattice distortion, Weyl angle (Ω_w), and Weyl distance (d_w) with the magnetic properties including the effective anisotropy field H_k and the saturation magnetization M_s. These changes can be directly related to the destroyed symmetries as the crystal structure is distorted. In-plane magnetoresistance measurements suggest through strong negative magnetoresistance, that the Weyl points that are destroyed as a function of temperature, exist further from the Fermi level, in agreement with the theoretical results. Controlling magnetostructural effects therefore allows for symmetry-selective creation and annihilation of Weyl points, creating a new degree of freedom for the manipulation of the magnetic and electronic properties in Weyl semimetal systems.

[1] I. Belopolski *et al.*, "Discovery of topological Weyl fermion lines and drumhead surface states in a room temperature magnet," *Science (1979)*, vol. 365, no. 6459, pp. 1278–1281, Sep. 2019, doi: 10.1126/science.aav2327. [2] K. Manna, Y. Sun, L. Muechler, J. Kübler, and C. Felser, "Heusler, Weyl and Berry," *Nat Rev Mater*, vol. 3, no. 8, pp. 244–256, Aug. 2018, doi: 10.1038/s41578-018-0036-5. [3] Hariharan Srikanth and Sayan Chandra, *Magnetic Measurement Techniques for Materials Characterization*. Springer, 2021.

AF-08. Withdrawn

AF-09. Magnetic Antiskyrmions in 2D van der Waals Magnets Engineered by Layer Stacking. *K. Huang*[1], E. Schwartz[1], D. Shao[1], A.A. Kovalev[1] and E. Tsymbal[1] *1. Department of Physics and Astronomy, University of Nebraska-Lincoln, Lincoln, NE, United States*

Magnetic skyrmions and antiskyrmions are topologically protected magnetic quasiparticles exhibiting a whirling spin texture in real space. Their formation usually requires a Dzyaloshinskii-Moriya interaction (DMI) driven by lack of structural inversion symmetry. Unlike the widely investigated skyrmions, antiskyrmions are rare due to the required anisotropic DMI with opposite signs along two perpendicular directions. Antiskyrmions offer some advantages over skyrmions as they can be driven without Hall-like motion [1] and have higher stability [2]. Here we propose to exploit the recently demonstrated van der Waals (vdW) assembly of 2D materials [3-5] that breaks inversion symmetry and creates conditions for anisotropic DMI in 2D magnets. We demonstrate, based on symmetry analyses and density functional theory (DFT) calculations, that this strategy is a promising platform to realize antiskyrmions. We exploit this strategy for CrI_3 – the recently discovered 2D vdW magnet [6]. The polar layer stacking of two centrosymmetric magnetic monolayers of CrI_3 (Fig. 1a,b) efficiently lowers the symmetry, resulting in anisotropic DMI that supports antiskyrmions. The DMI is reversible by switching the ferroelectric polarization inherited from the polar layer stacking, offering the control of antiskyrmions by an electric field. Furthermore, we find that the magnetic anisotropy and DMI of CrI_3 can be efficiently modulated by Mn doping, creating a possibility to control the size of antiskyrmions. Using atomistic spin dynamics and micromagnetic simulations with the parameters obtained from our DFT calculations, we predict the formation of antiskyrmions in a $Cr_{0.88}Mn_{0.12}I_3$ bilayer and switching their spin texture with polarization reversal (Fig. 1c,d). Our results open a new direction to generate and control magnetic antiskyrmions in 2D vdW magnetic systems.

[1] A. A. Kovalev and S. Sandhoefner, Front. Phys., Vol 6, p. 98 (2018). [2] L. Camosi et al., Phys Rev B, Vol. 97, p. 134404 (2018). [3] K. Yasuda et al., Science, Vol. 372, p. 1458 (2021). [4] M. Stern et al., Science, Vol. 372, p. 1462 (2021). [5] E. Y. Tsymbal, Science, Vol. 372, p. 1389 (2021). [6] B. Huang et al., Nature, Vol. 546, p. 270 (2017).

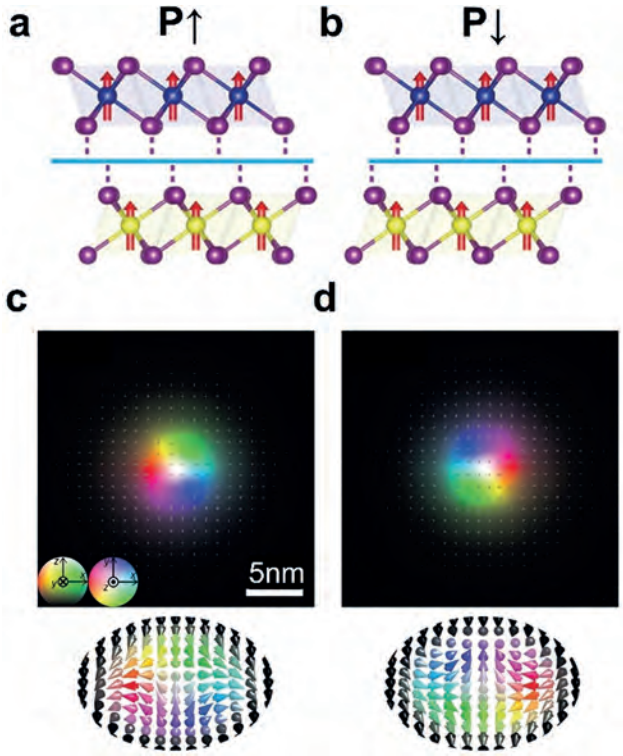

Fig. 1 (a,b) Side view of polar bilayer CrI_3 constructed by mirroring top monolayer to the bottom followed by in-plane sliding, resulting in two stable stackings with opposite polarization pointing up P↑ (a) or down P↓ (b). (c,d) Simulated antiskyrmion in polar bilayer $Cr_{0.88}Mn_{0.12}I_3$ for P↑ (c) and P↓ (d).

Session AG
INTERDISCIPLINARY TOPICS I: MAGNETIC FORCES AND NANOPARTICLES; BIOMEDICINE; EDUCATION AND OUTREACH

Sakhrat Khizroev, Chair
University of Miami, Coral Gables, FL, United States

INVITED PAPER

AG-01. Emerging Applications of Magnetic Nanoparticles for MRI Contrast: Positive T1 Contrast at Low Field and "Color" Contrast at High Field. *S. Oberdick*[1,2], K. Jordanova[1], J. Lundstrom[1,3], G. Parigi[4], M. Poorman[5], K. Keenan[1], S. Dodd[6], A. Koretsky[6] and G. Zabow[1] *1. NIST, Boulder, CO, United States; 2. Physics, CU Boulder, Boulder, CO, United States; 3. University of Illinois at Urbana-Champaign, Urbana, IL, United States; 4. Magnetic Resonance Center (CERM), University of Florence, Florence, Italy; 5. Hyperfine, Guilford, CT, United States; 6. NINDS, NIH, Bethesda, MD, United States*

Magnetic resonance imaging (MRI) is a non-invasive technique that produces three-dimensional images of human anatomy. MR images can be enhanced using contrast agents, which are exogenous magnetic materials that interact with resonant protons in tissue and modify image characteristics. Iron oxide-based magnetic nanoparticles (MNPs) have long been researched as MRI contrast agents and are usually thought of as negative contrast agents because they dephase signal from water protons, resulting in a region of decreased signal on an MR image. However, new technological advancements related to low field MRI scanners and, separately, microfabrication of MNP constructs, have created new opportunities for contrast generation that move beyond negative contrast. In this talk, I will describe new pathways for MNP-based MRI contrast using low field MRI and, also, "color" contrast with magnetic microstructures. First, I will describe possibilities for using MNPs as positive contrast agents with low field MRI (LF-MRI). LF-MRI scanners require less infrastructure than clinical MRI scanners and can be wheeled next to a patient's bedside, creating revolutionary possibilities for point-of-care diagnostics. While MNPs can be used as T1 contrast agents for clinical and high field MRI, the MNPs need to be specially synthesized with sizes of 3 nm or smaller to minimize proton dephasing effects. Here, I will discuss using FDA-approved contrast agents, like ferumoxytol, as well as commercially available iron oxide MNPs with sizes of 5 nm to 16 nm for positive T1 contrast at low field. I will present experiments using an FDA-approved, 64 mT MRI scanner to evaluate the potential of MNPs as contrast agents for LF-MRI. At 64 mT, MNPs show enhanced longitudinal relaxivity (r_1) and reduced transverse relaxivity (r_2) compared to 3 T. Moreover, MNPs have a size-dependent r_1 that is up to 8x larger than a common Gd-based contrast agent (Gd-BOPTA), suggesting that MNPs may outperform traditional T1 agents at lower fields [1]. These properties lead to enhanced T1 contrast at 64 mT for MNP-based contrast agents compared to clinical field strength (Figure 1a and 1b). Secondly, I will describe how hollow cylinder shaped MNP-polymer microparticles (Figure 2a) can be used as radio frequency (RF) multispectral MRI contrast agents at high magnetic fields (9.4 T). Multispectral, or "color" contrast is a unique form of contrast that uses three-dimensional magnetic microstructures to produce a distinct frequency readout [2]. I will describe a new way for producing MNP-polymer microparticles which generate spectral shifts which are tens of times larger than familiar NMR chemical shifts, providing an RF-identifier that is spectrally distinct from the environment. These contrast agents can also be used as biosensors by using shape reconfigurable "smart" hydrogels that expand or shrink in response to environmental conditions (Figure 2b). The change in shape causes a corresponding shift in the proton resonance, producing an MRI-addressable readout of the microenvironment. I will show proof-of-principle experiments showing a multispectral response to changes in pH (Figure 2c and 2d).

[1] S. D. Oberdick et al., "Iron Oxide Nanoparticles as Positive T1 Contrast Agents for Low-Field Magnetic Resonance Imaging at 64 mT," *Scientific Reports*, Under Review (2023) [2] G. Zabow et al., *Nature*, Vol. *453*, p. 1058 (2008)

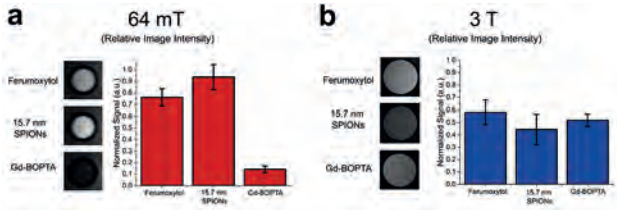

Fig 1. (a) Normalized image intensity from 64 mT MRI (T1-weighted inversion recovery 3D fast spin echo sequence) showing enhanced contrast for ferumoxytol and 15.7 nm SPIONs compared to Gd-BOPTA. (b) Normalized image intensity from 3 T MRI (inversion recovery sequence) showing comparable contrast for each of the three contrast agents.

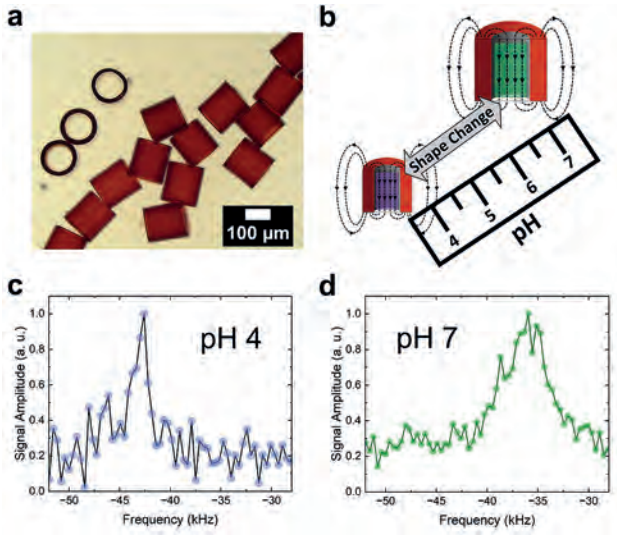

Fig. 2. (a) Optical microscope image of magnetic hydrogel particles with a hollow cylinder geometry used for multispectral contrast generation. (b) Physical changes in the contrast agents, caused by pH-induced hydrogel swelling, can be used to modify the magnetic fields within the cylinder. (c) The contrast agents produce a frequency readout of -43 kHz when contracted at pH 4. (d) At pH 7, the contrast agents expand, producing a shift in the frequency readout to -36 kHz.

CONTRIBUTED PAPERS

AG-02. T_1-T_2 Dual MRI Contrast by Thermal Plasma Synthesized Janus Nanomaterials. *K. Deka*[1], G.A. Deshpande[1], J. Fischer[2], M. Bock[2] and V.L. Mathe[1] *1. Deaprtment of Physics, Savitribai Phule Pune University, Pune, India; 2. Department of Radiology, University Medical Center Freiburg, Freiburg, Germany*

The precision of Magnetic Resonance Imaging (MRI) can be boosted by engaging a multifunctional nanosystem as T_1–T_2 dual contrast agent. The amalgamation of both T_1 and T_2 properties in one single contrast agent aids in getting cross-validated data during T_1-T_2 dual mode MRI and decreases the required dosage of the agent [1]. Presently, most of the regularly used T_1 CAs are gadolinium (Gd) based, but they possess the constraint of Gd toxicity. Magnetic iron oxide nanoparticles are known to be another class of familiar MRI contrast agents, largely owing to their suitable biocompatibility, but most of them display poor T_1 contrast and so cannot be employed as dual agents. Taking into account all these information, alternative imaging agents are being examined systematically for attaining T_1–T_2 dual contrast enhancement [2]. Manganese (Mn)-based compounds have drawn attention and been proven as potential MR imaging probes by several research-groups because of high spin number and labile water exchange of Mn [3, 4]. Therefore, in this study, Mn-based Janus nanosystem having a T_1 active moiety and a T_2 active moiety were developed by thermal plasma method as novel T_1-T_2 MR imaging agents. Thermal plasma technique was selected as it has been reported as a quick, eco-friendly and one-step process with no chemical waste. Furthermore, high purity yields are achieved by this synthesis technique as the reaction takes place in vaporous stage [5]. A series of characterizations were executed to understand the microstructure, composition and magnetic properties of the thermal plasma synthesized Janus system. The biocompatibility of the nanosystem was established by cell viability analysis. Lastly, its competence for T_1–T_2 contrast improvement was verified through MRI experiments at various concentrations [Fig. 1 and 2].

1. H, Saeidi, M. Mozaffari, S. Ilbey et al., Nanomaterials, Vol. 13(2), p.331 (2023) 2. K. Deka, A. Guleria, D. Kumar et al., Dalton Trans., Vol. 48(3), p. 1075 (2019) 3. L. G. Hevia, M. B. Lopez and J. Gallo, Chem. Eur. J., Vol. 25(2), p.431 (2019) 4. D. Pan, A. H. Schmieder, S. A. Wickline et al., Tetrahedron, Vol. 67(44), p.8431 (2011) 5. L. Kumaresan, K. S. Harshini, H. Amir et al., J. Alloys Compd., Vol. 942, p.169121 (2023)

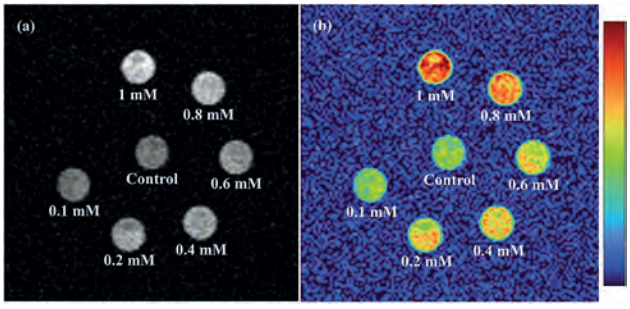

Fig. 1 (a) T_1 weighted MR image (b) Colour map of the image

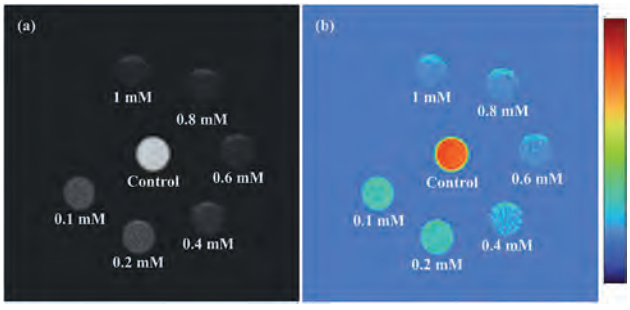

Fig. 2 (a) T_2 weighted MR image (b) Colour map of the image

AG-03. A modality for estimating the NMR relaxation time using angular correlation between successive γ rays. *W. Matsumoto*[1], F. Boyu[2], Y. Tamai[1], T. Ueki[1], M. Fushimi[1], K. Shimazoe[1], H. Takahashi[1] and M. Sekino[1] *1. Department of Bioengineering, The University of Tokyo, Bunkyo-ku, Japan; 2. Department of Nuclear Engineering and Management, The University of Tokyo, Bunkyo-ku, Japan*

MRI and NMR utilize the T2 relaxation time, determined by the phase dispersion speed of Larmor motion, to detect signal decay. However, the detection sensitivity is lower for nuclei with a smaller gyromagnetic ratio, thereby limiting observation of nuclei other than ^{1}H. In this study, we developed a novel approach using the angle between two γ rays emitted by ^{111}In, which provided a parameter equivalent to T2 for individual nuclei. We added superparamagnetic iron oxide (SPIO) to an indium chloride solution and prepared samples with different phase dispersion speeds. We observed paired γ rays from ^{111}In undergoing Larmor motion using detectors (Fig. 1) and obtained the angles between them based on a previous report[1]. We introduced the angular correlation function $R(t)$, where $N(\theta,t)$ is the total number of detected γ rays with an angle θ between the paired emissions, and t is the time difference. Subsequently, we obtained a cosine model that oscillates at twice the Larmor frequency ω, where A_{22} is a constant. $R(t) \equiv (N(90°,t) - N(180°,t)) \div N(90°,t) + N(180°,t) \fallingdotseq 3 \div 4 \times A_{22} \times \cos(2\omega t)$ (1) The direction of the second γ ray changes due to the electromagnetic field acting on the nucleus. The SPIO induces the phase dispersion due to the local field fluctuation, and leading to an isotropic direction. Therefore, $R(t)$ was assumed to decay exponentially. We defined a new model as shown in Eq. 2 and performed a regression analysis. Here, D and $D2$ are assumed as regression coefficients representing the phase dispersion speed resulting from the electric quadrupole and magnetic dipole interactions, respectively. $R(t) \fallingdotseq 3 \div 4 \times A_{22} \times \cos(2\omega t) \times e^{-Dt} \times e^{-D2t}$ (2) Higher SPIO concentrations, indicating faster phase dispersion, correspond to larger observed values of $D2$ (Fig. 1). This indicates that $D2$ represents the phase dispersion speed attributed to magnetic dipole interactions. The primary focus of this study was to explore the angle between γ rays emitted by ^{111}In to obtain a parameter equivalent to T2. We expect to establish a new modality that will enable the detailed observation of the behavior of specific nuclei, extending beyond the scope of ^{1}H.

1) K. Shimazoe, M. Uenomachi, H. Takahashi, *Communications Physics*, Vol.5, No.24 (2022).

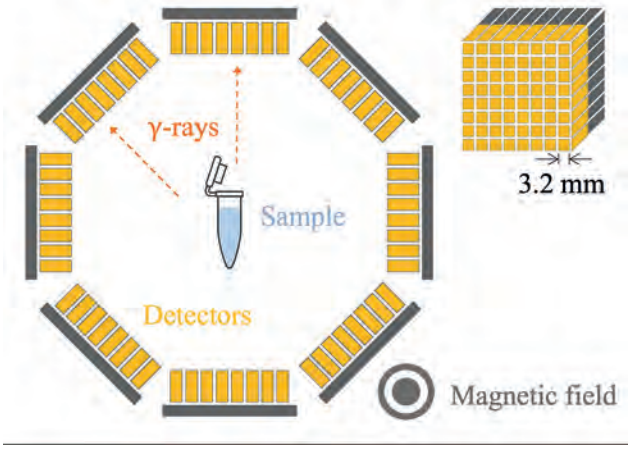

Fig. 1 γ-ray detector geometry.

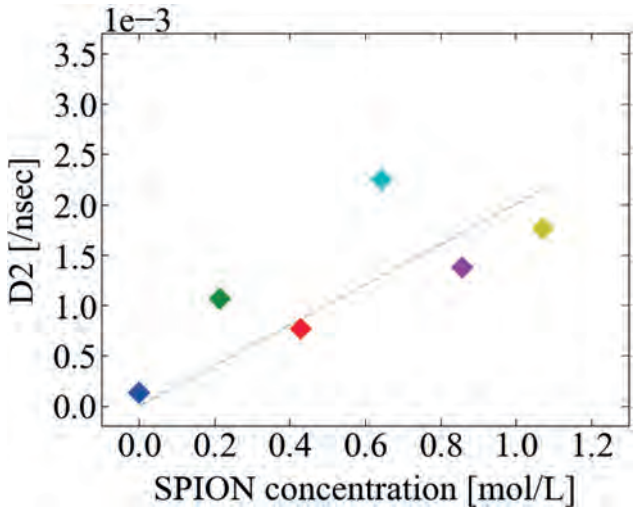

Fig. 2 Relationship between SPIO concentration and regression coefficient *D2*.

AG-04. Generation of Synthetic Magnetic Resonance Images via Bloch Simulation. *R. Ferrero*[1], M. Vicentini[1] and A. Manzin[1] *1. Istituto Nazionale di Ricerca Metrologica (INRiM), Torino, Italy*

Magnetic Resonance Imaging (MRI) is a widely diffused non-invasive diagnostic imaging technique used in clinics to acquire detailed information about the anatomy and functions of different organs, in both health and disease conditions. MRI provides excellent anatomical details due to its high soft-tissue contrast and the possibility to differentiate between several types of tissues by varying acquisition protocols. However, MRI measurements are strongly susceptible to differences in image acquisition parameters, protocols and used scanners, making complex the comparison of data obtained in large-scale trials and multi-site studies [1]. To validate the techniques adopted for analyzing the acquired images, reference data are required. These can be provided by computer-generated virtual models (digital phantoms) with known anatomy and properties, to be used as a gold standard for evaluating and improving MRI devices, image processing and reconstruction techniques [2, 3]. To this aim, we developed an MRI simulator based on the Bloch equations to produce realistic images, first, as a ground truth for signal generation and image production process and, second, as a validation tool for quantitative analysis. The solver is parallelized and developed to run on a CUDA compatible GPU-accelerated environment. The simulator enables us to compute, in a voxel-based domain representing the digital phantom, the Bloch equations, which describe the magnetization precessional motion under the effect of complex contrast-generating magnetic field sequences [4]. The exciting and encoding fields are inputted to the solver with a Python script based on the PyPulseq library [5]; the computed magnetization components are acquired at precise time intervals producing the MRI signal, from which the synthetic image is generated. The simulator is applied to study the sensitivity of image generation to magnetic field distortion and variations in T1 and T2 parameters.

[1] K. E. Keenan et al., Magn. Reson. Med., Vol. 79, p. 48–61 (2018). [2] C. Paganelli et al., Med. Phys., Vol. 45, p. 3161–3172 (2018). [3] J. Cohen-Adad et al., Magn Reson Med., Vol. 88, p. 849–859 (2022). [4] R. Kose et al., Magn. Reson. Med., Vol. 74, p. 250–257 (2020). [5] K. S. et al., J. Open Source Softw., Vol. 4, 1725 (2019).

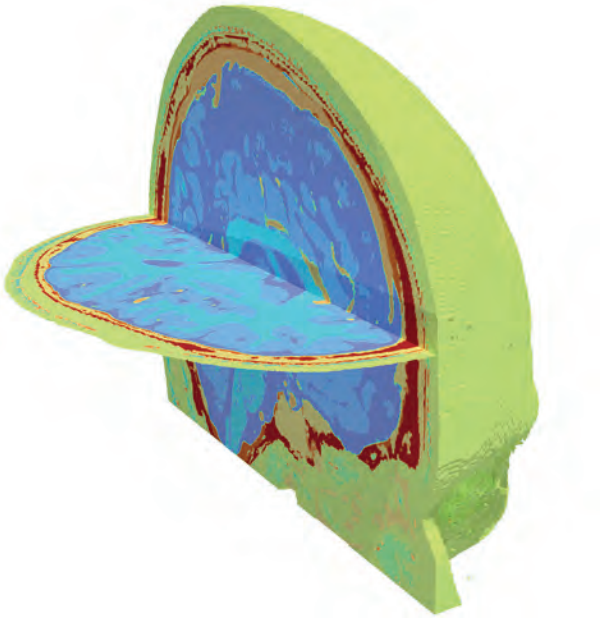

Fig. 1 Brain digital phantom with tissue segmentation in false colors. The horizontal slice corresponds to the MRI acquisition plane of Fig. 2

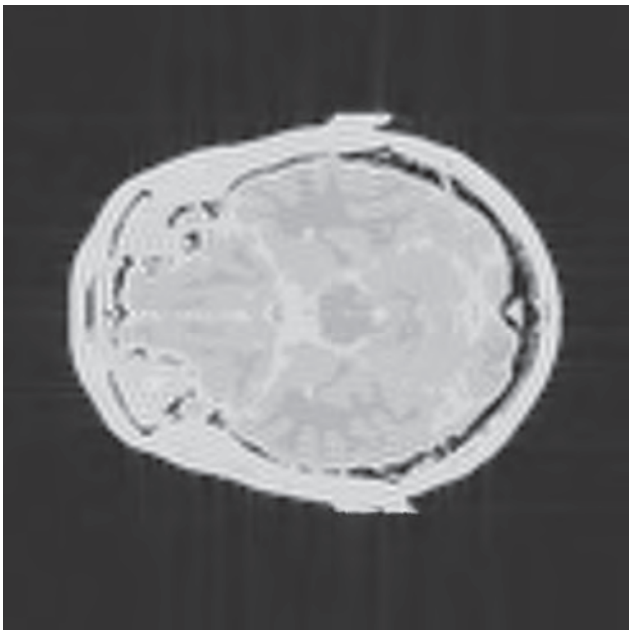

Fig. 2 Reconstructed image from simulated data of magnetization dynamics using a gradient echo sequence.

INVITED PAPER

AG-05. Magnetic Stray Field Landscapes from Engineered Domains for Full Motion Control of Magnetic Micro- and Nano Particles. *A. Ehresmann*[1] *1. Institute of Physics, Kassel University, Kassel, Germany*

Ferromagnetic and superparamagnetic micro- und nano-particles (MPs) are central functional elements in MP-based lab-on-chip devices in biotechnological applications. Key issues are (1) the full control over translatory and rotatory MP motion in their liquid environment, (2) the ability to track the full 3D trajectory of a particle, (3) eventually to quantify particle rotation and

angular orientation (in case of non spherically symmetric MPs), and (4) to carry out (1) - (3) for many particles in parallel. The combination of methods developed in recent years in Kassel addresses all of these items: Magnetic field landscapes (MFLs) emerging from magnetic domains in continuous layer systems [1] superposed by a dynamically varying external magnetic field enabled a controlled transversal MP motion along predefined tracks close to the substrate [2, 3]. Here light-ion bombardment induced magnetic patterning of in-plane exchange bias and Co/Au multilayers with perpendicular to plane magnetic anisotropies has been developed as a base technology [4] for fabrication of domains with defined geometry and remanent magnetization characteristics. As the use of this MP motion control strategy implies MP motion close to the substrate surface, MPs may be used as probes for (substrate) surface potentials and forces and for the quantification of interactions between MP and substrate surfaces mediated via the surrounding liquid. Changing interactions result in changing equilibrium distances between MP and substrate, necessitating a technology to measure the full 3D trajectories of an MP, in particular its distance to the surface. Here, a particular routine to analyze videos recorded through a standard microscope has been implemented, calibrating the sharpness of the MP image to the vertical MP coordinate with respect to the microscope's focal plane [5]. The use of MPs with non-spherically symmetric magnetic characteristics (e.g., so called Janus particles) enabled the control and optical detection of rotatory motion and particle orientation [6]. These MPs have been fabricated either by depositing magnetic layers on one side of non-magnetic spherically symmetric commercially available particles [7] or by using a combination of nanoimprint lithography and magnetic layer deposition for defined particle geometries. For self-fabricated and for commercially available particles there is a certain variation in particle size and magnetic characteristics resulting in variations of magnetophoretic mobilities. For statistically significant experiments, therefore, an automated motion characteristics analysis for many particles is mandatory. Here, machine learning routines for the video data analysis is key to success [8]. In the presentation I will discuss some aspects of the physics fundamentals behind the used technologies and some lab-on-chip functional elements, where specific functions have been realized by the design of particular magnetic domain configurations.

[1] Holzinger, Zingsem, and Koch et al., J. Appl. Phys., Vol. 114, p. 013908 (2012) [2] Ehresmann, Koch, and Holzinger, Sensors, Vol. 15, p. 28854 (2015) and references therein [3] Holzinger, Koch, and Burgard et al., ACS Nano, Vol. 9, p. 7323 (2015) [4] Mitin, Kovacs, and Schrefl et al., Nanotechnology, Vol. 29, p. 355708 (2018) and references therein [5] Huhnstock, Reginka, and Sonntag et al., Sci. Rep., Vol. 12, p. 20890 (2022) [6] Huhnstock, Reginka, and Tomita et al., Sci. Rep., Vol. 11, p. 21794 (2021) [7] Tomita, Reginka, and Huhnstock, J. Appl. Phys., Vol. 129, p. 015305 (2021) [8] Dingel, Huhnstock, and Knie et al., Comp. Phys. Comm., Vol. 262, p. 107859 (2021)

CONTRIBUTED PAPERS

AG-06. An Optimization Method of Magnetic Field Generating Magnetic Force Field for Magnetic Nanoparticles Control. *M. Fushimi*[1], H. Yoshioka[1] and M. Sekino[1] *1. The University of Tokyo, Tokyo, Japan*

Magnetically guided drug delivery systems (DDSs) are attracting attentions. Since magnetic fields are highly permeable to living organisms, it is expected to navigate magnetic nanoparticles to targets deep within the human body [1]. The magnetic force applied to a target depends on the magnetic field as well as the magnetic properties of the material, rendering their relation highly complicated. Thus, in practical situations, devices are designed to generate a desired magnetic force only at a specific point in a region [2], limiting the achievable navigation pattern. Therefore, in this study, we proposed a method to optimize the magnetic field generating the desired magnetic force distribution within a whole region of interest for a more flexible magnetic DDS. Generally, the magnetic moment of the magnetic material depends on the hysteresis of the external field. However, in the case of magnetic nanoparticles consisting of a single magnetic domain, the hysteresis property vanishes, and the magnetic moment is determined uniquely by the external field [3]. Since both the divergence and curl of the magnetic field are zero in the absence of a current source, the magnetic field as well as the magnetic force field is expanded by vector spherical harmonics [4]. We formulated the optimization problem as estimating the coefficients of the expansion by the nonlinear least-squares method [5]. The proposed method was tested by numerical simulations. The magnetic field that generates the desired magnetic force distribution shown in Fig. 2 (left) was estimated. As shown in Fig. 2 (right), a magnetic force distribution almost identical to the target was reproduced. The relative error measured in the L2 norm was 2.44 x 10^{-5}, confirming the validity of the method. The results of applying this method to a 3D problem will be presented at the conference.

[1] P. S. Williams *et al.*, *Molecular Pharmaceutics*, Vol. 6, No. 5, pp. 1290-1306 (2009) [2] H. Choi *et al.*, *Smart Materials and Structures*, Vol. 18, No. 5, p. 055007 (2009) [3] M. Kaneko *et al.*, *AIP Advances*, Vol. 8, No. 5, p. 056732 (2018) [4] A. J. Makinen *et al.*, *J. Appl. Phys.*, Vol. 128, p. 063906 (2020) [5] K. Levenberg, *Quarterly of Applied Mathematics*, Vol. 2, pp. 164-168 (1944)

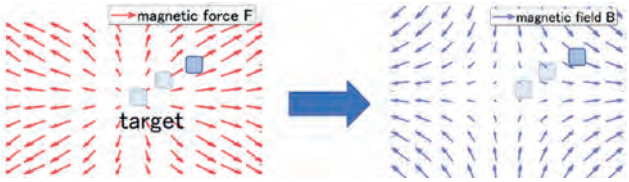

Concept of the magnetic DDS system. The magnetic field is optimized so that it generates the desired magnetic force field that can guide target magnetic nanoparticles.

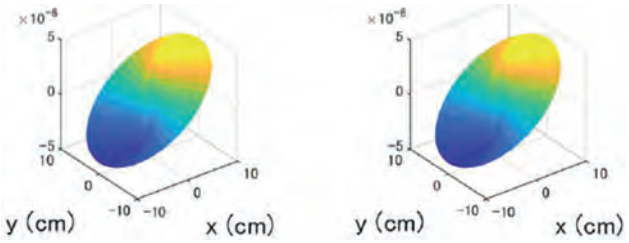

(Left) The desired magnetic force field and (Right) the magnetic force field generated by the estimated magnetic field.

AG-07. Optimization algorithm to generate robust magnetic force of the magnetic navigation system against position error of the magnetic robot. D. Lee[1], J. Kwon[1] and *G. Jang*[1] *1. Mechanical Engineering, Hanyang University, Seoul, The Republic of Korea*

Magnetic robots (MRs) have been investigated as a robotic endovascular intervention to replace conventional manual endovascular intervention [1]. Permanent magnet (PM) within wired or wireless magnetic robots interacts with an external magnetic field to generate magnetic force or torque which deliver them to a target lesion through complicated blood vessels and perform medical functions such as drilling, drug delivery, ballooning, and stenting etc. The electromagnets (EMs) of the magnetic navigation system (MNS) generate external magnetic field by applying and controlling the current to EMs. Prior researchers determined the current vector that generates the desired magnetic flux density and magnetic force at the interested position by multiplying the pseudo-inverse of the actuation matrix [2]. However, it is difficult to produce uniform magnetic gradients within the region of interest (ROI) [2]. If there is a discrepancy of the actual position of the MR within the ROI of the MNS, the unintended magnetic force may be induced, leading to loss of control of the MR. We proposed an optimization algorithm to generate robust magnetic force against position error to achieve good controllability of the MR in the ROI of the MNS as shown In Fig. 1. We mathematically formulate an objective function which minimizes

the norm of the spatial derivatives of the magnetic force. Fig. 2 shows the magnetic flux density and the magnetic force obtained by the pseudo-inverse matrix and the proposed method, respectively, to generate Bx of 3 mT and Fy of 0.3 mN at the interested position of (0, 0, 0). It shows that the magnetic flux density and magnetic force from the pseudo-inverse matrix method are very sensitive to position error. However, the proposed method generates the robust magnetic flux density and magnetic force against position error. We also performed an experiment with a MR moving in a complicated glass tube. It shows that the magnetic force generated by the proposed method can successfully navigate the MR in the complicated glass tube.

[1] B. J. Nelson, S. Gervasoni, P. W. Y. Chiu, L. Zhang and A. Zemmar, "Magnetically Actuated Medical Robots: An in vivo Perspective," in Proceedings of the IEEE, vol. 110, no. 7, pp. 1028-1037, 2022 [2] L. Yang, M. Zhang, H. Yang, Z. Yang and L. Zhang, "Hybrid Magnetic Force and Torque Actuation of Miniature Helical Robots Using Mobile Coils to Accelerate Blood Clot Removal," 2021 IEEE/RSJ IROS, pp. 7476-7482, 2021 [3] W. Lee, "Robotically adjustable magnetic navigation system and magnetic catheter robot for vascular intervention robotically adjustable magnetic navigation system and magnetic catheter robot for vascular intervention," February 2021

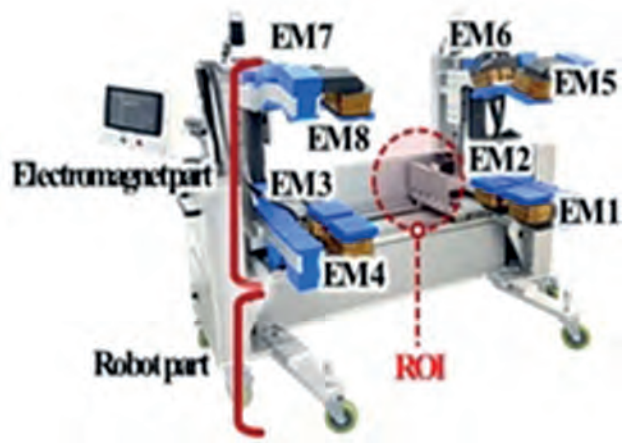

Fig. 1. EM-type MNS with eight cores

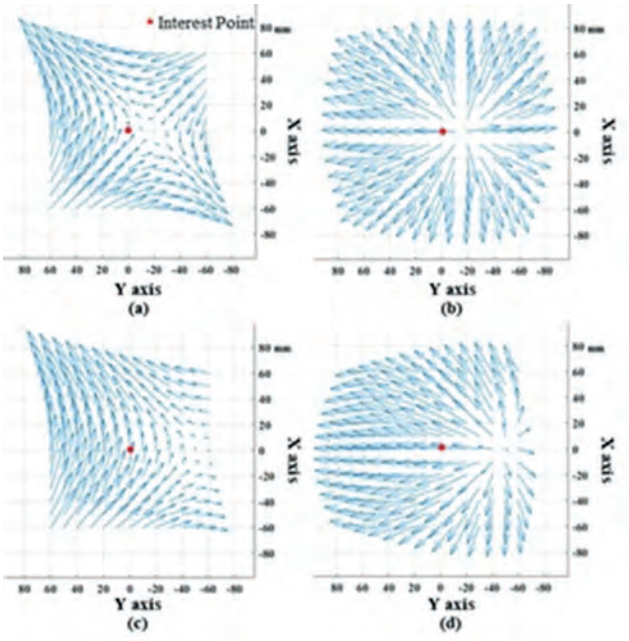

Fig. 2. Magnetic flux density and magnetic force determined by the pseudo-inverse matrix (a) (b), and by the proposed method (c) (d).

AG-08. Multifunctional effects in magnetic nanoparticles for precision medicine. G. Barrera[1], *P. Tiberto*[1] and P. Allia[1] *1. Advance Materials and Life sciences, INRIM, Torino, Italy*

The multifunctional properties of biocompatible magnetic nanoparticles pave the way to a variety of widespread applications in precision medicine and theranostics. Here, an effective combination of magnetic hyperthermia and thermometry will be shown to be implementable by using magnetic nanoparticles which behave either as a heat sources or as temperature sensors when excited at two different frequencies. Noninteracting magnetite nanoparticles are modeled as double-well systems and their magnetization is obtained by solving rate equations [1,2] in the case of Néel's relaxation of the magnetization. Two temperature sensitive properties (temperature-sensitive mean square voltage and ratio of spectral harmonics) derived from the cyclic magnetization are studied and compared for mono- and poly-disperse nanoparticles. The multifunctional effects enabling the combination of magnetic hyperthermia and thermometry are shown to depend on the interplay among nanoparticle size, intrinsic magnetic properties and driving-field frequency [3]. Figure 1a) shows, for any fixed nanoparticle diameter, how to determine in the magnetic anisotropy – frequency plane the values of ac field frequency at which the nanoparticles behave either as heaters or as temperature sensors. The selected temperature-sensitive quantities are shown in Figure 1b) where their perfect linear behavior in the temperature region of interest is highlighted. In conclusion, magnetic hyperthermia and thermometry can be effectively combined by properly tailoring the magnetic properties of nanoparticles and the driving-field frequencies. Therefore, it becomes possible to measure the temperature of a tissue in the very course of a hyperthermia treatment so that the therapy can be guided according to any specific need.

[1] P. Allia, G. Barrera, P. Tiberto, J. Magn. Magn. Mater. 496, 165927, 2020 [2] G. Barrera, P. Allia, P. Tiberto, Nanoscale 12 (11), 6360-6377, 2020 [3] G. Barrera, P. Allia, P. Tiberto, Nanoscale Advances, 2023, in press.

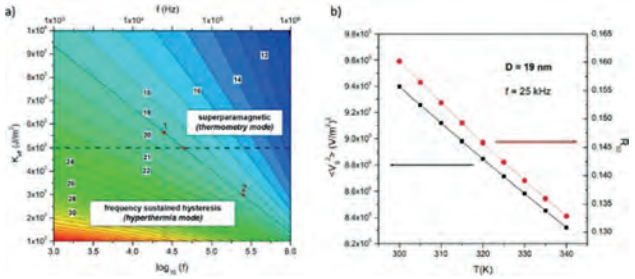

Fig. 1 a) Graphical representation in the frequency-magnetic anisotropy plane: lines are calculated as a function of nanoparticles diameter [3]; b) behaviour of the temperature-sensitive mean square voltage (black symbols and line) and of the harmonics ratio R53 (red symbols and line) for magnetite nanoparticles with D = 19 nm in the typical temperature interval of hyperthermia therapy.

AG-09. Design and Characterization of Colloidal Magnetic Nano-Objects for Thermal Magnetic Particle Imaging. *F.M. Abel*[1], M.T. Merritt[1,2], E. De Lima Correa[1], T.Q. Bui[1], A.J. Biacchi[1], M.J. Donahue[1], S.I. Woods[1], A.R. Hight Walker[1] and C. Dennis[1] *1. National Institute of Standards and Technology, Gaithersburg, MD, United States; 2. Morgan State University, Baltimore, MD, United States*

Magnetic particle imaging (MPI) is an imaging technique that utilizes the non-linear magnetic response of magnetic nano-objects (MNOs) to generate an image. If the MNOs also exhibit a change in magnetic response with temperature, then the technique lends itself to not only 3D imaging but also thermometry. Recently, ferrites having high crystal quality with oleic acid functionalization have been shown to exhibit greatly enhanced MPI signal and resolution when stimulated by AC magnetic fields with an

amplitude greater than a certain threshold [1,2]. To investigate the impact of size, solvents, stability, and surface functionalization of these types of MNOs, we have developed a one-pot colloidal synthesis method. MNOs with sizes between approximately 12 nm to 25 nm have been produced and physically characterized by X-ray diffraction, Raman spectroscopy, electron microscopy, and dynamic light scattering. Drive field amplitude dependent magnetic particle spectroscopy (MPS) measurements reveal a threshold behavior for the larger particles (20 nm and 25 nm) Fig. 1, in which a significant increase in signal and square-like AC hysteresis is observed. This is likely due to strong interactions between the MNOs that lead to chain formation, and its associated colloidal magnetic anisotropy [3], becoming energetically favorable at the threshold AC magnetic field amplitude. Surface functionalization was explored exchanging oleic acid (short ligand) for carboxylic acid terminated polystyrene (long ligand), both soluble in toluene. Additionally, an approach using a micelle to encapsulate the particles to make them soluble in water was used. In both cases the signal was reduced showing a nearly identical MPS response likely due to encapsulation of single or multiple particles into a larger molecular structure. The results suggest that a minimum critical particle size is required for the strong interactions to occur, and the length of the surface functionalizing molecules plays a role in the interactions. Finally, the temperature dependent MPS (278 K to 313 K) for the 20 nm oleic acid capped particles suggest that these MNOs are highly promising for near room temperature thermometry.

[1] Z. W. Tay et al. Small Methods., Vol. 5, p. 2100796 (2021) [2] K. L. Fung et al. Nano Lett., Vol. 23, p. 1717 (2023) [3] C. D. Dennis et al. Nanotechnology., Vol. 29, p. 215705 (2018)

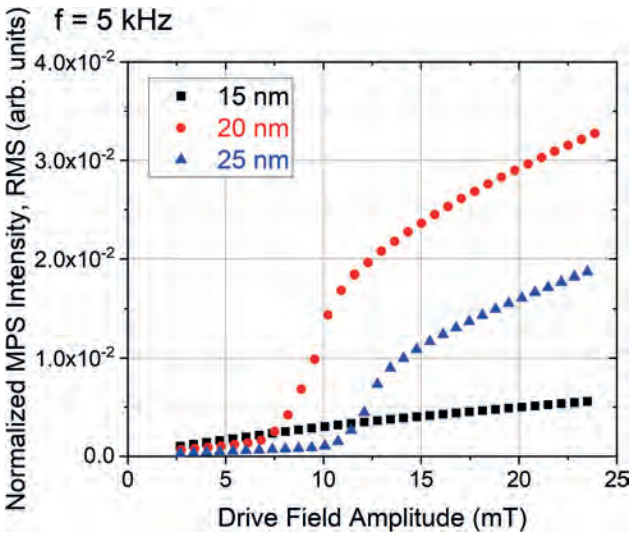

Fig. 1 Drive field dependent MPS measurements.

AG-10. Impact of Surface Stabilization on Colloidal and Magnetic Structure of Nanoflowers. J.A. Borchers[1], K. Krycka[1], B. dos Santos Correa[1], A. Sharma[2], E. Correa[1], Y. Dang[1], M.J. Donahue[1], C. Gruettner[3], R. Ivkov[2] and *C. Dennis[1] 1. NIST, Gaithersburg, MD, United States; 2. Johns Hopkins University School of Medicine, Baltimore, MD, United States; 3. Micromod Partikeltechnologie, GmbH, Rostock, Germany*

Functionalized magnetic nanoparticles (MNPs) have demonstrated utility in many research and commercial applications, especially biomedical applications such as magnetic nanoparticle hyperthermia (MNPH) and magnetic particle imaging (MPI). Here, we focus on correlating the physical, colloidal, and magnetic structure, static and dynamic magnetization, and heating performance of Synomag nanoflower MNPs, developed for both MNPH and MPI, with different surface stabilizations. The Synomag nanoflowers are comprised of iron oxide grains. To determine the relationship between their structure and function, we characterized the nanoflower MNPs using transmission electron microscopy, X-ray diffraction, dynamic light scattering, AC susceptibility, polarization analyzed small angle neutron scattering, specific loss power measurements, and magnetic particle spectroscopy, as well as magnetization versus field (M vs. H) and temperature (M vs. T) measurements. We performed similar measurements on coated and uncoated nanoflower MNPs comprised of cobalt ferrite grains to ascertain whether observed trends are enhanced by increasing the magnetic moment and/or magnetocrystalline anisotropy. Our comprehensive analysis reveals the influence of coating on the shape and size of the flux-closed clusters and chains of nanoflowers that develop in response to exposure to a static magnetic field of varying magnitude. Overall, uncoated nanoflowers form multi-dipole-like clusters and looser chains where the degree of multi-pole depends on the magnetic moment. In contrast, the coated nanoflowers form dipoles then branching chains of dipoles in increasing magnetic field. Our analysis details the important relationship between surface stabilization, magnetic moment, intra- and inter-particle structure, and function of these complex MNP systems and is being correlated with their performance.

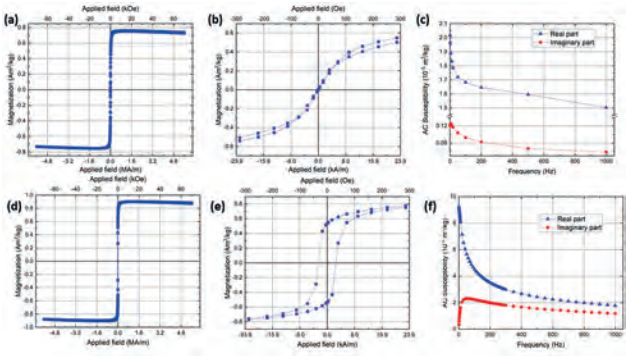

Fig 1 - Magnetization as a function of field at room temperature for the Synomag 50 nm (a) and Synomag-D 70 nm (d) samples with expanded view of the low field region in (b) and (e), respectively. The real and imaginary parts of the AC susceptibility are plotted as a function of frequency in (c) for the Synomag 50 nm and in (f) for the Synomag-D 70 nm.

AG-11. A mechanical model for teaching the Stoner-Wohlfarth model to undergraduate students. *V. Franco*[1], Á. Quintero-Suárez[1] and J. Law[1] *1. University of Seville, Seville, Spain*

The Stoner-Wohlfarth model [1] is the most natural way to connect the magnitudes of magnetic anisotropy and coercivity in an introductory undergraduate course. It shows that the interplay between Zeeman energy and the anisotropy energy gives rise to hysteresis. When this model is presented to undergraduate students, their main difficulty is to understand the influence of the applied field on the energy landscape. To solve this issue, there are several alternatives, like making different projections of the energy landscape as 2D views on the computer screen, but students tend to miss the connection between the presented 2D curve and how the projection would change with the magnetic field. Alternatively, a 3D plot of the whole energy surface can be made. While this option is suitable for grasping the most salient features, like the existence of one or two minima as a function of the orientation of magnetization, it is not ideal for identifying the fields at which the irreversible rotation of magnetization takes place. Computer programs can also be developed (Fig. 1), to make students interact with the model for different orientations of the applied field with respect to the easy axis [2], but this option is only suitable for individual work of the students in front of a computer, for lab work, but not for a general lecture. As a complement to the classroom, we have developed a mechanical model that represents the energy landscape of a single domain particle under an applied field (Fig. 2). The energy surface is built from 2D layers that represent the energy curve for given values of the field. These layers can be shown individually to the audience, making an evident connection between the value of the field and the position of that curve in the complete energy landscape. In combination with a small sphere, a slider in the 3D device allows one to follow the change

in the orientation of magnetization (minimum energy) with changing fields and clearly shows reversible and irreversible rotations of magnetization. The construction of this device is made by laser cutting and 3D printing.

[1] E. C. Stoner, E. P. Wohlfarth, A mechanism of magnetic hysteresis in heterogeneous alloys. *Philos. Trans. R. Soc. Lond. Ser. A* 240(826), 599–624 (1948). [2] V. Franco, Computer simulation of the Stoner-Wohlfarth Model. Laboratory practicals. University of Seville.

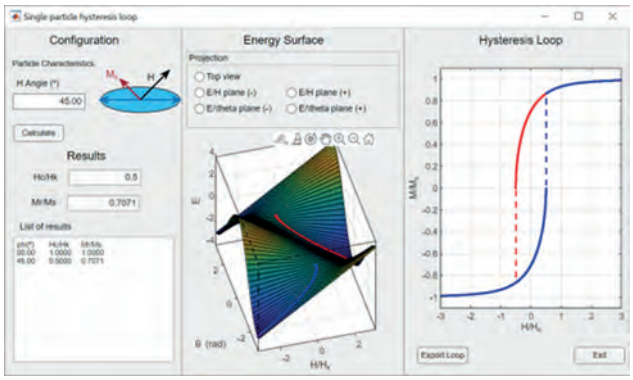

Fig. 1: Software used at the University of Seville [2].

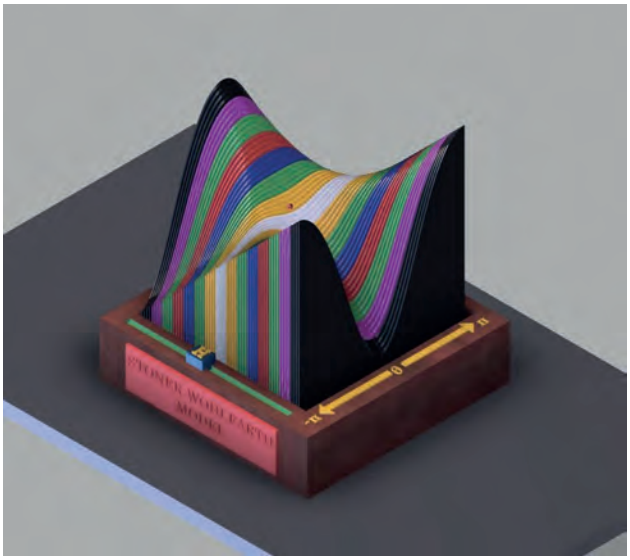

Fig. 2: Design of the mechanical model for interactive use.

AG-12. Talking about magnets – information retrieval with large language models. C. Wager[1], J. Fischbacher[2], A. Kornell[1], H.A. Moustafa[2], H. Oezelt[2], A. Kovacs[2], Q. Ali[1], M. Gusenbauer[2] and *T. Schrefl*[1]
1. Christian Doppler Laboratory for Magnet design through physics informed machine learning, University for Continuing Education Krems, Wiener Neustadt, Austria; 2. Department for Integrated Sensor Systems, University for Continuing Education Krems, Wiener Neustadt, Austria

We show how large language models can be used for data mining in the field of magnetism. Although trained with an enormous amount of text, generative pretrained transformers (GPTs) hallucinate when asked specific research questions. Open-source language models combined with semantic search overcome this problem and allow users to chat with their documents in a private and local manner. We used localGTP [1] to create an intelligent agent for magnetic materials. The presented methodology is an efficient method to explore and retrieve data from many research articles. The algorithm was tested in an exam-like evaluation on key questions on permanent magnets. Fig. 1 shows the underlying methodology. The text of pdf files is split into chunks. For each chunk, text embeddings are created and stored in a database. Likewise, the user query is encoded in a vector. By similarity search the related passages of the pdf files are identified. Finally, the large language model builds specific answers, which are based on the user provided documents. Queries may be composed of three parts: Context, question, and instruction. We collected open-source articles with the search term "permanent magnet*" AND "rare earth". In total 467 pdf files were used. We compared language models with 7, 13, and 30 billion parameters [2]. We prepared 10 exam questions for our intelligent agent and applied a marking scheme that gives negative points for wrong answers. The maximum positive points per question are 10, the minimum points per question are -4. Fig. 2 shows the exam scores. The best score is 80. It is obtained for large models and detailed queries. In addition to the answers, the algorithm presents the relevant text passages from the pdf files. If both do not match, the question is not covered in the pdf files. The financial support by the Austrian Federal Ministry of Labour and Economy, the National Foundation for Research, Technology and Development and the Christian Doppler Research Association is gratefully acknowledged.

[1] https://github.com/PromtEngineer/localGPT [2] https://github.com/melodysdreamj/WizardVicunaLM

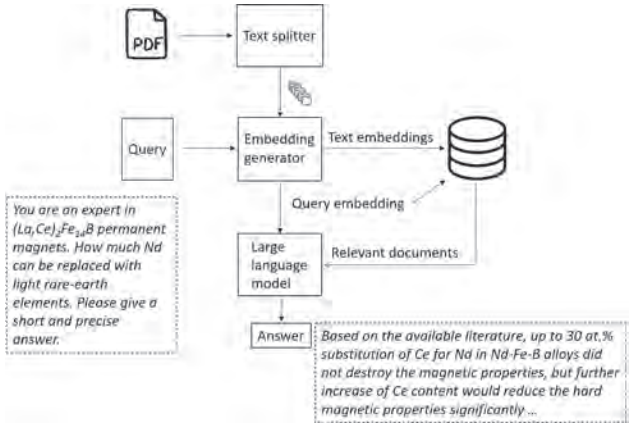

Fig. 1 Workflow for information retrieval from scientific papers.

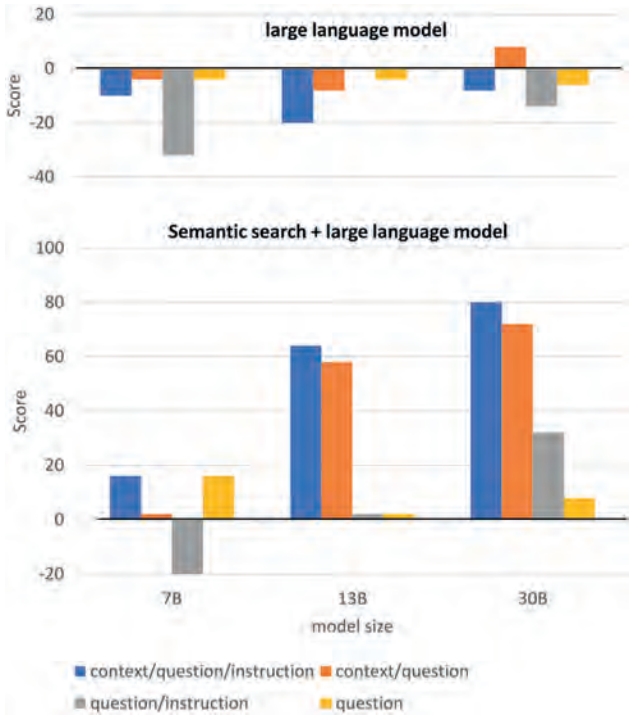

Fig. 2 Score for answering research questions. Queries were done with different degree of detail by dropping either the context, the instructions, or both.

Session AP
FUNDAMENTAL PROPERTIES II: MAGNETIC PHASE TRANSITIONS IN 2D SYSTEMS AND COMPLEX ALLOYS (Poster Session)

Lei Han, Chair
Tsinghua University, Beijing, China

AP-01. Valley polarized snake trajectories in anisotropic Weyl semimetals. *C. Yesilyurt[1] 1. Nanoelectronics Research Center, Istanbul, Turkey*

In the presence of spacially anti-symmetric out-of-plane magnetic fields, charged particles follow snake-like trajectories at the field boundary due to the coexistence of opposite-direction gauge potentials along the transport channel [1]. Previous works have shown that such configuration of gauge potentials can also be obtained with anti-symmetric pseudo-magnetic fields [2] or by applying a uniform magnetic field in the presence of a p-n junction [3]. The transport properties of snake states have been widely investigated in consideration of two-dimensional Dirac materials which generally respect crystal symmetry and exhibit isotropic energy dispersion. Here we calculate particle trajectories considering anisotropic Weyl semimetal with broken crystal symmetry and applied electrostatic potential where the barrier interface is parallel to the transport direction as illustrated in Fig. 1 (a). In the proposed model, the applied electrical potential (i.e., V0 = 2 EF, where Ef is the Fermi energy) effectively changes the carrier concentration on the half of the channel as illustrated in Fig. 1 (b) and results in Klein tunneling transport between electron and hole particles of which Fermi surfaces are shown in Fig. 1 (c). As a result, it is shown that the tilted anisotropic band structure of such materials breaks the valley degeneracy of snake state trajectories and thus two valleys with opposite chirality follow different paths with different velocities as shown in Fig. 1 (a).

[1] L. Oroszlány, P. Rakyta, and A. Kormányos et al. Phys. Rev. B 77, 081403(R), (2008) [2] L. S. Cavalcante, A. Chaves, D. R. da Costa, et al. Physical Review B, 94, 075432 (2016) [3] T. Taychatanapat, Jun You Tan, and Y. Yeo, et al. Nature Communications, 6, 6093 (2015)

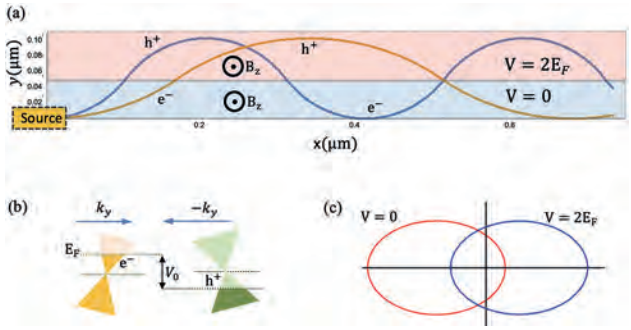

Fig. 1 The calculated valley-resolved snake state trajectories are presented in (a). The effect of applied electrical potential on the band structure and the Fermi surfaces is illustrated in (b) and (c) respectively.

AP-02. Complex magnetic ordering in $EuAl_4$ – A ^{151}Eu Mössbauer study. *D. Ryan[1], B. Kuthanazhi[2,3], N. Jo[4], B. Ueland[2,3], R.J. McQueeny[2,3], S. Riberolles[2,3], X. Wang[5] and P.C. Canfield[2,3] 1. Physics, McGill University, Montreal, QC, Canada; 2. Ames National Laboratory, Ames, IA, United States; 3. Physics and Astronomy, Iowa State University, Ames, IA, United States; 4. Physics, University of Michigan, Ann Arbor, MI, United States; 5. Neutron Scattering Division, Oak Ridge National Laboratory, Oak Ridge, TN, United States*

Whereas $EuGa_4$ exhibits simple basal-plane antiferromagnetic (AFM) ordering below T_N=16K, with the body centre moments antiparallel to the corner ones [1], $EuAl_4$ undergoes a complex sequence of changes on cooling, starting with a charge density wave (CDW) transition at 145K [2,3] and followed by no less than *four* magnetic transitions below 15K [2]. Time-of-flight Laue neutron diffraction identifed an incommensurate (δ_2,δ_2,0) magnetic structure below T_{N1} with a change to (δ_1,0,0) at T_{N3} but saw no distinct changes at either T_{N2} or T_{N4} [4]. Here we present a ^{151}Eu Mössbauer study of single-crystal $EuAl_4$ grown from excess aluminium. Fig.1 shows that the normalised spectral area (proportional to the Lamb-Mössbauer or '*f* '-factor) exhibts normal Debye behaviour (θ_D=201K), as shown by the dashed line. This suggests that the the CDW transition does not involve a significant change in the phonon spectrum at the Eu site. The spectrum at 5K shows a sharp, well-split magnetic pattern with a hyperfine field (B_{hf}) of 26.6T and an isomer shift of –10.7mm/s, values typical for divalent europium. We observe no significant changes on passing through the lowest transition (T_{N4}) but there is a marked change in the spectra at T_{N3} as the lines broarden towards the centre consistent with the development of an incommensurate modulated ordering[5]. Fig.2 shows that the higher-order harmonics become progressively weaker on further warming as the modulation becomes more closely sinusoidal. The amplitudes of the fundamental (Bk_1) and first harmonic (Bk_3) appear to pass through maxima near T_{N2} before the magnetic splitting is lost at T_{N1}. As with the earlier Laue study [4], we observe clear changes at T_{N1} and T_{N3}, the transitions with the strongest heat capacity signatures [2] and nothing at T_{N4}. The evolution of the order on warming from T_{N3} to T_{N1} appears to a progrssive rounding of the modulation as it becomes more sinusoidal in nature, with no obvious break at T_{N2}.

[1] T. Kawasaki *et al.* J. Phys. Soc. Jpn. 85, 114711 (2016) [2] Ai Nakamura *et al.* J. Phys. Soc. Jpn. 84, 124711 (2015) [3] S. Shimomura *et al.* J. Phys. Soc. Jpn. 88, 014602 (2019) [4] K. Kaneko *et al.* J. Phys. Soc. Jpn. 90, 064704 (2021) [5] P. Bonville et al. Eur. Phys. J. B 21, 349 (2001)

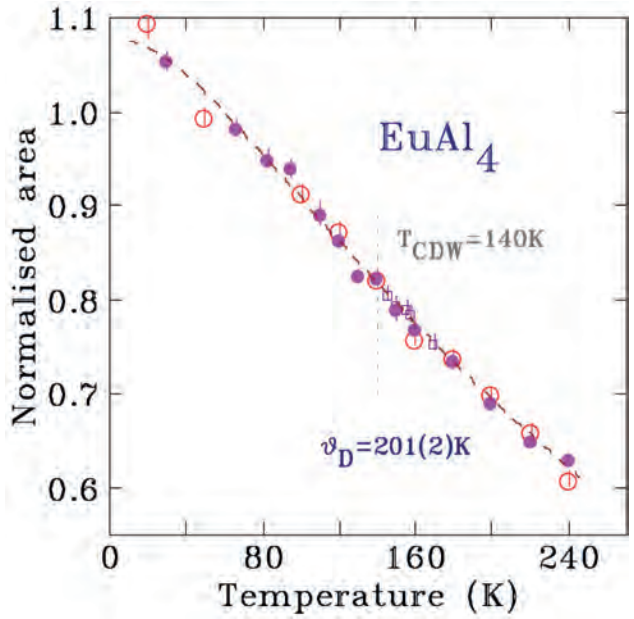

Normailsed spectral area showing normal Debye behaviour with θ_D=201K

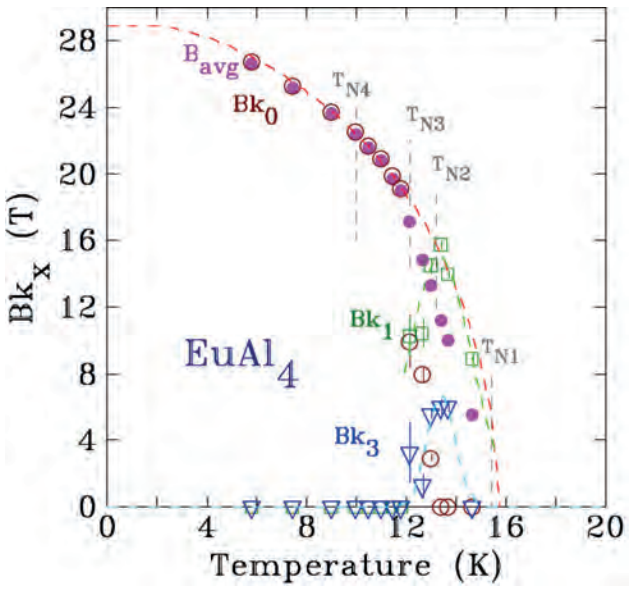

Temperature dependence of the hyperfine field components. There is a clear break at T_{N3} and the order is lost at T_{N1}. T_{N2} may mark a change in the form of the modulation as the harmonics die away on cooling.

AP-03. Twist p_z Orbital and Spin Moment of the Wavy-Graphene on $L1_0$-FePd Epitaxial Films. *H. Naganuma*[7,11], M. Uemoto[1], M. Nishijima[2], H. Adachi[1], H. Shinya[3,4], I. Mochizuki[5], M. Kobayashi[3], A. Hirata[6], B. Dlubak[9], T. Ono[1], P. Seneor[7,9], J. Robertson[8,7] and K. Amemiya[10]
1. Kobe University, Kobe, Japan; 2. The Electron Microscopy Center, Tohoku University, Sendai, Japan; 3. CSRN, The University of Tokyo, Tokyo, Japan; 4. RIEC, Tohoku University, Sendai, Japan; 5. Slow Positron Facility, KEK, Tsukuba, Japan; 6. Waseda University, Tokyo, Japan; 7. CSIS, Tohoku University, Sendai, Japan; 8. Cambridge University, Cambridge, United Kingdom; 9. CNRS/Thales, Palaiseau, France; 10. PF, KEK, Tsukuba, Japan; 11. CIES, Tohoku University, Sendai, Japan

A hexagonal graphene (Gr) and a tetragonal $L1_0$-FePd alloy heterointerface were bonded by van der Waals (vdW) forces.[1)] Interfacial perpendicular magnetic anisotropy was found at the Gr/$L1_0$-FePd interface.[2)] This study focuses on the Gr of the Gr/$L1_0$-FePd bilayer. X-ray absorption spectroscopy (XAS) of the C *K*-edge of Gr from two different angles was demonstrated. The figure shows the set-up geometry of XAS measurement. The π* orbital peak was observed not only as a glance incident (GI) angle but also as a nominal incident (NI) angle. The appearance of π* peak at NI can be considered as the formation of wavy Gr and vdW force of chemisorption-type. The densities of states (Dos) of p_x, p_y, and p_z from first-principles calculations indicated another reason for the appearance of π* peak at NI. The p_z orbital of C twists into the in-plane direction owing to its chemical bond with Fe or perturbation of the Fe ion to the C orbital. The twisted p_z orbital appears near the Fermi level. Therefore, π* peak at NI can be interpreted by three reasons: (i) the wavy Gr, (ii) the chemisorption-type of vdW force, and (iii) twisted p_z orbital near the Fermi level.[3)] The magnetic property of wavy Gr was evaluated by X-ray magnetic circular dichroism (XMCD) using the C *K*-edge. First-principles calculations interpreted that wavy Gr on $L1_0$-FePd has a spin magnetic moment of 0.018 m_B/C atoms but no orbital magnetic moment. The author (HN) acknowledges JSPS Core-to-Core Program (No. JPJSCCA20230005), QST-Tohoku University matching foundation, KAKENHI (No. 23H03803), PF Program (KA, HN.) (No. 2019S2-003), MEXT as a "Program for Promoting Researches on the Supercomputer Fugaku" (MU, TO) (No. JPMXP1020200205), RIKEN Center for Computational Science (No. hp200122/hp150273), and (HN, MK, SH) Spin-RNJ.

1) H. Naganuma *et al*, ACS Nano, 16, 4139 (2022). 2) H. Naganuma *et al*, Appl. Phys. Lett., 116, 173101 (2020). 3) H. Naganuma et al, The Journal of Physical Chemistry C (2023) *in press*.

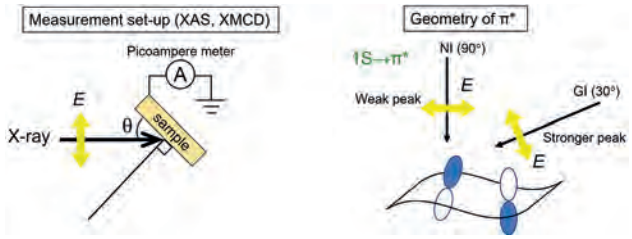

Setup geometry of the directionality of the XAS and XMCD

AP-04. Impurity effect on magnetic and thermal properties of *S*=3/2 spin gap system $Ba_3Ca(Ru_{1-x}Nb_x)_2O_9$. *Y. Ochiai*[2], I. Terasaki[1] and Y. Yasui[2]
1. Physics, Nagoya university, Nagoya, Japan; 2. Physics, Meiji university, Kanagawa, Japan

$Ba_3MRu_2O_9$ (M=Co, Zn, Ca, *etc*.) have the Ru_2O_9 dimers, made from face-shared RuO_6 octahedra, connected with corner-shared MO_6 octahedra to form triangular lattice in the *ab*-plane. $Ba_3MRu_2O_9$ exhibits various magnetic properties depending on the species of M^{2+} ions. In the case of M=Ca, it exhibits a non-magnetic state at low temperatures. The mechanism of the non-magnetic state in $Ba_3CaRu_2O_9$ was proposed that the *S*=3/2 spins of two Ru^{5+} ($4d^3$) ions become a dimer state through quantum mechanical singlet formation [1]. The phenomenon of two *S*=1/2 spins forming a nonmagnetic singlet state was reported in many materials such as Cu^{2+} ($3d^9$)

and V^{4+} ($3d^1$) compounds. On the other hand, the nonmagnetic singlet formation by two S=3/2 spins was reported in only two cases including this compound, making it a highly unusual phenomenon of interest [2]. In this study, we have investigated the magnetic and thermal properties of $Ba_3Ca(Ru_{1-x}Nb_x)_2O_9$, where the Ru^{5+} spins are partially substituted by the non-magnetic Nb^{5+} ions. From simple thinking, if one of the Ru^{5+}-dimers is replaced by Nb^{5+} ion, it is expected to appear the magnetism of the remaining Ru^{5+} spin. We have investigated the magnetic behavior induced by non-magnetic impurity doping. In the experiment, polycrystalline samples of $Ba_3Ca(Ru_{1-x}Nb_x)_2O_9$ varying the Nb concentration x were synthesized, and were confirmed to be a single phase by X-ray diffraction. Temperature (T) - dependences of magnetic susceptibility (χ) and magnetic specific heat (C_{mag}) have been measured for $Ba_3Ca(Ru_{1-x}Nb_x)_2O_9$. From the $\chi - T$ curves, we observed Curie-Weiss components in the low T-region due to Ru→Nb substitution. By analyzing the data, it is found that observed magnetic components are corresponding to paramagnetic ones derived from ~60% of the number of doped Nb^{5+} ions. We have evaluated the magnetic specific heat of doped samples, and reproduced the obtained $C_{mag} - T$ curves using the S=3/2 free spin model with internal magnetic field. It is also found that the magnetic specific heat is corresponding to ~60% of the number of doped Nb^{5+} ions. We discuss the origin of these discrepancy and induced magnetism by non-magnetic impurity doping in $Ba_3CaRu_2O_9$.

[1] J. Darriet *et al*., J. Solid State Chem. 19, 213 (1976). [2] D. Nishihara *et al*., JPSJ. 90, 114706 (2021).

AP-05. Magneto band-structure effect for two-dimensional spintronic devices. *W. Zhu*[1], C. Song[1] and F. Pan[1] *1. Materials Science and Engineering, Tsinghua University, Beijing, China*

Recent discovery of two-dimensional (2D) magnets with van der Waals (vdW) gapped layered structure prospers the fundamental research of magnetism and advances the miniaturization of spintronics[1–3]. Due to the significant anisotropy of vdW lattice and resulted 2D confinement effect, their band structure is able to be effectively modulated by the spin configuration, especially the direction of magnetic moment, which is named as magneto band-structure (MB) effect[4]. The MB effect leads to the large anomalous Hall effect in 2D vdW metal Fe_3GeTe_2[5] and the transition between indirect and direct band gap in semiconductor CrI_3[6], which shows potential for the high-performance spintronic devices based on 2D vdW magnets. Here, we report a significant magnetoresistance effect resulted by the MB effect in $Cr_2Ge_2Te_6$ thin flakes. The significant anisotropic lattice constructed by the interlayer vdW force and intralayer covalent bond induces anisotropic spin-orbit field, resulting in the spin orientation-dependent band splitting. Consequently, giant variation of resistance is induced between the magnetization aligned along in-plane and out-of-plane directions. Based on this, a colossal MR beyond 1000% was furtherly realized in lateral nonlocal devices with $Cr_2Ge_2Te_6$ acting as a magneto switch. Our finding provides a unique feature for the vdW magnets and would advance their applications in spintronics.

1. C. Gong, X. Zhang, Science, 363, eaav4450 (2019) 2. X. Lin, W. Yang and K. L. Wang, Nat. Electron., 2, 274 (2019) 3. H. Li, S. Ruan and Y. J. Zeng, Adv. Mater., 31, 1900065 (2019) 4. Z. Liao, P. Jiang and Z. Zhong, npj Quantum Mater., 5, 30 (2020) 5. K. Kim, J. Seo and E. Lee, Nat. Mater., 17, 794 (2018) 6. P. Jiang, L. Li and Z. Liao, Nano Lett., 18, 3844 (2018)

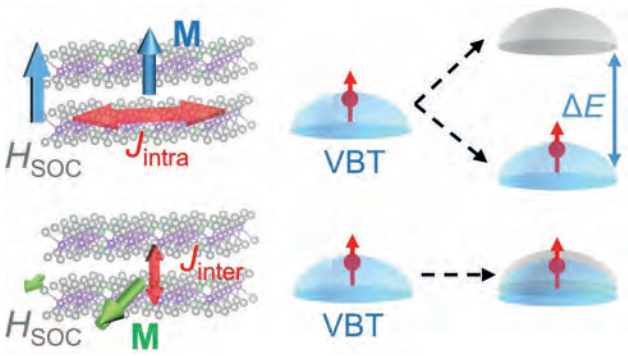

Fig. 1 Schematic of the band splitting induced by the interaction between the anisotropic crystalline field and the magnetization. The top of valance bands (VBT) occupied by spin majority and minority are colored in blue and grey, respectively.

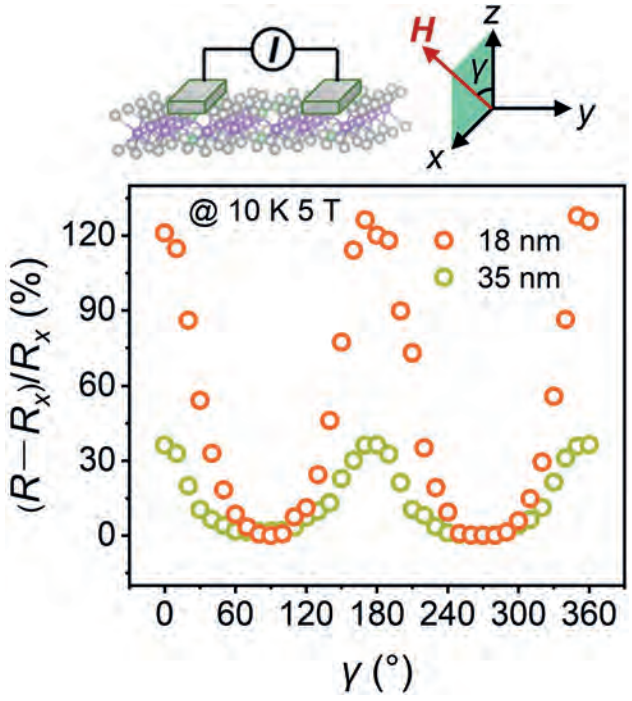

Fig. 2 Magnetoresistance effect induced by giant MB effect. The insets show the schematic and the definition of azimuthal angles and directions of the measurement.

AP-06. Exploring the critical behavior of the anomalous spin-glass transition in $Ga_{1-x}Mn_xS$. *T.M. Pekarek*[1], J.H. Blackburn[1], I. Miotkowski[2] and A.K. Ramdas[2] *1. Physics, Univ. of N. Florida, Jacksonville, FL, United States; 2. Physics, Purdue, W. Lafayette, IN, United States*

Single-crystalline $Ga_{1-x}Mn_xS$ is a quasi-two-dimensional system that exhibits an anomalous spin-glass transition temperature compared with the other well-known spin-glass systems. In contrast to the other known spin-glasses that all have three-dimensional structures, our host chalcogenide GaS system is quasi-two-dimensional. GaS has covalently bonded four-atom thick layers of the form (S-Ga-Ga-S) where the Mn ions substitutionally replace the Ga ions in the lattice. These 2-D layers are connected by van der Waals interactions between layers. Recent interest in utilizing spin-glass materials for applications in short-term, low-energy memory and processing power make this new 2-D system important for further exploration. We report on the critical behavior of the anomalous spin-glass transition in a single-crystalline $Ga_{0.91}Mn_{0.09}S$ system. Using the scaling equation of state describing the spin-glass transition in $Ga_{1-x}Mn_xS$, we obtained the relation $\chi_{nl} = C_1 H^{(2/\delta)}$ and

extract the value δ = 5.5 +/- 0.5 for this critical exponent. We find this value of delta for the critical temperature T_c = 11.2 K, combined with the other critical exponents γ = 4.0 and β = 0.8 form a self-consistent description of the spin-glass transition in this unusual 2-D spin-glass system. Interestingly, these results represent convincing evidence that, despite $Ga_{1-x}Mn_xS$ having a quasi-two-dimensional structure, $Ga_{1-x}Mn_xS$ undergoes a true spin-glass transition and is related to the class of semiconducting spin-glass materials with short-range interactions. The spin-glass transition in $Ga_{1-x}Mn_xS$ is characterized by critical exponents similar to the three-dimensional spin-glass systems and is therefore an excellent candidate for device applications. *This research was supported by UNF's Terry Presidential Professorship, the UNF Office of Undergraduate Research, a Purdue Univ. Academic Reinvestment Program, and by the National Science Foundation (NSF) Grants No. DMR-16-26332 and DMR-14-29428.

AP-07. Electronic, magnetic, and structural properties of MnCrNbAl and MnCrTaAl. *B. Schmidt*[1], P. Shand[1], P. Kharel[2] and P. Lukashev[1]
1. Physics, University of Northern Iowa, Cedar Falls, IA, United States; 2. Physics, South Dakota State University, Brookings, SD, United States

We present results of a computational study of electronic, magnetic, and structural properties of MnCrNbAl and MnCrTaAl, quaternary Heusler alloys exhibiting spin-gapless semiconducting properties. Our calculations indicate that these materials may crystallize in regular Heusler cubic structure, which has a significantly lower energy than the inverted Heusler cubic phase. The higher energy inverted phase is non-magnetic, while the lower energy regular phase is ferrimagnetic. The ferrimagnetic nature of the regular phase is due to a relatively small magnetic moment of Nb / Ta that is anti-aligned with the magnetic moments of Mn and Cr. Both MnCrNbAl and MnCrTaAl exhibit nearly spin-gapless semiconducting electronic structure at the ground state and retain their 100% spin-polarization at the larger than equilibrium lattice parameters. At the same time, the compressive strain (smaller lattice constants) have detrimental impact on spin-gapless semiconducting properties. Thus, both materials may be useful for practical spintronic applications, yet one should avoid using them in systems that may result in a compressive strain, as this may reduce their spin-polarization. We hope that these results will stimulate experimental efforts to synthesize these materials. Acknowledgments This research is supported by the *National Science Foundation* (NSF) under Grant Numbers 2003828 and 2003856 via DMR and EPSCoR.

AP-08. Theoretical understanding of magnetic phase transition in magnetocaloric $Er_{2-x}Yb_xIn$ compound. *R.K. Chouhan*[1], A. Biswas[1], A. Thayer[2] and Y. Mudryk[1] *1. Ames National Laboratory, US Department of Energy, Ames, IA, United States; 2. Blue Origin, LLC, Kent, WA, United States*

R_2In (R= rare-earth) compounds attract considerable research interests owing to their impressive magnetocaloric properties.[1-3] Namely, compounds with R = Pr, Nd, Eu exhibit large cryogenic magnetocaloric effect (MCE) due to anhysteretic magnetoelastic transformations at their corresponding T_C. Mixed rare-earth compounds present practical interest due to possibility of precise tuning of the MCE. Further, it remains unknown if the Ni_2In-type to Co_2Si-type transformation can be induced in rare earth alloys by external stimuli and/or chemical substitution. Thus, present work focuses on a series of titled pseudo-binary alloy with x varying between 0 and 2. The experimental study shows the change in room-temperature crystal structure from Ni_2In-type (Er_2In) to Co_2Si-type (Yb_2In) for x >= 1.5. The Er-rich samples exhibit second-order phase transition from paramagnetic to ferromagnetic state, which gradually disappears with the increase of x. We used density functional theory with the full potential linearized augmented plane wave method as implemented in WIEN2k, along with the localized treatment of 4f states using the Hubbard U approach. We utilized the spin-orbit coupling effect within the DFT calculations to understand the site specific contributions to the electronic structure of the alloys and their impact on ground state properties. Magnetic moment of Er was determined using the SOC calculation with the orbital moment contribution of 2.59 μ_B in addition to the 2.33 μ_B spin moment. Total energy calculation confirms the Ni_2In-type structure to be most stable at x=1 concentration by 8.5 meV as compared to the Co_2Si-type structure and suggests that the most favorable sites for Er and Yb are 2a and 2d, respectively. Our theoretical study also helps to understand the interesting experimentally observed magnetic properties of this series of compounds. This work was performed at Ames National Laboratory and supported by the Division of Materials Science and Engineering of the Office of Basic Energy Sciences, Office of Science of the U. S. Department of Energy (DOE). Ames National Laboratory is operated for the U.S. DOE by Iowa State University of Science and Technology under Contract No. DE-AC02-07CH11358.

1. F. Guillou, A. K. Pathak, D. Paudyal, Y. Mudryk, F. Wilhelm, A. Rogalev, and V. K. Pecharsky, Nature Communications 9, 2925 (2018). 2. A. Biswas, N. A. Zarkevich, A. K. Pathak, O. Dolotko, I. Z. Hlova, A. V. Smirnov, Y. Mudryk, D. D. Johnson, and V. K. Pecharsky, Physical Review B 101, 224402 (2020). 3. A. Biswas, R. K. Chouhan, A. Thayer, Y. Mudryk, I. Z. Hlova, O. Dolotko, and V. K. Pecharsky, Physical Review Materials 6, 114406 (2022). 4. W. Liu, F. Scheibel, T. Gottschall, E. Bykov, I. Dirba, K. Skokov, and O. Gutfleisch, Applied Physics Letters 119, 022408 (2021). 5. W. Cui, G. Yao, S. Sun, Q. Wang, J. Zhu, and S. Yang, Journal of Materials Science & Technology 101, 80 (2022).

AP-09. Magnetic fied-induced narrow first-order and metamagnetic phase transitions of Nd_5Ge_3: Magnetization, muon spin relaxation and neutron diffraction study. S. Samatham[1], *V. Yenugonda*[2], B. Gowrinaidu[3], P. Manuel[4], D. Khalyavin[4], S. Cottrell[4], A. Hillier[4] and K. Suresh[5]
1. Department of Physics, Chaitanya Bharathi Institute of Technology, Hyderabad, India; 2. Department of Physics, Indian Institute of Technology Kanpur, Kanpur, India; 3. Department of Physics, Government College Rajahmundry, Rajamahendravaram, India; 4. Rutherford Appleton Laboratory, ISIS Neutron and Muon Source, Oxfordshire, United Kingdom; 5. Department of Physics, Indian Institute of Technology Bombay, Powai, India

We investigate the magnetic nature of a hexagonal structured Nd_5Ge_3 using magnetization, muon spin relaxation and neutron diffraction measurements. A field dependent thermomagnetic irreversibility distinguishes the magnetic glass (MG) and reentrant spin glass (RSG) states at low temperatures. In zero field, the alloy undergoes a weak first-order magnetic phase transition from antiferromagnetic (AFM) to MG state, which ceases in H>10 kOe. Further, a transition from ferromagnetic (FM) to RSG persists up to about 50 kOe and above which a continuous transition from paramagnetic to FM state is reported. Phase diagram (*H-T*) identifies two regions; AFM + MG in low fields and FM + RSG states in high fields. The temperature dependent-magnetization, muon depolarization rate (λ), initial asymmetry (A_0) and the stretched exponent (β) show a clear anomaly at the Néel temperature and a low-T glassy state. From the neutron diffraction analysis, a field-driven metamagnetic transition (AFM to FM) is confirmed and the magnetic structure of FM state is presented [1-5]. This work was performed at the IIT Bombay and ISIS Neutron and Muon Sources, supported by Newton-India fund (Expt. RB No: 1610200) and DST-India and JNCASR-Bangalore (Expt. RB No: 1768039).

[1] T. Tsutaoka, A. Tanaka, Y. Narumi, M. Iwaki and K. Kindo, Physica B, 2010, 405, 180 – 185. [2] P. Schobinger-Papamontellos and K. Buschow, J. Magn. Magn. Mater., 1985, 49, 349 – 356. [3] B. Maji, K. G. Suresh and A. K. Nigam, Europhys. Lett., 2010, 91, 37007. [4] B. Maji, K. G. Suresh and A. K. Nigam, J. Phys.: Condens. Matter, 2011, 23, 506002. [5] Samatham et al., *Present work* (unpublished).

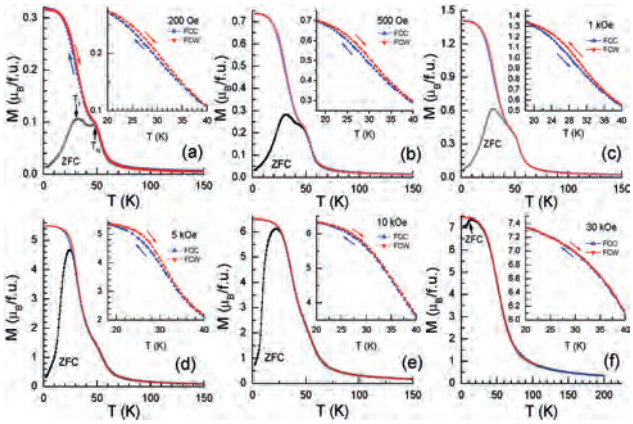

Fig. 1 (a) M-T data. Inset: The enlarged view of FCC and FCW magnetization curves, shows a narrow thermal hysteresis. (a-f) M-T in representative magnetic fields. T_N gets smeared out in fields while ZFC-M(T_t) is enhanced as H increases. FCC and FCW curves saturate below 15 K. Insets: Zoomed view of FCC and FCW. Above 15 K and below 40 K, a narrow but distinct thermal hysteresis of FCC/FCW is noticed up to a field of about 10 kOe.

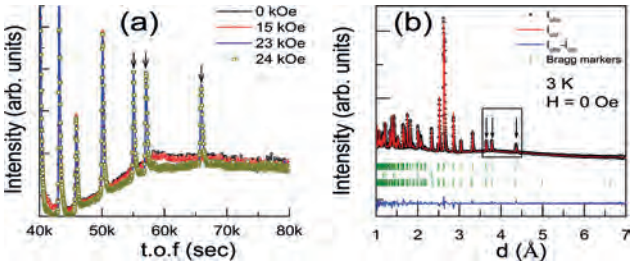

Fig. 2 (a) Neutron diffraction patterns at 3 K. The emergent magnetic peaks are marked by arrows. (b) Refined diffraction pattern at 3 K, after magnetic field is made zero from 60 kOe. The first and third rows indicate the positions of magnetic and nuclear reflections, while the second one describes the positions of reflections originating from Al. The magnetic peaks are indicated by arrows enclosed in a box.

AP-10. Superconducting exchange coupling with Vanadium interlayer.
S. Bhakat[1] and A. Pal[1] *1. Metallurgical Engineering and Materials Science, Indian Institute of Technology Bombay, Mumbai, India*

When a Superconductor(S), is sandwiched between two Ferromagnets (F), novel spin dependent phenomena arise at S/F interfaces, which is reflected through magnetotransport properties. Heterostructures of the kind - F/S/F constitute superconducting spin valves (SSVs), in which, the superconducting transition temperature (Tc) can be modified by controlling the relative orientation of the F layers. However, under certain conditions, by using Ferromagnetic Insulators (FI) in FI/S/FI′ type SSVs, one can observe the reverse phenomena - that of S controlling the relative orientation of FI layers. This phenomenon was theoretically predicted by de Gennes [1] in 1966 but has been experimentally observed recently in 2016 [2] with GdN as FI and Nb being the superconducting material. We demonstrated superconducting Vanadium(V) based SSV GdN(5nm)/V(xnm)/GdN(3nm) which shows two resistive states based on the relative orientation of the two GdN parallel or antiparallel to each other, and therefore can be used as a memory device.

[1].P.G. De Gennes. Coupling between ferromagnets through a superconducting layer. Physics Letters, 23(1):10 – 11, (1966). [2].Yi Zhu, Avradeep Pal, Mark G Blamire, and Zoe H Barber. Superconducting exchange Coupling between ferromagnets. Nature materials, 16(2):195–199, (2017).

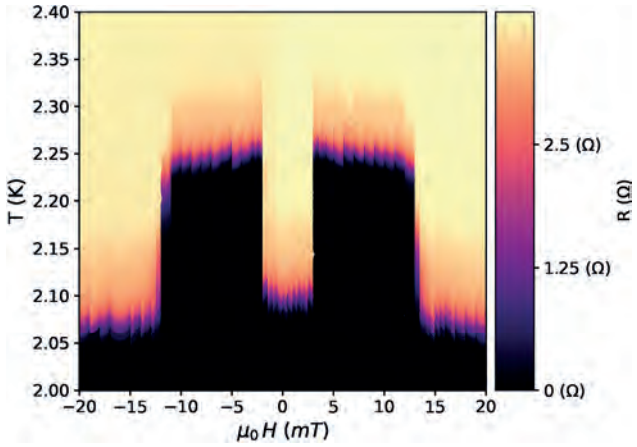

Fig.1 RT heat colormap of GdN(5 nm)/V(11 nm)/GdN(3 nm) from field range +20 mT to -20 mT and -20 mT to +20 mT.

AP-11. Withdrawn

AP-12. Study of Path Dependent Magnetic States in $CoS_{2-x}Se_x$ (x =0.24, 0.26, 0.28).
S. Karmakar[1], R. Joshi[1], K. Kumar[1] and R. Rawat[1] *1. UGC-DAE Consortium for Scientific Research, Indore, India*

The tuning of transition to near 0 K can lead to emergent magnetic states e.g. the emergence of superconductivity, non-fermi liquid behavior on driving a second-order transition to near 0 K, etc. In the case of first-order transitions, kinetics dominates the transformation leading to kinetically-arrested glass-like magnetic states [1]. Generally, such states have been reported for an order-order transition e.g. antiferromagnetic (AF) to ferrimagnetic transition in doped Mn_2Sb [2], AF to FM transition in FeRh [3,4] etc. The only exception to this generality is Se doped CoS_2 system ($CoS_{1.76}Se_{0.24}$) where it was observed for a PM to FM transition [5]. However, there is no other report on this aspect in this system. We investigated the composition dependence of kinetic arrest in $CoS_{2-x}Se_x$. The field-cooled cooling (fcc) and field-cooled warming (fcw) magnetization data in the figure show a broad first-order PM-FM transition. On the other hand, zero-field cooled warming (zfcw) data shows an increase in magnetization with the increase in temperature at low temperatures. It then merges to fcw curve and shows an FM to PM transition at higher temperatures. The low-temperature rise can be attributed to the transformation of the kinetically arrested PM state to the FM state. It was verified by systematic path-dependent magnetization measurements, which showed that the devitrification field increases with an increase in x.

1. S. B. Roy, P. Chaddah, V. K. Percharsky, K.A. Gschneidner Jr., Acta Mater., 56, 5895 (2008). 2. P. Kushwaha, R. Rawat, and P. Chaddah, Journal of Physics: Condensed Matter, 20(2), 022204 (2007). 3. P. Kushwaha, A. Lakhani, R. Rawat, P. Chaddah, Phys. Rev. B, 80, 174413 (2009). 4. P. Saha and R. Rawat, Appl. Phys. Lett., 112, 192409 (2018). 5. S.K. Mishra, and R. Rawat, Solid State Commun., 244, 33 (2016).

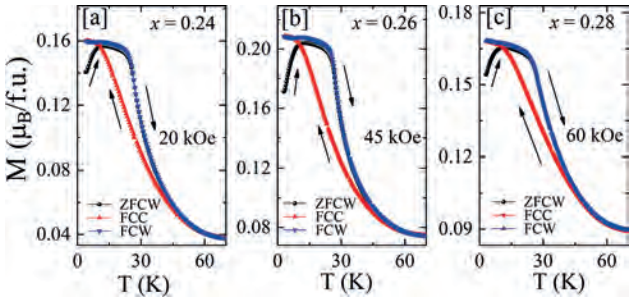

Temperature dependence of magnetization measured under labeled magnetic field during zero field cooled warming (zfcw), field cooled cooling (fcc), and field cooled warming (fcw) of $CoS_{2-x}Se_x$

Session AQ
HARD MAGNETIC MATERIALS I
(Poster Session)

Thomas Schrefl, Chair
Danube University Krems, Wiener Neustadt, Austria

AQ-01. Hard magnetic properties of $Fe_{16}N_2$ magnets. *T. Saito*[2] and H. Yamamoto[1] *1. Neoji-Consul, Kyoto, Japan; 2. Chiba Institute of Technology, Narashino, Japan*

Nd-Fe-B magnets are applied to various advanced electromagnetic devices, including hard disk drives, electric vehicles, and medical equipment [1]. The continuously growing demand for Nd-Fe-B magnets has raised concerns over their price and country risk of rare earth elements [2]. These severe concerns have led to the study of a new alternative magnet composed of no rare-earth elements. Recently, a new production technique for the $Fe_{16}N_2$ powder has been developed, and the newly-developed $Fe_{16}N_2$ powder is available [3]. This study's particular interest is whether this $Fe_{16}N_2$ powder can be utilized for the actual permanent magnets. The structures and magnetic properties of this $Fe_{16}N_2$ powder, with and without annealing, are characterized. The structure of the powder was examined by X-ray diffraction (XRD). The thermal property of the powder was measured using a differential thermal analysis (DTA). The magnetic property of the powder was measured by a vibrating sample magnetometer (VSM). The $Fe_{16}N_2$ powder was characterized by XRD. Figure 1 shows the XRD patterns of the powder and that annealed at 573 K. In the XRD pattern of the $Fe_{16}N_2$ powder, clear diffraction peaks of the α''-$Fe_{16}N_2$ phase are observed. On the other hand, diffraction peaks of the a-Fe and Fe_4N phases are found in the XRD pattern of the annealed specimens. The $Fe_{16}N_2$ powder had a relatively high coercivity of 2.65 kOe, but the annealed specimen showed a small coercivity due to the decomposition of the α''-$Fe_{16}N_2$ phase into the a-Fe and Fe_4N phase.

[1] G. Bailey, N. Mancheri, and K. Van Acker, J. Sustain. Metall. 3, 611 (2017). [2] T. Dutta, K. H. Kim, M. Uchimiya, E. E. Kwon, B. H. Jeon, A. Deep, and S. T. Yun, Environ. Res. 150, 182 (2016). [3] T. Ogawa, Y. Ogata, R. Gallage, N. Kobayashi, N. Hayashi, Y. Kusano, S. Yamamoto, K. Kohara, M. Doi, M. Takano, and M. Takahashi, Appl. Phys. Express, 6, 073007 (2013).

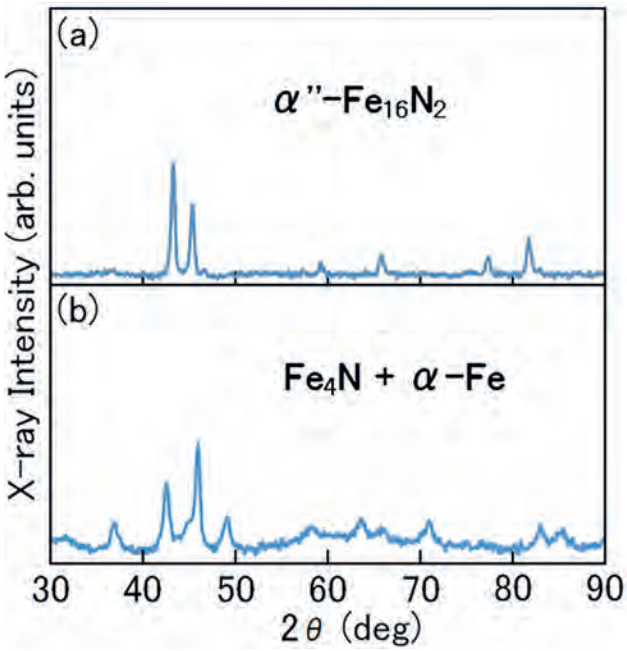

Figure 1 XRD patterns of (a) the $Fe_{16}N_2$ powder and (b) that annealed at 573 K.

AQ-02. Magnetic properties of $(Sm,Zr)(Fe,Co)_{10-x}Ti_x$ bulk magnets. *T. Saito*[1] and D. Hamane[2] *1. Chiba Institute of Technology, Narashino, Japan; 2. The University of Tokyo, Kashiwa, Japan*

Sm-Fe-N powders are usually prepared by the nitrogenation of Sm-Fe powders. However, it is known that Sm-Fe-N powders can not be processed into bulk magnets due to their poor thermal stability. It would be desirable if the magnetic properties of Sm-Fe alloys could be increased without the need for nitrogenation. In the present study, we prepared (Sm, Zr)(Fe, Co)$_{10-x}$Ti$_x$ melt-spun ribbons and subjected them to pulverization. Since the melt-spun ribbons are thermally stable, it would be possible to obtain Sm-Fe bulk magnets from them. The structures and magnetic properties of the (Sm, Zr)(Fe, Co)$_{10-x}$Ti$_x$ bulk magnets prepared by the spark plasma sintering (SPS) technique were investigated. $(Sm_{0.7}Zr_{0.3})$ $(Fe_{0.7}Co_{0.3})_{10-x}Ti_x$ (x =0-1) alloy ingots were prepared by induction melting in an argon atmosphere. The alloy ingots were induction melted and then ejected through an orifice with argon onto a copper wheel. The resultant melt-spun ribbons were comminuted into powders and then hot-pressed by the spark plasma sintering (SPS) method. The consolidation conditions were as follows: applied pressure of 100 MPa, temperatures at 873-1073 K, and duration for 300 s. The specimens were characterized using a vibrating-sample magnetometer (VSM), X-ray diffraction (XRD) using Cu-Kα radiation, and transmission electron microscopy (TEM). Figure 1 shows the hysteresis loops of the $(Sm_{0.7}Zr_{0.3})$ $(Fe_{0.7}Co_{0.3})_{10-x}Ti_x$ (x =0-1) magnets produced by the SPS method. Although the coercivity of the $(Sm_{0.7}Zr_{0.3})$ $(Fe_{0.7}Co_{0.3})_{10}$ magnet was low, the $(Sm_{0.7}Zr_{0.3})(Fe_{0.7}Co_{0.3})_9Ti$ magnet exhibited a high coercivity of 4.35 kOe. It was found that the magnetic properties of the

($Sm_{0.7}Zr_{0.3}$) ($Fe_{0.7}Co_{0.3}$)$_{10-x}Ti_x$ (x =0-1) magnets were dependent on the Ti content. The TEM studies revealed that the ($Sm_{0.7}Zr_{0.3}$)($Fe_{0.7}Co_{0.3}$)$_9$Ti magnet consisted of the fine Th_2Zn_{17}-type phase.

[1] J. M. D. Coey and H. Sun, J Magn. Magn. Mater. 87, L251 (1990). [2] M. Tokita, J. Soc. Powder Technol. Jpn, 30, 790 (1993). [3] T. Saito, J. Magn. Magn. Mater. 320, 1893 (2008).

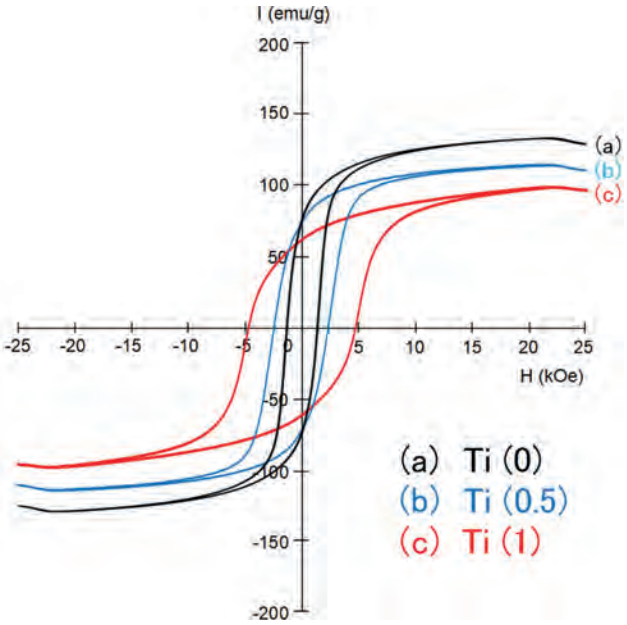

Figure 1 Hysteresis loops of the magnets: (a) Ti (0): ($Sm_{0.7}Zr_{0.3}$)($Fe_{0.7}Co_{0.3}$)$_{10}$, (b) Ti (0.5): ($Sm_{0.7}Zr_{0.3}$)($Fe_{0.7}Co_{0.3}$)$_{9.5}Ti_{0.5}$, and (c) Ti (1): ($Sm_{0.7}Zr_{0.3}$)($Fe_{0.7}Co_{0.3}$)$_9$Ti.

AQ-03. Fabrication and Magnetic Properties of Anisotropic Sm(Fe,X)$_{12}$ Powder and High Density Bulk Magnet. *J. Park*[1], T. Zhou[1,2] and C. Choi[1]
1. Department of Magnetic Materials, Korea Institute of Materials Science, Changwon, The Republic of Korea; 2. Pusan National University, Pusan, The Republic of Korea

The $ThMn_{12}$-type structured magnetic material demonstrates exceptional magnetic properties that surpass those of Nd-Fe-B magnets. For instance, Sm-Fe-Co film exhibits a M_s of 1.78 T, K of 12 T, and T_c of 859 K [1]. However, the low H_c observed in both film and powder forms has limited its utilization as a permanent magnet material. The properties of Sm-Fe-TM, particularly H_c, are highly influenced by the nanostructure. Recent advancements have led to the successful fabrication of Sm-Fe-V sintered magnets with an H_c exceeding 8 kOe by effectively controlling the grain boundary [2]. Nevertheless, there is a need to increase the M to enhance the $(BH)_{max}$. Consequently, this study focuses on investigating the impact of additional Sm content, phase stabilizing elements X, and intergranular phase on M and $(BH)_{max}$. To prepare the Sm(Fe,X)$_{12}$ ingots, induction melting and subsequent homogenization at 1000 °C were employed. Heat treatment was then conducted in a hydrogen environment. The resulting products were ground, sieved using a 100-mesh sieve, and further micronized through jet milling. The powder was pressed under 12.5 GPa and sintered at above 1100 °C to produce bulk magnets. Physical and magnetic properties were controlled by optimizing the experimental conditions. The fabricated Sm(Fe,X)$_{12}$ powders exhibited anisotropic behavior and a high purity $ThMn_{12}$ phase, constituting more than 94 wt.%. Fig. 1 depicts the XRD patterns for randomly oriented and field-oriented powders. The application of a sintering process led to an approximately tenfold increase in H_c for the produced bulks, elevating it from ~1000 to ~10000 Oe, owing to the formation of nano-sized intergranular phases. Conversely, the M_s decreased from 87 to 67 emu/g. Detailed investigations on the microstructure-related magnetic properties dependent on the fabrication conditions will be presented. Additionally, physical and magnetic properties of anisotropic bulk samples produced through field-oriented pressing and sintering will also be discussed.

1. Y. Hirayama, Y. K. Takahashi, and K. Hono, Scripta Materialia Vol. 138, p.62 (2017) 2. K. Otsuka, M. Kamata and T. Nomura, Materials Transactions Vol. 62, p.887 (2021)

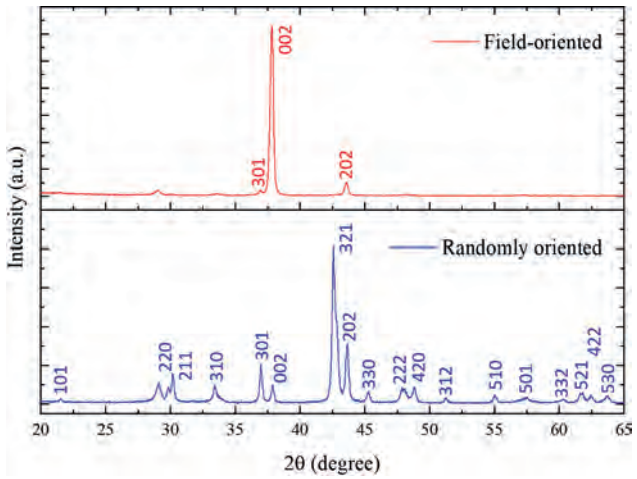

XRD patterns of the Field-oriented and randomly oriented jet-milled Sm(Fe,X)$_{12}$ powders.

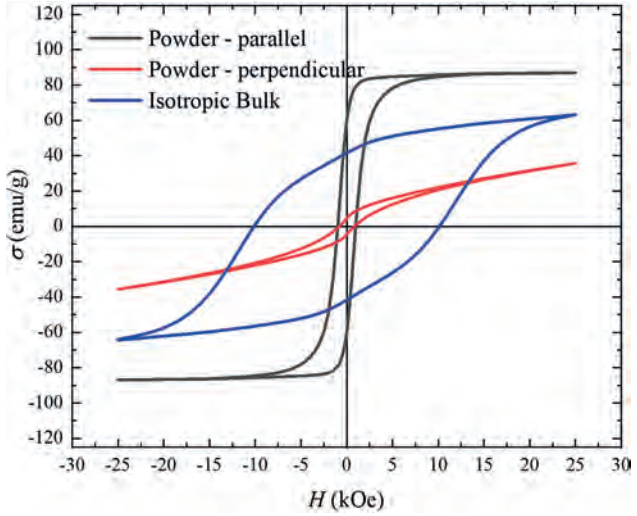

Magnetic hysteresis loops of the aligned powder in parallel and perpendicular directions and high-pressure pressed bulk.

AQ-04. Withdrawn

AQ-05. Influence of low sintering temperature of substituted M-type barium hexaferrite on its static and highfrequency magnetic properties. *K. Rana*[1,2], M. Tomar[1] and A. Thakur[2] *1. Physics, University of Delhi, Delhi, India; 2. Innovative Science Research Society (ISRS), Shimla, India*

Cobalt substituted M-type barium hexaferrite with nominal composition $BaCoFe_{12}O_{19}$ ($0.0 \leq x \leq 1.0$) in the steps of 0.2 were prepared via the chemical co-precipitation method. Thermal analysis was performed on pure BaM sample before undergoing thermal treatments to extract the beneficial information about their crystallization point. From TGA/DTA analysis it was confirmed that 910°C was an ideal sintering temperature for the pure BaM ferrite sample. On that basis, all six samples were sintered at the same

temperature. XRD confirmed the formation of the M phase in all the samples whereas the morphology of all the samples was investigated by using the FESEM technique. Magnetic parameters like saturation magnetization (M_s), coercivity (H_c), and squareness ratio (SQR) were examined by using VSM. The value of M was found to decrease from 65.74 emu/g to 54.30 emu/g at the very initial stage (x=0.2) due to the small amount of dopant but after that with an increase in the dopant content, M_s value was found to increase up to x= 0.8 and reached 65.39 emu/g. Moderate M_s value with a higher coercivity H_c of 3784 Oe was obtained for x=0.8. On the other hand, the variation of complex permittivity and complex permeability with composition was investigated over the X-band frequency range (8.2GHz-12.4GHz). Reliable and sustainable values of permittivity (more than10) and magnetic loss Tan_δ (at x=0.021) at x=0.8 makes this composition suitable for high-frequency application as well as electromagnetic shielding.

1. S Kumar, S Supriya and R Pandey, Journal of Magnetism and Magnetic Materials., 458, 30.38 (2018) 2. R Meena, S Bhattacharya and R Chatterjee, Materials Science and Engineering B., 171, 133-138 (2010)

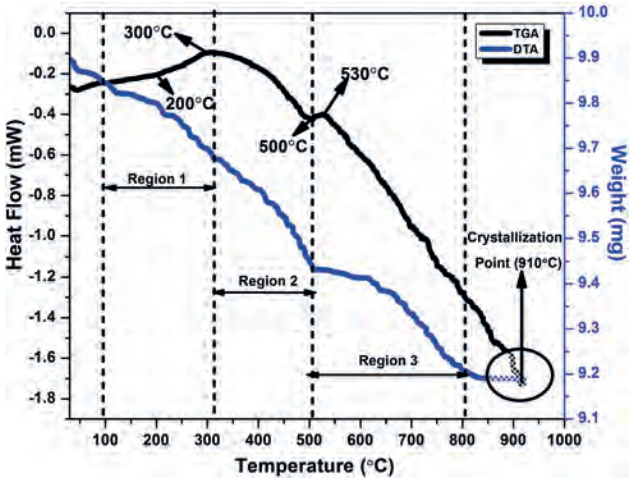

Fig 1. TGA/DTA analysis of pure BaM hexaferrite before undergoing appropriate heat treatments

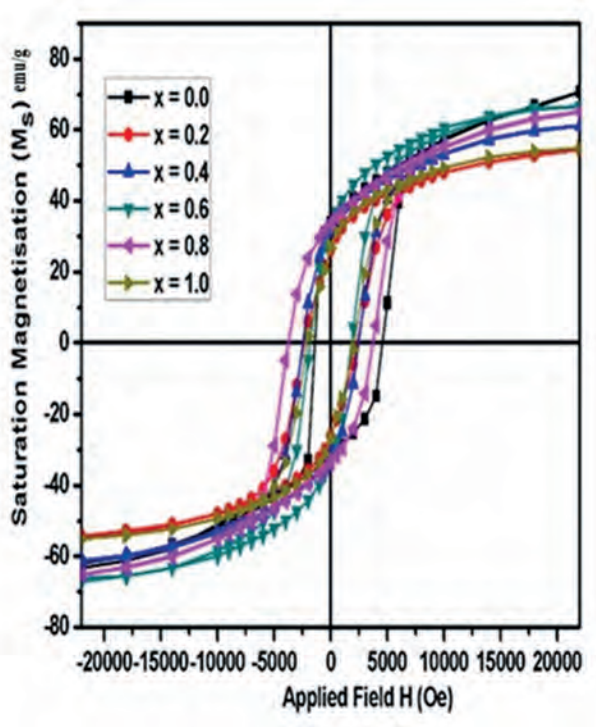

Fig.2 M-H loops of cobalt substituted BaM hexaferrite sintered at 910°C.

AQ-08. Enhanced Hard Magnetism of Synthetic $L1_0$-FeNi. I. Hlova[1], *Y. Mudryk*[1], O. Dolotko[1] and A. Biswas[1] *1. Ames National Laboratory, Ames, IA, United States*

An ordered tetragonal $L1_0$-FeNi, also known as meteoritic mineral tetrataenite – a promising rare-earth-free hard-magnetic compound – has been synthesized starting from a mechanochemically-activated disordered cubic $A1$-FeNi via formation of a chemically-ordered FeNiN intermediate and its subsequent denitrogenation and further purification of the product. Nature of a process control agent employed during the mechanochemical activation of $A1$-FeNi and ammonia flow velocity during the synthesis of the intermediate are two of the main factors controlling the nitrogenation. Denitrogenation with hydrogen at elevated pressures and at temperatures substantially below the order-disorder $L1_0$-FeNi to $A1$-FeNi transition preserves the chemical order spontaneously [HI1] established in the intermediate. Post-synthesis refinement of the $L1_0$-FeNi product includes removal of residual nitrides with a dilute acid to further improve hard-magnetic properties of the material. The thus synthesized $L1_0$-FeNi powders exhibit coercivity as high as 2.3 kOe and maximum energy product reaching 6 MGOe – the highest values ever reported for a synthetic tetrataenite.

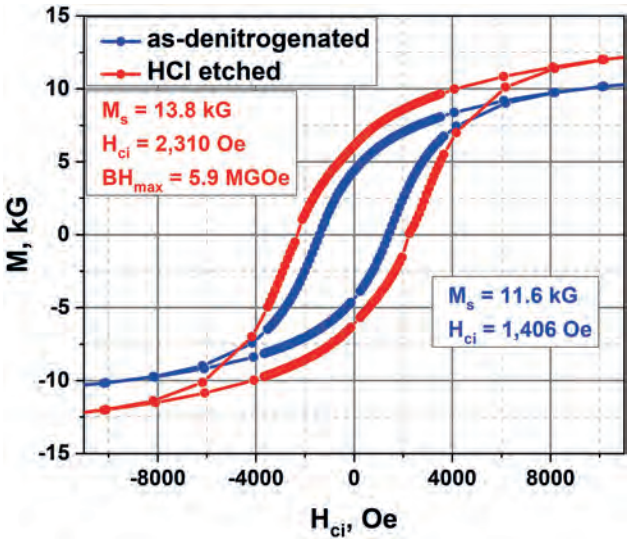

B-H loops of as-prepared $L1_0$-FeNi powders before (blue) and after (red) purification

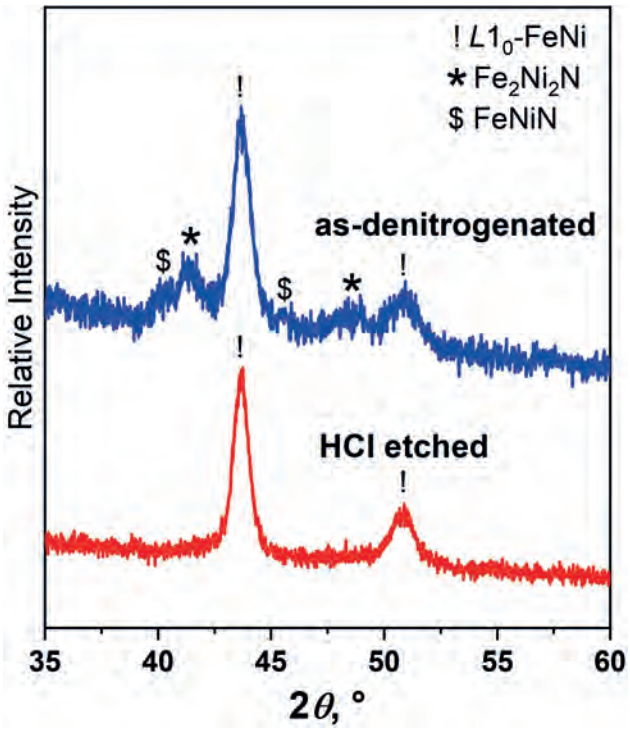

PXRD data of as-prepared $L1_0$-FeNi powders before (blue) and after (red) purification

AQ-09. Segregation of Al and its effect on coercivity in Nd-Fe-B. *X. Liu*[1] and C.I. Nlebedim[1] *1. Ames National Laboratory, Ames, IA, United States*

Doping a small amount of Al can effectively enhance coercivity in Nd-Fe-B magnets [1,2]. It is generally ascribed that Al decreases the melting point and promotes a homogenous distribution of Nd-Fe grain boundary phase (GBP). To gain more insight into the role of Al, we perform first-principles DFT (density functional theory) calculation and micromagnetic simulation to investigate the partitioning behavior of Al and its effect on coercivity in Nd-Fe-B magnet. The DFT calculation indicates that the substitution energy (E_{sub}) of Fe by Al is negative in $Nd_2Fe_{14}B$ (2:14:1) except for the 4e site, implying Al may partially enter the 2:14:1 lattice (Table 1). The calculated E_{sub} at different Fe sites reveals that Al atoms prefer to occupy the 4c and $8j_2$ sites (Table 1), in agreement with neutron diffraction results [3]. The partial replacement of Fe by Al enhances slightly the magnetocrystalline anisotropy but reduces magnetization in 2:14:1. Further, DFT calculations revealed that Al can stabilize the $Nd_6Fe_{13}Si$-type tetragonal phase $Nd_6Fe_{13}Al$ (6:13:1) at GB. The formation of the antiferromagnetic or weak ferrimagnetic 6:13:1 deplete Fe and reduces the amount of ferromagnetic Nd-Fe type GBP, which increases the pinning field of the magnetic domain wall at GB from 22 kOe to 35 kOe as indicated by our micromagnetic simulation. Micromagnetic simulation reveals also that Al-segregation on 2:14:1 grain surface and the formation of 6:13:1 suppress the nucleation of the reversal magnetic domain during demagnetization. Developing a novel processing route to promote homogenous distribution of Al and the formation of 6:13:1 phase at GB can effectively improve coercivity in Nd-Fe-B magnet.

1 O. Gutfleisch, M.A. Willard, E. Brück, C.H. Chen, S.G. Sankar, J.P. Liu, Magnetic Materials and Devices for the 21st Century: Stronger, Lighter, and More Energy Efficient, Advanced Materials. 23 (2011) 821–842. https://doi.org/10.1002/adma.201002180. 2 S. Pandian, V. Chandrasekaran, G. Markandeyulu, K.J.L. Iyer, K.V.S. Rama Rao, Effect of Al, Cu, Ga, Nb additions on the magnetic properties and microstructural features of sintered NdFeB, J Appl Phys. 92 (2002) 6082–6086. https://doi.org/10.1063/1.1513879. 3 E. Girt, Z. Altounian, I. P. Swainson, C Lupien, & J Yang, Structural properties of $Nd_2Fe_{14-\delta}Al_\delta B$ (δ= 0, 0.5). Physica B: Condensed Matter, (1997). *241*, 651-653.

Site	$16k_1$	$16k_2$	$8j_1$	$8j_2$	4c	4e
E_{sub}	-0.19	-1.49	-1.74	-2.05	-2.30	0.84

Table 1 Substitution energy (eV/Al unit cell) of Al in $Nd_2Fe_{13.75}Al_{0.25}$

AQ-11. A Design of Stainless Nd-based Permanent Magnets without Coatings and the Corrosion Mechanism Research. *M. Zhu*[1], Y. Wu[1], Y. Fang[1] and W. Li[1] *1. Central Iron and Steel Research Institute, Beijing, China*

Nd-Fe-B magnets have become the most consumed permanent magnet due to their excellent magnetic properties. However, the susceptibility to corrosion is a main disadvantage[1,2]. It is important to improve the corrosion resistance of uncoated sintered Nd-Fe-B magnets. In this work, the sintered Nd-Ni-Fe-Cr-B magnet was designed and fabricated. This sintered Nd-Ni-Fe-Cr-B magnet maintains a typical 2:14:1 tetragonal phase, and the metallurgical behavior of Ni and Cr is characterized by the distribution of Ni at the grain boundary and Cr in the main phase. To evaluate the effect of the co-addition of Ni and Cr on corrosion resistance, sintered Nd-Fe-B magnets with the same Nd content were also prepared. The results of the corrosion tests are encouraging: the mass loss of sintered Nd-Fe-B magnet (5.00 mg/cm^2) is ~11.40 times that of sintered Nd-Ni-Fe-Cr-B magnet (0.44 mg/cm^2) after corroded in accelerated corrosion test for 480 hours; The corrosion current of sintered Nd-Fe-B magnet (191.00 μA/cm^2) is ~17.36 times that of sintered Nd-Ni-Fe-Cr-B magnet (11.00 μA/cm^2) in 3.5 wt% NaCl solution. The impedance of NdNiFeCrB magnet (R_{ct0} is 2800.00 Ω) is greatly increased considerably by an order of magnitude compared to Nd-Fe-B magnet (R_{ct0} is 238.80 Ω). The metallurgical behavior of Ni and Cr, diminishing the potential difference between the grain boundary phase and the main phase, gives a huge improvement in the corrosion resistance of sintered Nd-Fe-B magnet. This work provides a direction for future research on magnets without coatings. Fig. 1 (a) The mass loss curves of samples; (b) The open circuit potential curves; (c) Potentiodynamic polarization plots. Fig. 2 In 3.5 wt% NaCl solution:(a) Nyquist plots of samples. The inset is the enlarged view of Nyquist plots of NdFeB magnet. (b) The equivalent circuit of NdNiFeCrB magnet. (c) The equivalent circuit of NdFeB magnet.

[1] Edgley DS, Le Breton JM, Steyaert S, et al. Teillet. Characterisation of high temperature oxidation of Nd-Fe-B magnet. J Magn Magn Mater

1997;173(1e2):29e42. [2] Lemarchand D, Delamare J, Vigier P. Thermomagnetic study of the high-temperature oxidation behavior of Nd-Fe-B permanent magnets and powders. J Appl Phys 1992;72:1996e2000.

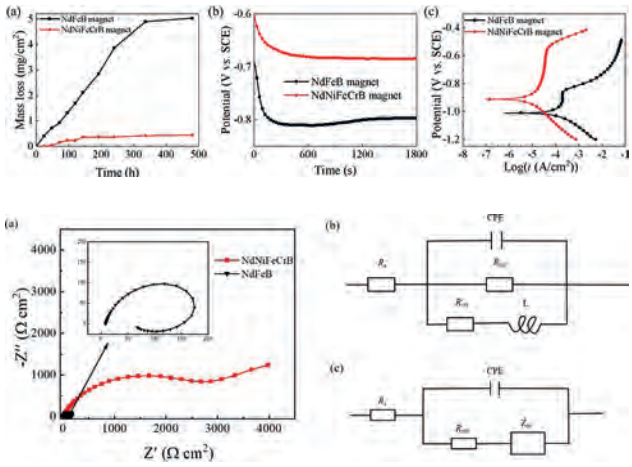

AQ-12. Recycling of Nd-Fe-B Magnets through Grain Boundary Diffusion with Rare Earth Fluorides. *C.I. Nlebedim*[1] and X. Liu[1]
1. Division of Critical Materials, Ames National Laboratory, Ames, IA, United States

Nd-Fe-B magnets have been playing more and more important role in clean energy field.[1,2] Given the concern regarding the scarcity of rare earth (RE) and environmental burden, the recycling and reuse of waste Nd-Fe-B are attracting more attention.[3,4] One challenge for reuse is the deteriorated magnetic properties of the waste magnet such as reduced coercivity. In this work, we explore the grain boundary diffusion process (GBDP) and/or optimized annealing as an approach to restore and/or enhance the coercivity of waste Nd-Fe-B magnets. The waste magnets of Nd-Fe-B were coated with/without REF_3 (RE=Y, La, Ce, Nd and Dy) and annealed at a temperature ranged from 600 to 900 °C for 2 hr. It was found that the coercivity can be improved from 11 kOe (without GBDP and annealing) to 14 kOe for all the samples annealed at 600 °C (Fig. 1). However, for the samples heat treated at 800 °C, their coercivity are sensitive to type of REF_3. For RE=Y and Ce, the coercivity is almost same (10 kOe) as the sample without REF_3 coating but with an annealing at 800 °C. The samples treated with RE=Nd has a coercivity comparable with that of the initial waste magnet (11.5 kOe). For RE=La and Dy, the coercivity was sharply reduced and enhanced, respectively (Fig. 1). Similar situation was also observed for all the samples treated at 900 °C (Fig. 1). These behaviors are ascribed to the various partitioning of each type of RE in Nd-Fe-B during annealing process under different temperature. The RE partitioning results in different RE element segregation, which modify both intrinsic properties of $Nd_2Fe_{14}B$ and microstructure. Optimized annealing and/or GBDP are promising approaches for reusing waste Nd-Fe-B magnets. This work is supported by the Critical Materials Institute (CMI), an Energy Innovation Hub funded by the U.S. Department of Energy (DOE), Office of Energy Efficiency and Renewable Energy, Advanced Manufacturing Office. The work was performed in Ames National Laboratory, operated for the U.S. Department of Energy by Iowa State University of Science and Technology under Contract No. DE-AC02-07CH11358

[1]. R.W. McCallum, L. Lewis, R. Skomski, M.J. Kramer, I.E. Anderson, Practical aspects of modern and future permanent magnets, Annu Rev Mater Res. 44 (2014) 451–477. https://doi.org/10.1146/annurev-matsci-070813-113457. [2] V. Franco, O. Gutfleisch, Magnetic materials for energy applications, JOM. 64 (2012) 750–751. https://doi.org/10.1007/s11837-012-0348-7. [3] V. Balaram, Rare earth elements: A review of applications, occurrence, exploration, analysis, recycling, and environmental impact, Geoscience Frontiers. 10 (2019) 1285–1303. https://doi.org/10.1016/j.gsf.2018.12.005. [4] R. Schulze, M. Buchert, Estimates of global REE recycling potentials from NdFeB magnet material, Resour Conserv Recycl. 113 (2016) 12–27. https://doi.org/10.1016/j.resconrec.2016.05.004.

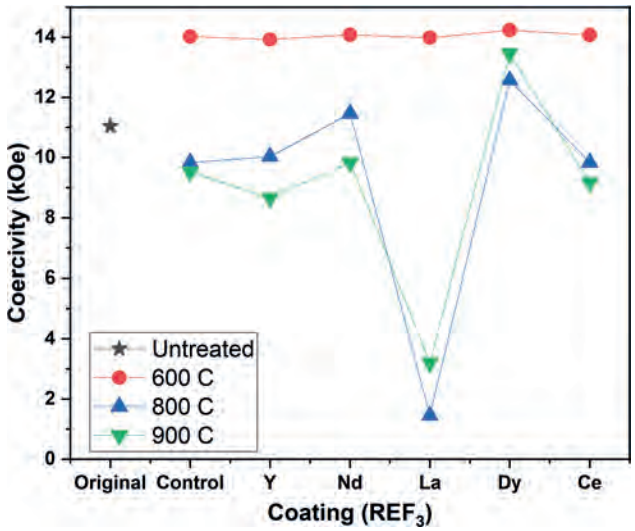

Fig. 1 Coercivity of Nd-Fe-B treated with REF_3 under different annealing temperature

AQ-14. Novel and ultra-sharp magnetization in Sm $(Ni_{0.5}Fe_{0.4}Al_{0.1})_5$. W. Yang[1], T. Zhu[1], Z. Luo[1], S. Liu[1], J. Han[1], H. Du[1], Q. Xu[1], C. Wang[1] and *J. Yang*[1] *1. Peking University, Beijing, China*

Many magnetic characteristics, such as spin reorientation, magnetic ordering and phase transition, magnetization compensation, remanence and coercivity, are closely dependent on the temperature of the magnetic materials[1-4]. Recently, temperature-dependent magnetization jump behaviors have been observed in several rare-earth transition-metal intermetallic compounds at very low temperatures, such as $Dy(Fe,M)_2$(M=Al,Si)[5], $Dy(Fe,Ga)_2$[6], $CeNi_{1-x}Cu_x$[7], $SmCo_{3.5}Cu_{1.5}$[8]. In this study, multi-element rare-earth transition-metal intermetallic compounds $Sm(Ni_{0.5}Fe_{0.4}Al_{0.1})_5$ has been successfully fabricated, and novel and ultra-sharp magnetization behaviors have been investigated. When T>4.1 K, the magnetization curve is smooth and the coercivity increases exponentially with decreasing temperature due to the decrease of the thermal activation, however, when T<4.1 K sharp magnetization steps appear and the coercivity decreases with further decreasing the temperature and tends to be constant when T<2.5 K. The hysteresis loops of a polycrystalline grain of about 1 mm are shown in Fig. 1. The hysteresis loop at 10 K is smooth, whereas at 2.2 K four ultra-sharp magnetization steps appear on the magnetization and demagnetization curves, respectively. The ultra-sharp magnetization steps can be explained using the mechanism of avalanche magnetization process launched by an instantaneous domain wall motion. The sample temperature of the polycrystalline grain has also been measured with increasing magnetic field at constant measurement temperature of 5 K and 2 K, as shown in Fig. 2. No temperature pulse is observed for the condition of 5 K, while for the condition of 2 K four temperature pulses are observed due to the ultra-sharp magnetization jumps, supporting the theory of avalanche magnetization mechanism.

[1] R. Grössinger, P. Obitsch and X.K. Sun et al., Mater. Lett., 2, 539 (1984). [2] T. Urakabe, T. Yamashita and T. Saito et al., J. Magn. Magn. Mater., 177, 1145 (1998). [3] C. Mazumdar, R. Nagarajan and L. C. Gupta et al., Appl. Phys. Lett., 77, 895 (2000). [4] S. Foner, E. J. McNiff and H. Oesterreicher et al., J. Appl. Phys., 49, 2061 (1978). [5] N. V. Mushnikov, N. K. Zajkov and A. V. Korolyov, J. Magn. Magn. Mater., 163, 322 (1996). [6] W. D. Zhong, Z. X. Liu and H. Y. Chen et al., Acta. Phys. Sin. Ch. Ed., 44, 1516 (1995). [7] N. Marcano, J. C. Gómez Sal and J. I. Espeso et al., Phys. Rev. Lett., 98, 166406 (2007). [8] M. Uehara, B. Barbara and B. Dieny et al., Phys. Lett., 114A, 23 (1986).

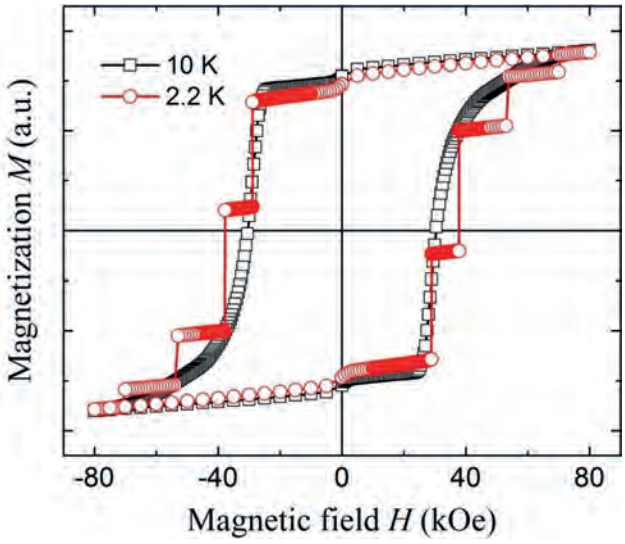

Fig. 1 Hysteresis loops of $Sm(Ni_{0.5}Fe_{0.4}Al_{0.1})_5$ at 2.2 K and 10 K.

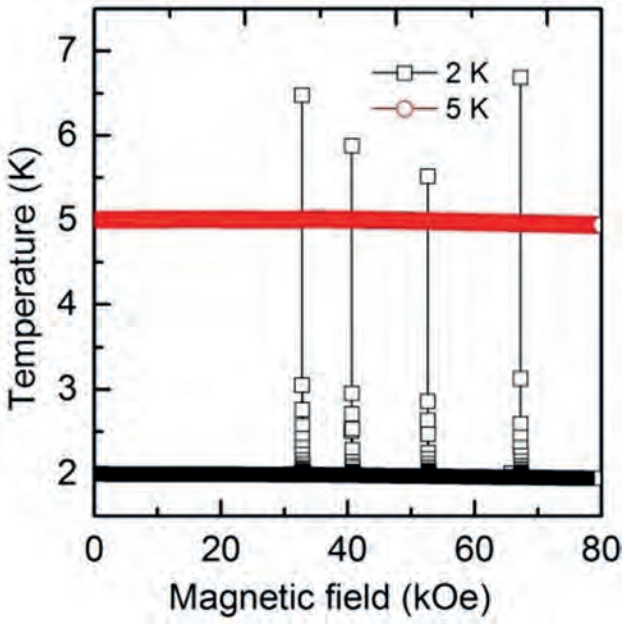

Fig. 2 Temperature of polycrystalline $Sm(Ni_{0.5}Fe_{0.4}Al_{0.1})_5$ with increasing magnetic field at constant measurement temperature of 5 K and 2 K.

AQ-15. Effect of TiC nanoparticle on microstructure and magnetic properties in Nd-Fe-B sintered Magnet. *H.G. Parmar*[1], I. Vela[1], X. Liu[1] and C.I. Nlebedim[1] *1. Ames National Laboratory, Ames, IA, United States*

High-performance Nd-Fe-B based hard magnets are extensively used in various applications including hybrid electric vehicles, wind turbines, and consumer electronics.[1,2] One weak point of Nd-Fe-B magnet is its low coercivity, which can be improved through partial replacement of Nd by Dy or Tb, or through microstructure engineering such as refinement of grain size and modification of grain boundary phases (GBP). TiC has been successfully applied in refining grain size in melt-spun Nd-Fe-B.[3] In this work, we study the effect of TiC on the microstructure and magnetic properties in sintered Nd-Fe-B. The strip-cast alloy of $Nd_{14.5}Fe_{bal}B_{5.9}Al_1Cu_{0.1}$ was crushed into fine particles with a size of 3-5 microns through hydrogen decrepitation and ball milling. The Nd-Fe-B powder was mixed with 1wt% TiC particles with a size of 200 nm as feedstock powder for the sintered magnet. The sintered magnets without- and with-TiC additive show coercivity of 10 kOe and 4.5 kOe, and maximum energy product of 42 MGOe and 21 MGOe, respectively (Fig. 1). The microstructure observation indicates that TiC can refine grain locally but do form some TiC particle cluster in magnet. The reduction of coercivity due to TiC is ascribed to the heterogeneous distribution of Nd-rich GBP. Properly engineering GBP is highly demanded for developing fine grain-sized Nd-Fe-B magnets *via* doping TiC. This work is supported by the Critical Materials Institute (CMI), an Energy Innovation Hub funded by the U.S. Department of Energy (DOE), Office of Energy Efficiency and Renewable Energy, Advanced Manufacturing Office. The work was performed in Ames National Laboratory, operated for the U.S. Department of Energy by Iowa State University of Science and Technology under Contract No. DE-AC02-07CH11358.

[1] M.J. Kramer, R.W. McCallum, I.A. Anderson, S. Constantinides, Prospects for non-rare earth permanent magnets for traction motors and generators, JOM. 64 (2012) 752–763. https://doi.org/10.1007/s11837-012-0351-z. [2] O. Gutfleisch, M.A. Willard, E. Brück, C.H. Chen, S.G. Sankar, J.P. Liu, Magnetic Materials and Devices for the 21st Century: Stronger, Lighter, and More Energy Efficient, Advanced Materials. 23 (2011) 821–842. https://doi.org/https://doi.org/10.1002/adma.201002180. [3] K. Gandha, X. Liu, W. Tang, I.C. Nlebedim, Enhancement in hard magnetic properties of (Nd, Pr)-Fe-B melt-spun ribbons, J Appl Phys. 128 (2020). https://doi.org/10.1063/5.0021135.

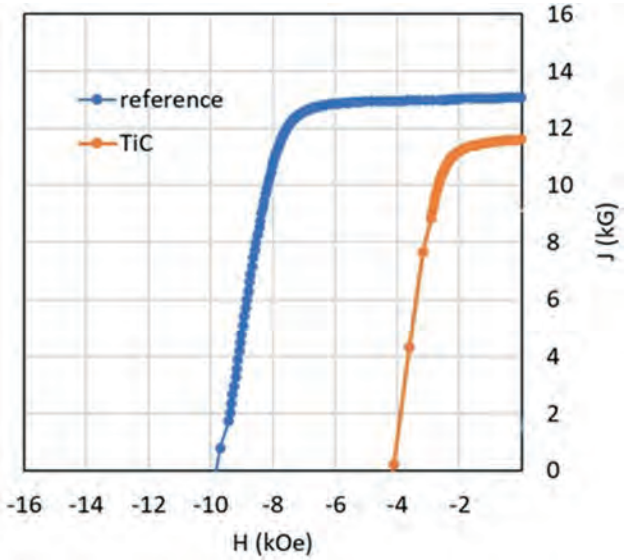

Figure 1 J-H curve for Nd-Fe-B sintered magnets without- and with-TiC nanoparticles

Session AR
SOFT MAGNETIC MATERIALS I
(Poster Session)

Nicoleta Lupu, Chair
National Institute of R&D for Technical Physics, Iasi, Romania

AR-02. Electrically Insulation of Three Fluid Jet Gas-Liquid Atomized FINEMET Powders with a High Resistivity Organosilane Coating to Preserve Magnetic Properties. F. Borza[1], D. Gherca[1], I. Murgulescu[1], M. Tibu[1], G. Stoian[1], M. Grigoras[1] and *N. Lupu[1] 1. National Institute of R&D for Technical Physics, Iasi, Romania*

The increasing demand for downsized high-output devices and hence, high-performance magnetic core materials corresponding to applications and usage environments requires intensive research on material composition, insulating films, etc. [1,2]. The aim of the work is to develop technology for reducing core loss, by producing FINEMET powder with particles size in the range where nanocrystalline state is directly achieved by using a new three-jet gas atomization technique (two jets of Ar gas and one jet of water) and a novel anhydrous method for insulating the surface of FINEMET powders with a focus on preserving the magnetic properties of the powders. FINEMET powders with diameter size of 20-32 μm, have been obtained directly in the nanocrystalline state. The electrically insulating layer was deposited by a self-assembled monolayer technique, using 1% 3-aminopropyltriethoxysilane (APTES) solution as coating agent. Fourier-transform infrared spectroscopy (FTIR) and Scanning Electron Microscopy (SEM) were used for both samples, before and after silanization process, to confirm the presence of APTES coating (Fig. 1). SEM, X-ray diffraction (XRD), and magnetic measurements have been performed to assess the structural and magnetic characteristics. The SEM images revealed the formation of particles with almost spherical shape. The X-Ray diffraction patterns show that in the range 20-32 μm the structure of particles is nanocrystalline. The Vibrating Sample Magnetometer (VSM) measurements performed at a maximum applied field of 8 kOe on uncoated and 1% APTES solution coated powders indicate that the magnetization for the pristine FINEMET powders reaches the saturation value of 142 emu/g and slightly decreases for the APTES insulated powder to 137 emu/g. The coercive force takes the value of 2.2 Oe for the uncoated powders and increases to7.6 Oe after insulating the powders with a thin APTES layer. These properties make the APTES coated FINEMET powders competitive in magnetic cores production. Work supported by the Romanian Ministry of Research, Innovation and Digitalization under NUCLEU Program – contract no. 33N/2019, project PN 19 28 01 01.

[1] C. Jiang, X. Li, S. S. Ghosh and H. Zhao, IEEE Transactions on Power Electronics, Vol. 35, p. 10821, (2020) [2] K. L. Alvarez, H.A. Baghbaderani, and J.M. Martín, J. Magn. Magn. Mater., Vol. 501, 166457, (2020)

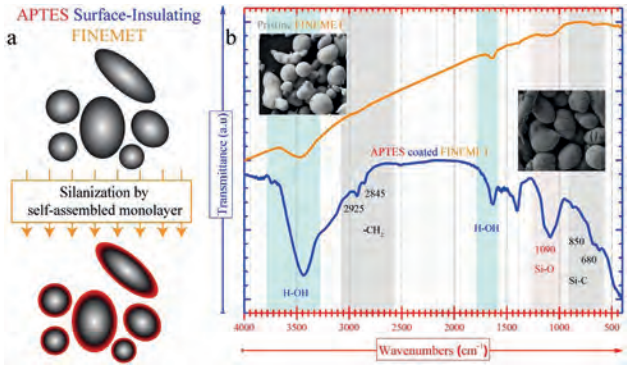

Fig. 1. FTIR spectra for (a) un-coated and (b) APTES coatedd powders.

AR-03. Direct Observation of Magnetic Domain Walls in Glass-Coated Amorphous Nanowires and Submicronic Wires. G. Ababei[1], G. Stoian[1], H. Chiriac[1], N. Lupu[1] and *T.A. Ovari[1] 1. Dept. of Magnetic Materials and Devices, National Institute of Research and Development for Technical Physics, Iasi, Romania*

Rapidly solidified amorphous nanowires with cylindrical symmetry have been extensively investigated in recent years [1]. Their main advantages originate in the typical one-step axial magnetization reversal process that takes place through the depinning and subsequent fast propagation of 180° domain walls. Here we report on the direct observation of magnetic domain walls in rapidly solidified amorphous nanowires with highly positive magnetostriction, i.e., $Fe_{77.5}Si_{7.5}B_{15}$ with $\lambda = 25 \times 10^{-6}$, and with nearly zero magnetostriction, e.g., $(Co_{0.94}Fe_{0.06})_{72.5}Si_{12.5}B_{15}$ with $\lambda = -1 \times 10^{-7}$, respectively. The studies have been performed by means of Lorentz transmission electron microscopy (LTEM) using a Libra 200 MC Carl Zeiss ultra-high-resolution microscope. This method also allowed us to observe the displacement of domain walls under various applied magnetic fields. The results show that all the investigated magnetic domain walls have vortex structures, irrespective of wire composition or diameter. In the case of nearly zero magnetostrictive samples, the symmetry of the vortex domain walls remains unchanged even under applied fields up to 100 kA/m applied under various angles with the wire axis. In the case of highly magnetostrictive nanowires and submicronic wires, the vortex structures of the domain walls are more sensitive to the magnitude and direction of the applied field. Moreover, the types of vortex structures in samples with different magnetostriction constants are different, in agreement with their different dynamic characteristics in the two types of materials. We have explained the results by considering the different magnetoelastic anisotropies as concerns both their magnitudes and nonlinear distributions in samples from the two investigated alloy compositions. Domain wall observation results have been correlated with domain wall velocity and mobility measurements to understand the role of domain wall structures on their dynamic properties, since domain wall propagation offers important application opportunities for such low dimensional amorphous magnetic materials. Work supported by UEFISCDI under contract no. PCE 1/2021 (project PN-III-P4-ID-PCE-2020-1856/MaDWallS).

[1] J. Alam, C. Bran, H. Chiriac, N. Lupu, T.A. Óvári, L.V. Panina, V. Rodionova, R. Varga, M. Vazquez, A. Zhukov, Cylindrical micro and nanowires: Fabrication, properties and applications, J. Magn. Magn. Mater., 513 (2020) 167074.

AR-04. Harmonic mesurement in FFP of Gd^{3+} -doped $MnFe_2O_4$ Nanoparticles for MPI Applications. T. Sakamoto[1], K. Nii[1], T. Moriwaki[1], Y. Fujita[1], H. Amano[1] and *Y. Ichiyanagi*[1,2] *1. Engneering Science, Yokohama National university, Yokohama, Japan; 2. Osaka University, Osaka, Japan*

Superparamagnetic nanoparticles with high magnetization and low coercivity are expected for the applications in the biomedical field [1]. Magnetic particle imaging (MPI) is one of the new ideas for diagnostic method, which directly visualizes the magnetic response [2]. In this study, DC magnetic field was applied as the gradient magnetic field and field-free point (FFP) was provided as the measurement point. The behavior of the harmonic response of magnetic nanoparticles under an AC magnetic field was observed. Gd-doped Mn-ferrite nanoparticles were prepared by our original wet-mixing method. Particle size *d* was controlled by varying the annealing temperature (d = 10, 14, 17, 21 nm), and the Gd doping amount was unified to 6.5%, which was found to respond particularly well to AC magnetic fields in previous studies. Magnetization measurements were performed on particle of various sizes. The coercivity(H_c) of the 10 nm and 14 nm particles was found to be small, while the initial permeability(μ) was large for the 14 nm and 17 nm particles. Based on the magnetic properties of the prepared samples, harmonic measurements under AC magnetic field were performed. As a result, the largest response was observed for the 14 nm particle. The 14 nm particles had the lowest coercivity, could follow external magnetic fields quickly, and would have the largest change in magnetization in the low-field region, resulting in the largest harmonic response and making them ideal properties for MPI applications. Furthermore, for practical applications, we have succeeded in creating FFP in a gradient magnetic field by placing two coils facing each other and applying DC current in opposite directions. The DC and AC coils were set in orthogonal orientations, and the third harmonic was measured while scanning them in horizontal coordinates(Fig.1). As a result, the harmonic response was maximum at the horizontal coordinate X = 0, the midpoint of the DC coil (Fig.2).

[1] A. Oshima, Y. Ichiyanagi et al., *J. Nanosci. Nanotechnol.*, 20, 7255-7262, (2020) [2] J. Borgert et al., *J. Cardiovasc. Comput.*, 149-153 (2005)

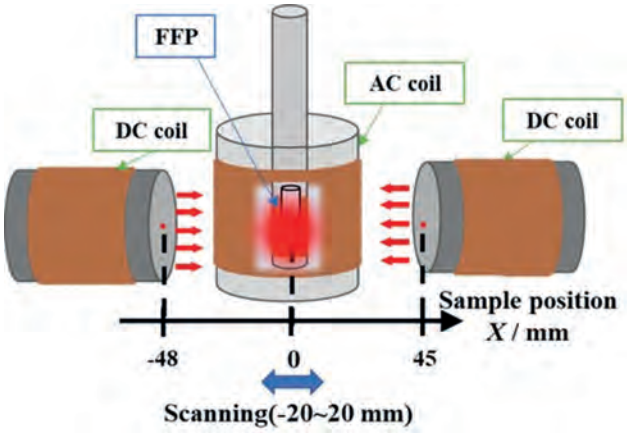

Fig. 1 Developed measurement system for the third harmonic components.

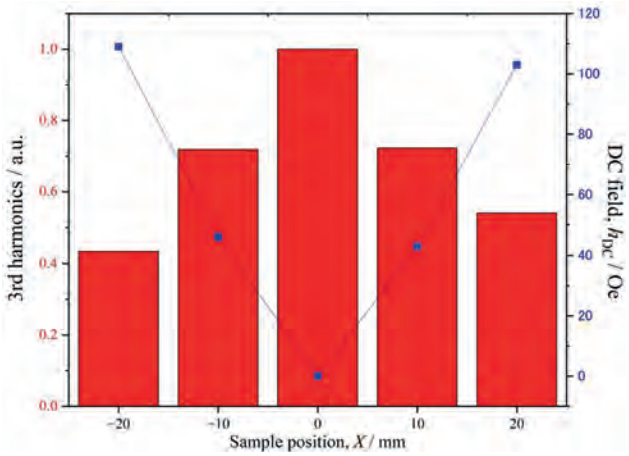

Fig. 2 Third harmonic response results when the measurement point was scanned horizontally.

AR-05. Influence of scanning strategy on magnetic properties of 630 stainless steel fabricated by directed energy deposition method. *K. Kinoshita*[1], M. Sakamoto[1] and S. Imatani[1] *1. Graduate School of Energy Science, Kyoto University, Kyoto, Japan*

The directed energy deposition (DED) process, which is a metal additive manufacturing (AM) process, is expected to be applied to large metal parts owing to its fast-forming speed [1]. Because of the application of 630 stainless steel (SUS630) AM products as structural materials in the aerospace industry, these products are expected to be highly reliable. During the DED process, objects are fabricated by scanning the laser, and the grains become columnar in the scanning direction [2] and are subjected to martensitic transformation by laser heating and cooling [3]. Therefore, the magnetic properties of these products may be modified by the DED process. In other words, these products may be evaluated nondestructively by measuring their magnetic properties. In this study, we investigated the dependence on the scanning strategy (SS) of the magnetic properties of SUS630 specimens manufactured using a DED machine. Each specimen was a prism with dimensions of 10 × 10 × 50 mm. The specimens for which the laser scanned back and forth in the *x*- and *y*- directions (Figure 1(a) and (b)) are denoted as X and Y, respectively. The specimen with the laser rotating and scanning in the *xy*-plane (Figure 1(c)) is denoted Z. Figure 2 shows the magnetization curves obtained for each specimen and their magnified views. The maximum magnetization, coercive force, and magnetic susceptibility near zero-magnetization depended on the SS. The martensite fraction and porosity measurements obtained using XRD, the internal structure analysis using the Bitter method and EBSD were conducted to investigate the variations in the magnetization curves based on the SS. The martensite fraction depended on the SS, and magnetic poles were generated in the martensitic phase block structure units. Furthermore, a numerical analysis using the magnetic micromechanics model [4] demonstrated that variation of the martensite structure owing to the SS produced differences in magnetic properties.

[1] M. Fujishima, Y. Oda, R. Ashida, K. Takezawa, M. Kondo, CIRP J. Manuf. Sci. Technol., Vol 19, p.200 (2017) [2] S. H. Kang, J. Suh, S. Y. Lim, S. Jung, Y. W. Jang, I. S. Jun, J. Nucl. Mater., Vol. 547, 152812 (2021) [3] D. S. Shim, H. Lee, Y. Son, W. J. Oh, J. Mater. Res. Technol., Vol. 13, p. 980 (2021) [4] K. Kinoshita, AIP Adv., Vol. 7, 056008, (2017).

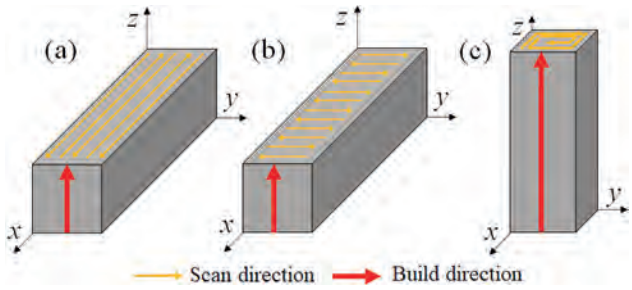

Figure 1: Scan strategy schematic used for specimen additive manufacturing.

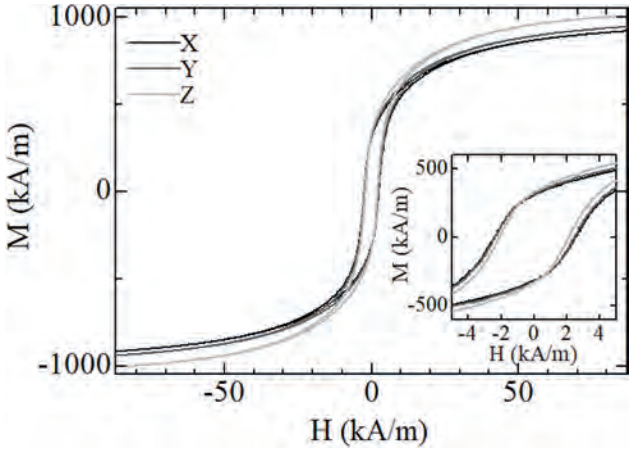

Figure 2: Magnetization curve corresponding to SUS630 with different scan strategies. Inset shows a magnified view of the hysteresis loop in the range of H = ±5 kA/m.

AR-06. High frequency magnetic properties of submicron-sized Fe-Ni-B amorphous particles synthesized by aqueous solution reduction method. *K. Wakabayashi*[1], T. Miyazaki[2], M. Nguyen[1], S. Muroga[1] and Y. Endo[1,3] *1. Graduate School of Engineering, Tohoku University, Sendai, Japan; 2. Faculty of Engineering, Tohoku University, Sendai, Japan; 3. Center for Science and Innovation in Spintronics, Tohoku University, Sendai, Japan*

Soft magnetic particles with micron-size are widely used in high frequency devices, i.e. inductor, noise suppressor because of high saturation magnetization and flexibility in shape. For the next-generation devices in several GHz range, eddy current becomes serious problem due to low resistivity. One of the effective ways to solve this problem is to reduce the particles size to less than the skin depth. Previously, we reported submicron-sized Fe-B amorphous particles synthesized by aqueous solution reduction method[1]. It found that ferromagnetic resonances were observed in the range of 1 to 3 GHz and their intrinsic permeability were 9-14. Herein, we newly synthesize submicron-sized Fe-B particles doped with Ni and evaluate their structures and magnetic properties. Figure 1 shows SEM image of as-made Fe-Ni-B particles. The particles were non-agglomerative and spherical shape with the median size of approximately 200 nm and the size distribution of 150-250 nm. Similar shape and median size were observed in the annealed particles at 400 for 1 h in Ar ambient. In both samples with and without annealing, the amorphous phase was confirmed by TEM observation. Figure 2 shows the complex permeability (μ′ and μ″) of the Fe-Ni-B particles composites. μ′ increased from 2 to 2.8 after annealing process. In case of μ″, broad peaks were observed in both samples. And value of μ″ was almost zero up to 1 GHz for the annealed sample. This indicates the high frequency magnetic properties were improved by annealing process, which might be attributed to the structure relaxation. In conclusion, these results suggest that submicron-sized Fe-Ni-B particles possess good high-frequency magnetic properties by annealing process.

[1] K. Murata, T. Miyazaki, H. Masumoto, Y. Endo: *T. Magn. Soc. Jpn. (Special Issues)*., 5, 1-5 (2021)

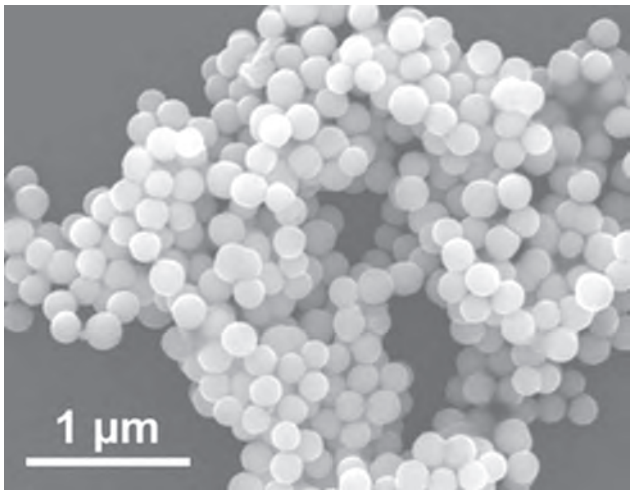

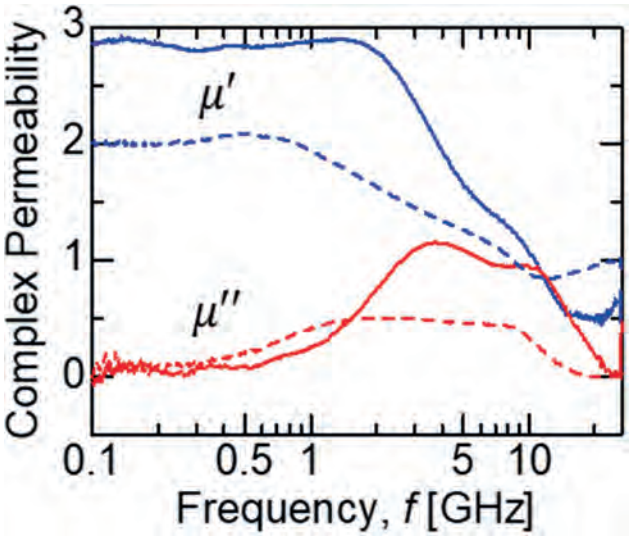

AR-07. Effects of Bulk Sulfur Content on Annealing Texture and Magnetic Properties in AlN-free and Mn-Contained Fe-3.2%Si Electrical Steels. *J. Ahn*[1], K. Lee[1], H. Gil[1], S. Yoo[2], Y. Ahn[2], G. Oh[2], C. Kang[2], N. Heo[3] and J. Kim[1] *1. Hanyang University, Ansan-si, The Republic of Korea; 2. Hyundai Steel R&D center, Dangjin, The Republic of Korea; 3. Thermvac, Hwaseong, The Republic of Korea*

The conventional grain-oriented electrical steels, which are used for the core materials of transformers, are composed of a sharp {110}<001> Goss texture. The {110} plane is parallel to the strip surface and the <001> direction to the rolling direction. Generally, the electrical steels are one-stage cold-rolled before final annealing. It is well known that the formation of Goss texture is deeply related to the role of precipitates (AlN and MnS) as inhibiters. It is the purpose of this study to investigate the effects of bulk sulfur content on the formation of Goss texture in AlN-free and Mn-contained Fe-3.2%Si electrical steels. The electrical steel strips of 0.2 mm thickness, which were obtained through a two-stage cold-rolling process, contained 10~30 (S1), 40~70 (S2), and 80~130 (S3) ppm sulfur. The pre-annealed strips were heated to 1200°C with a heating rate of 400°C/hr and held at the temperature for 10~15 hr under a reduction atmosphere. Fig. 1 shows the B-H analyzer measurement results for annealed strips. The Magnetic properties of the S2 steel were best: B_8 of 1.92 T and $W_{15/50}$ of 1.43 W/kg. The strip showed a sharp {110}<001> Goss texture, meaning the

existence of an optimal bulk sulfur content for the high magnetic properties. When the hot-rolled S2 steel plate was one-stage cold-rolled, the strip was composed of not Goss grains but {100} ones after final annealing. This implies that, because of the complete consumption of Goss grains, the selective growth of Goss grains could not occur even under the lowest surface energy condition of the {110} grains [1]. Changes in sulfur concentration with depth in a strip surface annealed at 1200°C for 15 min are shown in the SIMS analysis of Fig. 2. The surface-segregated sulfur concentration at the surface was interestingly lowest in the S2 steel and lower than that in the S1 steel. Such a sulfur concentration is advantageous for the active selective growth of Goss grains [2, 3]. Through additional experiments, the correlation between sulfur content and final annealing texture will be clarified in the electrical steels.

[1] N.H. Heo, K.H. Chai and J.G. Na, Acta Materialia, Vol. 48, 2901-2910 (2000) [2] D. Kohler, Journal of Applied Physics, Vol. 31, S408-S409 (1960) [3] N. H. Heo, K. H. Chai and J. G. Na, Journal of Applied Physics, Vol. 85, 6025-6027 (1999)

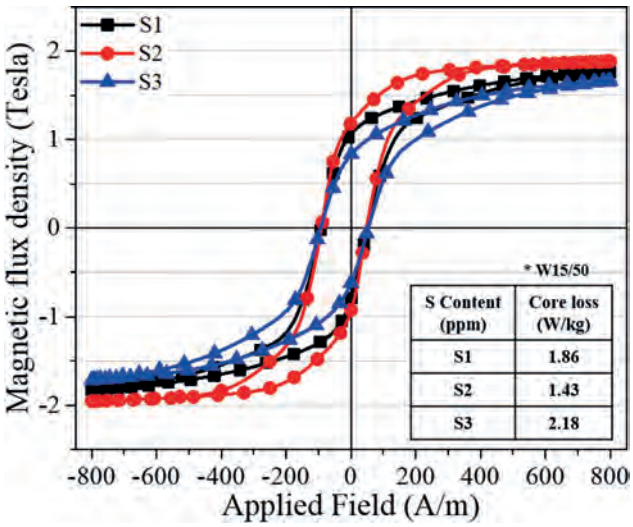

Fig. 1. Changes in magnetic properties with bulk sulfur content

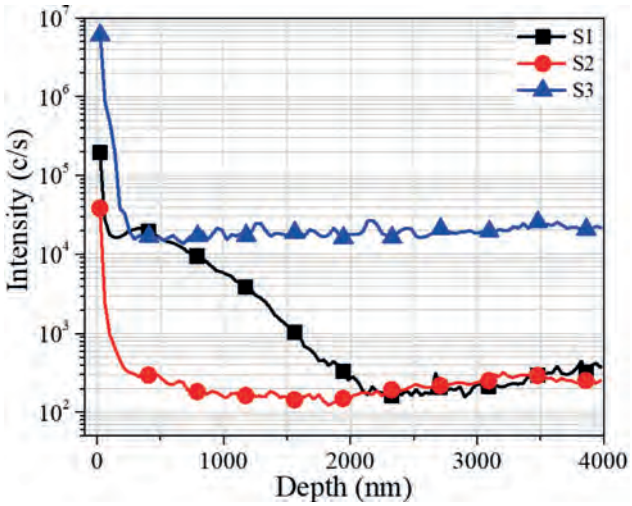

Fig. 2. The depth profile of the sulfur content

AR-08. Modelling of magnetization process of compacted Fe-based powder by Jiles-Atherton model. *D. Olekšáková*[1], P. Kollár[2] and M. Jakubčin[2] *1. Technical University of Košice, Prešov, Slovakia; 2. P. J. Šafárik University in Košice, Košice, Slovakia*

Anhysteretic magnetization is defined as the "thermal equilibrium" curve measured by the cooling the sample from Curie temperature in an incrementally increased dc field. The most important utilization of anhysteretic curves is in magnetic recording, where the superposition of high frequency field on the signal is used to overcome the hysteresis of the recording medium. The iron powder with particle size from 160 μm to 210 μm with irregular shape was obtained by the sieving method. The sample in the shape of ring was prepared by the compaction of the iron powder by the press at uniaxial pressure of 700 MPa at the temperature of 400 °C for 5 minutes in vacuum. Another sample was prepared at the same conditions, but after compaction was annealed at 1000 °C. Anhysteretic curves (fig. 1) were measured by modified dc hysteresisgraph. The ac field with decreased amplitude was applied at every measured point along the magnetization curve by the third toroidal winding to obtain experimental points of anhysteretic curve. According to the Jiles-Atherton model, after applying Maxwell-Boltzman statistics, represented by the modified Langevin function L we can write at internal magnetic field H_{int} for magnetization $M=M_s(K_1H_{int}+K_2M)$, where M_s is the saturation magnetization, K_1, K_2 are parameters, which can be fitted with experimental data of anhysteretic curves of our samples. Parameter K_1 depends on the room temperature T and the average magnetic moment of an effective domain m. Parameter K_2 is in accordance with a constant mean field parameter related with M. The experimentally obtained data of anhysteretic curve of the compacted iron powder samples were compared with the ones calculated by Jiles-Atherton model for ferromagnetic material. This research was funded by Slovak Research and Development Agency, grant numbers APVV-21-0228 and APVV-20-0072 and by Scientific Grant Agency of Ministry of Education of Slovak Republic and Slovak Academy of Science grant numbers VEGA 1/0403/23 and VEGA 1/0143/20.

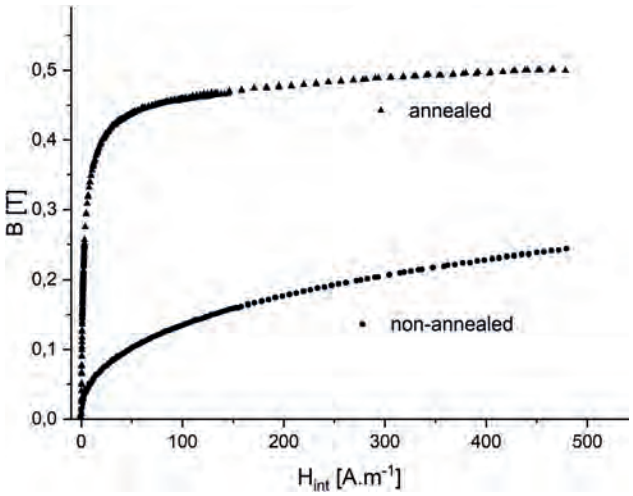

Fig. 1. Anhysteretic curves of compacted annealed and non-annealed sample

AR-09. Magnetization process of compacted iron powder in small magnetic fields. *P. Kollár*[1], D. Olekšáková[2], M. Tkáč[1], R. Maciaszek[1] and J. Füzer[1] *1. Institute of Physics, Faculty of Science, P. J. Šafárik University in Košice, Košice, Slovakia; 2. Institute of Manufacturing Management, Faculty of Manufacturing Technologies, Technical University of Košice, Prešov, Slovakia*

We investigated magnetization process of the soft magnetic compact consisting of iron particles of a size from 125 μm to 200 μm in small dc and ac magnetic fields. The hysteresis loops of the powder compact were measured at maximum magnetic field of 35 A/m from dc up to 800 Hz. Hysteresis loops in dc magnetic fields can be approximated by Rayleigh

law, $B=\mu_0\mu_r H+\mu_0 bH^2$, where μ_0 is the magnetic constant of free space, μ_r is the initial relative permeability and b is the Rayleigh constant. The dc hysteresis loop of the compact, similarly as for most ferromagnetic materials have typically sharp peaks, while in ac magnetic field the peaks are rounded. The phase shift between ac magnetic fields and magnetic induction (except of Rayleigh law) is responsible for resulting shape of the hysteresis loop in small magnetic fields. To determine the contribution of irreversible process to magnetization reversal in the range of validity of the Rayleigh law, we corrected the hysteresis loops measured in ac magnetic fields with respect to the phase shift φ and we obtained the hysteresis loops with shape typical for dc hysteresis loops and then we calculated the Rayleigh constant b, Fig. 1. The dc magnetization process is performed by displacement of domain walls hindered by obstacles (as inhomogeneities, dislocations) causing irreversible Barkhausen jumps. This fact is reflected in Rayleigh constant b. The value of this constant drops steeply with frequency, but the width of hysteresis loop increases (coercieve field), because the phase shift is growing steeply with frequency. The domain walls hindering is not responsible to a decisive degree for coercieve field above the frequency of 40 Hz, because the kinetic energy of domain walls does not allow them to permanently occupy the positions of the potential minimums and the phase shift dominantly affects the coercive field. This work was realized within the frame of the project "FUCO" financed by Slovak Research and Development Agency under the contract APVV-20-0072; and by Scientific Grant Agency of Ministry of Education of Slovak Republic and Slovak Academy of Science — projects VEGA 1/0143/20, VEGA 1/0225/20 and 1/0403/23.

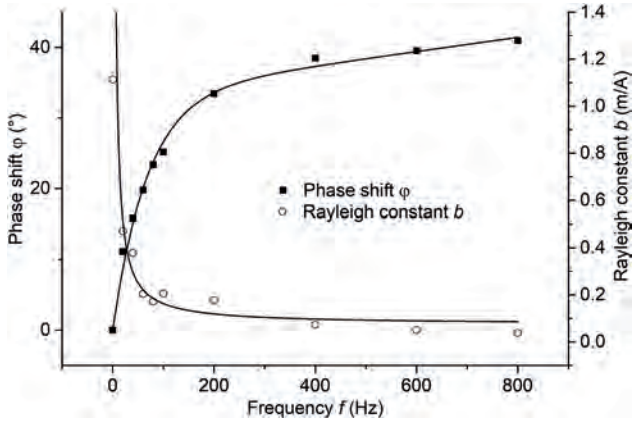

Fig. 1. Phase shift φ and Rayleigh constant *b* vs. frequency.

AR-10. Withdrawn

AR-11. A Study on the Elemental Distribution Behaviors of Fe-based Nanocrystal Ribbons using Atom Probe Tomography. *K. Lee*[1], J. Ahn[1], H. Im[2], J. Jeong[2] and J. Kim[1] *1. Department of Materials Science and Chemical Engineering, Hanyang University, Ansan, The Republic of Korea; 2. Metal Powder Department, Korea Institute of Materials Science, Chacngwon, The Republic of Korea*

High saturation magnetization (M_S) and permeability of soft magnetic materials are crucial requirements for high efficiency of electromagnetic devices. In recent, we reported the successful fabrication of Fe-based nanocrystalline ribbons with high Fe concentration [1]. However, the permeability of the ribbons was strongly dependent on the heating process because of their poor thermal stability. Thus it is necessary to understand the nucleation and growth behaviors of α-Fe grains in nanocrystalline ribbons with high Fe concentration. In the study of nanocrystalline Fe-B-C-Cu-Nb ribbons with Fe content greater than 80 at%, it was confirmed that the addition of C atoms helps to form an amorphous structure and Nb atoms inhibit the grain growth of α-Fe grains during crystallization [2]. However, a high Nb content was required to suppress the growth of grains below 20 nm, resulting in the reduction of the M_S. This indicates that Nb atoms cannot be effective enough to suppress the growth of α-Fe grains. To understand the effects of these adding elements on the crystallization, TEM and APT were used to measure the compositional distribution in five nanocrystalline ribbons with different compositions shown in Table 1. We particularly focused on the correlation between Si and Nb atoms. Fig. 1 shows the APT compositional mapping results of each elements in annealed specimen (e). Crystalline and amorphous regions can be distinguished by the differences in the Fe and B concentration. This indicates that B atoms diffuse from primary α-Fe grains and accumulate in the amorphous region. In addition, Cu clusters are found in the amorphous region and increase the Fe concentration at the Cu-amorphous interface, promoting α-Fe grain formation. The Nb concentration increases at the interfaces between crystal and amorphous regions. However, this segregation behaviors were observed to be dependent on the Si concentration. This paper will show changes in magnetic properties by the addition of Si and Nb atoms in nanocrystalline ribbons and discuss the microstructural explanation of the grain growth mechanism.

[1] K. Lee, M. Choi, G. Lee, M. Kim and J. Kim, "Changes in microstructure and magnetic properties of Fe–B–Cu–C ribbons according to annealing conditions," *IEEE Transactions on Magnetics*, vol. 55, no. 2, pp. 1-4, 2019. [2] K. Lee, J. Ahn and J. Kim, "Compositional effect on the magnetic and microstructural properties of Fe-based nano-crystalline alloys," *IEEE Transactions on Magnetics*, vol. 58, no. 2, pp. 1-4, 2022.

	Composition (at%)	T_{x1} (°C)	T_{x2} (°C)	ΔT_x (°C)	Ref.
(a)	$Fe_{84.3}B_{13.7}C_1Cu_1$	390	475	85	[3]
(b)	$Fe_{80}B_{12.5}C_1Cu_1Nb_{5.5}$	454	693	239	[2]
(c)	$Fe_{80}B_{12.5}C_4Cu_1Nb_{2.5}$	414	563	149	[2]
(d)	$Fe_{79.5}B_{12}Si_4Cu_1Nb_{2.5}Mo_1$	448	608	160	-
(e)	$Fe_{78}B_{10}Si_{8.5}Cu_1Nb_{2.5}$	457	624	167	-

Table. 1. Manufactured alloy ribbons composition

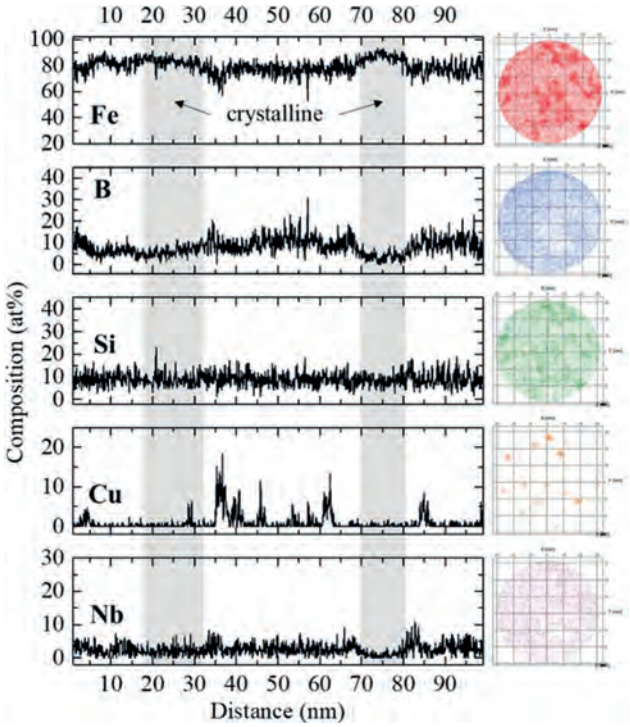

Fig. 1. Concentration profile of the annealed alloy ribbon, (e), using an APT

AR-12. Ferrite Magnetic Characteristic Simulation at Different Temperature with Recurrent Neural Network Model. H. Zhang[1], Q. Yang[2], *C. Zhang*[1], Y. Li[1] and Y. Chen[1] *1. Electrical Engineering, Hebei University of Technology, Tianjin, China; 2. Electronic Engineering, Tianjin University of Technology, Tianjin, China*

Ferrite is a widely applied magnetic core material in transformers and inductors. It exhibits strong temperature-dependence, with significant differences in loss under various temperature conditions[1-2]. Therefore, it is necessary to establish an accurate hysteresis model that takes into consideration the effects of temperature. In this paper, an improved Recurrent Neural Network model based on the Play hysteresis operator has been proposed, which is able to predict the hysteresis loops of ferromagnetic materials at different temperatures. The results demonstrated that the modified model has the benefits of high identification accuracy, fast convergence speed and extensively applicable. In order to evaluate the influence of temperature on the magnetic properties of ferrite, the ring sample has been adopted to measure the hysteresis loop of ferrite manufactured by Tokyo Denkikagaku Kogyo (TDK) from room temperature (25°C) to 120°C. The sample at different temperatures have reached the saturation magnetization state under the given excitation conditions. All hysteresis loops under the temperature of 25°C and 50°C were selected to constitute the training set of the neural network for material feature extraction. In order to determine whether the model is overfitting, the validation set of the model takes the measurement data at 75°C, while the experimental data at 100°C and 120°C were used as the test set to test the validation of the model. Fig.1 shows the schematic of the improved recurrent neural network. The improved model adopts the Mean Squared Error Loss (MSELoss) as the assessment benchmark. The MSELoss between predicted value and experimental value is 0.14% and 0.29% at 100°C and 120°C. Fig.2 shows a comparison between measured and predicted values of the ferrite at different magnetic flux densities at 100°C. Further results will be presented in the full paper. Moreover, these results suggest that the proposed model has significant scalability to various magnetic materials at different temperature, while it has the capacity to predict the magnetization characteristics at complex working conditions.

[1]Nouicer A, Nouicer E, Feliachi M. A neural network for incorporating the thermal effect on the magnetic hysteresis of the 3F3 material using the Jiles–Atherton model[J]. Journal of Magnetism and Magnetic Materials, 2015, 373: 240-243. [2]Savoie M, Shan J. Temperature-dependent asymmetric Prandtl-Ishlinskii hysteresis model for piezoelectric actuators[J]. Smart Materials and Structures, 2022, 31(5): 055022.

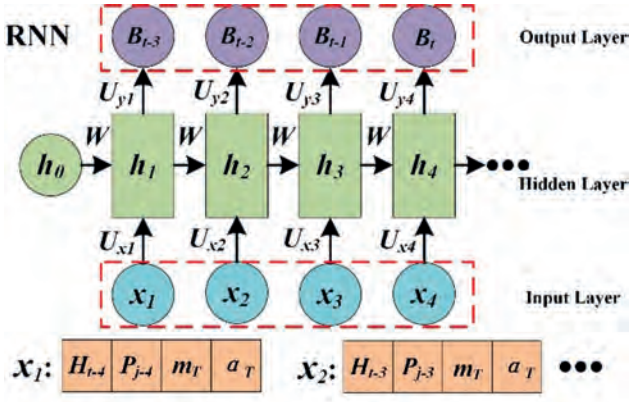

Schematic of the improved recurrent neural network

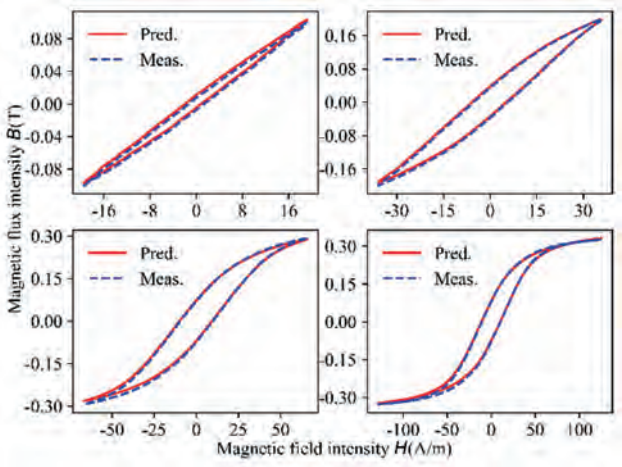

Comparison between Measured and Predicted Results at 100°C

Session AS
MULTI-FUNCTIONAL MAGNETIC MATERIALS AND APPLICATIONS I (Poster Session)

Thomas Feggeler, Co-Chair
Lawrence Berkeley National Laboratory, Berkeley, CA, United States
Hendrik Ohldag, Co-Chair
Lawrence Berkeley National Laboratory, Berkeley, CA, United States

AS-01. Anomalous Nernst effects in TbCo and GdCo alloys for heat flux sensing. *M. Odagiri*[1], H. Imaeda[1], S. Sumi[1], H. Awano[1] and K. Tanabe[1] *1. Toyota Technological Institute, Nagoya, Japan*

A heat flux sensor enables heat flux visualization unlike a temperature sensor. The commercialized heat flux sensor is based on the Seebeck effect and its price is very high. Recently, Zhou et al. have proposed a new heat flux sensor based on the anomalous Nernst effect (ANE)[1]. The ANE sensor has low cost and high flexibility due to being a film device. The sensitivity is generally evaluated as the ratio of the generated electric field to the heat flux density |E/j|, which is proportional to the transverse Seebeck coefficients S_{ANE} and inversely proportional to the thermal conductivity. Moreover, since the sensor needs a pair of two materials having positive and negative S_{ANE}, we should evaluate the sensitivity as the sum of the parameters in the two materials, $|E_+/j_+| + |E_-/j_-|$, where $E_+(E_-)$ and $j_+(j_-)$ are the electric field and heat flux density as $S_{ANE} > 0 (< 0)$, respectively. In this study, we have investigated the composition dependence of ANE in amorphas Gd(Tb)Co alloy films to improve the evaluation value. The Tb(Gd)Co films have some advantages of having positive and negative S_{ANE}, having low thermal conductivity. The sample structure is Si_3N_4(10 nm)/Gd_xCo_{1-x}(Tb_xCo_{1-x})(20 nm)/Si_3N(3 nm)/ glass sub. S_{ANE} was measured in the application of a perpendicular magnetic field and an in-plane thermal gradient(Fig. 1). $|S_{ANE}|$ increases with a slight doping of Gd(Tb) elements compared with that of pure Co. Moreover, the sign of S_{ANE} is changed at x = 0.22. Then, we estimated |E/j| in $Gd_{8.9}Co_{91.1}$ and $Gd_{23.7}Co_{76.3}$ alloy films. |E/j| was measured in the application of an in-plane magnetic field and a perpendicular heat flux. |E/j| in $Gd_{8.9}Co_{91.1}$ and $Gd_{23.7}Co_{76.3}$, and are 0.17 and 0.29 (μV/m)/(W/m^2), respectively. Consequently, if we fabricate a heat flux sensor using these materials, $|E_+/j_+| + |E_-/j_-| = 0.46$ μV/(W/m), which is almost 2 times larger than previous reports such as 0.20 μV/(W/m) in FeAl/Au[1] and 0.22 μV/(W/m) in SmCo/Au[2] even though $|S_{ANE}|$ in Gd(Tb)Co is smaller than those in FeAl and SmCo. Our results indicate that the sign of $|S_{ANE}|$ and the thermal conductivity play an important role in developing a heat flux sensor.

[1] W. Zhou and Y. Sakuraba, Appl. Phys. Express 13 (2020) 043001. [2] R. Modak et al., Sci. Technol. Adv. Mater., 23 (2022) 768.

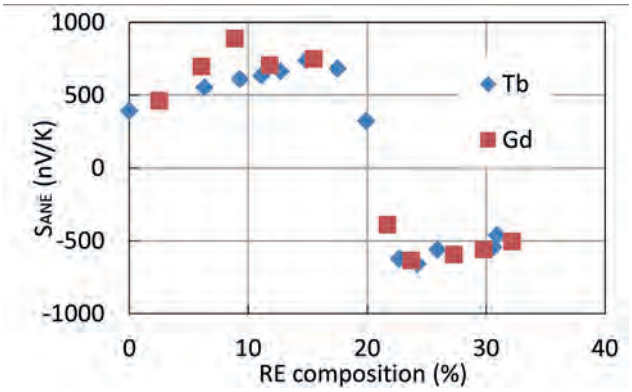

Composition dependence of S_{ANE}

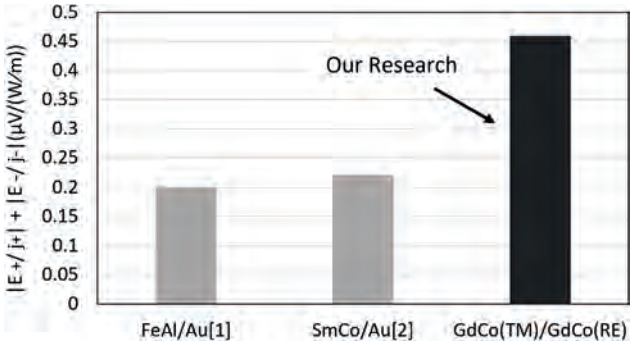

Comparison of sensitivity with previous studies

AS-02. Magnetic and magnetocaloric properties of $GdZn_{1-y}Ga_y$ (y= 0-0.2). A. Biswas[1], T. Del Rose[1] and *Y. Mudryk*[1] *1. Ames National Laboratory, Iowa State University, Ames, IA, United States*

The equiatomic RX (R= heavy rare-earth, X= elements of IB, IIB, IIIA groups) compounds exhibit strong variations in magnetic exchange interactions across the series and, depending on X, show clear dependence between the number of conduction electrons and type of magnetic ordering. For this reason, in addition to considerable research focused on the binary RX intermetallics, solid solutions of $RX'_{1-y}X''_y$ type, where X′ and X″ belong to different groups in the periodic table yet share a single crystallographic X-site, are interesting to explore with regard to such dependence. Our present work focuses on a series of such alloys, $GdZn_{1-y}Ga_y$ (y=0-0.2), in which Zn and Ga belong to two different groups: IIB and IIA, respectively. Our structural, magnetic, and magnetocaloric experimental study corroborates the earlier density functional theory calculation results,[1] confirming that substitution of Ga on the Zn site hardly affects the CsCl-type crystal symmetry and lattice parameters but drastically reduces the magnetic transition temperature. We also determined that all samples exhibit an appreciable magnetocaloric effect at their corresponding magnetic transition temperatures. From the comprehensive analysis of the magnetocaloric data, and with the evaluation of critical exponents we explicate the precise impact of introducing a IIIA element in the IIB element site for this series of compounds. Acknowledgement: This work was performed at Ames National Laboratory and was supported by the Division of Materials Science and Engineering of the Office of Basic Energy Sciences, Office of Science of the U.S. Department of Energy (DOE). Ames National Laboratory is operated for the U.S DOE by Iowa State University under Contract No. DE-AC02-07CH11358

1. L. Petit, Z. Szotek, D. Paudyal, A. Biswas, Y. Mudryk, V. K. Pecharsky, and J. B. Staunton, Physical Review B 101, 014409 (2020).

AS-03. Significant sensitivity improvement of a heat flux sensor based on anomalous Nernst effect by uneven structure. *H. Imaeda*[1], M. Odagiri[1], M. Sakamoto[1], S. Sumi[1], H. Awano[1] and K. Tanabe[1] *1. Toyota Technological Institute, Nagoya, Japan*

A heat flux sensor can visualize a heat flow unlike a temperature sensor, and is expected to be an elemental technique in thermal management technology. In particular, a heat flux sensor based on the anomalous Nernst effect (ANE) [1] is expected to be significantly cheaper and more flexible than a conventional one based on the Seebeck effect [2]. To improve the sensitivity of a heat flux sensor, the thermal electromotive force V_{ANE} must be increased. Although the sensitivity is improved by the enhancement of a thermopower in the viewpoint of material search in previous studies, the improvement rate is not so large. Here, we have investigated the significant sensitivity improvement by structural optimization using nanoimprint lithography. First, we performed the thermal simulation about the relationship between heat flows and temperature gradients in magnetic wires with varying heights and widths of the wires. The results show that the temperature gradients in the magnetic wires are proportional to the aspect ratio of the height to the width even though an applied heat flow is constant, suggesting that an ultrahigh-aspect-ratio wire is a suitable structure for realizing ultrahigh sensitivity. Next, we experimentally investigated the effect of the sample shape. We fabricated Co films on a plastic substrate with an uneven structure made by nanoimprint lithography. The Co films deposited on the side of the uneven structure can be regarded as an ultrahigh-aspect-ratio wire (Fig. 1). Figure 2 shows V_{ANE} the per heat flow j_h as a function of the height. The V_{ANE}/j_h increases with increasing height, which is roughly consistent with the simulation results. As a result, the voltage per heat flow [μV/(mW/m^2)] increased approximately 860 % higher than the flat substrate just by changing the sample structure. These results reveal the importance of the structural optimization to improve sensitivity.

[1] M. Mizuguchi et al., Sci. Tech. Adv. Mater. 20, 262 (2019). [2] W. Zhou and Y. Sakuraba, Appl. Phys. Express 13, 043001 (2020).

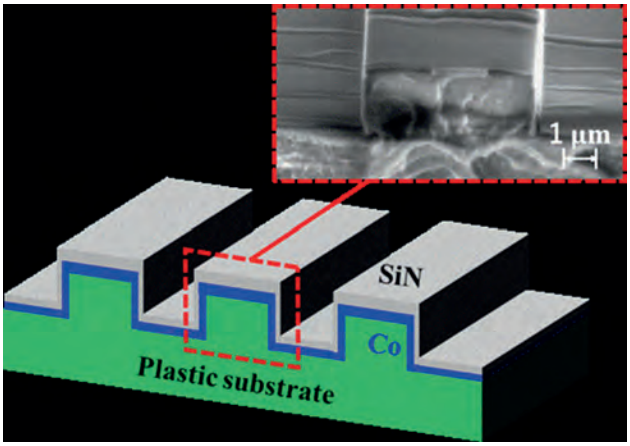

Schematic diagram of sample structure. The inset is an SEM image.

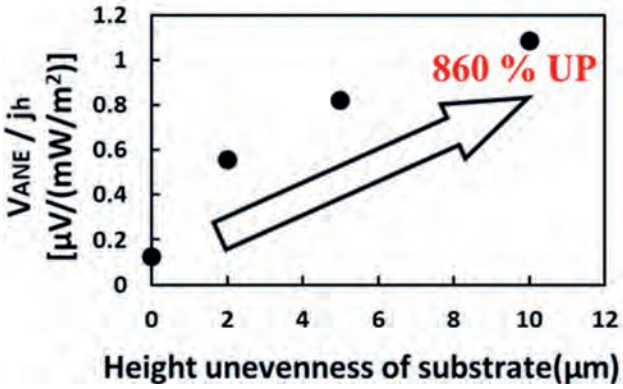

Relationship between uneven height and V_{ANE}/j_h

AS-04. Preparation, structural and magnetic properties of MnFePSi-based glass-coated microwires. M. Salaheldeen[1,2], *V. Zhukova*[1,3], M. Ipatov[1,3], A. Zhukov[1,3] and A. Wedeni[1,3] *1. Department of Polymers and Advanced Materials, Faculty of Chemistry, University of the Basque Country, UPV/EHU, San Sebastian, Spain; 2. Physics Department, Faculty of Science, Sohag University, Sohag, Egypt; 3. Department of Applied Physics, University of the Basque Country, UPV/EHU, San Sebastian, Spain*

Compared to the conventional vapour-compression refrigeration, magnetic refrigeration technology promises a 25% higher energy efficiency and does not use dangerous and environmentally unfriendly refrigerants such as ozone depleting chemicals (e.g., chlorofluorocarbons), hazardous chemicals (e.g., ammonia) or greenhouse gases (e.g., hydrofluorocarbons and hydrochlorofluorocarbons) [1,2]. This makes magnetic refrigeration one of the most promising technologies to replace vapour-compression refrigeration in the near future. There are several materials with a large MCE near room temperature [3]. Among all candidates for solid-state refrigerants, the $(Mn,Fe)_2(P,Si)$-based materials are among the most promising because they provide optimal conditions for practical applications (large MCE, low cost starting materials, and environmental benefits). The miniaturization of MCE devices based on small-size MCE particles, wires, ribbons, films, bi- and multilayers, pillars is quite important for future technological applications [4]. Therefore, fabrication of the $Mn,Fe)_2(P,Si)$-based materials thin wires from brittle MnFePSi alloy might be interesting from the point of view of application of MCE. Figure 1a presents the M(T) data of the as-prepared microwires for 0.05 T and their derivatives in the inset, showing the Curie temperature (T_C) of about 138 K. The magnetization and specific heat measurements are common methods for calculating the MCE performance of the materials. Here, isothermal magnetization curves were measured for determining the isothermal magnetic entropy change. Figure 1b presents the isothermal magnetic entropy change as a function of temperature for magnetic field change up to 5 T. This result indicates the possibility to prepare the magnetocaloric materials for magnetic refrigerators in the form of glass-covered microwires and showed that glass-coated microwires might be interesting for the MCE applications owing to high ratio of surface to volume.

[1] Smith, A., Bahl, C.R.H., Bjørk, R., Engelbrecht, K., Nielsen, K.K. and Pryds, N. “Materials Challenges for High Performance Magnetocaloric Refrigeration Devices”. Adv. Energy Mater., 2012 2: 1288-1318. [2] Franco, et al.” Magnetocaloric effect: From materials research to refrigeration devices. *Prog. Mater. Sci.* 2018, *93*, 112–232. [3] N. A. Zarkevich and V. I. Zverev, “Viable Materials with a Giant Magnetocaloric Effect,” *Crystals*, vol. 10, no. 9, p. 815, Sep. 2020, doi: 10.3390/cryst10090815. [4] Zhukov, A et al. “Advanced Functional Magnetic Microwires for Technological Applications.” *J. Phys. D Appl. Phys.* 2022, *55*, 253003. [5] L. Luo et al., “Enhanced Magnetocaloric Properties of Annealed Melt-Extracted Mn1.3Fe0.6P0.5Si0.5 Microwires,” Metals, vol. 12, no. 9, p. 1536, Sep. 2022, doi: 10.3390/met12091536.

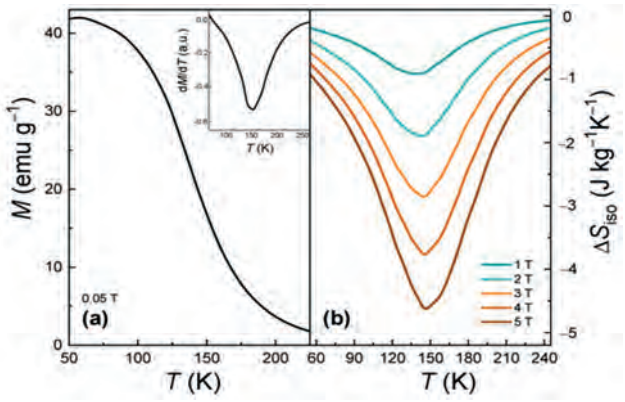

Temperature dependence of magnetization at 0.05 T and its derivatives in the inset (a) and Isothermal magnetic entropy change as a function of temperature for different magnetic field changes (b)

AS-05. Magnetic and magnetocaloric properties of the multi-component $Mn_{0.5}Fe_{0.5}Ni_{0.95}Cr_{0.05}Si_{0.95}Al_{0.05}$ intermetallic compound. *A. Bhatta*[1], J.F. Casey[2], S. Bhattacharjee[1], A. Pathak[2,3] and M. Khan[1] *1. Physics, Miami University, Oxford, OH, United States; 2. Physics, SUNY Buffalo State University, Buffalo, NY, United States; 3. GE Research, Niskayuna, NY, United States*

A selected group of solid-state materials are known to exhibit first-order phase transition where their magnetic and crystalline properties change simultaneously. This coupled phase transition is of strong interest due to the numerous functional properties associated with them. The magnetocaloric effect is one such property that can be exploited in energy-efficient magnetic refrigeration technology. Here we present an experimental study on the first-order phase transition and associated magnetocaloric properties of $Mn_{0.5}Fe_{0.5}Ni_{0.95}Cr_{0.05}Si_{0.95}Al_{0.05}$. The material is related to the $Mn_{1-x}Fe_{x-\delta}Ni_{\delta}Si_{1-y}Al_y$ family whose phase transition temperatures are tunable [1, 2]. X-ray diffraction data for the sample showed that both the orthorhombic and hexagonal crystalline phases coexist at room temperature. The first-order phase transition was observed at ~325 K during heating and at ~306 K during cooling, showing a thermomagnetic hysteresis of ~19 K. The entropy changes evaluated from the isothermal magnetization data peaked at 321 K during warming and at 312 K during cooling, showing a thermomagnetic hysteresis of ~9 K. Peak entropy changes of -16 J kg^{-1} K^{-1} and -42 J kg^{-1} K^{-1} were observed on heating for field changes of 20 kOe and 50 kOe, respectively. The associated refrigeration capacities were 74 J/kg and 194 J/kg. The experimental results and related discussion of this study will be presented.

[1] A. Biswas, A.K. Pathak, N.A. Zarkevich, X. Liu, Y. Mudryk, V. Balema, D.D. Johnson, and V.K. Pecharsky, Acta Mater. 180, 341 (2019). [2] Jacob Casey, Babajide Akintunde, Ranjit Chandra Das, Christopher Hanley, Brandon Reese, Mahmud Khan, Arjun K. Pathak, J. Magn. Magn. Mater. 579, 170862 (2023).

AS-06. New measurement method and instrument for direct measurement of the adiabatic temperature change to enable magnetic refrigeration. *B. Bosch-Santos*[1], C.F. Amigo[1], S.W. Young[1], R. Shull[1], J. Wu[1], M. Kedzierski[1] and C. Dennis[1] *1. National Institute of Standards and Technology, Gaithersburg, MD, United States*

Magnetic refrigeration based on the magnetocaloric effect has the potential to significantly improve energy efficiency of existing vapor-compression-based temperature control systems, while being environmentally benign. However, the existing measurement methods, direct (adiabatic temperature changes under magnetization/demagnetization) and indirect (heat capacity or isothermal magnetization measurements), have large uncertainties (30% or more) and a large discrepancy in values. For example, the adiabatic temperature change for gadolinium varies between 3.9 K to 5.8 K using a field change of about 2 T. To progress, this technology requires a clear connection between the properties of the magneto-caloric materials (MCMs) and their performance in the magnetic refrigeration cycle. Therefore, we are proposing a new instrument and measurement method to directly measure the refrigeration capacity of MCMs with acceptable uncertainties: a pressure-energy rig that uses the incompressibility of a fluid as an amplifier to increase the sensitivity of the measurement. In this method, a chamber is moved into/out of an applied magnetic field (Fig. 1). The sample chamber is made of pure diamagnetic glass to eliminate eddy current heating and minimize changes to the magnetic field seen by the sample, and is surrounded by a (high) vacuum jacket to make the chamber quasi-adiabatic. A glass “fence” is in the center of the sample chamber to hold the sample stationary while the actuator is operating, but maintains good thermal contact with the surrounding fluid. The sample surface, sample center, and chamber walls have their temperatures monitored to measure heat in/from the sample. A non-magnetic pressure sensor measures the pressure change in the fluid around the sample, and it can also be used to verify the maximum sample temperature change. The measurement technique is calibrated by comparison with the sample temperature rise from the injection of a known amount of heat, provided by a known applied current to a heater of known resistance located in the center of the sample. Preliminary results for Gd at room temperature are 2.5 K for a 1 T field change.

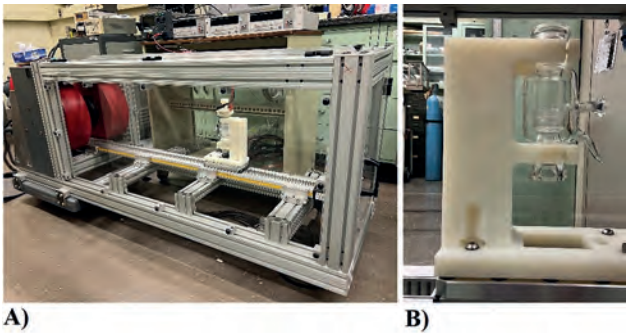

Fig. 1 - (a) Picture of the apparatus with (b) close-up of the chamber.

Session BA
RARE-EARTH SPINTRONICS

Alejandro O. Leon, Chair
Metropolitan University of Technology, Santiago, Chile

INVITED PAPERS

BA-01. Rare earth site occupancy: a path to designing anisotropy, compensation, and interfacial properties of ferrimagnetic iron garnets. *C.A. Ross[1] 1. Massachusetts Institute of Technology, Cambridge, MA, United States*

Magnetic garnet thin films provide unique functionality in spintronic, magnonic, and magnetooptical devices including magnetic memory, magnetic logic, and photonic integrated circuits. Yttrium iron garnet is the exemplary low-damping ferrimagnetic insulator, but replacement of Y with rare earths provides control over a wide range of properties. We will focus on the role of the RE site occupancy in determining the anisotropy, magnetization, compensation temperatures, and interface behavior of RE iron garnets (REIGs), both experimentally and through molecular field coefficient modeling. Bulk garnets have RE:Fe = 3:5, but epitaxy can stabilize nonstoichiometric compositions, for example in Tb-rich TbIG, excess Tb occupies octahedral sites driving the compensation temperature 90K higher and the Curie temperature 40K lower than bulk. A Dzyaloshinskii-Moriya interaction originating at the REIG/substrate interface is present in TbIG and TmIG films, yielding homochiral domain walls and enabling field-free high speed domain wall motion driven by spin orbit torques from a current in an adjacent Pt layer. In Sc-substituted TbIG/Pt, the spin mixing conductance of the garnet/Pt interface scales with the net Fe moment, but in DyIG/Pt, the proximity magnetism in the Pt layer is proportional to the net REIG moment. In EuIG, SmIG and TmIG (110)-oriented films, surface and interface anisotropies contribute to a thickness-dependent magnetic reorientation, and in EuIG an easy plane can be engineered perpendicular to the substrate plane, allowing out-of-plane magnetization rotation. Mixed REIGs such as EuTmIG exhibit ordering of the RE on non-equivalent dodecahedral sites, leading to a strong growth-induced anisotropy that yields a perpendicular easy axis even in unstrained films. Finally, we describe the structure and unusual properties of epitaxial TmIG/TbIG superlattices with layer thickness lower than one unit cell. The selection of RE element and site occupancy therefore gives extensive control over the anisotropy landscape, magnetization, spintronic, magnetooptical and interfacial properties of REIGs.

BA-02. 4f Local Moments in Spintronics. *G. Bauer[1,2] 1. AIMR, Tohoku University, Sendai, Japan; 2. KITS, UCAS, Beijing, China*

4f local moments are found in the lanthanides (except for lanthanum and lutetium with empty and full subshells). Gadolinium has a stable half-filled subshell with spin S=7 and orbital moment L=0. In all others, the spin-orbit interaction couples the L and S local momenta to a total J=L+S. Magnets containing 4f local moments are important for many applications [1]. However, since the 4f-orbitals are strongly localized to the nuclei, their use for the coupled spin and charge transport essential in spintronics, is not so obvious. An important material class is formed by the electrically insulating ferrimagnetic iron garnets (IG's) in which the dodecahedral sites are occupied by rare-earth ions. The competition between the rare earth and iron magnetic moments leads to the vanishing of the total angular momentum and magnetization at certain compensation temperatures [1]. The magnetization dynamics around the compensation points attracted much recent attention and will be addressed by other speakers in this symposium. On the other hand, the spin-orbit interaction that conduction electrons in metals and spin waves in ferromagnets experience when scattering at local moments formed by open 4f shells appears to have not yet been systematically studied. In this talk, I address spintronic effects associated with 4f local moments such as the spin Seebeck effect [2] and spin Hall magnetoresistance [3] of GdIG as well as the interface anisotropy and the equilibrium and non-equilibrium currents induced by 4f impurities in metals and at interfaces to metals [4-6].

[1] R. Skomski and J. M. D. Coey, Permanent Magnetism (Taylor & Francis, New York, 1999). [2] S. Geprägs et al., Nat. Commun. 7, 10452 (2016). [3] K. Ganzhorn et al., Phys. Rev. B 94, 094401 (2016). [4] A. O. Leon, A. B. Cahaya, G. E. W. Bauer; PRL 120, 027201 (2018). [5] A. O. Leon and G. E. W. Bauer, J. Phys.: Condens. Matter 32, 404004 (2020) [6] A.B. Cahaya et al., Phys. Rev. B 103, 064433 (2021).

BA-03. Compensated ferrimagnets for unconventional spintronics. *W. Jiang[1] 1. Physics Department, Tsinghua University, Beijing, China*

Compensated ferrimagnets with perpendicular-magnetic anisotropy, fast spin dynamics controlled by spin-orbit torques, and the ability to display topological spin textures are highly desirable for spintronic applications. This presentation demonstrates that rare-earth transition-metal compounds possess those attributes [1-3]. For example, we reveal the microscopic origin of the perpendicular anisotropy and interfacial Dzyaloshinskii-Moriya interaction in this rare-earth (RE)-based system [1]. Furthermore, the magnetization of multilayers containing FeTb and $SmCo_5$ can be efficiently switched by spin-orbit torque and exhibit skyrmion and skyrmionium-like spin textures [2,3]. Finally, we show that the rare-earth concentration in FeTb compounds controls the skyrmion size and density, as well as the anisotropy and magnetization of the material, pathing the way to tailor-made topological textures [4,5]. In the end, I will discuss the effective manipulation of magnetization compensation temperature by external means, together with the device realization by integrating with giant magnetoresistance and tunneling magnetoresistance.

[1] T. Xu et al., "Evolution of Compensated Magnetism and Spin-Torque Switching in Ferrimagnetic $Fe_{1-x}Tb_x$," Phys. Rev. Appl. 19, 034088 (2023). [2] T. Xu et al., et al., "Imaging the spin chirality of ferrimagnetic Néel skyrmions stabilized on topological antiferromagnetic Mn_3Sn," Physical Review Materials 5, 084406 (2021). [3] H.-A. Zhou et al., "Rare-Earth Permanent Magnet $SmCo_5$ for Chiral Interfacial Spin-Orbitronics," Adv. Funct. Mater. 31, 2104426 (2021). [4] T. Xu et al., "Systematic Control of Ferrimagnetic Skyrmions via Composition Modulation in Pt/$Fe_{1-x}Tb_x$/Ta Multilayers," ACS Nano 17, 7920 (2023)." [3] H.-A. Zhou et al., "Efficient Spintronics with Fully Compensated Ferrimagnets," Journal of the Physical Society of Japan 90 (8), 081006 (2021).

BA-04. Magnon transport and topological magnetic textures in rare-earth magnetic insulators. *S. Velez[1] 1. Universidad Autonoma de Madrid, Madrid, Spain*

Magnetic insulators, such as rare earth garnets ($R_3Fe_5O_{12}$; R=Y, Tm,.), have attracted a lot of interest because of their low Gilbert damping and high-frequency dynamics. Interestingly, unlike charge currents, spin currents can

couple and propagate through MIs, making possible to realize spintronic devices based on these materials. In this talk, we will discuss how we can exploit the charge to spin conversion phenomena in heavy metals for electrically injecting and detecting magnons carrying spin information [1-3] and for stabilizing and driving topological magnetic textures (Néel chiral domain walls and skyrmions) in thin film garnets [4,5]. We will discuss the key role of antisymmetric chiral interactions on the emergence of non-reciprocal phenomena in both magnon transport [3] and the dynamics of magnetic textures [4,5]. We will see that the performance of garnet devices is better than their metallic counterparts and demonstrate novel device functionalities enabled by chirality that could be exploited in future memory and spin-logic applications.

[1] J. M. Gómez-Pérez et al. Phys. Rev. B 101, 184420 (2019). [2] R. Schlitz and S. Vélez et al. Phys. Rev. Lett. 126, 257201 (2021). [3] J. Gao et al., Phys. Rev. Res. 4, 043214 (2022). [4] S. Vélez et al., Nat. Comm. 10, 4750 (2019). [5] S. Vélez et al., Nat. Nanotech. 17, 834 (2022). *email: saul.velez@uam.es

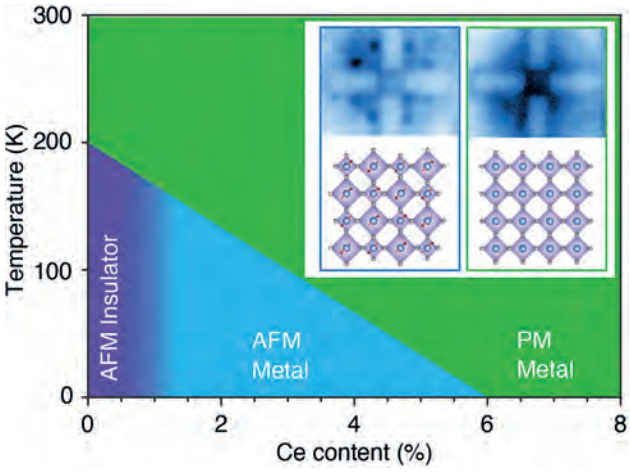

BA-05. Antiferromagnetic Metal Phase and Memory Behavior in a Rare-Earth Nickelate. *S. Doyle*[1], Q. Song[2], G.A. Pan[1], I. El Baggari[3], D. Ferenc Segedin[1], D. Córdova Carrizales[1], J. Nordlander[1], C. Tzschaschel[4], S. Xu[4], P. Shafer[5], L. Moreschini[6,7] and J. Mundy[1] *1. Physics, Harvard University, Cambridge, MA, United States; 2. Cornell University, Ithaca, NY, United States; 3. The Rowland Institute at Harvard, Harvard University, Cambridge, MA, United States; 4. Chemistry and Chemical Biology, Harvard University, Cambridge, MA, United States; 5. Lawrence Berkeley National Laboratory, Advanced Light Source, Berkeley, CA, United States; 6. Physics, University of California, Berkeley, Berkeley, CA, United States; 7. Materials Science Division, Lawrence Berkeley National Laboratory, Berkeley, CA, United States*

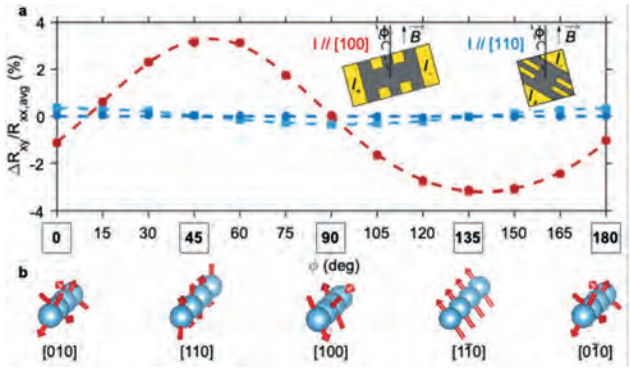

Antiferromagnetic materials emerged as promising candidates for spintronic devices due to their insensitivity to external fields and potential for high-speed switching. Recent work in spin orbitronics has identified ways to electrically control and probe the spins in metallic antiferromagnets, with particularly novel mechanisms present in noncollinear or noncentrosymmetric spin structures. Here we begin with a well characterized noncollinear antiferromagnet, the rare earth nickelate NdNiO3. In this compound, the onset of antiferromagnetic ordering is concomitant with a transition to an insulating state. We find that for low electron doping, however, the noncollinear magnetic order on the nickel site is preserved while electronically a new metallic phase is induced. We show that this new metallic phase has a distinctive fermiology, where most of the Fermi surface is gapped by the electronic reconstruction driven by the bond disproportionation. Furthermore, we demonstrate the ability to write to and read from the spin structure via a large zero-field planar Hall effect. Our results expand the already rich phase diagram of the rare-earth nickelates and open the door to creative spintronics applications in this family of correlated oxides.

Song, Q., Doyle, S., Pan, G.A. *et al.* Antiferromagnetic metal phase in an electron-doped rare-earth nickelate. *Nat. Phys.* 19, 522–528 (2023).

Session BB
NEUROMORPHIC COMPUTING II

Jayasimha Atulasimha, Co-Chair
Virginia Commonwealth University, Richmond, VA, United States
Joseph S. Friedman, Co-Chair
The University of Texas at Dallas, Richardson, TX, United States

INVITED PAPER

BB-01. Perpendicular Magnetic-Tunnel-Junction Nanopillars for True Random Number Generation. *L. Rehm*[1], M. Morshed[2], C.C. Capriata[3], S. Misra[4], J. Smith[4], M. Pinarbasi[5], A.W. Ghosh[2], B.G. Malm[3] and A.D. Kent[1] *1. Center for Quantum Phenomena, Department of Physics, New York University, New York, NY, United States; 2. Department of Electrical and Computer Engineering, University of Virginia, Charlottesville, VA, United States; 3. Division of Electronics and Embedded Systems, KTH Royal Institute of Technology, Stockholm, Sweden; 4. Sandia National Laboratories, Albuquerque, NM, United States; 5. Spin Memory Inc., Fremont, CA, United States*

True random number generators are of great interest for many applications such as cryptography, neuromorphic systems, Monte Carlo simulations, and more recently stochastic computing[1]. Different nanomagnetic devices such as superparamagnetic tunnel junctions[2], spin-orbit-torque-driven devices[3], and high-energy barrier tunnel junctions operated in the thermally assisted regime[4] have been studied for such applications. While they show promise, they exhibit strong sensitivities to environmental variations such as the temperature as well as process-related variations. We investigate the spin-transfer-torque-driven reversal of perpendicularly magnetized magnetic tunnel junction (pMTJ) nanopillars operated in the ballistic switching limit (nanosecond duration pulses) and find that these devices have great potential as true random number generators due to their reduced sensitivity to temperature variations compared to the same device operated with longer pulses (Fig. 1). We denote this a stochastic magnetic actuated random transducer (SMART) device because the applied pulse is activating the junction to generate a random bit, much like a coin flip[5,6]. Here the state of the junction in this ballistic limit is random mainly because of the thermal distribution of the initial magnetization state. We show that the experimentally obtained switching probability p characteristics of our SMART devices can be well described by a macrospin model, in which the related temperature sensitivity ($\mathrm{d}p/\mathrm{d}T$ for <ns duration pulses, see Fig. 1) only depends on the temperature and is independent of other material and device parameters. We also find that our SMART devices with a thermal stability factor $\Delta = 39$ are much less sensitive to variation in the pulse amplitude and process-related parameters, but more susceptible to variation in the write pulse duration compared to their operation in the thermally assisted regime. While operating our SMART devices at a switching probability of 0.5 (Fig. 2), we explore their stochastic nature by comparing their statistics to Bernoulli trials and show that we can successfully sample a uniform distribution[5], which is commonly used in computations that require random numbers. We determine the quality of the stochasticity of the SMART bitstreams using multiple statistical test such as the NIST test for random and pseudo random number generators for cryptographic applications and find that we pass all the tests after one XOR operation. Our results demonstrate that SMART devices are a great candidate for true random number generation due to their easily controllable characteristics, while being relatively robust towards most environmental changes. Funding: We acknowledge support from the DOE Office of Science (ASCR/BES) Microelectronics Co-Design project COINFLIPS.

[1]S. Misra *et al*., Advanced Materials 2022, 2204569 (2022) [2]K. Hayakawa *et al*., Physical Review Letters 126, 117202 (2021) [3]Y. Kim, X. Fong and K. Roy, IEEE Magnetics Letters, vol. 6, pp. 1-4 (2015) [4]A. Fukushima *et al*., Applied Physics Express 7, 083001 (2014) [5]L. Rehm *et al*., Applied Physics Letters 19 (2), 024035 (2023) [6]A. Shukla *et al*., 2023 24th International Symposium on Quality Electronic Design (ISQED), San Francisco, CA, USA, pp. 1-10 (2023)

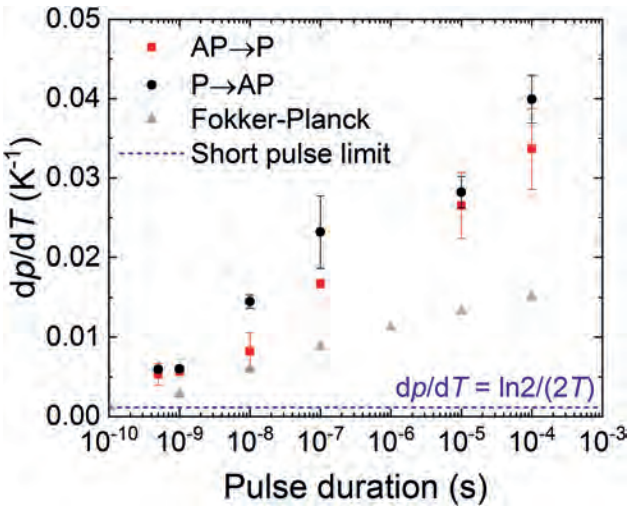

Fig. 1: Temperature sensitivity of the switching probability around p = 0.5 as a function of the applied write pulse duration at room temperature. An analytic macrospin model and Fokker-Planck analysis show that $\mathrm{d}p/\mathrm{d}T$ has a limiting value of $\mathrm{d}p/\mathrm{d}T = \ln 2/(2T)$ for pulse durations less than ~1ns.

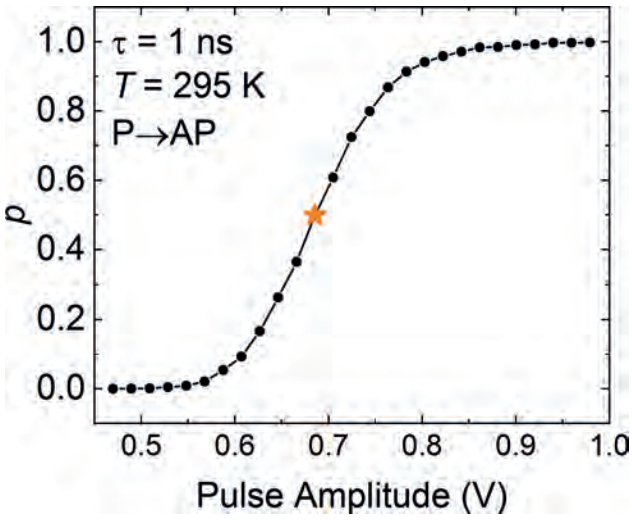

Fig. 2: SMART device characteristics. Switching probability *p* as a function of pulse amplitude of a 40 nm pMTJ at room temperature with pulse duration of 1 ns. Each point in the plot represents 10,000 switching attempts. SMART devices are operated at or near *p* = 0.5, indicated by the orange star.

CONTRIBUTED PAPERS

BB-02. Performance of Domain Wall-Magnetic Tunnel Junction Neuromorphic Computing Devices under Electron Beam and Heavy Ion Irradiation. *T. Leonard*[1], C. Bennett[2], T.P. Xiao[2], D. Hughart[2] and J.C. Incorvia[1] *1. UT Austin, Austin, TX, United States; 2. Sandia National Laboratories, Albuquerque, NM, United States*

Edge computing in space is a domain where new materials can make near-term impact, as CMOS suffers from radiation errors that are likely in space environments [1]. Contrarily, domain wall-magnetic tunnel junction (DW-MTJ) devices (Fig. 1) are radiation hard and can achieve neuromorphic behavior in a single device. These devices utilize domain wall (DW) motion to emulate neuromorphic behaviors such as integration, leaking, and multi-weight memory. We have shown that DW-MTJs can have highly tunable behavior depending on the geometry of the DW track and the MTJ [2]. However, DW-MTJs have not been experimentally demonstrated to be radiation hard to validate their potential for edge computing in space. While MTJs are known to be generally radiation-hard [3], the thin tunnel barrier within the MTJ can be degraded by high fluences of heavy ion irradiation. This has been investigated with continuous film stacks [4], but not in patterned DW-MTJ devices. Here we show DW-MTJ devices before and after two forms of irradiation. The performance of the devices is measured by the tunneling magnetoresistance (TMR) which can be used to determine the structural damage to the MTJ caused by radiation. The first experiment demonstrates the negligible effect electron beam (30 keV) total ionizing dose (TID) up to 200 Mrad had on these devices. Next, different devices were subjected to 2.2 MeV Ta heavy ion source. As displacements per atom (dpa) increases, TMR is reduced and eventually disappears as the tunnel barrier is degraded. Transmission electron microscopy (Fig. 2) and electron energy loss spectroscopy are performed on devices subjected to electron beam radiation and heavy ion irradiation to investigate the effects of displacement damage on the MTJ structure. In summary, DW-MTJ devices show high radiation hardness to both electron and displacement damage, but are not completely immune to displacement damage, defining the radiation window in which DW-MTJ devices can be used for edge computing in space. SNL is managed and operated by NTESS under DOE NNSA contract DE-NA0003525.

[1] V. Sharma & A. Rajawat. Review of Approaches for Radiation Hardened Combinational Logic in CMOS Silicon Technology. *IETE Tech. Rev. (Institution Electron. Telecommun. Eng. India)* 35, 562–573 (2018). [2] T. Leonard, S. Liu, M. Alamdar, H. Jin, C. Cui, O. G. Akinola, L. Xue, T. P. Xiao, J. S. Friedman, M. J. Marinella, C. H. Bennett & J. A. C. Incorvia. Shape-Dependent Multi-Weight Magnetic Artificial Synapses for Neuromorphic Computing. *Adv. Electron. Mater.* 8, 1–11 (2022). [3] E. A. Montoya, J. R. Chen, R. Ngelale, H. K. Lee, H. W. Tseng, L. Wan, E. Yang, P. Braganca, O. Boyraz, N. Bagherzadeh, M. Nilsson & I. N. Krivorotov. Immunity of nanoscale magnetic tunnel junctions with perpendicular magnetic anisotropy to ionizing radiation. *Sci. Rep.* 10, 1–8 (2020). [4] M. Alamdar, L. J. Chang, K. Jarvis, P. Kotula, C. Cui, R. Gearba-Dolocan, Y. Liu, E. Antunano, J. E. Manuel, G. Vizkelethy, L. Xue, R. Jacobs-Gedrim, C. H. Bennett, T. P. Xiao, D. Hughart, E. Bielejec, M. J. Marinella & J. A. C. Incorvia. Irradiation Effects on Perpendicular Anisotropy Spin-Orbit Torque Magnetic Tunnel Junctions. *IEEE Trans. Nucl. Sci.* 68, 665–670 (2021).

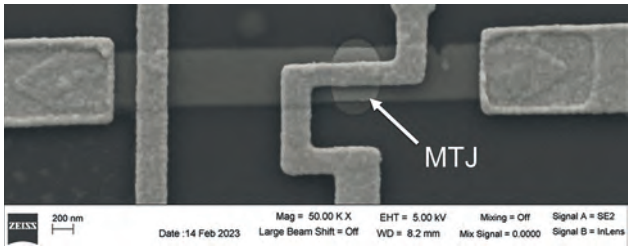

Fig. 1: SEM of representative device used in this study.

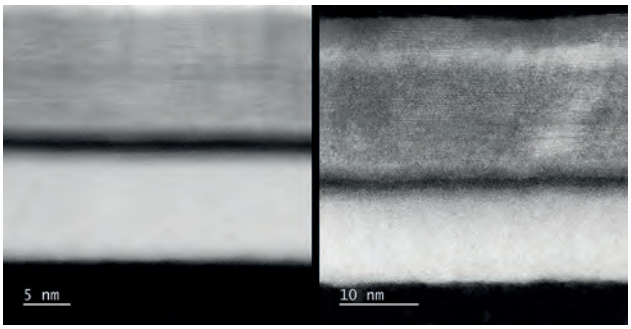

Fig. 2: TEM images showing pristine (left) and damaged (right) junctions.

BB-03. Switching Attempt Times of Superparamagnetic Tunnel Junctions as a Function of Diameter and Temperature. *H. Kaneko*[1,2], R. Ota[1,2], K. Kobayashi[1,2], S. Kanai[1,3], M. Elyasi[4,5], G. Bauer[4,6], H. Ohno[1,7] and S. Fukami[1,7] *1. RIEC, Tohoku Univ., Sendai, Japan; 2. Graduate School of Engineering, Tohoku Univ., Sendai, Japan; 3. National Institutes for Quantum Science and Technology, Takasaki, Japan; 4. WPI-AIMR, Tohoku Univ., Sendai, Japan; 5. IMR, Tohoku Univ., Sendai, Japan; 6. Kavli ITS, UCAS, Beijing, China; 7. CSIS, Tohoku Univ., Sendai, Japan*

Superparamagnetic tunnel junctions (s-MTJ) gather attention as critical building blocks for spintronic probabilistic computers [1-4]. The temperature dependence of the stochastic switching of the magnetization is an important design parameter that helps to gain insight into the microscopic mechanisms. Here we report stochastic switching of s-MTJs with various diameters D as a function of temperature T and discuss the underlying physics in terms of the attempt time $\tau_0(T)$ of the Arrhenius model. We fabricated a number of stacks, viz. buffer/ SyF/ Ta (0.2)/ CoFeB (1.0)/ MgO (1.1)/ CoFeB (1.5 or 1.8)/ cap (thickness in nm), deposited by sputtering and processed into circular MTJs with D of 20-100 nm. Both CoFeB layers have a perpendicular easy axis. The magnetization of the bottom CoFeB is fixed by the synthetic ferrimagnet (SyF), while that of the top CoFeB layer is designed to fluctuate at room temperature. We measure the rf transmitted voltage and the time-averaged (dc) resistance $\langle R \rangle$ of the s-MTJs at different T=20-130°C

and perpendicular magnetic fields H_z [Fig. 1]. Following Refs. [3, 5, 6], we derive $\tau_0(T)$ for six devices [Fig. 2]. We find that τ_0 increases with both T and D at a rate that is larger than expected for a macrospin. We attribute this discrepancy to spin-wave excitations: since the number of occupied spin wave modes increases with T and D, the stochastic torques on the magnetization also increase, thereby suppressing a full magnetization reversal. This work was supported in part by the JST-CREST Grant No. JPMJCR19K3, the JST-PRESTO Grant No. JPMJPR21B2, JST-AdCORP JPMJKB2305, JSPS Kakenhi Grant Nos. 19H05622, 19H00645, 19KK0130, 20H02178, and 21K13847. Shimadzu Research Foundation, Takano Research Foundation, GP-Spin at Tohoku University, and Cooperative Research Projects of RIEC.

[1] K. Y. Camsari *et al*., Phys. Rev. X 7, 031014 (2017). [2] W. A. Borders *et al*., Nature 573, 390 (2019). [3] K. Hayakawa *et al*., Phys. Rev. Lett. 126, 117202 (2021). [4] T. Funatsu *et al*., Nat. Commun. 13, 4079 (2022). [5] K. Kobayashi *et al*., Appl. Phys. Lett. 119, 132406 (2021). [6] W. F. Brown, Phys. Rev. 130, 1677 (1963).

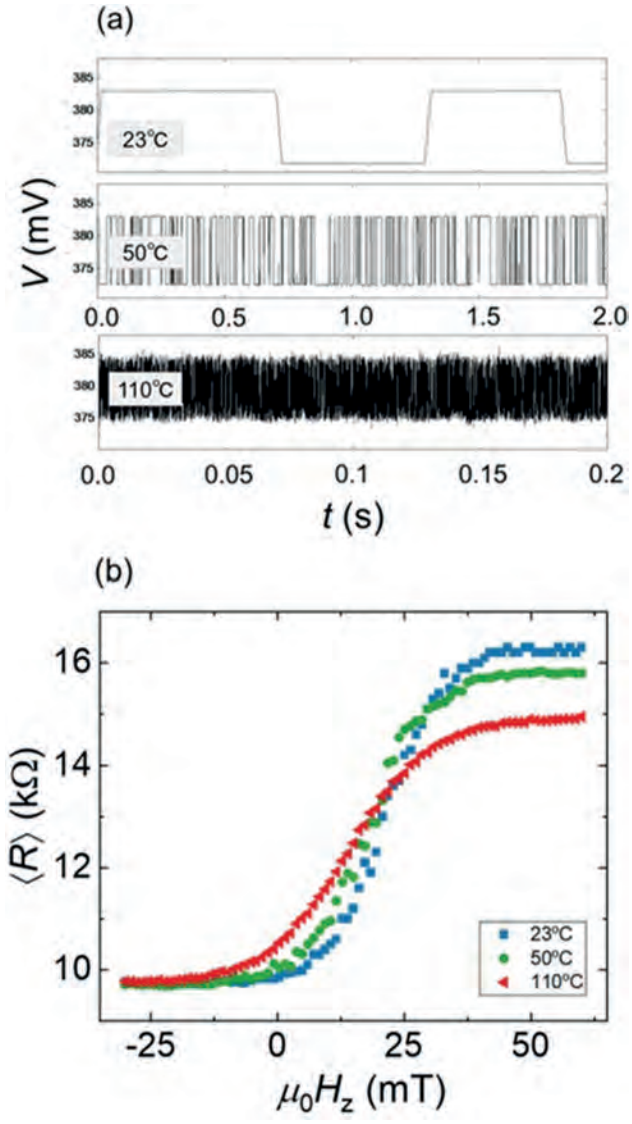

Fig. 1: (a) The rf transmitted voltage and (b) The time-averaged resistance $\langle R \rangle$ *vs.* H_z at three temperatures (T = 23, 50, 110 °C)

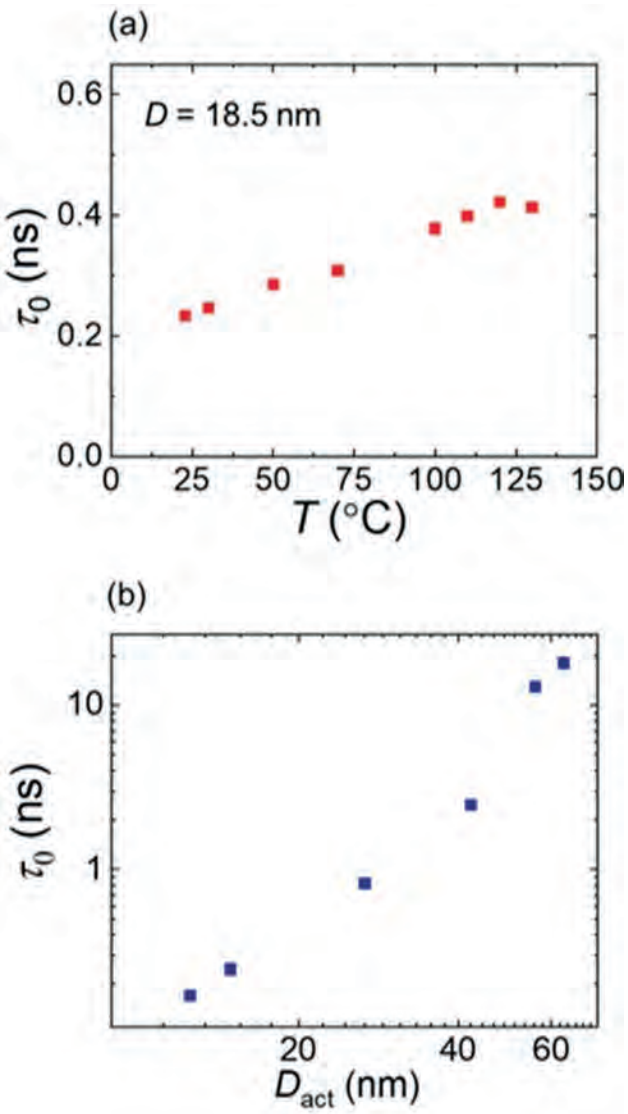

Fig. 2: (a)Temperature dependence of $\tau_0(T)$, (b)Diameter dependence of τ_0 (T = 30 °C)

BB-04. Magnetic Tunnel Junction Random Number Generators Applied to Dynamically Tuned Probability Trees Driven by Spin Orbit Torque. *A. Maicke*[1], S. Liu[1], J. Kwon[1], P.W. Bessler[1], J. Smith[2], J.B. Aimone[2], S. Misra[2], C.D. Schuman[3], S.G. Cardwell[2] and J.C. Incorvia[1]
1. University of Texas at Austin, Austin, TX, United States; 2. Sandia National Labs, Albuquerque, NM, United States; 3. University of Tennessee, Knoxville, Knoxville, TN, United States

Generating large amounts of random numbers on von Neumann machines can be prohibitively slow as data is transferred between logic and memory units. Further, the schemes which generate these numbers typically employ seeded mathematical functions where the output pseudorandom bitstream is in reality entirely deterministic. Instead, it is possible to leverage the inherent stochasticity of the thermally-driven magnetization dynamics of magnetic tunnel junction (MTJ) devices to both generate true random numbers and to generate them in-place [1-3]. Using an MTJ with perpendicular magnetic anisotropy (PMA), the probability of the magnetization state of a MTJ free layer to be up (1) or down (0) can be controlled via application of polarized spin-currents. Sampling the device at intervals gives a biased random bit sequence of 1's and 0's similar to a series of weighted coin flips. By changing the applied current between samples it is possible to adaptively bias the MTJ

'coin' to create more complex probability distribution functions (PDF) via a tree-structure (Fig. 1 [1]). However, when manufacturing MTJ devices there is no guarantee that a device will have precisely the intended design parameters [4]. It is thus uncertain that devices even from the same batch will identically sample the desired PDF. In particular, variations in either the parallel resistance (Rp) or TMR can affect the magnetization response to applied currents, or differences in anisotropy energy density (Ki) can change the degree of PMA. In this work, simulations are performed on 500 MTJ devices with varied TMR, Rp, and Ki with ranges based on data from manufactured STT-MRAM [4,5]. Each MTJ device samples 50,000 random numbers from an exponential distribution. Generated bitstream quality is evaluated via chi-squared fitting and quantified using p-values. It is found that devices perform well with realistic variations in TMR or Rp (Fig. 2), while variations in Ki can risk reducing the PMA too greatly and prevent recovery of the target PDF. SNL is managed and operated by NTESS under DOE NNSA contract DE-NA0003525

S. Misra, et al., Advanced Materials, art. no. 2204569 (2022) S. Liu, et al., IEEE Journal on Exploratory Solid-State Computational Devices and Circuits, vol. 8, p. 194-202 (2022) K. Y. Camsari, R. Faria, B. M. Sutton, and S. Datta, Physical Review X, vol. 7, no. 3, art. No. 031014, (2017) L. Xue, et al., 2018 IEEE Symposium on VLSI Technology, p. 117-118 (2018) L. Xue, A. Kontos, C. Lazik, S. Liang, M. Pakala, IEEE Transactions on Magnetics, vol. 51, no. 12, p. 1-3, (2015)

Fig. 1 Generating a random number using adaptively biased coins.

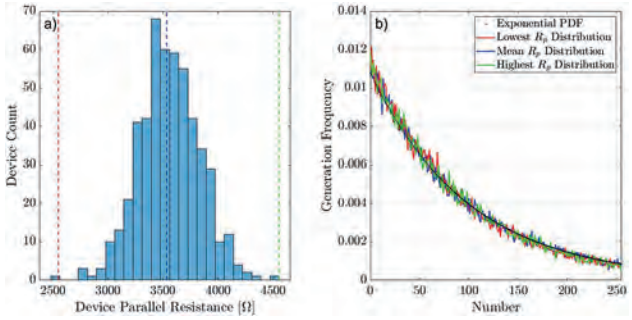

Fig 2 a) Rp distribution for simulated devices b) Observed PDF for select devices.

INVITED PAPER

BB-05. Probabilistic computing with voltage-controlled dynamics in magnetic tunnel junctions. *Y. Shao*[1], C. Duffee[1], E. Raimondo[2], N. Melendez[3], V. Lopez Dominguez[1], J. Katine[3], G. Finocchio[2] and P. Khalili Amiri[1] *1. Department of Electrical and Computer Engineering, Northwestern University, Evanston, Evanston, IL, United States; 2. Department of Mathematical and Computer Sciences, Physical Sciences and Earth Sciences, University of Messina, Messina, Italy; 3. Western Digital Corporation, San Jose, CA, United States*

Unconventional physics-based computing technologies are being widely studied, due to the limitations of existing solutions based on the von Neumann architecture in solving computationally hard problems[1]. Two examples of such problems are maximum satisfiability (MAX-SAT) and integer factorization, which have important applications in optimization and cryptography, respectively[2, 3]. To face larger instances of those problems, unconventional computing architectures are urgently needed. Probabilistic computing is a promising pathway to addressing this challenge[1, 4-11]. A key requirement for p-computing is the realization of fast, compact, and energy-efficient probabilistic bits. Stochastic magnetic tunnel junctions (MTJs) with low energy barriers, where the relative dwell time in each state is controlled by current, have been proposed as a candidate to implement p-bits. This approach presents challenges due to the need for precise control of a small energy barrier across large numbers of MTJs, and due to the need for an analog control signal. Here we demonstrate an alternative p-bit design based on perpendicular MTJs that uses the voltage-controlled magnetic anisotropy (VCMA) effect to create the random state of a p-bit on demand. The MTJs are stable (i.e., have large energy barriers) in the absence of voltage, and VCMA-induced dynamics are used to generate random numbers in less than 10 ns/bit. We then show a compact method of implementing p-bits by using VC-MTJs without a bias current. As a demonstration of the feasibility of the proposed p-bits and high quality of the generated random numbers, we solve up to 40-bit integer factorization problems using experimental bit-streams generated by VC-MTJs, as shown in Fig 1. Our proposal can impact the development of p-computers, both by supporting a fully spintronic implementation of a p-bit, and alternatively, by enabling true random number generation at low cost for ultralow-power and compact p-computers implemented in complementary metal-oxide semiconductor (CMOS) chips.

[1] G. Finocchio, M. Di Ventra, K. Y. Camsari, K. Everschor-Sitte, P. K. Amiri, and Z. Zeng, "The promise of spintronics for unconventional computing," *Journal of Magnetism and Magnetic Materials,* vol. 521, p. 167506, 2021. [2] N. Froleyks, M. Heule, M. Iser, M. Järvisalo, and M. Suda, "SAT competition 2020," *Artificial Intelligence,* vol. 301, p. 103572, 2021. [3] M. Mosca and S. R. Verschoor, "Factoring semi-primes with (quantum) SAT-solvers," *Scientific Reports,* vol. 12, no. 1, pp. 1-12, 2022. [4] W. A. Borders, A. Z. Pervaiz, S. Fukami, K. Y. Camsari, H. Ohno, and S. Datta, "Integer factorization using stochastic magnetic tunnel junctions," *Nature,* vol. 573, no. 7774, pp. 390-393, 2019. [5] N. A. Aadit *et al.*, "Massively parallel probabilistic computing with sparse Ising machines," *Nature Electronics,* pp. 1-9, 2022. [6] A. Grimaldi *et al.*, "Spintronics-compatible Approach to Solving Maximum-Satisfiability Problems with Probabilistic Computing, Invertible Logic, and Parallel Tempering," *Physical Review Applied,* vol. 17, no. 2, p. 024052, 2022. [7] B. Sutton, K. Y. Camsari, B. Behin-Aein, and S. Datta, "Intrinsic optimization using stochastic nanomagnets," *Scientific reports,* vol. 7, no. 1, pp. 1-9, 2017. [8] K. Y. Camsari *et al.*, "From charge to spin and spin to charge: Stochastic magnets for probabilistic switching," *Proceedings of the IEEE,* vol. 108, no. 8, pp. 1322-1337, 2020. [9] Y. Lv, R. P. Bloom, and J.-P. Wang, "Experimental demonstration of probabilistic spin logic by magnetic tunnel junctions," *IEEE Magnetics Letters,* vol. 10, pp. 1-5, 2019. [10] K. Y. Camsari, B. M. Sutton, and S. Datta, "P-bits for probabilistic spin logic," *Applied Physics Reviews,* vol. 6, no. 1, p. 011305, 2019. [11] J. Kaiser and S. Datta, "Probabilistic computing with p-bits," *Applied Physics Letters,* vol. 119, no. 15, p. 150503, 2021.

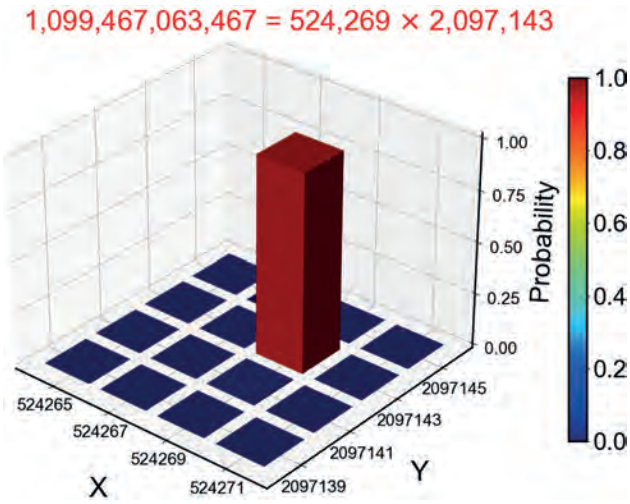

Fig. 1. Distribution for the probability of the input (X, Y) pair being at different combinations of numbers, when factorizing the semi-prime number 1,099,467,063,467.

CONTRIBUTED PAPERS

BB-06. Non-volatile binary radio-frequency synapses using vortex polarities. L. Mazza[2], *M. Menshawy*[1], V. Puliafito[2], M. Carpentieri[2], A. Jenkins[3], R. Ferreira[3], L. Benetti[3], A. Schulman[3], J. Grollier[1] and F.A. Mizrahi[1] *1. Unité Mixte de Physique, CNRS, Thales, Université Paris-Saclay, Palaiseau, France; 2. Politecnico di Bari, Bari, Italy; 3. International Iberian Nanotechnology Laboratory (INL), Braga, Portugal*

Spintronic devices have been identified as promising candidates for neuromorphic computing. Ross et al. [1] have demonstrated a fully spintronic neural network where magnetic tunnel junctions implement both neurons and synapses. In particular, magnetic junctions perform weighted sums – an operation at the core of neural networks – on radio-frequency (RF) signals, through the spin-diode effect. The synaptic weights are controlled by the resonance frequency of the devices. However, in [1], the control of the resonance frequency is volatile, which is an obstacle to building large artificial neural networks with low energy consumption. Here, we propose to implement non-volatile RF synapses using vortex-based magnetic tunnel junctions. In such a device, the free layer is in a vortex state which magnetic core is out-of-plane and can thus take two opposite directions, called polarities. We observe that each polarity has a different resonance frequency, leading to two synaptic weights of opposite signs. The polarity state is stable and thus the binary synapse is non-volatile. We control the polarity state (i.e. the weight) by sending an RF signal of large amplitude (about 1 mW). This leads the vortex to gyrate at a critical velocity where it reverses. We demonstrate that we can selectively program the synaptic weight be choosing the frequency of the RF signal. We connect magnetic tunnel junctions of different frequencies in series. The chain performs a weighted sum of RF inputs of different frequencies sent in parallel. Furthermore, leveraging the frequency-selectivity of the vortex polarity reversal, we can program each synapse by sending RF signals in the chain. This removes the need for individual accesses to the devices to program them. Our system uses frequency-multiplexing both to perform the weighted sum and to program the synaptic weights, which greatly simplifies the architecture and opens the path to scaling up the size of the network and the density of its connections. As binary neural networks can achieve high accuracy on state-of-the-art artificial intelligence tasks [2], these results open the path to large densely connected neural networks implemented in low energy consumption hardware.

[1] Ross, Andrew, et al. "Multilayer spintronic neural networks with radio-frequency connections." arXiv preprint arXiv:2211.03659 (2022). [2] Hubara, Itay, et al. "Binarized neural networks." Advances in neural information processing systems 29 (2016).

BB-07. Quantized Magnetic Domain Wall Synapse based Autoencoder for Efficient Unsupervised Learning. *M. Alam*[1], W. Misba[1] and J. Atulasimha[1,2] *1. Mechanical and Nuclear Engineering, Virginia Commonwealth University, Richmond, VA, United States; 2. Electrical and Computer Engineering, Virginia Commonwealth University, Richmond, VA, United States*

Autoencoders learn to effectively extract meaningful patterns and representations from unlabeled data through an encoder-decoder architecture in unsupervised learning manner. However, implementing them in edge devices that are capable of learning in real-time is extremely challenging due to limited hardware, computational resources, and energy. In this context, we propose a low resolution quantized magnetic domain wall (DW) synapse based autoencoder, designed to address these limitations. The proposed autoencoder model is evaluated based on anomaly detection task on NSL-KDD [1] data. Due to small on/off ratio of magnetic tunnel junctions (MTJs), which can be at most 7:1 at room temperature [2], current/voltage controlled DW devices that encode information in the resistance of MTJs have drawbacks including low resolution as well as stochastic nature [3]-[5]. Here, we simulate a notched DW device (Fig 1) for the proposed autoencoder synapses, where limited state (5-state) synaptic weights are controlled by spin orbit torque (SOT) current pulses on a magnetic racetrack in room temperature. Extensive micromagnetic simulations are performed to determine stochastic variations (Fig 2a) in each memory state of the DW device. Next, hardware-aware training of the autoencoder is performed, where the training algorithm is inspired by neural network training with low precision weights [6], [7]. While limited number of quantized states and the inherent stochastic nature of DW synaptic weights in nanoscale device is usually detrimental to training and testing accuracy, the hardware-aware training can leverage this imperfect device characteristics to generate a significant improvement in accuracy (90.7%) compared to accuracy (89.1%) obtained by floating point trained weights (Fig 2b). Therefore, with this approach, resource limited low energy autoencoders simulated with DW devices show improved performance. Acknowledgement: NSF grant ECCS: #1954589, CCI grant (award #VV-1Q23-008), and VCU Breakthrough.

[1] M. Tavallaee, E. Bagheri, W. Lu, and A. Ghorbani, "A Detailed Analysis of the KDD CUP 99 Data Set," *Submitted to Second IEEE Symposium on Computational Intelligence for Security and Defense Applications (CISDA)*, 2009. [2] S. Ikeda, J. Hayakawa, Y. Ashizawa, Y. M. Lee, K. Miura, H. Hasegawa, M. Tsunoda, F. Matsukura, and H. Ohno, "Tunnel magnetoresistance of 604% at 300K by suppression of Ta diffusion in CoFeB/MgO/CoFeB pseudo-spin-valves annealed at high temperature," Applied Physics Letters, 93(8), 2008. [3] X. Jiang, L. Thomas, R. Moriya, M. Hayashi, B. Bergman, C. Rettner, and S. S. Parkin, "Enhanced stochasticity of domain wall motion in magnetic racetracks due to dynamic pinning," Nature Communications, 1(1), pp. 1-5, 2010. [4] M. A. Azam, D. Bhattacharya, D. Querlioz, C. A. Ross and J. Atulasimha, "Voltage control of domain walls in magnetic nanowires for energy-efficient neuromorphic devices," *Nanotechnology*, *31*(14), p. 145201, 2020. [5] W. A. Misba, T. Kaisar, D. Bhattacharya, J. Atulasimha, "Voltage Controlled Energy Efficient Domain Wall Synapses with Stochastic Distribution of Quantized Weights in the Presence of Thermal Noise and Edge Roughness," *IEEE Transactions on Electron Devices*, *69*(4), pp. 1658-1666, 2021. [6] I. Hubara, M. Courbariaux, D. Soudry, R. El-Yaniv, and Y. Bengio, "Quantized neural networks: Training neural networks with low precision weights and activations," *The Journal of Machine Learning Research*, *18*(1), pp. 6869-6898, 2017. [7] W. A. Misba, M. Lozano, D. Querlioz, and J. Atulasimha, "Energy Efficient Learning With Low Resolution Stochastic Domain Wall Synapse for Deep Neural Networks," *IEEE Access*, *10*, pp. 84946-84959, 2022.

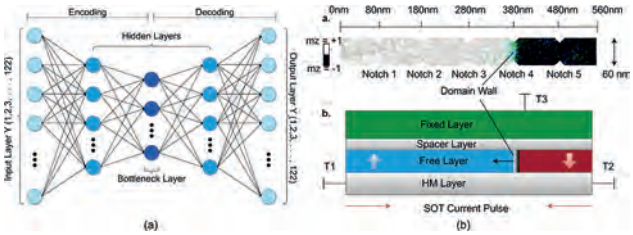

Figure 1: (a) Autoencoder architecture. (b) Schematic diagram of DW synapses.

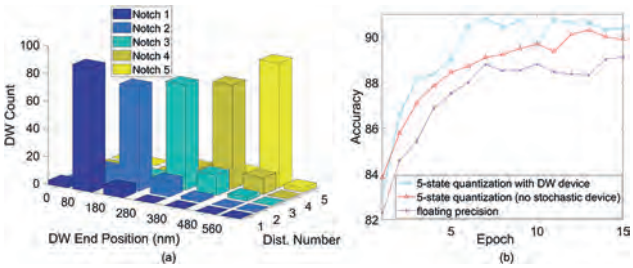

Figure 2: (a) Probabilistic distribution of DW positions and counts. (b) Accuracy against epoch for different synaptic states of autoencoder.

BB-08. A spiking neural network device based on Skyrmionic neurons and synapses. *M. Tey*[1], X. Chen[1], P. Ho[1] and A. Soumyanarayanan[1,2] *1. Institute for Materials Research and Engineering, Singapore, Singapore; 2. Physics, National University of Singapore, Singapore*

Hardware-accelerated spiking neural networks (SNNs) holds promise as a biologically-inspired, low-powered solution to realize edge artificial intelligence. Magnetic skyrmions - collective spin configurations with particle-like localization and non-zero topological charge - have the potential to underpin these next-generation devices owing to their nanoscale size, energy-efficient motion, and non-volatility at room temperature [1]. We propose an SNN design wherein both neuron and synapse are based on skyrmions that are stable at zero magnetic field [2]. In contrast to existing proposals, our device represents spike trains using skyrmions instead of electrical currents. Underpinning this device is the concept of a spatially-varying interlayer exchange coupling (IEC) layer, which allows for selective suppression of the skyrmion hall effect, fast skyrmion generation and motion. Our device comprises two skyrmion-hosting racetracks, separated by an IEC layer and stacked perpendicularly in a cross-bar manner (Fig. 1). The 'leaky' and 'integrate' behavior characteristic of the Leaky-Integrate-Fire model is represented by the time-dependent annihilation and accumulation of skymions in the readout region, while the 'fire' function will be triggered when an arbitrary number of skyrmions have accumulated in the readout. The synaptic weight is determined by the number of skyrmions in the bottom stack of the intersection region, and can be set by a selected number of current pulses through the bottom stack. Skyrmion cloning is enabled by the nucleation of skyrmions in the top stack due to stray fields arising from skyrmions in the bottom stack. Our findings are based on a blend of micromagnetic simulations and previous experimental evidence. Compatible with crossbar array architectures, our device is highly scalable and holds promise for the efficient and compact implementation of SNN-based neuromorphic computing.

1.Tey, M. S. N., Chen, X., Soumyanarayanan, A. & Ho, P. *ACS Appl Electron Mater* (2022) 4, 5088–5097. 2.Chen, X., Tai. T, Tan, H.R. *et al. Arxiv E-Prints (2023) 2301.07327.*

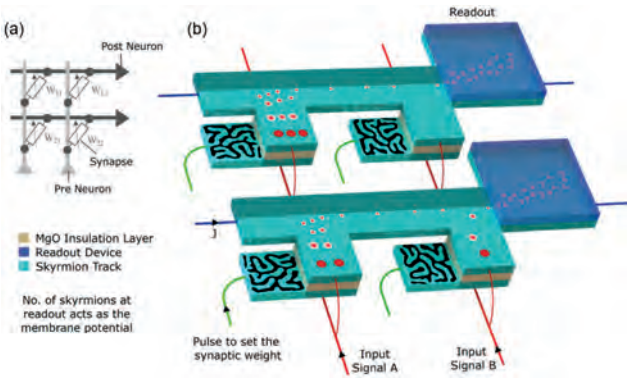

Fig. 1. (a) Overview of a 2x2 skyrmionic SNN. (b) Skyrmionic racetracks are stacked perpendicularly and separated by an insulating layer. Skyrmions generated in the bottom stack are cloned into the top stack. Pulse signals drive skyrmions to the readout. The number of readout skyrmions acts as the membrane potential.

BB-09. Integration of Magnetic Josephson Junction in Circuits for Neuromorphic Computing. *E. Jué*[2,1], D. Olaya[2,1], M.R. Pufall[3], I. Haygood[3], M. Castellanos Beltran[3], J. Biesecker[3], P. Hopkins[3], S. Benz[3], W.H. Rippard[3] and M.L. Schneider[3] *1. Department of Physics, University of Colorado, Boulder, Boulder, CO, United States; 2. Associate of the National Institute of Standards and Technology, Boulder, CO, United States; 3. National Institute of Standards and Technology, Boulder, CO, United States*

Nanoclustered magnetic Josephson junctions (nMJJ) are hybrid magnetic-superconducting devices that can be used as artificial synapses [1, 2]. This type of Josephson junction is made of a barrier with magnetic clusters and has the particularity to have a critical current that can be tuned with the magnetic order of the nanoclusters. This tunable critical current can be used to perform synaptic weighting in neuromorphic circuits. Until now, the functionality of the nMJJ as an artificial synapse has been demonstrated at the device level only. In this presentation, we present results of a new process and test circuits developed at NIST, which combine nMJJs with more traditional JJs. In this process, Josephson junctions are used as natural spiking neuron-like devices and the nMJJs are used as quasi-analog synapse-like devices [3]. Together, the two types of junctions allow for the development of neuromorphic circuits. The double-Josephson-junction process that has been developed will enable bio-inspired design to be taken all the way to the device level with the potential to enable new types of computation. We will present the results from circuits that test both synaptic function of the nanoclustered magnetic junctions in the previously demonstrated quasi-analog fashion, as well as the functionality of these devices when combined with single-flux-quantum pulses. For example, we expect a change in the amount of current coupled into the post synaptic neuron to change by roughly a factor of 12 when we vary the critical current of our nanoclustered magnetic Josephson junction from 1 mA to 10 microamps based on the WRSPICE models of our circuits.

[1] M. L. Schneider et al., "Ultralow power artificial synapses using nanotextured magnetic Josephson junctions," *Sci Adv*, vol. 4, no. 1, p. e1701329, 2018. [2] E. Jué, M. R. Pufall, I. W. Haygood, W. H. Rippard, and M. L. Schneider, "Perspectives on nanoclustered magnetic Josephson junctions as artificial synapses," *Appl Phys Lett*, vol. 121, no. 24, Dec. 2022. [3] P. Crotty, D. Schult, & K. Segall, "Josephson junction simulation of neurons", Physical Review E, 82(1), 011914, 2010.

Session BC
MAGNETO-IONICS
Chris Leighton, Chair
University of Minnesota, Minneapolis, MN, United States

INVITED PAPERS

BC-01. Magneto-Ionics with Alternative Ionic Species. C.J. Jensen[1], A. Quintana[1], G. Chen[1], Z. Chen[1], M. Robertson[2], A.A. Firme[3], P. Quarterman[4], A.J. Grutter[4], P.P. Balakrishnan[4], H. Zhang[4], D. Zheng[5], C. Liu[5], C. Ophus[6], A. Schmid[6], A. Davydov[4], X. Zhang[5] and *K. Liu*[1]
1. Georgetown University, Washington, DC, United States; 2. University of California, Davis, Davis, CA, United States; 3. University of Wyoming, Laramie, WY, United States; 4. NIST, Gaithersburg, MD, United States; 5. KAUST, Thuwal, Saudi Arabia; 6. Lawrence Berkeley Laboratory, Berkeley, CA, United States

Magneto-ionic (MI) effects have shown promise for energy-efficient nanoelectronics, where ionic migration may be used to achieve atomic scale control of interfaces in magnetic nanostructures. To date, magneto-ionics have been mostly explored in oxygen-based systems,[1-4] while there is a surge of interest in alternative ionic systems due to their different ionic migration mechanisms and characteristics.[5-8] We have recently demonstrated effective MI control of magnetic functionalities using a variety of ionic species: In nitride based Ta/CoFe/MnN/Ta films, chemically induced MI effect is combined with the electric field driving of nitrogen to electrically manipulate exchange bias.[9] Upon field-cooling the heterostructure, ionic diffusion of nitrogen from MnN into the Ta layers occurs. A significant exchange bias is observed, which can be further enhanced by ~ 20% after a voltage conditioning (Fig. 1). This enhancement can be reversed by voltage conditioning with an opposite polarity. Nitrogen migration within the MnN layer and into the Ta capping layer cause the enhancement in exchange bias, which is observed in polarized neutron reflectometry studies. Furthermore, we have achieved (001)-ordered Mn_4N thin films by sputtering Mn onto Mn_3N_2 seed layers on Si substrates. Nitrogen ion migration across the Mn_3N_2 /Mn layers leads to a continuous evolution of the layers to Mn_3N_2/Mn_4N, Mn_2N/Mn_4N, and eventually Mn_4N alone. The nitrogen ion migration is also manifested in a significant exchange bias, due to the interactions between ferrimagnetic Mn_4N and antiferromagnetic Mn_3N_2 and Mn_2N. In hydroxide based a-$Co(OH)_2$ films synthesized via electrodeposition, ferromagnetism can be induced by electrolyte gating with a low turn-on voltage (Fig. 2).[10] The α-$Co(OH)_2$, which is a room temperature paramagnet, is switched to ferromagnetic after electrolyte gating with a negative voltage. The system is fully, magnetically reversible upon positive voltage application. The origin of this transition is attributed to the ionic diffusion of hydroxyl groups, promoting the formation of metallic cobalt ferromagnetic regions. Our findings demonstrate one of the lowest turn-on voltages reported for propylene carbonate gated experiments. By tuning the voltage magnitude and sample area we demonstrate that the speed of the induced ionic effect can be drastically enhanced. In hydrogen based systems, a sensitive and reversible chirality switching of domain walls[7] is observed via hydrogen adsorption/desorption induced Dzyaloshinskii-Moriya Interaction (DMI). Furthermore, reversible writing/deleting of skyrmions[11] is shown via hydrogen adsorption/desorption induced magnetic anisotropy change. These effects demonstrate contrasts with oxygen-based MI effects in terms of operating principles, switching speed, and reversibility. Such MI systems are valuable platforms to gain quantitative understanding at buried interfaces. They also offer potentials for device applications based on electric modulation of magnetic functionalities. This work has been supported in part by the NSF (DMR-2005108, ECCS-1933527, ECCS-2151809), SRC/NIST SMART Center, DOE, and KAUST.

[1] U. Bauer, et al, Nat. Mater. 14, 174 (2015). [2] C. Bi, et al, Phys. Rev. Lett. 113, 267202 (2014). [3] D. A. Gilbert, et al, Nat. Commun. 7, 11050 (2016). [4] K. Duschek, et al. APL Mater. 4, 032301 (2016). [5] A. J. Tan, et al, Nat. Mater. 18, 35 (2019). [6] L. Herrera Diez, et al, Phys. Rev. Appl. 12, 034005 (2019). [7] G. Chen, et al, Phys. Rev. X 11, 021015 (2021). [8] J. de Rojas, et al, Nat. Commun. 11, 5871 (2020). [9] C. J. Jensen, et al, ACS Nano 17, 6745 (2023). [10] A. Quintana, et al, J. Mater. Chem. C 10, 17145 (2022). [11] G. Chen, et al, Nat. Commun. 13, 1350 (2022).

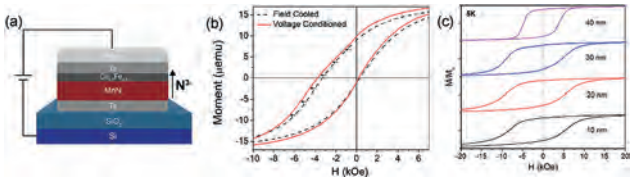

Fig. 1. (a) Schematic illustration of a MnN/CoFe heterostructure where N-ions are driven by an *E*-field, leading to (b) an enhancement of the exchange bias after voltage conditioning. (c) Exchange bias in nominally Mn_3N_2 (20nm)/Mn films with increasing Mn thickness, at 5 K after field cooling.

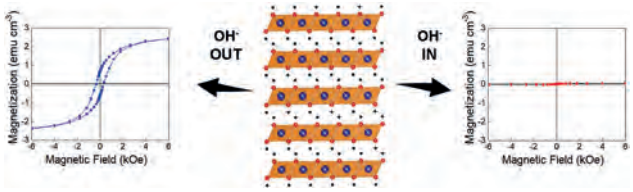

Fig. 2. Hydroxide-based magneto-ionics in electrodeposited α-$Co(OH)_2$ films. The α-$Co(OH)_2$, which is a room temperature paramagnet, is switched to ferromagnetic after electrolyte gating with a negative voltage. The system is fully, magnetically reversible upon positive voltage application.

BC-02. Solid/Liquid Electrolyte Engineering to Boost Cyclability During Magneto-ionic Actuation. Z. Tan[1], Z. Ma[1], L. Fuentes-Rodríguez[2], O. Liedke[3], M. Butterling[3], A. Attallah[3], E. Hirschmann[3], A. Wagner[3], L. Abad[4], N. Casañ[2], A. Lopeandia[1,5], E. Menéndez[1] and *J. Sort*[1,6]
1. Universitat Autonoma de Barcelona, Bellaterra, Spain; 2. Institut de Ciència de Materials de Barcelona, ICMAB, Bellaterra, Spain; 3. Institute of Radiation Physics, Helmholtz-Zentrum Dresden, Rossendorf, Germany; 4. Institut de Microelectrònica de Barcelona (IMB-CNM-CSIC). Campus de la UAB, Bellaterra, Spain; 5. Catalan Institute of Nanoscience and Nanotechnology (ICN2), CSIC and BIST, Bellaterra, Spain; 6. Institució Catalana de Recerca i Estudis Avançats, ICREA, Barcelona, Spain

Controlling magnetism with voltage has an enormous potential to boost energy efficiency in nanoscale magnetic devices since the use of electric field (instead of magnetic fields or electric currents) minimizes Joule heating effects and the associated energy power dissipation. Magneto-ionics, which refers to the control of magnetism via voltage-driven ion migration, is emerging as a new actuation mechanism in a variety of technological fields

ranging from spintronics to neuromorphic computing. To generate effective electric fields, either solid or liquid electrolytes are utilized. However, both types of electrolytes suffer from certain drawbacks. Thin solid electrolytes can have difficulties to withstand high electric fields without electric pinholes. In turn, the use of liquid electrolytes can result in poor cyclability, thus limiting applicability. Recently, we have developed a nanoscale-engineered magneto-ionic architecture (comprising a thin solid electrolyte in contact with a liquid electrolyte), that drastically enhances cyclability while preserving sufficiently high electric fields to trigger ion motion [1]. In particular, the insertion of a highly nanostructured Ta layer (with suitable thickness and electric resistivity) between a magneto-ionic target material (*i.e.*, Co_3O_4) and the liquid electrolyte, increases magneto-ionic cyclability from < 30 cycles (when no Ta is inserted) to more than 800 cycles. The Ta layer is very effective in trapping oxygen and hindering O^{2-} ions from moving into the liquid electrolyte, thus keeping O^{2-} motion mainly restricted between Co_3O_4 and Ta when voltage of alternating polarity is applied. The generated TaO_x interlayer is an excellent ionic conductor that improves magneto-ionic endurance by proper tuning of the types of structural defects. In this way, our approach combines the benefits of solid and liquid electrolytes in a synergetic manner. Beyond magneto-ionics, the reported strategy to enhance cyclability can be easily extrapolated to other systems relying on ion transport mechanisms (i.e., iontronic materials).

[1] Z. Tan et al., ACS Nano 17, 6973–6984 (2023).

BC-03. Solid-State Lithium Magnetoionics for Voltage Control of Perpendicular Magnetic Anisotropy and Skyrmions in Thin Films.

M. Ameziane[1,2], J. Huhtasalo[3], L. Flajšman[2], R. Mansell[2], V. Havu[2], P. Rinke[2] and S. van Dijken[2] *1. Paul Scherrer Institute, Zurich, Switzerland; 2. Aalto University, Espoo, Finland; 3. University of Helsinki, Helsinki, Finland*

The development of novel energy-efficient information technologies requires a paradigm shift in the design of hardware. In addition, the increased interest in brain-inspired computing architectures requires functionalities not inherent to conventional CMOS-based memory and logic, including logic-in-memory capabilities, nonlinearity, and plasticity [1]. Modulating magnetic properties with voltage is an efficient mechanism for the creation of ultralow power technologies for memory and logic. Exploiting the voltage-driven motion of ions has emerged as a promising approach for tuning the properties of magnetic thin films [2]. One major advantage of this approach is its capacity to achieve large magnetic responses at low voltages, yielding exceptionally high magnetoelectric coupling efficiencies. Magnetoionic devices, however, often suffer from slow kinetics and poor reversibility of the effects, impractical liquid architectures and sensitivity to ambient conditions. To circumvent these bottlenecks, here we draw inspiration from solid-state Li-ion batteries and supercapacitors to create magnetoionic devices for the reversible room-temperature voltage control of perpendicular magnetic anisotropy [3] and skyrmions [4] in magnetic thin films. In our structures, we employ LiPON, a common solid-state electrolyte, as the ion conduction medium, and $LiCoO_2$ as the ion storage layer. Exploiting Li ion migration in a battery-like ionic device comprising a Co/Pt thin film bilayer as one of the electrodes (Fig. 1a), we demonstrate reversible switching of the magnetization between in-plane and out-of-plane states at low voltages (Fig. 1b). The voltage-driven insertion and deinsertion of Li ions into and out of the Co film modulates the perpendicular magnetic anisotropy by affecting the hybridization of electron orbitals at the Co/Pt interface without substantially affecting the magnetization of Co. The experimental findings are corroborated by density functional theory calculations. The switching of the magnetization direction is achieved at sub-second timescales and the effects are fully reversible over hundreds of voltage-switching cycles. We adopt a similar approach to ionically control skyrmions with Li ions. Using a solid-state supercapacitor-like structure, we demonstrate the reversible nucleation and annihilation of skyrmions in a Pt/$Co_{20}Fe_{40}B_{20}$/Pt multilayer (Fig. 2a). Control of the skyrmion state can be achieved through accumulation and depletion of Li ions at the magnetic interface by applying voltage pulses (Fig. 2b) or dc voltages (Fig. 2c). The magnetic response of the device exhibits a hysteretic voltage dependence and short-term state retention, with a pronounced nonlinear response with respect to voltage pulse amplitude and pulse number. In addition, we show that skyrmions can be nucleated with single 60 µs pulses. Moreover, the magnetoionic device shows excellent electrical endurance under extensive voltage cycling. The solid-state Li-based ionic devices reported here combine functionalities that are attractive for post-von Neumann computing schemes. These results provide a design principle for future low power spin-based magnetoionic devices.

[1] D. V. Christensen, R. Dittmann, B. Linares-Barranco et al., *Neuromorph. Comput. Eng.*, Vol. 2, 022501 (2022). [2] M. Nichterwitz, S. Honnali, M. Kutuzau et al., *APL Mater*, Vol. 9, 030903 (2021). [3] M. Ameziane, R. Mansell, V. Havu et al., *Adv. Funct. Mater.*, Vol. 32, 2113118 (2022). [4] M. Ameziane, J. Huhtasalo, L. Flajšman et al., *Nano Lett.*, Vol. 23, p. 3167 (2023).

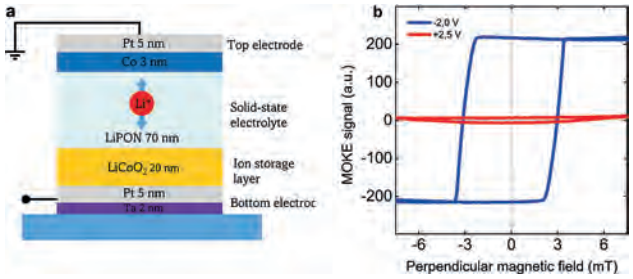

Fig. 1 | Ionic control of perpendicular magnetic anisotropy. (a) Schematic of the battery-like Co/Pt-based magnetoionic device. (b) Polar MOKE hysteresis curves demonstrating the voltage-driven switching of the magnetization of Co between out-of-plane and in-plane states at -2 V and +2 V, respectively.

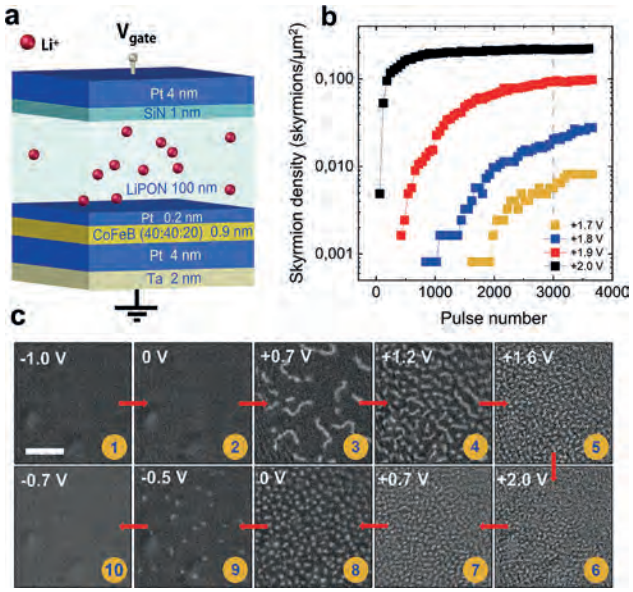

Fig. 2 | Ionic control of skyrmions. (a) Schematic of the Pt/$Co_{40}Fe_{40}B_{20}$/Pt-based magnetoionic supercapacitor. (b) Nucleation of skyrmions with voltage pulses as a function of pulse number and pulse amplitude. (c) Voltage dependence of the skyrmion state in a dc voltage sequence showing a hysteretic magnetic response.

CONTRIBUTED PAPERS

BC-04. Magneto-Ionic Control of Exchange Bias in Mn_4N/Mn_3N_2 Heterostructures. *Z. Chen*[1], C.J. Jensen[1], C. Liu[2], X. Zhang[2] and K. Liu[1]
1. Physics, Georgetown University, Washington, DC, United States; 2. King Abdullah University of Science & Technology, Thuwal, Saudi Arabia

Nitrogen-based magneto-ionics offers an alternative platform to the traditional oxide-based systems [1-4]. The manganese nitride ferrimagnet Mn_4N is particularly interesting as an emergent rare-earth-free spintronic material due to its uniaxial anisotropy, small saturation magnetization, high thermal stability, and large domain wall velocity. We have achieved high-quality Mn_4N films by sputtering Mn directly on top of an Mn_3N_2 seed layer at elevated temperatures. While Mn reacts with the nitrogen from Mn_3N_2 to form Mn_4N, Mn_3N_2 goes through a phase transition to Mn_2N and eventually to Mn_4N due to the nitrogen ionic motion. X-ray diffraction (Fig. 1) and transmission electron microscopy confirm the transition of the nitride phases. A large exchange bias, up to 3 kOe at 5 K, is observed due to mixed ferrimagnetic and antiferromagnetic nitride phases. Furthermore, the exchange bias can be tuned by up to 85% through either varying deposition conditions (thickness and nitrogen partial pressure) or post-annealing (Fig. 2). The change in exchange bias is attributed to the nitride phase change induced by nitrogen ionic motion. These results demonstrate a promising new platform with remarkable tunability for spintronic applications via nitrogen-based magneto-ionics. This work has been supported in part by the NSF (ECCS-2151809), SRC/NIST SMART Center, and KAUST.

[1]. D. A. Gilbert et al, Nat. Commun. 7, 11050 (2016). [2]. J. de Rojas et al, Nat. Commun. 11, 5871 (2020). [3]. P. D. Murray et al, ACS Appl. Mater. Interfaces 13, 38916 (2021). [4]. C. J. Jensen et al, ACS Nano 17, 6745 (2023).

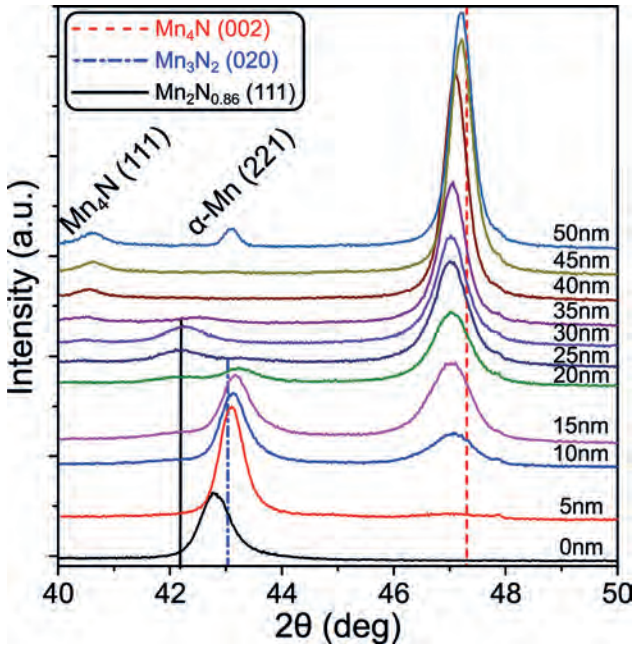

Figure 1. X-ray diffraction 2θ-ω scans showing Mn nitride phase evolution as the deposited Mn thickness changes.

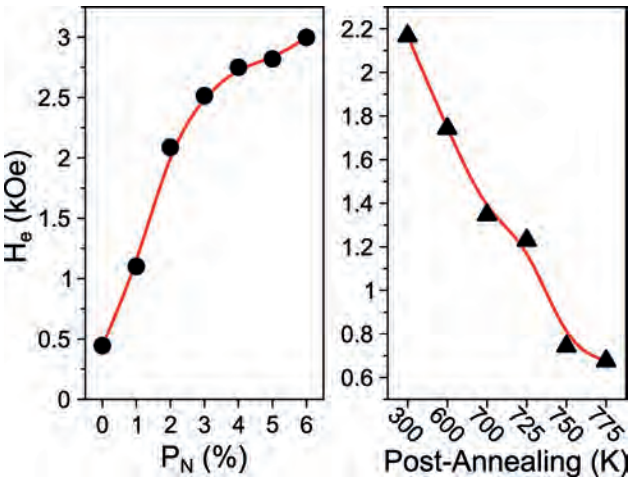

Figure 2. Exchange bias variation as nitrogen partial pressure (P_N) changes during deposition (left). Effects of post-annealing temperature on the exchanges bias (right). Solid lines are guides to the eye.

BC-05. Magneto-ionic physical reservoir computing. *M. Rajib*[1], D. Bhattacharya[2], M.F. Chowdhury[1], C.J. Jensen[2], G. Chen[2], K. Liu[2] and J. Atulasimha[1,3] *1. Mechanical and Nuclear Engineering Department, Virginia Commonwealth University, Richmond, VA, United States; 2. Department of Physics, Georgetown University, Washington, DC, United States; 3. Electrical and Computer Engineering Department, Virginia Commonwealth University, Richmond, VA, United States*

Physical Reservoir Computing (PRC) is an unconventional computing approach that leverages the nonlinear behaviors of reservoir blocks to perform classification and prediction of time-series data. Magneto-ionics, which involves the dynamic movement of ions through electrolytes at the magnet/electrolyte interface to modify physical and chemical properties, can potentially be utilized as a reservoir unit. Previous research has demonstrated successful control of perpendicular magnetic anisotropy (PMA) and the Dzyaloshinskii-Moriya Interaction (DMI) [1- 3], which presents ample opportunities for manipulating magnetization dynamics. In this study, we present magneto-ionic alteration of the domain state of Co/Ni multilayers interfaced with a GdOx layer, which can be utilized as a reservoir block for implementing reservoir computing. Here, the application of a voltage pulse that drives the oxides away from the interface reduces the PMA of the magnetic layer, as shown in Fig. 1(a). Conversely, applying a voltage of the opposite polarity drives oxide ions into the magnetic layer, thereby increasing the PMA. The evolution of PMA is dynamic with a timescale commensurate to the ion diffusion, manifesting an essential characteristic of a reservoir block called short-term memory. Figure 1(b) shows the normalized output observed with a MOKE microscope for the application of randomly distributed nine sine and square pulses. The outputs exhibit distinctive patterns for square and sine pulses, due to dynamic nature of PMA modulation. This clearly demonstrates the potential reservoir property of the magneto-ionic system. Figure 2 illustrates the corresponding changes in the domain pattern at the end of the first three pulses applied to the magneto-ionic system. Our work paves the way for magneto-ionic energy-efficient physical reservoir computing. This work has been supported in part by the NSF (CCF-1909030, ECCS-2151809 and DMR- 2005108).

[1] Bauer et al. Nature Mater 14, 174–181 (2015). [2] Chen et al, Nat. Comm. 13, 1350 (2022). [3] Fillion et al, Nat. Comm. 13, 5257 (2022).

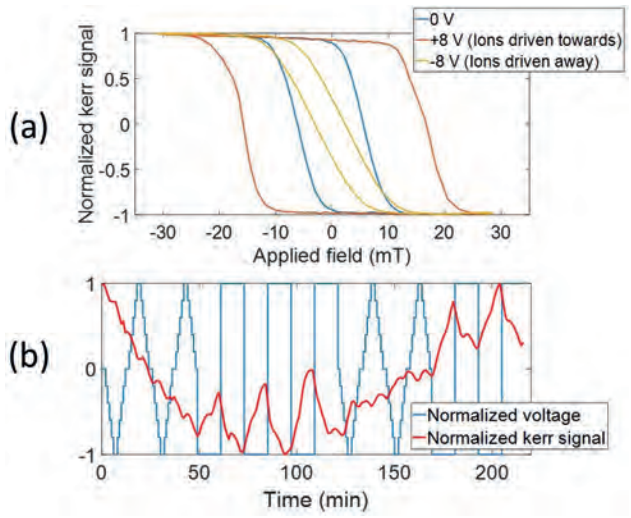

Figure 1. (a) PMA control in a Co/Ni thin film with positive and negative voltage pulse. (b) Output for randomly distributed nine voltage pulses

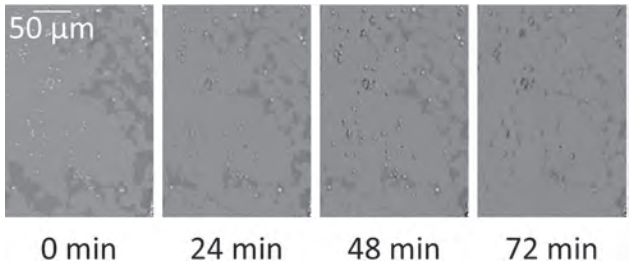

Figure 2. Change in magnetic domain for different voltage pulses

BC-06. Magneto-Ionic Enhancement of Exchange Bias and Modulation of Ferromagnetic Bi-stability. *M. Hasan*[1*], A.E. Kossak[1] and G. Beach[1]
1. Department of Materials Science and Engineering, Massachusetts Institute of Technology, Cambridge, MA, United States

Voltage control of exchange bias is desirable for spintronic device applications, however dynamic modulation of the unidirectional coupling energy in ferromagnet/antiferromagnet bilayers has not yet been achieved. Here we show that by solid-state hydrogen gating, perpendicular exchange bias can be enhanced by >100% in a reversible manner, in a simple $Co/Co_{0.8}Ni_{0.2}O$ heterostructure at room temperature. We show that this phenomenon is an isothermal analog to conventional field-cooling and that sizable changes in coupling energy can result from small changes in AFM grain stability. Using this method, we show for the first time, that a bi-directionally stable ferromagnet can be made unidirectionally stable, with gate voltage alone. We further demonstrate sub-millisecond hydrogen loading and potential for multistate operation. This work provides a means to dynamically reprogram exchange bias, with broad applicability in spintronics and neuromorphic computing, while simultaneously illuminating fundamental aspects of exchange bias in polycrystalline films.

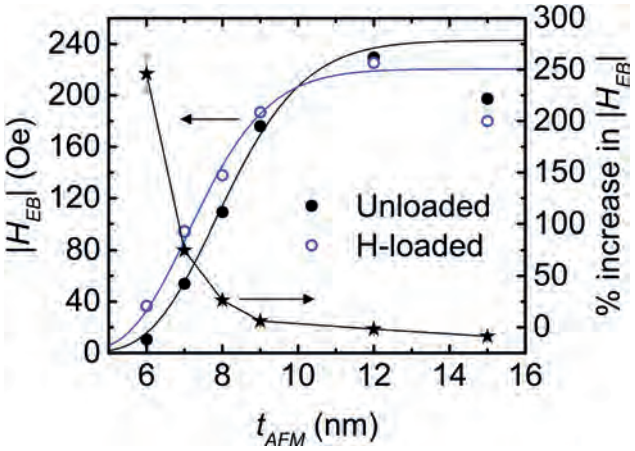

Fig. 1 Exchange-bias (H_{EB}) in the unloaded and Hydrogen-loaded states as a function of antiferromagnet thickness at 20 °C; right axis shows the percent change in H_{EB}

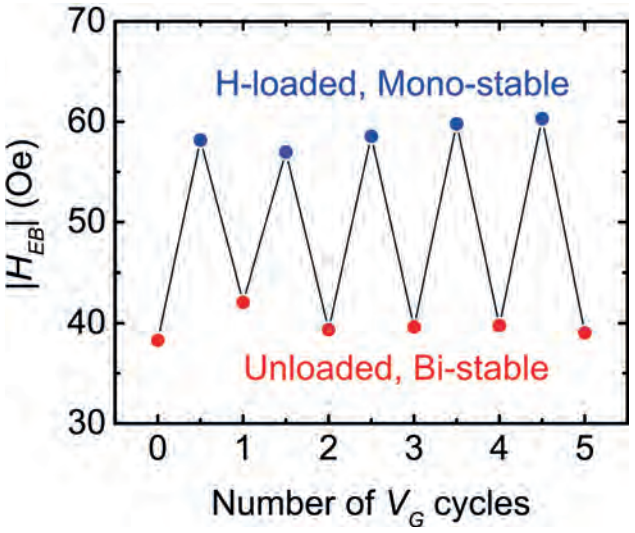

Fig. 2 Reversible toggling between bi-stable (ferromagnet stable in both up and down orientation) and mono-stable (ferromagnet stable only in up orientation) states by loading and unloading Hydrogen

BC-07. Magneto-Ionic Control of Perpendicular Magnetic Anisotropy for Energy-Efficient Spintronic Devices. *A. Islam*[1,2], A. Mahendra[1,2], S. Acharya[1,2], Y. Zhang[1,2] and S. Granville[1,2] *1. Robinson Research Institute, Victoria University of Wellington, Wellington, New Zealand; 2. MacDiarmid Institute for Advanced Materials and Nanotechnology, Wellington, New Zealand*

Magnetic materials with switchable magnetic domains and anisotropy are the key to energy-efficient spintronic devices [1]. Magnetization switching of ferromagnets can be achieved through a spin-orbit torque (SOT) generated using materials that have large charge-to-spin efficiencies, such as heavy metals. Some ferromagnets, such as Weyl semi-metal Co_2MnGa, have a large spin Hall angle [2] and can themselves generate sizeable SOTs [3]. In such materials, the magnetization direction determines the spin current and spin polarization directions [4], allowing for the possibility to control SOT by adjusting the magnetic anisotropy and hence the magnetization direction. Here, we will present the ionic liquid gating (Fig. 1a) switching of perpendicular magnetic anisotropy (PMA) of thin layers of stacks containing a conventional ferromagnet Ta/CoFeB/W and a ferromagnet Weyl semi-metal $MgO/Co_2MnGa/Pd$. Measurements were achieved with a magneto-optical Kerr effect (MOKE) system. A positive voltage causes CoFeB to completely

switch from perpendicular to in-plane anisotropy (Fig. 1b), whereas a negative voltage is required to reduce the anisotropy of Co_2MnGa, and it does not fully switch to in-plane (Fig. 1c). The CoFeB anisotropy change is reversible upon removing the voltage, but the Co_2MnGa cannot be reversed even with a reversed voltage. The relative slowness of the changes (~ seconds to hours) and the reversed-sign behaviour of the films show that the origin of the anisotropy change is magnetoionic, i.e. due to the change in oxidation state of the samples.

[1] A. Davidson, V. P. Amin, W. S. Aljuaid, P. M. Haney, and X. Fan, "Perspectives of electrically generated spin currents in ferromagnetic materials," *Phys. Lett. A*, vol. 384, no. 11, p. 126228, 2020, doi: 10.1016/j.physleta.2019.126228. [2] L. Leiva, S. Granville, Y. Zhang, S. Dushenko, E. Shigematsu, T. Shinjo, R. Ohshima, Y. Ando, and M. Shiraishi, "Giant spin Hall angle in the Heusler alloy Weyl ferromagnet Co2MnGa", *Phys. Rev. B*, vol. 103, L04114, 2021, doi: 10.1103/PhysRevB.103.L041114. [3] K. Tang, Z. Wen, Y. C. Lau, H. Sukegawa, T. Seki, and S. Mitani, "Magnetization switching induced by spin-orbit torque from Co2MnGa magnetic Weyl semimetal thin films," *Appl. Phys. Lett.*, vol. 118, no. 6, 2021, doi: 10.1063/5.0037178. [4] T. C. Chuang, D. Qu, S. Y. Huang, and S. F. Lee, "Magnetization-dependent spin Hall effect in a perpendicular magnetized film," *Phys. Rev. Res.*, vol. 2, no. 3, pp. 2–6, 2020, doi: 10.1103/PhysRevResearch.2.032053.

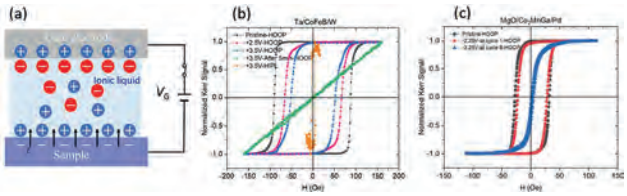

Figure 1: (a): Phenomenon of ionic liquid gating. (b), (c): Hysteresis curves of both stacks measured at various gate voltages using MOKE. The reduction of PMA signal is prominent for both stacks. HOOP is hysteresis with out-of-plane magnetic field and polar mode of MOKE. HIPL is hysteresis with in-plane magnetic field and longitudinal mode of MOKE.

BC-08. Magneto-ionic control of anisotropy and skyrmions in Co/Ni multilayers. *D. Bhattacharya*[1], M. Rajib[2], C.J. Jensen[1], G. Chen[1], J. Atulasimha[2] and K. Liu[1] *1. Department of Physics, Georgetown University, Washington, DC, United States; 2. Mechanical and Nuclear Engineering, Virginia Commonwealth University, Richmond, VA, United States*

Magneto-ionics utilizes ionic migration through magnet/electrolyte interfaces to modify physical and chemical properties and consequently, magnetic characteristics. Previous studies have shown effective ionic control of a variety of magnetic functionalities including perpendicular magnetic Anisotropy (PMA) and Dzyaloshinskii-Moriya Interaction (DMI) [1-3], presenting interesting opportunity to tailor spin textures such as magnetic skyrmions and domain walls. In this work, we demonstrate magneto-ionic control of PMA in $(Co/Ni)_N$ multilayers, which is in turn used to electrically manipulate magnetic skyrmions. To facilitate ionic motion, a GdOx layer was interfaced with the multilayer to be used as the solid-state electrolyte. After applying a voltage pulse across this oxide layer that moved oxygen away from the interface, the PMA decreased significantly (Fig. 1). This effect was found to be volatile, i.e. the PMA recovered when the voltage was reset to zero. However, PMA recovery was not instantaneous as this was mediated by ion diffusion to an equilibrium state. This is analogous to a short term memory effect useful to implement neuromorphic devices. The PMA could be increased by applying a voltage of the opposite polarity. However, PMA started to decrease after a certain voltage, possibly due to over-oxidation of the magnetic layers. In this multilayer system, the magnetic energy landscape can be easily fine-tuned by varying the number of bilayer repeats N. Utilizing this property, skyrmions were stabilized in a N=11 sample. Furthermore, skyrmion number and density could be controlled (Fig. 2) by tuning the PMA in the manner described above. These results highlight the potential of electric control of magnetic skyrmions in magneto-ionic devices. This work has been supported in part by the NSF (DMR- 2005108, ECCS-2151809 and CCF-1909030).

1. Chen et al, Nat. Comm. 13, 1350 (2022). 2. Fillion et al, Nat. Comm. 13, 5257 (2022). 3. Ameziane et al, Nano Lett. 23, 3167 (2023).

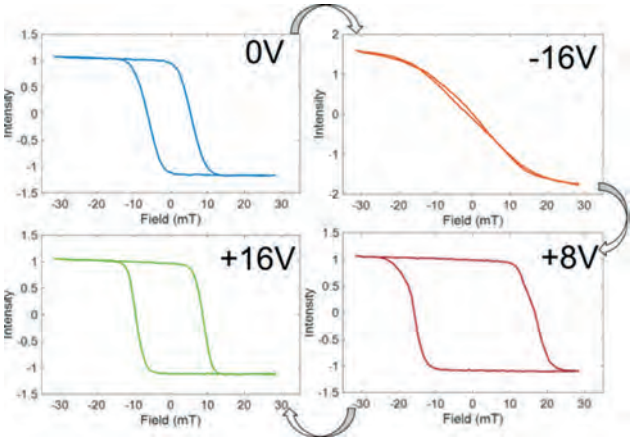

Figure 1. Controlling PMA in a Co/Ni thin film. Negative voltage drives oxygen away from the interface.

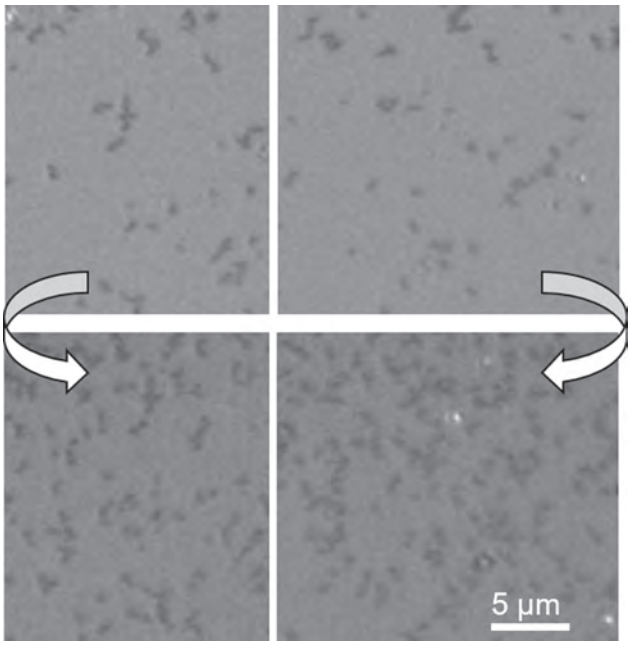

Figure 2. Voltage controlled creation of skyrmions in a $(Co/Ni)_{11}$ thin film sample.

Session BD
DOMAIN WALL, VORTEX, AND SKYRMION DYNAMICS AND DEVICES I

Wanjun Jiang, Co-Chair
Tsinghua University, Beijing, China
Dazhi Hou, Co-Chair
University of Science and Technology of China, Hefei, China

INVITED PAPERS

BD-01. Non-trivial Charge-dependent Spin Phenomena in Topological Spin Textures. *H. Han[1,2] 1. Center for X-ray Optics, Lawrence Berkeley National Laboratory, Berkeley, CA, United States; 2. Department of Materials and Science Engineering, Korea National University of Transportation, Chungju, The Republic of Korea*

Spin textures within the magnetic medium have attracted significant attention due to their potential application in future microelectronic devices. These spin textures are characterized by the topological charge q, which determines their unique physical properties [1]. For example, spin textures with a non-trivial topological charge ($q \neq 0$) exhibit high thermal stability known as topological stability. Additionally, the non-trivial topological charge gives rise to rich dynamic behaviors of spin textures such as skyrmion Hall effect [2] and the gyrotropic motion in patterned magnetic disks [3]. Here, we will show the topological charge-dependent physical properties of the spin textures utilizing magnetic transmission X-ray microscopy. We experimentally demonstrated the topological charge-dependent stability of the skyrmion [4] and vortex-antivortex pair [5, 6]. Additionally, we will show the Hall-like motion of the magnetic monopole known as Bloch point, depending on its topological charge [7]. We believe that our work will provide insight into topological spin textures and contribute to the spintronic devices based on spin textures.

[1] N. Nagaosa and Y. Tokura, *Nat. Nanotechnol.* 8, 899-911 (2013). [2] G. Chen, *Nat. Phys.* 13, 112-113 (2013). [3] S.-B. Choe et al., *Science* 304, 420-422 (2004). [4] S.-G. Je, H.-S. Han et al., *ACS Nano* 14(3), 3251-3258 (2020). [5] N. Gao et al. *Nat. Commun.* 10, 5603 (2019). [6] H.-S. Han et al., *Appl. Phys. Lett.* 118, 212407 (2021). [7] H.-S. Han et al., to be submitted.

BD-02. Skyrmion dynamics and the Skyrmion-Excited Spin Wave Fractal Network. *D.A. Gilbert[1,2] 1. Materials Science and Engineering, University of Tennessee, Knoxville, TN, United States; 2. Physics Department, University of Tennessee, Knoxville, TN, United States*

Magnetic skyrmions are topologically non-trivial chiral spin textures which are of interest for fundamental research and advanced spintronic architectures. As a result of their unique structure, skyrmions have coherent dynamic modes, for example gyration and breathing modes, which occur at gigahertz frequencies.[1, 2] During dynamic excitations, the constantly changing magnetization is compensated by the emission of spin-waves, which rapidly propagate away from the skyrmion. For an isolated skyrmion, the spin waves form an elegant double spiral structure, with a well-defined periodicity determined by the driving frequency.[3] For hybrid skyrmions, which have both Néel-like and Bloch-like windings along a single skyrmion tube and no chirality control,[4-6] there are twelve unique gyration modes, with an example shown in Fig. 1c, each with unique spin wave emissions that are related by mirror symmetry or 180° phase shifts. Within an ordered lattice of hybrid skyrmions, the interference pattern generated by the spin waves presents a unique, non-trivial structure. Specifically, the spin waves from the twelve gyration modes are unique but related, and are generated by skyrmion on a highly ordered hexagonal lattice, but the spin waves themselves lack translational symmetry. Using small angle neutron scattering (SANS) the skyrmion gyration dynamics and the spin wave emissions are directly measured, shown in Fig. 1a and b.[1] The skyrmion lattice itself changes very little during gyration, however the spin wave interference pattern is shown to be well represented by a fractal, with the interference fringes from the spin wave interference acting as the fundamental building blocks of the network. Consistent with the physics of spin waves, the structure is exceedingly small – with building blocks ≈40 nm in diameter – and extraordinarily fast – propagating in nanosecond timescales. Micromagnetic simulations confirm the proposed understanding, Fig. 1d. The fractal structure makes this system inherently chaotic and highly sensitive to variations within the skyrmion lattice, presenting an opportunity for spin-wave neural networks.[7]

[1] N. Tang et al., "Skyrmion-Excited Spin-Wave Fractal Networks," Advanced Materials, p. 2300416, (2023) doi: 10.1002/adma.202300416 [2] S. A. Montoya et al., "Resonant properties of dipole skyrmions in amorphous Fe/Gd multilayers," Physical Review B, vol. 95, p. 224405 (2017) [3] J. Chen, J. Hu, and H. Yu, "Chiral Emission of Exchange Spin Waves by Magnetic Skyrmions," ACS Nano, vol. 15, pp. 4372 (2021) [4] W. L. N. C. Liyanage et al., "Three-dimensional structure of hybrid magnetic skyrmions determined by neutron scattering," Physical Review B, vol. 107, p. 184412 (2023) [5] R. D. Desautels et al., "Realization of ordered magnetic skyrmions in thin films at ambient conditions," Physical Review Materials, vol. 3, 104406 (2019) [6] S. A. Montoya et al., "Tailoring magnetic energies to form dipole skyrmions and skyrmion lattices," Physical Review B, vol. 95, p. 024415 (2017) [7] Á. Papp, W. Porod, and G. Csaba, "Nanoscale neural network using non-linear spin-wave interference," Nature Communications, vol. 12, p. 6422, (2021)

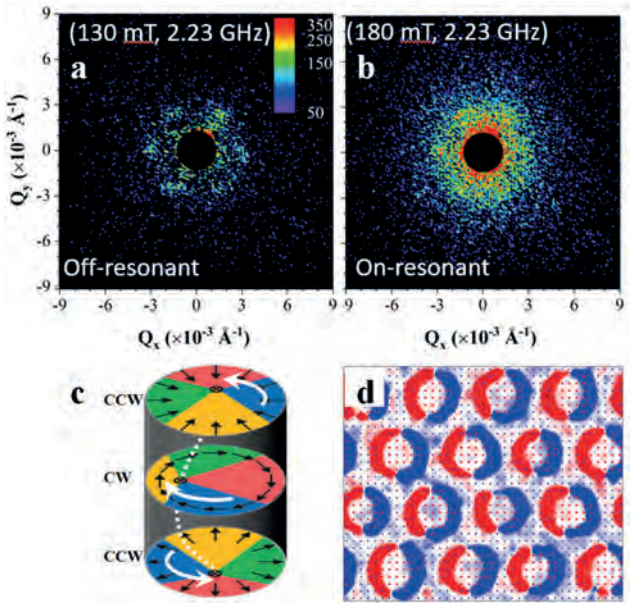

SANS scattering measurements of the skyrmion lattice in (a) the off-resonance condition and (b) on-resonance. (c) An exmple illustration of one of the twelve skyrmion gyration modes. (d) A micromagnetic simulation of the dynamic skyrmions and spin wave structure.

BD-03. Understanding Spin-texture Behavior in van der Waals Ferromagnets Using Cryo Lorentz Electron Microscopy. *Y. Li*[1]
1. Materials Science Division, Argonne National Laboratory, Lemont, IL, United States

Magnetic *van der Waals* (vdW) materials have unique crystal structures, which consist of layered atoms separated by vdW gaps, leading to strong intra-plane interaction and weak inter-plane vdW interaction[1]. This unique structure and strong intrinsic spin interactions give rise to fascinating physical phenomena, such as rich magnetic spin textures, namely, the Bloch or the Néel-type stripes, skyrmions, bubbles and merons[2-4]. It is essential to understand the behavior of spin textures in the vdW materials in response to external stimuli such as magnetic field, temperature and strain in order to control them by understanding the governing energy terms. Lorentz transmission electron microscopy (LTEM) allows for imaging the local spin textures and microstructure at high resolution in such materials and related heterostructures. In this talk, we will present the spin texture imaging of two types of vdW ferromagnets: (1) metallic Fe_3GeTe_2 and (2) semiconducting $Cr_2Ge_2Te_6$. Fe_3GeTe_2 (FGT) is itinerant ferromagnet in the 2D limit with strong perpendicular anisotropy and with the Curie temperature of around 230 K. We will show the creation and the control of magnetic spin textures in the vdW FGT by using in-situ cryo LTEM and as a function of temperature and magnetic field. We also gain insight into the order and interaction in the collective skyrmion lattice, showing short-range order and thermally hysteretic behavior. In addition, we will also report the formation of skyrmions in a field-free condition in an oxidized FGT (O-FGT) heterostructure due to the interfacial interaction between FGT and O-FGT. $Cr_2Ge_2Te_6$ (CGT) is another vdW ferromagnet with the Curie temperature of 65 K, which however has weaker uniaxial anisotropy compared to Fe_3GeTe_2. We will show formation of Bloch-type stripes and bubble domains in CGT. CGT is a known magnetostrictive material, and we will demonstrate the effect of local strain on stripe and bubble domains, which provides another approach to manipulate the order of spin texture in such materials.

[1] K.S. Burch, D. Mandrus, J.G. Park, Nature, 563 (2018) 47-52. [2] Y. Li, R. Basnet, K. Pandey, et al., JOM, 74 2310-2318 (2022). [3] A.R.C. McCray, Y. Li, R. Basnet, et al., Nano Lett., 22 7804-7810 (2022). [4] A.R.C. McCray, Y. Li, E. Qian, et al., Adv. Funct. Mater., 2023, 2214203 (2023).

[5] This work was supported by the U.S. Department of Energy, Office of Science, Office of Basic Energy Science, Materials Sciences and Engineering Division.

CONTRIBUTED PAPERS

BD-04. Domain Walls in the Presence of In-Plane Anisotropies: Structure Tuning and Domain Imprinting. K. Franke[1], E. Haltz[1,2], C. Ophus[3], A. Schmid[3] and *C. Marrows*[1] *1. School of Physics and Astronomy, University of Leeds, Leeds, United Kingdom; 2. Université Sorbonne Paris Nord, Villetaneuse, France; 3. National Center for Electron Microscopy, Lawrence Berkeley National Laboratory, Berkeley, CA, United States*

It is well-known that the Dzyaloshinskii-Moriya interaction stabilizes Néel type domain walls in perpendicularly magnetized thin films. We demonstrate, using micromagnetic simulations and analytical modeling, that the presence of a uniaxial in plane magnetic anisotropy can also lead to the formation of Néel walls in the absence of a Dzyaloshinskii-Moriya interaction. It is possible to abruptly switch between Bloch and Néel walls via a small modulation of either anisotropy [1]. This opens up a route toward electric field control of the domain wall type with small applied voltages through electric field controlled anisotropies, as well as rich current-driven dynamics [2]. In experimental work, we report on domain pattern transfer from a ferroelectric $BaTiO_3$ substrate with a (111)-orientation of the surface to an epitaxial Co [3] film grown on a Pd buffer layer. Spatially modulated interfacial strain transfer from ferroelectric/ferroelastic domains and inverse magnetostriction in the ferromagnetic film induce stripe regions with a modulation of the in-plane uniaxial magnetic anisotropy direction. Using spin-polarized low energy electron microscopy (SPLEEM), we observe the formation of two distinct anisotropy configurations between stripe regions, leading to angles of 60° or 120° between the magnetizations of adjacent domains. This results in four distinct magnetic domain wall types associated with different energies and domain widths, which in turn affects whether domain pattern transfer can be achieved. Again using SPLEEM, we investigated domain pattern transfer in a related multiferroic heterostructure consisting of a (111)-oriented $BaTiO_3$ substrate and an epitaxial Ni film [4]. After in situ film deposition and annealing through the ferroelectric phase transition, interfacial strain transfer from ferroelastic domains in the substrate and inverse magnetostriction in the magnetic thin film introduce a uniaxial in-plane magnetic anisotropy that rotates by 60° between alternating stripe regions. Combining experimental results with micromagnetic simulations we show that a competition between the exchange and magnetostatic energies in these domain walls have a strong influence on the magnetic domain configuration.

[1] K. J. A. Franke et al., Phys. Rev. Lett. 127, 127203 (2021). [2] E. Haltz et al., arXiv:2303.06142 [cond-mat.mes-hall]. [3] K. J. A. Franke et al., Phys. Rev. B 107, L140407 (2023). [4] K. J. A. Franke et al., Phys. Rev. Mater. 7, 034403 (2023).

BD-05. Withdrawn

INVITED PAPER

BD-06. Unraveling Stochastic Domain Wall Motion: Insights from LTEM Imaging in a Nanoscale Magnetic Galton Board System.
T.R. Cote[1,2], D. Sanz Hernandez[4], F. Montaigne[3], J. Grollier[4], L. Georgopoulos[1], C. Phatak[1,2], A. Petford-Long[1,2] and H. Arava[1]
1. Materials Science Division, Argonne National Laboratoy, Lemont, IL, United States; 2. Materials Science & Engineering, Northwestern University, Evanston, IL, United States; 3. CNRS Institut Jean Lamour, Université de Lorraine, Nancy, France; 4. Unité Mixte de Physique, Centre National de la Recherche Scientifique/Thales, Université Paris Saclay, Palaiseau, France

Taking inspiration from the traditional Galton board's design, we investigate a nanoscale magnetic equivalent of the classical system featuring a Permalloy honeycomb lattice.[1,2] Instead of propagating metal balls, magnetic domain walls are initiated at the top and are driven to the bottom of the lattice. Previous studies on this nanomagnetic Galton board unveiled stochastic behavior in domain wall motion, providing a promising foundation for use in unconventional computing.[3] However, the exact mechanism driving stochastic domain wall motion remains ambiguous. In this study, we apply Lorentz Transmission Electron Microscopy (LTEM) to directly image the magnetic microstructure at the vertices of the Galton board as shown in Figure 1 which drives the stochastic decision making. The findings pinpoint three primary influences on the decision-making in this nanomagnetic system: initial domain wall topology, vertex size, and local inhomogeneities within the patterned samples. Crucially, we have experimentally observed the presence of a lower bound to the curvature of a vertex that can support magnetic solitons at remanence, aligning with our Mumax simulations. In addition, we experimentally find stochasticity in modified Galton boards containing fewer lattice structures. This work not only provides a deeper understanding of the nanomagnetic Galton board's intricacies but also offers insights for other nanomagnetic networks such as artificial spin ices.

1. Zeissler, K. *et al. Sci. Rep.* 3, 1–7 (2013). 2. Walton, S. K. *et al. New J. Phys.* 17, 013054 (2015). 3. Sanz Hernández, D. *et al. Adv. Mater.* 33, (2021).

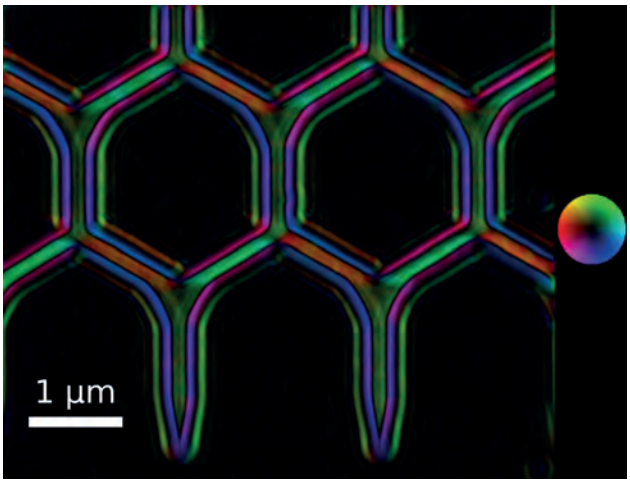

Fig. 1: A reconstructed magnetic induction map of a Galton board array for analysis of stochastic domain wall propagation.

BD-07. Magnetic droplet soliton pairs. S. Jiang[2], S. Chung[3], *M. Ahlberg*[1], A. Frisk[1], Q. Le[1], H. Mazraati[4], A. Houshang[1], O. Heinonen[5,6] and J. Akerman[1,7] *1. University of Gothenburg, Göteborg, Sweden; 2. School of Microelectronics, South China University of Technology, Guangzhou, China; 3. Department of Physics Education, Korea National University of Education, Cheongju, The Republic of Korea; 4. KTH Royal Institute of Technology, Stockholm, Sweden; 5. Argonne National Laboratory, Lemont, IL, United States; 6. Seagate Technology, Bloomington, MN, United States; 7. Tohoku University, Sendai, Japan*

Magnetic droplets are dissipative solitons found in perpendicular magnetized materials where a spin current counteracts the inherent damping. A typical device for droplet studies is the spin torque nano-oscillator, where a thick reference layer (RL) polarizes the applied current, which exert a torque on the free layer (FL) leading to the nucleation of a soliton. Droplets in these devices have been the subject of a large number of experimental and theoretical reports [1, 2]. However, the research has only been focused on magnetic excitations in the free layer. Here, we show that droplets form also in the reference layer at sufficient high currents. The experimental signature of droplet pairs (DP) is a clear decline in the resistance accompanied with strong low-frequency noise (Fig. 1). We use the measured data to construct a phase diagram of the magnetic states as a function of applied field and current. Furthermore, we use micromagnetic simulations to get more detailed insight in the droplet pair state. Figure 2 presents an example of the results. The simulations reveal that the dynamics of coexisting droplets can be described as periodic, pseudo-periodic or chaotic. The coexisting droplets are strongly interacting and constitute a platform for studies of non-linear soliton pair dynamics.

[1] Macià F., and Kent A. D. (2020). Magnetic droplet solitons. J. Appl. Phys., 128, 100901 [2] Sulymenko O. R., Prokopenko O. V., Tyberkevych V. S., Slavin A. N., and Serga A. A. (2018). Bullets and droplets: Two-dimensional spin wave solitons in modern magnonics (Review Article), Low Temp. Phys. 44, 602

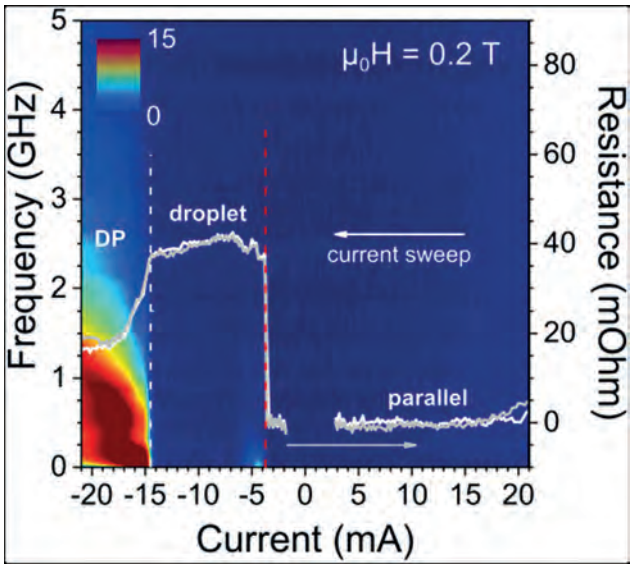

Figure 1. Device resistance and PSD revealing nucleation of an ordinary droplet followed by the emergence of a droplet pair, i.e. the nucleation of an additional droplet in the reference layer.

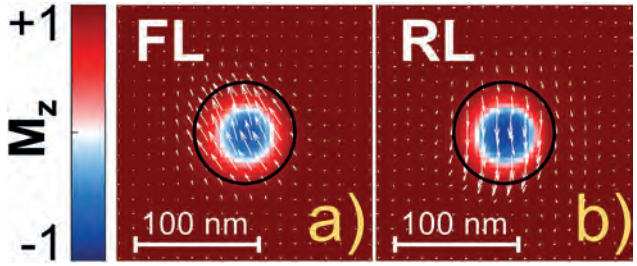

Figure 2. Micromagnetic simulation of coexisting droplets in the free (a) and reference layer (b). The applied field and current are $\mu_0 H$ = 0.5 T and I = -6 mA, respectively.

Session BE
3D MAGNETISM

Peter Fischer, Chair
Lawrence Berkeley National Laboratory, Berkeley, CA, United States

INVITED PAPERS

BE-01. Curvilinear and 3D micromagnetism: geometrically curved ferro- and antiferromagnets. *D. Makarov[1] 1. Helmholtz-Zentrum Dresden-Rossendorf e.V., Dresden, Germany*

Curvilinear magnetism is a framework, which helps understanding the impact of geometrical curvature on complex magnetic responses of curved 1D wires and 2D shells [1-3]. The lack of the inversion symmetry and the emergence of a curvature induced effective anisotropy and Dzyaloshinskii-Moriya interaction (DMI) stemming from the exchange interaction [4,5] are characteristic of curved surfaces, leading to curvature-driven magnetochiral effects. The exchange-driven chiral effects in curvilinear ferromagnets are experimental observables [6] and can be used to realize low-dimensional architectures with tunable magnetochiral properties based on standard magnetic materials. In particular, magnetochiral responses of any curvilinear ferromagnetic nanosystem are governed by the mesoscale DMI, which is determined via both the material and geometrical parameters [7]. Its strength and orientation can be tailored by properly choosing the geometry, which allows stabilizing distinct magnetic chiral textures including skyrmion and skyrmionium states as well as skyrmion lattices [8-10]. Interestingly, skyrmion states can be formed in a material even without an intrinsic DMI [8,10]. Recently, a novel non-local chiral symmetry breaking effect was discovered, which does not exist in planar thin film magnets: it is essentially non-local and manifests itself even in static spin textures living in curvilinear magnetic nanoshells [5]. The combined experimental and theoretical study revealed that the non-local chiral symmetry breaking effect is responsible for the coexistence and coupling of multiple magnetochiral properties within the same magnetic object [11]. The field of curvilinear magnetism is extended towards curvilinear antiferromagnets. Pylypovskyi et al. demonstrated that intrinsically achiral one-dimensional curvilinear antiferromagnets behave as a chiral helimagnet with geometrically tunable DMI, orientation of the Neel vector and the helimagnetic phase transition [12-14]. This positions curvilinear antiferromagnets as a novel platform for the realization of geometrically tunable chiral antiferromagnets for antiferromagnetic spinorbitronics. These new fundamental discoveries of non-local chiral symmetry breaking as well as curvilinear antiferromagnetism will be covered in this presentation.

[1] D. Makarov et al., Curvilinear micromagnetism: from fundamentals to applications (Springer, Zurich, 2022). [2] D. Makarov et al., Advanced Materials (Review) 34, 2101758 (2022). [3] D. D. Sheka et al., Small (Review) 18, 2105219 (2022). [4] Y. Gaididei et al., Phys. Rev. Lett. 112, 257203 (2014). [5] D. Sheka et al., Communications Physics 3, 128 (2020). [6] O. Volkov et al., Phys. Rev. Lett. 123, 077201 (2019). [7] O. Volkov et al., Scientific Reports 8, 866 (2018). [8] V. Kravchuk et al., Phys. Rev. B 94, 144402 (2016). [9] V. Kravchuk et al., Phys. Rev. Lett. 120, 067201 (2018). [10] O. Pylypovskyi et al., Phys. Rev. Appl. 10, 064057 (2018). [11] O. Volkov et al., Nature Commun. 14, 1491 (2023). [12] O. Pylypovskyi et al., Nano Letters 20, 8157 (2020). [13] O. Pylypovskyi et al., Appl. Phys. Lett. 118, 182405 (2021). [14] Y. A. Borysenko et al., Phys. Rev. B 106, 174426 (2022).

BE-02. 3D Magnetic Nanowire Networks for Neuromorphic Computing. *D. Bhattacharya[1], Z. Chen[1], C. Langton[1], E. Marlowe[1], C.J. Jensen[1], J. Malloy[1], C. Liu[2], E.C. Burks[3], D.A. Gilbert[4], X. Zhang[2], G. Yin[1] and K. Liu[1] 1. Department of Physics, Georgetown University, Washington, DC, United States; 2. Materials Science and Engineering, King Abdullah University of Science and Technology, Thuwal, Saudi Arabia; 3. Department of Physics, University of California, Davis, Davis, CA, United States; 4. Materials Science and Engineering, University of Tennessee, Knoxville, Knoxville, TN, United States*

Three-dimensional (3D) magnetic nanostructures may enable novel functionalities due to their unique geometry, intricate spin textures and non-trivial topology, which cannot be achieved in the conventional thin film structures [1, 2]. They have emerged as a promising platform to implement 3D information storage and neuromorphic computing. In this work, we have investigated quasi-ordered and random interconnected nanowire (INN) networks and demonstrated their potentials to be integrated into future computing paradigm. First, we have studied quasi-ordered, free-standing 3D Co nanowire networks fabricated using multiple-angle ion tracking of polycarbonate membranes and electrodeposition (Fig. 1a). First-order reversal curve (FORC) studies revealed intriguing magnetization reversal mechanisms in the networks including intersection-mediated domain wall pinning and propagation [3]. To obtain information about the local magnetic configurations of the networks during reversal, magnetoresistance (MR) measurement have been performed [4]. When only a few interconnected NWs were measured, multiple MR kinks and local minima were observed, a manifestation of discrete propagation of magnetic states in the networks (Fig. 1b). Furthermore, for a descending field sweep from positive saturation, a significant MR minimum is found at a *positive* field, in contrast to the usual case with a minimum in a *negative* field indicative of formation of domain walls (DWs) at the intersection. Magnetic imaging using off-axis electron holography also showed stabilization of DWs at the intersection. The pinning/depinning of the DWs can be further controlled by the driving current density. Another complex network with many intersections is also studied using MR-FORC. Sequential switching of NW sections separated by interconnects was observed where reversal of a part of the network allows access to new magnetization reversal pathways and consequently determines the final magnetic state at any given field (Fig. 1c). Therefore, the network can be conditioned to host different magnetic states by varying the sequence of applied magnetic field. The abundance and ease of stabilization of different magnetic states render these networks attractive for implementing multistate integrated memristor devices. We have also investigated the feasibility of utilizing random Ni NW networks as neuromorphic computing elements [5]. In this case, the Ni NWs were first electrodeposited and then drop casted on a prefabricated multielectrode array (Fig. 2). This offers a relatively simple way to prepare devices than the nuclear track etching method. Similar to the ordered network, the random network exhibits multiple discrete jump as a result of step-by-step switching. Each electrode pair shows unique MR feature as the network geometry varies. The network could be robustly driven to different magnetic states by applying current pulses of varying magnitudes and pulse-widths (Fig. 2). Thus, diverse programming of synaptic weights may be achieved by assigning different electrode pairs as inputs/outputs and controllably switching a certain subsection of the networks by applying current pulses. In summary, our results illustrate the potential of

3D interconnected nanowire networks for applications in spintronic memristors and synaptic devices. These findings open up possibilities for further research to unveil new functionalities towards neuromorphic computing. Work supported in part by the NSF (ECCS-2151809, DMR-2005108), SRC/NIST nCORE SMART Center, and KAUST.

[1] A. Fernández-Pacheco, et al. Nat. Commun. 8, 15756 (2017). [2] P. Fischer, et al, APL Mater. 8, 010701 (2020). [3] E. C. Burks, et al, Nano Lett., 21, 716 (2021). [4] D. Bhattacharya et al, Nano. Lett. 22, 10010 (2022). [5] D. Bhattacharya et al, APS March Meeting, Y54.00001 (2023).

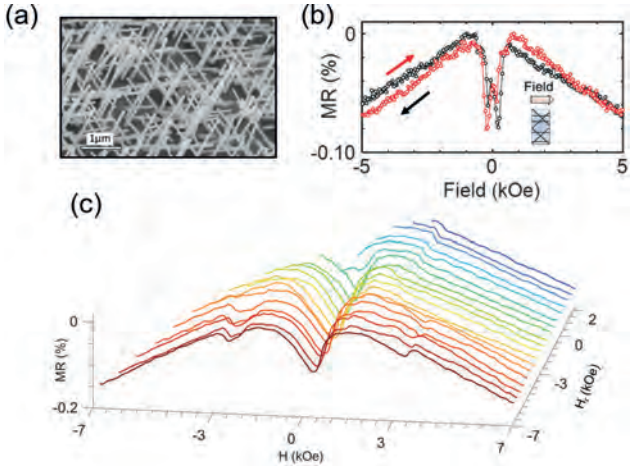

Figure 1. (a) Scanning electron microscopy image of a quasi-ordered Co nanowire network. (b) Multiple kinks in MR measurement showing step-by-step switching along descent-field (black) and ascent-field (red) sweeps. (c) Individual MR-FORCs showing history dependent switching and stochasticity.

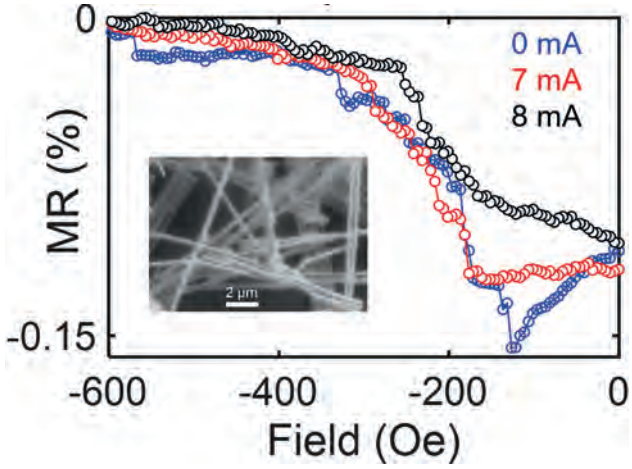

Figure 2. Current induced switching in a random magnetic nanowire network under different current densities. Inset shows zoomed-in view of the network.

CONTRIBUTED PAPERS

BE-03. Magnetic vortex structure in three-dimensional pyramidal Fe nanofilms studied with Kerr microscopy. *J. Juharni*[1], L.N. Pamasi[1], N. Hosoito[1], N. Mabarroh[1], A.N. Hattori[2], H. Tanaka[2], S. Yoshimura[3] and K. Hattori[1] *1. Nara Institute of Science and Technology, Ikoma, Japan; 2. Osaka University, Osaka, Japan; 3. Akita University, Akita, Japan*

The distinct characteristics and potential uses of magnetic vortex in ferromagnetic films have garnered significant interest in the field of magnetism [1]. The challenge of maintaining vortex stability in small sizes, which was constrained by patterned films on 2D plane [2], was overcome by implementing films on 3D structures [3]. This breakthrough was achieved through Landau-Lifshitz-Gilbert (LLG) simulation, which indicates a specific feature such as breaking points (BPs) in magnetization-magnetic field (M-H) curves implying the existence of stable vortex in 3D pyramidal shapes [4]. However, there is no experimental research indicating BPs in M-H curves due to the challenges encountered in the method used for sample growth. In our group, experimentally, we successfully produced 3D pyramidal Fe nanofilms using a combination of photolithography of Si substrates and Si surface treatments [5-6] for Fe deposition, resulting in BPs implying vortex formation [7]. Fig.1 shows the schematic of an Fe film on a 3D Si{111} pyramidal structure; 16 μm edge length and 50 nm of Fe thickness were prepared. Fig. 2 shows M normalized by the saturation magnetization (Ms) as a function of H applied in pyramid outer edge direction (|| Si[110]) measured by vibration sample magnetometer (VSM) at room temperature, displaying certain BPs corresponding vortex. To confirm the presence of magnetic vortex, we combined longitudinal magneto-optic Kerr effect (MOKE) microscopy, judging initial magnetization direction denoted by white arrows in Fig. 1. Clearly right (left) oriented magnetization close to the apex on the upper (downer) 3D-Fe pyramidal facet plane, indicating stable vortex is seen; note little information for right and left facets because M should be perpendicular to H. We noticed magnetization direction on 3D-Fe edge area close to 2D Fe oriented to left direction due to magnetic interaction between 3D and 2D Fe area, which would prevent the vortex formation. In the presentation, we will also demonstrate the results for patterned 3D-Fe pyramids without 2D Fe area.

[1] N. S. Kiselev, A. N. Bogdanov, R. Schafer, et al., J. Phys. D: Appl. Phys. 44, 392001 (2011) [2] R. P. Cowburn, D. K. Koltsov, A. O. Adeyey, et al., Phys. Rev. Lett. 83, 1042–1045 (1999) [3] M. Gavagnin, H. D, Wanzenboeck, D. Belic, et al, ACS nano. 7, 777 (2013) [4] A. Knittel, M. Franchin, T. Fishbacher, et al., New J. Phys. 12, 113048 (2010) [5] A. N. Hattori, S. Takemoto, K. Hattori, *et al.*, Appl. Phys. Express. 9, 085501 (2016) [6] S. Takemoto, A. N. Hattori, K. Hattori, *et al.*, Jpn. J. Appl. Phys. 57, 090303 (2018) [7] A. Irmikimov, L. N. Pamasi, A. N. Hattori, *et al.*, ACS Cryst. Growth Des. 21, 946 (2021)

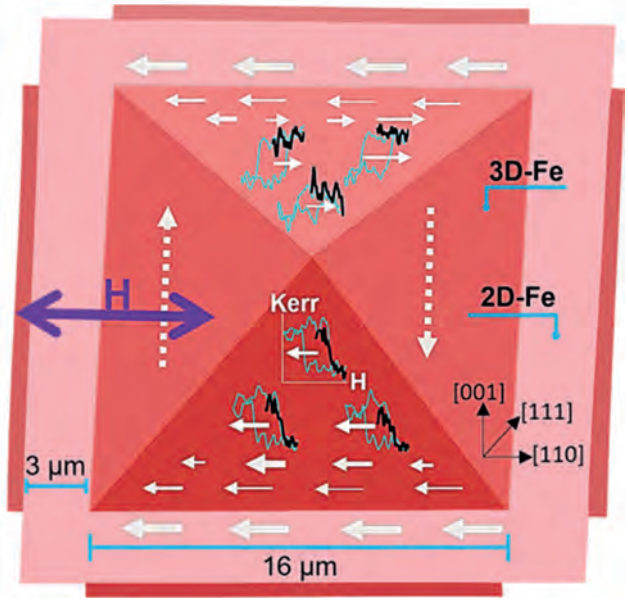

Figure 1. Schematic of 3D Fe with 2D-Fe. White arrows display initial magnetization directions.

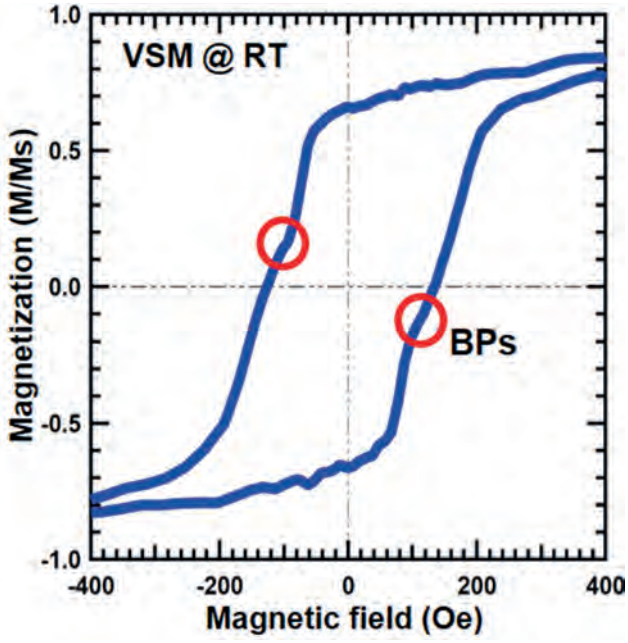

Figure 2. M-H curve of 3D Fe with 2D Fe. BPs are seen at red circles.

BE-04. 3-Dimensional Magnetostatic Interactions in Fe/Au Barcode Nanowire Arrays. *E. Jeong*[2*], A. Samardak[1], Y. Jeon[2], V. Samardak[1], A. Kozlov[1], K. Rogachev[1], A. Ognev[1], G. Kim[2], M. Ko[2], A. Samardak[1] and Y. Kim[2] *1. Far Eastern Federal University, Vladivostok, Russian Federation; 2. Korea University, Seoul, The Republic of Korea*

Memory devices, consisting of highly integrated magnetic nanoelements, have significant potential in computational technologies.[1-2] However, they face challenges related to magnetostatic fields between densely packed nanoelements. These fields can extend up to 100 μm within the array,[3] potentially affecting the magnetic properties of the entire device and damaging stored information. Therefore, research on the 3D magnetic characteristics of nanomaterials is necessary to address this. This study focused on analyzing interwire and intrawire 3D magnetostatic interactions using a multilayered barcode nanowire (BNW) array. We aimed to examine the complex magnetic interactions within the Fe/Au BNW array, synthesizing with the one-bath electrodeposition method. The composition and length of each segment of BNWs were facilely modulated by controlling applied current density and electrodeposition time. The length of Au segments varied from 30 to 200 nm, while the Fe segments remained fixed at lengths of 100 and 200 nm. Each segment's microstructural and compositional characterization was implemented using SEM, TEM, XRD patterns, and energy-dispersive X-ray spectroscopy (EDS). Then the magnetic properties were analyzed using VSM and MFM. The hysteresis curve indicated that the BNW exhibited soft magnetic properties: strong ferromagnetic Fe segments and weak ferromagnetic Au segments. MFM images demonstrated variations in the position of the magnetic poles when the external field was applied parallel or perpendicular to the easy axis of the BNW. Finally, we combined the above results with the first-order reversal curve (FORC) diagram and micromagnetic simulations. We identified three distinct types of magnetostatic interactions in 3D nano-geometry. These are interactions between: 1) opposite magnetic poles of adjacent Fe segments in the same BNW, 2) poles of the same Fe segment, 3) closest poles in the Fe segments of neighboring BNWs in 3D space. The overall dominating types according to the geometric parameters in a 3D BNW array are shown in Fig. 1. This result could be helpful in successfully engineering a magnetic memory cell and logic device.

1. B. Tao, C. Wan, and P. Tang, Nano Lett., Vol. 19, p.3019 (2019) 2. E. Grimaldi, V. Krizakoa, and G. Sala, Nat. Nanotechnol., Vol. 15, p.111 (2020) 3. A. Fernández-Pacheco, R. Streubel, and O. Fruchart, Nat. Commun., Vol. 8, p.15756 (2017)

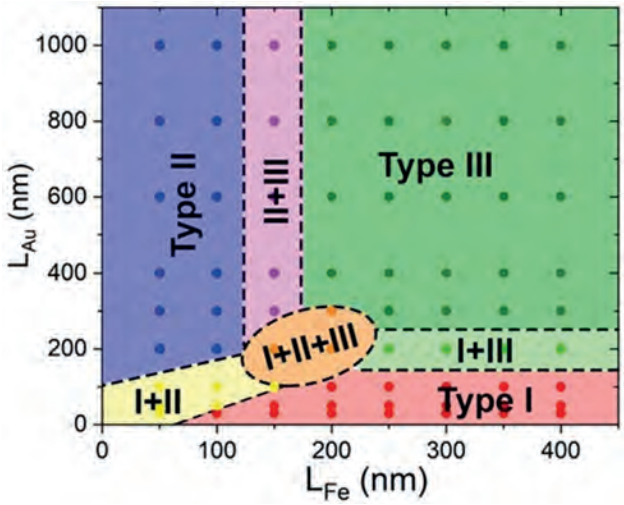

Fig. 1. Parametric diagram of dominating interaction type

BE-05. Domain Wall Formation and Dynamics in Interconnected Helical Nanowires. *J. Fullerton*[1] and C. Phatak[1,2] *1. Materials Science Division, Argonne National Laboratory, Lemont, IL, United States; 2. Department of Materials Science and Engineering, Northwestern University, Evanston, IL, United States*

It is now possible to fabricate complex, interconnected, three-dimensional (3D) nanostructures thanks to recent advances in nanofabrication, such as focused electron beam induced deposition (FEBID) [1]. These structures can possess intricate spin textures that can be controlled by altering the geometry of the system, potentially providing a new route to high density, low power computing and data storage devices [2]. A key nanostructure in the field of 3D nanomagnetism is the helical nanowire, largely studied due to its intrinsic geometric chirality and curvature [3, 4, 5]. We will outline complementary experimental and micromagnetic studies of nanostructures formed by several interconnected helical nanowires (see example in figure 1a), fabricated by FEBID and characterized by Lorentz transmission electron microscopy. Subsequently, we discuss the types of domain walls that form

at the intersections and how they are affected by applied fields. Figure 1a shows a micromagnetic simulation of a remanent magnetic state in an interconnected chain-like nanostructure, consisting of four nanohelices. In this structure three types of domain walls are seen (shown in more detail in figure 1b). A single and double transverse wall is shown in boxes i and iii, respectively (the double case being magnetostatically coupled together), and a helical domain wall is shown in box ii. These results show a further development of how 3D nanostructures could be utilized in domain wall applications and allow a fundamental study into the physics of shape and magnetic coupling in 3D.

[1] L. Skoric, et. al., Layer-by-layer growth of complex-shaped three-dimensional nanostructures with focused electron beams, Nano Lett., 20, 184 (2020). [2] A.Fernandez-Pacheco, et.al., Three-dimensional nano magnetism, Nat.Comm., 8, 15756(2017). [3] D. Sanz-Hernandez, et. al., Artificial double-helix for geometrical control of magnetic chirality, ASC Nano., 14, 8084 (2020). [4] C. Donnelly, et. al., Complex free-space magnetic field textures induced by three-dimensional magnetic nanostructures, Nat. Nanotechnol., 17, 136 (2022). [5] C. Phatak, et. al., Curved three-dimensional cobalt nanohelices for use in domain wall device applications, ACS Appl. Nano Mater., 3, 6009 (2020). This work was supported by the U.S. Department of Energy, Office of Science, Office of Basic Energy Sciences, Materials Sciences and Engineering Division. Use of the Center for Nanoscale Materials, an Office of Science user facility, was supported by the U.S. Department of Energy, Office of Science, Office of Basic Energy Sciences, under Contract No. DE-AC02-06CH11357

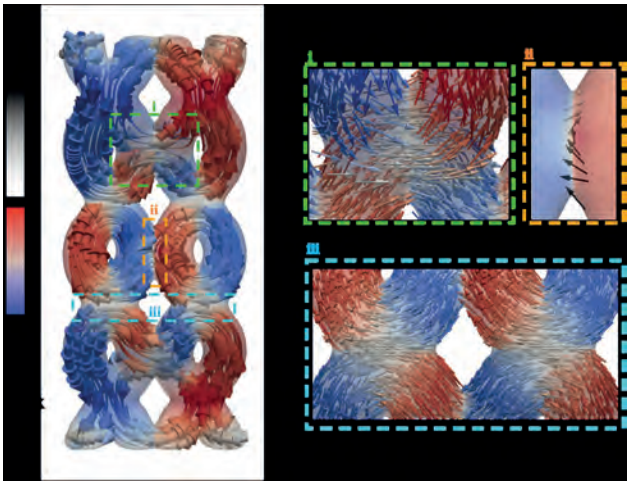

INVITED PAPER

BE-06. Magnetic Charge Ordering in 3D Artificial Spin-ice.
A. Van den Berg[1], M. Saccone[2], E. Harding[1], S. Singh[1], S. Giblin[1], F. Flicker[1] and *S. Ladak[1] 1. School of Physics and Astronomy, Cardiff University, Cardiff, United Kingdom; 2. Los Alamos National Laboratory, Los Alamos, NM, United States*

In this talk, I will outline experiments and modelling carried out upon a 3D artificial spin-ice system [1,2,3,4] which takes the geometry of a diamond-bond lattice, capturing the arrangement of spins in bulk pyrochlore systems. Monte-Carlo simulations of such structures, predict a rich phase diagram with a number of charge-ordered phases including a single and double charged monopole crystal [5]. By using magnetic force microscopy, I will show that the vertex states in experimental systems can be determined, and monopole transport upon the lattice surface can be directly visualised [2]. I will show that experimental demagnetised systems are found to host ferromagnetic stripes upon the surface, a configuration that forbids the formation of the expected double-charge monopole crystal ground state [5]. Instead, the system forms crystallites of single magnetic charge, superimposed upon an ice background. I will move onto discuss how the measured configuration can be understood in terms of an enhanced monopole chemical potential upon coordination-two vertices at the surface, and how this can be controlled with intricate 3D nanostructuring to realise the expected double-charge crystal ground state.

1. May, A. et al. Realisation of a frustrated 3D magnetic nanowire lattice. Communications Physics 2, 13 (2019) 2. May, A. et al. Magnetic charge propagation upon a 3D artificial spin-ice. Nature Communications 12, 3217 (2021) 3. Sahoo, S. et al. Observation of Coherent Spin Waves in a Three-Dimensional Artificial Spin Ice Structure. Nano Letters 21, 4629 (2021) 4. Van den Berg, A. et al. Combining two-photon lithography with laser ablation of sacrificial layers: A route to isolated 3D magnetic nanostructures, Nano Research 16, 1441 (2023) 5. Saccone, M. et al. "Exploring the phases of 3D artificial spin ice: From Coulomb phase to magnetic monopole crystal", arXiv:2211.04551 (2023)

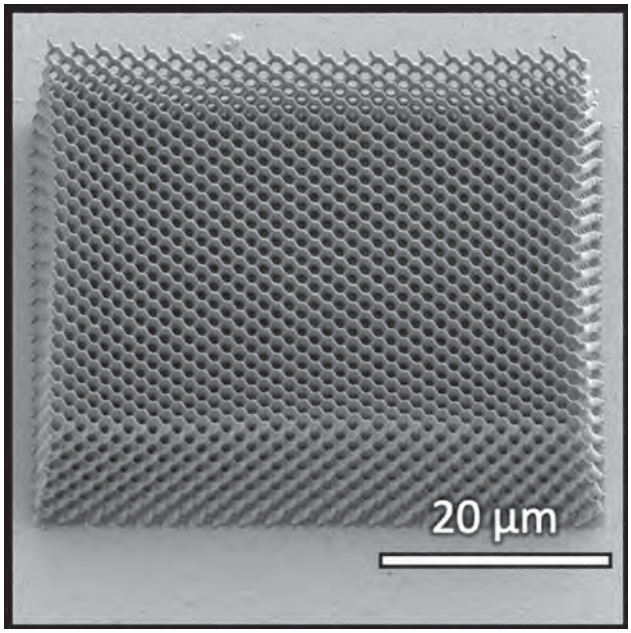

CONTRIBUTED PAPER

BE-07. 3D Printing of Flexible Magnetic Composites Using Digital Light Processing.
N. Tarabay[1], J.A. Lopez Medina[3] and C. Velez[2] *1. Department of Electrical Engineering and Computer Science, University of California, Irvine, Irvine, CA, United States; 2. Department of Mechanical and Aerospace Engineering, University of California, Irvine, Irvine, CA, United States; 3. Centro de Nanociencias y Nanotecnología, Universidad Nacional Autónoma de México, Ensenada, Mexico*

We present a controllable technique for 3D printing of Magneto Active Polymers (MAPs) at milli/micrometer scale using layer-based 3D printing of Digital Light Processing (DLP). Resulting MAPs contain nanoparticles (NPs) of NdFeB, AlNiCo18, AlNiCo38, $NiMnFe_2O_4$, or Fe_3O_4, employing weight ratios between 2-10% into a flexible resin with Young's modulus of ~1.9 MPa. Hard ferromagnetic MAPs presented intrinsic coercivities between 79-715 mT and BH_{max} products between 0.2-2 kGOe. Superparamagnetic MAPs presented saturation magnetizations between 0.5-1.5 mT. The 3D printing of MAPs is still in its early stages and has not been widely adopted in commercial applications [1] [2]. However, with the anticipated progress in technology and materials it is subjected to witness increased prevalence in the manufacturing of electronic devices [3], actuators [4] [5], and microrobotics [6]. We propose to leverage advances of DLP to obtain printed pixel sizes of 35 µm and fine tuning of magnetic response by

controlling NPs material and concentration. The dependence of the magnetic properties and NPs concentration was evaluated by measuring the magnetic moment using the Vibrator Sample Magnetometer (VSM). A printed membrane was created using flexible material as the outer layer and printed MAPs as the inner layer. Mechanical characterization of the membrane was conducted in a laser vibrometer under an oscillating magnetic field resulting in 275 nm displacement that peaks at 24 Hz. The results showed the potential of generating complex and flexible 3D structures at milli/micrometer scale.

[1] W. Clarissa, C. Chia and S. Zakaria, *Progress in Additive Manufacturing.,* Vol. 7, p. 325–350, (2022) [2] G. Ehrmann, T. Blachowicz and A. Ehrmann, *Polymers.*, Vol. 14, no. 18, p. 3895, (2022) [3] M. Cianchetti, C. Laschi and A. Menciassi, *Nature Reviews Materials.*, Vol. 3, p. 143–153, (2018) [4] M. Amjadi, K.-U. Kyung and M. Sitti, *Advanced Functional Materials.*, Vol. 26, p. 1678–1698, (2016) [5] S. Wu, W. Hu and M. Sitti, *Multifunctional Materials.*, Vol. 3, no. 4, p. 042003, (2020) [6] L. Hines, K. Petersen and M. Sitti, *Advanced Materials.*, Vol. 29, p. 1603483, (2017)

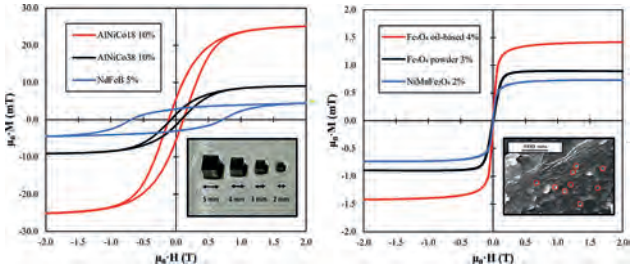

Fig.1 Printed material characterization. (a) hard MAPs in variable volume (insert) (b) soft MAPs and SEM cross section of Fe_3O_4 oil-based MAPs, the particles (red) size was measured and averaged to be 80 nm and validated by Dynamic Light Scattering.

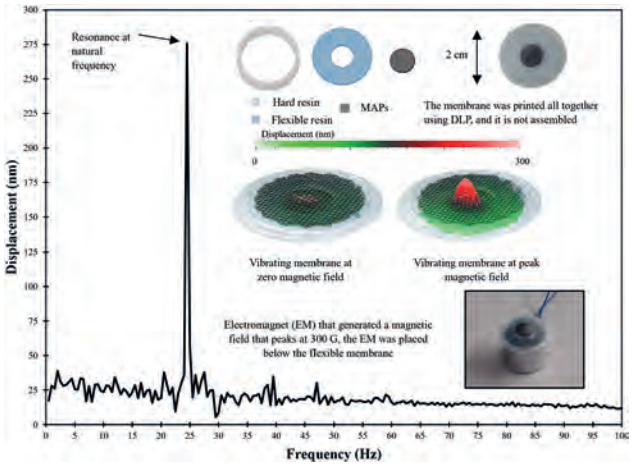

Fig.2 Vibration measurement of a printed flexible membrane (insert). The printed membrane is subjected to an oscillating controlled magnetic field generated by an electromagnet, and their resulting vibrations were measured and analyzed using a scanning laser vibrometer. Surface plot (frame) of the printed membrane showing the MAPs (red) vibrating in the presence of an oscillating magnetic field.

Session BF
FUNDAMENTAL PROPERTIES III: 2D AND TOPOLOGICAL MATERIALS II

Suvayan Saha, Chair
Saha Institute of Nuclear Physics, Kolkata, India

INVITED PAPER

BF-01. Robust negative longitudinal magnetoresistance and spin-orbit torque in sputtered Pt_3Sn and $Pt_3Sn_xFe_{1-x}$ topological semimetal.
D. Zhang[1] *1. Department of Electrical and Computer Engineering, University of Minnesota, Minneapolis, MN, United States*

Spintronic devices are promising candidates for future energy-efficient memory and computing systems. Contrary to topological insulators, topological semimetals possess a nontrivial chiral anomaly that leads to negative magnetoresistance and are hosts to both conductive bulk states and topological surface states with intriguing transport properties for spintronics. In this talk, I will present our recent works about spin orbital torque (SOT) generated from the sputtered Pt_3Sn and $Pt_3Sn_xFe_{1-x}$ topological semimetal [1]. We fabricate highly-ordered metallic Pt_3Sn and $Pt_3Sn_xFe_{1-x}$ thin films via sputtering technology. Systematic angular dependence (both in-plane and out-of-plane) study of magnetoresistance presents surprisingly robust quadratic and linear negative longitudinal magnetoresistance features for Pt_3Sn and $Pt_3Sn_xFe_{1-x}$, respectively. We attribute the anomalous negative longitudinal magnetoresistance to the type-II Dirac semimetal phase (pristine Pt_3Sn) and/or the formation of tunable Weyl semimetal phases through symmetry breaking processes, such as magnetic-atom doping, as confirmed by first-principles calculations. Furthermore, Pt_3Sn and $Pt_3Sn_xFe_{1-x}$ show the promising performance for facilitating the development of advanced spin-orbit torque devices. These results extend our understanding of chiral anomaly of topological semimetals and can pave the way for exploring novel topological materials for spintronic devices. Note: Delin Zhang's current address is Tiangong University, Tianjin, China

References 1. Delin Zhang, et al., arXiv:2305.05801 (2023) (Nature Communications in press)

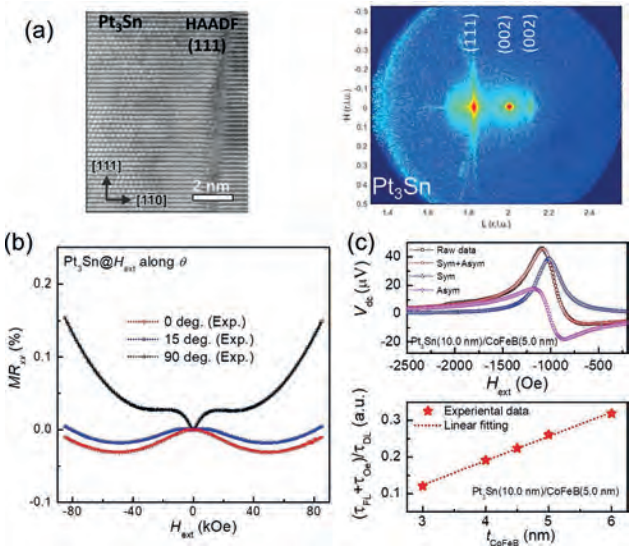

Fig. 1. (a) HAADF-STEM images of the Pt_3Sn thin film on the MgO substrate. Reciprocal space maps (RSM) around the (002) Bragg reflection of the MgO substrate of the Pt_3Sn thin film. (b) The experimental measured MR_{xx} vs. H_{ext} curves of Pt_3Sn for θ-angle dependence. (c) the room temperature ST-FMR spectra for the Pt_3Sn (10.0 nm)/CoFeB (5.0 nm) devices. The ratio $(\tau_{FL} + \tau_{Oe})/\tau_{AD}$ plotted against the thickness of the CoFeB layer. Through the linear fitting, spin torque efficiency θ_{SH} of ~ 0.4 is obtained for Pt_3Sn (10.0 nm).

CONTRIBUTED PAPERS

BF-02. ^{151}Eu Mössbauer study of flux-grown ferromagnetic and antiferromagnetic forms of $EuCd_2As_2$. *D. Ryan*[1], N. Jo[2], B. Kuthanazhi[3,4], S.L. Bud'ko[3,4] and P.C. Canfield[3,4] *1. Physics, McGill University, Montreal, QC, Canada; 2. Physics, University of Michigan, Ann Arbor, MI, United States; 3. Ames National Laboratory, Ames, IA, United States; 4. Physics and Astronomy, Iowa State University, Ames, IA, United States*

$EuCd_2As_2$ is a remarkably complex magnetic semimetal that may behave as a topological insulator or host two pairs of Weyl points, depending on the growth conditions and the final magnetic state [1]. It can be tuned from having an antiferromagnetic (AFM) ground state to a ferromagnetic (FM) one simply by changing growth conditions. Stoichiometric materials grown either from a NaCl/KCl flux or using tin as a solvent, exhibit AFM order below T_N=9.45(3)K, while (slightly) Eu-deficient materials grown from a NaCl/KCl flux exhibit FM order below T_c=30.3(K) [1]. Similar AFM→FM changes can also be induced by doping (<1%) with Ag or Na [2]. ^{151}Eu Mössbauer spectroscopy shows that the differences between the AFM and FM forms extend well beyond their ground state magnetic structures, and that while the AFM form undergoes a conventional AFM→paramagnetic transition, the FM form passes through a complex incommensurate modulated state before becoming paramagnetic. Fig.1 shows the spectra obtained for the AFM form where the spectral evolution is fully conventional: the lines remain sharp and the hyperfine field (B_{hf}) simply declines following

the expected $J=^{7}/_{2}$ Brillouin function. By contrast, Fig.2 shows the spectra for the FM form where the lines broaden immediately on warming above 5K, and the spectra increasingly develop excess weight towards the centre of the pattern; changes typical of an incommensurate modulated magnetic structure [3]. By ~20K the modulation is sufficiently strong that the magnetic order must be effectively AFM, or at least *ferri*magnetic, well before we reach the ordering temperature. Even though it is possible to establish the FM ground state predicted by DFT calculations [4] the competing AFM order reappears at higher temperatures. Neutron diffraction measurements will be required to establish the detailed nature of the ordering and follow its evolution with temperature.

[1] Na Hyun Jo *et al.* Phys. Rev. B101 (2020) 141402(R). [2] B. Kuthanazhi *et al.* Phys. Rev. Mater. 7 (2023) 034402. [3] P. Bonville *et al.* Eur. Phys. J. B 21 (2001) 349. [4] L.-L. Wang *et al.* Phys. Rev. B 99 (2019) 245147.

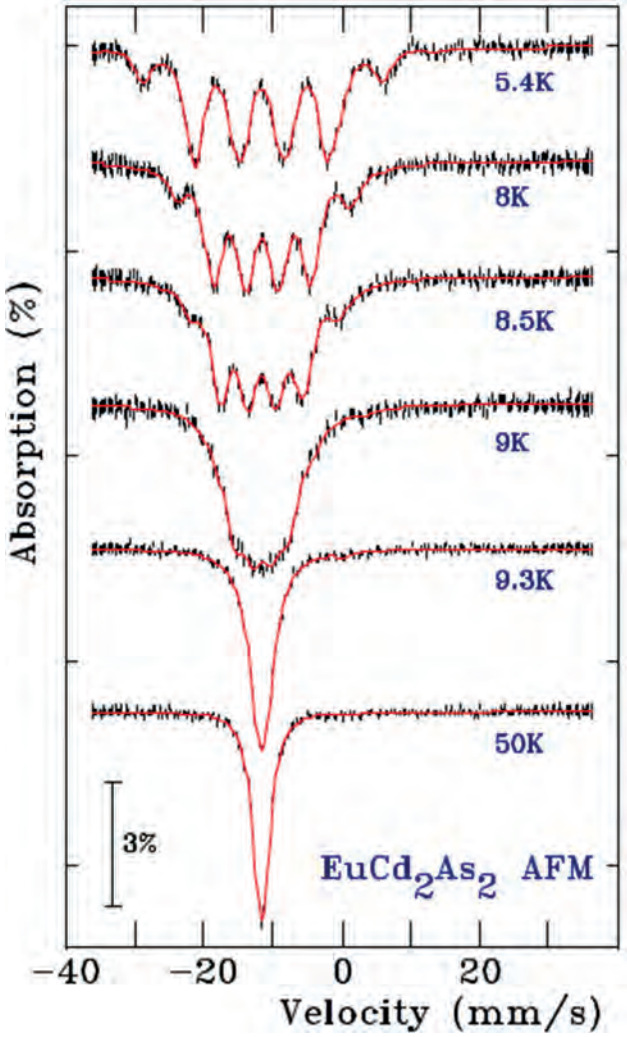

^{151}Eu Mössbauer spectra of the AFM form of $EuCd_2As_2$ showing a conventional evolution with increasing temperature.

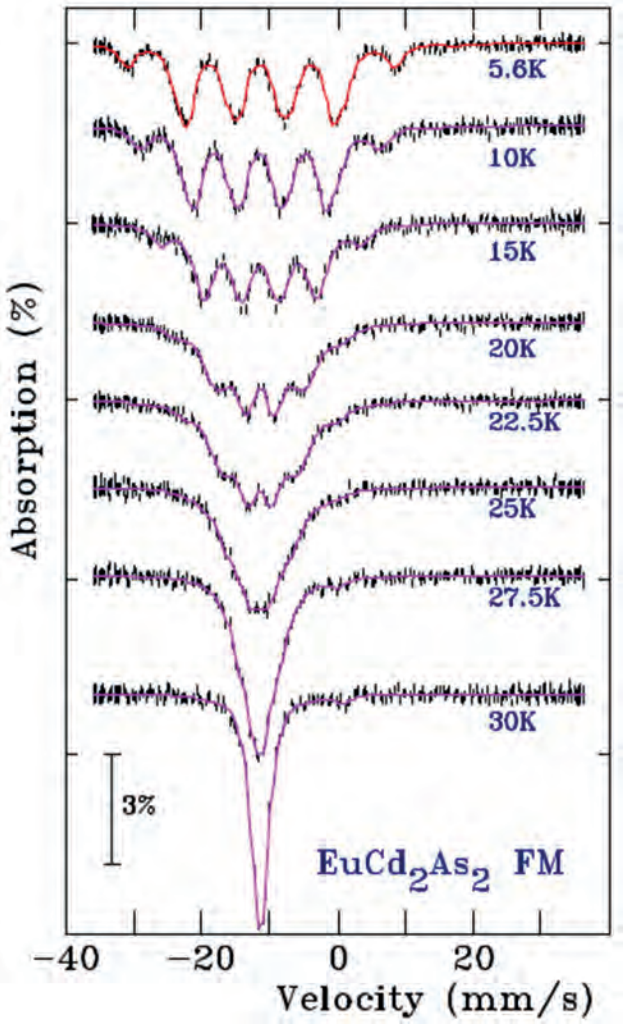

^{151}Eu Mössbauer spectra of the FM form of $EuCd_2As_2$ showing changes in the shape of the spectra that are characteristic of the development of an incommensurate modulated magnetic structure [3].

BF-03. Vortex phase transition and TAFF study of superconducting Fe (Te, Se) thin films. R. Kumar[1], A. Mitra[1] and *G.D. Varma*[1] *1. Physics, Indian Institute of Technology Roorkee, Roorkee, India*

Among all Iron based superconductors (IBS), Fe chalcogenides are more interesting because of their crystal structure simplicity, less toxic constituent elements, similarity of electronics state and fermi surface nesting with other IBS, which makes them the best candidate for probing the mechanism of superconducting [1-5]. In the present work, we have studied the effect of thickness on the structural and superconducting properties of Fe(Te, Se), fabricated on yttria-stabilized zirconia substrates by the pulsed laser deposition technique. The X-ray diffraction (XRD) results reveal that the grown films with different thicknesses are mainly (*00l*) orientated, which suggests the unidirectional growth of thin films. The electric transport measurements reveal that onset of superconducting transition is high for higher thickness thin film (Z2), around 13.16 K. From magnetoresistance measurements in the 0-8 T magnetic field range, the upper critical fields ($H_{C2}(0)$) have been obtained via Ginzburg Landau (GL) theory as well as by the Werthamer-Helfand-Hohenberg (WHH) model for 90%, 50% and 10% of normal state resistivity criterion [6]. The GL coherence lengths have also been calculated for the obtained $H_{C2}(0)$ values. Both the models suggest that the $H_{C2}(0)$ values are high for higher thickness thin films. Moreover, using the magnetoresistance measurements, the thermal activation energies (TAE) of both

the thin films have also been obtained via the conventional as well as by the modified thermally activated flux flow (TAFF) models. From the modified TAFF model analysis, the plots between $-\mathrm{dln}(\rho/\rho_{18})/\mathrm{dT}^{-1}$ versus T (Fig.(1)) have been used to estimate the TAE of both the grown thin films. From both conventional and modified TAFF models, TAE have been observed high for the higher thickness thin film. Furthermore, the results for vortex phase study reveals the transition from vortex liquid region to the vortex glass region at higher temperatures for higher thickness thin film.

1. Y. Kamihara, T. Watanabe, M. Hirano, and H. Hosono, J. Am. Chem. Soc. 130, 3296 (2008). 2. F. C. Hsu, J. Y. Luo, K. W. Yeh, T. K. Chen, T. W. Huang, P. M. Wu, Y. C. Lee, Y. L. Huang, Y. Y. Chu, D. C. Yan, and M. K. Wu, Proc. Nat. Acad. Sci. U.S.A.105, 14262 (2008). 3. H. Hosono and K. Kuroki, Physica C 514, 399 (2015). 4. W. Bao, Y. Qiu, Q. Huang, M. A. Green, P. Zajdel, M. R. Fitzsimmons, M. Zhernenkov, S. Chang, M. Fang, B. Qian, E. K. Vehstedt, J. Yang, H. M. Pham, L. Spinu, and Z. Q. Mao, Phys. Rev. Lett. 102, 247001 (2009). 5. M. Ozabaci, J. Supercond. Nov. Magn. 36, 445 (2023). 6. R. Kumar and G. D. Varma, Phys. Status Solidi B 257, 1900552 (2019).

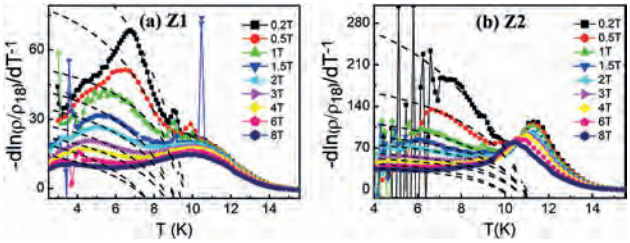

Figure (1). $-\mathrm{dln}(\rho/\rho_{18})/\mathrm{dT}^{-1}$ versus T (K) for the estimation of TAE using TAFF Model for (a) lower thickness film (Z1) and (b) higher thickness film (Z2).

BF-04. Spin-liquid State in Magnetically Diluted Jahn-Teller Active Spinel Pyrochlore ($ZnFe_2O_4$). *S.K. Jena*[1] and S. Thota[1] *1. Department of Physics, Indian Institute of Technology Guwahati, Guwahati, India*

Pyrochlore structures exhibit inherent magnetic frustration owing to their corner-shared tetrahedral geometry[1], which can be modulated to higher degrees by appropriate substitution of magnetic/non-magnetic elements[2]. However, the octahedral(*B*) site topology in the spinel lattice(AB_2O_4) that can accommodate a wide variety of elements may affect the exchange coupling between the magnetic ions significantly resulting in exotic magnetic phenomena such as spin-liquid(SL)/ice and spin-glass(SG) states[3]. $ZnFe_2O_4$(ZFO) is one such Pyrochlore oxide having extensive application in artificial neural network, computer science and genetics[4,5]. In the present work, bulk forms of polycrystalline ZFO was prepared all together doped with the Jahn-Teller active elements: dilute Cu^{2+}(*A* site) and Mn^{3+}(*B* site) with the intent to achieve altered exchange interaction with lifted ground state degeneracy. The neutron diffraction measurements(Fig.1) reveals tetragonal($I4_1/amd$) structural symmetry of the synthesized $Zn_{0.8}Cu_{0.2}FeMnO_4$ system which shows strong broadening for the (101), (002) and (110) magnetic reflections in the 20-40° 2θ range. Further, the ac-magnetic susceptibility(Fig.2) data shows three peaks (across 9K, 47K and 63K) in the loss spectrum; the former two peaks shift under varying frequency(*f*) indicative of SG phase much below the ferrimagnetic ordering ~80K. Yet, the Mydosh parameter $\Omega(= (T_{f2}-T_{f1})/[T_{f1}(log\, f_2 - log\, f_1)])$ calculated from the peak position(T_f) in $\chi''(T,f)$ corresponding to the highest (f_2) and lowest (f_1) frequencies depicts different kind of phase below 9K than that below the SG ordering (T_{SG}=47 K). A detailed thermo-remanent magnetization analysis(inset of Fig.2) reveals that in the SL region (which persists below 9K), in contrast to SG, the properties do not obey thermal activation process, in-line with the heat capacity results.

[1] E. Maniv, R. A. Murphy and J. G. Analytis, *Nat. Phys.* 17, 525 (2021) [2] J. S. Gardner, M. J. P. Gingras and J. E. Greedan, *Rev. Mod. Phys.* 82, 53 (2010) [3] S. K. Jena, M. S. Seehra and S. Thota, *J. Phys.: Condens. Matter 35*, 375802 (2023) [4] P. W. Anderson, *Phys. Rev.* 102, 1008 (1956) [5] M. T. Wolfinger, S. Will and P. F. Stadler, *EPL* 74, 726 (2006)

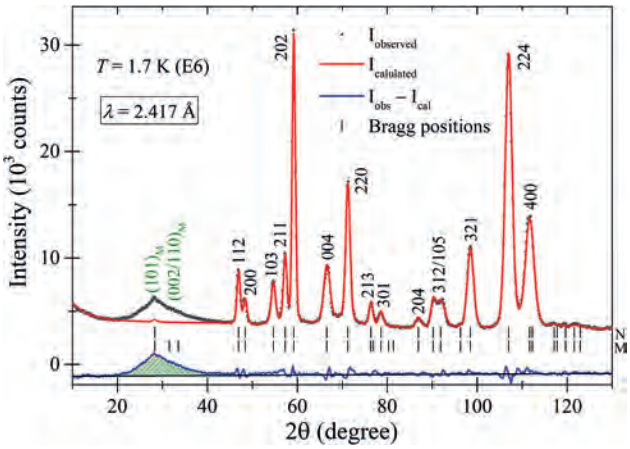

Fig. 1: Rietveld refinement of the powder neutron diffraction data of bulk $Zn_{0.8}Cu_{0.2}FeMnO_4$. The black vertical bars N and M mark the nuclear and magnetic reflections, respectively.

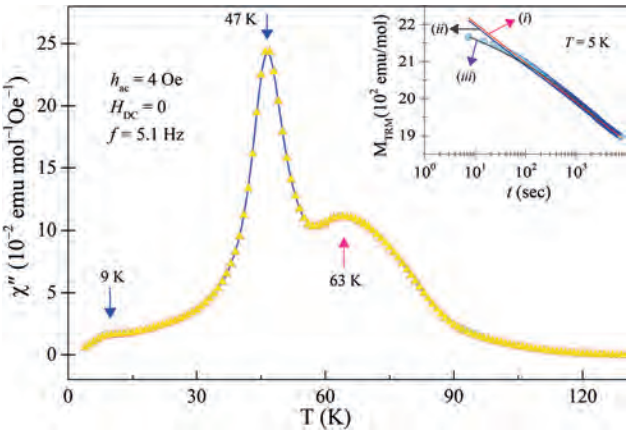

Fig. 2: Temperature dependence of the imaginary part of ac-susceptibility measured under 4 Oe ac-field and zero dc-bias. Inset shows the thermo-remanent magnetization performed at $T = 5$ K.

BF-05. Revealing unconventional quantum oscillations and non-trivial electronic states at EuO/$KTaO_3$ interface. *R. Km*[1], M. Duman[2], M.K. Chan[1], S. Chakraverty[2] and N. Harrison[1] *1. NHMFL, Los Alamos National Laboratory, Los Alamos, NM, United States; 2. Quantum Materials and Devices, Institute of NanoScience and Technology, Mohali, India*

The coexistence of electric-field controlled superconductivity and spin-orbit interaction in two-dimensional electron systems (2DES) based on complex oxides (e.g., $SrTiO_3$ and $KTaO_3$) hold great promise for next-generation of spintronics and quantum computing. The key to the success of these multi-functional 2DES for technological applications lies in a comprehensive understanding of their electronic properties. To address this, we recently investigated quantum oscillations of the $KTaO_3$-2DES in high magnetic fields and at low temperatures. $KTaO_3$ is a 5*d* transition metal oxide, exhibiting a lighter effective mass of electrons and a stronger spin-orbit interaction at its conducting surface/interface than its counterpart $SrTiO_3$ [1-3]. A high-mobility spin-polarized 2D electron gas (2DEG) with the superconducting feature is discovered at the EuO/$KTaO_3$ interface [4]. In this talk, I will present novel insights into the electronic states of the 2DEG at EuO/$KTaO_3$ interface investigated through Shubnikov-de Haas oscillations. To accurately resolve these oscillations, we performed transport measurements in high magnetic fields (60 T) and at low temperatures (down to 0.5 K). Remarkably, we observed a progressive increase in cyclotron mass and

oscillation frequency with the magnetic field, indicating the presence of non-trivial electronic bands. In addition to providing experimental evidence for topological-like electronic states in $KTaO_3$-2DES, these results shed light on the recent predictions[5] of topological states in the 2DES based on similar perovskite transition metal oxides.

[1] K. Rubi *et al*., Nature npj Quantum Materials 5, 1 (2020). [2] King, P. D. C. *et al*. Phys. Rev. Lett. 108, 117602 (2012). [3] K. Rubi *et al*., Phy. Rev. Research 3, 033234 (2021). [4] H. Zhang *et al*., Phys. Rev. Lett. 121, 116803 (2018); Liu *et al*., Science 371, 716 (2021). [5] M. Vivek *et al*., Phys.l Rev. B 95, 165117 (2017); Z. Liu, *et al*., npj Computational Materials 8, 208 (2022).

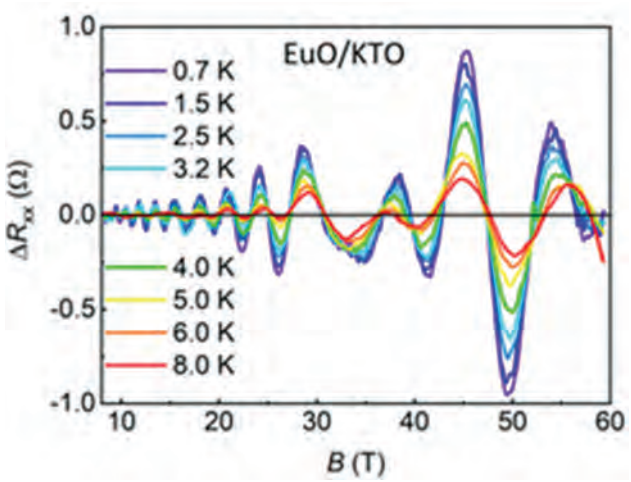

Oscillating resistance of EuO/$KTaO_3$ interface as a function of magnetic field at different temperatures. The oscillations amplitude decreases with increasing temperatures as an effect of the smearing out the edge of the Fermi-Dirac distribution function. The cyclotron mass is estimated from the temperature dependence of the oscillations amplitude.

BF-06. Spin-flop quasi metamagnetic, anisotropic magnetic, and transport behavior of Ho substituted $ErMn_6Sn_6$ kagome magnet. J.F. Casey[1], S. Samatham[2], C. Burgio[1], N. Kramer[1], A. Sawon[1], J. Huff[1] and *A. Pathak*[1,3] *1. Physics, Buffalo State University, Buffalo, NY, United States; 2. Physics, Chaitanya Bharathi Institute of Technology, Hyderabad, India; 3. GE Research, Niskayuna, NY, United States*

We report on the anisotropic-magnetic and electrical transport investigations of a kagome structured Ho doped $ErMn_6Sn_6$, i.e. $Er_{0.5}Ho_{0.5}Mn_6Sn_6$ single-crystal, by magnetization and electrical resistivity measurements. $Er_{0.5}Ho_{0.5}Mn_6Sn_6$ is found to order antiferromagnetically (AFM) at Néel temperature T_N ~ 350 K followed by a ferrimagnetic (FiM) order below T_C ~ 114 K along with a spin-orientation transition at T_t ~ 20 K. The magnetization measurements along *c*-direction ($H \| c$) reveal a narrow hysteresis between spin reorientation and field-induced FiM phases below T_t, a strengthened FiM phase in the region $T_t<T<T_C$ and AFM-FiM coexistence up to a field of about 30 kOe and an emerging FiM phase above 30 kOe in the temperature region $T_C<T<T_N$. On the contrary, the measurements along *ab*-plane ($H \| ab$), confirm a spin-flop quasi-metamagnetic transition from a weak AFM state to a field-induced FiM between T_N and T_C. The weak AFM interactions in ab-plan is because of the non-correlated individual contribution of R-Mn sublattices. The zero-field electrical resistivity shows metallic behavior with a quadratic temperature dependence at low temperatures indicating Fermi liquid behavior. The temperature-field (*T-H*) phase diagrams, constructed based on the magnetic features observed along the *c*-direction and in the *ab*-plane, depict the manifestation of the ground state magnetic properties of $Er_{0.5}Ho_{0.5}Mn_6Sn_6$ under the influence of magnetic fields [1-3]. ACKNOWLEDGMENTS- This work was performed at the State University of New York (SUNY), Buffalo State University, and supported by the National Science Foundation, Launching Early-Career Academic Pathways in the Mathematical and Physical Sciences (LEAPS-MPS) program under Award No. DMR-2213412.

[1] Kabir et al., Phy. Rev. Mater. 6, 064404 (2022). [2] Dhakal et al., Phy. Rev. B, 104, L161115 (2021). [3] Casey et al., Phy. Rev. Mater. (accepted).

BF-07. Large tuneable exchange fields due to purely paramagnetically limited domain wall superconductivity. *P. Banerjee*[1] and A. Pal[1,2] *1. Metallurgical Engineering & Materials Science, Indian Institute of Technology Bombay, Mumbai, India; 2. Centre of Excellence in Quantum Information Computing Science & Technology, Indian Institute of Technology Bombay, Mumbai, India*

Local application and precise tunability of large magnetic fields would bear an enticing prospect for generating and detecting Majorana fermions. Such functionality can be readily achieved using Superconductor (S) /Ferromagnet (F) bilayers, where superconductivity is strengthened on top of domain walls due to local lowering of the proximity-induced large effective exchange fields resulting in significant Tc enhancements and possible magnetic switching of this domain wall superconducting (DWS) phase. Using Nb and ferromagnetic insulating (GdN) bilayers and detailed magneto-transport measurements, we demonstrate previously unobserved phenomena of strengthening the DWS phase with shrinkage of cooper pairs. In the thinnest of Nb layers, we estimate in congruence with the theory of domain wall superconductivity that this tunability of proximity-induced exchange fields must be as high as 1.3T with an application of in-plane external fields of few mT.

BF-08. Magnetism in Molecule-based Systems: from Paramagnetic Complexes to Hard Magnets. R. Clérac[1], P. Perlepe[1], I. Oyarzabal Epelde[1,2], C. Mathonière[1], K.S. Pedersen[1,3], M. Rouzieres[1], N. Yutronkie[1,4], F. Wilhelm[4] and *A. Rogalev*[4] *1. CNRS, Centre de Recherche Paul Pascal, Pessac, France; 2. University of the Basque Country, San Sebastian, Spain; 3. Department of Chemistry, Technical University of Denmark, Kgs. Lyngby, Denmark; 4. European Synchrotron Radiation Facility, Grenoble, France*

The field of molecular magnetism offers an excellent playground for quantum phenomena, but applications of molecule-based magnets are usually hindered by low ordering temperatures and lack of sizeable coercivity. Only very few examples of molecule-based materials have demonstrated spontaneous magnetization above room temperature(RT) but with negligibly small coercivity. On the other side, one can imagine these magnetic systems as platforms for implementing additional functionalities within a single designed material. The versatility of coordination chemistry using abundant 3d metal ions and easily available organic ligands keeps all its promises to design next-generation magnets starting from paramagnetic complexes. The spin and orbital 3d magnetic moments, their anisotropy and transfer to ligands are crucial ingredients into rational approach to develop new building-blocks for future magnets. In this regard, X-Ray Magnetic Circular Dichroism (XMCD) is an essential tool to study molecule-based magnets, given its element and orbital specificity, in addition to its high sensitivity. These studies should be typically done at very low temperatures and high magnetic field nicely complementing macroscopic measurements. Paramagnetic complexes can be used as metal-ion precursors and linked together via redox-active ligands mediating strong magnetic interactions between them. These molecular assemblies can extend in two-dimensional arrays generating a highly delocalized network, e.g. $CrCl_2(pyrazine)_2$[1], that leads to the appearance of a ferrimagnetic order with an ordering temperature as high as 55 K. These remarkable magnetic properties can be further tuned by simply injecting electrons into the pyrazine scaffold through post-synthetic treatments, which results in an increase of the ordering temperature to a record 515 K with unprecedented 7500-Oersted coercivity at RT [2]. This presentation will divulge on the construction of molecule-based RT hard magnets from paramagnetic building blocks and the impact of advanced

magnetic characterization tools based on XMCD. Ongoing efforts are in progress to further tune the physical properties and engineering of these materials for future applications.

[1] K. S. Pedersen, et al., Nature Chemistry, Vol. 10, p.1056 (2018) [2] P. Perlepe, et al., Science, Vol. 370, p.587 (2020)

BF-09. Magnetic Ground States of Non-linear Antiferromagnetic Coordination Polymer Chains. *S. Vaidya*[1], R. Johnson[2], J. Singleton[3], J. Manson[4] and P. Goddard[1] *1. Physics, University of Warwick, Coventry, United Kingdom; 2. University College London, London, United Kingdom; 3. National High Magnetic Field Laboratory, Los Alamos, NM, United States; 4. Eastern Washington University, Washington, WA, United States*

Coordination polymers, in which lattices of magnetic metal ions are bridged by ligands, have proven to be an effective platform for exploring the properties of low-dimensional quantum magnets [1]. The ability to interchange the ligand species make these systems highly tuneable. Additionally, organic ligands such as pyrimidine (pym) allows the study of non-linear chain structures, which are not easy to realise in entirely inorganic structures. Previously, pym has been used to synthesise the staggered and chiral Cu(II) spin-1/2 antiferromagnetic chains, pym-$Cu(NO_3)_2(H_2O)_2$ [2] and $[Cu(pym)(H_2O)_4]SiF_6.H_2O$ [3], respectively. In these materials, the alternating orientation of the local spin environment gives rise to non-trivial staggered *g* tensors and Dzyaloshinskii-Moriya (DM) interactions which, on application of an external magnetic field, generate a staggered field and an unusual field-dependent energy gap [4]. In a theoretical tour de force it was shown that mapping the Hamiltonian to the sine-Gordon quantum-field theory accounts for this behavior in the staggered chain [5,6]. However, similar physics remains to be fully explained for the chiral chain. Recently, we synthesized the spin-1 Ni(II) analogues, $Ni(pym)(NO_3)_2(H_2O)_2$ (Fig. 1) and $[Ni(pym)(H_2O)_4]SO4$ (Fig. 2), of the staggered and chiral chains, in addition to third a non-linear structure $NiCl_2(pym)_2$. In these systems, an alternating single-ion anisotropy axis is expected to accompany the alternating local *g* tensors. We have used muon spin rotation and high field magnetisation experiments to infer the magnetic properties of these materials. Here, we present the ordered magnetic structure resulting from the competition of the exchange and the unusual alternating anisotropy axis.

[1] P. A. Goddard *et al*., *Phys. Rev. Lett.* 108, 077208 (2012) [2] R. Feyerherm *et al*., *Phys. Condens. Matter* 12, 8495 (2000) [3] J. Liu et al., *Phys. Rev. Lett.* 122, 57207 (2019) [4] D. C. Dender, et al., *Phys. Rev. Lett.* 79, 1750 (1997) [5] M. Oshikawa and I. Affleck, *Phys. Rev. Lett*. 79, 2883 (1997) [6] I. Affleck and M. Oshikawa, *Phys. Rev. B* 60, 1038 (1999).

Fig. 1 A single chain of $Ni(pym)(NO_3)_2(H_2O)_2$ viewed from the c-axis. Ni-pym-Ni chains run in the *ac*-plane with the Ni octahedra tilted out of the plane with a 2-fold staggered orientation.

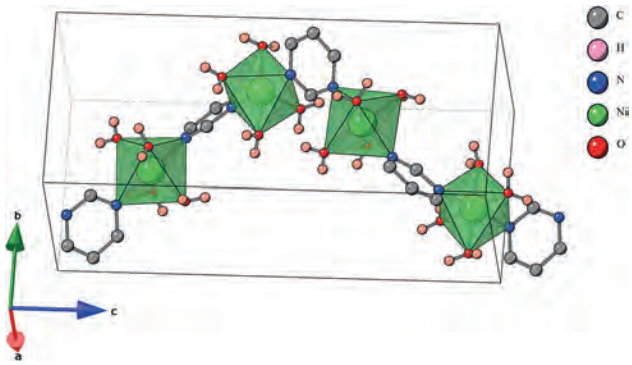

Fig. 2 Structure of $Ni(pym)(H_2O)_4]SO_4$ (SO_4 omitted for clarity). Ni octahedra along the Ni-pym-Ni chain are rotated by 90° between nearest neighbours resulting in a chiral chain structure.

BF-10. Magnetism of Multifunctional Metal-Organic Frameworks Incorporating Tailored Combinations of Multiple Rare-Earth Cations. *E. Bartolome*[5,4], A. Arauzo[1,2], M. Valvidares[3] and J. Giner Planas[4] *1. Instituto de Nanociencia y Materiales de Aragón (INMA), CSIC, Zaragoza, Spain; 2. Condensed Matter Physics, University of Zaragoza, Zaragoza, Spain; 3. ALBA Synchrotron, Barcelona, Spain; 4. Institut de Ciència de Materials de Barcelona (ICMAB-CSIC), Barcelona, Spain; 5. EUSS Research Group, Escola Universitària Salesiana de Sarrià (EUSS), Barcelona, Spain*

Metal-organic frameworks (MOFs) including different rare-earth (RE) ions are receiving growing attention, due to their interest for numerous applications, such as quantum computing, luminescence, anticounterfeiting, thermometry, etc. However, up to now the preparation of multi-metallic RE MOFs remained elusive. Recently, we were able to synthesize MOFs, based on a boron cluster-based ligand[1], incorporating any desired combination of up to eight different RE ions[2]. This milestone opens a flexible playground for the investigation of RE-based "compositionally complex materials". Herein, we demonstrate the remarkable potential of our strategy by presenting selected examples of multi-metallic MOFs with tailored RE-combinations. We synthesized and characterized the magnetic, thermal and optical properties of the first ever MOF containing 8 RE ions (Dy, Tb, Gd, Ce, Yb, Eu, La, Y), 8RE-mCB. Element-selective X-ray Absorption Spectroscopy and X-ray Magnetic Circular Dichroism (XMCD) allowed us to characterize spectroscopically each of the RE ions (Figure 1), and determine their orbital, spin and total magnetic moments. The measured susceptibility-temperature product $\chi T(T)$ and magnetization cycle $M(H)$ agree with the predictions for a diluted system of non-interacting ions, considering the MOF elemental composition. Ac susceptibility reveals that 8RE-mCB exhibits field-induced magnetic relaxation through a thermally-activated process and a direct relaxation mechanism. Moreover, the compound shows interesting magnetocaloric effect (MCE) performance, as evidenced by heat capacity measurements performed down to 0.3 K. In addition, we used our multivariate approach to combine Gd^{3+} (favourable for MCE) with other RE ions to obtain "self-refrigerated" {Gd-nRE} multifunctional MOFs for different applications, e.g. {Gd-Dy} MOFs with Single-Molecule Magnet nodes, {Gd-Tb} with qubit nodes, and {Gd-Eu, Tb, Eu/Tb} luminescent MOFs. We report the magneto-thermal properties of these multi-metallic compounds, compared to those of isostructural homonuclear analogues, investigated by dc and ac magnetometry, XMCD(H,T) and heat capacity.

1. Z. Li, R. Núñez, M. E. Light et al., Chem. Mater. vol. 34, p. 4795 (2022).
2. E. Bartolomé et al., "A metal-organic framework incorporating eight different size rare-earth metal elements: toward multifunctionality à la carte", submitted.

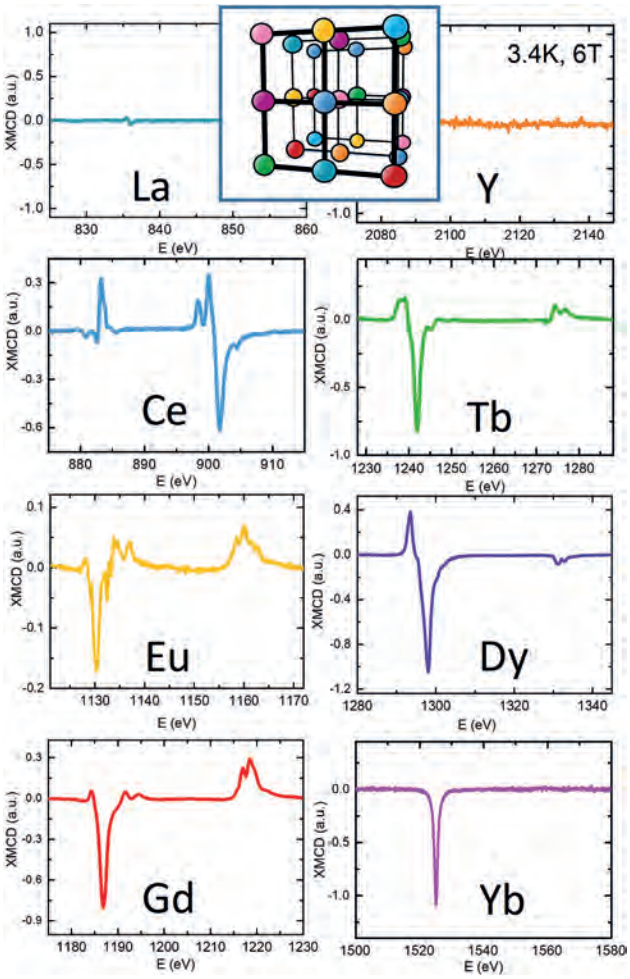

Figure 1. XMCD spectra at the $L_{2,3}$ edges of Y and $M_{4,5}$ edges of La, Ce, Eu, Gd, Tb, Dy and Yb in 8RE-mCB.

Session BG
SENSORS, HIGH FREQUENCY DEVICES, AND POWER DEVICES

Zhenchao Wen, Co-Chair
National Institute for Materials Science (NIMS), Tsukuba, Japan
Sara C. Mills, Co-Chair
U.S. Naval Research Laboratory, Washington, DC, United States

INVITED PAPER

BG-01. A Fresh Look at Magnetic Materials for Electric Machines: State of the Art and Beyond. *C. Chinnasamy*[1], V. Rallabandi[1] and V.G. Harris[2] *1. Oak Ridge National Laboratory, Knoxville, TN, United States; 2. Northeastern University, Boston, MA, United States*

In recent years, major R&D efforts have been directed towards the technology development of the magnetic material components, in particular the manufacturing feasibility of advanced magnetic materials and high-efficiency electric machines for consumer and transportation applications. With the ever-broadening choices of materials, it is incumbent upon design engineers to investigate targeted material properties, whether they be magnetic or mechanical in nature, to enable high-performance electric machines. Other essential characteristics include cost and availability restrictions, i.e., security of supply chain and natural abundance, that may affect non-performance parameters such as time-to-market for new designs or the cost of manufacturing across the U.S. and North America. Developing new magnetic materials using abundant-earth materials and secure supply chains will be of paramount import. In this presentation, we will discuss the breadth of the applications and the very demanding requirements in terms of existing and new magnetic materials requirement, and future road map. We will present the specific materials (amorphous vs nano vs metals vs ferrites vs composites vs multimaterial) properties, frequency ranges, new topologies requirements and specific designs created around RARE earths.

CONTRIBUTED PAPERS

BG-02. Barium Ferrite / Carbon Nanotube Composites for Millimeter-wave Electromagnetic Shielding Enhanced by Ferromagnetic Resonance Absorption. *B.M. Mears*[1], F.M. Freeman[1], Y. Yoon[1] and D. Arnold[1] *1. Electrical and Computer Engineering, University of Florida, Gainesville, FL, United States*

In this work, we report a flexible composite of barium ferrite (BaM) and multiwalled carbon nanotubes (CNT) in a polymer matrix of polydimethylsiloxane (PDMS) for the purpose of attenuation of electromagnetic interference (EMI) i.e., shielding. EMI is electromagnetic pollution that interferes with sensitive electronics, especially in the microwave range [1]. Shielding is accomplished primarily through absorption, which comes from a combination of the ferromagnetic resonance (FMR) response from the BaM and conductive losses from the CNT [2]. The composite is fabricated by mixing commercially available BaM nanoparticles and CNT into PDMS, screen printing the mixture into waveguide shims serving as both molds and sample holders, then curing at 80°C in a DC magnetic field for out-of-plan alignment of the magnetic BaM particles (Fig. 1a) [3]. The composites are electromagnetically characterized by fitting a sample fully in the cross-section of a rectangular waveguide and using a vector network analyzer (VNA) to measure scattering (S) parameters from 33-50 GHz (Fig. 1b). Using the measured S parameters, power reflected and absorbed can be calculated and used to characterize the composite's shielding effectiveness [4]. This measurement process also allows for the employment of the Nicolson-Ross-Weir (NRW) method to determine complex permittivity and permeability [5]. The resulting 2.422-mm-thick composite shows a peak absorption of 26.9 dB at the FMR frequency of 47.4 GHz (Fig. 2). When normalized for sample thickness, this corresponds to 11.3 dB/mm. The combination of high frequency and high absorption compares favorably to other BaM + CNT shielding composites in the literature including 8.4 dB/mm at 12.4 GHz [2] and 6.5 dB/mm at 52 GHz [6].

[1] D. Micheli, R. Pastore, and C. Apollo, IEEE Transactions on Microwave Theory and Techniques., Vol. 59, no. 10, pp. 2633-2646 (2011) [2] M. Zahari, B. H. Guan, and E. M. Cheng, Progress In Electromagnetics Research M., Vol. 52, pp. 79–87 (2016) [3] C. S. Smith, R. Bowrothu, and Y. Wang, IEEE Transactions on Magnetics., Vol. 57, no. 10 (2021) [4] L. Mohan, M. Setty, and S. Karakkad, IEEE Transactions on Nanotechnology., Vol. 20, pp. 61–68 (2021) [5] W. B. Weir, Proceedings of the IEEE., Vol. 62, no. 1, pp. 33–36 (1974) [6] O. S. Yakovenko, L. Y. Matzui, and L. L. Vovchenko, Nanomaterials., Vol. 11, no. 11, p. 2873 (2021)

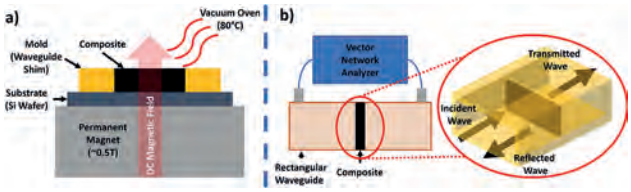

Curing step in fabrication process (a) and diagram of characterization method (b).

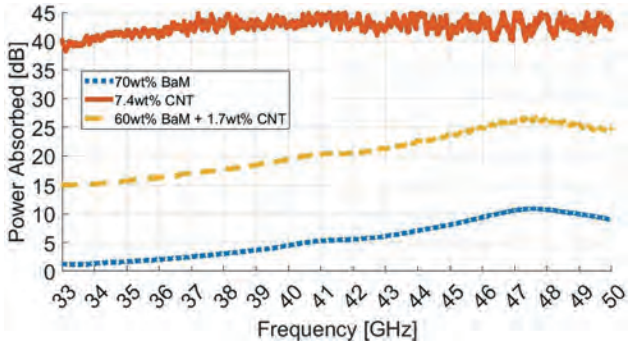

Power absorbed by 2.422mm thick PDMS composites of 70wt% BaM (blue dotted trace), 7.4wt% CNT (solid red trace), and 60wt% BaM + 1.7wt% CNT (dashed yellow trace)

BG-03. Selection of Magnetic Materials for AC Filter Inductors in PWM Inverters. *T. Yamaguchi*[1] and H. Matsumori[1] *1. Department of Electrical and Mechanical Engineering, Nagoya Institute of Technology, Nagoya, Japan*

In recent years, the wide-gap power devices such as SiC and GaN have improved the power density of the power converter [1, 2]. According to the report, the loss and volume of magnetic components in power converters is a large percentage and needs to be reduced. However, the design of magnetic components has been difficult and stagnant. The reason is that the waveform of the power converter (i,e., PWM inverter as shown in Fig. 1) is not a simple sine wave, but a waveform containing high frequency switching ripple. The high frequency switching ripple components cause a skin effect in the winding [3], and a dynamic minor loop on the major loop in the BH plane. Therefore, previous studies have investigated copper and iron loss analysis methods for power electronics operation [4, 5]. Using the loss analysis method, the authors attempted to reduce losses and the core volume for AC filter inductors under one magnetic material but didn't compare other materials for loss reduction, leaving the search for the best material incomplete [5]. Therefore, the authors evaluated the different magnetic materials [6], considering the differences in magnetic materials and permeability. The contributions in this paper reveal the loss and volume reduction performance when the AC filter inductor for the single-phase PWM inverter shown in Fig. 1 is designed using the best magnetic materials. According to the AC filter inductor design result as shown in Fig. 2, the magnetic core [Kool Mμ Hf (60μ, FeSiAl)], which has the best balance between loss and volume at 2.34W and 15.1cm3 respectively, improved losses by 34.3% (1.22W) compared to the worst case core [XFlux (60μ, FeSi)], which has the highest loss of 3.56W. Simulation and experimental results were also compared for the best inductor. The simulation result was relatively accurate with a calculation error of 10.9% (0.26W). It was shown that selecting the appropriate magnetic core can reduce inductor loss and volume. The final paper describes the differences in iron and copper loss distributions of the remaining magnetic cores and the core design method.

[1] D. Bortis, D. Neumayr and J. W. Kolar, "ηρ-Pareto optimization and comparative evaluation of inverter concepts considered for the GOOGLE Little Box Challenge," 2016 IEEE 17th Workshop on Control and Modeling for Power Electronics (COMPEL), Trondheim, Norway, pp. 1-5 (2016) [2] M. J. Kasper, J. A. Anderson, G. Deboy, Y. Li, M. Haider and J. W. Kolar, "Next Generation GaN-based Architectures: From 240W USB-C Adapters to 11kW EV On-Board Chargers with Ultra-high Power Density and Wide Output Voltage Range," PCIM Europe 2022; International Exhibition and Conference for Power Electronics, Intelligent Motion, Renewable Energy and Energy Management, Nuremberg, Germany, pp. 1-10 (2022) [3] J. Muhlethaler, "Modeling and Multi-Objective Optimization of Inductive Power Components. PhD thesis," Swiss Federal Institute of Technology (ETH Zurich) (2012) [4] J. Wang, N. Rasekh, X. Yuan and K. J. Dagan, "An Analytical Method for Fast Calculation of Inductor Operating Space for High-Frequency Core Loss Estimation in Two-Level and Three-Level PWM Converters," in IEEE Transactions on Industry Applications, vol. 57, no. 1, pp. 650-663, Jan.-Feb. (2021) [5] D. Mizutani, H. Matsumori, T. Kosaka, N. Matsui, T. Miyazaki and Y. Okawauchi, "AC filter inductor design for three-phase PWM inverter," 2020 23rd International Conference on Electrical Machines and Systems (ICEMS), Hamamatsu, Japan, pp. 1501-1505 (2020) [6] Magnetics Inc, "Magnetics - Powder Cores Manufacturer," https://www.mag-inc.com/Products/Powder-Cores

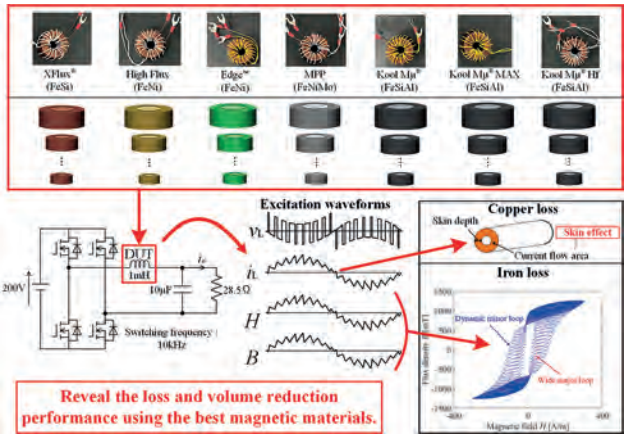

Fig. 1. Overview of this paper

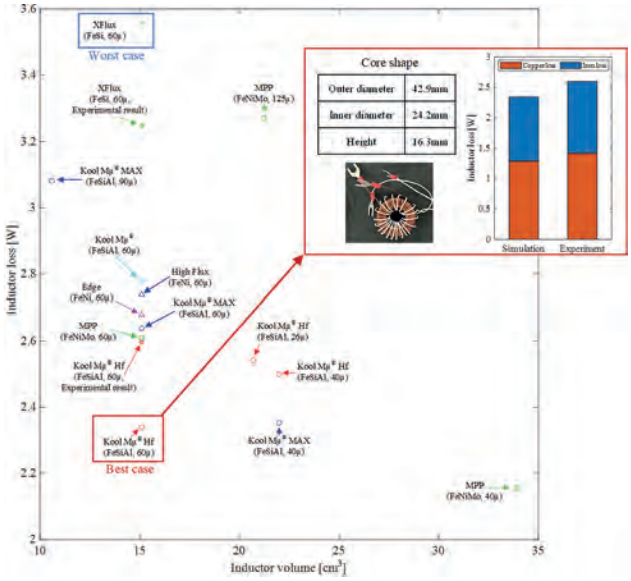

Fig. 2. Inductor loss-volume characteristics of each magnetic material

BG-13. Skyrmionic device for an offset-free 3D magnetic field sensor with high linear range enabled by spin-orbit-torques. *S. Koraltan*[1*], R. Gupta[2], C. Schmitt[2], A. Ducevic[1], F. Bruckner[1], C. Abert[1], A. Satz[3], K. Pruegl[3], M. Kirsch[3], S. Zeilinger[3], J. Güttinger[3], G. Jakob[2], M. Kläui[2] and D. Suess[1] *1. Physics of Functional Materials, University of Vienna, Vienna, Austria; 2. Institute of Physics, Johannes Gutenberg University Mainz, Mainz, Germany; 3. Infineon Technologies, Villach, Austria*

The discovery of tunnel magnetoresistance (TMR) has sparked considerable interest in developing novel spintronic devices [1]. TMR sensors are widely used in applications like hard-disk-drive read heads and automotive industry. However, a key challenge lies in the elimination of the offset observed at vanishing magnetic fields, limiting the resolution to measure absolute fields [2]. Recently, we proposed a differential measurement sensing concept that uses spin-orbit torques (SOT) to eliminate the sensing offset [3]. In contrast to the recent advances in SOT enabled sensors [4,5], we show a single device sensing principle of high and scalable linear range. We eliminate the sensing offset by a differential measurement scheme, and employ micromagnetic simulations using magnum.np to predict the sensor properties. The sensitivity and linear range are tunable by varying the injected in-plane SOT current. Experimental validation is performed on Ta/CoFeB/MgO trilayer [3] and $[W/CoFeB/MgO]_N$ multilayers [6]. The multilayers device exhibits a high density of skyrmions, as can be verified by anomalous Hall response to the out-of-plane field skyrmionic characteristics (Fig. 1). Micromagnetic simulations

allow to identify distinct skyrmion phases (Fig. 1). Experimentally measured transfer curves for opposing currents yield a sensor signal with cancelled offset; see Fig. 2. The skyrmionic stack, with hysteresis-free stripes breathing at high currents for out-of-plane (OOP) fields and in-plane (IP) fields, enables 3D sensing. Micromagnetic simulations reveal how skyrmions/stripes respond to injected currents and magnetic fields. In conclusion, our study presents a differential measurement sensing concept using SOT to cancel the sensing offset. Experimental validations on traditional and skyrmionic devices confirm its effectiveness and versatility in magnetic field sensing.

[1] - V. K. Joshi JESTECH (2016): 1503-1513. [2] - P. Ripka et al. *IEEE Sensors journal* 10.6 (2010): 1108-1116. [3] - S. Koraltan et al. (2023) arxiv.org/abs/2303.13261 under Review at Phys. Rev. Applied [4] - R. Li *et al. Nat Electron* 4, 179–184 (2021). [5] - Y. Xu et al. *Adv. Mater. Technol.* (2018), 3, 1800073. [6] - S. Koraltan et al. (2023) in prepation

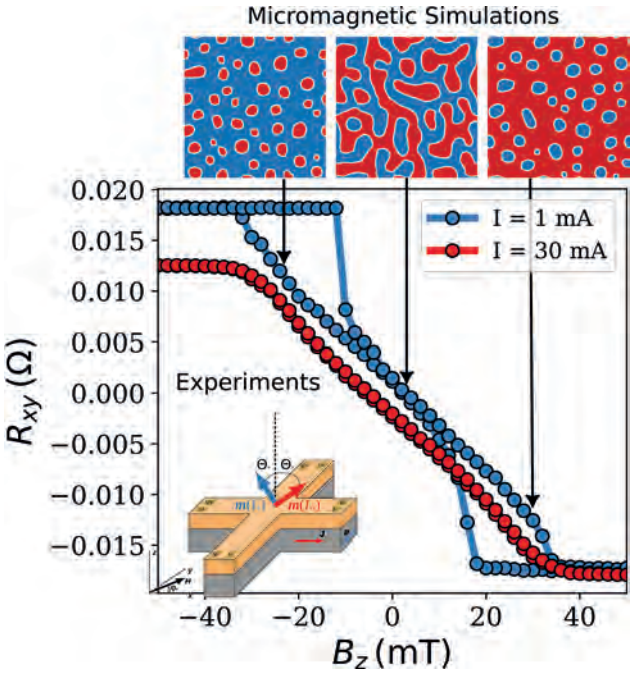

Fig. 1. Anomalous Hall response of skyrmionic device for low and high current regime for an OOP applied magnetic field with Micromagnetic simulations showing skyrmion and domain formation.

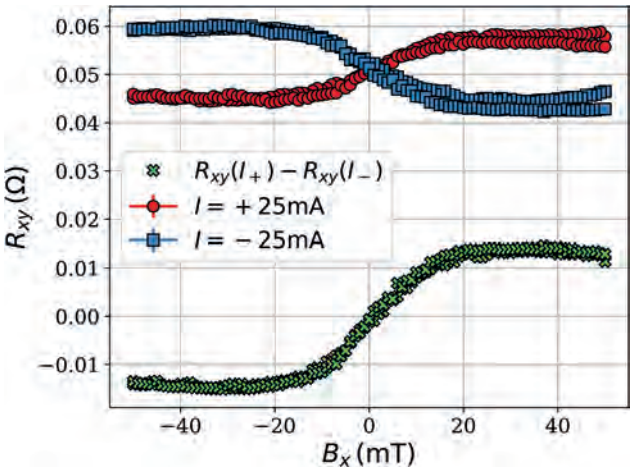

Fig. 2. Experimentally measured transfer curves for both current directions, and the offset free sensor signal as the difference between the two curves.

BG-04. Fast and Accurate Transient Simulation of Magnetic Gears. *A. Sahoo*[1] and V.K. Hari[1] *1. Department of Energy Science and Engineering, Indian Institute of Technology Bombay, Mumbai, India*

Magnetic gears, being contactless, offer distinct advantages over mechanical gears [1]. Power transmission in magnetic gears is achieved through the interaction of magnetic fields. Numerical simulation of a magnetic gear is essential for optimization and validation of a design. Finite element method (FEM)-based software are widely used for numerical simulations of magnetic gears. The simulations are usually magnetostatic in nature, performed at a given time instant. Transient simulations are required for the evaluation of dynamic performance, but the complex geometry of magnetic gears makes it computationally expensive and the simulation time is high. This article proposes an analytical method to perform transient simulation of a coaxial magnetic gear. The proposed method shows good agreement with FEM and is much faster. A coaxial magnetic gear is shown in Fig. 1, with the different spatial regions identified. An analytical method to calculate the magnetic field distribution in a coaxial magnetic gear was proposed by Lubin [2], which relies on solving the vector potential formulation of Maxwell's equations in the various spatial regions. The solution reported in [2] is magnetostatic in nature. This paper proposes a method to perform a time-domain transient analysis on a coaxial magnetic gear. The proposed method is derived by an appropriate and timely modification of specific terms in the magnetostatic solution, to result in a computationally efficient transient simulation. The proposed method also doesn't necessitate individual magnetostatic solutions for different time instances. Fig. 2 shows the results from the simulation of a coaxial magnetic gear with a speed ratio of 1:6. A magnetic gear is attached to a fan type load and is driven by a motor that supplies a step torque of -1 Nm at t=0.1s. The equations of motion are solved using Simulink [3] and the results are plotted in Fig. 2, compared with results from Comsol [4]. The proposed method is approximately 60 times faster than FEM when both are run on the same computer.

[1] K. Atallah and D. Howe, "A novel high-performance magnetic gear" IEEE Transactions on Magnetics, vol. 37, no. 4 I, pp. 2844:2846, Jul 2001. [2] T. Lubin, S. Mezani, and A. Rezzoug, "Analytical computation of the magnetic field distribution in a magnetic gear", IEEE Transactions on Magnetics, vol. 46, no. 7, pp. 2611:2621, 2010. [3] The Mathworks, Inc., Matlab version: 9.9.0.2037887 (R2020b) Update 8, Natick, Massachusetts, United States, 2022. https://www.mathworks.com [4] Comsol multiphysics ® v. 5.5, www.comsol.com, COMSOL AB, Stockholm, Sweeden.

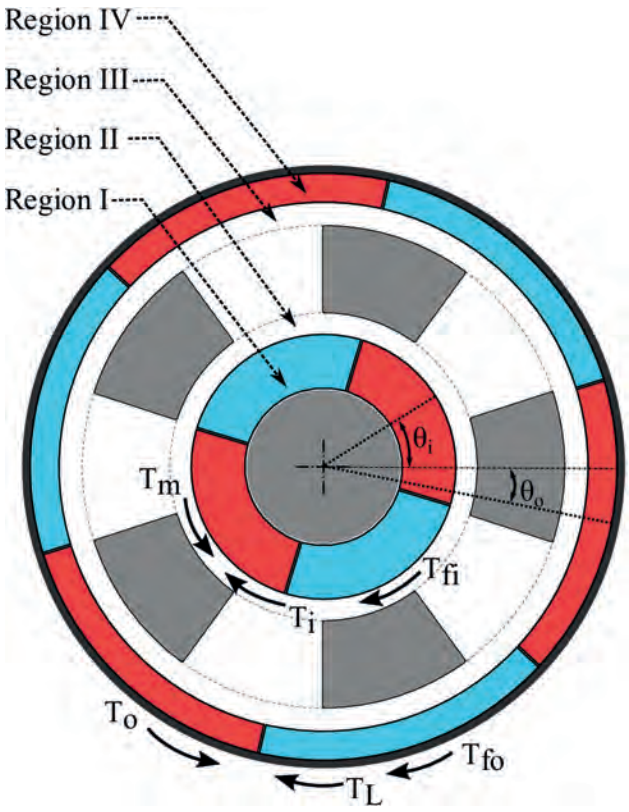

Fig.1: Magnetic gear geometry

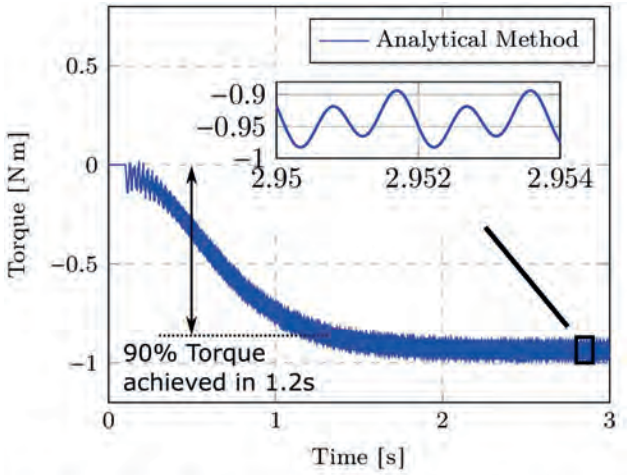

(a) Torque developed on the inner rotor (Analytical)

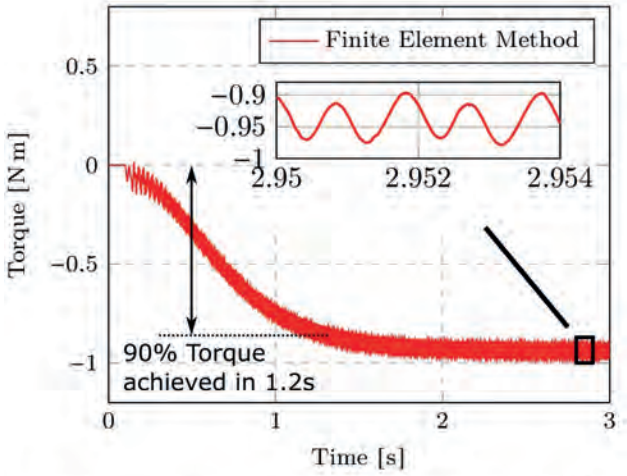

(b) Torque developed on the inner rotor (FEM)

Fig. 2: Simulation results

BG-05. A Novel Measurement-protection-integrated Current Transformer Based on Composite Core. *Z. Zhang*[1], B. Chen[1], C. Tian[1], Y. Chen[1] and S. Liu[2] *1. Wuhan University, Wuhan, China; 2. State Grid Shanghai Municipal Electric Power Company, Shanghai, China*

Current transformer is one of the most widely used equipment in power systems, including energy metering and relay protection[1, 2]. But when the core of the CT occurs saturation, the secondary current will be distorted, which may affect the accuracy of electric energy measurement or cause the malfunction of the relay protection equipment, thereby having certain impacts on the stability of the power grid[3, 4]. In order to address the problem, a novel measurement-protection-integrated current transformer based on composite core (MPICT) is proposed in this paper. The configuration of MPICT, mainly including composite core, secondary winding, magnetic sensor, operational amplifier, and power amplifier, is shown in Fig 1. The composite core used in MPICT includes a complete annular core and an annular core with several air gaps, which is called lower core and upper core respectively. A magnetic sensor is placed in the air gap of the upper core to measure the magnetic field strength. After sequentially processed by the operational amplifier and the power amplifier, the output of the magnetic sensor is added to the secondary current. In order to verify the effectiveness of the MPICT, the actual prototype are built. The rated primary current of the

prototype is 1000A, and the rated secondary current is 5A. The rated output is 15VA. The material of the lower core is amorphous alloy, while the upper core is made of silicon steel. The magnetic sensor used in the prototype is the tunnel magnetoresistance sensor with the model of TMR2651. Table 1 shows the errors of MPICT when the rms of primary currents are 10A, 50A, 200A, 1000A, 1200A, and 10000A, respectively. According to IEC 61869-2, MPICT can simultaneously meet the accuracy class 0.2S and 5P10. When the primary current is a short-circuit current with a transient factor of 2 and a primary time constant of 60ms, the composite error of MPICT is 2.98% that is still less than 5%. In summary, the novel current transformer designed in this paper can not only meet the accuracy class for measuring current transformers, but also satisfy the error limits for protective current transformers without significantly increasing the volume.

[1] R. Arseneau, IEEE Trans. Power Del., vol. 11, pp. 73–78 (1996). [2] P. Apse-Apsitis, K. Vitols, E. Grinfogels, etc, IEEE Electromagn. Compat. Mag., vol. 7, pp. 48–52 (2018). [3] A. V. Martins, R. M. Bacurau, A. D. dos Santos, etc, IEEE Trans. Instrum. Meas., vol. 69, pp. 1140–1147 (2020). [4] J. B. Leite and J. R. S. Mantovani, IEEE Trans. Smart Grid, vol. 9, pp. 1023–1032 (2018).

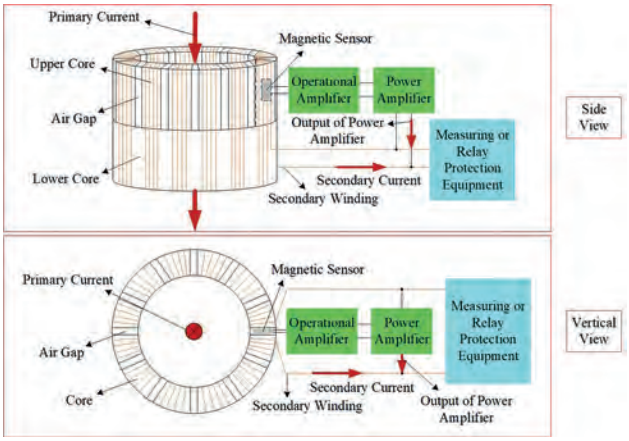

Table 1 Errors of MPICT

Burden	Accuracy	At current (% of rated)					Rated accuracy limit primary current
		1	5	20	100	120	
15VA	Ratio error/%	-0.06	-0.06	-0.06	-0.05	-0.05	-
	Phase displacement/minutes	3	3	3	1	1	
3.75VA	Ratio error/%	-0.02	-0.02	-0.02	-0.02	-0.02	-
	Phase displacement/minutes	2	2	2	1	1	
15VA	Composite error/%	-	-	-	-	-	2.63%

BG-06. A railgun concept for space launches and return travel from the Moon. *M. Trapanese*[1], M. Scozzaro[1], A. Iones[1] and F. Raimondi[1]
1. Palermo University, Palermo, Italy

A new era of space launches is ahead of us. The return of mankind to the moon will shortly happen. Research for a manned mission to Mars is in an advanced phase. A key critical point of these journeys is that any vehicle that is supposed to do a return mission from Mars or the Moon must have all the needed fuel from the journey's beginning. This limits strongly the payload that can be carried and increase the cost of the mission. However, in the near space, the energy from the light of the sun is plenty available. Sunlight can be simply transformed into electrical energy by photovoltaic systems and, as a result, an electromagnetic launcher located on the Moon could provide a viable approach to the return travel providing the necessary energy for the return by using a PV installation. The idea of electromagnetic space launch has been already proposed [1]. However, to the knowledge of the authors, the launcher proposed has been thought to be located on the earth, this approach has several limitations. Here, we propose a launcher to be located on the Moon for the return journey, this promises to solve several issues. This paper is one of a series of papers that will be published that will present the concept of a space launcher that is able to launch a vehicle from the Moon. The papers will address the power electronics, the thermal features, the mechanical features, the PV systems, and the electromagnetic device needed to accomplish such a task. In this paper, we start addressing the electromagnetic characteristic of a railgun supposed to be located on the Moon. We present the cylindrical geometry of the system adopted. The propulsion system is based on a synchronous motor and the system is provided with a levitation concept in order to limit friction problems. A comparison between a superconducting linear synchronous motor and a permanent magnet synchronous motor is performed. A careful thermal analysis of the motor is performed paying attention to the parasitic losses that are caused by the adopted geometry. Finally, we will compute the energy needed to launch a realistic vehicle from the moon. This figure will be input to design the power electronics system and the PV installation needed to achieve this goal.

[1] Ian R. McNab, "Launch to Space With an Electromagnetic Railgun", IEEE TRANSACTIONS ON MAGNETICS, VOL. 39, NO. 1, JANUARY 2003

BG-07. Origin of white noise in high-sensitive GMR sensor using AC modulation. *Y. Higashi*[1], A. Kikitsu[1], Y. Kurosaki[1] and S. Shirotori[1]
1. Toshiba Corporation, Kawasaki, Japan

High-sensitive magnetic sensors attract much attention for non-destructive inspection of defects in Li-ion battery and semiconductor circuit [1]. AC modulation is effective to improve detectivity of the magnetic sensors. Moreover Magneto-resistance (MR) sensor is attractive because it includes modulation system in sensor chip easily [2]. However the unique noise under modulation is occurred [3]. In the previous work, we successfully reduce noise in low frequency by optimized amplitude of modulation magnetic field with modeling signal and noise in symmetric response GMR under AC modulation [4]. In this study, we investigated the origin of white noise induced under AC modulation. Figure.1 shows power spectral density as a function of bias magnetic fields (H_b). Modulation magnetic field (H_{ac}) is 54.0 A/m at 10 kHz and measurement magnetic field (H_m) is 111 nT at 20 Hz. In the case of H_b = -21.6 A/m (red line), white noise from 100 Hz to near modulation frequency and the signal that contains high amplitude and many harmonic components of H_m occur simultaneously. On the other hand, there are no white noise and the signal that contains low amplitude and a few harmonic components of H_m at H_b = 7.2 A/m (blue line). It is found that there is a correlation between nonlinearity in the symmetric response GMR transfer curve (R(H)) and white noise. In consequence, we assume that domain walls in GMR induced by H_{ac} produce nonlinear region in R(H), so that passing Hac through this region cause many harmonic components which lead to white noise. With the optimized AC condition which avoids producing nonlinearity (H_{ac}= 79.2 A/m at 80 kHz), we successfully realized noise level almost equivalent to without modulation (black line) and symmetric response GMR with 6 pT/√Hz at 10 Hz (Fig.2). This work was supported by the Cabinet Office (CAO), Crossministerial Strategic Innovation Promotion Program (SIP), "An intelligent knowledge processing infrastructure, integrating physical and virtual domains" (funding agency: NEDO).

[1] K. Kimura et al.: *J. Inst. Electr. Eng. Jpn*., vol. 135, no. 7, pp. 437–440, 2015. [2] A.Bocheux et al.: SAS 2016 - Sensors Applications Symposium, Proceedings, pp. 149–153, 7479836 [3] Q.Du et al.: Appl.phys. Lett.102405(2020) [4] Y.Higashi et al., MMM OOA-06 (2022)

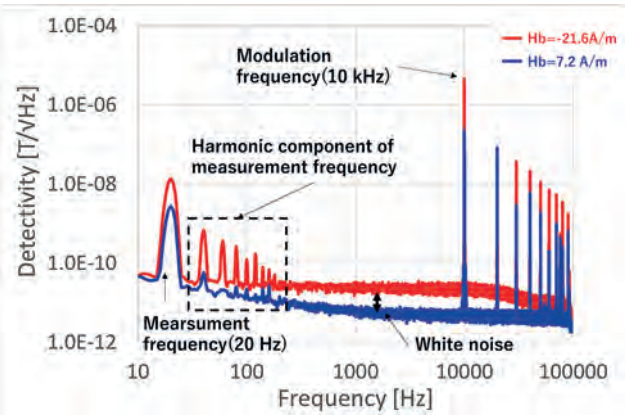

Fig.1 Each Power spectral density as a function of bias magnetic fields (H_b).

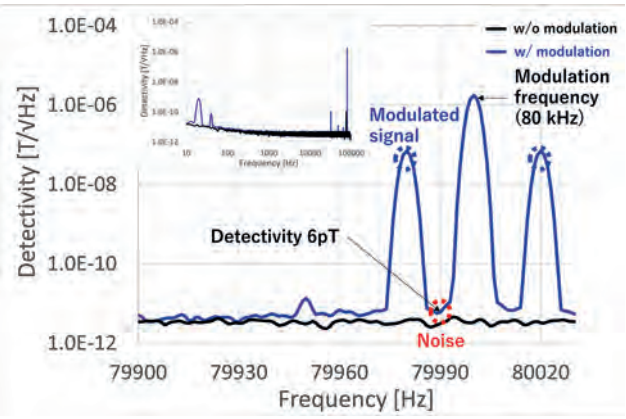

Fig.2 Each power spectral density with or without modulation.

BG-09. Butterfly motion of magneto-mechanical energy sensor for ambient ac field. *S. Yoon[1] 1. Korea Institute of Industrial Technology, Gwangju, The Republic of Korea*

Harnessing stray magnetic fields to generate electrical voltages offers significant potential for the development of sustainable power sources as well as power sensors. AC stray magnetic fields are frequently encountered in power-line cables, albeit with a fixed frequency and low amplitude (less than 5 gauss). Magneto-mechanical conversion has been recognized as the most efficient approach to convert magnetic fields into electric voltages [1-3]. In this study, we have conducted an experiment involving the mechanical bending of a piezo-plate under an alternating current (AC) magnetic field. Our objective was to achieve maximum bending effects in the piezo plate, and to accomplish this, we positioned both magnets anti-symmetrically. Therefore, the butterfly bending motion of the piezo-plate with magnets were carefully observed using an ultra-slow camera and validated through real-time voltage measurements obtained from the piezo. Furthermore, the effectiveness of the optimized magnet mass and its placement on the piezo-plate was confirmed through a 3D simulation. The experimental details will be thoroughly discussed in the presentation.

[1] N. Godard, L. Allirol, A. Latour, S. Glinsek, M. Gérard, J. Polesel, F. Domingues Dos Santos, and E. Defay, Cell Rep. Phys. Sci. Vol 1, 100068 (2020) [2] Q. Wang, K.-B. Kim, S.-B. Woo, Y. Song, and T.-H. Sung, Energies Vol 14, 2387 (2021) [3] H. Lee, R. Sriramdas, P. Kumar, M. Sanghadasa, M. G. Kang, and S. Priya, Energy Environ. Sci. Vol 13, 1462 (2020)

BG-12. Surface Acoustic Wave Actuated MEMS Magnetoelectric Antennas. *C. Zhang[1], H. Gu[1], Y. Ji[1] and T. Nan[1] 1. School of Integrated Circuits and Beijing National Research Center for Information Science and Technology (BNRist), Tsinghua University, Beijing, China*

State-of-the-art compact antennas based on acoustically actuated magnetoelectric antennas have emerged as a prominent research area, attracting considerable interest among researchers. The film bulk acoustic wave resonator (FBAR) based acoustically actuated magnetoelectric antennas exhibit outstanding antenna size miniaturization capability. However, the operation frequency of FBAR based magnetoelectric antennas is relatively high, over the gigahertz range, is difficult to adapt to the application requirements of hundreds of megahertz frequency band. Here, we demonstrate the prototype of surface acoustic wave (SAW) actuated magnetoelectric antennas which provides the solution for antenna needs in hundreds of megahertz frequency band. The devices consist of a bulk $LiNbO_3$ single crystal as piezoelectric substrate, a thin SiO_2 as insulating layer, and a FeGaB film as radiation layer. The radiation frequency of proposed SAW magnetoelectric antennas is about 430 MHz, corresponding to the Rayleigh wave resonant mode. By using gain-comparison method, the gain of -28 dBi can be calculated. The -3 dB relative bandwidth of the devices is about 1.61%. Our results show the feasibility of surface acoustic wave actuated magnetoelectric antennas and provide a new way for acoustically actuated MEMS magnetoelectric antennas design.

T. Nan, H. Lin and Y. Gao, Nature communications, Vol. 8, p. 296 (2017)

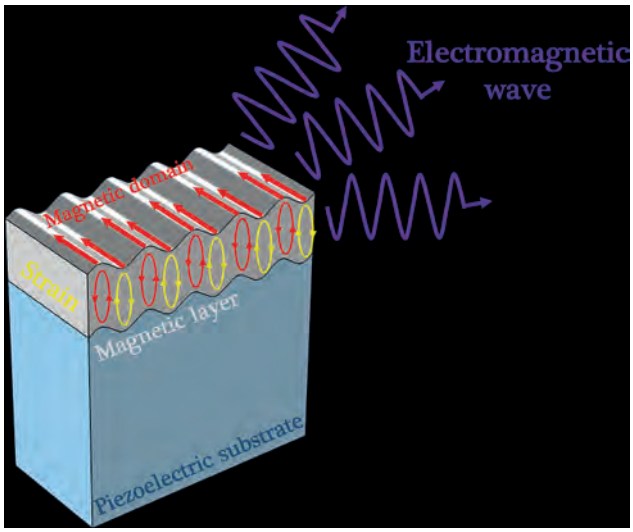

Fig. 1. The schematic of the surface acoustic wave actuated magnetoelectric antennas.

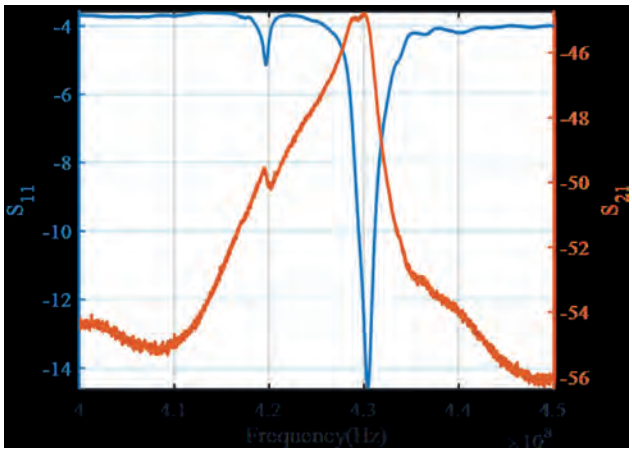

Fig. 2. The S11/S21 measurement results of the proposed magnetoelectric antennas.

Session BP
SPIN WAVES AND MAGNONICS I
(Poster Session)

Joseph Sklenar, Chair
Wayne State University, Detroit, MI, United States

BP-02. Observation of magnon-phonon coupling in propagating spin wave modes. *A.M. Park*[1], M. Song[1], Y. Soon[1], P.C. Van[2], J. Jeong[2] and K. Kim[1] *1. Physics, KAIST, Daejeon, The Republic of Korea; 2. Material Science and Engineering, Chungnam National University, Daejeon, The Republic of Korea*

Coupling between spin wave and acoustic wave enables long-range interaction of spin precession via angular momentum transfer by an acoustic wave. This property appeals to spintronic devices that seek a long-range transfer of spin information and can also enable quantum transduction between phonon and magnon in a single quantum limit. Among various modes of coupling between spin waves and acoustic waves, spin precession of the perpendicularly magnetized moments shows a strong coupling with circular shear deformation of the lattices due to the formation of a resonant acoustic standing wave in the substrate [1,2]. Furthermore, the precession of in-plane polarized magnetic moment also interacts with the standing acoustic wave but with the single transverse mode of the acoustic wave instead of circular shear deformation [3,4]. In this work, we observe the generation of bulk acoustic waves by propagating magnetostatic surface spin waves (MSSW) in the YIG/GGG system and the coupling between two wave modes. The spatial phase distribution of the propagating MSSW generates a corresponding phase difference of the acoustic wave, resulting in a propagation of the acoustic wave in the direction of the magnon wavevector. The periodic structure is implemented at the reflecting surface of the substrate to control the directional coupling of the propagating acoustic wave with the spin wave. Finally, we also discuss how double peaks, similar to that induced by the birefringence effect of acoustic waves [5], can form in the absorption spectra of the MSSW. Our result suggests a new control knob for coupling between spin and acoustic waves by focusing on the magnetostatic mode of spin wave oscillation.

[1] K. An, *et al., Phys. Rev. B*. 101, 060407(R) (2020) [2] M. Ye, & H. Dotsch, *Phys. Rev. B.*, 44, 9458, (1991) [3] N. Polzikova, *et al., Proc. IEEE Int. Freq. Cont. Symp.* (2014) [4] K. An, *et al.,* arXiv:2302.09936 (2023) [5] M. Muller, *et al.*, arXiv:2303.08429 (2023)

BP-03. Withdrawn

BP-04. Spin Waves realizing the classical analog of a quantum state superposition for computation and sensing. P. Micaletti[1] and *F. Montoncello*[1] *1. Department of Physics and Earth Sciences, University of Ferrara, Ferrara, Italy*

Spin Waves are the coherent oscillations of the magnetic moments of a medium, their propagation does not involve energy dissipation by Joule effect, and in periodic systems their wave function profile can be non-uniform and crucially dependent on the (tunable) symmetry of the underlying magnetization[1]. Their intrinsic wave nature, together with the quantization of their energy, suggests to use them to implement an entangled state superposition, which can collapse due to any symmetry breaking in the underlying magnetization texture[2,3]. The symmetry breaking can result from the measurement of any external quantity in sensing applications (e.g., a tiny external field or induced anisotropy) or from an intentional operation in computing applications[4]. With the help of micromagnetic simulations, we present an overview of two different situations: spin waves in a vortex magnetization state (Fig. 1 shows an illustration of a possible state superposition, exploiting the properties of spin waves in vortex magnetized rings[5]), and spin waves occurring as hybrids in a lattice of macrospins (elongated elements). In both cases, we suggest how to address the Bloch sphere through the complex amplitude of the spin-wave profiles, how to implement a gate operation which preserves the entanglement, and how to break the symmetry (i.e., the measurement) and force the system to collapse in one of the originally irreducible states, producing a result detectable, in principle, by any space-resolved spectroscopy (e.g., micro-focused Brillouin light scattering or X-ray microscopy[6,7]).

[1] R. Negrello, F. Montoncello, M.T. Kaffash et al., *APL Mater.* 10, 091115 (2022). [2] Dany Lachance-Quirion et al., *Appl. Phys. Express* 12, 070101 (2019). [3] M. Mohseni, V.I. Vasyuchka, V.S. L'vov, A.A. Serga and B. Hillebrands, *Communications Physics 5,* 196 (2022). [4] C. L. Degen, F. Reinhard, and P. Cappellaro *Rev. Mod. Phys*. 89, 035002 (2017). [5] G. Gubbiotti, M. Madami, S. Tacchi, et al., *Phys. Rev. Lett.* 97, 247203 (2006). [6] T. Sebastian, K. Schultheiss, B. Obry, B. Hillebrands and H. Schultheiss, *Front. Phys*. 3, 35 (2015). [7] Nick Träger, Felix Groß, Johannes Förster et al., *Scientific Reports* 10, 18146 (2020).

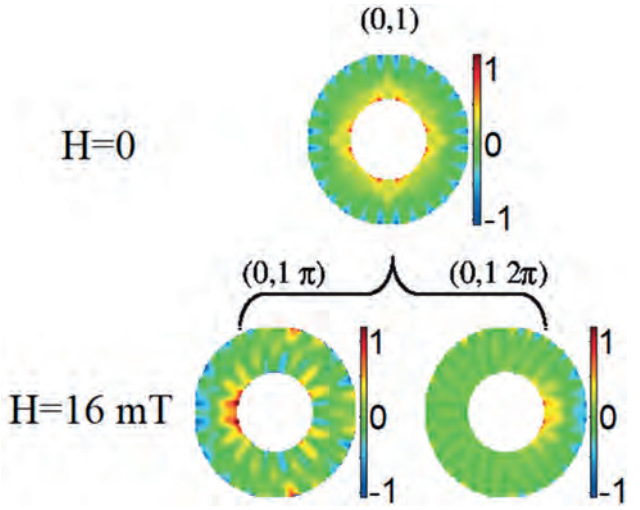

Example of implementation of a state superposition with a spin mode. Spin resonances in vortex magnetization have radial modes as possible solutions, which after the application of an external field (even extremely small) split into two complementary modes, due to the symmetry breaking: we show the mode with zero azimuthal nodes and one radial node labeled (0,1) for H=0, and then how it splits into the two irreducible modes localized at π and 2π (H=16 mT). At H=0 these modes can be considered in a superposition state, and form the circularly symmetric radial mode (0,1).

BP-05. Footprints of the specific artificial spin ice microstate on the dynamic properties of its spin waves. P. Micaletti[1] and *F. Montoncello*[1]
1. Department of Physics and Earth Sciences, University of Ferrara, Ferrara, Italy

We show the results of micromagnetic simulations, where the dynamic properties of the spin wave (SW) resonances (at zero wavevector) in an artificial spin ice (ASI) are studied as a function of the magnetic microstate at remanence (H=0). In particular, we select a few microstates with specific magnetic charge at an ASI vertex (including a flux-closure vortex one), and, after calculations by Fourier analysis, look to the corresponding spin wave spectrum and spin wavefunction profiles [1]. We discuss: (1) the modification of the nodal lines as a function of the macrospin separation and width, recognizing the phase-shift peculiar to the magnetic charge at vertex (Fig. 1); (2) the frequency gap between the edge mode and the fundamental mode; (3) the role of macrospin density in the array, as well as the macrospin width; (4) the role of the absolute size of a macrospin (in units of the exchange length) in determining how rich of modes (and peaks) is the spectrum [2]. We suggest a few experimental techniques (micro-focused Brillouin light scattering [3], X-ray microscopy [4]), to prove the described predictions. Our results aim to understand the footprints left in the dynamics by the specific orientation of the macrospin magnetization at the ASI vertices, so that a direct control of the SW propagation properties, particularly phase-shifts, might be pursued through specific macrospin reversals. This control is of crucial importance in the context of interferometric processing of SW information carriers, for magnonic logic devices and spin wave computing.

[1] R. Negrello, F. Montoncello, M.T. Kaffash, M.B. Jungfleisch, G. Gubbiotti, *APL Mater*. 10, 091115 (2022). [2] Pietro Micaletti and Federico Montoncello, *magnetochemistry* 9, 158 (2023). [3] T. Sebastian, K. Schultheiss, B. Obry, B. Hillebrands and H. Schultheiss, *Front. Phys*. 3, 35 (2015). [4] Nick Träger, Felix Groß, Johannes Förster, Korbinian Baumgaertl, Hermann Stoll, Markus Weigand, Gisela Schütz, Dirk Grundler and Joachim Gräfe, *Scientific Reports* 10, 18146 (2020).

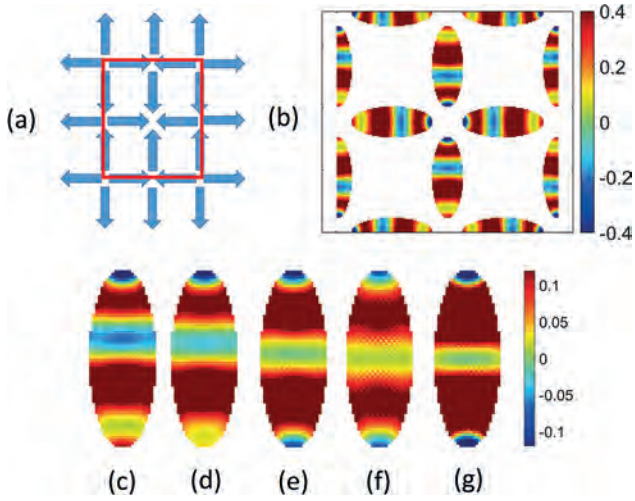

(a) ASI microstate with maximum charge at vertex (extract of an infinite array, in red the primitive cell); (b) Spin-wave profile in the selected ASI microstate; (c-g) Spin-wave profile on a single macrospins out of a square ASI lattice for increasing macrospin separation *s*, form (c) very close *s* = 96 nm, (d) *s* = 128 nm, (e) *s* = 256 nm, (f) s = 512 nm, (g) infinitely far (single macrospin). The region where the phase is negative progressively shifts to the center of the macrospin. Hence, the asymmetry of the mode profile in (b) and (c) is a local footprint of the global static ASI microstate (in this case, possessing same-pole vertices).

BP-06. Adjusting spin dynamics in ferromagnetic nanodisk arrays. *W. Bang*[1], M. Kaffash[2] and B. Jungfleisch[2] *1. Korea University of Technology and Education, Cheonan, The Republic of Korea; 2. Department of Physics and Astronomy, University of Delaware, Newark, DE, United States*

Because of the possible uses in magnonics devices, there has been significant interest in studying in spin dynamics in artificial spin ice (ASI) systems. We describe experimental and theoretical analyses of spin dynamics in the artificial spin ice arrays, which are made up of contacting or non-contacting honeycomb lattices of ferromagnetic nanodisks[1]. The honeycomb lattices on a co-planar waveguide are fabricated by electron-beam lithography, electron-beam evaporation of NiFe, and lift-off process. The spin-wave spectra and micromagnetic simulations obtained by broadband ferromagnetic resonance and Mumax[3], respectively. We show that the complicated spin dynamics in the ASI systems could be adjusted by the excitation frequencies. This study provides up new avenues for developing specialized applications in the magnonics. *Funding Work at Korea University of Technology and Education was supported by the National Research Foundation of Korea (NRF) grant funded by the Korea government (MSIT) (No. 2021R1G1A1092937).

Kaffash et al., Phys. Rev. B 101, 174424 (2020)

BP-07. Withdrawn

BP-08. Reinforcing spin wave amplitude non-reciprocity via multiple mechanisms. *J. Lim*[1,2], R. Klause[1,2], Y. Li[3], V. Novosad[3] and A. Hoffmann[1,4] *1. Materials Science and Engineering, University of Illinois Urbana-Champaign, Urbana, IL, United States; 2. Materials Research Laboratory, University of Illinois Urbana-Champaign, Urbana, IL, United States; 3. Materials Science Division, Argonne National Laboratory, Lemont, IL, United States; 4. Department of Physics, University of Illinois Urbana-Champaign, Urbana, IL, United States*

Achieving a large amplitude nonreciprocity in spin wave propagation is an important aspect for many applications of magnonics. We have studied spin wave propagation in ferromagnetic bilayers. It has been long established that the interlayer dipolar interaction in the ferromagnetic bilayer system can produce nonreciprocal dispersion relation of spin waves. We have found that ferromagnetic bilayer system can have an exclusive frequency band for spin waves propagating only along a specific direction in the presence of in-plane uniaxial anisotropy or in-plane static applied magnetic field. Also, we have shown that Oersted field from a patterned coplanar waveguide (CPW) on the film is coupled strongly to spin waves propagating along a specific direction compared to those propagating along the opposite direction [1]. Furthermore, we have found that these two different mechanisms of non-reciprocity can have ‘constructive interference’ or ‘destructive interference’ depending on the detailed design of the magnetic elements and the coupling antenna. By using these two mechanisms at the same time, we have achieved enhanced amplitude nonreciprocity bigger than those achieved from either of single mechanism. We also found that in a ‘destructively interfering’ geometry amplitude nonreciprocity was smaller than those from either of the single mechanisms. Figure 1 and Table 1 show a case of anti-parallel-aligned ferromagnetic bilayers. Within the exclusive frequency band, choosing different wavelength of excited spin waves corresponding to opposite signs of group velocity determines whether the two mechanisms have ‘constructive interference’ or ‘destructive interference’. This work is supported by the U. S. Department of Energy, Office of Science, Materials Science and Engineering Division under Contract No. DE-SC0022060.

[1] Y. Li, T.-H. Lo, J. Lim, J. E. Pearson, R. Divan, W. Zhang, U. Welp, W.-K. Kwok, A. Hoffmann and V. Novosad, “Unidirectional Microwave Transduction with Chirality Selected Short-Wavelength Magnon Excitations”, arXiv:2303.00936 (2023). https://doi.org/10.48550/arXiv.2303.00936.

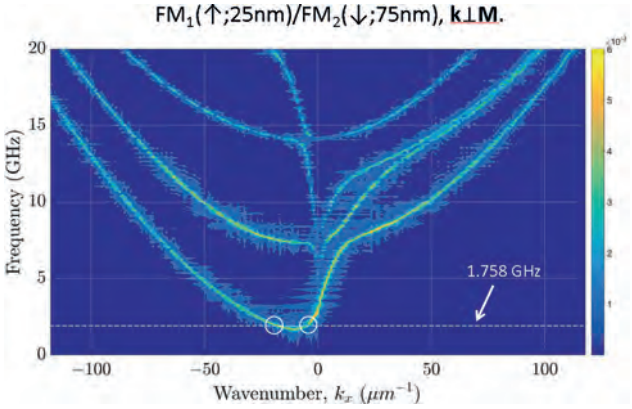

Figure 1. Dispersion relation of spin waves in ferromagnetic bilayer system with anti-parallel alignment.

$FM_1(\uparrow;25nm)/FM_2(\downarrow;75nm)$, k⊥M.

Frequency (GHz)	Wavelength (μm)	Sign of $\frac{d\omega}{dk_x}$	Isolation (dB)	Interference between two mechanisms
1.758	0.8	Positive	−28	Constructive
1.758	0.4	Negative	+1.6	Destructive

Table 1. Parameters for 'constructive' and 'destructive' interference and corresponding isolations.

BP-09. Directional Effects of Interfacial Dzyaloshinskii-Moriya Interactions for Spin Waves in Ferromagnetic Nanorings. *B. Hussain*[1] and M.G. Cottam[2] *1. Natural Sciences, University of Michigan-Dearborn, Dearborn, MI, United States; 2. Physics and Astronomy, University of Western Ontario, London, ON, Canada*

Thin ferromagnetic nanorings typically exhibit two states of magnetic ordering [1], depending on the interplay of the applied magnetic field with the exchange and dipole-dipole interactions: the low-field vortex state and the high-field bidomain onion state. Antisymmetric Dzyaloshinskii-Moriya interactions (DMI) may also play a role in the statics and dynamics, especially if the DMI is enhanced by interfacing a ferromagnetic layer with a heavy metal substrate [2]. We recently analyzed the spin waves (SWs) in both magnetic states of nanorings using a microscopic, or Hamiltonian-based, formalism. The discrete SW frequencies and spatial intensities were calculated, initially without DMI [3] and then with interfacial DMI included [4]. Here we report on novel SW results obtained when the directional properties of the interfacial DMI are varied through different choices for its axial vector. Interestingly, it is found that when the DMI axial vector lies in the plane of the nanoring (either parallel or perpendicular to the applied magnetic field) the static magnetizations in the vortex and onion states acquire a pronounced tilting out of the plane and the SW frequencies and intensities are modified. This behavior is quite different from that when the DMI axial vector is perpendicular to the plane of the nanoring as in [4], but it has some analogies with the zero-field configuration predicted in [5] for a disk structure. Numerical applications with interfacial DMI included are made to permalloy nanorings with diameters ranging up to 200 nm by generalizing the theoretical approach in [4]. Results are shown in Figs. 1 and 2 for the equilibrium orientations of the spins (color coded for the tilts) and for the lowest few SW frequencies.

[1] C. A. F. Vaz et al., J. Phys. Condens. Matter, Vol. 19, p.255207 (2007) [2] J.-H. Moon et al., Phys. Rev. B, Vol. 88, p.184404 (2013) [3] B. Hussain and M. G. Cottam, J. Phys. D, Vol. 54, p.165002 (2021) [4] B. Hussain and M. G. Cottam, J. Appl. Phys., Vol. 132, p.193901 (2022) [5] C. Q. Flores et al., Phys. Rev. B, Vol.102, p.024439 (2020)

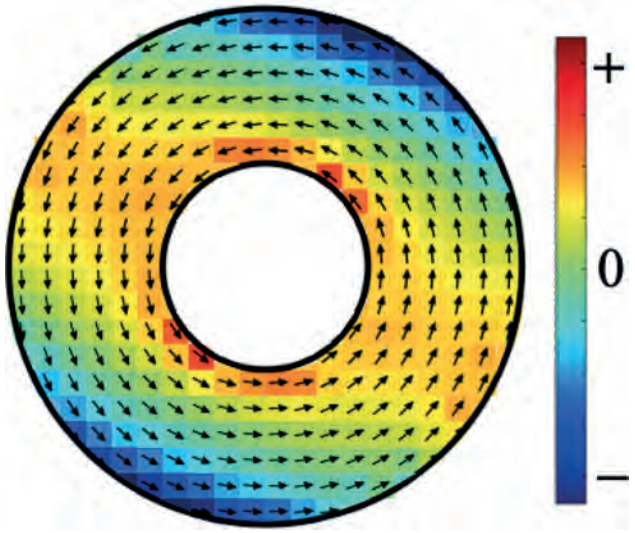

Fig. 1. Spin orientations (arrows) for a nanoring with outer radius 40 nm and inner radius 16 nm in a vortex state with applied field 0.005 T. The out-of-plane tilts up (+) and down (-) are represented by color code.

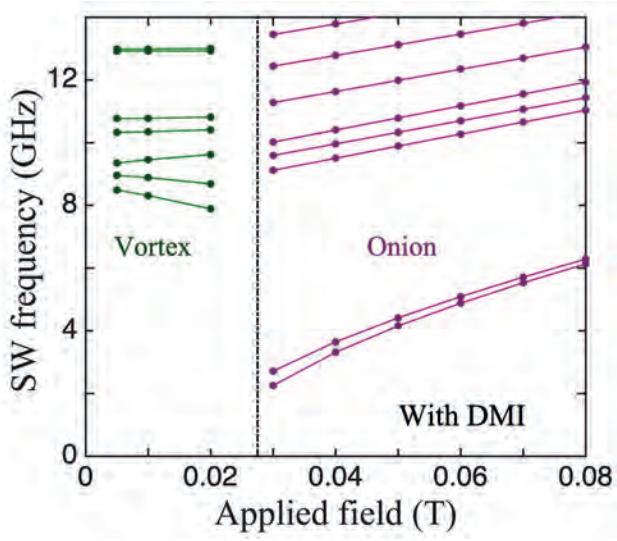

Fig. 2. SW frequencies plotted versus the applied field for a permalloy nanoring with outer radius 60 nm, inner radius 24 nm, and thickness 4 nm when the DMI axis is in-plane, perpendicular to the field. The vertical line shows the transition field between the states.

BP-10. Conversion of propagating magnon polarization into charge current. *Y. Shiota*[1,2], T. Taniguchi[3], D. Hayashi[1], R. Hisatomi[1,2], T. Moriyama[4] and T. Ono[1,2] *1. Institute for Chemical Research, Kyoto University, Uji, Japan; 2. Center for Spintronics Research Network, Kyoto University, Uji, Japan; 3. National Institute of Advanced Industrial Science and Technology (AIST), Tsukuba, Japan; 4. Department of Material Physics, Nagoya University, Nagoya, Japan*

Because the magnons carry angular momenta, various magnonic applications have been proposed, including logic gates, information storage/transducers, magnon-based computings, and so on [1]. Recently, propagating magnon-induced domain wall (DW) motion has been demonstrated in perpendicularly-magnetized ferromagnets [2,3]. In the ferromagnets, however, the DW can be moved in only one direction relative to the magnon propagation because ferromagnetic magnons possess only right-handed precession mode. It is theoretically predicted that bidirectional DW motion can be achieved by utilizing the polarization degree of freedom of magnon [4]. Therefore,

magnons in ferri- and antiferromagnetic materials, which possess both right- and left-handed precession modes, have attracted much attention. In our previous study, we reported the polarization-selective excitation of antiferromagnetic resonance in perpendicularly magnetized synthetic antiferromagnets (p-SAF) using a wide band crossed microstrip circuit that generates circularly polarized microwave fields [5]. Here, we demonstrate the detection of propagating magnon polarization in p-SAF by inverse spin Hall effect (ISHE). We prepared the films consisting of a Co/Ni-based p-SAF sandwiched by Pt layers which show the spin-to-charge current interconversion through the ISHE. Then we fabricated the devices with the Hall bar structure of p-SAF and microwave antenna, as shown in Fig. 1. The magnon excitation is achieved by applying the microwave current to the stripline antenna and the measurements of ISHE voltage V_{ISHE} have been performed using a lock-in detection technique. No V_{ISHE} resulting from the propagating magnon was detected under the perpendicular magnetic field ($\theta_H = 0°$). However, the sign reversal of the V_{ISHE} peaks depending on the magnon polarization was successfully observed under the tilted magnetic field ($\theta_H = 30°$). We also found that it is important to sandwich the p-SAF structure with the upper and lower Pt layers for detecting the magnon polarization. Our results open a new way for detecting the polarization of coherently-excited propagating magnon in antiferromagnets.

[1] A. Barman *et al., J. Phys; Condens. Matter.* 33, 413001 (2021). [2] J. Han *et al., Science* 366, 1121-1125 (2019). [3] Y. Fan *et al., Nat. Nanotechnol.* (2023) https://doi.org/10.1038/s41565-023-01406-2. [4] S.-H. Oh *et al., Phys. Rev. B* 100, 174403 (2019). [5] Y. Shiota *et al., Phys. Rev. Appl.* 18, 014032 (2022).

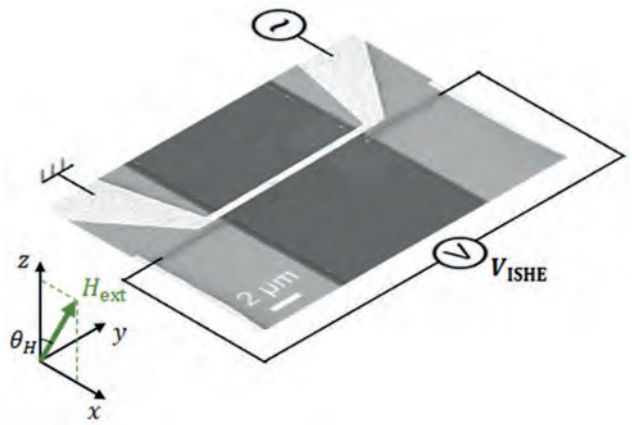

Fig. 1 Schematic of device structure and measurement setup.

BP-11. Precise determination of ferromagnetic exchange in thin films. *J. Wisser*[1], M. Tanksalvala[1], J.M. Shaw[1] and H. Nembach[1] *1. NIST, Boulder, CO, United States*

The exchange stiffness constant, A_{ex}, is a fundamental property of magnetic materials. However, there are few ways to measure this property in technologically-relevant magnetic thin films. We show that the most commonly used method, perpendicular standing spin wave (PSSW) analysis via ferromagnetic resonance (FMR) spectroscopy, requires implicit assumptions be made about the interface anisotropies in the film stack. As shown in Figure 1(a), we observe five PSSWs in 100 nm-thick $Ni_{80}Fe_{20}$ (Py) films. We used the exchange boundary condition for unequal interfacial spin pinning in [1] and the Kittel equation for FMR to generate the dependence of the PSSW exchange field ($H^{ex}_n = H_0 - H^{res}_n$) on PSSW wavevector, k, shown in Figure 1(b). The resulting variation in calculated A_{ex} values depending on how the surface anisotropy, K_s, is divided between the top and bottom film surfaces is shown in Figure 1(c). Ta-seeded Py films with Cu/Ta, TaO/Ta, and Pt caps exhibit different exchange stiffnesses, even though A_{ex} is a bulk property of magnetic materials. Furthermore, depending upon how K_s is distributed between the two interfaces, the calculated A_{ex} value can vary by up to 5%. Using Brillouin light scattering (BLS) spectroscopy we are able to determine the exchange stiffness parameter without any implicit assumptions about K_s. [2] This method is also effective in ultra-thin films, whereas PSSW analysis requires the observation of many modes, and consequently is only possible in thicker films, which are not relevant for current spintronics applications. This work paves the way for precise measurements of Aex for a more thorough understanding of magnetic materials as well as more precise inputs for modeling of spintronic device performance.

[1] R. F. Soohoo, Phys. Rev. 131, 594 (1963). [2] G. A. Riley, J. M. Shaw, T. J. Silva, and H. T. Nembach, Applied Physics Letters 120, 112405 (2022).

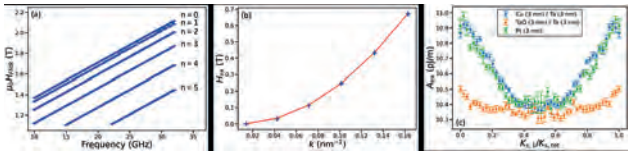

Figure 1: (a) FMR resonance field vs frequency for a 100 nm-thick Py film capped with Cu (3 nm)/Ta (3 nm) with labeled indices for PSSWs. (b) The resulting exchange field vs PSSW wavevector used to determine the exchange stiffness (data in blue, fit in red).(c) Variation of the calculated exchange stiffness with fractional interface anisotropy for each capping material.

BP-13. Broken Symmetry Induced Magnon-Magnon Coupling in a Synthetic Ferrimagnet. *M. Hossain*[1], H. Chen[1], S. Bhatt[1], M. Kaffash[1], J. Sklenar[2], J. Xiao[1] and B. Jungfleisch[1] *1. University of Delaware, Newark, DE, United States; 2. Wayne State University, Detroit, MI, United States*

Synthetic antiferromagnetic materials offer a rich magnon energy spectrum in which optical and acoustic magnons branches can hybridize. In previous works, magnon-magnon interactions have been tuned using symmetry breaking external magnetic fields or dipolar interactions. Here, we demonstrate an out of plane mirror symmetry breaking induced hybridization of acoustic and optical magnons in a synthetic ferrimagnet consisting of two dissimilar antiferromagnetically coupled ferromagnetic metals. The ferromagnetic layers used in this study were 10nm thick CoFe and Py of similar thickness. The ferromagnetic metals were separated by a non-magnetic metal, Ru, with thickness varied from 0 to 1nm. The hybridized excitation is studied using microwave spectroscopy through spin torque ferromagnetic resonance (STFMR) and Brillouin light scattering (BLS) spectroscopy. Two distinct magnon modes hybridized at degeneracy points as indicated by an avoided level crossing. The avoided level crossing gap depends on the interlayer exchange interaction between the magnetic layers, which can be controlled by adjusting the non-magnetic interlayer thickness. An exceptionally large avoided level crossing gap of 4 GHz is revealed, exceeding the coupling strength that is typically found in other magnonic hybrid systems based on a coupling of magnons with photons or magnons and phonons. This research was supported by NSF through the University of Delaware Materials Research Science and Engineering Center, DMR-2011824

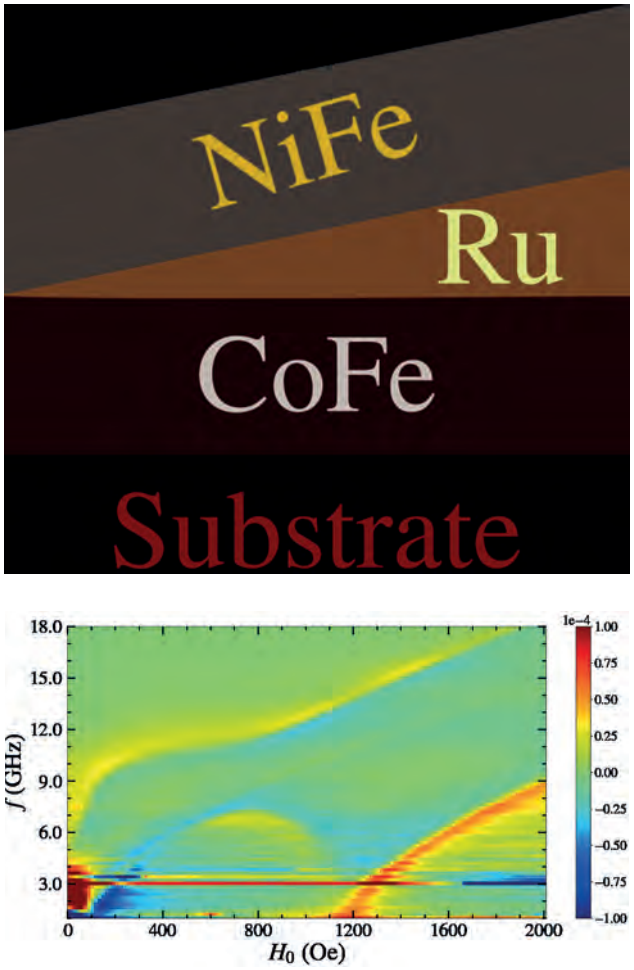

BP-14. Observation of magnon-phonon coupling in two-dimensional ferromagnetic Fe_3GeTe_2. *N. Bansal*[1], Q. Li[1], P. Nufer[1], L. Zhang[2,3], A.A. Haghighirad[4], Y. Mokrousov[3,5] and W. Wulfhekel[1,4] *1. Physics Institute (PHI), Karlsruhe Institute of Technology, Karlsruhe, Germany; 2. School of Physics and Electronic Engineering, Jiangsu University, Zhenjiang, China; 3. Peter Gruenberg Institut (PGI-1) and Institute for Advanced Simulation (IAS-1) Forschungszentrum Juelich GmbH, Juelich, Germany; 4. Institute for Quantum Materials and Technologies, Karlsruhe Institute of Technology, Karlsruhe, Germany; 5. Institute of Physics, Johannes Gutenberg-University Mainz, Mainz, Germany*

The quasiparticle excitations such as magnon and phonon can both be observed in magnetic materials. Magnon polarons [1-4] are the quasiparticles formed through the coupling of magnons and phonons. Fe_3GeTe_2 (FGT) is a ferromagnetic two-dimensional van der Waals material with a Curie temperature of up to 230 K [5,6] which makes it a promising candidate for the development of spintronic devices [7]. We use inelastic electron tunneling spectroscopy (IETS) at 35 mK to investigate phonon-magnon coupling in FGT. IETS is a powerful tool for determining the inelastic scattering of hot carriers with magnons or phonons with the second derivative of the tunneling current with respect to the bias voltage being proportional to the density of states of phonons and/or magnons. We observed three low-energy excitations below 10 meV using non spin-polarized IETS, as shown in Fig. [1]. These excitations are further supported by the spin-polarized IETS, which further demonstrate their spin-dependent nature by displaying a sizable spin contrast across a domain wall. Interestingly, calculations using density functional theory (DFT) do not reveal any peaks in the density of states (DOS) for phonons or magnons below 10 meV, ruling out the possibility that either phonons or magnons solely are responsible for these excitations. To understand our experimental results, we compared the low-energy bands between phonons and magnons, which show band crossings. Moreover, the energies of these crossings match our experimental results. These band crossings can result in van Hove singularities when there is a significant magnon-phonon interaction. Consequently, magnon polarons can be identified as the low-energy excitations that were detected. Our results provide insights into the potential application of acoustic magnonics in FGT.

[1] Berk, C., *et al.* Nat. Commun. 10, 2652 (2019) [2] Vaclavkova, D., *et al*. Phys. Rev. B 104, 134437, (2021). [3] Li, J., *et al*. Phys. Rev. Lett. 125, 217201, (2020). [4] Nambu, Y., *et al*. Phys. Rev. Lett. 125, 027201, (2020). [5] Deiseroth, H., *et al.* European Journal of Inorganic Chemistry 2006, 1561-1567, (2006). [6] Fei, Z., *et al*. Nat. Mat. 17, 778-782, (2018). [7] Deng, Y. *et al.* Nature 563, 94-99, (2018).

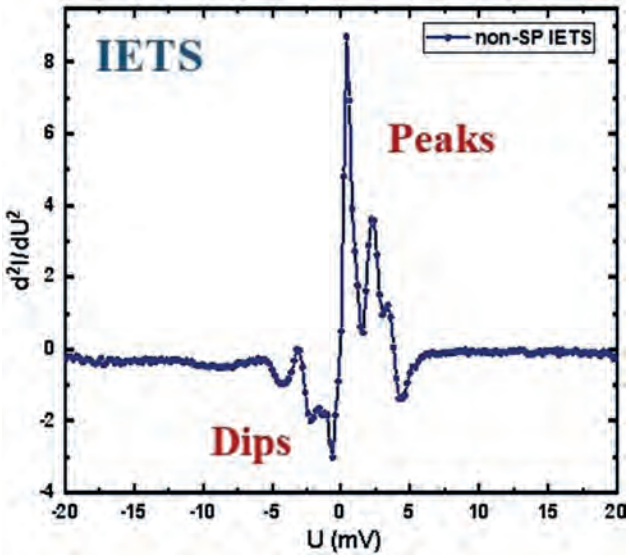

BP-15. Amplification of propagating spin waves interacting with a rapidly cooling magnon gas. *P. Artemchuk*[1], V. Tyberkevych[1] and A.N. Slavin[1] *1. Department of Physics, Oakland Universiy, Rochester, MI, United States*

When a hot magnon gas cools down rapidly, it demonstrates non-trivial thermodynamic behavior [1]. This includes formation of Bose-Einstein condensate of magnons due to increase of chemical potential of the magnon gas [1,2]. Here, we show that the distribution of magnons over energies in a rapidly cooling non-equilibrium magnon gas can be accurately described using Bose-Einstein distribution with local (in energy space) temperature $T(f) = (h/k_B)(\partial\xi(f)/\partial f)^{-1}$ and chemical potential $\mu(f) = hf - k_BT(f)\xi(f)$ that depend on the magnon frequency f. Here h is the Plank constant, k_B is the Boltzmann constant, and $\xi(f) = \log(1+1/n(f))$ is a function of the local population of magnons n(f). The simulation results obtained using the model described in [1] (see Fig.1) show that the effective temperature T(f) weakly depends on the magnon frequency, while the effective chemical potential $\mu(f)$ changes significantly with both magnon frequency and time during the thermalization of the magnon gas. At low magnon frequencies, the chemical potential $\mu(f)$ approaches, but never exceeds the minimum magnon energy hf_{min}. On the contrary, at frequencies f > 150 GHz, $\mu(f)$ substantially exceeds hf_{min} at intermediate times 1.0 ns < t < 10 ns. This "overshoot" of $\mu(f)$ over hf_{min} has profound effect on magnon gas dynamics. Our analysis shows, that 4-magnon scattering processes $f_k + f_1 \leftrightarrow f_2 + f_3$ lead to exponential growth of the magnon mode f_k when $\mu(f_2) + \mu(f_3) - \mu(f_1) > hf_k$. In the "overshoot" case, this condition is satisfied in the low-frequency part of the magnon spectrum. As a result, 4-magnon scattering leads to accelerated thermalization of low-energy magnon states, including formation of magnon BEC, and to coherent amplification of propagating spin waves. The latter effect has been observed recently in [3].

[1] M. Schneider, T. Brächer, D. Breitbach, et al., *Nature Nanotech.* 15, 457 (2020). [2] M. Schneider, D. Breitbach, R.O. Serha, et al., *Phys. Rev. Lett.* 127, 237203 (2021). [3] D. Breitbach, M. Schneider, F. Kohl, et al., arXiv:2208.11455 (2022).

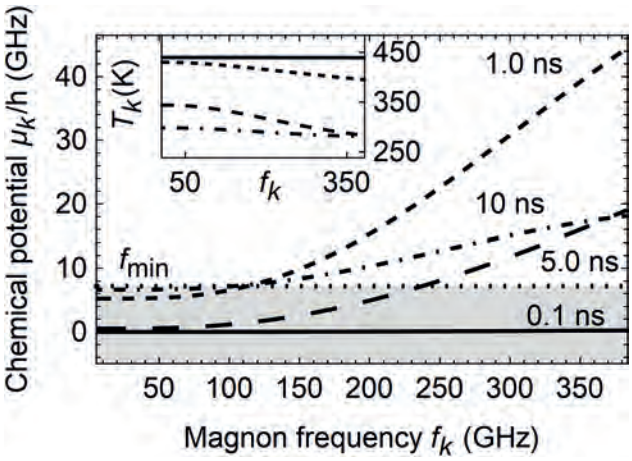

Fig. 1. Dependence of the effective chemical potential μ(f) (main graph) and effective temperature T(f) (inset) on the magnon frequency f at different time moments since the start of the rapid cooling process. The shaded area marks chemical potential below minimum magnon energy.

BP-16. Withdrawn

Session BQ
SPIN HALL AND RELATED EFFECTS I
(Poster Session)

Michael Dornu Kitcher, Chair
Massachusetts Institute of Technology, Cambridge, MA, United States

BQ-01. Withdrawn

BQ-03. Experimental Measurement Scheme for Spin Swapping Effect. *K. Kim*[1], M. Kim[1,2], W. Shim[1] and S. Choe[1] *1. Department of Physics and Astronomy, Seoul National University, Seoul, The Republic of Korea; 2. Center for Spintronics, Korea Institute of Science and Technology (KIST), Seoul, The Republic of Korea*

Spin swapping effect generates a transverse spin current by exchanging the original directions of the spin polarization and flow direction. While theoretical expectations have been made for decades, experimental evidence has started to emerge recently. The spin swapping and spin Hall effects share a common origin, but they generate the spin currents with different spin orientations. Due to the symmetry-breaking component generated by the spin swapping effect, there has been great attention as a breakthrough.in technological applications such as magnetoresistive random access memory. In this study, we propose a way to measure the spin swapping effect. For this study, we fabricated a ferromagnetic Co/Au/Co double layer film using DC magnetron sputtering. The double Co layers are antiferromagnetically coupled, but the coupling strength is weak enough to allow independent movement of domain walls in each magnetic layer. One of the Co layers functions as a magnetically hard layer, while the other acts as a soft layer. In experiments, the magnetization in the hard layer was saturated in the direction ±z and a domain wall was placed in the soft layer. When electric current was injected into this film, σ_x spins were generated from the hard layer by the spin swapping effect and then, injected to the soft layer. In contrast, the spin Hall effect in the Au layer generates σ_y spin injection into the soft layer. The effects from the σ_x and σ_y spins were then examined by measuring the spin orbit torque efficiency ε on the magnetic domain-wall motion in the soft layer. Fig. 1 shows the measurement results of ε_+ and ε_-, where $\varepsilon_\pm$ was measured under ±z saturation of the hard layer. The contribution of the spin swapping effect can be then retrieved as $(\varepsilon_+ - \varepsilon_-)/2$ as shown by Fig. 2. The figure clearly shows the typical characteristics of the spin swapping effect in this experimental situation. Therefore, the present observation provides a way to measure the spin swapping effect.

1. Lifshits, M. B., & Dyakonov, M. I. (2009). Swapping spin currents: Interchanging spin and flow directions. *Physical review letters*, *103*(18), 186601.

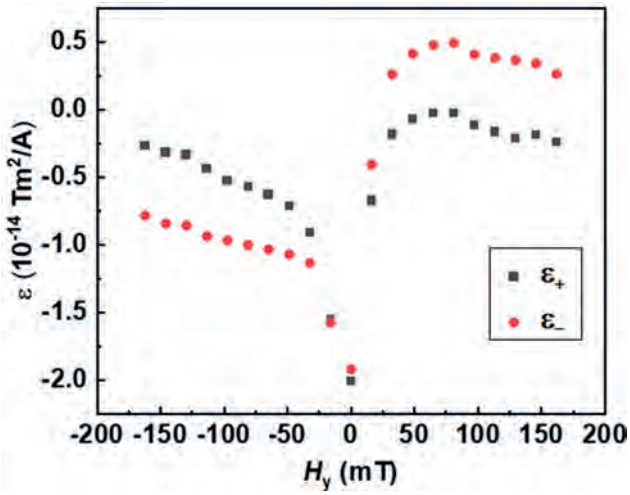

Measurement result of ε_+ and ε_- with respect to H_y

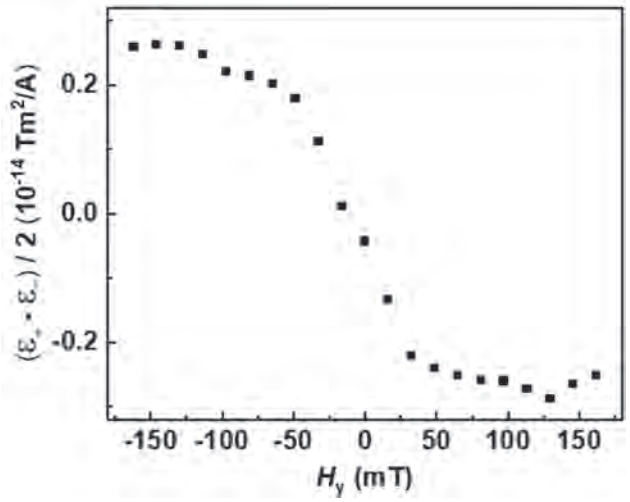

$(\varepsilon_+ - \varepsilon_-)/2$ with respect to H_y

BQ-04. Current Induced Magnetization Switching in Ferromagnetic Heusler Alloy Co_2MnAl-based Magnetic Trilayers. *M. Wang*[1], C. Pan[1], X. Qiu[1] and Z. Shi[1] *1. Shanghai Key Laboratory of Special Artificial Microstructure Materials and Technology and Pohl Institute of Solid State Physics and School of Physics Science and Engineering, Tongji University, Shanghai, China*

Spin-orbit torque (SOT) has emerged as a promising candidate for efficient magnetization manipulation of spintronic devices in the past decade [1]. In the request for high SOT efficiency, various materials and mechanisms have been explored. Recently, researchers have found ferromagnet (FM) as a high-efficiency spin source to achieve current-induced magnetization switching in the FM/Ti/FM trilayers [2,3]. In this regard, FM Heusler alloy

Co_2MnAl (CMA), a predicted Weyl semimetal [4] with strong anomalous Hall effect (AHE), anomalous Nernst effect and Spin Hall effect [5-7], shows great potential for SOT application. Here, current-induced magnetization switching is realized in a multilayer CMA/Ti/CoFeB(CFB)/MgO (Fig. 1). The perpendicularly-magnetized CFB layer serves as a spin-current analyzer. The Ti spacer layer is deployed to decouple the ferromagnetic layers and to develop perpendicular magnetic anisotropy of CFB, but allows efficient spin current transmission [2,8]. The switching current density is 1.362 and 1.905 × 10^7 A/cm^2 for ordered and disordered CMA, respectively. Furthermore, the spin Hall efficiency ξ has been determined to be -0.072 and -0.029 via the current-induced AHE hysteresis loop shift technique for the ordered and disordered CMA (Fig. 2). The ξ of ordered CMA is larger than that of Ta, CFB and NiFe [2]. At last, we attribute the low switching current density and enhanced spin Hall efficiency to the increase of spin-orbit interaction strength with the ordered structure.

[1] A. Manchon, J. Zelezny, I. M. Miron, Reviews of Modern Physics, Vol. 91, p.035004 (2019). [2] S. C. Baek, V. P. Amin, Y. W. Oh, Nat Mater, Vol. 17, p.509 (2018). [3] J. Ryu, R. Thompson, J. Y. Park, Nature Electronics, Vol. 5, p.217 (2022). [4] J. Kübler and C. Felser, EPL (Europhysics Letters), Vol. 114, p.47005 (2016). [5] Y. M. Ji, W. X. Zhang, H. B. Zhang, New Journal of Physics, Vol. 24, p.053027 (2022). [6] A. T. Breidenbach, H. Yu, T. A. Peterson, Physical Review B, Vol. 105, p.144405 (2022). [7] P. Li, J. Koo, W. Ning, Nat Commun, Vol. 11, p.3476 (2020). [8] Y. W. Oh, S. H. Chris Baek, Y. M. Kim, Nat Nanotechnol, Vol. 11, p.878 (2016).

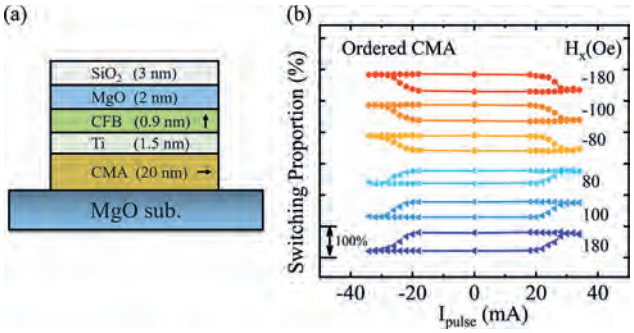

Fig. 1. (a) Structure of the ferromagnetic trilayer, black arrows represent the magnetization direction. (b) External field-dependent magnetization switching in ordered CMA sample.

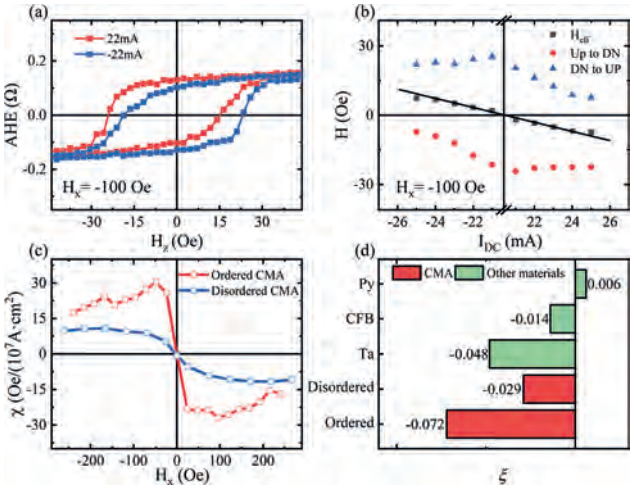

Fig. 2. (a) AHE loop for ordered CMA sample with I_{DC}= ±22 mA. (b) Fields for down-to-up and up-to-down magnetization reversals as functions of I_{DC} in ordered CMA, black squares are the center of the AHE loops. (c) Current-induced effective field per current density as a function of applied in-plane field for ordered and disordered CMA. (d) Comparison of spin Hall efficiency.

BQ-05. Role of a 2D Magnetic Interlayer on Thermally Driven Spin Current in Pt/YIG Systems. C. Hung[1], A. Chanda[1], V. Kalappattil[2], D. Zhou[3], D. Arena[1], M. Wu[2], M. Terrones[3], H. Srikanth[1] and *M. Phan*[1]
1. Physics, University of South Florida, Tampa, FL, United States;
2. Physics, Colorado State University, Fort Collins, CO, United States;
3. Physics, Pennsylvania State University, State College, PA, United States

The ferrimagnetic insulator $Y_3Fe_5O_{12}$ (YIG) is known as the benchmark system for exploring the longitudinal spin Seebeck effect (LSSE) in Pt/YIG bilayers because of its ultralow Gilbert damping. Current effort is to enhance the spin current injection across the Pt/YIG interface by reducing the conductivity mismatch between the Pt and YIG and increasing the spin mixing conductance [1,2]. Theoretical study suggests the insertion of a recently discovered two-dimensional (2D) dilute magnetic semiconductor, such as vanadium-doped transition metal dichalcogenide (TMD) monolayers V-WS_2 and V-WSe_2 [3,4], can enhance the LSSE in YIG/Pt [5]. The light-tunable magnetic property of this 2D-TMD might also enable an optical control of the spin current in spin-caloritronic devices [6]. To explore this experimentally, we have studied the LSSE in Pt/YIG and Pt/ML V-WS_2/YIG heterostructures with different V-WS_2 surface coverages. We observed a reduction in LSSE voltage when the V-WS_2 monolayer (ML) was inserted in between the Pt and YIG. The LSSE voltage decreased with increasing the V-WS_2 surface coverage. The presence of the V-WS_2 monolayer was found to increase the out-of-plane (OOP) surface magnetic anisotropy and Gilbert damping of the YIG film as probed by magnetometry and ferromagnetic resonance (FMR) measurements, respectively. The increase of these parameters decreased the magnon propagation length of YIG, thus decreasing the LSSE in Pt/YIG. Our study provides physical insights into the spin to charge conversion phenomenon via a 2D magnetic interface.

[1] S. K. Lee et al., Adv Funct Mater 30, 2003192 (2020). [2] V. Kalappattil et al., Mater Horiz 7, 1413 (2020). [3] F. Zhang et al., Advanced Science 7, (2020). [4] Y. T. H. Pham et al., Advanced Materials 32, 2003607 (2020). [5] D. Thi-Xuan Dang et al., Journal of Physical Chemistry Letters 13, 8879 (2022). [6] M. H. Phan et al., Appl Phys Lett 119, (2021).

BQ-06. Terahertz Probing of Interfacial Curie Temperatures in Spintronic Thin-Film Stacks. *O. Gueckstock*[1,2], R. Rouzegar[1,2], D. Engel[3], S. Eisebitt[3,5], S. Auffret[4], V. Baltz[4], G. Jakob[6], M. Kläui[6], T.S. Seifert[1] and T. Kampfrath[1,2] *1. Freie Universität Berlin, Berlin, Germany; 2. Fritz-Haber-Institute of the Max Planck Society, Berlin, Germany; 3. Max Born Institute, Berlin, Germany; 4. University Grenoble Alpes, Grenoble, France; 5. Technische Universität Berlin, Berlin, Germany; 6. Johannes-Gutenberg-Universität Mainz, Mainz, Germany*

Transport of spin angular momentum and spin-charge-current interconversion are fundamental operations for future spin-electronic devices. To trigger spin transport from a ferromagnetic metal F into an adjacent paramagnetic layer P on the ultrafast time scales of electron relaxation processes, femtosecond laser pulses are ideally suited [1,2]. In this approach, the inverse spin Hall effect converts the spin current into an in-plane charge current that gives rise to the emission of an electromagnetic pulse with frequencies extending into the terahertz (THz) range (Fig. 1). As the ultrafast currents are confined to only ~1 nm around the F/P interface, the emitted THz pulse is expected to be a highly sensitive probe of interface properties. Here, we investigate the impact of the F/P interface morphology and sample temperature on the THz-emission signal. We find that the variation of the THz emission signal with sample temperature depends critically on the disorder of the F/P interface. We conclude that the Curie temperature of F at the F/P interface is strongly reduced relative to the bulk by the higher degree of disorder at the F/P interface.

[1] T. Seifert *et al.*, Applied Physics Letters 120, 180401 (2022). [2] R. Rouzegar *et al.*, Physical Review B 106, 144427 (2022).

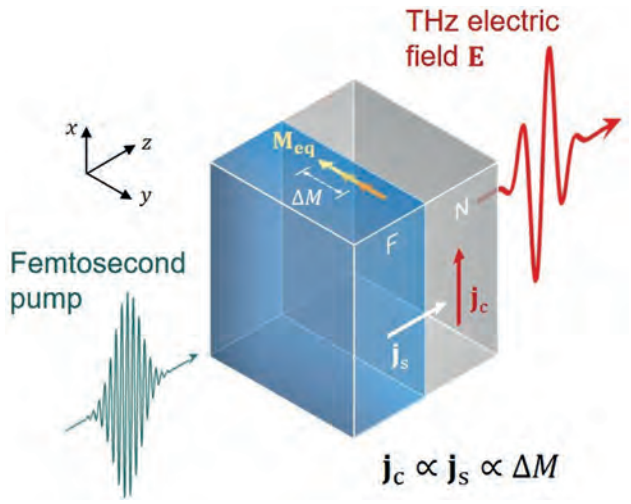

A femtosecond pulse generates a spin current j_s in the magnetic layer F that propagates into the paramagnetic layer P, where it gets converted into a transverse charge current j_c. Subsequently, an electromagnetic pulse with frequencies extending to the THZ range is ejected.

BQ-07. Origin of the unconventional temperature dependence of the spin Hall effects in a compensated ferrimagnetic insulator. C. Hung[1], A. Chanda[1], C. Holzmann[2], M. Albrecht[2], N. Schulz[1], D. Detellem[1], N. Alzahrani[1], D. Arena[1], *M. Phan*[1] and H. Srikanth[1] *1. Physics, University of South Florida, Tampa, FL, United States; 2. Institute of Physics, University of Augsburg, Augsburg, Germany*

Recently, ferrimagnetic insulator (FMI)/heavy metal (HM) based bilayer heterostructures have attracted immense interest in the field of spintronics due to their exciting magneto-physical phenomena e.g., spin Hall magnetoresistance [1] (SMR), spin orbit torque switching [2], interfacial Dzyaloshinskii-Moriya interaction [3], topological Hall effect [4] etc., which arise because of the complex interplay of the spin Hall effect, the inverse spin Hall Effect, the Rashba-Edelstein effect, and the magnetic proximity effect. Especially, the rare-earth iron garnet (REIG) based FMIs have shown extraordinary room temperature spin transport properties owing to their complicated spin textures. In this regard, the compensated REIG gadolinium iron garnet (GdIG) is of particular interest as both collinear and canted magnetic phases coexist in this system with a magnetic compensation temperature close to the room temperature. To induce perpendicular magnetic anisotropy (PMA) in the magnetic garnets, the modification of the strain between the substrate and the magnet garnet is necessary [5]. Although there are lots of study on the spin transport properties of REIGs especially around room temperature, the origin of the unconventional spin transport behavior over a broad temperature range specifically in magnetically compensated REIGs is yet to be explored. We have performed a comprehensive investigation of the temperature dependent anomalous Hall effect (AHE) in GdIG to understand the influence of its temperature dependent complex spin textures on the spin transport properties. The HMs (Pt and W) that contain opposite sign of spin Hall angle are utilized to discuss the potential Stoner stability influence on the AHE. Interestingly, there are two anomalous Hall polarity changes in these PMA GdIG. One of the polarity changes is correlated to the magnetic compensation temperature and the other one is related to the competition between the surface and bulk magnetism of GdIG. At low temperatures, GdIG undergoes a spin reorientation which causes the unusual anomalous Hall effect. These results offer the fundamental understanding of the AHEs in GdIG, which can be usefull for spintronics applications.

[1] Y. Ji, J. Miao, K. K. Meng, al -, Y.-T. Chen, S. Takahashi, and H. Nakayama, *Theory of Spin Hall Magnetoresistance (SMR) and Related Phenomena*, Journal of Physics: Condensed Matter 28,103004 (2016). [2] J. Ding, T. Liu, H. Chang, and M. Wu, *Sputtering Growth of Low-Damping Yttrium-Iron-Garnet Thin Films*, IEEE Magn. Lett. 11, 1-5 (2020). [3] C. O. Avci, E. Rosenberg, L. Caretta, F. Büttner, M. Mann, C. Marcus, D. Bono, C. A. Ross, and G. S. D. Beach, *Interface-Driven Chiral Magnetism and Current-Driven Domain Walls in Insulating Magnetic Garnets*, Nature Nanotechnology. 14, 561-566(2019). [4] T. N. Nunley, S. Guo, L. J. Chang, D. Lujan, J. Choe, S. F. Lee, F. Yang, and X. Li, *Quantifying Spin Hall Topological Hall Effect in Ultrathin Tm3Fe5 O12/ Pt Bilayers*, Phys. Rev. B 106, 014415(2022). [5] C. Holzmann, A. Ullrich, O.-T. Ciubotariu, and M. Albrecht, *Stress-Induced Magnetic Properties of Gadolinium Iron Garnet Nanoscale-Thin Films: Implications for Spintronic Devices*, ACS Appl. Nano. Mater. 2022, 1023 (2022).

BQ-08. Interfacial Static and Dynamic Exchange Coupling in a Heterostructure of CoFeB and a Perpendicular Ferrimagnetic Insulator Thulium Iron Garnet. *W. Misba*[1], D.B. Gopman[2], M. Gross[3], J.E. Shoup[2], K. Hayashi[3], C.A. Ross[3] and J. Atulasimha[1] *1. Virginia Commonwealth University, Richmond, VA, United States; 2. National Institute of Standards and Technology, Gaithersburg, MD, United States; 3. Massachusetts Institute of Technology, Cambridge, MA, United States*

Heterostructures consisting of a ferrimagnetic insulator and a ferromagnetic material gained much traction due to their great potential in energy efficient applications based on spin pumping, which can generate pure spin currents [1,2]. Moreover, spin waves excited due to non-collinear magnetization precession in the heterostructure can obviate the need to fabricate nano-antennas to generate microwave frequencies which are prone to Ohmic losses. We use a 40 nm thick film of Thulium Iron Garnet (TmIG) as the ferrimagnet which shows perpendicular magnetic anisotropy of magnetoelastic origin when deposited on a gallium gadolinium garnet (GGG) substrate using pulsed laser deposition [3]. Next, the GGG/TmIG (40 nm)/CoFeB(x)/W(0.4 nm)/CoFeB(0.8 nm)/MgO(1 nm)/W(5 nm) heterostructure is fabricated using ion beam sputter deposition method, where x varies from 0.84 nm to 4 nm. Detailed ferromagnetic resonance (FMR) and magneto optical Kerr microscopy (MOKE) studies were performed for all the samples before and after annealing (300°C) to investigate dynamic and static coupling. Figure 1 shows the angular dependence of the resonance field and resonance linewidth at 14 GHz for an annealed sample including a 3 nm CoFeB overlayer, where the angle = 0 (90) reflects the magnetic field applied within (normal to) the plane. The CoFeB linewidth dipped at the point of the crossover of the two modes indicating excitation and propagation of spin waves from the interface which effectively introduces spin torques and suppresses the damping. FMR studies on other samples also indicate similar dynamic coupling where the two modes avoid crossing as indicated from divergent linewidth. Furthermore, the MOKE study shows signs of static exchange coupling as seen from the pronounced difference in the perpendicular hysteresis loops between a pristine GGG/TmIG sample and the heterostructure with CoFeB (3 nm) in Fig. 2. These findings are important for spintronic devices working in exchange coupled spin wave system. ACKNOWLEDGEMENT: NSF EECS 1954589

[1] S. Klingler, M. D. Stiles and M. Weiler, Phys. Rev. Lett., Vol. 120, p. 127201 (2018) [2] P.-C. Chang, V. R. Mudinepalli and W.-C. Lin, Journal of Alloys and Compounds, Vol. 875, p. 159948 (2021) [3] A. Quindeau, G. S. D. Beach and C. A. Ross, Adv. Electron. Mater., Vol. 3, p.1600376 (2017)

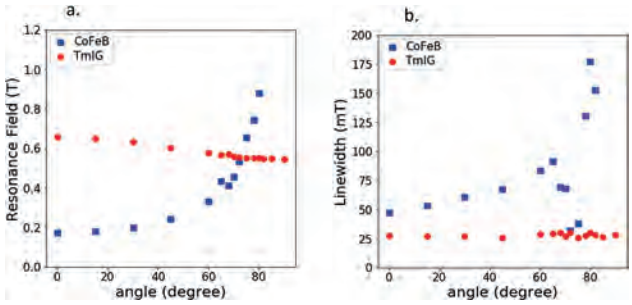

Fig.1: (a) Ferromagnetic resonance and (b) resonance linewidth vs angle at f = 14 GHz for two observed resonance modes including a CoFeB (3nm) layer

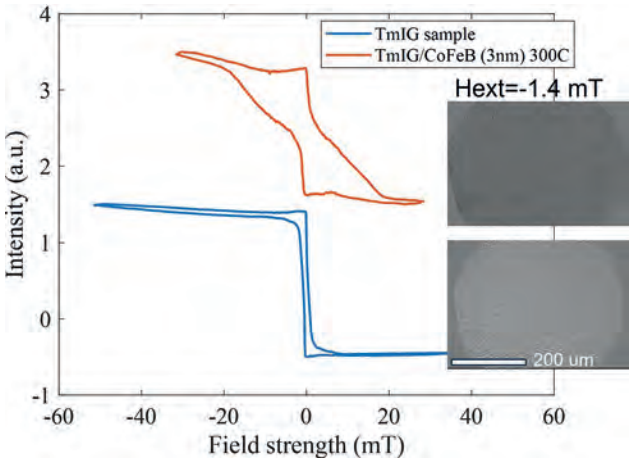

Fig. 2: Polar MOKE for TmIG and TmIG/CoFeB samples

BQ-09. Unexpected Enhancement of the Field-like Spin-orbit Torque in Ultrathin Ferromagnetic Regime. *J. Yoon*[1], M. Kim[1,2], S. Lee[1], D. Kim[2] and S. Choe[1] *1. Physics and Astronomy, Seoul Nationl University, Seoul, The Republic of Korea; 2. Center for Spintronics, Korea Institute of Science and Technology, Seoul, The Republic of Korea*

Spin-orbit torques (SOTs) have been extensively studied in spintronics over the past decade [1]. They originate from two well-known sources: the spin Hall effect (SHE) in a normal metal layer adjacent to a ferromagnetic layer, and the Rashba-Edelstein effect (REE) occurring at metallic interfaces due to electrostatic potential gradients [2]. The theoretical framework suggests that SOTs associated with the SHE should display a linear relationship with the reciprocal of the ferromagnetic thickness. In contrast, SOTs arising from the REE are expected to be independent of the ferromagnetic layer's thickness [3]. However, previous research has consistently reported a linear dependence of both damping-like torque (DLT) and field-like torque (FLT) on the reciprocal of the ferromagnetic thickness [4]. Notably, these studies have not explored the behavior in the atomically thin regime of ferromagnetic materials. In our study, we prepared two series of samples with ferromagnetic thickness reduced to the atomically thin regime, enabling us to perform simultaneous measurements of DLT and FLT. The detailed structure of series A and B is as follows: Ta(5 nm)/Pt(3 nm)/Co(t_{Co}^{eff})/Ta(3 nm)/Au(1.5 nm) and Ta(2 nm)/Pd(2 nm)/Co(t_{Co}^{eff})/Pt(2.5 nm) respectively. In series B, both DLT and FLT displayed the reciprocal of the ferromagnetic thickness, indicating the dominant contribution of bulk SHE in the SOT. However, series A exhibited a non-linear correlation with t_{Co}^{eff}, showing enhanced behavior as t_{Co}^{eff} decreased, suggesting the predominant influence of the REE. Further details will be presented during the on-site session.

[1] Cheng Song, Ruiqi Zhang, Liyang Liao, Yongjian Zhou et al. Prog. Mater. Sci., Vol. 118, p. 100761 (2021) [2] V. P. Amin, and M. D. Stiles, Phys. Rev. B. Vol. 94, p. 104420 (2016) [3] A. V. Khvalkovskiy, V. Cros, D. Apalkov et al. Phys. Rev. B., Vol. 87, p. 020402(R) (2013) [4] Yongxi Ou, Chi-Feng Pai, Shengjie Shi.et al., Phys. Rev. B., Vol. 94, p. 140414(R) (2016)

BQ-10. Enhanced spin current generation near magnetic transition in amorphous cobalt silicon. *C. Hsu*[1,2], H. Kleidermacher[1,3], E. Blenkinsop[1], J. Webster[1], S. Hsu[1], S. Sayed[1], A. N'Diaye[2], F. Hellman[1] and S. Salahuddin[1,2] *1. University of California Berkeley, Berkeley, CA, United States; 2. Lawrence Berkeley National Lab, Berkeley, CA, United States; 3. Stanford University, Stanford, CA, United States*

Large spin-orbit torque has been observed in fully amorphous iron silicide [1]. While the concentration dependence of spin-orbit torque in iron silicide can potentially arise from the change in density of states near the Fermi level, the role of magnetism in magnetic element silicide has not been fully understood. Here, we report large spin-orbit torque in fully amorphous cobalt silicide through in-plane harmonic Hall measurement. By varying the concentration between cobalt and silicon, we observed that the peak of spin-orbit torque efficiency coincides with the transition of the magnetic phase from nonferromagnetic to ferromagnetic characterized through x-ray magnetic circular dichroism. Our observation of an enhanced spin current near the magnetic transition of amorphous cobalt silicon potentially demonstrates a new way of engineering and understanding spin current generation in amorphous magnetic element silicide systems.

[1] Cheng-Hsiang Hsu, Julie Karel, Niklas Roschewsky et al. Large spin-orbit torque generated by amorphous iron silicide, 17 September 2022, PREPRINT (Version 1) available at Research Square [https://doi.org/10.21203/rs.3.rs-1946953/v1]

BQ-11. Negative effective Gilbert's damping constant through spin pumping in FM/HM bilayer system. *P. Sharma*[1], K. Begari[1], B. Lim[1] and C. Kim[1] *1. Department of Physics and Chemistry, Daegu Gyeongbuk Institute of Science and Technology (DGIST), Daegu, The Republic of Korea*

Pure spin current generation and detection are of great interest in Spintronics devices due to their high data storage capacity and low power consumption, making them ideal for next-generation MRAM applications [1-3]. Spin pumping has emerged as a powerful tool for spin current generation (spin accumulation) in bilayer systems comprising ferromagnetic materials (FM) and Heavy Metals (HM) [3-5]. Typically, spin pumping is accompanied by an enhancement of the damping constant(α). However, for low-power applications, a lower damping constant is preferred. This can be achieved by applying an external direct current (DC) to the Heavy Metal layer, generating an anti-damping torque due to Rashba spin-orbit interaction [6,7]. Nevertheless, this procedure reduces the efficiency of device operation. Recently, non-equilibrium spin accumulation induced by spin pumping at the interface has been reported, reducing the Gilbert's damping parameter (anti-damping) without using external DC [4,6,8]. In This study, we report anti-damping in SiO_2/NiFe(10nm)/Ta(5nm) and SiO_2/NiFe(10nm)/W(5nm). The FMR spectra of NiFe, NiFe/Ta, and NiFe/W were acquired using a coplanar waveguide for a frequency range of 6 GHz to 12 GHz. Fig.1 shows the FMR spectra of a NiFe sample. The damping Constant(α) was evaluated by fitting the frequency versus linewidth(ΔH) plot (Fig.2). The values of α for NiFe and NiFe/Ta and NiFe/W are extracted to be 0.01261± 0.00042, 0.00968± 0.000083 and 0.01085±0.000081, resulting in effective damping ($\alpha_{FM/HM}$-α_{FM}) values of -0.00293 and -0.00176 for NiFe/Ta and NiFe/W, respectively. It is evident that a negative effective Gilbert's damping constant was obtained through spin pumping in the FM/HM bilayer system. Furthermore, high interfacial spin mixing conductance ($g^{eff}_{\uparrow\downarrow}$) values of -1.17454E+19 m^{-2} and -6.56985E+18 m^{-2} were calculated for NiFe/Ta and NiFe/W, respectively. The accumulated spin in HM layer can be converted and measured as charge current across the sample due to the inverse spin hall effect.

1. I. M. Miron, K. Garello, G. Gaudin, Nature, Vol. 476, p.189(2011) 2. L. Liu, C.-F. Pai, Y. Li, Science, Vol.336, p.555(2012) 3. K. Ando, S. Takahashi, J. Ieda, Journal of applied physics, Vol. 109, p. 103913(2011)

4. N. Behera, P. Guha, D. K. Pandya, ACS applied materials & interfaces, Vol. 9, p.31005(2017) 5. B. Panigrahi, S. K. Sahoo, S. Syamlal, Solid State Communications, Vol. 348, p.114743(2022) 6. N. Behera, S. Chaudhary and D. K. Pandya, Scientific reports, Vol.6, p.1(2016) 7. J. R. Sánchez, L. Vila, G. Desfonds, S. Gambarelli, Nature communications, Vol.4, p.2944(2013) 8. P. Gupta, B. B. Singh, K. Roy, Nanoscale, Vol.13, p.2714(2021)

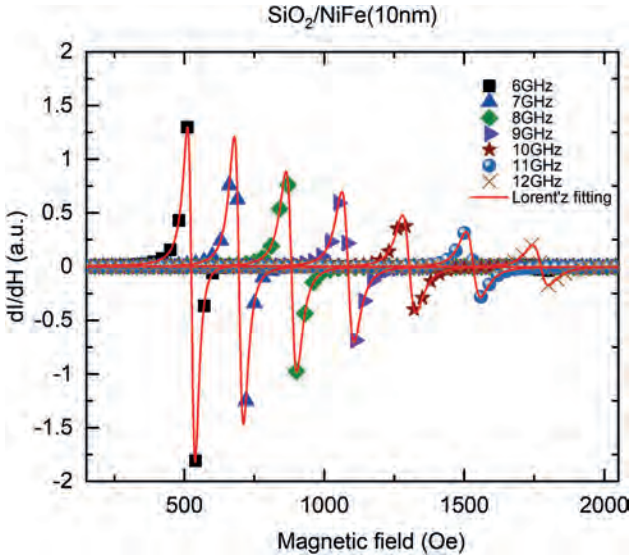

Fig.1: FMR spectra of NiFe sample at different microwave frequencies

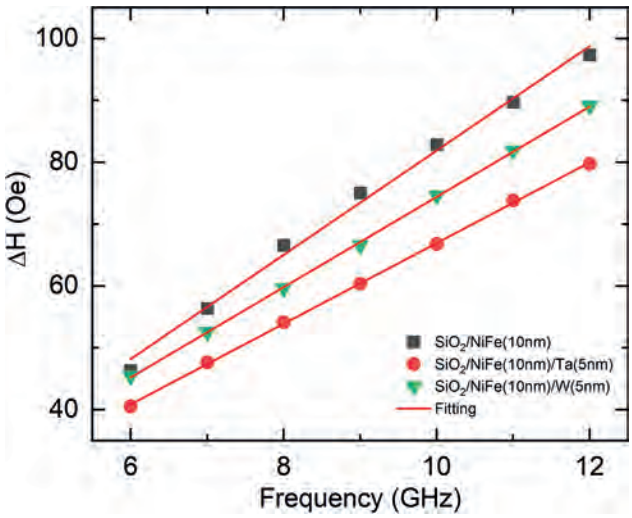

Fig.2: Frequency vs Linewidth(ΔH) plot for NiFe, NiFe/Ta and NiFe/W

Session BR
SKYRMIONS AND ANTIFERROMAGNETS
(Poster Session)

Yi Li, Co-Chair
Argonne National Laboratory Lemont, IL, United States
Wei Zhang, Co-Chair
University of North Carolina at Chapel Hill, Chapel Hill, NC, United States

BR-01. Origin and Mechanism of Unusual Anomalous Hall Effect Response in GdFeCo-Ta-TbFeCo. R.C. Bhatt[1,2], L. Ye[1,2], N. Huang[1,2] and *T. Wu*[1,2] *1. Graduate School of Materials Science, National Yunlin University of Science and Technology, Douliu, Taiwan; 2. Taiwan SPIN Research Center, National Yunlin University of Science and Technology, Douliu, Taiwan*

This study aims to understand the underlying process of magnetization reversal and the origin of the complex anomalous Hall effect (AHE) in sandwich structures of RE-TM FIM, specifically GdFeCo and TbFeCo, with different coercivities. We fabricated two film structures A and B, as shown in Fig. 1, using magnetron sputtering. Sample A had a negligible difference in FeCo content, while sample B had the same FeCo content with a thickness of 10 nm. The M-H loops confirmed the magnetization reversal of the two layers with significant differences in their coercivities (Fig. 1). Although structures A and B exhibited similar M-H loops, the temperature-dependent AHE loops had different shapes due to the presence of FeCo and Tb-dominant phases in TbFeCo, respectively. Both structures showed a Hall sign reversal near 232 K, indicating the compensation temperature (T_{comp}) of GdFeCo. Moreover, at high fields above T_{comp}, the transition from a collinear to a non-collinear magnetic configuration in GdFeCo led to a decrease in the AHE resistance of the system. The spin-flop field (H_{SF}) increased as both structures moved away from T_{comp}. The triple AHE loops resulted from the significant Zeeman field-induced spin-flopping, leading to a non-collinear magnetic configuration in GdFeCo. The abnormal AHE behavior in these sandwich ferrimagnetic structures could be explained by considering the magnetic arrangements of Gd, Tb, and FeCo sublattices at different applied fields. Additionally, we presented a model (Fig. 2) to simplify understanding the origin of the complex AHE loops in these sandwich systems. This study provides insights into the mechanism behind the phenomenal temperature-dependent AHE response of technologically important RE-TM FIM films for spintronics applications.

1. Y. Hirata *et al.*, Phys. Rev. B, Vol. 97, p. 220403 (2018) 2. K. Cai *et al.*, Nat. Electron., Vol. 3, p. 37 (2020) 4. L.-X. Ye, R.C. Bhatt, N.-C. Huang, J. Magn. Magn. Mater., Vol. 565, p. 170282 (2022) 5. R.C. Bhatt, L.-X. Ye, N. T. Hai, J. Magn. Magn. Mater., Vol. 537, p. 168196 (2021) 6. R.C. Bhatt, L.-X. Ye, N.-C. Huang, J. Magn. Magn. Mater., Vol. 580, p. 170881 (2023)

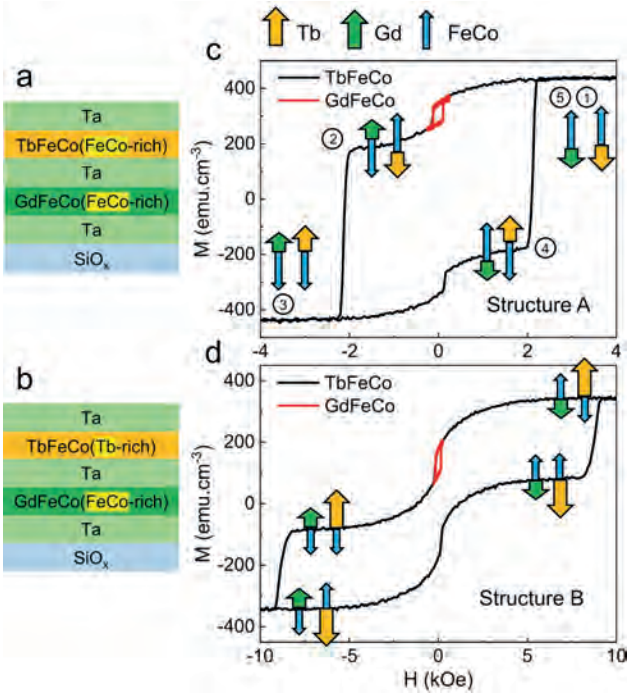

Fig. 1. Schematic of two film structures (a) A and (b) B. Their corresponding magnetization hysteresis curves are shown in (c) and (d), respectively.

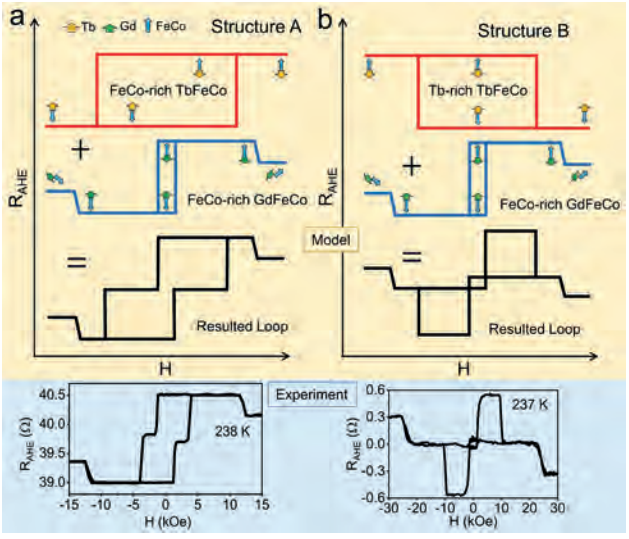

Fig. 2. The two-magnet model for explaining the complex AHE loops. Panel (a) and (b) represent the scheme for structures A and B, respectively. The models fit well with the experimental data.

BR-02. Magnetoresistance Hysteresis in Altermagnet Candidate α-MnTe Grown by MBE on III-V Semiconductors. *S. Bey*[1], S. Bac[1], B. Márkus[2,1], J. Wang[1], D. Beke[2,1], S.P. Bennett[4], A. Ievlev[5], M. Zhukovskyi[3], T. Orlova[3], L. Forró[2,1], X. Liu[1] and B. Assaf[1]
1. Department of Physics and Astronomy, University of Notre Dame, Notre Dame, IN, United States; 2. Stravropoulos Center for Complex Quantum Matter, University of Notre Dame, Notre Dame, IN, United States; 3. Notre Dame Integrated Imaging Facility, University of Notre Dame, Notre Dame, IN, United States; 4. Materials Science and Technology, U.S. Naval Research Laboratory, Washington, DC, United States; 5. Center for Nanophase Materials Sciences, Oak Ridge National Laboratory, Oak Ridge, TN, United States

Hexagonal MnTe is a candidate altermagnet, a new class of collinear antiferromagnets that have alternating momentum dependent spin-polarization. In MnTe, the real space spin-sublattices lack inversion centers [1-3], enabling this spin-polarization despite the zero net magnetic moment of the material. Systematic investigation of growth conditions and carrier doping in MnTe films is crucial to understand fundamental physics related to the spin polarized band structure of this material. In this work, we report the synthesis and magnetotransport measurements of 160nm thick MnTe thin films on GaAs(111) and InP(111). We only observe an unusual magnetoresistance (MR) hysteresis with angular dependence in films grown on GaAs. The samples were determined to be single-phase from X-ray diffraction (XRD). They were characterized using transmission electron microscopy (TEM), secondary ion mass spectroscopy (SIMS) and High-Resolution XRD. From XRD, shown in Fig. (1), the MnTe sample grown on GaAs is fully relaxed. The epitaxial relationship was found to be Mn(0001)||GaAs(111) and MnTe[11-20]||GaAs[1-10]. Using the linear Hall resistance in transport measurements up to B=12T at T=10K we find that the MnTe film on GaAs is p-type with p_{2D}=7.86X10^{14}cm^{-2} and the MnTe film on InP is n-type with n_{2D}=3.16X10^{16} cm^{-2}. We then measured angular dependent magnetoresistance with the current J applied along the film plane parallel to the MnTe[11-20]||GaAs[1-10] direction and the magnetic field B rotated between out-of-plane and in-plane. B || J when it is applied in-plane. In the sample on GaAs, we observe a low field hysteresis in the MR for all field angles, as shown in Fig. 2. The MR vs. Field for the InP sample is also plotted in Fig. 2, showing that we do not see this hysteresis behavior under the same conditions. Our current efforts focus on understanding the origin of this MR hysteresis and its relationship to doping, strain, anisotropy and interface structure and chemistry. The aim of our work is to establish reproducible conditions under which altermagnetic properties are observed in MnTe transport measurements.

[1] L. Šmejkal, J. Sinova, and T. Jungwirth. Phys. Rev. X., Vol. 12, 031042 (2022) [2] I.I. Mazin. Phys. Rev. B Vol. 107, L100418 (2023) [3] R. D. Gonzalez Betancourt, J. Zubáč, R. Gonzalez Hernandez. Phys. Rev. Lett., Vol. 130, 036702 (2023)

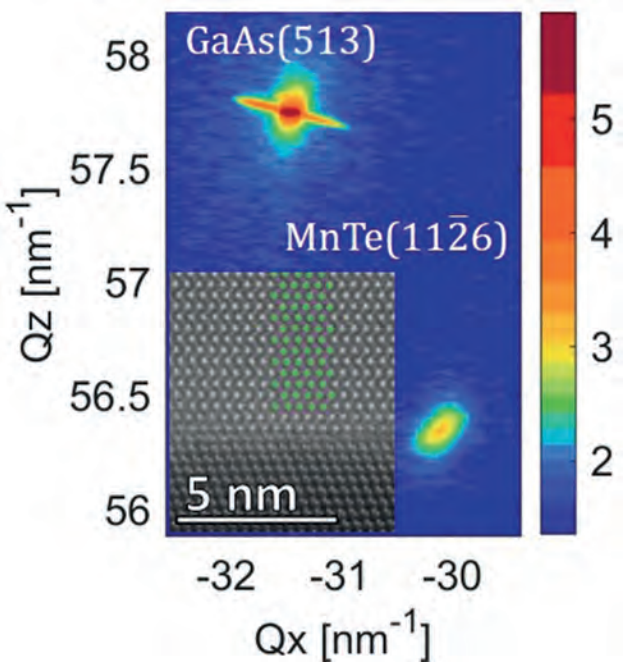

Fig. 1 RSM and TEM of MnTe film on GaAs

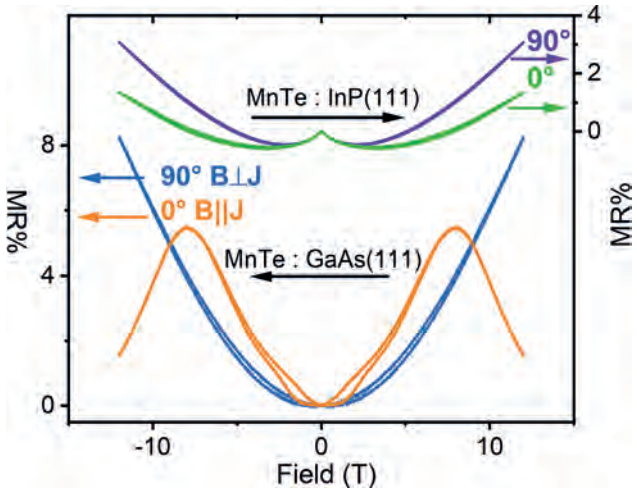

Fig. 2 Magnetoresistance vs field at 10K for MnTe on GaAs(111) and MnTe on InP(111)

BR-03. Large Transverse Magnetoresistance in AFM/FM Perovskite Oxide Bilayers: A Potential System for Low-Field Controllable AFM Spin Transport. *M.R. Natale*[1], S. Bleser[1], D.Y. Sasaki[2], I. Nihal[2], M. Roos[1], Y. Takamura[2] and B.L. Zink[1] *1. Physics and Astronomy, University of Denver, Denver, CO, United States; 2. Materials Science and Engineering, University of California Davis, Davis, CA, United States*

Epitaxially grown $La_{1-x}Sr_xFeO_3$/ $La_{1-x}Sr_xMnO_3$ heterostructures can be carefully engineered to show reliable "spin flop" coupling of the ferromagnetic and antiferromagnetic order. This arrangement, where the LSMO magnetization and LSFO Neel order are mutually perpendicular, has been repeatably shown using soft x-ray magnetic microscopy measurements [1,2]. $La_{1-x}Sr_xMnO_3$ has well-established magneto-transport effects [3], while $LaFeO_3$, a nominally insulating AFM and parent structure of $La1_{-x}Sr_xFeO_3$, has been explored as possible tunnel junctions [4]. These heterostructures enable control of the Neel vector with low fields by coupling with the FM sublayer. In this report, we probe the effects this novel ordering has on the magneto-transport properties of $La_{0.5}Sr_{0.5}FeO_3$/ $La_{0.7}Sr_{0.3}MnO_3$ by implementing the Hall Bar

geometry and the DC-current reversal method [4,5]. The Hall Bar is patterned using e-beam lithography and 10nm of Pt is deposited by RF sputtering. We measure transverse and longitudinal voltages as a function of both field and temperature in multiple field-orientations. Both transverse and longitudinal configurations result in very distinct behavior, with potential spin Hall magnetoresistance observed in the transverse configuration. Exploring interfacial effects between Pt/ $La_{0.5}Sr_{0.5}FeO_3$, we remove the main current channel. The resulting signals show charge can flow through the LSFO but show entirely different symmetry with field orientation. The symmetry with no Pt channel is explained with a combination of the planar Hall effect and magnetoresistance in the LSMO, while the novel patterns with a Pt channel allows spin current effects suggesting a type of spin conversion through the LSFO.

[1] F. Yang, et al. Phys. Rev. B. 83, 014417 (2011) [2] E. Folven, et al. Nano. Lett. 12, 300361 (2012) [3] L.M. Wang, et al. Phys. Rev. B. 74, 184412 (2006) [4] F.Y. Bruno, et al. Nat. Commun. 6, 6306 (2015) [5] W.X. Wang, et al. Appl. Phys. Lett. 105, 182403 (2014) [6] S. Velez, et al. Phys. Rev. B. 94, 174405 (2016)

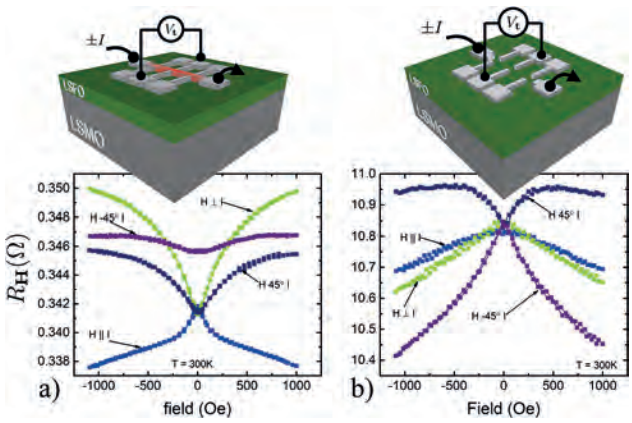

Fig 1: Transverse R_H measured LSFO/LSMO bilayer with (a) and without (b) the main Pt spin injection channel. Observed symmetry without the Pt channel is consistent with LSMO planar Hall effect and magnetoresistance, while behavior with the Pt channel indicates controllable spin transport in LSFO.

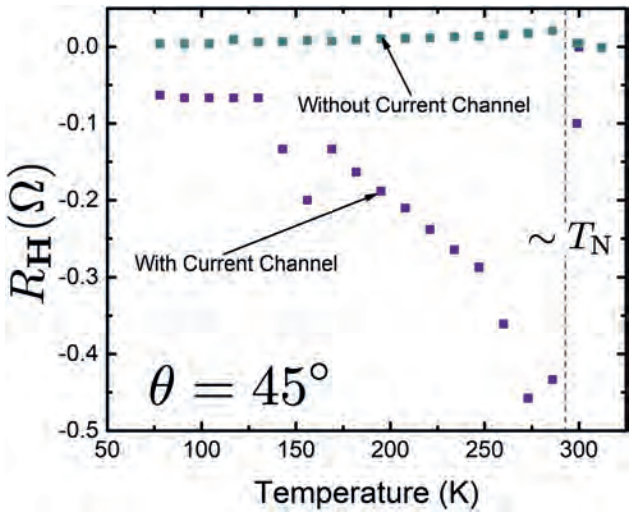

Fig 2: R_H vs. Temperature for the devices shown in Fig. 1. The large onset of a negative signal just below 300 K in the device that probes spin transport likely indicates the location of the Neel temperature in this thin LSFO.

BR-04. Anisotropic Magnetoresistance in Thin Film FeRh|Pt and FeRh|SiN Bilayers with Varying Film Thicknesses. *E. Blake*[1], C. Fitzpatrick[1], A. Pedroza[1], S.K. Patel[2], H. Ren[2], P. Sparks[1], E. Fullerton[2] and J. Eckert[1] *1. Physics, Harvey Mudd College, Claremont, CA, United States; 2. Center for Memory and Recording Research, University of California San Diego, La Jolla, CA, United States*

Anisotropic magnetoresistance (AMR) measurements can reveal effects on spin orientation in spin-orbit coupled systems by probing the dependence of resistivity on the angle between the current direction and the high magnetic susceptibility direction. FeRh is a characteristic metallic magnetic material, demonstrating a first order hysteretic metamagnetic phase transition from the low temperature antiferromagnetic (AFM) to the high temperature ferromagnetic (FM) phase at ~370K. It has been reported that electronic band structure can be affected by changes in spin orientation in a collinear antiferromagnet, meaning the band structure of FeRh can be tuned [1,2]. Because of the tunability of FeRh, the material has garnered interest for AFM-based spintronic devices. The AMR in the AFM phase of FeRh|Pt bilayers has been shown to undergo a symmetry change. After the symmetry change, the AMR magnitude increases strongly with increasing magnetic field and decreasing temperature [3]. This effect may be impacted by spin-orbit coupling interactions between the FeRh and Pt layers. To resolve the role of the interfaces on the complex transport, we explore FeRh(001) films of different thicknesses with different capping layers (Pt and SiN). We have explored AMR in both the FM and AF phases with current along the [100] and [110] directions. The 40 nm films in the AF phase show AMR with two-fold symmetries, however, in thinner 20nm films, lower symmetries start to emerge. We will discuss possible origins and the role of capping layers on these phenomena.

1. T. Suzuki, R. Chisnell, A. Devarakonda, Y.-T. Liu, W. Feng, D. Xiao, J. W. Lynn, J. G. Checkelsky, *Nature Phys* 12, 1119–1123 (2016). 2. J. Gibbons, T. Dohi, V. Amin, F. Xue, H. Ren, J. Xu, H. Arava, S. Shim, H. Saglam, Y. Liu, J. Pearson, N. Mason, A. Petford-Long, P. Haney, M. Stiles, E. Fullerton, A. Kent, S. Fukami, A. Hoffmann, *Phys. Rev. Applied* 18, 024075 (2022) 3. S. Shim, M. Mehraeen, J. Sklenar, J. Oh, J. Gibbons, H. Saglam, A. Hoffmann, S. Zhang, N. Mason, *Phys. Rev. X* 12, 021069 (2022)

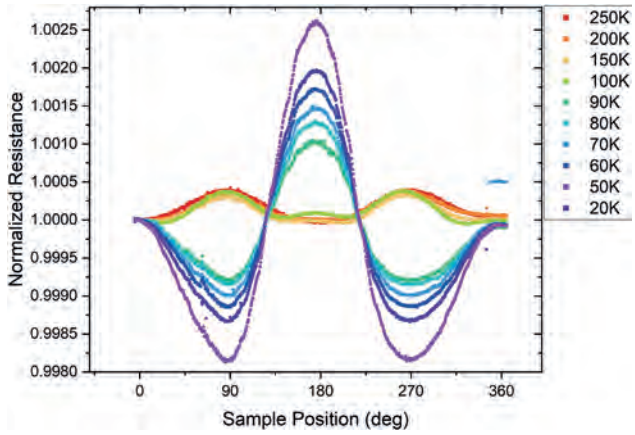

Resistance versus angle between current and applied field (AMR) for 20nm FeRh sample with 2nm SiN capping layer at 8T field. Multiple temperature series are shown. Note the distinct character change in the AMR signal between 100K and 90K.

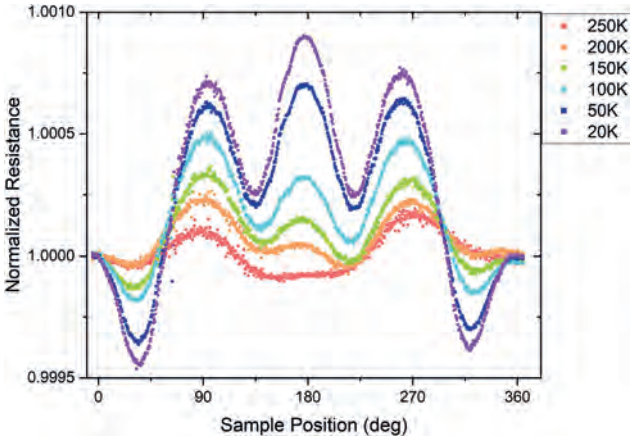

Resistance versus angle between current and applied field (AMR) for 20nm FeRh sample with 2nm Pt capping layer at 8T field. Multiple temperature series are shown.

BR-05. Withdrawn

BR-06. Temperature dependent spin Seebeck voltages in thermally-evaporated chromium thin films. *S. Bleser*[1], M.R. Natale[1], R. Greening[1], X. Fan[1] and B.L. Zink[1] *1. University of Denver, Denver, CO, United States*

We recently demonstrated that the longitudinal spin Seebeck effect (LSSE) [1] shows large spin-charge conversion and large spin Seebeck voltages in evaporated chromium (Cr) thin films relative to sputtered platinum (Pt) at room temperature. However, determining the exact nature and control of thermal gradients in LSSE experiments is imperative, especially at the interface [2,3]. In this work, we adopt the Hall bar geometry and current-driven heating [4,5] for LSSE experiments in a vacuum cryostat for better manipulation of thermal gradients. We present LSSE voltages, V_{LSSE}, between 78K to 350K for a 10 nm Cr thin film deposited at room temperature on a bulk polycrystalline yttrium-iron-garnet (YIG) substrate and make comparisons to a sputtered 25 nm Pt thin film on a YIG substrate from the same batch. Furthermore, we present dimensionless sensitivity measurements, dR/dT*(T/R), that reveal two distinct peaks centered at ≈ 350K and ≈ 200K for the 10 nm Cr thin film. These two peaks likely indicate the separate Neel temperatures of the incommensurate and commensurate spin density wave antiferromagnetic states, coexisting in a strain-driven mixed state in the evaporated film. We compare our evaporated Cr LSSE measurements to 10 nm sputtered Cr thin film [6]. Below 200K, our evaporated Cr thin film shows a larger V_{LSSE} than the sputtered Cr thin film suggesting that a combination of finite-size effects and strain that lead to a modification to the spin-density wave nature of Cr could explain the larger V_{LSSE} seen in our Cr thin film.

[1] Bleser, Greening, Roos, *et al*. J. Appl. Phys 131, 113904 (2022). [2] Sola, A., Bougiatioti, P., Kuepferling, M. et al. Sci Rep 7, 46752 (2017). [3] A. Sola et al. IEEE Transactions on Instrumentation and Measurement, vol. 68, no. 6, pp. 1765-1773, June 2019. [4] W.X. Wang, S. H. Wang, L. K. Zou, et al. Appl. Phys. Lett. 105, 182403 (2014). [5] Michael Schreier, et al. Appl. Phys. Lett. 103, 242404 (2013). [6] D. Qu, *et al*. Phys. Rev. B 92, 020418(R) (2015).

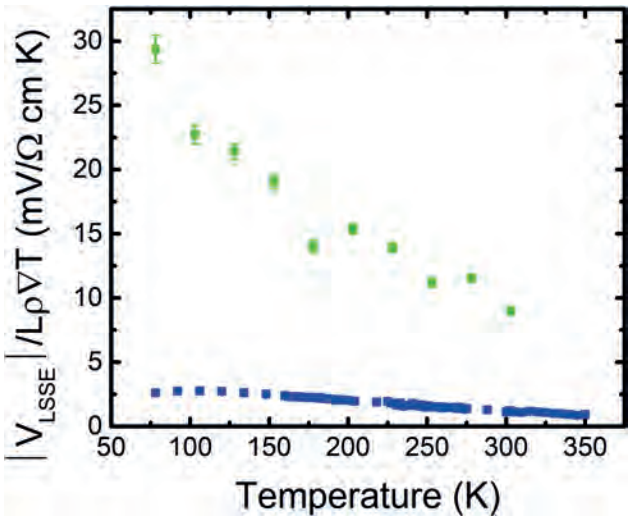

The absolut LSSE voltage, V_{LSSE}, normalized by length, L, resistivity, ρ, and thermal gradient, ∇T, vs T for a 10 nm evaporated Cr film (Blue symbols) and a 25 sputtered Pt film (Green symbols).

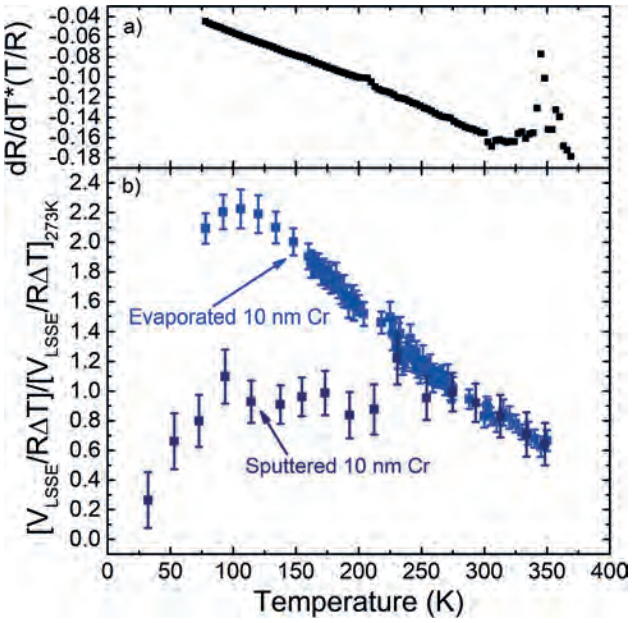

a) The dimensionless sensitivity, dR/dT*(T/R), for a 10 nm evaporated Cr film vs T. Two distinguishable peaks are centered at ≈350K and ≈200K. b) Comparison of the temperature dependence of the LSSE voltage, V_{LSSE}, divided by film resistance, R, and temperature difference, ΔT, for a 10 nm sputtered Cr film (navy blue symbols) and 10 nm evaporated Cr film (blue symbols). The LSSE voltage are relative to measurements made at 273K. The sputtered Cr data is adapted from [6].

BR-07. Glassy behavior determined by transport in antiferromagnet $Fe_{1/3}NbS_2$. *S. Shim*[1,2], M. Huq[3], K. Lu[1,2], A. Murzabekova[1,2], F. Mahmood[1,2], G. MacDougall[1,2] and N. Mason[4,2] *1. Physics, University of Illinois at Urbana-Champaign, Urbana, IL, United States; 2. Materials Research Laboratory, University of Illinois at Urbana-Champaign, Urbana, IL, United States; 3. Physics & Astronomy, Amherst College, Amherst, MA, United States; 4. Pritzker School of Molecular Engineering, University of Chicago, Chicago, IL, United States*

Antiferromagnets have gained significant interest as next-generation material for spintronics applications, due to their absence of stray fields, non-volatility, and THz dynamics. Recent work has demonstrated that

the antiferromagnetic metal Fe1/3NbS2 can be electrically switched with extremely low current densities [1], and that such electrical switching can be facilitated when the spin glass and antiferromagnetic order are coupled [2]. The coexistence of spin glass and antiferromagnetic order is usually confirmed with magnetometry [2, 3], but it is rarely confirmed with transport measurements. Here, we show that anisotropic magnetoresistance (AMR) can probe glassy behavior in Fe1/3NbS2. We observe that below the spin-glass freezing temperature the AMR differs for field-cooled versus zero-field-cooled devices. Such history-dependent AMR arises from the coupling between the antiferromagnetic and spin-glass phases, where the resistance depends on the relative orientation of antiferromagnetic order to the spin-glass-pinned uncompensated moments. Moreover, we observe that the AMR shifts in phase depending on which direction the field is applied during the field cooling process (Figure 1), further confirming the coupling between the antiferromagnetic and spin-glass phases. Our observation shows the potential of AMR as a sensitive probe for complex, coexisting magnetic orders. This research was primarily supported by the NSF through the University of Illinois at Urbana-Champaign Materials Research Science and Engineering Center DMR-1720633 and was carried out in the Materials Research Laboratory Central Research Facilities, University of Illinois.

[1] N. L. Nair et al., Nat. Mater. 19, 153 (2020) [2] E. Maniv et al., Sci. Adv. 7, 1 (2021) [3] E. Maniv et al., Nat. Phys. 17, 525 (2021)

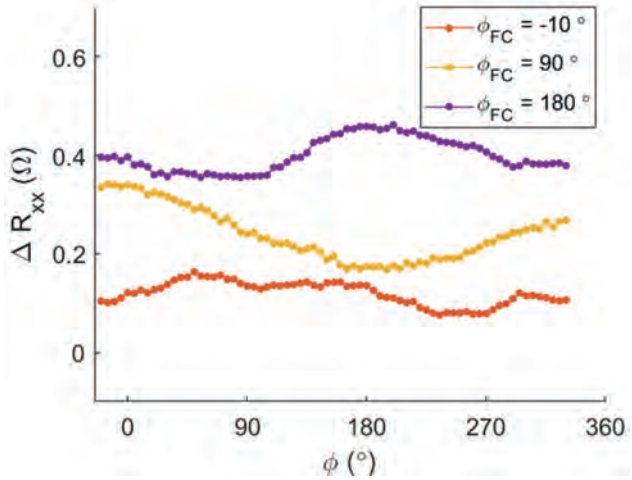

Figure 1: In-plane anisotropic magnetoresistance (AMR), measured at T = 10 K under H = 9 T, where φ is the angle between the current and the magnetic field. The in-plane AMR shifts in phase depending on φ_{FC}, the direction of the applied field during the field cooling (FC) process. The AMR curves are vertically shifted for clarity.

BR-08. Withdrawn

BR-09. The Nucleation of Magnetic Skyrmion Bubbles in Synthetic Antiferromagnetic Microwires Using Air-bridge Vertical Spin Injection Devices. *R. Aboljadayel*[1], C.E. Barker[1], M. Rosamond[1], S. Finizio[2], G. Burnell[1] and C. Marrows[1] *1. University of Leeds, Leeds, United Kingdom; 2. Paul Scherrer Institut, Villigen, Switzerland*

Magnetic skyrmions are small topologically protected nontrivial spin textures found in specially engineered chiral magnetic materials. Skyrmions' unique properties, such as their small size, stability and responsiveness to electrical currents, make them ideal information carriers for future low-power technology and spintronics applications such as racetrack memory devices and quantum computation [1]. However, skyrmions in ferromagnetic materials hold some limitations. For example, the stray magnetic field limits their sizes and operation speed. Furthermore, the Magnus force resulting from their finite topological charge adds a transverse component to their motion in the direction of the applied current, limiting their functionality [2]. However, it has been proposed that antiferromagnetic (AF) skyrmions can overcome these issues and increase the skyrmion's mobility and stability due to the absence of the skyrmion Hall effect [3-4]. Here we report our successful attempt to observe the nucleation of skyrmion bubbles in a synthetic AF (Ta/[Ru/Pt/CoB/Ru/Pt/CoFeB]$_5$/Ru/Pt) microwire on X-ray transparent membranes (Fig. 1). We fabricated specially-engineered air-bridge vertical spin injection devices (Fig. 2) to control the creation of the skyrmion bubbles which were found to be stable under zero field. The ferromagnetic (FM) layers in this stack have strong perpendicular magnetic anisotropy and DMI and are antiferromagnetically coupled by indirect exchange through the non-magnetic spacer (Ru/Pt). Furthermore, the thicknesses of the FM layers are tuned so that they have equal and opposite magnetic moments. This zero net magnetisation makes it challenging to characterise such systems using most standard techniques. Therefore, we utilised the element specificity of soft X-ray scanning transmission X-ray microscopy (STXM) to study the two sublattices (CoFeB and CoB) independently by tuning the X-ray energy to the Fe and Co L_3-edge. We will also highlight the growth of the synthetic AF stack and the fabrication process of devices.

[1] A. Fert et al., Nat Rev Mater 2, 17031 (2017) [2] R. Chen et al., Nano Lett., 20, 5, 3299–330 (2020) [3] M. Fattouhi et al., Phys. Rev. Applied 16, 014040 (2021) [4] W. Legrand et al., Nat. Mater. 19, 34-42 (2020)

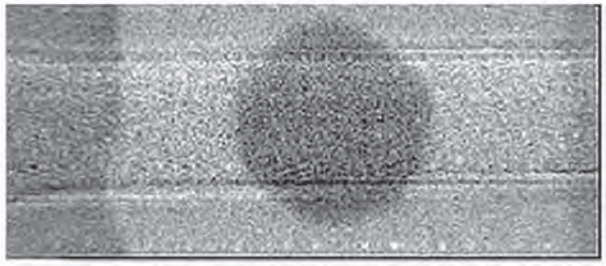

STXM image of the skyrmion nucleated when applying pulse trains of 10 bipolar 5ns pulses of the current density of 1.923x10^{12}Am^{-2} with an in-plane field of 120mT.

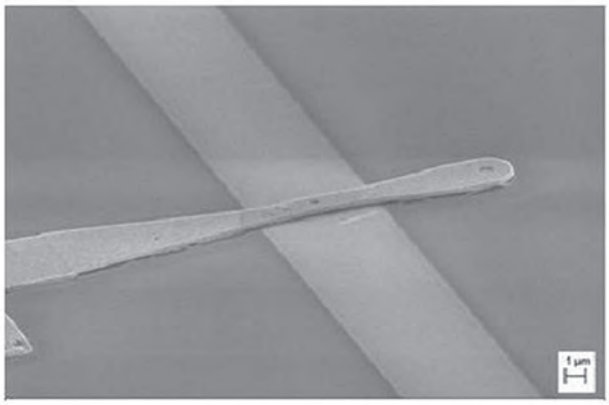

SEM image of the vertical injector

BR-10. Voltage control of the skyrmion phases and its Brownian motion. *M. Kasagawa*[1], S. Miki[1,3], K. Hashimoto[1], R. Ishikawa[2], M. Goto[1,3], H. Nomura[1,3] and Y. Suzuki[1,3] *1. Graduate School of Engineering Science, Osaka University, Osaka, Japan; 2. Ulvac-Osaka University Joint Research Laboratory for Future Technology, ULVAC, Osaka, Japan; 3. OTRI-Osaka, Osaka, Japan*

Magnetic skyrmions are recently expected to function as information carriers in ultra-low-power Brownian calculators because they exhibit Brownian motion near room temperature [1,2]. In order to realize such devices, voltage control of skyrmions is essential. Prior studies of voltage control of skyrmions, gate manipulation [3,4], diffusion [5], and control of

creation and annihilation [6] of skyrmions by applying DC voltage have been reported. However, its microscopic mechanism is not precise because there is also DMI modulation, which is not just a VCMA effect [4]. Therefore, in this study, we searched for clues to elucidate the mechanism of the voltage effect of skyrmion and investigated the voltage dependence of skyrmion creation and annihilation, as well as diffusion. Two types of stacked structures, Si/SiO_2 substrate/Ta /$Co_{16}Fe_{64}B_{20}$/Ta/MgO/SiO_2 and Si/SiO_2 substrate/Ta/Pt/$Co_{16}Fe_{64}B_{20}$/Ta /MgO/SiO_2, were fabricated by sputtering. Here, Pt was inserted to increase DMI. Then, Cr(1 nm)/Au(5 nm) ultrathin film electrodes were deposited on these samples. While applying a voltage to each sample in the perpendicular direction, we observed the voltage change of Kerr hysteresis and the diffusion of skyrmions by MOKE microscopy. About the correlation between temperature and voltage for skyrmions, the creation temperature of skyrmions decreases with positive voltage and increases with negative voltage. The presentation will discuss voltage hysteresis, temperature-voltage phase diagram, and frequency dependence of diffusion coefficient when AC voltage is applied. This work was supported by CSRN-Osaka, JSPS KAKENHI Grant Number JP20H05666, 23KJ1477, 23KJ1477, Japan and JST CREST Grant Number JPMJCR20C1, and MEXT Initiative to Establish Next-generation Novel Integrated Circuits Centers (X-NICS) Grant Number JPJ011438.

[1] Y. Jibiki *et al*., Appl. Phys. Lett., 117, 082402 (2020), [2] K. Raab *et al*., Nature Communications, 13, 6982 (2022), [3] K.Hashimoto *et al.*, MMM, EOC-06, Minneapolis (2022), S.Miki *et al.*, Intermag, HOD-14, Sendai (2022), [4] C. Fillion *et al.*, Nature Communications, 13, 5257 (2022), [5] T. Nozaki *et al*., Appl. Phys. Lett., 114, 012402 (2019), [6] R.Ishikawa *et al*., Appl Phys. Lett, 121, 252402 (2022)

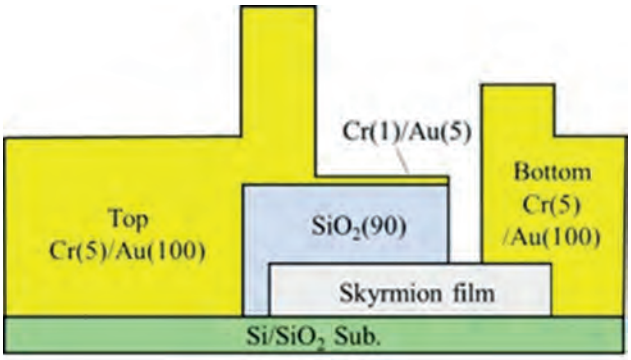

Cross sectional view of sample configuration (nm)

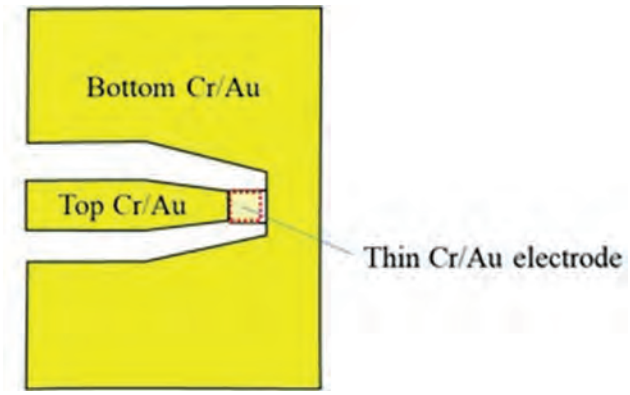

Top view of sample configuration (nm)

BR-11. Near-Landauer Reversible Skyrmion Logic with Voltage-Based Propagation. B. Walker[1], *K. Muthukrishnan*[1], R. Thapa[1], X. Hu[1], M.P. Frank[2], F. Garcia-Sanchez[3], A.J. Edwards[1] and J.S. Friedman[1]
1. Electrical and Computer Engineering, The University of Texas at Dallas, Richardson, TX, United States; 2. Sandia National Laboratories, Albuquerque, NM, United States; 3. Departamento de Fisica Aplicada, Universidad de Salamanca, Salamanca, Spain

Magnetic skyrmions are topological quasiparticles whose non-volatility, detectability, and mobility make them exciting candidates for low-energy computing. Previous works have demonstrated the feasibility and efficiency of current-driven skyrmions in cascaded logic structures inspired by reversible computing [1-3]. As skyrmions can be propelled through the voltage-controlled magnetic anisotropy (VCMA) effect with much greater efficiency, we propose a VCMA-based skyrmion propagation mechanism that drastically reduces energy dissipation (Fig. 1) [4]. Additionally, we demonstrate the functionality of skyrmion logic gates enabled by our novel voltage-based propagation and estimate its energy efficiency relative to other logic schemes (Fig. 2). Finally, we simulate these circuits at non-zero temperatures (up to 150 K), demonstrating their thermal robustness. The minimum dissipation of this VCMA-driven magnetic skyrmion logic at 0 K is found to be ~6× the room-temperature limit predicted by Landauer's principle, indicating the potential for sub-Landauer dissipation through further engineering.

[1] M. Chauwin, X. Hu, F. Garcia-Sanchez, N. Betrabet, A. Paler, C. Moutafis, J. S. Friedman, Skyrmion Logic System for Large-Scale Reversible Computation, Physical Review Applied 12:6, 064053 (2019). [2] B. W. Walker, C. Cui, F. Garcia-Sanchez, J. A. C. Incorvia, X. Hu, J. S. Friedman, Skyrmion Logic Clocked via Voltage-Controlled Magnetic Anisotropy, Applied Physics Letters 118, 192404 (2021). [3] X. Hu, B. W. Walker, F. Garcia-Sanchez, A. J. Edwards, P. Zhou, J. A. C. Incorvia, A. Paler, M. P. Frank, J. S. Friedman, Logical and Physical Reversibility of Conservative Skyrmion Logic, IEEE Magnetics Letters 13, 4503805 (2022). [4] B. W. Walker, F. Garcia-Sanchez, A. J. Edwards, X. Hu, M. P. Frank, F. Garcia-Sanchez, J. S. Friedman, Near-Landauer Reversible Skyrmion Logic with Voltage-Based Propagation, ArXiv, Jan 2023, doi:10.48550/arXiv.2301.10700

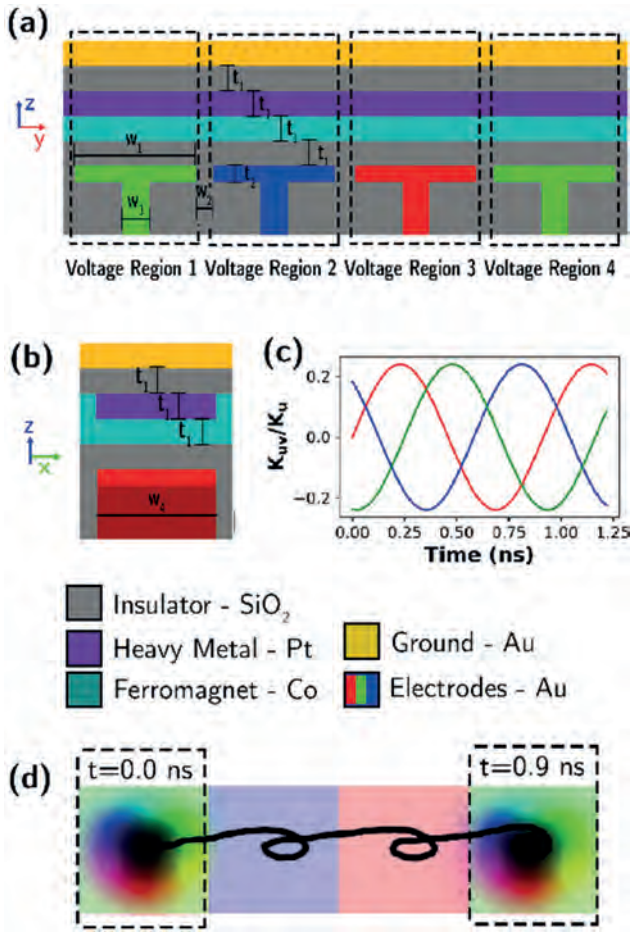

Skyrmion propagation with VCMA. An electric field is applied across a heavy metal/ferromagnet interface (teal/purple) via electrodes (red/green/blue) separated by a dielectric (grey). The skyrmion exists in the ferromagnet layer. (a) Y-Z Device Cross Section (b) X-Z Device Cross Section (w1 = 19 nm, w2 = 1 nm, w3 = 11 nm, w4 = 20 nm, t1 = 0.8 nm, t2 = 0.5 nm) (c) VCMA anisotropy waveform applied to electrodes of corresponding color. (d) Micromagnetic simulation of skyrmion propagation; black path indicates skyrmion trajectory.

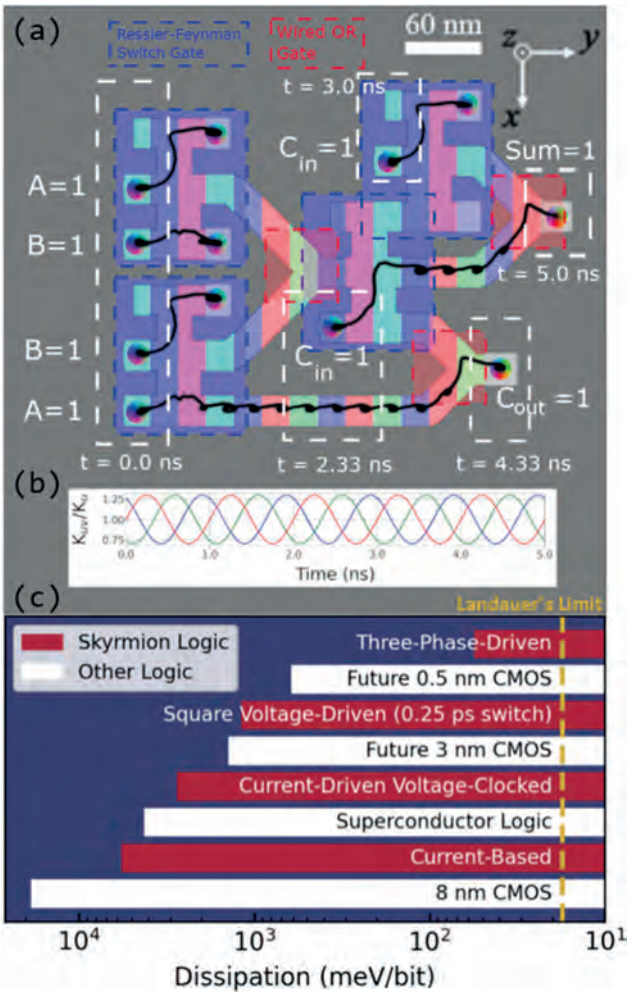

(a) Micromagnetic simulation results of full adder using voltage-based propagation with input combination A=1, B=1, Cin=1. The black path indicates skyrmion trajectory. (b) VCMA anisotropy waveform applied to electrodes of corresponding color. (c) A comparison of total dissipation per bit processed for skyrmion logic technologies (red) and other logic technologies (white). While temperature is not considered, considerable progress has been made in the efficiency of skyrmion-based logic as it approaches the room-temperature Landauer limit (gold line).

BR-13. Chiral Inversion of Resonant Modes in Gd_xFe_{1-x} Ferrimagnetic Alloy. C. Chen[1], C. Zheng[1], Y. Liu[1] and *J. Zhang*[1] *1. School of Physics, Tongji University, Shanghai, China*

Antiferromagnetic materials exhibit higher frequencies (up to THz) compared to ferromagnetic materials and demonstrate better magnetic field stability due to the absence of stray fields. They possess a twin sublattice structure, and their intrinsic magnetic excitation modes exhibit both left-handed and right-handed precession modes. However, controlling their magnetic order with an external magnetic field is challenging as their net magnetic moment is zero. In contrast, ferrimagnetic materials, with a twin sublattice structure and partial net magnetic moment, provide a suitable platform for studying antiferromagnetic spin dynamics. In ferrimagnetic alloys with specific composition ratios, compensation temperatures for magnetic moment and angular momentum exist due to thermal excitation. Moreover, as the composition ratio changes, points of magnetic moment compensation (PM) and angular momentum compensation (PA) are observed. In this study, we employed atomic-scale micromagnetic simulation techniques considering the lattice spatial structure to investigate the chirality reversal characteristics of GdxFe1-x ferrimagnetic alloys at different composition

ratios and the variations of spin wave precession near the PA point under an external magnetic field. Our results indicate that the chirality of the resonant mode in GdxFe1-x alloys undergoes reversal with an increase in Gd ratio. Additionally, the energy degeneracy points of the two resonant modes deviate from zero magnetic field, distinguishing them from antiferromagnetic materials, owing to the different saturation magnetization strengths of the two sublattices in GdxFe1-x alloys. That is to say, the chirality of the spin resonance mode changes with variations in the external magnetic field under the same composition ratio. We also provide a theoretical explanation for this phenomenon.

[1] Kim C, Lee S, Kim H G, et al. Distinct handedness of spin wave across the compensation temperatures of ferrimagnets (vol 9, 980, 2020)[J]. Nature materials, 2020(10):19. [2] Rezende S M, Azevedo A, RL Rodríguez-Suárez. Introduction to antiferromagnetic magnons[J]. Journal of Applied Physics, 2019, 126(15):151101. [3] Ishibashi M, Shiota Y, Funada S, et al. Spin Wave Resonance in Perpendicularly Magnetized Synthetic Antiferromagnets[J].

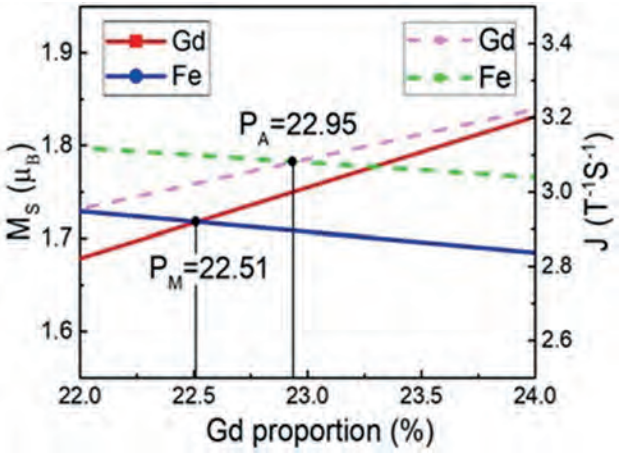

Fig. 1 Theoretical calculated saturation magnetizations (solid lines) and angular momentums (dashed lines) as the functions of the proportion x for Gd and Fe atoms, respectively.

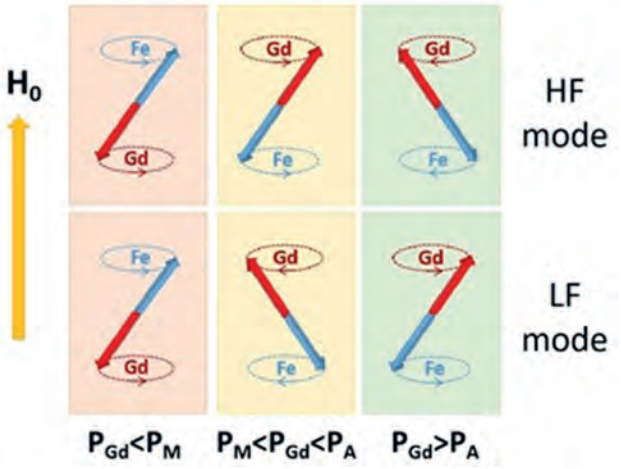

Fig (2) Schematic diagrams of chirality change of resonant modes with the proportion x.

BR-14. Withdrawn

BR-15. Simultaneous High Charge-Spin Conversion Efficiency and Large Spin Diffusion Length in Antiferromagnetic RuO_2. Y. Zhang[1], *H. Bai*[1], L. Han[1], C. Chen[1], Y. Zhou[1], F. Pan[1] and C. Song[1] *1. Tsinghua University, Beijing, China*

Developing superior materials for spin generation, transport and detection is crucial to the progress in spintronics. Relying on strong spin-orbit coupling (SOC), materials with powerful charge-spin conversion ability (i.e. large spin Hall angle θ_{SH}) can either be applied to spin generators primarily based on spin Hall effect (SHE), or play a role in spin detectors via inverse spin Hall effect (ISHE). On the other hand, long spin diffusion length (λ_{SD}) is highly desired for the sake of efficient spin transport and spin logic devices. However, a trade-off between θ_{SH} and λ_{SD} have to be made in traditional SHE-based spin source materials due to SOC. To be more specific, heavy metals with strong SOC, e.g., Pt, β-Ta and β-W, possess relatively large θ_{SH} as well as limited λ_{SD}, while semiconductors like GaAs and some light metals with weak SOC like Cu and Ag have small θ_{SH} and long λ_{SD}. Here, we prove that collinear antiferromagnetic RuO_2(100) film is able to address this key issue and break the inverse relationship of θ_{SH} versus λ_{SD}. Based on spin torque-ferromagnetic resonance (ST-FMR) and spin pumping (SP) measurements, we demonstrate that the θ_{SH} of RuO_2(100) film is 0.183, and the λ_{SD} is over 12 nm being an order of magnitude longer than that of Pt, β-W and β-Ta. By conducting control experiment, nonrelativistic altermagnetic spin splitting effect (ASSE) is ascertained to be the crucial mechanism accounting for the large θ_{SH} and long λ_{SD} in RuO_2 simultaneously, as compared to spin Hall effect (SHE). Besides the fundamental significance, our findings would advance the development of spintronics towards higher efficiency and lower power consumption.

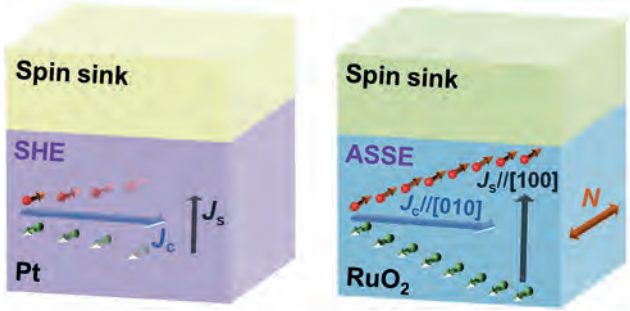

Comparison of spin source materials with different charge-spin conversion mechanisms.

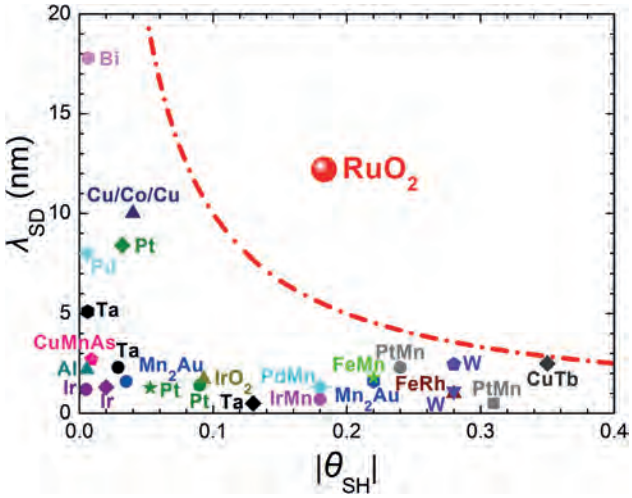

Evaluation of various spin source materials according to both the absolute value of spin Hall angle $|\theta_{SH}|$ and spin diffusion length λ_{SD}. Each color corresponds to one type of material system, where various symbols indicate data acquired from different literature. The reference line of $|\theta_{SH}\lambda_{SD}| = 1$ nm is represented by the red dash dot line demonstrating the inverse relationship between θ_{SH} and λ_{SD} followed by materials with SHE except for RuO_2 with ASSE.

Session BS
SPIN ORBITRONICS I
(Poster Session)

Gen Yin, Chair
Georgetown University, Washington, DC, United States

BS-01. Withdrawn

BS-02. Magnetization reversal induced by spin-orbit torque in perpendicularly magnetized (Mn-Cr)AlGe/W bilayer system. *T. Kubota*[1], T. Kato[2], S. Honda[3], Y. Sonobe[2,4] and K. Takanashi[5,1] *1. Tohoku University, Sendai, Japan; 2. Nagoya University, Nagoya, Japan; 3. Kansai University, Suita, Japan; 4. Waseda University, Tokyo, Japan; 5. Japan Atomic Energy Agency, Tokai, Japan*

Materials showing perpendicular magnetization and low saturation magnetization are essentially required for future spintronics applications such as magnetoresistive random access memories. An intermetallic compound, (Mn-Cr)AlGe (MCAG) is focused in this study. The crystal structure of this material is a Cu_2Sb-type tetragonal phase which exhibits magnetocrystalline anisotropy (K_u) to the *c*-axis direction. One attribute of the material is its ease of transfer to practical devices, i.e, sufficiently large K_u can be obtained in a few-nanometer thick (001)-textured MCAG films using thermally oxidized silicon substrates[1]. In this study, layered samples consisting of MCAG and W layers were fabricated for spin-orbit torque (SOT) applications, and the magnetization reversal process was investigated using Hall-bar devices with electrical measurements and a magneto-optical Kerr effect (MOKE) imaging technique. The stacking structure of the samples is Si, SiO_2 substrate/seed/MgO 10 nm/MCAG *t* /W 5 nm/MgO 0.8 nm/Ta 1 nm, where *t* was changed from 5 to 20 nm. The samples were deposited at room temperature by magnetron sputtering and annealed at 400 °C in a vacuum furnace. They were patterned into cross shapes using lithography techniques. A hysteresis loop obtained by the Hall voltage measurements are shown in Fig. 1 for t = 10 nm with an in-plane magnetic field (H_x) of 100 mT along the current direction. Magnetization reversal is clearly observed after applying pulse currents of about ±24 mA. Sign reversal of the hysteresis was also confirmed for the opposite direction of H_x, which suggests a successful SOT induced magnetization reversal for the relatively thick MCAG layer. Fig. 2 shows a MOKE image of a device after the SOT reversal. Dark contrast was observed in the most region of the horizontal Hall-bar suggesting the reversed magnetization, however, some region around a cross remains bright. Such a situation implies a loss of SOT due to current shunting at the cross point. The detail dependence on the pulse as well as on the Hall-bar width will be discussed in the presentation.

[1] T. Kubota *et al*., Appl. Phys. Lett. 118, 262404 (2021).

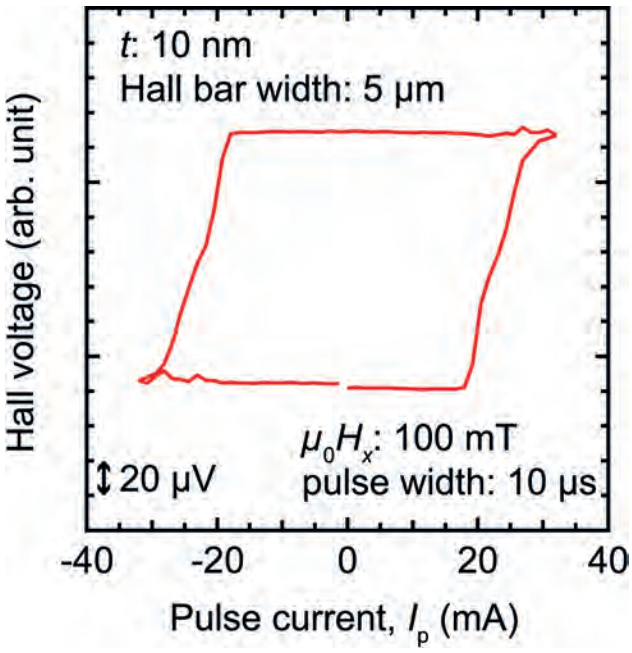

A hysteresis loop of Hall voltages as a function of pulse currents.

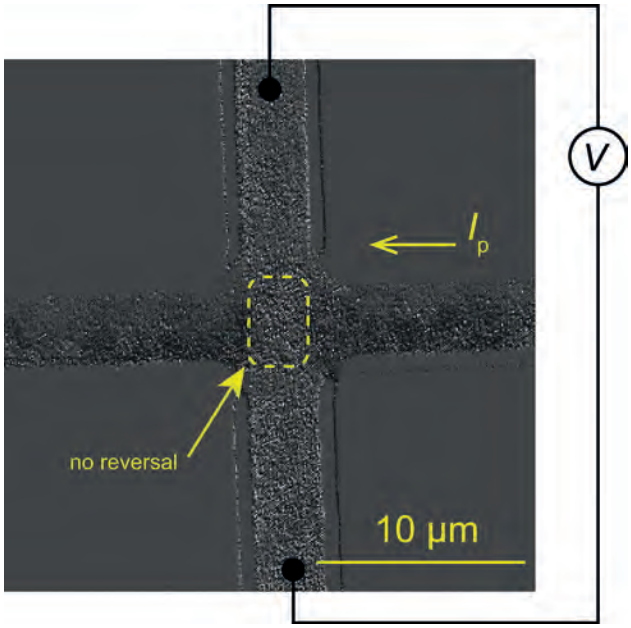

A MOKE image of a device after the SOT magnetization reversal.

BS-03. Tunable spin-orbit torque in Cu based heterostructures by HfO_2 gating. *M. Kim*[1], C. Yun[1], S. Yu[1], J. Park[1], Y. Jo[1] and K. Rhie[2] *1. Applied Physics, Korea University, Sejong, The Republic of Korea; 2. Display and semiconductor physics, Korea University, Sejong, The Republic of Korea*

Current-induced spin-orbit torque (SOT) is governed as an efficient mechanism to manipulate the magnetization in magnetic material [1]. In principle, the sizable SOT is believed to originate from the bulk spin Hall effect (SHE) and/or the interfacial spin Rashba-Edelstein effect (SREE) in heavy metal (HM) based magnetic heterostructure with strong spin-orbit coupling (SOC). However, recent reports indicated that the light metal (LM) such as Cu, Cr can also generate non-negligible SOTs and these sizable charge to spin conversions are attributed to the orbital angular momentum (OAM) induced orbital Hall effect (OHE) and/or orbital Rashba-Edelstein effect (OREE) [2]. The OAM dominating SOT generation has been experimentally explored in various LM-base systems [3]. By broken inversion symmetry at the interface of LM and oxide layer such as CuOx, the OREE can emerge independent of the SOC. Due to natural oxidation may impact the degree of potential gradient significantly, which can lift the orbital quenching [4]. In this work, we study the impact of the controlled potential at interface of light metal/oxide by gating system on the nature of the OREE as well as its efficiency in terms of damping-like and field-like effective fields in ferromagnets. We prepare Co/Cu/CuOx inplane-magnetic heterostructures and for the controlling electric potential between Cu/CuOx, HfO2 layer as gating insulator which is known as high dielectric constant oxide. We observe the impact of induced external voltage on the interface of Cu/CuOx which indicate the change of potential may affects significantly to OREE. We believe that our results could be a boost up the generated spin-current by exploiting the interfacial Rashba-Edelstein effect as well as provide valuable information for building energy-efficient spin/orbitronic devices utilinzing the spin and orbital effect.

[1] L. Liu, C. F. Pai, and R. A. Buhrman, *Science (80-.)*., vol. 336, pp. 555–558 (2012) [2] D. Lee *et al.*, *Nat. Commun.*, vol. 12, pp. 1–8 (2021) [3] S. Lee *et al.*, *Commun. Phys.*, vol. 4, pp. 3–8 (2021) [4] S. Ding *et al.*, *Phys. Rev. Lett.*, vol. 125, p. 177201 (2020)

BS-04. Spin Synergistic Torque Switching in CoTb Ferrimagnetic Perpendicular Magnetic Tunnel Junction. *W. Zhu*[1,2], M. Tang[1,2] and X. Qiu[1,2] *1. School of Physics Science and Engineering, Tongji University, Shanghai, China; 2. Shanghai Key Laboratory of Special Artificial Microstructure Materials and Technology, Tongji University, Shanghai, China*

Perpendicular magnetic tunnel junction (p-MTJ) consists as the essential building block of various spintronic devices [1]. Instead of applying magnetic field, all electrical operation of p-MTJ is greatly desired for the highly efficient and high-density spintronic applications [2]. However, the magnetization switching driven by the spin-transfer torque (STT) reduces the lifetime of the MTJ [3], and the switching speed is slow as compared to that driven by spin-orbit torque (SOT) [4]. On the other hand, although SOT has many advantages [5], an extra magnetic field required to accomplish the SOT switching severely limits its application [6]. To solve this dilemma, here we combine the STT and the SOT to realize the spin synergistic torque (SST) to achieve field-free switching [7] of the p-MTJ at a very low current density. We have successfully fabricated a ferrimagnetic CoTb based p-MTJ, and the device structure and current application method are shown in Figure 1 (a). The tunneling magnetoresistance (TMR) characteristics of MTJ are shown in Figure 1 (b) and Figure 1 (c). The CoTb promises a faster response speed and maintains a large coercivity in a large temperature range, as shown in Figure 1 (d). Next, we demonstrated that STT can independently drive the magnetization switching of MTJ, as shown in Figure 2 (a). It is also able to synergistically drive the magnetization reversal of MTJ under low STT current density by simultaneously applying SOT and STT, as shown in Figure 2 (b), (c), and (d). By combining the advantages of both the SOT and the STT, STT sheds great prospects for practical low-power and high-speed spintronic devices. Key Words: magnetic tunnel junction ferrimagnetic CoTb spin synergistic torque

[1] Thomas, L. et al. J. Appl. Phys., Vol 115, 172615 (2014). [2] Ikeda, S. et al. Electron Devices Meet. (IEDM) 33.2.1–33.2.4 (IEEE, 2015). [3] Amara-Dababi, S. et al. Appl. Phys. Lett., Vol 99, 083501 (2011). [4] Garello, K. et al. Appl. Phys. Lett., Vol 105, 212402 (2014). [5] Manchon A, et al., Rev. of Mod. Phys., Vol 91(3), 035004 (2019). [6] Liu L, Pai C-F, Li Y, et al. Science., Vol 336, p. 555-558 (2012). [7] Wang, M., Cai, W., Zhu, D. et al. Nat Electron., Vol 1, p.582–588 (2018).

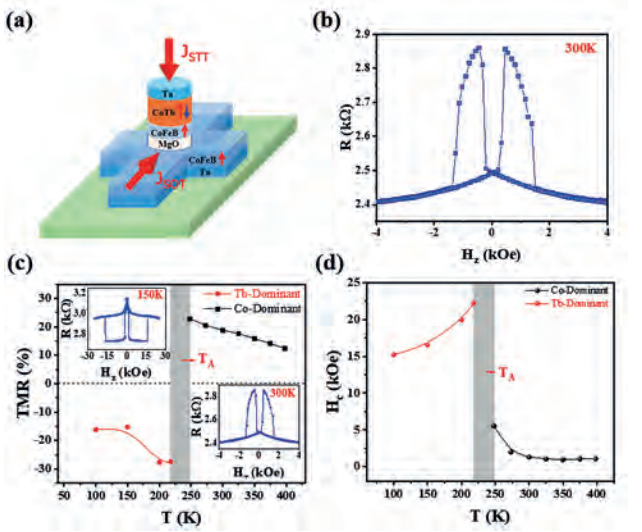

(a) The structure of MTJ and the method of applying current. (b) TMR of MTJ at 300K. (c) Properties of the TMR of MTJ around the compensation point. (d) The MTJ has stable coercivity in the Co-dominant temperature range.

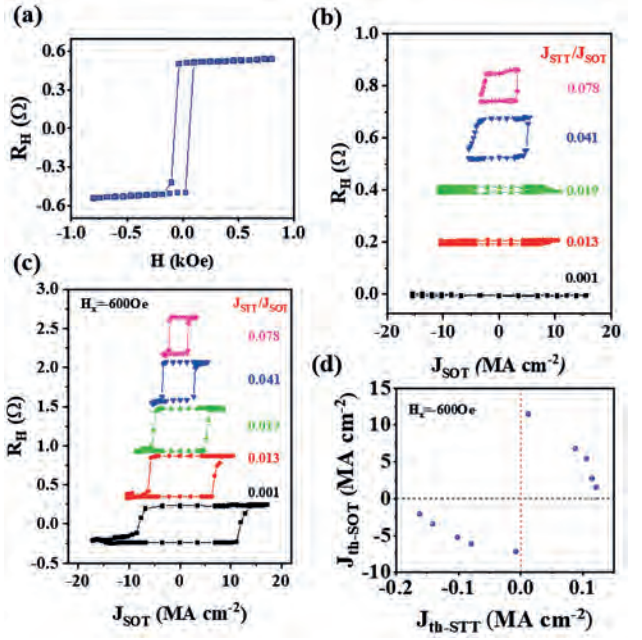

(a) AHE of MTJ. (b) Field free switching of MTJ driven by SST (c) Magnetization switching of MTJ driven by SST under an external magnetic field. (d) The relationship between STT and SOT on critical switching current density under external magnetic field.

BS-06. Tuning effective spin hall angle of Pt/Co/Pt based perpendicularly magnetized system. *S. Maji*[1], K.P. Chauhan[1], I. Bhat[1], A. Mukhopadhyay[1], S. Kayal[1] and P. Kumar[1] *1. Physics, Indian Institute of Science, Bangalore, India*

Thin films with perpendicular magnetic anisotropy (PMA) attained huge attraction among the spintronics researchers due to their application on high density data storage devices [1,2]. The HM converts the longitudinal charge current (J_x) into a transverse spin (J_s) current due to the spin hall effect. The spin current gives spin-orbit torque (SOT) to the FM magnetization. The strength of SOT largely depends on effective the spin hall angle (θ_{sh}) of the HM. Therefore, tuning effective spin hall angle is very important to achieve current induced magnetization reversal (CIMR) at very low current density. Several HMs has been studied to quantify the θ_{sh} [3-5]. In this work, we prepared Ta/Pt/Co/Pt and Ta/Pt/Co/Au PMA multilayers and introduced Au layer at both sides of Co layer to prepare Ta/Pt/Co/Au/Pt, Ta/Pt/Au/Co/Pt and Ta/Pt/Au/Pt/Au multilayers (Fig. 1) and studied critical current density (J_c) required for magnetization reversal. The detailed measurement scheme can be found here [6]. The J_c with respect to in plane magnetic field (H_x) has been displayed in Fig. 2. The J_c decreases with increase in H_x for all the samples. The bottom and top Pt layers in S1 generate competing spin polarized current that minimizes SOT strength acting on magnetization of Co and as a result $J_c = 3.13 \times 10^{11}$ A/m^2 obtained for switching is maximum at $H_x = 100$ mT among all samples. Introduction of Au layer between top Co/Pt interface (sample S2) the J_c drops only 5% at same H_x. In sample S3, the Au layer is introduced between bottom Pt/Co interface the current density drops significantly (~50 %). In sample S4, Au layer generates negligible spin current and the bottom Pt layer acts as primary source of spin polarized current. In S4, the obtained J_c was not reduced significantly in. comparison with S1. The introduction of Au layer at bottom Pt/Co interface in S5 leads to reduction of J_c ~49% with respect to S1. The lowering of J_c can be due to the reduction of spin memory loss or spin back flow at the Pt/Co interfaces of S3 and S5. Introduction of a thin layer of Au between bottom Pt/Co can significantly increase the the SOT strength and lower the J_c.

1. Parkin *et. al.*, Science, 320, 190–194 (2008) 2. Fert *et. al.*, Nature nanotechnology 8, 152–156170 (2013) 3. Mohanan *et. al.*, Physical Review B 96, 104412 (2017) 4. Obstbaum *et. al.*, Phys. Rev. Lett. 117, 167204 (2016) 5. Liu *et. al.*, Science 336, 555 (2012) 6. Kayal *et. al.*, Journal of Magnetism and Magnetic Materials 558, 169499 (2022)

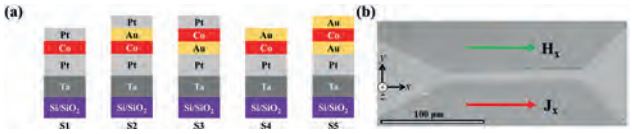

(a) The multilayers. (b) The fabricated device

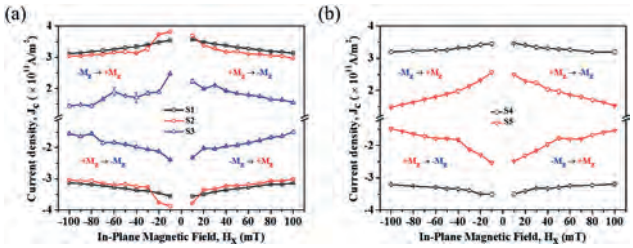

J_c as a function of H_x

Session XA
EVENING SESSION 1: REALISM IN MICROMAGNETICS

Michael Joseph Donahue, Chair
National Institute of Standards and Technology, Gaithersburg, MD, United States

INVITED PAPERS

XA-01. From 1D to 3D Computational Micromagnetics for Realistic Simulations of Magnetic Nanomaterials and Nanodevices. *A. Manzin*[1], R. Ferrero[1] and M. Vicentini[1] *1. Istituto Nazionale di Ricerca Metrologica (INRIM), Torino, Italy*

Computational micromagnetic modelling is a powerful tool to address the design of nanostructured magnetic materials and devices for applications in health, energy, automotive, ICT and metrology sectors, as well as to guide the interpretation of novel magnetic phenomena at the nanoscale [1]. However, the numerical implementation of efficient micromagnetic solvers is a very complex task, especially for the simulation of several-micron-sized magnetic nanostructures or large-scale arrays of nanomagnets. The main reason of such complexity is the multiscale nature of the problems to be investigated, which involve both long-range magnetostatic interaction and rapidly decaying exchange interaction. Several strategies have been implemented to speed-up micromagnetic simulations, such as fast-multipole and FFT-based techniques for the magnetostatic field computation. At the same time, efforts have been made towards multiscale modelling, coupling atomistic models to micromagnetic calculations [2]. In the last decade, many parallel micromagnetic solvers have also been developed, able to run on massively parallel architectures based on graphical processing units (GPUs) [3, 4]. To perform reliable and efficient micromagnetic simulations, we have combined GPU-accelerated computing with non-standard numerical techniques (e.g. multipole expansion approaches for magnetostatic field calculation, finite-difference methods for exchange field estimation on irregular grids, domain symmetry exploitation, geometric integration based on Cayley transform) as well as machine learning tools. This talk will present the implemented strategies, including hybrid 1D-3D, 2D-3D or totally 3D modelling approaches [5, 6], and their application in nanomagnetism, from nanostructured magnetic materials (magnetic nanoparticle clusters, nanopatterned thin films, spin-ice systems) to magnetoresistive and spintronic devices. Acknowledgements: This work is funded by the Italian Ministry of University and Research under Project PRIN 2020LWPKH7 IT.

[1] A. Fernández-Pacheco et al., *Nature Communications* 8 (2017), 15756. [2] S. C. Westmoreland et al., *Scripta Materialia* 148 (2018), 56-62. [3] S. Fu, W. Cui, M. Hu, R. Chang, M. J. Donahue, V. Lomakin, *IEEE Trans. Magn.* 52 (2016), 7100109. [4] J. Leliaert, J. Mulkers, *J. Appl. Phys.* 125 (2019), 180901. [5] A. Manzin, R. Ferrero, *J. Magn. Magn. Mater.* 492 (2019), 165649. [6] R. Ferrero, A. Manzin, *J. Magn. Magn. Mater.* 518 (2021), 167409.

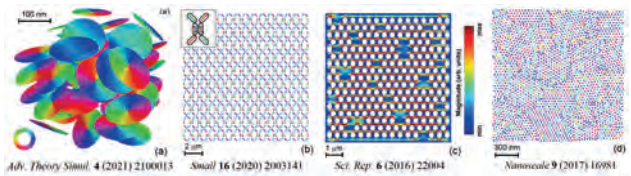

Figure 1: An excursus of applications of the micromagnetic modelling tools developed at INRIM: (a) magnetic nanodisks for hyperthermia; (b) artificial spin-ice; (c) ferromagnetic resonance in magnonic crystals; (d) high-density magnetic nanodots.

XA-02. Pushing the Boundaries of Micromagnetic Modeling: Multiphysics Integration and High-Performance Computation. *V. Lomakin*[1] *1. Center for Memory and Recording Research and Department of Electrical and Computer Engineering, University of California, San Diego, San Diego, CA, United States*

Magnetic materials and devices are integral to numerous applications in physics and engineering, making it essential to develop advanced numerical tools for understanding and designing complex systems. Micromagnetic modeling requires the integration of various elements, such as physics formulations, mathematical foundations, and high-performance numerical methods and their implementations. This talk delves into the latest developments addressing these components in realistic micromagnetic modeling. On the formulation level, we demonstrate the importance of integrating multiphysics formulations in micromagnetics to accurately represent complex physics behavior. We showcase the coupling of the Landau-Lifshitz-Gilbert (LLG) equation, which governs magnetization dynamics, with Maxwell's equations describing eddy current dynamics. By examining linear and non-linear coupled magnetization-eddy current dynamics, we highlight some of the significant differences that emerge compared to considering separate physics types, including current diffusion, skin depth, and modified damping effects. Further examples include magnon-phonon coupling, spin diffusion effects, and temperature influences. From a solver perspective, in addition to the general non-linear time domain LLG formulation, we introduce a linearized LLG formulation for time and frequency domains and a non-linear formulation for time-harmonic excitations. On the space and time discretization levels, we discuss finite element method based formulations with implicit adaptive time stepping, featuring high-performance algorithms and codes for calculating effective magnetic fields and time integration on parallel computing architectures. Finally, we showcase the application of computational micromagnetic tools in realistic modeling of various complex magnetic materials and devices, such as magnetic memories with granularity and roughness, magnetic write heads, polycrystalline layers, large patterned films, extensive arrays of spin torque and spin Hall oscillators, and magnonic structures. Our findings demonstrate the ability to handle highly intricate configurations with non-uniform meshes containing tens to a hundred million elements, ultimately pushing the boundaries of realistic micromagnetic modeling through multiphysics integration and high-performance computation.

Session CA
RECENT ADVANCES IN CAVITY MAGNONICS

Andrew David Kent, Chair
New York University, New York, NY, United States

INVITED PAPERS

CA-01. Coherent Microwave Emission Using Cavity Magnonics. *C. Hu*[1] *1. Department of Physics and Astronomy, University of Manitoba, Winnipeg, MB, Canada*

Cavity Magnonics is an emerging field studying the light-matter interactions involving cavity photons and magnons [1]. Via the quantum physics of spin-photon entanglement on the one hand, and classical electrodynamic coupling on the other, magnon-photon coupling connects some of the most exciting modern physics, such as quantum information and quantum optics, with one of the oldest science on the earth, the magnetism [2]. This talk reports our latest progress in this frontier. By developing a gain-embedded cavity magnonics platform [3], we create a gain-driven polariton (GDP) that is activated by an amplified electromagnetic field. Utilizing the gain-sustained photon coherence of the GDP, we demonstrate polariton-based coherent microwave amplification (~ 40 dB) and achieve high-quality coherent microwave emission ($Q > 10^9$), which exceed the performance of spin-torque oscillators and many state-of-the-art masers.

[1] Michael Harder, et al., "Coherent and Dissipative Cavity Magnonics", J. Appl. Phys. 129, 201101 (2021) (invited tutorial). [2] Babak Zare Rameshti, et al., "Cavity Magnonics", Physics Reports, 979, 1-61 (2022). [3] Bimu Yao, Y.S. Gui, J.W. Rao, Y.H. Zhang, Wei Lu, and C.-M. Hu, "Coherent Microwave Emission of a Gain-Driven Polariton", Phys. Rev. Lett., 130, 146702 (2023) (Editor's Suggestion).

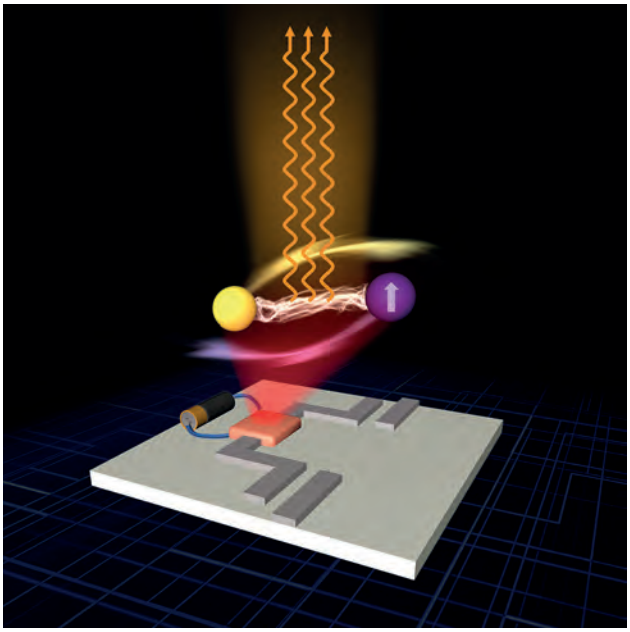

Schematic diagram of creating a gain-driven polariton: A voltage (battery) is applied to a microwave amplifier (peach-colored block). It drives the photon (yellow) in the microwave cavity (grey strip) to strongly interact with a magnon (violet) and form a gain-driven polariton, which in turn emits coherent microwaves.

CA-02. Strong photon-magnon coupling using a lithographically defined organic ferrimagnet. *G.D. Fuchs*[1] *1. Cornell University, Ithaca, NY, United States*

Hybrid quantum coupling between superconducting circuits elements and magnon modes has emerged as an interesting avenue to develop nonreciprocal quantum devices, leverage magnons as a quantum bus, and study non-Hermitian quantum dynamics. One of the challenging aspects of this research area is that in most cases, magnon loss rates far exceed the loss rates of high-quality microwave resonators and other quantum circuit elements. I'll discuss recent experiments in which we demonstrate a hybrid system composed of superconducting resonator photons and magnons hosted by the organic ferrimagnet vanadium tetracyanoethylene ($V[TCNE]_x$). Our work is motivated by the challenge of scalably integrating an arbitrarily-shaped, low-damping magnetic system with planar superconducting circuits, thus enabling a new class of quantum magnonic circuit designs. We take advantage of the properties of $V[TCNE]_x$, which has ultra-low intrinsic damping, can be grown at low processing temperatures on arbitrary substrates, and can be patterned via electron beam lithography. We demonstrate the scalable, lithographically integrated fabrication of hybrid quantum magnonic devices consisting of a thin-film superconducting resonator coupled to a low-damping, thin-film $V[TCNE]_x$ microstructure [1]. Our devices operate in the strong coupling regime, with a cooperativity as high as 1181 at T~0.4 K, suitable for scalable quantum circuit integration. This work paves the way for the exploration of high-cooperativity hybrid magnonic quantum devices in which magnonic circuits can be designed and fabricated as easily as electrical wires. This work is supported by the DOE office of Basic Energy sciences through the Center for Molecular Quantum Transduction (DE-SC0021314) and the QIS program (DE-SC0019250).

[1] Q. Xu, H. F. H. Cheung, D. S. Cormode, T. O. Puel, H. Yusuf, M. Chilcote, M. E. Flatté, E. Johnston-Halperin, and G. D. Fuchs, "Strong photon-magnon coupling using a lithographically defined organic ferrimagnet," arXiv:2212.04423 (2022).

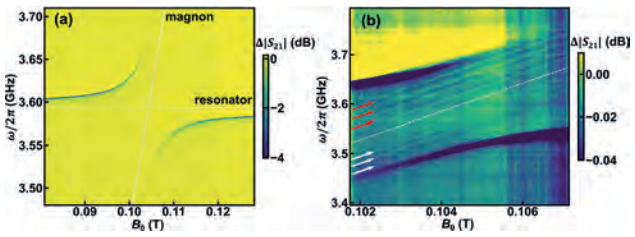

CA-03. Exciton-coupled coherent magnons in a 2D magnetic semiconductor. *Y. Bae*[1] *1. Columbia University, New York, NY, United States*

Two-dimensional (2D) magnetic semiconductors possess tightly bound excitons with large oscillator strength and long-lived coherent magnons due to the presence of bandgap and spatial confinement [1]. While magnons and excitons are energetically mismatched by orders of magnitude, their

coupling can lead to efficient optical access to spin information. The ability to overcome energy mismatch between magnon and exciton combined with optical excitation and detection renders 2D magnetic semiconductors attractive candidates for quantum transducers. In this presentation, I will discuss strong magneto-electronic and magnetoelastic coupling and the implications of these couplings in the 2D van der Waals antiferromagnetic semiconductor, CrSBr. Because of both magnetic and semiconducting properties in CrSBr, excitons are highly sensitive to spin environments. Optical excitation of coherent spin waves can dynamically modulate the dielectric environment and excitons can sensitively detect these changes. During the process of optical excitation, the strong magnetoelastic coupling in CrSBr creates transient strain fields that selectively launch a narrow range of wavevector and frequency in both coherent magnons and acoustic phonons.

[1] Bae, Y. J., Wang, J., Scheie, A. Diederich, G., Cenker, J., Ziebel, M.E., Bai, Y., Ren, H., Delor, M., Xu, X., Kent, A., Roy, X., Zhu, X.Y., Nature 609, 282–286 (2022)

CA-04. Direct probing of strong magnon-photon coupling in a planar geometry. M. Kaffash[1], A. Rai[1], D. Wagle[1], T. Meyer[2], J. Xiao[1] and *B. Jungfleisch[1] 1. University of Delaware, Newark, DE, United States; 2. THATec Innovation GmbH, Ludwigshafen, Germany*

Unleashing the full potential of quantum technologies requires the development of quantum computation, memories, interconnects, detectors, and transducers. Understanding the coupling between disparate quantum systems is particularly important. The emergent properties of such hybrid systems promise to advance a wide range of quantum information applications. Due to their highly tunable dispersion and the possibility to couple with different excitations, including optical photons, phonons, and spins, magnons are ideal candidates for coherent information processing and transduction. Here, we demonstrate direct probing of strong magnon-photon coupling using Brillouin light scattering spectroscopy in a planar geometry [1]. The magnonic hybrid system comprises a split-ring resonator loaded with epitaxial yttrium iron garnet thin films of 200 nm and 2.46 μm thickness. The Brillouin light scattering measurements are combined with microwave spectroscopy measurements where both biasing magnetic field and microwave excitation frequency are varied. Clear avoided level crossings are observed, evidencing the hybridization of the magnon and microwave photon modes in the strong coupling regime, Fig. 1. We also identify contributions of higher-order magneto-static surface spin waves. The detection of magnonic hybrid excitations by Brillouin light scattering demonstrates a coherent conversion of microwave to optical photons, which could be harnessed for an up-conversion of quantum signals from the optical to the microwave regime in hybrid quantum systems. Furthermore, we show the influence of damping and field-like torques on the magnon–photon coupling process by classically integrating the generalized Landau–Lifshitz–Gilbert equation with RLC equation in which a phase correlation between dynamic magnetization and microwave current through combined Ampère and Faraday effects are considered [2]. The magnitude of the level repulsion can be controlled in samples with damping parameters in the order of 10^{-3} by changing the direction of the dc current density if a certain threshold is reached. This analysis also reveals a regime where a level attraction in the real part of the hybridized modes can be observed. Our results suggest that an on-demand manipulation of the magnon-photon coupling strength can be achieved in yttrium iron garnet/Pt hybrid structures. Research supported by the U.S. Department of Energy, Office of Basic Energy Sciences, Division of Materials Sciences and Engineering under Award DE-SC0020308. The authors acknowledge the use of facilities and instrumentation supported by NSF through the University of Delaware Materials Research Science and Engineering Center, DMR-2011824.

[1] M. T. Kaffash, D. Wagle, A. Rai, T. Meyer, J. Q. Xiao, and M. B. Jungfleisch, Direct probing of strong magnon–photon coupling in a planar geometry, Quantum Sci. Technol. 8, 01LT02 (2023). [2] A. Rai and M. B. Jungfleisch, Control of magnon–photon coupling by spin torque, J. Magn. Magn. Mater 571, 170558 (2023).

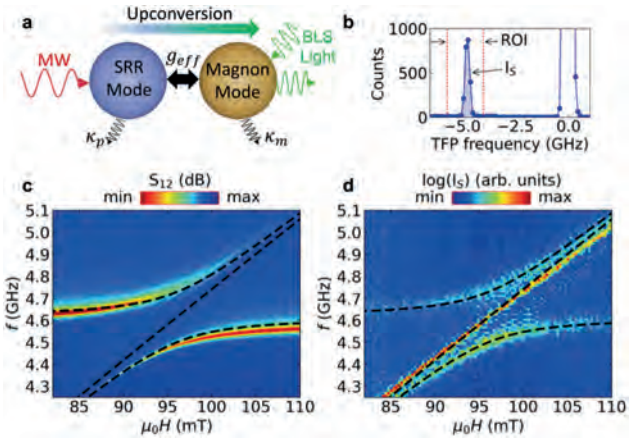

Figure 1: (a) Schematic illustration of the coupling process between the microwave photon (MW) mode of the split-ring resonator (SRR) with the magnon mode of the YIG film. (b) A typical BLS spectrum with the reference peak at 0 GHz and the Stokes signal at around -5 GHz. (c,d) False color-coded spectra of the magnon-photon hybridization of the 2.46 μm-thick YIG film. Results were obtained by (c) microwave absorption measurements, where S12 is plotted versus f and μ_0H, (d) microfocused BLS spectroscopy. The black dashed lines are fits to a coupled two-harmonic oscillator model. Adapted from Ref. [1].

CA-05. Time-domain Coherent Magnon Interference with On-chip Superconducting Hybrid Magnonic Circuits. M. Song[1,2], T. Polakovic[3], T.W. Cecil[4], J. Pearson[1], R. Divan[5], W. Kwok[1], U. Welp[1], A. Hoffmann[6], K. Kim[2], V. Novosad[1] and *Y. Li[1] 1. Materials Science Division, Argonne National Laboratory, Lemont, IL, United States; 2. Department of Physics, Korea Advanced Institute of Science and Technology, Daejeon, The Republic of Korea; 3. Physics Division, Argonne National Laboratory, Lemont, IL, United States; 4. High Energy Physics Division, Argonne National Laboratory, Lemont, IL, United States; 5. Center for Nanoscale Materials, Argonne National Laboratory, Lemont, IL, United States; 6. Department of Materials Science and Engineering, University of Illinois Urbana-Champaign, Urbana, IL, United States*

Cavity magnonics is an emerging research field which cultivates strong coupling of magnetic excitations, or magnons, with microwave photons for exploring their coherent interactions [1-2]. This field is a sub-branch of hybrid dynamic systems with primary applications in quantum information science, with the main goal of coherent manipulation of entanglements within decoherence time. Up to now, there are many cavity systems and magnetic systems that have been investigated for building hybrid magnonic systems. However, in order to manipulate magnon states in time domain, critical high performance and on-demand control of magnon-photon interaction is needed. Superconducting microwave resonators provide a new paradigm for building high-performance hybrid magnonic systems [3] because 1) they provide high quality factor and thus long photon coherence time; 2) they allow for flexible coplanar design and engineering of magnon-photon interactions with lithographic fabrications; 3) they are compatible for embedding superconducting quantum components such as qubits in the hybrid magnonic system. Here, we develop a superconducting circuit platform, incorporating chip-mounted single-crystal YIG spheres that are mounted in lithographically defined holes on silicon substrates with superconducting resonators, for implementing microwave-mediated distant magnon-magnon interactions [4]. For a single 250-μm-diameter YIG sphere, we achieve a magnon-photon coupling strength of 130 MHz with both the magnon and photon coherence time approaching 1 μs at 1.6 K, corresponding to a cooperativity of 13000. In a two-sphere-one-resonator circuit, we achieve a resonator mediated magnon-magnon coupling strength of 14 MHz in the dispersive coupling regime where the magnon-photon frequency detuning is ten times larger than their coupling strength. In addition, we use the two-YIG-sphere-one-superconducting-resonator system to demonstrate

time-domain coherent magnon interference. Using two vertical microwave antennas that are placed adjacent to each YIG sphere, we can independently control and read out the magnon excitation state of the two spheres. By sending a microwave pulse to one sphere and measuring the time trace of microwave output from the other antenna, we can measure the Rabi-like oscillation of magnon excitations between the two remote YIG spheres that are strongly coupled from their dispersive coupling to the superconducting resonator bus. In addition, we show that by sending two microwave pulses with a certainly time delay, their interactions to the YIG sphere lead to coherent interference, i.e. constructive or destructive interference depending on the relative phase delay of the two pulses. This allow us to program the magnon-magnon hybrid states by changing the frequency of the pulse microwave and the time delay. Our results provide a high-performance, circuit integrated cavity magnonic system for building coherent magnon networks and processing hybrid magnon excitations in the time domain. We anticipate the hybrid YIG-sphere-superconducting-resonator architecture to be applied in more realistic quantum magnonics study, particularly for microwave-to-optic coherent transduction and nonreciprocal microwave information processing. Work at Argonne and UIUC was supported by the U.S. DOE, Office of Science, Basic Energy Sciences, Materials Sciences and Engineering Division under contract No. DE-SC0022060. Use of the Center for Nanoscale Materials (CNM), an Office of Science user facility, was supported by the U.S. Department of Energy, Office of Science, Office of Basic Energy Sciences, under Contract no. DE-AC02-06CH11357.

[1] Y. Li, *et al.*, Hybrid magnonics: Physics, circuits, and applications for coherent information processing, *J. Appl. Phys.*, 128, 130902 (2020) [2] B. Z. Rameshti *et al.*, Cavity Magnonics, *Phys. Rep.,* 979, 1-61 (2022) [3] Y. Li, *et al.*, Strong coupling between magnons and microwave photons in on-chip ferromagnet-superconductor thin-film devices, Phys. Rev. Lett. 123, 107701 (2019) [4] Y. Li *et al.*, Coherent coupling of two remote magnonic resonators mediated by superconducting circuits, *Phys. Rev. Lett.* 128, 047701 (2022)

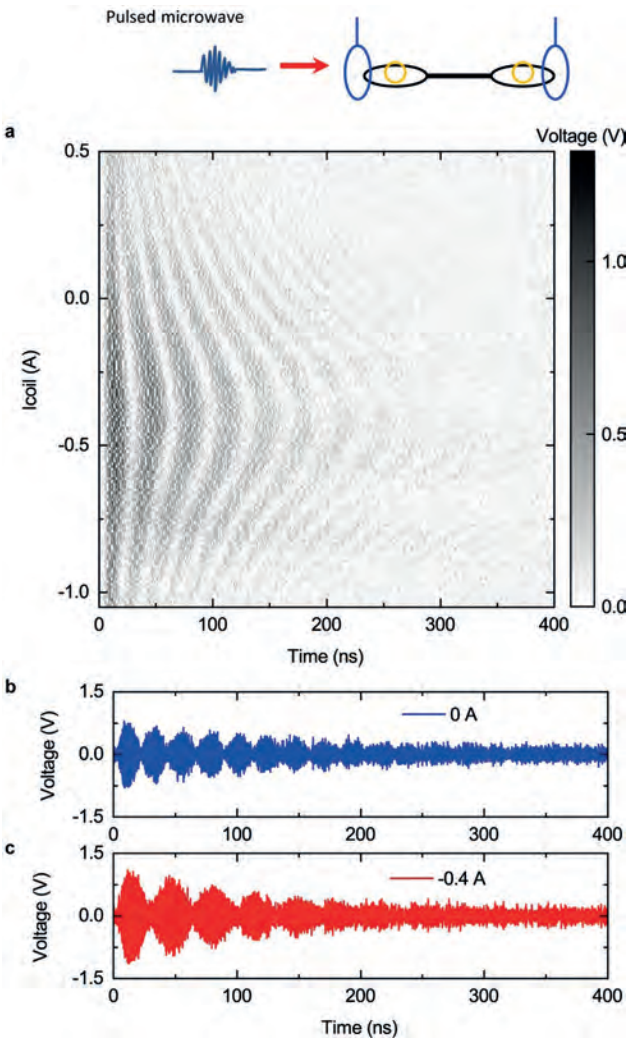

(a) Rabi-like oscillation of magnon excitations between two remotely coupled YIG spheres on a superconducting resonator. (b) Time trace of magnon excitations from one YIG sphere measured by a fast oscilloscope.

Session CB
SKYRMIONS

Jiadong Zang, Chair
University of New Hampshire, Durham, NH, United States

INVITED PAPER

CB-01. Voltage-controlled Skyrmion Brownian Devices with Zero-Or Ultralow-Energy Consumption. *R. Ishikawa*[1], S. Miki[2], M. Goto[2], H. Nomura[2], E. Tamura[2] and Y. Suzuki[2] *1. ULVAC-Osaka University Joint Research Laboratory for Future Technology, ULVAC, Suita, Japan; 2. Graduate School of Engineering Science, Osaka University, Toyonaka, Japan*

Skyrmions are topologically protected spin-wave solitons that behave as particles[1,2]. Examples of the use of skyrmions as information carriers include racetrack memory[3] and skyrmion logic[4]. In these devices, information is processed by transporting skyrmions mainly by electric current. However, current-based methods are not suitable for ultimate energy conservation due to the dissipation of Joule heat. In contrast to these previous studies, this study attempts to realize ultralow-power devices that use voltage to control skyrmions and Brownian motion to drive them. Such a computer is called a Brownian computer[5] and is a type of information heat engine that functions by a mechanism similar to those of biological systems. In this talk, I will report on the progress of our work to realize the token-based Brownian computer[6] proposed by Peper. In this study, we used skyrmions in Ta/Co-Fe-B/Ta/MgO/SiO_2 films deposited by magnetron sputtering. Skyrmions approximately 1 μm in size were used in this study to enable optical observation. First, a method using an amorphous Co-Fe-B layer[7] and annealing in air[8] was developed to form skyrmions that exhibit a large diffusion coefficient (60 μm^2/sec) approximately 500 times greater than that inour initial films[9,10]. Next, we have developed a method for forming a confinement potential using a SiO_2 cap[7] and irradiation of a focused ion beam[10]. These methods succeeded in freely controlling the potential energy landscape felt by the skyrmions while maintaining a large diffusion coefficient. Using these techniques, we fabricated a device that mimics a cellular automaton[11]. As shown in Fig. 1, when several skyrmions are confined in a five-square cell, a repulsive force acts between the skyrmions, causing them to avoid each other and move in a Brownian motion. As a result, this device can be viewed as an Ising annealing machine, and arrangements of skyrmions with high probabilities of appearance provide solutions to the minimization problem coded into the Hamiltonian of this system (specifically, AND and OR calculations are performed). At this point, a flow of information (transfer entropy) occurs between skyrmions. An analysis of the information flow with the positions of the skyrmions converted to binary values revealed that this few-skyrmion system is a non-Markovian system. In other words, this system can be viewed as a hidden Markov system and is expected to have memory and computational capabilities. A detailed analysis revealed that such a simple skyrmion system partially performs the XOR operation between past and current bit states. This is an example of zero-energy natural computation in physical systems. To combine these zero-energy devices to form an ultralow-energy device, we studied the voltage control of the motion and interaction of skyrmions. Control of the diffusion of skyrmions by voltage[9] and their generation and annihilation[12,13] has been reported. Here, we show the results of gating Brownian motion using voltage (Fig. 2). A narrow (200 nm) gate electrode was fabricated on top of a skyrmion channel. When no voltage is applied, the skyrmions pass freely under the gate; however, when a voltage of approximately 2 volts is applied, the skyrmions cannot approach the electrode. This led to the successful experiment of Maxwell's demon, which rectified thermal motion. This is a demonstration example of an information heat engine with ultralow power consumption. The Brownian computer, which is composed of zero-energy natural computing and the information heat engine described above, is expected to be an intelligent computer with ultralow energy consumption. This work was supported by JSPS KAKENHI Grant Number JP20H05666, 23KJ1477, Japan and JST CREST Grant Number JPMJCR20C1.

[1] T. H. R. Skyrme, Nucl. Phys. 31, 556 (1962). [2] U. K. Rößler, A. N. Bogdanov, and C. Pfleiderer, Nature 442, 797 (2006). [3] A. Fert, V. Cros, and J. Sampaio, Nat. Nanotechnol. 8(3), 152 (2013). [4] X. Zhang, M. Ezawa, and Y. Zhou, Sci. Rep. 5, 9400 (2015). [5] C. H. Bennett, Int. J. Theo. Phys, 21, 12 (1982). [6] J. Lee, F. Peper, S. D. Cotofona *et al*., Int. J. Unconv. Comput. 12, 341 (2016). [7] Y. Jibiki, M. Goto, E. Tamura, ..., R.I., *et al*., Appl. Phys. Lett. 117, 082402 (2020). [8] M. Goto, R.I., H. Nomura, *et al*., AIP Advances 13, 025216 (2023). [9] T. Nozaki, Y. Jibiki, M. Goto, *et al*., Appl. Phys. Lett. 114, 012402 (2019). [10] S. Miki, K. Hashimoto, J. cho, ..., R.I., *et al.,* Appl. Phys. Lett. 122. 202401 (2023). [11] R.I., M. Goto, H.Nomura, *et al*., Appl. Phys. Lett. 119, 072402 (2021). [12] M. Schott, A. Bernand-Mantel, O. L. Ranno, *et al*., Nano Lett. 17, 3006 (2017). [13] R.I., M.Goto, H. Nomura, *et al*., Appl. Phys. Lett. 121, 252402 (2022)

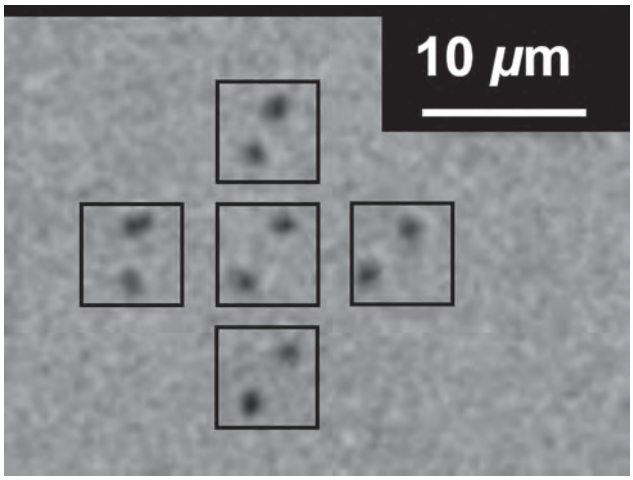

Fig.1 A device that mimics a cellular automaton using skyrmions

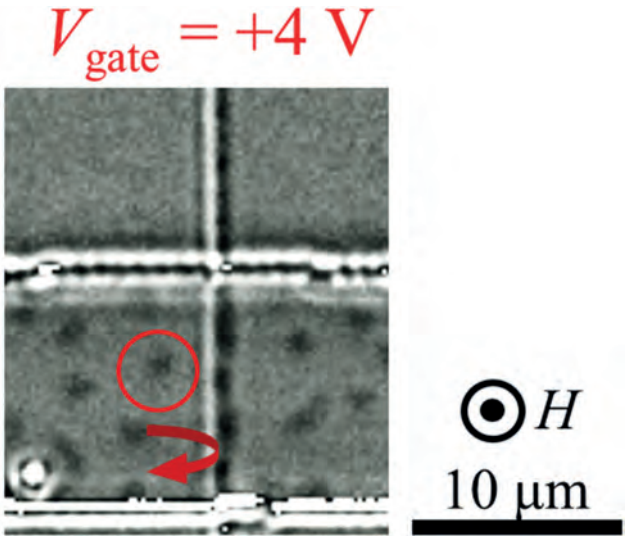

Fig.2 A gating device of skyrmion in Brownian motion by voltage

CONTRIBUTED PAPERS

CB-02. The evolution of magnetic phases leading to Skyrmions in a Fe/Gd multilayer system probed through simultaneous transport and scattering experiments. *A. Us Saleheen*[3], A. Singh[1], D.W. Raftrey[2], M. McCarter[3], R. Tumbleson[2], S. Montoya[4], S. Kevan[3], S.A. Morley[3] and S. Roy[3] *1. Materials Science Division, Lawrence Berkeley National Laboratory, Berkeley, CA, United States; 2. University of California Santa Cruz, Santa Cruz, CA, United States; 3. Advanced Light Source, Lawrence Berkeley National Laboratory, Berkeley, CA, United States; 4. University of California San Diego, San Diego, CA, United States*

Skyrmions in magnetic materials are topologically non-trivial magnetic textures [1]. The realization of skyrmions in thin-film multilayer systems over a broad range of temperature and magnetic field has opened up the possibility for next-generation logic and memory devices [2,3]. We report the evolution of magnetic phases leading to skyrmions in a Fe/Gd multilayer thin-film through simultaneous resonant soft X-ray scattering (RSXS) and Hall effect measurements. Upon application of a field sequence, ordered stripe domains emerged from the labyrinthine domains (Fig. 1b). The stripe domains transform into a skyrmion lattice phase---as evident from the six-fold scattering pattern---by applying magnetic field perpendicular to the sample's plane (Fig. 1d). The onset of the six-fold pattern coincides with a pronounced dip in the Hall resistance vs. magnetic field [R_{xy}(H)] data. The scattering pattern disappears at around H = 256 mT, whereas the R_{xy}(H) curve saturates at around 289 mT at T = 270 K. An additional feature is present in the R_{xy}(H) curve just before saturation. A comparison between the magnetic field dependence of magnetization [M(H)] and R_{xy}(H) reveals that the additional feature is absent in the M(H) data (Fig. 2). This indicates that the feature may represent a topological contribution to the Hall effect, also known as the topological Hall effect (THE). Previous investigations into this system revealed that the skyrmion lattice breaks into disordered isolated skyrmions before transitioning to a fully field polarized state [3, 4]. Our results indicate that the disordered isolated skyrmions give rise to larger THE. No six-fold pattern can be observed when the field is swept in the negative direction after saturation in the positive direction (Fig. 1i-r). However, the R_{xy}(H) curves measured in both field directions are identical. Based on these results, we shed light into the effects of ordered and disordered skyrmion lattice on the transport properties of this system.

[1] Nagaosa, N., Tokura, Y., Nature Nanotech 8, 899–911 (2013) [2] Finocchio, G. et al., J. Phys. D: Appl. Phys. 49, 423001 (2016) [3] Fert, A., Reyren, N. & Cros, V. Nat Rev Mater 2, 17031 (2017) [3] Desautels, R. et al., Phys. Rev. Materials 3, 104406 (2016) [4] Montoya, S. et al., Phys. Rev. B 95, 024415 (2017)

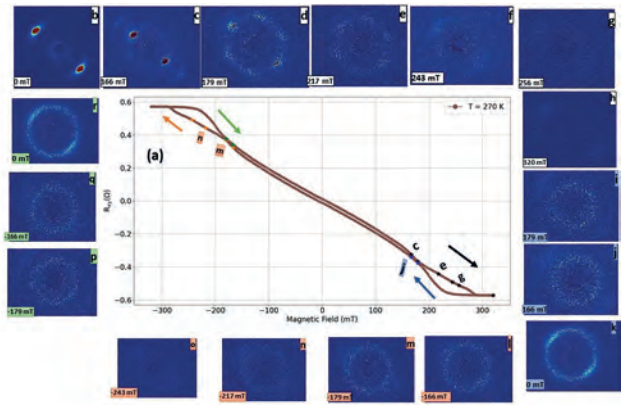

Fig. 1. (a) Hall resistance vs. magnetic field [R_{xy}(H)] at T = 270K. (b-r) RSXS scattering patterns at selected magnetic fields.

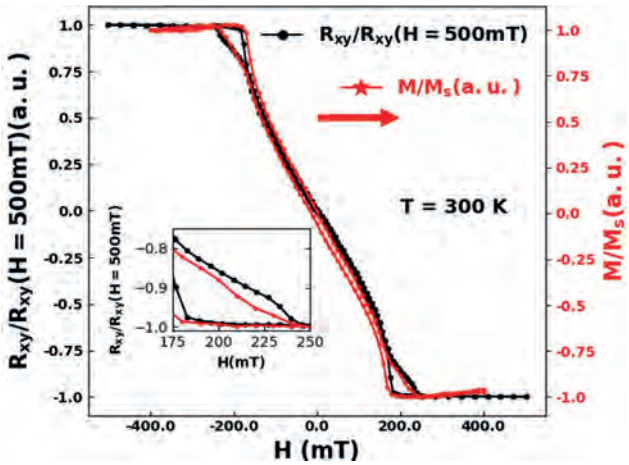

Fig. 2. Normalized Hall resistance and magnetization vs. magnetic field. (Inset) A zoomed view of the data.

CB-03. Central Role of Structural Disorder on the Chiral Helimagnetic Order in $Cr_{1/3}NbS_2$. *X. Li*[1,2], B. Ding[1], X. Xi[1], W. Wang[3] and Y. Lau[1,2] *1. Institute of Physics, Chinese Academy of Sciences, Beijing, China; 2. University of Chinese Academy of Sciences, Beijing, China; 3. Tiangong University, Tianjin, China*

Chiral soliton lattice (CSL) is a one-dimensional topological spin texture that is potentially useful for spintronic applications in magnetic memory and logic. $Cr_{1/3}NbS_2$ is a typical CSL system with a theoretical helical period of ~48 nm.[1,2] However, previous reports found large dispersion of the magnetic properties for $Cr_{1/3}NbS_2$.[2-4] In some cases, $Cr_{1/3}NbS_2$ can even be ferromagnetic.[5] Here, we reveal the central role of Cr atom occupancy and structural disorder which directly modulate the Dzyaloshinskii–Moriya (DM) interaction and subsequently control the chiral helimagnetic order in $Cr_{1/3}NbS_2$. Figure 1(a) shows a typical scanning transmission electron microscope (STEM) image of (100)-oriented $Cr_{1/3}NbS_2$ lamella. The atomic arrangement of Cr is clearly different from the ideal crystal structure with space group $P6_322$. To account for the STEM observation, we find that Cr atoms should occupy three non-equivalent crystallographic positions, as shown in an illustration in Fig. 1(b). Under-focused Lorentz-TEM image with no applied field in Fig. 1(c) reveals a longer-than-expected helimagnetic period of ~86.3 nm for $Cr_{1/3}NbS_2$ at 93 K, suggesting that the disorder of the Cr sublattice can modulate the helimagnetic period. We identify regions that host CSL with

opposite chirality from the bright and dark stripes that appear with an applied field of 0.09 T in Fig. 1(d). These observations indicate that the occupancy of Cr atoms is not completely random to ensure a given chirality of the crystal structure over a length scale of several helical periods. This work establishes a link between the arrangement of the Cr atoms and the chiral helimagnetic order in $Cr_{1/3}NbS_2$.

1. T. Miyadai, K. Kikuchi, H. Kondo, et al., J. Phys. Soc. Jpn. 52 (4), 1394-1401 (1983). 2. Y. Togawa, T. Koyama, K. Takayanagi, et al., Phys. Rev. Lett. 108 (10), 107202 (2012). 3. V. Dyadkin, F. Mushenok, A. Bosak, et al., Phys. Rev. B 91 (18), 184205 (2015). 4. X. Li, Z. Li, H. Li, et al., Appl. Phys. Lett. 120 (11), 112408 (2022). 5. Y. Kousaka, T. Ogura, J. Jiang, et al., APL Materials 10 (9), 090704 (2022).

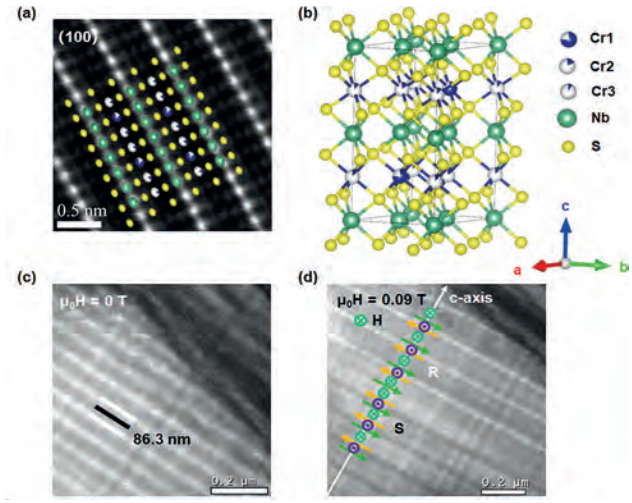

Fig. 1. (a) Atomic configuration along (100) direction for $Cr_{1/3}NbS_2$ detected by high-angle annular dark-field (HAADF) imaging. (b) Simulated crystal structure based on the HAADF image in (a). (c) Underfocused Lorentz-TEM micrographs for $Cr_{1/3}NbS_2$ with 0 T (c) and 0.09 T (d) applied field at 93 K. S means CSL with left-handed, and R is right-handed.

CB-04. Ordered creation and motion of skyrmions with surface acoustic wave. *C. Song*[1], R. Chen[1] and F. Pan[1] *1. Tsinghua University, Beijing, China*

Magnetic skyrmions with a well-defined spin texture have shown unprecedented potential for various spintronic applications owning to their topologically non-trivial and quasiparticle properties [1]. To put skyrmions into practical technology, efficient manipulation, especially the inhibition of skyrmion Hall effect (SkHE) has been intensively pursued. In spite of the recent progress made on reducing SkHE in several substituted systems, such as ferrimagnets and synthetic antiferromagnets [2-5], the organized creation and current driven motion of skyrmions with negligible SkHE in ferromagnets remain challenging. Here, by embeding the [Co/Pd] multilayer into a surface acoustic wave (SAW) delay line where the longitudinal leaky SAW is excited to provide both the strain and thermal effect [6,7], we experimentally realized the ordered generation of magnetic skyrmions. The resultant current-induced skyrmions movement with negligible SkHE was observed. Two aspects of issues are critical to realize the orderly alignment and movement of skyrmions. One is the magnetic structure design that the [Co/Pt] multilayers with proper perpendicular magnetic anisotropy, interfacial Dzyaloshinskii-Moriya interaction, and film thickness. The other is the integrated delay line structure which can provide SAWs and thermal effect simultaneously. Thus, owning to the energy redistribution derived from the strain gradient during the excitation of SAWs, magnetic skyrmions are confined at the anti-nodes of the SAW and move nearly in a straight line under the current pulses [8]. The unprecedented reduction of SkHE in ferromagnets is expected to drive the progress of skyrmion-based applications. Our findings open up an unprecedentedly new perspective for manipulating topological solitons, which would trigger the future discoveries in skyrmionics and spin acousto-electronics.

[1] X. Z. Yu, et al. Nat. Mater. 10, 106 (2011). [2] S. Woo, et al. Nat. Commun. 9, 959 (2018). [3] W. Legrand, et al. Nat. Mater. 19, 34 (2020). [4] T. Dohi, et al. Nat. Commun. 10, 5153. (2019). [5] R. Y. Chen, C. Song, et al. Nano Lett. 20, 3299 (2020). [6] T. Yokouchi, et al. Nat. Nanotechnol. 15, 361 (2020). [7] R. Y. Chen, C. Song, et al. Adv. Funct. Mater. 32, 2111906 (2022). [8] R. Y. Chen, C. Song, et al. Nat. Commun. (accepted); arXiv. 2212.06997.

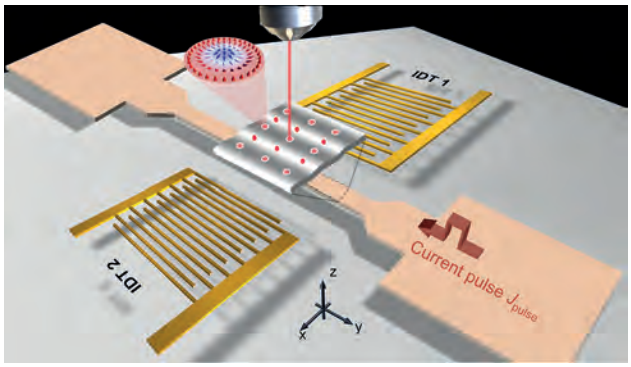

Schematic of the integrated device with a pair of IDTs on both sides of the magnetic multilayer channel.

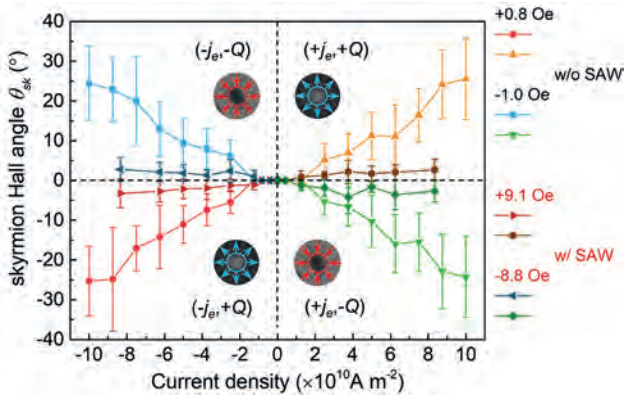

Phase diagram of the skyrmion Hall angle θ_{sk} as a function of current density measured with and without SAWs for skyrmions with topological charge $Q = +1$ and $Q = -1$.

INVITED PAPER

CB-05. Magnetic skyrmions toward advanced microelectronic applications. *C. Hwang*[1] *1. Korea Research Institute of Standards and Science, Daejeon, The Republic of Korea*

One of the serious problems in current Si-based CMOS technology is its power consumption as the device scale goes down to few nano meter. A promising alternative is the spin-based device such as MRAM. However, the current MRAM technology used in actual device application needs more innovative way to cut down its power consumption. One possibility is to use the magnetic domain wall but it requires the notch to hold the domain wall edge at room temperature but the distance between the notches limits the high density of the information. Magnetic skyrmion has drawn a lot of attention ever since the report on the possibility of the replacement of magnetic domain wall with magnetic skyrmion. For the last ten years, most works on this magnetic skyrmion are limited to the random generation of it by

very broad external perturbation and its characteristic movement. Recently we have shown several device applications of magnetic skyrmion such as magnetic skyrmion race-track memory[1] or magnetic skyrmion transistor[2] based on our determintistic recipe for the magnetic skyrmion generation[1,2,3] based on our microspic understanding of the formation of it. In this talk, we add an interesting but very practical application in neuromorphic device. This application is possible with the magnetic anisotropy control with the voltage pulse in our magnetic multilayer system[2]. In generation part, we can make so called "magnetic skyrmion reservoir", where the current pulse can kick out a single magnetic skyrmion on the track where it can move. In detection part, we can even preset the number of magnetic skyrmions holded in detection area, where the level of multi-values is determined by this number. One advantage of this method is that the signal is quite linear with respect to the number of magnetic skyrmions, which is quite different from the current devices based on ReRAM or CMOS with Si. We can increase or decrease the signal by adding or subtracting magnetic skyrmions so that we have symmetric signal distribution. Using MOKE microscopy, we can visualize the whole process including LIF operation.

[1] S. Yang et al, Adv. Mater. VOL. 33, p.2104406(2021) [2] S. Yang et al, Adv. Mater. VOL. 35, p.2208881(2023) [3] K. Moon et al., NPG Asia Materials VOL. 13, p.20 (2021)

CONTRIBUTED PAPERS

CB-06. Residual anomalous Hall effect and its spin-textural origin in chiral multilayers. *G. Krishnaswamy*[1], T. Yingzhe[1,2], X. Wong[1], E. Chue[1,2], H. Tan[2], H. Tan[2], R. Lim[2], X. Chen[2], N. Yakovlev[1] and A. Soumyanarayanan[1,2] *1. Department of Physics, National University of Singapore, Singapore; 2. Institute of Materials Research & Engineering, A*STAR, Singapore, Singapore*

The residual anomalous Hall effect (RAHE) – often equated with the topological Hall effect (THE) – is treated as evidence for the presence of skyrmions in chiral magnetic systems [1]. We show that the large RAHE occurs not just in chiral but also achiral multilayers using bespoke concurrent optical magnetometry and electrical characterization, complemented by Lorentz transmission electron microscopy measurements. Further, these measurements are performed on a series of samples with varying interfacial chiral interactions and anisotropy to correlate the domain structure with their electrical response. The RAHE is found to be maximized in the regime of maximum isolated disconnected domains. Our experimental results and theoretical calculations reveal that the RAHE occurs as a consequence of non-destructive accumulation of the AHE from isolated multi-domains and can be explained without invoking homochirality or topological properties of spin-textures. The experiments corroborate qualitatively with the theory and offer better quantitative agreement when compared to THE theories, thus supporting the universality of such a mechanism.

[1] Nagaosa, N., Tokura, Y. Topological properties and dynamics of magnetic skyrmions. Nature Nanotech8, 899–911 (2013) [2] Soumyanarayanan, A., Raju, M., Gonzalez Oyarce, A. et al. Tunable room-temperature magnetic skyrmions in Ir/Fe/Co/Pt multilayers. Nature Mater 16, 898–904 (2017). [3] Raju, M., Yagil, A., Soumyanarayanan, A. et al. The evolution of skyrmions in Ir/Fe/Co/Pt multilayers and their topological Hall signature. Nat Commun 10, 696 (2019) [4] Kimbell, G., Kim, C., Wu, W. et al. Challenges in identifying chiral spin textures via the topological Hall effect. Commun Mater 3, 19 (2022).

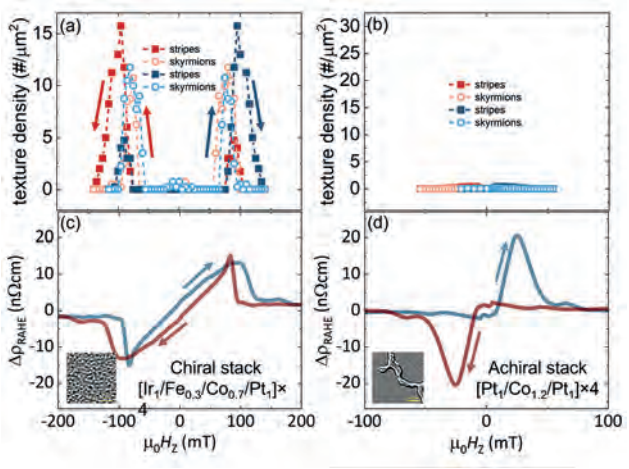

Texture density represented for both skyrmions and stripes obtained from LTEM imaging for a (a) chiral stack consisting of [Ir(1nm)/Fe(0.3nm)/Co(0.7nm)/Pt(1nm)]x4 multilayer and (b) an achiral stack consisting of [Ir(1nm)/ Co(1.2nm)/Pt(1nm)]x4. The corresponding residual anomalous Hall resistivity measurements are provided for the (c) chiral and (d) achiral cases respectively. The inset images in (c) and (d) show a 2 x 2 mm² field of view image of LTEM at the field of corresponding to the maximum textures which depict the domain morphology and chirality.

CB-07. Chiral Coupling of Two Orthogonal Magnetizations in a Single Ferrimagnetic GdCo Layer. *S. Ko*[1], J. Park[2], H. Kim[1,3], J. Park[1], A. Lee[4], J. Yuk[2], A.M. Park[1] and K. Kim[1] *1. Physics, Korea Advanced Institute of Science and Technology, Daejeon, The Republic of Korea; 2. Material Science and Engineering, Korea Advanced Institute of Science and Technology, Daejeon, The Republic of Korea; 3. Physics, Korea University, Seoul, The Republic of Korea; 4. Korea Basic Science Institute, Daejeon, The Republic of Korea*

Chiral coupling in magnetic materials offers exciting prospects for the development of noncolinear spin structures, such as chiral magnetic domain walls or chiral magnetic skyrmions, which can be utilized in magnetic memory and logic devices [1]-[2]. Typically, the chiral coupling is induced by Dzyaloshinskii-Moriya interaction (DMI), which requires more than two magnetic layers [3]-[4]. However, in our study, we present a novel form of chiral magnetic coupling that arises within a single magnetic layer. To investigate this phenomenon, we prepared a Gd-rich ferrimagnetic GdCo single layer consisting of Si/SiN(200nm)/$Gd_{28.7}Co_{71.3}$(50nm)/Pt(8nm)/Ti(2nm). Our measurement using a vibrating sample magnetometer (VSM) demonstrated coexistence of in-plane (IP) and out-of-plane (OOP) magnetization within a single GdCo layer (Fig. 1(a)). Remarkably, these two mutually orthogonal magnetizations are chirally coupled, evident from the dependence of the Hall voltage on the OOP magnetic field for different initial IP magnetizations (Fig. 1(b)). Our results revealed a distinct shift in the hysteresis loop, either positively or negatively, depending on the initial direction of the IP magnetization (+y direction (←)(green) or -y direction (→)(purple)). This loop shift is attributed to the chiral coupling between the IP and OOP moments. As described schematically in Fig. 1(b), the GdCo layer exhibits a preference for the chirality of ←↓ or →↑ between the IP and OOP moments, thereby a large coercive field is required to achieve the state with the opposite chirality. To reveal the origin of the chiral coupling, we performed the scanning transmission electron microscopy (STEM) and electron energy loss spectroscopy (EELS) measurements. The results show that there is an elemental inhomogeneity in the lateral direction which could generate non-vanishing out-of-plane magnetic moments. Furthermore, we also find the gradual decrease of the GdCo composition ratio in the vertical direction, which could give the bulk DMI [5]. Our study presents compelling evidence

for the emergence of chiral magnetic coupling within a single magnetic layer, opening new avenues for exploring chiral effects in magnetic materials for advanced magnetic devices.

[1] K.-S. Ryu *et al*., *Nature Nanotechnology* 8, 527-533 (2013). [2] M. Song *et al*., *IEEE Transactions on Electron Devices* 68, 1939 (2021). [3] D.-S. Han *et al*., *Nature Materials* 18, 703-708 (2019). [4] C. O. Avci *et al*., *Physical Review Letters* 127, 167202 (2021). [5] D.H. Kim *et al*., *Nature Materials* 18, 685–690 (2019).

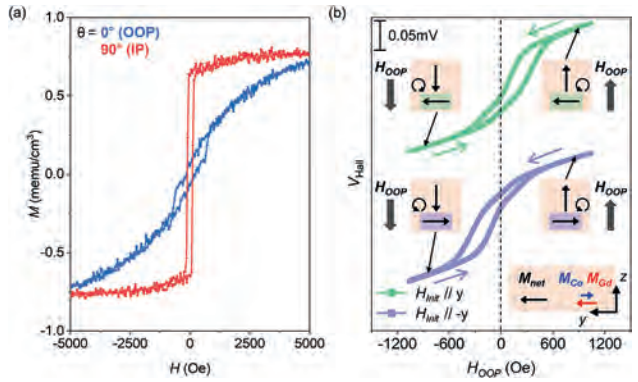

CB-08. Skyrmions in Magnetic Multilayer Thin Films Are Half-Integer Hopfions. *W. Parker*[1*], J.A. Reddinger[1] and B. McMorran[1] *1. Physics, University of Oregon, Eugene, OR, United States*

Magnetic skyrmions have attracted intense research for their novel physics and potential applications as spintronic information carriers. In practice, their use in real world devices has been hindered by the difficulty of stabilizing them in ambient conditions and of achieving low current density driven motion. This is in part because skyrmions while are fundamentally 2-dimensional, they exist in physical systems with 3-dimensional extent. In multilayer thin film geometries, whose ability to tunably stabilize skyrmions at ambient conditions makes them a promising host material, skyrmions' domain walls twist from Bloch-type at the center to Néel-type at the surface, with opposite helicities at the top and bottom. This is a result of surface-volume stray field interactions, and strongly affects both the velocity and angle of current-driven motion. Here we show that this varying helicity creates a topologically non-trivial and mathematically novel structure which is related to the magnetic hopfion but has a half-integer Hopf index. By analogy to the hopfion, to construct it we extend a skyrmion along its central axis, then wrap the resulting tube around the z-axis to form a torus. In the simplest integer case, the cross-sectional skyrmion is a bimeron (topological charge ±1), and the resulting hopfion has a Hopf index of ±1. In our case, we must use a charge ±1/2 texture, the meron. Wrapped in the same way, the center of the meron forms the Bloch component of the skyrmion's domain wall, while its edges form the Néel caps, core, and exterior. Remarkably, the field lines of this configuration form the Hopf fibration, forming links on concentric tori beginning with a single circle at the Bloch core. Meanwhile, the preimages - curves along which magnetization is constant - form a set of nested hyperboloids filling space. Here we describe the real-space and topological properties of the half-integer hopfion found in multilayer thin films, an important step towards understanding and predicting their stability, formation, and current-driven dynamics.

B. Göbel, I. Mertig, O. Tretiakov, Physics Reports., Vol. 895, p.1-28 (2021) N. Kent, N. Reynolds, D. Raftrey, Nature Communications., Vol. 12, p. 1562 (2021) I. Lemesh, G. Beach, Phys. Rev. B., Vol. 98, p.104402 (2018) A. Kamchatnov, Sov. Phys., Vol. 82, p. 117-124 (1982)

Fig. 1. The cross-sectional meron texture of a Bloch skyrmion with Néel caps.

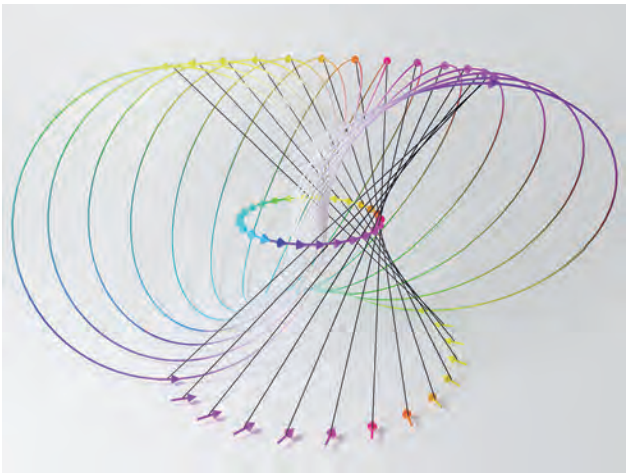

Fig. 2. Black lines are curves of constant magnetization, colored curves are the Hopf fibers.

INVITED PAPER

CB-09. Quantum Computation Based on Magnetic Skyrmions. *C. Psaroudaki*[1] *1. Physics, École Normale Supérieure, Paris, France*

Sixty years after its proposal in particle physics, the concept of a skyrmion as a topological quasi-particle, has now found a highly suitable application in the form of whirl-like nano-objects observed in helimagnetic materials. In this talk, I will review the appealing properties of skyrmions for magnetic storage of classical information, including their nanoscale size, topological stability, lifetime, and tunable energetics. The discovery of stable nanometer-scale skyrmions at low temperatures has sparked interest in their quantum properties for information processing, while improved quantum sensors and novel skyrmion-hosting materials enable their experimental exploration. I will discuss a new class of primitive building blocks for realizing quantum logic elements based on nanoskyrmions. In a skyrmion qubit, information is stored in the quantum degree of helicity, and the logical states can be adjusted by electric and magnetic fields, offering a rich operation regime with high anharmonicity. Scalability, qubit parameter tunability, and readout by nonvolatile techniques converge to make the skyrmion qubit highly attractive as a logical element of a quantum processor. Using skyrmions in the quantum regime introduces an entirely new direction in the filed of skyrmionics and an unexplored avenue for quantum computing. The challenges are now practical, primarily to identify suitable materials with the required characteristics and engineer architectures for the specific functionalities.

Christina Psaroudaki and Christos Panagopoulos, Phys. Rev. Lett. 127, 067201 (2021) Christina Psaroudaki and Christos Panagopoulos, Phys. Rev. B 106, 104422 (2022)

Session CC
MULTIFERROIC MATERIALS AND MAGNETOELECTRIC PHENOMENA

Paola Tiberto, Co-Chair
INRIM, Torino, Italy
Jordi Sort, Co-Chair
Universitat Autonoma de Barcelona, Cerdanyola del Valles, Spain

INVITED PAPERS

CC-01. Novel tetragonal phase and multiferroism in (1-x)$BiFeO_3$-(x) $BaTiO_3$ films. *L. Martin[1,2] 1. Materials Science and NanoEngineering and Rice Advanced Materials Institute, Rice University, Houston, TX, United States; 2. Materials Sciences Division, Lawrence Berkeley National Laboratory, Berkeley, CA, United States*

While bulk $BiFeO_3$ has a rhombohedral perovskite structure with the polarization lying along the {111}, the room temperature structure and polarization can be manipulated using strain and chemistry due the presence of numerous structural polymorphs. Under sufficiently large compressive (tensile) strains researchers have found super-tetragonal-like (orthorhombic) structures. Changing the structure can also change the resulting polarization and magnetism and thus the study of the polymorphism in this system has been a matter of great attention. Considerable work has been done on the super-tetragonal-like structure (with large $c/a \approx 1.25$ and predicted polarization as large as ~150 $\mu C/cm^2$), but it has been found that growing a phase-pure version of this material is challenging and limited to very thin films before it relaxes back to the parent structure. On the other hand, chemical substitution has also been widely used to modify $BiFeO_3$ since the polarization (structure) is strongly influenced by the $6s^2$ lone pair electrons of bismuth meaning that *A*-site substitution can greatly impact the structure and properties. Here, we explore such concepts by examining the evolution of the structure and polar and magnetic properties of (1-x)$BiFeO_3$–(x) $BaTiO_3$ (x = 0-0.3) solid solution thin films. Films of varying compositions have been deposited using pulsed-laser deposition on a range of perovskite substrates. While for all values of x films grown on scandate substrates exhibit the expected rhombohedral (monoclinic) structure seen in most films (albeit with slightly larger lattice parameter), growth of films with x = 0.1, 0.2, and 0.3 on $SrTiO_3$ (001) substrates produces a new phase. Detailed X-ray diffraction, piezoresponse force microscopy, and scanning transmission electron microscopy reveal this new phase to be tetragonal and different from the previously observed super-tetragonal-like phase. Insights on this new structure are gleaned from first-principles calculations. Subsequent dielectric and polarization-electric field hysteresis loop studies show that the novel tetragonal phase exhibits a lower dielectric constant and increased polarization (as large as 120 mC/cm^2) and coercive field (~500 kV/cm) as compared to parent-phase $BiFeO_3$. In turn, the magnetic nature of the material is studied via inelastic light scattering, exchange bias, SQUID magnetometry, angle-dependent X-ray absorption spectroscopy and magnetic linear and circular dichroism, and scanning NV magnetometry measurements. A comparatively large in-plane magnetization is observed. Finally, the potential for magnetoelectric coupling in this system is probed. Overall, these findings suggest the discovery a new phase of $BiFeO_3$ that, to the best of our knowledge, has not been observed before and works to provide understanding for why it forms and how it evolves from the parent phase.

CC-02. Magnetoelectric order in Antiferromagnetic $SrMnO_3$ Thin Films. *T. Banerjee[1] 1. Zernike Institute for Advanced Materials, University of Groningen, Groningen, Netherlands*

Emergent phenomena in quantum materials exploiting strong correlation effects and topology is an active area of research. Specifically, multiferroic materials have found renewed interest particularly for topological magnetism and for logic-in-memory applications such as in the prototype MESO structure demonstrated by Intel. In this talk, a correlated oxide perovskite, SrMnO3, which is a rare example of a multiferroic and an antiferromagnet, theoretically predicted to exhibit a very strong magnetoelectric coupling due to strain will be discussed. The predicted large phase space of new and accessible states in strained SrMnO3 thin films opens avenues in exploring topological magnetism in this material. Investigation of magnetic order is less studied in strained SrMnO3, primarily because it is unresponsive to modest magnetic fields and requires using large scale infrastructure such as synchrotron facilities or high resolution imaging techniques to unravel the magnetic ordering. However, in recent years Spin Hall Magnetoresistance (SMR) has become an established method to probe surface magnetic order and for extracting useful parameters such as magnetic anisotropy and spin mixing conductance in ferromagnetic, antiferromagnetic and chiral magnetic insulators. We use SMR and extend its potential in an unique way to reveal a new feature in the phase response of the SMR. Importantly both the phase and amplitude of the SMR oscillations are needed to draw conclusions on the observed magnetic order in the differently strained thin films of SMO. Interestingly, we find that strain modifies the magnetic anisotropy, magnetic order and domain structures in these films. DFT studies predict a multiferroic phase above 1% epitaxial strain with a strong magnetoelectric coupling which corroborates with our findings. Our work is important for the development of antiferromagnetic spintronics and orbitronics and promising for electric field control of magnetic order in multiferroic materials relevant for alternative computing applications

[1] J.J.L. van Rijn, D. Wang, B. Sanyal, T. Banerjee, *Phys. Rev. B* 106, 214415 (2022) [2] A. Das, V. E. Phanindra, A.J. Watson, T Banerjee, *Appl. Phys. Lett.* 118, 052407 (2021) [3] P. Zhang, A. Das, J.J.L. van Rijn, A.J. Watson, *Appl. Phys. Lett.* 121, 152401, (2022)

CONTRIBUTED PAPERS

CC-03. Pressure effect on 4d-4f coupled multiferroic compound, $Ba_3HoRu_2O_9$. *T. Basu[1], E. Kushwaha[1], M. Kumar[1], G. Roy[1] and A. Santos[2] 1. Rajiv Gandhi Institute of Petroleum Technology, Jais, India; 2. Neutron Scattering Division, Oak Ridge National Lab, Oak Ridge, TN, United States*

We demonstrate domain dynamics of the 6H-perovskite multiferroic Ba3HoRu2O9 system via comprehensive magnetic, dielectric, and neutron powder diffraction measurements. Further, we have investigated the title compound under external pressure to tune this 2nd magnetic phase and multiferroicity. This system undergoes long-range antiferromagnetic ordering

at T_{N1} ~ 50 K (with a propagation wave vector of K_1 = ½ 0 0) followed by another phase transition at ~10 K (T_{N2}). Both Ru and Ho-moments order simultaneously below T_{N1}, followed by spin reorientations at lower temperatures, demonstrating a strong Ru(4d)-Ho(4f) magnetic correlation [1,2]. Below T_{N2} two magnetic phases co-exist, in which one magnetic phase containing an up-up-down-down structure (with a propagation wave vector of K_1 = ¼ ¼ 0) is predicted to be responsible for spatial inversion symmetry breaking to govern ferroelectricity below T_{N2}. The coexistence of two magnetic phases arises due to phase competition as a result of different competing exchange interactions. The 2nd magnetic phase (up-up-down-down spin-structure) is attributed to finite-size magnetic domains instead of true long-range-ordering. The external pressure has a pronounced effect on the magnetic ordering of the 2nd phase. We will discuss the results of external pressure and domain dynamics.

[1] T. Basu, et al., Phys. Rev. Materials, 3, 114401 (2019). [2] T. Basu, *et al.,* Phys. Rev. B, 102, 020409(R) (2020).

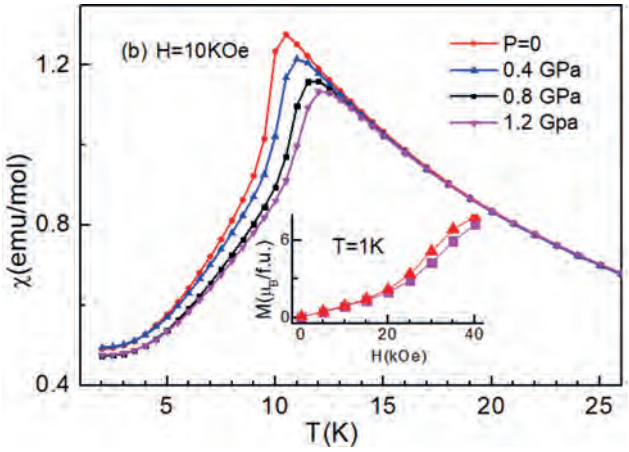

CC-04. Exploring the Ferroelectric Order and Linear High-Field Magnetoelectric Coupling in $Na_2Co_2TeO_6$: Implications for a Kitaev Compound. *S. Mukherjee*[1] and S. Giri[1] *1. School of Physical Sciences, Indian Association for the Cultivation of Science, Kolkata, India*

We present findings of ferroelectric (FE) ordering in $Na_2Co_2TeO_6$, accompanied by a linear magnetoelectric effect. The ferroelectric order, observed at approximately 72 K (T_{FE}), surpasses the antiferromagnetic ordering (T_N) at 26 K. This confirmation comes from both pyroelectric and bias-electric field measurements. Additionally, we observe a notable electrocaloric effect around T_{FE}. The onset of the FE order triggers a magnetic entropy change (ΔS_M) that reaches a maximum at approximately 35 K, which is considerably higher than T_N. This suggests a predominant short-range ordering beyond T_N. A structural transition from a high-temperature $P6_322$ space group to a polar $P6_3$ structure is proposed at T_{FE}, explaining the emergence of polar order. We discuss the distortion of the CoO_6 octahedra and the layered honeycomb structure around T_{FE} and T_N, which relates to the significance of magnetic frustration, the occurrence of FE order, the multi-caloric effect, and the potential for a Kitaev spin liquid state. The compound's multifunctional properties have attracted significant attention and hold fundamental interest. (1)

1. S Mukherjee et al., *Physical Review Materials*, 6, 054407 (2022).

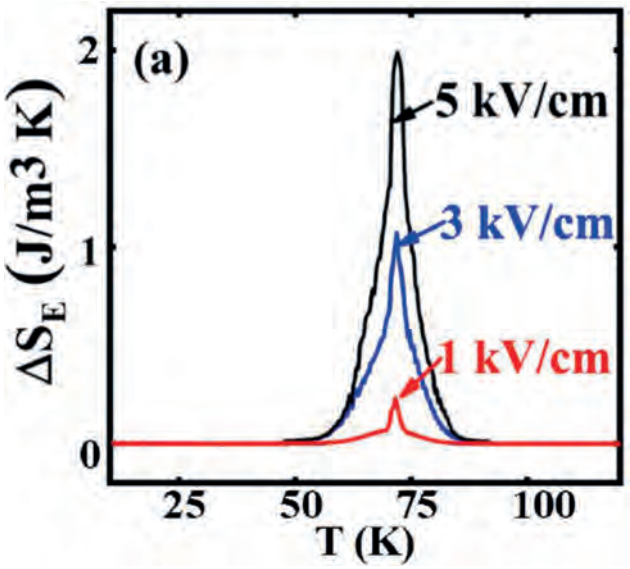

(a) Thermal variation of ΔS_E at different electric field

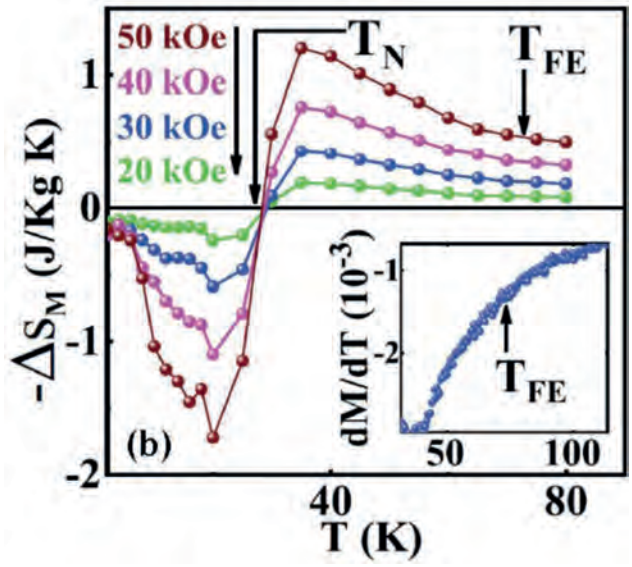

Thermal variation of ΔS_M at different magnetic field

CC-05. The Anisotropic Variation of Magnetic Moment Arrangement with Respect to Temperature in Monolayer $NbOI_2$. *G. Zhang*[1] and Q. Chen[1] *1. School of Physics, Southeast University, Nanjing, China*

The monolayer $NbOI_2$ has been obtained experimentally through mechanical exfoliation recently, and it exhibits highly in-plane anisotropic electrical and optical properties[1]. 2D $NbOI_2$ is also ferroelectric material with ultra-strong second-harmonic generation (SHG)[2] and huge piezoelectric responses[3] which are newly discovered. The electronic and magnetic properties are studied in our work by first-principles calculations on the basis of density functional theory. We discovered a new phase of $NbOI_2$, whose magnetism originates from the separation of Nb atom dimers and the disappearance of Nb-Nb bonding status. Based on the anisotropic Heisenberg model, the Néel temperature (T_N) of the monolayer $NbOI_2$ is predicted to be 43 K, and the magnetic susceptibility has a valley value at 10 K [see Fig.1]. This is because of the significant difference of magnetic alignment in two directions [see Fig.2] results from the anisotropy of magnetic exchange-coupling strength, and we provided detailed physical pictures to understand these extraordinary phenomena. This discovery provides a new construct for

exploring unusual phase transitions in two-dimensional systems, and demonstrates the great potential of $NbOI_2$ for applications in multiferroics-based flexible memory devices.

[1] Y.Q. Fang, F.K. Wang and R.Q. Wang, et al. Advanced Materials, 33, 2101505 (2021) [2] I. Abdelwahab, B. Tilmann, Y.Z. Wu, et al. Nature Photonics, 16, 644-650 (2022) [3] Y.Z. Wu, I. Abdelwahab, K.C Kwon, et al. Nature Communications, 13, 1884 (2022)

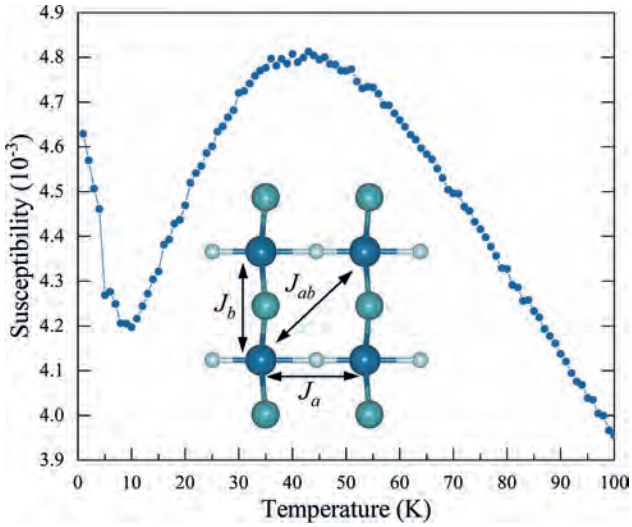

The simulated susceptibility as a function of temperature for the $NbOI_2$ monolayer. The inset is schematic of the exchange interaction.

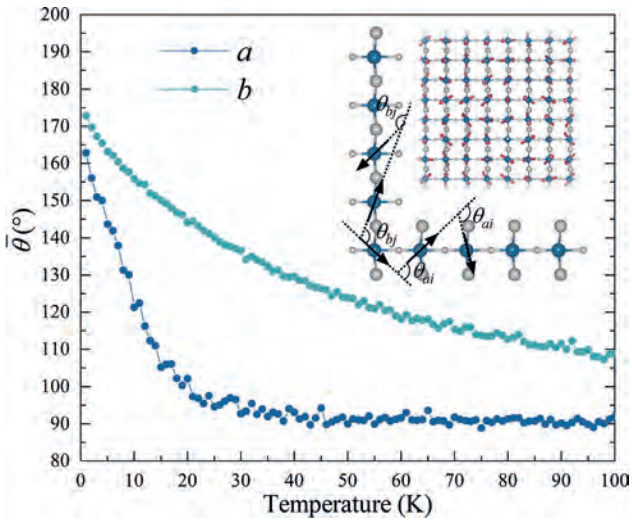

Calculated mean values of the angle between neighboring magnetic moments (θ) along *a* and *b* directions with respect to temperature, and schematics for calculation of θ.

CC-06. Manipulating Metastability: Quenched Control of Topological Skyrmions in Multiferroics. *N.P. Nazirkar*[2], R. Harder[1] and E. Fohtung[2]
1. Advanced Photon Source, Argonne National Lab, Lemont, IL, United States; 2. Materials Sciences and Engineering, Rensselaer Polytechnic Institute, Troy, NY, United States

The topological properties of quasiparticles, such as skyrmions and vortices, have the potential to offer extraordinary metastability through topological protection, and drive motion with minimal electrical current excitation. This has promising implications for future applications in spintronics. Skyrmions frequently appear either in lattice form or as separate, isolated quasiparticles [1]. Magnetic ferroelectrics, a subset of multiferroics that exhibit magnetically induced ferroelectricity, possess intriguing characteristics like magnetic (electric) field-controlled ferroelectric (magnetic) responses. Previous research based on Landau theory indicated the potential to stabilize metastable phases in multiferroic barium hexaferrite [2]. We have successfully stabilized these metastable phases through magnetic quenching of hexaferrite nanoparticles, leading to the creation of compelling topological structures. The structural changes in individual $BaFe_{12}O_{19}$ nanocrystals were scrutinized using Bragg coherent diffractive imaging, granting us insight into the emergent topological structures in field-quenched multiferroics. Additionally, we explored why these structures are energetically preferable for the formation of metastable topological structures [3].

[1] Magnetic Skyrmion Materials, Yoshinori Tokura and Naoya Kanazawa, Chemical Reviews 2021 121 (5), 2857-2897, DOI: 10.1021/acs.chemrev.0c00297 [2] D. Karpov, Z. Liu, A. Kumar, B. Kiefer, R. Harder, T. Lookman, and E. Fohtung, Phys. Rev. B 100, 054432 – Published 22 August 2019 [3] Karpov, D., Liu, Z., Rolo, T. *et al. Nat Commun* 8, 280 (2017). https://doi.org/10.1038/s41467-017-00318-9

CC-07. A Robust High-temperature Multiferroic Device with Tunable Magnetic Chiral Fluctuation. *Z. Lim*[1,2], C. Li[3], G. Omar[1] and A. Ariando[1]
*1. Physics, National University of Singapore, Singapore; 2. Soft Materials Department, IMRE, A*STAR, Singapore, Singapore; 3. Department of Materials Science and Engineering, Southern University of Science and Technology (SUSTECH), Shenzhen, China*

We integrated $Pt/La_{0.5}Ba_{0.5}MnO_3$ ultrathin films with the $PbZr_{0.2}Ti_{0.8}O_3$ ferroelectric and obtained several unprecedented results. Apart from strong Topological Hall Effect (THE) measurable across a wide temperature range, we also demonstrate reversible ON/OFF tuning of THE signal by ferroelectric polarization switching, indicating creation and annihilation of magnetic Skyrmions by short voltage pulses. Regarding the exact mechanism of magnetoelectric coupling, although the concept of selective electrostatic doping between e_g orbitals of manganite cations has been well-known, our magnetoelectric polarity is found opposite to the earlier observations, which is best explained by a novel phase transition between C-type antiferromagnetic and ferromagnetic. The crucial innovation here originates from our opposite choice of layer stacking sequence which reverses the sign of tetragonal strain of the manganite unit cell, therefore providing a complementary insight where strain and polarization switching act in tandem. The relationship between the phase transition and tuning of THE is supported by micromagnetic simulations.

1. *Nature* 408, pages 944 (2000) 2. *Physical Review Letters*, 104, 127202 (2010) 3. *Science* 336, 198 (2012) 4. *Nature Communications* 7, 12669 (2016) 5. *Nature Materials* 17, 1087 (2018) 6. *Nature Materials* 18, 1054 (2019) 7. *Physical Review Letters* 124, 107201 (2020)

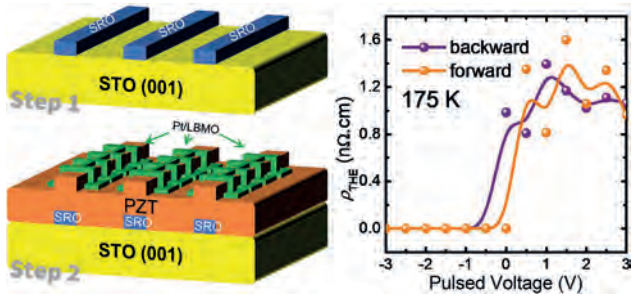

Left panel: Device structure fabrication. Step 1: bottom electrode SRO was deposited in a pulsed laser deposition (PLD) chamber and patterned *ex-situ* by standard photolithography and ion milling. Step 2: The same sample was continued in PLD for growth of PZT and LBMO, followed by Pt sputtering. Finally the top Hall bar was defined by standard photolithography and ion milling. Right panel: Change in the Topological Hall Effect (THE) versus pulsed voltage applied across the PZT.

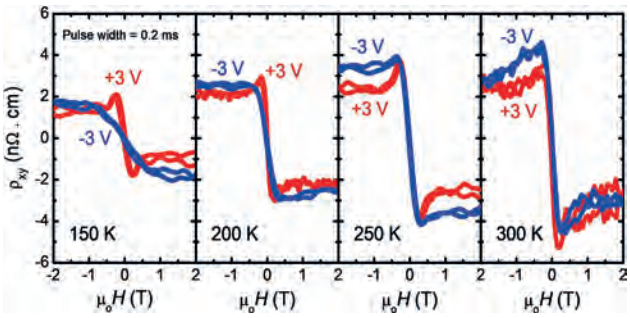

Temperature dependent Hall Effect measurement on Pt/LBMO after application of +/-3V pulse voltages across the PZT.

CC-08. Withdrawn

CC-09. Tuning magnetic anisotropy by a ferroelectric phase transition in ferromagnetic-piezoelectric heterostructure with giant magnetoelectric effect. *P. Finkel*[1] and T.R. Mion[1] *1. NRL, Washington, DC, United States*

Magnetoelectric materials and, to a larger extent, multiferroic heterostructures offer a novel route for electric field control of magnetism. We explored the induced magnetic anisotropy of an FeCo/Ag multilayer thin film deposited on the surface of 001 poled $(Pb(In_{1/2}Nb_{1/2})O_3$-$Pb(Mg_{1/3}Nb_{2/3})O_3$-$PbTiO_3$ PIN-PMN-PT single crystal as it is electrically driven through a ferroelectric-ferroelectric phase transition. In PIN-PMN-PT an effective giant piezoelectric coefficient >10,000 pm/V occurs during the phase transition providing strain >0.25% along a principle strain direction. This effect translates into anisotropic strain to the magnetoelastic thin film inducing a giant magnetoelastic effect driven by the induced magnetic anisotropy along the principle strain direction. We measured an effective converse magnetoelectric coefficient ~1.4 x 10^-5 s/m when driven through the phase transition which was more than double the values obtained in the linear piezoelectric rhombohedral phase. The controllable and repeatable nature of the phase transition allows an interactive driving of the induced magnetization making the phenomenon attractive for application in spintronic devices.

CC-10. Magnetoelectric CoV_2O_6 Spin ice lattice – Role of Fe inter-play in Co-based spin chains. *K. Preethi Meher*[1] *1. Central University of Tamilnadu, Thiruvarur, India*

Figure (a) Magnetization as a function of applied magnetic field (m_0H) at 5 K. (b) dM/dH as a function of applied magnetic field (m_0H) and (c) Capacitance as a function of the applied magnetic field. CoV_2O_6, a Brannerite-type material, exists in both monoclinic (a) and triclinic (g) forms. It is said to exhibit quasi-1D ferromagnetic chains of octahedrally-coordinated Co^{2+} ions in the higher spin state [1,2]. The monoclinic form of CoV_2O_6 contains only VO_6 octahedra (V^{5+} in 3d° electronic configuration) with equivalent Co^{2+} sites. However, in triclinic form, CoV_2O_6 contains two types of inequivalent Co^{2+} sites that co-exist with both VO_4 tetrahedra and VO_6 octahedra. Both forms are long-range antiferromagnets with Neel's temperature of 15 K and 7 K respectively. Magnetodielectric coupling correlated to the magnetization plateaus observed in monoclinic-CoV_2O_6 single crystals was reported by Singh *et al [3]*. $Co_{0.5}Fe_{0.5}V_2O_6$ single crystals were synthesized using the high-temperature melt method. Before the crystals were measured by me, detailed Laue studies were conducted to identify the polymorph stabilized. Here, the 1D Co^{3+} chains are going to be disrupted by Fe^{3+} substitution within the chains thereby altering the average spin state. Also, Co with large single ion isotropy is replaced, almost half by Fe with relatively smaller single ion isotropy. This has considerable ramifications on the structural, magnetic, and magneto-dielectric properties in comparison to the parent phase. Capacitance measurements exhibited two sharp steps coinciding with the plateau edges H_{c1}~1.65T (Antiferromagnetic to Ferrimagnetic state) and H_{c2}~3.3 T (Ferrimagnetic state to Ferromagnetic state) observed in M-H curves (shown in Figure).

1. Markulla et al, Phys. Rev.B.86, 134401 (2012); 2. Mulibana et al, AIP Advances, 13, 025023 (2023) 3. Singh et al, Phys. Rev.B, 8, 024410 (2012)

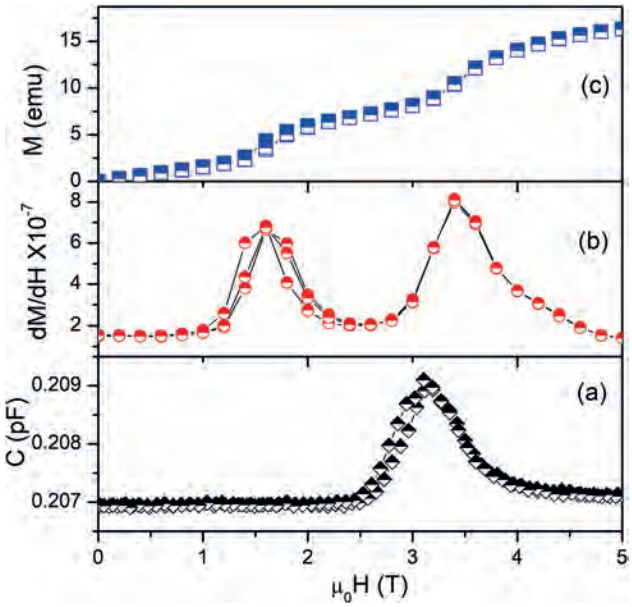

CC-11. Light-induced Ferromagnetic Resonance Shift in Magnetoelectric Heterostructure. *P. Pathak*[1], A. Kumar[2] and D. Mallick[1] *1. Electrical Engineering, Indian Institute of Technology Delhi, New Delhi, India; 2. Physics, Indian Institute of Technology Delhi, New Delhi, India*

Recently, coherent resonant control of the spin magnetic moment in nanoscale spintronic oscillators using ferromagnetic resonance (FMR) has expedited the exploration of next-generation neuromorphic-based spintronic and signal processing devices [1]. To achieve different neuromorphic functions, direct control of FMR is highly desirable. However, conventional methods of spin control through FMR typically involve the use of a radio frequency (RF) magnetic field [2] or high-density spin-polarized current [3], resulting in higher power consumption. Lately, considerable endeavour towards FMR control with an external electric field using magnetoelectric (ME) materials is explored extensively due to large strain-mediated ME coupling and low power consumption [4]. However, the primary obstruction in this method is the requirement of the high-saturation electric field that could cause device malfunction due to dielectric breakdown [5]. Additionally, the necessity to make electrical contacts in ME heterostructure leads to complexity as the dimension of ME-based microwave devices continues to shrink. To overcome these issues, we demonstrate light-induced FMR tunability in Ni/PMN-PT ME heterostructure. We showed that light generates piezo strain in PMN-PT without any bias voltage and controls the spin dynamics of the Ferromagnetic Ni thin film. Depending on the direction of the external applied magnetic field with respect to the PMN-PT crystalline directions, upward and downward volatile FMR shift is demonstrated (Fig 1). It is also observed that FMR shift can be induced by increasing the irradiation time at constant illumination power (Fig 2). This technique presents a remote means to control the spin magnetic moment for next-generation light-controlled ME-based microwave devices, allowing easier integration of these devices into complex architectures by eliminating the need for direct electrical contacts or bulky external components.

[1] J. Grollier, D. Querlioz, K. Camsari, Nature electronics 3, 360 (2020). [2] M. Romera, P. Talatchian, S. Tsunegi, Nature 563, 230 (2018) [3] S. Iihama, T. Taniguchi, K. Yakushiji, Nature electronics 1, 120 (2018). [4] M. Liu, O. Obi, J. Lou, Advanced Functional Materials 19, 1826 (2009) [5] T. Wu, A. Bur, K. Wong, Applied Physics Letters 98, 262504 (2011)

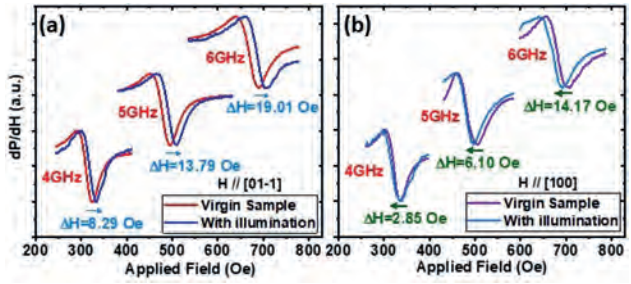

Light-induced (a) Upward and (b) Downward FMR Shift

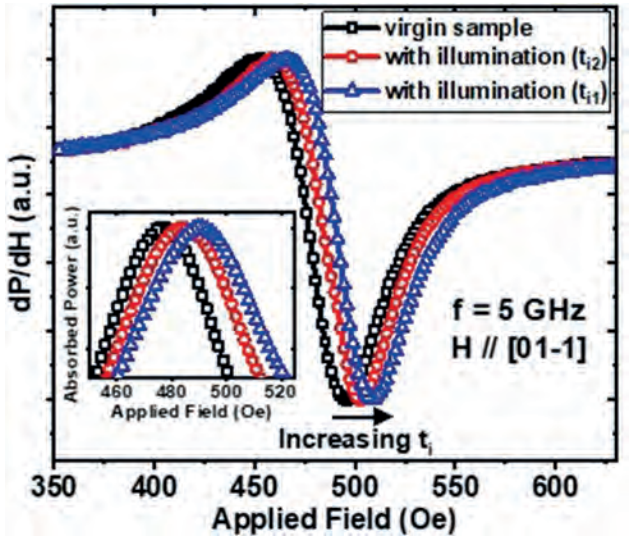

Effect of illumination time on FMR absorption spectra with inset curve showing half-power absorbed power spectra

Session CD
MAGNETIZATION DYNAMICS II: SPIN PUMPING AND FMR

Marco Coisson, Chair
INRIM, Torino, Italy

CONTRIBUTED PAPERS

CD-01. Magneto-dynamic modulation via antiferromagnetic coupling structure on permalloy/Holmium interface. M. Tian[1], Q. Chen[1], P. Wong[2], R. Liu[3], F. Silly[4], M. Silly[5], P. Ohresser[5], B. You[3], J. Du[3], A. Wee[6], J. Rojas-Sanchez[7], Z. Huang[1], W. Zhang[2] and *Y. Zhai*[1] *1. Key Laboratory of Quantum Materials and Devices of Ministry of Education, School of Physics, Southeast University, Nanjing, China; 2. School of Microelectronics, Northwestern Polytechnical University, Xi'an, China; 3. National Laboratory of Solid Microstructures, Nanjing University, Nanjing, China; 4. Université Paris-Saclay, Gif sur Yvette, France; 5. Synchrotron SOLEIL, Gif sur Yvette, France; 6. National University of Singapore, Singapore; 7. Université de Lorraine, Nancy, France*

Magneto-dynamics and its interfacial modulation have attracted much attention in energy-efficient and non-volatile spintronic devices, in which the antiferromagnetic coupling at the interface plays a significant role in the spin dynamic behaviors. Here, we utilize rare-earth Holmium(Ho) to interface with transition-metal alloy $Ni_{80}Fe_{20}$(Py), and achieve a naturally-formed antiferromagnetic coupling between Py and interfacial Ho via the magnetic proximity effect, as confirmed by elements specified synchrotron radiation X-ray magnetic circular dichroism (XMCD) hysteresis loop. Even when the temperature decreases to 4.2 K, i.e., far below the Curie temperature of Ho, the antiferromagnetically-coupled interface is still preserved. Using ferromagnetic resonance analysis, we reveal that the Gilbert damping parameters of the Py/Ho bilayers are much larger than those of the Py/Pt and Py/Pd, suggesting a superior spin transparent efficiency on such an interface with an antiferromagnetic coupling. More importantly, upon the insertion of 2-nm-thick Cu, the antiferromagnetic coupling disappears, associated with the evident suppression of Gilbert damping. This strengthens the key role of the antiferromagnetically-coupled interface in the magneto-dynamics of the transition-metal/rare-earth bilayers, providing a promising way of magneto-dynamics modulation in antiferromagnetic based devices.

CD-02. Impact on Gilbert damping in ultrathin ferromagnetic film from surface magnetic anisotropy. *S. Yoshii*[1], R. Ohshima[1], Y. Ando[1] and M. Shiraishi[1] *1. Kyoto University, Kyoto, Japan*

The ability to control the Gilbert damping parameter of ferromagnetic (FM) thin films, which governs the length over which spin information can be transmitted, is crucial for designing spintronic and magnonics devices. Thus, devising methods to adjust the Gilbert damping constant α has been a significant research target for several decades. Although numerous approaches have been explored to control α, there are presently only few articles that report a large modulation in Gilbert damping. In our recent works, the strong impact of surface state of FM films on the magnetization damping in ultrathin, i.e., less than 2 nm-thick, Co films was reported [1]. As the next milestone for further control of α we demonstrate the significant modulation of Gilbert damping of 2 nm-thick FM films by altering the surface magnetic anisotropy (SMA) [2], which opens the door for achieving the optimal method of controlling α in ultrathin ferromagnetic films. The samples of MgO (2 nm)/Co (t_{Co} nm)/nonmagnetic (NM) buffer layer (3 nm) were prepared on SiO_2 substrates by electron deposition as shown in Fig. 1, where Ti, Al, Cu and SiO_2 (as the reference) were selected as the buffer layers and the t_{Co} was varied from 2 nm to 20 nm. The broadband ferromagnetic resonance measurement of the prepared samples was performed to estimate the t_{Co}-dependence of α, of which result is shown in Fig. 2. In the samples with the ultrathin Co layer, the significant difference of α was obtained by choosing the different buffer layers. This substantial modulation of α in ultrathin Co film is attributed to the change of the SMA of Co films, which will be discussed in the presentation. Since the large modulation of α in ultrathin $Co_{25}Fe_{75}$ film expected to possess ultralow intrinsic α[3] by altering its SMA was also confirmed [4], this modulation principle can be versatile method of designing α.

[1] S. Yoshii, M. Shiraishi *et al*., Sci. Rep. 10, 15764 (2020). [2] S. Yoshii, M. Shiraishi *et al*., Phys. Rev. B 106, 174414 (2022). [3] Martin A. W. Schoen *et al*., Nat. Phys. 12, 839-842 (2016). [4] S. Yoshii, M. Shiraishi *et al*., in preparation.

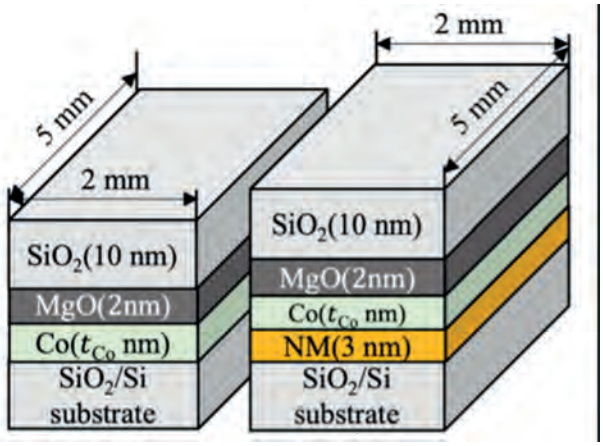

Fig. 1 Sample structures

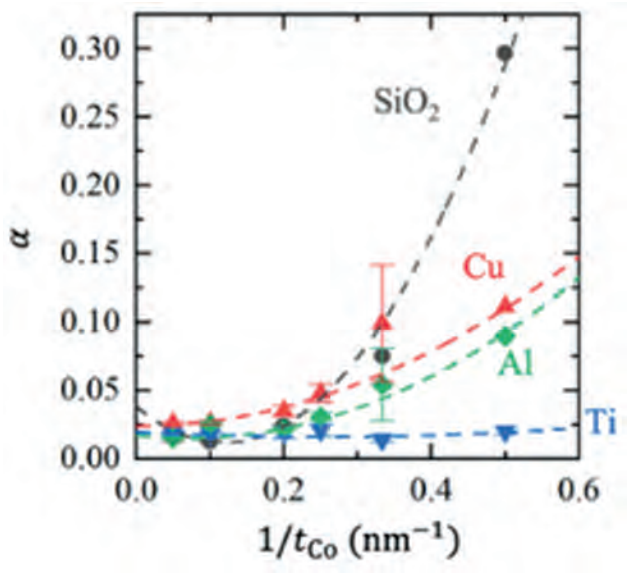

Fig. 2 Co thickness dependence of Gilbert damping constant

CD-03. Amplification of electron-mediated spin currents by stimulated spin pumping. B.J. Assouline[1], M. Brik[1], N. Bernstein[1] and *A. Capua*[1]
1. Applied Physics, Hebrew University of Jerusalem, Jerusalem, Israel

Spin current amplifiers are necessary building blocks in spintronic networks. The advances in magnon spintronics as well as the expected advantages in efficient data processing, speed, and integration [1] have attracted much recent attention, and a variety of technologies for amplifying magnonic spin currents have emerged [2,3]. Despite their necessity, amplifiers of spin currents that are mediated by electron transport have received little attention. Here we propose a process of stimulated spin pumping that we show to be capable of amplifying electron-mediated spin currents [4]. The process closely resembles the optical stimulated emission during which a coherent photon is emitted. Stimulated emission is a nonadiabatic (NA) process [5]. Namely, it is a hybrid time–frequency process whereby energy is transferred between an atomic system and a driving electromagnetic (EM) radiation before the two equilibrate. Recently, the NA regime was demonstrated in ferromagnets (FMs) by combining the rf-driven FMR and the time-resolved magneto-optical Kerr effect [6]. In these experiments, a variety of phenomena that are more familiar in their optical form were observed, including a controllable frequency chirping of the magnetization, induction of coherence in the inhomogeneously broadened spin ensemble, tuning of the intrinsic relaxation times, and mode locking of the spin ensemble [6]. The stimulated spin pumping amplification process described here takes the NA regime in FMs a step further. The mechanism relies on exciting first the spin transfer torque (STT) oscillator by a dc spin Hall effect. It is asynchronous since it does not require prior preparation of the phase of the excitation. Consequently, the injected ac spin current is amplified or absorbed depending solely on the dc bias current level. We show that the operation of the DC-STT based spin current amplifier is reminiscent of the operation of the optical amplifier, such as the erbium-doped fiber amplifier or the semiconductor optical amplifier, and that the similarity to the optical amplifier extends to the gain saturation profiles.

[1] P. Pirro, V. I. Vasyuchka, A. A. Serga, and B. Hillebrands, Advances in coherent magnonics, Nat. Rev. Mater. 6, 1114 (2021). [2] T. Brächer, P. Pirro, and B. Hillebrands, Parallel pumping for magnon spintronics: Amplification and manipulation of magnon spin currents on the micron-scale, Phys. Rep. 699, 1 (2017). [3] D. Malz, J. Knolle, and A. Nunnenkamp, Topological magnon amplification, Nat. Commun. 10, 3937 (2019). [4] B. Assouline, M. Brik, N. Bernstein, and A. Capua, "Amplification of electron-mediated spin currents by stimulated spin pumping", Physical Review Research 4, L042014 (2022). [5] I. I. Rabi, Space quantization in a gyrating magnetic field, Phys.Rev. 51, 652 (1937). [6] A. Capua, C. Rettner, S.- H. Yang, T. Phung, and S. S. P. Parkin, Ensemble-averaged Rabi oscillations in a ferromagnetic CoFeB film, Nat. Commun. 8, 16004 (2017).

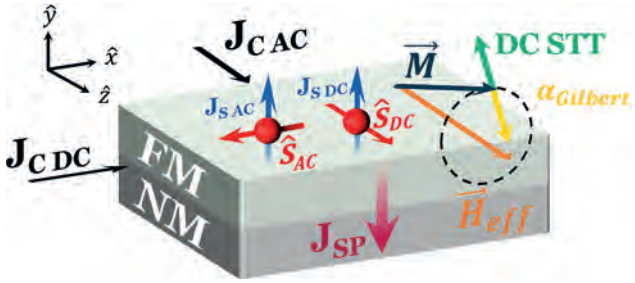

DC-STT based spin current amplification scheme.

CD-04. Structural and magnetic properties of thin cobalt films with mixed hcp and fcc phases. *G.I. Patel*[1], F. Ganss[1], R. Salikhov[1], S. Stienen[1], L. Fallarino[2,1], R. Ehrler[3], R. Gallardo[4], O. Hellwig[1,3], K. Lenz[1] and J. Lindner[1] *1. Institute of Ion Beam Physics and Materials Research, Helmholtz-Zentrum Dresden-Rossendorf, Dresden, Germany; 2. CIC energiGUNE, Vitoria-Gasteiz, Spain; 3. Institute of Physics, Chemnitz University of Technology, Chemnitz, Germany; 4. Departamento de Fisica, Federico Santa María Technical University, Valparaíso, Chile*

Cobalt is a magnetic material that finds extensive use in various applications, ranging from magnetic storage to ultrafast spintronics. Usually, it exists in two phases with different crystal lattices, namely in hexagonal close-packed (hcp) or face-centered cubic (fcc) structure. The crystal structure of Co films significantly influences their magnetic and spintronic properties. We report on the thickness dependence of the structural and magnetic properties of sputter-deposited Co on a Pt seed layer. It grows in an hcp lattice at low thicknesses, while for thicker films, it becomes a mixed hcp-fcc phase due to a stacking fault progression along the growth direction. The X-ray based reciprocal space map technique has been employed to distinguish and confirm the presence of both phases. Moreover, the precise determination of Landé's g-factor by ferromagnetic resonance provides valuable insights into the structural properties. In our detailed experiments, we observe that a structural variation results in a nonmonotonic variation of the magnetic anisotropy along the thickness. The work offers information of great significance and insight for both fundamental physics and potential applications of thin films with perpendicular magnetic anisotropy.

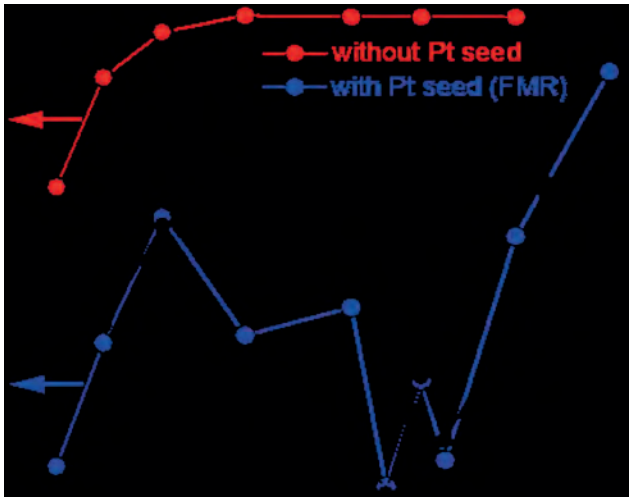

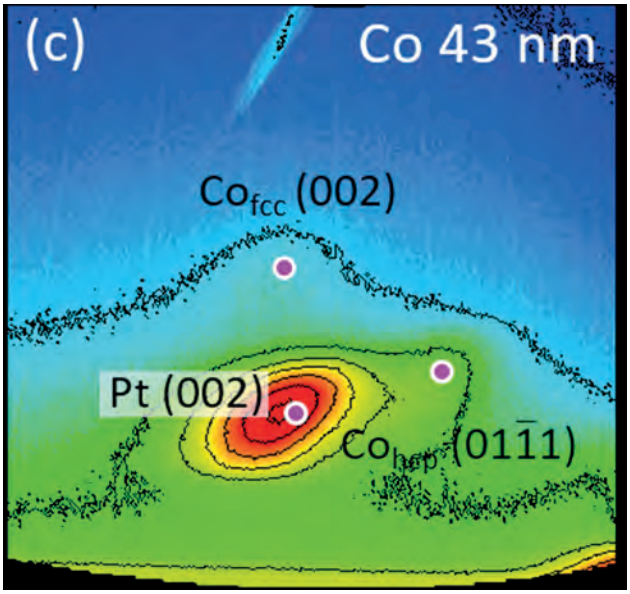

CD-05. Spin Pumping into A15 Spin Hall Candidates as Unconventional Superconductors. *Y. Qian*[1,2], A. Hoffmann[1], V. Novosad[2] and Y. Li[2] *1. Materials Science and Engineering, University of Illinois Urbana-Champaign, Urbana, IL, United States; 2. Materials Science Division, Argonne National Laboratory, Lemont, IL, United States*

Superconducting spintronics is a rapid-growing field, bridging spintronics and superconductivity for studying quantum phenomena in materials. In particular, spin injection in superconductors has attracted wide interest in dissipationless spin transport and the search for spin triplets in topological quantum computing. In this work, we explore spin pumping effect from permalloy (Py, $Ni_{80}Fe_{20}$) thin films into A15 superconductors, Ti_3Pt single crystal and $Ta_{1.5}Sb$ thin films. They are candidates of topological superconductors because of their strong topological-induced spin-orbit coupling. For the first sample, we polish the surface of the Ti_3Pt crystal down to a surface roughness of ~3 nm. Before the Py sputtering, we ion mill the surface of the Ti3Pt crystal in vacuum to clean the surface. For the second sample, we sputtered both the Py and $Ta_{1.5}Sb$ films without breaking the vacuum in order to ensure good interfacial coupling. Additionally, Py/Si samples were also sputtered as reference samples for extracting the spin pumping effect. The samples were tested with field modulation ferromagnetic resonance (FMR) measurements. We observe that both Ti_3Pt and $Ta_{1.5}Sb$ samples exhibited the same resonance field as compared with the control samples, indicating a reliable quality of the Py growth. For the linewidth, we notice an increase of inhomogeneous broadening in the Py/Ti_3Pt sample as compared with the Py/Si sample (Fig.1). However, the Py/$Ta_{1.5}Sb$ sample shows a change of slope by more than 30% as compared with the Py/Si sample (Fig.2). Our results show that spin pumping into A15 crystal is enabled in thin films with less roughness but is difficult for crystals with large roughness and potentially with dead layers. The results are very important in studying spin injection into unconventional superconductors and can be a potential approach for the search for spin triplets in superconductors. Work at Argonne was supported by the U.S. DOE, Office of Science, Basic Energy Sciences, Materials Sciences and Engineering Division under contract No. DE-SC0022060

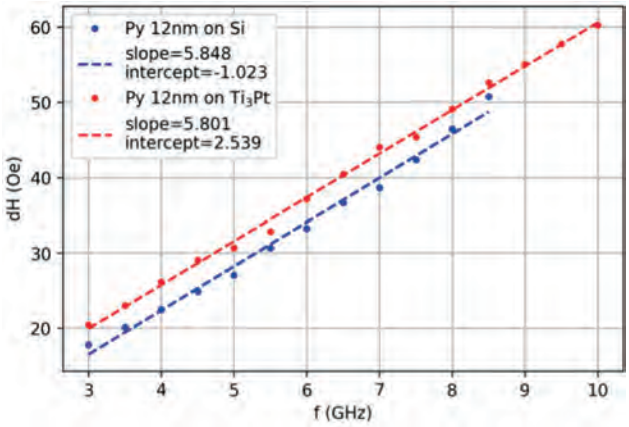

Full width half maximum line width Py/Ti_3Pt and Py/Si as a function of frequency.

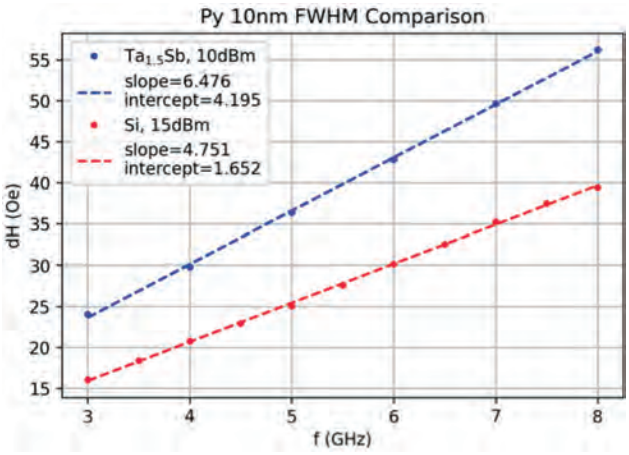

Full width half maximum line width Py/$Ta_{1.5}Sb$ film and Py/Si as a function of frequency.

CD-06. Vertically Graded Single-Layer Fe-Ni Alloys with Low Damping and Sizeable Spin-Orbit Torques. *R.E. Maizel*[1], S. Wu[1], P.P. Balakrishnan[2], A.J. Grutter[2], C. Kinane[3], A. Caruana[3], P. Nakarmi[4], B. Nepal[4], D.A. Smith[1], Y. Lim[1], J.L. Jones[1], W.C. Thomas[1], J. Zhao[5], M. Michel[5], T. Mewes[4] and S. Emori[1] *1. Physics, Virginia Polytechnic Institute, Blacksburg, VA, United States; 2. Center for Neutron Research, National Institute of Standards and Technology, Gaithersburg, MD, United States; 3. ISIS-Neutron and Muon Source, STFC Rutherford Appleton Laboratory, Didcot, United Kingdom; 4. Department of Physics and Astronomy, University of Alabama, Tuscaloosa, AL, United States; 5. Department of Geosciences, Virginia Polytechnic Institute, Blacksburg, VA, United States*

Power-efficient spintronic memories and oscillators require a large spin-orbit torque (SOT) and low damping. Typical heavy metal-ferromagnetic (-FM) bilayers attain a sizeable SOT at the expense of high damping, stemming from the ultrathin FM, ~1 nm. Here, we examine an alternative mechanism of producing sizeable SOT with low damping by continuously breaking bulk inversion symmetry [1-3] in thicker single-layer FMs. Fe with low intrinsic damping [4] and Ni with modest spin-orbit coupling [5] were co-sputtered to attain vertical compositional gradients in 10 nm thick single-layer FMs. We focus on three structures: (1) compositionally symmetric $Fe_{50}Ni_{50}$ [Fig. 1(b)], (2) vertically asymmetric $Fe_{100-x}Ni_x$ with Fe on the bottom [Fig. 1(c)], and (3) vertically asymmetric Fe_xNi_{100-x} with Ni on the bottom [Fig. 1(d)]. Out-of-plane ferromagnetic resonance (FMR) shows that asymmetric $Fe_{100-x}Ni_x$ and Fe_xNi_{100-x} have low intrinsic damping parameters of ≈0.003, indistinguishable from symmetric $Fe_{50}Ni_{50}$ despite the steep

intentional inhomogeneity. Angular-dependent DC-bias spin-torque FMR measurements [Fig. 1] indicate a sizeable SOT efficiency of ≈0.09 ± 0.02 in $Fe_{100-x}Ni_x$ and ≈-0.05 ± 0.02 in Fe_xNi_{100-x}, with the inverted compositional gradients yielding opposite SOT directions [Fig. 1 (c,d)]. Surprisingly, we also see a comparable efficiency of ≈-0.07 ± 0.02 in symmetric $Fe_{50}Ni_{50}$ [Fig. 1(b)] despite no intentional compositional gradient. Grazing-incidence X-ray diffraction shows a vertical strain gradient in $Fe_{50}Ni_{50}$, suggesting that the sizeable SOT efficiency could originate from the strain – rather than compositional – gradient. Indeed, we observe a possible correlation between the magnitude of the SOT efficiency and the vertical strain gradient in the three FeNi samples [Fig. 2]. Our results point to a new route to enable power-efficient SOT devices.

[1] Liu, L., et al., Phys Rev. B., Vol. 101, p. 220402 (2020) [2] Tang, M., et al., Adv. Mater., Vol. 32, p. 2002607 (2020) [3] Zhu, L., et al., Adv. Func. Mater., p. 2103898 (2021) [4] Wu, S., et al., Phys Rev. B., Vol, 105, p. 174408 (2022) [5] Du, C., et al., Phys Rev. B., Vol. 90, p. 140407 (2014)

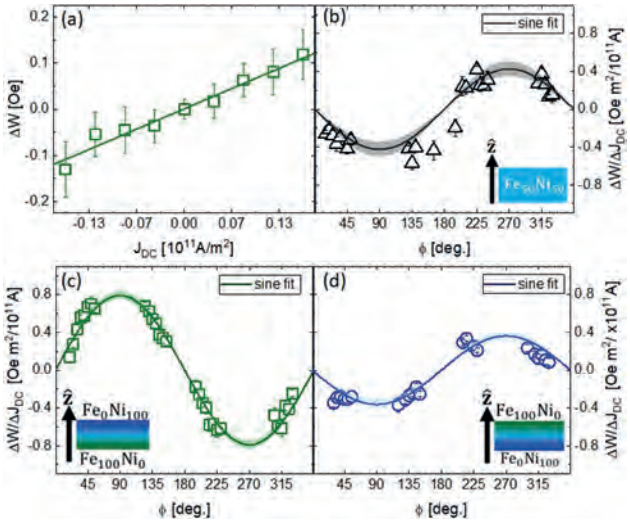

Fig. 1: (a) Change in linewidth, ΔW, with DC bias, J_{DC} in $Fe_{100-x}Ni_x$ at fixed in-plane field angle, φ=45°. Angular dependence of $\Delta W/\Delta J_{DC}$ for: (b) $Fe_{50}Ni_{50}$, (c) $Fe_{100-x}Ni_x$, and (d) Fe_xNi_{100-x}.

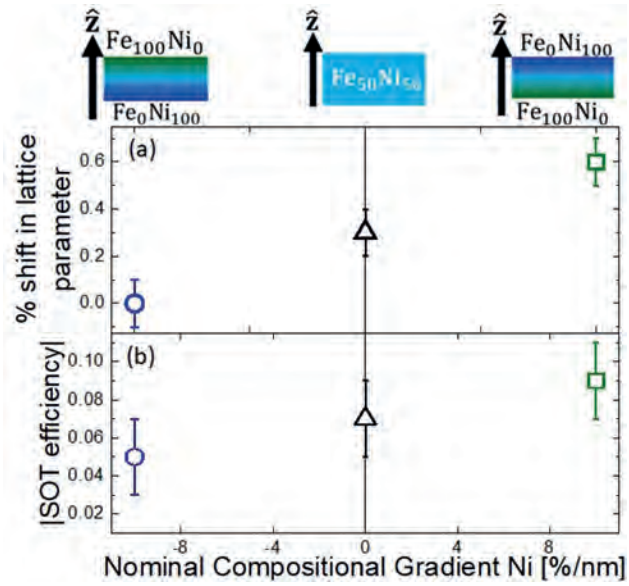

Fig. 2 (a) Percent change in the lattice parameter with thickness and (b) magnitude of SOT efficiency for the three FeNi samples.

INVITED PAPERS

CD-07. High-Bandwidth, Element-Specific Ferromagnetic Resonance Spectroscopy with an Ultrafast EUV Source. *M. Tanksalvala[1] 1. PML, NIST, Boulder, CO, United States*

Magnetic multilayer and device structures are the fundamental building blocks of spintronic devices. X-ray ferromagnetic resonance (XFMR) measurements are important for measuring these systems since they can decouple the magnetic state of the constituent elements if the magnetic layers contain different magnetic elements.[1] For over a decade, element-specific XFMR measurements have been performed at synchrotron facilities but suffer from limited access and a limited bandwidth of only a few GHz due to the time duration of the electron bunches. We have developed an instrument that addresses both of these limitations, providing element-specific XFMR measurements that we so far demonstrate to 40 GHz, with promise to extend to 100 GHz or higher. This laboratory-scale instrument uses high-harmonic generation (HHG) to produce extreme ultraviolet (EUV) light with a pulse duration on the order of 10 fs, and with photon energies spanning the M-edges of most magnetic elements. It also combines the laser oscillator used for the HHG system with a frequency comb generator to produce a microwave excitation that is synchronized to the EUV pulses with approximately 2 ps RMS of phase jitter. The low jitter, combined with the ultrafast pulse duration, enables us to demonstrate 40 GHz XFMR measurements. As a first example, we show a reflection-mode measurement on 10 nm thick permalloy (on a silicon substrate) at 8.5 GHz, highlighting the high bandwidth and element-specificity of the instrument. Since this instrument operates in reflection-mode, it is a milestone toward measuring the dynamics of the magnetic state and spin transport between individual layers of active devices on arbitrary and opaque substrates. The higher bandwidth also enables measurements of materials with high magnetic anisotropy, as well as ferrimagnets, antiferromagnets, and short-wavelength (high wavevector) spinwaves in nanostructures. To realize the ultimate goal of imaging transport in active devices, we can augment the present instrument with nanoscale lensless imaging techniques such as ptychography or holography, which have already shown merit for EUV-based nano-device characterization.[2,3]

[1] C. Klewe, Q. Li, M. Yang, et al., *Synchrotron radiation news,* 33.2 (2020) [2] M. Tanksalvala, C. L. Porter, Y. Esashi, et al., *Science Advances,* 7.5, eabd9667 (2021) [3] R. M. Karl Jr, G. F. Mancini, J. L. Knobloch, et al., *Science Advances* 4.10, eaau4295 (2018)

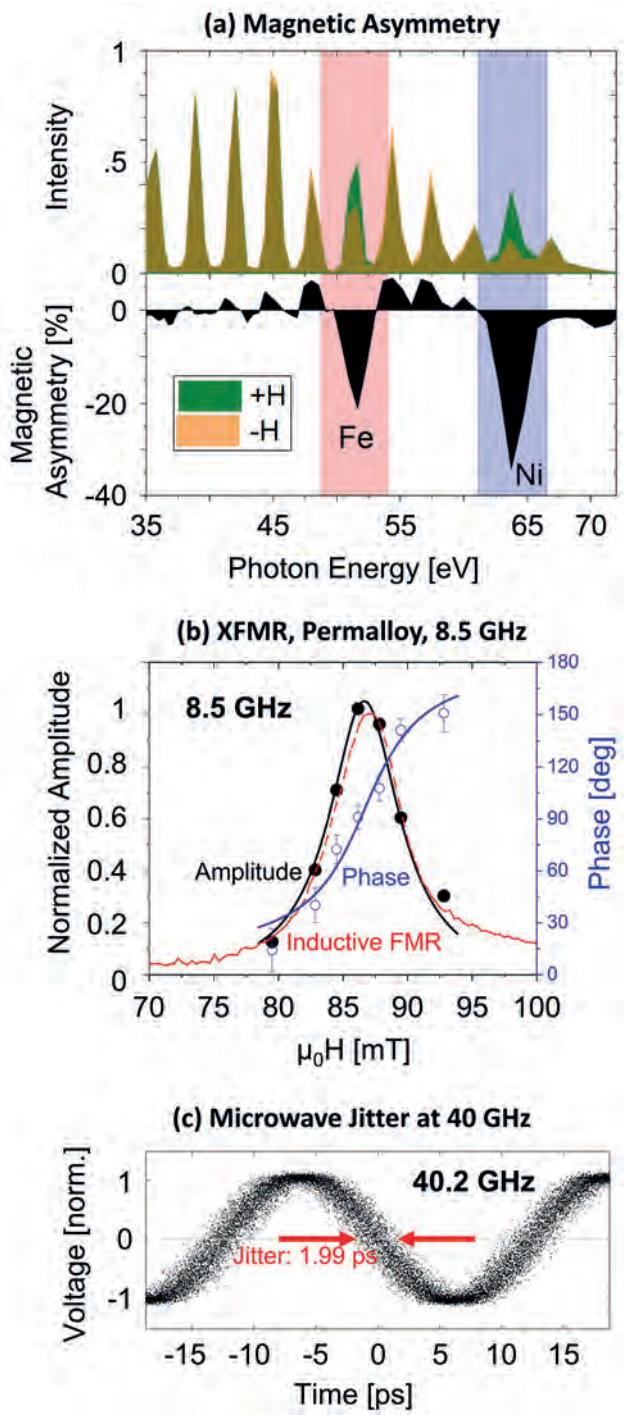

(a) Magnetic asymmetry in a Ni-Fe alloy, highlighting the ability to isolate the magnetic moments of individual elements within magnetic multilayers. (b) XFMR showing the ferromagnetic resonance of permalloy at the Ni M-edge, measured at 8.5 GHz. Overlayed are the simultaneous fits of the amplitude and phase to the Cauchy (Lorentzian) function. An in-situ measurement of the inductive FMR of the same sample is included as the red curve. (c) Data from a sampling oscilloscope showing a 40 GHz microwave output that is synchronized to the EUV pulses with an RMS phase jitter of 2 ps.

CD-08. Cation-Specific Magnetization Dynamics Probed by X-ray Ferromagnetic Resonance. *S. Emori[1] 1. Virginia Tech, Blacksburg, VA, United States*

Many technologically useful magnetic oxides are ferrimagnetic insulators, which consist of chemically distinct cations. In this presentation, we will demonstrate a unique approach to examine the dynamics of different magnetic cations [1] in such a complex ferrimagnetic oxide – namely, NiZnAl-ferrite ($Ni_{0.65}Zn_{0.35}Al_{0.8}Fe_{1.2}O_4$ [2]). We employ time-resolved x-ray ferromagnetic resonance (X-FMR) [3,4] to separately probe $Fe^{2+/3+}$ and Ni^{2+} cations from distinct sublattices. Unlike conventional methods that average over all cations, X-FMR acquires a time-resolved signal from each magnetic cation species. Our high-precision X-FMR results show that the excited cation moments remain rigidly collinear to within ≈2° and have identical spin relaxation to within <10%. Thus, our work validates the oft-assumed "ferromagnetic-like" dynamics in the resonantly driven ferrite: the magnetic moments from different cations precess as a coherent, collective magnetization – despite nonmagnetic Zn^{2+} and Al^{3+} diluting the exchange interactions. The demonstrated X-FMR method is a powerful tool to examine fundamental dynamics in multi-component magnetic systems.

[1] C. Klewe, *et al*. *Appl. Phys. Lett.* Vol. 122, p. 132401 (2023). [2] S. Emori, *et al*. *Adv. Mater.* Vol. 29, p. 1701130 (2017). [3] S. Emori, *et al. Nano Lett.* Vol. 20, p. 7828 (2020). [4] C. Klewe, *et al*. *Synchrotron Radiation News*, Vol. 33, p. 12 (2020).

CONTRIBUTED PAPERS

CD-09. Withdrawn

CD-10. Large Anomalous Frequency Shift in Perpendicular Standing Spin Wave Modes Induced by Thin Metallic Overlayers. *B. Lee*[1], T. Fakhrul[1], C.A. Ross[1] and G. Beach[1] *1. Material Science and Engineering, Massachusetts Institute of Technology, Cambridge, MA, United States*

Interface-driven phenomena in magnetic insulators is gaining attention owing to the possibility to control magnetization dynamics and magnetic textures in low-dissipation materials. Pure spin signals can be transported in magnetic insulators through magnon excitations, and controlling the nature of these excitations may lead to new insights into magnetization dynamics and novel spin wave devices. In this work, the influence of metallic overlayers on the spin wave dynamics of thin Bi-substituted yttrium iron garnet films is studied using Brillouin light scattering spectroscopy. [1] It is found that the magneto-static Damon-Eschbach modes exhibit a significant frequency shift when Pt, Au, or Cu films are deposited upon them, which arises from an interfacial contribution to the effective magnetic anisotropy. [2] In addition, there is an unexpectedly large shift in the perpendicular standing spin wave mode frequencies that cannot be explained by anisotropy-induced surface spin pinning. Rather, the experimental observations are consistent with the interface-induced decrease in the effective thickness where the standing waves are confined, increasing the exchange contribution to the mode frequency. It is suggested that this additional confinement may result from spin pumping at the insulator/metal interfaces, which results in a locally-over-damped interface region. To motivate a possible physical origin of the observation, we propose a phenomenological model that can describe the observation in terms of an interfacial region where the spin-orbit coupling plays a crucial role and the local effective damping associated with spin-pumping torque is relatively large, which would qualitatively explain the anomalously large metal-induced frequency shifts. These results uncover a previously unidentified interface-driven change in magnetization dynamics that may be exploited to locally control and modulate magnonic properties in extended films.

[1] B. H. Lee, T. Fakhrul, C. A. Ross, and G. S. D. Beach, Phys. Rev. Lett. Vol. 130, p126703 (2023). [2] A. J. Lee, A. S. Ahmed, B. A. McCullian, S. Guo, M. Zhu, S. Yu, P. M. Woodward, J. Hwang, P. C. Hammel, and F. Yang, Phys. Rev. Lett. Vol. 124, p107201 (2020).

Session CE
SPIN ORBITRONICS II
Albert Min Gyu Park, Chair
Korea Advanced Institute of Science and Technology, Daejeon, The Republic of Korea

INVITED PAPER

CE-01. Spin Orbit driven effects in Graphene/Ferromagnet interfaces. A. Gudín[1], I. Arnay[1], P. Olleros-Rodríguez[1], B. Muñiz[1], A. Guedeja-Marron[2], M. Varela[2], M. Valvidares[3], M. Jugovac[4], S. Bluegel[5], G. Bihlmayer[5], M. Valbuena[1], J. Camarero[1], R. Miranda[1] and *P. Perna*[1] *1. IMDEA Nanoscience, Madrid, Spain; 2. Universidad Complutense de Madrid, Madrid, Spain; 3. ALBA synchotron, Cerdanyola, Spain; 4. ELETTRA synchotron, Trieste, Italy; 5. PGI and IAS, Forschungszentrum Jülich, Jülich, Germany*

A major challenge for future spintronics is to develop suitable spin transport channels with superior properties such as long spin lifetime and propagation length. Graphene (Gr) can meet these requirements, even at room temperature [1]. While technologically challenging, the introduction of giant spin-orbit coupling (SOC) in the electronic bands of graphene via proximity with intercalated layers potentially allows the realization of highly efficient, electrically tunable, nonvolatile memories as well as opens up new pathways towards the realization of spintronic devices exploiting novel exotic electronic and magnetic states. A plethora of SOC driven properties have been recently demonstrated in graphene-based magnetic heterostructures controlled via proximity with intercalated layers, e.g., a strong perpendicular magnetic anisotropy (PMA) [2,3] and an unexpected giant Dzyaloshinskii-Moriya interaction (DMI) at Gr/Co interface [4,5], tailored spin-charge conversion [6] or the generation of single spin-polarized flat bands by inserting an europium ultrathin layer [7] and enables the electrical control of the SOC driven properties even by the interface with ferroelectric layers [8]. In this work, I will discuss on element dependent and averaged surface/interface SOC induced magnetic properties of epitaxial Gr/FM stacks grown on heavy metal/insulating oxide supports. From one side, we have provided evidence of an enhancement of the PMA driven by the strong orbital moment anisotropy. On the other side, we have experimentally found an energy splitting of in-plane spin polarized Gr π bands, consistent with an Rashba-SOC at the Gr/Co interface, which is either the fingerprint or the origin of the Dzyaloshinskii Moriya interaction. The induced SOC in Gr is due to the interaction of the HM with the C atomic layer via hybridization with ultra-thin Co layer. At larger Co thicknesses (~10 ML), neither in-plane or out-of-plane spin splitting is observed, indicating a Gr/Co interface decoupled from the Co/HM. Moreover, via 4f europium doping, we demonstrate the possibility to generate single-spin polarized bands. The doping is controlled by Eu positioning, allowing for the formation of a localized single spin-polarized low-dispersive parabolic band if Eu is on top, and a π* flat band with single spin character when Eu is intercalated underneath graphene. All this is then translated in a measurable induced magnetic moment in Gr, in the generation of competing effects for charge, orbital and spin conversion, and in driving the appearance of non-trivial, exotic topological spin textures and emerging symmetry-broken phases. Financial support from the EU FLAG-ERA SOgraphMEM and Spanish AEI through projects PCI2019-111867-2 and 111908-2, PID2021-122980OB-C52 (ECLIPSE-ECoSOx) and CNS2022-136143 (SPINCODE) is acknowledged.

[1] Han, et al. Graphene Spintronics, Nat. Nanotech. 9, 794 (2014). [2] Yang et al. Nano Lett. 16, 145 (2016); Ajejas, et al., ACS Appl. Mater. & Interfaces, 12, 4088 (2020); [3] Blanco-Rey, et al. ACS Appl. Nano Mater. 4, 4398 (2021). [4] Ajejas, et al., Nano Lett. 18(9), 5364-5372 (2018); Yang, et al., Nat. Mater. 17, 605 (2018). [5] Muñiz, et al. (2023), https://doi.org/10.48550/arXiv.2206.04351. [6] Anadon, et al. APL Materials 9, 061113 (2021). [7] Jugovac, et al. Advanced Materials, 2301441 (2023) https://doi.org/10.1002/adma.202301441 [8] Lancaster, et al. ACS Applied Materials & Interfaces 15, 16963 (2023).

CONTRIBUTED PAPERS

CE-02. Field-free spin-orbit torque switching in synthetic antiferromagnetic system using interfacial Dzyaloshinskii-Moriya interaction. *Y. Saito*[1], S. Ikeda[1,2], N. Tezuka[3], H. Inoue[1] and T. Endoh[1,4] *1. Center for Innovative Integrated Electronic Systems, Tohoku University, Sendai, Japan; 2. Center for Science and Innovation in Spintronics, Tohoku University, Sendai, Japan; 3. Department of Materials Science, Graduate School of Engineering, Tohoku University, Sendai, Japan; 4. Department of Electrical Engineering, Graduate School of Engineering, Tohoku University, Sendai, Japan*

Charge-to-spin conversion via spin Hall effect has the potential to achieve efficient manipulation of magnetization by electrical current. However, there are two major challenges in realizing high-performance spin-orbit-torque (SOT) devices. First is that perpendicular magnetization is difficult to achieve SOT switching without an external magnetic field. Second is the need for heavy metal electrodes with both large damping-like SOT efficiency (ξ_{DL}) and low resistivity. Many methods have been proposed for observing the field-free switching and advance partially for SOT-based systems toward real applications. However, any new approaches utilizable toward real applications for simultaneous achieving of field-free switching and high SOT efficiency are still highly demanded and worthy of deep and systematic investigations. In this work, an interfacial Dzyaloshinskii-Moriya interaction is introduced into perpendicularly magnetized synthetic antiferromagnetic (AF) system [1-4] by changing the type of capping or underlayer in the [capping layer]/Co/Pt/Ir/Pt/Co/[underlayer] structures (Figs. 1(a) and 1(b)). The anomalous Hall effect and current-induced magnetization switching were measured by the 4-point probe method in a Hall cross (Fig. 1(c)) at room temperature. As shown in Figs. 2(a)–2(d), field-free switching in synthetic AF system is observed in the cases of W, Ta, $Ir_{22}Mn_{78}$ capping layers or $Ir_{22}Mn_{78}$ underlayer. Among the synthetic AF system with field-free switching, the $Ir_{22}Mn_{78}$ capping layer case shows the largest ξ_{DL} = 28.1%. We also found that the observed large ξ_{DL} is related to the enhancement of spin absorption in antiferromagnetic Co magnetization configuration in synthetic AF system compared to that in ferromagnetic Co magnetization configuration. In this presentation, we will discuss the possible mechanism for observed field-free switching and the design of the synthetic AF structures for future nonvolatile high-speed memories and logic circuits. This work was supported by the CIES Consortium, Spin-RNJ, RIEC, X-NICS (No. JPJ011438), and JSPS KAKENHI JP21K18189.

[1] Y. Saito, N. Tezuka, S. Ikeda, and T. Endoh, Phys. Rev. B 104, 064439 (2021). [2] Y. Saito, S. Ikeda, and T. Endoh, Appl. Phys. Lett. 119, 142401 (2021). [3] Y. Saito, S. Ikeda, and T. Endoh, Phys. Rev. B 105, 054421 (2022). [4] Y. Saito, S. Ikeda, and T. Endoh, Appl. Phys. Exp. 16, 013002 (2023).

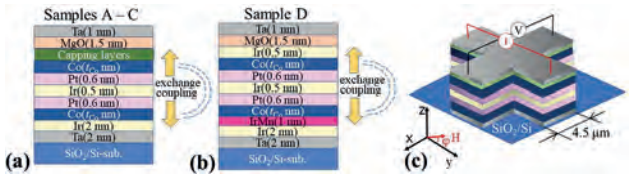

Fig. 1 (a) (b) Schematic of prepared film structures and (c) typical device image.

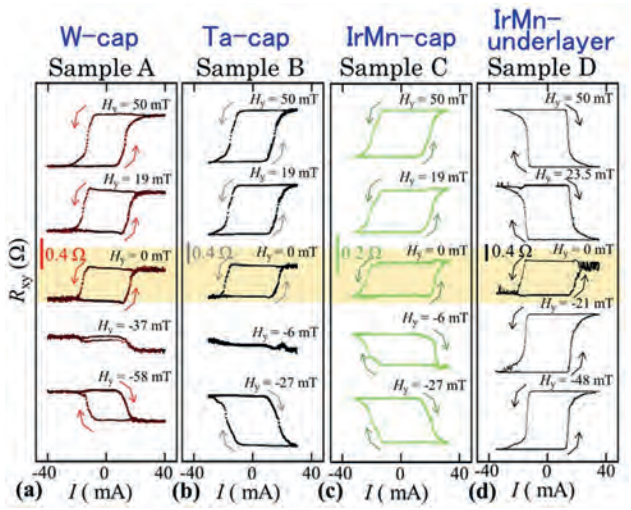

Fig. 2 Typical current-induced SOT switching.

CE-03. Dzyaloshinskii-Moriya Spin Density. *A.O. Leon*[1] and A.B. Cahaya[2] *1. Departamento de Fisica, Universidad Tecnologica Metropolitana, Santiago, Chile; 2. Universitas Indonesia, Jakarta, Indonesia*

The Dzyaloshinskii-Moriya interaction (DMI) is an antisymmetric exchange that stabilizes magnetization textures, such as skyrmions and merons, assists spin-orbit torques, and modifies several magnetic properties [1,2]. The DMI was predicted in 1958 [3], but the emergence of this coupling in complex materials and interfaces, as well as the tunning of its strength and symmetries, are still under active investigation. This presentation investigates the DMI of metals and interfaces containing rare-earth atoms (lanthanides), such as Dy and Tb. These atoms are heavy and possess a strong spin-orbit interaction which induces antisymmetric exchange, i.e., a DMI [4,5]. The starting point of our study is a model consisting of two magnetic atoms in an electron gas, one of them being a rare earth [5]. Each atom creates a conduction-electron spin polarization along its spin direction, but the rare earth tilts this spin polarization due to the spin-orbit coupling [5]. The result is an anisotropic spin density, orthogonal to both atomic spins, that we name Dzyaloshinskii-Moriya Spin Density (DM-SD). Figure 1 shows this spin density. Then, when adding a third impurity to the electron gas, its spin locally interacts with the DM-SD giving rise to the DMI. Therefore, the DM-SD is the antisymmetric equivalent of the RKKY spin density that mediates the isotropic exchange between two distant spins in metals. The simplicity of this model allows its use in more general situations, such as rare-earth-containing interfaces between magnetic insulators and transition-metal magnets. Furthermore, if the rare-earth atom is replaced by a transition metal with a partially unquenched orbital momentum, the magnitude of the DM-SD is reduced from the one of rare earths. AOL acknowledges financial support in Chile from ANID FONDECYT 11230120.

[1] S. Blundell, Magnetism in Condensed Matter (Oxford University Press, Oxford, 2012). [2] Spintronics Handbook: Spin Transport and Magnetism: Volume One: Metallic Spintronics, edited by E. Y. Tsymbal and I. Zutic (CRC, Boca Raton, FL, 2019). [3] I. Dzyaloshinsky, A thermodynamic theory of "weak" ferromagnetism of antiferromagnetics, J. Phys. Chem. Solids 4, 241 (1958). [4] S. M. Goldberg and P. M. Levy, Anisotropy in binary metallic spin-glass alloys. II. Rare earths, Phys. Rev. B 33, 291 (1986). [5] A. B. Cahaya and A. O. Leon, Dzyaloshinskii-Moriya spin density by skew scattering, Phys. Rev. B 106, L100408 (2022).

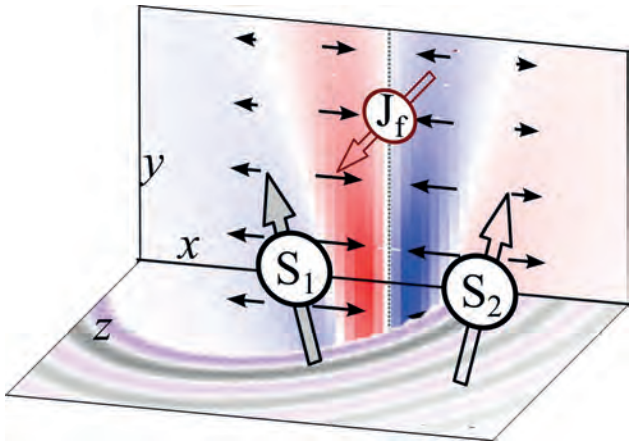

Figure 1. The Dzyaloshinskii-Moriya Spin Density (DM-SD). There is a conduction-electron spin density collinear to each atomic spin. In addition, the spin-orbit coupling of heavy atoms, such as rare earths, rotates these densities creating an anisotropic contribution, i.e., the DM-SD. The big arrows stand for atomic spins, while the small black arrows are the conduction-electron spin density, namely, the DM-SD.

CE-04. Investigating Orbital Hall Effect Materials for Efficient Magnetization Control with In-plane and Perpendicular Magnetic Anisotropic Ferromagnets. *R. Gupta*[1], A. Bose[1], C. Bouard[2], D. Go[1,4], F. Kammerbauer[1], S. Martin[2], G. Jakob[1], Y. Mokrousov[1,4], M. Drouard[2] and M. Kläui[1,3] *1. Insitutie of Physics, Johannes Gutenberg University Mainz, Mainz, Germany; 2. ANTAIOS, Meylan, France; 3. Department of Physics, Center for Quantum Spintronic, Trondheim, Norway; 4. Peter Grünberg Institut and Institute for Advanced Simulation, Forschungszentrum Jülich and JARA, Jülich, Germany*

The spin Hall effect (SHE) and orbital Hall effect (OHE) are promising mechanisms for magnetization control in spintronic devices [1-6]. Ru shows one of the highest orbital Hall conductivities among 3d, 4d, and 5d elements, surpassing Pt's spin Hall conductivity by a factor of four [7, 8]. This presentation discusses differentiating between SHE and OHE and explores OHE's impact on spin-orbit torques and magnetization switching. Ferromagnetic/OHE heterostructures with in-plane and perpendicular magnetic anisotropy were used. Preliminary findings reveal a significant orbital Hall torque generated by Nb and Ru, with a strong and long-range dependence on in-plane magnetized ferromagnets [9, 10]. Comparing Nb (or Ru)/Ni and Nb (or Ru)/FeCoB heterostructures, a pronounced enhancement in damping-like torque efficiency is observed, along with a sign reversal in Nb/(Ni or FeCoB) samples (Figure 1). To evaluate magnetization switching efficiency in out-of-plane magnetic anisotropic ferromagnets with various OHE materials, anomalous Hall effect devices with 100 nm diameter magnetic dots and perpendicular magnetic anisotropy were fabricated (inset of Figure 2). The magnetic stacks comprised Ta/OHE/Pt/$[Co/Ni]_3$/Co/MgO/CoFeB/Ta/Ru layers on different OHE layers (Ru, Nb, Cr), with a Ta/Pt/$[Co/Ni]_3$/Co/MgO/CoFeB/Ta/Ru reference sample. Experimental results demonstrate that Ru exhibits higher damping-like torque efficiency and lower switching current density compared to Pt, Nb, and Cr (Figure 2) [11]. These findings highlight the significant enhancement of magnetization switching efficiency in spin-orbit torque-based devices by utilizing OHE in Ru, aligning with first-principles predictions. This enhancement holds the potential for improving device performance and reducing power consumption.

1. Sinova et al., Rev. Mod. Phys. 87, 1213 (2015) 2. Bernevig et al., Phys. Rev. Lett. 95, 066601 (2005) 3. Kontani et al., Phys. Rev. Lett. 102, 016601

(2009) 4. Go et al., Phys. Rev. Lett. 121, 086602 (2018) 5. Ding et al., Phys. Rev. Lett. 125, 177201 (2020) 6. Lee et al., Nat. Commu. 12, 6710 (2021) 7. Tanaka et al., Phys. Rev. B 77, 165117 (2008) 8. Salemi et al., Phys. Rev. Mat. 6, 095001 (2022) 9. Bose et al., Phys. Rev. B 107, 134423 (2023) 10. Go et al., Phys. Rev. Lett. 130, 246701 (2023) 11. Gupta et al., (2023), in preparation

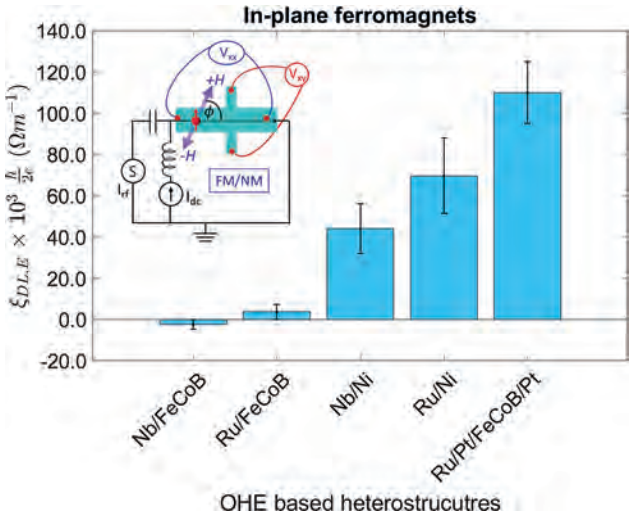

Figure 1: Efficiency of damping-like torque per unit electric field for different OHE based heterostructures. Inset: Schematic of Hall bar structure used for spin-orbit torques experiments for in-plane ferromagnet/OHE heterostructures.

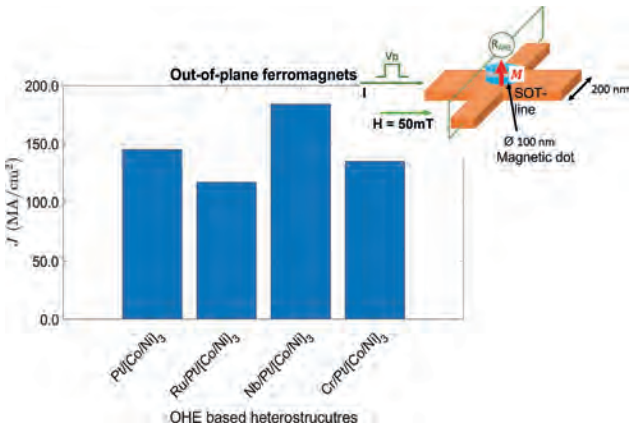

Figure 2: Switching current density observed for out-of-plane ferromagnet/OHE heterostructures. Inset: Schematic of anomalous Hall effect device with magnetic dots of 100 nm for magnetization switching experiments.

INVITED PAPER

CE-05. Unconventional Spin-Orbit Torques (SOT) in Sputtered Thin Films and Multilayers for Advanced Spintronics. F. Xue[1], M. DC[2,3], W. Hwang[1], W. Tsai[2] and *S. Wang*[1,2] *1. Electrical Engineering, Stanford University, Stanford, CA, United States; 2. Materials Science and Engineering, Stanford University, Stanford, CA, United States; 3. Intel Corp., Hillsboro, OR, United States*

Many emerging nonvolatile memory technologies have been proposed to further improve the energy efficiency of tomorrow's computing systems. Spin orbit torque magnetoresistive random access memory (SOT-MRAM) and its variants are one class of emerging nonvolatile memory technology which promises SRAM-like performance at higher bit cell density and energy efficiency [1-3]. High spin-orbit torques (SOTs) generated by in-plane currents in heavy metals and topological materials and interfaced with a ferromagnetic layer show great potentials of high endurance and robustness for next generation MRAM [4,5]. From a system perspective, such MRAM is a memory technology well suited for energy efficient in-memory computing (IMC) [5]. SOT switching of magnetization is known for ultrafast operation in the nanosecond (ns) and subnanosecond (sub-ns) regimes. An important problem that remains to be solved, though, is that the SOT switching mechanisms still require a stray magnetic field to achieve deterministic switching. To circumvent the above limitation, we and a few other groups are developing unconventional spins generated in MnPd3 [6], IrMn [7], and CuPt [8] thin films, among others. Specifically, we observe conventional SOT due to y spin, and out-of-plane and in-plane anti-damping-like torques originated from z spin and x spin, respectively, as shown in Fig. 1. Notably, we have demonstrated complete field-free deterministic switching of perpendicular cobalt via out-of-plane anti-damping-like SOT [6]. Density functional theory calculations show that the observed unconventional torques are due to the low symmetry of the (114)-oriented MnPd3 films. We also found significant in-plane unconventional spin currents from sputtered ultrathin $[Pt/Co]_N$, which are either highly textured on single crystalline MgO substrates or randomly textured on SiO2 coated Si substrates [9]. The unconventional spin currents generated in the low-dimensional Co films result from the strong orbital magnetic moments, which have been observed by X-ray magnetic circular dichroism (XMCD) measurement. The x-polarized spin torque efficiency reaches up to -0.083 and favors complete field-free switching of CoFeB magnetized along the in-plane charge current direction. The micromagnetic simulation additionally demonstrates its lower switching current than that in type-y configuration, especially for narrow pulse widths. Our work provides additional pathways for electrical manipulation of spintronic devices in the pursuit of high speed, high-density, and low-energy non-volatile memory.

[1] J.K. De Brosse, L. Liu, and D. Worledge, "Spin Hall effect assisted spin transfer torque MRAM," US Patent 8,889,433. [2] M. Wang, W. Zhao et al., "Field-free switching of a perpendicular magnetic tunnel junction through the interplay of spin-orbit and spin-transfer torques," Nature Electron., vol. 1, no. 11, pp. 582–588, 2018. [3] N. Sato, F. Xue, R. M. White, C. Bi, and S. X. Wang, "Two-terminal spin–orbit torque magnetoresistive random access memory," Nature Electron., vol. 1, no. 9, pp. 508–511, Sep. 2018. [4] M. DC, J.P. Wang et al., "Room-temperature high spin-orbit torque due to quantum confinement in sputtered Bi x Se (1-x) films," Nature Mater. 17, 800–807, 2018. [5] W. Hwang, F. Xue et al., "Energy-Efficient Computing with High-Density, Field-Free STT-Assisted SOT-MRAM (SAS-MRAM)," IEEE TRANSACTIONS ON MAGNETICS, 59(3), 3400106, 2023. [6] M. DC, S.X. Wang et al., "Observation of anti-damping spin-orbit torques generated by in-plane and out-of-plane spin polarizations in MnPd3," Nature Mater., 22, 591, 2023. [7] J. Zhou, X. Shu, J. Chen et al., "Magnetic asymmetry induced anomalous spin-orbit torque in IrMn," PHYSICAL REVIEW B 101, 184403, 2020. [8] L. Liu, C. Zhou, et al., "Symmetry-dependent field-free switching of perpendicular magnetization," Nature Nano. 16(3), 277-282, 2021. [9] F. Xue, S.-J. Lin, M. Song, et al., "Field-free spin-orbit torque switching assisted by in plane unconventional spin torque in ultrathin [Pt/Co]N," Nature Comms., in press, 2023.

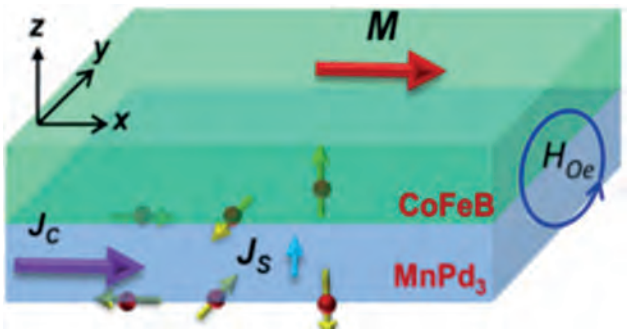

Figure 1: The out-of-plane anti-damping torque from z-spin current of MnPd3 enables up-down deterministic switching of CoFeB magnetization, a key ingredient in SOT-MRAM. This could lead to lower switching current density and thus energy-efficient computing and Edge AI. Field-free switching enables robust MRAM for diverse applications such as automobiles and aerospace.

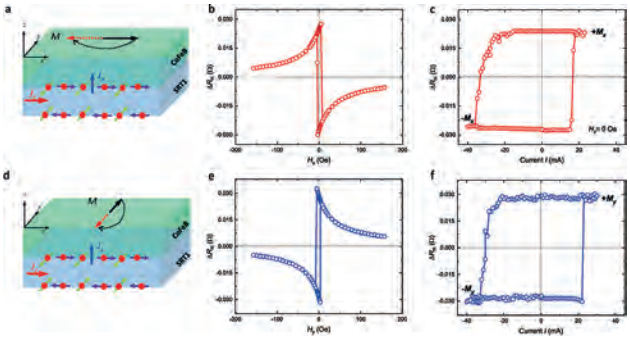

Figure 2: Type-x and type-y SOT switching behaviors in the SRT1/Mg/CoFeB samples deposited on (100) MgO single crystal substrates: a, A schematic depiction of type-x SOT switching with spin polarizations of sx and sy. b,c, Field switch and field-free current-induced switching in type-x configuration based on DPHE measurement in (100)MgO/SRT1/Mg(2)/CoFeB(2.5)/MgO(1.5)/Ta(2) devices with magnetic anisotropy in x direction. d, A schematic depiction of type-y SOT switching with spin polarizations of sx and sy. e,f, Field switch and field-free current-induced switching in type-y configuration based on DPHE measurement in (100)MgO/SRT1/Mg(2)/CoFeB(2.5)/MgO(1.5)/Ta(2) devices with magnetic anisotropy in y direction. SRT1 = $[Pt(1nm)/Co(0.159nm)]_5$.

CONTRIBUTED PAPERS

CE-06. Strain induced anisotropy of interfacial Dzyaloshinski-Moria Interactions. *E. Savostin*[2] and V. Lomakin[1] *1. ECE, UCSD, La Jolla, CA, United States; 2. MAE, UCSD, La Jolla, CA, United States*

This work presents a formulation and theoretical study of strain-induced anisotropy in interfacial Dzyaloshinskii-Moriya interactions (DMI) (Fig. 1). Recent experiments [1] show a strong variation of the DMI constant at uniaxial deformation of the ferromagnetic films. We employ Levy-Fert's analytical spatial model [2] to describe the DMI and derive a quantum Hamiltonian for the system. Using the linear spin wave theory and applying the Holstein-Primakoff transformation [3], we obtain the spin wave dispersion relations as a function of the DMI anisotropy in the high-frequency approximation (Fig. 2). Furthermore, we extend the analysis by considering an anisotropic DMI expression and its effects on the magnetic phase diagrams. We employ a formulation that combines the Landau-Lifshitz-Gilbert equation and the elastic wave equations. This allows investigating the interplay between the DMI anisotropy and strain-induced effects on the magnetic properties of the system such as anisotropic deformations of skyrmions and new emerging magnetic phases. We implement the formulation in finite difference and finite element based coupled micromagnetic-elastodynamic code providing solutions for the magnetization, stress, and velocity. Using this formulation and code, we investigate the dynamical properties of systems with elastically induced anisotropy of DMI. We demonstrate that presence of DMI anisotropy drastically increases magnetic response to applied monochromatic elastic waves and provides additional modes in spin waves. The interplay between the DMI anisotropy and magnetoelastic effects provides a rich landscape for studying emergent phenomena such as spin waves, skyrmions, and domain walls.

[1] N.S. Gusev, A.V. Sadovnikov, S.A. Nikitov, M.V. Sapozhnikov, and O.G. Udalov, Phys. Rev. Lett. 124, 157202 (2020). [2] A. Fert and P. M. Levy, Phys. Rev. Lett. 44, 1538 (1980) [3] T. Holstein and H. Primakoff, Phys. Rev. 58, 1098 (1940)

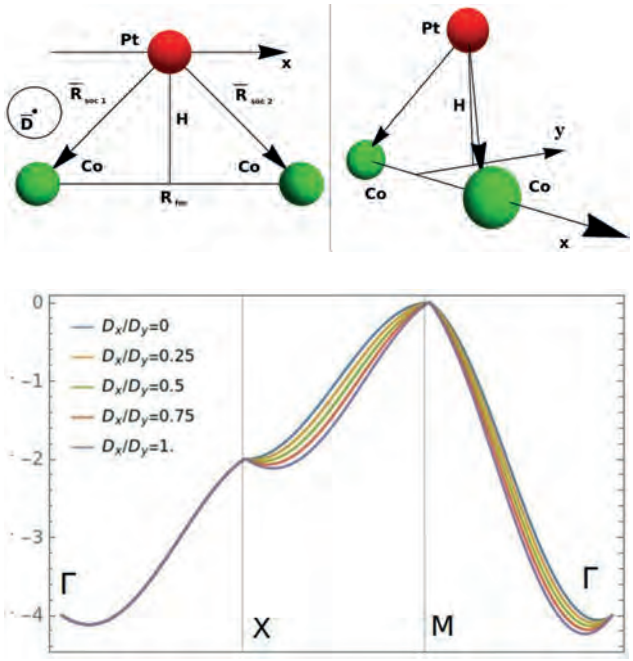

CE-07. Gradient-Induced Symmetry Breaking in Pt/Co Multilayer Structures. *H. Ko*[1] and Y. Kim[1] *1. Korea University, Seoul, The Republic of Korea*

Inversion symmetry breaking heterostructures comprising a nonmagnetic metal and a ferromagnetic layer are gaining attention. Recent research demonstrated that an increasing number of stack N leads to the augmentation of chiral interaction in [Co/Pd/Pt]N superlattices [1]. In this investigation, we examined the magnetic characteristics of [Pt/Co]4 layers where the thickness of the Pt layer is either increasing or decreasing. Samples were fabricated using DC magnetron sputtering under a base pressure of 5x10-9 Torr at room temperature. Three types of stacks were prepared as follows: Type 1: Si/SiO2 (Substrate)/Ta2/[Pt2/Co(t)/Pt2/Co(t)/Pt2/Co(t)/Pt2/Co(t)]/Pt2/Ta2; Type 2: Si/SiO2 (Substrate)/Ta2/[Pt2/Co(t)/Pt1.6/Co(t)/Pt1.2/Co(t)/Pt0.8/Co(t)]/Pt0.4/Ta2; Type 3: Si/SiO2 (Substrate)/Ta2/[Pt0.4/Co(t)/Pt0.8/Co(t)/Pt1.2/Co(t)/Pt1.6/Co(t)]/Pt2/Ta2, where Co thickness t was 0.4, 0.6, or 0.8 nm. The samples underwent post-annealing at 300°C for 1 hour under a pressure of 1x10-6 Torr. The magnetic properties were investigated using a vibrating sample magnetometer (VSM). The saturation magnetization (MS) of the samples was 2500 emu/cm3, approximately 2.5 times larger than that of the Ta/Pt3/Co1.2/Ta sample. The increased MS can be attributed to the proximity effect [2]. The MS of the samples increased as the number of Pt/Co interfaces increased, where the proximity effect takes place. Particularly, for samples with a Co thickness of 0.8 nm, magnetization switching occurred gradually rather than instantaneously. Moreover, the interfacial Dzyaloshinskii-Moriya interaction (DMI) energy

was determined using Brillouin light scattering (BLS) spectroscopy and polar magneto-optic Kerr effect (p-MOKE). BLS measurement showed low DMI energy density but it was not a sufficient measurement for multilayer thin film. The findings demonstrate that the breaking of symmetry in [Pt/Co] multilayers leads to the enhancement of magnetic properties through the proximity effect, which is associated with the Pt/Co interfaces.

[1] W. S. Ham et al., Dzyaloshinskii–Moriya interaction in noncentrosymmetric superlattices, npj Comput. Mater. 7, 129 (2021) [2] L. J. Zhu et al., Irrelevance of magnetic proximity effect to spin-orbit torques in heavy-metal ferromagnet bilayers, Phys. Rev. B 98, 134406 (2018)

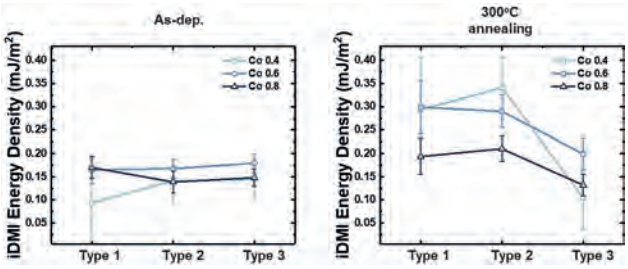

CE-08. Spin-orbit torque in antiferromagnetic Mn_3Pt with various structural ordering. *C. Zhang*[1], L. Yu[1], M. Al-Mahdawi[2] and M. Oogane[1,2] *1. Department of Applied Physics, Tohoku University, Sendai, Japan; 2. Center for Science and Innovation in Spintronics, Tohoku University, Sendai, Japan*

Non-collinear antiferromagnets (AFMs) exhibit remarkable magneto-transport properties due to their topological spin structures[1-3]. One intriguing phenomenon is the magnetic spin Hall effect, which enables spin polarization manipulation through spin structure tuning. Previous studies on Mn_3Pt, a well-known non-collinear AFM, have reported the current-induced x, y, z spin polarizations[4,5]. However, the effect of the structural ordering of Mn_3Pt on the spin polarization remains uncertain, hindering the material development and a comprehensive understanding of the underlying mechanisms. In this study, we modify the order parameters of $L1_2$ Mn_3Pt and investigate its effect on spin-orbit torque (SOT). We first focus on the post annealing temperature (T_a) dependence on the structural ordering of Mn_3Pt in Mn_3Pt/Py/RuCr stacks, which is deposited on MgO (001) substrates by co-sputtering with a substrate temperature of 350 °C. The structural properties of the Mn_3Pt films are analyzed with X-ray diffraction (XRD) measurements, and degree of ordering is quantified using the order parameter *S*. We find that *S* increases from 0.4 to 0.8 as T_a ranges from 400 to 550 °C. When T_a becomes larger than 600 °C, the collapse of the $L1_2$ structure is observed. We then use second harmonic Hall measurements to evaluate the SOT originated from the x and y spin polarization, which are defined as x-SOT and y-SOT, respectively. For T_a values below 550 °C, both x-SOT and y-SOT increase with increasing T_a. However, beyond 600 °C, x-SOT starts to decrease, while y-SOT continues to increase. These results indicate that x-SOT is influenced by the structural ordering of the $L1_2$ Mn_3Pt phase, likely originating from the magnetic spin Hall effect. On the other hand, the increase of y-SOT is more likely to be correlated with increasing resistivity, which can be explained by the spin-dependent scattering. The insights into the interplay between structural ordering and spin polarization in this study are expected to contribute to the design and optimization of antiferromagnetic systems for future applications. This work was partially supported by the X-nics project, and CSIS, CIES, and the GP-Spin program at Tohoku University

[1] V. Baltz *et al.*, Rev. Mod. Phys. 90, 015005 (2018). [2] M. B. Jungfleisch, Phys. Lett. A 382, 865 (2018). [3] L. Šmejkal *et al.*, Nat. Phys. 14, 242 (2018). [4] H. Bai *et al.*, Phys. Rev. B 104, 104401 (2021). [5] L. Yu *et al*., Appl. Phys. Express 15, 033002 (2022).

CE-09. Unconventional higher-order spin-orbit torques in monolayer Fe_3GeTe_2. *F. Xue*[1,2], M.D. Stiles[2] and P.M. Haney[2] *1. Department of Physics, University of Alabama at Birmingham, Birmingham, AL, United States; 2. Physical Measurement Laboratory, National Institute of Standards and Technology, Gaithersburg, MD, United States*

In ferromagnetic systems lacking inversion symmetry, an applied electric field can control the ferromagnetic order parameters through the spin-orbit torque. The prototypical example is a bilayer heterostructure composed of a ferromagnet and a heavy metal that acts as a spin current source. In addition to such bilayers, spin-orbit coupling can mediate spin-orbit torques in ferromagnets that lack bulk inversion symmetry. A recently discovered example is the two-dimensional monolayer ferromagnet Fe_3GeTe_2. In this work, we use first-principles calculations to study the spin-orbit torque and ensuing magnetic dynamics in this material. Johansen *et al.* recently predicted that this material's C_{3z} symmetry leads to novel bulk lowest order spin-orbit torques derived from the Cartesian expansion. By expanding the torque versus magnetization direction as a series of vector spherical harmonics, we find that higher order terms (up to l=4) are significant and play important roles in the magnetic dynamics. They give rise to deterministic, magnetic field-free electrical switching of perpendicular magnetization.

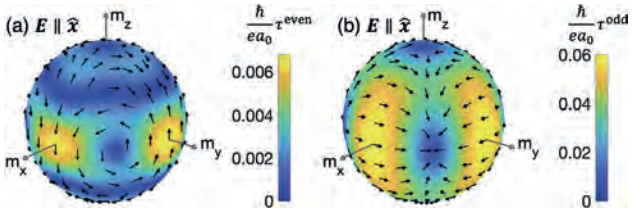

Angular dependence of the time-reversal even (a) and odd (b) torkance on the magnetization direction (θ,φ) under an external electric field along the x direction at the Fermi level. The arrow (color) on the sphere indicates the direction (magnitude) of the torkance at the given magnetization. We use k_BT =2 meV, η=25 meV in the calculation.

CE-10. Bulk spin-orbit effect in single rare earth-transition metal alloy on the magnetization switching. *P. Lee*[1,2], S. Mangin[2] and C. Lai[1] *1. Materials Science and Engineering, National Tsing Hua University, Hsinchu, Taiwan; 2. Physics, Institute Jean Lamour, Nancy, France*

In the early work[1], we have shown the spin-orbit torque (SOT) switching on the single TbCo layer with or without the heavy metal (HM) in different thicknesses to identify the damping-like torque of bulk SOT effects generated in the TbCo layer. Here, we prepared two structures for the detailed investigation as shown in Figure 1(a) left. For both structures, the interplay of self-torque and the spin-orbit torque generated in HM was clearly observed. Since the spin hall angle is opposite from the bulk TbCo, the addition of SOT from top W and self-torque from $Co_{70}Tb_{30}$ leads to smoothly enhanced switching efficiency when the thickness of $Co_{70}Tb_{30}$ is increased. On the other hand, the competition of SOT from bottom W and self-torque in $Co_{70}Tb_{30}$ of W/$Co_{70}Tb_{30}$ devices was revealed by increasing the thickness of $Co_{70}Tb_{30}$. The comparison of two W-based structures reveals two critical points: (1) The self-torque effect in TbCo requires a threshold thickness (6 nm) to establish and (2)The sign of spin hall angle in $Co_{70}Tb_{30}$ is independent of the layer position which is very different from the traditional heavy metal and we attributed it to the bulk spin hall effect. Next, we measured the effective DMI effect for both systems by loop shift measurements[2]. With the increased $Co_{70}Tb_{30}$ thicknesses, we can clearly observe that the effective DMI fields are enhanced accordingly, as shown in Figure 2. It has been reported that the thick ferrimagnets have an additional contribution to the DMI effect from the bulk nature[3] due to the composition gradient, whatever the materials of the interfaces on the ferrimagnetic layer are, the consistent increment of the DMI effect is observed. According to our results, we can straightforwardly find a positive correlation between TbCo thickness and effective DMI fields, meaning that the composition gradient is critical for bulk SOT efficiency in amorphous systems. These results broaden

the scope of spin-orbitronics and provide a novel avenue for developing single-layer-based SOT memory with simplified architecture and improved scalability.

[1] P.-W. Lee, C.-C. Huang, S. Mangin, and C.-H. Lai, "Effects of self-torque in rare earth-transition metal alloy on the magnetization switching by spin-orbit torque," Journal of Magnetism and Magnetic Materials, vol. 563, 2022, doi: 10.1016/j.jmmm.2022.169879. [2] C.-F. Pai, M. Mann, A. J. Tan, and G. S. D. Beach, "Determination of spin torque efficiencies in heterostructures with perpendicular magnetic anisotropy," Physical Review B, vol. 93, no. 14, 2016, doi: 10.1103/PhysRevB.93.144409. [3] D. H. Kim et al., "Bulk Dzyaloshinskii-Moriya interaction in amorphous ferrimagnetic alloys," Nat Mater, vol. 18, no. 7, pp. 685-690, Jul 2019, doi: 10.1038/s41563-019-0380-x.

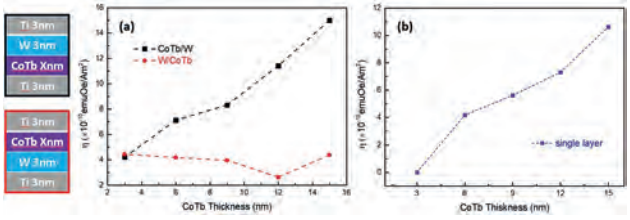

SOT switching efficiency comparison for (a) W-based system and (b) single layer system

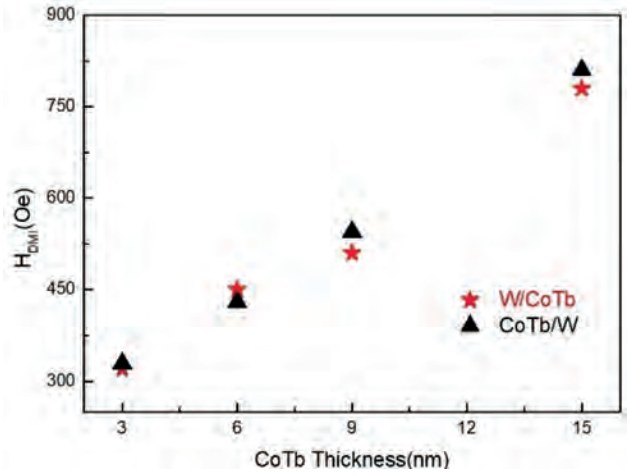

Effective DMI field as a function of CoTb thickness.

CE-11. Self-generated anomalous Hall spin-orbit torque.

E.A. Montoya[1,2], X. Pei[2] and I.N. Krivorotov[2] *1. Physics and Astronomy, University of Utah, Salt Lake City, UT, United States; 2. Physics and Astronomy, University of California, Irvine, Irvine, CA, United States*

Spin-orbit torques (SOTs) can be generated in bilayers of ferromagnetic (FM) and non-magnetic (NM) materials with broken inversion symmetry. SOTs enable the energy-efficient manipulation of magnetization by electric current, which is promising for future information technology – with applications in non-volatile memory [1], microwave-assisted magnetic recording [2], spin torque nano-oscillators (STNO) [3], and neuromorphic computing [4]. The most well-studied SOTs originate from spin Hall effect in the NM layer and Rashba effect at the NM/FM interface [5,6]. Recently, we have demonstrated that the planar Hall current in a FM can lead to a giant SOT applied to the same FM [7], an example of a new class of self-generated spin-orbit torques. In this talk, we will report the discovery of a giant self-generated SOT associated with the anomalous Hall effect (AHE) in the FM. This anomalous Hall torque displays an unusual angular symmetry that is distinct from the previously discovered SOTs. We demonstrate that the strength of the anomalous Hall torque can be tuned by filling of the FM electronic bands in the same manner as the AHE magnitude [8]. Finally, we demonstrate a new type of spin torque oscillator – the anomalous Hall nano-oscillator.

[1] N. Sato, F. Xue, R. M. White, *et al*., Nature Electronics, Vol. 1, p. 508 (2018) [2] H. T. Nembach, P. Martín Pimentel, S. J. Hermsdoerfer, *et al*., Applied Physics Letters, Vol. 90, p. 062503 (2007) [3] M. Haidar, A. A. Awad, M. Dvornik, *et al*., Nature Communications, Vol. 10, p. 2362 (2019) [4] J. Grollier, D. Querlioz, K. Y. Camsari, *et al*., Nature Electronics, Vol. 3, p. 360 (2020) [5] L. Liu, C.-F. Pai, Y. Li, *et al*., Science, Vol. 336, p. 555 (2012) [6] I. Mihai Miron, G. Gaudin, S. Auffret, *et al*., Nature Materials, Vol. 9, p. 230 (2010) [7] C. Safranski, E. A. Montoya, and I. N. Krivorotov, Nature Nanotechnology, Vol. 14, p. 27 (2019) [8] Z. Shi, H.-Y. Jiang, S.-M. Zhou, *et al*., AIP Advances, Vol. 6, p. 015101 (2016)

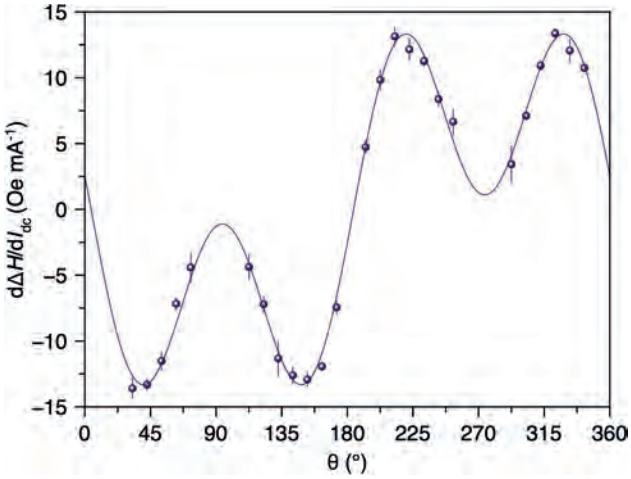

Spin-orbit torque angular dependence for magnetization in the yz-plane for Ta/Au/$Ni_{90}Fe_{10}$ nanowire.

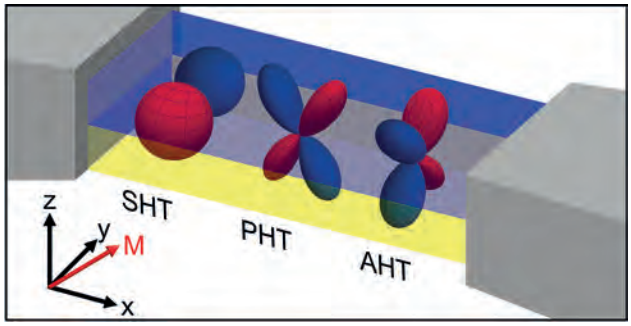

Spin orbit torque symmetries for spin Hall torque (SHT), planar Hall torque (PHT), and anomalous Hall torque (AHT). Red and blue lobes represent anti-damping and additional damping torques, respectively, for positive conventional current flowing in the x-direction.

Session CF
FUNDAMENTAL PROPERTIES IV: 2D AND TOPOLOGICAL MATERIALS

Rakshit Jain, Chair
Cornell University, Ithaca, NY, United States

INVITED PAPERS

CF-01. Decoding Spin Interactions in a Helical Spin Structure.
B. Wilfong[1], D. Graf[5], G.M. Stephen[6], R. Barua[4], S.P. Bennett[2], J. Prestigiacomo[2], D. Heiman[3] and *M.E. Jamer*[1] *1. Physics, United States Naval Academy, Annapolis, MD, United States; 2. Naval Research Laboratory, Washington, DC, United States; 3. Physics, Northeastern University, Boston, MA, United States; 4. Department of Mechanical & Nuclear Engineering, Virginia Commonwealth University, Richmond, VA, United States; 5. National High Magnetic Field Laboratory, Tallahassee, FL, United States; 6. Laboratory for Physical Sciences, College Park, MD, United States*

Fe_3Ga_4 is an exciting compound since the helical spin structure (HSS) results in a competition between two ground states - one ferromagnetic (FM) and one antiferromagnetic (AFM).[1] Through this ground state competition, there are multiple magnetic transitions of interest, where one is a meta-magnetic transition FM to AFM at 70 K, then an AFM to FM transition at 370 K.[2,3] The HSS in Fe_3Ga_4 allows for the metallicity to be retained in the AFM state, which makes this compound a candidate for room-temperature AFM spintronic applications and the helimagnetism can support topological skyrmion particles similar to MnSi and FeGe. While there is interest in exploring the topological Hall effect,[4] this presentation focuses on the axis-dependent magnetoresistance (MR) taken at the National High Magnetic Field Laboratory to further understand magnetic interactions. In this talk, we will discuss the magnetic ordering through magnetization and MR measurements on oriented single crystal Fe_3Ga_4 to further explore the HSS structure. The transport depends strongly on the crystal axes, which provides information on the exchange interactions of the spins with field and temperature. Furthermore, the changes in the MR between the *b*- and *c*-axes as a result of the temperature and field state of the HSS leads to three unique regions of the magnetic coupling of the Fe atoms. Along the *b*-axis, there is a positive MR at low fields and temperatures in the low temperature FM state that behaves similarly to a hopping model, which is not evident along the *c*-axis. The intermediate field region is overwhelmed by the electron-magnon scattering at higher temperatures, then the MR becomes linear at the highest fields for both axes. The MR results lead to important insights about this interesting spiral material leading to further understanding of the exchange in Fe_3Ga_4.

[1] J. Alloys and Comp. 894, 162421 (2022). [2] J. Alloys and Comp. 917, 165532 (2022). [3] J. Magn. and Magn. Mater. 563, 169964 (2022). [4] Phys. Rev. B 104, 094418 (2021).

CF-02. Quantum Annealers to Advance Understanding of Frustratred Magnetic Lattices.
A. Lopez-Bezanilla[2], A.D. King[1] and C. Nisoli[2] *1. D-Wave Quantum, Burnaby, BC, Canada; 2. Los Alamos National Laboratory, Los Alamos, NM, United States*

Quantum annealer technology is initiating a revolution in quantum computing and revolutionizing the field of magnetism research. D-Wave Quantum's specialized qubit-based computer harnesses superposition and entanglement to explore the ground and low-energy states of Ising-type systems. With quantum annealers, magnetic lattices find an ideal hardware platform to dynamically explore their manifold of configurations through the influence of quantum fluctuations. After providing an overview of the processor's fundamental operation, this presentation will delve into several ongoing studies that showcase the scientific advantages offered by this quantum technology. By manipulating individual magnetic moments, we can demonstrate Gauss' law for emergent magnetic monopoles in two dimensions and explore entropic monopole-monopole screening interactions [1]. Through experiments on a frustrated kagome qubit lattice, we have observed out-of-equilibrium behavior of quasi-particles resulting from successive annealing cycles [2]. In back-and-forth travel between quantum and classical worlds, fractional excitations wander within a topologically protected environment. Additionally, we replicate order-by-disorder-like phenomena in a frustrated quantum system, where an increase of the effective temperature paradoxically enhances long-range correlations between magnetic moments. Finally, a material prototyping study reveals multiple magnetic textures in a Penrose tiling when subjected to a modulating magnetic field [3].

[1] A.D. King, C. Nisoli, et al. Science, eabe282 (2021) [2] A. Lopez-Bezanilla, C. Nisoli, Science Advances Vol 9, Issue 11 (2023) [3] A. Lopez-Bezanilla, J. Carrasquilla, K. Boothby et al., Nature Communications 14, 1105 (2023)

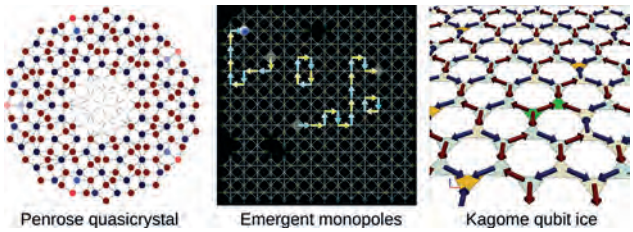

CONTRIBUTED PAPERS

CF-03. Correlation of Griffiths Phase with Magnetic Phase Transition in Nanocrystalline $La_{0.4}(Ca_{0.5}Sr_{0.5})_{0.6}MnO_3$.
S. Saha[1], S. Bandyopadhyay[2] and I. Das[1] *1. Condensed Matter Physics, Saha Institute of Nuclear Physics, Kolkata, India; 2. Department of Physics, University of Calcutta, Kolkata, India*

There is an immense deal of research interest for the past few decades on the origin of Griffiths phase (GP) due to its rich underlying physics [1-4]. A GP is a short-range ferromagnetic (FM) ordering appeared owing to the presence of FM clusters in the temperature region $T_C < T < T_G$ in a system [2]. T_C and T_G are magnetic transition and Griffiths temperature, respectively. Recently, the evolution of GP in nanomaterial has drawn attention owing to its dramatic variation of magnetic properties with decreasing particle size. However, a comprehensive study on the origin of GP and its correlation with the magnetic phase transition due to the formation of nano grains or grain boundary defects in such compounds is rare. Thus, a detailed investigation of a new compound $La_{0.4}(Ca_{0.5}Sr_{0.5})_{0.6}MnO_3$ has been carried out. It reveals the appearance of FM clusters, below $T_G = 350$ K and above $T_C = 274$ K, result in the emergence of GP in this nanomaterial (Fig. 1). Novel emphases in studying the isothermal magnetization, magnetocaloric effect (MCE) and critical analysis have been given besides the conventional study of temperature dependence inverse

magnetic susceptibility, with an aim to probe the GP and to reveal the origin of such novel phase formation. The GP slows down the spin dynamics in that region and the spin interaction is Ising-type (inset Fig. 1) [5]. Albeit, from the critical analysis, unusual critical exponents are observed, which does not follow a particular spin-interaction. Thus, a correlation between the unusual critical parameters with the GP has been furnished. Moreover, minimum 5 Mn-ions reside in each FM cluster that has also been confirmed by matching the simulation curves with the experimental MCE curves (Fig. 2). On the basis of various experimental observations and related theoretical study based on different proposed models, it has been observed that the strain field, developed owing to the surface pressure effect along with grain boundary defects of core-shell structure, plays a pivotal role in nanomaterial to grow and stabilize the GP.

1. M. B. Salamon, P. Lin, and S. H. Chun, Phys. Rev. Lett. 88, 197203 (2002) 2. R. B. Griffiths, Phys. Rev. Lett. 23, 17 (1969) 3. P. Tong, B. Kim, D. Kwon, Phys. Rev. B 77, 184432 (2008) 4. S. Ubaid-Kassis, T. Vojta, and A. Schroeder, Phys. Rev. Lett. 104, 066402 (2010) 5. T. Vojta, J. Phys. A: Math. Gen. 39, R143 (2006)

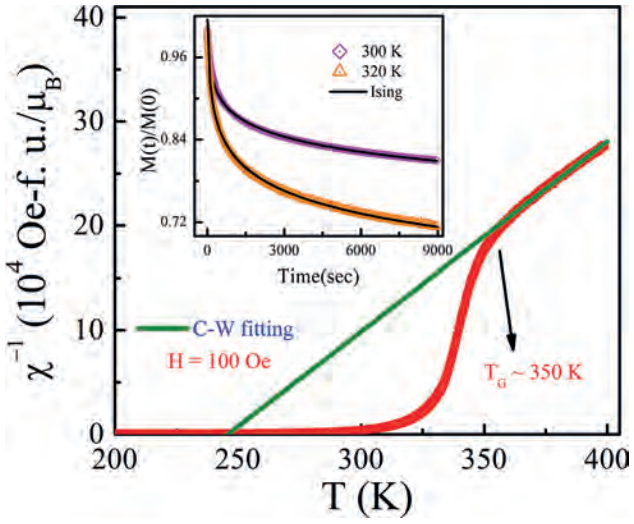

Inverse magnetic susceptibility and Griffiths phase. Inset: Ising fit of IRM at GP

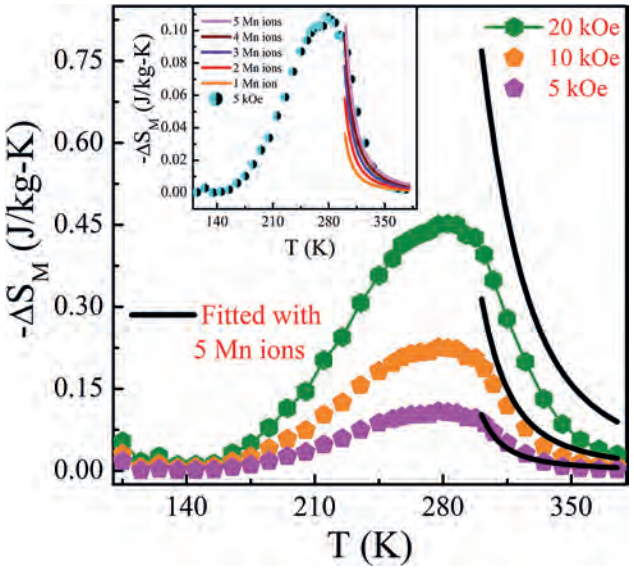

MCE theoretical matching for 5 Mn-ions. Inset: 1 to 5 Mn-ions fitting for H = 5 kOe

CF-04. Magnetic properties of microwave-processed ferromagnetic La_2CoMnO_6. M. Marimuthu[1] and *R. Mahendiran*[1] *1. Physics, National University of Singapore, Singapore*

The double perovskite La_2CoMnO_6 is a ferromagnetic insulator with a high Curie temperature (T_C = 220-225 K) exhibiting magnetoelectric property [1]. The origin of ferromagnetism in this compound is positive superexchange interaction among Co^{2+} and Mn^{4+} ions which order next to each other in a rock-salt type pattern. However, the ordering of these transition metal cations is severely affected by synthesis conditions[2,3]. The presence of Co^{2+} at the Mn^{4+} site and vice versa, known as antisite disorder, promotes local antiferromagnetic interaction which competes with long-range ferromagnetism. Traditionally, this compound is synthesized via a solid-state reaction of oxide precursors at a high temperature (T ≥ 1000°C) or a low-temperature wet chemical synthesis route, both of them take several days to obtain a well-sintered pellet. Here, we report the fast synthesis of single phase La_2CoMnO_6 (monoclinic structure, $P2_1/n$ space group) within 45 minutes by irradiating oxides precursors using microwave radiation of frequency 2.45 GHz and a microwave power of 1600 Watt. The exact mechanism of microwave synthesis is not fully understood yet though dielectric heating due to microwave losses can not be ruled out. Investigation of magnetization (M) reveals that the sample orders ferromagnetically at 220 K and M = 5.18 μ_B/f.u at 10 K and H = 5 T which is lower than 6 μ_B/f.u. expected for fully ordered B-site cations. We intend to alter the synthesis condition (change in microwave power or final temperature) to study its influence on saturation magnetization, Curie temperature, and ferromagnetic resonance to quantitatively understand the anti-site disorder effect, which will be reported in this conference. Acknowledgments: This work was supported by the Ministry of Education, Singapore through Grant No. A-8000924-00-00.

[1] M. P. Singh et al., Appl. Phys. Lett. 91,042504 (2007); J. Krishnamurthy, and J. Venimadhav, J. Appl. Phys. 111, 024102 (2012). [2] G. Blasse, J. Phys. Chem. Solids 26, 1969 (1965); R. I. Das and J.B. Goodenough, Phys. Rev. B 67, 014401 (2003). [3] L. Lopez-Mir *et al*. Phys. Rev. B, 95, 224434 (2017); K. Manna, S. Elizabeth, and P. S. Anil Kumar, J. Appl. Phys. 119, 043906 (2016).

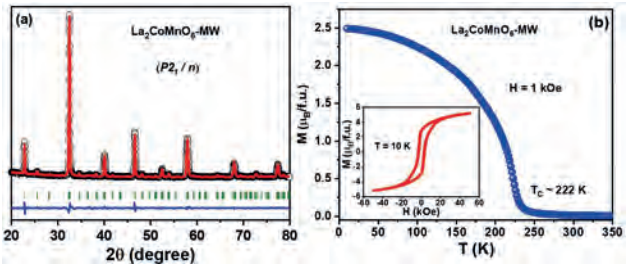

Fig. 1 (a) Powder X-ray diffraction (symbol) and Rietveld fit (line) for the microwave synthesized La_2CoMnO_6, (b) Temperature dependence of magnetization (M) under a magnetic field of H = 1 kOe. Inset: M versus H at 10 K.

CF-05. First-principle Calculations of Magnetic Properties of $Ho_6(Fe,Mn)Bi_2$ Compounds for Magnetic Refrigeration Applications. *A.J. Garcia-Adeva*[1], E. Apiñaniz[1], A. Herrero Hernandez[2], I.R. Aseguinolaza[2] and A. Oleaga[2] *1. Departamento de Física Aplicada, Universidad del País Vasco (UPV/EHU), Vitoria, Spain; 2. Departamento de Física Aplicada, Universidad del País Vasco (UPV/EHU), Bilbao, Spain*

Ternary intermetallic compounds have received a great deal of attention, since these compounds show interesting magnetic properties that are of interest for refrigeration applications. In particular, our research group has pursued a comprehensive study of the intermetallic family R_6TX_2, where R is a rare earth element, T is a transition metal, and X is either of Bi, Te, or Sb [1, 2, 3, 4]. Many members of this family exhibit two magnetic phase transitions with relevant magnetocaloric effect that extend, in some

cases, around room temperature. They also possess very complex magnetic properties, which is a subject of fundamental interest in itself. Indeed, most of these compounds exhibit a paramagnetic (PM) to ferromagnetic (FM) phase transition at an intermediate temperature. Moreover, there is a second phase transition at very low temperature to a non-collinear spin order. The case of Ho_6 (Fe,Mn)Bi_2 is especially striking since the PM to FM transition temperature changes from 72 K for the Fe compound to 203 K for the Mn one and it grows linearly upon Fe substitution by Mn [1]. It would be desirable to be able to devise microscopic theoretical models that would help us understanding these intriguing magnetic properties and act as a guide in the search of novel materials which possess adequate magnetic properties for refrigeration applications. Unfortunately, microscopic analytical models for these compounds are extremely difficult to develop and they only provide qualitative results in real systems. For this reason, we have studied the Ho_6MnBi_2 and Ho_6FeBi_2 crystals on the framework of the density functional theory in order to theoretically investigate their intriguing magnetic properties. The equation of state (Fig. 1), magnetic moments, and total and projected magnetic densities of states (Fig. 2) have been calculated. Also, by using a combination of both first principle calculations and simple analytical mean field theory, the exchange couplings between magnetic ions and the corresponding Curie temperatures of the magnetic phase transition have been calculated and a good agreement with our previous experimental results is found.

[1] A. Herrero, A. Oleaga, A. Salazar, A. Garshev, V. Yapaskurt, A. Morozkin, Journal of Alloys and Compounds 821 (2020) 153198. doi:10.1016/j.jallcom.2019.153198. [2] A. Oleaga, A. Herrero, A. Salazar, A. Garshev, V. Yapaskurt, A. Morozkin, Journal of Alloys and Compounds 843 (2020) 155937. doi:10.1016/j.jallcom.2020.155937. [3] A. Herrero, A. Oleaga, I. Aseguinolaza, A. Garcia-Adeva, E. Apiñaniz, A. Garshev, V. Yapaskurt, A. Morozkin, Journal of Alloys and Compounds 890 (2022) 161849. doi:10.1016/j.jallcom.2021.161849. [4] A. Herrero, I. R. Aseguinolaza, A. Oleaga, A. J. Garcia-Adeva, E. Apiñaniz, A. V. Garshev, V. O. Yapaskurt, A. V. Morozkin, Dalton Transactions 52 (17) (2023) 5780–5797. doi:10.1039/D3DT00223C.

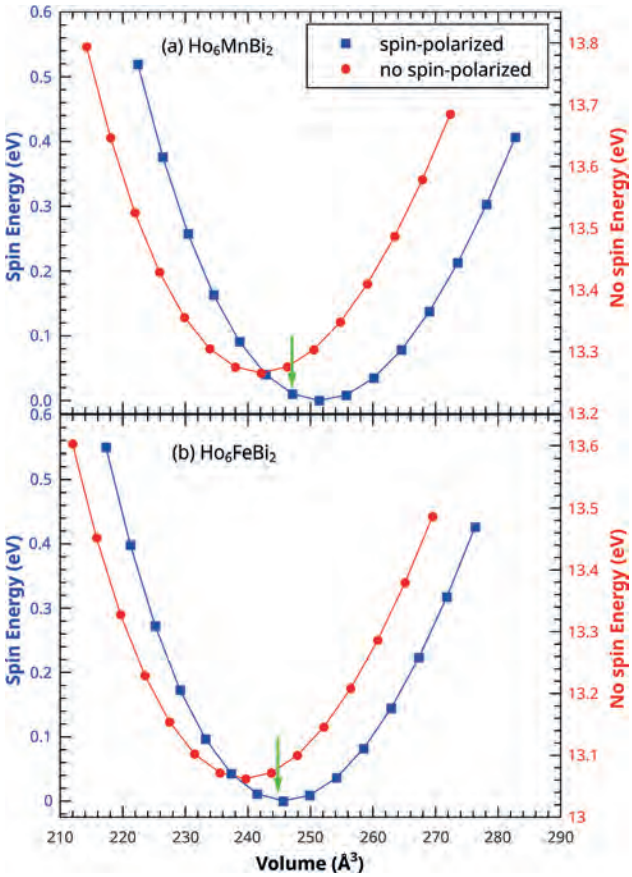

Fig. 1: Equation of state.

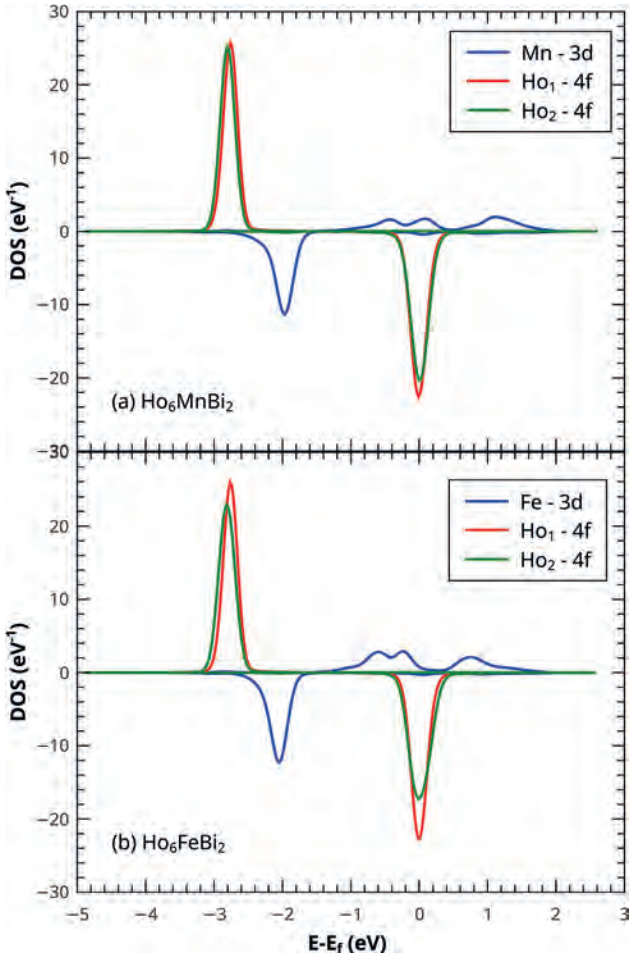

Fig. 2: Projected magnetic density of states

CF-06. Transport and magnetic transitions in Dirac fermion system via the Zeeman field. *H. Lin*[2], T. Ma[1] and J. Meng[1] *1. Physics, Beijing Normal University, Beijing, China; 2. School of Physics, Zhejiang University, Hangzhou, China*

Since Slater argued that a gap could be opened by magnetic ordering with spin-dependent electronic energy, applying a magnetic field has been a powerful means to elucidate novel phenomena. Using the determinant quantum Monte Carlo method, we investigate phase transitions induced by the Zeeman field in a disordered interacting two-dimensional Dirac fermion system. The interplay between Coulomb repulsion U, disorder Δ, and magnetic fields B, drives the otherwise semimetallic regime to insulating phases exhibiting different characters. And the critical Zeeman field B_c is largely reduced by the presence of the electronic interaction and quenched disorder. As the magnetic field continues to increase, the B-induced symmetry breaking introduces an antiferromagnetic(AFM) phase, and eventually the system enters a fully spin-polarized state. Due to the promoting effect of U on polarization in the presence of the magnetic field, strong interactions with B≠0 would suppress the AFM order, while weak interactions would enhance the AFM order. U_c~4.5 which is the critical strength inducing the metal-Mott insulator transition in a clean system divides these two ranges.

[1] J. Meng, R. Mondaini, T. Ma, and H.-Q. Lin, Phys. Rev. B 104, 045138 (2021). [2] J. Meng, L. Zhang, T. Ma, and H.-Q. Lin, Phys. Rev. B 105, 205121 (2022)

CF-07. Control of the asymmetric band structure in Mn_2Au by a ferromagnetic driver layer. *Y. Lytvynenko*[1,2], O. Fedchenko[1], S. Chernov[1,3], S. Babenkov[1], D. Vasilyev[1], O. Tkach[1,4], A. Hloskovsky[3], T. Peixoto[3], C. Schlueter[3], V. Grigorev[1,5], M. Filianina[1,5], S. Sobolev[1], A. Kleibert[6], M. Kläui[1], J. Demsar[1], G. Schönhense[1], M. Jourdan[1] and H. Elmers[1] *1. Institute of Physics, Johannes Gutenberg-University, Mainz, Germany; 2. Institute of Magnetism of the NAS and MES of Ukraine, Kyiv, Ukraine; 3. Deutsches Elektronen-Synchrotron DESY, Hamburg, Germany; 4. Sumy State University, Sumy, Ukraine; 5. Department of Physics, Stockholm University, Stockholm, Sweden; 6. Paul Scherrer Institute, Swiss Light Source, Villigen, Switzerland*

Antiferromagnets (AFMs) have recently attracted scientific interest due to their potential applications in the field of spintronics. The orientation of the staggered magnetization of collinear AFM, i.e., the Néel vector, could be used as an information carrier similar to the magnetization vector in ferromagnets. A promising approach for Néel vector manipulation is based on the Néel spin-orbit torque (NSOT), which corresponds to a staggered effective field generated by an electric current in the bulk of metallic AFMs with a specific crystal lattice symmetry and strong spin-orbit interactions, such as CuMnAs and Mn_2Au [1]. At the microscopic electronic structure level, the manipulation of the Néel vector results in changes in the electronic properties [2], which, in Mn_2Au, show up as an asymmetry in the electronic band structure, $E(k) \neq E(-k)$ [3, 4]. In this work, the hard X-ray angle-resolved photoemission spectroscopy reveals the momentum-resolved band structure in an epitaxial $Mn_2Au(001)$ film capped by a 2 nm thick ferromagnetic Permalloy (Py) layer. By magnetizing the Py layer, the exceptionally strong exchange bias aligns the Néel vector in the $Mn_2Au(001)$ film [5]. Uncompensated Mn interfacial magnetic moments in Mn_2Au are identified as the origin of the exceptional exchange bias using X-ray magnetic circular dichroism in combination with photoelectron emission microscopy. Using time-of-flight momentum microscopy, we measure the asymmetry of the band structure, $E(k) \neq E(-k)$, in Mn_2Au resulting from the homogeneous orientation of the Néel vector. Comparison with theory shows that the Néel vector, determined by the magnetic moment of the top Mn layer, is oriented antiparallel to the Permalloy magnetization. Our experimental results demonstrate that hard X-ray photoemission spectroscopy can measure the band structure of epitaxial layers beneath a metallic capping layer. We thus confirm that the ferromagnetic capping layer controls the bulk band structure of the AFM film [6].

1. J. Zelezny, H. Gao, K. Vyborny, et al., Phys. Rev. Lett. 113, 157201 (2014) 2. A. G. Linn, P. Hao, K. N. Gordon, et al., npj Quant. Mat. 8, 19 (2023) 3. H. J. Elmers, S. V. Chernov, S. W. D'Souza, et al., ACS Nano 14, 17554 (2020) 4. O. Fedchenko, L. Smejkal, M. Kallmayer, et al., J. Phys.: Cond. Matt. 34, 425501 (2022) 5. S. P. Bommanaboyena, D. Backes, L. Veiga, et al., Nat. Comm. 2, 6539 (2021) 6. Y. Lytvynenko, O. Fedchenko, S. Chernov, et al., arXiv:2306.14713 (2023)

CF-08. Withdrawn

CF-09. Study of Spin Glass State in Co doped $NdMnO_3$. *F.H. Bhat*[1] and G. Anjum[2] *1. Physics, Islamic University of Science and Technology, Awantipora, India; 2. Physics, S P College, Srinagar, India*

The spin glass (SG) behaviour in $NdMn_{0.6}Co_{0.4}O_3$ has been studied using temperature dependent ac susceptibility measurement of in-phase (χ'_{ac}) and out of phase component (χ_{ac}''). The measurement was performed in an *ac* field of 4 Oe and 0 Oe *dc* field at frequencies of 111 Hz, 311 Hz, 1011 Hz, and 1311 Hz. The peak position in χ'_{ac}, corresponding to T_f, moves towards higher temperatures with it's magnitude decreasing as the frequency increases. This is a strong indication of the existence of SG state and absence of long range feromagnetic (FM) ordering. Temperature variation for out of phase component or imaginary part of ac susceptibility χ_{ac}'' at different frequencies is just opposite to χ_{ac}' and agrees with the existence of SG state. The parameter

called relative shift in freezing temperature (δT_f) per decade of frequency on a logarithmic scale is a handy tool to distinguish between different SG systems. It's value for the sample under study is found to be $\delta T_f = 0.0089$ which agrees with the one reported for canonical SG systems [1,2]. In order to confirm the existence of canonical SG state in the $NdMn_{0.6}Co_{0.4}O_3$ sample the ac susceptibility data was further analyzed using Arrhenius, Vogel Fulcher, and Power –law. Using Arrhenius law the relaxation time τ_0 of a single spin flip of the fluctuating entities was found to be $\tau_0 \sim 10^{-122}$ s and the barrier height $E_a/k_B = 37407$, these are quite unrealistic values thus ruling out the existence of superparamagnetic state in $NdMn_{0.6}Co_{0.4}O_3$. The value of τ_0 obtained using Vogel Fulcher and Power –law is of the order of $\sim 10^{-13}$ s which is distinctive value of canonical SG system. Further, the value of $z\nu'$ ~7 for the sample under study, where z is the dynamical exponent and ν' is the critical exponent of the spin correlation length. For canonical SG system $z\nu'$ lies in the range of 4 -12. The criterion introduced by Tholence [3] $\delta T_{Th} = (T_f - T_0)/T_f$ is used to compare different SG systems. As per this criterion, the value of δT_{Th} obtained for $NdMn_{0.6}Co_{0.4}O_3$ ~0.07 which are one order of magnitude less than the values reported for clsuter glass state [1]. These values are comparable to those obtained for canonical SG system like CuMn [3].

1. J. A. Mydosh, *Spin Glasses: An Experimental Introduction* (1993). 2. N. Khan, A. Midya, P. Mandal, and D. Prabhakaran, J. Appl. Phys. 113, (2013)183909. 3. J. Souletie and J. L. Tholence, Phys. Rev. B 32, 516 (1985).

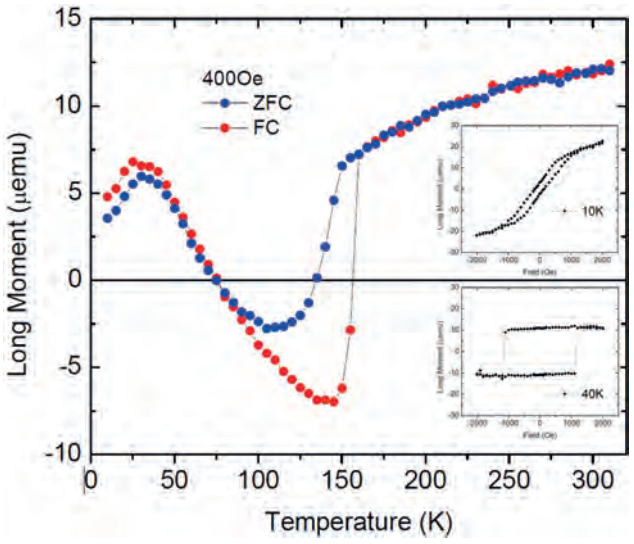

Fig. 1 SQUID measurements of Magnetization vs. Temperature of 3Ta/3Pt/0.8Co/1.8Gd/3Pt (nm) in perpendicular field orientation. M = 0 at roughly 80K and glassy feature is present at low temperatures. Insets show M vs. H at 10K and 40K indicating change in anisotropy.

CF-10. Glassy magnetism in bilayer Co/Gd metallic ferrimagnets.

L.A. Hernandez[1], R. Greening[1], M. Roos[1], X. Fan[1] and B.L. Zink[1]
1. Physics and Astronomy, University of Denver, Denver, CO, United States

Metallic ferrimagnets, where two antiferromagnetically coupled subsystems are not fully compensated, are a growing area of interest in spintronics and related fields [1]. This interest encompasses diverse applications, from skyrmion memories, to all-optical switching, to ionic gating that changes the magnetization compensation temperature [2,3,4]. While use of metallic alloys combining rare earth and transition metal components is a fairly common route to creating these films, some recent work employs bilayers, often grown in heterostructures with heavy metal components to introduce perpendicular magnetic anisotropy [5]. In this talk we present SQUID magnetometry, with supporting anomalous Hall effect measurements, on Ta/Pt/Co/Gd/Pt thin-film heterostructures, which show clear features of glassy magnetism [6]. As shown in Fig. 1, splitting between magnetization vs. temperature measured in field cooled (FC) and zero-field cooled (ZFC) states appears below approximately 30 K, where the M vs. H loop also clearly indicates a mixed anisotropy. For low cooling fields a large, reversed splitting between FC and ZFC remains until much higher temperatures, finally collapsing well above the temperature where the total film magnetization is zero. These two temperatures, as shown in Fig. 2, likely indicate the magnetization and angular momentum compensation points in this Co/Gd metallic ferrimagnet [7, 8]. The source of the frustration driving the emergence of this glassy phase in the nominal absence of random alloy disorder is not yet clear, but could have impact on applications based on these metallic ferrimagnets.

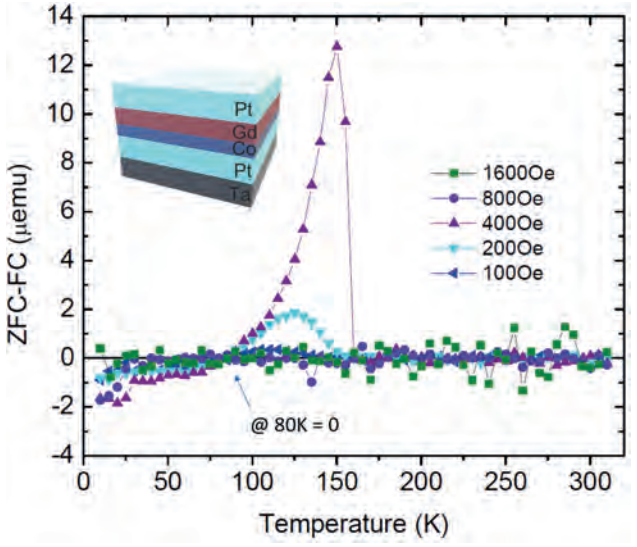

Fig. 2 Difference of ZFC and FC values plotted vs. Temperature. Multiple ZFC/FC runs at increasing field values are shownfor perpendicular orientation. A crossing of 0 at 80K is consistent through all field values. Inset shows thin-film heterostructure.

[1] J. Finley and Luqiao Liu, *Appl. Phys. Lett.* 116, 110 50 1 (2020) [2] J. Brandao, D. A. Dugato, M.V. Puydinger dos Santos, J. C. Cezar, *ACS Appl, Nano Mater.* 2019, 2, 7532-7539 [3] X. Ren, L. Liu, B. Cui, B. Cheng, W. Liu, T. An, R. Chu, M. Zhang, T. Miao, X. Zhao, G. Zhou, J. Hu, *Nano Lett.* 2023, XXXX, XXX, XXX-XXX [4] M. Binder, A. Weber, O. Mosendz, G. Woltersdorf, M. Izquierdo, I. Neudecker, J.R. Dahn, T. D. Hatchard, J. U. Thiele, C. H. Back, M. R. Scheinfein, *Phys. Rev. B* 74, 134404 (2006) [5] R. Bläsing, T. Ma, SH. Yang, C. Garg, F. K. Dejene, A. T. N'Diaye, G. Chen, K. Liu, S. S. P. Parkin, *Nat Commun* 9, 4984 (2018). [6] V. Tsurkan, M. Baran, R. Szymczak, H. Szymczak, R. Tidecks, *Physica B* 296 (2001) 301-305. [7] J. Barker, U. Atxitia, *J. Phys. Soc. Jpn.* 90, 081001 (2021) [8] L. Hernandez, R. Greening, X. Fan, B. L. Zink, "Glassy magnetism in bilayer Co/Gd metallic ferrimagnets" *In preparation*

Session CG
BIOMEDICAL APPLICATIONS I

Arno Ehresmann, Chair
University of Kassel, Kassel, Germany

INVITED PAPER

CG-01. Wireless Brain Stimulation With Magnetoelectric Nanoparticles.
P. Liang[1], E. Zhang[2], M. Abdel-Mottaleb[3], S. Chen[4,1], V. Andre[3], M. Shotbolt[3] and *S. Khizroev*[2,5] *1. Cellular Nanomed, Irvine, CA, United States; 2. Electrical and Computer Engineering, University of Miami, Coral Gables, FL, United States; 3. Biomedical Engineering, University of Miami, Coral Gables, FL, United States; 4. Chemical, Environmental and Materials Engineering, University of Miami, Coral Gables, FL, United States; 5. Biochemistry and Molecular Biology, University of Miami, Miami, FL, United States*

Due to their magnetoelectric effect, magnetoelectric nanoparticles (MENPs) enable a pathway to a noninvasive wireless brain-machine interface (BMI) with record high spatial and temporal resolutions, without a need for genetic modification.[1] However, to fully realize the enormous potential of this approach, several technological roadblocks need to be overcome. Besides the need to further maximize the magnetoelectric effect,[2] these roadblocks relate to the capability to target the neuronal membrane, minimize the nanoparticles' agglomeration, and control the magnetic field energy localization with metastable physics.[3] This presentation discusses *in vitro* and *in vivo* studies to demonstrate wireless targeted deep brain stimulation with MENPs. It also gives a perspective on the future potential impacts of this technology. For example, according to the Principle of Reciprocity, MENPs can be used not only to wirelessly write information in the brain, i.e., stimulate or modulate neural circuits, but also to wirelessly read it back, i.e., record neural activity. To realize the latter, MENPs will need to be integrated with high-resolution magnetic imaging technologies such as magnetic resonance imaging (MRI) or the recently emerged magnetic particle imaging (MPI). Furthermore, having the potential to enable a two-way wireless BMI with high spatial and temporal resolutions, MENPs have the potential to shed light on the computing architecture of the brain as well as revolutionize the field of neurological medicine.

1. K. Yue, R. Guduru, J. M. Hong, P. Liang, M. Nair and S. Khizroev, Plos One 7 (9) (2012). 2. P. Wang, E. Zhang, D. Toledo, I. T. Smith, B. Navarrete, N. Furman, A. F. Hernandez, M. Telusma, D. McDaniel, P. Liang and S. Khizroev, Nano Lett 20 (8), 5765-5772 (2020). 3. E. Zhang, M. Abdel-Mottaleb, P. Liang, B. Navarrete, Y. A. Yildirim, M. A. Campos, I. T. Smith, P. Wang, B. Yildirim, L. Yang, S. Chen, I. Smith, G. Lur, T. Nguyen, X. Jin, B. R. Noga, P. Ganzer and S. Khizroev, Brain Stimul 15 (6), 1451-1462 (2022).

CONTRIBUTED PAPERS

CG-02. Wireless Multi-channel Control over Motor Cortex with Magnetoelectric Nanoparticles.
E. Zhang[1], M. Abdel-Mottaleb[2], M. Alberteris[1], B. Navarrete[1], V. Andre[2], M. Shotbolt[2], I. Smith[2], B. Noga[3], P. Liang[4] and S. Khizroev[1] *1. Electrical and Computer Engineering, University of Miami, Coral Gables, FL, United States; 2. Biomedical Engineering, University of Miami, Coral Gables, FL, United States; 3. Neurosurgery, University of Miami, Miami, FL, United States; 4. Cellular Nanomed, Irvine, CA, United States*

The brain is an incredibly complex organ with 100 billion neurons and 100 trillion connections that make it difficult to study while intact. Despite this, localized brain stimulation is clinically relevant in restoring sensory and motor functions and in treating neurological diseases[1] such as Parkinson's and essential tremor. However, the risks associated with implanting electrodes in brain tissue (e.g., surgical complications, inflammation, and degrading performance) confine the technique to last resort medical cases and prohibits exploring functional and enhancement applications. Alternative neurostimulation methods based on magnetic fields, ultrasound[2], guided electric fields, and optogenetics[3] have recently come about. However, modern magnetic methods such as magnetomechanical[4] and Transcranial Magnetic Stimulation[5] have tradeoffs with temporal and spatial resolution, especially for deep brain regions. Recently proposed Magnetoelectric Nanoparticles (MENPs) can offer the best of both worlds[6], obtaining both high spatial localization and low latency activation. The particles work as nanoscale transducers, efficiently converting external, low-power magnetic fields into short range, stimulating electric fields. This approach is blood brain barrier permeable, reducing the need for extensive surgery, and can be guided into place by magnetic fields, antibodies, and magnetic robots[7]. Existing studies have successfully shown broadscale activation of neural responses, sufficient to trigger neural activity in vitro[6] and adjust behavioral responses in vivo[8]. This study further enhances the method by demonstrating precision control over 7 motor responses corresponding to a 1 mm2 region of a rat motor cortex. The response differentiation is controlled completely externally through varied magnetic spatiotemporal profiles, which opens the possibility for a non-surgical, wireless, multichannel brain-machine interface.

1 J.M. Bronstein, M. Tagliati, R.L. Alterman, Arch. Neurol. 68(2), (2011). 2 Y. Tufail, A. Yoshihiro, S. Pati, Nat. Protoc. 6(9), 1453–1470 (2011). 3 K. Deisseroth, Nat. Methods 8(1), 26–29 (2011). 4 D. Gregurec, A.W. Senko, A. Chuvilin, ACS Nano 14(7), 8036–8045 (2020). 5 M. Hallett, Neuron 55(2), 187–199 (2007). 6 E. Zhang, M. Abdel-Mottaleb, P. Liang, Brain Stimulat. 15(6), 1451–1462 (2022). 7 H. Zhou, C.C. Mayorga-Martinez, S. Pané, Chem. Rev. 121(8), 4999–5041 (2021). 8 K.L. Kozielski, A. Jahanshahi, H.B. Gilbert, Sci. Adv. 7(3), eabc4189 (2021).

CG-03. Optimized Design of Transcranial Magnetic Stimulator Coils with Reduced Influence of Individual Variabilities of Head Geometry.
S. Liu[1], A. Kuwahata[2] and *M. Sekino*[1] *1. Department of Bioengineering, Graduate School of Engineering, The University of Tokyo, Tokyo, Japan; 2. Graduate School of Engineering, Tohoku University, Sendai, Japan*

Transcranial magnetic stimulation (TMS) is an emerging treatment for depression with a painless and noninvasive neuromodulation function [1]. The winding path of the TMS coil can be realized in several ways [2]. For instance, the H1 coil is designed for deep brain stimulation [3], the hat-like coil is designed to suppress temperature rise during stimulation [4], and the fdTMS coil comprehensively considers energy, depth, and focality [5]. However, a practical TMS coil satisfying both high energy efficiency and robustness against individual variabilities in head shape has not yet been realized. The purpose of this study is to optimize an energy-efficient TMS coil that is robust against individual differences in head shape. The optimization scheme is shown in Fig. 1. Multiple MRI anatomical images are used to optimize the shape to facilitate fitting of the scalp at the target stimulation position. Subsequently, the winding path of this shape is optimized through the following steps. First, the forward model $E=A\Psi$ for the scalar stream function Ψ and target induced electric field E is established. Second, the Tikhonov regularization is used to solve the stream function Ψ numerically, given E. Finally, the coil winding path is extracted from the contour lines of Ψ [6]. This coil was compared with two commercially-available TMS coils by simulating the eddy current distribution in the digital brain model. The results are shown in Fig. 2. Under the same energy consumption condition, compared with planar figure-eight and butterfly coils, the proposed head-fit coil has stimulus area increases of 87% and 67%, respectively, with the corresponding efficiency drops of only 2% and 3%. The expansion of the stimulation area indicates that stimulation to the target area can be ensured even with a slight movement of the head during 20–30 min of treatment. Furthermore, considering the shape of the scalp of different subjects facilitates close fitting of the head. Our method allows the design of TMS coils suitable for practical TMS therapy.

[1] J. P. Lefaucheur et al., Clin. Neurophysiol., vol. 125, no. 11. Elsevier Ireland Ltd, pp. 2150–2206, 2014. [2] Z. De Deng, S. H. Lisanby, and A. V. Peterchev, Brain Stimul., vol. 6, no. 1, pp. 1–13, Jan. 2013. [3] H. M. Gellersen and K. K. Kedzior, BMC Psychiatry, vol. 19, no. 1, pp. 139, 2019. [4] L. M. Koponen, J. O. Nieminen, and R. J. Ilmoniemi, Brain Stimul., vol. 10, no. 4, pp. 795–805, 2017. [5] L. J. Gomez, S. M. Goetz, and A. V. Peterchev, J. Neural Eng., vol. 15, no. 4, pp. 1–31, 2018. [6] G. N. Peeren, J. Comput. Phys., vol. 191, no. 1, pp. 305–321, 2003.

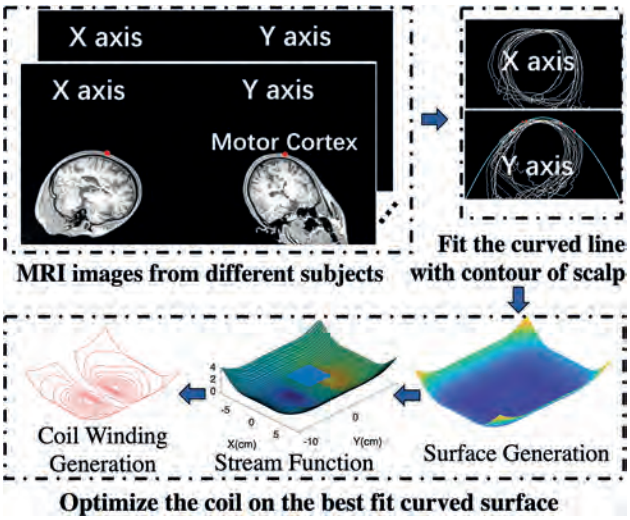

Fig. 1. Schematic for the optimization of the TMS coils using stream function

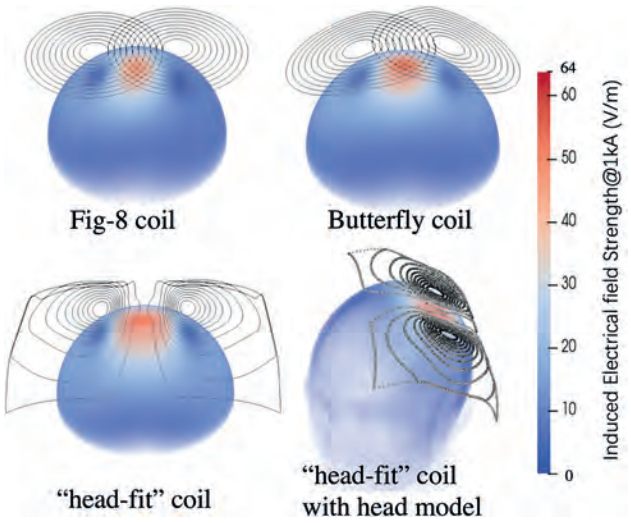

Fig. 2. Simulation result on the hemisphere model for the figure-eight coil, butterfly coil, and the head-fit coil

CG-04. Assessing Drug Loaded Magnetic Nanoparticles Concentration with Magnetoelectric Based Lab-On-A-Chip Device for Diagnostic Applications.
P. Pathak[1*], V.K. Yadav[1], S. Das[2] and D. Mallick[1] *1. Electrical Engineering, Indian Institute of Technology Delhi, New Delhi, India; 2. CARE, Indian Institute of Technology Delhi, New Delhi, India*

Lately, magnetic nanoparticles (MNPs) have gained significant attention in the field of nanomedicine, offering great potential for various biological applications. These MNPs incorporated into nanomedicines, have demonstrated the ability to precisely target specific regions while minimizing potential harm to healthy tissues[1]. To ensure the therapeutic efficacy of these nanomedicines, it is crucial to accurately measure the quantity of transported MNPs and the concentration of the attached drugs, as this step determines whether the desired dosage reaches the target site. Unfortunately, the current quantification methods rely on large external electromagnets, which not only incur high costs but also inefficient in energy usage[2]. Recently, magnetoelectric (ME) devices have emerged as a promising alternative in the field of biomedicine. These devices have gained attention due to their ability to sort and deliver MNPs and offer an ultra-low energy pathway without the need for high-powered external electromagnets [3]. However, the quantitative assessment of captured or released MNPs and the concentration of attached drugs has not been extensively explored, which hampers the broader application of ME devices in critical biomedical applications. This study introduces the development of an ME heterostructure-based sensor that utilizes a combination of nickel (Ni) and PMN–PT piezoelectric substrate (Fig 1). Injected MNPs are attracted by the field gradient generated by Ni thin film. Subsequently, the concentration of the captured MNPs and attached drugs is measured by the optothermal-pyroelectric property of PMN-PT. At zero external bias, it exhibits varying photoresponse upon exposure to an incident infrared (IR) pulse, which directly correlates with the concentration of injected MNPs (Fig 2). The photocurrent generated by the device demonstrates an almost linear relationship with the concentration of MNPs. By employing such a device, new possibilities arise for controlled drug delivery, hyperthermia treatments, and cell labeling applications.

[1] J. Huang, Y. Li, A.Orza, Advanced Functional Materials, 26, 3818 (2016). [2] A. Cheung, A.Neyzari, Cancer Research, 44, 4736 (1984). [3] R.Khojah, Z.Xiao, Advanced Materials, 33, 2006651 (2021).

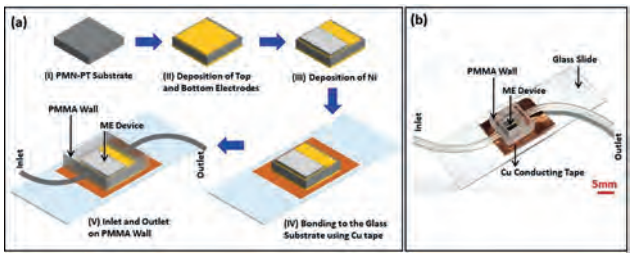

(a) Fabrication Flow of the developed ME based sensor and (b) Fabricated Device

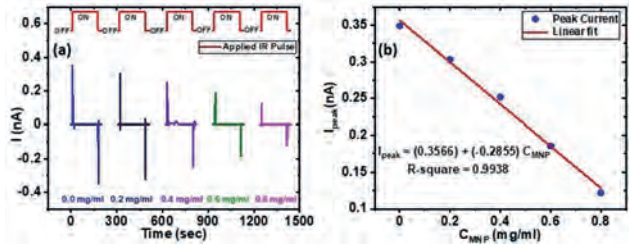

(a) Photoresponse and (b) corresponding peak current variation against different MNP concentration

CG-05. Novel Multi-Magnetic Material Transcranial Magnetic Stimulation (TMS) Coil Designs for Small Animals Application.
M. Tashli[1], A. Mhaskar[2,1], G. Weistroffer[3], D. Kumbhare[4], M. Baron[5,6] and R.L. Hadimani[1,7] *1. Mechanical and Nuclear Engineering, Virginia Commonwealth University, Richmond, VA, United States; 2. Biomedical Sciences, Mills E. Godwin High School, Richmond, VA, United States; 3. Biomedical Engineering, Virginia Commonwealth University, Richmond, VA, United States; 4. Neurosurgery, Louisiana State University Health Center, Shreveport, LA, United States; 5. McGuire Research Institute, Hunter Holmes McGuire VA Medical Center, Richmond, VA, United States; 6. Neurology, Virginia Commonwealth University, Richmond, VA, United States; 7. Martino's Biomedical Imaging Center, Harvard Medical School, Boston, MA, United States*

Transcranial magnetic stimulation (TMS) is a non-invasive therapeutic approach used to treat various psychiatric and neurological disorders. It is FDA approved treatment of depression, obsessive-compulsive disorder and smoking cessation [1]–[3]. Recently, there has been a notable increase in research exploring the potential of TMS for addressing a broader range of neurological and psychiatric disorders. However, in order to effectively apply TMS to these conditions, it is crucial to ensure that the electric field is focused to specific regions within the brain [4]. Several coil configurations have been proposed aiming to enhance the focality of TMS coils. However, a limited number of these designs have incorporated soft magnetic materials as coil cores, as well as explored different core shapes, to further enhance the concentration of the E-field due to saturation magnetization limit of the cores. In this study, we examined innovative TMS coil designs utilizing finite element analysis in Ansys Maxwell software. Our study involved a comparison of the focality and intensity of the electric field for different coil configurations (Fig. 1) using our anatomically accurate rat head model [5]. Permendur alloy having a high permeability, high saturation magnetization and low coercivity was used as the core material for all simulations. In addition to adding a diamagnetic Graphite plate with a hole, that has a susceptibility of -1.6×10^{-5} [6], to increase the coil focality as shown in Fig. 2. a, b and c. Simulation results in Fig. 1, indicate significant E-Field distribution variation when changing the coil configuration, aiming to concentrate the E-Field to the targeted region in rat head model without stimulating adjacent regions. It was observed that the parabolic shape coil has the best focality compared to other coils, besides achieving the stimulation strength required at the rat's gray matter.

[1] M. S. George *et al.*, *Arch. Gen. Psychiatry*, vol. 67, no. 5, pp. 507–516, May 2010 [2] D. W. Dodick *et al., Headache J. Head Face Pain*, vol. 50, no. 7, pp. 1153–1163, Jul. 2010 [3] O. of the Commissioner, "FDA permits marketing of transcranial magnetic stimulation for treatment of obsessive-compulsive disorder," *FDA*, Mar. 24, 2020. [4] J. Selvaraj *et al., IEEE Trans. Magn.*, vol. 54, no. 11, pp. 1–5, Nov. 2018 [5] C. Nimonkar *et al.*, IEEE *Trans. Magn.*, vol. 58, no. 2, pp. 1–4, Feb. 2022 [6] Young and Freedman, "Young & Freedman, University Physics with Modern Physics with Mastering Physics | Pearson -11th-Edition

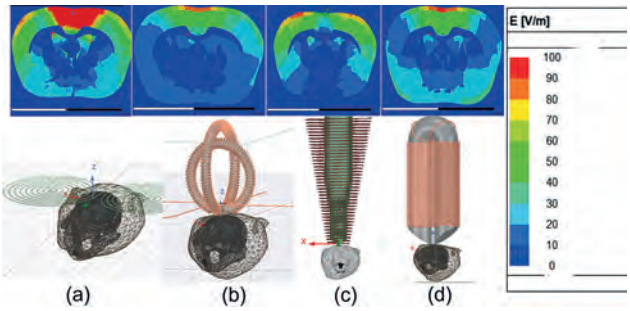

Fig. 1. TMS coil configurations with the associated electric field distribution on the rat's gray matter. a) Figure of 8 coil. b) Double C core. c) V-tip core. d) Parabolic shape core.

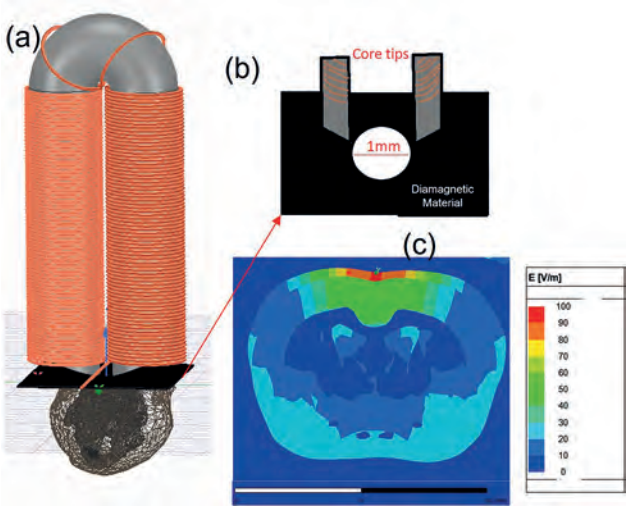

Fig. 2. (a) Parabolic core with shielding (b) Diamagnetic plate schematic (c) Electric field distribution (Coronal view) taken at the vertex.

CG-06. Development of a High-Efficiency and Wide-Irradiation Coil for Transcranial Magnetic Stimulation Therapy at Home.
M. Fushimi[1], Y. Kawasaki[1], K. Yamamoto[1] and M. Sekino[1] *1. The University of Tokyo, Tokyo, Japan*

Transcranial magnetic stimulation (TMS) is a noninvasive brain stimulation modality that induces an electric field inside the brain by a coil positioned around the head [1, 2]. TMS treatment at home is desirable to maintain effectiveness of e.g., the neuropathic pain treatment through continued routine stimulation [3]. To perform TMS therapy at home, it is critical to use a stimulation coil that is robust against misalignment. The bowl-shaped coil [4] is one such coil, but it has a disadvantage that the generated current intensity is smaller than that of the well-known figure-8 coil [5]. To increase the induced current, a larger current must be applied to the coil, resulting in a larger driving circuit as well as faster heating of the coil. In this study, we first investigate the bowl-shaped coils with varying scale parameters and clarify that it is important to minimize the influence of the return current. Next, we design the double-D-shaped coil which has a horizontal return

path to suppress the influence of the return current while maintaining the coil inductance as shown in Fig. 1. By numerical simulation, we confirmed that the double-D-shaped coil achieved wider range of electrical stimulation as shown in Fig. 2. On the other hand, the inductance of the designed coil was calculated to be 8.5 uH, which is comparable to commercially available coils. We also performed numerical simulations incorporating individual brain anatomy of six patients. The double-D-shaped coil contained about twice larger area with more than 99% of maximum electric field magnitude than that of the figure-8 coil as the average of the six cases. Furthermore, we fabricated the designed coil by 3D printing and evaluated its performance, the details of which will be shown in the presentation. Our newly developed double-D coil is capable of wide-area stimulation and is robust in positioning, opening the possibility of TMS treatment at home.

[1] A. T. Barker *et al.*, *Lancet*, Vol. 1, No. 8473. pp. 1106-1107 (1985) [2] S. Groppa *et al.*, *Clinical Neurophysiology*, Vol. 123, pp. 858-882 (2012) [3] A. Hirayama *et al.*, *The Journal of the International Association for the Study of Pain*, Vol. 122, No. 1, pp. 22-27 (2006) [4] K. Yamamoto *et al.*, *Journal of Applied Physics*, Vol. 117, p. 17A318 (2015) [5] S. Ueno *et al.*, *Journal of Applied Physics*, Vol. 64, pp. 5862-5864 (1988)

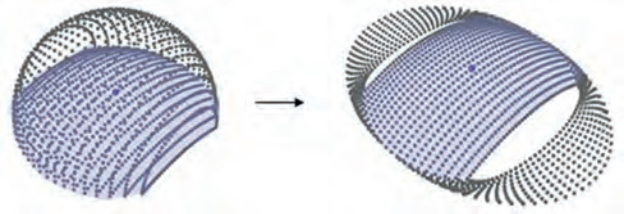

The coil shape of (left) the previously proposed bowl-shaped coil and (right) the proposed double-D-shaped coil.

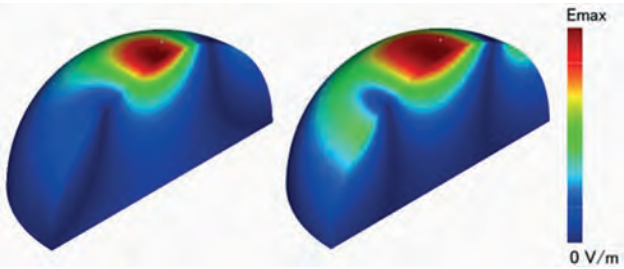

The induced electric field distribution of (left) the figure-8 coil and (right) the double-D-shaped coil normalized by the maximum field magnitude.

CG-07. Anti-CD3ε Conjugated Magnetic Nanoparticles (Fe_3O_4) for Targeted Inhibition of Cytokine Storm: Intravenous and Dermal Stamp Patch Based Transdermal Approaches. *M. Hasan*[1,2], J. Choi[1] and S. Lee[1] *1. Department of Digital Healthcare Engineering, Sangji University, Wonju, The Republic of Korea; 2. Department of Biochemistry and Molecular Biology, Bangabandhu Sheikh Mujibur Rahman Science and Technology University, Gopalganj, Bangladesh*

Inhibiting T cell-mediated inflammation by inducing immune tolerance is a key step to preventing cytokine hypersecretion. Monoclonal antibodies (mAbs) against the CD3ε subunit of the T cell receptor (TCR) complex induce immune tolerance. Conjugation of anti-CD3ε with magnetic nanoparticles will avoid Fc-dependent interaction with TCR[1]. Besides, targeted distribution will be enhanced by using external magnets. We aim to conjugate anti-CD3ε with MNP (dextran-coated Fe_3O_4, dia. 50 nm) and evaluate the inhibition of cytokine oversecretion through intravenous and transdermal microneedle patch delivery. The effective treatment strategy of reducing cytokine oversecretion or cytokine storm was assessed on a concanavalin A (ConA) induced hyperinflammation BALB/c mouse model[2]. Intravenous injection, transdermal microneedles, and dermal stamp roller administered anti-CD3ε-MNP (Ab-MNP). Electron microscopes, immunofluorescence staining, and nanoparticle tracking analysis (NTA) validated the Ab-MNP conjugation complex[3]. Compared to MNPs, 90% of Ab-MNPs had increased in size from 54.7 ± 0.5 to 71.7 ± 2.7 nm (Fig. 1). Different dosages of Ab-MNPs were administered to mice before administering concanavalin-A, an inducer of inflammation. Pre-administration of Ab-MNPs, not MNPs or anti-CD3 mAb alone, significantly reduced (up to 85%) the serum levels of interferon-γ and interleukin-6 in ConA-treated mice. Furthermore, we validated the transdermal stamp patch as an effective delivery system for Ab-MNPs (Fig. 2). This study showed that an Ab-MNP complex is helpful in pathologies associated with T cell-mediated hyperinflammation, such as organ transplantation and COVID-19.

[1] C. Kuhn, H. L. Weiner, Immunotherapy 8, 889-906 (2016) [2] E. Y. Abu-Rish, A. T. Mansour, and H. T. Mansour, Scientific reports, 10, 4007 (2020) [3] J.-G. Choi, M. Hasan, and S.-S. Lee, Current Applied Physics, 48, 79-83 (2023)

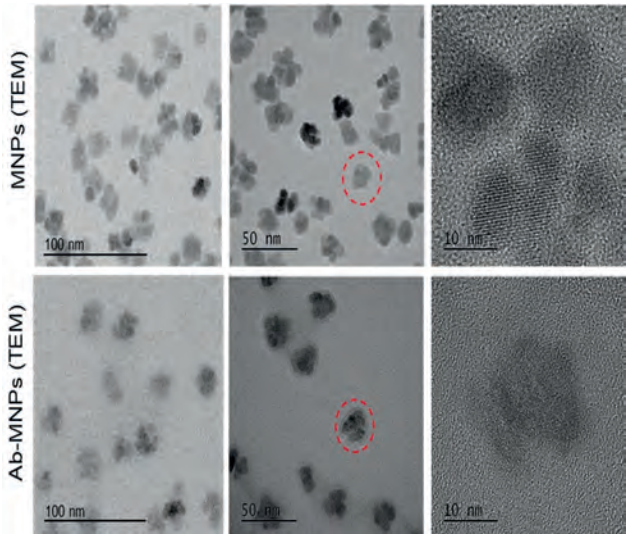

Fig. 1: Transmission electron microscope images revealed the structural differences after conjugation with antibodies.

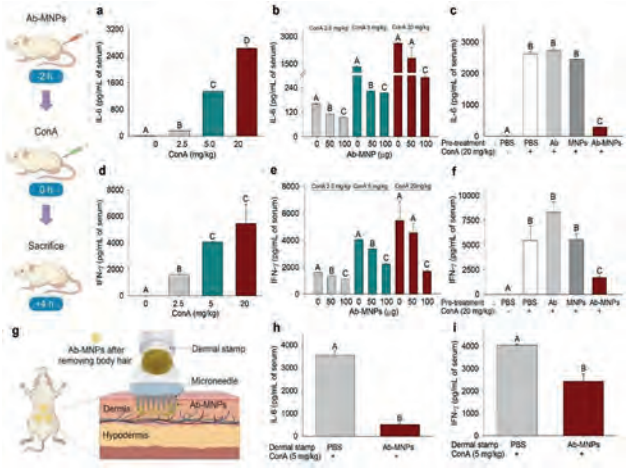

Fig. 2: Inhibition of concanavalin A (ConA)-induced increase in the level of proinflammatory cytokines in mice by intravenous tail vein injection and transdermal delivery of Ab-MNPs using microneedle stamp patch. The data are shown as mean ± standard error of the mean (SEM). $^{A\text{-}D}$ Different letters indicate significant differences between groups ($p < 0.05$).

CG-08. Multifunctional platform for phothermal hyperthermia combined with luminescence nanothermometry probes. M. Horcajo Fernandez[1], D. Arranz[1], R. Weigand[2] and *P. de la Presa*[1] *1. Institute of Applied Magnetism, Complutense University of Madrid, Madrid, Spain; 2. Departament of Optics, Complutense University of Madrid, Madrid, Spain*

The design of multifunctional magnetic nanoparticles that can generate and monitor heat release in real-time during thermal therapy is a major challenge in nanomedicine. In this work, a trimodal system that combines magnetic hyperthermia (MH), photothermal therapy (PT) and luminescence nanothermometry (LT) has been set up in a single platform. Magnetite NPs were optimized focusing on MH and PT, then, the NPs have been coated with silica embedded Nd^{3+} or Er^{3+} cations in order to enhance the PT and also to act as LT probe. Erbium has excitation lines at 790 nm and 980 nm, and luminescence around 500 nm and 650 nm. Neodymium is another interesting luminescent probe, with excitation around 800 nm and emission at the second biological window. Such hybrid system could act as heat mediator and imaging probe for in-vitro and in-vivo experiments, since these wavelengths belong to the biological windows, as well as an in-situ thermometer during the PT. The samples were prepared by a modified hydrothermal method [1], the multifunctional system is composed of magnetite NPs as core funcionalized with citrate for colloidal stability (IONs), then coated with a silica shell that servses as insulating between the magnetic core and the luminescent probe (IONs@SiO_2), and, finally, an additional silica shell containing either Nd^{3+} or Er^{3+} (IONs@SiO_2:RE). The structure and morphology have been investigated by XRD and HRTEM, and the magnetic properties by SQUID magnetometry. The heating efficiency has been measured under laser irradiation at 808 nm [2]. Figure 1 shows the Specific Absortion Rate (SAR) obtained in PT, and, as it can be seen, are higher than 200 W/g and are independent of the coataing. On the other side, the SAR measured with MH at 300 kHz and 100 Oe is around 20 W/g for uncoated NPs and almost negligible for the coated ones. High frequency magnetometry characterizations allows us to understand this behavior. The luminescence properties of the multifunctional platform is discussed in the work. Acknowledgments This work was supported by PID2021-123112OB-C21 and TED2021-129688B-C21.

[1] Marcus Vinícius-Araujo, Navadeep Shrivastava, Ailton A. Sousa-Junior, Sebastiao A. Mendanha, Ricardo Costa De Santana, and Andris F. Bakuzis, ACS Appl. Nano Mater. 2021, 4, 2190–2210. [2] Arranz D, Weigand R, de la Presa P. Towards the Standardization of Photothermal Measurements of Iron Oxide Nanoparticles in Two Biological Windows. Nanomaterials. 2023; 13(3):450.

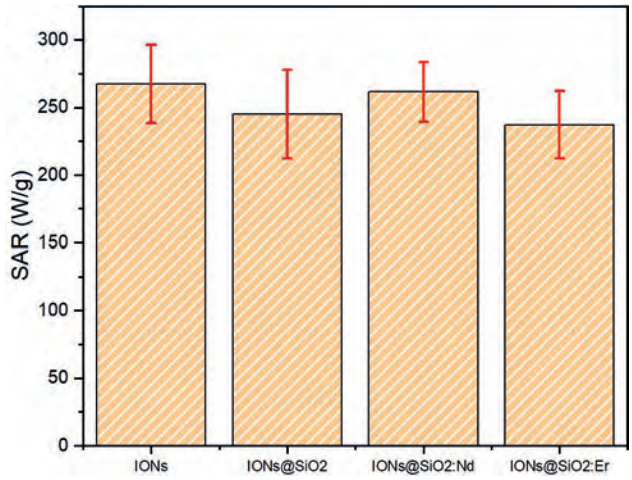

Figure 1: Photothermal SAR of the samples IONs, IONs@SiO_2, IONs@SiO_2:Nd and IONs@SiO_2:Er.

CG-09. Wireless Temperature Measurement Using Magnetic Nanoparticle during Magnetic Hyperthermia Operation. *A. Kuwahata*[1,2], R. Shinohara[3], T. Kagami[2] and S. Yabukami[2,1] *1. Graduate School of Engineering, Tohoku University, Sendai, Japan; 2. Graduate School of Biomedical Engineering, Tohoku University, Sendai, Japan; 3. School of Engineering, Tohoku University, Sendai, Japan*

Magnetic hyperthermia (MH) using magnetic nanoparticles (MNPs) and alternating magnetic fields (AMF) enables less invasive cancer therapy compared to other treatment technologies such as radiation and laser irradiation. To achieve non-invasive therapy, the temperature monitoring in vivo [1] and feedback control of AMF heating power [2] during MH operation is required to avoid overheating. However, there is no clinical device capable of monitoring temperature under the application of large AMF. In this study, we investigated the temperature-dependent magnetic characteristics of MNPs (Resovist®) under varying temperatures and large AMF applications to design a magnetic theranostics device that enables simultaneous MH treatment and wireless temperature monitoring in vivo. Figure 1 presents the experimental setup for a wireless temperature monitoring system based on magnetization (low-frequency excitation coil) in the MH operation system with large AMF (high-frequency heating coil). The resonance circuits are utilized to eliminate interaction between both systems. Figure 2(a) displays the accuracy of temperature measurement at different field strengths and frequencies. We identified the optimized parameters of 6.0 mT for low-frequency magnetic fields and 1.886 kHz for frequency. Figure 2(b) demonstrates the wireless temperature measurement of MNPs and reference temperature as a function of time during MH operation. The accuracy of wireless temperature measurement, ±1.3°C, is sufficient for controlling the heating power of the MH system for magnetic-cancer theranostics. This technique will facilitate the theranostics for non-invasive cancer treatment using MH, and we will develop a clinical prototype through future animal experiments.

[1] A. Kuwahata *et al.*, AIP Advances 13, 025142 (2023). [2] A. Shikano *et al.*, *T. Magn. Soc. Jpn. (Special Issues)* 6, 100-104 (2022).

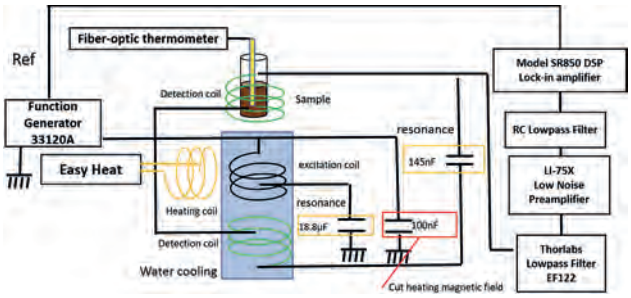

Wireless temperature monitoring system during magnetic hyperthermia operation. Magnetic signals (1.5-6 mT and 0.235-9.43 kHz) of magnetic nanoparticles are measured under magnetic heating (10 mT and 270 kHz) and converted to temperature of magnetic nanoparticles.

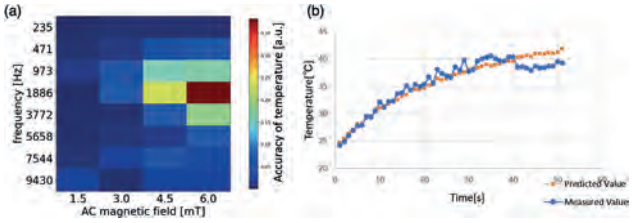

(a) Accuracy of wireless temperature measurement of various frequency and strength of magnetic fields. (b) Wireless temperature monitoring compared with reference temperature measured by fiber-optic thermometer.

CG-10. Enhanced Magnetic Hyperthermia in $CoFe_2O_4$ Nanorods.
J. Mohapatra[1], J. George[1], *N.A. Molwani*[1], P. Joshi[1] and J. Liu[1]
1. Department of Physics, University of Texas at Arlington, Arlington, FL, United States

Localized heat induction using magnetic nanoparticles under an alternating magnetic field (AMF) is an emerging technology that is applied in cancer treatment, thermally activated drug release, and remote activation of cell functions.[1-3] The intrinsic and extrinsic magnetic parameters influencing the heating efficiency of magnetic nanoparticles (MNPs) should be effectively engineered to enhance the induction heating efficiency of the MNPs. In this work, an efficient magnetic hyperthermia agent with a high specific absorption rate (SAR) value is obtained. Monodispersed $CoFe_2O_4$ nanorods of length (25- 250 nm) and diameter (10-28 nm) are synthesized via a thermolysis technique using oleylamine as a multifunctionalizing agent (surfactant, solvent, and reducing agent). $CoFe_2O_4$ nanorods of 70 nm length encapsulated with citric acid show a very high SAR value of 860 W/g for an AMF of 625 Oe. The improved heating effects of nanorods are related to shape-induced predominant changes in magnetic properties. Coercive loss increases with the length of a nanorod due to increased effective magnetic anisotropy, improving heating effects. When the length of the nanorod is increased above 70 nm, the coercivity increased above the applied AMF, which led to a decreased ac hysteresis loop area and a rapid decrease in the SAR values. Our findings open new avenues for manipulating the magnetic properties of MNPs and establishing a qualitative relationship between effective magnetic anisotropy and heating efficiency

1. Z. Ma, J. Mohapatra, K. Wei, J. P. Liu and S. Sun, *Magnetic Nanoparticles: Synthesis, Anisotropy, and Applications*, *Chemical Reviews*, 2023, 123, 7, 3904–3943. 2. J. Mohapatra, S. Nigam, J. George, A. C. Arellano, P. Wang and J. P. Liu, *Principles and applications of magnetic nanomaterials in magnetically guided bioimaging*, *Mater. Today Phys.*, 2023, 32, 101003. 3. J. Mohapatra, M. Xing and J. P. Liu, *Inductive Thermal Effect of Ferrite Magnetic Nanoparticles*, *Materials* 2009, 12(19), 3208.

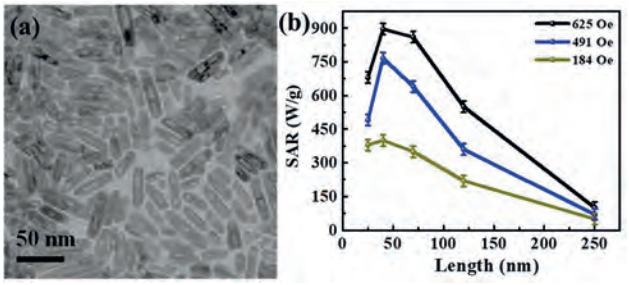

Figure 1: (a) TEM image of $CoFe_2O_4$ nanorods (length ~70 nm and diameter ~15 nm) prepared via a high-temperature thermal decomposition approach. (b) The SAR as a function of $CoFe_2O_4$ nanorods lengths with the variation of applied ACMF amplitude (184-625 Oe).

CG-11. Ferromagnetic Resonance-based Heat Dissipation in Dumbbell-like Au–Fe_3O_4 Nanoparticles. *L. Tonthat*[1], A. Kuwahata[1] and S. Yabukami[1] *1. Tohoku University, Sendai, Japan*

Ferromagnetic resonance (FMR) has emerged as a promising approach for heat dissipation in magnetic nanoparticles (MNPs) for cancer therapy [1]. Previous studies demonstrated the ultrafast heating capabilities of gold-coated iron oxide MNPs [2,3] based on FMR [1]. However, there is a research gap regarding the influence of particle morphology on heating efficiency. In this study, we investigated a novel class of dumbbell-like gold and iron oxide NPs (Au-Fe_3O_4 NPs), motivated by the potential benefits of increasing effective magnetic anisotropy, resulting in increased heat generation. Pure Fe_3O_4 NPs (~11nm) were synthesized under the same condition but without using ~5nm Au seeds. The TEM image confirms the successful synthesis of dumbbell-like morphology, exhibiting distinct sizes of ~5nm and ~15nm for Au and Fe_3O_4 segments, respectively. We examined the temperature rise of the samples (each sample ~6.4mg) for different DC fields (H_{DC}=0~1600Oe) under an RF field (f_{AC}=4GHz, H_{AC}=1.3Oe) for a heating duration of ~13s using our experimental setup (Fig.1). Notably, the temperature versus time exhibited a similar trend: a rapid increase when RF field was turned on, followed by a sudden drop when RF field was turned off. The temperature rise varied with DC field and reached a maximum value of 23.4°C at H_{DC}=400Oe for Au-Fe_3O_4 NPs. Importantly, this value surpassed the sum of the maximum value observed for ~11nm Fe_3O_4 NPs (11.1°C at H_{DC}=1000Oe) and ~5nm Au NPs (3.5°C, nearly constant with increasing DC field). Moreover, compared with our previously developed Au-coated Fe_3O_4 NPs [1] (17.0°C at H_{DC}=1200Oe, H_{AC}=4Oe, f_{AC}=4GHz), the dumbbell Au-Fe_3O_4 NPs exhibited significantly higher temperature rise, highlighting their enhanced potential for magnetic hyperthermia. This observed difference in heat generation can be attributed to the effects of size, shape, and efficient exchange coupling between the Au and Fe_3O_4 segments in the dumbbell NPs. Ongoing experiments and analyses aim to further elucidate these complex mechanisms.

(1) L. Tonthat, A. Kuwahata, T. Ogawa and S. Yabukami, "Ultrafast Heating Rate of Ultrasmall Gold-coated Iron Oxide Magnetic Nanoparticles by Ferromagnetic Resonance," IEEE Transactions on Magnetics, doi: 10.1109/TMAG.2023.3287550 (early access). (2) L. Tonthat, M. Kimura, T. Ogawa, et al: "Development of gold-coated magnetic nanoparticles as a theranostic agent for magnetic hyperthermia and CT imaging applications," AIP Advances, 13(2), 2023. (3) L. Tonthat, T. Ogawa and S. Yabukami: "Ultrasmall Fe_3O_4@Au Composite Nanoparticles with Different Sizes of Fe_3O_4 for Magnetic Hyperthermia," IEEE Transactions on Magnetics, doi: 10.1109/TMAG.2023.3287505 (early access).

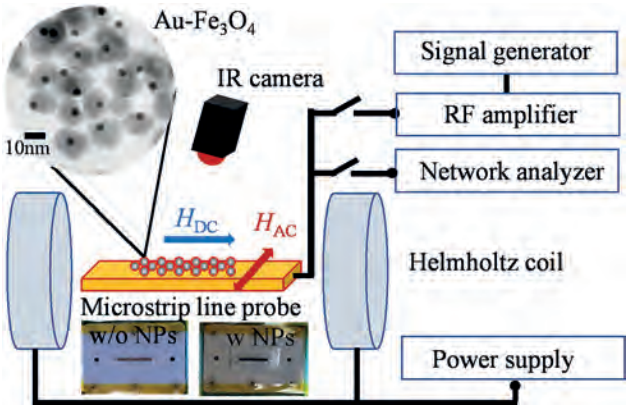

Fig.1 Experimental setup.

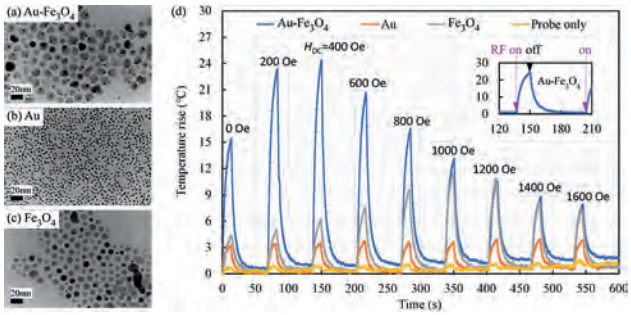

Fig.2 TEM images of (a) Au-Fe_3O_4, (b) Au, (c) Fe_3O_4 NPs, and (d) the temperature rises under RF magnetic field of f_{AC}=4 GHz, H_{AC}=1.3 Oe for different DC field strengths.

Session CP
DOMAIN WALL, VORTEX, AND SKYRMION DYNAMICS AND DEVICES II (Poster Session)

Xianzhe Chen, Chair
University of California, Berkeley, Berkeley, CA, United States

CP-01. Correlation between Dzyaloshinskii-Moriya interaction and lattice constant through in-vacuum measurement at Pt/Co single interface. *J. Yu*[1], S. Lee[1], J. Chang[1], M. Kim[1], J. Yoon[1], J. Shin[1], W. Shim[1] and S. Choe[1] *1. Physics and Astronomy, Seoul National University, Seoul, The Republic of Korea*

The Dzyaloshinskii-Moriya interaction (DMI) is an asymmetric exchange interaction that occurs at interfaces [1]. In conventional magnetic systems, the DMI is present at both top and bottom interfaces adjacent to magnetic layer. However, the presence of multiple interfaces makes it challenging to distinguish the individual contributions of DMI from each interface, which hinders our understanding of the mechanism behind its emergence. In this study, we propose an novel approach to measure the DMI at single interface through in-vacuum magneto-optical Kerr effect (MOKE) system. By utilizing in-vacuum MOKE system, we were able to accurately quantify the DMI at Pt/Co single interface through the observation of asymmetric domain-wall motion [2]. In the experiment, the thickness of Pt layer t_{Pt} was varried from 1.5 nm to 8.0 nm, as shown in Fig. 1. Interestingly, the magnitude of the DMI-induced effective magnetic field H_{DMI} gradually increases with increasing $t_{Pt.}$ This observation indicates that the DMI exhibits a strong dependence on the thickness of the non-magnetic layer. This result is in clear contrast to the theoretical expectation [3], which suggests that the DMI has a very localized origin close to the magnetic layer at the interface. To investigate the origin of the increase in DMI, we conducted a XRD examination and observe a strong correlation between the DMI and the lattice constant.

[1] A. Fert, V. Cros and J. Sampaio, Nat. Nanotechnol. 8, 152 (2013). [2] S.-G. Je, K.-J. Lee, and S.-B. Choe, Phys. Rev. B 88, 214401 (2013). [3] H. Yang, A. Thiaville, and M. Chshiev, Phys. Rev. Lett 115, 267210 (2015).

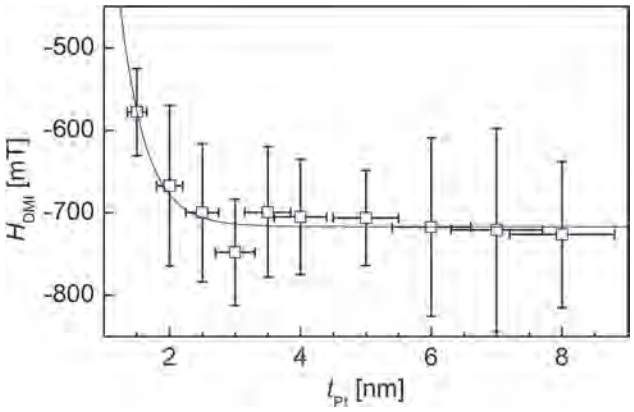

Fig. 1. Plot of H_{DMI} with respect to t_{Pt}.

CP-02. Withdrawn

CP-03. Stochasticity of magnetic domain-wall motion in tech-relevant speed regime. *M. Kim*[1], S. Lee[1], M. Kim[1] and S. Choe[1] *1. Department of Physics and Astronomy, Seoul National University, Seoul, The Republic of Korea*

The magnetic domain-wall (DW) motion has been studied widely, since the magnetic DW devices have received great attention recently for the next generation devices. Even though the magnetic domain is able to represent binary systems—magnetized up and down, the magnetic DW devices still require stable controllability. In magnetic domain systems, the DW moves through quenched disorders, resulting in inherent stochasticity. A large stochasticity may lead to collapse of domains and thus, loss of reproducibility, followed by malfunctions of devices. Therefore, understanding of the stochastic nature is crucial for high performance with proper controllability. Here, we investigated the universality of stochasticity in magnetic DW motions driven either by electric current or magnetic field. It is well known that as the driving force increases, the number of depinning events increases and thus, the stochasticity decreases. However, interestingly, within the tech-relevant DW speed regime (1~100 m/s), the stochasticity increases as the magnetic field increases. Such increase could be explained with the context of the creep scaling criticality. The present observation suggests a way to reduce stochasticity in the tech-relevant DW speed regime.

Junyeon Kim, Soong-Geun Je and Sug-Bong Choe, *Appl. Phys. Express,* Vol. 8, 063001 (2015) Pascal Chauve, Thierry Giamarchi, and Pierre Le Doussal, Phys. Rev. B, Vol. 62, 6241 (2000) Alejandro B. Kolton, Alberto Rosso and Thierry Giamarchi et la., Phys. Rev. B, Vol. 79, 184207 (2009) Alejandro B. Kolton, Alberto Rosso and Thierry Giamarchi et la., Phys. Rev. Lett., Vol. 97, 057001 (2006) Ezequiel E. Ferrero, Laura Foini and Thierry Giamarchi et la., Phys. Rev. Lett., Vol. 118, 147208 (2017) Matías Pablo Grassi, Alejandro B. Kolton and Vincent Jeudy et la., Phys. Rev. B, Vol. 98, 224201 (2018)

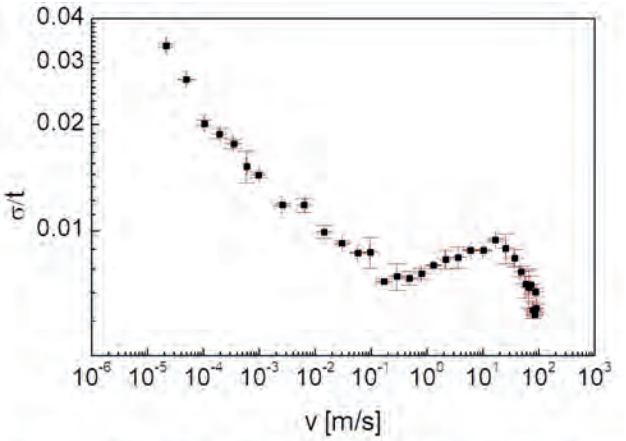

FIG. 1. The stochasticity of the domain wall arrival time is represented by the relative standard deviation. The stochasticity decreases as the domain wall velocity increases in the slow domain wall speed regime. The stochasticity has the kink at the tech-relevant domain wall speed regime.

CP-04. Magnetic texture-based design of artificial neurons and synapses. D. Das[1], C. Yunuo[1], J. Wang[1] and *X. Fong*[1] *1. National University of Singapore, Singapore*

The non-volatile nature and energy efficiency of the spintronics devices make them a suitable candidate for futuristic computing devices. Inspired by the efficiency of the biological brain, researchers are motivated to develop energy-efficient hardware by mimicking the biological neuronal functionality. Magnetic domain wall (DW) and skyrmion devices are two promising candidates for such neuro-inspired computing devices for their non-volatile nature and energy efficiency. Compared to the DW, skyrmions are smaller in size and have lower depinning current density. The skyrmion has an ultra-small-scale size with lower depinning current density than the DW, and it suffers from unwanted Magnus force which forces the skyrmion to move along a curved trajectory. This force becomes dominant for the higher current density which leads to the failure of the device. However, the micromagnetic simulation shows that the Magnus force can be completely nullified in a synthetic antiferromagnetically (SAF) coupled bilayer system. In this work, using micromagnetic simulation, we compare the DW and skyrmion-based neuron and synaptic devices. We demonstrate the leaky-integrate-and-fire (LIF) functionality for both the DW and skyrmion-based neuron devices. The membrane potential in the neuron is represented by the position of the DW/skyrmion in the devices. The leak functionality is achieved by incorporating an uniaxial anisotropy gradient in the devices. In the presence (absence) of an incoming spike the DW/skyrmion moves along the forward (backward) direction of the length of the device. Our simulations show that a similar device without the anisotropy gradient can be used as a synapse for the DW-based devices, however, a longer device is needed for the skyrmion-based synapse device. Both DW and skyrmion-based synapse device shows highly linear and symmetric weight update characteristics which is an essential criterion for an ideal synapse. Here, we compare the energy requirements of the DW and skyrmionic devices to perform the neuronal and synaptic functionality. We also perform a system-level simulation on a spiking neural network (SNN) using our proposed neuron and synapse devices.

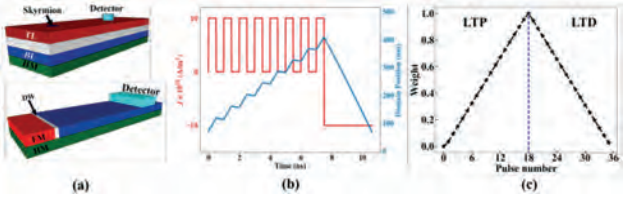

CP-05. Real-time detection of fast current driven domain wall motion by using magneto-optical readout method in GdFe magnetic wire memory. *N. Suzuki*[1], K. Wainai[1], K. Nomura[1], M. Mohammadi[1], S. Sumi[1], K. Tanabe[1] and H. Awano[1] *1. Toyota Technological Institute, Nagoya, Japan*

Magnetic wire memory is attraction attention as a future power-saving memory. There are many reports on problems such as how small a current can drive a domain wall and how fast it can be driven. However, there are no reports on the real-time detection of the driving magnetic domains. A TMR head is generally considered for this detection. However, it is difficult to fabricate a high-performance TMR head on this magnetic wire, and the increase in wiring is also a problem. Therefore, we tried a readout technology that uses the magneto-optical (MO) recording, the maximum linear velocity of the recorded magnetic domains with respect to the optical head was 50 m/sec, but in the magnetic wire memory, it is 2000 m/sec [1], which is 40 times faster. In this experiment, as shown in Fig. 1, the magnetization state of the sample is checked using a polarizing microscope, and the readout laser beam of 780 nm wavelength is focused on the magnetic wire sample through the same objective lens (OBL). The reflected light was detected through a photodetector and an avalanche photodiode (APD), and the current driven domain wall motion was observed. A 3 μm wide and 120 μm long magnetic wire consisting of Pt (5 nm) / $Gd_{22}Fe_{78}$ (20 nm) / SiN (10 nm) layers on a Si substrate with a thermal oxide film was used for the measurement. Fig. 2 shows the detected MO signal waveforms of the domain wall motion when a pulse current with a current density of 3.07×10^{11} A/m^2 and a pulse width of 10 nsec is applied. As shown in Figure 2, the measurement was done when the recorded domain passed through the laser spot, indicating that the passage of the domain in the laser spot could be detected in real time. The Gaussian distribution of the waveform also confirms that the speed of the domain wall motion is always constant during the application of current.

[1] S.Ranjbar et al., Materials Advances., vol. 3, p.7028 (2022)

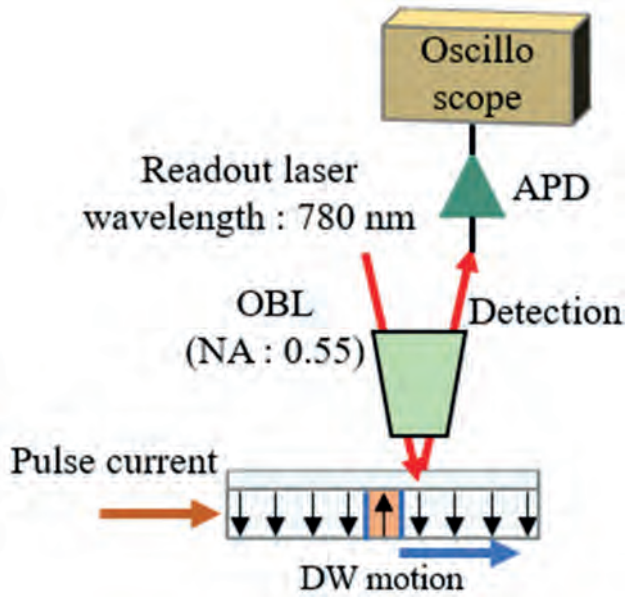

Fig. 1 MO detection method for the current driven domain wall motion in the racetrack memory.

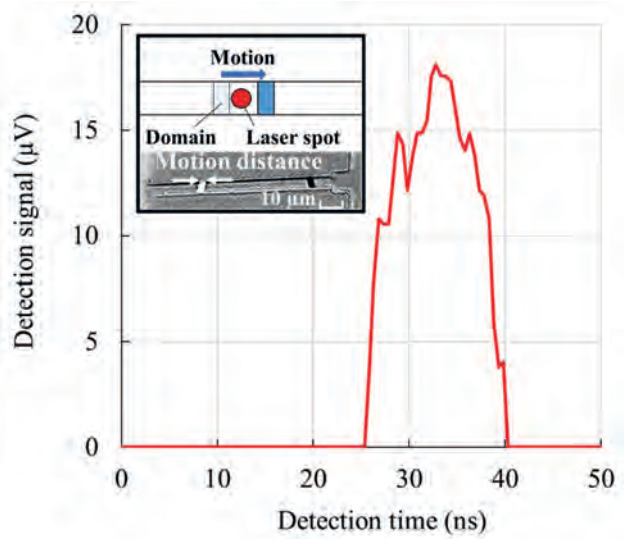

Fig. 2 MO signal waveform detected in real-time. The inset of Fig. 2, the domain wall passed through the laser spot by applying a pulse current of 10 nsec. The motion distance of the domain wall is about 3.6 μm.

CP-06. Dynamics of Disordered Magnetic Helices Probed With Coherent Soft X-Ray Scattering. *R. Tumbleson*[3,2], E. Holingworth[1], A. Singh[2], D.W. Raftrey[3,2], M. McCarter[2], A.U. Saleheen[2], S.A. Morley[2], P. Fischer[2], F. Hellman[1], S. Kevan[2] and S. Roy[2,3] *1. Physics, University of California - Berkeley, Berkeley, CA, United States; 2. Lawrence Berkeley National Laboratory, Berkeley, CA, United States; 3. Physics, University of California - Santa Cruz, Santa Cruz, CA, United States*

The skyrmion hosting material FeGe stabilizes magnetic spin textures as a result of the competition between the Heisenberg exchange interaction and the Dzyaloshinskii-Moriya interaction. In this talk, I present X-ray photon correlation spectroscopy results on the phase transition from a disordered helical state towards a paramagnetic state in an amorphous FeGe thin film. By using highly coherent soft X-rays, we are sensitive to the thermal magnetic fluctuations that drive the phase transition.

CP-07. Effects of embedded topological defects on the resonance modes of magnetic skyrmions. *T. Staggers*[1] and S. Pollard[1] *1. Physics and Materials Science, University of Memphis, Memphis, TN, United States*

The resonant behavior of magnetic skyrmions, topologically protected spin structures stabilized by the Dzyaloshinskii-Moriya Interaction (DMI) in materials with broken inversion symmetry, has been extensively explored due to various rotational and breathing modes that emerge in the GHz regime, making them attractive for microwave applications [1]. Additionally, topological defects in the form of Bloch lines play a key role in the dynamics of magnetic domains and domain walls. Recently it has been shown that films with a sufficiently strong DMI can support Bloch-lines characterized by an integer topological charge known as domain wall skyrmions (DWSky's) [2]. Further, these DWSky's embedded in traditional Néel skyrmions can play significant roles in the current driven dynamics of magnetic skyrmions [3]. Here, we explore the role of DWSky's embedded within a skyrmion on the skyrmion resonance modes in a confined geometry using micromagnetic simulations, as demonstrated in Fig. 1. We find the emergence of a mode described by the oscillation of the DWSky's along the skyrmion's boundary, as well as a suppression of the skyrmion's breathing mode. Further, a shift to higher frequencies in the traditional skyrmion's resonance modes is observed. The effects of temperature, damping, DMI strength, DWSky packing density, and disorder are explored in these systems. Finally, we demonstrate that a weak field tuned to various resonance modes may result in splitting or annihilation of embedded topological structures. This work has been supported in part by NSF grant ECCS-2138271.

[1] V. L. Zhang *et al.*, *AIP Adv*, vol. 7, no. 5, p. 055212 (2017) [2] R. Cheng *et al.*, *Phys Rev B*, vol. 99, p. 184412 (2019) [3] F. Nasr *et al.*, *Phys Rev B*, vol. 104, p. 174441 (2021)

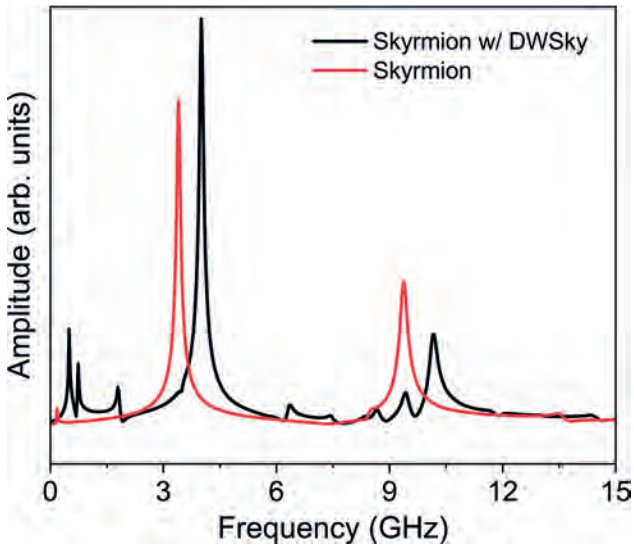

Fig. 1: Resonance spectra comparing skyrmion and one with an embedded DWSky.

CP-09. Controlling Stable Bloch Points with Electric Currents. *M. Lang*[2,1], S. Pathak[2], S. Holt[2], M. Beg[3] and H. Fangohr[2,1] *1. Engineering and Physical Sciences, University of Southampton, Southampton, United Kingdom; 2. Computational Science, Max Planck Institute for the Structure and Dynamics of Matter (MPSD), Hamburg, Germany; 3. Department of Earth Science and Engineering, Imperial College, London, United Kingdom*

Bloch points are point singularities in the magnetization configuration, which play an important role in many magnetization reversal processes and can be found as equilibrium configurations in several systems. Beg et al. [1] showed that an isolated stable Bloch point of two different types can exist in a two-layer FeGe nanodisk when the two layers have opposite chirality.

In a recent work [2], we have demonstrated that two-layer FeGe nanostrips with layers of opposite chirality can host arbitrarily many Bloch points in any combination of the two different types. In the present work, we use spin currents to manipulate the Bloch points in this two-layer system. We use micromagnetic simulations to study the effects of spin-transfer torques. We demonstrate that Bloch points can move collectively (Fig. 1) and study their motion in more complex geometries. In particular, we investigate pinning of the Bloch point at a notch (Fig. 2).

[1] Beg et al. Sci Rep 9, 7959 (2019) [2] Lang et al. Sci Rep 13, 6910 (2023)

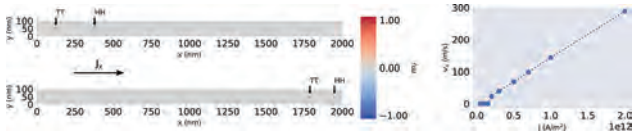

Fig. 1 (left) Two Bloch points in a nanostrip can be moved collectively by applying a spin current. We initialize a tail-to-tail (TT) and a head-to-head (HH) Bloch point [2] near the left sample boundary. When applying spin current in +x direction both Bloch points move along the current direction without any Hall effect. (right) After depinning, the velocity of a single Bloch point increases linearly with the current density.

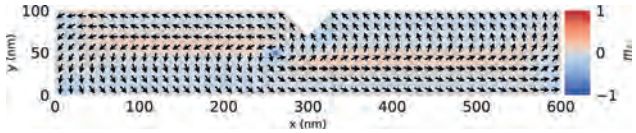

Fig. 2 Pinning of the Bloch point at a notch.

CP-10. Atomistic Study of Local Forces and Dynamics of Multi-sublattice Skyrmions. *E.A. Tremsina*[1,2] and G. Beach[2] *1. Department of Electrical Engineering and Computer Science, Massachusetts Institute of Technology, Cambridge, MA, United States; 2. Department of Material Science and Engineering, Massachusetts Institute of Technology, Cambridge, MA, United States*

Magnetic solitons, or quasiparticles formed by a local twist in the magnetization, are great candidates for use in novel spintronic devices, specifically, those in ferri- and antiferromagnetic materials which exhibit ultra-fast dynamics. The key question for the use of solitons in practical applications is their dynamic stability and maximum speed of propagation through magnetic media. For one-dimensional solitons (domain walls), the high-speed dynamics are quite well understood[1] and are limited in antiferromagnetic (AFM) materials by relativistic-like effects, namely velocity saturation towards a velocity v_m akin to the speed of light, and Lorentz-like width contraction, as seen in Fig. 1(a)-(b). Two-dimensional solitons (skyrmions) instead exhibit geometrically more complicated dynamic distortions, the exact nature and symmetries of which have not yet been explained using real simulation data for multi-sublattice systems. Here, the unique capabilities of fully atomistic modelling in the VAMPIRE software[2], in conjunction with the Thiele formalism are used to perform an extensive and systematic study of domain wall and skyrmion dynamics driven by spin orbit torque. A physical explanation for skyrmion deformations, which are attributed to the local imbalance of the gyrotropic, dissipation and driving forces, is derived using simulation data for antiferromagnetic (AFMSk), as well as ferrimagnetic (FiMSk) skyrmions [3]. These results expand the understanding of the fundamental properties of magnetic skyrmions, in particular, their dynamical stability, ability to reach high velocities and dependence thereof on material parameters, paving the way for their potential use in spintronic applications.

1. L. Caretta L, *et al., Science*, 370(6523):1438-1442 (2020). 2. R.F. L.Evans, *et al., Journal of Physics: Condensed Matter*, *26*(10), 103202 (2014). 3. E. Tremsina & G. Beach, *Phys. Rev. B, 106,* L220402 (2022).

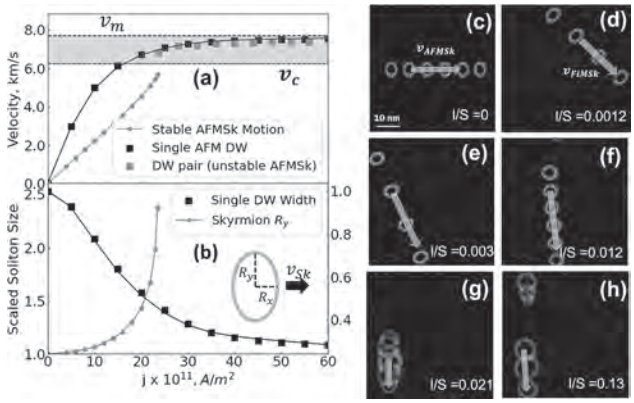

Figure 1. Simulated current-driven dynamics of AFMSk and AFM DW, showing (a) velocity and (b) extracted dimensions, versus applied current density. AFMSk show eliptical elongations, and their velocity is limited by a critical value v_c, found to be always less than limiting velocity for DW. (c)-(h) simulated 2D profiles of the motion of AFMSk(c) and FiMSk(d-h), showing deformation and trajectory deflection due to the presence of the Magnus force, all as a function of scaled angular momentum $\delta S/S_{net}$.

CP-12. Analysis of information current between skyrmions in cellular automaton-type device. *K. Emoto*[1], H. Mori[1], R. Ishikawa[2], S. Miki[1,3], M. Goto[1,3], H. Nomura[1,3], E. Tamura[1,3] and Y. Suzuki[1,3] *1. Graduate school of Engineering Science, Osaka University, Toyonaka, Japan; 2. ULVAC, Inc., Suita, Japan; 3. OTRI-Osaka, Osaka University, Toyonaka, Japan*

Recently, magnetic skyrmions are expected to apply to ultra-low power consumption computing due to their stochastic behavior and repulsive interactions[1]. In such devices using stochastic dynamics, evaluation of the information current between skyrmions is essential to understand the function of the complex system. In this study, we evaluated the information current by means of mutual information[2] and transfer entropy[3] between skyrmions. We fabricated the cellular automaton-type device. The skyrmion film consisting of Ta (5.0 nm)|$Co_{16}Fe_{64}B_{20}$ (1.2 nm)|Ta (0.22 nm)|MgO (2.0 nm)|SiO_2 (3.0 nm) was deposited on a thermally oxidized silicon substrate by the magnetron sputtering, and a square-shaped SiO_2(0.083 nm) film was added by a lift-off method. In such a sample, the skyrmions are confined within an additional deposition area[4]. Due to repulsive interactions, the confined two skyrmions in the box form a two-state state in the possible diagonal configurations. The trajectories of the Brownian motion of skyrmions are treated as probabilistic data, and the amount of mutual information between skyrmions is determined. We then observe information flow under certain degree of flustratoin between the boxes. The fabricated device was observed at 26.5°C with the magneto-optical Kerr effect microscope and frame rate of 125 fps. Fig. 2 shows the transfer entropy versus time in semi-log representation for the 1220 frames data. The pink dots (blue dots) represent the transfer entropy from skyrmion A(B) at step n to skyrmion B at step n+j. a_n (b_n) represents the random variable for the location of skyrmion A(B) and n.j. represents the discrete time. The transfer entropy of $a_n \rightarrow b_{n+j}$ has a peak. This peak represents the time delay in information transfer. The data for 1220 frames is considered to have a statistical error. Therefore, we obtained data for new 16,000 frames. The results of the evaluation of the interactions between the two skyrmions will be discussed on the day. This work was supported by JST CREST Grant number JPMJCR20C1, Japan and JSPS KAKENHI Grant Number JP20H05666, 23K13660, CSRN-Osaka.

1)R.Ishikawa, et al., Appl. Phys. Lett. 119, 072402 (2021) 2)T.Sagawa and M.Ueda, New J. Phys. 15 125012(2013) 3)T.Schreiber, Phys. Rev. Lett. 85, 461 (2000) 4)Y.Jibiki, et al., Appl. Phys.Lett. 117, 082402 (2020)

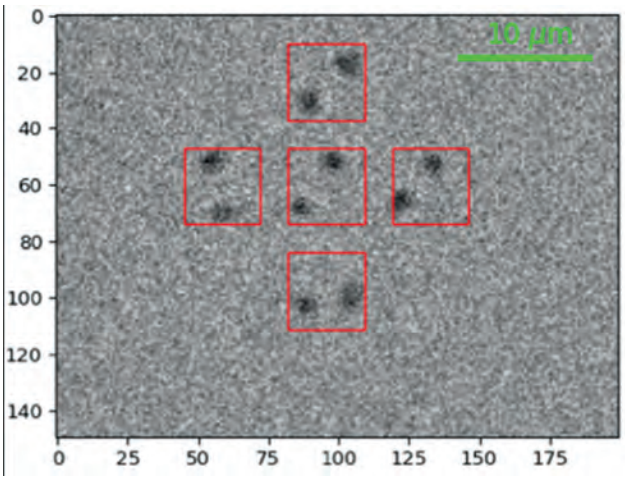

Fig.1 Skyrmions confined in the pattern

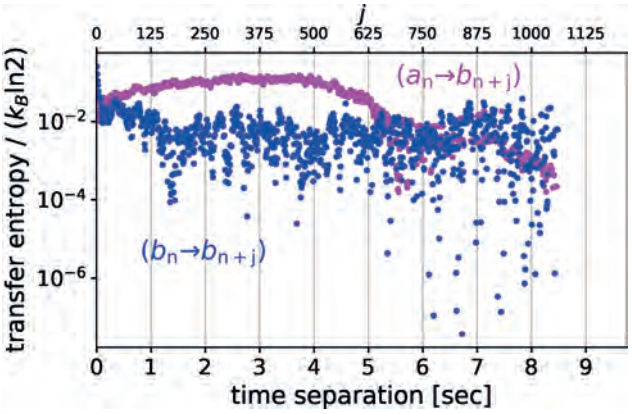

Fig.2 Transfer entropy between skyrmions of different squares for 1220 frames

Session CQ
MAGNETIZATION DYNAMICS III: MICROMAGNETICS AND MODELING (Poster Session)

Chuanpu Liu, Chair
Colorado State University, Fort Collins, CO, United States

CQ-01. Power-Phase Relation in Ultra-compact 'Magnon Microwave Antenna' for Generation of Microwaves with Tuneable Frequencies.
A. Samanta[1,2] and *S. Roy*[1,2] *1. Micropower Devices and Nanomagnetics Group, Tyndall National Institute, Cork, Ireland; 2. School of Physics, National University of Ireland - University College Cork, Cork, Ireland*

A spin wave(SW)/magnon based nanopatterned magnetic antenna, known as "Magnon Microwave Antenna"(MMA) [1] is operated in the microwave frequency range. Since the MMA are designed with magnetic nanoheterostructures[patterned magnetostrictive(MS) nanowire (NWs) arrays on piezoelectric (PE) substrate], the operation of MMA relies on interaction between phonons (from PE layer), magnon (from MS layer) and photons (electromagnetic radiation). When the MMA is placed in an alternating external electric field, a sinusoidal stress has been generated in PE layer, that travels along the surface of PE substrate and acts as surface acoustic wave (SAW). The developed SAW has then been transferred to the MS NWs which in turn excites the magnetization in the same to form collective SW excitations/magnons. Subsequently, the generated SWs further radiates photons at the SAW frequency and which can be used to transfer information and energy in the nanoscale regime[1],[2]. The MMA consists of 5 FeGa NWs patterned on $LiNbO_3$ separated by distances = 40-160 nm and is designed in COMSOL[3] to obtain the SAW frequency. S_{11} and S_{22} parameters estimate the SAW frequency as 551.35 MHz, that propagates along the longitudinal direction. The micromagnetic simulations with MuMax3[4] are performed by discretizing NWs into cell sizes considering typical FeGa material parameters (M_S=1.32MA/m, A_{ex}=16pJ/m, K_u=0kJ/m^3). Along with the M_x component, the associated power and phase profiles of the SWs at the 0.3 GHz frequency of s = 40 nm configuration are shown in Fig. 1 (a), (b) and (c), respectively. M_X profile shows that the multidomains are formed along x-component due to the SAW excitation. The power profile shows that the 0.3 GHz SW mode is quantized in a complex pattern, while the phase profile at that frequency exhibits a complex propagation mode of the SW. We note that s=40 nm configuration has a distribution of four different magnetodynamical resonance modes, whereas for s = 90 nm configuration the phonon-magnon-photon coupling generates a single synchronized 0.56 GHz resonance microwave frequency. Funding support: SFI-21/FFP-A/10003-MERIT.

[1] A. Samanta and S. Roy, "Generation of Microwaves With Tuneable Frequencies in Ultracompact 'Magnon Microwave Antenna' via Phonon-Magnon-Photon Coupling," *IEEE Trans. Electron Devices*, vol. 70, no. 1, pp. 335–342, 2023. [2] R. Fabiha, J. Lundquist, S. Majumder, E. Topsakal, A. Barman, and S. Bandyopadhyay, "Spin Wave Electromagnetic Nano-Antenna Enabled by Tripartite Phonon-Magnon-Photon Coupling," *Adv. Sci.*, vol. 9, no. 8, p. 2104644, 2022. [3] A. B. COMSOL, "COMSOL Multiphysics Version 6.0." 2022. [4] A. Vansteenkiste, J. Leliaert, M. Dvornik, M. Helsen, F. Garcia-Sanchez, and B. Van Waeyenberge, "The design and verification of MuMax3," *AIP Adv.*, vol. 4, no. 10, p. 107133, 2014.

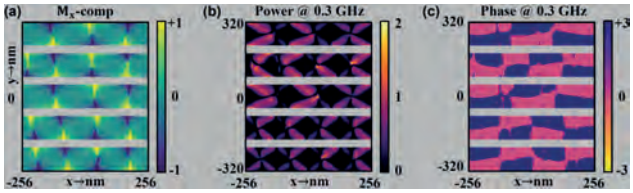

For 40 nm configuration: (a)M_x component, (b)power and (c)phase profiles of SW at 0.30 GHz mode profile.

CQ-02. Antiferro/ferromagnetic coupling of ultrathin middle-MgO layer in multilayered CoFeB/MgO magnetic tunnel junction by first-principles calculation and micromagnetic simulation.
H. Naganuma[1,2], C. Kaneta[1], T. Nguyen[2], H. Honjo[1], K. Nishioka[1], S. Ikeda[1] and T. Endoh[1,3] *1. CIES, Tohoku University, Sendai, Japan; 2. CSIS, Tohoku University, Sendai, Japan; 3. Graduate School of Engineering, Tohoku University, Sendai, Japan*

Perpendicular magnetic tunnel junctions (*p*-MTJs) with CoFe(B)/MgO multi-interface have advantages in scaling due to their large perpendicular magnetic anisotropy and high write efficiency. We reported that the quad-interface MTJs achieved enough thermal stability down to 18 nm for SRAM-type spin transfer torque magnetic random-access memory (STT-MRAM) [1] and the hexa-interface MTJs overcame the scaling issue for eFlash-type STT-MRAM. [2] In this multilayer technique, understanding the magnetic coupling of the ultra-thin middle-MgO layer is important because our previous calculation, assuming a continuous middle-MgO layer, [3] indicated that an antiferromagnetic coupling state appeared in the thermal barrier curve, which degrades data retention characteristics. However, owing to the very thin middle-MgO, a possibility that (i) through holes in the middle-MgO layer and (ii) the atom diffusion exists. However, these holes are difficult to investigate by scanning transmission electron microscope (STEM), which is a direct observation method. In this study, a microscopic calculation was performed by micromagnetic simulations assuming that the middle-MgO layer in the quad-interface MTJ has holes, and a first-principles calculation assuming the diffusion of Fe atoms into the middle-MgO layer was performed. A small amount of Fe diffusion into the middle-MgO layer tends to result in an antiferromagnetic coupling state. When the middle-MgO layer with magnetically coupled holes is considered, the antiferromagnetic coupling state does not appear in the thermal barrier curve, and the ferromagnetic coupling tends to have appeared. From these calculation results, it can be considered in the actual multilayered MTJ samples that the ultra-thin middle-MgO layer has holes and showed ferromagnetically coupled, which increases data retention. The authors acknowledge JSPS Core-to-Core Program (No. JPJSCCA20230005), QST-Tohoku University matching foundation, X-NICS (No. JPJ011438), the Core Research Cluster program, and the MRAM program in CIES, Tohoku Univ.

[1] H. Naganuma *et al*., VLSI, T12-4 (2020). [2] H. Honjo *et al.*, IEDM Technical Digest 19.3, (2022). [3] H. Naganuma *et al*., AIP Advances, 12, 125317 (2021).

CQ-03. magnum.np - a PyTorch based GPU enhanced Finite Difference Micromagnetic Simulation Framework. F. Bruckner[1], *S. Koraltan*[1], C. Abert[1] and D. Suess[1] *1. Physics of Functional Materials, University of Vienna, Vienna, Austria*

magnum.np is a micromagnetic finite-difference library based on PyTorch, which makes it easy to maintain and extend. It is perfectly suited for the investigation of novel algorithms and modeling approaches, and simulation of very large systems. On the other hand, magnum.np benefits from the devices abstraction and optimizations of PyTorch enabling the efficient execution of micromagnetic simulations on a number of computational platforms including GPU and potentially TPU systems. We demonstrate a competitive performance to state-of-the art micromagnetic codes such as *mumax3* and show how our code enables the rapid implementation of new functionalities. Furthermore, handling inverse problems becomes possible by using PyTorch's autograd feature. Figure 1 shows visualizes the high-level structure of the code. High-level optimizations like Just-In-Time compilation via e.g. *torch.compile* allow competitive performance without changing the simplicity of the code. Fig. 2 presents detailed timings of the Exchange Field calculation. Magnum.np is open-source under the GPL3 licence and can be found at \url{https://gitlab.com/magnum.np/magnum.np}. Different demo scripts are part of the source code and can be tested online using Google Colab, without the need for local installations or specialized hardware like GPUs.

[1] - Florian Bruckner, Sabri Koralta, Claas Abert, Dieter Suess, "magnum.np -- A PyTorch based GPU enhanced Finite Difference Micromagnetic Simulation Framework for High Level Development and Inverse Design" https://arxiv.org/abs/2302.08843 (2023) - under Review

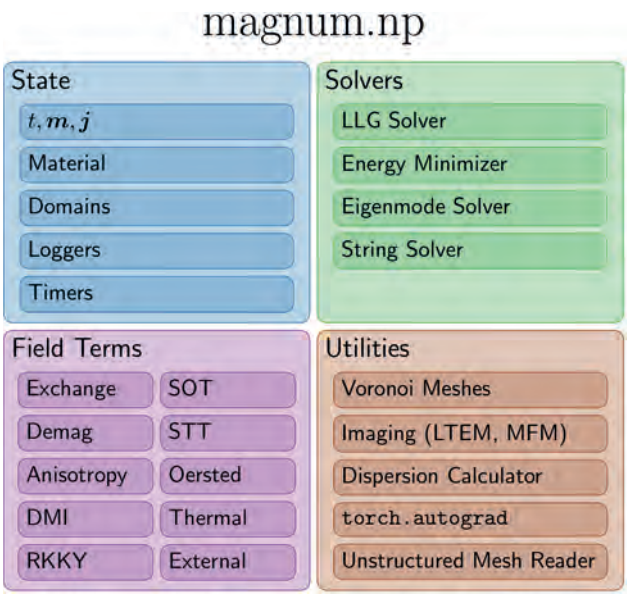

Fig.2. Overview of basic architecture of magnum.np and available main features.

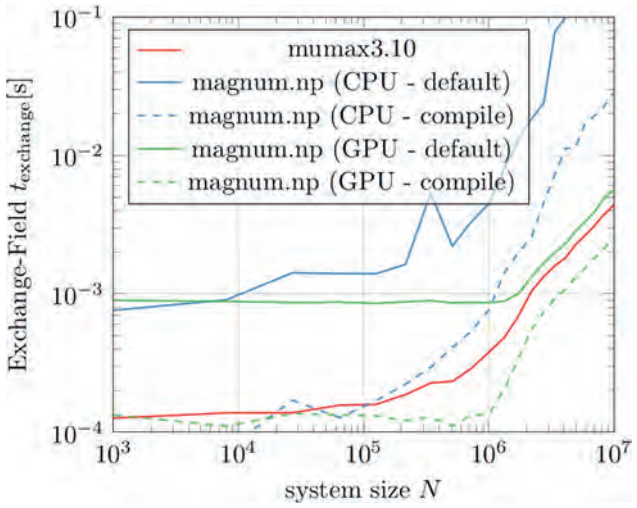

Fig.2. Performance of magnum.np compared to mumax3 for the calculation of the exchange field. Magnum.np can be operated both single and double precession, on CPU and GPU. Torch.compile enables very fast pythonic code with future improvements.

CQ-04. Direct-Current Electrical Detection of Surface-Acoustic-Wave-Driven Ferromagnetic Resonance. *C. Chen*[1] and C. Song[1] *1. School of Materials Science and Engineering, Tsinghua University, Beijing, China*

Surface acoustic wave (SAW) provides a promising platform to study spin-phonon coupling, which can be achieved by SAW-driven ferromagnetic resonance (FMR) for efficiently acoustic manipulation of spin. A well-established model for SAW-driven FMR is based on the magneto-elastic effective field, which is proportional to the magneto-elastic coupling coefficient and strain component[1,2]. Plenty of techniques and equipment have been developed to investigate magneto-elastic effective field, including vector network analyzer[3,4] magneto-optical methods[5] and X-ray magnetic circular dichroism-photoemission electron microscopy[6]. However, these methods need complicated analysis and cost-prohibitive equipment, which drastically block future widespread application and are incompatible with modern microelectronic circuits. Here, by integrating ferromagnetic stripes with SAW delay lines, we report direct-current detection for SAW-driven FMR based on electrical rectification. By analyzing FMR rectified voltage, we straightforwardly characterize and extract the effective fields, which exhibits advantages of better integration compatibility and lower cost. Large nonreciprocal rectified voltage is obtained, which is attributed to the coexistence of in-plane and out-of-plane effective fields. The effective fields can be modulated by controlling the longitudinal and shear strains within the films to achieve almost 100 % nonreciprocity ratio. Besides the fundamental significance, our finding provides a unique opportunity for designable spin acousto-electronic device and its convenient signal readout.

[1] M. Weiler, L. Dreher and C. Heeg, Phys. Rev. Lett., 106, 117601 (2011). [2] L. Dreher, M. Weiler and M. Pernpeintner, Phys. Rev. B, 86, 134415 (2012). [3] R. Sasaki, Y. Nii and Y. Iguchi, Phys. Rev. B, 95, 020407 (2017). [4] S. Tateno and Y. Nozaki, Phys. Rev. Appl., 13, 034074 (2020). [5] M. Jaris, W. Yang and C. Berk, Phys. Rev. B, 101, 214421 (2020). [6] B. Casals, N. Statuto and M. Foerster, Phys. Rev. Lett., 124, 137202 (2020).

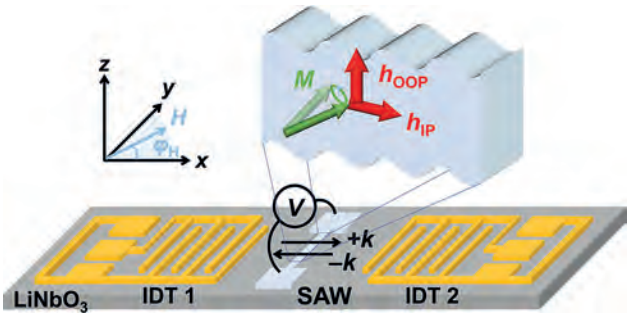

Fig. 1 Experimental setup for detecting SAW-driven FMR. SAWs are launched on piezoelectric $LiNbO_3$ substrate by interdigital transducers (IDT). The zoom-in view shows the strain within the stripe induced by SAW and effective fields, including in-plane h_{IP} and out-of-plane field h_{OOP}, acting on the magnetization to drive FMR.

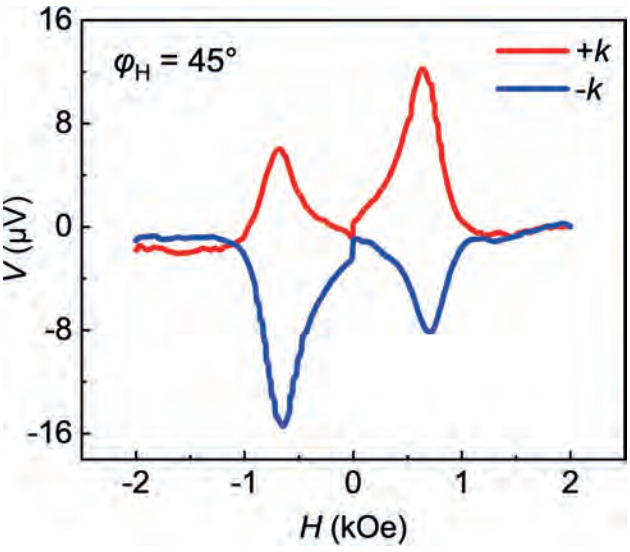

Fig. 2 Typical SAW-driven FMR spectrum measured at φ_H = 45° under the excitation of SAW (frequency = 2.79 GHz) in the Ni(16 nm)/Si(19 nm) sample. *+k* and *–k* represent wave vectors of SAW propagating along *+x*- and *–x*-direction, respectively.

CQ-05. Simulating interactions between antiferromagnetic NiO and circularly polarized THz light. *T. Jeffrey*[1], B. Jungfleisch[2] and J. Sklenar[1] *1. Physics and Astronomy, Wayne State University, Detroit, MI, United States; 2. Physics and Astronomy, University of Delaware, Newark, DE, United States*

In the field of antiferromagnetic spintronics, studying the behaviors exhibited by antiferromagnets in the presence of external fields is key to understanding the dynamics of antiferromagnetic materials. For many of these materials, antiferromagnetic resonance frequencies occur in the THz range in comparison to the GHz range for ferromagnetic resonance. NiO is an antiferromagnetic material of interest due to its resonance frequency near 1 THz [1,2]. Using frequency-domain THz spectroscopy, we have measured the antiferromagnetic resonance of three different orientations of monocrystalline NiO (111), (110), and (100). All three orientations show an absorption peak near 1 THz, however the amplitude of the (110) absorption peak suggests that this orientation couples more strongly to the circularly polarized THz wave. To investigate the origin of the enhanced absorption in the (110) sample we perform simulations for each orientation. The magnetization of the NiO is represented using two layers with an antiferromagnetic interlayer coupling. Because the moments of the NiO lie within the (111) planes, the circularly polarized THz field must be oriented so that it is oblique to the plane where the moments lie. For example, the (110) sample sees the THz field interacting with the planes of magnetization at an angle of 35.26 degrees, as this is the angle between the (111) and (110) planes. Using our experimental data as a consistency check, the goal of these simulations is to create a guide so that we can optimize how to excite magnetization dynamics in an easy-plane antiferromagnet using circularly polarized THz light.

[1] Moriyama, Takahiro, et al. Physical Review Materials 3.5 (2019): 051402. [2] Moriyama, Takahiro, et al. Physical Review Materials 7.5 (2023): 054401.

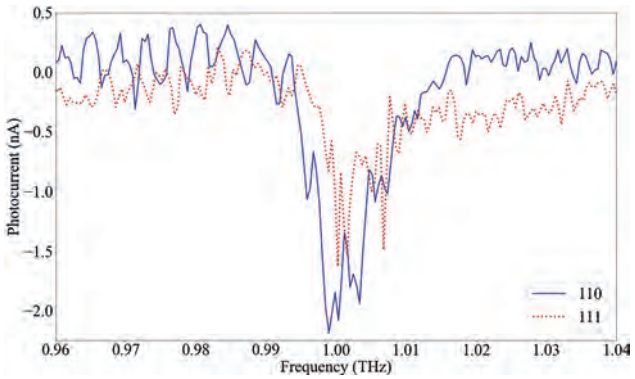

Figure 1. Frequency-domain THz spectroscopy results of the antiferromagnetic resonance for NiO orientations (110) and (111).

CQ-07. Electronic Heat Bath Simulations for Ultrafast Spin Dynamics. *J. Ross*[1], R. Chantrell[1] and R. Evans[1] *1. School of Physics, Engineering and Technology, University of York, York, United Kingdom*

Magnetic modelling for ultrafast simulations at the atomistic scale makes common use of Langevin Dynamics to model the effect of thermal fluctuations on the precession of the magnetic moment. Such a model is simplistic and assumes thermal noise is uncorrelated in space or time [1]. In general, however, the thermal fluctuations in a material are correlated through collective occupation of electron, phonon, and magnon modes in the system. Here, we present an improved thermostat for ultrafast atomistic scale magnetic simulations using a Monte Carlo (MC) solution to a two-electron Boltzmann transport equation (BTE) with both time and advection steps. The main divergence of our method from the literature is the implementation of a dynamic electron environment in Cartesian space. Electron equilibrium is maintained through the relaxation time approximation conserving energy and momentum in Cartesian space. Unlike other MC methods which redraw electron distributions according to the BTE evolution [2], our electron distribution changes purely from two-electron and electron-phonon scattering events [3]. The use of this dynamically determined electron environment allows for coupling of spatially and temporally correlated thermal and spin transport phenomena to the atomistic magnetic moment. Currently, our environment simulates charge and heat transport in metals on ultrafast time scales during severe non-equilibrium caused from applied electric fields or laser pulses. The electron-electron and electron-phonon relationship is parametrized into the relaxation time approximation using constants derived from experimental data [4,5]. Our environment successfully reproduces the popular *two-temperature model* (Fig 1), with the added advantage of resolving energy-dependent lifetimes of excited states (Fig 2). In the future, this will offer the ability to include correlated spin effects not possible in Langevin Dynamics.

[1]. R. F. L. Evans, W. J. Fan and P. Chureemart, *J. Phys.: Condens. Matter., Vol.* 26, p.103202 (2014) [2]. W. Miao, Y. Guo and X. Ran, Phys. Rev. B., Vol. 99, p.205433 (2019) [3]. B. Y. Mueller and B. Rethfield, Phys. Rev. B., Vol. 87, p.035139 (2013) [4]. M. van Kampen, J. T. Kohlhepp and W. J. M. de Jonge, J. Phys.: Condens. Matter., Vol. 17, p.6823 (2004) [5]. L. Jiang and H. Tsai, ASME. J. Heat Transfer., Vol. 127, p.1167 (2005)

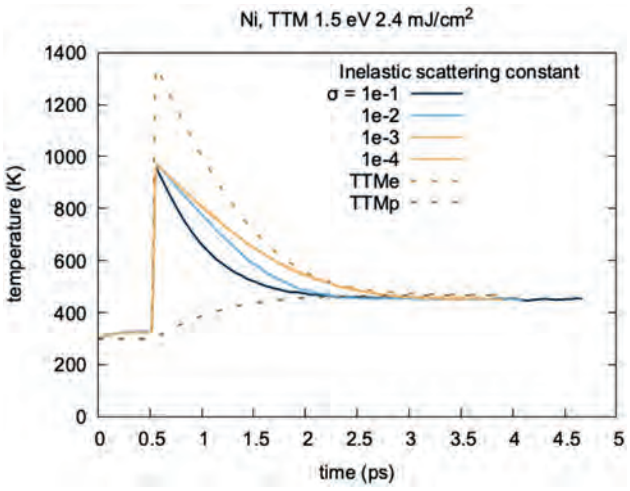

Figure 1. Simulated electron temperatures (solid lines) following laser exposure compared to the standard TTM (dashes). The varying dynamics are a result of varying the inelastic electron-electron scattering constant.

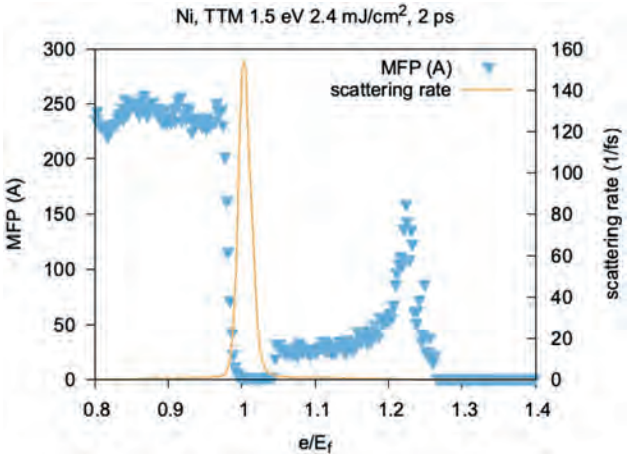

Figure 2. Mean free path and scattering rate 2 ps after laser excitation as a function of energy.

CQ-08. ML-based Magnetization Field Classification. *S. Pathak*[1], K. Rahir[2], S. Holt[1], M. Lang[2,1] and H. Fangohr[1,2] *1. Computational Science, Max Planck Institute for the Structure and Dynamics of Matter (MPSD), Hamburg, Germany; 2. Faculty of Engineering and Physical Sciences, University of Southampton, Southampton, United Kingdom*

Magnetic materials at the nanoscale have attracted considerable interest both from academia and industry. A key aspect is the thorough understanding of the emerging magnetization field configurations, and their behaviour within samples and devices. However, an in-depth study such as plotting a magnetic phase diagram [1, 2] as a function of geometry, material parameter or applied field, can lead to creation of a large amount of data. Its evaluation typically requires considerable human effort and time. We report that it is possible to automate this process, to a certain degree, using an unsupervised machine learning (ML) algorithm. In this study, we use Agglomerative Clustering in magnetic phase diagram discovery of a FeGe disc with changing external magnetic field. First, we obtain the equilibrium magnetisation configurations by changing the field values from 0 to 1.2 T using micromagnetic simulations. Second, we obtain a feature space by passing the simulation data through the pre-trained layers of VGG-16 [3]. As the final step, we perform the Agglomerative Clustering on the feature space to sort the configurations in different classes. We find that the algorithm performs well when compared to the published results [1] on the same material geometry and range of external fields (Fig. 1). Although, the different classes obtained through the process do show some mixing of the equilibrium magnetisation configurations (Fig. 2). Our study shows that ML can be used to aid researchers in evaluating large amounts of magnetisation data. In our case, the algorithm clustered a thousand simulation results into individual classes without any training or human supervision, greatly reducing human effort for the task.

[1] M. Beg *et al.*, *Sci. Rep.* 5, no. 1 (2015) [2] S. Pathak *et al.*, *Phys. Rev. B.* 103, no. 10 (2021) [3] K. Simonyan *et al.*, *ICLR*, (2015)

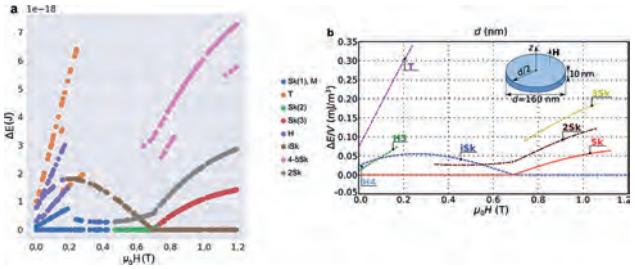

Fig 1: Plot of total energy of the equilibrium magnetisation states at a given external field compared to the ground state. (a) The result obtained through the ML clustering algorithm. (b) Published results [1] on the same geometry.

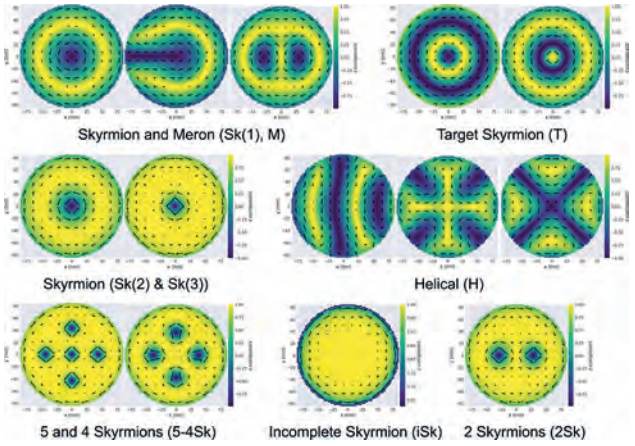

Fig 2: Magnetisation classes obtained through the ML clustering algorithm.

CQ-09. Efficient Micromagnetic Modelling of Strongly Interacting Nanomagnets. *A. Manzin*[1], R. Ferrero[1] and M. Vicentini[1] *1. Istituto Nazionale di Ricerca Metrologica, Torino, Italy*

This work presents a GPU-parallelized 3D micromagnetic solver for the efficient calculation of magnetization dynamics in 3D distributions of magnetic nano-objects, strongly interacting in the space in a random or ordinated configuration. The nano-objects can be magnetic nanoparticles for biomedical applications, which can also have complex shape and size leading to multi-domain state [1]. Moreover, the handled nano-objects can be magnetic nanodevices, like magnetoresistive or spintronic sensors displaced in the environment, system or body to be monitored [2]. In the developed micromagnetic solver, curved surfaces can be accurately modelled thanks to the use of a finite difference approach enabling the calculation of the exchange and magnetostatic fields on non-structured meshes [3]. To allow the accurate simulation of many objects, the magnetostatic field is locally separated into two contributions, i.e. a short-range and a long-range one. The first contribution, which includes the magnetostatic interactions internal to each object, is obtained by numerically solving the Green's integral equation. The second contribution, which takes into account the inter-object magnetostatic interactions, is determined by approximating each object as a collection of magnetic dipoles, associated with mesh elements. The accuracy and computational efficiency of the micromagnetic solver are analysed by comparison

to a standard 3D-FFT code [4], putting in evidence the reliability and flexibility of the proposed methodology in handling many objects, without any restrictions on their shape and orientation in the space [5]. The figures below provide an example of application, i.e. the calculation of the hysteresis loops of magnetic nanorings randomly distributed with variable volume concentrantion, to explore their applicability in magnetic hyperthermia.

[1] H. Gavilán et al., Nanoscale, Vol. 13, p. 15631-15646 (2021). [2] S. Jung et al., Nature, Vol. 601, p. 211-216 (2022). [3] A. Manzin and R. Ferrero, J. Magn. Magn. Mater., Vol. 492, 165649 (2019). [4] R. Ferrero and A. Manzin, J. Magn. Magn. Mater., Vol. 518, 167409 (2021). [5] A. Manzin, R. Ferrero and M. Vicentini, Adv. Theory Simul., Vol. 4, 2100013 (2021).

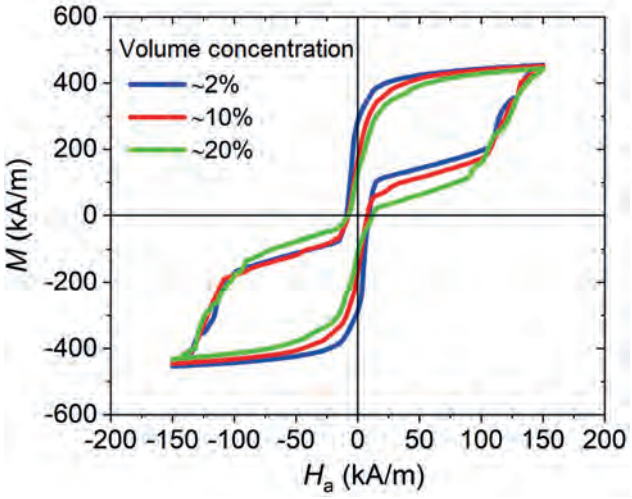

Calculated hysteresis loops of magnetite nanorings with external diameter of 150 nm, internal diameter of 90 nm and thickness of 30 nm, randomly distributed in the space with variable volume concentration.

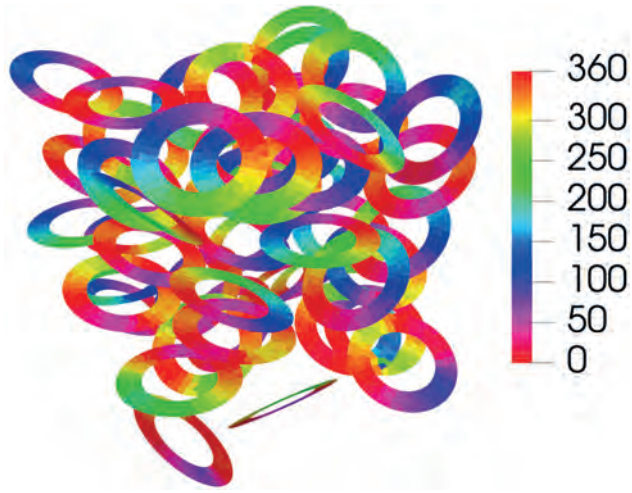

Remanence magnetization spatial distribution for a volume concentration of 20%.

CQ-10. Optical Detection of Antiferromagnetic Resonance in van der Waals Antiferromagnets. *A. Melendez*[1], S. Das[1], I. Kao[2], F. Ayala Rodriguez[1], W. Liu[3], B. Lv[3], S. Singh[2] and C. Hammel[1] *1. Physics, The Ohio State University, Columbus, OH, United States; 2. Physics, Carnegie Mellon University, Pittsburgh, PA, United States; 3. University of Texas Dallas, Dallas, TX, United States*

In recent years, antiferromagnets have been shown to be advantageous as components in high frequency and robust spintronic devices[1-2]. However, detection and characterization of antiferromagnetic dynamics is challenging due to high resonant frequencies and lack of net magnetization. One method to detect antiferromagnetic dynamics is the use of atomic-scale color centers, which are optically active point defects in crystals. Color centers constitute sensitive noninvasive probes with the ability to detect local fields and fluctuations emanating from dynamics in magnetic systems[3]. In addition to nitrogen-vacancy (NV) centers in diamond, recently discovered color centers in hexagonal boron nitride (h-BN) hold promise for achieving close proximity to a sample surface which aids in sensing the short-range magnetic field fluctuations produced by antiferromagnetic dynamics[4]. Moreover, dynamics at frequencies well above the color center resonance frequency can be indirectly detected through magnon scattering that produces local magnetic noise at the color center resonance frequency[3,5]. Here we present the first optical detection of antiferromagnetic resonance in the van der Waals materials $CrCl_3$ and CrSBr. This measurement allows inferences to be made about the parameters that govern the dynamics in thin samples that would otherwise be challenging to measure using conventional FMR. This technique provides a powerful tool for studying dynamics driven at the interface between thin antiferromagnets and neighboring systems that couple to the antiferromagnetic state.

1. T. Jungwirth, *et al.,* Nature Nanotech. Vol. 11, p.231-241 (2016) 2. V. Baltz, *et al.,* Rev. Mod. Phys. Vol. 90, 015005 (2018) 3. H. Wang, *et al.,* Sci. Adv. Vol. 8, eabg8562 (2022) 4. A. Gottscholl, *et al.,* Nat. Mater. Vol. 19, p.540-545 (2020) 5. B.A. McCullian, *et al.,* Nat. Commun. Vol. 11, 5229 (2020)

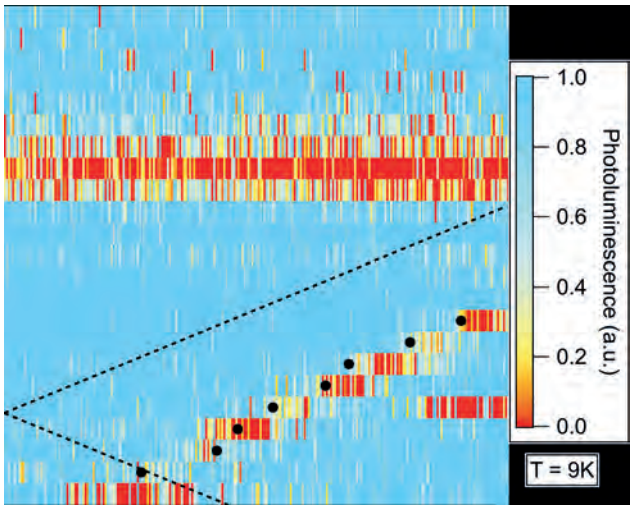

Optical detection of antiferromagnetic resonance in ~10μm $CrCl_3$ using NV centers as a function of field and frequency, showing acoustic (lower) and optical (upper) AFMR modes. Dynamics were excited by a microwave stripline at 9K with field applied in plane.

CQ-11. Helicity-dependent optical control of the magnetization state emerging from the Landau-Lifshitz-Gilbert equation. B.J. Assouline[1] and *A. Capua*[1] *1. Applied Physics, Hebrew University of Jerusalem, Jerusalem, Israel*

Ferromagnetic resonance experiments are usually carried out at the GHz range. In contrast, optical fields oscillate much faster, at ~400-800 THz. Therefore, it seems unlikely that such fast-oscillating fields may interact with magnetic moments. However, the amplitude of the magnetic field in ultrashort optical pulses can, temporarily, be very large such that the magnetization may respond extremely fast. For example, in typical experiments [1-3] having ~ 40 fs - 1 ps pulses at 800 nm, with energy of 0.5 mJ that are focused to a spot size of ~ 0.5 mm^2, the peak magnetic flux density can be as high as ~ 5 T, for which the corresponding Gilbert relaxation time reduces to tens of picoseconds in typical ferromagnets. Here we show that ultrashort optical pulses may control the magnetization state by merely considering the optical magnetic field in the Landau-Lifshitz-Gilbert equation [4]. We find that the strength of the interaction is determined by {eta} = {alpha}*{gamma}*H/{f_opt}, where {f_opt}

and {alpha} are the angular optical frequency and the Gilbert damping, respectively, and {gamma} and H the gyromagnetic ratio and the amplitude of the optical field. Accordingly, the loss of spin angular momentum to the lattice is key to the interaction. Moreover, we show that for circularly polarized pulses, the polarity of the optically induced torque is determined by the optical helicity. From a quantitative analysis, we find that a sizable effective out-of-plane field is generated, which is comparable to that measured experimentally in ferromagnet/heavy-metal material systems [5].

[1] C. D. Stanciu, F. Hansteen and T. Rasing, Physical Review Letters 99, 047601 (2007). [2] D. Steil, S. Alebrand and M. Aeschlimann, Physical Review B 84, 224408 (2011). [3] G. Kichin, M. Hehn and S. Mangin, Physical Review Applied 12, 024019 (2019). [4] B. Assouline, A. Capua, arXiv:2306.04617 (2023). [5] G.-M. Choi, A. Schleife, and D. G. Cahill, Nature Communications 8, 15085 (2017).

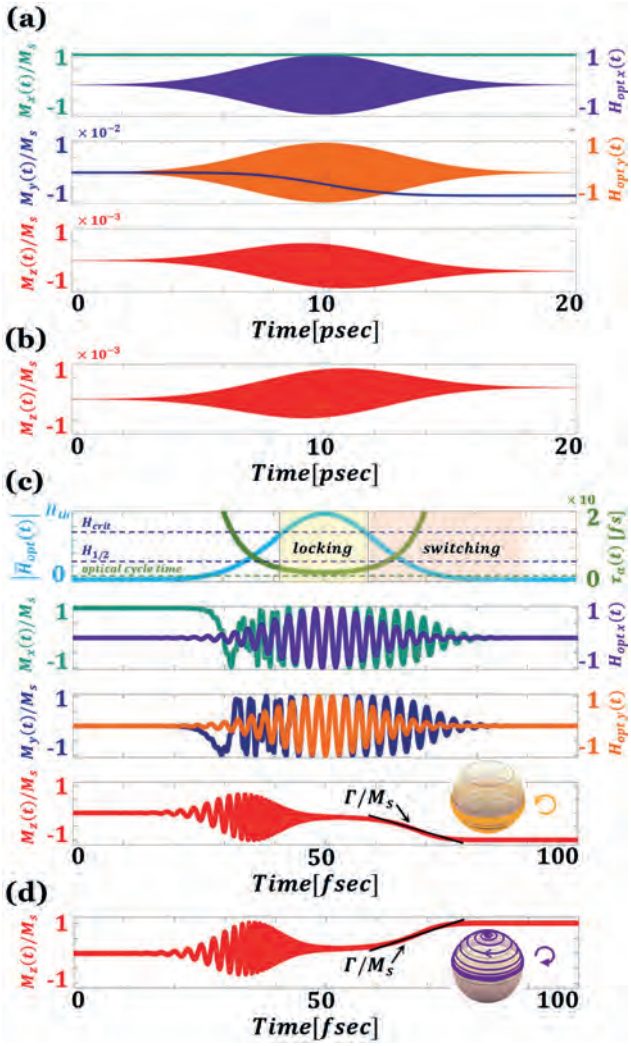

Magnetization dynamics induced by an RCP Gaussian pulse. Top and middle panels depict the temporal evolution of the transverse components of the magnetization and the optical field in normalized units. Bottom panel depicts the longitudinal component of the magnetization, (b) for the application of an LCP pulse. (c) Magnetization reversal induced by an RCP Gaussian pulse of higher amplitude.

CQ-12. High-frequency response of magnetic nanoparticle arrays studied with micromagnetic simulations. K. Brzuszek[2], C.A. Ross[1] and *A. Janutka*[2] *1. Department of Materials Science and Engineering, Massachusetts Institute of Technology, Cambridge, MA, United States; 2. Department of Theoretical Physics, Wroclaw University of Science and Technology, Wroclaw, Poland*

Using micromagnetic simulations, we study the magnetic response of composites of magnetic nanoparticles (MNPs) embedded in dielectric matrices to high-frequency (0.1÷1.0 GHz) field. Such systems are considered as core materials for power microconverters of reduced conductivity, thus, of lowered eddy-current-related loss. The ultimate reduction of the conductivity is achievable using superparamagnetic cores which are composites of highly-separated MNPs. In spite of their relatively-low permeability, such materials can offer noticeable performance of microinductors or microtransformers relative to air-core devices [1]. Our simulations include thermal fluctuatios and magnetostatic interactios between MNPs both playing crucial role in the magnetization dynamics of MNPs. Use of numerical approach is motivated by considering the driving field of high amplitude which exceeds limitations of the linear response regime. Additionally, we do not restrict our simulations of high-frequency driving to the macrospin approximation for MNPs, thus, including the competition between the magnetocrystalline and shape anisotropies inside MNPs. Applying periodic boundary conditions, we test 3D arrays of spherical high-magnetization MNPs of uniaxial magnetic anisotropy ($Fe_{65}Co_{35}$, [2]) and of cubic anisotropy (Fe), as well as MNPs of lower magnetization (Fe_3O_4) in terms of the amplitude of the magnetic response function (Fig. 1) and the dynamical magnetization-field curves (Fig. 2). We evaluate and compare high-frequency susceptibilities of the nanocomposites and determine conditions of opening the dynamical hysteresis loop with regard to reducing magnetic loss.

[1] M. Kin, H. Kura, T. Ogawa, AIP Advances 6 (2016) 125013, [2] K. Brzuszek, C. A. Ross, A. Janutka, J. Magn. Magn. Mat. 573 (2023) 170651

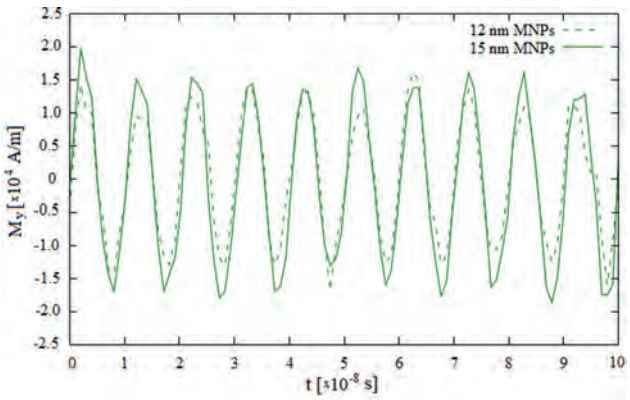

Magnetization vs. time for array of 12nm (dashed line) and 15 nm (solid line) MNPs driven with 10mT field of 0.1GHz frequency at T=300K.

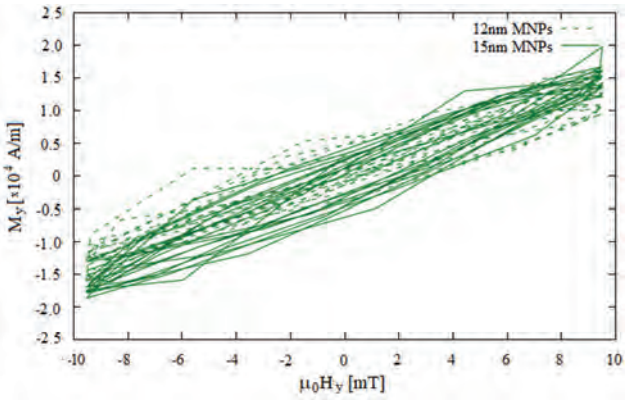

Dynamical M-H curve for arrays of 12nm (dashed line) and 15 nm (solid line) MNPs driven with 10mT field of 0.1GHz frequency at T=300K.

CQ-13. Ferromagnetic resonance investigation of CoFeB/W bilayers on SiO_2, MgO, and Al_2O_3 substrates. *U. Karki*[1], J. Cox[2], T. Mewes[1] and J.B. Mohammadi[2] *1. Physics and Astronomy, The University of Alabama, Tuscaloosa, AL, United States; 2. Physics, Loyola University, New Orleans, LA, United States*

Investigating the dynamic response of ferromagnetic materials adjacent to non-ferromagnetic materials is significantly important to understand the underlying physics that impact spintronic device performance [1]. Ferromagnetic resonance measurements allow us to determine perpendicular magnetic anisotropy (PMA), required to achieve high density magnetic memory. In addition, it provides information about magnetic damping, important for device performance metrics such as critical current for spin-torque switching. Understanding the interfacial properties of CoFeB/W is verry important as it has been widely used in Perpendicular Magnetic Tunnel Junctions (PMTJs). Using W as capping layer were reported to enhance effective perpendicular anisotropy and make storage layer robust and hence it promises as reliable candidate for next generation low power high performance memory and logic devices [2-4]. Here, we report on ferromagnetic resonance study of *as deposited* CoFeB/W bilayers on the most used substrates (i.e., SiO_2, MgO, and Al_2O_3). Our results show a linear decrease of effective magnetization with the inverse of CoFeB thickness, indicating interfacial PMA. Moreover, MgO substrates facilitate strong interfacial PMA compared to SiO2 and Al_2O_3 substrates. We will present in detail about the contribution of interfacial perpendicular anisotropy (K_i) on the total perpendicular magnetic anisotropy (K_u) of CoFeB/W on different substrates and dependence of relaxation mechanism and higher order anisotropies [5, 6] on ferromagnetic film thickness.

1. Liu, X.Y., et al., *Ferromagnetic resonance and damping properties of CoFeB thin films as free layers in MgO-based magnetic tunnel junctions.* Journal of Applied Physics, 2011. 110(3). 2. Ikeda, S., et al., *A perpendicular-anisotropy CoFeB-MgO magnetic tunnel junction.* Nature Materials, 2010. 9(9): p. 721-724. 3. Kim, J.H., et al., *Ultrathin W space layer-enabled thermal stability enhancement in a perpendicular MgO/CoFeB/W/CoFeB/MgO recording frame.* Scientific Reports, 2015. 5. 4. Miura, S., et al., *Insertion Layer Thickness Dependence of Magnetic and Electrical Properties for Double-CoFeB/MgO-Interface Magnetic Tunnel Junctions.* Ieee Transactions on Magnetics, 2019. 55(7). 5. Shaw, J.M., et al., *Perpendicular Magnetic Anisotropy and Easy Cone State in Ta/Co60Fe20B20/MgO.*Ieee Magnetics Letters, 2015. 6. 6. Mohammadi, J.B., et al., *Strong interfacial perpendicular anisotropy and interfacial damping in Ni0.8Fe0.2 films adjacent to Ru and SiO2.* Journal of Applied Physics, 2019. 125(2).

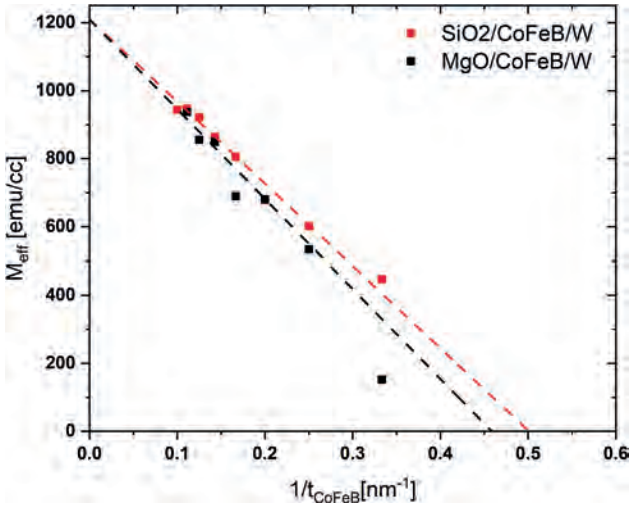

Effective magnetization (M_{eff}) vs reciprocal thickness of CoFeB ($1/t_{CoFeB}$) on substrates SiO_2 and Al_2O_3.

CQ-14. Complex field-reversal dynamics in nanomagnetic systems. *M.D. Saccone*[1] and F. Caravelli[1] *1. T4/CNLS, Los Alamos National Laboratory, Los Alamos, NM, United States*

The broad field of metamaterials uses nanoscale fabrication techniques to create systems with collective behaviors that mimic or go beyond those exhibited in natural materials. The innate properties of metamaterial "atoms" differ from literal atoms and molecules, often introducing second order kinetic behaviors that give rise to new complexity. Nanomagnetic materials, which started as analogies to frustrated magnetism built from thin, patterned films of ferromagnetic materials, are now being considered for device physics which depend heavily on the systemic dynamics and coupling to external magnetic field. A recent model of how nanomagnetic domains flip, the Glauber mean-field model, is used here to understand how systems of nanomagnets flip directions when opposed by external field. This reversal is solvable on one dimensional chains and trees at zero temperature, the cascade of spin flips giving rise to harmonic power spectra. The same cascades in two and three dimensions form fractal clusters whose shape depends on the strength of the field and the tuning of interactions between nanomagnets. The results suggest experiments in physical nanomagnets that can produce fractal structures which are potentially useful to neuromorphic applications and could better explain recent results in pyrochlore magnetic systems that suggest fractal structures emerge in the dynamics.

Saccone, Michael, and Francesco Caravelli. "Complex field reversal dynamics in nanomagnetic systems." *arXiv preprint arXiv:2302.04857* (2023).

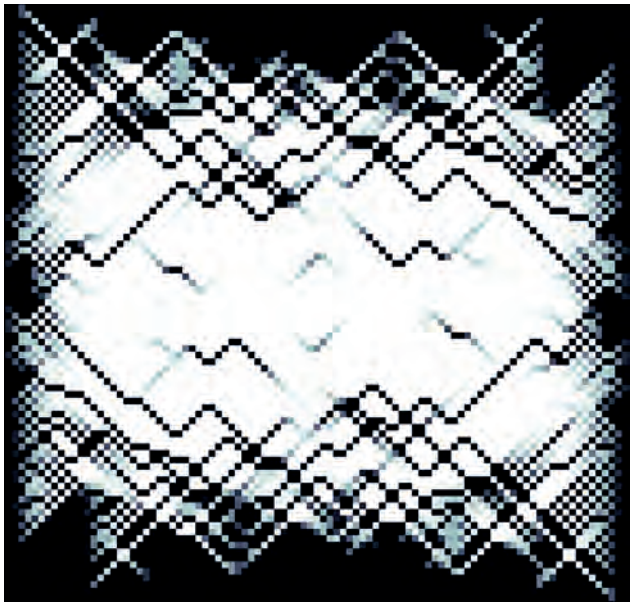

Session CR
MICROSCOPY & CHARACTERIZATION II
(Poster Session)

Claas Abert, Chair
University of Vienna, Vienna, Austria

CR-01. On the origin of systematic errors in VSM Torque Curves.
A. Sapkota[1], L. Rodriguez[2], K. Dieckow[1], D. Binod[2], C. Howlader[2,4], J. Tate[2,3] and W. Geerts[1,2] *1. Physics, Texas State University, San Marcos, TX, United States; 2. Materials Science, Engineering and Commercialization, Texas State University, San Marcos, TX, United States; 3. Ingram School of Engineering, Texas state University, San Marcos, TX, United States; 4. Electroninks, Austin, TX, United States*

Magnetic anisotropy (K_2) is a basic and crucial property that affects the magnetic performance of permanent magnetic materials. Torque measurements are normally used to measure a sample's K_2 and can be taken using a torque magnetometer (TM) or indirectly measuring the magnetic dipole moment perpendicular to the field using a vibrating sample magnetometer (VSM) [1]: $\tau = \mu_0 M_y H_x$ Most TM only operate at room temperature. However, a biaxial VSM allows straightforward torque measurements at varying temperatures. VSM torque curves comprise a 2θ background caused by the small misalignments of the sample on the sample rod, and/or a non-azimuthal symmetric sample shape. These errors originate from the position dependence of the pickup coil sensitivity matrix S: $X_x=S_{xx}M_x + S_{xy}M_y$, $X_y=S_{yx}M_x + S_{yy}M_y$ Where (X_x, X_y) and (M_x,M_y) are the pickup coil signals and sample magnetic dipole vectors. The $S_{xx}(S_{yy})$ and $S_{xy}(S_{yx})$ represent the coil's sensitivities and cross-talks respectively. Fig. 1 shows the contour plot of the calculated cross-talk for a Mallinson coil set [2] which is only zero for a perfectly-centered cylindrical symmetric sample. It is clear that the cross talk of an elongated wire sample (red line) or a dot sample that describes a circular trajectory (black circle) in between the pickup coils depend on the sample-holder angle and contributes to a large 2θ term in the X_y. Here, the magnetic torque of a strontium ferrite/PA-12 3D printed samples [3] was explored using biaxial VSM. Torque curves were taken from 16-22kOe every 2kOe on a 4.8 mm wire and a 1.2 mm dot sample using a MicroSense EZ9 VSM. Fourier analysis was used to determine the second harmonics from each torque curve. The wire sample's τ-1/H curve shows a slope. Note that, strontium ferrite saturates above 19 kOe, and the true torque curve of a wire sample and a VSM torque curve of a dot sample with a length of 1.2mm show almost no slope. So, we conclude that this slope originates from a shape cross-talk contribution to the X_y. This work was supported in part by NSF through DMR- MRI Grant under awards 2216440 and in part by DOD instrumentation grant (78810-W911NF-21-1-0253).

[1] B.C Dodril et al., "Magnetic Anisotropy: Measurements with a Vector Vibrating Sample Magnetometer", Lake Shore Cryotronics, Inc., 575 McCorkle Blvd., Westervile, Ohio, USA. [2] Binod D.C. MSc. Thesis, Texas State University, Dec. 2019; Kolton Dieckow, MSc. Thesis, Texas State University, May 2021. [3] Tanjina Ahmed. Ph.D. dissertation, Texas State University, February 2023.

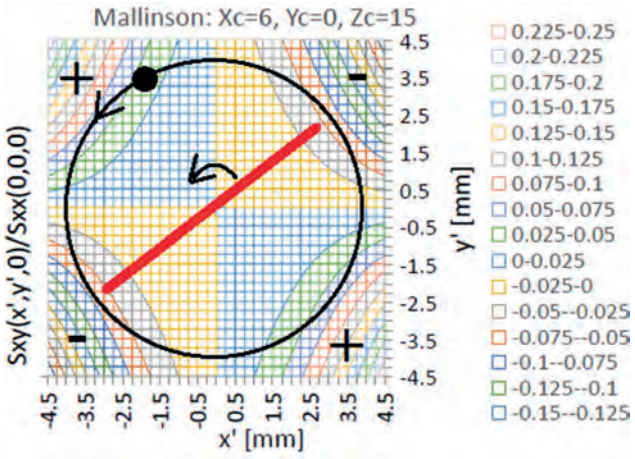

Fig. 1: Effect of Shape and Wobble on cross-talk

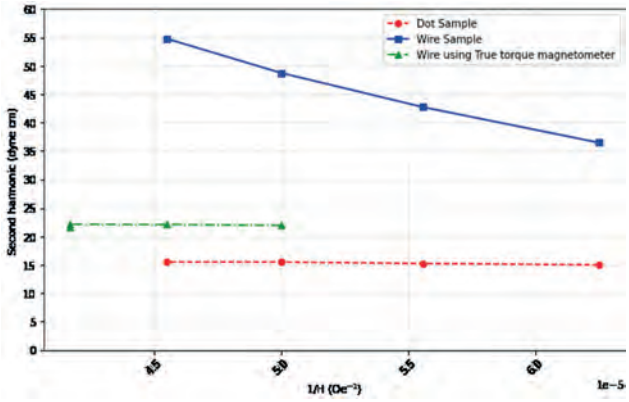

Fig 2: measured normalized τ versus 1/H

CR-02. Computational Modelling of a Triaxial Vibrational Sample Magnetometer.
L. Rodriguez[1], A. Sapkota[2], J. Tate[1] and W. Geerts[1,2] *1. MSEC, Texas State University, San Marcos, TX, United States; 2. Physics, Texas State University, San Marcos, TX, United States*

Magnetic Field Assisted Additive Manufacturing (MFAAM) has enabled the ability to 3D print magnetic materials in a wide multitude of shapes which have a complex anisotropy energy surface containing contributions generated from different origins such as sample, particle, and agglomerate shape anisotropy, flow and field induced anisotropy, and particle crystal anisotropy. Magnetic anisotropy describes how a magnetic materials magnetic properties vary depending on the direction of observation. The various 3D printed material shapes facilitated the need to measure the x, y, and z components of the magnetic dipole moment simultaneously. This work aims to develop a triaxial vibrational sample magnetometer (VSM) by adding a z-coil set to a preexisting biaxial VSM employing a modified Mallison coil set. The optimum size and location of the sensing coils are determined from modelling the sensitivity matrix of the z-coil set using the framework

provided by [1]. The magnetic scalar potential at a field point (z,r) for a coil at the origin is given by: $V_c(z,r)=\sum_{(l=1,3,5)}B_l/r^{(l+1)}P_l(z/r)$ Where P_l is the Legendre polynomial and B_1, B_2, and B_3 are constant that depend on the coil's length, inner and outer diameter. Assuming that the sample is vibrating in the z-direction the diagonal components of the sensitivity matrix are given by: $S_{ii}=\partial^2/\partial i\partial z(V_c(z,r))$ Where i is, x, y or z. Mathematica [2] was used to model the two configurations sketched in Fig. 1. For the 4 coil configuration the sensitivity Szz increases with smaller inner diameter, i.e. reduction from 6 to 5 mm results in an increase of Sz with 20%. This configuration allows for the use of coils with larger OD as the coils are placed outside the gap. Szz doubles when increasing the OD with a factor 1.4. For the on axis two coil configuration the OD and ID of the coils are limited by pole piece distance and sample size. Calculated Szz for the two coil configuration were typically higher. This work was supported in part by NSF through DMR- MRI Grant under awards 2216440 and in part by DOD instrumentation grant (78810-W911NF-21-1-0253).

[1] J. P. C. Bernards, "Design of a detection coil system for a biaxial vibrating sample magnetometer and some applications," *Rev. Sci. Instrum.*, vol. 64, no. 7, pp. 1918–1930, Jul. 1993, doi: 10.1063/1.1143977. [2] Wolfram Research, Inc., Mathematica, Version 13.3, Champaign, IL (2023)

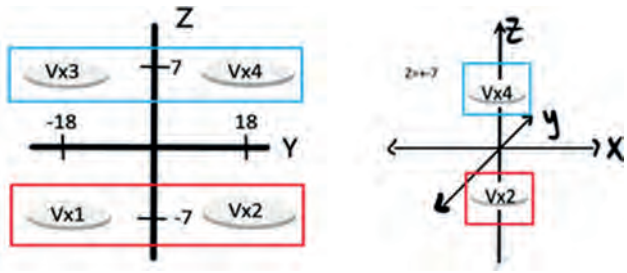

Fig. 1: four coil configuration (left) and two coil configuration (right)

CR-03. Magneto Optical Characterization of TCO Films using Standard and Enhanced Cavity Configurations. *M. Syed*[1], S. Reza[1], P. Miller[1] and B. Roop[1] *1. Physics & Optical Engineering, Rose-Hulman Institute of Technology, Terre Haute, IN, United States*

Carrier response in conducting samples is typically investigated using measurements like Hall Effect and 4-point probe measurements. We use a very sensitive AC Faraday rotation (FR) setup to show that magneto-optic techniques can also be utilized to study thin film samples whose magnetic response is challenging to characterize. Samples included in this study are widely used in technological and research applications. The setup employs a stabilized He-Ne laser (633 nm) along with an AC magnetic field that enables lock-in detection (1). We investigate a series of transparent conducting oxide (TCO) samples deposited on a glass substrate. The TCO samples include the widely used Indium Tin Oxide (ITO) and the relatively newer Fluorine doped ITO films, usually referred to as FTO. These films have a magnetic response due to the presence of free carrier concentration and therefore measurement of this response (Verdet constant) is related to their carrier concentration (2). The response may be strong in relative terms (as in per unit length of the film), but is still challenging to measure given that the thickness range of these films which is usuallysub-micron. Since magneto optic responses like FR depend on the length of the sample length traveled by light, these sub-micron films pose considerable challenges. In this work we share and discuss the details of design and characterization of an optical cavity that allows multiples passes of light through the sample, effectively increasing the path length of the sample and thereby amplifying the FR signal from the sample. In addition, we share results from the cavity measurement and compare them to the single-pass conventional geometry to highlight the enhancement of the FR response due to the cavity. We have already shown that employing an AC version of FR along with lock-in detection enables us to measure small values of FR with high confidence (3). Cavity enhancement of these very small values represents a major step forward in extending the usefulness of FR as a characterization technique. To our knowledge this work represents a novel effort in the area of FR measurements of TCO films.

1. Jain, J. Kumar, F. Zhou, L. Li, Am. J. Phys. 67, 714 (1999). 2. J. Pankove, *Optical Processes in Semiconductors*, Dover, p.346 (1975). 3. C. Patterson, M. Syed, Y. Takemura, Journal of Magnetism and Magnetic Materials 451, 248-253 (2018).

CR-04. Magnetometry of Buried Co-based Nanolayers by Hard X-ray Photoelectron Spectroscopy. *A. Hloskovsky*[1], C. Schlueter[1] and G. Fecher[2] *1. Photon Science / DESY, Hamburg, Germany; 2. Max Planck Institute for Chemical Physics of Solids, Hamburg, Germany*

The intensity and shape of photoelectron lines of magnetic materials depend on the relative orientation of the sample magnetization, the X-ray beam polarization and the spectrometer axis, i.e. the electron emission direction. In the hard X-ray regime, the beam polarization can be conveniently modified utilizing the phase shift produced by a diamond phase plate in the vicinity of a Laue or Bragg reflection. A single-stage in-vacuum phase retarder is installed and commissioned in 2020 at the HAXPES beamline P22 at PETRA III (Hamburg, Germany) [1]. The electronic and magnetic properties of CoFe, CoFeB and Co-based Heusler nanolayers were studied using the linear and circular magnetic dichroism in the angular distribution of photoelectrons. The layers were remanently magnetized in-situ and Co $2p_{1/2}$ and $2p_{3/2}$ core levels were probed at room temperature [2-3]. Both the polarization-dependent spectra and the dichroism indicate that the lines of the multiplet extend over the entire spectral range. In particular, the dichroism does not vanish between the two main parts of the spin–orbit doublet. It is demonstrated that magnetic dichroism in HAXPES is an effective and powerful technique to perform element specific magnetometry of deeply buried ferromagnetic and antiferromagnetic magnetic materials, which are inaccessible with conventional soft X-ray photoelectron spectroscopy. Co spectrum has a an additional weak shoulder at 4 eV from the main $2p_{3/2}$ line. The feature becomes much clearer in the difference spectrum. This may be an indication of a correlation-induced satellite of majority spin nature in Co.

1. C. Schlueter, A. Gloskovskii, K. Ederer et al., AIP conference proceedings 2054(1), 040010 (2019). 2. G. H. Fecher, D. Ebke, S. Ouardi et al., *SPIN* 04, 1440017 (2014). 3. P. Swekis, A.S. Sukhanov, Y.-C. Chen, A. Gloskovskii et al., *Nanomaterials* 11, 251 (2021).

CR-05. Withdrawn

CR-06. Withdrawn

CR-07. Structural, Magnetic, and Magnetocaloric effect in Al doped $ErCr_{1-x}Al_xO_3$ (x = 0.25, 0.5) orthochromites. *J. Sultana*[1], A. Sawon[2], G. Brzykcy[2], A. Pathak[2] and S. Mishra[1] *1. Physics and Materials Science, The University of Memphis, Memphis, TN, United States; 2. Physics, Buffalo State(The State University of Newyork), Buffalo, NY, United States*

This paper investigates the structural, magnetic, and magnetocaloric characteristics of Al-doped $ErCr_{1-x}Al_xO_3$ (x=0.25, 0.5) orthochromites, which belong to the family of rare earth chromite's ($RCrO_3$) known for their intriguing physical properties. The samples were synthesized using the sol-gel auto combustion method, resulting in pure orthorhombic phases with the Pbnm space group, as confirmed by X-ray diffraction. The lattice parameters and volume exhibited a decrease with the substitution of Al^{3+} ions due to the smaller ionic radius of Al^{3+} (0.535Å) compared to Cr^{3+} (0.615Å). Fourier transform infrared spectroscopy analysis verified the presence of Ho–O, Cr–O, and Cr–Cr bonds in all samples. Magnetic measurements were carried out in the temperature range of 5K to 300K under magnetic fields up

to 0.2T to investigate the impact of Al^{3+} doping on the Neel temperature (T_N) for $ErCr_{1-x}Al_xO_3$ (x=0.25, 0.5). The results revealed a significant decrease in T_N below 100K for the Al doped $ErCr_{1-x}Al_xO_3$ samples, indicating a suppression of the magnetic ordering transition caused by the introduction of Al^{3+} dopants. Isothermal magnetization data at various temperatures were used to evaluate changes in the magnetic entropy and relative cooling power (RCP) in bulk $ErCrO_3$ with Al^{3+} substitution. $ErCrO_3$ had a maximum magnetic entropy of 11.60 $Jkg^{-1}K^{-1}$ at 11K and an RCP of 240.7Jkg^{-1} at 5T applied field. After Al doping, it was found that $ErCr_{0.75}Al_{0.25}O_3$ had a maximum magnetic entropy of 11.52$Jkg^{-1}K^{-1}$ at 11K with a 5T applied field and RCP of 283.85Jkg^{-1}, whereas $ErCr_{0.5}Al_{0.5}O_3$ had a maximum magnetic entropy of 11.63 $Jkg^{-1}K^{-1}$ at 5K with a 5T applied field and RCP of 321.5Jkg^{-1}. The observed variations in maximum magnetic entropy changes are attributed to the Al^{3+} substitution and its influence on the Cr^{3+}-Cr^{3+} exchange coupling, which is influenced by alterations in the Cr1-O1-Cr1 bond angle and Cr1-O1 bond lengths. Notably, Al^{3+} doped $ErCrO_3$ has not been previously reported in the literature. The significant entropy changes and relative cooling power observed in Al^{3+} substituted $ErCrO_3$ highlight its potential as a promising material for low-temperature magnetic refrigeration applications.

CR-08. Withdrawn

CR-09. Magnetic Imaging Method of Individual Barcode Nanowires using Diamond Nitrogen-Vacancy Centers. *E. Oh*[1], J. Yoon[2], J. Moon[1], J. Chung[2], Y. Kim[9], K. Kim[2], H. Kang[3], Y. Jeon[10], S. Lee[4], K. Han[5,6], D. Lee[7,6], C. Lee[8], Y. Kim[1,9] and D. Lee[2] *1. Department of Materials Science and Engineering, Korea University, Seoul, The Republic of Korea; 2. Department of Physics, Korea University, Seoul, The Republic of Korea; 3. KU-KIST Graduate School of Converging Science and Technology, Korea University, Seoul, The Republic of Korea; 4. Center for Multidimensional Carbon Materials (CMCM), Institute for Basic Science (IBS), Ulsan, The Republic of Korea; 5. Department of Neuroscience, Korea University College of Medicine, Seoul, The Republic of Korea; 6. BK21 Graduate Program, Department of Biomedical Sciences, Korea University College of Medicine, Seoul, The Republic of Korea; 7. Department of Anatomy, Korea University College of Medicine, Seoul, The Republic of Korea; 8. Department of Electrical and Computer Engineering, Seoul National University, Seoul, The Republic of Korea; 9. Institute for High Technology Materials and Devices, Korea University, Seoul, The Republic of Korea; 10. Institute of Engineering Research, Korea University, Seoul, The Republic of Korea*

Investigating magnetic properties in low-dimensional nanostructures in solid-state physics is in the limelight [1]. One-dimensional magnetic nanostructures like nanowires and barcode magnetic nanowires (BMNs) which consist of multiple segments with alternating properties within a single structure have gained attention for their potential applications in bioengineering [2]. Despite significant advancements in the manufacturing of magnetic nanowires, analyzing individual nanowires in detail and imaging them under microscope are still challenges. Previous studies have examined the magnetic properties of nanowire arrays, but individual nanowires can exhibit different behavior due to magnetostatic interactions between them [3]. Additionally, traditional microscopy techniques for imaging internal magnetic structures require a high vacuum and cryogenic environment and do not provide quantitative magnetic information. This study aimed to characterize and image individual magnetic nanowires and BMNs under ambient temperature using wide-field quantum microscopy with diamond nitrogen-vacancy (NV) centers. Solid-state spin qubits based on diamond NV centers have high sensitivity to local magnetic fields, and NV centers can accurately quantify sensing results without additional calibration. They can retain their sensing abilities over a wide temperature range, including room temperature, making them suitable for bioengineering applications. Employing the diamond NV center-based microscopy, the in situ characterization of the magnetic properties of individual nanowires is possible [4]. Each segment of BMNs appeared similar in their optical images, but the magnetic images revealed distinct magnetic field profiles depending on the material composition and sequences of layer, allowing us to characterize each material layer individually. The novel imaging method of this research paves the way for the characterization method to analyze individual magnetic nanowires.

[1] A. Buchter, J. Nagel, D. Rüffer, Phys. Rev. Lett., 111, 067202 (2013) [2] Y. S. Jeon, H. M. Shin, Y. J. Kim, ACS Appl. Mater. Interfaces., 11, 23901 (2019) [3] A. Y. Samardak, Y. S. Jeon, V. Y. Samardak, Small., 18, 2203555 (2022) [4] J. Yoon, J. H. Moon, J. Chung, Small., 2304129 (2023)

CR-10. Quantitative Imaging of Nanoscale Spin Textures in Epitaxial Quantum Materials. *M. Sim*[1], Z. Lim[1], M. Pardo-Almanza[2], Y. Fujisawa[2], H. Tan[3], X. Chen[3], Y. Okada[2], A. Ariando[1] and A. Soumyanarayanan[1,3] *1. Department of Physics, National University of Singapore (NUS), Singapore, Singapore; 2. Quantum Materials Science Unit, Okinawa Institute of Science and Technology (OIST), Okinawa, Japan; 3. Institute of Materials Research and Engineering (IMRE, A*STAR), Singapore, Singapore*

Quantum materials and heterostructures have emerged as a fascinating playground for magnetism, topology, and their interplay with spin-charge interconversion. The presence of interfacial chiral interactions in such materials may give rise to topological spin textures [1-3], which is expected to manifest in Hall transport measurements as an additional "topological" component. Coined as the topological Hall effect (THE), the magnitude of such a "bump" in the Hall signal is expected to correspond to the imaged density of chiral spin textures. While unusual Hall effects have been reported in myriad chiral magnetic films, several concerns have emerged – notably including order-of-magnitude discrepancies between the expected and measured density of spin textures, and other plausible explanations of the observed phenomena. In this work, we utilise variable temperature magnetic force microscopy (MFM) imaging to probe the formation of spin textures in epitaxially grown transition metal chalcogenides CrTe and oxide superlattice films of SRO/SIO. To this end, we establish a toolbox of quantitative analysis techniques to characterize the nature and extent of these spin textures, determine their field and temperature dependent evolution, and explore their potential anomalous and topological contributions to Hall transport measurements.

[1] M. Gibertini et al., Nature Nanotechnology, 14, 408-419 (2019) [2] J. Matsuno et al., Science Advances, 2, e1600304 (2016) [3] K. Yasuda et al., Nature Physics, 12, 555-559 (2016)

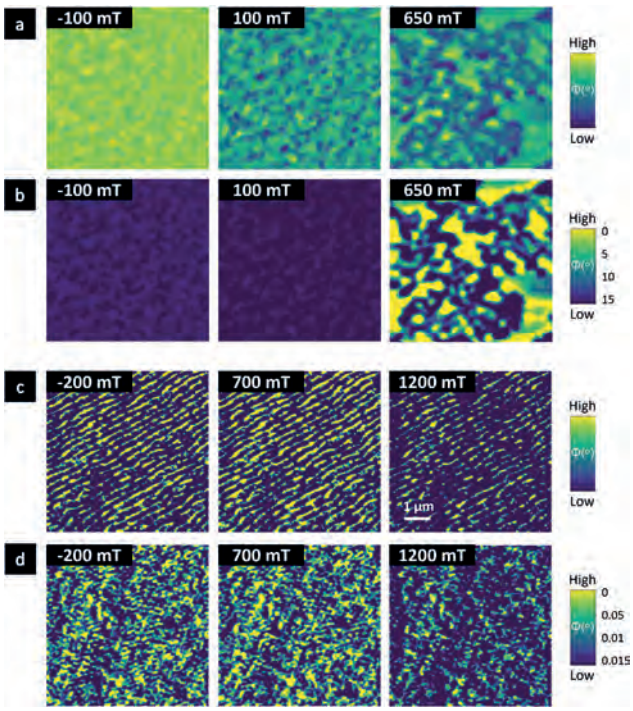

Figure 1: Field evolution of MFM-imaged features in CrTe at 10 K (a,b) and SRO/SIO at 20 K (c,d) before (a,c) and (b,d) after applying quantitative MFM analysis.

CR-11. Hybrid Bimodal Magnetic Force Microscopy. *D. Fernández Brito*[1], J.A. Lopez Medina[2], E.A. Murillo Bracamontes[4], M.A. Palomino Ovando[1] and J.J. Gervacio Arciniega[3,1] *1. Facultad de Ciencias Físico Matematicas, Benemérita Universidad Autónoma de Puebla, Puebla, Mexico; 2. Fisicoquimica, Centro de Nanociencias y Nanotecnologia - Universidad Nacional Autonoma de Mexico, Ensenada, Mexico; 3. Física, Consejo Nacional de Humanidades Ciencias y Tecnologías, Puebla, Mexico; 4. Nanoestructuras, Centro de Nanociencias y Nanotecnologia - Universidad Nacional Autonoma de Mexico, Ensenada, Mexico*

Magnetic Force Microscopy (MFM) is an Atomic Force Microscopy (AFM) technique that characterizes, at a nanometric scale, the magnetic properties of ferromagnetic materials. Conventional MFM works by scanning in two different AFM modes. The first one is tapping mode, in which the cantilever has short-range force interactions with the sample, with the purpose of obtaining the topography. Then, the lift AFM mode starts, raising the cantilever to maintain a fixed distance between the tip and the surface of the sample, only interacting with the magnetic field forces of the sample, which are long-ranged. In recent years, there have been attempts to improve the MFM technique. Bimodal MFM was first theoretically developed [1] and later experimentally proven [2]. In bimodal MFM, the AFM internal piezoelectric is used to cause the cantilever oscillations in two resonance modes simultaneously, the first mode detects the topography, while the second is more sensitive to the magnetic forces between the tip and the sample. However, it has been proven that the cantilever vibrations induced by the internal AFM piezoelectric ceramic are not optimal, affecting the bimodal MFM characterizations. Moreover, the Secondary Resonance Magnetic Force Microscopy (SR-MFM) [3] was developed. In this technique, a coil located below the sample generates an external magnetic field. This alternating magnetic field excites the cantilever at a second frequency to apply the Bimodal MFM mode. Nonetheless, for ferromagnetic materials with a low coercive field, the external field used in SR-MFM technique can modify the magnetic domains of the sample. In this work, a *Hybrid Bimodal Magnetic Force Microscopy* (HB-MFM) technique is proposed. In HB-MFM, the bimodal MFM is used, but the second resonance frequency of the cantilever is induced by the magnetic field of the ferromagnetic sample due to its vibrations caused by a piezoelectric element placed under the sample. The advantages of this new technique are demonstrated through the preliminary results obtained by HB-MFM on a hard disk sample. Additionally, traditional two pass MFM and HB-MFM measurements were compared.

[1] T. R. Rodríguez and R. Garcia, Appl. Phys. Lett. Vol. 84, p. 449 (2004) [2] J. W. Li, J. P. Cleveland, and R. Proksch Appl. Phys. Lett. Vol 94, p. 163118 (2009) [3] D. Liu, K. Mo and X. Ding, Appl. Phys. Lett. Vol 107, p. 103110 (2015)

Session CS
MAGNETIC SENSORS AND HIGH FREQUENCY DEVICES
(Poster Session)

Laura Rehm, Chair
New York University, New York City, NY, United States

CS-01. AC Susceptibility Measurement of Magnetic Nanoparticles Using an Optically Pumped Magnetometer. *T. Sasayama*[1], S. Taue[2] and T. Yoshida[1] *1. Department of Electrical and Electronic Engineering, Kyushu University, Fukuoka, Japan; 2. School of System Engineering, Kochi University of Technology, Kochi, Japan*

INTRODUCTION The imaging of magnetic nanoparticle (MNP) distributions is a promising biomedical imaging technique to detect targets, e.g., cancer cells. One such method is magnetic particle imaging (MPI), which images targets by detecting magnetic signals from MNPs [1]. In this application, the magnetic signal from MNP is small (typically less than 1 pT); therefore, a high-sensitivity magnetic sensor is required. Although optically pumped magnetometers (OPMs) are high-sensitivity magnetic sensors, their dynamic range is small and they are difficult to use directly in general MPI. Therefore, as a first step for an MPI system, we develop a system for detecting magnetic signals from MNPs in AC magnetic field using an OPM, that is, an AC susceptibility measurement system. METHODS Fig. 1 shows the experimental setup for measuring the AC susceptibility of MNPs. To solve the problem of dynamic range, we employed a flux transformer to enhance the sensitivity in the strong excitation magnetic field. First, an MNP sample was excited using an excitation coil. Second, the magnetic field from the MNP sample was detected using a pickup coil. Third, the magnetic field was generated using an input coil. Finally, the magnetic field was detected using OPM. A Resovist (Fujifilm RI Pharma) MNP sample was arranged inside the pickup coil. Two types of MNP samples, suspended (liquid phase) in water and immobilized using calcium sulfate hemihydrate (solid phase), were prepared. RESULTS Fig. 2 shows the result of AC susceptibility. The parameter χ' in the liquid phase decreased rapidly when the frequency was $f > 200$ Hz, whereas χ' in the solid phase decreased slowly in all frequency regions. Similarly, χ'' in the liquid phase increased rapidly when $f > 200$ Hz, whereas in the solid phase, it increased slowly in all frequency regions. The results agreed well with previous studies [2]. These results indicate that the proposed method can be applied to MPI.

[1] B. Gleich and J. Weizenecker, "Tomographic Imaging using the Nonlinear Response of Magnetic Particles," Nature, vol. 435, pp. 1214–1217, 2005. [2] Y. Higuchi, S. Uchida, A. K. Bhuiya, T. Yoshida, and K. Enpuku, "Characterization of magnetic markers for liquid-phase detection of biological targets," IEEE Trans. Magn. vol. 49, no.7, pp. 3456-3459, 2013.

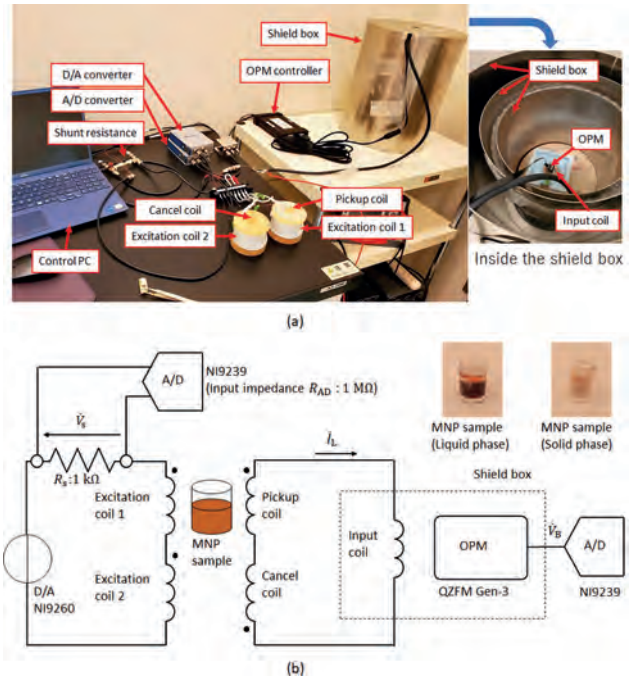

Fig. 1. Experimental setup for AC susceptibility measurement of MNPs. (a) Photograph and (b) schematic diagram.

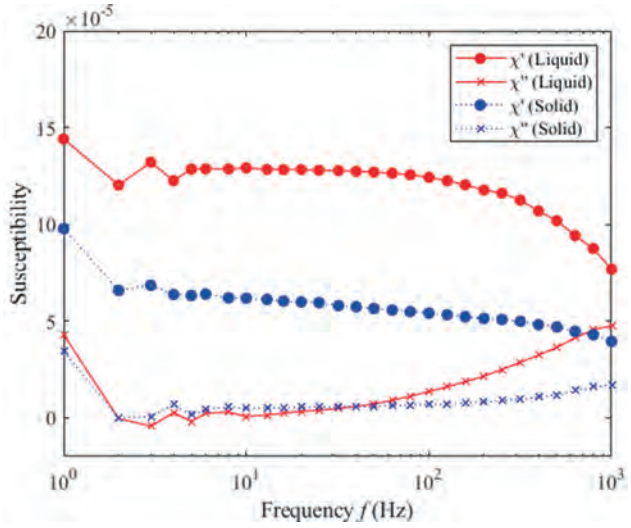

Fig. 2. AC susceptibility results of the Resovist MNP sample in liquid and solid phases.

CS-02. Ultralow power magnetic tactile sensor development using the modified MRAM architecture. J. Cho[1], W. Ju[1], D. Kim[1], D. Lee[1] and *J. Kim[1] 1. Division of Nanotechnology, Daegu Gyeongbuk Institute of Science and Technology (DGIST), Daegu, The Republic of Korea*

Sensors are ubiquitous, and minimizing power consumption is crucial since they need to operate continuously. For instance, in the case of a tactile sensor, it is essential to address power consumption issues due to its operation cycles, and it also needs to precisely respond to various inputs [1]. One of the emerging candidates with ultralow power consumption and ultrafast operation speed is the use of a modified spin-transfer torque magnetoresistive random access memory (STT-MRAM) architecture. When directly compared to other conventional memory groups such as DRAM, STT-MRAM exhibits excellent performance characteristics, including a writing energy per bit (< 100 fJ), write speed (< 10 ns), read speed (< 10 ns), and non-volatile characteristics [2]. Here, we demonstrate a highly low-power tactile sensor based on a modified perpendicular-type magnetic tunnel junction (pMTJ) architecture as depicted in Fig. 1 (a). Contrary to conventional pMTJs, the modified pMTJ structure has an antiferromagnetic interlayer exchange coupling (IEC) between the storage layer (SL) and the reference layer (RL). Furthermore, a conventional pMTJ structure is also fabricated to read the resistance of the sensor cell when the magnetization directions of SL are changed due to external magnetic fields. Once the changes in the external magnetic field disappear, the magnetization of the information storage layer returns to its original state. Figure 1(b) shows the full stack of the modified pMTJ architecture and the magnetic hysteresis loops for various splits. For the cases of Ta insertion at the interface between the CoFeB layer and the Co layer, the magnetizations of SL are almost linearly varied as a function of the external field. These structures are good to develop "analog-type tactile sensors". For the cases without Ta insertions, the squareness of hysteresis loops is observed, and these structures are good to develop "digital-type sensors". Finally, the full electrical evaluations of the magnetic tactile sensors are experimentally demonstrated and the results will be discussed. This work was supported by the DGIST R&D Program of the Ministry of Science, ICT, and Future Planning (23-IT-01, 23-CoE-NT-02, and 23-SENS-01).

[1] P. Y. Dibal, *et. al*., Internet of Things 21, 100655 (2021) [2] S.-W. Chung *et al.*, 2016 IEEE International Electron Devices Meeting (IEDM), pp. 27.1.1-27.1.4 (2016)

CS-03. Anomalies in the Magnetostrictive Modulation of Love Surface Acoustic Waves. J.D. Aguilera[2], L. Soria[2], R. Loriente[2], R. Ranchal[2,3], I. Gràcia Tortadés[1], S. Vallejos[1], A. Hernando[2], P. Palacios[2], D. Matatagui[2] and *P. de la Presa[2] 1. Instituto de Microelectrónica de Barcelona, Barcelona, Spain; 2. Institute of Applied Magnetism, Complutense University of Madrid, Madrid, Spain; 3. Material Physics, Complutense University of Madrid, Madrid, Spain*

A wide range of high-performance, small, low cost, and low consumption sensors are based on the variation of the parameters characterizing a surface acoustic wave (SAW) propagating through a piezoelectric substrate [1]. In this work, we study the response of a SAW device which is made sensitive to magnetic fields by depositing a magnetostrictive nanofilm onto it. Only a few precedents to this idea can be found in literature [2-3]. The SAW device is composed of a ST-cut quartz substrate on which two sets of interdigitated electrodes and a 3.6 μm film of amorphous SiO_2 excite and guide the shear horizontal SAW close to the interface (Love wave). A 100 nm thick polycrystalline Galfenol ($Fe_{72}Ga_{28}$) layer is deposited by sputtering onto the area between the IDTs. A feedback loop circuit provides a resonant SAW frequency f_r around 160 MHz which can be tracked in real time. Fig. 1 shows the frequency shift observed as the applied magnetic field sweeps from -40 to 40 mT (and back) forming a 45º or 0º angle with the propagation of SAWs. For 4º (blue), f_r follows a hysteretic behavior induced by the strain linked to the nanofilm magnetization M_s, with f_r increasing with M, apparently reaching saturation at the higher applied fields, and the coercive field corresponding to the two central minima. In 0º configuration (red), saturation is not reached, and a new relative maximum appears as the field is reversed, so in this case f_r cannot be directly related to this component of the magnetization in a simple way. Other works [3] have reported a single frequency peak at zero applied field, using a FeCoSiB magnetostrictive ribbons. We believe that using a harder magnetic material as Galfenol has permitted the discrimination of two different peaks in this work, thanks to the higher coercive field derived from its polycrystalline structure. Therefore, this is the first step towards tailoring SAW magnetic sensors with different responses to magnetic field by a careful design of the magnetostrictive film, obtaining tunable sensitivity peaks at selected fields.

[1] Mandal, D.; Banerjee, S. *Surface Acoustic Wave (SAW) Sensors: Physics, Materials, and Applications*. Sensors 2022, 22, 820. [2] Fahim, et al., *A simple and novel SAW magnetic sensor with PVA bound magnetostrictive nanopowder film.* Sensors and Actuators A: Physical, 2021. 331: p. 112926. [3] Meyer, et al., *Thin-film -based SAW magnetic field sensors*, Sensors, 2021. 24, art. no. 8166,.

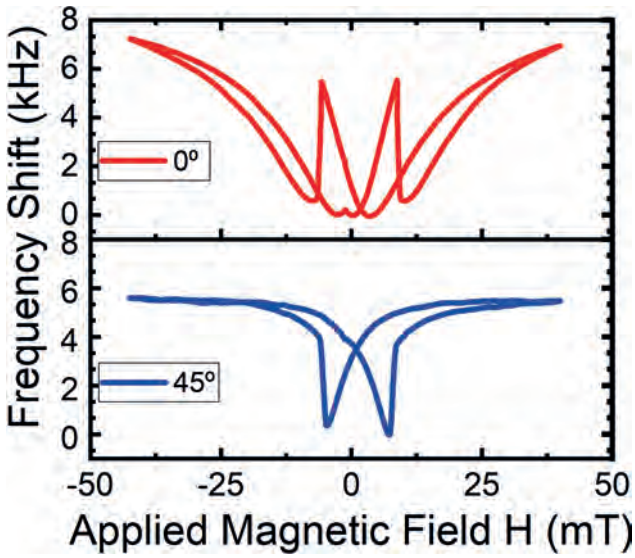

Figure 2: Frequency shift against field for 0° (red) and 45° (blue) configuration.

CS-04. High-frequency magnetic response of crystalline and nanocrystalline antiferromagnetic NiO. A. Janutka[1] and *K. Brzuszek[1] 1. Department of Theoretical Physics, Wroclaw University of Science and Technology, Wroclaw, Poland*

Using micromagnetic simulations, we consider response of bulk and polycrystalline NiO to high-frequency (up to 100GHz) magnetic field with relevance to potential applicattion of the antiferromagnet as core material to microconverters of power which have to operate at very-high frequency (due to small magnetic flux). Our interest in verifying applicability of a Mott insulator to the power conversion follows from the need for avoiding eddy-current-related losses which are critically important at high frequencies. We treat such an opportunity as an alternative to previously considered core materials created of superparamagnetic composites of metallic or semiconducting (magnetite) nanoparticles embedded in dielectric matrices for applications at sub-GHz frequencies [1]. Among other antiferromagnets, NiO is of Neel temperature well above room temperature. Though, the dynamical susceptibility of antiferromagnets is low, achievable product of susceptibility and frequency ("performance factor" [2]) can considerable, which makes NiO potential core material for operating at extremely-high (sub-THz) frequencies. Our numerical simulations of field-driven systems of many domains/nanocrystals of NiO with random orientations of antiferromagnetic-sublattice layers confirm that of similar order ($\nu^{\circ}\chi(\nu) \sim 10^8$ s^{-1}) while higher than for superparamagnetic nanocomposites performance factor is reachable with the antiferromagnet. Due to strong exchange field of the antiferromagnet, thermal fluctuations influence

weakly the susceptibility up to room temperature even for nanocrystalline material, whereas, the magnetic response is linear for much wider ranges of frequencies and driving-field amplitudes than for ferromagnetic-nanoparticle-based systems.

[1] K. Brzuszek, C. A. Ross and A. Janutka, J. Magn. Magn. Mat. 573, 170651 (2023) [2] C. R. Sullivan, D. V. Harburg, J. Qiu, C. G. Levey and D. Yao, IEEE Trans. Power Electron. 28 (2013) 4342–4353

CS-05. Tuning of Magnetoplasmon Coupling between Graphene Scatterers for the Optimal Design of Adjustable Metasurfaces.
S.A. Amanatiadis[1], T. Ohtani[3], *Y. Kanai*[2] and N.V. Kantartzis[1] *1. Department of Electrical and Computer Engineering, Aristotle University of Thessaloniki, Thessaloniki, Greece; 2. Department of Engineering, Niigata Institute of Technology, Kashiwazaki, Japan; 3. Asahikawa CIty, Asahikawa, Japan*

The purpose of this study is to extract and thoroughly analyze the resonance frequencies of magnetically-biased graphene scatterers in the THz band. Specifically, the application of an external magnetostatic bias field on graphene induces anisotropic effects caused by Lorentz forces acting on electrons. These effects reveal intriguing phenomena such as gyrotropy, non-reciprocity, and the support of magnetoplasmons [1]. Initially, a simple graphene disk is examined, and the fundamental frequencies are extracted for various applied bias fields. This process involves employing an appropriate eigenvalue formulation that enables the linear modeling of the 2D material's frequency-dispersive characteristics [2]. The extracted results for the first mode of the scatterer are depicted in Fig. 1, clearly illustrating that precise bias control can finely tune both the resonance frequency and the electromagnetic field pattern. The accurate evaluation of resonance modes in graphene scatterers enables the optimal design of more complex devices, such as metasurfaces. Specifically, tuning the bias fields appropriately modifies the device's performance based on the proximity of the operational frequency to the scatterer resonance. However, the periodic pattern of metasurfaces requires the utilization of multiple elementary cells in a periodic arrangement. Hence, our analysis extends to investigating the coupling between adjacent scatterers to assess their combined performance. Notably, the spiral electromagnetic pattern generated by the magnetically-biased scenario activates coupling in specific directions. Consequently, the metasurface exhibits increased adjustability, even in the case of a simple graphene disk scatterer, with additional degrees of freedom.

[1] D. L. Sounas, and C. Caloz, IEEE Trans. on Microw. Theory Tech., Vol. 60, p. 901 (2012) [2] P. Lalanne, *et al*., J. Opt. Soc. Am. A, Vol. 36, p. 686 (2019)

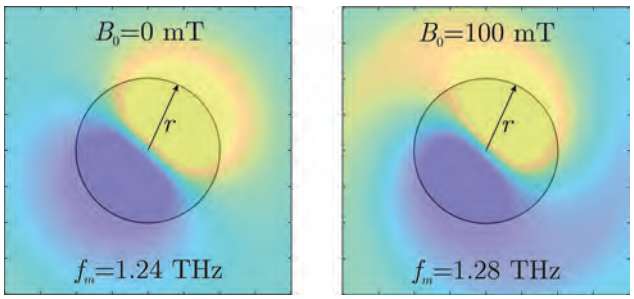

Fig. 1: The first resonance of a magnetically-biased graphene disk scatterer under different applied magnetostatic fields.

CS-06. A micromagnetic study of the fractional resonance response driven by voltage-controlled magnetic anisotropy.
A. Giordano[1], A. Grimaldi[1], E. Raimondo[1], R. Tomasello[2], M. Carpentieri[2] and G. Finocchio[1] *1. University of Messina, Messina, Italy; 2. Politecnico di Bari, Bari, Italy*

Spintronic diodes (STDs) exhibit potential advantages over semiconductor. They are compact (nanoscale size), CMOS-compatible, energy-efficient [1][2]. In particular, the STDs allows to use many driving forces to tune their rectification response, such as the voltage controlled magnetic anisotropy (VCMA) [3]. Here, we have predicted a fractional parametric resonance response driven by the simultaneous excitation of VCMA and ac spin-transfer torque for spintronic diodes working in the passive regime. This resonance is characterized by the ferromagnetic resonant frequency, the standard parametric excitation at twice the resonance frequency and several other sub-harmonic peaks, all of which are an integer fraction (1/2, 1/3, etc.) of the main resonance frequency. We have performed a systematic study of the resonance response of the MTJ as a function of VCMA amplitude. The dynamics is driven by the presence of VCMA and simultaneity by spin-transfer-torque driven by an ac in-plane spin-polarized current density (Jac =0.1MA/cm^2), and both current density and VCMA have the same frequency. The figure 1 shows the results that are obtained by considering the current value fixed and varying only the value of VCMA (KVCMA =0, 50, 100 mT). In absence of VCMA, we obtained a frequency resonance of 4.88GHz. With adding of VCMA, not only the same frequency, we obtained other frequencies minor, until to 7 for the value of VCMA higher and in this case is present also an peak at twice the ferromagnetic frequency (labelled -1). This work opens a new direction for the use of spintronic diodes in the field of communication, as a single device would have the ability to detect more information carriers.

[1] G. Finocchio et al., "Perspectives on spintronic diodes," Applied Physics Letters, vol. 118, no. 16. 2021, doi: 10.1063/5.0048947. [2] P. N. Skirdkov and K. A. Zvezdin, "Spin-Torque Diodes: From Fundamental Research to Applications," Annalen der Physik, vol. 532, no. 6. Wiley-VCH Verlag, Jun. 01, 2020, doi: 10.1002/andp.201900460 [3] Y. J. Chen et al., "Parametric resonance of magnetization excited by electric field," Nano Lett., vol. 17, no. 1, pp. 572–577, Jan. 2017, doi: 10.1021/acs.nanolett.6b04725

CS-07. Evaluation of structure and magnetic properties in amorphous dust core for high frequency device application.
M. Nguyen[1], S. Yoshida[2], S. Okamoto[2,3], T. Miyazaki[4] and Y. Endo[1,5] *1. Department of Electrical Engineering, Graduate School of Engineering, Tohoku University, Sendai, Japan; 2. Institute of Multidisciplinary Research for Advanced Materials, Tohoku University, Sendai, Japan; 3. National Institute for Material Science (NIMS), Tsukuba, Japan; 4. Faculty of Engineering, Tohoku University, Sendai, Japan; 5. Center for Science and Innovation in Spintronics, Tohoku University, Sendai, Japan*

Amorphous metallic alloys are made by rapidly quenching from the melt, therefore, their atomic structures lack the long-range order of a crystalline nature and leading to having no magneto-crystalline anisotropy. Compared to Fe-Si and Fe-Ni binary alloys, the amorphous shows high electrical resistivity, drawing much attention as soft magnetic materials for high frequency applications. This paper reports the phase transformation and magnetic property of amorphous FeSiBCr powder cores by annealing process. Also, reducing the core loss by changing compacting pressures and binder contents will be evaluated. Phase transformation was confirmed by observing sharp peaks in XRD patterns for the cores at the annealing temperature above 550 ^{o}C, comparing a hollow peak for the lower annealed temperature ones. The real part of relative permeability μ' increased at higher annealing temperature up to 450 ^{o}C and then decreased for the annealed ones at 500 and 550 ^{o}C. These results were caused by the crystalline structure and/ degradation of the insulation layer at higher temperatures. Dynamic coercivity H_c and core loss P_{cv} gradually decreased at higher annealing temperatures in case of the amorphous structure, whereas they both abruptly increased for all cores in case of the crystalline structure. These results suggest that the strong relationship between microstructure and magnetic properties of FeSiBCr powder

core, and so that the optimum condition of low core loss with high μ′ could be controlled. Core loss P_{cv} decreased from 322 to 193 kW/m^3 as the binder content decreased from 3 to 0.3 %. In addition, due to a poor plastic deformation ability of amorphous powder, a high compacting pressure in 1980 MPa was done. At higher compacting pressure, dynamic H_c decreased from 10.4 to 8.7 A/m and the real part of relative permeability increased from 25.2 to 38.3. The reduction of P_{cv} from 200 to 168 kW/m^3 measured at frequency of 200 kHz and flux density of 50 mT was confirmed which is less than half value comparing to current commercial material. The low core loss with high permeability in a wide frequency range of FeSiBCr amorphous provides broad prospects for electronic component applications at high frequency.

1. R. Yapp, B.E. Watts and F. Leccabue, J. Magn. Magn. Mater., 215-216, 300 (2000) 2. 4mp.pdf (pacificsowa.co.jp) Acknowledgement This work was supported in part by MEXT Program for Creation of Innovative Core Technology for Power Electronics Grant Number JPJ009777 and Data Creation and Utilization-Type Material Research and Development Project (Digital Transformation Initiative Center for Magnetic Materials) Grant Number JPMXP1122715503. This work was supported in part by CSIS, CSRN, and CIES, Tohoku University.

CS-08. High-frequency Loss Modeling of Nanocrystalline Core Considering Nonuniform Distribution of Flux Density. W. Meng[1], Y. Li[1], *C. Zhang*[1], H. Sun[1] and Z. Wan[1] *1. School of Electrical Engineering, Hebei University of Technology, Tianjin, China*

In recent years, nanocrystalline cores were used for high-frequency transformers due to the attractive properties of nanocrystalline materials. However, the flux density distribution is nonuniform along the core because the inner and outer reluctance of the core are different [1]. At present, the calculation of core loss in high-frequency transformers mainly uses two methods: loss separation model and empirical formula [2]. But both methods do not consider the nonuniform distribution of flux density in the core, which may cause huge calculation errors of core losses. In this paper, the core losses of U-shape cores with various wound thicknesses are measured and analyzed. The outer profile of the measured core keeps unchanged, and the inner thickness increased. Based on the measurement results, an improved loss separation model is introduced in detail to characterize the nonuniform distribution of flux density through the cross section. Fig. 1 shows the cross section of the core is discretized into several equal segments. The summation of the fluxes in each path is equal to the total flux. Eventually, according to Ohm's law for magnetic circuit, we can obtain the relationship between reluctance, flux density and shape parameters. That is, the distribution function of the flux density is obtained. The improved model is expressed as the superposition of n layers core loss, and each layer is calculated using the loss separation method. Fig. 2 shows the error comparison between the traditional loss separation model and the improved model under f = 5 kHz, B = 0.5 T. It can be seen that the loss calculation error is low when considering the non-uniform distribution of flux density. The prediction accuracy is improved significantly compared with the traditional model. More details are shown in the full paper.

[1] Agheb, E. and H. K. Hoidalen, IET Electric Power Applications., vol. 7, pp.381-390(2013) [2] T. Wang and J. Yuan, IEEE Transactions on Magnetics., vol. 58, pp.1-9(2022)

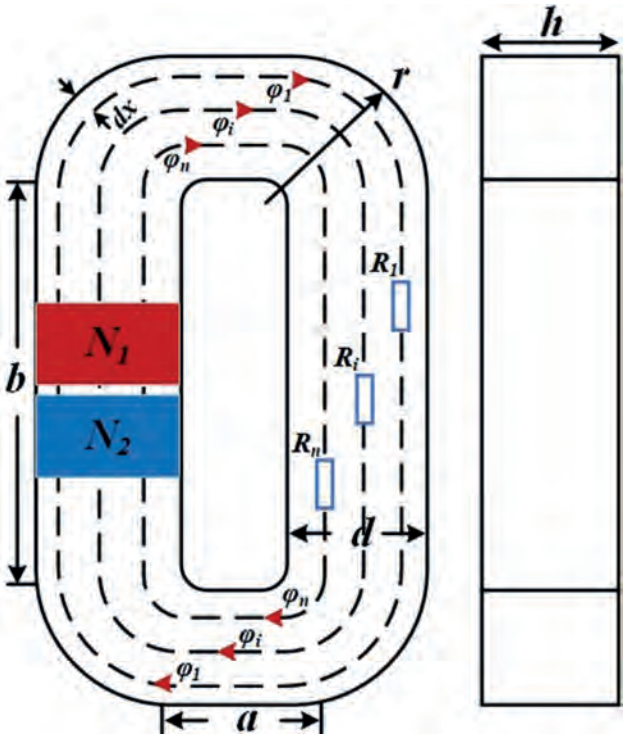

Fig.1 Schematic diagram of the nanocrystalline core

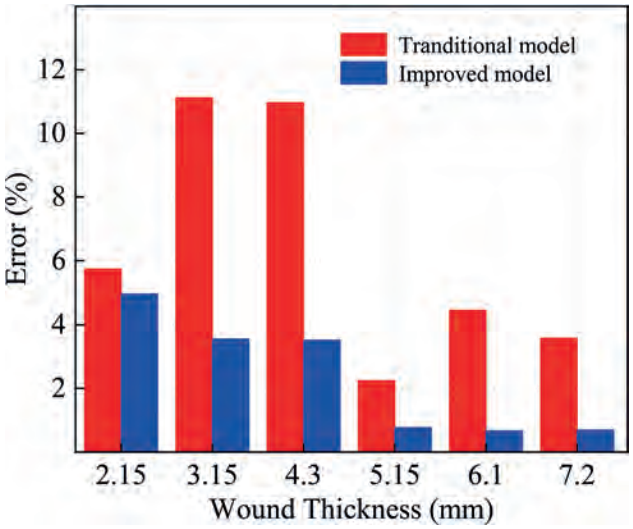

Fig. 2 Error comparison between the improved model and the traditional model

Session DA
EMERGING TOPICS IN MAGNETIC TUNNEL JUNCTIONS: ALTERMAGNETISM, PROBABILISTIC COMPUTING AND ENERGY EFFICIENT SWITCHING

Weigang Wang, Chair
University of Arizona, Tucson, AZ, United States

INVITED PAPERS

DA-01. Antiferromagnetic Tunnel Junctions for Spintronics.
E. Tsymbal[1] *1. University of Nebraska-Lincoln, Lincoln, NE, United States*

Antiferromagnetic (AFM) spintronics has recently emerged as a subfield of spintronics, where an AFM Néel vector is used as a state variable. Due to being robust against magnetic perturbations, producing no stray fields, and exhibiting ultrafast dynamics, antiferromagnets can serve as promising functional materials for spintronic applications. To realize this potential, efficient electric control and detection of the AFM Néel vector are required. This invited talk features antiferromagnetic tunnel junctions (AFMTJs) as spintronic devices where such a control and detection can be realized (Fig. 1). The critical requirements for efficient AFMTJs are (i) AFM electrodes exhibiting a spin-split Fermi surface and hence momentum-dependent spin polarization, and (ii) crystallinity of the junction conserving a transverse wave vector in the tunneling process. If these two conditions are satisfied, AFMTJs support a tunneling magnetoresistance (TMR) effect, resulting from the matching (mismatching) of the spin-polarized Fermi surfaces of the two AFM electrodes dependent on the relative alignment of their Néel vectors (Fig. 2). To demonstrate this behavior, we explore three different types of AFMTJs based on collinear (RuO_2) and noncollinear (Mn_3Sn and $GaNMn_3$) AFM electrodes. RuO_2 has a rutile structure with an A-type AFM order supporting a spin-polarized band structure. As a result, for an $RuO_2/TiO_2/RuO_2$ (001) AFMTJ, reversal of the Néel vector from parallel to antiparallel creates a spin mismatch between the Fermi surfaces of the two electrodes, leading to a TMR effect as large as 500% [1]. Noncollinear antiferromagnets, such as Mn_3X (X = Sn, Ge, Ga, Pt) can also be efficiently used as electrodes in AFMTJs. For example, Mn_3Sn has a noncollinear AFM order where Mn atoms form a kagome lattice with neighboring Mn moments misaligned by 120°. Such an AFM structure supports momentum dependent spin polarization. As a result, AFMTJs with Mn_3Sn electrodes and a vacuum barrier are predicted to exhibit TMR as high as 300% [2]. Very recently, a large TMR has been experimentally observed in $Mn_3Pt/MgO/Mn_3Pt$ [3] and $Mn_3Sn/MgO/Mn_3Sn$ [4] AFMTJs, confirming this theoretical prediction. Another class of noncollinear antiferromagnets are antiperovskites $XNMn_3$ (X = Ga, Sn, Ni). For example, $GaNMn_3$ has a cubic structure with a frustrated Mn kagome lattice in the (111) plane favoring a Γ_{5g} noncollinear AFM order with a spin-split Fermi surface. For a $GaNMn_3/SrTiO_3/GaNMn_3$ (001) AFMTJ, we predict an extraordinarily large TMR exceeding 10^{4}% [5], due to perfectly spin-polarized electronic states of $GaNMn_3$ matching the low-decay-rate evanescent states of $SrTiO_3$. Finally, AFMTJs allow not only the detection of the Néel vector by TMR but also its control by a spin transfer torque (STT) generated by the momentum-dependent spin polarization [6]. Theoretical calculations applied to $RuO_2/TiO_2/RuO_2$ (001) AFMTJs predict a field-like STT being comparable to that in Fe/MgO/Fe MTJs and capable of the deterministic switching of the Néel vector. Overall, AFMTJs have potential to become a new standard for spintronic devices providing a few orders of magnitude faster switching speed and packing density than conventional MTJs. *Acknowledgements*: this work has been performed in collaboration with my former group members, Prof. Ding-Fu Shao of Institute of Solid-State Physics, Chinese Academy of Sciences, Dr. Gautam Gurung of Trinity College, University of Oxford, and Prof. Jia Zhang of Huazhong University of Science and Technology.

[1] D.-F. Shao et al., Nat. Commun., Vol. 12, p. 7061 (2021). [2] J. Dong et al., Phys. Rev. Lett., Vol. 128, p. 197201 (2022). [3] P. Qin et al., Nature, Vol. 613, p. 485 (2023). [4] X. Chen et al., Nature, Vol. 613, p. 490 (2023). [5] G. Gurung, D.-F. Shao, and E. Y. Tsymbal, arXiv:2306.03026 (2023). [6] D.-F. Shao et al., Phys. Rev. Lett., Vol. 130, p. 216702 (2023).

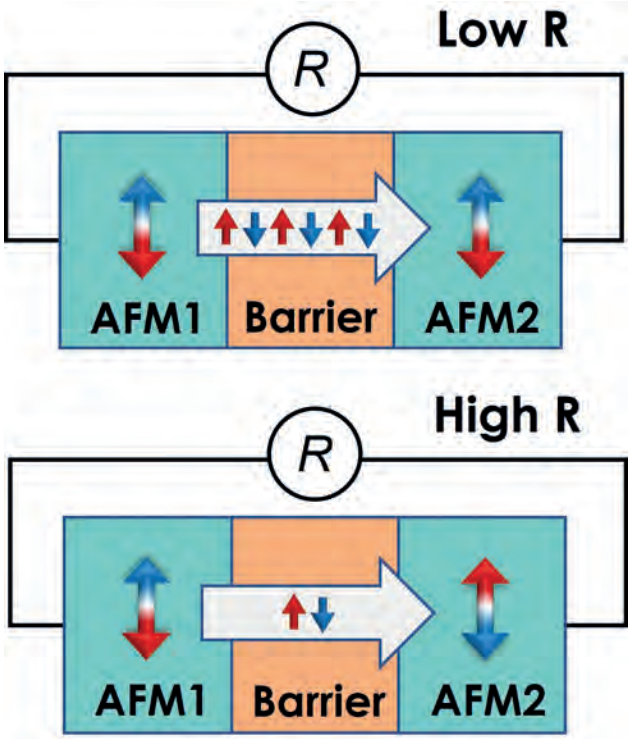

FIG. 1 Schematic of an AFMTJ where two AFM electrodes (AFM1 and AFM2) are separated by a tunnel barrier. Resistance is high or low depending on the relative orientation of the Néel vectors (indicated by double arrows).

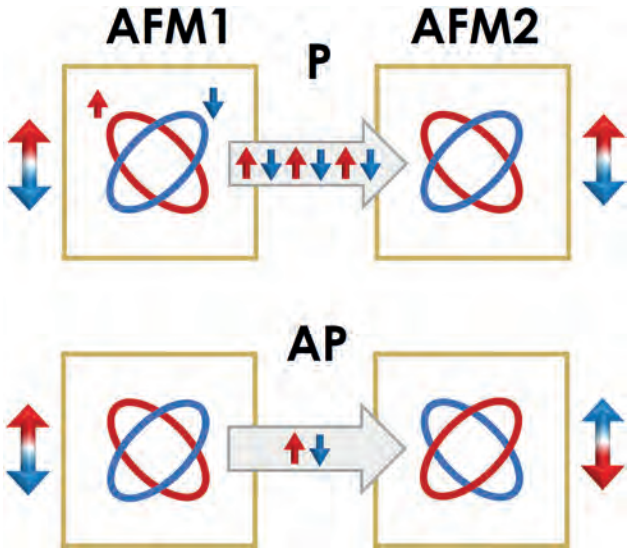

FIG. 2 Momentum-dependent spin splitting: the spin-up and spin-down Fermi surfaces are different in momentum space. Conductance is large when the Néel vectors of AFM1 and AFM2 are parallel (P) and small when they are antiparallel (AP).

DA-02. Spin-torque switching and tunnel magnetoresistance using an antiferromagnetic Weyl semimetal. *S. Miwa*[1], X. Chen[2,1], T. Higo[2,1], K. Tanaka[2,3], R. Arita[3,4] and S. Nakatsuji[2,5] *1. The Institute for Solid State Physics, The University of Tokyo, Kashiwa, Japan; 2. Department of Physics, The University of Tokyo, Bunkyo, Japan; 3. Research Center for Advanced Science and Technology, The University of Tokyo, Meguro, Japan; 4. Center for Emergent Matter Science, RIKEN, Wako, Japan; 5. Institute for Quantum Matter, Johns Hopkins University, Baltimore, MD, United States*

Tunnel magnetoresistance (TMR) and spin-transfer torque (STT), due to longitudinal spin-polarized current, provide the read and write protocols for the two-terminal magnetoresistive devices. In addition to the well-established ferromagnetic spintronics, antiferromagnets have attracted considerable interest as next-generation active elements for further improvements in operating speed and integration density. While no STT method has been experimentally demonstrated, several write means, including spin-orbit torque, have been developed using the same methods as for ferromagnets. For readout, in addition to anisotropic magnetoresistance and spin Hall magnetoresistance, the anomalous Hall effect has recently become available for antiferromagnets [1]. Tunnel anisotropic magnetoresistance (TAMR) has been studied for junctions based on a single antiferromagnetic electrode [2]. However, TAMR is generally observed at low temperatures and at much lower temperatures than the TMR, even when it is available at room temperature. Therefore, it is very important to develop both TMR and spin-transfer torque using all-antiferromagnetic MTJs. In principle, TMR effect in all-antiferromagnetic tunnel junction is feasible in terms of momentum-dependent spin polarization [3]. However, it is difficult to prepare such time-reversal odd and controllable spin state in collinear antiferromagnet. Therefore, no reports have been published on the TMR effect using an all-antiferromagnetic MTJ. In addition, the observation and manipulation of the longitudinal spin-polarized current is necessary as a basis for the design of the memory device based solely on antiferromagnets, but, again, it has never been carried out for antiferromagnets. The antiferromagnetic Weyl semimetal $D0_{19}$-Mn_3Sn [1] is a unique antiferromagnet that exhibits time-reversal-odd and controllable spin states. The non-collinear chiral magnetic texture in Mn_3Sn can be viewed as a ferroic order of a cluster magnetic octupole and breaks time-reversal symmetry macroscopically. Figure 1a shows the crystal and magnetic structures of Mn_3Sn. The magnetic moments of Mn lie in the (0001) plane and form an inverse triangular spin structure. By rotating each spin 180 degree, the octupole polarization can reverse its direction (Fig. 1b). In this respect, the antiferromagnetic Weyl semimetal Mn_3Sn is a suitable for the development of antiferromagnetic tunnel junctions. In this talk, we show that high-quality epitaxial thin films of the Weyl antiferromagnet Mn_3Sn could be prepared by molecular beam epitaxy, and that the epitaxial Mn_3Sn thin film realizes full switching of the octupole polarization by STT from the spin-Hall effect [4]. Furthermore, we clarify the existence of anisotropic, longitudinal spin-polarized current [5] in Mn_3Sn using Fe/MgO/Mn_3Sn-MTJ and finally achieve TMR in an all-antiferromagnetic tunnel junction consisting of Mn_3Sn/MgO/Mn_3Sn [6]. The TMR ratio of the all-antiferromagnetic MTJ is larger than that estimated from the observed spin polarization of Mn_3Sn. Theoretically, the Weyl antiferromagnetic MTJ can produce a substantially large TMR ratio as a result of the time-reversal, symmetry-breaking polarization characteristic of octupole polarization. Our work lays the foundation for the development of antiferromagnetic spintronics. We thank S. Sakamoto, M. Shiga, T. Nomoto, H. Tsai, H. Idzuchi, R. Ando, H. Kosaki, T. Matsuo, D. Nishio-Hamane, and Y. Otani of the University of Tokyo, K. Kondou of RIKEN for collaborative research. This work was supported by JST-MIRAI Program, JST-CREST, JSPS-KAKENHI, Spin-RNJ, and MEXT-XNICS.

[1] S. Nakatsuji *et al.*, Large anomalous Hall effect in a non-collinear antiferromagnet at room temperature. Nature 527, 212 (2015). [2] B. G. Park *et al.*, A spin-valve-like magnetoresistance of an antiferromagnet-based tunnel junction, Nat. Mater. 10, 347 (2011). [3] D.-F. Shao *et al.*, Spin-neutral currents for spintronics. Nat. Commun. 12, 7061 (2021). [4] T. Higo *et al.*, Perpendicular full switching of chiral antiferromagnetic order by current. Nature 607, 474 (2022). [5] J. Železný *et al.*, Spin-polarized current in noncollinear antiferromagnets, Phys. Rev. Lett. 119, 187204 (2017). [6] X. Chen *et al.*, Octupole-driven magnetoresistance in an antiferromagnetic tunnel junction. Nature 613, 490 (2023).

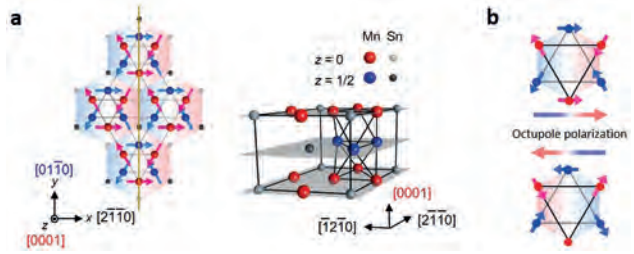

Fig. 1 (a) Spin and crystal structures of Mn_3Sn. The inverse triangular spin-structure can be viewed as a ferroic ordering of cluster magnetic octupole. (b) Magnetic cluster octupole units with different octupole polarization directions.

DA-03. Record for tunnel magnetoresistance of 631% at room temperature with barrier interface control technology. *H. Sukegawa*[1] *1. National Institute for Materials Science, Tsukuba, Japan*

Tunnel magnetoresistance (TMR) observed in magnetic tunnel junctions (MTJs) has a history of almost half a century since the first report by Julliere in 1975 [1], and is the basis for many of today's spintronic applications. Significant progress in the room temperature (RT) TMR ratios has been achieved with two breakthroughs that have determined the practical applications: the first was the observation of RT TMR ratios above ten percent in 1995, and the second was the observation of the giant TMR effect due to the coherent tunneling mechanism in 2004. These observations have greatly contributed to the development of high-capacity recording using TMR heads in hard disk drives. The establishment of magnetization switching technology, such as spin-transfer torque switching and spin-orbit torque switching, and the introduction of perpendicular magnetization for MTJs have also accelerated the development of high-density magnetoresistive random access memories (MRAMs). Achieving a much larger TMR ratio at RT is essential for realizing novel spintronic devices in the future, such as very high-density MRAMs with 3-dimensional architecture and nonvolatile magnetic logics. However, the progress in the RT TMR ratio has stagnated for 15 years after the report of 604% in a CoFeB/MgO/CoFeB MTJ [2].

To overcome the stagnation in TMR and to search for the limit of the RT TMR ratio, we have recently revisited a Fe/MgO/Fe(001) type MTJ, which is known as the simplest coherent tunneling MTJ structure. The standard theories have predicted TMR ratios above 1000% in the Fe/MgO/Fe(001) MTJs, while the experimental demonstration has lagged behind even at low temperatures (300~400%). To bridge the gap in between, we engineered MTJ structures focusing on the simultaneous control of the barrier interface states for both the top and bottom sides: e.g., the use of epitaxial technology combining sputtering and electron beam evaporation, the insertion of Mg and CoFe alloy nano-layers, and the use of a $MgAl_2O_4$ (MAO) based barrier instead of MgO. We observed a significant increase in the TMR ratios of Fe-based MTJs due to the improved coherent transport by the interface control: 417% at RT and 914% at 3 K in Fe/MgO/Fe [3], and 429% at RT and 1034% at 10 K in Fe/Mg-rich MAO/Fe [4]. In particular, the latter reached the typical theoretical TMR ratio at low temperature, demonstrating the importance of interface control for the giant TMR observations. In addition, by introducing a $Co_{50}Fe_{50}$ (CoFe)/MgO/CoFe structure, a TMR ratio of up to 631% at RT (1134% at 10 K) was demonstrated (Fig. 1) [5]. These significant improvements in the TMR ratio are crucial steps for the development of future spintronic applications. Along with the increase in TMR ratio, the unsolved effect, namely TMR oscillation, is more pronounced in the high-quality epitaxial MTJs. The TMR ratio oscillates significantly as a function of barrier thickness with a period of ~0.3 nm, and the peak-to-valley differences at RT reach 80% in Fe/MgO/Fe, 125% in Fe/MAO/Fe, and 141% in CoFe/MgO/CoFe. Such large oscillations cannot be explained by standard coherent tunneling theories. Therefore, further clarification of the oscillatory behavior may provide an important clue to truly large TMR ratios, e.g., >1000% at RT. The presentation includes the works in collaboration with T. Scheike, Z. Wen, and S. Mitani. The works were partly supported by JSPS KAKENHI Grant Nos. 16H06332, 21H01750, 21H01397, and 22H04966 and is partly based on results obtained from a project, JPNP16007, commissioned by the New Energy and Industrial Technology Development Organization (NEDO).

[1] M. Julliere, Phys. Lett. A 54, 225 (1975). [2] S. Ikeda *et al.*, Appl. Phys. Lett. 93, 082508 (2008). [3] T. Scheike *et al.*, Appl. Phys. Lett. 118, 042411 (2021). [4] T. Scheike *et al.*, Appl. Phys. Lett. 120, 032404 (2022). [5] T. Scheike *et al.*, Appl. Phys. Lett. 122, 112404 (2023)

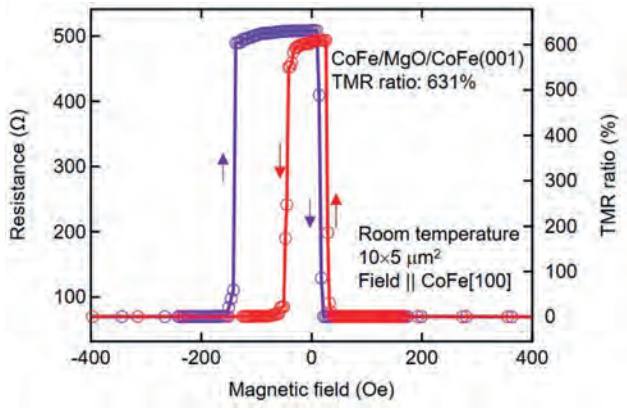

Fig. 1: TMR-field curve at RT of developed epitaxial CoFe/MgO/CoFe(001) MTJ.

DA-04. Spin-Transfer-Torque MRAM: The Next Revolution in Memory. *G. Hu*[1] *1. IBM Research, Yorktown Heights, NY, United States*

Spin-Transfer-Torque (STT) MRAM is an emerging memory technology with a unique combination of non-volatility and high write endurance, owing to the spintronics nature of its switching mechanism. STT-MRAM products have been commercially available for both standalone memory [1] and eFlash-replacement applications [2-3] by successfully integrating magnetic tunnel junctions with standard CMOS technology. Optimization of the conventional CoFeB based single MTJ devices is expected to meet the performance requirement of the next generation embedded MRAM product for RAM-like applications on the horizon. As the industry moves towards denser and faster STT-MRAM products, materials and device innovations are needed to further improve the switching efficiency and lower the switching current of STT-MRAM devices. This talk will first give a brief overview of the current status of the STT-MRAM technology, covering the key advances that enabled today's STT-MRAM technology and the latest product announcements in the field. The second part of the talk will focus on materials innovations and remaining challenges to further expand STT-MRAM's application space. Especially, we will report on our recent progress on demonstrating reliable switching of STT-MRAM devices with sub-5 ns write pulses [4-5] and a new device structure enabling a significant switching current reduction [6-7], as key developments towards the use of STT-MRAM for last-level-cache applications.

[1] S. Aggarwal, et al., "Demonstration of a Reliable 1 Gb Standalone Spin-Transfer Torque MRAM For Industrial Applications," 2019 IEEE International Electron Devices Meeting (IEDM), 2019, pp. 2.1.1-2.1.4 [2] K, Lee, et al., "1Gbit High Density Embedded STT-MRAM in 28nm FDSOI Technology," 2019 IEEE International Electron Devices Meeting (IEDM), 2019, pp. 2.2.1-2.2.4 [3] W. J. Gallagher, et al., "22nm STT-MRAM for Reflow and Automotive Uses with High Yield, Reliability, and Magnetic Immunity and with Performance and Shielding Options," 2019 IEEE International Electron Devices Meeting (IEDM), 2019, pp. 2.7.1-2.7.4 [4] G. Hu et al., "Spin-transfer torque MRAM with reliable 2 ns writing for last level cache applications," 2019 IEEE International Electron Devices Meeting (IEDM), 2019, pp. 2.6.1-2.6.4 [5] E R. J. Edwards et al., "Demonstration of narrow switching distributions in STTMRAM arrays for LLC applications at 1x nm node," 2020 IEEE International Electron Devices Meeting (IEDM), 2020, pp. 24.4.1-24.4.4 [6] G. Hu et al., "2X reduction of STT-MRAM switching current using double spin-torque magnetic tunnel junction," 2021 IEEE International Electron Devices Meeting (IEDM), 2021, pp. 2.5.1-2.5.4 [7] C. Safranski et al., "Reliable Sub-nanosecond MRAM with Double Spin-torque Magnetic Tunnel Junctions," 2022 Symposium on VLSI Technology, 2022, T01-4

DA-05. Using Stochasticity and Randomness in Magnetic Tunnel Junctions for Energy-Efficient Computing Beyond Memory. *J.C. Incorvia*[1], T. Leonard[1], S. Liu[1], H. Jin[1], J. Kwon[1], C. Cui[1], N. Zogbi[1], A. Maicke[1], S. Karki[1], P.W. Bessler[1], Z. Khodzhaev[1], V.C. Rogers[1], C. Bennett[2], T.P. Xiao[2], S.G. Cardwell[2], C.D. Schuman[3], S. Agarwal[2], M.J. Marinella[2], J. Smith[2], S. Misra[2] and J.B. Aimone[2] *1. Electrical and Computer Engineering, University of Texas at Austin, Austin, TX, United States; 2. Sandia National Laboratories, Albuquerque, NM, United States; 3. Electrical Engineering and Computer Science, University of Tennessee, Knoxville, TN, United States*

We are at an opportune time, when magnetic tunnel junctions (MTJs) have reached a level of maturity in industry for spin transfer torque-magnetic random access memory (STT-MRAM) and hard disk drives (HDDs), and computing is rapidly welcoming new materials and devices to tackle critical spaces where silicon devices are reaching their limits. Training and inference for AI, noise-resilient and radiation-tolerant computing on the edge, solving NP-hard problems, reducing costly analog-to-digital conversion, and efficiently processing naturally probabilistic data, are all areas that the MTJ can move into beyond memory. The scalability and endurance possible with MTJs, as well the high tunability of their properties using materials, interfaces, and geometry, make the MTJ a strong candidate device to tackle these problems. Here, we will present our recent results on using MTJs for these applications. We will show that by incorporating a domain wall (DW) into the MTJ in the DW-MTJ device, it can act as an artificial synapse and artificial neuron. The device prototypes behave as stochastic neurons, which we show can out-perform processing of noisy datasets compared to ideal numerical neurons (Fig. 1a-b) [1]. We show the DW-MTJ also maps onto an integrate-and-fire neuronal model with automatic reset. We will show our recent efforts pushing the DW-MTJ forward for combinatorial logic for edge computing, simulating a 256×256 systolic array of DW-MTJs in

micromagnetics, benchmarked against Google's TPU [2]. Focusing on the two-terminal MTJ, we will compare the different methods for using the MTJ as a random number generator (RNG) via STT, spin orbit torque, field, or voltage-controlled magnetic anisotropy (Fig. 1c-d) [3]. The simulations show a small set of MTJ RNGs can be used to in various probabilistic algorithms in the presence of device-to-device variability. Benchmarking the MTJ solution to these problems will be shown, compared to both CMOS and other emerging device choices. These results lay the groundwork for leveraging MTJs beyond memory. SNL is managed and operated by NTESS under DOE NNSA contract DE-NA0003525.

[1] T. Leonard, S. Liu, H. Jin, and J. A. C. Incorvia. "Stochastic Domain Wall-Magnetic Tunnel Junction Artificial Neurons for Noise-Resilient Spiking Neural Networks." *Applied Physics Letters* 122, 262406 (2023). DOI 10.1063/5.0152211. [2] N. Zogbi, S. Liu, C. Bennett, S. Agarwal, M. J. Marinella, J. A. C. Incorvia, and T. P. Xiao. "Massively Parallel Matrix Multiplication using Voltage Controlled Magnetic Anisotropy Domain Wall Logic." *IEEE Journal on Exploratory Solid-State Computational Devices and Circuits (JxCDC)* 9, 1 (2023). DOI 10.1109/JXCDC.2023.3266441. [3] S. Liu, J. Kwon, P. W. Bessler, S. G. Cardwell, C. Schuman, J. D. Smith, J. B. Aimone, S. Misra, and J. A. C. Incorvia. "Random Bitstream Generation using Voltage-Controlled Magnetic Anisotropy and Spin Orbit Torque Magnetic Tunnel Junctions." *IEEE Journal on Exploratory Solid-State Computational Devices and Circuits (JxCDC)* 8, 2 (2023). DOI 10.1109/JXCDC.2022.3231550.

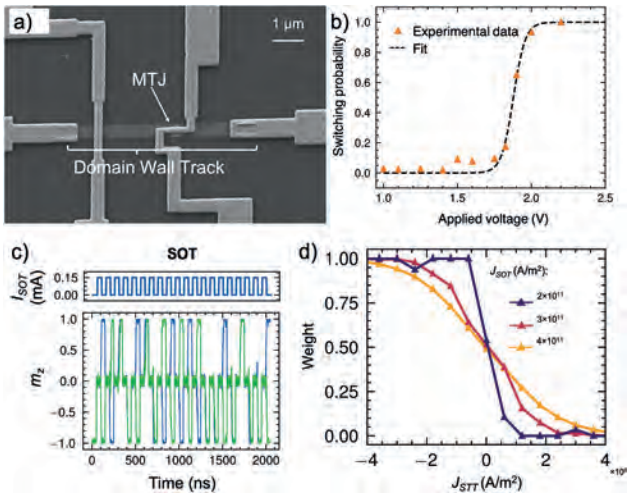

Figure 1. a) Top-down image of the domain wall-magnetic tunnel junction (DW-MTJ) stochastic neuron prototype, showing the perpendicular anisotropy MTJ on top of a DW track. b) Data (orange) of DW switching probability vs. applied voltage pulse amplitude (pulse duration held constant at 30 ns with 10 ns rise/fall times), showing an s-curve behavior. c) Micromagnetic simulation of spin orbit torque (SOT) driven perpendicular MTJ, where the SOT brings the free layer magnetization m_z to the in-plane state, and subsequently m_z switches back to one of the two perpendicular directions when the SOT current is removed. Two overlapping data runs over time shows the randomness. d) Simulations showing that the weight curve of the RNG can be controlled with both STT and SOT, where here the SOT current acts as an effective temperature for simulated annealing. a) and b) are reproduced from Ref. [1], c) and d) are reproduced from Ref. [3].

Session DB
ANTIFERROMAGNETS: ELECTRIC SWITCHING AND SPIN-ORBIT TORQUES
Matthew Daniels, Chair
National Institute of Standards and Technology

INVITED PAPER

DB-01. Coherent Antiferromagnetic Spintronics. *J. Han*[1], R. Cheng[2], L. Liu[3], H. Ohno[1] and S. Fukami[1] *1. Tohoku University, Sendai, Japan; 2. University of California, Riverside, Riverside, CA, United States; 3. Massachusetts Institute of Technology, Cambridge, MA, United States*

Spintronics based on ferromagnetic materials has demonstrated remarkable potential in the current memory and computing technologies. The tunneling magnetoresistance and the current-induced spin torques gave birth to the magnetic random-access memory, while the coherent spin wave attracts attention for wave-based computing with gigahertz frequency. Antiferromagnets have been considered as alternative materials to build higher-performance spintronic devices due to the absence of stray field, the immunity to magnetic perturbation, and the ultrafast dynamics with terahertz frequency, forming a paradigm so-called the antiferromagnetic (AFM) spintronics. In the first chapter of AFM spintronics, a lot of efforts had been spent on the switching and readout of static magnetic order. Meanwhile, spin coherence, the key to explore the wave features of spin polarization and to integrate spintronics with quantum technologies, had been largely untouched, leaving AFM spintronics in its infancy compared to its well-established ferromagnetic counterpart. To usher the next chapter of AFM spintronics featured by coherence, it is essential to induce and harness the coordinating dynamics of the antiferromagnetically coupled magnetic moments. In the recent few years, spin transport and manipulation based on the coherent AFM dynamics have emerged, exhibiting unique functions that are not achievable in ferromagnets [1]. In this talk, we categorize and analyze the fundamental effects of coherent AFM spintronics, including spin pumping from coherent AFM magnons, spin transmission via phase-correlated AFM magnons, electrically induced spin rotation/switching and ultrafast spin–orbit effects in antiferromagnets. We also illustrate how these effects lead to potential applications in unconventional computing, terahertz signal generation, and ultrafast memory. In particular, we discuss our recent progresses in the directions of AFM magnon transport [2] and non-collinear AFM dynamics driven by the spin-orbit torque (SOT) [3, 4]. In the former part, we focus on the spin transmission in an AFM insulator with easy-plane magnetic anisotropy, α-Fe_2O_3 thin film. Contrary to the conventional understanding that its magnon eigenmodes are linearly polarized and thus less likely to transmit spins due to their vanishing angular momentum, we found efficient spin transmission over micrometer distances, which arises from the interference of two linearly polarized propagating magnons forming a circularly polarized effective magnon [2]. This birefringence-like transport provides new opportunities for vector-based computing and non-volatile control of spin transmission. In the latter part, we present the unconventional spin dynamics of a non-collinear antiferromagnet Mn_3Sn driven by the SOT. We found continuous rotation of the chiral-spin structure as a response to the driving current [3]. We also demonstrated a handedness anomaly in the SOT-driven dynamics of Mn_3Sn: when spin current is injected, the collective magnetic order parameter (that is, the octupole moment) rotates in the opposite direction to the individual moments, leading to a SOT switching polarity distinct from ferromagnets [4]. These two studies unveil the unique properties and functionalities of non-collinear antiferromagnets in sharp contrast to ferromagnets and collinear antiferromagnets, which provide additional pathways for electrical manipulation of magnetic materials. A portion of this work has been supported by JSPS Kakenhi 19H05622 and 22F32037.

1. J. Han, et al. Nat. Mater. 22, 684 (2023). 2. J. Han, et al. Nat. Nanotechnol. 15, 563 (2020). 3. Y. Takeuchi, et al. Nat. Mater. 20, 1364 (2021). 4. J.-Y. Yoon, et al. Nat. Mater. accepted (2023).

CONTRIBUTED PAPERS

DB-02. Phase Field Modelling of Magnetoelasticity in Antiferromagnets. *R.A. Mackay*[1,2], J. Barker[1,2] and S.P. Fitzgerald[3,2] *1. School of Physics and Astronomy, Univerity of Leeds, Leeds, United Kingdom; 2. The Bragg Centre for Materials Research, Leeds, United Kingdom; 3. School of Mathematics, University of Leeds, Leeds, United Kingdom*

Conventional ferromagnetic data storage devices are fast approaching the lower limit of their minimum individual bit sizes. Antiferromagnetic spintronic devices have the potential to surpass this limit; antiferromagnets are highly resistant to stray magnetic fields and have THz-order spin dynamics, respectively meaning denser packing of bits is available as well as fast reading/writing of information to these bits. The formation and dynamics of magnetic domains in these materials, however, remain relatively unexplored at device level, despite experimental observation of their existence [1]. It is thought that these domains are magnetoelastic in origin [2]. To explain these observations and to increase the efficiency of future devices, we will explore the domain formation and dynamics using a phase field modelling approach based on the free energy which allows exploration of the domain formation and dynamics at a device-level length scale. To demonstrate our model, we will look at a thin film of the antiferromagnet NiO grown on a substrate of MgO. In this thin film of NiO we have two antiferromagnetically coupled magnetic sublattices. Since NiO and MgO have different lattice constants, we inevitably get a "mismatch" strain in both materials. Following [3], we separate this strain into two components, the spontaneous strain (from the magnetoelastic coupling in the antiferromagnet) and the elastic strain (from the strain coupling between magnet and substrate). Using this "mismatch" strain together with the magnetoelastic coupling and other relevant free energy terms (i.e. antiferromagnetic coupling, anisotropies etc.), this scenario was input into our phase field model, the results of which can be seen in Fig. 1 and Fig. 2. Antiferromagnetic domains can clearly be observed, vindicating our model, and giving us a future base on which to improve our model further.

[1] D. Kriegner, X. Marti and T. Jungwirth, Nat. Commun., Vol. 7, p. 11623, 6 (2016) [2] H. Gomonay and V. M. Loktev, J. Phys.: Condens. Matter, Vol. 14, p. 3959–3971, 4 (2002) [3] H. Meer, O. Gomonay and C. Schmitt, Phys. Rev. B, Vol. 106, p. 094430 (2022)

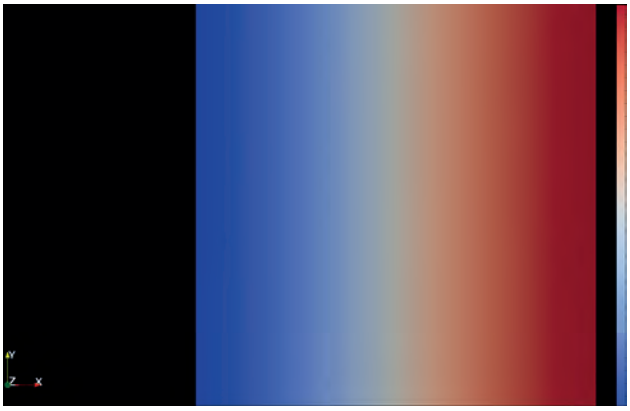

Fig. 1: Y-component of the magnetisation of the first magnetic sublattice. This is mirrored antiferromagnetically on the second sublattice. Magnetic domains can be observed.

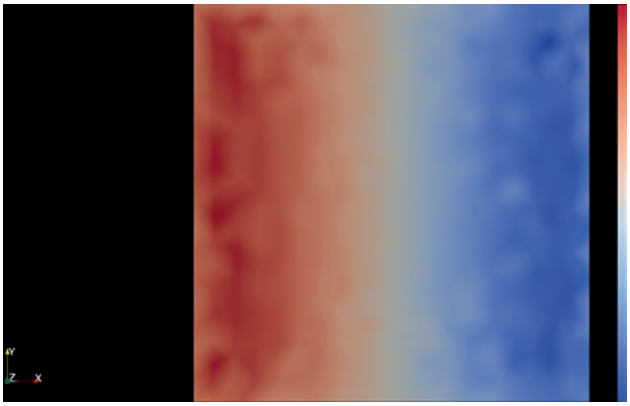

Fig. 2: XY-component of the strain tensor. This mimics the domain structure, a clear indication that the magnetoelastic coupling is the main driver of the domain structure.

DB-04. Spin current generation in collinear antiferromagnet RuO_2.

T. Nguyen[1,2], T. Vu[3], Y. Saito[2], S. DuttaGupta[4,1], H. Naganuma[1,2], S. Ikeda[1,2] and T. Endoh[1,2] *1. Center for Science and Innovation in Spintronics, Tohoku University, Sendai, Japan; 2. Center for Innovative Integrated Electronic Systems, Tohoku University, Sendai, Japan; 3. Institute for Materials Research, Tohoku University, Sendai, Japan; 4. Saha Institute of Nuclear Physics, West Bengal, India*

Investigations on spin-orbit torque (SOT)-induced magnetization switching in different material systems has attracted immense interest owing to its prospect for high-performance MRAMs. RuO_2 is a prospective candidate belonging to the transition metal oxide family, showing spin-split effect (SSE)-induced spin current generation and SOTs, in addition to the conventional spin Hall effect [3, 4]. Recent works have reported SSE-induced SOTs in RuO_2/FM bilayers for various crystal orientations [5, 6], although a detailed understanding of the mechanism of SSE-induced SOTs is lacking. Herein, we investigate the spin current generation in epitaxial RuO_2 (100) film and investigate effective SOT fields, including Slonczewski-like term (H_{SL}) and field-like term (H_{FL}) in a RuO_2/Co-Fe-B bilayer by harmonic Hall measurement. RuO_2 (4 nm)/Co-Fe-B (1.2 nm) bilayer was fabricated on an *a*-Al_2O_3 (0001) substrate by DC/RF sputtering. Fig. 1 shows the XRD φ scans for the substrate and RuO_2 film, meaning that the RuO_2 (100) film was grown on the with the epitaxial relationship: RuO_2[010]//α-Al_2O_3 [11-20], [-2110], [1-210], where three domains were repeatedly rotated 120°. Symmetry analysis of the spin Hall conductivity (SHC) of RuO_2 (100) with this 3-domain structure showed that SHC is independent of the Néel vector orientation, and only depends on the angle between the applied current (J_C) and crystal axis. If J_C is applied at an angle β with the *X*-axis (Fig. 2 (a)), the spin current (J_S) along *Z*-axis: J_{S_z}~ (cosβ-sinβ)J_C with both *X* and *Y* polarizations could be detected by the harmonic Hall measurement. The magnitude J_{S_z} will equal when J_C//[1-100]$_{Sub}$ (β=90°), compared with the case J_C//[11-20]$_{Sub}$ (β=0°). Fig. 2 (b) shows J_C dependence of H_{SL}, H_{FL} for these two cases. Both $|H_{SL}|$ and $|H_{FL}|$ increase with J_C, implying their current-induced origin. We obtain comparable magnitudes of $|H_{SL}|$ and $|H_{FL}|$ for both cases, for similar J_C, consistent with the symmetry analysis. These findings suggest a novel route towards SOT-induced magnetization switching without using materials with large spin-orbit coupling.

[1] H. Honjo *et al.*, IEDM Technical Digest 28.5, (2019). [2] M. Natsui *et al*., JSSC 56, 1116 (2020). [3] R. González-Hernáldez *et al*., Phys. Rev. B 126, 127701 (2021). [4] A. Bose *et al.*, Nature Electronics 5, 267 (2022). [5] H. Bai *et al.*, Phys. Rev. Lett. 128, 197202 (2022). [6] S. Karube *et. al.*, Phys. Rev. Lett. 129, 137201 (2022).

Figure 1:

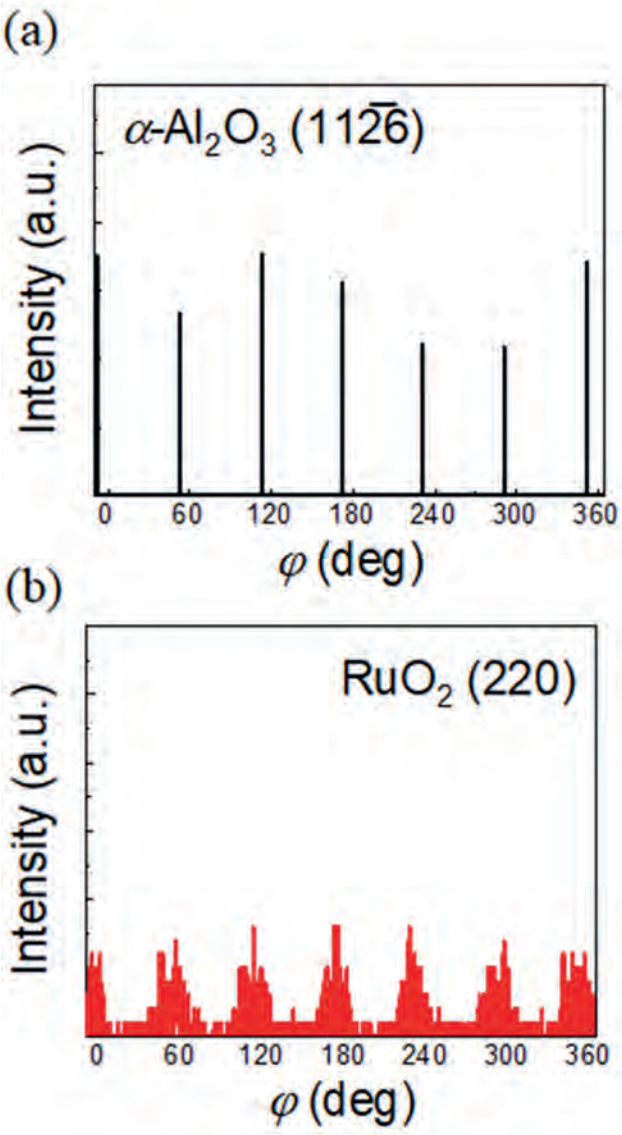

XRD φ-scans for the substrate (a) and RuO_2 films (b).

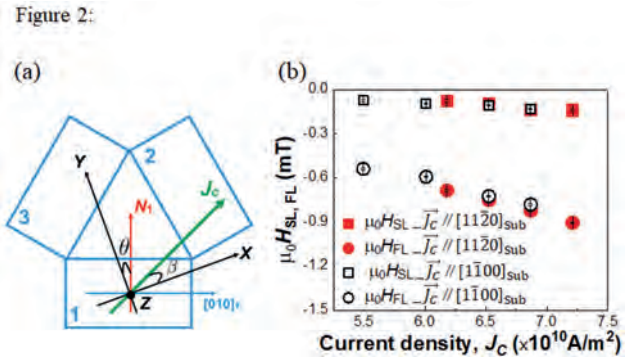

(a) Illustration of 3-domain structure. (b) J_C dependence of H_{SL}, H_{FL} for two cases.

DB-05. Spin-charge conversion via altermagnetic spin splitting effect in RuO_2. *H. Bai*[1] and C. Song[1] *1. Tsinghua University, Beijing, China*

The relativistic spin Hall effect (SHE) and inverse spin Hall effect (ISHE) enable the efficient generation and detection of spin current. Nevertheless, the spin polarization is limited to the direction orthogonal to both charge and spin current. In contrast, a novel relativistic mechanism of spin-charge conversion, termed as altermagnetic spin splitting effect (ASSE), was theoretically predicted. [1,2] On one hand, the controllable generation of spin current and the resultant spin splitting torque (SST) can combine advantages of conventional spin transfer torque (STT) and spin-orbit torque (SOT). On the other hand, ASSE enables detection of spin current with multi-directional polarization, as well as the controllable THz emission. This talk presents experimental evidence of SST and the inverse effect in collinear antiferromagnetic RuO_2 films. First, according to spin torque ferromagnetic resonance (ST-FMR) measurements of RuO_2 films, we exhibit that spin current direction is correlated to the crystal orientation of RuO_2 and spin polarization direction is parallel to the Néel vector, indicating the existence of SST in RuO_2. [3] Second, based on spin Seebeck effect and THz emission measurements, we demonstrate that inverse ASSE can convert spin current polarized along Néel vector into charge current, which manifests as Néel vector-dependent spin Seebeck voltage signals and THz emission signal. [4] These findings not only present a new member for the spin torques besides traditional STT and SOT, but also proposes RuO_2 for both promising spin source and spin sink in spintronic devices.

[1] M. Naka, *et al*., Nat. Commun. Vol.10, p.4305 (2019). [2] R. González-Hernández, *et al*., Phys. Rev. Lett. Vol.126, p.127701 (2021). [3] H. Bai, *et al*., Phys. Rev. Lett. Vol.128, p.197202 (2022). [4] H. Bai, *et al*., Phys. Rev. Lett. Vol.130, p.216701 (2023).

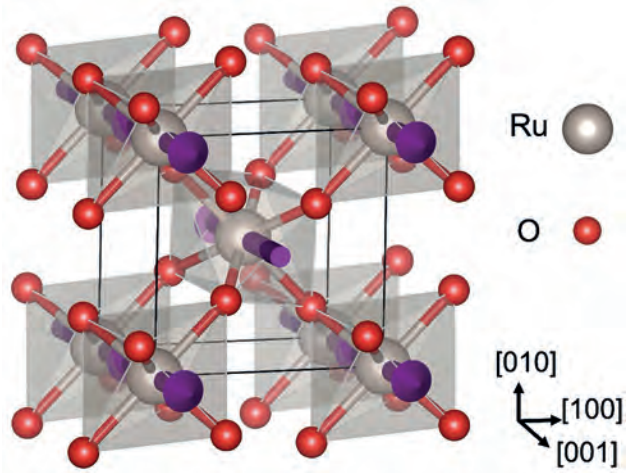

The crystal and magnetic structure of RuO_2.

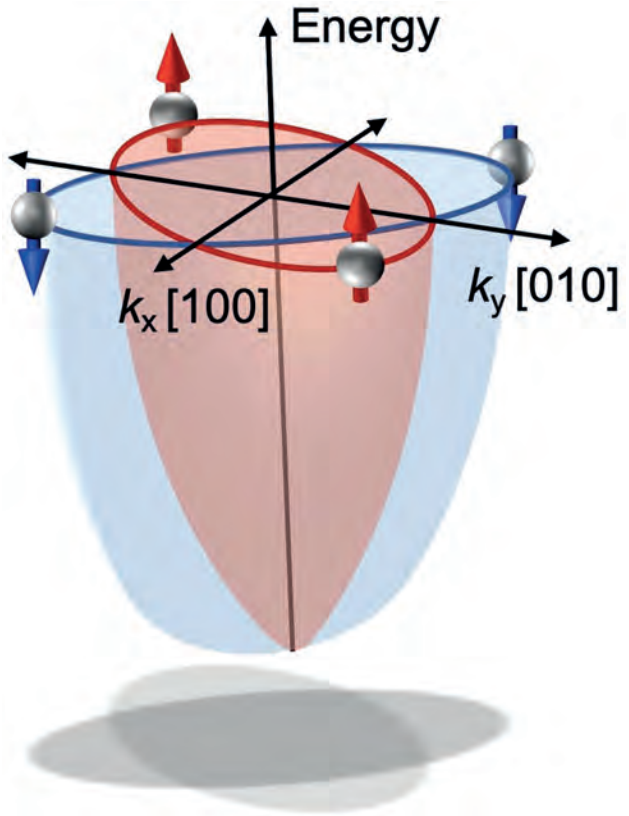

The Fermi-level of RuO_2 at $k_z = 0$ with anisotropic spin splitting.

DB-06. Electrical Manipulation of Spin-splitting Antiferromagnet Mn_5Si_3. *L. Han*[1], C. Song[1] and F. Pan[1] *1. Tsinghua University, Beijing, China*

The recently discovered spin-splitting antiferromagnets (AFMs) inherit advantages of both ferromagnets and AFMs, which provide unprecedented opportunities for the long-desired non-volatile, high-density, and ultra-fast memories[1-3]. Notably, unique features of spin-splitting AFMs such as the alternating spin-splitting band structure[3], the spin-splitter torque[4], the large tunneling magnetoresistance[5], as well as the anomalous Hall effect[6] are all determined by the direction of Néel vector and can be controlled by 180° switching of the Néel vector. Traditionally, current-induced staggered

spin-orbit fields can achieve 90° switching in AFM CuMnAs and Mn_2Au, but it requires special AFM sublattice symmetry breaking and the 180° switching is missing. Besides, the electrical 90° or 120° switching have been realized in NiO, α-Fe_2O_3, et al., where the Néel vectors are first driven into rotation by spin-orbit torque (SOT), and then redirected along one of local easy axes due to magnetic anisotropy. The desired deterministic 180° switching is very difficult to be realized in this way because both opposite Néel vectors have the same magnetic anisotropy. In this work, we propose a new mechanism for the deterministic electrical 180° switching of the Néel vector via damping-like SOT by designing asymmetric switching barriers and experimentally achieved it in spin-splitting AFM Mn_5Si_3[7-8]. We prove theoretically and experimentally that 180° switching of the Néel vector indeed tunes the spin-splitting bands and flips the Berry curvature, and subsequently brings about opposite anomalous Hall conductivity (AHC), which can be used as an unconventional electrical readout approach of the Néel vector. With these write and read methods ready, we successfully fabricate a prototype device that realizes robust write and readout cycles, paving the way for the long-desired electrical-controllable AFM memory.

[1] R. González-Hernández, L. Šmejkal, K. Výborný, Phys. Rev. Lett., Vol. 126, p. 127701 (2021). [2] H.Y. Ma, M. Hu, N. Li, Nat. Commun., Vol. 12, p. 2846 (2021). [3] L. Šmejkal, J. Sinova, T. Jungwirth, Phys. Rev. X., Vol. 12, p. 031042 (2022). [4] H. Bai, L. Han, X.Y. Feng, Phys. Rev. Lett., Vol. 128, p. 197202 (2022). [5] L. Šmejkal, A.B. Hellenes, R. González-Hernández, Phys. Rev. X. Vol. 12, p. 011028 (2022). [6] Z. Feng, X. Zhou, L. Šmejkal, Nat. Electron., Vol. 5, p. 735 (2022). [7] H. Reichlová, R.L. Seeger, R. González-Hernández, http://arxiv.org/abs/2012.15651. [8] I. Kounta, H. Reichlova, D. Kriegner, Phys. Rev. Mater. Vol. 7, p. 024416 (2023).

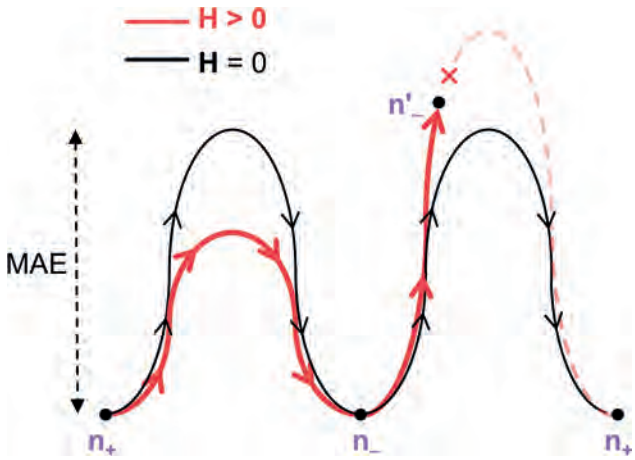

Schematic of using magnetic field to design asymmetric switching barrier

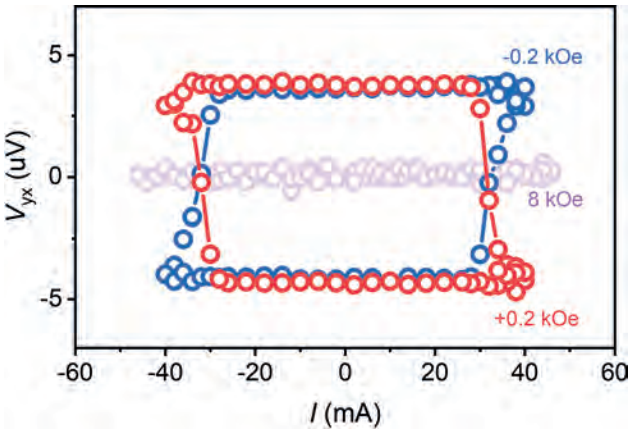

Hall voltage collected when sweeping electrical pulse of different magnitude and polarity with assistant field of –0.2 kOe, 0, and 0.2 kOe, respectively.

DB-07. Exotic Spin-Orbit Torque in Antiferromagnetic Topological Insulator $MnBi_2Te_4$. *J. Tang*[1] and R. Cheng[2,1] *1. Department of Physics and Astronomy, University of California, Riverside, Riverside, CA, United States; 2. Department of Electrical and Computer Engineering, University of California, Riverside, Riverside, CA, United States*

We formulate and quantify the spin-orbit torque (SOT) in intrinsic antiferromagnetic topological insulator $MnBi_2Te_4$ of a few septuple-layer thick in charge-neutral condition, which exhibits pronounced layer-resolved characteristics and even-odd contrast. A striking feature of our SOT is that it is not accompanied by a conduction current, thus devoid of Joule heating. We further study the SOT-induced magnetic resonances, where in the tri-septuple-layer case we identify a peculiar exchange mode that is blind to microwaves but can be exclusively driven by the predicted SOT. As an inverse effect of the SOT, topological charge pumping generates a pure adiabatic current, which occurs concomitantly with the SOT and gives rise to an effective reactance for MnBi2Te4, enabling a lossless conversion of electric power into magnetic dynamics.

[1] J.Y. Tang and R. Cheng, Voltage-driven exchange resonance achieving 100% mechanical efficiency, Phys. Rev. B 106, 054418 (2022)

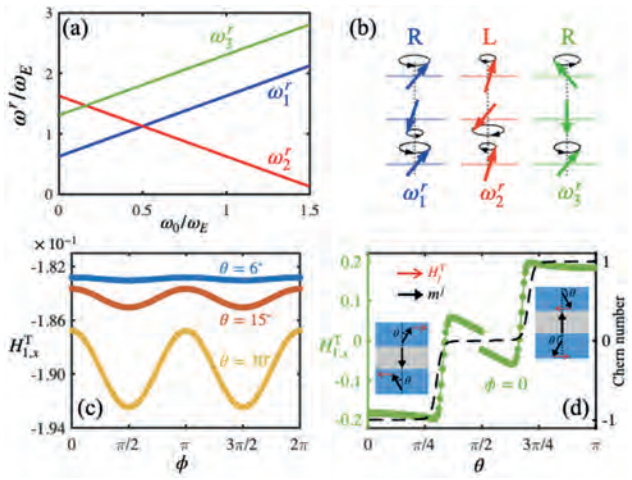

(a) Resonance frequencies of 3-SL $MnBi_2Te_4$ varying with a perpendicular magnetic field. (b) SL-specific magnetic precessions in each eigenmode. The SOT field strength in the ω^r_3-mode configuration as a function of: (c) φ for different θ; (d) θ for φ=0. The total Chern number is also shown (black dashed curve). m^2 is opposite for θ ∈ [0, π/2) and (π/2, π]. Parameters: γ_{ex} = 75 meV, $\hbar\omega_E$ = 0.272 meV and $\hbar\omega_A$ = 0.084 meV.

DB-08. Coexistence of magnon-induced and rashba-induced unidirectional magnetoresistance in antiferromagnet. Z. Zheng[1] and *J. Chen[1] 1. Department of Material Science and Engineering, National University of Singapore, Singapore*

Antiferromagnets (AFMs) are of great interest to the next-generation spintronic devices [1], due to their attractive properties like ultra-fast dynamics, negligible magnetization, and immunity to external magnetic field. However, the naturally compensated magnetization in antiferromagnet hinders the read-out function. Efficient alternatives to read AFM order are still in urgent need. In this work, we show that a kind of non-linear magnetoresistance, i.e., unidirectional magnetoresistance (UMR) [2], can read out the Néel order in an AFM insulator. The experiments are implemented in a device made of $YFeO_3$/Pt bilayer film. When an applied current passes through Pt layer, a pure spin current j_s is generated to drive the Néel vector, to do precession away from the equilibrium position, allowing the detection of second harmonic signals. Fig. 1a plots the angle dependence of the second harmonic longitudinal voltage $V_{2\omega,xx}$ with H = 8 T at 300 K together with the spin Seebeck effect and UMR contribution. Our magnetic-field-dependent UMR measurement in Fig. 1b shows an anomalous tendency: 1) when increasing H from 0.75 T to 3 T (blue zone), the extracted UMR resistance R_{UMR} first increases and then decreases. It reaches maximum at H = 2 T as indicated by the red arrow. 2) with further increase of H above 3 T (pink zone), R_{UMR} increases monotonically. We attributed this anomalous tendency to the coexistence of two individual AFM UMR origins in the same sample: 1) magnon-induced UMR; 2) Rashba-induced UMR. The contribution of magnon-induced UMR is verified by the micromagnetic calculation of the magnon number difference as a function of applied magnetic field (Fig. 1c). And the role of Rashba-induced UMR is also proved by the tight-binding model shown in Fig. 1d. This work provides a convincing alternative to read out the Néel order in AFM material and may inspire more novel AFM functional devices.

[1] V. Baltz, et al. Rev. Mod. Phys. 90 (2018), 015005. [2] C. O. Avci, et al. Nat. Phys. 11 (2015), 570.

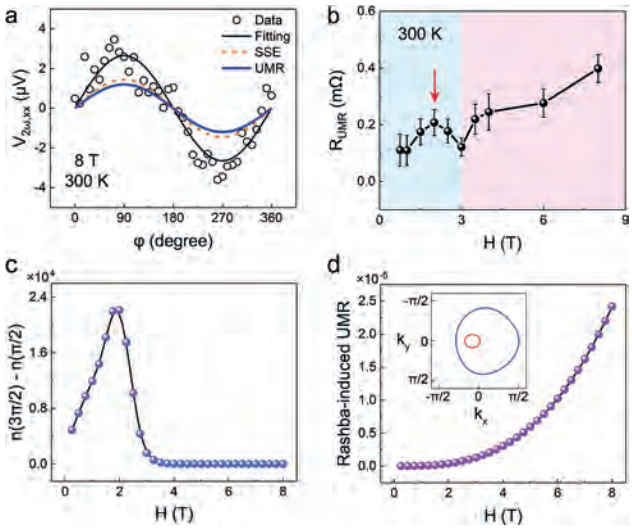

Figure 1: (a) and (b) Angle dependence and field dependence of UMR signal in AFM insulator. (c) Calculated field-dependent magnon number difference between φ = 3π/2 and φ = π/2. (d) Calculated Rashba-induced UMR as a function of magnetic field.

DB-09. Unidirectional Spin Hall Magnetoresistance in Antiferromagnetic Heterostructures. *Y. Cheng*[1], J. Tang[2], J. Michel[3], S. Chong[1], F. Yang[3], R. Cheng[3] and K. Wang[1] *1. Electrical and Computer Engineering, UCLA, Los Angeles, CA, United States; 2. Department of Physics & Astronomy, University of California Riverside, Riverside, CA, United States; 3. Physics, The Ohio State University, Columbus, OH, United States*

Unidirectional spin Hall magnetoresistance (USMR) has been widely reported in the heavy metal / ferromagnet (HM/FM) bilayer systems. We observe the USMR in Pt/α-Fe_2O_3 bilayers where the α-Fe_2O_3 is an antiferromagnetic (AFM) insulator. Systematic field and temperature-dependent measurements confirm the magnonic origin of the USMR. The appearance of AFM-USMR is driven by the imbalance of creation and annihilation of AFM magnons by spin-orbit torque due to the thermal random field. However, unlike its ferromagnetic counterpart, theoretical modeling reveals that the USMR in Pt/α-Fe_2O_3 is determined by the antiferromagtic magnon number with a non-monotonic field dependence as compared with that of ferromagnetic materials. The magnonic origin of USMR is further confrimed by the temperature-dependent measurements. This first evidence of USMR in HM/AFI bilayers significantly expands our materials base to include the large family of AF insulators and paves the way for the highly sensitive detection of AF spin state in emerging the AF spintronics through USMR.

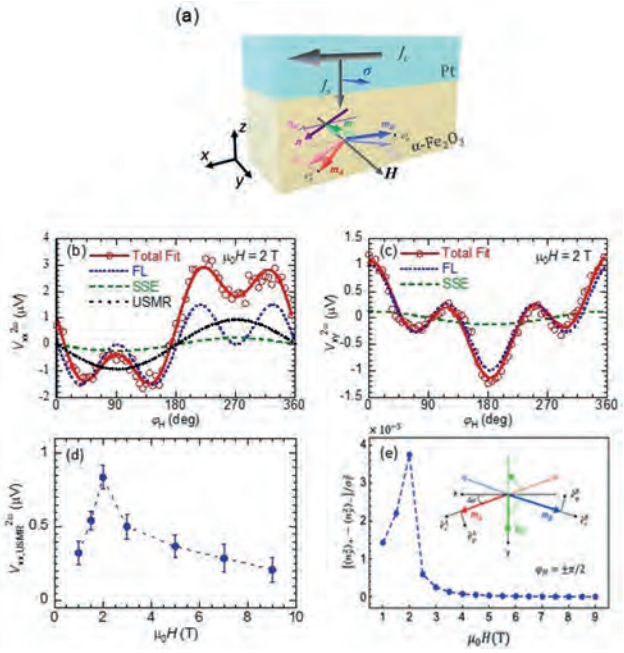

Figure 1. (a) Schematic of current induced spin orbit torque in two spin sublattices. In-plane angular dependence of second harmonic voltage (b) $V_{xx}^{2\omega}$ and (c) $V_{xy}^{2\omega}$ for the Pt(5 nm)/*a*-Fe_2O_3(30 nm) bilayer at 300 K with 2 T applied field. The blue, green, and black curves are contributions from the field-like torque, spin Seebeck effect, and USMR, respectively. (d) The extracted magnetic field dependence of USMR contribution in the $V_{xx}^{2\omega}$. (e) Magnetic field dependence of antiferromagnetic magnon number difference between $\varphi_H = +\pi/2$ and $-\pi/2$, which qualitatively agrees with the non-monotonic trend of the USMR contribution in the $V_{xx}^{2\omega}$ in (d). The magnetic fluctuation originates from the thermal random fields in the two orthogonal directions. σ_T^2 is the thermal coefficient.

DB-11. A Multi-state Analog Magnetic Memory Neuromorphic Processor Based on an Artificial Antiferromagnetic Domain Wall Device. *Y. Huang*[1], Y. Huang[1], C. Cheng[1], Y. Wu[1], Y. Lin[1], W. Chang[2] and Y. Tseng[1] *1. National Yang Ming Chiao Tung University, Hsinchu, Taiwan; 2. Powerchip Semiconductor Manufacturing Corporation, Hsinchu, Taiwan*

Multi-State spin-orbit torque (SOT) switching is a promising artificial intelligence component since it enables the creation of integrated SOT synaptic neuronal units compatible with neuromorphic computing networks[1,2]. Multi-State can mimic the behavior of synapses and increase the storage density of each storage unit through multiple discrete storage levels within a single unit. In this work, the synthetic antiferromagnetic (SAF) structure CoFeB/Ta/CoFeB ferromagnetic tri-layer is shown to be metastable under field-free switching with the pulsed current. By continuously applying a pulse current to modulate the RKKY effective field, the amplitude and polarity of the effective field acting on the domain wall can be changed to drive the reciprocal motion of the domain wall. Utilizing the current-induced gradual switching of the SAF's ferromagnetic tri-layer, we built an artificial neuron where the fitted sigmoid function in the typical field-free switching loop represents the activation function of the hidden layer. At the same time, weight updating is accomplished through the resistance states extracted from memristive switching induced by electrical current pulses. We further implemented an artificial neural network (ANN) with hundreds of excitatory neurons to train and deduce each letter symbol separately. Our structure allows the classification of images from the modified National Institute of Standards and Technology (NIST) dataset with an accuracy of up to 93.27%.

[1]. J. Grollier et al., *Nat. Electron.* 3, 360 (2020). [2]. K. Dong et al., *Phys. Rev. Applied* 19, 024034 (2023).

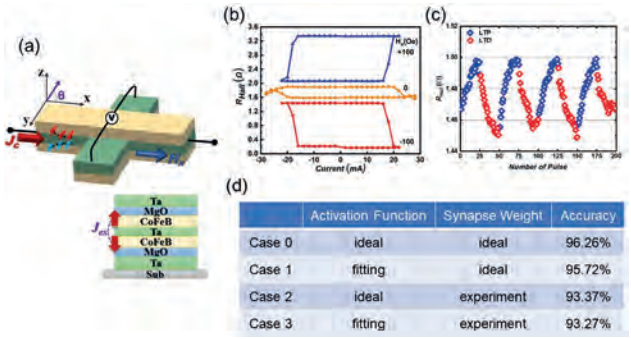

	Activation Function	Synapse Weight	Accuracy
Case 0	ideal	ideal	96.26%
Case 1	fitting	ideal	95.72%
Case 2	ideal	experiment	93.37%
Case 3	fitting	experiment	93.27%

Fig.1 (a) Schematic of Ta/MgO(2)/CoFeB(1.2)/Ta(1.0)/CoFeB(1.2)/MgO(2)/Ta (thickness in nanometers) Hall bar devices and corresponding measurement configuration. (b) SOT-induced switching for the antiferromagnetic coupling sample versus different external magnetic fields, where field-free switching is achievable. (c) SOT-driven memristor for neuromorphic computing. R_H variations are tuned by programming consecutive pulse sequences. (d) ANN performance comparison of accuracy for training 17900 images with different combinations of synapses and neurons.

DB-12. Withdrawn

Session DC
MAGNETO-IONIC AND NEW MAGNETOELECTRIC MATERIALS

Kai Liu, Co-Chair
Georgetown University, Washington, DC, United States
Dhritiman Bhattacharya, Co-Chair
Georgetown University, Washington, DC, United States

INVITED PAPER

DC-01. Hysteresis and Reversibility Across the Voltage-Driven Perovskite-Brownmillerite Ferromagnet-Antiferromagnet Transition in Ultrathin $La_{0.5}Sr_{0.5}CoO_{3-\delta}$ films. W.M. Postiglione[1], G. Yu[1], V. Chaturvedi[1], K. Heltemes[1], A. Jacobson[1], H. Zhou[2], M. Greven[1] and *C. Leighton[1] 1. University of Minnesota, Minneapolis, MN, United States; 2. Argonne National Lab, Argonne, MN, United States*

Perovskite cobaltites are archetypes for electrochemical control of properties in electrolyte-gated devices [1-7]. Voltage-driven redox cycling can be performed between fully oxygenated perovskite and oxygen-vacancy-ordered brownmillerite phases, enabling wide modulation of structure [1-7], magnetism [1,2,3,7], electronic transport [1,2,7], thermal transport [4,5], and optical properties [6,7]. The vast majority of studies, however, focus only on the perovskite and brownmillerite *endpoints*. Here we focus on hysteresis and reversibility across the entire perovskite ↔ brownmillerite transformation, combining gate-voltage hysteresis loops, minor loops, quantitative *operando* synchrotron X-ray diffraction, and temperature-dependent (magneto) transport, using ultrathin epitaxial $La_{0.5}Sr_{0.5}CoO_{3-\delta}$ (LSCO) films (Fig. 1). Gate-voltage (V_g) hysteresis loops and *operando* synchrotron diffraction reveal a wealth of new findings, including asymmetric redox kinetics tied to differing oxygen diffusivities, non-monotonic transformation rates due to the first-order transformation, and limits on reversibility related to structural degradation. Minor hysteresis loops additionally enable rational design of the gate-voltage cycle for optimal reversibility of magnetism and transport. Combining this knowledge, we demonstrate state-of-the-art cycling of electronic/magnetic properties, encompassing 10^5 transport ON/OFF ratios at room temperature, and reversible metal-insulator-metal and ferromagnet-antiferromagnet-ferromagnet cycling (see Fig. 2), all at 10-unit-cell thickness with high 300-K stability [8].

[1] Leighton, Nat. Mater. 18, 13 (2019). [2] Lu, Zhang, Zhang, Qiao, He, Li, Wang, Guo, Zhang, Duan, Li, Wang, Yang, Yan, Arenholz, Zhou, Yang, Gu, Nan, Wu, Tokura, Yu, Nature 546, 124 (2017). [3] Ning, Zhang, Occhialini, Comin, Zhong, Ross, ACS Nano 14, 8949 (2020). [4] Lu, Huberman, Zhang, Song, Wang, Vardar, Hunt, Waluyo, Chen, Yildiz, *Nat. Mater.* 19, 655 (2020). [5] Zhang, Postiglione, Xie, Zhang, Chaturvedi, Heltemes, Zhou, Feng, Leighton and Wang, Nat. Commun. 14, 2626 (2023). [6] Chakraborty, Postiglione, Ghosh, Mkhoyan, Leighton and Ferry, Adv. Opt. Mater. 2300098 (2023) [7] Chaturvedi, Postiglione, Chakraborty, Yu, Tabis, Hameed, Biniskos, Jacobson, Zhang, Zhou, Ferry, Greven and Leighton, ACS Appl. Mater. Interf. 13, 51205 (2021). [8] Postiglione, Yu, Chaturvedi, Heltemes, Jacobson, Zhou, Greven and Leighton, in preparation (2023).

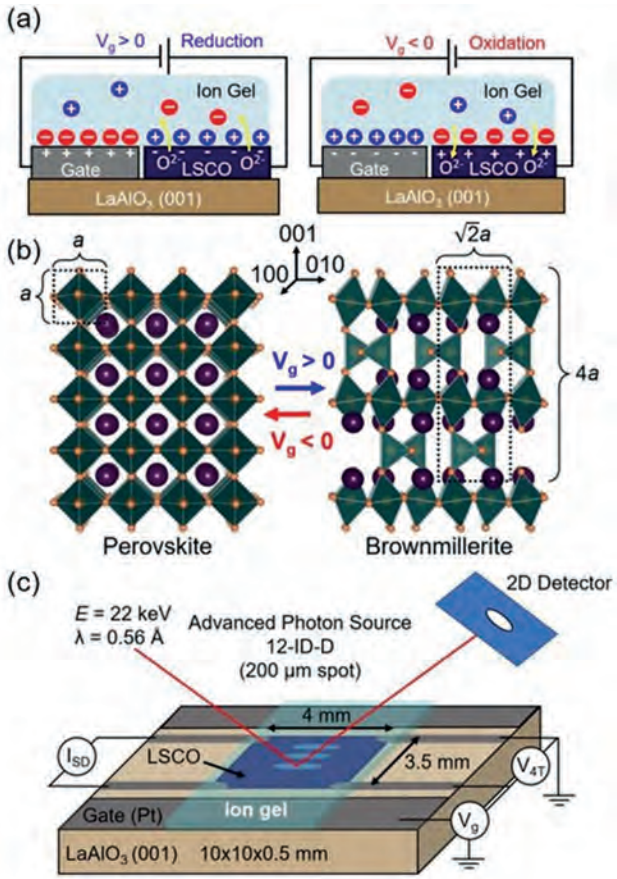

Fig. 1: Device (a), crystal structure (b), and experimental set-up (c) schematics.

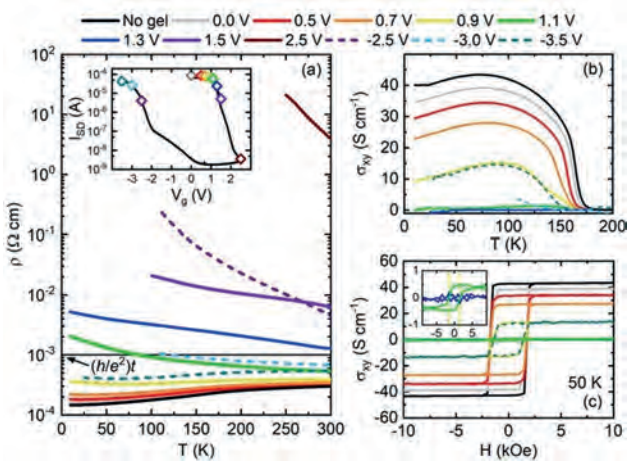

Fig. 2: (a) Temperature (*T*) dependent resistivity (ρ) at the various gate voltages color-coded on the source-drain current hysteresis loop in the inset. (b) Corresponding *T* dependence of the anomalous Hall conductivity (σ_{xy}) at various V_g. (c) Corresponding magnetic field (*H*) dependence of the 50-K σ_{xy} at various V_g. Note the reversible cycling from ferromagnetic metal to antiferromagnetic insulator, back to ferromagnetic metal.

CONTRIBUTED PAPERS

DC-02. Fast and giant modulation of magnetism in 3d-4f magnets by small voltages. *X. Ye*[1], H. Singh[1], H. Zhang[1], B. Gault[3], R. Kruk[2], K.P. Skokov[1], H. Hahn[2] and O. Gutfleisch[1] *1. Technical University of Darmstadt, Darmstadt, Germany; 2. Institute of Nanotechnology, Karlsruhe Institute of Technology (KIT), Karlsruhe, Germany; 3. Department of Microstructure Physics and Alloy Design Max-Planck-Institut für Eisenforschung GmbH (MPIE), Dusseldorf, Germany*

Controlling magnetism and magnetic properties by small voltages have become one of the core research topics pursued in magnetoelectric actuation, spintronics and data storage. In magnetically-ordered metals and alloys, however, the voltage effect is usually limited to the scale of atomic layers due to strong electric-field screening [1]. Substantial efforts have been devoted to break this thickness limitationas represented by magneto-ionics [2-4]. Previously, we proposed to control their magnetism and magnetic properties by electrochemically-driven insertion/extraction of hydrogen atoms in interstitial sites. The uniqueness of this concept lies in controlling the absorption and desorption of electrically neutral hydrogen atoms by means of electrochemical potentials. We demonstrated that by applying voltages as low as 1 V the magnetocrystalline anisotropy and coercivity of Sm-Co magnets with micrometer-sized particles by more than 1 T [5,6]. In this talk, we will extend the concept to thin films of Sm-Co magnet with nanocrystalline structure as well as ferrimagnetic alloy. We achieved the reversible switching of coercivity between 2.9 T and nearly zero tesla, as well as the voltage control of demagnetization and re-magnetization. Importantly, the tuning speed has been increased by several orders of magnitude to ms. In the latter case, we can switch the perpendicular anisotropy to in-plane anisotropy in amorphous ferrimagnetic thin films, which resolves the mechanism behind perpendicular anisotropy in amorphous thin films. Experimental and density functional theory calculation results show that the change of magnetic anisotropy originates from the change of crystal field and magnetic exchange interactions.

[1] F. Matsukura, Y. Tokura, H. Ohno, *Nature Nanotech.* 10, 209-220 (2015). [2] A. Tan, M. Huang, C. O. Avci, F. Büttner, M. Mann, W. Hu, C. Mazzoli, S. Wilkins, H. L. Tuller, G. S. D. Beach, Nat. Mater. 18, 35 (2019). [3] Navarro-Senent, A.Quintana, E. Menendez, E. Pellicer, J. Sort, *APL Mater.* 7, 030701 (2019). [4] M. Nichterwitz, S. Honnali, M. Kutuzau, S. Guo, J. Zehner, K. Nielsch, K. Leistner. *APL Mater.* 9, 030903 (2021) [5] X.L.Ye, H. Singh, H.B Zhang, H. Geßwein, M.R. Chellali, R. Witte, A. Molinari, K. Skokov, O. Gutfeisch, H. Hahn, R. Kruk. *Nature Comm.* 11, 4849 (2020). [6] X.L.Ye, F.K. Yan, L. Schaefer, D. Wang, H. Geßwein, W. Wang, M.R.Chellali, L. Stephenson, K. Skokov, O. Gutfleisch, D. Raabe, H. Hahn, B. Gault, R. Kruk. *Adv. Mater.* 33, 2006853 (2021).

DC-03. Voltage-Modulated Magnetization and Angular Momenta in Pd/Co/Pd Trilayers. *A.E. Kossak*[1], A. Kaczmarek[1] and G. Beach[1] *1. Department of Materials Science and Engineering, Massachusetts Institute of Technology, Cambridge, MA, United States*

The high energy cost of current-controlled spintronic devices has motivated the search for alternative methods of in-situ exploitation of magnetic materials. Chief among them is voltage-controlled magneto-ionic gating. Despite the rampant discovery of tunable magnetic properties, e.g., the RKKY interaction,[1] magnetic anisotropy,[2,3] and exchange bias,[4] there are very few studies that give a quantitative understanding of the reversible and irreversible effects of ionic infiltration. In this study, we use in-situ vibrating sample magnetometry (VSM) and x-ray magnetic circular dichroism (XMCD) to reveal both the reversible and irreversible control of magnetization and angular momenta in Pd/Co/Pd trilayers by solid-state hydrogen-ion gating.[2] We demonstrate that the typical,[1–4] less than 0.25 mm^2, devices can be scaled 100 times in size and therefore within the resolution of a VSM. Using these large devices, we perform in-situ gating VSM measurements and show that the previously demonstrated magneto-ionic control of magnetization is only controlled by the magnetic anisotropy and that the saturation magnetization remains constant. However, over the span of thousands of cycles, the cyclic insertion and removal of hydrogen does cause a decrease in the saturation magnetization. The rate at which this occurs, however, is not enough to explain the formerly observed irreversible enhancement in coercivity.[3] Using XMCD, we can attribute this to a hydrogen-induced modification of the spin and orbital angular momenta. Our results further show that the nature of the magneto-ionic gating is heavily dependent on the interface as Pt/Co/Pd trilayers show little to no change with the insertion of hydrogen. Hence, both the proximity-induced magnetization at the heavy-metal/Co interface and the Co magnetization can be easily controlled only in the case of Pd. These quantitative results shine a light on the previously open questions regarding the magneto-ionic gating of Co/Pd heterostructures and provide a basis for scaling these devices more than 2 orders of magnitude.

[1] A. E. Kossak, M. Huang, P. Reddy, *et al.* Sci. Adv., Vol. 9, p.eadd0548 (2023). [2] A. J. Tan, M. Huang, C. O. Avci, *et al.* Nat. Mater. Vol. 18, p.35–41 (2018). [3] A. E. Kossak, D. Wolf and G. S. D. Beach Appl. Phys. Lett. Vol. 121, p.222402 (2022). [4] J. Zehner, D. Wolf, M. U. Hasan, *et al.* Phys. Rev. Mater. Vol. 5, p.L061401 (2021).

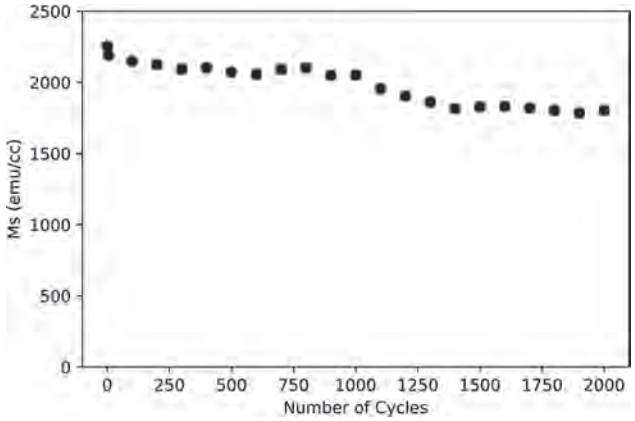

Fig. 1 Saturation magnetization from VSM as a function of gating cycles for a 5x5 mm device.

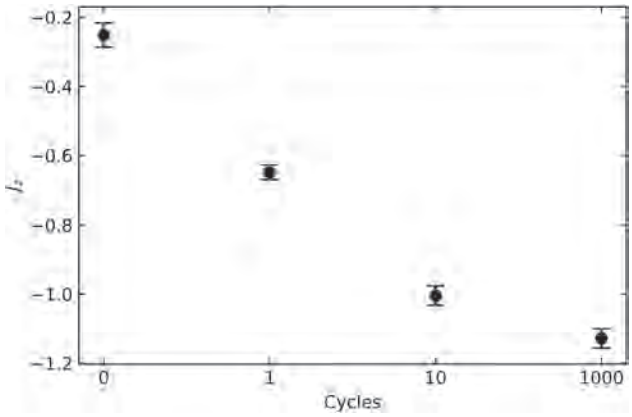

Fig. 2 Total angular momenta from XMCD as a function of gating cycles.

DC-04. Identifying axion insulator by quantized magnetoelectric effect in antiferromagnetic tunnel junction. *R. Cheng*[1,2] and Y. Li[1] *1. Electrical and Computer Engineering, University of California, Riverside, Riverside, CA, United States; 2. Physics and Astronomy, University of California, Riverside, Riverside, CA, United States*

Even-layer MnBi2Te4 is believed to be a topological axion insulator in its antiferromagnetic ground state, featuring unique magnetoelectric responses. However, direct identification of axion insulators remains experimentally elusive because the observed vanishing Hall resistance, while indicating the onset of the axion field, is insufficient to distinguish the system from a trivial normal insulator. Using integrated numerical-analytical methods, we theoretically predict a viable setup to unambiguously identify the axion insulator state through simple and accurate transport measurement. The proposed device is a tunnel junction involving an atomically thin MnBi2Te4 spacer, in which an AC magnetic field of radio frequency could induce a significant tunnel current owing to the topological magnetoelectric effect. We claim that the tunnel current serves as a smoking-gun signal confirming antiferromagnetic MnBi2Te4 to be an axion insulator.

[1] Yu-Hang Li and Ran Cheng, Phys. Rev. Res. 4, L022067 (2022). [2] Yu-Hang Li and Ran Cheng, Phys. Rev. Res. 5, 029001 (2023).

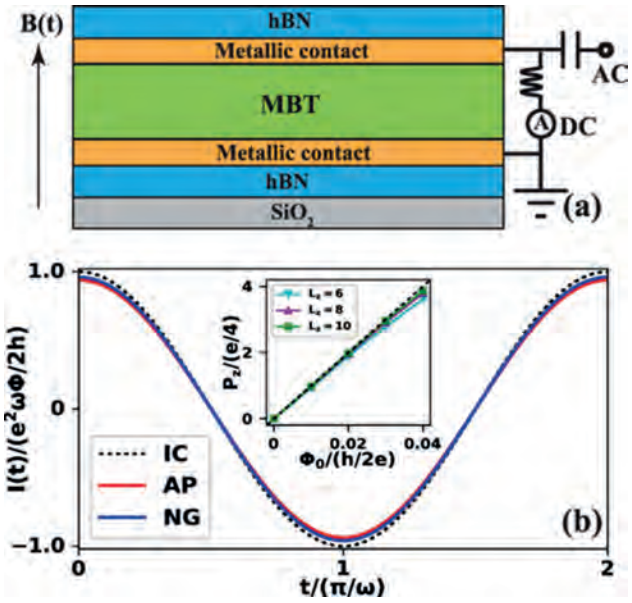

(a) Schematics of the proposed setup. The metallic leads are connected to a bias tee to separate the harmonic ac output from the dc output which is short circuited. (b) Tunnel current induced by an ac magnetic field quantified by the time-dependent nonequilibrium Green's function (NG) (solid blue) and the adiabatic variation of the surface charge polarization (AP) (solid red), respectively. The ideal case (IC) (dotted black) calculated for an infinite system is plotted to benchmark the accuracy of the NG and AP results. System size: Lx=Ly=20 and Lz=6. Inset: Surface charge polarization as a function of the magnetic flux for thicknesses Lz=6, 8, and 10.

DC-05. Nanoscale imaging of skyrmion lattices under external electric fields. *M. Han*[1] and Y. Zhu[1] *1. Condensed Matter Physics & Materials Science, Brookhaven National Laboratory, Upton, NY, United States*

Electric field control of magnetic skyrmions is an important capability because it can enable energy-efficient, nonvolatile device operation and potentially enhanced density of data storage [1]. Multiferroic Cu_2OSeO_3 (CSO) is an insulator with a magnetoelectric coupling [2], a good testbed for electric field control of skyrmions. Although x-ray and neutron scattering studies reported skyrmion lattice stabilization and rotation under electric fields [3,4], direct imaging of skyrmion lattices under external electric fields is desired to understand underlying physics. Using *in situ* electrical and magnetic biasing in a transmission electron microscope (TEM) at liquid helium temperatures, we demonstrate a deterministic control of hexagonally packed skyrmion lattices in insulating chiral magnet CSO by electric fields [5]. We fabricated the TEM sample devices using a commercial TEM grid with pre-written electrodes (TEM windows) using focused ion beam (FIB) technique, as shown in Figure 1. Based on our direct imaging (Figure 2), we found that the skyrmion responses to external electric fields are highly dependent on the crystallographic orientation. Our results show the electric field can effectively control the stability and lattice orientation of skyrmions, providing an important foundation for designing skyrmions-based spintronic devices.

[1] Back, C. et al., J. Phys. D: Appl. Phys. 53, 363001 (2020). [2] Seki, S. et al., Science 336, 198 (2012). [3] Okamura, Y. et al., Phys. Rev. B 95, 184411 (2017). [4] White, J. S. et al., Phys. Rev. Lett. 113, 107203 (2014). [5] Han, et al., submitted (2023). [6] The work was supported by the U.S. DOE Basic Energy Sciences, Materials Science and Engineering Division under Contract No. DESC0012704.

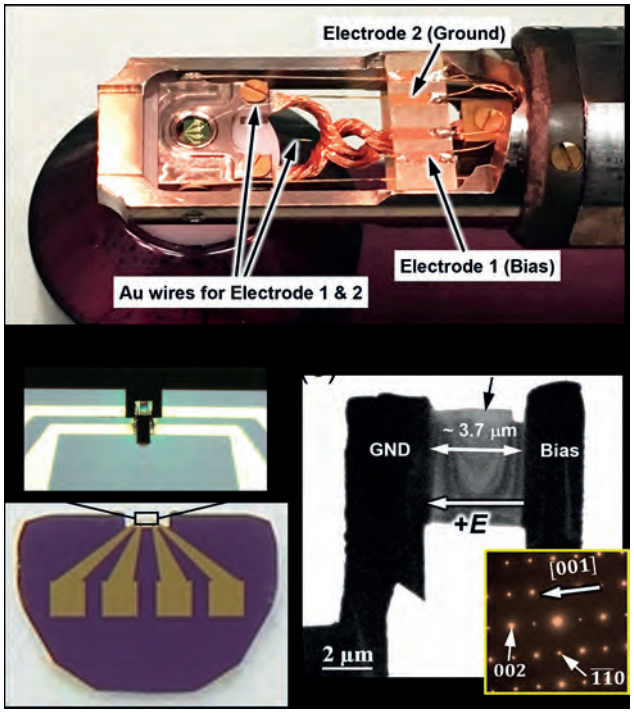

Fig. 1. TEM sample device made of multiferroic CSO. (a) a photograph of cryo-holder with a sample connected electrically. (b) an optical image of TEM sample fabricated by FIB. (c) TEM image of a (110)-oriented CSO sample. The inset shows electron diffraction patterns. The electric field was applied along the [001].

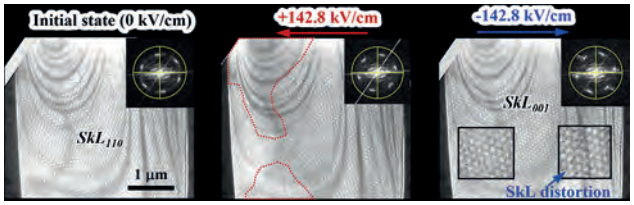

Fig. 2. Lorentz TEM images under magnetic field of 92.7 mT at 13.9 K: initial state (a), a positive electric field of 142.8 kV/cm (b), and a negative electric field of 142.8 kV/cm (c). The insets are fast Fourier transforms. The two insets in (c) show undistorted (left) and distorted (right) skyrmion lattices. A positive electric field (b) destroys SkL in the area highlighted with red lines. The wave vector of skyrmion lattice along the [110] in the initial state was rotated to the [001] direction by the negative electric field (c).

DC-06. Tuning Coercivity and Domain Wall Velocity in CoPd Multilayers via Hydrogen-Loading. M. Bischoff[1], O. Hellwig[2,3], K. Leistner[1] and *M. Goessler*[1] *1. Institute of Chemistry, Chemnitz University of Technology, Chemnitz, Germany; 2. Institute of Physics, Chemnitz University of Technology, Chemnitz, Germany; 3. Institute of Ion Beam Physics and Materials Research, Helmholtz Zentrum Dresden Rossendorf, Dresden, Germany*

Magneto-ionics offers a low-power alternative for the electric control of magnetic properties, which is of great importance for future magnetic data storage. Hydrogen-based magneto-ionics in particular has gained traction recently, because of the large magnetization changes and low switching times promised [1,2]. Here, we investigate CoPd multilayer stacks with perpendicular magnetic anisotropy (PMA) [3], a well-known system researched for magnetic data storage, as a platform for hydrogen-based magneto-ionics. We use our established *in situ* electrochemical cell setup [4] in combination with polar magneto-optical Kerr effect (MOKE) microscopy to observe magneto-ionic effects in CoPd multilayers. This method not only allows us to detect changes in hysteresis loops upon hydrogen-loading, but also provides image data of the underlying domain wall (DW) dynamics. First, we show that coercivity can be increased in CoPd multilayer stacks via electrochemical hydrogen-loading by up to 20%. This increase is highly reversible over several hydrogen-loading/unloading cycles and occurs at low voltages of about 2V. A direct correlation of coercivity with hydrogen concentration in the stacks is found, which allows us to use hydrogen for a continuous tuning of magnetic properties. Furthermore, we demonstrate that hydrogen also influences magnetization dynamics in such multilayer stacks, as DW velocity is decreased upon hydrogen-loading by a factor of ~10 for various driving fields (see Figure 1). We show MOKE microscopy data evidencing that hydrogen-loading can even be used to bring DW motion to a complete halt. On the other hand, for a hydrogen-saturated multilayer stack, hydrogen-unloading can be used to accelerate DWs. We discuss the observed changes in coercivity and DW velocity in terms of hydrogen-induced variations in interfacial anisotropy, taking recent literature findings on similar systems into account [5][6]. The prospects of an analogous magneto-ionic mechanism in platinum-based PMA multilayer stacks are addressed in the outlook.

[1] M. Gößler, M. Albu, R. Würschum *et al., Small* 15 1904523 (2019) [2] A. J. Tan, M. Huang, G. S. D. Beach *et al.*, *Nat. Mater.*, 18, 35, (2019) [3] S. Pan, O. Hellwig, A. Barman, *Phys. Rev. B* 98 214436 (2018) [4] J. Zehner, I. Soldatov, K. Leistner *et al.*, *Adv. Electron. Mater.*, 9, 030903 (2020) [5] K. Klyukin, G. S. D. Beach, B. Yildiz, *Phys. Rev. Mater.* 4 (2020) 104416 [6] A. E. Kossak, D. Wolf, G. S. D. Beach, *Appl. Phys. Lett.* 121 222402 (2022)

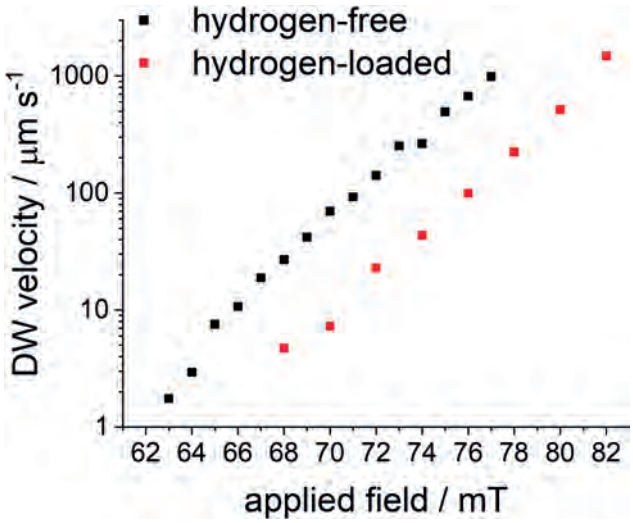

Fig. 1: Magneto-ionic control of DW velocity as a function of applied field via hydrogen-loading in a $[Co(0.4nm)/Pd(0.7nm)]_5$ multilayer stack.

DC-07.: Intrinsic exchange bias in van der Waals alloy Cr0.45Pt0.55Te2. *R. Bailey-Crandell*[1], A. Williams[2], W. Huey[2], W. Zhou[1], J.E. Goldberger[2] and R.K. Kawakami[1] *1. Physics, Ohio State Univeristy, Columbus, OH, United States; 2. Chemistry, Ohio State University, Columbus, OH, United States*

Two-dimensional van der Waals magnetic materials are of recent interest for scientific and technological applications. The novelty in two dimensional magnetic materials means there are new paradigms and functionalities that have yet to be explored, including atomically thick layered structures. Here we report evidence of a novel magnetic structure in exfoliatable van der waals magnetic alloy Cr0.45Pt0.55Te 2 (CPT). We use magneto-optic measurements to observe hysteresis loops in exfoliated CPT samples. The most notable attribute of CPT's hysteresis is that the loop is not centered at zero.

We interpret this as an exchange bias effect, reminiscent of heterostructures of ferromagnets and antiferromagnets, but intrinsic to this material. We explain this effect as a layer-by-layer system of coupled ferromagnetic layers, exerting exchange bias on each other. This work demonstrates layer by layer exchange bias effects that pave the way for further understanding exchange in two dimensional systems.

DC-08. Withdrawn

DC-09. GdWN3: A New Magnetic Nitride Perovskite. *R.W. Smaha*[1], K. Yazawa[1,2], S. Bauers[1] and A. Zakutayev[1] *1. National Renewable Energy Laboratory, Golden, CO, United States; 2. Colorado School of Mines, Golden, CO, United States*

Metal-rich nitrides, such as Fe16N2 and Sm2Co17N3, are promising materials for permanent magnetic applications. However, developments in nitride magnets have been stymied by the difficulty of synthesizing them, given the comparative stability of N2. As such, the phase space of nitrides is vastly underexplored compared to those of oxides and halides. Recent advances in experimental methods for synthesizing nitride materials, particularly thin film methods employing radiofrequency co-sputtering to increase the effective synthesis temperature, have led to a rapid increase in the number of known ternary nitride phases. The greater covalency of nitrogen than oxygen and halogens makes nitrides attractive for semiconducting and other functional applications in renewable energy, and incorporating rare earth cations into novel ternary nitrides may enable novel functionality for magnetic, (opto) electronic, spintronic, and other applications. Rare earth nitride perovskites offer an intriguing path forward for multiferroics since there is evidence of piezoelectricity in $LaWN_3$ [1,2] and low temperature magnetic order in $CeMoN_3$.[3] I present the synthesis, crystal structure, and magnetic characterization of a new thin film rare earth nitride perovskite: $GdWN_3$. Its crystallization dynamics and magnetic properties, as well as the development of design rules for the stabilization and functionalization of new nitride perovskites, will be discussed.

[1] K.R. Talley et al., Science 374, 1488 (2021). [2] R.W. Smaha et al., arXiv:2305.00098 (2023). [3] R. Sherbondy, R.W. Smaha et al., Chem. Mater. 34, 6883 (2022).

DC-11. Understanding the origins of induced net magnetism in the strained interface of a thin-film antiferromagnetic perovskite. *S.A. Morley*[1], S.M. Griffin[1], P. Quarterman[3], B. Kirby[3], J.A. Borchers[3] and D. Lederman[2] *1. Lawrence Berkeley National Laboratory, Berkeley, CA, United States; 2. Physics Department, University of California Santa Cruz, Santa Cruz, CA, United States; 3. NIST Center for Neutron Research, Gaithersburg, MD, United States*

Emergent physics at material interfaces that are not sustained in the bulk is a new and promising avenue, not only for the exploration of fundamental physics but also for original device architectures which can have a variety of functional properties such as superconductivity [1,2], ferroelectricity [3] or emergent low-dimensional magnetism [4]. Epitaxial canted antiferromagnetic perovskite NaNiF3 thin films have been grown on substrates with a lattice mismatch that induces a tensile strain [5]. Polarized neutron reflectometry and magnetometry both indicate the presence of a ferromagnetic interfacial layer (Fig. 1). Perovskites can accommodate modest amounts of strain through octahedral rotations and distortions, the nature of which depends on the amount of strain, the nature of the octahedral chemistries, and the geometry of the structural confinement (e.g. uniaxial -vs- biaxial strain). We use density functional theory to explain the origin of the observed emergent magnetic moment at the interface.

[1] N. Reyren *et al.* Superconducting Interfaces Between Insulating Oxides. *Science*317,1196-1199(2007). [2] Liu, C. *et al.* Two-dimensional superconductivity and anisotropic transport at $KTaO_3$ (111) interfaces. *Science* 371, 716–721 (2021). [3] Ye, F., Zhang, Y., Addiego, C. *et al.* Emergent properties at oxide interfaces controlled by ferroelectric polarization. *npj Comput Mater* 7, 130 (2021) [4] Salluzzo, M. et al. Origin of interface magnetism in $BiMnO_3/SrTiO_3$ and $LaAlO_3/SrTiO_3$ heterostructures. *Phys. Rev. Lett.* 111, 087204 (2013). [5] Morley, S. A., Marquez, H., and Lederman, D. Epitaxial strain and the magnetic properties of canted antiferromagnetic perovskite NaNiF3 thin films. *APL Materials*, 8(1), 011101 (2020).

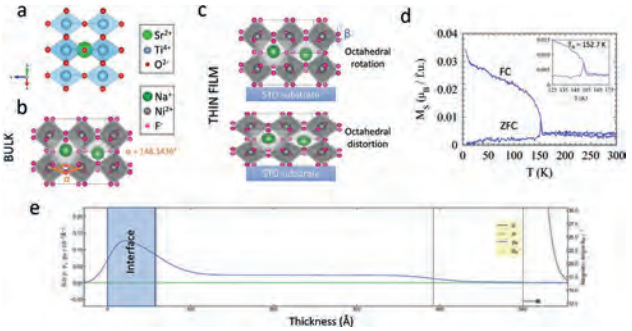

Figure 1. (a) Schematic of the crystal structure of SrTiO3 (STO) substrate, (b) the bulk crystal structure of NaNiF3 perovskite, (c) the possible ways the NaNiF3 can accommodate strain when grown on STO through octahedral rotations (top) or distortions (bottom). (d) Zero-field cooled (ZFC) and field-cooled (FC) magnetometry indicating an additional ferromagnetic contribution below T ≈ 60 K (kink in FC) (e) the modelled magnetic density ρ_m, obtained from polarized neutron reflectometry at T = 5K, indicating a 50 Å magnetic layer at the interface.

Session DD
MAGNETIZATION DYNAMICS IV: ULTRAFAST MAGNETISM

Ezio Iacocca, Chair
University of Colorado Colorado Springs, Colorado Springs, CO, United States

INVITED PAPERS

DD-01. Unraveling Optically Induced Ultrafast Modification of Nanoscale Magnetic Textures. *R. Kukreja[1] 1. Materials Science and Engineer, University of California, Davis, CA, United States*

Ultrafast optical control of magnetization has emerged as a new paradigm for the next generation memory and data storage devices. Numerous studies have been performed to understand the mechanism of transfer of angular momentum at such fast timescales. However, it has been recently recognized that spatial domain pattern and nanoscale heterogeneities can play a critical role in dictating the ultrafast behavior [1-4]. These experimental findings have been possible due to recent advances in x-ray and extreme ultraviolet sources which combine the power of coherent x-rays with femtosecond (fs) temporal resolution [5]. I will discuss some of the key studies performed at x-ray free electron lasers (XFELs) sources in the recent years which have shed light on the magnetic behavior at ultrafast and ultrasmall frontier. I will also describe some of our recent experimental results at European XFEL and FERMI where we uncovered symmetry-dependent behavior of the ultrafast response [6,7]. Our results on the same sample with the same experimental conditions but different ground state (isotropic labyrinth domains vs anisotropic stripe domains) shows that the symmetry of magnetic texture dictates the magnitude and timescale of the ultrafast response. These results clarify the previous controversy in the literature for time-resolved magnetic studies for different samples showing distinct responses. We also utilized time-resolved magnetic scattering to test recent predictions of >10 km/s domain wall speeds. We observed fluence threshold dependence for distortions of diffraction pattern which are not seen for magnetization quenching, consistent with a picture of domain wall motion with pinning sites. Supported by simulations, we show that a speed of ~66 km/s for highly curved domain walls can explain the experimental data (see Fig. 1) [7]. We thus show that these intriguing observations suggest preferential texture-dependent paths for the spin transport and provide us with a unique way to manipulate spin degrees of freedom in far-from-equilibrium regime.

1. Zusin PRB 106, 144422 (2022) 2. Hennes et al., PRB 102, 174437 (2020) 3. Vodungbo et al. J. Nat Comm. 3, 999 (2012) 4. Pfau, B. et al. Nat. Comm. 3, 1100 (2012) 5. Spencer Jeppson and Roopali Kukreja. APL Materials 9, 100702(2021) 6. Hagström et al. PRB 106, 224424(2022) 7. Rahul Jangid et al. arXiv 2303.16131 (2023)

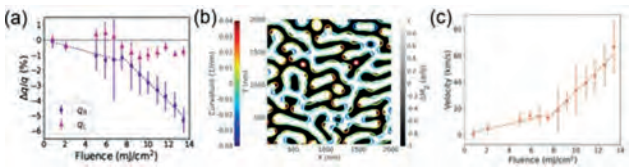

DD-02. Soliton nucleation in ultrafast periodically pumped 1D ferromagnetic chain by the pseudo-spectral Landau-Lifshitz equation. *K. Rockwell[1], J. Hirst[2], T. Ostler[3] and E. Iacocca[1] 1. Center for Magnetism and Magnetic Materials, University of Colorado Colorado Springs, Colorado Springs, CO, United States; 2. Materials and Engineering Research Institute, Sheffield Hallam University, Sheffield, United Kingdom; 3. Department of Physics and Mathematics, University of Hull, Hull, United Kingdom*

Ultrafast magnetism gives rise to intriguing far-from-equilibrium processes, including soliton nucleation [1] and novel phases of matter [2]. Experiments in ultrafast magnetism are typically complemented with input from atomistic spin dynamics (ASD) simulations, or micromagnetics [3]. However, ASD requires significant computing and storage resources, and the micromagnetic model inflates the magnon frequency due to the continuum approximation. Thus, the dynamics between the two regimes have been difficult to resolve. We introduce a pseudo-spectral Landau Lifshitz equation (PS-LLE) to bridge the gap between ASD and micromagnetics. We apply this method to investigate ultrafast dynamics due to a pump grating with a period of 80 nm in a perpendicular magnetic anisotropy, quasi-one-dimensional chain. ASD predicts the nucleation of solitons, as shown in Fig. 1(a). The PS-LLE model also shows soliton nucleation in qualitative agreement with ASD, shown in Fig. 1(b). However, the micromagnetic model fails because of the inflated magnon frequencies and group velocities due to the continuum approximation, shown in Fig. 1(c). The PS-LLE also predicts other nonlinear phenomena including modulational instability [4] and dispersive shock waves [5]. Thus, with the capacity for multiscaled grids between atomistic and continuum models, our PS-LLE method opens the door for the exploration of nonlinear and far-from-equilibrium magnetization dynamics, including modulational instability [4], short-wavelength excitations [6], and three-dimensional topological textures [7].

[1] E. Iacocca *et al.*, Nature Communications 10, 1756 (2019) [2] F. Büttner, *et al.*, Nature Materials 20, 30–37 (2021) [3] T. Ostler, *et al.*, Nature Communications 3, 666 (2012) [4] B. Rumpf and A. Newell, Phys. Rev. Lett. 87, 054102 (2001) [5] G. El and M. A. Hoefer, Physica D 333, 11-65 (2016) [6] N. Zhou Hagström *et al.*, Phys. Rev. B 106, 224424 (2022);R. Jangid et al., arXiv:2303.16131 [7] A. Rana *et al.*, Nature Nanotechnology 18, 227-232 (2023)

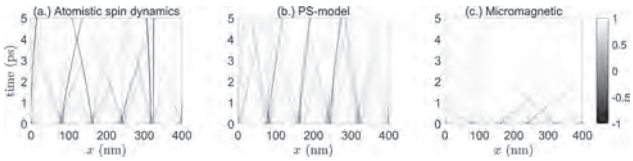

Figure 1: Comparison of soliton nucleation between ASD (a), PS-LLE (b), and micromagnetic (c).

DD-03. Effects of Inertia in Spin Dynamics of Anisotropic Ferromagnets.
A.S. Semisalova[1], M. Cherkasskii[1,2] and M. Farle[1] *1. Faculty of Physics and CENIDE, University of Duisburg-Essen, Duisburg, Germany; 2. Institute for Theoretical Solid State Physics, RWTH Aachen University, Aachen, Germany*

The interaction of magnetic moments with an external magnetic field is determined by the torque created by the effective magnetic field and the damping torque which drive the damped precession of magnetization, described by the phenomenological Landau-Lifshitz-Gilbert (LLG) equation. The LLG equation has been successfully used to explain the experimental behavior of ferro-, ferri- and antiferromagnets for decades despite neglecting the inertia of magnetization. Recently, effects of magnetization inertia in ferromagnets have been revisited and shown to give rise to an additional motion of magnetization – a THz-frequency nutation, superimposed on the regular GHz-frequency precession [1,2,3,4]. Also, magnetic nutation occurs at the level of atomic magnetic moments on ps time scales due to a non-uniform spin configuration and spatially inhomogeneous effective magnetic field induced by surface anisotropy in nanomagnets [5]. The manipulation of magnetization of thin films and nanoparticles on such short timescale broadens the functionality of ferromagnets and paves the way to new ultrafast spintronic and magnonic applications opening a prominent field of research of inertia effects [4,6]. In this contribution, I will show how to resolve effects of inertia on spin dynamics and magnetic resonances in anisotropic ferromagnets [7]. Within the inertial LLG equation [1], the ferromagnetic resonance frequency is found to be reduced in comparison to the non-inertial case for both aligned (saturated) and non-aligned (below the saturation field in hard-axis configuration) modes. We illustrate this phenomenon using model systems of single-crystalline thin films with cubic and uniaxial magnetocrystalline anisotropy and derive a resonance frequency for an arbitrary shape and magnetocrystalline anisotropy. Notably, for an out-of-plane applied magnetic field the frequency dependence of the precession resonance field of a thin film becomes non-linear, in contrast to conventionally used Kittel formula. We also find that the nutation resonance frequency increases with the magnetic anisotropy and the applied magnetic field for saturated film. However, below the saturation field, nutation resonance frequency reduces with the applied field for the hard-axis configuration similarly to the non-aligned mode of precession resonance. While these higher-order corrections due to inertia can be neglected for most of the conventional ferromagnetic resonance techniques (up to 40-60 GHz), we conclude that the magnetization inertia needs to be taken into account for an accurate evaluation of magnetic parameters such as magnetic anisotropy and g-factor, and for an interpretation of spin dynamics experiments at higher frequencies [7]. Financial support from German Research Foundation (project SE 2853/1-1 | AL 618/37-1 (Project-ID 392402498) and CRC/TRR 270 (Project-ID 405553726) is gratefully acknowledged.

[1] M.-C. Ciornei, J. M. Rubí, J.-E. Wegrowe, Phys. Rev. B 83, 020410(R) (2011) [2] D. Thonig, O. Eriksson, M. Pereiro, Sci. Rep.7, 931 (2017) [3] M. Cherkasskii, M. Farle, A. Semisalova, Phys. Rev. B 102, 184432 (2020) [4] K. Neeraj, N. Awari, S. Kovalev et al., Nat. Phys. 17, 245 (2021) [5] R. Bastardis, F. Vernay, H. Kachkachi, Phys. Rev. B 98, 165444 (2018) [6] R. Mondal, L. Rózsa, M. Farle et al., J. Magn. Magn. Mater. 579, 170830 (2023) [7] M. Cherkasskii, I. Barsukov, R. Mondal et al., Phys. Rev. B 106, 054428 (2022)

CONTRIBUTED PAPERS

DD-04. Antiferromagnetic Switching in Mn_2Au Using a Novel Laser Induced Optical Torque on Ultrafast Timescales.
J. Ross[1], P. Gavriloaea[2], T. Adamantopoulos[3], R. Otxoa[2], O. Chubykalo-Fesenko[2], R. Chantrell[1], Y. Mokrousov[3] and R. Evans[1] *1. Physics, Engineering and Technology, University of York, York, United Kingdom; 2. CSIC, Madrid, Spain; 3. Peter Grünberg Institut and Institute for Advanced Simulation, Forschungszenstrum Jülich, Jülich, Germany*

We present on the atomistic-scale simulation of a novel laser-induced spin-orbit torque for the use of precessional switching Mn_2Au domains 90 and 180 degrees. Classes of high-Neel temperature antiferromagnets which respond asymmetrically to external controls represent an important step for Terahertz level generation, manipulation, and characterisation of magnetic textures. Mn_2Au is one such material, and provides a generous platform for both high and low level model development and research. Currently, Mn_2Au domains are known to respond to the induced spin Hall effect (spin orbit torque) [1], and simulated to respond to laser excited spin-current generation (spin transfer torque) [2]. Recent *ab initio* calculations studying the broken inversion symmetry of Mn_2Au allows for a non-zero staggered spin-orbit field induced from optical laser excitation, which is separate from spin Hall and spin-current effects [3]. The driving mechanism takes advantage of the sizeable 'exchange enhancement' characteristic of antiferromagnets [4], allowing for small picosecond switching with fluences on the order of mJ/cm^2. The symmetry of these novel torques are highly dependent on the time-varying atomic magnetisation directions and laser polarisation, which results in precessional toggle switching—a large departure from traditional current-induced spin orbit torques (Fig 1,2). We calculate switching phase diagrams as functions of fluence, damping constant, and pulse duration for the two main exchange Hamiltonians present in the literature [2,4], for both 0K and finite temperature.

[1]. S. Yu. Bodnar, L. Šmejkal and I. Turek, Nat. Comms., Vol. 9, p.348 (2018) [2]. M. Weißenhofer, F. Foggetti and U. Nowak, Phys. Rev. B., Vol. 107, p.174424 (2023) [3]. F. Freimuth, S. Blügel and Y. Mokrousov, Phys. Rev. B., Vol. 103, p.174429 (2021) [4]. P. E. Roy, R. M. Otxoa and J. Wunderlich, Phys. Rev. B., Vol. 94, p.014439 (2016)

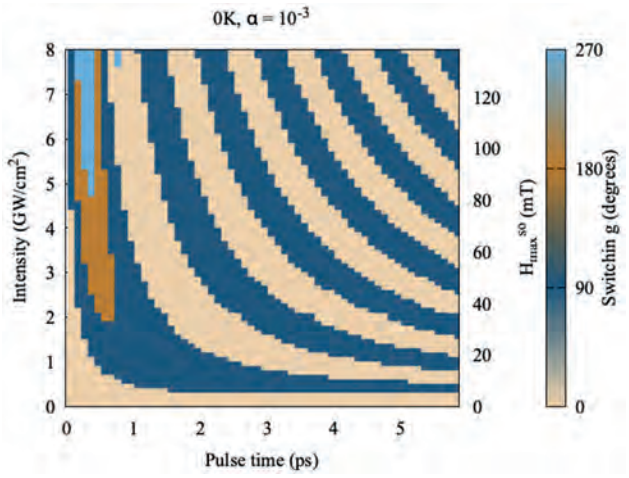

Figure 1. Switching phase diagram with varying laser intensity and pulse length with corresponding maximum spin-orbit field. Colours represent the final state of the Neel vector. Damping constant 0.001.

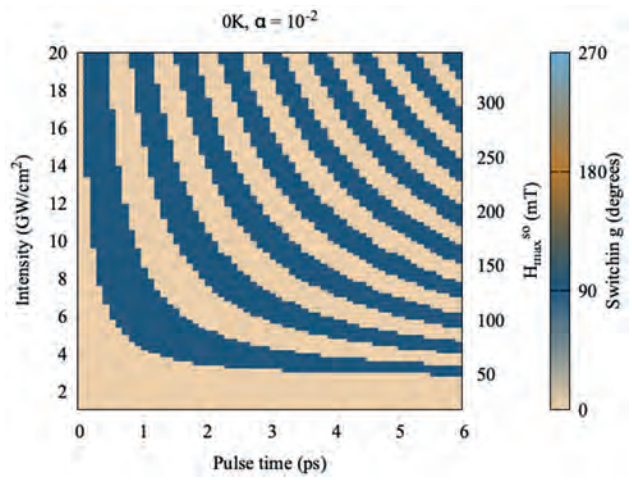

Figure 2. Switching phase diagram for damping constant 0.01. Colours represent the final state of the Neel vector. Shows a nearly linear relationship between necessary intensity and damping.

DD-05. The MagneDyn beamline at the FERMI free electron laser.
M. Malvestuto[1] 1. Elettra Sincrotrone Trieste, Trieste, Italy

The scope of this communication is to outline the main marks and performances of the MagneDyn beamline [1] at the Free Electron Laser FERMI which was designed and built to perform ultrafast magnetodynamic studies in solids. Open to users since 2019, MagneDyn operates with variable circular and linear polarized femtosecond pulses delivered by the externally laser-seeded FERMI free-electron laser (FEL). The very high degree of polarization, the high pulse-to-pulse stability, and the photon energy tunability in the 50-300 eV range allow to perform advanced time-resolved magnetic dichroic experiments at the K-edge of light elements, e.g. carbon and at the M- and N-edge of the 3d-transition-metals and rare earth elements, respectively. To this end two experimental end-stations are available. The first is equipped with an in-situ dedicated electromagnet, a cryostat, and an extreme ultraviolet (EUV) Wollaston-like polarimeter[2,3]. The second, designed for carry-in users instruments, hosts also a spectrometer for pump-probe resonant X-ray emission and inelastic spectroscopy experiments with a sub-eV energy resolution. A Kirkpatrick–Baez active optics system provides a minimum focus of ~20x20 μm² FWHM at the sample. A pump laser setup, synchronized with the FEL-laser seeding system, delivers sub-picosecond pulses with photon energies ranging from the mid-IR to near-UV for optical pump-FEL probe experiments with a minimal pump-probe jitter of few femtoseconds. The overall combination of these features renders MagneDyn a unique state-of-the-art tool for studying ultrafast magnetic phenomena in solids.

[1] Malvestuto, M. *et al.* The MagneDyn beamline at the FERMI free electron laser. *Rev Sci Instrum* 93, 115109 (2022). [2]Caretta, A. *et al.* A novel free-electron laser single-pulse Wollaston polarimeter for magneto-dynamical studies. *Struct Dynam-us* 8, 034304 (2021). [3] Laterza, S. *et al.* All-optical spin injection in silicon investigated by element-specific time-resolved Kerr effect. *Optica* 9, 1333 (2022).

DD-06. Experimental evidence for ultrashort-lived spin polarons in EuSe.
S.C. van Kooten[1], G. Springholz[2] and A.B. Henriques[1] 1. Instituto de Física, Universidade de São Paulo, São Paulo, Brazil; 2. Institute of Semiconductor and Solid State Physics, Johannes Kepler Universität Linz, Linz, Austria

Recently, we demonstrated ultrafast optical magnetization through the photo-excitation of huge spin polarons (SPs) in magnetic semiconductors, whose individual magnetic moment can reach many thousands of Bohr magnetons [1,2]. However, the exact nature of the electronic states occupied by electrons forming SPs is not completely understood. Here, we investigate the selection rules for SP recombination using our recently developed method to investigate the temporal evolution of SPs [3], based on time-resolved Faraday rotation. We find that, in EuSe, light induces not only previously observed long-lived SPs [1], with a lifetime of around a microsecond, but also an even larger concentration of short-lived SPs, with a lifetime of a few hundred picoseconds, as demonstrated by the time-dependent SP density in Fig. 1. To explain this stark, four order-of-magnitude difference in lifetime, we consider that the lifetime of an electric dipole-allowed, spin-allowed, electronic transition with emission of a photon of energy $h\nu$ is in the order of [4] $\tau \sim h/\alpha^3 h\nu$ where $\alpha = 1/137$ is the fine structure constant and h is Planck's constant. For $h\nu = 2$ eV, corresponding to the EuSe bandgap, this gives $\tau \sim 1$ ns, about the same lifetime as the short-lived SPs from Fig. 1, indicating that the short-lived SP decays through an electric dipole-allowed, spin-allowed transition. Therefore, electron-hole recombination of short-lived SPs must occur before the spin of the photoexcited electron relaxes and minimizes its Zeeman energy in the effective exchange field. Our measurements also show that the lifetime of short-lived SPs is temperature-independent, providing additional support for this conclusion. Conversely, when the photoexcited electron relaxes its spin before recombining, a spin-flip becomes necessary for electron-hole recombination. The exchange field exerted by the atoms inside the SP further impedes the occurrence of such a spin-flip, leading to the much larger recombination time for long-lived SPs.

[1] A. B. Henriques, X. Gratens, P. A. Usachev et al., Phys. Rev. Lett., Vol. 120, p. 217203 (2018). [2] X. Gratens, Y. Ou, J. S. Moodera et al., Appl. Phys. Lett., Vol. 116, p. 152402 (2020). [3] S. C. P. van Kooten, G. Sprinholz, and A. B. Henriques, Phys. Rev. B, Vol. 105, p. 224427 (2022). [4] A. S. Davydov, Quantum Mechanics (Pergamon Press, Oxford, 1965), p.300.

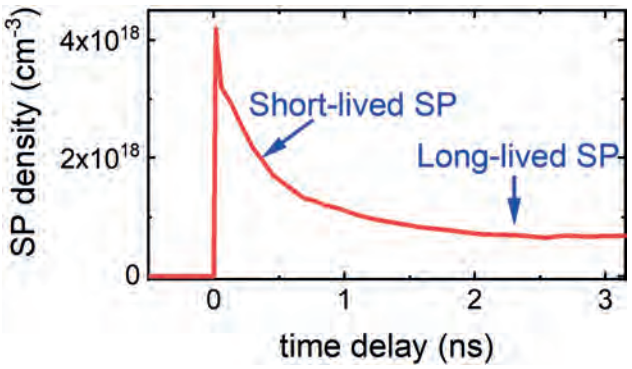

Fig. 1, temporal evolution of the SP density after excitation by a pump pulse. Short-lived SPs decay rapidly within a nanosecond, while the density of long-lived SPs appears as a constant level on the timescale considered.

DD-07. Vortex Motion Mediated Back-and-Forth Magnetization Switching in Ferrimagnets.
X. Zhang[1], Z. Xu[1] and *Z. Zhu[1,2] 1. ShanghaiTech University, Shanghai, China; 2. Shanghai Engineering Research Center of Energy Efficient and Custom AI IC, Shanghai, China*

Ferrimagnet (FiM) attracts research interests due to its highly tunable properties [1]. In this work, we show that there is additional tunability provided by the spatial nonuniform magnetization dynamics in FiM. We have developed an atomistic model to study the spin transfer torque (STT) induced magnetization switching of the FiM ($FeCo_{1-x}Gd_x$), where the Gd atoms are randomly distributed [2, 3]. In the sample with x = 0.15, the switching process with $J_c = -1\times10^{11}$ A/m² and $J_c = -0.6\times10^{11}$A/m² are shown in Fig. 1(a) and 1(b), respectively. We find that the switching starts with the formation of the first switched region and then propagates through the domain wall (DW) motion. This DW induced switching behavior leads to a more interesting phenomenon when two DWs meet each other, i.e., a back and forth magnetization switching as shown in region 1, where its color alternates between red and

blue between t = 40 to 70 ps. In addition, different J_c results in different positions of this region, e.g., region 2 appears under a smaller J_c. These results can also be visualized in the atomic magnetization dynamics which is shown in Fig. 2(a). A spatial resolved magnetization profile in the x-y plane is shown in Fig. 2(b) with t = 55 ps and $J_c = -1\times10^{11}$ A/m^2. It is found that the initialization and motion of the vortex which is highlighted in yellow are responsible for the back and forth switching. To understand these results, we first check the atom distribution since its spatially nonuniform nature coincides with the nonuniform switching process. We find that the switching occurs in the FeCo-rich region which can be understood by analyzing STT and net magnetization. This initially switched regions then affect the DW shape and the vortex dynamics. Our work shows that the FiM under spin torque exhibits rich magnetization dynamics, which will stimulate the development of FiM-based multifunctional device.

[1] Zhu, Zhifeng, et al. *Phys. Rev. B* 97, 184410 (2018). [2] Zhu, Zhifeng, et al. *Phys. Rev. Appl.* 13, 034040 (2020). [3] Zhang, Xue, et al. *Phys. Rev. B* 106, 184419 (2022).

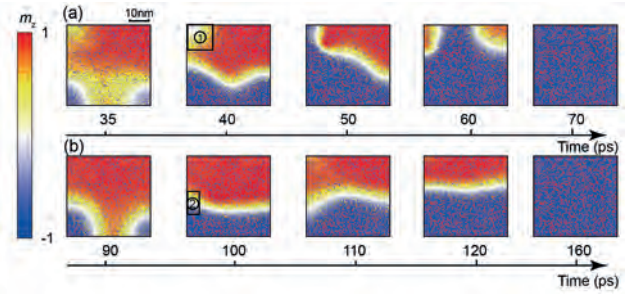

Fig. 1 (a) Snapshot images of the sample with x = 0.15 under (a) $J_c = -1\times10^{11}$ A/m^2 and (b) $J_c = -0.6\times10^{11}$ A/m^2, respectively.

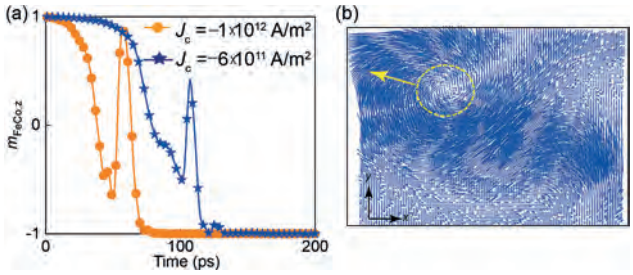

Fig. 2 (a) Atomic magnetization dynamics in region 1 (orange circle) and region 2 (blue star). (b) Illustration of the magnetic vortex in region 1. The yellow arrow denotes its path of motion.

Session DE
SPIN HALL AND RELATED EFFECTS II

Shun Kanai, Chair
Tohoku University, Sendai, Japan

INVITED PAPERS

DE-01. Giant Efficiency and Anisotropy of Spin Hall Effect in Bismuth. *R. Ohshima[1,2] 1. Kyoto University, Kyoto, Japan; 2. CSRN Kyoto, Kyoto, Japan*

Spin-orbit interaction (SOI) plays a major role in condensed matter physics and has attracted attention for spin-charge interconversion, the topological surface state with spin-momentum locking, and so on. An index of the spin conversion efficiency (spin Hall angle, θ_{SH}) is considered to be dependent on the magnitude of the SOI because the spin Hall effect, a charge-to-spin conversion effect is attributed to the SOI. Indeed, it has been reported that the magnitude of θ_{SH} of heavy elements such as Pt, Ta, and W was very large ($\theta_{SH} > 0.1$). Therefore, bismuth (Bi) has been intensively studied because of its largest SOI among the nonradioactive elements. However, only negligibly small spin Hall angle has been reported in Bi despite its large SOI, which is one of the biggest mysteries in spintronics and spin-orbitronics for the decade. Here, we demonstrate the large θ_{SH} (0.17-0.27) in Bi by introducing the rhombohedral (110) structure, whereas negligibly small θ_{SH} in rhombohedral (111) Bi which has been usually used in the previous reports [1]. Spin-torque ferromagnetic resonance and harmonic Hall measurements were applied to estimate the θ_{SH} of Bi. The self-induced spin-orbit torque in an adjacent ferromagnet of Bi was considered to increase accuracy of the estimation [2]. The large anisotropy of θ_{SH} is attributable to the large anisotropy of the effective *g*-factor (spin magnetic moment) in Bi due to its anisotropic crystal structure and the crystalline SOI. Considering the electron evacuation via the quantum size effect and anisotropic effective *g*-factor enables us to explain the quite small θ_{SH} in rhombohedral (111) Bi in the previous reports. This study was in collaboration with Yuki Fuseya from University of Electro-Communications, Shoya Sakamoto, Masanobu Shiga, and Shinji Miwa from The University of Tokyo, Naoki Fukumoto, Motomi Aoki, Masayuki Matsushima, Ei Shigematsu, Teruya Shinjo, Yuichiro Ando, and Masashi Shiraishi from Kyoto University.

[1] N. Fukumoto, R. Ohshima *et al*., Proc. Natl. Acad. Sci. USA (PNAS) 120, e2215030120 (2023). [2] M. Aoki, R. Ohshima *et al*., Phys. Rev. B 106, 174418 (2022).

DE-02. Ultrastrong Magnon-Magnon Coupling and Chiral Symmetry Breaking in a 3D Magnonic Metamaterial. *J.C. Gartside*[1], T. Dion[2], K.D. Stenning[3], A. Vanstone[1], H.H. Holder[1], R. Sultana[4], M. Kaffash[4], G. Alatteili[5], V. Martinez[5], T. Kimura[2], B. Jungfleisch[4], E. Iacocca[5], W.R. Branford[1] and H. Kurebayashi[3] *1. Physics, Imperial College London, London, United Kingdom; 2. Solid State Physics Laboratory, Kyushu University, Fukuoka, Japan; 3. University College London, London, United Kingdom; 4. Physics & Astronomy, University of Delaware, Newark, DE, United States; 5. Physics, University of Colorado, Colorado Springs, Colorado Springs, CO, United States*

Strongly-interacting nanomagnetic arrays are ideal systems for exploring the frontiers of magnonic control. They provide functional reconfigurable platforms and attractive technological solutions across storage, GHz communications and neuromorphic computing. Typically, these systems are primarily constrained by their range of accessible states and the strength of magnon coupling phenomena. Increasingly, magnetic nanostructures have explored the benefits of expanding into three dimensions. This has broadened the horizons of magnetic microstate spaces and functional behaviours, but precise control of 3D states and dynamics remains challenging. Here, we introduce a 3D magnonic metamaterial, compatible with widely-available fabrication and characterisation techniques. By combining independently-programmable artificial spin-systems strongly coupled in the z-plane, we construct a reconfigurable 3D metamaterial with an exceptionally high 16N microstate space and intense static and dynamic magnetic coupling. The system exhibits a broad range of emergent phenomena including ultrastrong magnon-magnon coupling with normalised coupling rates of $\omega/\gamma = 0.57$ and magnon-magnon cooperativity up to C = 126.4, GHz mode shifts in zero applied field and chirality-selective magneto-toroidal microstate programming and corresponding magnonic spectral control.

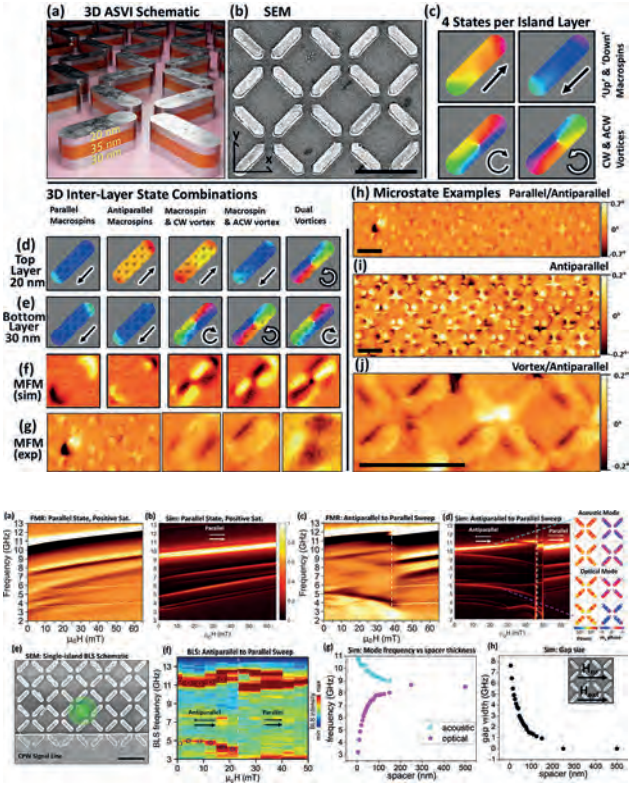

CONTRIBUTED PAPERS

DE-03. Spin/orbital Hall and Nernst effects in bulk, interface, and impurity-doped systems: First-principles study. *K. Nawa*[1,2], Y. Tsujide[1], S.H. Rhim[3], M. Hayashi[4] and K. Nakamura[1] *1. Mie University, Tsu, Japan; 2. National Institute for Materials Science, Tsukuba, Japan; 3. The University of Ulsan, Ulsan, The Republic of Korea; 4. The University of Tokyo, Bunkyo-ku, Japan*

Spin Hall effect is known as a phenomenon to generate pure spin current and has been widely studied in the last decades. Recent interests in magnetic materials research extends to an orbital current, which is another degree of freedom in solid states. Pioneering work from theory by Salemi *et al*. [1] provided an insight into electrically-driven spin and orbital Hall effects and thermally-driven spin and orbital Nernst effects in monocrystalline metals, where an appearance of the largest contribution of these effects can be interpreted qualitatively from the number of *d* electrons in metals. Here, we aim to investigate modulations of spin/orbital currents by structural changes from first-principles all-electron full-potential linearized augmented plane wave method [2]. Monoatomic single bulk crystal of 40 elements in the periodic table, bilayer interfaces, and impurity-doped systems are considered. The intrinsic spin/orbital Hall conductivities (SHC, OHC) are evaluated from Kubo formula and the spin/orbital Nernst conductivities (SNC, ONC) are from Mott formula. As given in Table I, in bulk Pt the SHC and OHC are obtained as 1928 and 3757 $\Omega^{-1}cm^{-1}$, where the value of OHC is greater than that of SHC, as is consistent with previous work [1]. For a $Co_{(1)}/Pt_{(9)}$ bilayer (number of atomic layers is given in parenesis in monolayer unit), the SHC becomes small compared to that in bulk Pt, but no change in OHC, which may indicate that the OHC is less affected by symmetry breaking at the interface. Similar to the SHC and OHC, the ONC is larger than the SNC in bulk Pt and the change of ONC in $Co_{(1)}/Pt_{(9)}$ is negligibly smaller than that of SNC. When the Pt is doped as an impurity to the Cu ($Cu_{1-x}Pt_x$, $x \sim 3\%$), the OHC increases from 31 $\Omega^{-1}cm^{-1}$ (Cu) to 275 $\Omega^{-1}cm^{-1}$ ($Cu_{0.97}Pt_{0.03}$), which is twice larger than the value estimated from a linear relationship of composition between Cu and Pt in bulk. Similar enhancement is confirmed in SNC and ONC for $Cu_{0.97}Pt_{0.03}$, where the SNC (ONC) is 450% (300%) over the value of liner relationship of Cu and Pt limits, whereas only the SHC follows linearly. The physical origin of effects of structural changes on SHC, OHC, SNC, and ONC will be discussed.

[1] L. Salemi, *et al.*, Phys. Rev. Mater. 6, 095001 (2022). [2] K. Nakamura, *et al.*, Phys. Rev. B 67, 014420 (2003).

	SHC [$\Omega^{-1}cm^{-1}$]	OHC [$\Omega^{-1}cm^{-1}$]	SNC [A/(K m)]	ONC [A/(K m)]
Bulk Pt	1928	3757	–0.83	3.73
$Co_{(1)}/Pt_{(6)}$	1510	3701	–0.64	3.31
Bulk Cu	90	31	0.04	–0.28
$Cu_{0.97}Pt_{0.03}$	180	275	0.08	–0.46

Calculated SHC, OHC, SNC, and ONC.

DE-04. Spin Superfluidity: Geometrically Enhanced Efficiencies and the Nonlocal Manifestation of Spin Hall Magnetoresistance in Nonlocal Devices. *M.D. Kitcher*[1] and G. Beach[1] *1. Materials Science and Engineering, Massachusetts Institute of Technology, Cambridge, MA, United States*

Spin superfluidity (SSF) has been theorized to be supported by easy-plane magnetic insulators [1]. Despite the sub-exponential decay of SSF efficiencies with transport distance, claims of SSF based on such experiments have been plagued by competing explanations such as unwanted heating effects [2]. Many seminal studies focused on devices with a sandwich geometry, which enables the injection and detection of spin polarized along the hard axis of conventional easy-plane films [3]; however, the required sidewall deposition is challenging. Recently, SSF studies on lateral nonlocal devices have noted that additional geometric factors should influence their spin transfer efficiency, but these were limited to the simplest scenarios [4]. Finally, while SSF has been predicted to engender a nonlocal magnetoresistance, questions remain regarding its connection to the spin Hall magnetoresistance (SMR) or the dependence of this nonlocal resistance on the dimensional factors at play in the lateral geometry [5]. In this work, we present our analysis of the spin and current transfer efficiencies of SSF devices in a lateral geometry for the general case. Using the Landau-Lifshitz-Gilbert formalism and magneto-circuit theory, we show that both the spin and current transfer efficiencies enabled by SSF are dependent on the ratio of width of the injector relative to the length of the uncovered transport channel, as well as ratio of the width of the injector to that of the detector; consequently, the transfer efficiencies can remain at the theoretical maximum for arbitrary long channels by making injectors proportionally wide. Moreover, simultaneously increasing the width of the injector and the spin-mixing conductance at the detector–film interface has an unbounded effect on the efficiencies. These unique geometric dependencies allow for an unambiguous observation of SSF. Furthermore, we find that the corresponding nonlocal resistance is completely analogous to the local SMR as described by the spin drift-diffusion model; the current transfer efficiency is proportional to the geometric mean of the SMRs at the injector and detector. Thus, probing SSF in lateral devices offers a new way to elucidate local and nonlocal SMR phenomena.

[1] E. B. Sonin, Sov. Phys. JETP 47, 1091 (1978); Adv. Phys. 59, 181 (2010). [2] R. Lebrun et al., Nature 561, 222 (2018). [3] S. Takei and Y. Tserkovnyak, Phys. Rev. Lett. 112, 227201 (2014). [4] H. Skarsvåg, C. Holmqvist, and A. Brataas, Phys. Rev. Lett. 115, 237201 (2015). [5] S. Takei and Y. Tserkovnyak, Phys. Rev. Lett. 115, 156604 (2015).

DE-05. First-principles analysis of transverse spin diffusion in a disordered Pt film. *K. Belashchenko*[1], G.G. Baez-Flores[1], W. Fang[1], A.A. Kovalev[1], M.D. Stiles[2] and P.M. Haney[2] *1. Department of Physics and Astronomy, University of Nebraska-Lincoln, Lincoln, NE, United States; 2. Physical Measurement Laboratory, National Institute of Standards and Technology, Gaithersburg, MD, United States*

Spin current and spin accumulation in a free-standing disordered Pt film carrying in-plane charge current are studied using the first-principles nonequilibrium Green's function approach. Disorder is treated within the Anderson model in a supercell embedded between the leads. The spin-Hall conductivity extracted from the data is insensitive to disorder strength, and its magnitude and energy dependence agree with the known intrinsic contribution. The results are compared with the spin-diffusion model, revealing qualitative differences. The effective spin-diffusion length extracted from the spin accumulation profile is about 1.3 nm (which is similar to or even shorter than the mean-free path), insensitive to disorder strength, and a few times shorter than the bulk spin-diffusion length for longitudinal transport extracted from separate Landauer-Buttiker calculations. Furthermore, the profiles we find for the spin accumulation and the spin current are not generally consistent with the semiclassical diffusion equations. These discrepancies indicate violations of the standard semiclassical description of spin transport arising from the intrinsic spin Hall effect in thin layers, which have implications for the understanding of spin-orbit torques. We also find that orbital accumulation only penetrates into the bulk of Pt in the presence of spin-orbit coupling and is otherwise a purely surface effect.

DE-06. Influence of non-uniform magnetization perturbation on spin-orbit torque measurements. *R. Greening*[1] and X. Fan[1] *1. Physics, University of Denver, Denver, CO, United States*

Measurements of spin–orbit torques in a ferromagnetic/nonmagnetic multilayer are typically based on an assumption that the entire ferromagnetic layer uniformly responds to the spin–orbit torque. This assumption breaks down when the thickness of the ferromagnetic layer is comparable to the dynamic exchange coupling length, which can be as short as a few nanometers in certain measurement geometries. If the ferromagnets thickness is comparable

to its dynamic exchange coupling length, the magnetization tilting due to the spin–orbit torque is not necessarily uniform across the film thickness [1]. On the other hand, the calibration procedures in these experiments are often conducted by applying a magnetic field that rotates the magnetization uniformly. It is therefore important to take into consideration the nonuniform magnetization perturbation when quantifying the magnitude of the spin–orbit torque. The nonuniform magnetization perturbation coupled with a nonuniform contribution from each magnetic sublayer due to the magnetoresistance or the Kerr effect may impact the accuracy in the extrapolation of spin–orbit torque, particularly if a thick ferromagnetic layer is used. In this presentation, we will present the results of numerical models to investigate such an impact in three frequently used experimental techniques: the magneto-optic-Kerr-effect (MOKE) method [2], the second-harmonic anomalous hall (AH) method [3], and the spin torque ferromagnetic resonance (ST-FMR) method [4]. We show that the second-harmonic and magneto-optic-Kerr-effect methods are prone to be influenced by the nonuniform magnetization reorientation, while the spin torque ferromagnetic resonance method is remarkably less impacted due to enhanced susceptibility at resonance [5].

[1] W. Wang, T. Wang, and V.P. Amin, Nature Nanotechnology. Vol. 14, p.819-824 (2019) [2] X. Fan, H. Celik, and J. Wu, Nature Communications. Vol.5, (2014) [3] C. O. Avci, K. Garello, and M. Gabureac, Phys. Rev. B. Vol. 90, p.224427 (2014) [4] L. Liu, T. Moriyama, and D. Ralph, Phys. Rev. Letters. Vol. 106, P.036601 (2011) [5] R. Greening and X. Fan, J. Magn. Magn. Materials. Vol. 563, p.169877 (2022)

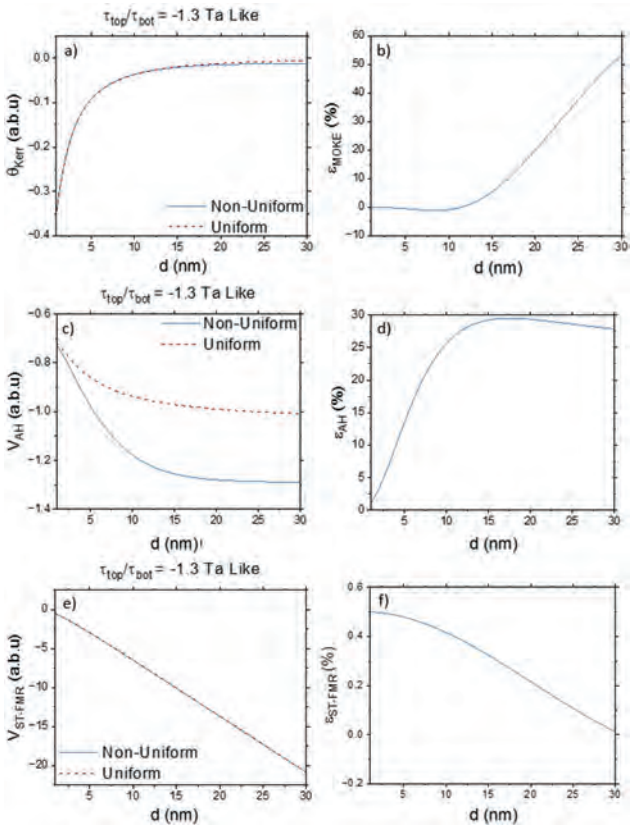

Fig 1 simulated thickness dependence response for three different experiments and the precent difference between 'uniform' and 'non-uniform' magnetization distributions for: MOKE (a,b), AH (c,d) and ST-FMR (e,f).

	M_S (T)	α	A_{exc} (J · m)	$\omega_{off\ res.}$ (2πGHz)	λ_{MOKE} (nm)	$\lambda_{2nd\ Harm.}$ (nm)	λ_{ST-FMR} (nm)
Fe	2.24	0.02	1.9×10^{-11}	8	3.1	2.6	36
Ni	0.54	0.04	8.3×10^{-12}	8	8.4	5.0	31
Co	2.00	0.02	2.4×10^{-11}	8	3.9	3.2	48

Material dependent exchange lengths for various ferromagnets under three different experiments.

DE-07. Zero-field polarity-reversible Josephson supercurrent diodes enabled by a proximity-magnetized Pt barrier. *K. Jeon*[1,2], J. Kim[2], J. Yoon[2], J. Jeon[2], H. Han[2], A. Cottet[3], T. Kontos[3] and S. Parkin[2] *1. Chung-Ang University (CAU), Seoul, The Republic of Korea; 2. Max Planck Institute of Microstructure Physics, Halle/Saale, Germany; 3. Laboratoire de Physique de l'Ecole Normale Supérieur, Paris, France*

Simultaneous breaking of inversion and time-reversal symmetries in a conductor yields a non-reciprocal electronic transport[1,2,3], known as the diode or rectification effect, that is, low (ideally zero) conductance in one direction and high (ideally infinite) conductance in the other. So far, most of the diode effects observed in non-centrosymmetric polar/superconducting conductors[4,5,6,7] and Josephson junctions[8,9,10] require external magnetic fields to break the time-reversal symmetry. Here we report zero-field polarity-switchable Josephson supercurrent diodes[11], in which a proximity-magnetized Pt layer by ferrimagnetic insulating $Y_3Fe_5O_{12}$ serves as the Rashba(-type) Josephson barrier. The zero-field diode efficiency of our proximity-engineered device reaches up to ±35% at 2 K, with a clear-square root dependence on temperature. Measuring in-plane field-strength/angle dependences and comparing with Cu-inserted control junctions, we demonstrate that exchange spin-splitting and Rashba(-type) spin-orbit coupling at the Pt/$Y_3Fe_5O_{12}$ interface are key for the zero-field giant rectification efficiency[11]. Our achievement advances the development of field-free absolute Josephson diodes.

[1] *Phys. Rev.* 37, 405 (1931), [2] *J. Phys. Soc. Jpn.* 12, 570 (1957), [3] *Phys. Rev. Lett.* 87, 236602 (2001), [4] *Nat. Commun.* 9, 3740 (2018), [5] *Sci. Adv.* 3, e1602390 (2017), [6] *Nature* 584, 373 (2020), [7] *Nat. Commun.* 13, 4266 (2022), [8] *Nat. Nanotech.* 17, 39 (2021), [9] *J. Phys.: Condens. Matter* 34 154005 (2022), [10] *Nat. Phys.* 18, 1228 (2022), [11] *Nat. Mater.* 21, 1008 (2022).

DE-08. Orbital torque in Cr/CoFeB/MgO stack compatible with SOT-MRAM application. *S. Chiba*[1,2], Y. Marui[1], H. Ohno[1,3] and S. Fukami[1,3] *1. Laboratory for Nanoelectronics and Spintronics, RIEC, Tohoku Univ., Sendai, Japan; 2. Graduate School of Engineering, Tohoku Univ., Sendai, Japan; 3. CSIS, Tohoku Univ., Sendai, Japan*

Spin-orbit torque (SOT) in nonmagnet (NM)/ferromagnet (FM) heterostructures is actively investigated for various applications such as SOT-magnetoresistive random access memory (MRAM). While most of the studies so far have focused on SOT induced by the spin Hall effect (SHE) in heavy metals with a large spin Hall conductivity (SHC) such as W and SOT-MRAM was demonstrated with a W/CoFeB/MgO stack [1], there is a quest for materials with even larger torque efficiency and lower resistance. Recently, orbital Hall effect (OHE) was theoretically predicted as an alternative mechanism generating the current-induce torque [2]. Numerical calculation suggests that Cr and V, which are expected to meet the major requirements of SOT-MRAM applications when using as a replacement of W, has one order of magnitude larger orbital Hall conductivity than SHC in heavy metals [3]. However, in spite of increasing attention on orbital torque [4], systematic studies in stacks compatible with SOT-MRAM applications are missing. In this work, we evaluate the orbital torque in a Cr/CoFeB/MgO stack as a function of Cr and CoFeB thicknesses and discuss the prospect and challenge for SOT-MRAM applications. Figure 1 shows the stack

structure we studied. t_{CoFeB} is varied from 2 to 14 nm and t_{Cr} from 2 to 20 nm. Effective spin orbital Hall conductivity (s_{xy}) is measured using a harmonic Hall technique. Figure 2 shows the obtained effective spin orbital Hall conductivity (s_{xy}) as a function of t_{Cr} and t_{CoFeB}. s_{xy} increases with t_{Cr} and t_{CoFeB}, and shows sign change from minus to plus with t_{Cr}. According to the previous studies, the sign of s_{xy} should be minus (plus) when the torque caused by SHE (OHE) is dominant [3], indicating that OHE is dominant for our stacks with thicker Cr and CoFeB. Also, s_{xy} reaches 2300 ± 200 $W^{-1}cm^{-1}$ (effective spin Hall angle ~ 0.1) at CoFeB(14 nm)/Cr(17.5 nm), which is comparable to or higher than heavy metals such as Pt and W. This study reveals that the orbital torque possesses a potential for SOT-MRAM applications but has some challenges such as reduction of typical thickness where a large orbital torque is activated. This work is partly supported by MEXT X-NICS JPJ011438 and JSPS Kakenhi 19H05622.

[1] M. Natsui *et al*., IEEE J. Solid-State Circuits 56, 1116 (2021). [2] D. Go *et al*., Phys. Rev. Research 2, 013177 (2020). [3] D. Jo *et al*., Phys. Rev. B 98, 214405 (2018). [4] S. Lee *et al*., Commun. Phys. 4, 234 (2021).

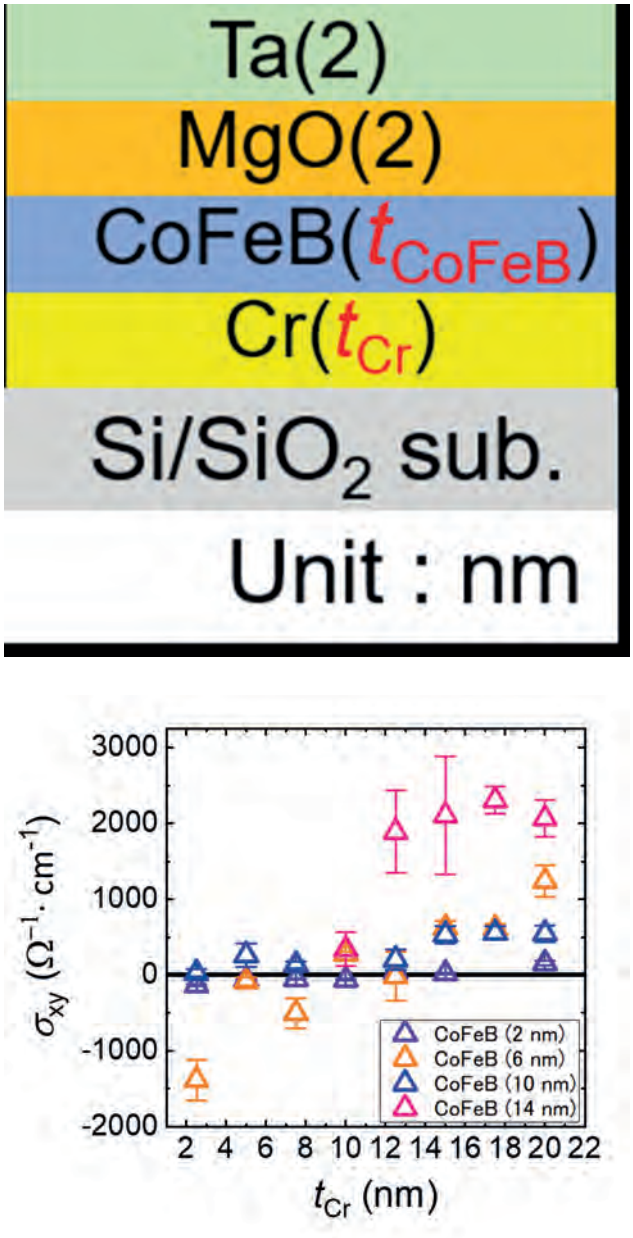

DE-10. Artificial helical spin structures in AFM/FM/AFM multilayers set by SOT control of AFM. *W. Choi*[1], S. Yoon[1], J. Ha[1], H. Kim[2] and J. Hong[1] *1. Physics & Chemistry, Daegu Gyeongbuk Institute of Science & Technology, Daegu, The Republic of Korea; 2. Korea Research Institute of Standards and Science, Daejeon, The Republic of Korea*

Antiferromagnetic (AFM) material is known to exhibit zero net magnetization and low magnetic susceptibility due to the compensating alignments of magnetic moments, for which applications of AFM have been limited. However, it is notable that AFM thin film can effectively pin the magnetic moments of the neighboring ferromagnet (FM) layer in the AFM/FM bilayer structure giving rise to the well-known exchange bias effect. Recent advances in spintronics to establish exchange bias in the heavy metal (HM)/AFM/FM systems by SOT of spin Hall current bring a prospect of finer control of exchange coupling in a spatially localized area. With these, multiple exchange couplings with independently controlled pinning directions can be implemented as desired in the patterned microscopic device structure, resulting in the modified non-collinear spin structures. In the present work, we demonstrate that double exchange bias pinning at two different directions can indeed be applied to a single FM layer to induce modified magnetic behaviors as the non-collinear helical spin structure is formed in the FM layer. Multilayers of HM/AFM1/FM/AFM2 were deposited, where the exchange couplings at the interface between FM and AFM1 was controlled by spin Hall current from HM layer at room temperature. While the spins at the other interface with AFM2 is pinned in a fixed direction. Magnetic hysteresis loops of the FM layer were measured as the spins in AFM2 was controlled, and the change in the magnetic hysteresis could be clearly recognized. Chirality of the helical structure could also be set in either clockwise or counterclockwise directions, and it is reflected in the measurement of in-plane magnetic domain motion as it propagates along the linearly patterned layer, where the domain wall is tilted with respect to the patterned line direction depending on the chirality of the helical spins. Magnetic domains wall showed opposite tilt directions for clockwise and counterclockwise chiral orientations. Unique magnetic behaviors of artificial helimagnetic structure are expected to be useful for the operation mechanisms of spintronic devices.

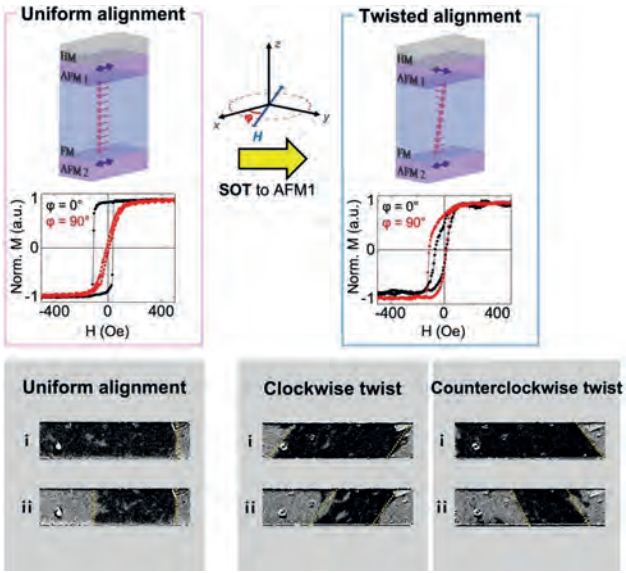

Fig. 1 Spin structures and their corresponding magnetic behaviors.

DE-11. Measurement of the Orbital Hall Effect in Cu and Al by spin-torque FMR and optical FMR. *Y. Ben Tal*[1], A. Rothschild[1], N. Am-Shalom[1], N. Bernstein[1], B.J. Assouline[1] and A. Capua[1] *1. Applied Physics, The Hebrew University in Jerusalem, Jerusalem, Israel*

In the orbital Hall effect (OHE)[1,2], a charge current is converted into an orbital current in a fashion that is reminiscent of the spin Hall effect. It emerges from momentum space orbital texture when current is passed through the crystal and does not require spin orbit coupling, making it especially attractive for low power applications. The OHE was theoretically predicted to be very significant and ubiquitous in a variety of technologically relevant materials[3], but its nature remained elusive for a long time. Recently, we have reportedon the OHE in Cu and Al[4] which was demonstrated using the Ferris ferromagnetic resonance (FMR) technique[5]. In this work, we compare the measurements of the OHE in Cu and Al using an optically probed spin torque FMR (OSTFMR) and FMR (OFMR) using a Pt orbit to spin conversion layer. We find an effective spin Hall angle of 0.16 and –0.065 in Cu/Pt and Al/Pt, respectively, while the two techniques agree within 5%. A comparison is made to the Ferris FMR technique. Al and Cu are two key metals in the semiconductor industry and have been traditionally used for interconnects. Our results mark another step toward utilizing the OHE in practical applications.

1 S. Zhang, PRL 94, 066602 (2005). 2 A. Bernevig, PRL 95, 066601 (2005). 3 D. Go PRL, 121, 086602 (2018) 4 A. Rothschild, PRB 106, 144415 (2022) 5 A. Rothschild, AIP Advances, 13, 065319 (2023)

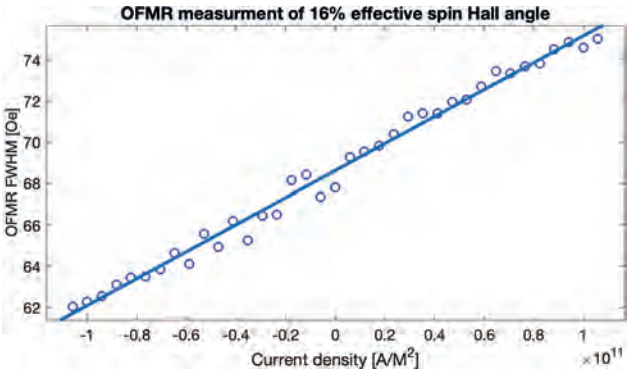

Session DF
FUNDAMENTAL PROPERTIES V: MAGNETIC PHASES IN TOPOLOGICAL MATERIALS AND COMPLEX ALLOYS

Xianzhe Chen, Chair
University of California, Berkeley, Berkeley, CA, United States

INVITED PAPERS

DF-01. Gate-tunable anomalous Hall effect in a 3D topological insulator/2D magnet van der Waals heterostructure. *R. Jain*[1], M. Roddy[1], V. Gupta[1], B. Huang[1], Y. Ren[2], X. Zhang[1], H. Alnaser[3], A. Vashist[3], D. Xiao[2], D. Muller[1], V. Deshpande[3], T. Sparks[3] and D.C. Ralph[1] *1. Cornell University, Ithaca, NY, United States; 2. University of Washington, Seattle, WA, United States; 3. University of Utah, Salt Lake city, UT, United States*

Interactions between three-dimension topological insulators (TIs) and magnets can induce exotic topological phases like the quantum anomalous Hall [1] or axion insulator states [2] and might be used to harness the properties of topological-insulator surface states in spintronic devices. Coupling of a topological-insulator surface state to a magnetization that is perpendicular to the surface is predicted to open an exchange gap at the Dirac point, thereby inducing Berry curvature in the electronic states near this gap. If the electron chemical potential is swept through the states near the exchange gap, this Berry curvature should cause an anomalous Hall effect (AHE) peak when the chemical potential lies in the gap. For an ideal scenario at low temperatures, the peak value of the Hall conductivity for an exchange gap on just one surface of a TI flake should reach a quantized value of e^2/h. This work reports the first experimental demonstration of strong and controllable interaction between the topological surface states (TSS) of a 3D topological insulator ($BiSbTeSe_2$) and an adjacent insulating 2D magnet layer ($Cr_2Ge_2Te_6$) in an all van-der Waals (vdW) heterostructure. Experimental demonstrations of such interactions between topological insulators and magnets are essential for identifying suitable material platforms that can realize and control topological magneto-electric effects, which are of great interest in developing next-generation electronic devices. For the first time in any proximity-coupled topological insulator (TI)/magnet bilayer structure, this work provides the experimental observation of an abrupt hysteretic anomalous Hall effect whose amplitude can be continuously tuned via gate voltage, with a strong peak near the Dirac point of TSS. This behavior is the signature of the anomalous Hall effect, predicted to originate from the Berry curvature associated with an exchange gap induced by the interaction between the topological surface state and an insulating magnet. This interaction can also lead to changes in the magnetic properties of the ferromagnet in proximity to a topological insulator. We observe gate-tunable magnetic anisotropy of the 2D magnet in proximity to TI, which shows a peak near the Dirac point. This is consistent with predictions of changes in magnetic anisotropy due to the opening of an exchange gap in TI/magnet bilayer structures. Our results provide a pathway to realize proximity effects in clean vdW heterostructures of topological insulators and 2D magnets, which could pave the way for novel magnetoelectric phenomena.

[1] R. Yu, W. Zhang, H.-J. Zhang, S.-C. Zhang et al. "Quantized anomalous Hall effect in magnetic topological insulators," Science, vol. 329, no. 5987, pp. 61–64, 2010 [2] M. Mogi, M. Kawamura, R. Yoshimi et al. "A magnetic heterostructure of topological insulators as a candidate for an axion insulator," Nature Materials, vol. 16, no. 5, pp. 516–521, 2017 [3] Vishakha Gupta*, Rakshit Jain* et al. Nano letters 2022, 22, 17, 7166–7172

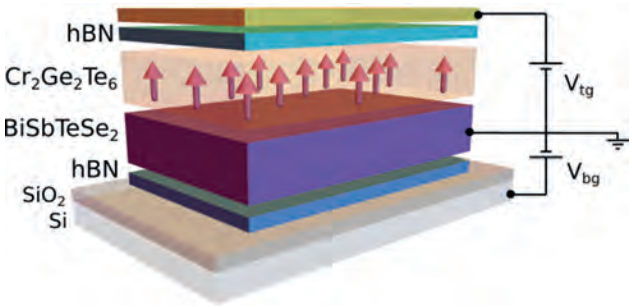

Fig. 1. Schematic of the device geometry and electrostatic gating geometry. TI and 2D magnet flakes with few-layer thickness are double-encapsulated between hBN layers on a Si/SiO_2 substrate

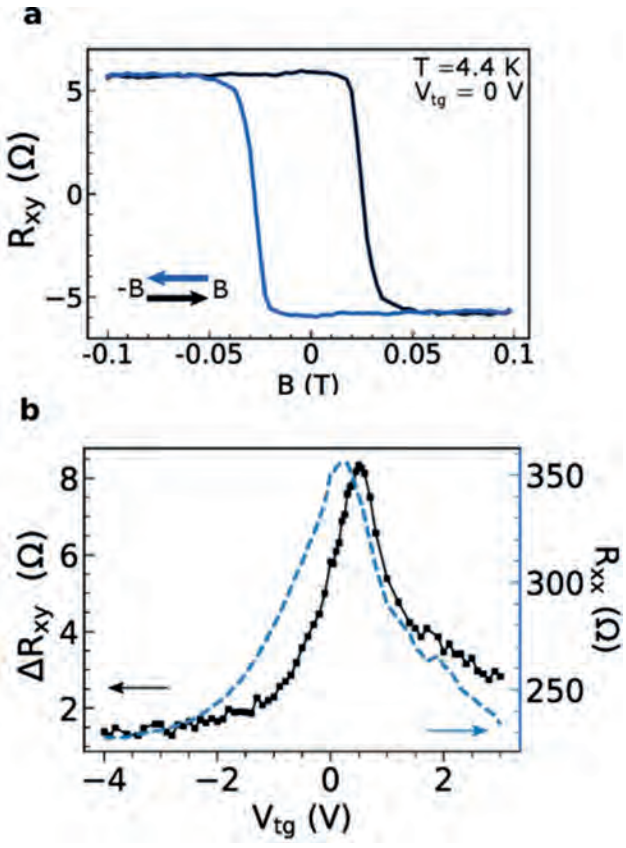

Fig. 2. (a) AHE contribution to Rxy at Vtg = 0 after subtraction of linear background. (b) Size of AHE signal (black solid line) ΔRxy as a function of top-gate voltage. The trend matches closely with the observed top-gate dependence of Rxx (blue dashed line) measured at zero magnetic field.

DF-02. Terahertz spintronic emission from 2D transition metal dichalcogenides and their van der Waals heterostructures.

K. Abdukayumov[1], M. Micica[2], F. Ibrahim[1], S.M. Massabeau[7], C. Vergnaud[1], A. Marty[1], J. Veuillen[3], P. Mallet[3], I. de Moraes[1], D. Dosenovic[4], A. Ouerghi[5], V. Renard[6], F. Mesple[6], F. Bonell[1], H. Okuno[4], M. Chshiev[1], J. George[7], H. Jaffres[7], S. Dhillon[2] and *M. Jamet*[1] *1. Univ. Grenoble Alpes, CEA, CNRS, Grenoble INP, IRIG-Spintec, Grenoble, France; 2. Laboratoire de Physique de l'Ecole Normale Supérieure, ENS, Université PSL, CNRS, Sorbonne Université, Université de Paris, Paris, France; 3. Université Grenoble Alpes, CNRS, Grenoble INP, Institut NEEL, Grenoble, France; 4. Université Grenoble Alpes, CEA, IRIG-MEM, Grenoble, France; 5. Université Paris-Saclay, CNRS, Centre de Nanosciences et de Nanotechnologies, Palaiseau, France; 6. Université Grenoble Alpes, CEA, CNRS, IRIG-PHELIQS, Grenoble, France; 7. Unité Mixte de Physique, CNRS, Thales, Université Paris-Saclay, Palaiseau, France*

Terahertz (THz) Spintronic emitters based on ferromagnetic/metal junctions have become an important technology for the THz range, offering powerful and ultra-large spectral bandwidths [1,2]. These developments have driven recent investigations of two-dimensional (2D) materials for new THz spintronic concepts. 2D materials, such as transition metal dichalcogenides (TMDs) and their van der Waals heterostructures, are ideal platforms for spin-to-charge conversion (SCC) as they possess strong spin-orbit coupling (SOC) and reduced symmetries [3]. Moreover, SCC and the resulting THz emission can be tuned with the number of layers, electric field, strain or by stacking different TMDs. In this work [4], we have grown single crystalline mono and multilayers of 1T-$PtSe_2$ on graphene, followed by amorphous CoFeB, with atomically sharp interfaces. We used a full set of characterization tools to demonstrate the structural and chemical preservation of $PtSe_2$ after CoFeB deposition. SCC was then studied on these advanced 2D samples using THz emission spectroscopy depicted in Fig. 1a as a function of $PtSe_2$ thickness (from 1 to 15 ML), that showed the generation of efficient THz electric fields. In comparison, THz emission from CoFeB/WSe_2 and CoFeB/VSe_2 are negligible. The THz emission with $PtSe_2$ is shown to arise from the 1T crystal structure and large spin-orbit coupling. The measured peak electric fields as a function of number $PtSe_2$ are shown in Fig. 1b. The THz electric field clearly shows a two-step dependence with $PtSe_2$ thickness, which we interpret as the transition from the inverse Rashba Edelstein effect (IREE) in the semiconducting regime to the inverse spin Hall effect (ISHE) in the semimetallic regime (around 3 to 4 MLs). As shown by ab initio, the IREE arises from the large Rashba spin splitting at the $PtSe_2$/graphene interface by the combination of large spin-orbit coupling and electron transfer from graphene to $PtSe_2$, generating an interface electric field. By fitting the thickness dependence, we can extract the out-of-plane spin diffusion length in $PtSe_2$ to be 2-3 nm and find that SCC by IREE at the $PtSe_2$/Gr interface is twice as efficient than that of ISHE in bulk $PtSe_2$. This is summarized in Fig. 1c and 1d where IREE takes place in the $PtSe_2$ monolayer in contact with graphene and ISHE in the semimetallic bulk $PtSe_2$ respectively. To summarize, owing its unique thickness dependent electronic structure, $PtSe_2$-ferromagnetic heterostructures have shown THz emission and has enabled to observe the transition from IREE to ISHE in a single 2D material system. This opens up novel applications of these structures to THz spintronics. For example, by further adjusting the Fermi level position by gating the semiconductor material, it will be possible to modulate and dramatically enhance the SCC efficiency, and achieve electronically controlled spintronic THz emission. Moreover, we have recently extended this work to van der Waals heterostructures containing $PtSe_2$: $PtSe_2$/$MoSe_2$ and $PtSe_2$/Bi_2Se_3 bilayers, where very strong Rashba SOC has been predicted [5,6].

[1] T. Seifert, S. Jaiswal, U. Martens et al., Nat. Photon. Vol. 10, p.483 (2016) [2] E. Rongione, L. Baringthon, D. She et al., Adv. Sci. 2023, p.2301124 [3] D. Xiao, G.-B. Liu, W. Feng et al., Phys. Rev. Lett. Vol. 108, p.196802 (2012) [4] K. Abdukayumov, M. Mičica, F. Ibrahim et al., arXiv:2305.06895, submitted to Adv. Mater. [5] L. Xiang, Y. Ke, Q. Zhang, Appl. Phys. Lett. Vol. 115, p.203501 (2019) [6] S. Sattar, J. Andreas Larsson, ACS Appl. Electron. Mater. Vol. 2, p.3585 (2020)

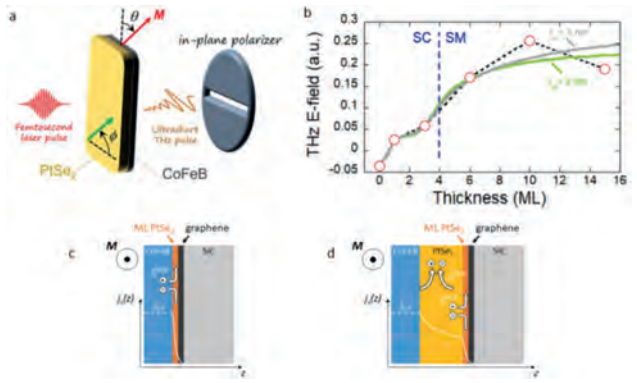

Figure 1: a) Optical excitation of CoFeB/$PtSe_2$/graphene junctions for THz generation. b) Normalized peak THz field obtained from samples with different number of $PtSe_2$ layers. Transition from semiconductor (SC) to semimetal (SM) can be estimated around 4 monolayers. c) and d) Illustration of the spin-to-charge conversion in CoFeB/$PtSe_2$/graphene samples. In the sample with 1 monolayer $PtSe_2$ a) the contribution is due to IREE and thick $PtSe_2$ sample b) where both ISHE and IREE are presented. White curve: profile of js(z). js(0) is the effective spin current injected in $PtSe_2$ from optically pumped CoFeB.

DF-03. Ferroelectric Switching of Berry Curvature Dipole in a Topological Crystalline Insulator at Room Temperature.

T. Nishijima[1] *1. Department of Electronic Science and Engineering, Kyoto University, Kyoto, Japan*

The physics related to Berry curvature is now a central research topic in condensed matter physics. The Berry curvature dipole (BCD) is an important and intriguing physical parameter that characterizes the antisymmetric distribution of Berry curvature. The BCD exists under inversion symmetry breaking, which induces current-driven out-of-plane magnetization and nonlinear Hall effect (NLHE) [1,2]. However, the creation and controllability of BCDs have been limited to below room temperature (RT) and nonvolatile switching of BCDs has not yet been achieved, hindering further progress in topological physics. To achieve room temperature demonstration of nonvolatile BCD control, we focused on a topological crystalline insulator (TCI), a type of topological insulator whose nontrivial band topology is protected by crystal symmetries [3]. The rock-salt structure IV–VI material, $Pb_{1-x}Sn_xTe$ (PST) is a TCI when $x > \sim 0.3$. On the (001) surface of PST, there are four Dirac cones and two mirror planes, and each mirror plane protects two of the four Dirac cones. Interestingly, ferroelectric displacements of anions and cations on the (001) surfaces and resulting mirror symmetry breaking have been reported. Since topological features of PST are protected by mirror symmetries, this ferroelectric distortion of the lattice results in the opening of band gap in Drac cones and finite BCD perpendicular to the ferroelectric distortion. Therefore the BCD in PST is expected to be controllable and nonvolatile, owing to its association with ferroelectricity. In this work, we have investigated NLHE induced by BCD in PST. A $Pb_{0.48}Sn_{0.52}Te$ single crystal was grown with Sb-doping to compensate for the Sn site vacancies, resulting in an insulating behavior of increasing resistance with decreasing temperature. The result of BCD induced NLHE measurement from the PST shows a quadratic dependence on applied current at room temperature, 300K, which is a manifestation of the NLHE (Fig. 1). As a control experiment, we chose PbTe (PT), a topologically trivial material. As a result, NLHE was not observed in the PT even at 5 K, which is evidence that the topological surface state of PST is the key to the NLHE. To explore the relevance of the NLHE and ferroelectric distortion in the PST, we performed NLHE measurement after applying pulsed electric fields to control the ferroelectric distortion and its direction. Sweeping the pulsed electric field, a clear hysteresis loop is obtained (Fig. 2), which is attributed to the ferroelectric-like behavior of the BCD [4]. The discovery of this ferroelectric control of the BCD in PST could contribute to further progress in topological materials science and the engineering of novel topological devices.

[1] I. Sodemann and L. Fu, Phys. Rev. Lett., Vol. 115, p.216806 (2015) [2] Q. Ma, S.Y. Xu and P. Jarillo-Herrero, Nature, Vol. 565, p.337 (2019) [3] Y. Ando and L. Fu, Annu. Rev. Condens. Matter Phys., Vol. 6, p.361 (2015) [4] T. Nishijima, S. Kuroda and M. Shiraishi, Nano Lett., Vol. 23, p.2247 (2023)

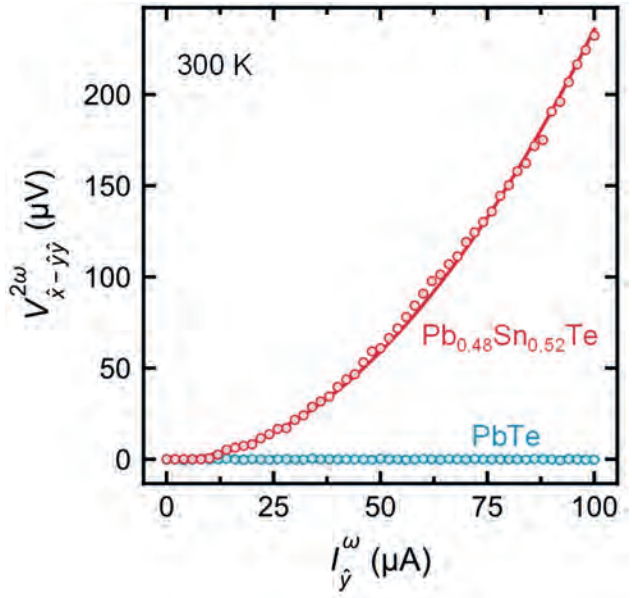

Nonlinear Hall voltage on the ac current along *y* at 300 K. The results are colored red and blue for PST and PT, respectively.

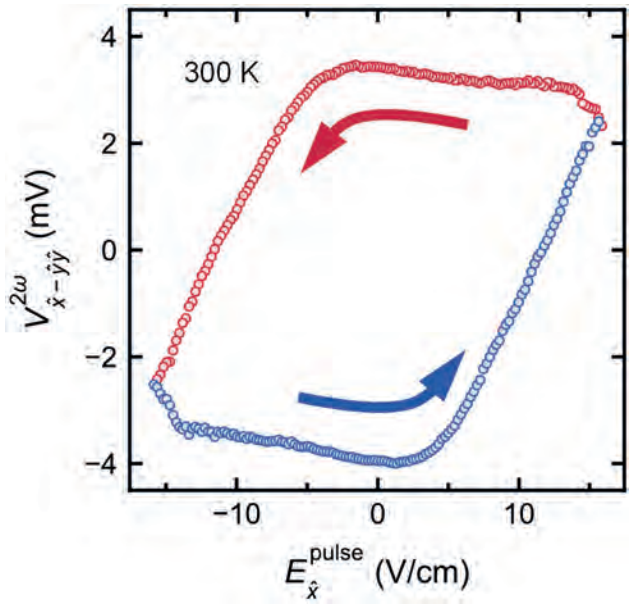

Nonlinear Hall voltage measured with a sweeping pulsed electric field. Red (blue) circles show the down sweep (up sweep).

CONTRIBUTED PAPERS

DF-04. Topological Weyl semimetal and Griffith's phase-like behavior of CrFeVGa: A Combined Theoretical and Experimental Studies.

J. Nag[1], P. Sreeparvathy[1], R. Venkatesh[2], P. Babu[3], K. Suresh[1] and A. Alam[1] *1. Physics, IIT Bombay, Mumbai, India; 2. Physics, UGC-DAE Consortium for Scientific Research, Indore, India; 3. Physics, UGC-DAE Consortium for Scientific Research, Mumbai Centre, Mumbai, India*

We report a combined theoretical and experimental study of a new topological semimetal CrFeVGa with an emphasis on the role of atomic disorder on the magneto-electronic properties and its applications. The disorder possibly leads in quenching the magnetization (net moment ~ 5×10^{-3} μ_B/f.u.) and gives rise to other anomalies. AC and DC magnetization data reveal the occurrence of Griffith's phase-like behavior in the presence of small magnetic clusters with a weak antiferro-/ferri- magnetic ordering. Resistivity data indicates a disorder-mediated semiconducting to semimetallic transition in CrFeVGa. Hall measurements show some anomalous behavior (including large AHC of 270 S cm^{-1}, anomalous Hall angle =0.07 degree at 2 K) with significant contribution from the semimetallic bands of the electronic dispersion. Hall data analysis also reveals the presence of some non-negligible topological Hall contribution, which is significant at very low temperatures. The possibility of spin texture in this system is also supported by anomalous low-temperature specific heat data. *Ab-initio* calculations help in getting a deeper insight into the topological nature of CrFeVGa and hence the origin behind the anomalous Hall response. A combination of the broken time-reversal symmetry and non-centrosymmetric feature of CrFeVGa allows the possibility of topological Weyl nodes. The non-trivial band topology stems from the 'p' and 'd' states of Vanadium atom, which overlap near E_F. The presence of multi-Weyl points (24 pairs) near E_F causes a large Berry curvature and hence reasonably high AHC. Simulated special quasi random structure predict the B2 disorder to be mainly responsible for the quenching of net magnetization. These fascinating properties of CFVG like high mobility and AHC etc. as a magnetic Weyl semimetal illustrate its potential for possible future applications in spintronics. The coexistence of so many emerging features in a single compound is rather rare and thus opens up a new avenue for future topological and spintronics based research.

Jadupati Nag, P.C. Sreeparvathy, R. Venkatesh, P.D. Babu, K.G. Suresh, and Aftab Alam; Phys. Rev. Applied 19, 044071 (2023)

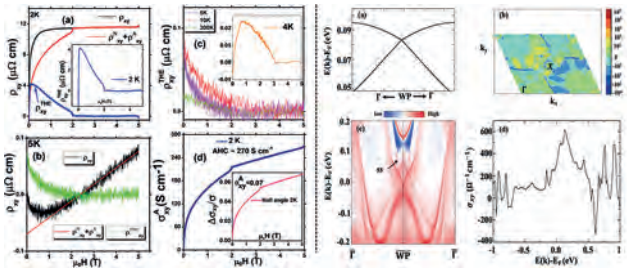

(Left) ρ_{xy} vs. H at 5 K along with the normal, anomalous and topological Hall contributions. (Right) simulated Berry curvature at the E_F and energy-dependent AHC.

DF-05. Impact of strain on induced magnetism and perpendicular magnetocrystalline anisotropy in $MoSe_2$ with a Mo vacancy.

T. Ochirkhuyag[1], B. Narangerel[1], O. Bayarsaikhan[2], G. Munkhsaikhan[2] and D. Odkhuu[1,3] *1. Incheon National University, Incheon, The Republic of Korea; 2. School of Applied Sciences, Mongolian University of Science and Technology, Ulaanbaatar, Mongolia; 3. Institute of Physics and Technology, Mongolian Academy of Sciences, Ulaanbaatar, Mongolia*

Two-dimensional (2D) structures that exhibit intriguing magnetic phenomena such as perpendicular magnetocrystalline anisotropy (PMA) and its switchable feature are of great interest in spintronics research. In this talk, we will present

the results of our recent first-principles calculations on magnetism and PMA induced in 2D $MoSe_2$ by a Mo-site vacancy. In contrast to the $MoSe_2$ without and with a Se vacancy, the presence of a Mo vacancy induces significant magnetic moments to its first neighboring Se and Mo atoms due to the charge deficit. Remarkably, a very large PMA more than 1000 μeV/Mo-vacancy is predicted. We further explore the impact of strain effects on PMA and find that PMA reorients into an in-plane magnetization under a practically achievable biaxial tensile strain of only 1% while it is quite robust against the compressive strains. This magnetization reversal is mainly driven by the strain-induced changes in the spin-orbit coupled $3d-4p$ orbital states of the nearest-neighbor Mo and Se atoms to a Mo vacancy. These findings open interesting prospects for exploiting strain engineering to manipulate magnetism and magnetization orientation of 2D materials. The research is funded by the Office of Naval Research and the Office of Naval Research Global of the US Department of Defense Grant N62909-23-1-2035.

DF-06. Room-temperature nonlinear Hall effect driven by Berry curvature dipole in $NbIrTe_4$. *J. Lee*[1,2], A. Wang[3], S. Chen[4], M. Kwon[5], J. Hwang[6], M. Cho[5], K. Son[7], D. Han[7], J. Choi[7], Y. Kim[5], S. Mo[1], C. Petrovic[4], C. Hwang[8], S. Park[9], C. Jang[7] and H. Ryu[7] *1. Advanced Light Source, Lawrence Berkeley National Laboratory, Berkeley, CA, United States; 2. Max Planck POSTECH Center for Complex Phase Materials, Pohang University of Science and Technology, Pohang, The Republic of Korea; 3. Chongqing University, Chong Qing Shi, China; 4. Brookhaven National Laboratory, Upton, NY, United States; 5. Kyunghee University, Seoul, The Republic of Korea; 6. Kangwon National University, Gangwondo, The Republic of Korea; 7. Korea Institute of Science and Technology, Seoul, The Republic of Korea; 8. Pusan National University, Busan, The Republic of Korea; 9. Soongsil University, Seoul, The Republic of Korea*

The realization of a nonlinear Hall effect in a non-magnetic material with broken centrosymmetry in the absence of external magnetic field has attracted huge research interest due to its potential application to versatile electronic devices. In this talk, we provide experimental evidence of the nonlinar Hall effect in $NbIrTe_4$ that persists up to room temperature. More interestingly, the Hall conductivity changes its sign at 150 K. The combined study using angle-resolved photoemission spectroscopy and first-principles calculations reveals that the Berry curvature hotspots in the partially occupied spin-orbit split bands are modified by the chemical potential shift as a function of temperature, leading to the novel nonlinear Hall effect. Our findings shed light on the correlation between the electronic structure and the Berry curvature dipole, providing an effective approach to control the nonlinear Hall effect in centrosymmetry-broken nonmagnetic materials.

DF-07. Theory-Led Pathways to Two-Dimensional Magnetism. *S.M. Griffin*[1] *1. Lawrence Berkeley National Laboratory, Berkeley, CA, United States*

The recent discovery of intrinsic long-range magnetic order in atomically thin layers has triggered an explosion of interest, defying traditional Mermin-Wagner-Hohenberg theorem predictions that state such order should not be stable in purely 2D isotropic systems. The development of compact, spin-based electronics gives them potential for energy-efficient microelectronics. However, most 2D magnetic materials demonstrate weak magnetocrystalline anisotropy (MCA) and coercive fields, underscoring the urgent need for new materials with stronger and more controllable MCA. Here I present our recent results of achieving high MCA in two classes of 2D magnetic materials – intercalated transition-metal dichalcogenides [1] and bulk kagomé metals [2]. Using first-principles calculations to build up effective Hamiltonians, I will describe the origins of 2D magnetism in these materials, routes to controlling the emergent properties, and the onset and interplay of non-trivial topology in both real and reciprocal space.

[1] S. Husremovic, C. K. Groschner, K. Inzani, et al. "Hard ferromagnetism down to the thinnest limit of iron-intercalated tantalum disulfide." Journal of the American Chemical Society 144, 12167 (2022) [2] L. Prodan, D. M. Evans, S. M. Griffin et al. "Large ordered moment with strong easy-plane anisotropy and vortex-domain patterns in the kagomé ferromagnet Fe_3Sn." Appl. Phys. Lett. (In Press) (2023)

DF-08. 2D ferromagnetic $Fe_{5-x}GeTe_2$ films on graphene with Curie temperature above room temperature. H. Lv[1], *J. Herfort*[1], M. Ramsteiner[1], A. Kassa[1], A. da Silva[1], M. Hanke[1], A. Trampert[1], R. Engel-Herbert[1] and J. Lopes[1] *1. Paul-Drude-Institute of Solid State Eelectronics, Berlin, Germany*

Van der Waals (vdW) heterostructures combining layered ferromagnets and other 2D crystals are promising building blocks for the realization of ultra-compact devices with integrated magnetic, electronic, and optical functionalities [1]. Their implementation in various technologies depends strongly on the development of a bottom-up scalable synthesis approach allowing for realizing highly uniform heterostructures with well-defined interfaces between different 2D-layered materials. It is also required that each material component of the heterostructure remains functional, which ideally includes ferromagnetic order above room temperature for 2D ferromagnets. Here, we present our recent results on van der Waals (vdW) epitaxy of the 2D itinerant ferromagnetic metal $Fe_{5-x}GeTe_2$ ($x \sim 0$) on single crystalline epitaxial graphene using molecular beam epitaxy. It is demonstrated that the large-area growth of $Fe_{5-x}GeTe_2$/graphene heterostructures is achieved. Morphological and structural characterization using methods such as atomic force microscopy, synchrotron-based grazing incidence X-ray diffraction, and scanning transmission electron microscopy (STEM) revealed that epitaxial $Fe_{5-x}GeTe_2$ films exhibiting very good surface morphology, high crystalline quality, and a sharp interface to graphene could be realized. Temperature-dependent magneto-transport measurements and superconducting quantum interference device (SQUID) magnetometry were employed to assess the magnetic properties of the samples. It is revealed that the ferromagnetic order persists well above 300 K with a predominant perpendicular magnetic anisotropy. In addition, epitaxial graphene on SiC(0001) continues to exhibit a high electronic quality. Our comprehensive results [2] represent an important advance beyond nonscalable flake exfoliation and stacking methods, thus marking a crucial step toward the implementation of ferromagnetic 2D materials in practical applications.

[1] J. F. Sierra, J. Fabian, R. K. Kawakami, S. Roche, S. O. Valenzuela, Nat. Nanotechnol. 2021, 16, 856. [2] H. Lv, A. da Silva, A. I. Figueroa *et al.,* Small 2023, 2302387.

Session DG
DOMAINS AND ANISOTROPY IN MAGNETIC JUNCTIONS

Razan Aboljadayel, Chair
University of Leeds, Leeds, United Kingdom

CONTRIBUTED PAPERS

DG-01. Perpendicular Magnetic Tunnel Junctions with a Monoatomic-Layer-Controlled CoPt(111) layer and a MgO(111) Barrier. *J. Song*[1,2], T. Scheike[1], C. He[1], Z. Wen[1], T. Ohkubo[1], K. Kim[3], H. Sukegawa[1] and S. Mitani[1,2] *1. National Institute for Materials Science (NIMS), Tsukuba, Japan; 2. Graduate School of Science and Technology, University of Tsukuba, Tsukuba, Japan; 3. Samsung Advanced Institute of Technology, Suwon, The Republic of Korea*

The development of magnetic tunnel junctions (MTJs) with large tunnel magnetoresistance (TMR) and strong perpendicular magnetic anisotropy (PMA) is essential for ultra-high density magnetoresistive random access memories (MRAMs). Nowadays, the bcc(001)-type MTJs, i.e., Fe/MgO/Fe and CoFeB/MgO/CoFeB, which exhibit enhanced TMR ratios due to the Δ_1 coherent tunneling effect and PMA at a MgO interface, are used as MRAM cells. [1] However, the limited material choices within the (001)-type MTJs and the limited interfacial PMA energies restrain further progress in perpendicular MTJs (p-MTJs). Recently, theoretical calculations have predicted that the fcc(111)-type p-MTJs using a MgO(111) barrier and Co-based PMA alloys, such as $L1_1$-CoPt, exhibit large TMR ratios over 2000% due to an interfacial resonant tunneling effect [2]. In this work, we report the first TMR observation by developing an epitaxial $L1_1$-CoPt(111)/MgO(111)/CoFeB p-MTJ using monoatomic monolayer control by sputtering. All stacks were deposited by magnetron sputtering (base pressure less than 10^{-6} Pa) on a single crystal sapphire(0001) substrate. The typical stack structure was substrate/Ru (40)/$[Co\ (0.2)/Pt\ (0.3)]_{20}$ (10)/Co (0.2)/MgO (1)/CoFeB (1.1)/W (0.2)/CoFeB (0.6)/MgO (1)/Ta (5)/Ru (12) (units in nm) (Fig. 1). The CoFeB/W/CoFeB/MgO is for the perpendicular magnetization of the top layer. The bottom CoPt layer were sputter deposited by repeating of a Co (1 ML ~ 0.2 nm)/Pt (1~5 ML) unit. The epitaxial growth of an $L1_1$-based ordered structure and a MgO barrier with (111) orientation was confirmed by X-ray diffraction and scanning transmission electron microscopy, indicating the well-controlled CoPt and MgO(111) growth. The epitaxial CoPt layer shows a high PMA energy of ~1 MJ/m^3. The prepared MTJs have a TMR ratio of 24% at room temperature (Fig. 2). This work demonstrate a novel MTJ structure towards a large TMR ratio and a strong PMA beyond the conventional bcc(001) MTJs.

[1] S. Ikeda, K. Miura and H. Ohno, Nature Mater. 9, 721 (2010). [2] K. Masuda, H. Itoh and Y. Miura, Phys. Rev. B. 103, 064427 (2021).

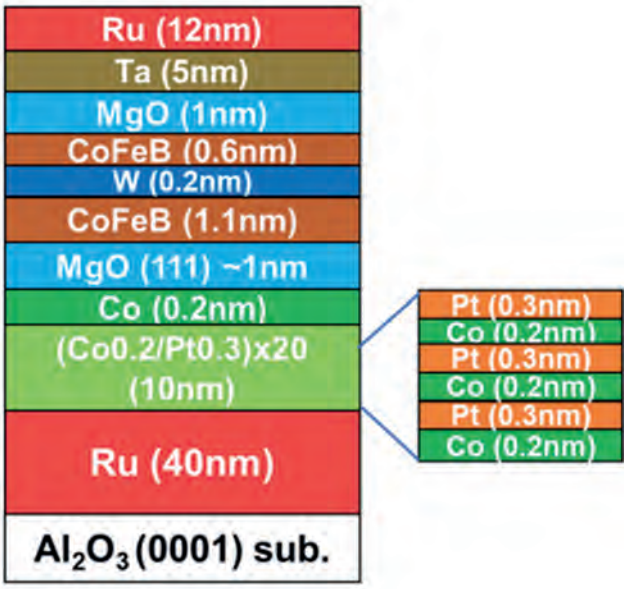

Fig. 1 Schematic illustration of epitaxial fcc(111) p-MTJ stack with CoPt.

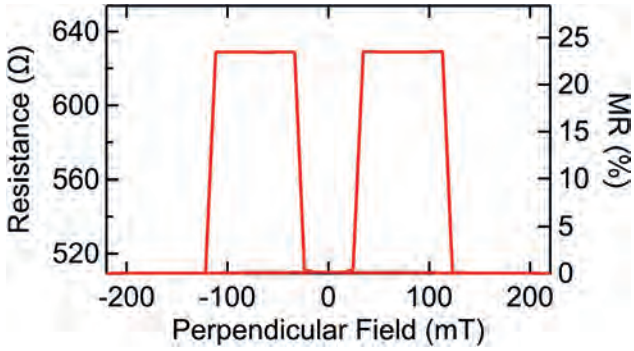

Fig. 2 TMR-field curves at room temperature.

DG-02. Giant Tunneling Magnetoresistance in Magnetic Tunnel Junctions with a Single Ferromagnetic Electrode. *K. Samanta*[1], D. Shao[2], T.R. Paudel[3] and E. Tsymbal[1] *1. Department of Physics and Astronomy, University of Nebraska-Lincoln, Lincoln, NE, United States; 2. Key Laboratory of Materials Physics, Institute of Solid-State Physics, HFIPS, Chinese Academy of Sciences, Hefei, China; 3. Department of Physics, South Dakota School of Mines and Technology, Rapid City, SD, United States*

Magnetic tunnel junctions (MTJs) are key components of spintronic devices, such as magnetic random-access memories. Normally, MTJs consist of two ferromagnetic electrodes separated by an insulating spacer layer. The key

functional property of MTJs is the tunneling magnetoresistance (TMR) effect that is a change in resistance when magnetization of the two electrodes alters from parallel to antiparallel. Here, we demonstrate that TMR can occur in MTJs with a single ferromagnetic electrode, provided that the counter electrode is an antiferromagnetic metal with a spin-split band structure. The latter property requires broken PT and Ut symmetries (where P is space inversion, T is time reversal, U is spin flip, and t is half a unit cell translation). Using RuO_2 as a representative example of such an antiferromagnet (Fig. 1a) and CrO_2 as a ferromagnetic metal (Fig. 1b), we design an all-rutile $RuO_2/TiO_2/CrO_2$ (110) MTJ whose symmetry supports a non-vanishing TMR (Fig. 2a). Our first-principles calculations of the electronic structure and conductance predict that reversal of magnetization of CrO_2 significantly changes the resistance of the MTJ (Fig. 2b). The predicted giant TMR ~ 560% stems from spin-dependent conduction channels in CrO_2 (110) and RuO_2 (110), whose overlap alters with CrO_2 magnetization orientation (Figs. 1c-e), and symmetry matching of the electronic bands in the electrodes and the TiO_2 barrier. Our results demonstrate a possibility of a sizable TMR effect in MTJs with a single ferromagnetic electrode and offer a simple practical test for using the collinear antiferromagnet RuO_2 in functional spintronic devices.

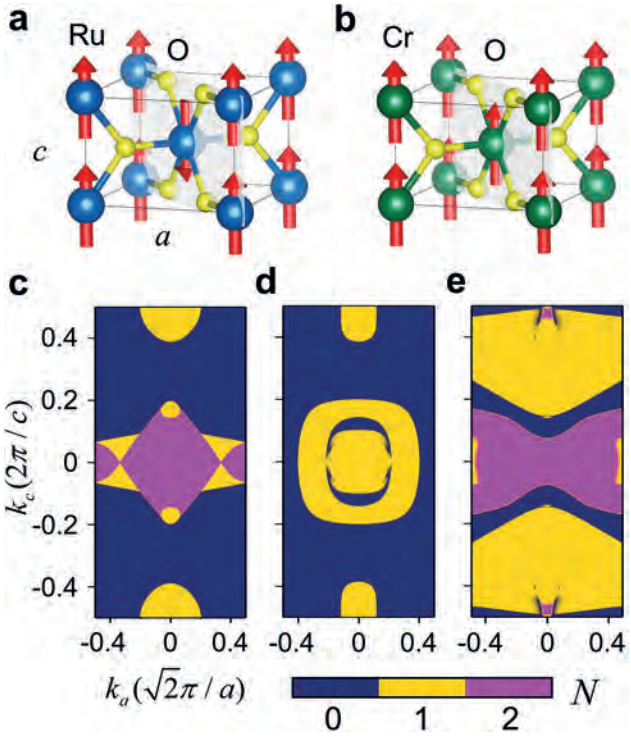

FIG. 1 (a,b) Atomic and magnetic structure of antiferromagnetic RuO_2 (a) and ferromagnetic CrO_2 (b) with (110) plane indicated. (c,d,e) Number of conduction channels N in the 2D Brillouin zone for up- (c) and down- (d) spin in RuO_2 and majority spin in CrO_2 (e).

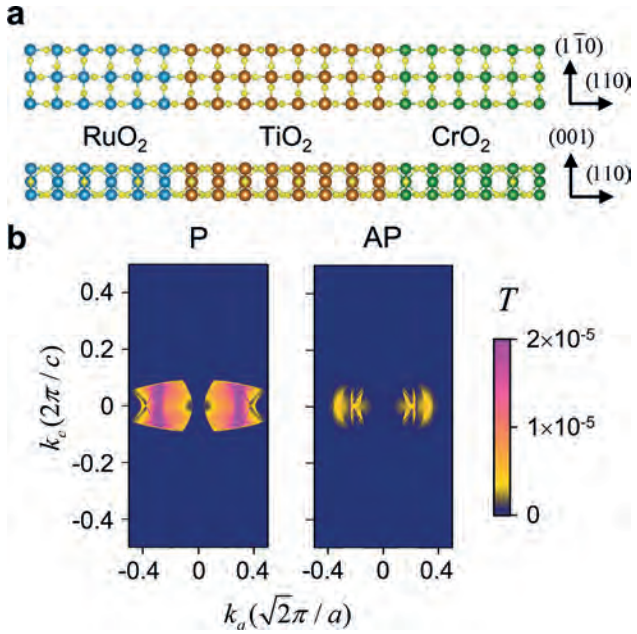

FIG. 2 (a) Atomic structure of $RuO_2/TiO_2/CrO_2$ (110) MTJ (top and side view). (b) Calculated $k_{\parallel}$-resolved transmission T across the junction for parallel (P) and antiparallel (AP) alignment of CrO_2 magnetization with respect to RuO_2 Néel vector. The corresponding TMR ratio $(T_P - T_{AP})/T_{AP} \sim 560\%$.

DG-03. Unconventional Magnetoresistance and its Implications in Spin-Torque Characterization. *H. Zhang*[1] and R. Cheng[1,2] *1. Department of Electrical and Computer Engineering, University of California Riverside, Riverside, CA, United States; 2. Department of Physics and Astronomy, University of California Riverside, Riverside, CA, United States*

Magnetoresistance (MR) is essential in characterizing spin torques, especially in spin-torque ferromagnetic resonance (ST-FMR) and harmonic Hall analysis. Some experiments utilize a ferromagnetic (FM) metal that hosts anisotropic MR, where current in an adjacent material generates spin torques exerting on the magnetization and changes the MR. The variation of MR can in turn be used to quantify the spin torques, such as the out-of-plane anti-damping torque recently discovered in WTe_2 attributed to unconventional mechanisms[1]. A different type of experimental setup involves an insulating FM driven and detected by a heavy metal[2]. In such a system, there is no shunting current in the FM insulator, so the spin Hall effect in the heavy metal generates the spin torque and at the same time detects the FM dynamics through the change of the spin Hall MR. However, when it comes to an FM insulator driven by a non-spin-Hall system, such as $WTe_2/Cr_2Ge_2Te_6$ bilayer, there has been no clear understanding of the MR, let alone using the MR to characterize the spin torques. In this work, we first investigate the unconventional form of MR in a non-spin-Hall geometry. Next, by solving the Landau-Lifshitz-Gilbert equation and conducting harmonic expansion of the unconventional MR, we derive a series of expressions for measurable ST-FMR and harmonic Hall signals. Verified by detailed numerical results, our finding lays the theoretical foundation for characterizing spin torques originating from unconventional mechanisms beyond the spin Hall effect, which can not only guide ongoing experimental endeavors but also stimulate future experimental designs.

1. D. MacNeill, G. Stiehl, M. Guimaraes, *et al*., *Nat. Phys.* 13, 300–305 (2017). 2. Y. Chen, S. Takahashi, H. Nakayama, *et al.*, *Phys. Rev. B* 87, 144411 (2013). 3. E. Cogulu, H. Zhang, N. Statuto, *et al*., *Phys. Rev. Lett.* 128, 247204 (2022). 4. H. Zhang and R. Cheng, *J. Magn. Magn. Mater.* 556, 169362 (2022).

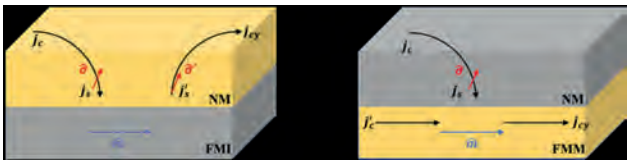

Fig 1. Schematics of (a) Spin-Hall MR system, (b) AMR system.

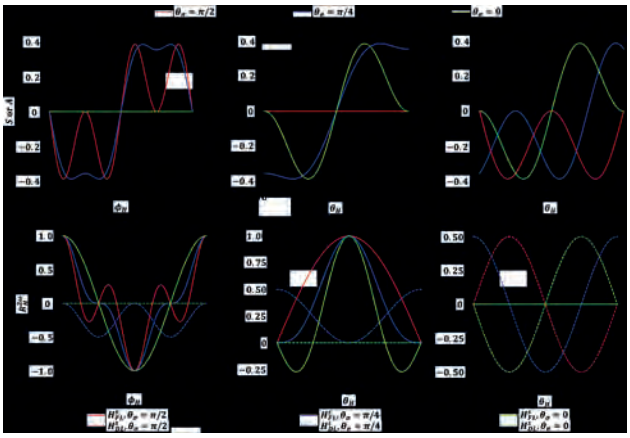

Fig 2. Symmetric *S* and antisymmetric *A* components of the ST-FMR rectification voltage [(a)-(c)] and second harmonic Hall resistance [(d)-(f)] in three orthogonal angular scans of magnetic field with different polar angles θ_σ of the spin polarization σ. (a) and (d), (b) and (e), (c) and (f) correspond to magnetic field rotation in the *xy*, *xz* and *yz* planes, respectively. $H^s_{FL}(H^s_{DL})$ represents the field-like (damping-like) spin torque contribution. The top and bottom legends belong to (a)-(c) and (d)-(f), respectively.

INVITED PAPER

DG-04. Nanoscale domain wall devices with magnetic tunnel junction read and write. *V. Nguyen*[1], E. Raymenants[1,2], D. Wan[1], Y. Canvel[1], D. Giuliano[1,2], B. Vermeulen[1,2], S. Rao[1], K. Wostyn[1] and S. Couet[1]
1. IMEC, Leuven, Belgium; 2. KU Leuven, Leuven, Belgium

The discovery of fast domain wall (DW) motion governed by spin-orbit torque (SOT) and the Dzyaloshinskii-Moriya interaction (DMI) in ultrathin magnetic layers on heavy metals was a breakthrough in the development of next-generation, scalable, and energy-efficient data storage [1] and spin logic [2] devices. However, the absence of an electrical method to efficiently write/read DWs in nanoscale devices hinders the practical implementation of this device concept. As demonstrated in current MRAM technology, the magnetic tunnel junction (MTJ)-based on a CoFeB/MgO free layer (FL) [3] which offers efficient spin-transfer torque (STT) write and a high tunneling magnetoresistance (TMR) readout signal could provide an approach to electrically write/read DWs at nanoscale devices. However, such MTJ stack design posed significant challenges to realizing a DW device that particularly related to low DW speed and poor manufacturability for a DW conduit-based CoFeB/MgO layer using industrial integration platforms [4]. Here, we present functional DW devices with electrical read/write operations using the hybrid free layer (HFL) MTJ stack design, c.f., Fig. 1 [6]. In this MTJ stack design, the first free layer consists of a conventional CoFeB/MgO-based free layer. The second free layer, which typically consists of a ferromagnet (i.e., Pt/Co) or a synthetic antiferromagnetic (i.e., Pt/Co/Ru/Co), is exploited to enable high-velocity DW motion. We first demonstrate that single MTJs with an HFL stack can offer a reliable TMR readout signal and efficient STT writing and can thus be used as the outputs and inputs of a DW device. We then demonstrate full electrical control of a nanoscale DW device comprising multiple MTJ pillars that share a common free layer. In this device, we show that STT can be used locally nucleate DWs at the input MTJ and a DW can be read out via TMR at the output MTJ, while the DWs can propagate between input and output via field or SOT-driven DW motion [5, 6]. As an example, Figure 2 (a, d) presents field-driven domain expansion where the nucleated domain expands from the center pillar P2 to both outer pillars (*i.e., observed a change of TMR in both P1 and P3*). In contrast to field-driven DW motion, we then show that the direction of DW motion is selectively manipulated by current polarity. Figure 2 (b, e) shows a change of TMR in P3 indicating DW motion from P2 to P3 with a positive current while DW moves from P2 to P1 with a negative current. Finally, we show that these DW devices can be used to investigate the SOT-driven DW dynamics in nanoscale devices. Our DW devices show good TMR read-out and efficient STT writing, comparable to current STT-MRAM devices. The devices are fabricated in imec's 300 mm CMOS fab on full wafers which clears the path for large-scale integration. This proof-of-concept thus offers potential solutions for high-performance and low-power DW-based devices for logic and memory applications [1, 2].

1. Parkin et al., Science 320, 190 (2008) 2. Luo et al., Nature 579, 214 (2020) 3. Ikeda, et al., Nat. Mater. 9, 721 (2010) 4. Raymenants, Nguyen et al., 2018 IEDM, 36.4 5. Raymenants, Nguyen et al., 2020 IEDM, 21.5 6. Raymenants, Nguyen et al., Nat. Elec., 4, 392 (2021)

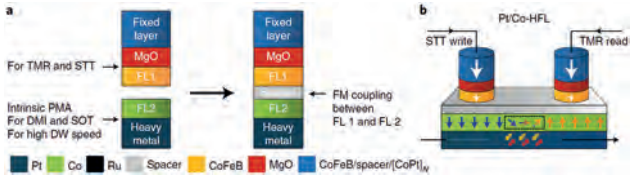

Figure 1. (a) Schematics of the hybrid free layer MTJ stack design for nanoscale DW devices. The HFL design consisting of CoFeB/MgO-based first free layer for efficient STT write and high TMR read operations, and the second free layer consisting of a material is optimized for high DW velocity driven by SOT. The two free layers are ferromagnetically coupled through a spacer layer via interlayer exchange coupling. (b) An example presents schematic of DW-based devices with Pt/Co-second free layer. Figure was taken from [6].

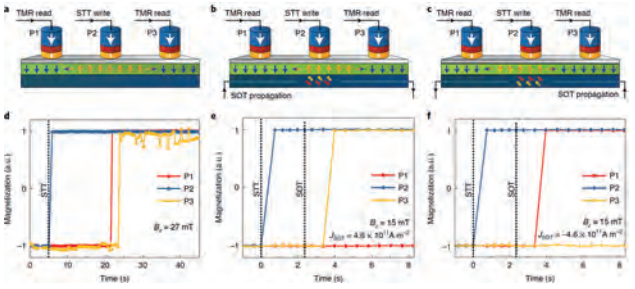

Figure 2. Schematic and measurement sequences explaining the motion of DW from pillar-to-pillar via TMR detection. (a, d) Field driven DW motion where domain was nucleated in P2 by STT, after which external field expanded it to the outer pillars, P1 and P3. SOT-driven DW motion from P2 to P3 with positive current (b, e) and from P2 to P1 with negative current (c, f). No DW propagation was observed to P1 for positive current or P3 for negative current. Figure was taken from [6].

CONTRIBUTED PAPERS

DG-05. Towards Fully Electrically Controlled Domain-Wall Logic.
B. Vermeulen[1,2], E. Raymenants[1], V. Pham[3,1], B. Caerts[2], S. Pizzini[3], B. Soree[1,4], S. Couet[1], K. Wostyn[1], V. Nguyen[1] and K. Temst[2,1] *1. IMEC, Leuven, Belgium; 2. Department of Physics and Astronomy, KU Leuven, Leuven, Belgium; 3. Université Grenoble Alpes, CNRS, Institut Néel, Grenoble, France; 4. Department of Electrical Engineering (ESAT), KU Leuven, Leuven, Belgium*

Domain-wall (DW) logic can benefit from magnetic tunnel junctions (MTJs) for write/read operations and from fast spin-orbit-torque (SOT)-driven DW motion for information propagation, enabling non-volatile logic and majority operations [1]. In 2020, Luo et al. demonstrated DW inverter and NAND/NOR gates in a Pt/Co/AlOx stack via magnetic imaging, where the Dzyaloshinskii-Moriya interaction (DMI) induces chiral coupling between perpendicular magnetic anisotropy (PMA) regions via an in-plane (IP) oriented region [2,3]. However, nanoscale electrical write/read access is lacking, and selective oxidation is used to convert the magnet from IP to PMA, which is not compatible with the fabrication of PMA MTJs. Here, to achieve a full electrical operation of nanoscale DW logic [4], we propose a combination of a Hybrid Free Layer (HFL) concept to implement MTJ write/read units [5] with He ion irradiation to enable a PMA-to-IP conversion. The HFL consists of coupled free layers (FLs) (Fig.1a). FL1 is based on CoFeB/MgO to provide good spin-transfer torque (STT) write and tunneling magnetoresistance (TMR) read operations (Fig.1b). FL2 consisting of Pt/Co is selected to provide high PMA and DMI for fast DW motion. We first study the properties of 100-nm HFL MTJ pillars as a function of the CoFeB and Co thicknesses. STT and TMR are shown to mainly depend on the CoFeB thickness, offering flexibility to tune the Pt/Co stack without compromising the MTJ properties. Through DW dynamics measurements, we find a DMI of ~0.7 mJ/m^2 for the HFL and compare it with a single Pt/Co stack [3]. Finally, we show that He ion irradiation can convert the HFL stack from PMA to IP (Fig.2), providing an approach compatible with PMA MTJs. To enable DW logic, a mask approach or focused ion beam for local PMA-to-IP conversion at nanoscale are discussed.

[1] D. E. Nikonov, G. I. Bourianoff and T. Ghani, IEEE Electron Device Letters, Vol. 32, pp.1128-1130 (2011) [2] Z. Luo, T. P. Dao, A. Hrabec, et al., Science, Vol. 363, pp.1435-1439 (2019) [3] Z. Luo, A. Hrabec, T. P. Dao, et al., Nature, Vol. 579, pp.214-218 (2020) [4] B. B. Vermeulen, M. G. Monteiro, D. Giuliano, et al., [Submitted] (2023) [5] E. Raymenants, O. Bultynck, D. Wan, et al., Nature Electronics, Vol. 4, pp.392-398 (2021)

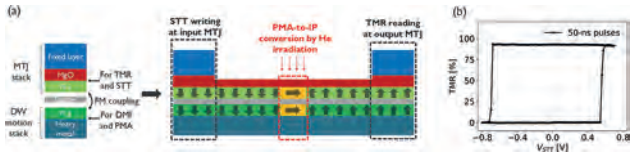

Fig.1: HFL concept (a) Combination of an MTJ stack with a DW track. DW logic gates are made by local in-plane regions. (b) TMR versus STT voltage on HFL stack (no offset compensation).

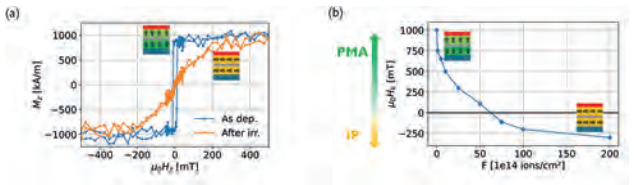

Fig.2: PMA-to-IP conversion by 30-keV He ion irradiation on a HFL stack (a) Out-of-plane magnetization M_z versus field $\mu_0 H_z$, as deposited and after 10^{16} ions/cm^2 fluence. (b) Anisotropy field as a function of fluence F.

DG-06. Constant Bit Shift Motion of Recorded Magnetic Domains in Magnetic Nanowire Device with Step Trap Sites.
D. Kato[1], M. Takahashi[1], K. Ogura[1], Y. Iguchi[1] and Y. Miyamoto[1] *1. Science & Technology Research Labs., NHK (Japan Broadcasting Corp.), Tokyo, Japan*

We have been studying the magnetic nanowire (NW) memory, which utilizes current-driven domain wall motion to shift the recorded magnetic domains, to achieve large capacity and ultra-high data transfer rate. In our previous work[1], we tried to install periodic ratchet-structured trap sites along the NW for the constant domain shift. However, since these ratchets induced the Bloch-domain wall mode and their trapping energy was too high, the stable shift of multiple domains was obstructed. While the NW with step-structured trap sites exhibited the chiral domain wall mode and offers the prospect of achieving a constant-length shift of the multiple domains[2]. In this study, we report the stable current-driven domain wall motion in the NW with step trap sites, which was investigated by magneto-optical Kerr effect microscopy (MOKE). Figure 1 shows a microscopic image of the fabricated NW memory device. To define the unit shift length, periodic SiN(4) step structures with a width of 3 μm and a pitch of 6 μm were formed under the NW consisting of Pt(3)/[Co(0.35)/Tb(0.8)]$_4$ (units in nm). A writer for recording domains was placed orthogonally to the NW and inserted with an insulating spacer. Figure 2 shows the differential MOKE images of successful memory operation: (a) The NW was initialized upward by an external magnetic field of 1 kOe. (b) The recording pulse current density of 30.0 MA/cm^2 and the shift pulse current density of 1.3 MA/cm^2 were simultaneously applied to the NW to record the first downward domain. (c)-(e) After the shift of preceding domains, the second to the fifth downward domains were recorded in the same way. (f)-(g) The negative recording pulse and the same shift pulse were simultaneously applied to the NW to record the sixth and seventh upward domains. (h)-(i) The eighth to the ninth downward domains were recorded. These results show that the magnetic domains can be stably shifted at the installed unit steps, and it was confirmed that each domain maintained its length while being shifted, which is preferable for the memory operation.

[1]M. Takahashi et al.: MMM2022, IPA-05 (2022) [2]K.Ogura et al.: SSDM2023 (will be presented)

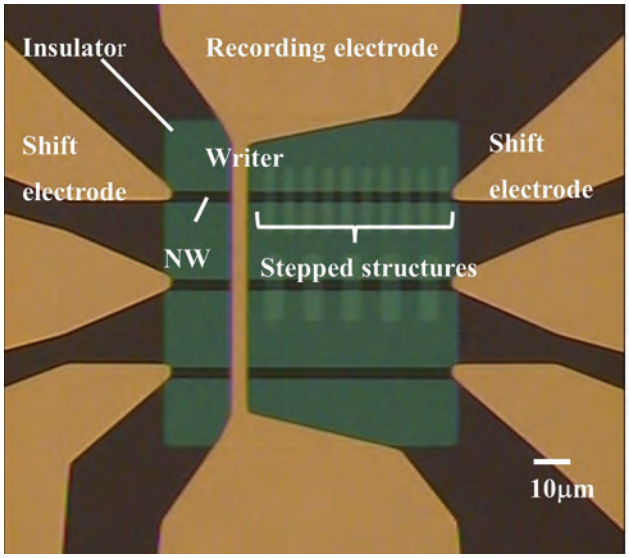

Fig.1 Fabricated magnetic nanowire memory with step trap sites

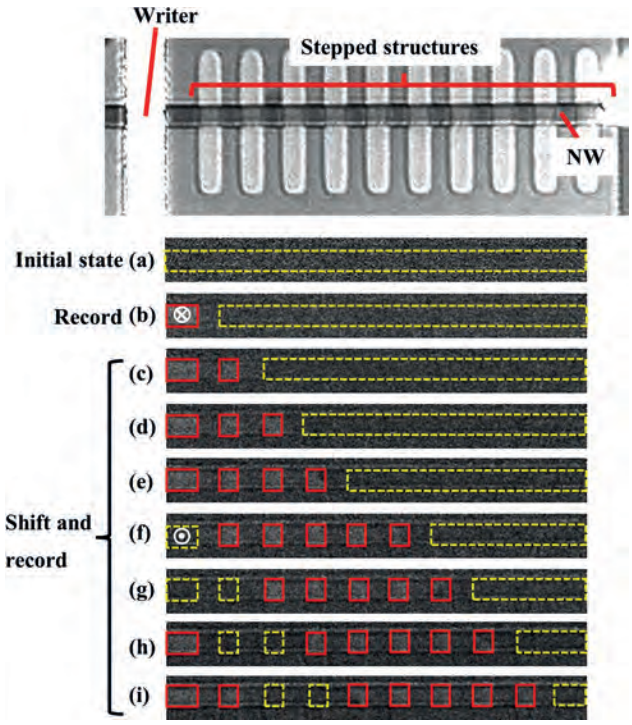

Fig.2 Differential images of magneto-optical Kerr microscope for memory operation

DG-07. Drastically Enhancement for Stable and Fast Domain Wall Motion in GdFe Nanowires by Laser-Annealing Treatment of Wire Edges. *M. Mohammadi*[1], S. Sumi[1], Y. Miyose[1], K. Tanabe[1] and H. Awano[1] *1. Memory Engineering Laboratory, Toyota Technological Institute, Nagoya, Japan*

One of the key challenges in the racetrack memory (RM) technology is achieving high velocities for domain walls (DWs) while maintaining low power consumption. Recent studies on GdFeCo nanowires, have found that the drive power and the DW motion velocity of the RM depend on the DW shape [1]. In our study, we propose a novel laser-annealing (LA) process to modify wire edges and to reduce the pinning effect for a smoother DW movement along the nanowire. In this regard, a film stack of Pt (5nm)/$Gd_{26}Fe_{74}$(20nm)/SiN(10nm) were deposited by magnetron sputtering. The DW velocity in the wire (3 μm wide and 50 μm long) was measured by applying single voltage pulses and then observing the DW motion using a Kerr microscope. The current-induced domain walls motion (CIDWM) measurements have shown that LA process significantly enhances the velocity of DW motion. Specifically, when subjected to a current density of 3×10^{11} A/m^2 and a pulse width of 3 ns, the LA of both edges of the nanowire results in a threefold increase in DW velocity compared to non-LA condition. The velocity of DWs increase from approximately 600 m/s to 1800 m/s, as depicted in Fig.1. Furthermore, as depicted in Fig.2, the DW motion remains stable for the laser-annealed condition across a wide range of applied currents, spanning from 3×10^{11} A/m^2 to 7×10^{11} A/m^2. This achievement, i.e. the stability and consistency of the domains velocity (as the components of a RM) in a wide range of applied current, is a significant progress in the field of operation and industrialization of RM. Our results also revealed that LA process induces changes in the shape of DWs, transforming them from curved to rectangular shape. This improvement may due to this reason that the DW in the center of the magnetic nanowire moves easily, however the edges don't move easily [1,2]. LA process smoothly heat and modifies pinning sites present at the wire edges, reducing their influence on DW movement. To the best of our knowledge, this is the first demonstration of the effectiveness of LA process in enhancing the velocity of DW motion in a ferrimagnetic nanowire.

[1] S. Ranjbar, S. Kambe, S. Sumi, et al, Mater. Adv. Vol.3, p.7028 (2022).
[2] S. Ranjbar, S. Sumi, K. Tanabe, et al, APL Mater, Vol.10, p.091102 (2022).

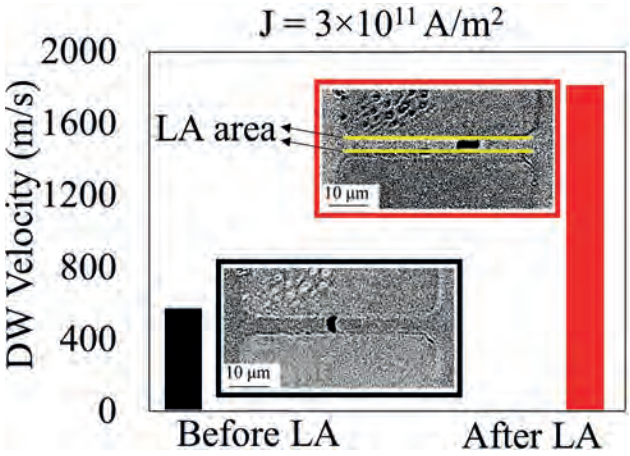

Fig.1: Displacement of DWs before and after LA process.

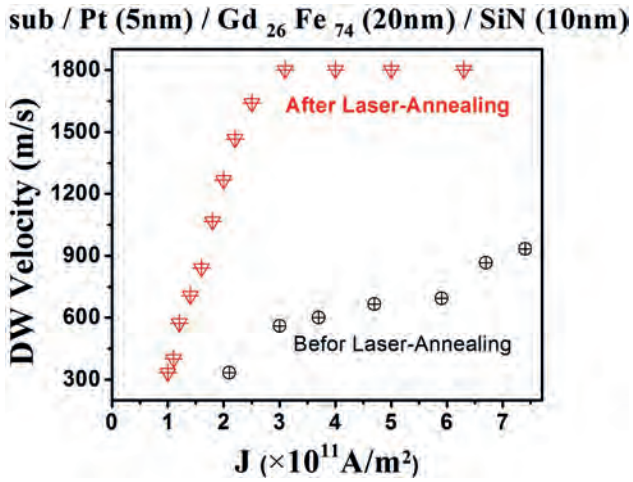

Fig.2: DW velocity vs. current density.

DG-08. A Path Towards Synthetic Antiferromagnets in Nanoscale Domain Wall Devices. *D. Giuliano*[2,1], V. Nguyen[2], Y. Canvel[2], Y. Li[2], A. Palomino[2], R. Carpenter[2], S. Rao[2], C. Fleischmann[2,1], K. Temst[1,2], K. Wostyn[2] and S. Couet[2] *1. Physics and Astronomy, KU Leuven, Leuven, Belgium; 2. Imec, Leuven, Belgium*

Domain wall (DW) memory, where information is encoded in magnetic domains within a nanotrack (Fig. 1a-b), offers a promising solution for high storage capacity [1-3]. Recently, a full electrical control of a nanoscale DW device has been demonstrated [4] using Magnetic Tunnel Junctions (MTJs) as the read/write elements. However, the use of ferromagnets as storage tracks poses challenges to the DW motion, such as sensitivity to the stray field generated by the MTJ. To address such issues, Synthetic Antiferromagnets (SAF) have been studied to simultaneously enhance DW speed, density, and to minimize the impact of stray fields [5]. However, using a SAF-based DW track in nanoscale devices is still unexplored. Here, we show that a SAF (Pt/Co/Ru/Co) can be implemented as a DW track material in nanoscale devices with CoFeB/MgO-based MTJ read/write components thanks to the hybrid free layer (HFL) design [4]. We then demonstrate that the switching behavior of a SAF can be electrically detected via Tunneling Magnetoresistance (TMR). In our devices, the CoFeB layer ferromagnetically couples to the top Co layer of the SAF, allowing the detection of its switching via a TMR measurement. Fig. 2 b-c show the TMR loops as function of field

measured on SAF-HFL MTJs (Fig.2a), revealing two distinct loops driven by different switching mechanisms. In Fig. 2b, upon positive saturation, for decreasing field values (blue curve), the top layer switches at positive field values, indicating signature of antiferromagnetic (AF) coupling in forming the AF configuration. Conversely, Fig. 2c shows the top layer switching at negative values, signifying the breaking of AF coupling. To understand this behavior, we used micromagnetic simulations of an uncompensated SAF structure (Fig.2d) where we observe two distinct switching mechanisms depending on the top layer anisotropy (Fig.2 e-f). The results provide valuable insights into the electrical detection of SAF in nanoscale MTJs, paving the way for high-performance DW devices.

1. S. S. Parkin et al., *Science 320,* 6 (2008). 2. D. Kumar et al., *Physics Reports* 958, 1–35 (2022). 3. R. Blasing *et al.*, *Proc. IEEE* 108, 1303–1321 (2020). 4. E. Raymenants et al., *Nature Electronics* 4, 392–398 (2021). 5. S. S. Parkin and S.H. Yang, *Nature Nanotechnology* 10, 195–98 (2015).

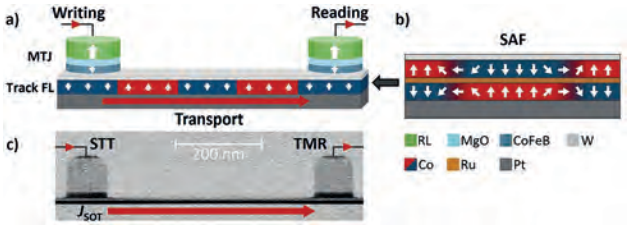

Fig. 1: a) HFL-MTJ-based DW memory; (b) representation of a SAF and (c) TEM image of a DW device.

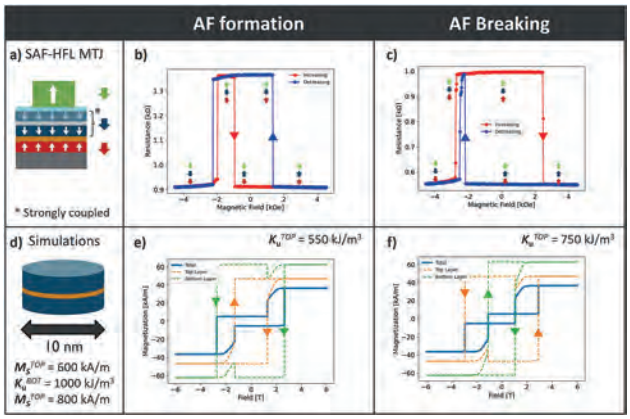

Fig. 2: MTJ (a); measured RH loops (b-c) and simulations (d-e) indicating AF formation and AF breaking switching mechanisms.

DG-09. Bias Dependence of Tunneling Magnetoresistance in Magnetic Tunnel Junctions with Antiferromagnetic Pt_xMn_{1-x}. *A.T. Habiboglu*[1], B. Hong[1], P. Khanal[1], B. Larsen[1], B. Zhou[1], J. O'Brien[1], C. Eckel[1], K. Warrilow[1], A. Enriquez[1] and W. Wang[1] *1. Physics, University of Arizona, Tucson, AZ, United States*

Antiferromagnets have attracted considerable attention due to their promissing properties such as the absence of stray field and the potential for ultrafast switching. Recent advancements revealed non-zero spin polarization in non-collinear antiferromagnets, enabling fabrication of Magnetic Tunnel Junctions (MTJs) with antiferromagnetic electrodes[1,2]. The investigation of voltage-controlled magnetic anisotropy (VCMA) in antiferromagnets has gained interest, with theoretical calculations on VCMA effect in PtMn[3-5]. In our study, we fabricated antiferromagnetic MTJs using Pt_xMn_{1-x} as one of the electrodes. Fig. 1 shows TMR curves measured at various voltages on an MTJ with an antiferromagnetic layer (Buffer\CoFeB\MgO\PtMn\Capping). Sharp switching in Fig. 1a corresponds to CoFeB layer switching, disappearing with increasing bias voltage. In Fig. 1b, the magnetic signal at a larger magnetic field arises from changes in antiferromagnet's magnetic orientation, with stronger signals at higher voltages. To address Joule heating, measurements were conducted at a similar negative and positive voltage values (Fig. 1c). Positive voltage data (Fig. 1c Black) exhibited a TMR signal ten times higher than negative voltage data (Fig. 1c Red), indicating minor role of Joule heating. Signals above 50 Oe originate from magnetic orientation of Pt_xMn_{1-x} electrode, suggesting voltage-controlled magnetic anisotropy and/or spin-polarization of Pt_xMn_{1-x} plays an important role. We investigated a different structure (Buffer\CoFeB\MgO\PtMn\CoFeB\Capping) where sharp switching similar to tunneling anisotropic magnetoresistance based on exchange spring effect[6] was observed (Fig. 2a). Interestingly, TMR changes sign above 200 mV (Fig. 2b), different from MTJs based on IrMn. These results enhance understanding of antiferromagnetic systems and provide insights for advanced spintronics devices. Supported by the National Science Foundation.

X. Chen, T. Higo and K. Tanaka, *Nature*, Vol. 613, p.490 (2023) P. Qin, H. Yan and X.Wang, *Nature*, Vol. 613, p.485 (2023) R. Cheng and Q. Niu, *Phys. Rev. B - Condens. Matter Mater. Phys.*, Vol. 89, p.1 (2014) Y. Su, M. Li and J. Zhang, *J. Magn. Magn. Mater.*, Vol. 505, p.166758 (2020) P.-H. Chang, W. Fang and T. Ozaki, *Phys. Rev. Mater.,* Vol. 5, p.54406 (2021) B. G. Park, J. Wunderlich and X. Martí, *Nat. Mater.*, Vol. 10, p.347 (2011)

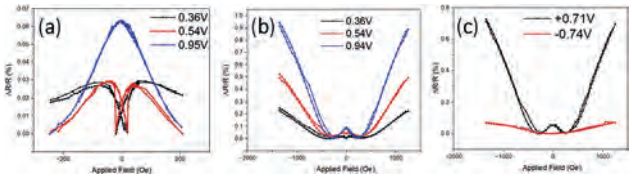

Fig. 1 Room temperature (RT) TMR loops measured with different bias voltages within relatively low (a) and high (b) magnetic field ranges. TMR loops measured at similar positive and negative voltage values are shown in (c).

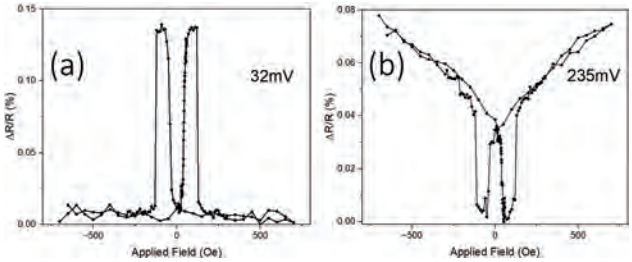

Fig. 2: TMR measurements at RT with relatively low (a) and high (b) bias voltages.

DG-10. Three Types of Nano Crystal Domain Structures in Fully Epitaxial fcc-Co/MgO/Co(111) Magnetic Tunnel Junctions. *C. He*[1], K. Masuda[1], J. Song[1,2], T. Scheike[1], Z. Wen[1], H. Sukegawa[1], Y. Miura[1], T. Ohkubo[1], K. Hono[1] and S. Mitani[1,2] *1. National Institute for Materials Science (NIMS), Tsukuba, Japan; 2. University of Tsukuba, Tsukuba, Japan*

The tunnel magnetoresistance (TMR) effect in magnetic tunnel junctions (MTJs) has been extensively studied for practical spintronic devices such as non-volatile magnetoresistive random access memories (MRAMs). To date, large TMR ratios exceeding 100% have been reported in bcc-(001) MTJs, e.g. Fe/MgO/Fe and CoFeB/MgO/CoFeB, which have been explained by coherent tunneling through "bulk" Δ_1 states [1,2]. A recent theoretical calculation predicted a large TMR ratio above 2000% in the fcc-Co(111)/MgO(111)/Co(111) MTJ due to the "interfacial" resonance effect of *d-p* antibonding states [3]. More recently, a first TMR ratio (35%) has been demonstrated by Song *et al.* [4] in a fully epitaxial fcc(111) MTJ with a ($Co_{90}Fe_{10}$) CoFe/MgO/CoFe structure. In this study, we have systematically investigated the detailed microstructure and its relationship to the TMR properties in the CoFe/MgO/CoFe(111) MTJ using a combination of atomic-resolution scanning transmission electron microscope (STEM) observations and first-principles calculations. We report a rich degree of freedom in the epitaxial relationships and a different TMR mechanism in

the (111)-oriented MTJ. There are three types of lattice matching between CoFe and MgO layers, including a cube-on-cube type (Type-I), a twin-like type (Type-II) and an unexpected in-plane rotation type (Type-III) (Fig. 1). The (111)-oriented MgO barrier is achieved by the extension of (111) atomic planes through different adjacent MgO crystal domains. The formation mechanisms of these three types of MgO domains are reasonably explained by crystallographic analyses. In addition, first-principles calculations revealed that the formation of the Type-III domain significantly suppresses the TMR ratio. Our observations and calculations provide important insights into the design of (111) MTJs, which can overcome the limitations of the conventional bcc(001) MTJs. This work was partly supported by JST CREST (JPMJCR19J4), JSPS KAKENHI Nos. 21H01750, 22H04966, 20K14782 and 23K03933.

[1] S. Ikeda, J. Hayakawa, Y. Ashizawa *et al*., Appl. Phys. Lett. Vol. 93, p.082508 (2008). [2] X. G. Zhang & W. H. Butler, Phys. Rev. B Vol. 70, p.172407 (2004). [3] K. Masuda, H. Itoh and Y. Miura, Phys. Rev. B. Vol. 103, p.064427 (2021). [4] J. Song, T. Scheike, C. He *et al*., https://www.intermag2023digest.com/AOA-09.pdf.

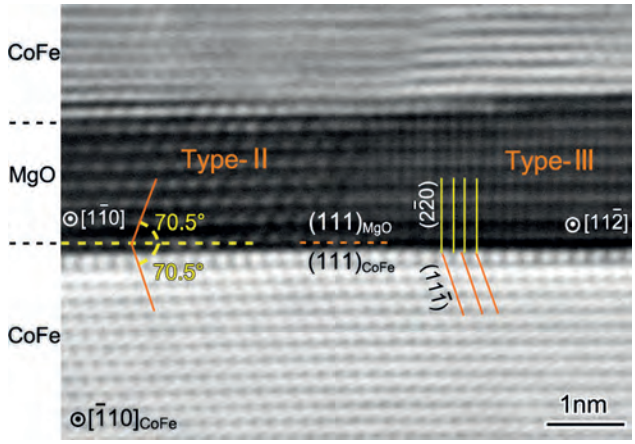

Fig. 1 Atomic-resolution STEM image showing two types of (111)-orientated MTJs. The left one has a twin-like orientation (Type-II) while the right one has an unexpected orientation (Type-III).

DG-11. Design of Domain Wall Magnetic Tunnel Junction Logic Devices and Circuits Using Voltage Controlled Magnetic Anisotropy.

N. Zogbi[1], S. Liu[1], C. Bennett[2], S. Agarwal[2], M.J. Marinella[3], J.C. Incorvia[1] and T.P. Xiao[2] *1. Electrical and Computer Engineering, University of Texas at Austin, Austin, TX, United States; 2. Sandia National Laboratories, Albuquerque, NM, United States; 3. Arizona State University, Phoenix, AZ, United States*

To achieve digital logic using spintronic architectures for edge computing, the device should be all-spintronic, require no magnetic fields to read or write, and be cascadable to form large circuits. The three-terminal domain wall-magnetic tunnel junction (DW-MTJ) logic gate fulfills these requirements and implements a universal gate within a single device [1]. Data is encoded based on the position of the DW, which also forms the free layer of the MTJ. When reading the state of the MTJ, the DW will propagate to its initial state on the free layer. This read current is also used to concatenate logic: if another device is connected to the MTJ and the amplitude of the current is strong enough, the DW of the connected device will propagate. But, challenges remain for the reliability of DW-MTJ logic. Prior designs relied on the inertia of the DW as a way to complete a read operation, which creates errors when conducting multiple reads and writes. Also, implementing different logic functions required modifying the device footprint. Here, instead of relying on DW inertia, we incorporate voltage controlled magnetic anisotropy (VCMA) electrodes into the device (Fig. 1). We also design the device for a constant footprint vs. logic operation and fanout [2]. Using the micromagnetic simulation software MuMax3, we show highly improved reliability, with 100% accuracy when conducting multiple reads and writes. We then simulate a 256×256 systolic array of DW-MTJs and benchmark it against Google's TPU. The results show that using a micro-pipelining technique (Fig. 2), the efficiency and throughput of the systolic array are on par with state-of-the-art CMOS accelerators for neural network inference. These results show that the newly designed nonvolatile spintronic logic devices can be used for edge computing applications while offering robustness under extreme environments. SNL is managed and operated by NTESS under DOE NNSA contract DE-NA0003525.

[1] M. Alamdar, T. Leonard, and J. A. Incorvia, Applied Physics Letters., Vol. 118, p.12401 (2021) [2] N. Zogbi, J. A. Incorvia, and T. P. Xiao, IEEE Journal on Exploratory Solid-State Computational Devices and Circuits., Vol. 9, p.65 (2023)

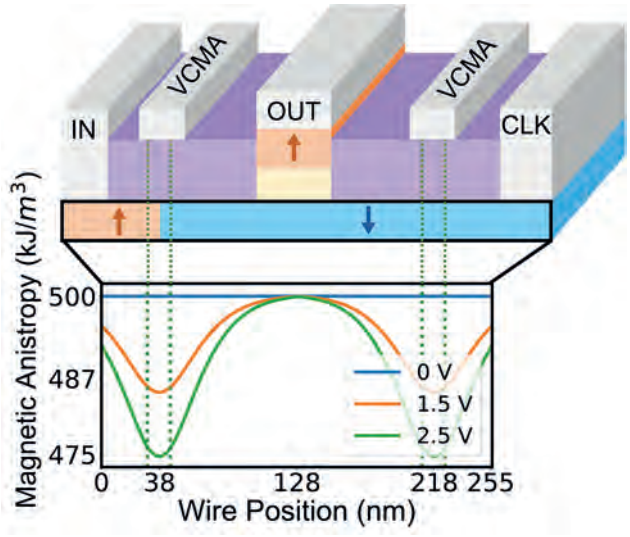

Fig. 1: DW-MTJ logic device schematic with magnetization shown by the arrows. The VCMA electrodes apply voltage through the purple oxide, below is the calculated magnetic anisotropy at various applied voltages.

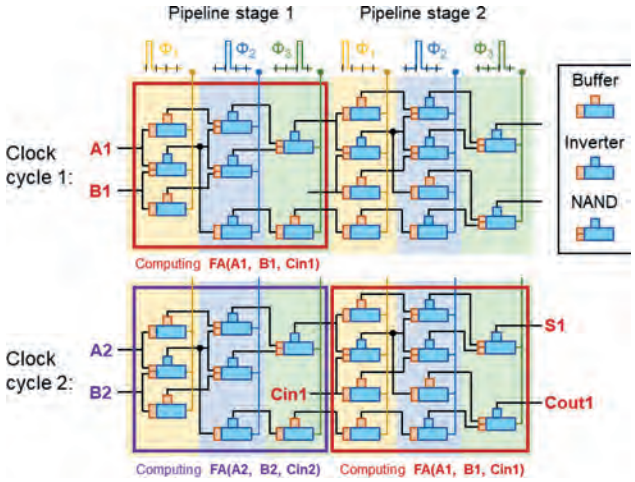

Fig. 2: Illustration of a DW-MTJ full adder and the micro-pipelining technique.

Session DP
STRUCTURED MATERIALS AND MAGNETIC RECORDING
(Poster Session)

Yayoi Takamura, Co-Chair
University of California, Davis, Davis, CA, United States
Varaprasad Bollapragada, Co-Chair
Carnegie Mellon University, Pittsburgh, PA, United States

DP-01. Geometrical Structure induced Magnetic Anisotropy in Three-dimensional Ferromagnetic Iron Nanofilms. *K. Hattori*[1], L.N. Pamasi[1], J. Juharni[1], N. Hosoito[1], N. Mabarroh[1], A.N. Hattori[2], H. Tanaka[2] and S. Yoshimura[3] *1. Nara Institute of Science and Technology, Ikoma, Japan; 2. SANKEN, Osaka University, Ibaraki, Japan; 3. Faculty of Engineering Science, Akita University, Akita, Japan*

Ferromagnetic nanofilms with architected three-dimensional (3D) shapes could be a cutting edge in an enormous application such as data storage, medical diagnosis, and quantum information processing [1,2]. One of the attractive advantages in the 3D-shaped ferromagnetic nanofilms should be to create stable magnetic vortex rather than 2D-patterned nanofilms [3], because of the reduction of a static magnetic energy in magnetic loop where magnetic orientations change slowly in 3D geometrical (e.g. pyramidal shaped) films. Indeed, the realization of magnetic vortex on 3D pyramidal films has been discussed in Landau-Lifshitz-Gilbert (LLG) simulation [4], predicting a specific feature of breaking points (BPs) in magnetization vs. magnetic field (M-H) relations due to creation of stable vortex. In experiment, however, no clear BPs have been confirmed owing to less accuracy in the synthesis of 3D pyramidal films. Recently, our group successfully created 3D pyramidal Fe nanofilms using a combination of photolithography of Si substrates [5,6] and Fe deposition on the 3D pyramidal Si templates in vacuum, which result in BPs implying vortex stabilization (Fig. 1) [7]. To extend the stabilization to control of vortex, systematic study for 3D geometrical structures is required. In this presentation, we will discuss magnetic anisotropic properties of Fe films (150 nm thickness) depending on 3D shape, from square pyramid (edge width W is equal to edge length L = 16 um) to rectangle facet-line structures with different aspect ratio (W/L = 2-10) in M-H curves measured by vibration sample magnetometer. We found that M-H curves were not drastically changed at H parallel to the facet-line direction, while they became cant with increasing the aspect ratio at H perpendicular to the facet line (Fig. 2). The results imply that the vortex across the facet line would be stabilized at the line but not for the vortex along the line. The control of vortex on 3D designed nanofilm will open a new field toward spintronic devices.

[1] F. Nasirpouri, M. A. Engbarth, S. J. Bending, et al., Appl. Phys. Lett. 98, 222506 (2011). [2] F. Nasirpouri, S.-M. Peighambari-Sattari, C. Bran, et al., Sci. Rep. 9, 9010 (2019). [3] R. P. Cowburn, D. K. Koltsov, A. O. Adeyey, et al., Phys. Rev. Lett. 83. 1042 (1999). [4] A. Knittel, M. Franchin, T. Fishbacher, et al., New J. Phys. 12,113048 (2010). [5] A. N. Hattori, S. Takemoto, K. Hattori, et al., Appl. Phys. Express 9, 085501 (2016). [6] S. Takemoto, A. N. Hattori, K. Hattori, et al., Jpn. J. Appl. Phys. 57, 090303 (2018). [7] A. Irmikimov, L. N. Pamasi, K. Hattori, *et al.*, ACS Cryst. Growth Des. 21, 946 (2021).

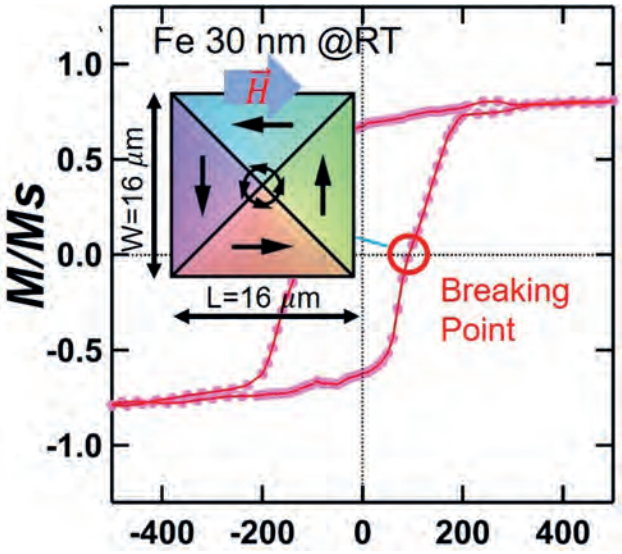

Typical M-H curve with BPs for 3D Fe pyramids, with magnetization schematics.

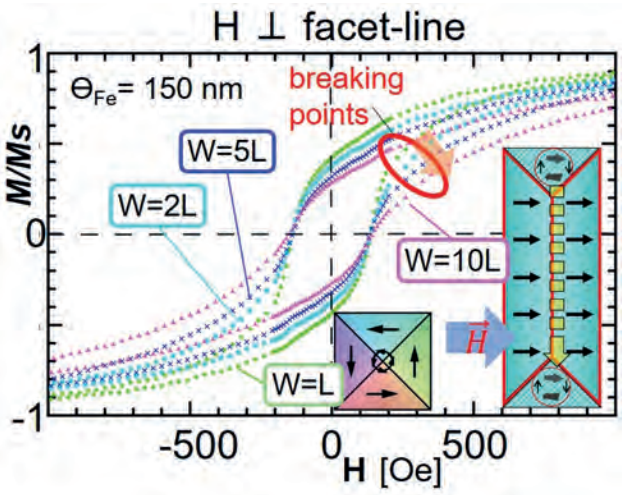

M-H curves for 3D Fe facet-line structure of different aspect ratio under H perpendicular to the facet line direction.

DP-02. Exchange bias mediated by semiconductor with spin-orbit coupling. *A.B. Cahaya*[1], A.A. Anderson[1], A. Azhar[2] and M.A. Majidi[1] *1. Physics, Universitas Indonesia, Depok, Indonesia; 2. Physics and Astronomy, The University of Manchester, Manchester, United Kingdom*

The data writing efficiency on magnetic memory requires effective manipulation of one ferromagnetic layer while fixing the other. By attaching an antiferromagnet into the ferromagnetic layer, an exchange bias can be induced

and the particular ferromagnetic layer become fixed. The microscopic origin is the exchange interaction between ferromagnetic spins and uncompensated spins of antiferromagnet at the magnetic interface[1]. Recently, exchange bias is observed in $La_{0.67}Sr_{0.33}MnO_3/LaAlO_3/SrTiO_3$ heterostructure, which not includes any antiferromagnet[2]. Theoretical study of predicts that interface magnetoelectric effect can induces exchange bias without antiferromagnet[3]. The interface magnetoelectric is mediated by conduction electrons in heterostructure system with spin-orbit coupling. However, $LaAlO_3$ is a semiconductor with large bandgap. In this research we study the exchange bias in the interface of $La_{0.67}Sr_{0.33}MnO_3/LaAlO_3/SrTiO_3$. By modeling $LaAlO_3$ as non-magnetic semiconductor with spin-orbit coupling induced by broken symmetry at the interface, we show that there is interface magnetoelectric effect near $La_{0.67}Sr_{0.33}MnO_3/LaAlO_3$ interface. The magnetoelectric effect enables the coupling of interface spins and electric field at the magnetic heterostructure and induces exchange bias.

[1] R L Stamps 2000. Mechanisms for exchange bias. J. Phys. D: Appl. Phys. 33 R247 (2000), https://doi.org/10.1088/0022-3727/33/23/201 [2] Lü, W., Saha, et al. Long-range magnetic coupling across a polar insulating layer. Nat Commun 7, 11015 (2016). https://doi.org/10.1038/ncomms11015 [3] A. B. Cahaya, et al. Electrically controllable exchange bias via interface magnetoelectric effect. IEEE Trans. Magn. (2023), https://doi.org/10.1109/TMAG.2023.3283526.

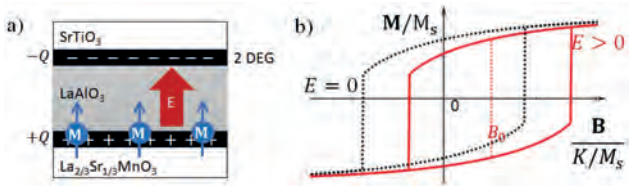

(a) Two dimensional electronic gas (2DEG) at magnetic heterostructure induces electric field. (b) The coupling of magnetization and electric field in magnetoelectric effect enables exchange bias.

DP-03. Study on strength of a 3D structure composed of multiple magnetic microbeads chains. Y. Lin[1], C. Liang[1], *Y. Li*[1] and H. Hsieh[1]
1. Mechanical and Aerospace, Chung-Cheng Institute of Technology, National Defense University, Taoyuan, Taiwan

Magneto-rheological materials have gained much attention because of their prominent controllable properties and potential applications in various fields. To enhance the application of (MRF) based devices, this work is aimed to numerically investigate the strength of 3D solid structure consisting of multiple microbeads chains in the presence of an external magnetic field. The properties of microbeads are density ρ=1500 kg/m^3, diameter d = 4.5 μm with magnetic susceptibility χ= 1.6, saturation magnetization M= 350-400 Oe with an absence of magnetic hysteresis. All the governing equations are numerically solved by COMSOL Multiphysics. Fig. 1 shows the sketch and stress distributions for the 3D solid-like structure composed of multiple microbeads chains subjected to a field strength of 62.8 Oe. When a force of 1x10^{-14} N is applied to a specific microbead, the stress propagates to the other beads around it. Figs. 1(a) and 1(b) respectively demonstrate the regular and staggered pattern of the microbeads formation, which may occur under different field configurations. The total number of the microbead is 99, which constitutes four microbeads layers, each has four rows of microbeads chains. Fig. 1(c) shows the stress distribution on the central line of the four microbeads chains in the first layer of regular pattern. The maximum stress of nearly 0.09 N/m^2 is shown on Node 3 and Node 4 (denoted as N3 and N4, respectively) in Row 2 (denoted as R2) chain. For the stress distribution of staggered pattern shown in fig.1 (d), the maximum stresses on the N3 and N4 in Row 2 decrease to 0.03 N/m^2, while each node of Row 4 bears an insignificant stress. The results show that the staggered pattern can reduce the stress on the nodes between the microbeads and may prevent the rupture of the 3D solid-like structure generated by the MRF. The effects of magnetic field strength, susceptibility, and number of microbeads on the 3D structure will be discussed in the full manuscript.

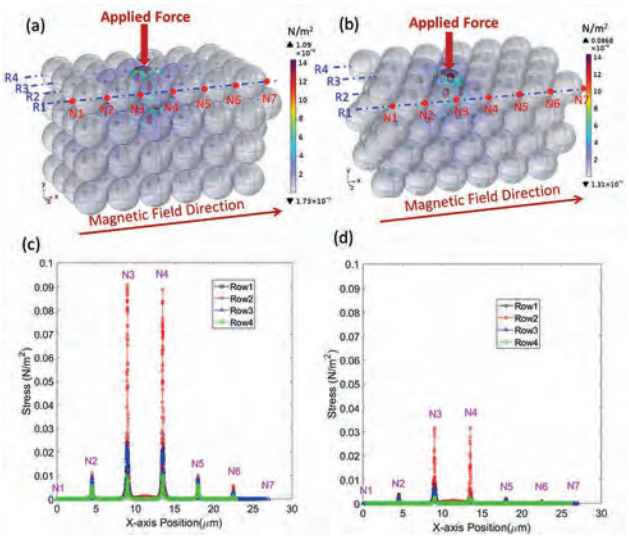

Sketch of 3D structure consisting of multiple microbeads chains in (a) regular and (b) staggered arrangement. (c) and (d) are the stress distributions on the central line of the microbeads chain in the first layer of the 3D structure in (a) and (b), respectively.

DP-05. Phase Enhancement and Crystallinity Tuning of Iron Oxide Nanorods via Annealing. *S.B. Attanayake*[1], A. Chanda[1], R. Das[2], M. Phan[1] and H. Srikanth[1] *1. Physics, University of South Florida, Tampa, FL, United States; 2. South East Technological University, Waterford, Ireland*

Presence of multiple phases of iron oxides in low-dimensional form highlights the significance of them being investigated extensively to tune the phase fractions for their applications in different fields ranging from cancer treatments to spintronics applications[1,2]. While high aspect ratio iron-oxide nanorods exhibited exotic magnetic and inductive heating properties,[3] epitaxially grown highly oriented Fe_3O_4 nanorods showed enhanced perpendicular magnetic anisotropy, which is desirable for magnetic data storage and spintronic applications. In this context, we have performed a comprehensive investigation of the influence of thermal treatment on the magnetic properties of iron oxide nanorods at different temperatures (225 °C – 325 °C) for a fixed duration of time of 3 hours. As-grown nanorods showed Fe_3O_4 with a lower level of crystallinity but with a quite indistinct Verwey transition around 120 K. The sharpness of the Verwey transition boosted and settled at 123 K as the as-grown nanorods were annealed at 250 °C for 3 hours, reflecting an enhanced magnetization, which drastically decreased in samples annealed at higher temperatures. The decreasing magnetization hinted at the presence of an antiferromagnetic (AFM) phase observed to be α-Fe_2O_3 through X-ray diffractometry and later confirmed with the presence of the Morin transition at the 250 K – 260 K range through magnetometry. While the Fe_3O_4 phase was observed to reach its full crystallinity at 250 °C, annealing at higher temperatures produced the α-Fe_2O_3 AFM phase that coexisted and completed with the Fe_3O_4 FM phase, thus reducing the net magnetization. Our study sheds light on the complex magnetism in multiphase nanosystems and paves a new pathway for tunable magnetization of iron oxide nanostructures through phase control.

[1]S. B. Attanayake, A. Chanda, R. Das, N. Kapuruge, H. R. Gutierrez, M.-H. Phan and H. Srikanth, J. Phys.: Condens. Matter 34, 495301 (2022). [2]S. B. Attanayake, A. Chanda, T. Hulse, R. Das, M.-H. Phan and H. Srikanth, Nanomaterials 13, 1340 (2023). [3]R. Das et al., J. Phys. Chem. C 120, 10086–10093 (2016).

DP-06. Synergistic effects of reduced graphene oxide and nickel doping on the magnetic and sensing properties of Ni- Co_3O_4 – rGO nanoparticles. *L.J. Cardenas Flechas*[1] and M. Rincón Joya[2] *1. Mechanical Engineering, Universidad de América, Bogotá, Colombia; 2. Physics, Universidad Nacional de Colombia, Bogotá, Colombia*

This research focuses on developing sensors using a nanocomposite material called Ni-Co_3O_4-rGO, which exhibits both electrical and magnetic properties. The material is synthesized using two different methods to thoroughly investigate its characteristics. The electrical resistivity of the sensors is measured precisely using the four-probe method. To evaluate the sensor's functionality, it is exposed to vapors of methanol, ethanol, and acetone, enabling researchers to examine its responsiveness and selectivity in different environments. Additionally, the study explores the magnetic behavior of the nanocomposite material through magnetic hysteresis analysis, revealing the presence of both paramagnetic and ferrimagnetic characteristics. This finding suggests that the material possesses magnetic properties that can be utilized for specific applications or interactions with external magnetic fields. Moreover, the research emphasizes the impact of reduced graphene oxide (rGO) on the nanocomposite's magnetic properties. By incorporating rGO into cobalt oxide nanoparticles, the material's magnetization is enhanced, enabling effective interaction with electrical, magnetic, and electromagnetic energies. This characteristic expands the potential applications of the nanocomposite beyond conventional sensing, highlighting its versatility across various technological domains.

[1] Min, S., Zhao, C., Chen, G., & Qian, X. (2014). One-pot hydrothermal synthesis of reduced graphene oxide/Ni (OH) 2 films on nickel foam for high performance supercapacitors. Electrochimica Acta, 115, 155-164. [2] Liu, Y., Fergus, J. W., & Cruz, C. D. (2013). Electrical properties, cation distributions, and thermal expansion of manganese cobalt chromite spinel oxides. Journal of the American Ceramic Society, 96(6), 1841-1846. [3] Iranshahi, S., & Mosivand, S. (2022). Cobalt/graphene oxide nanocomposites: Electro-synthesis, structural, magnetic, and electrical properties. Ceramics International, 48(9), 12240-12254. [4] Cardenas-Flechas, L.J.; Freire, P.T.C.; Paris, E.C.; Moreno, L.C.; Joya, M.R. Temperature-induced structural phase transformation in samples of Co 3 O 4 and Co 3-x Ni x O 4 for CoO. Materialia 2021, 18, 101155. [5] Cardenas Flechas, L.J.; Raba Paéz, A.M.; Rincon Joya, M. Synthesis and evaluation of nickel doped Co3O4 produced through hydrothermal technique. DYNA 2020, 87, 184–191. [6] Cárdenas Flechas, L. J. Síntesis y caracterización de nanoestructuras de Co3O4 dopadas con Ni para aplicación en detección de gases (Doctoral dissertation, Universidad Nacional de Colombia). Flechas, L. J. C., Martín, E. X., Sanchez, J. A. P., Ribera, J. M. C., & Joya, M. R. (2023). Effect of nickel and rGO on the photocatalytic properties of Co3-xNixO4 prepared with citric acid and CTAB. Materials Today Communications, 106406.

DP-07. Withdrawn

DP-08. Domain Wall Creep for Assessing Exchange-Bias in Ferromagnet/Antiferromagnet Thin Films. *M. Hasan*[1] and G. Beach[1] *1. Department of Materials Science and Engineering, Massachusetts Institute of Technology, Cambridge, MA, United States*

Exchange-bias (EB) is an important phenomenon that has found use in devices such as spin-valves and magnetic read-heads, and has been proposed as a component for emerging applications such as field-free spin orbit-torque switching, domain-wall based devices etc. For engineering such devices, understanding EB and characterizing it thoroughly is essential. Most commonly, EB is measured via acquisition of hysteresis loops (HL) using vibrating sample magnetometry or magneto optic kerr effect (MOKE) magnetometry. However, magnetization in thin films reverse via localized nucleation of domains and their subsequent growth, two aspects that are not normally seperably in a HL measurement. The outcome of such measurements is tied to the nucleation process at a local defect, which may or may not reflect the properties of the area surrounding the nucleation sites. Domain wall (DW) dynamics, on the other hand, is influenced only by the properties at the location of the DW. Because EB acts as an effective field on the ferromagnet, its effect on DW motion is also of the same nature, enabling the extraction of local EB from DW motion. In this work, we show that by combining focused laser MOKE and domain wall creep dynamics it is possible to measure EB at nucleation sites and away from these sites independently. Our measurements confirm that the EB at nucleation sites can vary widely and be significantly different from areas away from them. Utilizing DW creep dynamics in regions away from nucleation sites can yield EB values that truly represent the area being measured. Furthermore, we show that relying just on focused laser MOKE can misrepresent the local properties and/or lead to wrong conclusions. Our results showcase the usefulness of DW creep measurements for assessing EB in thin films, as well as highlight the importance of being aware of the local nucleation pattern for high resolution MOKE measurements.

DP-09. 3D Structure of Dipole Antiskyrmion in Fe/Gd Multilayers. *J.A. Reddinger*[1] and B. McMorran[1] *1. Physics, University of Oregon, Eugene, OR, United States*

Fe/Gd multilayers host a variety of magnetic textures including magnetic bubbles, skyrmions, and antiskyrmions. Fe/Gd lacks any Dzyaloshinskii-Moriya Interaction but interfacial. Instead its textures are primarily stabilized by dipole and exchange interactions, leading to interesting 3D structures. In previous works, we have studied the 3D structure of the skyrmion in Fe/Gd using a combination of data collected by NIST's Scanning Electron Microscope with Polarization Analysis (SEMPA) and Lorentz Transmission Electron Microscopy (LTEM) and the micromagnetic simulation software Mumax3. By applying the same analysis to antiskyrmions found in Fe/Gd, we uncover the antiskyrmion's more complex structure and develop a 3D analytical model. Fig 1 shows a real space image of the antiskyrmion's surface magnetization collected by SEMPA. The most notable feature here is the preference for the in-plane magnetization to point outwards from the core. This is a closure domain, analogous to the Néel caps found in dipole skyrmions. Fig 2 shows micromagnetics simulation of the antiskyrmion. The top and bottom layers feature the closure domains with bottom layer in-plane magnetization pointing mostly inwards vs the top layer's pointing mostly outwards. The middle layer features a symmetric antiskyrmion with balanced inplane magnetization. This structure agrees with SEMPA and LTEM data. An analytical model is developed from simulation. The magnetization's angle of inclination is given by: $\Theta(r,z,\varphi) = 2*\arctan((r/k)^{\wedge}\alpha)$, where $k(z,\varphi)$ is the domain wall radius, $\alpha(z,\varphi)$ is the domain wall thickness. The magnetization's in-plane angle is given by: $\Phi(r,z,\varphi) = \Phi\_0 + \mathrm{mod}[\varphi + \arctan((\sin(\varphi)\cos(\varphi)) / (\sin(\varphi)\sin(\varphi) - p)), \pi]$, where Φ_0 and p are functions of r and z.

A. Vansteenkiste, J. Leliaert and M. Dvornik, AIP Advances, Vol 4, Issue 10 (2014) S. A. Montoya, S. Couture and J. J. Ches, Physical Review B, Vol 95, Issue 2 (2017)

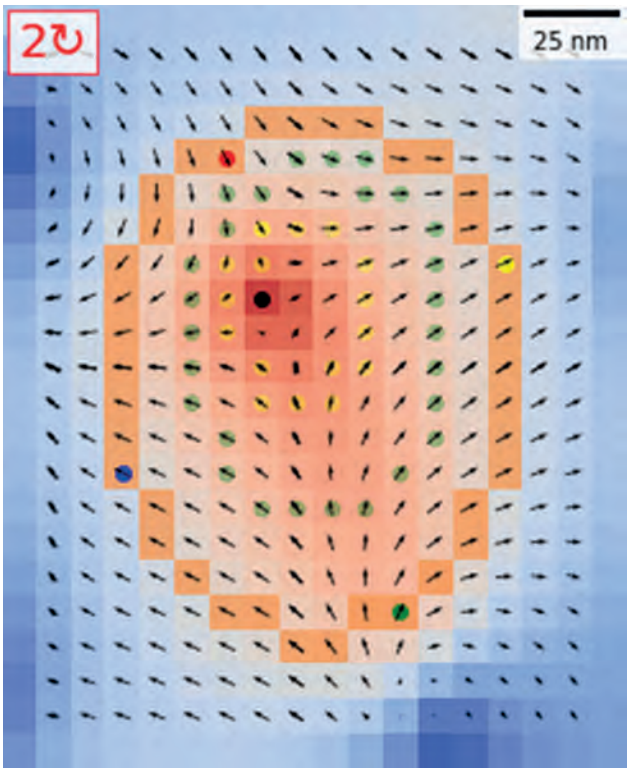

Fig 1. SEMPA surface magnetization data of an antiskyrmion in Fe/Gd. The asymmetry of the in-plane magnetization through the domain wall is analogous to the skyrmion's closure domain.

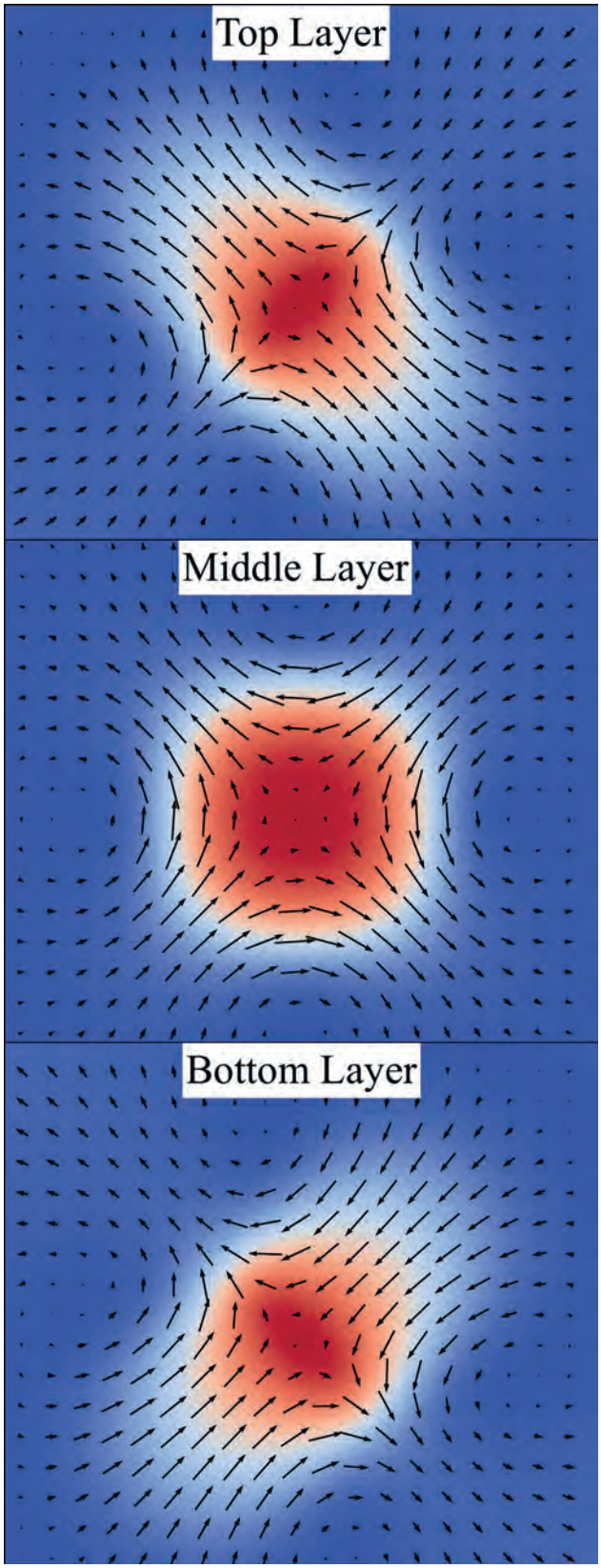

Fig 2. Micromagnetic simulation of an antiskyrmion in Fe/Gd. Notable features: depth dependent eccentricity, depth/azimuth dependent domain wall thickness, atypical closure domains. Colormap shows mz component, red out of page, blue into page.

DP-10. Withdrawn

DP-11. Comparison of Magnetization Thermal Stability for MAMR Media with Different Layer Anisotropy Structures. *T. Tanaka*[1], X. Ya[2], S. Onaka[1] and Y. Kanai[3] *1. ISEE, Kyushu University, Fukuoka, Japan; 2. Artificial Intelligence and Big Data College, Chongqing College of Electronic Engineering, Chongqing, China; 3. Department of Engineering, Niigata Institute of Technology, Kashiwazaki, Japan*

Microwave-assisted magnetic recording (MAMR) [1] is a technology which can potentially increase the areal recoding density. Layer anisotropy structured media, such as notched and graded types, have been proposed [2] for improving MAMR writability as well as MAMR recording characteristics. Our previous study has shown that enhanced MAMR writability can be observed in four-layered media when one of the top three layers has a large anisotropy field[3]. In the present study, microwave-assisted magnetic recording characteristics and magnetization thermal stability for layer anisotropy structure media were compared. Fig. 1(a) illustrates the layer anisotropy structure of three types of recording media assumed in this study. Recording characteristics were evaluated in terms of signal-to-noise ratios (SNR), where a 30-nm-wide SPT head with a spin torque oscillator with the frequency at 22 GHz [4] and Voronoi grain medium model ($<D>$ = 5.4 nm) were assumed in recording process. Fig. 2(a) presents SNRs as a function of weight averaged H_k for the media, which indicates that SNR reaches a maximum at $H_{k.ave}$ = 21 kOe for Large H_{k1} media because of moderate microwave assistance without wide writings. SNR comparison among the three type meida is explains that MAMR writability is sensitive to layer anisotropy structures. Fig. 2(b) compares magnetization thermal stability indexes $<\Delta E>/k_BT$ @ 300 K. Here, averaged energy barrier height $<\Delta E>$ were numerically estimated using the nudged elastic band method. The indexes decrease with decrease in the linear density reflecting the effect of the demagnetizing fields for recorded bits. The figure indicates that magnetization thermal stability for Large H_{k1} media retains greater than 70, but is the lowest among the three types of layer anisotropy structure media. The probable reason is that coherency (R) in magnetization switching was slightly lower for Large H_{k1} media (R = 0.80) compared with the other media (R = 0.81 and 0.84 for Large H_{k2} and Large H_{k3}, respectively).

[1]J. G. Zhu et al., *IEEE Trans. Magn.*, 44, pp. 125-131(2008).[2]X. Bai and J. G. Zhu, *IEEE Magn. Lett.*, 7, p. 4507904(2016).[3]K. Kurihara et al., MMM2022 Abstruct book, IPA-07 (2022).[4]Y. Kanai et.al, *IEEE Trans. Magn.*, 55, 3000613(2019).

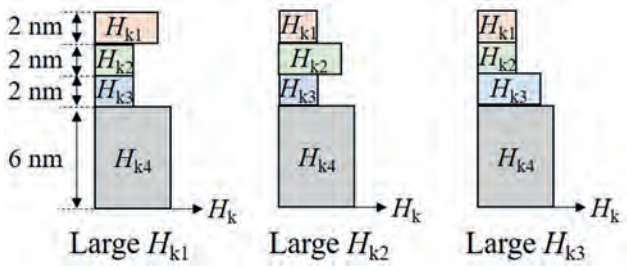

Fig. 1 Three types of layer anisotropy structures.

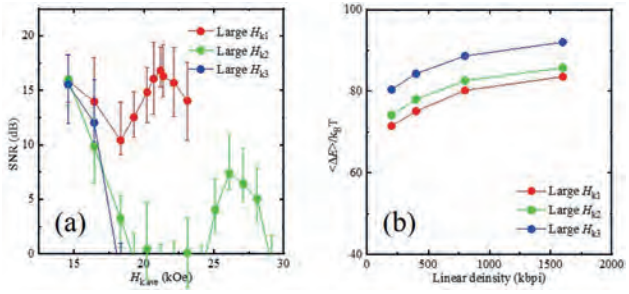

Fig. 2 (a) MAMR characteristics and (b) magnetization thermal stability indexes.

DP-12. Suppression of in-plane (001) texture component in FePt-oxide granular films by adding a carbon buffer layer. *K. Tham*[1], R. Kushibiki[1] and S. Saito[2] *1. Tanaka Kikinzoku Kogyo K. K., Tsukuba, Japan; 2. Electronic Engineering, Tohoku University, Sendai, Japan*

The $L1_0$ type FePt phase is attracting attention as the heat assisted magnetic recording medium material due to its high uniaxial crystalline magnetic anisotropy energy of 5×10^7 erg/cm^3 at room temperature. To obtain a granular structure with fine columnar and isolated magnetic grains, high *c*-axis orientation, and high degree of order, the research of adding various grain boundary materials (GBMs), such as C[1,2], SiO_2[3], TiO_2[4], MgO[5], Ta_2O_5[6], B_2O_3[7] into FePt thin films have been widely conducted. Based on our previous study, most of FePt granular films with oxides have high ratio of in-plane (001) texture component[8] than that of with C. Many reports show that the in-plane component is induced by surface roughness, grain size, crystal orientation of MgO underlayer[9]. To address this issue, we have carried out an experiment to avoid a direct contact between MgO underlayer and oxide GBM by adding a buffer layer in between those layers. In this paper, we will report the evaluation result of nanostructure and magnetic properties of the granular films added with a carbon buffer layer. Fig. 1 shows *M-H* loops of FePt-B_2O_3 granular films with various C buffer thickness. Film structure is shown in the inset. Larger hysteresis can be observed with addition of a C buffer layer (0.6 nm). With further increase in thickness of the C buffer layer (1.0 nm), the hysteresis becomes smaller. This suggests that the employment of the thin C buffer layer is effective to improve magnetic properties. Fig. 2 shows in-plane XRD profiles for FePt-B_2O_3 granular films with various various C buffer thickness. For all films, mainly, the (110), (200), and (220) diffractions from $L1_0$-FePt phase are observed, which indicates that FePt grains have *c*-plane sheet texture. Concerning other diffractions, the integral intensities of (001) diffraction for FePt-B_2O_3 granular films with the C buffer layer (> 0.6 nm) is significantly reduced which indicates that the ratio of FePt grains with their *c*-axes parallel to film normal is reduced by using the C buffer layer.

1) J. S. Chen et al., *Appl. Phys. Lett.*, 91, 132506 (2007). 2) A. Perumal et al., *J. Appl. Phys.*, 105, 07B732 (2009). 3) E. Yang et al., *J. Appl. Phys.*, 104, 023904 (2008). 4) Y. F. Ding et al., *Appl. Phys. Lett.*, 93, 032506 (2008). 5) Y. Peng et al., *J. Appl. Phys.*, 99, 08F907 (2006). 6) B. C. Lim et al., *J. Appl. Phys.*, 105, 07A730 (2009). 7) T. Saito et al., *Jpn. J. Appl. Phys.*, 59, 045501 (2020). 8) K. K. Tham et al., 2021 IEEE INTERMAG, 1-5 (2021), doi: 10.1109/INTERMAG42984.2021.9580144. 9) J. Wang et al., *Acta Mater.*, 91, 41 (2015).

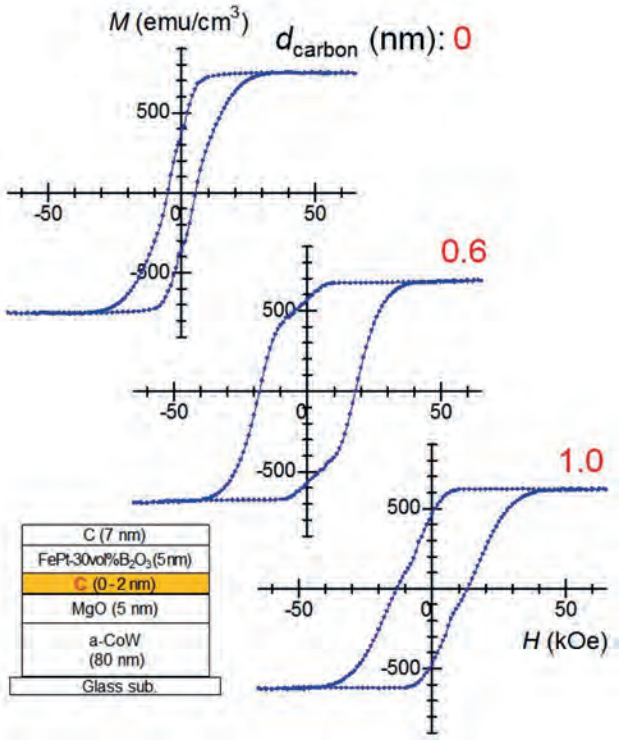

***M-H* loops of FePt-B_2O_3 granular films with various C buffer thickness. Film structure is shown in the inset.**

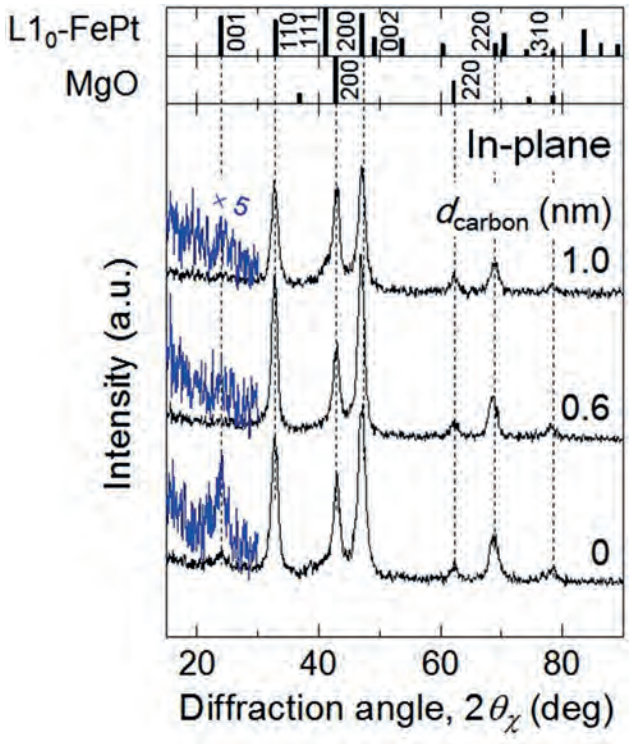

In-plane XRD profiles for FePt-B_2O_3 granular films with various C buffer thickness.

Session DQ
INTERDISCIPLINARY TOPICS II: MAGNETIC FORCES AND NANOPARTICLES; BIOMEDICINE; EDUCATION AND OUTREACH
(Poster Session)

Frank M Abel, Chair
National Institute of Standards and Technology, Gaithersburg, MD, United States

DQ-01. Integration of Fiber Tracts in Anatomically Accurate Brain Models during Transcranial Magnetic Stimulation. C.J. Lewis[1], C.M. Harris[2,4], N. Mittal[1], C.L. Peterson[1] and *R.L. Hadimani*[2,3]
1. Biomedical Engineering, Virginia Commonwealth University, Richmond, VA, United States; 2. Mechanical and Nuclear Engineering, Virginia Commonwealth University, Richmond, VA, United States; 3. Psychiatry, Harvard Medical School, Boston, MA, United States; 4. Center for Biological Data Science, Virginia Commonwealth University, Richmond, VA, United States

Introduction: White matter derived fiber tractography approaches have been used to establish subcortical architecture and have shown influence in transcranial magnetic stimulation (TMS) response [1,2]. We are unaware of any studies which have successfully implemented fiber tracts into segmented head models for finite element analysis (FEA). This study aims to evaluate how integrated fiber tracts into FEA simulations of TMS influences resting motor threshold (RMT). Methods: 9 non impaired participants from the previously mentioned studies [1,2] underwent diffusion tensor imaging (DTI), structural magnetic resonance imaging (MRI), and TMS. DSI studio [3] was used to create fiber tracts in the region of interest from DTI and export 3-D modeled tracts into Sim4life [1,2]. Sim4life FEA simulations were prepared with tracts implemented into the head model, expanding on the methods of Mittal, et al. [2]. The induced electric field strength (EFS) on the fiber tracts were obtained from FEA simulations along the depth of each embedded fiber tract. Linear regression and linear mixed effects models (LMEM) were created in R Studio to evaluate the effects of the induced electric field strength on RMT [1,2]. Results: The maximum induced EFS on the tract was found to correlate with RMT for both the biceps and first dorsal interosseous (FDI) evaluated against RMT as evident by an increase in R^2 however these results did not reach significance. The incorporation of the induced electric field strength along the tract depth did not influence FDI RMT in linear mixed effects modeling ($\chi 2 = 0$, $p = 1$). Conclusion: The improvement in R^2 with linear regression modeling suggests the incorporation of fiber tracts into FEA simulations of TMS provides a more accurate predictor of RMT when EFS is considered alone. The lack of improvement in the prediction of RMT with (LMEM) suggests the incorporation of fiber tracts into FEA of induced EFS does not improve the prediction of RMT when other effects are considered. This may be indicative of the diversity of fiber tract function apart from transmission between the motor cortex and spinal cord.

References: [1] Mittal, N., Thakkar, B., Hodges, C. B., Lewis, C., Cho, Y., Hadimani, R. L., & Peterson, C. L. (2022). Effect of neuroanatomy on corticomotor excitability during and after transcranial magnetic stimulation and intermittent theta burst stimulation. Human Brain Mapping, 43 (14), 4492– 4507. https://doi.org/10.1002/hbm.25968 [2] N. Mittal, C. Lewis, Y. Cho, C. L. Peterson and R. L. Hadimani, "Effect of Fiber Tracts and Depolarized Brain Volume on Resting Motor Thresholds During Transcranial Magnetic Stimulation," in IEEE Transactions on Magnetics, vol. 58, no. 8, pp. 1-6, Aug. 2022, Art no. 5000306, doi: 10.1109/TMAG.2022.3148214. [3] Yeh FC. Population-based tract-to-region connectome of the human brain and its hierarchical topology. Nature communications. 2022 Aug 22;13(1):1-3.

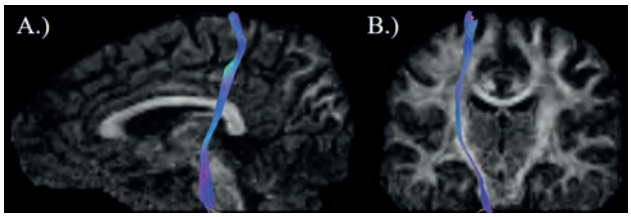

Fig 1. Fiber Tracts in Sagittal View (A) and Coronal View (B)

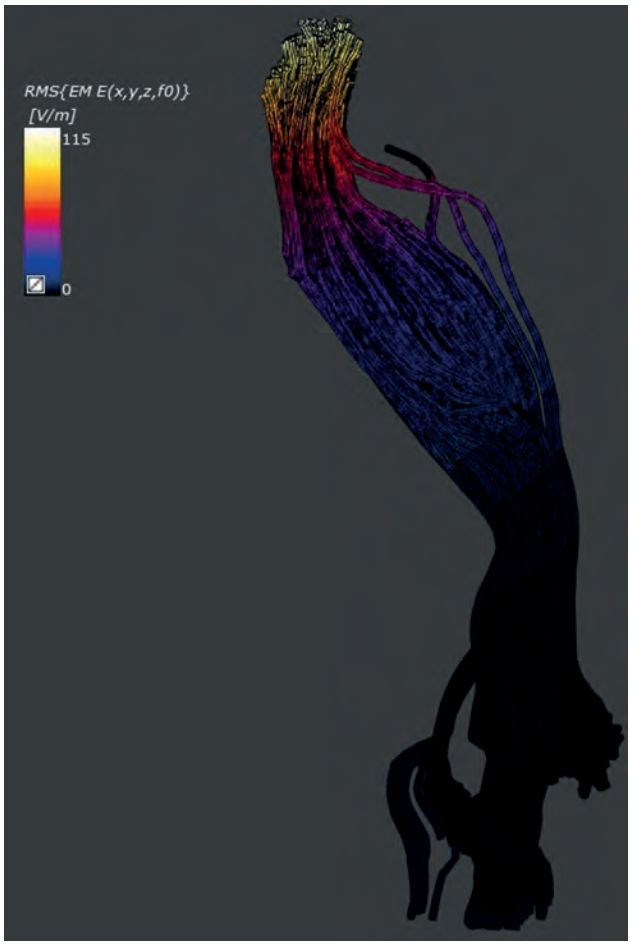

Fig 2. Sim4life FEA of Fiber Tractograpy

DQ-02. Withdrawn

DQ-03. The Effect of Functional Magnetic Resonance Imaging Connectivity on Transcranial Magnetic Stimulation Outcomes in Schizophrenia Participants. C.J. Lewis[1], N. Mittal[1,2], A.K. Pandurangi[4], U.M. Mehta[5] and *R.L. Hadimani[2,3] 1. Biomedical Engineering, Virginia Commonwealth University, Richmond, VA, United States; 2. Mechanical and Nuclear Engineering, Virginia Commonwealth University, Richmond, VA, United States; 3. Psychiatry, Harvard Medical School, Boston, MA, United States; 4. Psychiatry, Virginia Commonwealth University, Richmond, VA, United States; 5. Psychiatry, National Institute of Mental Health & Neurosciences, Bangalore, India*

Introduction: SRepetitive transcranial magnetic stimulation (rTMS) has previously been shown to treat both the positive and negative symptoms of schizophrenia [1]. The dosage parameter for rTMS is the resting motor threshold (RMT) which is known to vary with limited understanding. Previous investigations have used functional magnetic resonance imaging (fMRI) to predict RMT in healthy participants [2]. The goal of this study was to investigate the extent RMT could be predicted from fMRI when anatomy and the presence of schizophrenia are considered. Methods: 54 participants with schizophrenia and 43 controls of a previous investigation were included [1]. Participants underwent fMRI, structural MRI, and TMS [1]. FSL was used for fMRI preprocessing of the scans into 25 independent components. 7 components were chosen for analysis based on relationships to the motor cortex (Fig 1). Principal component analysis (PCA) was used to identify interactions between the selected channels for input parameters along with depolarized gray matter volume (DGMV) in linear mixed effects models (LMEM) for associations with RMT [3]. Results: *Control Population* PCA identified relationships between fMRI channels 3 and 4, 1 and 7, 5 and 7, and channels 3 and 5. DGMV, fMRI channel 2, the interaction between fMRI channels 5 and 7, and the interaction between fMRI channels 1 and 7 were required for the LMEM to converge and were therefore assessed as significant. The interaction between fMRI channels 3 and 5 was also associated with RMT ($p < 0.001$). RMT and DGMV were found to be negatively correlated using Spearman's correlation ($p < 0.001$). *Schizophrenia Population* PCA identified relationships between fMRI channels 1 and 3, 1 and 6, 3 and 4, 3 and 6, and channels 4 and 6. fMRI channel 2 was associated with RMT ($p < 0.001$). No other parameters were associated with RMT. The different PCA identified fMRI channels suggest functional networks are influenced by the presence of schizophrenia. Similarly, RMT had different relationships with fMRI and MRI parameters between the two groups suggesting schizophrenia changes brain organization.

References: [1] C. J. Lewis, E. Cheng, U. M. Mehta, A. K. Pandurangi and R. L. Hadimani, "The Effect of Coil to Cortex Distance and Induced Electric Field Strength on Resting Motor Thresholds in Schizophrenia Patients," in IEEE Transactions on Magnetics, doi: 10.1109/TMAG.2023.3282784. [2] Rosso C, Perlbarg V, Valabregue R, Obadia M, Kemlin-Méchin C, Moulton E, Leder S, Meunier S, Lamy JC. Anatomical and functional correlates of cortical motor threshold of the dominant hand. Brain Stimul. 2017 Sep-Oct;10(5):952-958. doi: 10.1016/j.brs.2017.05.005. Epub 2017 May 17. PMID: 28551318. [3] Chen A, McCarron M, Schooner L, Brasfield K, Chesley J, et al. (2022) Transcranial Magnetic Stimulation for Schizophrenia: A Meta-Analysis. Clin Psychiatry. 8.11.169. [4] Cheng Y, Zamrini E, Ahmed A, Wu W-C, Shao Y, Zeng-Treitler Q. Medication-Wide Association Study Plus (MWAS+): A Proof of Concept Study on Drug Repurposing. Medical Sciences. 2022; 10(3):48. https://doi.org/10.3390/medsci10030048

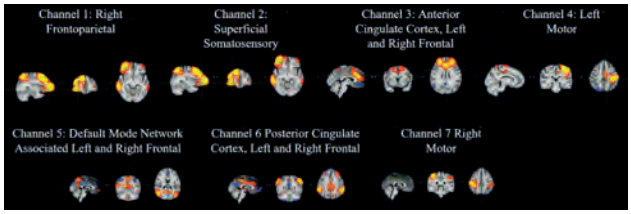

Fig 1. fMRI Channels

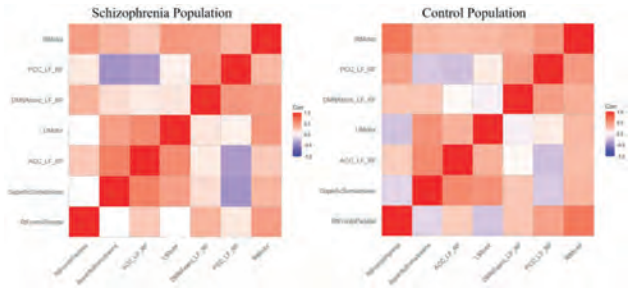

Fig 2. Correlation Matrix of fMRI Nodes

DQ-04. Ferrofluid droplets for visualizing tides in educational settings. *Z. Boekelheide[1] 1. Physics, Lafayette College, Easton, PA, United States*

It is commonly known that Earth's ocean tides are related to the Moon's gravity. However, many students misunderstand the mechanism[1]. Tidal effects specifically refer to effects of *nonuniform* forces. In the case of Earth's ocean tides, the nonuniform force is the Moon's gravity, stronger on the side of Earth closest to the Moon and weaker on the side farthest from the Moon, which causes slight stretching of Earth's oceans. Ferrofluid droplets falling towards a permanent magnet have been used as a clever way to visualize how tidal forces can cause stretching/elongation of the droplets[2]. Is this a demonstration (i.e. the stretching is truly caused by tidal effects) or a visual analogy (i.e. stretching and tidal effects occur but are not causative)? Because the magnetic self-energy of a ferrofluid droplet is decreased by elongation in the presence of even a *uniform* magnetic field[3,4], the observed elongation is not necessarily caused by tidal effects. It can be shown that elongation of a ferrofluid droplet due to tidal effects is very sensitive to the distance to the permanent magnet ($\sim 1/r^8$), while that due to self-energy effects is less sensitive. Thus, elongation of a droplet falling towards a permanent magnet is expected to be initially dominated by magnetic self-energy effects; tidal effects could begin to dominate as the droplet approaches the magnet. The crossover between regimes depends on experimental parameters (strength of magnet, susceptibility of ferrofluid) and the dominant mechanism of ferrofluid droplet elongation is a question that is accessible to student hands-on, open-ended experimentation. Students with access to simple lab equipment such as electro- and permanent magnets, commercial ferrofluid, and smartphone cameras (high-speed cameras if available) can design and execute their own experiments to test the dominant mechanism of ferrofluid droplet elongation.

[1] John R. Taylor, Classical Mechanics, University Science Books (2005). [2] Dianna Cowern, "SLOW MOTION SCIENCE! Ferrofluid dropping on magnet", https://www.youtube.com/watch?v=04v4qWVtdPs, YouTube (2017) [3] B. D. Cullity and C. D. Graham, Introduction to Magnetic Materials, 2nd ed. IEEE Press (2009) [4] M. Beleggia, M. De Graef, and Y. T. Millev, J. of Phys. D: Applied Physics, 39, 891 (2006).

Elongation of a ferrofluid droplet in a quasi-uniform magnetic field (Helmholtz coil).

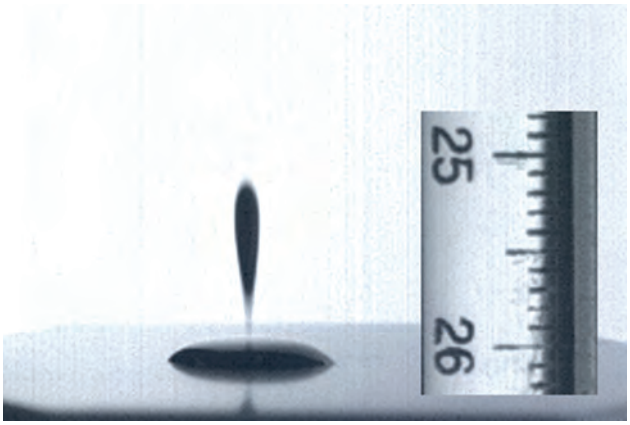

Elongation of a ferrofluid droplet in a nonuniform magnetic field (as it approaches a permanent magnet).

DQ-05. Mn-Zn ferrite nanoparticles as an agent for imaging and hyperthermia treatment. N. Kataoka[1], T. Ishikawa[1], T. Kondo[1], A. Usui[3], Y. Hosokai[4] and *Y. Ichiyanagi*[1,2] *1. Physics, Yokohama National University, Yokohama, Japan; 2. Osaka University, Toyonaka, Japan; 3. Medicine, Tohoku University, Sendai, Japan; 4. Radiological Sciences, International University of Health and Welfare, Otawara, Japan*

$Mn_{1-x}Zn_xFe_2O_4$ ($0 \le x \le 1.0$) nanoparticles surrounded by amorphous SiO_2 were prepared by an original wet chemical method, and DC magnetization measurements revealed that the maximal magnetic value M_S (38.9 emu/g at 300 K) was observed for x = 0.2. AC magnetic measurements were performed for five different particle sizes of $Mn_{0.8}Zn_{0.2}Fe_2O_4$ nanoparticles between 13 and 30 nm. From the temperature dependence of the imaginary part of magnetic susceptibility, a peak was observed at the particle size of 18 nm. T_2 relaxation curves were measured for various particle sizes of $Mn_{0.8}Zn_{0.2}Fe_2O_4$ nanoparticles in magnetic field of 0.3 T, resonance frequency of 13 MHz of MRI system at room temperature. As a result, compared to agarose as the background, the obtained particles exhibited a significant T_2 shortening effect for all the samples (Fig.1). Interestingly, he highest relaxation rate observed for 18-nm nanoparticles, which were most effective particle size for hyperthermia treatment in our previous report. A clear, significant contrast with the background of agarose was observed for the samples with particle size of 18 nm even with a short echo time of approximately 50 ms. Furthermore, the third harmonic responses of Mn-Zn ferrite nanoparticles were measured under an AC magnetic field, suggested their application for magnetic particle imaging. Mn-Zn ferrite nanoparticles indicate their potential for theranostics agents.

[1] T. Kondo, K. Mori, M. Hachisu, T. Yamazaki, D. Okamoto, M. Watanabe, K. Gonda, H. Tada, Y. Hamada, M. Takano, N. Ohuchi, and Y. Ichiyanagi, "AC Magnetic Susceptibility and Heat Dissipation by $Mn_{1-x}Zn_xFe_2O_4$ Nanoparticles for Hyperthermia Treatment" *J. Appl. Phys.,* 117 17D157, 2015. [2] Sota Hamada, Kota Aoki, Keita Kodama, Kentaro Nashimoto, Yuko Ichiyanagi, "AC magnetic susceptibility and heat dissipation of Zn-doped Mg-ferrite nanoparticles", *J. Magn. Magn. Mater.* 559 (2022) 169536

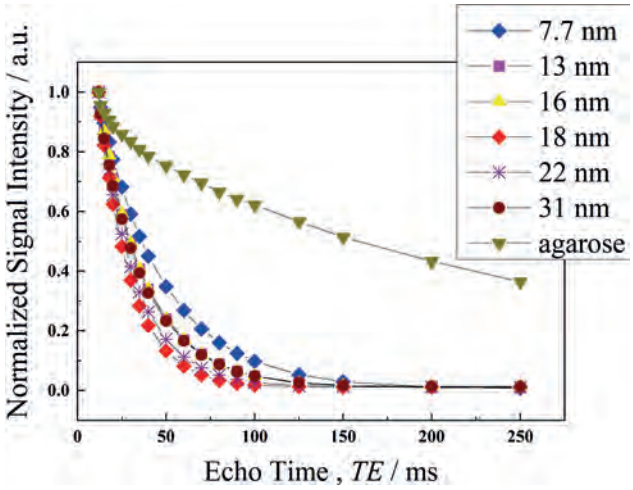

Fig.1 *T*2 relaxation curves of Mn-Zn ferrite nanoparticles for various particle sized and agarose samples are shown for comparison.

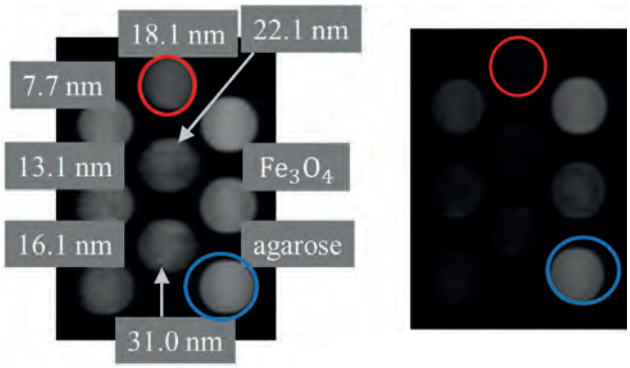

Fig.2 Phantom image of a *T*2-weighted image for Mn-Zn ferrite nanoparticles and agarose samples.

DQ-06. Magnetic response of the magnetic nanoparticles/protein aggregation for protein detection. K. Kaneko[1], T. Murayama[1], J. Honda[1], L. Tonthat[1], K. Okita[1] and *S. Yabukami*[1] *1. Tohoku University, Sendai, Japan*

1. Introduction There is a strong need for rapid detection of proteins, such as many biomarkers for diagnosing metastatic cancer, mitochondrial disease, hypertension, etc. We successfully detected bacteria using the magnetic properties of antigen-antibody reaction aggregates and obtained a high correlation with PCR [1][2]. However, since proteins are far smaller than bacteria, detecting differential magnetic signals with and without the protein is more challenging. In the present study, we have found the new phenomenon that highly dense proteins are likely to aggregate magnetic nanoparticles like a new binder. This is probably because the proteins help to bind with magnetic nanoparticles in certain conditions. The popular proteins (GDF-15) are detected with several concentrations, and we analyze the mechanism by which the protein facilitates the aggregation of magnetic nanoparticles. 2. Experimental procedure Magnetic nanoparticles (Nanomag-D, 500 nmΦ) with an antibody were reacted protein (GDF-15). The samples of GDF-15 were prepared to 0, 1, 10, and 100 ng/ml. The electromagnet made the aggregations with a sharp magnetic yoke. Our magnetic sensor detected the aggregates' magnetic response [1]. 3. Experimental results Fig. 1 shows optical micrographs of magnetic nanoparticles/antigen aggregates with stepwise protein (GDF-15) concentration changes. The magnetic nanoparticles/antigen

aggregation progressed and became dark brown as the antigen increased. This means that the highly dense proteins concentrated more magnetic nanoparticles. Nearly the same trend was observed for the four holders in the system, indicating reproducibility. Fig. 2 shows the magnetic response of the aggregates driven by the switching magnetic field. As the protein concentration increased, the amount of magnetization increased significantly, indicating that the protein concentration could be detected. The results in Fig. 1 and 2 reveal the application of proteins enhanced the magnetic nanoparticles/protein aggregation.

[1]Loi Tonthat et. al., AIP Advances, Vol.9, No. 12, 125325 (2019). [2]K. Okita et. al., International Symposium on Integrated Magnetics 2023 CP-02 (iSIM 2023).

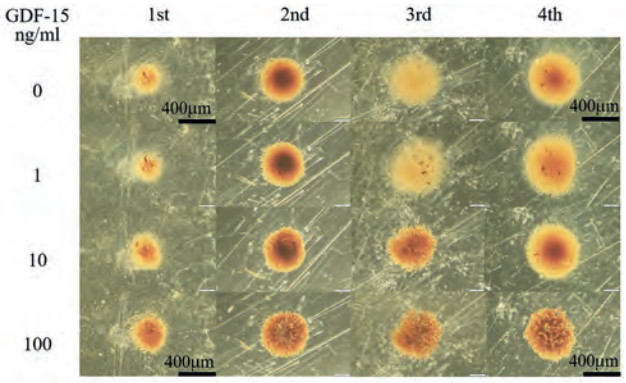

Fig. 1 optical micrographs of magnetic nanoparticles/antigen aggregates.

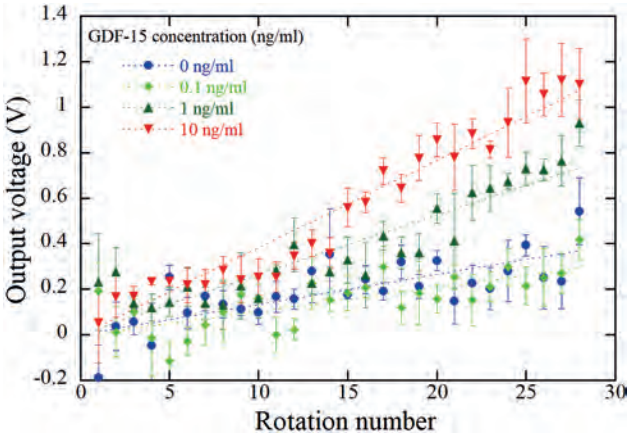

Fig. 2 Magnetic response when the magnetization is reversed by a switching magnetic field.

DQ-07. Surface receive coil dedicated for rat kidney with high sensitivity in vivo magnetic resonance imaging. *M. Takahashi*[1], M. Fushimi[2], S. Yabukami[1], M. Sekino[2] and A. Kuwahata[1] *1. Tohoku University, Sendai, Japan; 2. The University of Tokyo, Tokyo, Japan*

The monitoring of kidney diseases by measurements of renal function and structure is important in clinical nephrology for understanding therapy mechanisms [1, 2]. Although magnetic resonance imaging (MRI) is a non-invasive imaging technology, there is a lack of signal-to-noise ratio (S/N) and spatial resolution [3]. In this study, we proposed a customized surface coil to enhance high sensitivity for rat kidneys in MRI with a static magnetic field strength of 7 T. Figure 1 shows the design of the coil shape by inverse problem approach using bfieldtools [4, 5]. For the initial settings, the coil surface is a square area of 30 mm with a circular hole of 10 mm diameter to obtain a clear image of kidney in the region of interest (ROI, a cube with 10 mm sides with a depth of 10–20 mm from the coil surface) (Fig. 1(a)). We found the unique coil design (Fig. 1(b)) and fabricated the coil by connecting each loop of the designed loops in series with tuning and matching circuits optimized at 300 MHz for 7 T MRI (Bruker, Ettlingen, Germany). Figure 2 shows the experimental result of a biomedical phantom and a rat in vivo MR image. We compared the phantom image with the proposed coil to the image with a conventional volume coil (Fig. 2(a) and (b)) and the proposed coil improved S/N by 1.4-fold compared to the volume coil. We also observed the kidney of a rat injected a contrast agent (magnetic nanoparticles, Resovist® diluted 100 times) by using the proposed coil and volume coil (Fig. 2(c) and (d)). The proposed coil improved S/N by 3-fold compared to the volume coil. We explore further clinical studies to diagnose kidney diseases by optimizing the S/N, spatial resolution, and the concentration of the contrast.

[1] A. Pohlmann, Niendorf, T, https://doi.org/10.1007/978-1-0716-0978-1 (2021) [2] J. H. Seo, Y. Ryu, and J. Y. Chung, *Sensors* 22, 4274 (2022) [3] E. J. Baldelomar, J. R., Charlton, S. C. Beeman, *et al*., *Am. J. Physiol. Renal Physiol*. 314, F399–F406 (2018) [4] A. J. Mäkinen, R. Zetter, J. Iivanainen, *et al*., *J. Appl. Phys*. 128, 063906 (2020) [5] R. Zetter, A. J. Mäkinen, J. Iivanainen, *et al*., *J. Appl. Phys*. 128, 063905 (2020)

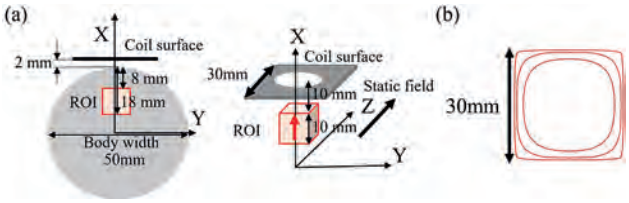

Fig. 1. Design of the coil shape by inverse problem approach: (a) initial settings for optimization and (b) proposed coil.

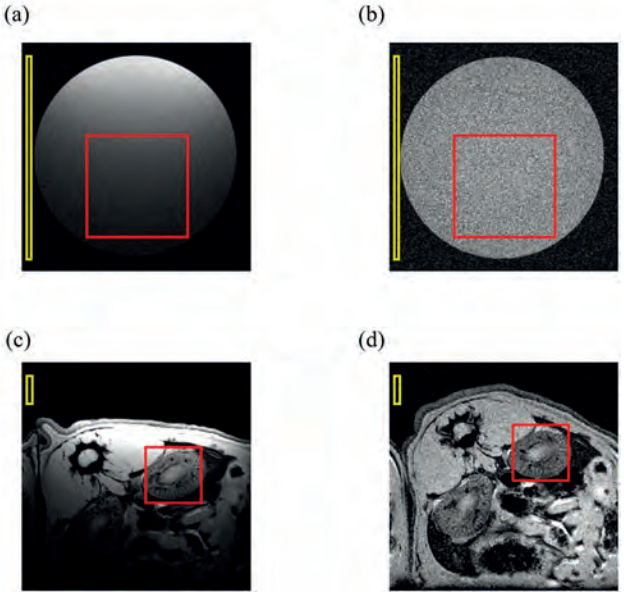

Fig. 2. MR images of a biomedical phantom and a rat kidney. Cylindrical biomedical phantom obtained by (a) proposed coil and (b) conventional volume coil (3D gradient recalled echo (GRE) sequence). Rat kidney obtained by (c) proposed coil and (d) conventional volume coil (2D GRE sequence). Red and yellow area show ROI (kidney) and the region for noise calculation, respectively.

DQ-08. Enhancing heating efficiency of magnetic hyperthermia by using pulsed magnetic fields. *Y. Adachi*[1], A. Kuwahata[1] and E. Nakamura[2,1]
1. Engeneering, Tohoku_university, Sendai, Japan; 2. High Energy Accelerator Research Organization (KEK), Tsukuba, Japan

For magnetic hyperthermia cancer therapy using magnetic nanoparticles (MNPs) [1, 2], an alternating magnetic field (AMF) can not deliver magnetic field deeply into the body. Magnetic relaxation of MNPs is important for magnetic energy dissipation and thermal energy generation. However, the sinusoidal magnetic field excitation does not always generate heat effectively. Therefore, it is necessary to use magnetic field waveform that can dissipate more energy to obtain more considerable hysteresis loss. In this study, we proposed a pulsed magnetic field to generate heat in MNPs effectively. We designed a short pulsed magnetic field formation circuit to compare the heating power with conventional magnetic field. Figures1(a) and (b) show the pulsed magnetic field formation circuit and experimental setup. Figure 1(c) shows the pulsed magnetic field of 7.5 mT_{pp} with 60 ns falling time (0.13 T/μs) in 200 kHz repetitive frequency and the conventional sinusoidal wave. Figure 2 shows the heating characteristics of 250 μL of MNPs (Resovist®) by the pulsed magnetic field. The temperature increment tends to be proportional to the square of the magnetic field amplitude and to the frequency (Figs. 2(a) and (b)). A comparison of the temperature increment between the pulsed and sinusoidal magnetic field waveforms, normalized by the magnetic energy per unit volume $E_{mag} = \int B(t)^2/2\mu_0 dt$, shows that the heating efficiency is approximate four times higher by applying the pulsed magnetic field (Fig. 2(c)). This result indicates the delay of the magnetic relaxation caused by the steep rising of the pulse and the enhancement of MNP heating by the higher frequency band of magnetic harmonic signals [3]. This fact suggests the potential to treat tumors located in deeper regions. we explore further studies of the development of an effective pulsed magnetic field generator for clinical applications. Figure 1. (a) Pulsed magnetic field generator, (b) picture of pulsed magnetic field generator, and (c) applied pulsed and sinusoidal magnetic field. Figure 2. (a) Temperature dependence on magnetic field strength, (b) temperature dependence on magnetic field frequency, and (c) heating efficiency with pulsed and sinusoidal magnetic fields.

[1] D. Kouzoudis *et al.*, *frontiers in Materials* 8, 638019 (2021) [2] A. Shikano *et al.*, *T. Magn. Soc. Jpn.* 6, 100-104, (2022) [3] A. Kuwahata *et al.*, *AIP Advance* 13, 025145 (2023)

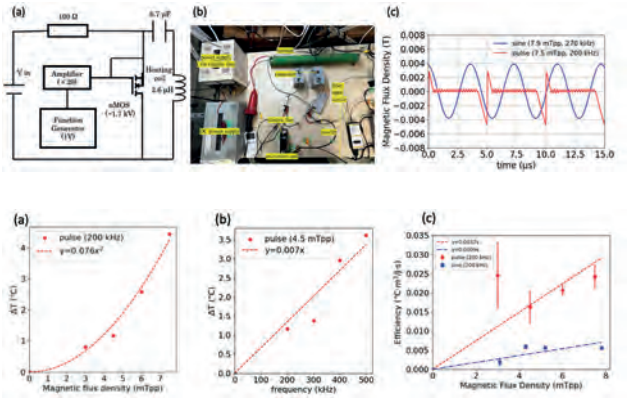

DQ-09. Micromagnetic Stimulation (μMS) of the Vagus Nerve: An in vivo Study. R. Saha[1], D. Van Helden[2], *M.S. Hopper*[1], W. Low[3], T. Netoff[4], J. Osborn[2] and J. Wang[1] *1. Department of Electrical and Computer Engineering, University of Minnesota, Minneapolis, MN, United States; 2. Department of Surgery, University of Minnesota, Minneapolis, MN, United States; 3. Department of Neurosurgery, University of Minnesota, Minneapolis, MN, United States; 4. Department of Biomedical Engineering, University of Minnesota, Minneapolis, MN, United States*

To treat diseases associated with vagal innervation of peripheral organs, selective activation of efferent and afferent vagal fibers is necessary. Due to the nerve's complex anatomy, fiber-specific activation proves challenging. Spatially selective neuromodulation using micromagnetic stimulation (μMS) is showing significant promise. This neuromodulation technique uses microcoils (μcoils) powered by a time-varying current to generate magnetic fields, inducing a highly directional electric field in the nerve. In this study on rodent cervical vagus, a solenoidal-shaped μcoil was oriented at an angle to the left and right branches of the nerve. The aim was to measure changes in mean arterial pressure (MAP) and heart rate (HR) from the femoral artery after vagus μMS. The μcoils were powered by a 3 A single-cycle sinusoidal current with pulse widths (PW) of 100, 500, and 1000 μsec at a frequency of 20 Hz. Under isoflurane anesthesia, μMS of the left vagus at 1000 μsec PW led to an average MAP drop of 21.4 mmHg (SD = 28.5 mmHg, n=7). Similarly, μMS of the right vagus under isoflurane resulted in an average MAP drop of 2.24 mmHg (SD = 13.6 mmHg, n=7). This MAP reduction is consistent with electrical vagus stimulation, regulating heart contractility and blood vessel constriction. Anesthesia was switched to urethane as no significant HR changes were observed under isoflurane. No changes in MAP or HR were noted during μMS of the cervical vagus under urethane anesthesia. From our experiments, the left branch seems more susceptible to μMS than the right. However, we believe that due to the spatial selectivity of μMS, the fibers associated with changes in MAP and HR on the right remained inactive. The choice of anesthesia evidently influenced the efficacy of μMS on hypertension-linked vagal fibers. Finally, the absence of HR modulation upon μMS could offer alternative treatment options using VNS with fewer heart-related side-effects.

R. Saha, S. Faramarzi and R. Bloom, Journal of Neural Engineering., Vol. 19, Num. 1 (2022)

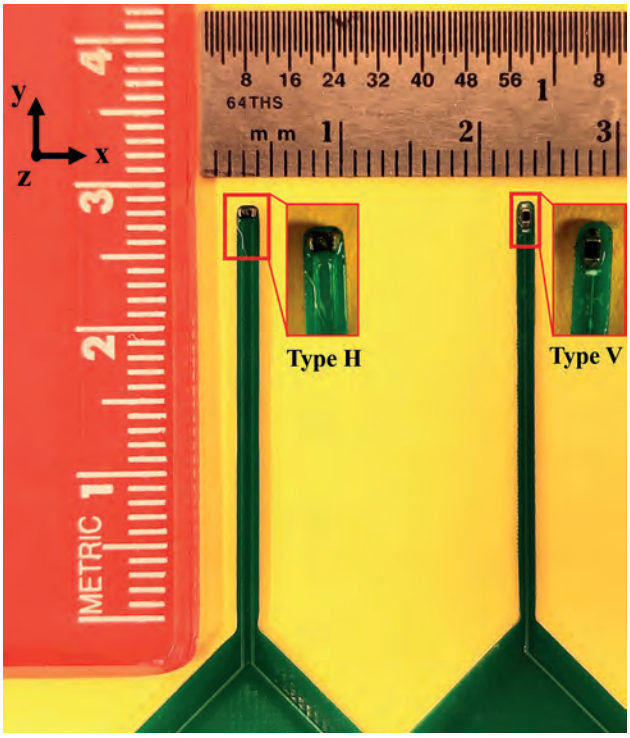

Fig. 1: The MagPen was prototyped with two µcoil orientations: Type H (horizontal) and Type V (vertical). Close-up insets show the tips for both orientations. The µcoils are positioned at the board tip and coated with Parylene-C.

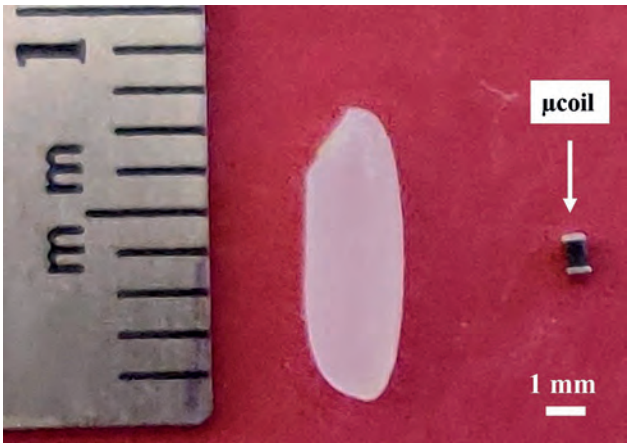

Fig. 2: The sub-mm µcoil compared to a single Basmati rice grain.

DQ-10. In Silico Experiments to Guide Preclinical Tests of Magnetic Hyperthermia. M. Vicentini[1], R. Ferrero[1] and *A. Manzin*[1] *1. Istituto Nazionale di Ricerca Metrologica, Torino, Italy*

Magnetic hyperthermia has shown great potential as an adjuvant to radiotherapy and chemotherapy, enabling a selective heating of diseased tissues with limited side effects in healthy ones. This technique is based on the administration of magnetic nanoparticles (MNPs) within a tumour region and on their activation with AC magnetic fields, with frequency between 50 kHz and 1 MHz [1]. The MNP activation leads to a release of heat that raises the tumour temperature, promoting the damage of cancer cells. Preclinical tests on mice and rats are commonly used to evaluate the efficacy of this therapeutic technique [2], investigating how to maximize heat deposition and minimize side effects connected to the occurrence of hotspots due to electromagnetic field exposure [3]. To these aims, several factors have to be taken into account, including the fulfilment of biophysical constraints when selecting magnetic field parameters (frequency and peak amplitude), the geometry of the field applicator and its placement with respect to the body, and the dependence of MNP thermal efficiency on the experimental conditions [4]. In this framework, we perform *in silico* tests of magnetic hyperthermia treatments in a high-resolution digital phantom of a 30 g mouse, to study the role of AC magnetic field sources and of MNP administered dose. In the simulations, we compare different magnetic field applicators, varying their geometry (solenoid, pancake, Helmholtz-type) and the AC supply conditions (frequency and peak amplitude of the supply current). The analysis is carried out by means of in-house finite element solvers [5, 6], which enable us to evaluate the magnetic field spatial distribution within the target region, the possible eddy current heating and the thermal effects due to MNP excitation, under different magnetic field application conditions.

[1] H. Gavilán et al., Chem. Soc. Rev., Vol. 50, p. 11614–11667 (2021). [2] H. F. Rodrigues, G. Capistrano and A. F. Bakuzis, Int. J. Hyperthermia, Vol. 37, p. 76–99 (2020). [3] M. Vicentini et al., Comput. Methods Programs Biomed., Vol. 223, 106975 (2022). [4] E. A. Périgo et al., Applied Physics Reviews, Vol. 2, 041302 (2015). [5] A. Manzin, R. Ferrero and M. Vicentini, Adv. Theory Simul., Vol. 4, 2100013 (2021). [6] M. Vicentini, R. Ferrero and A. Manzin, Adv. Theory Simul., 2300234 (2023).

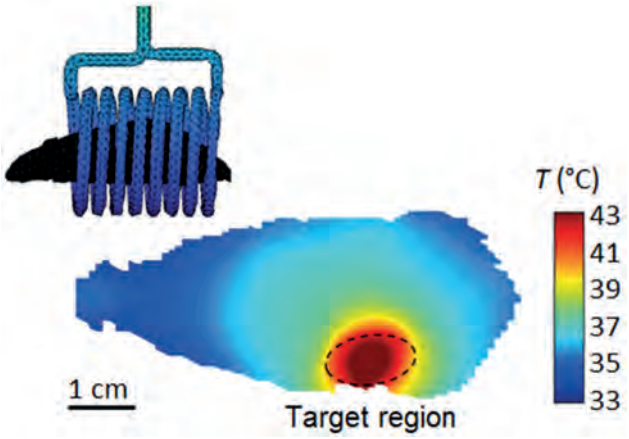

Map of equilibrium temperature in a mouse treated with magnetite nanoparticles activated with a 300 kHz magnetic field generated by a 100 A current. The specific loss power is around 400 W/g.

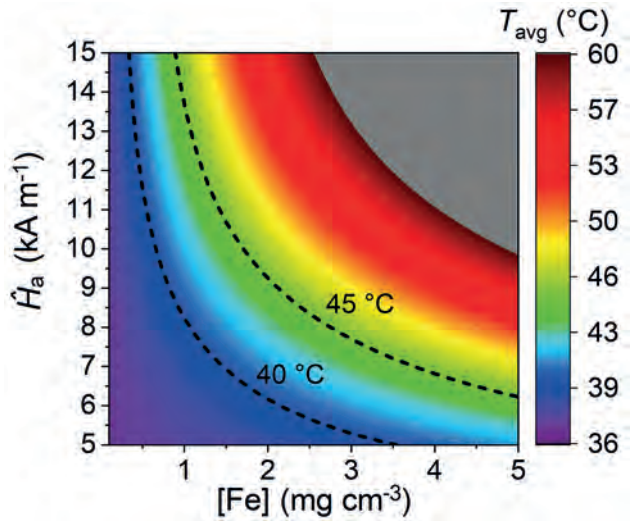

Diagram of average temperature within the mouse target region treated with magnetite nanoparticles, versus iron concentration [Fe] and AC magnetic field peak amplitude, for a frequency of 300 kHz.

DQ-11. Estimating Location of the Hook-Wire for Breast-Conserving Surgery Using a Magnetometer. O. Debnath[1], A. Kuwahata[2], Y. Sunaga[1], S. Chikaki[1], M. Kaneko[3], M. Kusakabe[4] and *M. Sekino*[1] *1. The University of Tokyo, Tokyo, Japan; 2. Tohoku University, Sendai, Japan; 3. Osaka University, Osaka, Japan; 4. Matrix Cell Research Institute Inc., Ibaraki, Japan*

Early-stage breast cancer is excised in breast-conserving surgery. Some surrounding healthy tissue is also excised as a margin to confirm that all the cancer cells are removed [1]. An implantable device is necessary to mark the lesion for excision [2-4]. A hook-wire is inserted into the lesion for marking it before surgery under an image navigation, and then surgeons excise the lesion. It is important to check whether the margin is sufficient, to avoid a recurrence of cancer. In this study, we propose a method to estimate the location of hook-wire in the excised tissue to check if the tissue has a sufficient margin. We used a magnetometer equipped with a neodymium magnet for magnetizing the hook-wire and a Hall sensor for detecting the resulting fields [5]. The magnetometer was fixed, and the phantom containing the hook-wire was rotated and vertically displaced, as shown in fig. 1. To estimate the positional vector of hook-wire from the measured magnetic field, the relationship between the measured magnetic field and the positional vector were mathematically modeled. The stochastic gradient descent optimization algorithm was used to optimize the positional vector, minimizing the difference between the estimated magnetic field based on the model function and the experimentally measured values. Fig. 2 shows how the measured magnetic field strength is varied with variation of α. The total distance between the magnetometer and hook-wire was 20 mm when α was 0°. A maximum magnetic field strength of 58.7 μT was obtained when α was 20°. The developed algorithm worked perfectly and gave less than 1% error. The average error of the x-axis was 2.27%, the y-axis error was 28%, and the z-axis error was 2.62%. The main challenge in resecting nonpalpable tumors is to obtain clear margins and minimize the resection of healthy breast tissue, with associated good surgical outcomes. The results showed that the location of the tip of the hook-wire could be successfully estimated. Surgeons can remove the tissue precisely having the hook-wire using a magnetometer with the help of this algorithm.

[1] Sebastian M, Akbari S, Anglin B, Alice P, Springerplus, 4-198, 2015. [2] Peek MCL, Zada A, Ahmed M, Baker R, Sekino M, Kusakabe M, Douek M, J. Magn. Magn. Mater., vol. 460, 2018, pp. 334-339. [3] Ahmed M, Anninga B, Goyal S, Young P, Pankhurst Q A Douek M, British. J. Surg, vol. 102, 2015, pp. 646-652. [4] Xiao Y, Debnath O B, Chikaki S, Kuwahata A, Peek M, Saito I, Maeda S, Kusakabe M, Sekino M (2020) AIP Adv., vol. 10, 2020, pp. 1-5. [5] Sekino M, Kuwahata A, Ookubo T, Shiozawa M, Ohashi K, Kaneko M, Saito I, Inoue Y, Ohsaki H, Takei H, Kusakabe M, Breast Cancer Patients" in Sci. Rep. 8, 2018.

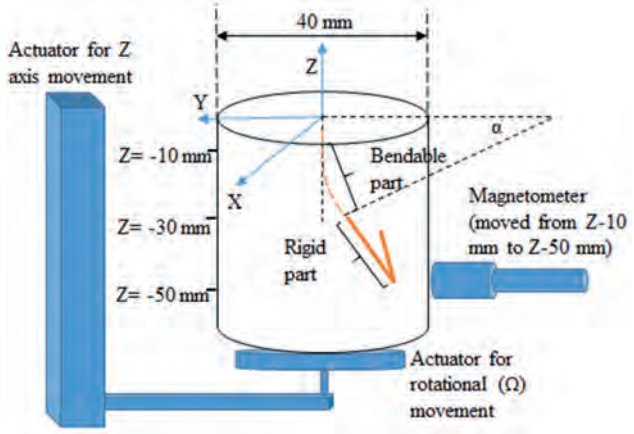

Fig. 1 Measurement setup showing the location of the hook-wire and the magnetometer.

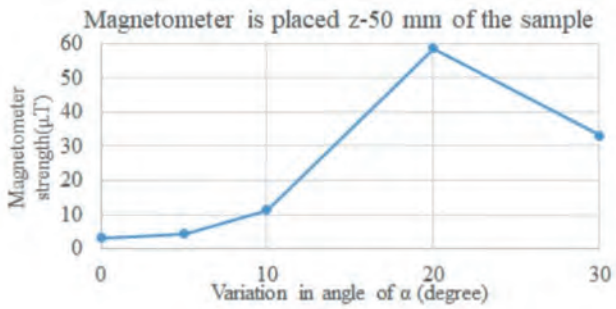

Fig. 2 magnetic field strength data with varied angle.

DQ-12. Withdrawn

DQ-13. Mapping the Design Space for Heating with Magnetic Nanowires. *A. Harpel*[1] and B. Stadler[1] *1. University of Minnesota, Minneapolis, MN, United States*

Magnetic nanowires (MNWs) are desirable for heating applications due to their square hysteresis loops and their size which allows for tunable switching fields. However, because MNWs are readily modified, a vast design space is available when applying magnetic nanowires to different heating applications. Here, major and minor hysteresis loops have been measured for ferromagnetic nanowire arrays. These experimental results have been used to project heating rates and energy loss per cycle for nanowires depending on the equipment constraints used to heat the nanowires. These constraints include maximum frequency and applied magnetic field. In this work, these heating maps allow for informed design and fabrication of nanowires for cryopreservation applications, especially when paired with simulation. However, these heat rate maps are broadly applicable for understanding the thermal behavior of nanowires in broader applications including electronics and hyperthermia.

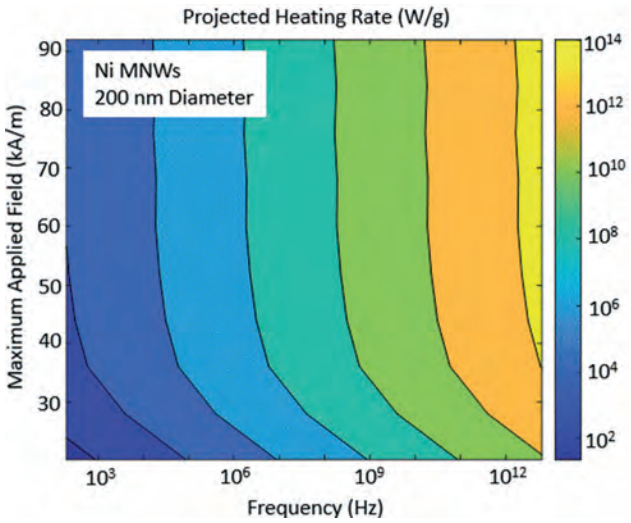

Fig. 1: The projected heating rate map is shown for an array of 200 nm Ni MNWs.

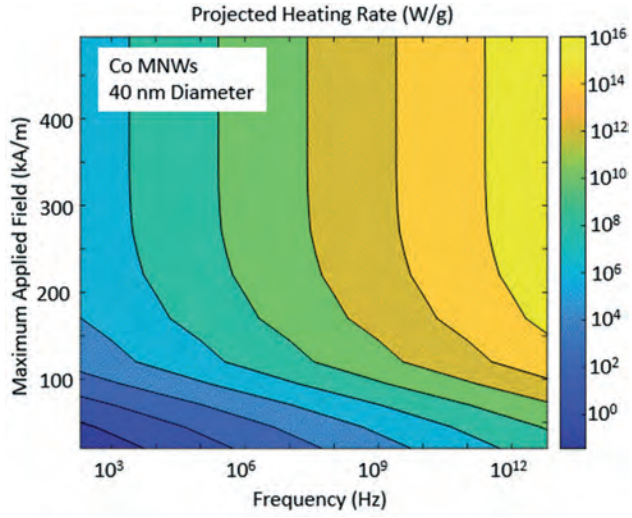

Fig. 2: The projected heating rate map is shown for an array of 40 nm diameter Co MNWs. Depending on the diameter and material of the wire, the ideal equipment for heating can change, as demonstrated by the scale differences and change in topology of the heat rate maps for cobalt and nickel MNWs of different diameters.

DQ-14. Magnetics and Music: the Voice of the Machine. *A. Emelianoff*[1,2] *1. Lutherie Postmoderne, Montreal, QC, Canada; 2. CIRMMT McGill, Montreal, QC, Canada*

Magnetoacoustics implicates the use of magnetic technologies for music and sound arts. I am an artist and musician, developing electronic systems to audify magnetic and electromagnetic activity. This activity fascinates as a sound medium because of its permeability, the way that sources of energy affect and are affected by each other. In particular, EM sounds are rejected as noise in music, but they can be embraced: glitch and noise are effectively the voice of the machine. As the performer, I walk the line between 'controller' and 'catalyzer', having partial authority over the sound results but having to accept artifacts or surprises from the system, such as static discharges. This questions the agency of the performer vs. a slippery medium such as electro-magnetics. Extracting and organizing sound from magnetic sources allows a new insight into the behavior of energy and matter, as well as creating a new, elusive language for music. Many artists have touched these media to some degree, but I see it as a frontier field and would like to advance to a higher level of development. Through electronic and physical media, I seek to expose, catalyze, amplify or transform unique activity and subtle influences in matter. *Spirit of Light* is a magnetic turntable machine which sonifies the movement of magnets and the topography of steel discs through inductive pickups. The title refers to the metaphysical and cross-sensory (synaesthetic or poetic) depictions of electricity in its early years, and to the cross-modal experience created by the machine and sound system. It produces sound directly from the movement of permanent magnets but also captures the kinetic and electrical activity of the whole machine. All sound is routed through MaxMSP and spatialized through a multichannel sound system. The resulting sounds are haunting, hypnotic, pulsing and completely unique. I've given several concerts with this device. The programming committee for the conference has already accepted to have me present a sound demo of the Spirit of Light machine at the entrance to one of the tutorial sessions. I would like to create a poster as well to fully participate in the conference.

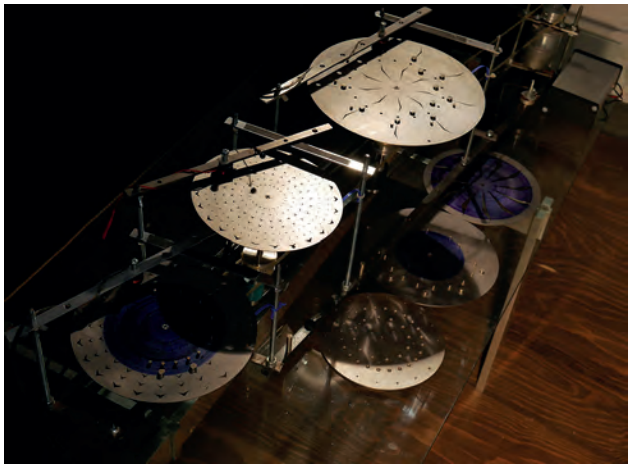

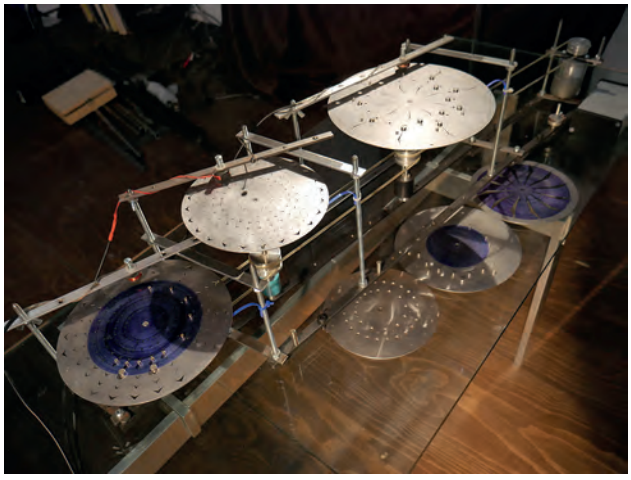

DQ-15. Magnetic Nanoparticles (MNPs) Based Additively Manufactured Computational and Memory Devices. *R.A. Mendonsa*[1], S. Liang[1] and J. Wang[1] *1. Electrical Engineering, University of Minnesota, Minneapolis, MN, United States*

Magnetic nanoparticles (MNPs) have been shown in a suspension to change resistance in orders of magnitude based on an applied field [1]. We have prepared the MNPs samples with matrices of PEDOT:PSS or H_2O, and Co MNPs (Figure 1(a)) and carried out the magnetoresistive measurements as shown in the Figure 1(b). A switch-based model is used to understand the mechanism for the change in resistance as studied in Figure 1(c). We further propose devices for memory and computation based on MNPs. Building blocks for these devices are then fabricated using additive manufacturing techniques and measurements of change in resistance under the influence of a magnetic field are conducted. Niche application of additive manufacturing

techniques to the fabrication of these devices are proposed. Further modelling is done to understand power consumption of these proposed devices. An example of a device for the purpose of a memory based on the above principle is shown in Fig. 2. The device uses MNPs suspended in a liquid matrix. The application of a magnetic field is used to move the MNPs to or away from electrical contacts. Depending on the change of position of the MNPs, a connection is either made or broken, which can act as a 1 or a 0. The measured change in resistance observed in such devices is more than an ordered of magnitude depending on the choice of MNP and matrix solution.

Meyer, J., Rempel, T., Schäfers, M., Wittbracht, F., Müller, C., Patel, A. V., & Hütten, A. *Smart materials and structures*, 22(2), (2013) 025032.

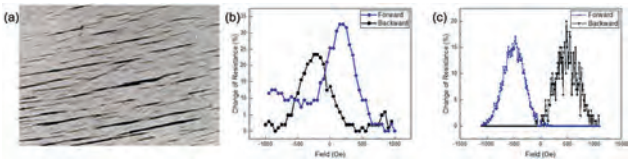

Fig.1 – Prepared sample (a) and results (b) from sample vs. simulated results (c) using the switch-based model

Fig.2 – Schematic of a device and operation, showing resistance switching from low to high (a) and high to low (b)

DQ-16. Photo-actuated Ferrofluid Cavities for Nonreciprocal Acoustic Wave Transmission. M. Yao[1], *A. Neogi*[1], Z. Wang[1], Y. Jin[2] and Q. Wang[1]
1. University of Electronic Science and Technology of China, Institute of Fundamental and Frontier Sciences, Chengdu, China; 2. University of North Texas, Department of Physics, Denton, TX, United States

Nonreciprocity in the propagation of acoustic waves through a medium can be achieved through the nonlinearity of the medium[1] or broken time symmetry[2] due to the active motion of the inertial frame of reference. As in electrical or photonic systems, magnetic fields typically do not alter acoustic modes. However, manipulating fluid motion[3] or viscoelastic properties[4] of a magnetoactive medium such as ferrofluids can lead to a novel pathway to control acoustic waves by a magnetic field. The density and viscosity of ferrofluids are known to be drastically modified in the presence of a magnetic field and induce a broken spatial parity relative to the direction of motion of a propagating acoustic wave[5]. A finite temperature gradient in the presence of a magnetic field can also lead to a finite fluid flow due to the magnetocaloric effect for breaking the T-symmetry of a medium[6]. A dynamic magnetoactive fluidic ring cavity-based meta-atoms supporting ultrasonic waves were designed with a thermoelectric cooler in a magnetic field. A laser-induced photoabsorption leads to a temperature and viscosity gradient resulting in a rotational ferromagnetic fluid flow due to the Kelvin-body force in the presence of a magnetic field. It violates the PT symmetry for the acoustic wave co-propagate and counter-propagate with the fluid motion within the cavity. A semicircular ring resonator cavity (Figure 1), was designed using numerical simulation to confine the acoustic modes in the 400-600 kHz range (Figure 2a and 2b). Figure 2c shows a 20 dB nonreciprocal transmission at 550 kHz from an 800 mW laser irradiation. This fluid flow rate, viscosity and density variation in the presence of a dc magnetic field and a dynamic temperature gradient can yield efficient nonreciprocal propagation without any nonlinear effects or the use of metamaterials. Thermomagnetic control of intracavity fluid dynamics and convection enables a remotely light-controlled, multifunctional acoustic device and shows promise for use in various acoustic devices.

1. Bogdan-Ioan Popa and Steven A. Cummer, Nature Communications., 5, 3398 (2014) 2. Piyush J. Shah, Derek A. Bas and Ivan Lisenkov, Science Advances., 6, eabc5648 (2020) 3. Kunihiro Ichimura, Sang-Keun Oh and Masaru Nakagawa, Science., 288, 5471 (2000) 4. R.E Rosensweig, R Kaiser and G Miskolczy, Journal of Colloid and Interface Science., 29, 680-686 (1969) 5. M. S. Pattanaik, V. B. Varma and S. K. Cheekati, Scientific Reports., 11, 24167 (2021) 6. Jaswinder Singh Mehta, Rajesh Kumar and Harmesh Kumar, Journal of Thermal Science and Engineering Applications., 10, 020801 (2017)

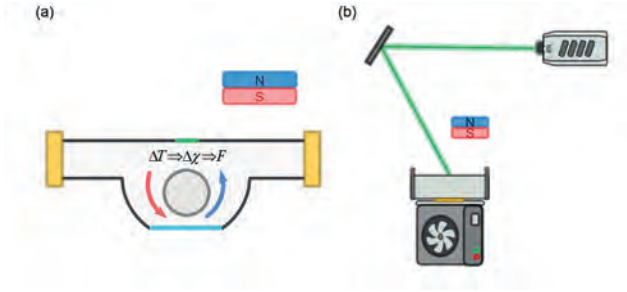

Fig.1 (a) Design of ferrofluid cavity (b) Experiment setup

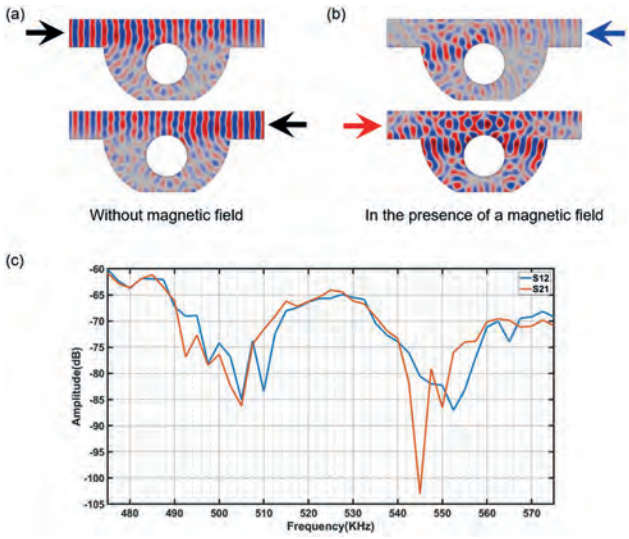

Fig.2 (a) Reciprocal and (b) nonreciprocal transmission in acoustic simulation (c) Nonreciprocity in acoustic experiments

Session DR
SHIELDING, LEVITATION AND PROPULSION
(Poster Session)

Mai Phuong Nguyen, Chair
Tohoku University, Sendai, Japan

DR-01. Effect of EM Absorbers Placed on Aperture Side within Enclosure on Shielding Effectiveness. *J. Kwon[1] 1. Radio Research Department, ETRI, Daejeon, The Republic of Korea*

Metallic enclosures are used to mechanically protect and electromagnetically shield the interior critical devices, equipment, and systems from external electromagnetic fields. Various apertures, such as those for air ventilation, operator access, and cabling, are indispensable. However, the external field should penetrate the enclosure through apertures. Then the electromagnetic field within metallic enclosures increases at resonant frequencies due to their high Q-factor, lowering their shielding effectiveness. To minimize this adverse effect of the aperture on the shielding of the enclosure, the design of metallic enclosures with apertures must consider the electromagnetic coupling mechanism through apertures. In this study, a lossy material such as an electromagnetic absorber is used to improve the shielding property of the metallic enclosure with an aperture. A structure for analyzing the shielding properties of the enclosure with absorber is shown in Fig. 1. An aperture is placed in the center of the enclosure's front panel. In order to calculate the shielding characteristics, a set of horn antenna was used for measuring the electromagnetic field. The frequency for calculation was set from 1 to 5 GHz. The absorber used in this study is the Eccosorb LS series [4] and provided the material data by CST.[5] Fig. 2 shows the SE according to the absorber. Three different absorbers (LS22, LS26, LS30) with 20 mm thickness were used. A solid line was displayed using a moving average to clearly show the SE. In the case of LS22, the SE is over 20 dB. The higher the absorption performance of the absorber, the higher the SE, and the higher the frequency, the higher the SE. **Acknowledgement**: This work was supported by Institute of Information & communications Technology Planning & Evaluation (IITP) grant funded by the Korea government(MSIT) (No. 2020-0-00917, Development of Key Technologies for Low-cost EMP Protective Materials, Components, Devices(MCD) & Facilities Vulnerability Assessment)

[1] JH Kwon, CH Hyoung, JH Hwang and HH Park, "Impact of absorbers on shielding effectiveness of metallic rooms with apertures," MDPI Electronics, vol. 10, no. 3, Jan. 2021. [2] C.R. Paul, Introduction to Electromagnetic Compatibility, 2nd Ed., John Wiley & Sons, Inc, 2006 [3] H. W. Ott, Electromagnetic Compatibility Engineering, 1st Ed., John Wiley & Sons, Inc, 2009 [4] Laird, www.laird.com [5] CST Studio, www.cst.com

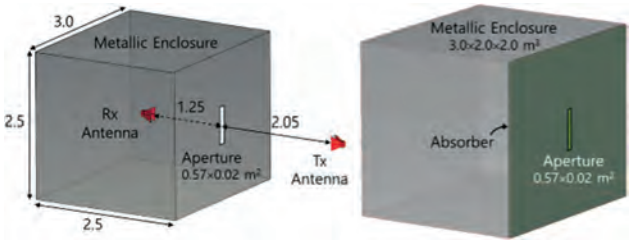

Fig. 1. Structure of enclosure with/without absorber

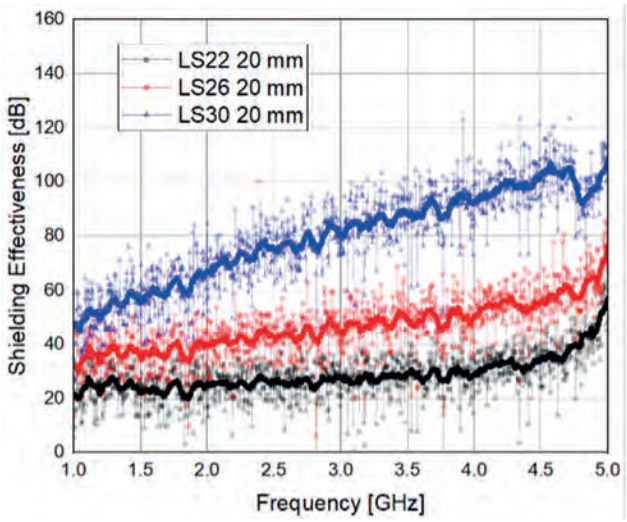

Fig. 2. Calculated Result of SE due to the type of absorber

DR-02. A Study on Reduction of Magnet Usage and Cogging Torque through the Intersect Consequent Model. H. Kim[1], S. Song[1], D. Jung[2], *D. Choi*[1] and W. Kim[1] *1. Department of Electrical Engineering, Gachon University, Seongnam-si, The Republic of Korea; 2. Halla University, Wonju-si, The Republic of Korea*

Since the use of rare-earth permanent magnets in electric motors has greatly improved their performance since the 2000s, concerns have arisen about the high cost and unstable supply of these magnets due to China's monopoly. As a solution, alternative resources that do not use rare-earth materials or electric motor models that use small amounts of rare-earth magnets are being proposed[1]. One such model is the Consequent Pole Synchronous Motor (CPSM), which can reduce magnet usage by 50% compared to conventional Synchronous Permanent Magnet Motors (SPMSM)[2-3]. However, reducing magnet usage inevitably leads to decreased performance and increased cogging torque due to magnet asymmetry. Cogging torque is a hindrance to motor rotation caused by the magnetic attraction between the stator and rotor[4]. Therefore, in this paper, we propose the Intersect CSP model, which uses a design that alternates N and S poles per rotor pole with 50% magnet usage while reducing cogging torque. This design also includes a gap between the rotor poles to reduce axial leakage flux between magnets, and the stator lamination length is increased by the same amount as the rotor gap to maximize magnet flux linkage. We selected an EPS motor with 6 poles and 9 slots as the analysis model, and used finite element analysis to analyze the induced voltage and cogging torque by increasing the rotor gap and stator lamination length. To achieve the same output as the existing SPMSM model while reducing cogging torque, we set induced voltage and cogging torque as the objective functions for optimization.

[1] Feng, D.Y.; Liu, Z.W.; Zheng, Z.G.; Zhong, X.C.; Zhang, G.Q. Hard Magnetic Properties and Thermal Stability for TbCu7-Type SmCo6. 4Si0.3Zr0.3 Alloys with Sm Substituted by Various Rare-Earth Elements. IEEE Trans. Magn. 2015, 51, 2100604 [2] Sirimanna, S.; Balachandran, T.; Haran, K. A Review on Magnet Loss Analysis, Validation, Design

Considerations, and Reduction Strategies in Permanent Magnet Synchronous Motors. Energies 2022, 15, 6116. [3] Shou, J.; Ma, J.; Zhang, Z.; Qiu, L.; Xu, B.; Luo, C.; Li, B.; Fang, Y. Vibration and Noise Optimization of Variable-Frequency-Driven SPMSM Used in Compressor Based on Electromagnetic Analysis and Modal Characteristics. Energies 2022, 15, 7474. [4] Song, S.W.; Jeong, M.J.; Kim, K.S.; Lee, J.; Kim, W.H. A study on reducing eddy current loss of sleeve and improving torque density using ferrofluid of a surface permanent magnet synchronous motor. IET Electr. Power Appl. 2022, 16, 463–471.

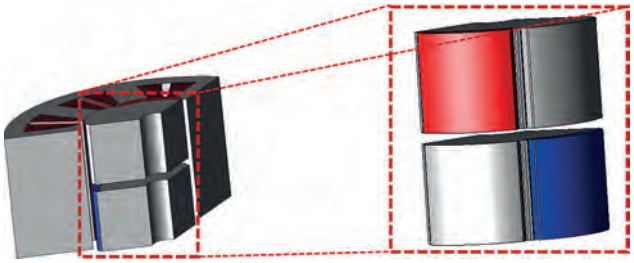

DR-03. Comparison and Analysis of Electromagnetic Characteristics According to the Slot-Number of 210kW-class MG-PMSM for Urban Railway Vehicle. I. Jo[1], J. Lee[1], *H. Lee*[2], J. Lee[2], J. Lim[2], S. Kim[1] and C. Park[2] *1. Hanyang University, Seoul, The Republic of Korea; 2. Korea National University of Transportation, Uiwang-si, The Republic of Korea*

Magnetic geared permanent magnet synchronous motor(MG-PMSM) is a system that combines a magnetic gear and a PMSM integrally, and consists of an inner PM rotor, pole pieces rotor, an outer PM, and a stator. Since this system transmits power in a non-contact method, it has high efficiency and power density performance, so many recent studies are being studied. In particular, current urban railway vehicle are equipped with complex vertical mechanical gear and a relatively low-efficiency induction motor, so replacement with a new system is absolutely necessary [1]-[4]. Therefore, this paper presents considerations for selecting the optimal combination of pole-number, pole pieces-number, and slot-number to apply MG-PMSM as a traction motor for 210kW-class urban railway vehicles, and compares and analyzes the electromagnetic field characteristics accordingly. In this paper, first, considering the operating frequency and PM eddy current loss, the inner PM pole-number was fixed to 12 poles, and then synchronizable combinations(pole-number and pole-pieces number) were selected [5]. Among them, combinations that minimize unbalanced magnetic force and torque ripple coefficient were selected to reduce noise and vibration. At this time, considering winding feasibility and manufacturability, four slot combinations were adopted, and analysis models were derived within the same specification and electric loading. Fig. 1 shows the fast fourier transform(FFT) of outer air gap magnetic flux density for the four models. The 9 and 27-slot have sub-harmonic(3rd order) by the winding method, and in addition, the 9-slot exhibits larger magnitude of this harmonic due to the modulated magnetic flux. Since this harmonic wave has a larger wavelength than the fundamental wave(6th order), the flux line penetrates deeply into the inner rotor, increasing the eddy current loss of inner PM, as shown in Table 1 [6]. For 54-slot, the rated average torque(required torque: 6.6kNm) can be maximized because leakage of the armature flux can be minimized by being designed equal to the outer PM pole number.

[1] I.-H. Jo, J. Lee, C.-B. Park, etc., Energies., Vol. 15, p. 1-13 (2022) [2] C.-B. Park, H.-W. Lee, T. Kim, etc., AIP Advances., Vol. 10, p. 1-8 (2020) [3] J.-H. Lim, G. Jeong, C.-B. Park, etc., Applied Science., Vol. 11, p. 1-18 (2021) [4] I. -H. Jo, H. -W. Lee, C. -B. Park, etc., IEEE Transactions on Magnetics., Vol. 55, p. 1-5 (2019) [5] B. Praslicka, M. C. Gardner, H. A. Toliyat, etc., IEEE Journal of Emerging and Selected Topics in Power Electronics, Vol. 10, p. 1813-1822, (2022) [6] N. Bianchi, S. Bolognani and E. Fomasiero, 2007 IEEE International Electric Machines & Drives Conference., p. 634-641 (2007)

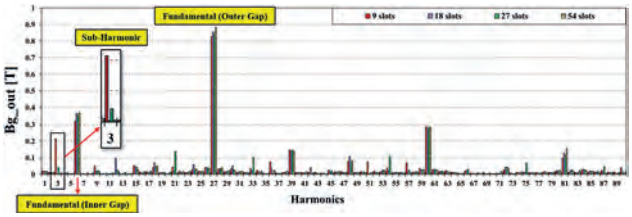

FFT of outer airgap flux density of the four models

Total Loss [W/m³]	Inner PM-Number : Pole pieces-Number : Outer PM-Number : Slot-Number			
	12 : 33 : 54 : 9	12 : 33 : 54 : 18	12 : 33 : 54 : 27	12 : 33 : 54 : 54
	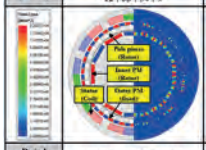	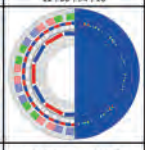	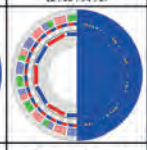	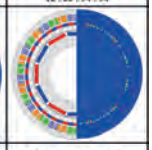
Rated Torque	6.85 [kNm] (218.07 [kW])	6.95 [kNm] (221.25 [kW])	6.87 [kNm] (218.71 [kW])	7.45 [kNm] (237.17 [kW])
Torque Ripple	15.1 [%]	2.2 [%]	4.5 [%]	1.3 [%]
Core Loss	2.56 [kW]	1.96 [kW]	1.69 [kW]	1.73 [kW]
Mag. Loss	36.66 [kW]	9.39 [kW]	12.29 [kW]	11.50 [kW]
Efficiency	84.76 [%]	95.12 [%]	93.99 [%]	94.72 [%]

Electromagnetic analysis results for MG-PMSM models

DR-04. Withdrawn

DR-05. Study on the Reduction of Eddy Current Loss of Permanent Magnet Synchronous Motor considering PWM. *Y. Lee*[1], I. Jang[2], I. Yang[3], N. Jo[1] and W. Kim[1] *1. Department of Electrical Engineering, Gachon University, Seongnam-Si, The Republic of Korea; 2. Electric Powertrain Core Technology Team, Hyundai Mobis, YoungIn-Si, The Republic of Korea; 3. Department of Electrical Engineering, Hanyang University, Seoul-Si, The Republic of Korea*

Recently, permanent magnet synchronous motors to which PWM (Pulse Width Modulation) control is applied are mainly used. PWM control is a technique that can modulate not only the frequency of the output voltage but also the magnitude, and is a control method that generates pulses for turning on and off each phase switch. In addition, it is a technology that uses switching to control analog circuits with digital output, which is effective for motor control. In general, when designing a motor using FEM, a sinusoidal current waveform is used. When the motor is driven through PWM control, current contains harmonic components compared to sinusoidal current, and these harmonic components have a great influence on eddy current loss generated in permanent magnets. When designing a motor, it is possible to obtain more accurate analysis results by using a current waveform considering PWM control instead of using a conventional sinusoidal waveform. In this paper, the eddy current loss of the permanent magnet, which has a great effect on the performance of the motor, is compared using the division of the permanent magnet, and the eddy current loss of the permanent magnet is derived and compared using the sinusoidal current waveform and the current waveform considering PWM control. In a synchronous motor, since the rotating speed of the rotor and the speed of the stator rotating magnetic field are the same, eddy current loss for the fundamental wave does not occur. However, when harmonics exist, eddy current loss of permanent magnets occurs due to harmonics. Due to the harmonic components of the PWM current, the Total Harmonic Distortion(THD) of the line-to-line voltage under load increased by about 167% compared to the simulation result through the sinusoidal current waveform in comparison to the existing sinusoidal current waveform, and the torque ripple also increased by about 33%. When the magnet was not divided, the model using a sinusoidal current waveform measured 5.79W, and the model using a current waveform considering PWM measured 7.26W. When the magnet was divided, the model using a sinusoidal current waveform measured 0.416W and PWM The model using the considered current waveform measured 0.604W.

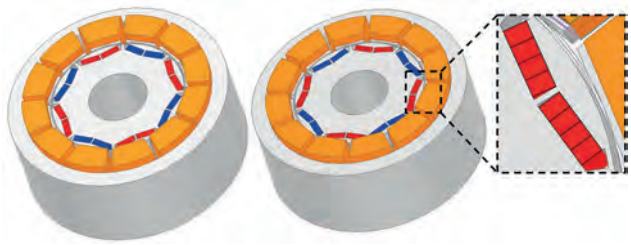

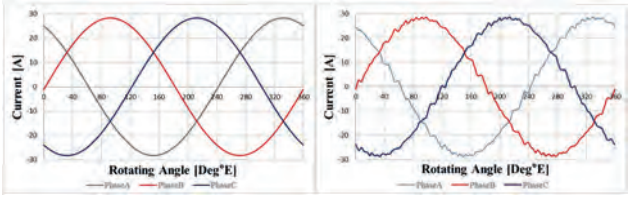

DR-07. Electromagnetic Drag Force Analysis According to Changes in Material and Shape Characteristics of Steel Tubes for Superconducting EDS Propulsion Type Hyperloop System. S. Kim[1], *H. Lee*[3], J. Lee[1] and W. Cho[2] *1. Electrical Engineering, Hanyang University, Seoul, The Republic of Korea; 2. Steel Structure Research Group, POSCO, Pohang-si, The Republic of Korea; 3. Department of Railway Engineering, Korea National University of Transportation, Uiwang-si, The Republic of Korea*

Based on the Hyperloop alpha[1] concept proposed by Elon Musk, various organizations such as HTT, TransPod, and Hyperloop Technology[2] are researching Hyperloop. In South Korea, KRRI has constructed an EDS superconducting propulsion system that installs superconducting electromagnets (SCM) on the vehicle and propulsion, levitation, and guidance coils on the ground[3]. The Hyperloop must maintain a sub-vacuum state inside the tube for drag-free driving, and steel tubes that can maintain this sub-vacuum state at all times must be applied. However, such a steel tube forms a driving resistance due to the magnetic field of a SCM. Therefore, this paper analyzed how this driving resistance changes depending on the material properties and shape characteristics of the steel tube. The theoretical background of the electromagnetic drag force (EDF) generated when a current-carrying coil moves on a conductor plate was first reviewed to analyze the electromagnetic drag generated by the steel tube. Based on this theoretical background, it was confirmed that the EDF received by a coil moving on a conductor plate is greatly affected by the skin effect and is influenced by the electrical conductivity and magnetic permeability of the material. However, since the permeability of steel materials generally varies nonlinearly with the strength of the magnetic field, electromagnetic analysis was performed using finite element analysis to consider the nonlinear characteristics. Based on the conductivity and B-H curve data of various steels that can be applied to the Hyperloop tube, the results of the finite element analysis were compared. For Hyperloop propulsion tubes, the hydrodynamic limit, the Kantrowitz limit[4], determines the minimum value of the tube diameter according to the pod diameter. Therefore, the EDF characterization was performed by increasing the diameter from the minimum tube diameter, and the EDF characterization was also performed by changing the tube thickness. In addition, the segmentation method of the tube to reduce the generated EDF was also analyzed.

[1] SpaceX, 2013. Hyperloop Alpha [2] Nanalyze, "3 Companies Building Elon Musk's Hyperloop," 2019. https://www.nanalyze.com/2016/04/3-companies-building-elon-musks-hyperloop/ (accessed June. 23, 2023). [3] K. S. Lee, 2018. Core technology development of subsonic capsule train, KRRI research report 2018-078 of Korea Railroad Research Institut, pp. 1-732. [4] M. Bizzozero, Y. Sato, M. A. Sayed, 2021. "Aerodynamic study of a Hyperloop pod equipped with compressor to overcome the Kantrowitz limit." *Journal of Wind Engineering and Industrial Aerodynamics*, 218, 104784. ISSN 0167-6105.

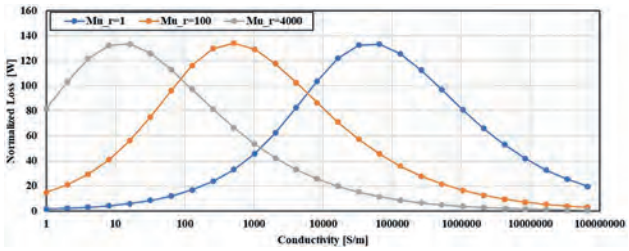

Loss analysis result according to the electrical conductivity and magnetic relative permeability

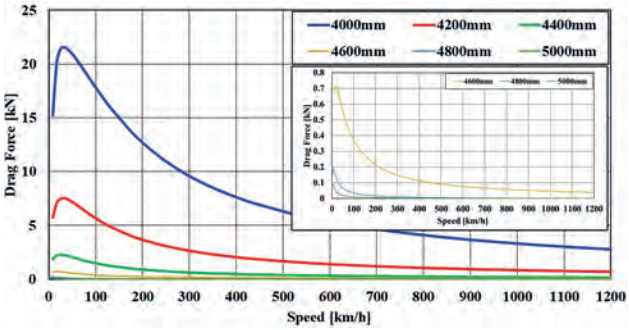

Drag forces analysis result according to the tube diameter

DR-08. Withdrawn

DR-09. Experimental verification for electromagnetic and thermal characteristics of a high-speed permanent magnet motor with two different rotors. *J. Woo*[1], J. Shin[2], K. Shin[1] and J. Choi[1] *1. Power System Engineering, Chonnam National University, Yeosu, The Republic of Korea; 2. Electrical Engineering, TNE Korea Co, Cheongju, The Republic of Korea*

Operating high-speed motors at relatively low frequencies is often advantageous from a control perspective. Therefore, these motors usually feature a two-pole and six-slot structural design. In such a case, the current harmonic component is considerably affected by the pulse-width modulation inverter owing to the small inductance, which in turn significantly affects the electromagnetic loss [1]. In high-speed motors, electromagnetic losses can cause demagnetization of the permanent magnet (PM) owing to overheating [2-3]. In this study, electromagnetic characteristics was determined using an improved electromagnetic loss analysis method that considers the current harmonics and magnetic field behavior of two motors with different rotor sizes. Subsequently, a thermal-characteristics analysis was performed based on the derived electro-magnetic loss to assess the effect of electromagnetic loss on heat generation. Fig. 1 shows the process of calculating core losses considering magnetic field behavior. The electromagnetic loss on the rotor side was determined by considering the current harmonics and the core loss using an improved electromagnetic loss analysis method based on magnetic field behavior analysis. Thermal analysis was performed through the finite element method (FEM) based on the calculated electromagnetic loss. Figs. 2 (a) and (b) show the maximum winding temperatures for both motors. Fig. 2 (c) shows the thermal measurement test results of the prototype model under an 18.67 kW water-cooling condition at the motor winding. Fig. 2 (d) shows the FEM analysis results of temperature measurement according to the drive rating. The proposed thermal analysis method was validated through an experiment using the initial prototype model, and the efficiency improvement of the high-speed PM motor and heat reduction design result through application to the improved model. Detailed analysis results will be provided in a comprehensive manuscript.

[1] Huynh, C.; Zheng, L.; Acharya, D. Losses in High Speed Permanent Magnet Machines Used in Microturbine Applications. J. Eng. Gas Turbines Power 2008, 131, 022301 [2] C. Micallef, S. J. Pickering, K. A. Simmons, and K. J. Bradley, "Improved cooling in the end region of a strip-wound totally enclosed fan-cooled induction electric machine," IEEE Trans. Ind. Electron., vol. 55, no. 10, pp. 3517–3524, Oct. 2008. [3] Cheol Han, Jang-Young Choi, Ji-Hun Ahn, Ji-Hwan Choi and Seok-Myeong Jang, "The harmonics influence and efficiency improvement in high-speed permanent magnet synchronous motor using 2-d finite element method" IEEE INTERMAG CONFERENCE 2012, Vancouver, Canada, May 7-11, 2012

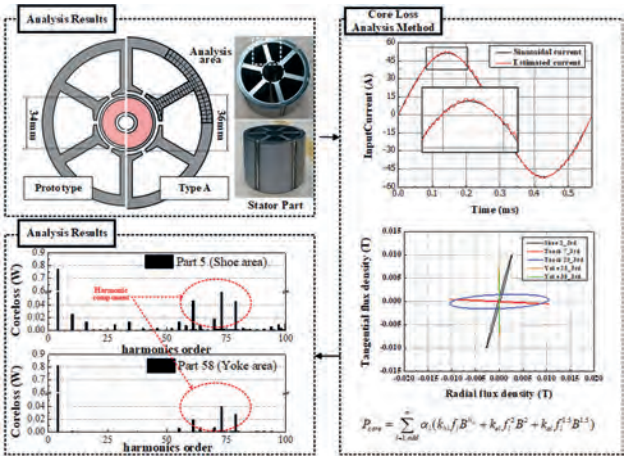

Core loss analysis method considering phase current waveform

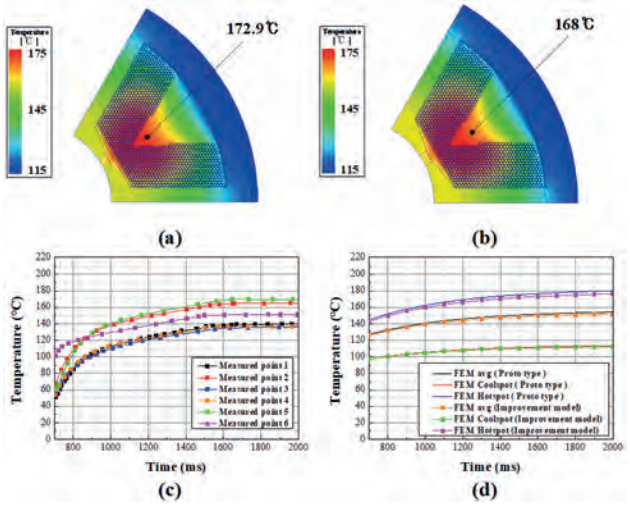

Highest heating point of (a) prototype model and (b) improved model winding; (b) experimental and (c) finite element method (FEM) analysis results of temperature measurement according to drive rating

DR-10. Design of Magnetization Yoke to Reduce the number of Double Spoke Type PMSM Magnetization Using I-Core. *D. Choi*[1], D. Nam[1], Y. Lee[1], N. Jo[1] and W. Kim[1] *1. Gachon University, Seongnam, The Republic of Korea*

This paper conducted a study on the reduction of the number of split Magnetization and the prevention of irreversible demagnetization using the I-Core of a double spoke type motor. Recently, as interest in spoke-type motors using ferrite permanent magnets has increased, the need for research on magnetization and irreversible demagnetization in double spoke-type rotor shapes has emerged. However, in the existing spoke-type rotor shape, the magnet was deeply embedded in the rotor, making it difficult to magnetization. As it is important to use permanent magnets excluding rare earths in the future, the use of spoke-type motors becomes important, and design to consider magnetization and prevent irreversible demagnetization accordingly is important. Therefore, this paper proposed a magnetization yoke shape design in consideration of magnetization and irreversible demagnetization on using I-Core of Double Spoke type PMSM to solve this problem.

DR-11. Effects of Permanent Magnets on Batteries in an Electrical Vehicle. *A.P. Singh*[1] and C.I. Nlebedim[1] *1. Critical Material Institute, Ames National Laboratory, Ames, IA, United States*

There is a global effort to decarbonize the transportation sector in which transportation electrification plays a very critical role. Development of sustainable technologies in the energy storage and drive-train aspects of electric vehicles (EVs) is required for transport electrification. Permanent magnet (PM) motors are preferred for electric vehicles but often require Nd-Fe-B magnets [1] which are prone to supply disruption, hence poses a long-time sustainability challenge. Although efforts have been made to replace some (or all) of the Nd-Fe-B magnets with the cheap and abundant ferrite/other low-performing magnets [2-3], success has been limited because it can affect the performance of the energy storage devices which is often not acceptable to manufacturers. However, a compromise in magnets strength will not only affect the energy consumption of the system but also the battery's efficiency and its lifetime in the long run. Thus, this work offers a modeling approach to study the effects of PM performance on the energy storage device in an EV. A computationally efficient model is developed for simulating the performance of the PM motor (drivetrains) and battery (energy-storage) systems in terms of the state of charge (SOC) of the battery and total energy consumption in a drive cycle. A schematic of the modeling approach is shown in Fig. 1 with the interaction between the two systems. The magnet properties, particularly remanence/recoil permeability, are varied with fixed coercive field in a permanent magnets motor and evaluate its performance in terms of efficiency using a finite element analysis. A permanent magnet motor with rating/performance equivalent to Nissan-Leaf-2012 and the vehicle parameters from [4] are considered in this analysis. To evaluate the magnets performance in an EV, a standard drive cycle (UDDS, here) is used for computing total energy consumptions and SOCs (Fig. 2) with two PMs with B_r (1.1 T and 0.8T). This research was supported by the Critical Materials Institute, an Energy Innovation Hub funded by the U.S. Department of Energy, Office of Energy Efficiency and Renewable Energy, Advanced Materials and Manufacturing Technologies Office.

[1] V. T. Buyukdegirmenci, A. M. Bazzi, and P. T. Krein, "Evaluation of Induction and Permanent-Magnet Synchronous Machines Using Drive-Cycle Energy and Loss Minimization in Traction Applications," *IEEE Trans.Inds. App.*, vol. 50, pp. 395-403, 2014. [2] A. P. S. Baghel, and I. C. Nlebedim, "A Hybrid Rotor Design with Reduced Rare Earth Magnet for Traction Motors," *JOM*, vol. 75, pp. 557-565, 2022. [3] Y. Chen, T. Cai, X. Zhu, D. Fan and Q. Wang, "Analysis and Design of a New Type of Less-Rare-Earth Hybrid-Magnet Motor with Different Rotor Topologies," *IEEE Transactions on Applied Superconductivity*, vol. 30, pp. 1-6, 2020. [4] K. N. Genikomsakis and G. Mitrentsis, "A computationally efficient simulation model for estimating energy consumption of electric vehicles in the context of route planning applications," *Transport. Res. Part D: Transp. Environ.*, vol. 50, pp. 98-118, 2017.

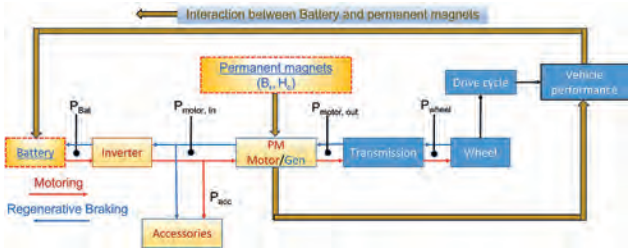

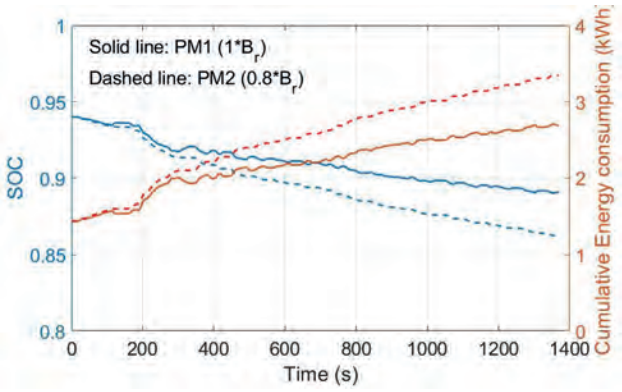

DR-13. Thermal Reduction Method for Outer Rotor Assembly of Magnetic-Geared Permanent Magnet Synchronous Motor for Tram Traction. J. Lim[1], *H. Lee*[1], J. Lee[1], I. Jo[2], S. Kim[2], T. Kim[3] and C. Park[1]
1. Korea National University of Transportation, Uiwang-si, The Republic of Korea; 2. Hanyang University, Seoul, The Republic of Korea; 3. University of Michigan-Dearborn, Dearborn, MI, United States

Currently, major cities in South Korea are considering the introduction of eco-friendly and affordable public transportation. One of the first alternatives is tram. It is eco-friendly as it does not use internal combustion engines, and it can utilize the same roads as automobile roads, saving huge construction costs compared to existing subways [1-4]. However, due to the limited space available for mounting the traction motor in tram compared to subways, the size of the traction motor needs to be reduced. To achieve this, gears are used to increase the rotational speed of the motor and transmit it to the wheels at a lower actual speed. At this time, the direct contact between the teeth of the gears causes wear and tear, which is why they need to be maintained regularly [5]. If there is a problem with the gears, it will cause the railway vehicle to break down and fail to operate, which will increase traffic congestion on existing roads and cause accidents [6]. This paper propose a Magnetic Geared-Permanent Magnet Synchronous Motor (MG-PMSM) for traction of trams that can replace the existing mechanical gears and traction motors. Unlike conventional drive systems, this consists of magnetic gears and traction motors as one system. Rare earth neodymium permanent magnets are inserted in the inner rotor and stator, and the gear ratio varies with the number of permanent magnets. Since there is no direct contact between the gear teeth, it has an advantage over conventional systems in terms of maintainability, and it can also solve vehicle breakdowns and operational disruptions caused by broken gears. However, when a 45kW-class MG-PMSM for tram traction was manufactured and tested, it was found that the Poly Ether Ether Ketone(PEEK) supporters inserted between the outer rotor, which are made of soft magnetic material, were melted. Also, when viewing the outer rotor assembly from the outside, it was found that the edge parts of PEEK were intensively deformed by heat. Therefore, this paper investigates why heat from the core, a soft magnetic material, melted the PEEK, proposes a solution, and validates it usung FEA to present an alternative model.

[1] https://www.intelligenttransport.com/transport-articles/23541/efficient-tram-flexible-bus/ (Accessed June 2023) [2] Z. Xiao, H. Chen and J. Guo, "Joint Optimization of Speed and Voltage Trajectories for Hybrid Electric Trams", IEEE Transactions on Industry Applications, Vol. 57, No. 6, p6427 (2021) [3] Y. Zhang, Z. Wei and H. Li, "Optimal Charging Scheduling for Catenary-Free Trams in Public Transportation Systems", IEEE Transactions on Smart Grid, Vol. 10, No. 1 (2019) [4] M. Echarri, L. Azpilicueta and V. Ramos, "From 2G to 5G Spatial Modeling of Personal RF-EMF Exposure Within Urban Public Trams", IEEE Access, Vol. 8, p100930 (2020) [5] C. Bae Park, H. Woo Lee and G. Jeong, "Performance verification of DR-PMSM for traction system according to permanent magnet shape", AIP advances, Vol. 10, No. 2, (2020) [6] Y. Fang, Y. Jiang and W. Fei, "Disruption Recovery for Urban Public Tram System: An Analysis of Replacement Service Selection", IEEE Access, Vol. 8, p31633 (2020)

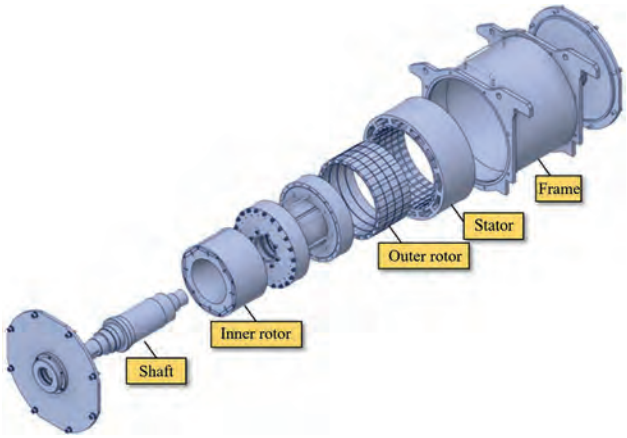

3D Configuration of MG-PMSM

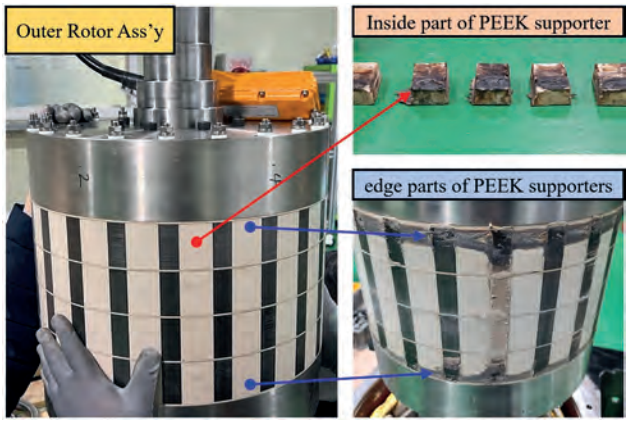

PEEK melting point on the outer rotor

DR-14. A Study on Eddy Current Loss Reduction in Single Phase Claw-Pole Motor. *N. Jo*[1], H. Pyo[1], Y. Lee[1], D. Kim[2] and W. Kim[1]
1. Gachon University, Gyeonggi-do, The Republic of Korea; 2. Hanyang University, Seoul, The Republic of Korea

Single-phase Claw-Pole motors can be largely divided into stator types and rotor types depending on their structure. In the case of the rotor type, the winding or permanent magnet is wrapped around the rotor, which is disadvantageous for maintenance, repair, and cost reduction due to additional factors such as brushes and slip rings. In the case of the stator-type Claw-Pole, the ring winding is wrapped in the shape of a stator Claw-Pole in a permanent magnet-type rotor, making it easy to manufacture winding and molds, but the eddy current loss is very large due to the non-stacked steel plate structure using SMC by the stator. The driving principle of the stator type is that the polarity of the up and down Claw is determined by the armature winding magnetic force and the current direction, and a magnetic torque between the magnetic pole formed on the Claw and the permanent magnet generates a rotating force in one direction. Applying the slit structure to the stator core can have the same effect as stacking of existing motors. Air insulation due to the slit structure creates induced electromotive force, which is a source of eddy current, and reduces eddy current loss by increasing electrical resistance compared to the same area. Therefore, the slit structure was applied and analyzed according to the location as shown in Figure 1 to the Claw and stator back yoke parts with relatively many changes in magnetic flux, relatively small magnetic resistance, and the Slit 1 model and Slit 3 model were combined to reduce eddy current. As shown in Figure 2, the Slit 1 model has a 17.4% decrease in Claw and current losses compared to the existing model, the Slit 2 and Slit 3 models have a 8.77% decrease in stator and current losses, respectively. In addition, Claw-Pole motors increase torque and efficiency by reducing eddy current loss because performance

degradation caused by eddy current loss occurs relatively more than conventional motors. Depending on the slit position of the proposed model, the torque compared to the existing model increased by 1.3%, 17.2%, 3.2%, and 2.5%, respectively.

[1] Dae-Sung Jung.(2014). The Study on the design of Claw Pole Stepping Motor considering Axial flux. Journal of the Korean Institute of Illuminating and Electrical Installation Engineers, 28(9),28-34. [2] H. -J. Pyo, J. W. Jeong, J. Yu, D. -W. Nam, S. -H. Yang and W. -H. Kim, "Eddy Current Loss Reduction in 3D-Printed Axial Flux Motor Using 3D-Printed SMC Core," 2020 IEEE Energy Conversion Congress and Exposition (ECCE), Detroit, MI, USA, 2020, pp. 1121-1125, doi: 10.1109/ECCE44975.2020.9235442. [3] Lim Seung-bin, "Magnetic Equivalent Circuit Method and Three-Dimensional Yuhan-Yo" "Effective Shape Optimization of Crow-Fall Motor Using Small Method," Degree Paper (Doctor), Graduate School of Hanyang University, Seoul, 2007

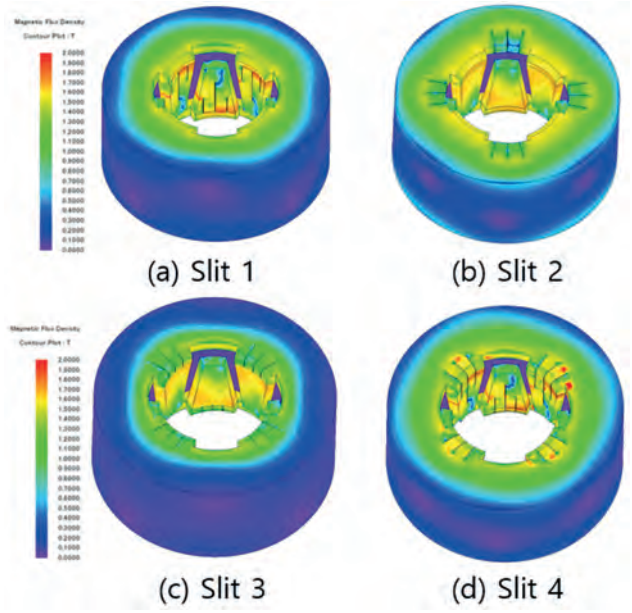

Stator magnetic flux saturation according to Slit position

Modle	Eddy Loss [W]		Torque [mNm]	Efficiency [%]
	Claw	Stator back yoke		
Slit 1	0.71	1.83	24.76	61.54
Slit 2	0.84	1.56	24.86	62.35
Slit 3	0.86	1.3	25.22	63.89
Slit 4	0.68	1.7	25.06	62.5

Performance Comparison of Proposed Models

DR-15. Electromagnetic characteristics analysis of winding process error in parallel delta-connection BLDC motor. *H. Shin*[1] and M. Koo[1]
1. Korea Institute of Industrial Technology, Gimje-si, The Republic of Korea

As a cooling fan motor for engine cooling of a passenger car using an engine as the main power source, a brush DC type motor using a low voltage of 12V is generally used. However, as users' demands for increased mileage and improved noise and fuel efficiency have increased, the number of vehicles employing BLDC motors with easy speed control and high energy efficiency is increasing [1]. As the delta connection is advantageous for the low-voltage and high-current source compared to the Y connection, it is widely used in low voltage motors for vehicles like engine cooling fan BLDC motors. In addition, it is a trend that is widely applied because it is advantageous to manufacture products that consider productivity, such as winding process. When parallel winding is applied, the phase current flowing through the coil wires can be distributed as much as the number of parallel windings, and in the case of delta connection, the value of inter-line resistance can be reduced up to three times compared to that of Y connection [2]. Since BLDC motors generally monitor the current in the inverter in real time through a sensor, it is relatively easy to analyze the motor winding characteristics through current characteristics analysis [3]. However, in the case of a motor having a two-parallel delta connection structure, since it is difficult to diagnose a motor fault only with the line current characteristics, in this paper, the error occurred in a low-voltage cooling fan BLDC motor with a parallel delta connection. The analysis of the effect of the wiring error on the no-load characteristics and load characteristics of the motor will be dealt with.

[1] TY Lee, MK Seo, YJ Kim and SY Jung, IEEE Transactions on applied superconductivity, vol.26, no.4, (2016) [2] Duane Hanselman, E-Man Press LLC, 2012 [3] JS Park, BG Gu, JH Kim, JH Choi and IS Jung, 4th International Conference on Power Engineering, Engergy and Electrical Drives, 2013

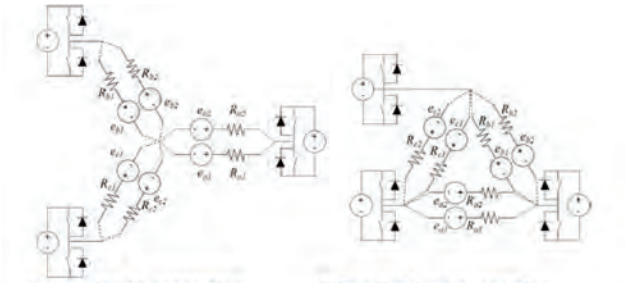

Fig.1 Winding schematic of parallel condition

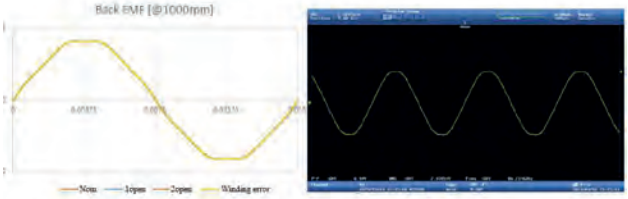

Fig.2 Comparison of BEMF analysis and measurement results according to wiring errors

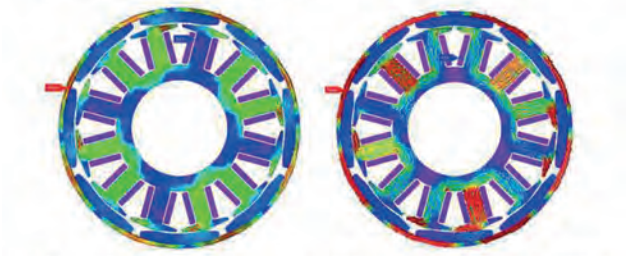

Fig.3 Comparison of magnetic flux density distribution

DR-16. Analysis of Multilayer Shielding Panels With Absorbing Materials Between Two Conducting Plates. J. Kwon[1] and *H. Park*[2]
1. Electronics and Telecommunications Research Institute, Daejeon, The Republic of Korea; 2. The University of Suwon, Hwaseong, The Republic of Korea

Shielding enclosures or facilities are used to protect electronic devices and systems against external electromagnetic waves and noises. These shielding enclosures or facilities are mostly manufactured as an assembly of conducting panels. As the conducting panels age over time, cracks or gaps arise between

them, which reduce the shielding effectiveness of enclosures or facilities [1]-[3]. Therefore, there is a need for a way to maintain the shielding properties of enclosures and facilities even if unwanted cracks or gaps occur in the conductor panels. This paper proposes a multilayer panel structure in which an absorber made by magnetic or dielectric materials is placed between two conductor panels as depicted in Fig. 1. In addition, the shielding characteristics of the proposed multilayer panel structure were analyzed using an analytic solution based on the mode matching method. When there are slots in the conductor plates, it was confirmed that the shielding property was improved by having an absorbing material between the conductor plates. Fig. 2 compares the case without and with the absorbing material in the two conductor plates when the width of slots on the conducting plate is 100 mm and the thickness of absorbing material is h = 30 mm. It can be seen that, despite the presence of slots in both conductor plates, the electric field is reduced as the frequency increases due to the absorbing material. In addition, in order to confirm the accuracy of the analytical solution based on the mode matching method, it was compared with the 3D numerical simulation results using CST Microwave Studio. They matched each other well. Acknowledgement**:** This work was supported by Institute of Information & communications Technology Planning & Evaluation (IITP) grant funded by the Korea government(MSIT) (No. 2020-0-00917, Development of Key Technologies for Low-cost EMP Protective Materials, Components, Devices(MCD) & Facilities Vulnerability Assessment)

1. H. A. Méndez, “Shielding theory of enclosures with apertures,” IEEE Trans. EMC, vol. 20, pp. 296–305, May 1978. 2. J. H. Kwon, et. al, ‘Improving shielding effectiveness of enclosure with apertures using absorbers’, 2019 IEEE Symp. EMC+SIPI, New Orleans, LA, USA, July 2019, 3. Jong-Hwa Kwon, Chang-Hee Hyoung, Jung-Hwan Hwang and Hyun Ho Park, “Impact of absorbers on shielding effectiveness of metallic rooms with apertures,” MDPI Electronics, vol. 10, no. 3, Jan. 2021.

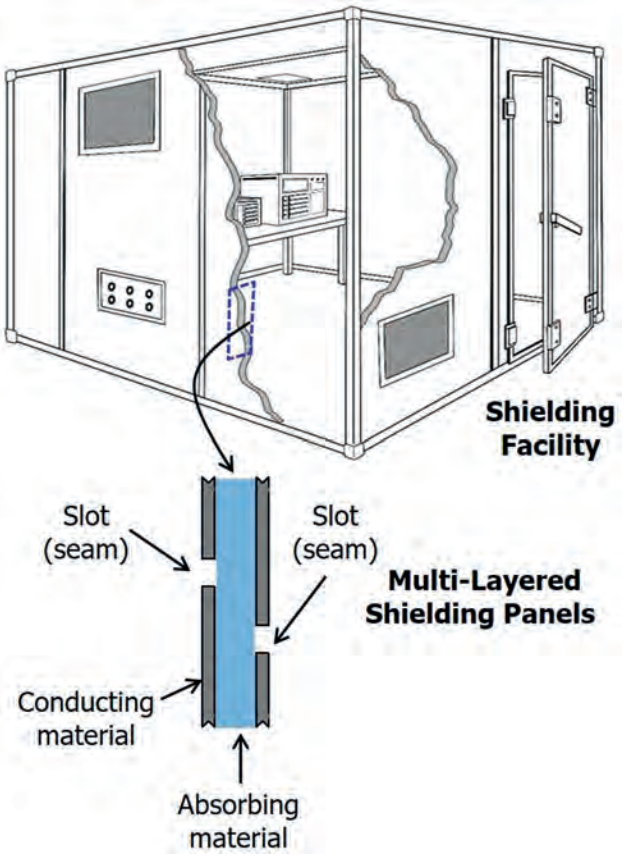

Proposed shielding panel with absorbing materials

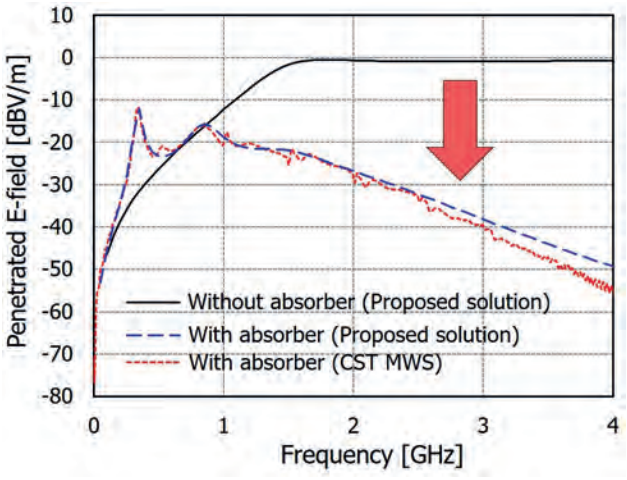

Analysis results of penetrated electric fields through the shielding panels

Session YA
EVENING SESSION 2: MAGNETO-IONICS

Karin Leistner, Chair
Technische Universität Chemnitz, Chemnitz, Germany

INVITED PAPERS

YA-01. Oxygen-based Magneto-ionics: Mechanisms, Recent Developments and Perspectives. *L. Herrera Diez*[1] *1. Centre for Nanoscience and Nanotechnology CNRS- Université Paris Saclay, Palaiseau, France*

The ability to manipulate magnetic properties through ionic motion in ferromagnetic/oxide structures in a non-volatile way, rather than the volatile purely electronic means, presents exciting opportunities for the development of functionalities like reconfigurable multistate memories and the implementation of cumulative gate effects in spintronics devices. Oxygen-based magneto-ionics takes inspiration from memristor technologies and offers one of the most advanced approaches today for controlling magnetic properties using ionics. In this talk, I will discuss the chemical-physical mechanisms underlying the observed effects on magnetic properties and explore the various available device geometries. Furthermore, I will provide an overview of recent advancements and novel functionalities enabled by oxygen-based magneto-ionics in spintronics devices, while also addressing the challenges and opportunities associated with this field.

YA-02. When Smaller is Better: Advancing Magneto-ionics with Protons. *G. Beach*[1] *1. Department of Materials Science and Engineering, Massachusetts Institute of Technology, Cambridge, MA, United States*

Voltage control of magnetism has the potential to substantially reduce power consumption in spintronic devices, while offering new functionalities through field-effect operation. The last decade has seen the emergence and rapid development of a new means of achieving such control, through the marriage of magnetic and ionic functionality in materials, in what has come to be termed magneto-ionics [1,2]. The most prominent examples have been based on electric field driven O^{2-} displacement, which can trigger reversible interfacial redox reactions in ferromagnet/oxide stacks [3] or stoichiometric changes in bulk magnetic oxides [4]. These electrochemical changes yield dramatic changes in a wide range of magnetic properties, but often at unattractive timescales and at the expense of structural degradation. This talk will focus on utilizing the smallest ion, H^+, to achieve fast, nonvolatile, voltage-controlled magnetic property switching in a manner that largely mitigates the irreversibility and structural degradation inherent to oxygen redox-based devices. We show that H_2O hydrolysis in ambient atmosphere catalyzed by a rare-earth oxide/noble metal interface can serve as a solid-state proton pump that enables nondestructive magnetic property gating with a modest voltage [5]. Unlike other ions, H^+ not only exhibits a high mobility in well-selected oxides, but upon meeting a metal/oxide interface, it can be incorporated into a metallic heterostructure as interstitial H. After providing a mechanistic overview of the process, the talk will detail examples of interfacial and bulk magneto-ionic switching in thin-film heterostructures, including anisotropy at ferromagnet/heavy-metal interfaces [5], ferrimagnetic order in CoGd alloys [6], interlayer exchange coupling in Co/Ru/Co stacks [7], and exchange bias in ferromagnet/antiferromaget bilayers [8]. The talk will close with a discussion of device opportunities and the challenges that remain to be solved in order to realize them.

[1] U. Bauer, *et al.*, *Nature Nano.* 8, 411 (2013). [2] U. Bauer, *et al.*, *Nature Mater.* 14, 174 (2015). [3] M. Nichterwitz, *et al.*, *APL Materials*, 9, 030903 (2021). [4] C. Leighton, *Nature Mater.* 18, 13 (2019). [5] A. J. Tan, *et al*, *Nature Mater.* 18, 35 (2019). [6] M. Huang, *et al.*, *Nature Nano.*, 16, 981 (2021). [7] A. Kossak, *et al.*, *Sci. Adv.*, 9, eadd0548 (2023). [8] M. U. Hassan, *et al.*, *submitted* (2023).

Session EA
ORBITRONICS: FROM ORBITAL CURRENTS CREATED BY CHARGE CURRENTS TO CREATION BY LIGHT OR RF EXCITATION

Mairbek Chshiev, Chair
SPINTEC, Univ. Grenoble Alpes, CEA, CNRS, Grenoble, France

INVITED PAPERS

EA-01. Orbitronics: Light-induced Orbit Currents in Terahertz Emission Experiments. Y. Xu[1], F. Zhang[1], *H. Jaffres*[2], Y. Liu[1], R. Xu[1], Y. Jiang[1], H. Cheng[1], A. Fert[2] and W. Zhao[1] *1. Beihang University, Beijing, China; 2. Universite Paris-Saclay, Palaiseau, France*

Recent progress in orbitronics reveals the possibility of using orbit current as an information carrier. Several recent works have highlighted the importance of the orbital degree of freedom in condensed matter physics and kicked off the emergent research field of orbitronics [1]. Orbitronics exploits the transport of orbital angular momentum through materials by orbit currents which can be exploited as an information carrier in solid-state devices. As for the conversion between spin and charge current by SHE or SREE, it has been theoretically predicted and experimentally shown that a charge current can be converted into an orbit current via the orbital Hall effect (OHE) or the orbital Rashba-Edelstein effect (OREE) [2–4]. THz emission from magnetic heterostructures offers a unique opportunity for studying the orbital effects [5]. Here we show that orbital currents can be created by femtosecond light pulses on Ni layers and then converted to charge current pulses for the emission of terahertz pulses. Based on the new experimental method, we study the production of light-induced orbit current and their exploitation for terahertz emission from NM/Ni bilayers with NM = Cu, Ta or Pt. We find terahertz emission of the same polarity with Cu, Ta, and Pt as NM in NM/Ni bilayers despite the opposite SHE of Ta with respect to Pt (this common polarity is also opposite to the polarity of the AHE-induced emission by a Ni monolayer). We ascribe these results to an efficient light-induced emission of orbit currents in Ni, and we have presented a detailed analysis of them in the simpler situation of Cu/Ni from which, in addition, we can extract information on the velocity and orbital flip time of the orbit carriers. The main general results are that orbit currents can be generated not only by conversion from charge or spin currents but also induced by light. In THz emission experiments, the analysis of the emission delays can bring precious information on the dynamics of the orbit carriers. All these results open new routes for developing future devices using orbit currents.

[1] D. Go, D. Jo, H.-W. Lee, et al., Europhys. Lett. 135, 37001 (2021). [2] D. Go, D. Jo, T. Gao, et al., Phys. Rev. B 103, L121113 (2021). [3] H. Kontani, T. Tanaka, D. S. Hirashima, et al., Phys. Rev. Lett. 102, 016601 (2009). [4] D. Lee et al., Nat. Commun. 12, 1 (2021). [5] Y. Xu, F. Zhang, Y. Liu, et al., arXiv:2208.01866.

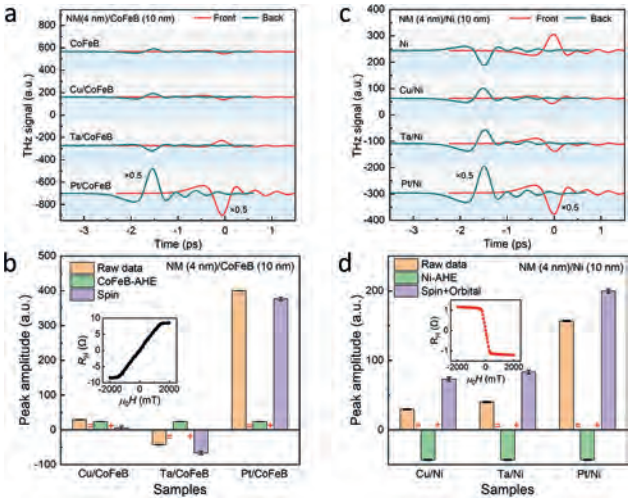

Fig. 1 A comparison between THz signals from NM/CoFeB and NM/Ni heterostructures. a) THz waveforms emitted from CoFeB (10 nm), Cu (4 nm)/CoFeB (10 nm), Ta (4 nm)/CoFeB (10 nm), and Pt (4 nm)/CoFeB (10 nm) measured with front and back sample excitations. b) THz waveforms emitted from Ni (10 nm), Cu (4 nm)/Ni (10 nm), Ta (4 nm)/Ni (10 nm), and Pt (4 nm)/ Ni (10 nm) measured with front and back sample excitation. c-d) Schematic illustration of the decomposition of the back THz signals of NM/CoFeB in panel a) or NM/Ni in b) into the sum of the signals in CoFeB or Ni single layers (we call it AHE, see later) and the added contribution introduced by NM in bilayers (we call it spin + orbital). The insets display the Hall resistance RH as a function of the out-of-plane magnetic fields H for CoFeB and Ni layers in insets of c) and d), respectively.

EA-02. Generation of Orbital Currents Driven by Spin Pumping. E.S. Santos[1], J.E. Abrão[1], J.B. Mendes[2] and *A. Azevedo*[1] *1. Physics, Federal University of Pernambuco, Recife, Brazil; 2. Physics, Federal University of Viçosa, Viçosa, Brazil*

The ability to manipulate magnetic moments without the need of magnetic field has been vital for the advancement of spintronic devices. This can be accomplished through the utilization of spin transfer torque (STT) to the local magnetization. STT can be achieved either by a flow of spin-polarized charge current or by a flow of pure spin current, utilizing the phenomenon known as spin-orbit torque (SOT). Although charge and spin currents are extensively employed in spintronic device technology, the orbital angular momentum (OAM) degree of freedom of electrons has largely been disregarded until now. Despite the expectation that the crystal fields would suppress the OAM, some theoretical studies have predicted the existence of non-equilibrium OAM flow perpendicular to a charge current. This surprising phenomenon occurs even in cases where OAM is quenched in solids or in materials with a weak spin orbit coupling (SOC). Termed the orbital Hall effect (OHE), this perpendicular OAM flow serves as the orbital counterpart of the spin

Hall effect (SHE). The fundamental physics governing orbital dynamics lies in the coupling between the orbital degree of freedom and the crystalline lattice, particularly in the presence of an external electric field. This coupling enables the transfer of angular moment from the lattice to the OAM. In materials with strong SOC, the out-of-equilibrium OAM can be transferred to the spin degree of freedom. Similar to SHE, OHE can be caused by bulk or interface phenomena, as shown in recent experiments where an electric current flows through an interface between a heavy-metal and a light-metal oxide. For a review about the phenomena of orbital dynamics, see Ref.[1]. In this talk, we will present experimental results of the excitation of orbital current by means of spin pumping driven by ferromagnetic resonance (FMR) on YIG/Pt/CuO_x heterostructures [2]. The spin current injected at the YIG/Pt interface couples with the angular momentum of Pt, facilitated by its strong SOC, and subsequently diffuses to the Pt/CuOx interface, where the inverse orbital Rashba-Edelstein effect (IORRE) occurs. We show that, due to the strong SOC of Pt, the pure spin current injected into Pt becomes intertwined with the local orbital states, resulting in the generation of an upward pure spin-orbital current (with no flow of charge). A portion of this current is then converted within Pt into a transverse charge current through either the inverse SHE or the inverse OHE. The remaining spin-orbital current flowing upwards is transformed into a transverse charge current via the inverse OREE at Pt/CuOx. The YIG/Pt/CuOx sample exhibits an ISHE-like voltage measurement that shows more than a fivefold gain compared to the sample without the CuOx coating. The same result was obtained by means of thermal-driven spin pumping technique. We also performed an extensive investigation on the interaction between spin, orbital and charge in FM/NM/CuO_x, using Permalloy or Co as FM (ferromagnet) and Pt, W, Ti, and Cr as NM (non-magnetic). Through a comparison of experimental results between FM/HM with FM/HM/CuOx configurations, we found substantial changes in the ISHE-type signal, suggesting a pivotal role played by HM/CuOx interface.

[1] Dongwook Go et al. Orbitronics: Orbital currents in solids, EPL 135 37001 (2021). https://doi.org/10.1209/0295-5075/ac2653. [2] E. Santos, et al. Inverse Orbital Torque via Spin-Orbital Intertwined States Phys. Rev. Applied 19, 014069 (2023). https://doi.org/10.1103/PhysRevApplied.19.014069.

EA-03. Orbital Torque and Orbital Pumping. *K. Lee*[1] *1. Department of Physics, KAIST, Daejeon, The Republic of Korea*

The orbital Hall effect [1,2] describes the generation of orbital currents flowing perpendicular to external electric field, analogous to the spin Hall effect. As orbital currents carry angular momentum as spin currents do, the injection of orbital current into a ferromagnet can result in torque on the magnetization [3], which provides a way to detect the orbital Hall effect. With this motivation, we examine current-induced spin-orbit torques in various ferromagnet/heavy metal bilayers by theory and experiment [4]. Analysis of the magnetic torque reveals the presence of a contribution from the orbital Hall effect, which competes with a contribution from the spin Hall effect. In particular, we find that net torque in Ni/Ta bilayers is opposite in sign to the spin Hall theory prediction but instead consistent with the orbital Hall theory. This orbital torque can enhance net spin-orbit torque via efficient orbital-to-spin conversion [5]. We also present a theory of orbital pumping, which is the Onsager reciprocity of orbital torque.

[1] H. Kontani et al., Giant orbital Hall effect in transition metals: Origin of large spin and anomalous Hall effects. Phys. Rev. Lett. 102, 016601 (2009). [2] D. Go and D. Jo, C. Kim, and H.-W. Lee, Intrinsic spin and orbital Hall effects from orbital texture. Phys. Rev. Lett. 121, 086602 (2018). [3] D. Go and H.-W. Lee, Orbital torque: Torque generation by orbital current injection. Phys. Rev. Research 2, 013177 (2020). [4] D. Lee et al., Orbital torque in magnetic bilayers. Nat. Commun. 12, 6710 (2021). [5] S. Lee et al., Efficient conversion of orbital Hall current to spin current for spin-orbit torque switching. Commun. Phys. 4, 234 (2022).

EA-04. First-Principles Investigation of Orbital Edelstein Effect in Co/Al Heterostructure. *S. Nikolaev*[1], M. Chshiev[2] and A. Fert[3] *1. Osaka University, Osaka, Japan; 2. SPINTEC, Univ. Grenoble Alpes, CEA, CNRS, Grenoble, France; 3. UMR CNRS-Thales, Paris, France*

Orbitronics is an emerging field of research aimed at creating and manipulating orbital currents, as opposed to the field of spintronics which is focused on the generation and control of spin currents instead. Various theoretical studies have shown that orbital degrees of freedom can mediate non-equilibrium transport phenomena such as the orbital Hall and orbital Edelstein effects and that the injection of orbital currents into a ferromagnet can excite magnetization dynamics [1-3]. Recent experiments have reported on the enhanced spin-orbit torque in a Pt/Co bilayer upon adding a well-protected Al layer on top of Co, which does not occur when a Cu layer is placed instead of Al [4]. In particular, the field-like and damping-like components of the spin-orbit torques at the interfacial Co layer were shown to be increased up to 9 and 4 times, respectively. As spin-orbit coupling is small in light elements such as Al, these experiments suggest that the enhanced spin-orbit torque can originate from the orbital Edelstein effect at the interface rather than from the spin Hall effect, which is conventionally regarded as one of the main sources to generate spin currents. In this study, we carry out a theoretical analysis of the orbital Edelstein effect in the Co/Al and Co/Cu heterostructures by combining first-principles calculations and linear response theory. As follows from the results shown in Fig. 1, the Co/Al heterostructure reveals a giant orbital texture at the interfacial Co layer with a clear helical locking of the in-plane orbital momentum in the reciprocal space, which is found to be much smaller at the Co/Cu interface. According to our calculations, the origin of the chiral orbital texture can be attributed to a non-trivial hybridization due to the formation of surface states at the interfacial Al layer. Importantly, such a large orbital texture preserves itself even in the absence of spin-orbit coupling but cancels out when summed over the Brillouin zone yielding zero orbital magnetic moments in equilibrium at each Co layer. Upon including spin-orbit coupling, the orbital texture at the interface is found to be slightly enhanced and to be exceedingly larger than the corresponding spin texture. We further employ the Kubo formalism using the Wannier functions technique to calculate the orbital magnetoelectric susceptibility in response to an applied electric current. Our calculations unveil that the orbital texture can bring about the out-of-equilibrium orbital polarization producing large field-like spin-orbit torques. In conclusion, our results demonstrate that the enhanced spin-orbit torque in the Co/Al heterostructure can be attributed to the orbital texture that gives rise to the orbital Edelstein effect at the interface, thus providing a rigorous theoretical interpretation for recent experiments [4].

[1] T. Tanaka *et al*, Phys. Rev. B, Vol. 77, p. 165117 (2008) [2] D. Go and H.-W. Lee, Phys. Rev. Research, Vol. 2, p. 013177 (2020) [3] D. Go *et al*, Phys. Rev. Research Vol. 2, p. 033401 (2020) [4] S. Krishnia *et al*, arXiv:2205.08486v2

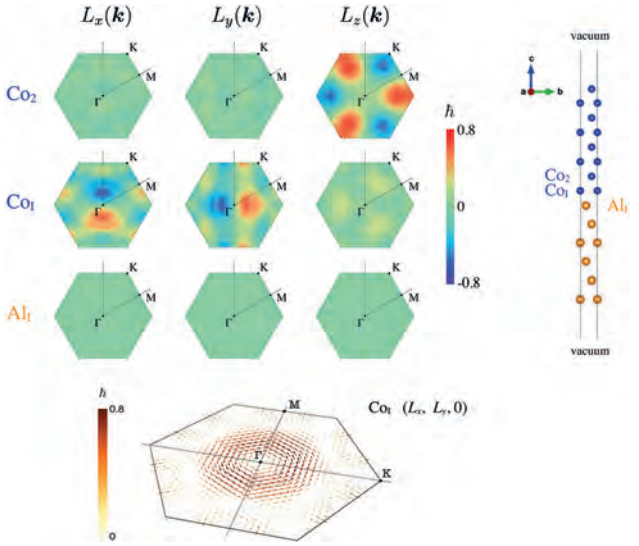

Fig. 1. Layer-resolved orbital textures calculated for the Al(111)/Co(0001) heterostructure.

EA-05. Orbital Torques and Orbital Magnetoresistance in Transition-Metal Elements. *G. Sala*[1] *1. University of Geneva, Geneva, Switzerland*

For a long time, the orbital angular momentum has been considered a frozen degree of freedom in condensed matter because of the symmetry constraints imposed by the crystal field. However, recent theoretical and experimental works have shown that the orbital momentum does participate in transport phenomena [1-3]. In particular, non-equilibrium orbital angular momentum can be induced by electric currents by means of the so-called orbital Hall and orbital Rashba-Edelstein effects, which do not require spin-orbit coupling. This discovery has triggered a paradigm shift with fundamental and technological implications. It offers a new perspective on the physical mechanisms underlying the generation and transport of angular momentum in crystals [4]. In addition, it opens up the intriguing possibility of exciting orbital dynamics that have no spin counterparts [5]. Finally, it promises a more efficient generation of spin-orbit torques by engineering the interplay of spin and orbital currents [6-8]. These findings aroused great interest in the spintronic community. In this talk, I will discuss the most recent experimental results on the orbital generation and transport in transition-metal elements. In particular, I will focus on spin-orbit torques and magnetoresistance measurements that provide clear evidence of orbital effects in 3*d* transition metals. I will conclude with an outlook on possible future steps necessary to explore the orbital physics.

[1] Go, Phys. Rev. Lett., Vol. 121, p. 086602 (2018 [2] Salemi, Phys. Rev. Materials, Vol. 5, p. 074407 (2021) [3] Ding, Phys. Rev. Lett., Vol. 125, p. 177201 (2020) [4] Go, Phys. Rev. Res., Vol. 2, p. 033401 (2020) [5] Han, Phys. Rev. Lett., Vol. 128, p. 176601 (2022) [6] Lee, Comm. Phys., Vol. 4, p. 234 (2021) [7] Lee, Nat. Comm., Vol. 12, p. 66710 (2021) [8] Sala, Phys. Rev. Res., Vol. 4, p. 033037 (2022)

Session EB
NEUROMORPHIC JUNCTIONS AND NEW DESIGN

Atsufumi Hirohata, Chair
University of York, York, United Kingdom

CONTRIBUTED PAPERS

EB-01. Stochastic Charge Transport and Noise Characteristic in AlO_x Magnetic Tunnel Junctions. *C. Chen*[1], B. Huang[1], Y. Tang[1], C. Gonzalez-Ruano[2], F. Aliev[2] and J. Hong[3] *1. Department of Physics, National Central University, Taoyuan City, Taiwan; 2. Departamento de Física de la Materia Condensada, Universidad Autónoma de Madrid, Madrid, Spain; 3. Department of Physics, Tamkang University, New Taipei City, Taiwan*

The metal/oxide heterostructures offer a reversible manipulation on the magnetic property and resistive switching (RS) for the low power consumption devices. [1,2] Building on this concept, the combination of magnetic tunnel junctions (MTJs) with RS enables the creation of multi-level thermal stable bits using both magnetic and electric fields, such as the merging of Magnetic Random Access Memory (MRAM) and Resistive Random Access Memory (RRAM). [3] However, studying the transport mechanism becomes challenging as the oxide layer scales down to sub-nanometer dimensions for RS systems. Random telegraph noise (RTN) is extensively studied in RRAM and MOSEFTs devices for accurately detecting charge dynamics through oxygen vacancies or interface traps [4,5] Recently, RTN has also been utilized to achieve probabilistic manipulation in magnetic tunnel junctions, resulting in the development of probabilistic bits (p-bits). [6] Beyond magnetic responses, Memristor based on stochastic events can also approach the similar mechanism. [7] In this study, we investigated RTN in AlO_x magnetic tunnel junctions with resistive switching. We observed stochastic behavior resulting from charge capture and emission via oxygen vacancies, as well as spin-dependent tunneling related to trap location within the tunneling barrier. To further examine these findings, we employed tight-binding model by our self-developed "JunPy" package. [8] The experimental results were successfully examined by the simulation model for spin-dependent tunneling magnetoresistance (TMR) with different RS states. Our study gives the promising application on the design of the spintronics devices with probabilistic and thermal stable multi-bit. This work is supported by the National Science and Technology Council, Taiwan (NSTC 108-2112-M032-003-MY2 / 108-2628-M-008-004-MY3 / 111-2112- M-008-025).

[1] U. Bauer et al., Nature materials., Vol.14, p.174 (2015). [2] A. Sawa, Materials today., Vol.11, p.28 (2008). [3] J.-Y. Hong et al., Scientific Reports., Vol.11, p.6027 (2021). [4] K. Ralls et al., Physical review letters., Vol.52, p.228 (1984). [5] D. Ielmini et al., Applied Physics Letters., Vol.96, p.053503 (2010). [6] K. Hayakawa et al., Physical review letters., Vol.126, p.117202 (2021). [7] K. S. Woo et al., Nature Communications., Vol.13, p.5762 (2022). [8] Y.-H. Tang et al., Physical Review B., Vol.96, p.064429 (2017).

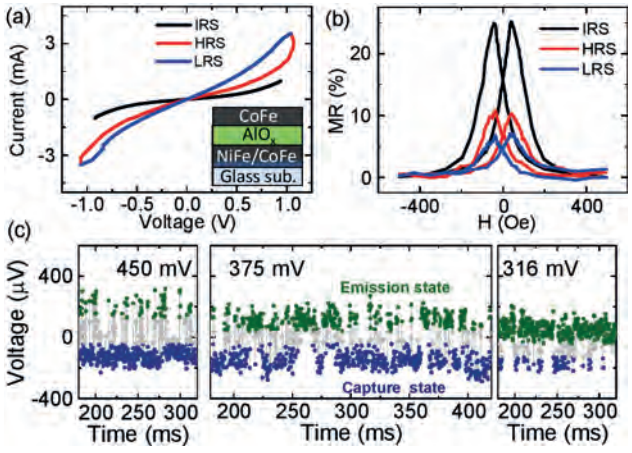

Fig 1. (a) The I-V curve and (b) MR curve of AlO_x MTJs with initial, high, and low resistance states (IRS, HRS, LRS). (c) The time domain of RTN at different bias voltage in LRS, showing the stochastic transition of charge capture and emission events.

EB-02. Bias voltage robustness in double-free-layer stochastic magnetic tunnel junction. *R. Ota*[1,2], K. Kobayashi[1,2], K. Hayakawa[1,2], S. Kanai[1,3], K.Y. Camsari[4], H. Ohno[1,3] and S. Fukami[1,3] *1. Research Institute of Electrical Communication, Tohoku University, Sendai, Japan; 2. Grad. School Eng., Tohoku University, Sendai, Japan; 3. Center for Science and Innovation in Spintronics, Tohoku University, Sendai, Japan; 4. Department of Electrical and Computer Engineering, UC Santa Barbara, Santa Barbara, CA, United States*

Stochastic magnetic tunnel junction (s-MTJ) is a promising ingredient in spintronics-based energy-efficient probabilistic bits (p-bits) [1,2]. For a typical p-bit cell [3], the s-MTJ is preferred to be robust against external disturbances, namely magnetic field and bias voltage, where a synthetic antiferromagnetic free layer structure was reported to be promising for magnetic field-robust operation [4]. Recent theoretical work proposed a bias voltage-robust s-MTJ with a double-free-layer (DFL) structure [5]. In this work, we experimentally study the voltage robustness of DFL s-MTJs with various thicknesses and the underlying mechanism. A stack structure, Ta (28)/ CoFeB (t_{bottom})/ MgO (1.1)/ CoFeB (t_{top})/ Ta (5)/ Ru (5) (nominal thickness in nm), is deposited by sputtering. We prepare several stacks having in-plane easy axis with various thickness pairs (t_{bottom}, t_{top}). The stacks are processed into elliptical MTJs with geometrically averaged diameters of ~120 nm [Fig. 1]. We monitor the random telegraph noise, reflecting parallel and antiparallel configurations, in the rf transmitted voltage under various bias voltages V_{dc}. Figure 2 shows the variation of the ratio of relaxation times for two configurations (τ_{AP}/τ_P) with V_{dc}, which is the robustness against bias voltage. While a conventional single-free-layer (SFL) s-MTJ [4] and a DFL s-MTJ with (t_{bottom}, t_{top}) = (2.5, 2.0) show significant V_{dc} dependence due to the spin-transfer torque, another DFL s-MTJ with (t_{bottom}, t_{top}) = (2.0, 2.5) is almost independent of V_{dc}. We derive an analytical solution of τ_{AP}/τ_P for the DFL s-MTJs and find τ_{AP}/τ_P is robust against V_{dc} when the thermal stability factors of the two layers are

close, consistent with the experimental results considering the thickness of magnetic dead layers t^d of the two layers (t^d_{bottom}, t^d_{top}) = (0.2, 0.7). This work was supported in part by the JST-CREST JPMJCR19K3, the JST-PRESTO JPMJPR21B2, JST-AdCORP JPMJKB2305, JSPS-Kakenhi 19H05622, Shimadzu Research Foundation, and Cooperative Research Projects of RIEC.

[1] K. Y. Camsari *et al*., Phys. Rev. X Vol. 7, p.031014 (2017) [2] W. A. Borders *et al*., Nature Vol. 573, p.390 (2019). [3] K. Y. Camsari *et al*., IEEE Electron Device Lett. Vol. 38, p.1767 (2017) [4] K. Kobayashi *et al*., Phys. Rev. Appl. Vol. 18, p.054085 (2022) [5] K. Y. Camsari *et al*., Phys. Rev. Appl. Vol. 15, p.044049 (2021)

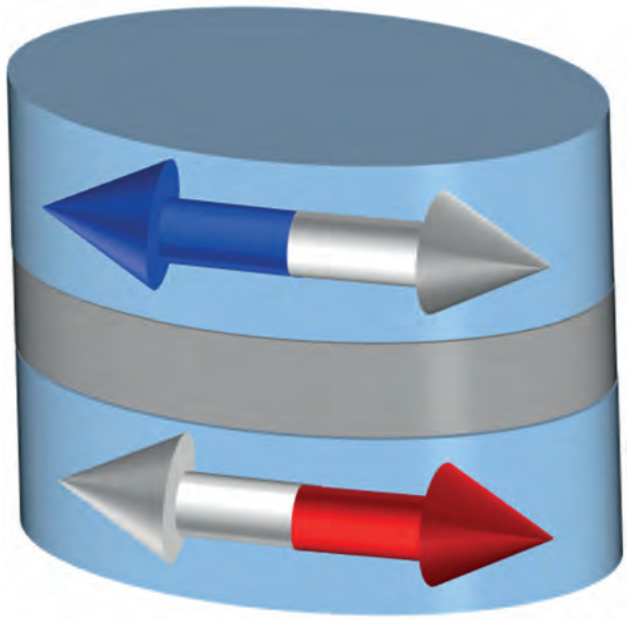

Fig. 1 Schematic image of DFL s-MTJ.

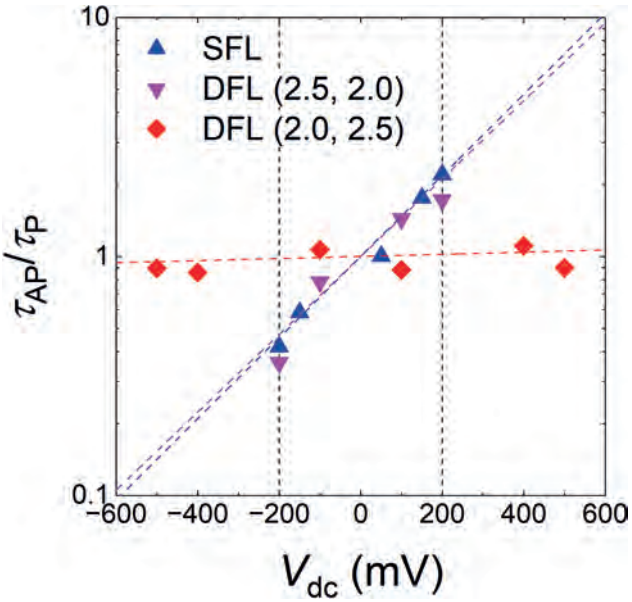

Fig. 2 τ_{AP}/τ_P *vs.* V_{dc} in DFL s-MTJ with (t_{bottom}, t_{top}) = (2.5, 2.0) and (2.0, 2.5) along with a conventional SFL s-MTJ. Lines are exponential fits.

EB-03. Reduced sensitivity to process-voltage-temperature variations in stochastic magnetic actuated random transducer devices.

M. Morshed[1], L. Rehm[2], A. Shukla[3], S. Ganguly[4], S. Rakheja[3], A.D. Kent[2] and A.W. Ghosh[1] *1. University of Virginia, Charlottesville, VA, United States; 2. New York University, New York, NY, United States; 3. University of Illinois at Urbana-Champaign, Champaign, IL, United States; 4. Virginia Commonwealth University, Richmond, VA, United States*

True random number generators (TRNGs) are fundamental building blocks for many applications, such as cryptography, Monte Carlo simulations, neuromorphic computing, and probabilistic computing [1]. Conventional complementary metal-oxide semiconductor (CMOS)-based TRNGs have large footprints and are energy hungry [2]. Nanomagnet-based TRNGs offer a new opportunity in this regard. Most studied nanomagnet-based TRNGs employ magnetic tunnel junctions (MTJs) that utilize low-barrier magnets (LBMs) operating in the superparamagnetic limit. LBMs have energy barriers comparable to thermal energy ($E_b \sim k_BT$), which allow the magnetic state to fluctuate spontaneously and require low energy to operate. However, they can suffer from slow dynamics, are extremely sensitive to process variations, and are hard to build in practice. Recently, medium-barrier magnet (MBMs) based perpendicular MTJs (pMTJs) operated with nano-second pulses — denoted, stochastic magnetic actuated random transducer (SMART) devices — have emerged as potential candidates to circumvent these drawbacks [3,4]. We present a systematic analysis of spin-torque-driven switching of the MBM-based pMTJs ($E_b \sim 20 – 40\ k_BT$) as a function of pulse duration (1ps to 1ms) by numerically solving their dynamics using a 1-D Fokker–Planck equation. We also investigate the impact of voltage, temperature, and process variations (e.g., MTJ's dimension and material parameters) on the switching probability of the device. Our results show SMART devices activated by short-duration pulses (≲ 1ns) are much less sensitive to process-voltage-temperature variations than the same devices operated with longer pulses (see Fig. 1). Our results agree well with recent experiments and show a path toward building a fast, energy-efficient, and robust TRNG hardware unit for solving optimization problems.

[1]. S. Misra, L. C. Bland, and J. B. Aimone, Adv. Mater., 2204569 (2022) [2]. K. Yang, D. Fick and D. Sylvester, IEEE ISSCC, pp. 280-281 (2014) [3]. L. Rehm, C. C. M. Capriata and A. D. Kent, Phys. Rev. Appl., 19, 024035 (2023) [4]. A. Shukla, L. Heller, and S. Rakheja, *ISQED,* pp. 1-10 (2023)

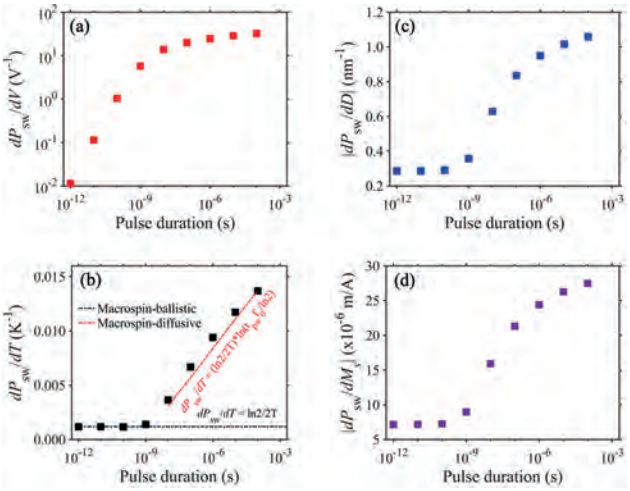

Fig. 1. Change of P_{sw} = 0.5 with respect to (a) voltage, (b) temperature, (c) MTJ diameter, and (d) saturation magnetization. In the short pulse regime, SMART devices are less sensitive to process-voltage-temperature variations.

INVITED PAPER

EB-04. Fully spintronic RF neural network. A. Ross[1], N. Leroux[1], A. De Riz[1], D. Markovic[1], D. Sanz Hernandez[1], J. Trastoy[1], P. Bortolotti[1], D. Querlioz[2], L. Martins[3], L. Benetti[3], M.S. Claro[3], P. Anacleto[3], A. Schulman[3], T. Taris[4], J. Begueret[4], S. Saïghi[4], A. Jenkins[3], R. Ferreira[3], A.F. Vincent[4], *F.A. Mizrahi*[1] and J. Grollier[1] *1. Unité Mixte CNRS/ Thales, Palaiseau, France; 2. Université Paris-Saclay, CNRS, Centre de Nanosciences et de Nanotechnologies, Palaiseau, France; 3. International Iberian Nanotechnology Laboratory (INL), Braga, Portugal; 4. Univ. Bordeaux, CNRS, Bordeaux INP, IMS, Talence, France*

Spintronic nano-synapses and nano-neurons perform neural network operations with high accuracy thanks to their rich, reproducible and controllable magnetization dynamics. These dynamical nanodevices could transform artificial intelligence hardware, provided that they implement state-of-the art deep neural networks. However, there is today no scalable way to connect them in multilayers. Here we show that the flagship nano-components of spintronics, magnetic tunnel junctions, can be connected into multilayer neural networks where they implement both synapses and neurons thanks to their magnetization dynamics, and communicate by processing, transmitting and receiving radio frequency (RF) signals. We build a hardware spintronic neural network composed of nine magnetic tunnel junctions connected in two layers, and show that it natively classifies nonlinearly-separable RF inputs with an accuracy of 97.7% [1]. Using physical simulations, we demonstrate that a large network of nanoscale junctions can achieve state-of the-art identification of drones from their RF transmissions, without digitization, and consuming only a few milliwatts, which constitutes a gain of several orders of magnitude in power consumption compared to currently used techniques. Based on these results, we propose an architecture to perform convolutions on images in a fully parallel way. As, convolutional neural networks are key to many state-of-the-art applications and are limited by the sequential way in which they are implemented in conventional hardware, this is an important step. Furthermore, we provide several paths for device optimization of the neurons and synapses, including how to obtain non-volatile weights and neurons with fixed frequency. This study lays the foundation for deep, dynamical, spintronic neural networks.

[1] Ross, Andrew, et al. “Multilayer spintronic neural networks with radio-frequency connections.” arXiv preprint arXiv:2211.03659. Accepted for publication in Nature Nanotechnology.

CONTRIBUTED PAPERS

EB-05. Easy-plane magnetic tunnel junction as an entropy source for computing. *J.Z. Sun*[1], C. Safranski[1], P. Trouilloud[1], C. D’Emic[1], P. Hashemi[1] and G. Hu[1] *1. IBM T. J. Watson Research Center, Yorktown Heights, NY, United States*

A nano-structured magnetic tunnel junction (MTJ) operating in superparamagnetic limit with easy-plane dominant anisotropy can convert thermal fluctuation of the magnetic moments into electric tunnel conductance fluctuation with nearly white spectrum beyond a GHz in bandwidth and could be useful as a compact electronic entropy source for computing. We explore the base-line behavior of such easy-plane dominant MTJs using materials and fabrication routes similar to spin-transfer-torque magnetic random-access memory (STT-MRAM). The measurement observations, both on analog time-series and the corresponding binary digitized bit-streams are analyzed for their randomness and spectrum content, and compared to behaviors generated from a 4-moment coupled macrospin Langevin model in comparable materials and operating parameters space. We show experimentally that stochastic bit-streams can be generated using these MTJs at a bit-rate around 1Gb/sec, and we establish the likely important factors in need for further materials and device optimization – chief of them the reduction of any unintended in-plane magnetic anisotropy energy in such junctions in comparison to thermal energy.

EB-06. Hybrid MRAM/SRAM Bit Cell with Self-Terminating MTJ Readout. *D. Biswas*[1], S.R. Evans[1], M.J. Rickard[1], A. Fowler[1], Y. Makris[1], N. Hassan[1], A.J. Edwards[1] and J.S. Friedman[1] *1. Electrical and Computer Engineering, The University of Texas at Dallas, Richardson, TX, United States*

One of the principal challenges related to the application of magnetic random access memory (MRAM) [1,2] is that current must be passed through the magnetic tunnel junctions (MTJs) every time they are read, incurring large dynamic power costs. This is particularly problematic in applications such as FPGA configuration memory that require a constant presentation of a voltage output, similar to static random-access memory (SRAM). It would therefore be ideal to provide a mechanism for MTJs to be latched after being read, with minimal read current pulses, thus eliminating dynamic read energy and minimizing static power and latency (Fig. 1a). We propose a hybrid MRAM/SRAM bit cell [3] comprising a differential pair of MTJs and a CMOS latch (Fig 1b). The MTJ pair may be fabricated as a single or multiple devices depending on technology constraints (Fig 2a-c). The circuitry is designed such that when power is restored, a brief current is supplied through the MTJs to create a voltage divider such that the voltage at node Vb determines the initial state of the latch. As the latch settles to a value determined by the MTJ resistance states, the current through the MTJs is automatically terminated in order to minimize the dynamic read energy. Finally, by asserting the Data and W_en signals, write current can be passed through the MTJs to set them in opposite states. We demonstrated successful operation of the bit cell [3]. We further demonstrate that the bit cell remains functional even with TMR as low as 100% (Fig. 2d). We therefore proposed and demonstrated the first hybrid MRAM/SRAM that can directly plug into existing SRAM arrays without additional area overhead, with no additional static power draw, and with instant-on data restoration.

[1] D. Apalkov, A. Khvalkovskiy, S. Watts, V. Nikitin, X. Tang, D. Lottis, K. Moon, X. Luo, E. Chen, A. Ong et al., “Spin-transfer torque magnetic random access memory (stt-mram),” ACM Journal on Emerging Technologies in Computing Systems (JETC), vol. 9, no. 2, pp. 1–35, 2013. [2] S. Ikegawa, F. B. Mancoff, J. Janesky, and S. Aggarwal, “Magnetoresistive random access memory: Present and future,” IEEE Transactions on Electron Devices, vol. 67, no. 4, pp. 1407–1419, 2020. [3] S. R. Evans, M. J. Rickard, A. Fowler, Y. Makris, N. Hassan, A. J. Edwards, D. Biswas, J. S. Friedman, Non-Volatile Memory Circuit with Self-Terminating Read Current, Government Microcircuit Applications & Critical Technology Conference, Mar. 2023.

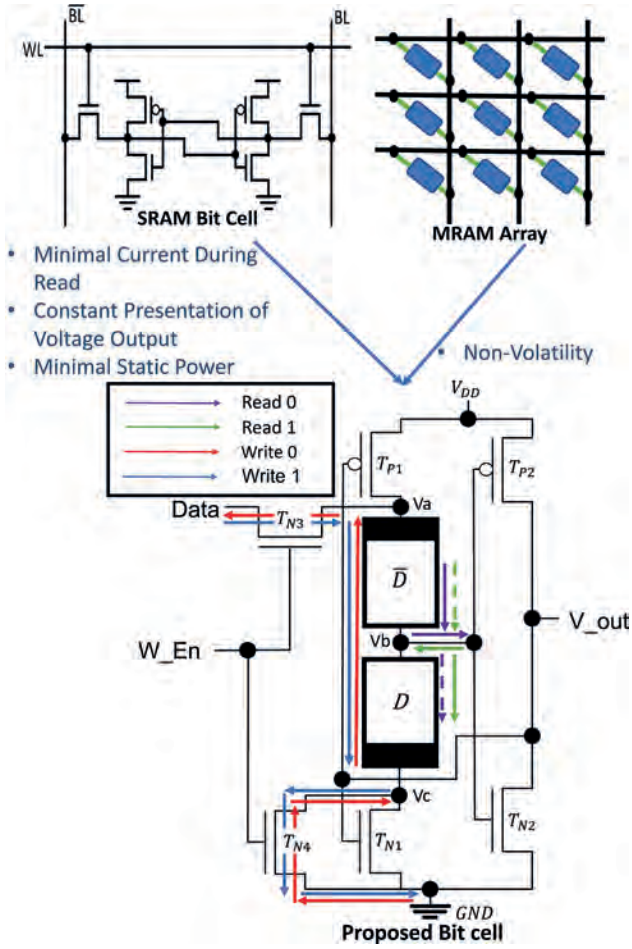

(a) A hybrid MRAM/SRAM cell should combine the non-volatility of MTJs with the power efficiency of SRAM. (b) The proposed bit cell comprises a differential pair of non-volatile MTJs supported by six access transistors that latch the state and output a constant voltage.

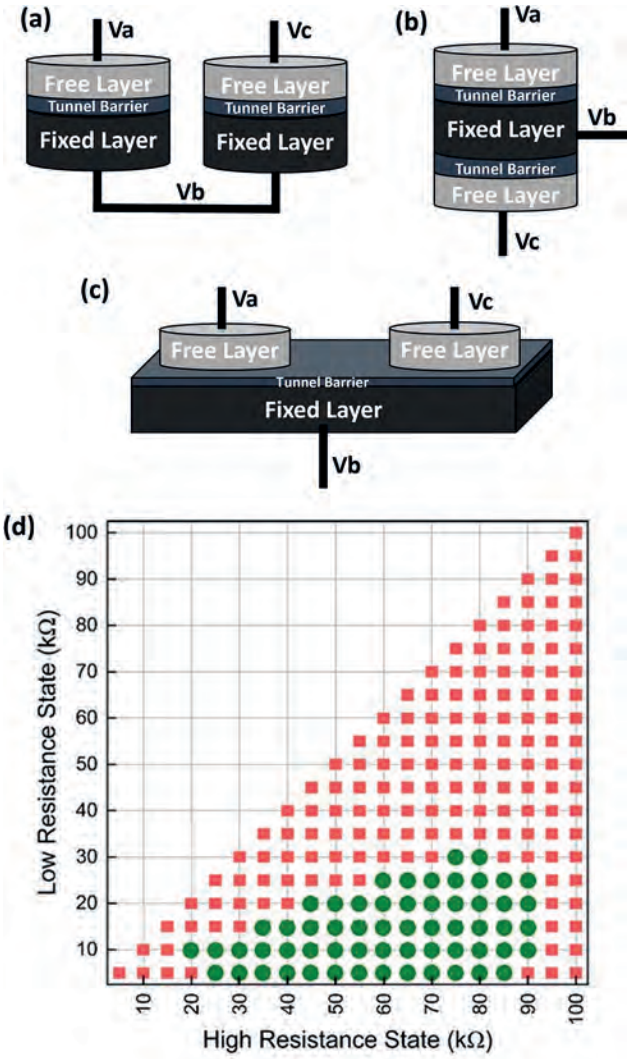

(a-c) Three fabrication methods of the differential MTJ pair. (d) MTJ resistance states were varied between 10 kOhm and 100 kOhm in simulation. Circles (squares) indicate proper (improper) functionality of the bit cell.

EB-07. Spintronic physical unclonable functions based on magneto-resistive memory. *J. Kang*[1], D. Han[1], D. Koh[1], S. Ko[1], K. Lee[2], J. Lee[3], C. Park[4], J. Ahn[4], M. Yu[4], M. Pakala[4], S. Lee[1], J. Park[2], K. Kim[1] and B. Park[1] *1. Korea Advanced Institute of Science and Technology, Daejeon, The Republic of Korea; 2. Korea University, Seoul, The Republic of Korea; 3. Hyundai Motor Company, Hwaseong, The Republic of Korea; 4. Applied Materials, Santa Clara, CA, United States*

Physical unclonable functions (PUF) are a promising candidate for future security primitives that offers secure communication and authentication for electronic devices [1]. They harness device-to-device variations during the manufacturing process or randomness of a physical entity to generate cryptographic keys. Conventional silicon-based PUFs such as the arbiter PUF and ring-oscillator PUF which utilize delay time or frequency differences as an entropy source undergo low randomness and reliability particularly under environmental fluctuations [2]. To resolve these issues, spintronic PUFs have been proposed to improve randomness and to generate highly reliable binary bits [3]. However, more commercialized form of spintronic PUF including nanoscale integration and higher on/off ratio through tunneling magneto-resistance (TMR) is yet to be realized. Here, we experimentally demonstrate nanoscale magneto-resistive memory-based PUF by randomizing the

reference layer of the 70 nm-sized synthetic antiferromagnetically coupled magnetic tunneling junctions. Figure 1a shows minor hysteresis loops of 64-bit magneto-resistive memory based PUF with the TMR ratio ~ 130 % for each unit cell. Polarity of the hysteresis loop which corresponds to the direction of the reference layer is randomly distributed after the randomization process, allowing us to utilize resistance distribution as an entropy source of the magneto-resistive memory-based PUF. The resulting PUF exhibits ideal uniformity, uniqueness of 0.988 and 0.500 respectively. They also show reconfigurability, reliability under environmental fluctuations. Furthermore, resilience against machine learning attacks are shown, promoting the development of spintronic PUF more into the industrial level.

[1] Y. Gao, S. F. Al-Sarawi, D. Abbott, *Nat. Electron.* 2020, *3*, 81. [2] J. L. Zhang, G. Qu, Y. Q. Lv, Q. Zhou, *J. Comput. Sci. Technol.* 2014, *29*, 664. [3] S. Lee, J. Kang, J.-M. Kim, *Adv. Mater.* 2022, *34*, 2203558

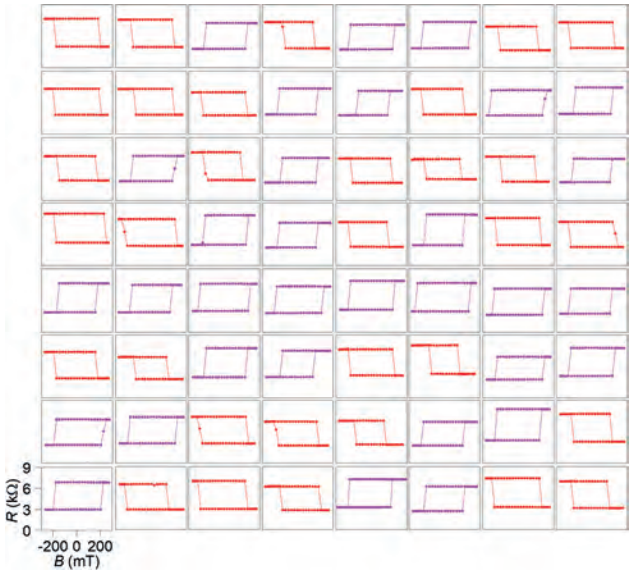

Fig. 1. Hysteresis loops of 64-bit magneto-resistive memory PUF. The curves are measured after the randomization process. Different polarity of hysteresis loops indicate different direction of reference layers.

EB-08. High Data Rate Spin-Wave Transmitter. *K. Xue*[1] and R. Victora[1]
1. Electrical and Computer Engineering, University of Minnesota, Minneapolis, MN, United States

Spin-wave devices have recently become a strong competitor in computing and information processing owing to their excellent energy efficiency [1]-[2]. A lot of effort has been made to explore magnons, the quanta of spin-waves, as an information carrier [3]-[4] and great progress has been made in exciting and transporting these spin-waves [5]. However, most waveguide designs remain immature in terms of data rate and information capacity as they could only send and detect simple spin-wave pulses. In this work, using micromagnetic simulations, we first demonstrate a spin-wave transmitter that could operate reliably at a data rate of 2 Gbps over a distance of about 7500 nm. This transmitter is essentially a rectangular yttrium iron garnet sample that is saturated along its in-plane transverse direction. Magnons are excited on one side of the sample by forcing the edge cells to precess coherently along the saturation direction at some predefined operating frequency (or carrier frequency). The precession angle switches between 0° and 10° according to an input bit sequence so that the information is encoded into the amplitude of the spin-waves. This is also known as amplitude-shift keying (ASK) in the radio frequency communication field. This device can be integrated into either pure-magnon circuits or electronic networks. For the latter case, Fig. 1 shows its signal-to-noise ratio (SNR) and bit error rate (BER) performance versus propagation length. The signal is collected by using a giant magneto-resistance (GMR) based detector. A total of 1116 bits are transmitted and a carrier frequency of 10 GHz is chosen. The smaller BER data are calculated by first fitting the SNR-BER relation to the equation in [6] and then extrapolating the BER curve. A monotonic dependence on propagation length is seen for both SNR and BER. The dashed line in Fig. 1 (b) demonstrates that these high data rate signals can travel a considerably long distance (~7500 nm) while maintaining high quality (BER < 10^{-6}).

[1] G. Csaba, Á. Papp and W. Porod, *Physics Letters*, Section A: General, Atomic and Solid State Physics, 381(17), 1471–1476 (2017). [2] A. Chumak, P. Kabos and M. Wu, *IEEE Transactions on Magnetics*, 58(6) (2022). [3] Q. Wang, M. Kewenig and M. Schneider, *Nature Electronics*, 3(12), 765–774 (2020). [4] A. Mahmoud, F. Vanderveken and C. Adelmann, *AIP Advances*, 10(3) (2020). [5] R. Salikhov, I. Ilyakov and L. Körber, *Nature Physics*, 19(April) (2023). [6] Y. Jiao, Y. Wang, and R. H. Victora, *IEEE Transactions on Magnetics*, 51(11), 11–14 (2015).

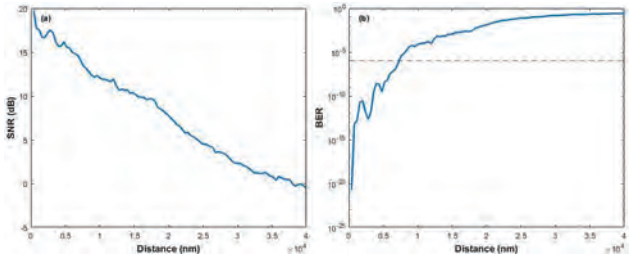

Fig. 1. Dependence of (a) SNR and (b) BER on propagation distance. The dashed line in (b) indicates a BER of 10^{-6}.

EB-09. Properties of ideal soft magnetic material, FeAlSi films for ultra-sensing spintronics device application. *S. Akamatsu*[1,2], B. Lee[3], Y. Hou[1], M. Oogane[2], G. Beach[3] and J. Moodera[1,4] *1. Plasma Science and Fusion Center, Massachusetts Institute of Technology, Cambridge, MA, United States; 2. Graduate School of Engineering, Tohoku University, Sendai, Japan; 3. Department of Materials Science and Engineering, Massachusetts Institute of Technology, Cambridge, MA, United States; 4. Physics, Massachusetts Institute of Technology, Cambridge, MA, United States*

Sendust alloys, known for their superior soft magnetic properties, are ideal candidates for tunnel-magneto resistance (TMR) sensors [1]. In the pursuit of understanding their electron transport properties and spin dynamics, we investigated Sendust (FeAlSi) films using inelastic electron tunneling spectroscopy (IETS) and Brillouin Light Scattering (BLS). This allowed us to observe Damon-Eshbach (DE), perpendicular standing spin wave (PSSW) mode magnons, ascertain the stiffness constant and band features, thereby contributing to a better understanding of the spin dynamics of FeAlSi, The IETS and BLS measurements were carried out using thin film stack structures on MgO substrates: MgO(20) / FeAlSi (30) / MgO(2) / $Co_{40}Fe_{40}B_{20}$(3) / Ru(0.85) / $Co_{75}Fe_{25}$(5) / $Ir_{22}Mn_{78}$(10) and MgO(20) / FeAlSi(30) / MgO(1.5) / Ta(1) (in nm). $Fe_{73.7}Al_{11.7}Si_{14.6}$ (at%) FeAlSi films were deposited and annealed at 400 °C, as optimized in our previous work [1]. The high-quality tunnel junction stacks showed excellent bias stability and TMR ratios of 121% (at 295K) and 180% (at 1.6 K). IETS and BLS [2] were measured to reveal rich features in FeAlSi films of various thicknesses. The symmetric peaks displayed in IET spectra at low V_{Bias}, were assigned to magnon modes at the FeAlSi/MgO interface and MgO phonon, consistent with previous works [3, 4]. High bias spectra presented asymmetric peaks, attributed to be arising from the band structure of the magnetic films. The interface magnons between FeAlSi and MgO were studied using BLS, that clearly showed the DE and PSSW mode peaks, as theory predicts. The estimated exchange stiffness constant for FeAlSi was 12.2 (pJ/m), close to that in Fe [5]. This work at MIT is supported by NSF, ONR, AFoSR, ARO, whereas SA visit to MIT is facilitated by the JSPS Grants-in-Aid for Scientific Research, X-nics project, and the GP-Spin, CIES and CSIS in Tohoku University. Fig. 1. IET spectra (The second derivative of current dependence on bias voltage V_{Bias}). Fig. 2. BLS spectra as a function of H. Inset: The dependence of peak positions for DE and PSSW modes on H.

[1] S. Akamatsu et al., Appl. Phys. Lett. 120, 242406 (2022). [2] Byung Hun Lee et al., Physical Review Letters 130.12 126703 (2023). [3] V. Drewello et al., Journal of Applied Physics 111.7 07C701 (2012). [4] Guo-Xing Miao et al., Journal of applied physics 99.8 08T305 (2006). [5] C. Vittoria et al., Journal of magnetism and magnetic materials 37.2 L111-L115 (1983).

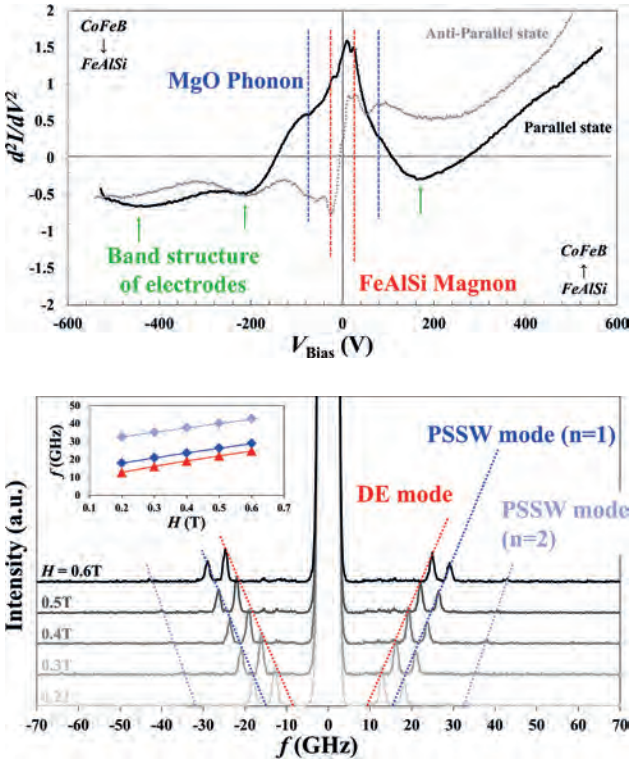

EB-10. Enhancing Performance of Anisotropic Magnetoresistive Sensors through Interface Engineering. *R.F. Constantino*[1,2], G. Brites[1,2], P. Araujo[1,2], R. Macedo[1] and S. Cardoso[1,2] *1. Instituto de Engenharia de Sistemas E Computadores – Microsistemas e Nanotecnologias (INESC MN), Lisbon, Portugal; 2. Instituto Superior Técnico, Universidade de Lisboa, Lisbon, Portugal*

Anisotropic magnetoresistance (AMR) sensors have revolutionized applications with their exceptional characteristics [1][2], however room for further improvement still exists. Strategies for Py film growth and interface enhancement have been explored, emphasizing the significance of capping and buffer layer materials. When Ta is used as a buffer, Py exhibits favorable magnetic properties in unpatterned and microfabricated samples [3] [4]. However, interdiffusion between Py and Ta leads to the formation of a magnetic dead layer [5]. To mitigate this effect, an additional dusting layer between the Py and adjacent layers [7][8] and magnetic annealing can be employed [9], that will also impact electron scattering, crystalline structure, and surface roughness. In this study, we examined unpatterned multilayers and microfabricated AMR devices with Pt and MgO layers at the Py interfaces. R(H) curves were obtained, and various parameters including ΔR, Rmin, magnetoresistance, coercive field (H_C), and H_k values were extracted. Figure 1 presents representative AMR(H) curves for patterned devices with MgO and Pt dusting and Figure 2 the AMR ratio summary for the samples before and after magnetic annealing. Samples with additional MgO layers initially exhibit a decrease in the AMR ratio compared to the reference Ta/NiFe/Ta stack (AMR = 2.06%). However, the results show that this reduction can be reversed through annealing, achieving AMR ratios of 2.47%. Conversely, samples with Pt extra layers display an increase in the AMR ratio, ranging from 2.13% to 2.2% with t=1 nm, however annealing at 350°C for 2 hours did not further increase the AMR. Further discussions will cover additional annealing temperatures (280-350°C) and times (up to 5 hours). This research enhances our understanding of AMR sensors, with implications for material testing, interface engineering, and industrial applications.

[1] 1. 1. Khan MA, Sun J, Li B. Engineering Research Express. 2021;3:022005. [2] 1. Zheng C, Cardoso de Freitas S, Freitas PP. IEEE Transactions on Magnetics. 2019;55:1–30. [3] 1. Guo Y, Ouyang Y, Sato N. IEEE Sensors Journal. 2017;17:3309–15. [4] 1. Svalov AV, González Asensio B, Chlenova AA. Vacuum. 2015;119:245–9. [5] 1. Kowalewski M, Butler WH, Moghadam N. Journal of Applied Physics. 2000;87:5732–4. [6] 1. Huangfu J, Liu Y, Feng C. Rare Metals. 2012;31:117–20. [7] 1. Li M, Han G, Ding L. Journal of Magnetism and Magnetic Materials. 2012;324:1–3. [8] 1. Liu YF, Cai JW, Sun L. Applied Physics Letters. 2010;96:092509. [9] 1. Lu QH, Huang R, Wang LS. Journal of Magnetism and Magnetic Materials. 2015;394:253–9.

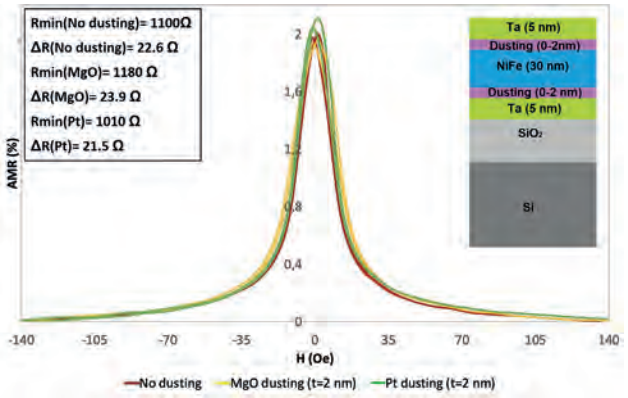

Fig. 1: Representative AMR(H) transfer curves obtained in micro-patterned AMR sensors with no dusting and 2 nm thick MgO and Pt dusting layers.

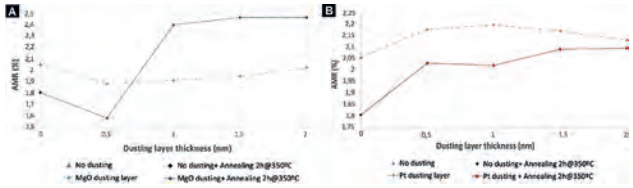

Fig. 2: Average AMR values obtained in micropatterned AMR sensors with [A] MgO and [B] Pt dusting layers of thicknesses t=0-2nm before and after magnetic annealing at 350°C for 2h

EB-11. Withdrawn

EB-12. Higher-Order Nonlinear Transverse Spin Hall Magnetoresistance. *T. Shiino*[1], P.C. Van[2], H. Kim[3], J. Choi[1], K. Lee[3], K. Kim[3], J. Jeong[2] and B. Park[1] *1. Department of Materials Science and Engineering, KAIST, Daejeon, The Republic of Korea; 2. Department of Material Science and Engineering, Chungnam National University, Daejeon, The Republic of Korea; 3. Department of Physics, KAIST, Daejeon, The Republic of Korea*

We report our finding of current-induced higher-order *n*-fold ($n > 4$) inplane rotational symmetries in the XY plane in transverse spin-Hall magnetoresistance (TSMR) of platinum (Pt)/yttrium-iron-garnet (YIG) bilayers. The higher-order *n*-fold TSMR behavior, which is contrasted to unidirectional magnetoresistance [1], was observed in the large current regime. The significant nonlinearity is represented by the square-wave-like angle dependence of the second-harmonic TSMR curves (see Fig. 1). The square-wave-like

curve can be expressed by the summation of cos($n\varphi$) curves. We discuss the possible origin of the angle dependence considering higher-order contributions from spin-orbit torques.

[1] G. Liu et al., Phys. Rev. Lett., Vol. 127, 207206 (2021)

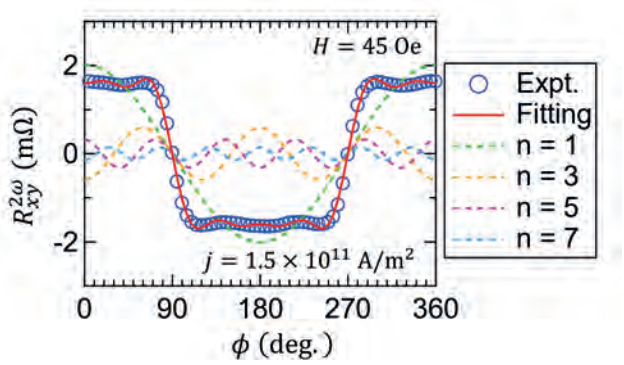

Fig. 1 Angle dependence of the second-harmonic Hall resistance.

Session EC
SOFT MAGNETIC MATERIALS II: AMORPHOUS AND NANOCRYSTALLINE MATERIALS

Nicola Morley, Co-Chair
University of Sheffield, Sheffield, United Kingdom
Alpha N'Diaye, Co-Chair
Lawrence Berkeley National Laboratory, Berkeley, CA, United States

INVITED PAPER

EC-01. Nucleation barriers and Hysteresis in Soft Magnetic Alloys.
A. Renuka Balakrishna[1] *1. Materials Department, University of California, Santa Barbara, Santa Barbara, CA, United States*

In 1914, a magnetic alloy with an unusually high magnetic permeability and low coercivity was discovered at the Bell Telephone Laboratories. This magnetic alloy resulted from a series of investigations on the iron-nickel alloy system, in which the nickel content and manufacturing conditions, such as heat treatment, magnetic annealing and mechanical loads, were systematically varied. Under a very specific combination of the alloy composition (78.5% nickel content) and manufacturing conditions, the magnetic alloy (now known as the permalloy) demonstrates a drastic increase in the magnetic permeability and a decrease in coercivity. In the past, this unusual behavior of the permalloy has been attributed to the anisotropy constant, however, there is still no theory that explains this drastic decrease in coercivity in magnetic alloys. In a departure from prior work, we hypothesize that a combination of a large local disturbance (needle microstructure) and material constants (e.g., anisotropy, magnetostriction) contributes to the drastic decrease in hysteresis in magnetic alloys. We recently developed a nonlinear framework based on the micromagnetics theory to test this hypothesis, and our findings provide insights into the longstanding permalloy problem and suggest a new mathematical relationship between material constants for which magnetic hysteresis is minimum.

[1] AR Balakrishna and RD James. Design of soft magnetic materials. npj Computational Materials, 8(1):1–10, 2022. [2] AR Balakrishna and RD James. A tool to predict coercivity in magnetic materials. Acta Materialia, 208:116697, 2021. [3] AR Balakrishna and RD James. A solution to the permalloy problem—a micromagnetic analysis with magnetostriction. Applied Physics Letters, 118(21):212404, 2021.

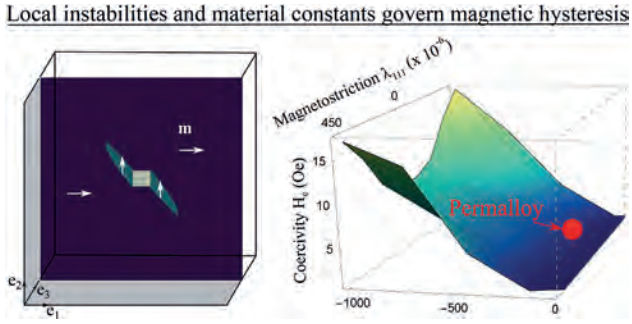

CONTRIBUTED PAPERS

EC-02. Extreme Temperature Stability of Induced Anisotropies in Co-rich Nanocrystalline Ribbon.
T. Paplham[1], A. Leary[2], Z. Wang[1] and P. Ohodnicki[1,3] *1. Mechanical Engineering and Materials Science, University of Pittsburgh, Pittsburgh, PA, United States; 2. NASA Glenn Research Center, Cleveland, OH, United States; 3. Department of Electrical and Computer Engineering, University of Pittsburgh, Pittsburgh, PA, United States*

A shear loop desirable for inductive applications has been shown to be achievable in nanocrystalline tape-wound cores by applying a saturating magnetic field or large mechanical stress to the ribbon during the initial thermal processing [1-6]. While the temperature stability of field-annealed Co-rich amorphous and nanocrystalline cores has been previously studied [5], this work more comprehensively examines the anisotropy energy as a function of temperature and time held at temperature for both field- and stress-induced anisotropies. Trends in the anisotropy energy for the Co-rich system will be connected to microstructure and mechanisms for observed changes will be suggested. We will also examine the role that an applied field during the reannealing step, mimicking the operating condition of the core, plays in overall stability. Understanding of the thermo-temporal stability of field- and stress-induced anisotropy is critical for extreme temperature environments such as in aerospace and space exploration applications, e.g., the surface of Venus [7], where temperatures are comparable to the primary crystallization temperature of the nanocrystalline core material.

[1] H. Kronmüller, Physica Status Solidi (b), Vol. 118, p. 661 (1983) [2] G. Herzer, Materials Science and Engineering: A, Vol. 181-182, p. 876 (1994) [3] A. Leary, V. Keylin and A. Devaraj, Journal of Materials Research, Vol. 31, p. 3089 (2016) [4] P.R. Ohodnicki, J. Long, and D.E. Laughlin, Journal of Applied Physics, Vol. 104 (2008) [5] P.R. Ohodnicki, D.E. Laughlin and M.E. McHenry, Journal of Applied Physics, Vol. 105 (2009) [6] S. Kernion, P.R. Ohodnicki and J. Grossmann, Applied Physics Letters, Vol. 101 (2012) [7] P. Beauchamp, M. Gilmore and R. Lynch, IEEE 2021 Aerospace Conference (2021)

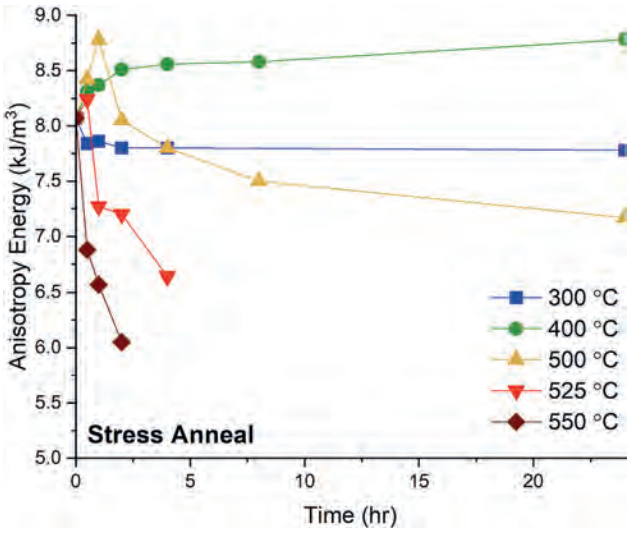

Fig. 1: Initial results for anisotropy energies in an example stress-annealed Co-rich nanocrystalline alloy as a function of reannealing time and temperature, as estimated by strip tests of reannealed ribbon segments.

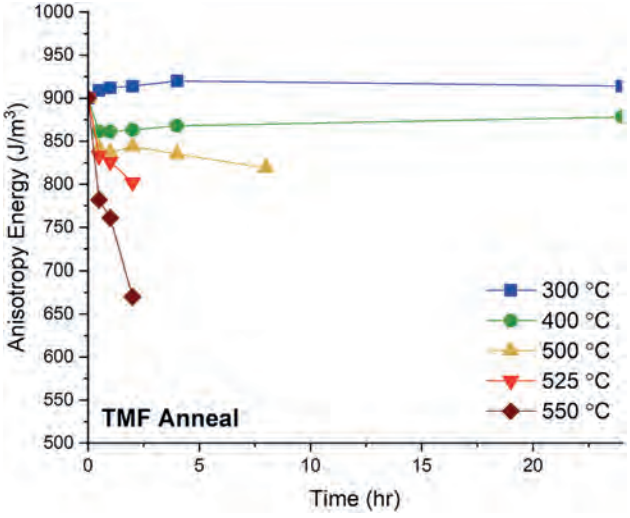

Fig. 2: Initial results for anisotropy energies in an example transverse magnetic field-annealed Co-rich nanocrystalline alloy as a function of reannealing time and temperature, as estimated by strip tests of reannealed ribbon segments.

EC-03. Theory of amorphous chiral spin textures: a case study of amorphous FeGe. *T. Bayaraa*[1,2] and S.M. Griffin[1,2] *1. Materials Science Division, Lawrence Berkeley National Laboratory, Berkeley, CA, United States; 2. Molecular Foundry, Lawrence Berkeley National Laboratory, Berkeley, CA, United States*

Magnetic spin textures are both fundamentally intriguing and relevant to novel information storage and processing units, such as the racetrack memory which harnesses electromagnetism in solids to link topological properties to electronic transport phenomena. Recent results from our collaborators found evidence of 3D chiral spin textures, such as helical spins and skyrmions with different chirality and topological charge, stabilized in amorphous FeGe thin films [1]. Here, we look at the emergence of chiral spin textures in amorphous FeGe by means of first-principles calculations and ab-initio molecular dynamics simulations. We investigate how the atomic arrangement of randomness affects the electronic, magnetic, and topological properties of amorphous FeGe, and present new theoretical insights into the accurate prediction and modeling of amorphous quantum materials.

[1] Streubel, R., Bouma, D. S., Bruni, F., Chen, X., Ercius, P., Ciston, J., N'Diaye, A. T., Roy, S., Kevan, S. D., Fischer, P., Hellman, F., Chiral Spin Textures in Amorphous Iron–Germanium Thick Films. Adv. Mater. 2021, 33, 2004830.

EC-04. Temperature influence on magnetic properties and magnetoimpedance effect of Co- rich glass-coated microwires. P. Corte-Leon[1,3], I. Skorvanek[2], F. Andrejka[2], M. Jakubcin[2], V. Zhukova[1,3] and *A. Zhukov*[1,3] *1. Dept. Polymers and Advanced Materials, University of Basque Country, UPV/EHU, San Sebastian, Spain; 2. Institute of Experimental Physics, Slovak Academy of Sciences, Kosice, Slovakia; 3. Dept. Applied Physics I, Escuela de Ingeniería de Gipuzkoa EIG, University of Basque Country, UPV/EHU, San Sebastian, Spain*

Recently studies of glass-coated microwires with excellent soft magnetic properties (low coercivities of about 5 A/m, high magnetoimpedance, MI, ratio up to 600%), the reduced dimensions, good mechanical properties, excellent corrosion resistance and biocompatibility have attracted substantial attention owing to emerging applications [1,2]. One of such promising applications deals with design of multifunctional composite materials with magnetic wires inclusions suitable for nondestructive and contactless stress and temperature monitoring [2]. Consequently, studies of temperature dependence of the MI effect become essentially pertinent. However, there are only a few publications on temperature dependence of MI and magnetic properties of Co-rich amorphous wires [3]. We report our most recent experimental results on the influence of temperature on the magnetic properties and MI effect of $Co_{69.2}Fe_{3.6}Ni_1B_{12.5}Si_{11}Mo_{1.5}C_{1.2}$ glass-coated microwires with vanishing magnetostriction coefficient. Specially designed experimental system allowed impedance measurements of the microwire and evaluation of the MI ratio in a temperature, T, range from ambient temperature up to 300 °C at frequencies up to 110 MHz [4]. The MI effect measurements were performed at a frequency range from 5 MHz up to 110 MHz. Hysteresis loops of the microwires were measured by means of vibration sample magnetometer (VSM) MicroSense EV9 and by fluxmetric method. The MI has been presented as MI ratio, $\Delta Z/Z$, determined as [4]: $\Delta Z/Z = [Z(H) - Z(H_{max})] / Z(H_{max})$, (1) being Z the impedance of the microwire, H and H_{max}, the applied DC magnetic field and the maximum field, respectively. We observed that upon heating the hysteresis loop changed its shape from inclined to rectangular (see Fig.1a). These changes in hysteresis loop shape correlate with modification of $\Delta Z/Z(H)$ dependencies from double-peak to single-peak (see Fig.1b). The origin of observed temperature dependences can be explained taking into account contributions from the Hopkinson effect, the relaxation of the internal stresses and temperature dependence of the named internal stresses.

1. D. Kozejova, L. Fecova, P. Klein, R. Sabol, R. Hudak, I. Sulla, D. Mudronova, J. Galik, R. Varga, J. Magn. Magn. Mater. 470, 2 (2019). 2. A. Allue, P. Corte-León, K. Gondra, V. Zhukova, M. Ipatov, J.M. Blanco, J. González, M. Churyukanova, S. Taskaev, A. Zhukov, Compos. Part A Appl. Sci. and Manuf. 120, 12 (2019). 3.L.V. Panina, A. Dzhumazoda, S.A. Evstigneeva, A.M. Adam, A.T. Morchenko, N.A. Yudanov and V.G. Kostishyn, J. Magn. Magn. Mater. 459, 147 (2018). 4.P. Corte -Leon, I. Skorvanek, F. Andrejka, V. Zhukova, J.M. Blanco, M. Ipatov, A. Zhukov, J. Alloys Compd. 946 (2023) 169419, doi: 10.1016/j.jallcom.2023.169419.

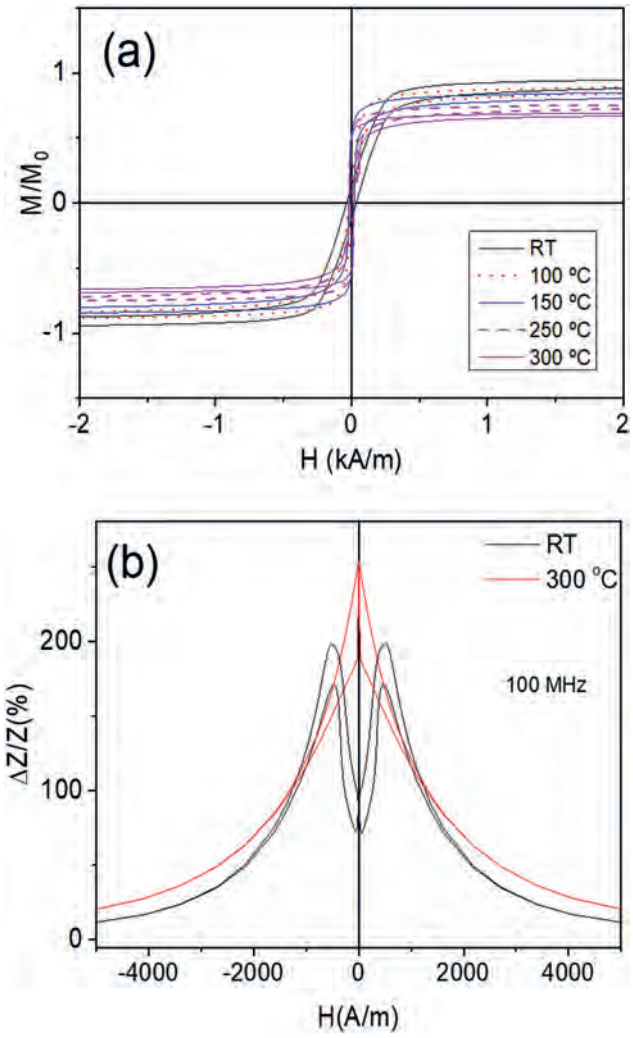

Modification of the hysteresis loops (a) and ΔZ/Z(H) dependencies upon heating of studied microwires.

INVITED PAPER

EC-05. Design of soft magnetic materials for low energy loss in the high-frequency range. *K. Ono*[1] *1. Osaka University, Suita, Japan*

Research and development toward low-loss soft magnetic materials have been active. Current design guidelines for low-loss soft magnetic materials are mainly low coercivity to reduce hysteresis loss and high resistance to reduce eddy current loss. As the use of soft magnetic materials shifts to the high-frequency range, losses conventionally referred to as excess loss and abnormal eddy current loss are attracting attention. Our research aims to elucidate the mechanisms of these excess losses physically and data-scientifically and to establish new design guidelines for soft magnetic materials. Magnetostriction is an essential factor that prevents low energy loss in soft magnetic materials.[1] We also study the relationship between magnetostriction and the energy dissipation mechanism of soft magnetic materials. [2] We clarify the mechanism of energy loss of soft magnetic materials due to magnetostriction. When an alternating magnetic field is applied to soft magnetic materials, the motion of the magnetic domain wall generates strain through magnetostriction. Since this strain is relaxed by viscous stress, the magnetic domain wall motion dissipates the elastic energy induced by the magnetic field. The energy loss mechanism due to magnetostriction is formulated and found to be consistent with the experimental results. These results develop a design guideline for improving the energy efficiency of soft magnetic materials in the high-frequency range. This work was mainly conducted by Dr. Hiroshi Tsukahara and we also thank Prof. Kiyonori Suzuki for his collaboration. This work was supported by MEXT Program: Data Creation and Utilization-Type Material Research and Development Project (Digital Transformation Initiative Center for Magnetic Materials) Grant Number JPMXP1122715503 and TOYOTA Motor Corporation.

[1] R. Balakrishna, and R.D. James, *npj Comput Mater.,* 8, 4 (2022). [2] H. Tsukahara, H. Imamura, C. Mitsumata, K. Suzuki, and K. Ono: *NPG Asia Mater.*, 12, 29 (2020).

CONTRIBUTED PAPERS

EC-06. Giant Magneto-Impedance Effect in Core-Shell CoP@Cu Microwires in a Wide Range of Frequencies. C. Iglesias[1], J. Marques de Lima[1], E. Padrón-Hernández[1], J. Sinnecker[2], S. Rezende[1] and *F. de Araujo Machado*[1] *1. Departamento de Física, UFPE, Recife, Brazil; 2. CBPF, Rio de Janeiro, Brazil*

The penetration depth in high magnetic permeability metallic materials drives the ac electrical current to the surface of the conductor even for moderate values of frequencies (*f*). This phenomenon is strongly dependent on *f* and yields values for the magneto-impedance that can vary over one order of magnitude by changing the applied magnetic field (*H*) by few Oersteds only. This phenomenon was named giant magneto-impedance (GMI) and the domain wall (DW) dynamics and the ferromagnetic resonance (FMR) were found to be the main sources for the *f*-dependence of the GMI. In this work, the longitudinal (*H* parallel to the length of the wire) GMI was investigated in 18.9 mm long core-shell structured micro-wires made of thin copper wires (core) and electrodeposited CoP alloys (shell) at room temperature. The measurements were carried out using strip-line waveguides for *f* varying from 1 MHz up to 9 GHz. Values of GMI of about 100 % were observed for frequencies close to 30 MHz. Moreover, at the microwave regime the FMR yielded resonance parameters that were nicely fit to the Kittel's formula currently used for thin slabs yielding for the CoP alloy a saturation magnetization of 1007 emu/cm^3. The magnetic shell can be mapped into a thin slab in the present case because the ratio of the diameter of the core (~ 190 μm) to the thicknesses (2 - 5 μm) of the shell is significantly high (> 40) while the magnetization is oriented along the micro-wire. The crossing over from the DW to the FMR regime was found to be around 50 MHz. Above this frequency the FMR starts to play a major rule yielding splits in the GMI spectra that increase for increasing values of *f*. The splittings were also found to be highly influenced by the anisotropy field and by the demagnetizing field. A phenomenological model that accounts for the overall response of the GMI with *f* as well as the observed split is also presented. The CoP alloys were found to be stable for over two decades and as good candidates for applications in devices required to cover a broad range of frequencies as well as in 5G technologies and as microwave absorbers. This work was partially supported by CNPq, CAPES, FACEPE and FINEP (Brazilian Agencies).

EC-07. Stress-annealing influenced anelastic microstructural transformations in Co-based amorphous wires. S. Corodeanu[1], G. Ababei[1], M. Grigoras[1], T.A. Ovari[1], H. Chiriac[1] and *N. Lupu*[1] *1. National Institute of Research and Development for Technical Physics, Iasi, Romania*

Fe-based and Co-based soft magnetic amorphous/nanocrystalline wires are of particular interest nowadays for a wide variety of applications. This work focusses on the influence of stress annealing on the microstructural transformations and magnetic properties of zero magnetostrictive $Co_{68.15}Fe_{4.35}Si_{12.5}B_{15}$ amorphous wires with Φ = 120 μm. In the as-cast state, the wires exhibit high magnetic permeability (μ_r > 6.5 x 10^4), low coercive field (H_c < 8 A/m) and a saturation induction, B_s, of 0.68 T.

The magnetic permeability suffers very small variations with the magnetic field for wires annealed between 400°C and 550°C (below and around crystallization temperature, $T_x \approx 550$°C) under longitudinal tensile stresses (Fig. 1). However, μ_r and the magnetic field range in which μ_r remains constant depend strongly on the annealing temperature and the annealing tensile stress. Such a specific behaviour suggests the presence of creep induced anisotropies, as an effect of atomic bonds reorientation under the influence of the anelastic strains. Moreover, the changes induced by stress annealing are reversible. The samples annealed at lower temperatures show a higher sensitivity of the magnetic properties on the applied stresses, while HR-TEM and DSC measurements indicate the presence of very small α-(Fe,Co) clusters of 2÷4 nm in stress annealed samples at higher temperatures, regardless of the method used to anneal the samples (by current annealing or in furnace). All these aspects will be discussed in regard to potential applications of such wires. *Financial support from the MCID Nucleu (PN 23 11 01 01) and PFE (Contract No. 5PFE/2022) Programmes is highly acknowledged.*

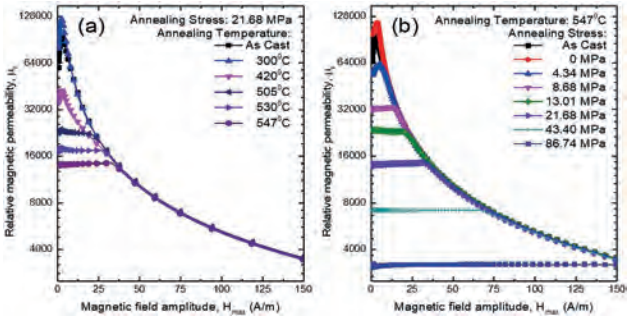

Fig. 1. Relative magnetic permeability dependence on the amplitude of the a.c. magnetic field for stress annealed wires.

EC-08. Soft Magnetic Properties of Nanostructured Fe-rich Alloys Upon the Formation of BCC Nanocrystallites. A. Talaat[2,1], *P. Corte-Leon*[2,1], V. Zhukova[2,1], M. Ipatov[2,1] and A. Zhukov[2,1] *1. Department of Applied Physics I, UPV/EHU, San Sebastian, Spain; 2. Department of Polymers and Advanced Materials, UPV/EHU, San Sebastian, Spain*

Soft magnetic materials and advanced component technologies play an increasingly important role within the electrical transmission and distribution system. Recent demands for next generation power electronics devices with greater efficiency and compact size require the development of new types of soft magnetic core materials with comparable or even superior attributes over existing state-of-the-art soft magnetic materials. Glass-coated microwires are magnetically soft composites that feature an amorphous structure with high electrical resistivity which is critical for reduced eddy current losses at high frequency, flexible and insulating glass-coating, and tunable saturation magnetization values upon the specific alloy chemistry which can result in a dramatic size reduction of magnetic components. In this work, the role of BCC Fe-nanocrystallites formation and their features in optimizing the soft magnetic properties upon alloying different chemical elements is presented. Fe-rich glass-coated microwires with nominal compositions of $Fe_{71.8}B_{13.27}Si_{11.02}Nb_{2.99}Ni_{0.92}$, $Fe_{72.8}Si_{14}B_{9.1}Nb_{3.1}Cu_1$, and $Fe_{80}Si_{10}B_{10}$ have been prepared by the modified Taylor-Ulitovsky technique in different wire dimensions. The correlation between magnetoelastic anisotropy and characteristic magnetic properties are systematically analyzed for a wide range of annealing temperatures under various heating and cooling profiles. Magnetic softening and reduced coercivities have been achieved, and observed results are discussed within the underlying mechanism of induced anisotropies and their impacts on structural and magnetic properties.

EC-09. Controllable magnetic anisotropy in Fe-rich microwires. *P. Corte-Leon*[1,2], V. Zhukova[1,2], J. Blanco[2], A. Talaat[1,2], M. Ipatov[1,2] and A. Zhukov[1,2] *1. Department of Polymers and Advanced Materials, UPV/EHU, Donostia, Spain; 2. Department of Applied Physics I, UPV/EHU, Donostia, Spain*

Generally, Fe and Fe-Ni based glass-coated microwires present magnetic bistability and single domain wall (DW) propagation. The use of fast and controllable DW propagation has been proposed in a number of promising applications, such as racetrack memories, magnetic logic or magnetic tags [1]. This work focuses on the controllability of the magnetic properties in Fe-rich amorphous microwires by induced magnetic anisotropy. Although as-prepared Fe-rich amorphous microwires exhibit low Giant magneto-impedance (GMI) effect and rectangular hysteresis loops, stress-annealing, Joule heating, and combined stress-annealed followed by conventional furnace annealing can substantially improve the GMI effect (by more than an order of magnitude) [2]. On the other hand, Fe-rich microwires with moderate stress-annealing induced anisotropy can present both GMI effect and single domain wall propagation. Additionally, partial reversibility of the stress-annealing induced anisotropy is observed. The stress-annealing induced anisotropy depends on stress-annealing conditions: temperature, stress and time. The dependence of stress-annealing induced anisotropy on stress-annealing conditions allowed us to tune the magnetic anisotropy along the length of a microwire subjected to stress annealing with a temperature gradient. Non-uniform DW propagation is observed in a microwire with graded magnetic and the DW can be trapped in the microwire region with strong enough stress-annealing induced magnetic anisotropy.

[1] S.S.P. Parkin, M. Hayashi, L. Thomas, Science 320, 190-194, (2008). [2] A. Zhukov, P. Corte-Leon, L. Gonzalez-Legarreta, M. Ipatov, J.M. Blanco, A. Gonzalez, and V. Zhukova, J. Phys. D: Appl. Phys. 55, 253003, (2022).

Session ED
SPIN WAVES AND MAGNONICS II
Jack C Gartside, Chair
Imperial College London, London, United Kingdom

CONTRIBUTED PAPERS

ED-03. Acousto-Plasmo-Magnonics in a 2D Artificial Magnonic Crystal. *S. Pal*[1], P.K. Pal[1], R. Fabiha[2], S. Bandyopadhyay[2] and A. Barman[1]
1. Condensed Matter and Materials Physics, S.N.Bose National Centre for Basic Sciences, Kolkata, India; 2. Department of Electrical andComputer Engineering, Virginia Commonwealth University, Richmond, VA, United States

We report a new phenomenon of strong non-linear coupling (with cooperativity factor far exceeding unity) between spin waves (SWs) and hybridized phonon-plasmon waves in a 2D artificial magnonic crystal (AMC). The AMC consists of a periodic array of elliptical magnetostrictive cobalt nanomagnets (~100 nm major axis, ~90 nm minor axis and 6 nm thickness) deposited on a silicon substrate with an intervening thin film of aluminium that acts as a source of surface plasmons (Fig. 1(inset)). Hybridized phonon-plasmon waves [1] are generated in this system under ultrashort laser pulses and they strongly couple with the intrinsic SW modes of the system to spawn a new breed of waves – acousto-plasmo-spin waves (APSW) - resulting from tripartite coupling of magnons, phonons and plasmons. We study this phenomenon with time-resolved magneto-optical-Kerr-effect microscopy [2]. The strong non-linear coupling results in the formation of an APSW "frequency comb" spanning two octaves [3] and occurring at frequencies of 1, 2, 3 and 4 GHz (Fig. 1). The frequency period (1 GHz) is equal to the (measured) frequency of the hybridized phonon-plasmon wave that mediates the tripartite coupling between phonons, plasmons and magnons. The comb is insensitive to the presence or absence of any magnetic field (Fig. 2). This tripartite coupling also produces parametric amplification in this system; the APSW modes exhibit 200X power amplification arising from the transfer of energy from the hybridized phonon-plasmon modes to the naturally occurring SW modes in the magnonic crystal. This opens up an emerging path for designing novel active metamaterials with tailored and enhanced responses. It may enable high-efficiency magneto-mechanical-plasmonic frequency mixing in the GHz–THz frequency regime and provide a novel avenue to study non-linear coupling, parametric amplification, and frequency comb physics with applications as hardware accelerators in artificial intelligence systems [4].

[1] A. Ahmed, R. Gelfand, S.D.Storm et al., Nano Lett., 22, 5365 (2022) [2] A. Barman and J. Sinha, Spin Dynamics and Damping in Ferromagnetic Thin Films and Nanostructures, Springer, Berlin, ISBN 978-3-319-66295-4, p. 52-54, (2018) [3] S. Pal, P.K.Pal, R.Fabiha et al., Adv. Func. Mater., 2304127 (2023) [4] J. Feldman, N.Youngblood, M.Karpov et al., Nature, 589, 52-58 (2021)

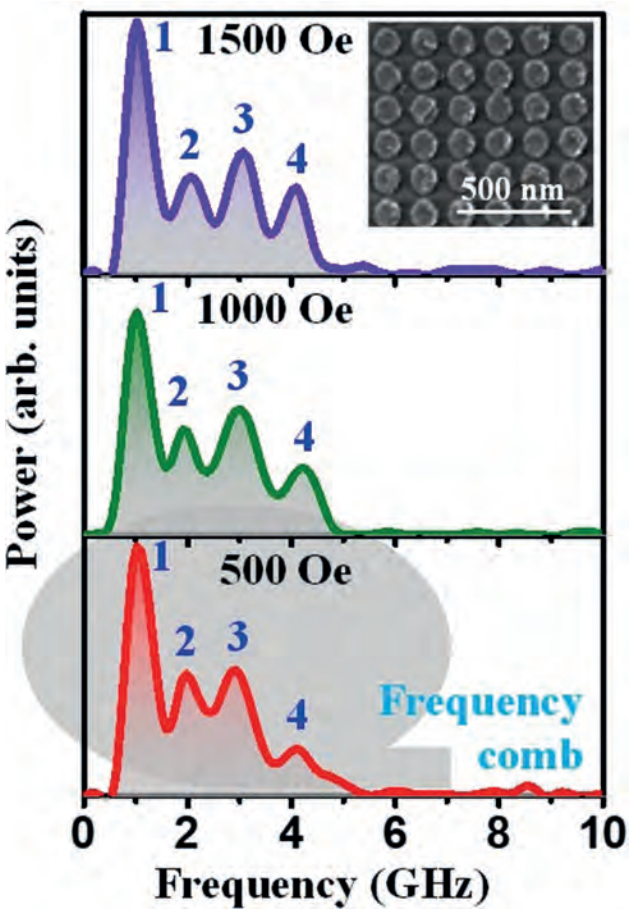

Fig.1: A frequency comb with four "teeth" at 1, 2, 3 and 4 GHz, reproduced from [3]. The inset presents the SEM image of the cobalt nanomagnet arrays.

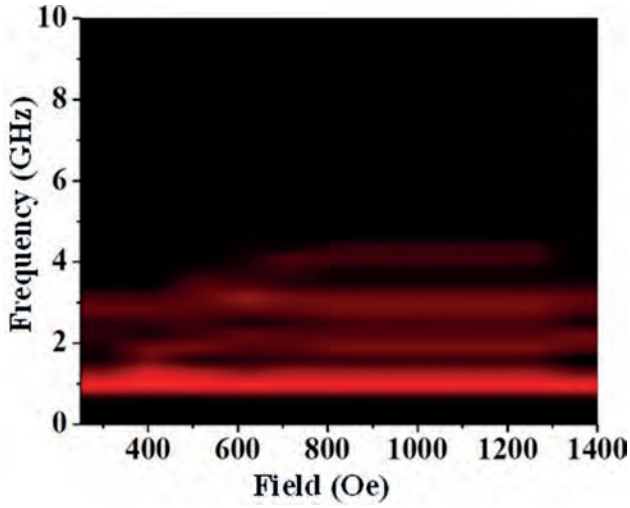

Fig. 2: Surface plot of APSW power spectra as a function of bias magnetic field reproduced from [3].

ED-05. Magnetic Resonance Imaging of Coherent Spin Waves in Ferrimagnetic Insultor TmIG Thin Films. R. Timalsina[1], H. Wang[2], B. Giri[2], A. Erickson[1], X. Xu[2] and *A. Laraoui[1,2] 1. Department of Mechanical & Materials Engineering, University of Nebraska-Lincoln, Lincoln, NE, United States; 2. Department of Physics and Astronomy and the Nebraska Center for Materials and Nanoscience, University of Nebraska-Lincoln, Lincoln, NE, NE, United States*

Magnetic insulators are of great interest for magnonic platforms because they have low damping and can allow long-distance information transmission that is free of Joule heating [1]. Yttrium iron garnet (YIG) is a ferrimagnetic (FMI) insulator with a mm long spin-wave (SW) coherence length and low damping (~10^{-4}) [1]. When YIG is interfaced with heavy metals, spin transport phenomena have been observed extending its application to spintronics [2]. However, insulators with perpendicular magnetic anisotropy (PMA) are desirable for such applications because they allow for lower current densities. Thulium iron garnet (TmIG: $Tm_3Fe_5O_{12}$) is an FMI insulator with PMA [3] and has been extensively studied recently for spintronics when interfaced with heavy metals [4]. However, its magnon properties (SW wavelength and coherence length) are missing. In this work we use nitrogen vacancy (NV) based magnetometry in combination with broadband ferromagnetic resonance (FMR) spectroscopy to study SW propagation in TmIG thin films (thickness: 2 – 35 nm) grown by pulsed laser deposition on gadolinium-gallium-garnet (GGG) and substituted GGG (sGGG) substrates. We performed FMR measurements on TmIG films and found a damping value ~ 10^{-3} and a SW group velocity of 2-3 km/s depending on the amplitude of applied magnetic field [5]. To image the surface propagating SWs, we used optical detected magnetic resonance (OMDR) of NV ensembles doped into the surface of a diamond chip facing a TmIG(35 nm)/GGG film. We observed an amplification of local microwave magnetic field due to coupling of NV spins with the stray-field produced by the surface SWs seen by the enhancement of the NV ODMR peaks and an increase of NV Rabi oscillation frequency. By scanning the hybrid TmIG-diamond system we observed the propagation and interference of the SWs with wavelengths in the sub-micrometer scale and a SW propagation length up to 70 μm [5]. Our result provides a platform for the development of high-speed chip based spintronic devices and offers new material possibilities for quantum magnonics [6]. Acknowledgement: This work is supported by the NSF/EPSCoR RII Track-1: Emergent Quantum Materials and Technologies, Award OIA-2044049.

[1] A. V. Chumak, V. I. Vasyuchka, A. A. Serga AA, et al., Nature Physics, 11(6):453–461 (2015). [2] M. Collet, X. de Milly, O. d'Allivy Kelly, et al., Nature Communications 7, 10377 (2016). [3] C. N. Wu, C. C. Tseng, Y. T. Fanchiang, et al., Scientific Reports 8, 11087 (2018). [4] Q. M. Shao, Y. W. Liu, G. Q. Yu, et al., Nature Electronics 2, 182-186 (2019). [5] R. Timalsina, H. Wang, B. Giri, et al., under preparation (2023). [6] D. D. Awschalom, C. R. Du, R. He, et al., IEEE Transactions on Quantum Engineering, vol. 2, pp. 1-36, Art no. 5500836 (2021).

INVITED PAPER

ED-06. Resonant Dynamics, Spin Wave Generation, and Spin Wave Annealing in Three-Dimensional Skyrmionic Lattices. *T. Srivastava[1,2]*, Y. Sassi[2], F. Ajejas[2], A. Vecchiola[2], I. Ngouagnia[3], H. Hurdequint[3], K. Bouzehouane[2], N. Reyren[2], V. Cros[2], T. Devolder[1], J. Kim[1] and G. de Loubens[3] *1. Centre de Nanosciences et de Nanotechnologies, CNRS, Université Paris-Saclay, 91120, Palaiseau, France; 2. Unité Mixte de Physique, CNRS, Thales, Université Paris-Saclay, 91767, Palaiseau, France; 3. SPEC, CEA, CNRS, Université Paris-Saclay, 91191, Gif-sur-Yvette, France*

Skyrmions in magnetic materials are nanoscale, chiral topological solitons which exhibit a number of dynamical phenomena that have garnered much interest for fundamental reasons and technological applications alike [1]. While most studies to date have focused on their motion as rigid particles under different stimuli like spin currents or thermal fluctuations, only a few experimental reports [2,3] exist on their internal mode dynamics owing to large damping coefficients. Here we present the resonant dynamics of ultrathin film [Pt/CoFeB/AlOx] × 20 multilayers hosting stable skyrmion lattices under ambient conditions while exhibiting low Gilbert damping α= 0.02 [4]. We identify distinct spin wave modes associated with skyrmions by combining magnetic force microscopy (MFM) and ferromagnetic resonance (FMR) experiments with micromagnetic simulations as shown in Fig.1. At low frequency (≤ 2 GHz), we observe a number of modes related to the precession of the uniform background state of individual layers close to or at the surfaces of the stack, along with eigenmodes localized to the skyrmion edges. At intermediate frequencies (2 – 8 GHz), the precession of the uniform background near the centre of the stack dominates the response. We report the experimental observation of a new dynamical mode at high frequency (> 12 GHz), which is most visible in the skyrmion lattice phase. FMR spectroscopy reveals clear peaks in the susceptibility above 12 GHz over a range of applied magnetic fields, which we find through micromagnetics simulations to correspond to a coherent precession of the skyrmion core. The skyrmions here have a distinct three-dimensional structure due to the competition between the different existing magnetic interactions in these multilayers. Moreover, the simulations show that this core precession generates spin waves, with wavelengths in the range of 50 to 80 nm, that flow into the ferromagnetic background, illustrating the potential of skyrmions to convert uniform radiofrequency waves into nanoscale excitations. These spin waves interfere with those generated at neighbouring skyrmion cores, yielding a collective dynamical state governed by the subtle interplay between the skyrmion diameter, the wavelength of the emitted SWs, and the skyrmion lattice periodicity. Using micromagnetic simulations we also examine the role of spin wave interactions with the skyrmion cores. As the applied field increases and skyrmions begin to annihilate, leaving vacancies in the hexagonal lattice, the excitation of the high-frequency mode can "anneal" the lattice, resulting in a glassy state as shown in Fig.2. The spin wave interactions are found to provide a dynamical repulsive force between the skyrmion cores, which results in a more homogeneous arrangement in terms of density, but at the expense of crystalline order. These results also shed new light on how dynamical excitations can influence phase transitions associated with the melting of skyrmion lattices [5].

[1] A. Fert et al., Nat. Rev. Mater., 2, 17031 (2017) [2] L. Flacke et al., Phys. Rev. B, 104, L100417 (2021) [3] B. Satywali, et al., Nat. Commun., 12, 1909 (2021) [4] T. Srivastava et al., APL Mater., 11, 061110 (2023) [5] P. Huang et al., Nat. Nanotechnol.,15, 761 (2020)

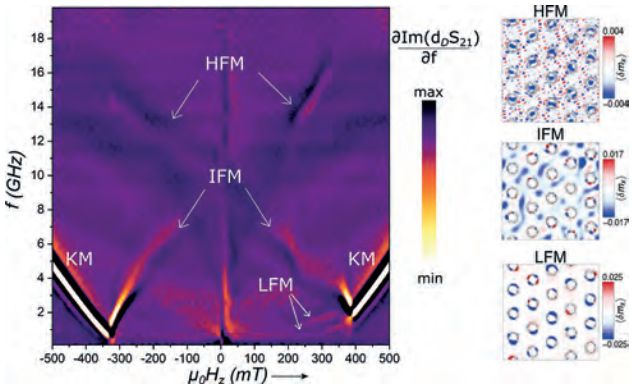

Fig.1. (Left) Broadband ferromagnetic resonance: Frequency-field dispersion map measured by VNA-FMR over a frequency range of 0.1 GHz to 20 GHz with the applied out-of-plane field swept from -500 mT to 500 mT. Three families of modes are observed at low frequency (LFM), intermediate frequency (IFM) and high frequency (HFM). (Right) Micromagnetic simulations: Two-dimensional view of the magnetic response$\langle \delta m_x \rangle$ in layer 10 of the modes for LFM, IFM, and HFM.

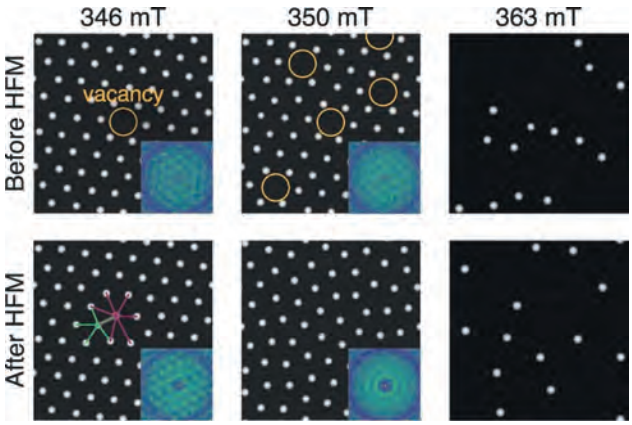

Fig.2. Simulated MFM images of skyrmion lattices under different applied fields, before and after the excitation of a high-frequency mode (HFM) that generates spin waves. The insets show discrete Fourier transforms of the spatial order.

CONTRIBUTED PAPERS

ED-07. Time-Resolved Spin-Wave Imaging Using Ultrafast Electron Microscopy. *C. Liu*[1,2], F. Ai[3], S. Reisbick[2], A. Pofelski[2], M. Han[2], V. Lomakin[3] and Y. Zhu[2,1] *1. Department of Physics and Astronomy, Stony Brook University, Stony Brook, NY, United States; 2. Condensed Matter Physics and Material Science, Brookhaven National Laboratory, Upton, NY, United States; 3. Department of ECE, UC San Diego, La Jolla, CA, United States*

Spin waves or magnons in ferromagnetic thin films stand as a candidate for next-generation information carrier in spintronics and magnonics devices, advantaged from the low energy consumption without Ohmic heating. It promises high-speed data procession in both conventional and quantum information transmission. Nowadays, several experimental techniques have been developed to study spin-wave properties. For example, BLS microscopy, TR-MOKE and XMCD-STXM are frequently used to study dynamics of magnetization and magnons. Yet, the temporal and spatial resolution of spin dynamic imaging are still limited by the wavelength and the focus capability of the photon probes. As a result, imaging of local spin-wave dynamics with sufficient resolution remains a challenge. We demonstrated a new way to study spin-wave dynamics using ultrafast electron microscopy (UEM). With the development of the laser-free electron pulser at Brookhaven National Laboratory, direct visualization of magnetization dynamics in ferromagnetic materials with nanometer-picosecond spatiotemporal resolution can be achieved using Lorentz transmission electron microscopy (LTEM). In this work, we studied the dynamic of spin-wave propagation in patterned permalloy (Py, $Ni_{80}Fe_{20}$) thin films. The Py films were deposited on top of a TEM Silicon Nitride window by means of e-beam lithography. Transverse microwave signals were sent to the sample via an impedance matched radio frequency (RF) sample holder to initiate spin waves. The RF current was carried by an Au antenna that cross the permalloy thin films, generating oscillating magnetic field that applied to the sample as a local excitation (Fig.1). For the first time, dynamics and propagation properties of spin waves are observed (Fig.2) using electron probe. The results will be reported and discussed. We also preformed micromagnetic simulations to help us understanding of the results.

S. Wintz et al, Nature Nanotechnology., Vol. 11, p.948-953 (2016) K. Wagner et al, Nature Nanotechnology., Vol. 11, p.432-436 (2016) X. Fu et al, Sci. Adv., Vol. 6: eabc3456 (2020) J. W. Lau et al, Rev. Sci. Instrum., Vol. 91, 021301 (2020) S. A. Reisbick et al, Ultramicroscopy., Vol. 235, 113497 (2022) S. A. Reisbick et al, Ultramicroscopy., Vol. 249, 113733 (2023) The work was supported by the U.S. DOE Basic Energy Sciences, Materials Science and Engineering Division under Contract No. DESC0012704

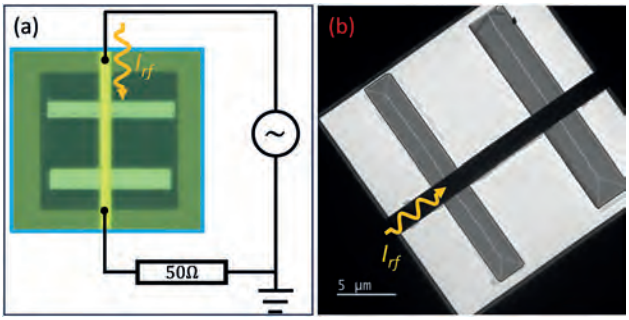

Fig.1. Schematic of the sample. (a) Schematic of the RF circuit with an optical micrography shows the window area of the sample. (b) Example LTEM image of the sample.

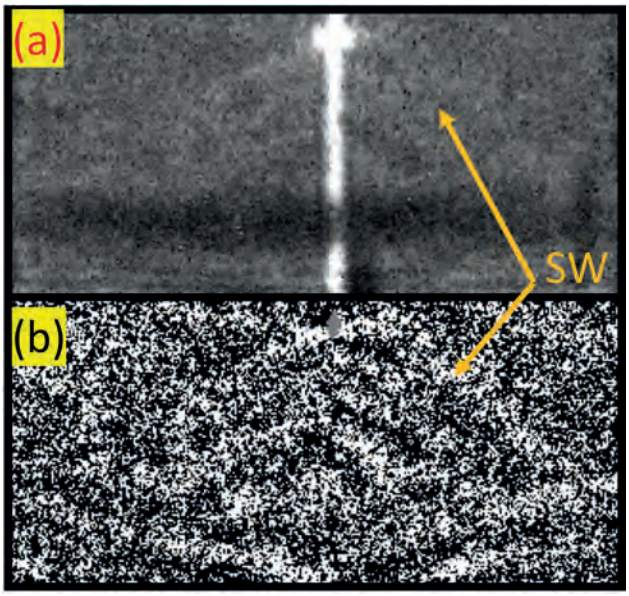

Fig.2. Time-resolved snapshot of LTEM image showing the spin-wave fronts. (a) LTEM image. (b) Normalized LTEM image.

ED-08. Observation of nonlinear acoustic-to-optic magnonic interaction in a synthetic antiferromagnet. *M. You*[1], M. Song[1], A.M. Park[1], D. Lee[2], S. Kim[2] and K. Kim[1] *1. Physics, Korea Advanced Institute of Science and Technology (KAIST), Daejeon, The Republic of Korea; 2. Physics and Energy Harvest Storage Research Center, University of Ulsan, Ulsan, The Republic of Korea*

Understanding magnonic nonlinearity originating from the three-magnon or four-magnon process in ferromagnetic metals and insulators is essential for enriching the knowledge about complex interactions of magnons [1-4]. In addition, controlling the magnonic systems in a nonlinear regime enables new technological progress in hybrid magnonic systems, for instance, by using nonlinear magnon-polariton anti-crossing gap closing and bi-stability in the magnon dispersion [5, 6]. Recent report shows magnon-magnon interaction in the synthetic antiferromagnet, which is drawn attention to the new magnonic platform [7]. However, nonlinear magnonic excitation in synthetic antiferromagnet (SAF) remains largely unknown despite its unique characteristics that encompass both the ferromagnetic and antiferromagnetic properties of spin waves. In this work, we investigate the nonlinear magnon-magnon interaction in SAF composed of two ferromagnetic CoFeB layers antiferromagnetically coupled by Ru insertion layer via Ruderman-Kittel-Kasuya-Yoshida (RKKY) interaction. Two distinct magnon modes coexist inside the system: the acoustic (in-phase rotation) and optic magnons (out-of-phase rotation). These propagating magnons show the anti-crossing gap in the spin wave resonance spectra when the angle between the in-plane field and the magnon wave vector is around 45° [7]. By sweeping RF-excitation power from -20 dBm to +10 dBm, we find an abnormal distortion in the magnonic dispersion caused by an abrupt transition from acoustic to optic mode near the anti-crossing gap. We observe the discontinuous transition between acoustic to optic mode and vice versa. Furthermore, the magnonic dispersion shows hysteretic behavior with respect to external field sweep direction revealing the bistability between acoustic and optic modes. This observation reveals the strong and nonlinear acoustic-to-optic magnonic interaction in SAF, which can be potentially useful for magnonic technologies such as frequency shifters, magnon transistors, and future hybrid magnonic device.

[1] J. J. Carmiggelt et al., *Appl. Phys. Lett.* 119, 202403 (2021). [2] R. Dreyer et al., *Nat. Commun*. 13, 4939 (2022). [3] C. Koerner et al., *Sci.* 375, 1165 (2022). [4] Z. Haghshenasfard et al., *JMMM*. 426, 380-389 (2017). [5] O. Lee et al., *Phys. Rev. Lett*. 130, 046703 (2023). [6] Y. -P. Wang et al., *Phys. Rev. Lett*. 120, 057202 (2018) [7] Y. Shiota et al., *Phys. Rev. Lett*. 125, 017203 (2020)

ED-09. Coherent control of collective nuclear quantum states via transient magnons. *G. Meier*[1], L. Bocklage[2] and R. Röhlsberger[3] *1. Max Planck Institute for the Structure and Dynamics of Matter, Hamburg, Germany; 2. DESY, Hamburg, Germany; 3. Helmholtz-Institut Jena, Jena, Germany*

Ultrafast and precise control of quantum systems at x-ray energies involves photons with oscillation periods below one attosecond. Coherent dynamic control of quantum systems at these energies is one of the major challenges in hard x-ray quantum optics. Here, we demonstrate that the phase of a quantum system embedded in a solid can be coherently controlled via a quasi-particle with sub-attosecond accuracy. In particular, we tune the quantum phase of a collectively excited nuclear state via transient magnons with a precision of one zeptosecond. These small temporal shifts are monitored interferometrically via quantum beats between different hyperfine-split levels. The experiment demonstrates zeptosecond interferometry and shows that transient quasi-particles enable accurate control of quantum systems embedded in condensed matter environments [1].

L. Bocklage, J. Gollwitzer, C. Strohm, C. F. Adolff, K. Schlage, I. Sergeev, O. Leupold, H.-C. Wille, G. Meier, R. Röhlsberger, "Coherent Control of Collective Nuclear Quantum States via Transient Magnons", Science Adv. 7, eabc3991 (2021)

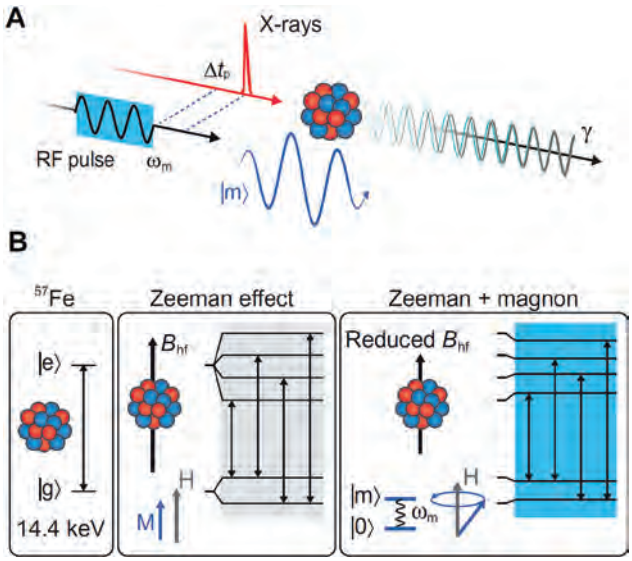

Nuclear dynamics with magnon excitation. An ^{57}Fe nucleus is excited by an x-ray pulse and subsequently emits a photon. The emitted photon is a superposition of nuclear dipole transitions, here shown for two frequencies (green and gray). An RF burst with delay Δtp excites the magnon (blue) and leads to a nanosecond shift of the resonance line. (B) Nuclear-level scheme with magnon excitation. Level scheme of a ^{57}Fe nucleus with the transition from the ground to the excited state. The magnetic hyperfine-field B_{hf} splits the nuclear transition by the Zeeman effect. Four circularly polarized transitions are excitable in this experimental geometry. When a coherent magnon is excited in the magnetic material at its resonance ω_m the hyperfine field is reduced, leading to a shift of the nuclear transitions.

ED-10. Two-Qubit Magnon-Mediated Quantum Gates. *C. Trevillian*[1] and V. Tyberkevych[1] *1. Physics, Oakland University, Rochester, MI, United States*

Coupled systems of magnons and qubits are studied as bases of hybrid quantum computing architectures [1 – 3], as magnons interact strongly with bosonic and fermionic excitations. As such, magnons have much shorter lifetimes than other excitations of similar characteristic energies and are not well-suited as qubits or quantum memories. Even so, magnons can be useful for coherent information manipulation and transduction between disparate qubits, i.e., as mediators of quantum interactions, due to such strong interaction with other excitations. Here, we study the limits of manipulating quantum information via magnon-mediated interactions. We show that we can realize arbitrary quantum operations using only interactions with magnons on a system of noninteracting qubits. We consider a hybrid quantum system of two noninteracting qubits and one magnonic mode, shown schematically in Fig. 1. By controlling only the magnonic mode, namely, by using different initial states and changing the magnon resonance frequency $\omega_m(t)$, the operations are performed. When $\omega_m(t)$ is near the qubit resonance frequency $\omega_{q1,2}$ such that the frequency gap $\Delta\omega_{1,2}=\omega_m(t)-\omega_{q1,2}$ compares to the magnon-qubit coupling rate $g_{1,2}$, interaction occurs by resonant coupling. Our results show that it is possible to realize arbitrary single-qubit gates by invoking different protocols of dynamic magnon-mediated interactions. Furthermore, we developed an algorithm to describe the protocol of *any* two-qubit magnon-mediated quantum gate. Fig. 2 shows one example of this: a two-qubit controlled-phase gate. This means that by ensuring that the magnon and qubit systems are unentangled before and after the protocols, we can form universal sets of quantum gates and perform any quantum operations that are mediated by magnons. This work may help realize universal magnon-mediated quantum computers where qubit interactions and computations are performed by manipulating only the magnonic modes.

[1] Y. Li, W. Zhang, V. Tyberkevych, *et al.*, J. Appl. Phys., vol. 128, no. 130902, 2020. doi:10.1063/5.0020277 [2] D. D. Awschalom, C. R. Du, R. He, *et al.*, IEEE Trans. Quantum Eng., vol. 2, no. 5500836 doi:10.1109/TQE.2021.3057799 [3] J. Xu, C. Zhong, X. Han, *et al.*, Phys. Rev. Lett., vol. 126, iss. 20, no. 207202, 2021. doi:10.1103/PhysRevLett.126.207202

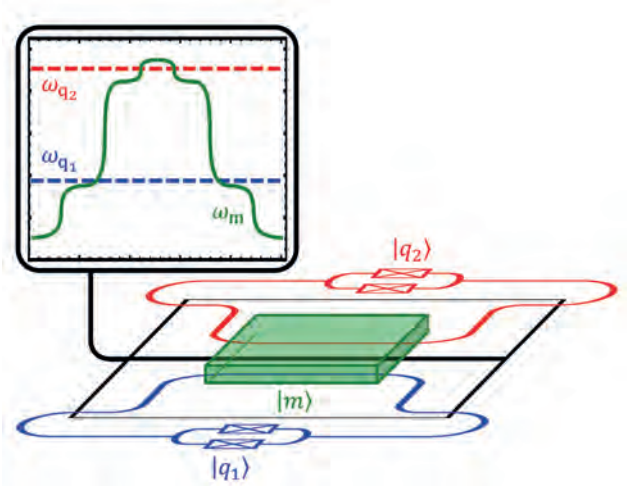

Fig. 1. Schematic of the two-qubit hybrid quantum system. The window shows the protocol $\omega_m(t)$ applied in Fig. 2.

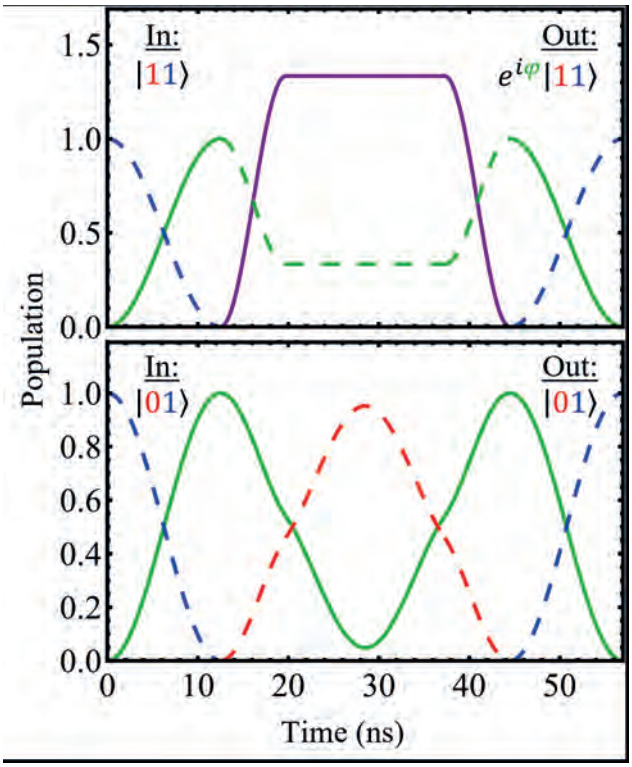

Fig. 2. Population evolution as protocol $\omega_m(t)$ is applied. In/out states described by $|q_2\rangle|q_1\rangle = |q_2\, q_1\rangle$. Top: phase φ acquired by $|11\rangle$. Bottom: identity is applied to $|01\rangle$.

ED-11. Hybrid Magnonics in Hybrid Perovskite Antiferromagnets.

A. Comstock[1], C. Chou[2], Z. Wang[3], T. Wang[1], R. Song[4], J. Sklenar[5], A. Amassian[1], W. Zhang[6], H. Lu[3], L. Liu[2], M. Beard[7] and D. Sun[1] *1. North Carolina State University, Raleigh, NC, United States; 2. Massachusetts Institute of Technology, Cambridge, MA, United States; 3. The Hong Kong University of Science and Technology, Kowloon, China; 4. Duke University, Durham, NC, United States; 5. Wayne State University, Detroit, MI, United States; 6. University of North Carolina, Chapel Hill, NC, United States; 7. National Renewable Energy Laboratory, Golden, CO, United States*

Hybrid magnonic systems are a newcomer for pursuing coherent information processing owing to their rich quantum engineering functionalities. One prototypical example is hybrid magnonics in antiferromagnets with an easy-plane anisotropy that resembles a quantum-mechanically mixed two-level spin system through the coupling of acoustic and optical magnons. Generally, the coupling between these orthogonal modes is forbidden due to their opposite parity. Here we show that the Dzyaloshinskii–Moriya-Interaction (DMI), a chiral antisymmetric interaction that occurs in magnetic systems with low symmetry, can lift this restriction. We report that layered hybrid perovskite antiferromagnets with an interlayer DMI can lead to a strong intrinsic magnon-magnon coupling strength up to 0.24 GHz, which is four times greater than the dissipation rates of the acoustic/optical modes. Our work shows that the DMI in these hybrid antiferromagnets holds promise for leveraging magnon-magnon coupling by harnessing symmetry breaking in a highly tunable, solution-processable layered magnetic platform.

Session EE
MAGNETIC NANOPARTICLES AND EXCHANGE BIAS SYSTEMS

Yayoi Takamura, Co-Chair
University of California, Davis, Davis, CA, United States
Denys Makarov, Co-Chair
Helmholtz-Zentrum Dresden-Rossendorf, Dresden, Germany
Volker Neu, Co-Chair
IFW Dresden, Dresden, Germany

INVITED PAPERS

EE-01. From Nano to Macro – Increasing Actuator Performance Starting with High-Remance Magnetic Nanostructures. *A. El-Ghazaly*[1], Y. Chen[2] and L. Cestarollo[2] *1. Electrical and Computer Engineering, Cornell University, Ithaca, NY, United States; 2. Materials Science and Engineering, Cornell University, Ithaca, NY, United States*

Magnetic devices, such as mechanical actuators, strongly depend upon their nanoscale behavior. In this talk, we will demonstrate this by investigating the macroscale deformation characteristics, including actuator response, deflection amount, and mechanical hysteresis, of magnetic soft actuators made with magenetic nanoparticles in an elastomer matrix [1]. The properties of the actuator strongly depend on the strength of the magnetization of the nanoparticles, the magnetic remanence of their assembled nanostructures, and their distribution within the elastomer. Anisotropic 1-dimensional nanostructures, i.e. nanochains, formed from the nanoparticles are hypothesized to produce the maximimum actuation response with maximum deflection and minimum mechanical hysteresis. Furthermore, we have developed a self-assembly technique for high-remanent Fe-Co nanochain structures for magnetic actuators [2, 3]. Fe-Co was chosen due to its theoretical high saturation magnetization, 230 emu/g. By synthesizing Fe-Co in high-concentration solutions, no external field is required to develop single paticle-wide nanochains with aspect ratios >10:1. Compared to nanoparticles, nanochains achieve 2x the remanence. An optimal volume concentration of nanochains exists (6 vol.%) that minimizes the antiferromagnetic chain-to-chain interactions while maximizing remanence ($0.43*M_s$). Capitalizing on these results, an optimized soft actuator was made with the nanochains and shown to provide large actuation at fields <100 mT.

[1] L. Cestarollo, S. Smolenski, A. El-Ghazaly, *ACS Applied Materials & Interfaces*, 2022. [2] Y. Chen, A. El-Ghazaly, *Small*, 2023. [3] Y. Chen, K. Srinivasan, M. Choates, L. Cestarollo, A. El-Ghazaly, "Enhanced Magnetic Anisotropy for Reprogrammable High-Force Density Micro-Actuators," (under review)

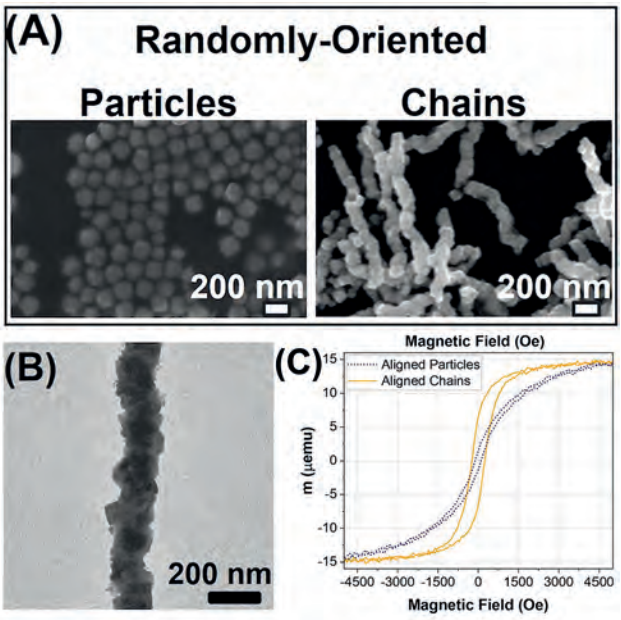

Fig. 1 – A) randomly-oriented, Fe-Co nanoparticles and nanochains synthesized in low and high-concentration solutions, respectively. B) TEM image of a single nanochain, showing seamless nanochain formation. C) magnetic hysteresis comparison of nanopartles and nanochains when pre-aligned by a magnetic field.

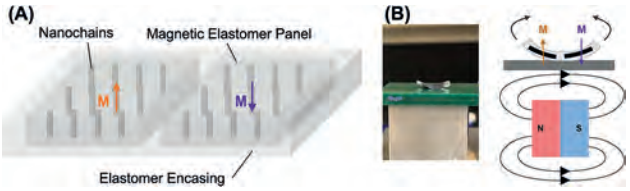

Fig. 2 – A) Example soft actuator structure, where individual magnetic elastomer panels can be programmed to have either up or down magnetization. B) Image of the actuator behavior in an in-plane magnetic field that torques both oppositely-magnetized panels upward.

EE-02. Laser-Induced Field-Free Exchange Bias Reversal. *F. van Riel*[1], B. Koopmans[1] and D. Leitao[1] *1. Applied Physics and Science Education, Eindhoven University of Technology, Eindhoven, Netherlands*

Exchange bias (EB) at a ferromagnetic/antiferromagnetic interface is extensively applied in magnetoresistive (MR) sensors for providing a robust reference axis. For application in navigation, robotics or biomedicine[1,2], it is required to detect multiple magnetic field components, and do so preferably at a single point in space[3]. Here, we propose a method for changing the reference axis orientation by directly acting on the EB layer. We employ fs laser pulses that enable local and ultrafast magnetization switching[4]. The framework of all-optical helicity-independent switching in Co/Gd multilayers[5] is studied in combination with EB from an IrMn layer[6]. Heat from the laser simultaneously quenches the EB and reverses the Co/Gd magnetization, and upon remagnetization it resets the EB orientation at the interface. We demonstrate field-free and field-assisted reversal of the EB with a single fs laser pulse in stacks that mimic an MR sensor's pinned layer. For optimized pulse fluence and field, a reversal can be realized (Fig. 1). Kerr microscopy of the switched areas revealed an internal ring structure, dependent on the fluence (Fig. 2). Moreover, toggling between 180° EB orientation is observed when firing repeated pulses at the same spot (inset Fig. 2). A decrease in EB magnitude occurs after being subjected to the first pulse, but its value stabilizes after several successive pulses and subsequent EB reversal. The difference between positive and negative values is likely a preferential orientation imprinted in the IrMn during growth. Current efforts to understand the underlying switching mechanisms will serve as stack design rules to deliver optimized performance for application in MR sensors.

[1] C. Zheng, K. Zhu, S. Cardoso de Freitas et al., IEEE Transactions on Magnetics, Vol. 55(4), p.1-30 (2019) [2] C. Becker, D. Karnaushenko, T. Kang et al., Science Advances, Vol. 5(12) (2019) [3] R. Li, S. Zhang, S. Luo et al., Nature Electronics, Vol. 4(3), p.179-184 (2021) [4] I. Radu, K. Vahaplar, C. Stamm et al., Nature, Vol. 472(7342), p.205 (2011) [5] M.L.M. Lalieu, M.J.G. Peeters, S.R.R. Haenen et al., Physical review B, Vol. 96(22), p.220411 (2017) [6] Z. Guo, J. Wang, G. Malinowski et al., arXiv preprint, arXiv:2302.04510 (2023)

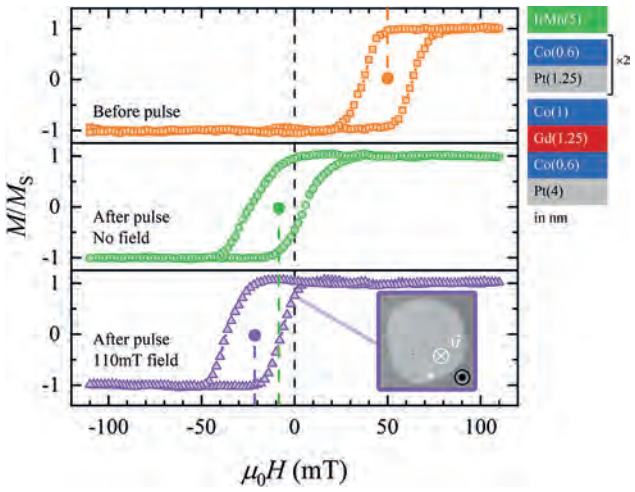

Fig. 1: *M*(*H*) loops before and after being subject to a single 40mJ/cm² pulse. Data obtained with Kerr microscopy from the center of the laser spot.

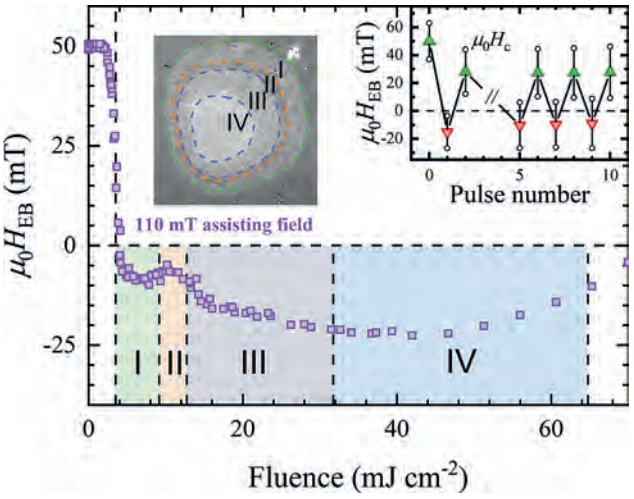

Fig. 2: Fluence dependence of the EB reversal, with 110mT assisting field. Inset shows EB and coercivity (bars) as a function of the number of pulses (alternating the assisting field sign between each pulse). Data obtained with Kerr microscopy from *M*(*H*) loop fits, extracted from the center of the laser spot.

EE-03. Tunable magnetization dynamics of magnetic nanoparticles for temperature sensing and biomedical imaging. *T.Q. Bui*[1], S. Oberdick[3,2], F.M. Abel[1], A.J. Biacchi[1], E. Correa[1], K.N. Quelhas[1], M. Henn[1,4], W.L. Tew[1], A.R. Hight Walker[1], C. Dennis[1], M.J. Donahue[1] and S.I. Woods[1] *1. National Institute of Standards and Technology (NIST), Gaithersburg, MD, United States; 2. University of Colorado, Boulder, Boulder, CO, United States; 3. National Institute of Standards and Technology (NIST), Boulder, CO, United States; 4. University of Maryland, College Park, MD, United States*

Magnetic nanoparticles (MNPs) are becoming increasingly important as tracers for biomedical magnetic imaging[1], magnetic hyperthermia[2], and thermometry[3]. For these applications, MNP tracers are driven by AC magnetic fields and detected by their modulated magnetization. The ability to engineer MNPs to be either weakly or strongly interacting provides access to wide-ranging magnetization dynamics characteristic of superparamagnetic to superspin-glass-like magnetic systems, important from both technological and theoretical perspectives. One prominent example of a strongly interacting system is iron oxide nanoparticle chains (Figure 1), enabled by strong dipolar interactions, that exhibit enhanced magnetization response relative to their isolated counterparts due to the rapid correlated magnetization reversal of the MNPs along the length of the chain[4]. The chaining and magnetization dynamics span broad timescales and are governed by a complex set of parameters, including magnetic field amplitude, frequency, temperature, and the local environment in which the MNPs are suspended (liquid, solid). Here, we present mechanistic characterization using time-resolved magnetometry, high-frequency magnetic AC susceptibility, and electron microscopy over a range of temperatures (240-310 K), magnetic field amplitudes (1-20 mT_{RMS}), and timescales (20 ns to 10 seconds) to elucidate magnetization dynamics for both weakly and strongly interacting magnetic nanoparticle systems synthesized by our group. Frequency and time domain measurements for MNPs show the presence of both Néel and Brownian dynamics, and the temperature dependence reveals their intrinsic coupling (Figure 2). To resolve this coupling, we present stochastic Monte Carlo methods to simulate the field and temperature dependence of magnetization dynamics.

[1] Gleich *et al*. 2005 *Nature*, 435, p. 1214-7; Stephen *et al. 2011 Mater today,* 14(7-8), p. 330 [2] Liu *et al*. 2020, *Theranostics*, 10, P. 3793 [3] Bui *et al.* 2023 10.48550/arXiv.2301.08539; Bui *et al.* 2022 *Appl. Phys. Lett.* 120, p.012407 [4] Tay *et al. 2021, Small Methods*, 5, 2100796; Fung *et al. 2023, Nano Letters,* 23, p. 1717

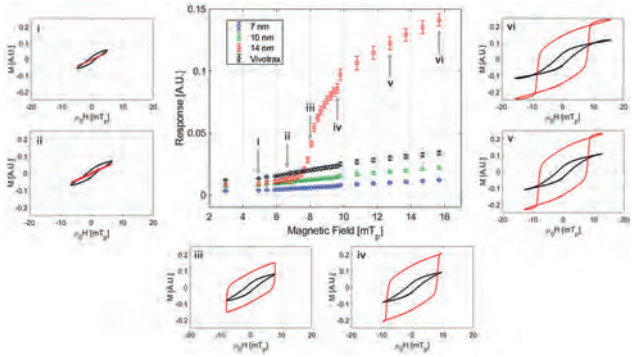

Figure 1: Magnetization response threshold behavior for strongly-interacting magnetic nanoparticle chains.

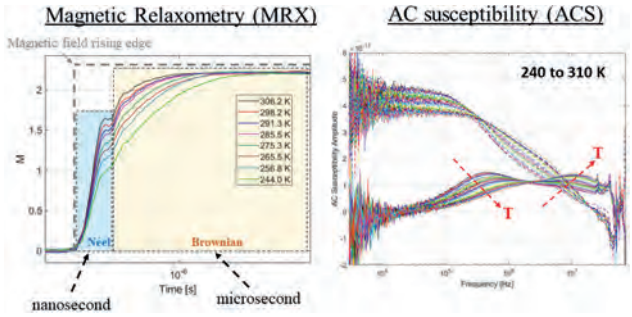

Figure 2: Time (MRX) and frequency (ACS) response of weakly-interacting magnetic nanoparticles.

CONTRIBUTED PAPERS

EE-04. Superparticles with excellent superparamagnetic and hyperthermia properties for advanced biomedical applications.
S.B. Attanayake[1], M. Nguyen[2], A. Chanda[1], T. Randall Lee[2], H. Srikanth[1] and M. Phan[1] *1. Physics, University of South Florida, Tampa, FL, United States; 2. Department of Chemistry, University of Houston, Houston, TX, United States*

Iron-oxide-based magnetic nanostructures are well-known for their non-toxicity and bio-degradability, along with their potential applications in different fields ranging from cancer treatments to spintronics devices.[1] On the contrary, due to the small size of these nanoparticles, they tend to penetrate highly sensitive areas of the body such as the Blood Brain Barrier (BBB), leading to complexities.[2] Additionally, the smaller nanoparticles, with their inherent higher reactivity, have a higher probability of retention, which can lead to genotoxicity and biochemical toxicity.[3] However, with an increase in particle size (> ~30 nm), the excellent superparamagnetic properties that are desirable for biomedical applications including magnetic hyperthermia therapy and drug delivery are lost. These grand challenges have motivated us to explore the development of large superparamagnetic nanoparticles with average diameters in the range of 150-400 nm comprised of small nanocrystallites 10–15 nm in diameter. These so-called "superparticles" contain both magnetite and maghemite phases. Here, we have systematically studied the influence of the size of the superparticles and their crystallite size on their magnetic and hyperthermia responses. We found that the particles having an average diameter of ~160 nm with the smallest crystallite diameter of 10 nm showed the highest potential, reaching the promising 40-44 °C mark. The significant enhancement of the Specific Absorption Rates (SAR > 330 W/g) generated with a low 0.5 mg/ml concentration indicates that a minimal amount of nanoparticles is needed for cancer treatment. We also found that for similar crystallite sizes, the smaller superparticles were more efficient than the larger ones. While all samples showed nearly the same saturation magnetization, the coercivity decreased with both superparticle size and crystallite size. This study enables us to determine the ideal particle-to-crystallite size combination to harness the superparamagnetic and hyperthermia properties for advanced biomedical applications of magnetic iron oxide nanoparticles.

[1] R. Das, J. Alonso, Z. Nemati Porshokouh, V. Kalappattil, D. Torres, M.H. Phan, E. Garaio, J.Á. García, J.L. Sanchez Llamazares, and H. Srikanth, "Tunable High Aspect Ratio Iron Oxide Nanorods for Enhanced Hyperthermia," Journal of Physical Chemistry C 120(18), 10086–10093 (2016). [2] R.P. Moura, A. Almeida, and B. Sarmento, "The role of non-endothelial cells on the penetration of nanoparticles through the blood brain barrier," Prog Neurobiol 159, 39–49 (2017). [3] R. D, and P. Rao, "Nanoparticles: Is Toxicity a Concern?," EJIFCC 22(4), 92 (2011).

EE-05. Simulating Spin Configurations in Arrays of Spinel Ferrite Nanoparticles.
N. Kim[1], H. Chen[2], H. Wang[2], S. Majetich[1,2], Y. Ijiri[3], K. Krycka[4], J.A. Borchers[4] and J. Rhyne[4] *1. Materials Science and Engineering, Carnegie Mellon University, Pittsburgh, PA, United States; 2. Physics, Carnegie Mellon University, Pittsburgh, PA, United States; 3. Physics and Astronomy, Oberlin College, Oberlin, OH, United States; 4. NIST, Gaithersburg, MD, United States*

Spin configurations of magnetic nanoparticles impact their use in biomedical and other device applications [1–3]. While polarization-analyzed small-angle neutron scattering (PASANS) provides direct evidence of 3D nanoscale magnetic correlations [1–3], we use simulations of internal spin arrangements to further constrain the data. Experimental data for FCC-like assemblies of spinel ferrite nanoparticles show a Bragg peak, indicating interparticle magnetic correlations parallel to the applied field. $CoFe_2O_4$ appear to be uniformly magnetized, with some canting of particle moments relative to the field direction. Fe_3O_4 assemblies also have a characteristic dip in the magnetic scattering perpendicular to the field, stemming from a shell of spins [1–3]. Fe_3O_4 core/Mn ferrite shell nanoparticles have even more complex scattering. Python was used to calculate 3D FT for different spin configurations within a FCC lattice of different dimensions and orientations [4]. Each crystal contained 10 – 30 nanoparticles along the x, y and z directions. 10,000 randomly oriented FCC packed crystals were simulated with relative peak intensities modulated by all experimental autocorrelation function [5]. Figure 1 shows the (111) Bragg peak for the uniformly magnetized 8 nm diameter $CoFe_2O_4$ nanoparticles with an edge-to-edge distance of 1 nm, fitting the experimental results. We also examined possible magnetic configurations for the magnetic core-shell model of 7 nm Fe_3O_4 nanoparticles with a shell thickness of 0.3 nm and edge-to-edge distance of 1 nm. Results showed the additional dip in the perpendicular PASANS intensity as expected from experimental data at the (111) Bragg peak (Figure 2). These results indicate the ability to test potential spin configurations for shell development, assisting in interpreting experimental results to explain the mechanisms responsible for spin canting.

[1] K. L. Krycka et al., Phys Rev Lett Vol. 104, p. 207203, (2010). [2] K. Hasz, Y. Ijiri, K. L. Krycka, J. A. Borchers, R. A. Booth, S. Oberdick, and S. A. Majetich, Phys Rev Vol. 90, p. 180405, (2014). [3] S. D. Oberdick A. Abdelgawad, C. Moya, S. Mesbahi-Vasey, D. Kepaptsoglou, V. K. Lazarov, R. F. L. Evans, D. Meilak, E. Skoropata, J. van Lierop, I. Hunt-Isaak, H. Pan, Y. Ijiri, K. L. Krycka, J. A. Borchers, and S. A. Majetich., Vol 8, p. 3425, (2018). [4] K. Krycka, J. Borchers, Y. Ijiri, R. Booth, and S. Majetich, J Appl Crystal Vol 45, p. 554, (2012). [5] S. A. Majetich, T. Wen, and R. A. Booth, ACS Nano Vol 5, p. 6081, (2011).

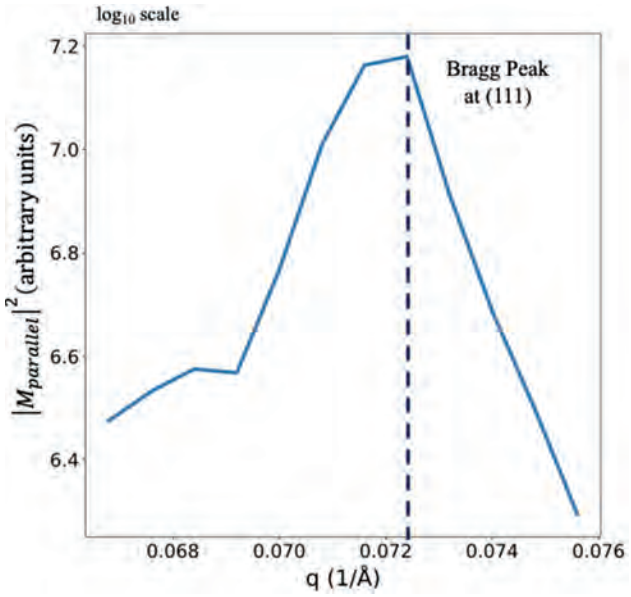

Fig. 1: Simulation results for uniformly magnetized $CoFe_2O_4$ nanoparticles showing the magnetic scattering from spins parallel to the applied field.

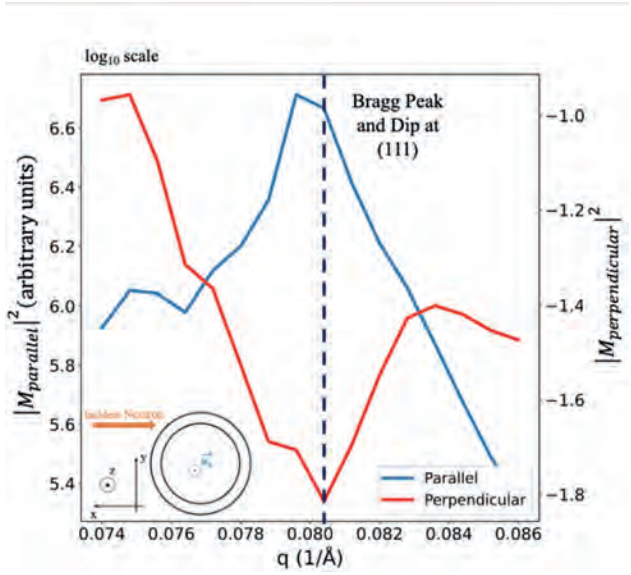

Fig. 2: Simulation results for the magnetic core-shell model of Fe_3O_4 nanoparticles. $M_{perpendicular}$ refers to scattering due to magnetic correlations along y and z.

EE-06. Gænice: a general model for magnon band structure of artificial spin ices. G. Alatteili[1], V. Martinez[1], A. Roxburgh[1], J.C. Gartside[2], O. Heinonen[3], S. Gliga[4] and *E. Iacocca*[1] *1. University of Colorado Colorado Springs, Colorado Springs, CO, United States; 2. Imperial College London, London, United Kingdom; 3. Seagate Technology, Bloomington, MN, United States; 4. Paul Scherrer Institute, Villigen PSI, Switzerland*

Artificial spin ices (ASIs) are arrays of nanomagnets that can be arranged in virtually any geometry exhibiting different forms of frustration [1]. ASIs can also be considered magnonic crystals [2], exhibiting band structure depending on their magnetization state [3] and hosting nonlinear magnon scattering processes [4]. However, the band structures appear due to non-local dipole interactions, making it impossible to solve analytically and extremely time consuming numerically. Here, we introduce a general-scope eigenvalue solver based on a tight-binding semi-analytical approach, called Gænice [5], and demag factor retrieved from micromagnetic simulations [6]. Our model allows us to solve arbitrary geometries, including three-dimensional ASIs. We study the particular case of a square ASI composed of trilayered nanoislands [7]. This reasonably complicated problem returns many interesting features at FMR that find good quantitative agreement with experiments [7], shown in Figure 1. In addition, we can predict the eigen-frequencies in a large parameter space, including lattice separation which is particularly time-consuming by micromagnetic methods, and full band structures as a function of the microstate. This material is based upon work supported by the National Science Foundation under Grant No. 2205796.

[1] S. H. Skjærvø *et al.*, Nat. Rev. Phys. 2, 13 – 28 (2020) [2] S. Gliga, E. Iacocca, and O. G. Heinonen, APL Materials 8, 040911 (2020) [3] E. Iacocca *et al.*, Phys. Rev. B 93, 134420 (2016); T. D. Lasnier and G. M. Wysin, Phys. Rev. B 101, 224428 (2020) [4] S. Lendinez *et al*., Nature Communications 14, 3419 (2023) [5] G. Alatteili *et al.*, In preparation. [6] V. Martinez and E. Iacocca, In preparation. [7] T. Dion *et al.*, In preparation.

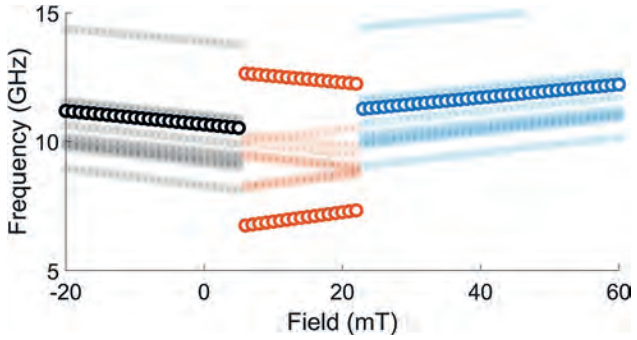

Figure 1. Field dependent eigenfrequencies predicted by Gænice for a trilayer ASI. From -20 mT to 5 mT, the two layers are strongly coupled and magnetized against the external field. From 5 mT and 22 mT, the layers are antiparallel, resulting in in-phase and out-of-phase modes with opposite tunability. From 22 mT to 60 mT, the two layers are both magnetized along the field direction. Weaker modes are depicted with faint symbols.

EE-07. Giant Uniaxial Magnetic Anisotropy and Zero-Field-Cooled Exchange Bias in Half-Metallic Compensated Ferrimagnetic $CrFeS_2$ Single Crystals. J. Liang[1,2], X. Xi[1], W. Wang[3] and *Y. Lau*[1,2] *1. Beijing National Laboratory for Condensed Matter Physics, Institute of Physics, Chinese Academy of Sciences, Beijing, China; 2. University of Chinese Academy of Sciences, Beijing, China; 3. Tiangong University, Tianjin, China*

Half-metallic compensated ferrimagnets (HMCF) [1] with 100 % spin polarization and zero net moment are ideal candidates for spintronic applications. Up to now, only a few of these materials have been identified and experimentally synthesized [2,3]. Hexagonal NiAs-structured $CrFeS_2$ has long been theoretically predicted [4] to be a HMCF but it is only until very recently that polycrystalline $CrFeS_2$ was first synthesized and studied [5]. Here, we report on the experimental realization of $CrFeS_2$ single crystals, which has allowed us to unveil the highly anisotropic nature of its magnetic and transport properties. Figure 1(a) illustrates the crystal structure of hexagonal $CrFeS_2$ where antiferromagnetically coupled Cr and Fe atoms are expected to randomly occupy the 2a atomic site. The remanent magnetization against temperature $M(T)$ for $CrFeS_2$ in Fig. 1(b) undergoes sign change on heating, which is a hallmark of compensated ferrimagnetism. We extract the magnetic compensation temperature T_{comp} ~ 185 K. $CrFeS_2$ also shows large anomalous Hall effect with Hall angle up to 2 %, which again undergoes sign change near T_{comp}. At 300 K, $CrFeS_2$ has a coercive field of ~2.5 T with a huge in-plane hard-axis anisotropy field estimated to be > 30 T. The giant uniaxial magnetic anisotropy in $CrFeS_2$ is attributed to the magnetocrystalline anisotropy induced by the hexagonal lattice. Furthermore, a large zero-field-cooled

exchange bias of about 0.8 T emerges in $CrFeS_2$ single crystal at 5 K, which resembles another compensated ferrimagnet Mn_2PtGa [6]. The direction of the exchange bias can be controlled by initially setting the "up" (M_{z+}) or "down" (M_{z-}) magnetic state of $CrFeS_2$ at 300 K, as shown in Fig. 1(c). The unique combination of all these fascinating features makes $CrFeS_2$ a very interesting candidate for applications in rare-earth-free exchange-biased hard magnets and ferrimagnetic tunnel junctions.

References: [1] H. van Leuken and R. A. de Groot, Phys. Rev. Lett. 74, 1171 (1995). [2] H. Kurt, K. Rode, P. Stamenov, et al., Phys. Rev. Lett. 112, 027201 (2014). [3] R. Stinshoff, A. K. Nayak, G. H. Fecher, et al., Phys. Rev. B 95, 060410 (2017). [4] N. H. Long, M. Ogura, and H. Akai, J. Phys.: Condens. Matter 21, 064241 (2009). [5] S. Semboshi, R. Y. Umetsu, Y. Kawahito, et al., Sci. Rep. 12, 10687 (2022). [6] A. K. Nayak, M. Nicklas, S. Chadov, et al., Phys. Rev. Lett. 110, 127204 (2013).

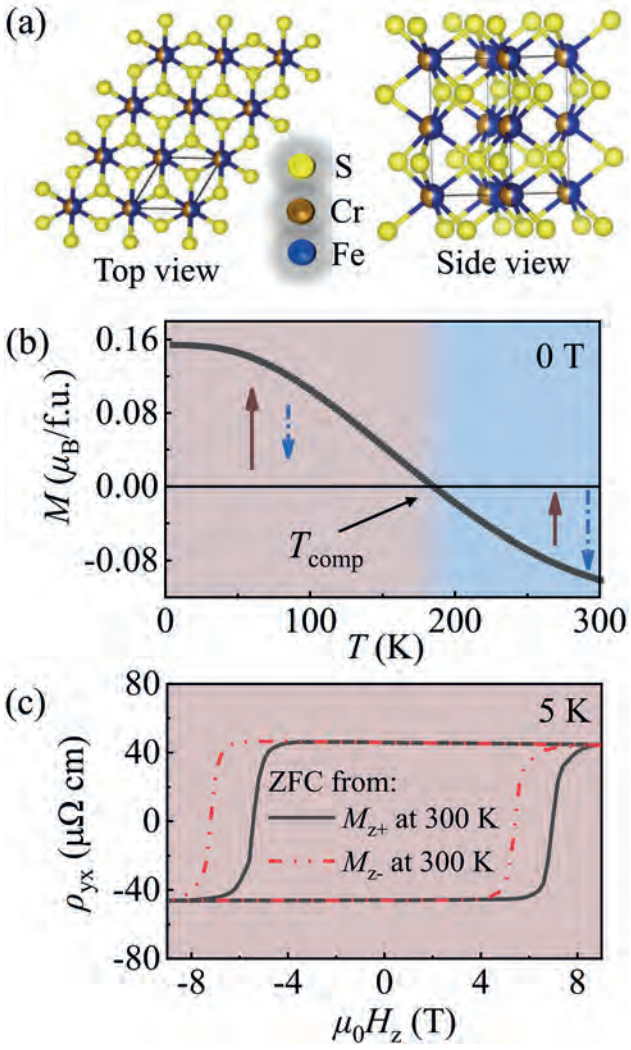

Fig.1: (a) Hexagonal NiAs-type structure of $CrFeS_2$ (b) $M(T)$ loop for $CrFeS_2$ single crystal with no applied field (c) Zero-field cooled (ZFC) exchange bias effect in $CrFeS_2$ single crystal after setting "up" (M_{z+}) and "down" (M_{z-}) magnetic states at 300 K.

EE-08. Effect of *fcc* to *bcc* Transformation on Exchange Bias in Single-Layer $FeCoNiMnAl_x$ Thin Films. *W. Beeson*[1], D. Bista[1], G. Yin[1] and K. Liu[1] *1. Department of Physics, Georgetown University, Washington, DC, United States*

High entropy alloys have emerged as an exciting platform to explore magnetic phases in systems with competing interactions.[1] For example, the Fe-Co-Ni-Mn system has been shown to exhibit a rich magnetic phase diagram consisting of ferromagnetic (FM), antiferromagnetic (AF), and spin-glass (SG) phases.[2] Simulations have shown that addition of Al to FeCoNiMn induces a change in the magnetic ordering of Mn from AF to FM,[3] presenting a handle for tuning the magnetic interactions in this system. In this work we have observed an exchange bias effect in sputtered $FeCoNiMnAl_x$ films, and investigated the evolution of magnetic phase and ordering of Mn with the Al addition. Single-layer 50 nm FeCoNiMn films exhibit a *fcc* phase from X-ray diffraction, shown in Fig. 1, and a large exchange bias of 500 Oe after field-cooling to 2.5 K (Fig. 2a), attributed to the coexistence of FM and AF/SG phases. After addition of 10 at.% Al, the films transform into a *bcc* phase, coinciding with a large increase in the saturation magnetization and suppression of the exchange bias to 70 Oe. The decrease in exchange bias suggests a reduction of the AF/SG phase, mediated by the structural change which promotes FM ordering of Mn. First-principles calculations have been carried out on $FeCoNiMnAl_x$ using the experimentally determined crystal structures. The simulated magnetic moments show strong qualitative agreement with the experimental trend, shown in Fig. 2b, and confirms the transition of the ground-state magnetic ordering of Mn from AF to FM upon *fcc* to *bcc* transition.

1. O. Schneeweiss, M. Friák, M. Dudová, Phys. Rev. B, 96, 014437, (2017). 2. J. Yu, W. Wu, H. Zhang, Phys. Rev. Mater., 6, L091401, (2022). 3. T. Zuo, M.C. Gao, L. Ouyang, Acta Mater., 130, 10, (2017).

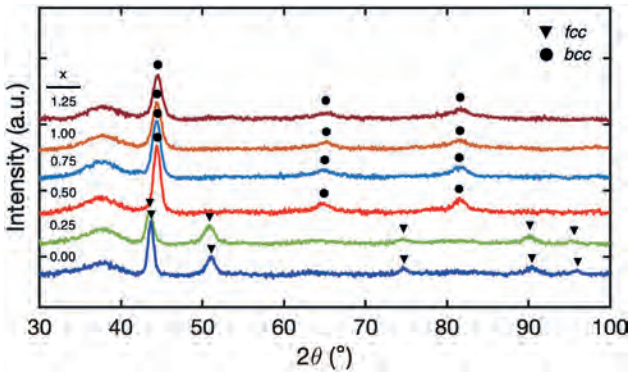

Fig. 1. Grazing-incidence X-ray diffraction scans of 50-nm $FeCoNiMnAl_x$ films for different values of x.

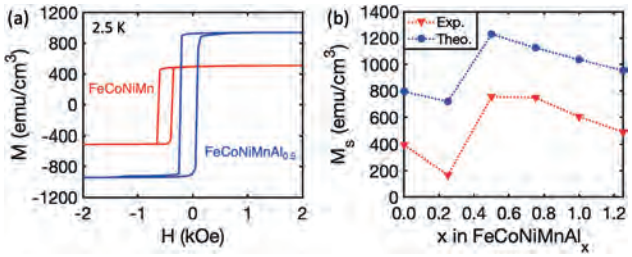

Fig. 2. (a) In-plane hysteresis loops for 50-nm FeCoNiMn and $FeCoNiMnAl_{0.5}$ films taken at 2.5 K after field-cooling in 500 Oe applied field. (b) Experimental and theoretical values of the saturation magnetization for $FeCoNiMnAl_x$.

EE-09. Modelling of magnetic nanoparticle dipole-dipole interactions in random clusters for hyperthermia application. *R. Ferrero*[1], M. Vicentini[1] and A. Manzin[1] *1. Istituto Nazionale di Ricerca Metrologica (INRiM), Torino, Italy*

Magnetic nanoparticles (MNPs) have been intensively studied for potential application in cancer therapies based on magnetic hyperthermia [1, 2], due to their ability to release heat via hysteresis losses when excited by alternating current (AC) magnetic fields with frequency in the range 50 kHz – 1 MHz. The magnetic behavior of isolated MNPs can be well described by micromagnetic analytical models. However, the energy losses predicted by such models provide only a rough estimation of the MNP specific loss power (SLP) [3]. It is indeed very difficult to include the effect of magnetostatic dipole-dipole interactions into analytical models when the MNPs are randomly clustered, thus leading to an inaccurate evaluation of their heating properties. That is the reason for studying the influence of MNP clustering and their dynamic response to different exciting conditions by means of numerical models that solve the Landau Lifshitz Gilbert (LLG) equation. However, full micromagnetic simulations are computationally intensive and not suitable to describe thousands of MNPs [4, 5]. An appropriate solution to investigate the magnetization dynamics and hysteresis losses of a large ensemble of MNPs with LLG equation is the macrospin model, valid under the assumption of single-domain MNPs [6, 7]. In this work, a micromagnetic solver based on the stochastic LLG equation and on the macrospin approximation is implemented to study the response of MNPs to different AC magnetic fields and applied to calculate the hysteresis losses and the SLP of Fe_3O_4 NPs with a size between 10 and 40 nm. The analysis is performed on very diluted MNPs as well as on strongly interacting MNPs, with variable volume concentration. As a result of the simulations, indications on how increasing the SLP are provided, focusing on the role of MNP size, arrangement in random clusters, and AC magnetic field parameters (frequency and amplitude).

[1] H. Gavilán et al., Chem. Soc. Rev., Vol. 50, p. 11614–11667 (2021). [2] X. Liu et al., Theranostics, Vol. 10, p. 3793–3815 (2020). [3] R. R. Wildeboer, P. Southern and Q. A. Pankhurst, J. Phys. D: Appl. Phys., Vol. 47, 495003 (2014). [4] R. Ferrero et. al., Nanomaterials, Vol. 11, 2179 (2021). [5] R. Ferrero et al., Scientific Reports, Vol. 9, 6591 (2019). [6] J. Leliaert et al., Med. Biol. Eng. Comput., Vol 53, p. 309– 317 (2015). [7] C. Haase and U. Nowak, Phys. Rev. B, Vol. 85, 045435 (2012).

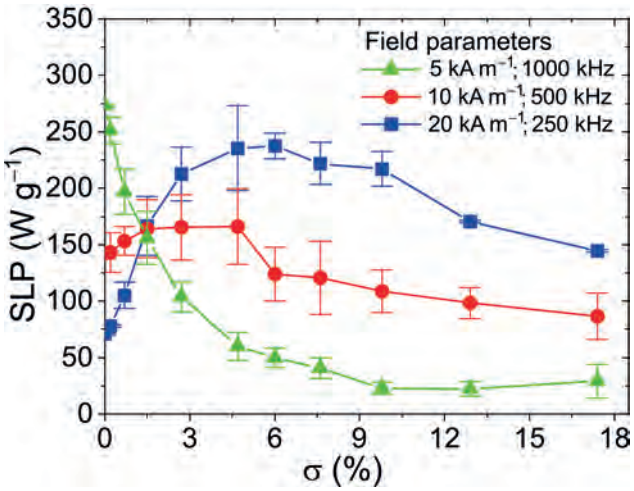

Fig 1. SLP calculated for variable volume concentrations of Fe_3O_4 NPs with 15 nm size, arranged within random clusters. Different magnetic field conditions are considered.

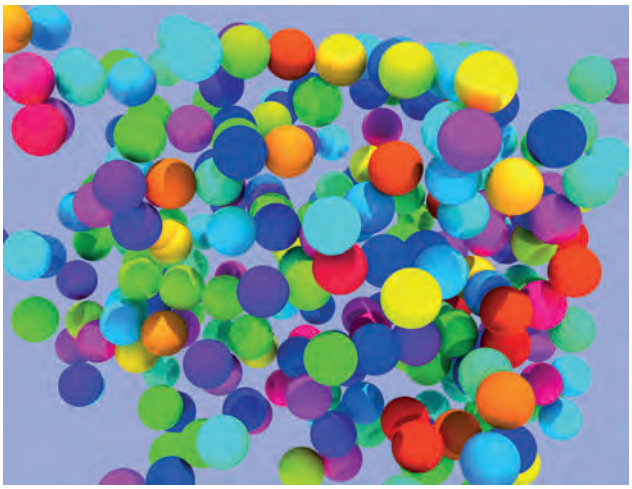

Fig. 2. Example of magnetization distribution at remanence, for σ = 9.8% under an AC magnetic field with frequency of 250 kHz and amplitude of 20 kA m^{-1}.

Session EF
HARD MAGNETIC MATERIALS II

J. Ping Liu, Chair
University of Texas at Arlington, Arlington, TX, United States

CONTRIBUTED PAPERS

EF-01. Production of $Sm_2Fe_{17}N_3$ magnets. *T. Saito[1] 1. Chiba Institute of Technology, Narashino, Japan*

$Sm_2Fe_{17}N_3$ phase, one of the newer permanent magnetic materials, has been prepared by nitrogenation of the Sm-Fe alloy powder [1]. The resultant $Sm_2Fe_{17}N_3$ intermetallic compound has been produced in powder form. However, the conventional powder metallurgical process cannot be applied to the production of $Sm_2Fe_{17}N_3$ bulk magnets because $Sm_2Fe_{17}N_3$ intermetallic compound is not stable at high temperatures and decomposes into a-Fe and SmN above 873 K. A recently developed consolidation technique, called the spark plasma sintering (SPS) method, can consolidate powders into bulk form in a relatively short time and at a lower temperature [2]. It has been demonstrated that $Sm_2Fe_{17}N_3$ magnets can be produced by the SPS method [3]. However, the reported magnetic properties of $Sm_2Fe_{17}N_3$ magnets were not yet comparable to the original $Sm_2Fe_{17}N_3$ powder. This study aimed to improve the magnetic properties of $Sm_2Fe_{17}N_3$ magnets. In this study, $Sm_2Fe_{17}N_3$ powder was blended with Zn powder and additive before the consolidation. The $Sm_2Fe_{17}N_3$ powder, with and without additives, was placed in a carbon die and then magnetically aligned before the consolidation by the SPS method. The $Sm_2Fe_{17}N_3$ powder was sintered by the SPS method. The anisotropic $Sm_2Fe_{17}N_3$ magnets were successfully produced by the SPS method. The magnetic properties of the $Sm_2Fe_{17}N_3$ magnets deeply depended on the processing condition. Figure 1 shows the hysteresis loops of the $Sm_2Fe_{17}N_3$ magnets produced by the SPS method with and without the Zn powder and additive. It was found that the small amounts of Zn powder and additive improved the coercivity and remanence of the $Sm_2Fe_{17}N_3$ magnets. A high-performance anisotropic $Sm_2Fe_{17}N_3$ magnet was successfully produced by the SPS method with the Zn powder and additive. The resultant $Sm_2Fe_{17}N_3$ bulk magnets exhibited a high coercivity of 6.70 kOe.

[1] J. M. D. Coey and H. Sun, J Magn. Magn. Mater. 87, L251 (1990). [2] M. Tokita, J. Soc. Powder Technol. Jpn, 30, 790 (1993). [3] T. Saito, J. Magn. Magn. Mater. 320, 1893 (2008).

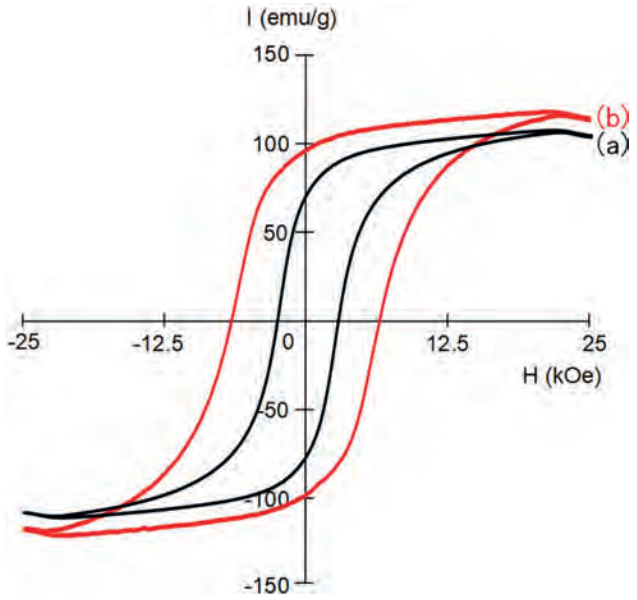

Figure 1 hysteresis loops of (a) the $Sm_2Fe_{17}N_3$ magnet and (b) the $Sm_2Fe_{17}N_3$ magnet with the Zn powder and additive.

EF-02. Engineering grain boundary for high performance Dy-free-NdFeB sintered magnets with Pr-Al-Cu additions. *W. Tang[1], G. Ouyang[1], J. Wang[1], H. Dasari[2], M.J. Kramer[1,2], J. Cui[1,2] and I. Anderson[1,2] 1. Ames National Laboratory, Ames, IA, United States; 2. Materials Science & Engineering, Iowa State University, Ames, IA, United States*

Efficient high power density electric drive motors require permanent magnets with high energy product, good thermal stability, and less critical materials. $Nd_2Fe_{14}B$-based sintered magnets are one of the primary candidates for these applications. However, Nd-Fe-B based magnets without heavy rare earth elements (HREE) have poor magnetic properties above 150°C, target operating temperature for most electric vehicles (EV). HREE, such as, Dy, have been added to the magnets to enhance the coercivity H_{cj} and improve their performance at elevated temperatures. The operating temperature of the magnets depends on the amount of Dy added. For the magnet to be operable at 200°C, the amount of Dy required could exceed 10 wt.%. Unfortunately, Dy is a critical element. Therefore, the development of Dy-lean or free Nd-Fe-B magnets capable of high temperature operation becomes a great interest to the EV industry. It is well accepted that the H_{cj} of these magnets is controlled by the nucleation of reversal domains at locally low-anisotropy surfaces of the individual 2:14:1 grain. The H_{cj} is sensitive to grain boundary structure, grain boundary chemistry, and grain size. Engineering microstructure techniques are one of the most effective methods to develop Dy-lean or free Nd-Fe-B magnets. Our previous studies on Pr-Cu eutectic alloy-doped Neo magnets show that the addition of Pr-Cu can greatly improve H_{cj}. In this work, Dy-free sintered magnets were fabricated by mixing Nd-Fe-B powder with various amounts of Pr-Al-Cu powder followed by the sintering and annealing procedures. It was found that the addition of Pr-Al-Cu is more

effective to enhance H_{cj} and simultaneously maintain a higher $(BH)_{max}$ than that of Pr-Cu. With increasing Pr-Al-Cu from 0 to 10 wt.%, as shown in Fig 1, the H_{cj} of obtained magnets increases from the original 14.5 to 19.1 kOe, and $(BH)_{max}$ decreases from 45.3 to 37.2 MGOe. Relatively, the magnet with 7.5 wt% Pr-Al-Cu achieves the best overall H_{cj} and $(BH)_{max}$. The thermal stability of the magnets with different additions of Pr-Al-Cu was studied. The microstructure and Pr-Al-Cu roles in the magnets will be analysed and discussed.

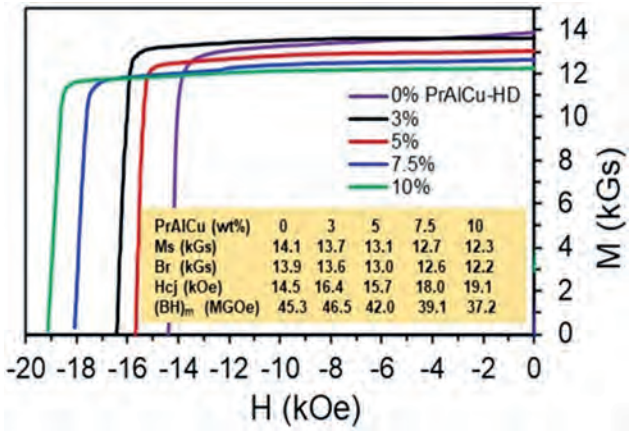

Fig1. ***Demagnetization curves of the magnets with different additions of Pr-Al-Cu***

EF-03. Achieving optimal processing of grinding sludge in the manufacturing of Sm_2Co_{17} magnets to contribute to a waste-free economy. *S. Khoshsima*[1], F. Kafexhiu[1], T. Tomse[1], K. Zuzek[1,2] and S. Sturm[1,2] *1. Nanostructured Materials, Institute Jozef Stefan, Ljubljana, Slovenia; 2. Jozef Stefan International Postgraduate School, Ljubljana, Slovenia*

Samarium-Cobalt (SmCo) magnets possess outstanding qualities, such as remarkable resistance to oxidation/corrosion, high thermal stability (Tc ≥ 747 °C), and exceptional magneto-crystalline anisotropy, making them valuable across various industries. However, the market share of SmCo magnets remains relatively low due to challenges associated with limited material resources, sustainability concerns, and environmental risks [1-3]. An important source of secondary resources comes from the waste generated during the machining and polishing of SmCo magnets. This waste contains impurities and a significant amount of carbon, posing difficulties for recycling and reusing. This research focuses on the recycling and reprocessing of SmCo waste derived from permanent magnets, employing an innovative separation method that combines pyrolysis and arc-melting to reduce the carbon content and facilitate its reuse in SmCo magnet production. Various techniques for characterization and thermal pretreatment are utilized to analyze and prepare the waste for further processing. The results demonstrate a successful reduction in carbon content within the waste (from 0.79 to 0.2 wt.%), paving the way for a more sustainable and environmentally friendly production cycle of SmCo magnets.

1-O. Gutfleisch, M.A. Willard, E. Brück, et al., Adv. Mater. 23 (2011) 2-J.-H. Yi, Rare Met., 33, 633–640 (2014) 3-N. Swain, S. Mishra, J. Clean. Prod. 220 (2019)

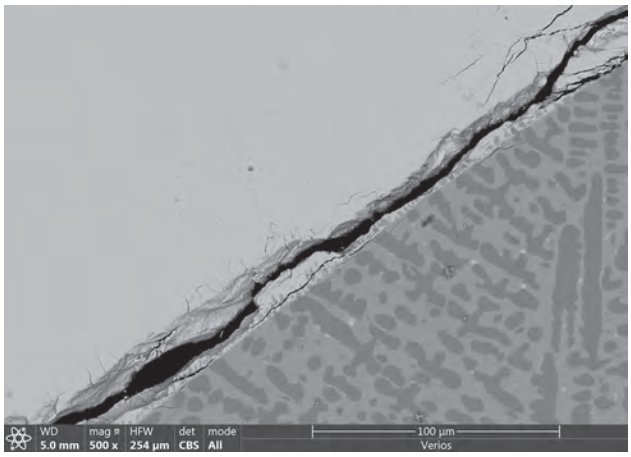

Microstructure of the arc-molten button: The backscatter image of the Sm_2O_3 oxide layer.

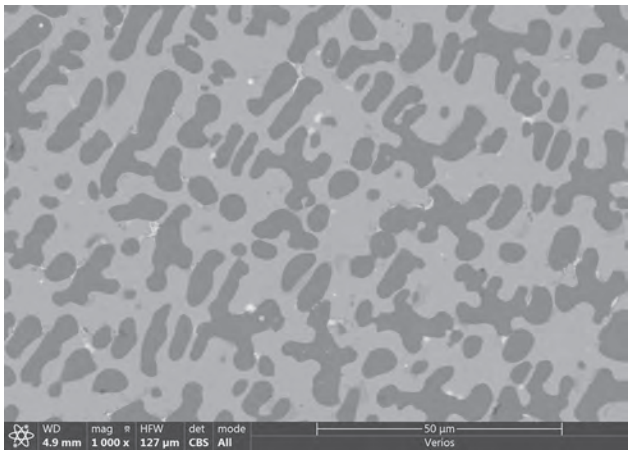

Microstructure of the arc-molten button: Backscatter images of the dendrite-like microstructure of the inner metallic core of the molten button

EF-04. Magnetic and crystalline microstructures of dual-main-phase (Nd, Ce)-Fe-B sintered magnets. Y. Xiao[1], *Y. Fang*[1], T. Liu[1], M. Zhu[1] and W. Li[1] *1. Central Iron and Steel Research Institute, Beijing, China*

In recent years, rare earth permanent magnets (REPM) with high Ce content have been successfully prepared by dual-main-phase (DMP) technology[1-7]. However, the correlation between the magnetic microstructure, composition process, and crystalline structure of the DMP (Nd, Ce)-Fe-B magnets is still not clear. In this work, three kinds of strips with nominal compositions of $Nd_{30.5}Fe_{bal}B_{0.95}M_{0.45}$ (denoted as N), $Ce_{30.5}Fe_{bal}M_{1.1}B_{0.96}$ (denoted as C), $Nd_6Ce_{24}B_{0.95}Fe_{68.6}M_{0.45}$ (denoted as NC) were synthesized by a strip-casting process. Two types of Ce-rich DMP magnets with Nd-Fe-B/Ce-Fe-B and Nd-Fe-B/$(Nd_{0.2}Ce_{0.8})$-Fe-B as the basic component were prepared, respectively. Both magnets have the same Ce content of 40 wt % of the total rare earth content, denoted as N-C40 and N-NC40, respectively. The remanence B_r of the magnet N-NC40 is 12.68 kGs, which is an increase of 6.38% compared with 11.92 kGs of the magnet N-C40. The intrinsic coercivity H_{cj} of the magnet N-C40 is 3.97 kOe, while that of N-NC40 reaches 5.31 kOe, which improves about 33.75% more than that of N-C40. The maximum energy product $(BH)_{max}$ of N-NC40 is 32.99 MGOe, and it is 42.94% higher than that of N-C40, which is 23.08 MGOe. Magnetic force microscope (MFM) investigations reveal that the DMP (Nd, Ce)-Fe-B magnets show maze-like patterns. However, much finer domain structures mixing with coarse ones can be observed obviously in the sintered magnets. The size distribution of the domain width of the magnet is not uniform obviously.

The average domain width is 0.912 μm, and the fine domain width has only 0.216 μm. The smaller domain width and more branch domain patterns exist in poorer coercivity DMP magnets. This is caused by the non-uniform Ce composition of poorer property DMP magnets and the grain boundary microstructure that is not conducive to improving the coercivity. Furthermore, it is found that some domains of rare-earth-rich grain boundary phases exhibit the characteristics of plate-like patterns rather than no-contrast by using MFM, indicating their ferromagnetism at room temerature. Obvious correlations between the crystalline microstructure, chemical composition of phases, and magnetic structure were demonstrated for the DMP magnets.

[1] M. Zhu, W. Li, J. Wang, L. Zheng, Y. Li, K. Zhang, H. Feng and T. Liu, IEEE Transactions on Magnetics, 50, 1-4 (2014) [2] Q. Jiang, L. He, W. Lei, Q. Zeng, S. Ur Rehman, L. Zhang, R. Liu, J. Li, S. Ma and Z. Zhong. Journal of Magnetism and Magnetic Materials, 475, 746-753(2019) [3] Y. Zhang, T. Ma, M. Yan, J. Jin, B. Wu, B. Peng, Y. Liu, M. Yue and C. Liu. Acta Materialia. 146, 97-105(2018) [4] L. Zhang, M. Zhu, Y. Guo, L. Song and W. Li. Journal of Alloys and Compounds, 891, 161921 (2021). [5] J. Jin, M. Yan, W. Chen, W. Zhang, Z. Zhang, L. Zhao, G. Bai and J-M Greneche. Acta Materialia, 204, 116529(2021) [6] G-Y Kim, T-H Kim, H-R Cha, S-H Lee, D-H Kim, Y-D Kim and J-G Lee. Journal of Materials Science & Technology, 126, 71-79(2022) [7] W. Li, L. Zhao and Z. Liu. Journal of Magnetism and Magnetic Materials, 476, 302-310(2019)

EF-05. Withdrawn

EF-06. Efficient Hybrid NdFeB – SmFeN Bonded Magnets. *H.G. Parmar*[1], M.P. Paranthaman[2] and C.I. Nlebedim[1] *1. Critical Materials Institute, Ames National Laboratory, Ames, IA, United States; 2. Critical Materials Institute, Oak Ridge National Laboratory, Tennessee, IA, United States*

The commercial bonded magnets are fabricated by injection molding and compression molding, which have a typical magnet powder loading fraction between 65 and 80 vol%, respectively[1]. In order to improve the energy product of bonded magnets, one can either increase the loading fraction/filling fraction or use high energy product powder. In fact, the filling fraction also impact the alignment of particles and, the energy product of bonded magnets [2]. The same size particles can provide a close-packed arrangement providing 74% packing by volume[3]. Hence, we have used bi-modal packing of 40mm Sm-Fe-N and 105mm Nd-Fe-B particles to improve packing density in a hybrid Nd-Fe-B/Sm-Fe-N bonded magnets, fabricated by warm compaction using nylon as the binder. In this approach, filling fraction and density are improved by the smaller Sm-Fe-N particles that fill the gap between the bigger Nd-Fe-B particles. It is reported that Sm-Fe-N has an excellent hard magnetic properties and high oxidation resistance[4]. Sm-Fe-N exhibits a high saturation magnetization (1.57 T), high anisotropy field (14 T) and Curie temperature (750K), which are comparable or superior to Nd-Fe-B[5]. It is known that Nd-Fe-B/Sm-Fe-N hybrid magnets show a thermal stability with magnetic properties better than that of Nd-Fe-B bonded magnets. As shown in Fig.1, SmFeN has particle size of ~40 μm, while NdFeB has ~105 μm. We have fabricated 70 Vol % of magnetic powder loading fraction bonded magnet using warm compaction. We have also performed in-situ alignment of particles during the process. Hence, this process removes the post alignment steps for bonded magnet fabrication. We have varied the SmFeN powder percentage form 0-100% and studied the effect of small size particle variations on magnetic properties. Fig.2 shows the M-H loop of 50% SmFeN and 50% NdFeB hybrid magnets. The magnet has a density of 5.9 g/cm^3 and energy product of 18.8 MGOe. The present study provides a pathway for making highly efficient bonded magnets.

[1] B. M. Ma, J. W. Herchenroeder, B. Smith, M. Suda, D. N. Brown, and Z. Chen, "Recent development in bonded NdFeB magnets," *J Magn Magn Mater*, vol. 239, no. 1, pp. 418–423, 2002, doi: https://doi.org/10.1016/S0304-8853(01)00609-6. [2] K. Gandha *et al.*, "Additive manufacturing of anisotropic hybrid NdFeB-SmFeN nylon composite bonded magnets," *J Magn Magn Mater*, vol. 467, pp. 8–13, 2018, doi: https://doi.org/10.1016/j.jmmm.2018.07.021. [3] S. Torquato, T. M. Truskett, and P. G. Debenedetti, "Is Random Close Packing of Spheres Well Defined?," *Phys Rev Lett*, vol. 84, no. 10, pp. 2064–2067, Mar. 2000, doi: 10.1103/PhysRevLett.84.2064. [4] C. N. Christodoulou and N. Komada, "High coercivity anisotropic Sm2Fe17N3 powders," *J Alloys Compd*, vol. 222, no. 1, pp. 92–95, 1995, doi: https://doi.org/10.1016/0925-8388(94)04924-6. [5] M. Katter, J. Wecker, C. Kuhrt, L. Schultz, and R. Grössinger, "Magnetic properties and thermal stability of Sm2Fe17Nx with intermediate nitrogen concentrations," *J Magn Magn Mater*, vol. 117, no. 3, pp. 419–427, 1992, doi: https://doi.org/10.1016/0304-8853(92)90099-A.

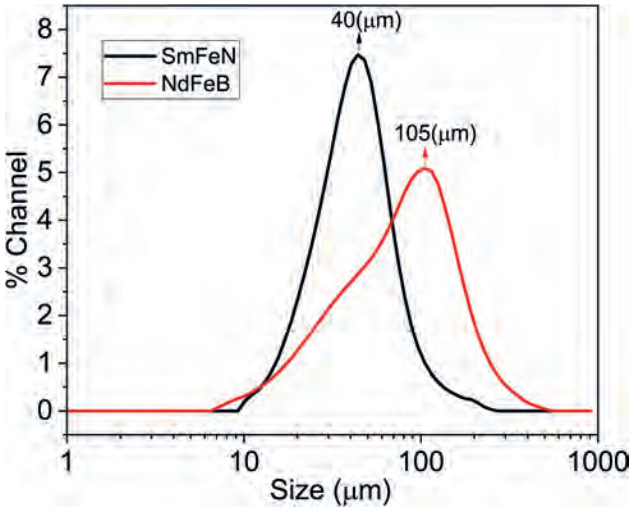

Particles size of NdFeB particles and SmFeN particles

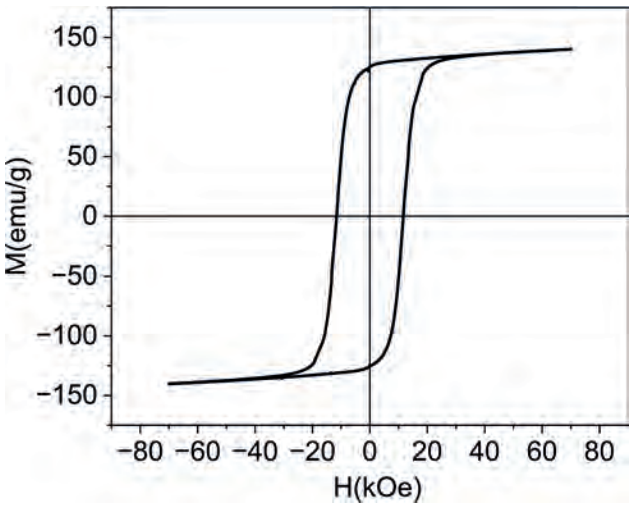

Room temperature M-H loop of bonded magnet

EF-07. Correlating the Degree of Alignment and Physical Interactions During the Processing of Anisotropic Bonded Magnets. *C.I. Nlebedim*[1], X. Liu[1] and M.P. Paranthaman[2] *1. Division of Critical Materials, Ames National Laboratory, Ames, IA, United States; 2. Nanomaterials Chemistry Group, Oak Ridge National Laboratory, Oak Ridge, TN, United States*

We will present the correlation between multiple physical parameters that can be controlled during the processing of anisotropic bonded magnets. The parameters of interest include magnetic loading fraction, changes in binder viscosity, applied magnetic field and the degree of alignment. Understanding and controlling the relationship between these parameters is important for developing high performance bonded magnets, while reducing the rare earth (RE) contents. The use of sintered Nd-Fe-B magnets in compact electronic

devices often require extensive machining, hence significant waste generation [1], [2]. Since bonded magnets can serve in some of the applications and can be made near net-shape, their use reduces machining waste, hence saves REs. Also, since the magnet fraction in bonded magnets is less, compared to sintered magnets, there is additional opportunity to reduce the use of critical REs. Consequently, bonded magnets offer an avenue for addressing the potential disruption in the supply of RE for permanent magnets. 40 vol.% and 50 vol.% bonded anisotropic MQA powder and ethylene-vinyl acetate (EVA) copolymer were extruded. Differential scanning calorimetry was used to study the melting characteristics of the EVA, with/without the powders. Magnetic hysteresis loops and magnetization vs. temperature (M vs. T) were studied in a SQUID magnetometer, which was also used to align the samples. Fig. 1 shows the M vs. T for the 40 vol.% and 50 vol.% samples, at the different alignment fields. At m_0H = 1 T, both samples reached maximum alignment at ~340 K. We will show that alignment began at the onset of the EVA melting peak (~310 K) and is maximum at the end (i.e., ~340 K). By comparing Fig. 1a and 1b, the change in magnetization between the heating and cooling steps is less in the 50 vol.% sample, compared to the 40 vol.% sample. This suggests that the work done by the applied field to align the samples with 50 vol.% MQA is less than that for the 40 vol.% sample. This behavior is due to competing interactions, i.e., Zeeman energy, magnetostatic energy, and the drift force between molten binder and particles. We will show how this interaction can be leveraged in producing bonded magnets.

[1] T. Xu and H. Peng, "Formation cause, composition analysis and comprehensive utilization of rare earth solid wastes," *J. Rare Earths*, vol. 27, no. 6, pp. 1096–1102, Dec. 2009. [2] I. C. Nlebedim *et al.*, "Studies on in situ magnetic alignment of bonded anisotropic Nd-Fe-B alloy powders," *J. Magn. Magn. Mater.*, vol. 422, pp. 168–173, Jan. 2017.

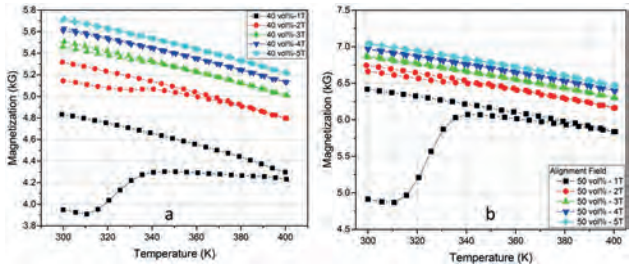

EF-08. Intrinsically hard magnetic $TbCu_7$-type Sm-Fe based compounds with high anisotropy field. *D. Angayarkanni Ramamurthy*[1,2], D. Ogawa[1], P. Tozman Karanikolas[1], H. Sepehri-Amin[1,2], K. Hono[1,2] and Y. Takahashi[1] *1. Research Center for Magnetic and Spintronic Materials, National Institute for Materials Science, Tsukuba, Japan; 2. Graduate School of Science and Technology, University of Tsukuba, Tsukuba, Japan*

Sm-Fe based compounds are considered to be the next generation permanent magnets as it enables balanced use of rare earth (RE) elements besides Nd [1]. Recently, the $ThMn_{12}$-type $SmFe_{12}$ compounds have been extensively studied due to their low RE content and high Fe content. However, $SmFe_{12}$ is unstable and always requires large amounts of stabilizing elements, resulting in a trade-off between phase stability and the magnetic property [2]. On the other hand, the metastable $TbCu_7$-type Sm-Fe based compounds are intriguing because of their disordered structure, which allows Fe to be accommodated beyond the stoichiometry of $SmFe_7$, i.e., Fe:Sm>7. Additionally, this material exhibits a strong uniaxial magneto-crystalline anisotropy after nitriding [3]. Nevertheless, very little attention has been paid to this compound, and the evaluation of its intrinsic properties is important to understand its potential as a permanent magnet. In this study, we present a systematic investigation on the phase formation and intrinsic magnetic properties of $TbCu_7$-type $SmFe_9$ epitaxial films, deposited on Al_2O_3 (0001) single crystal substrates with Mo buffer layer. From XRD, it is observed that all the peaks correspond to the $TbCu_7$ phase of Sm-Fe compound with *c*-axis texture (Fig. 1). The epitaxial growth of the thin film was confirmed using φ scan, which shows 6-fold symmetry of (102) peak (Fig. 1b). Nitrogen treatment was then performed on this epitaxial film at elevated temperature at different N_2 pressure. Peak shift was observed in all peaks corresponding to $TbCu_7$ type phase after nitrogen treatment (Fig. 1c). There is a slight increase in the lattice parameters *c* and *a* of $SmFe_9N_\delta$ from 0.4181 nm to 0.4281 nm and from 0.4885 nm to 0.4986 nm respectively. The intrinsic magnetic properties such as saturation magnetization (M_s) and anisotropy field (H_A) of $SmFe_9N_\delta$ are estimated from *M* vs *H* hysteresis loop (Fig. 2) and anomalous Hall effect torque method [4]. We found previously unreported high values of H_A ~22 T and M_s of 1.45 T, showing that this system has potential as a future permanent magnetic material.

1. K. Binnemans, P. T. Jones, T. Muller, J. Sustain.Metall.,Vol. 4, p.216-146 (2018) 2. Y.K. Takahashi, H. Sepehri-Amin, T. Ohkubo, Sci. Technol. Adv. Mater., Vol. 22, p.449–460 (2021) 3. S. Sato, K. Nishikawa, E. Node, J. Alloys compd., Vol. 929, P. 167280 (2022). 4. T. Ono, S.Okamoto N.Kikuchi, Appl. Phys. Exp., Vol. 11, 033002 (2018)

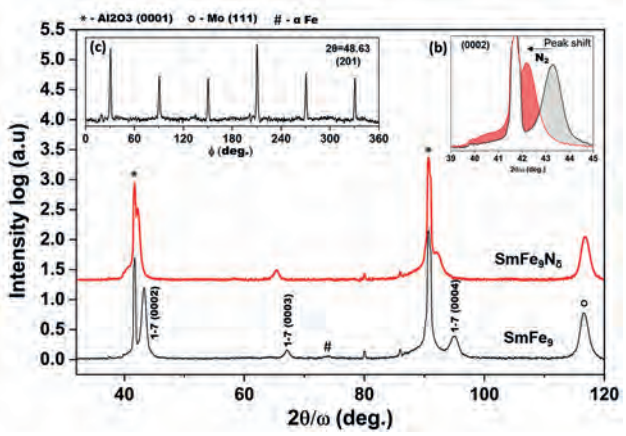

Fig. 1 XRD of $SmFe_9$ and $SmFe_9N_\delta$ epitaxial thin films, peak shift (b) and φ-scan (c)

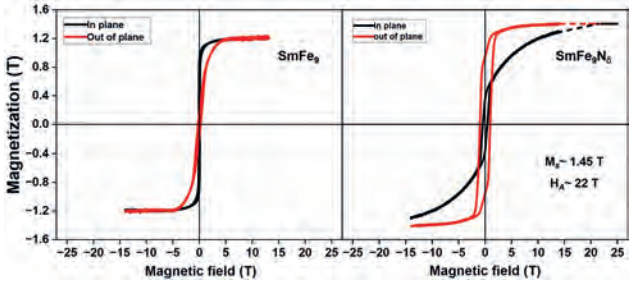

Fig. 2 M vs H hysteresis loop of $SmFe_9$ and $SmFe_9N_\delta$

EF-09. Electronic structure and magnetocrystalline anisotropy of W-type hexaferrites. *R. Islam*[1], S.P. Madsen[1] and M. Christensen[2] *1. Mechanical and Production Engineering, Aarhus University, Aarhus, Denmark; 2. Center for Materials Crystallography, Department of Chemistry and Interdisciplinary Nanoscience Center (iNANO), Aarhus University, Aarhus, Denmark*

Extending the range of superior permanent magnets will ease supply strain on the present rare-earth-based permanent magnets. The hard-magnetic properties of rare-earth magnets are unrivaled, but the search for alternatives is still of the utmost importance, especially for those that contain little to no rare-earth elements. W-type $SrFe_{18}O_{27}$ (SrW) hexaferrite has received a lot of attention as a prospective "gap" magnet due to its high magnetization and unique magnetic properties, with appreciable magnetocrystalline anisotropy energy (MAE) derived from the seven magnetic sublattices of Fe cations [1,2]. Here, we report first-principles density functional theory

calculations of the electronic structure and intrinsic magnetic properties of $SrFe_{18}O_{27}$ (SrW), $SrNi_2Fe_{16}O_{27}$ (SrNW), $SrZn_2Fe_{16}O_{27}$ (SrZW) and $SrNiZnFe_{16}O_{27}$ (SrNZW) hexaferrite compounds. The GGA+U approach was employed to improve the description of strongly correlated 3*d* electrons. The MAE constant K_1 of the SrW, SrNW, SrZW and SrNZW hexaferrites are computed, and examined based on the electronic structure and evaluated individual contributions of different Fe sublattices. The calculated K_1 values indicate that the compounds are uniaxial with easy axis along the (001) direction. Detailed analysis of the electronic structure reveals that MAE is significantly influenced by orbital distortion. The results highlight the challenge of simultaneously enhancing K_1 and magnetization M_s in W-type hexaferrite compounds. However, SrZW compounds show intriguing properties with moderate K_1 and high M_s values, which may outperform the conventional M-type ferrite magnets in some applications. This work is supported by the Independent Research Fund Denmark – Green Transitions COMPASS project (1127-00235B) and DeiC National HPC (g.a. DeiC-AU-N2-2023011 and DeiC-AU-L5-0010).

1. H. Ueda, H. Shakudo, H. Santo, Y. Fujii, C. Michioka and K. Yoshimura, Journal of the Physical Society of Japan 87, 104706 (2018). 2. M. I. Mørch, J. V. Ahlburg, M. Saura-Múzquiz, A. Z. Eikeland and M. Christensen, IUCrJ 6, 492-499 (2019).

EF-10. The Magnetic Anisotropy of Field-Assisted 3D Printed Nylon Strontium Ferrite Composites. *O.K. Arigbabowo*[2], M. Khadka[1], J. Tate[2,1] and W. Geerts[2,3] *1. Ingram School of Engineering, Texas State University, San Marcos, TX, United States; 2. Materials Science, Engineering, and Commercialization, Texas State University, San Marcos, TX, United States; 3. Department of Physics, Texas State University, San Marcos, TX, United States*

Magnetic Field Assisted Additive Manufacturing (MFAAM), 3D printing in a magnetic field, has the potential in fabricating high magnetic strength anisotropic bonded magnets. Here, 10, 35, and 54wt% strontium ferrite bonded magnets using polyamide 12 (nylon 12) binder were developed by twin screw compounding process and then printed via MFAAM samples in zero, and in 0.5 Tesla (H parallel to the print direction). The hysteresis curves were measured using a MicroSense EZ9 Vibrating Sample Magnetometer (VSM) for 3 different mount orientations of the sample on the sample holder - Vertical at 0 degrees (H perpendicular to print bed normal n_p), Vertical at 90 degrees (H parallel to n_p), and Horizontal at 0 degrees (H parallel to extrusion print direction). The hysteresis curve's squareness S (M_r/M_s) is shown in Fig. 1 for samples printed in zero field and samples printed parallel to the print field. The no-field samples exhibited a weak anisotropy with an easy axis perpendicular to the print direction. This anisotropy is caused by the effect of shear flow on the orientation of the magnetic platelets in the 3D printer head. Such anisotropy was also observed in the twin extruded filaments [1]. For the MFAAM samples, the S values are largest in the VSM measuring orientation vertical-90 indicating an easy axis parallel to the print bed normal. The alignment of the magnetic particles happens when the molten suspension is in the extruder. When the material is printed it is folded over on the print bed and its easy axis rotates 90 degrees parallel to the print bed normal. Little realignment of the particles happens after it is printed, suggesting a sharp drop in temperature once the composite touches the print bed, indicating that field-induced effects dominate the anisotropy of MFAAM deposited samples. This work was supported in part by NSF through DMR- MRI Grant under awards 2216440 and in part by DOD instrumentation grant (78810-W911NF-21-1-0253).

[1] Tanjina Ahmed, Maria Belduque, Binod D.C., Jitendra Tate, Wilhelmus Geerts, AIP Adv. 11 (2021) 015048, 1-5.

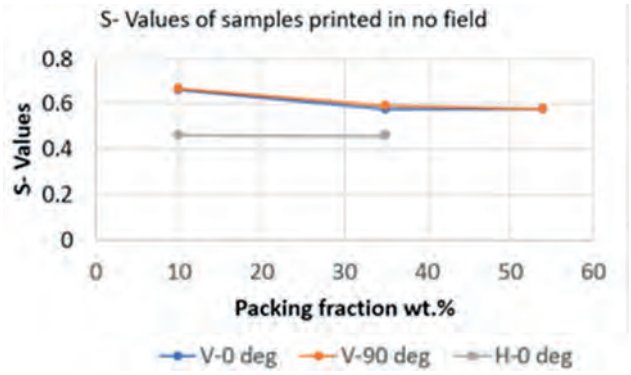

Fig. 1(a) S-values of samples printed in no-field

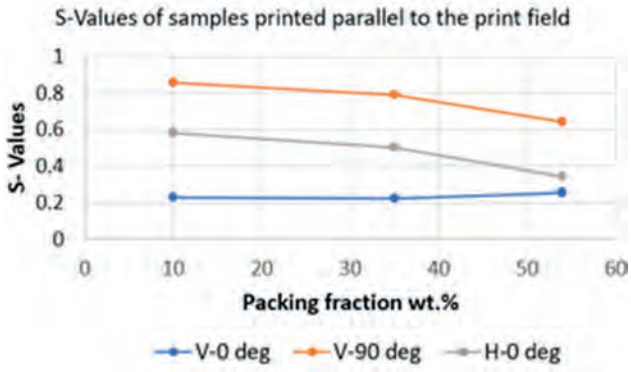

Fig. 1(b) S-values of samples printed parallel to the print field

EF-11. Crystal Anisotropy of Strontium Ferrite and PA-12 3D Fused Fillament Fabrication (FFF). *G.L. Espinosa Rodriguez*[1], J. Alvarado[2], O.K. Arigbabowo[3], J. Tate[2,3] and W. Geerts[1,3] *1. Physics, Texas State University, San Marcos, TX, United States; 2. Ingram School of Engineering, Texas State University, San Marcos, TX, United States; 3. Materials Science, Engineering, and Commercialization, Texas State University, San Marcos, TX, United States*

Strontium Ferrite (SF) is a widely used hard magnetic ferrimagnetic material that can be used for 3D printer filaments for Magnetic Field Assisted Additive Manufacturing (MFAAM) of permanent magnets. The filaments studied here are composed of a SF/PA-12 thermoplastic composite that is produced using a twin-screw extruder. SF powder is mixed with PA-12 with a 40 wt.% ratio for the SF, PA-12 is used as an adhesive for the SF particles. The single crystalline SF platelets have a magnetic anisotropy with an easy axis perpendicular to the platelet. Recently it was discovered that extruded filaments are anisotropic with an easy plane along the r-directions [1]. This is supported by computational work of others which suggests shear flow orient the SF platelets near the filament's cylindrical surface parallel to the flow [2]. So, we expect the filament's outside cylindrical surface to be more anisotropic than its center. To further explore this, the magnetic hysteresis of various parts of the filament were studied. A dissecting tool is used to remove the core of a 1.5 mm long cut of the filament (Fig. 1a-b). Both the core (removed part) and donut (outer shell) are characterized by an EZ9 vibrating smaple magnetometer. The squareness ($S=M_r/M_s$) of the hysteresis curves measured parallel to the filament's z- (S_z) and r-axis (S_r) are compared. It was found that the S_r/S_z is larger for the donut than for the core samples confirming the above-mentioned hypothesis. Note that two different platelet orientation distributions are possible (Fig.2). To further investigate this, an incision was made on one side of the donut sample and the cut open donut was flattened and glued to an 8 mm round cover glass (Fig. 1c-d). The hysteresis curves were measured for different field directions, i.e., parallel to the r and parallel to the θ directions. As the S is larger in the r-direction we conclude that the c-axis of the particles line up in filament's r-direction due to shear flow near

the walls of the extrusion die (Fig. 2a). This work was supported in part by NSF-DMR (2216440) by DOD (78810-W911NF-21-1-0253) and by an NSF REU grant (2051066).

[1] Tanjina Ahmed, Maria Belduque, Binod D.C., Jitendra Tate, Wilhelmus Geerts, AIP Adv. 11 (2021) 015048, 1-5. [2] S. Yashiro, H. Sasaki, and Y. Sakaida, Compos. Part A Appl. Sci. Manuf., vol. 43, no. 10, pp. 1754–1764, 2012; Martin Trebbin, Dagmar Steinhauser, Jan Perlich, Adeline Buffet, Stephan V. Roth, Walter Zimmermann, Julian Thiele, Stephan Forster, Proc Natl Acad Sci U S A. 2013 Apr 23; 110(17): 6706–6711.

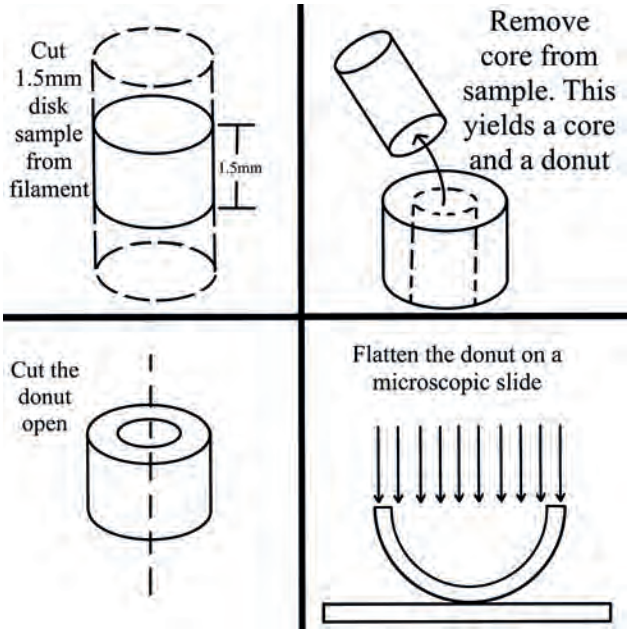

Fig. 1: Sample preparation method.

Fig. 2: Circular or star alignment.

EF-12. 4*f*-electrons driven giant magnetic and optical anisotropy in site-substituted M-type strontium-hexaferrite. *D. Paudyal*[1] and C. Bhandari[1] *1. Ames Laboratory, Ames, IA, United States*

By performing density functional calculations, we find a giant magnetocrystalline anisotropy (MCA) constant in abundant element substituted M-type hexaferrite, in the energetically favorable strontium site, assisted by a quantum confined electron transfer from substituted site to specific iron (2a) site. Remarkably, the calculated electronic structure shows that the electron transfer leads to the formation of 3+ valence state in substituted site and Fe2+ at the 2a site producing an occupied 4*f*1 state below the Fermi level that adds a significant contribution to MCA and magnetic moment. A 50% substitution of Sr forms a metallic state, while a full substitution retains the semiconducting state of the strontium-hexaferrite (host). In the latter, the band gap is reduced due to the formation of charge transferred states in the gap region of the host. The optical absorption coefficient shows an enhanced anisotropy between light polarization in parallel and perpendicular directions. Calculated formation energies, including the analysis of probable competing phases, and elastic constants confirm that both compositions are chemically and mechanically stable With successful synthesis, the site-hexaferrite can be a new high-performing critical-element-free permanent magnet material adapted for use in devices such as automotive traction drive motors. This work is supported by the Critical Materials Institute, an Energy Innovation Hub funded by the U.S. Department of Energy, Office of Energy Efficiency and Renewable Energy, Advanced Manufacturing Office. The Ames National Laboratory is operated for the U.S. Department of Energy by Iowa State University of Science and Technology under Contract No. DE-AC0207CH11358.

C. Bhandari and D. Paudyal, 4*f*-electrons driven giant magnetic and optical anisotropy in site-substituted M-type strontium-hexaferrite, under review in Physical Review Applied.

EF-13. Magnetic Hardening of Iron Carbide Nanocrystals. J. Mohapatra[1], X. Meiying[1], *P. Joshi*[1], N.A. Molwani[1], J. Ruiz[1] and J. Liu[1] *1. Department of Physics, University of Texas at Arlington, Arlington, TX, United States*

In all ferromagnetic materials, the coercivity limit is scaled with their anisotropy field, however, the experimental coercivity values are significantly below the magnetic anisotropy field (only 20-40% of the anisotropy field values), which limits the energy density. Our recent investigations on singe-domain and single-crystalline nanowires have led to a paradigm shift in the understanding of coercivity and its mechanism, including the discovery of a novel approach for utilizing 100 % anisotropy field to develop an extraordinarily high coercivity in cobalt nanowires.[1-3] Here we extend our exploration to develop high coercivity in iron carbide (Fe_5C_2) material by synthesizing its nanorods. It is found that when the nanocrystals have an increased aspect ratio, the coercivity at room temperature increases up to 1 kOe for iron carbide nanorods with an aspect ratio of 10. The lower coercivity for smaller aspect ratios is due to an increased demagnetizing field along the long axis of nanorods, especially for equiaxed nanocrystals for which the aspect ratio is unity and the demagnetizing field is the same in all directions. Magnetic hardening is more pronounced at cryogenic temperatures in iron carbide nanorods with an observed coercivity value of 2 kOe.

1. K. Gandha, J. Mohapatra and J. P. Liu, *Coherent magnetization reversal and high magnetic coercivity in Co nanowire assemblies*, *J. Magn. Magn. Mater.*, 2017, 438, 41-45. 2. J. Mohapatra, M. Xing, J. Elkins, J. Beatty and J. P. Liu, *Extraordinary Magnetic Hardening in Nanowire Assemblies: the Geometry and Proximity Effects*, *Adv. Funct. Mater.*, 2021, 31, 2010157. 3. J. Mohapatra, J. Fischbacher, M. Gusenbauer, M. Y. Xing, J. Elkins, T. Schrefl and J. P. Liu, *Coercivity limits in nanoscale ferromagnets*, *Phys. Rev. B*, 2022, 105, 214431.

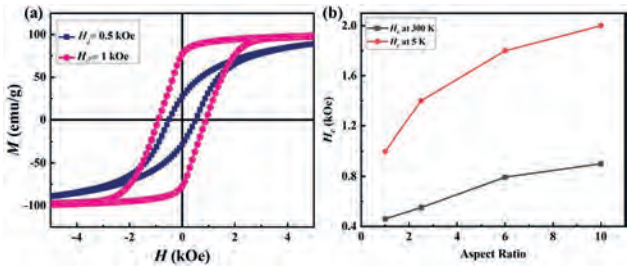

Figure 1: (a) Room temperature magnetization loops of aligned Fe_5C_2 nanorods measured parallel and perpendicular to the nanorods along the axis. (b) Aspect ratio dependence of coercivity of Fe_5C_2 nanorods.

EF-14. Thermal Stability and Intrinsic Magnetism of Mn-Bi-Ge alloys: A Potential Gap Permanent Magnet. U. Enkhtur[1], *T. Ochirkhuyag*[1], K. Odbadrakh[2] and O. Dorj[1,3] *1. Department of Physics, Incheon National University, Incheon, The Republic of Korea; 2. National Institute for Computational Sciences, Oak Ridge, TN, United States; 3. Institute of Physics and Technology, Mongolian Academy of Sciences, Ulaanbaatar, Mongolia*

Since neodymium–iron–boron ($Nd_2Fe_{14}B$) permanent magnet was developed in 1982,[1] a permanent magnet with higher performance has not been reported yet. Ever since, search for permanent magnet materials that do not contain rare-earth elements, but compatible to ferrites in price, is underway. In this talk, first we will review the properties that make a material good permanent magnet, including saturation magnetization (M_s), uniaxial magnetocrystalline anisotropy (K_u), maximum energy density product (BH_{max}), Curie temperature (T_C), and thermodynamic stability and discuss our approach to designing new permanent magnets free of rare-earth elements. We will then report our recent results of the systematic density-functional theory, density-functional perturbation theory, and Monte Carlo simulations in a low-temperature MnBi structure with 3*d* transition and simple metal doping elements. While the stability of MnBi structure retains with the early transition metal Ti and simple metal Ge among the 11 metal substitutional elements, the Ge substitute can turn a biaxial magnetic anisotropy (-0.2 MJ m^{-3}) of MnBi into a uniaxial magnetic anisotropy, yielding a maximum value of K_u = 3.7 MJ m^{-3} at x = 3, and simultaneously enhance the Curie temperature up to T_C = 785 K at x = 1 in $Mn_{16}Bi_{16-x}Ge_x$. These values are superior to those of the widely investigated rare-earth free permanent magnets such as MnBi and MnAl, and even comparable to the state-of-the-art permanent magnet $Nd_2Fe_{14}B$. * The research is funded by Office of Naval Research and Office of Naval Research Global of the US Department of Defense Grant N62909-22-1-2045.

[1] M. Sagawa, S. Fujimura, H. Yamamoto, Y. Matsuura, and S. Hirosawa, J. Appl. Phys. 57, 4094 (1985).

Session EG
NEW APPLICATIONS AND SENSORS AND OTHER EMERGING TOPICS

Minh-Hai Nguyen, Chair
Kepler Computing, Milpitas, CA, United States

INVITED PAPER

EG-01. Induction Heating of Magnetic Nanoparticles for Catalytic Hydrogen Production. *C. Frandsen[1] 1. Physics, Technical University of Denmark, Kgs. Lyngby, Denmark*

As of today, most of the world's hydrogen is produced from natural gas through steam methane reforming (SMR), a highly endothermic process, in which hydrogen and carbon monoxide are produced in chemical reactors by converting methane and steam at temperatures of up to 950 °C [1]. Conventionally, this process is heated by gas burners on the outside of the reactor tube, causing ~1% of the world's CO_2 emission [1]. Induction-heating by magnetic hysteresis of nanoparticles placed inside chemical reactors, as illustrated in Fig. 1, is an interesting alternative approach for the heating of high-temperature endothermic catalytic reactions such as SMR [1-4]. Magnetic nanoparticles have the potential to heat locally "from the inside" of the reactor, hence supplying heat where it is needed while avoiding large temperature gradients across the catalyst bed [1-4]. At the same time, the induction heating may be supplied by electricity from renewable sources and may allow for fast reactor startup times potentially exploiting periods of surplus electricity [1-4]. This talk addresses induction heating by magnetic nanoparticles in connection to catalytic hydrogen production. Our recent work shows how CoNi nanoparticles on an alumina support can act both as catalyst and as magnetic susceptor to drive SMR at high methane to hydrogen conversion rate at high temperatures [1-4]. Based on magnetic measurements of CoNi nanoparticles with well-defined compositions and particle sizes, it is shown how Co:Ni composition can be tuned for optimal performance at given operating temperatures and induction field amplitudes [1]. Moreover, it is shown how Co:Ni composition can be chosen such that Curie temperature prevents overheating [1]. The talk further discusses the applicability of induction heating to drive catalytic reactions [1-4] and compares induction heating with conventional heating [1-4] and resistive heating [5,6] in the case of SMR and more generally.

[1] M. R. Almind *et al.*, *ACS Applied Nano Materials,* Vol. 4, p. 11537 (2021). [2] M. G. Vinum *et al.*, *Angewandte Chemie,* Vol. 130, p. 10729 (2018). [3] M. R. Almind *et al.*, *Catalysis Today,* Vol. 342, p. 13 (2020). [4] P. M. Mortensen *et al.*, *Industrial and Engineering Chemistry Research,* Vol. 56, p. 14006 (2017). [5] S. T. Wismann *et al.*, *Science,* Vol. 364, p. 756 (2019). [6] S. T. Wismann *et al.*, *Chemical Engineering Journal,* Vol. 425, p. 131509 (2021).

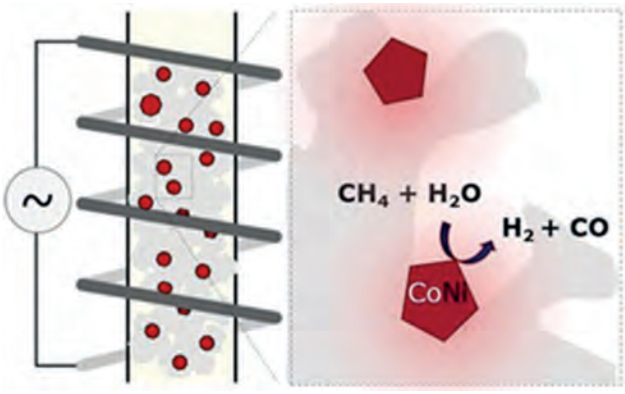

Fig. 1. Induction-heated catalytic CoNi nanoparticles driving the SMR process for hydrogen production.

CONTRIBUTED PAPERS

EG-02. Materials Informatics for Magnetic Materials Discovery. *N. Morley[1]*, R. Rowan-Robinson[1] and Z. Leong[1] *1. Materials Science and Engineering, University of Sheffield, Sheffield, United Kingdom*

The climate emergency has established the need for sustainability within existing and new technologies, which is driving a demand for material innovation. New materials need to be economically sourced from abundant elements, whilst still obtaining the functional characteristics of the existing leading materials. Functional Magnetic Materials (FMMs) are central to new green technologies and an excellent example of a sector with great industrial demand for innovation. At the present, existing hard magnets: NdFeB and SmCo, consist of elements on the critical list, while soft magnets are limited due to processing costs and eddy losses. The need for innovation is clear: by improving the material properties of FMMs, industries can fully capitalise on the aforementioned engineering advances in green technologies, thus saving money and benefiting the environment. Traditional material discovery methods, where existing material compositions are tweaked and optimised, are too slow and costly, and not practical or sufficient to address the current material challenges. Material informatics will overcome these existing problems, by using data-driven solutions to reduce the use of natural resources and expensive experiments. Our research has focused on using Natural Language Processing (NPL) to data mine open access papers to create a FMM database. This has been achieved by combining the linear approach NPL, which searches for defined compositions and parameters within papers, with semantic networks, to allow the compositions related parameters to be correctly linked together. In doing this we are able to data mine papers, which contain more than one composition and magnetic parameter for the database. Having created this database, machine learning (ML) algorithms are trained on it, which are then used to observe trends within the data, along with predicting compositions with specific magnetic parameters. These compositions are then fabricated and characterised using high throughput techniques, including combinatorial sputtering, XRD, FMR and MOKE magnetometry. This allows us to verify the ML results, quickly and cheaply, along with discovering new FMMs.

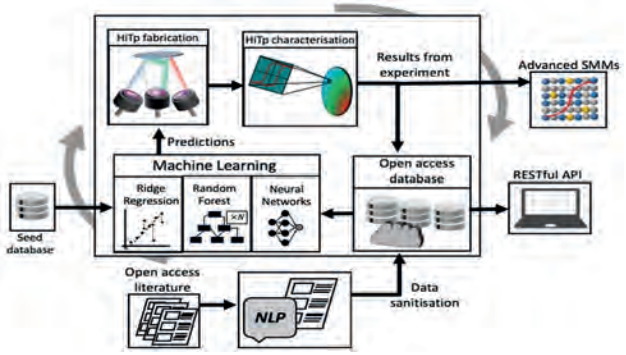

Scematic of Materials Informatics for Magnetic Materials Discovery

EG-03. Withdrawn

EG-04. Demonstration of a Magnetic Odometer for Downhole Robots.
H.R. Seren[1], M. Deffenbaugh[1] and M. Larbi Zeghlache[2] *1. Houston Research Center, Aramco Americas, Houston, TX, United States; 2. EXPEC-ARC, Saudi Aramco, Dhahran, Saudi Arabia*

Untethered autonomous robots can significantly simplify the inspection and data collection inside wells [1-2]. One obstacle for downhole robots is navigation. Many commonly used navigation techniques such as echo-location or global positioning system do not work inside the steel cased wells that reach several kilometers of depth. Therefore, new technologies are needed to accomplish this goal [3-4]. In this presentation, we will present a magnetic odometer that can be used in steel cased wells and pipelines. Steel casings inside the wells have a residual magnetic field during manufacturing, handling, and installation. This field vary as a function of position inside casings. The magnetic odometer uses these residual fields to calculate the speed and location of robots [5]. The odometer consists of two magnetometers that are placed along the direction of motion with a known distance between them. Two time series data are acquired. 1D feature search algorithm is used to compare the two data sets, locate matching features, and find the time lag between them. Thus, the average speed can be found by dividing the known length between the sensors by the time lag in acquisitions. To test this concept, we built a tool where two low-cost 9-dof inertial measurement units (IMUs) are placed with 20 in distance from each other inside a PVC pipe (Fig.1). A microcontroller circuit was employed to collect and store the data. The circuitry and the sensors were powered using 3 AA lithium batteries. The tool was connected to a wire and tested along a 40-ft steel casing. Magnetic fields were collected from the two sensors with 100 Hz rate. Acceleration was also measured from one of the IMUs. The speed from the magnetic odometer was integrated over time to find displacement. As a comparison, the accelerometer data was integrated over time twice to also find displacement. It's observed that the magnetic odometer provided more reliable displacement measurement compared to accelerometer based calculation (Fig.2).

[1] A. Saeed, B. Mellerowicz, K. Bywaters, International Petroleum Technology Conference (2022) [2] H. Seren, E. Buzi, L Al-Maghrabi, IEEE Trans. on Instr. and Meas., Vol. 67(4), p. 798-803 (2017). [3] H. Seren, M. Deffenbaugh, IEEE Sensors Letters, Vol. 6(4), p.1-4 (2022). [4] H. Santos, M. Meggiolaro, ABCM International Congress of Mechanical Engineering (2015). [5] H. Seren, M. Deffenbaugh, M. Larbi Zeghlache, Middle East Oil, Gas and Geosciences Show (2023).

Magnetic odometer test tool

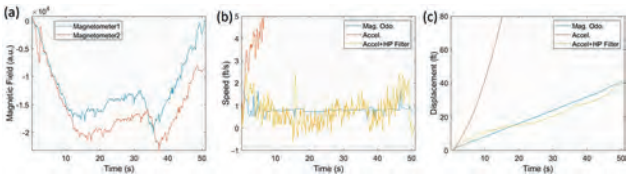

(a)Measured magnetic fields of the casing; (b,c)Speed and displacement of the tool based on the magnetic odometer, accelerometer, and high pass filtered accelerometer data

EG-06. Electroless Deposition of NiFe on Flexible Substrate: Towards Wearable Magnetic Devices for High-Temperature Applications.
K. Akhil[1], I.P. Seetoh[1], X. Chen[1], G. Lim[1] and C. Lai[1] *1. Temasek Laboratories, Nanyang Technological University, Singapore, Singapore*

The electroless deposition (ELD) of NiFe on flexible substrates has gained attention as a promising approach for developing wearable devices for high-temperature applications. This study investigates the feasibility of ELD as a low-cost and scalable method that does not require vacuum conditions, focusing on its ability to provide good magnetic properties on flexible substrates. ELD offers a solution-based approach that allows for uniform coating thicknesses on various substrates without the need for external current flow. In this research, we explore the deposition of NiFe alloys using ELD on Polyimide (PI) which is a thermally stable flexible substrate. Initial experiments involved electroless deposition (ELD) of NiFe on a polyimide (PI) substrate, followed by annealing up to 500°C. The resulting film's crystallinity and magnetic properties were evaluated. The ELD process involves immersing the substrate in a solution containing dopamine HCl and Tris-HCl resulting in thin films with catechol and amine groups. Then the substrate was activated using $PdCl_2$ and HCl before the ELD with iron and nickel sources, along with complexing agents. This vacuum free process can produce NiFe films with thicknesses of 30-300nm which was then patterned to different structures using conventional lithography techniques. The NiFe films were annealed at 200°C, 350°C, and 500°C. Magnetic properties, including saturation magnetization (M_s) and coercivity (H_c), were measured using a vibrating sample magnetometer (VSM) for these annealed samples and the pristine sample. These measurements offer insights into the magnetic behavior and quality of the deposited NiFe films. The X-ray diffraction (XRD) measurement shows that crystallinity improves for NiFe films in the Polyimide substrate as well and the polyimide was able to withstand until 500°C.This research contributes to the field of magnetism and magnetic materials, by opening possibilities for the development of magnetic devices on flexible substrates for high-temperature applications

P Pip, C Donnelly and C Gunderson, *Small* 16.44, 2004099, (2020) Zighem, F., and D. Faurie, *Journal of Physics: Condensed Matter* 33.23, 233002, (2021) A Ferreira, CM Costa and MA Correa, *Journal of Alloys and Compounds* 956, 170333, (2023)

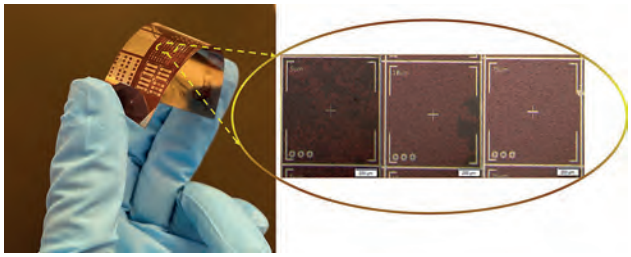

Fig.1 NiFe Thin films deposited on flexible substrate by ELD and patterned as hall bar structures of 05µm, 10µm and 05µm.

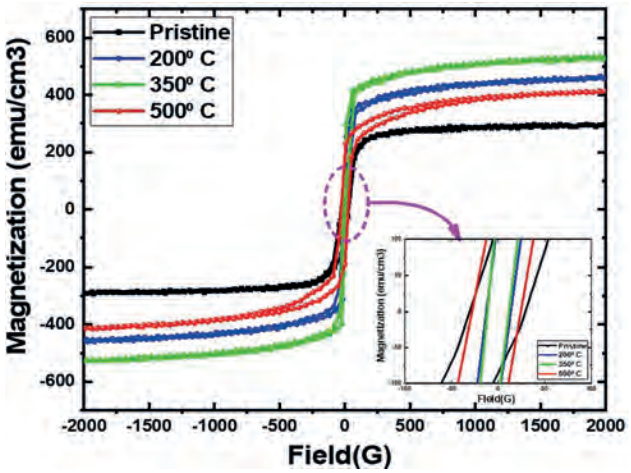

Fig.2 VSM results showing the MH curves of pristine sample and annealed samples

INVITED PAPER

EG-05. High-Frequency Electromagnetic Characterization of Magnetic Nanoparticles. *J. Marqués-Fernández*[1], J.C. García-Martínez[1], M. Salvador[1] and M. Rivas[1] *1. Applied Physics, Universidad de Oviedo, Gijón, Spain*

Magnetic lateral-flow immunoassays (MLFIAs), a variant of lateral flow immunoassays (LFIAs), have applications in rapid disease diagnosis, environment monitoring, and food safety with numerous advantages in terms of reliability, sensitivity and quantifiability while maintaining the affordability and rapidity of the traditional LFIAs [1]. The MLFIAs require quantifying nanograms of magnetic nanoparticles (MNPs), contributing to the measured magnetic permeability in parts per million. Previous work has quantified MNPs in controlled environments with laboratory-grade equipment, including large and expensive impedance analyzers and vector network analyzers. The affordability and ease of use of magnetic LFIA call for portable, sensitive and reliable devices. We use frequency-domain measurements, which allow high precision and sensitivity while reducing cost, complexity and improving ease of use. Our measuring method uses the self-resonant frequencies (SRFs) of multiple coils, which influences both the magnetic permeability and the electric permittivity of the MNPs, increasing the detectable signal and, thus, the sensitivity. At the same time, this implementation considers the sensors' self-inductance and self-capacitance, allowing for high-frequency measurements improving precision [2] using negative impedance oscillators and digital frequency counters. To assess this new working mode, we used full three-dimensional electromagnetic simulations to ensure electromagnetic field uniformity across the sensing surface at the SRF to achieve the same sensitivity to the magnetic permeability and the electric permittivity [2]. The sensing coils present some physical limitations which impact the measurements' stability. Three leading causes of these problems are physical deformations caused by thermal expansion and mechanical stress, environmental refraction index variations, and electromagnetic radiation from external sources. All these noise sources reduce stability and certainty, which has limited the usage of these sensors. We have developed a multi-sensor solution to reduce the influence of physical factors. Using the measurement from identical sensors close to each other, we can reduce all external noise sources and improve sensitivity and stability. We have developed a data analysis routine which, in addition to noise reduction, enables error detection important in critical applications not reachable before. These calculations use relative type measurement and contrast detection. Working with multi-sensor devices, enabled by the low cost and ease of measurement of our technique, new possibilities for mapping magnetic permeability and electric permittivity of different materials have been opened with high sensitivity and stability.

[1] Salvador, M. Springer: Cham, Switzerland, 2021; pp. 771–804. [2] J.L. Marqués-Fernández et al., Sensors 23, 2372 (2023)

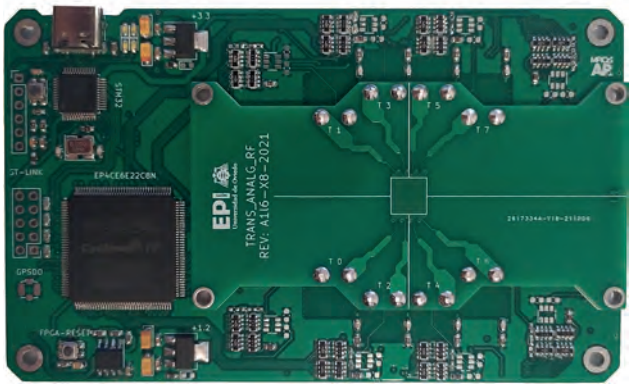

Prototyped electronic system for the measurement of magnetic nanoparticles at high frequency.

CONTRIBUTED PAPERS

EG-07. Design and Characterization of High-Resolution Embedded Magnetic Thermometers for Thermal Magnetic Particle Imaging. *F.M. Abel*[1], T.Q. Bui[1], E. De Lima Correa[1], A.J. Biacchi[1], M.J. Donahue[1], S.I. Woods[1], A.R. Hight Walker[1] and C. Dennis[1] *1. National Institute of Standards and Technology, Gaithersburg, MD, United States*

Temperature measurement within optically opaque 3D volumes is important for the development of many new technologies, e.g. additive manufacturing (AM), heat exchangers, and temperature tracking in medicine. Thermal magnetic particle imaging (T-MPI) aims to create such a measurement method by utilizing the temperature dependent nonlinear response of magnetic nano-objects (MNOs) to measure temperature. Colloidal MNOs have been demonstrated to have good thermosensitivity (change in magnetization with temperature), high sensitivity (signal to noise), and good spatial resolution. However, for AM or other applications where an embedded thermometer is necessary a colloidal system will not work. Randomly embedding MNOs into a solid matrix produces mostly sinusoidal responses with time at moderate drive fields (about 10 mT to 20 mT RMS), resulting in poor noise ratio and poor spatial resolution. Here, we have developed an approach to utilize recent findings that chain formation in colloidal environments produce significant improvements in spatial resolution and signal to noise [1,2] likely due to development of a "new" colloidal anisotropy at a critical drive field value [3]. We have magnetically aligned strongly interacting ferrites in a polystyrene-toluene solution followed by solidification due to evaporation in the presence of a DC magnetic field. Samples using this method have been produced with film-like morphologies, in channels of 3D printed objects, and alignment on the surface of cylindrical sapphire crucibles. These aligned ferrite-polystyrene nanocomposites have been characterized by magnetic particle spectroscopy (MPS) Figure 1, B-H loops, and temperature dependent MPS for a sample in a sapphire crucible. The results clearly demonstrate that magnetic alignment of strongly interacting ferrites in a polystyrene-toluene solution followed by solidification in a DC magnetic field results in similar enhanced signal to noise and spatial resolution as dynamically chaining ferrites in colloidal environments, with some thermosensitivity.

[1] Z. W. Tay et al. Small Methods., Vol. 5, p. 2100796 (2021) [2] K. L. Fung et al. Nano Lett., Vol. 23, p. 1717 (2023) [3] C. D. Dennis et al. Nanotechnology., Vol. 29, p. 215705 (2018)

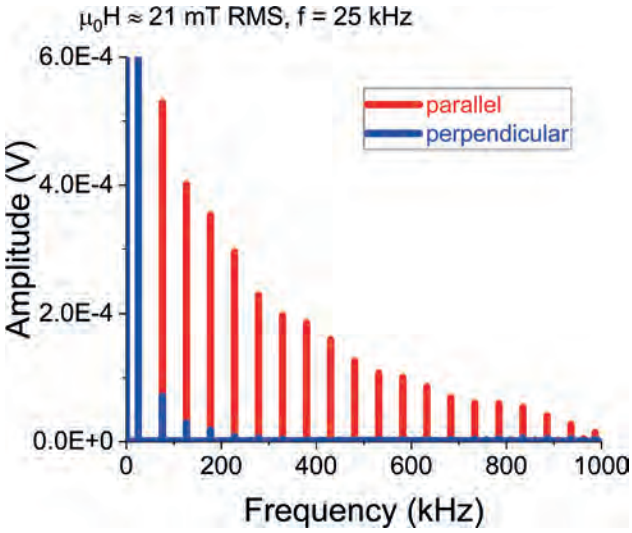

Fig. 1 Fouri transform of time domain MPS signal of ferrites aligned in a polystyrene nanocomposite film measured parallel to the chain-like structures and perpendicular.

EG-08. Symmetry and energetics of relaxation pathways in nanomagnetic clusters. F. Barrows[2], I. Tapia[1], P. Mellado[1] and *H. Arava*[3] *1. Adolfo Ibáñez University, Santiago, Chile; 2. Los Alamos National Laboratory, Los Alamos, NM, United States; 3. Materials Science Division, Argonne National Laboratory, Lemont, IL, United States*

Arrays of single domain nanomagnetic islands are potential building blocks for logic gates to implement probabilistic computation using artificial spin ice[1][2]. In clusters made out of lithographically prepared nanomagnets, the anisotropy of magnetic interactions and the symmetry of the magnetic array combine to give rise to several output magnetic states. The probability of obtaining a particular magnetic configuration in finite clusters has been experimentally manipulated by implementing energy barriers in the relaxation pathway. Here, we examine the magnetic symmetries of the relaxation process on four island clusters which are symmetric and arranged in a vertex or a loop. Via analysis of the point group symmetries of the magnetic configurations we can compare an abstract representation of the relaxation process, identifying high energy configurations with reduced symmetries. Finally, by considering a single nanomagnet as a dumbbell, we study the effect of interactions, entropy, and symmetry in the staircase associated with the relaxation path of small clusters of nanomagnets. We show that the hierarchy of energy scales found in experiments can be analytically captured by extending the monopole theory for spin ice to a multipole one[3][4], which exposes metastability's origin and analytically captures all the magnetic regimes in the relaxation process.

[1]Arava, Hanu, et al. "Computational logic with square rings of nanomagnets." *Nanotechnology* 29.26 (2018): 265205. [2] Arava, Hanu, et al. "Engineering relaxation pathways in building blocks of artificial spin ice for computation." Physical Review Applied 11.5 (2019): 054086. [3] Möller, Gunnar, and Roderich Moessner. "Magnetic multipole analysis of kagome and artificial spin-ice dipolar arrays." Physical Review B 80.14 (2009): 140409. [4] Chern, Gia-Wei, Paula Mellado, and O. Tchernyshyov. "Two-stage ordering of spins in dipolar spin ice on the kagome lattice." Physical review letters 106.20 (2011): 207202.

EG-09. Withdrawn

EG-10. Electromagnetic Noise Suppression of 26–30 GHz Range Harmonics from Switching Semiconductor Chips Using Spinodally Decomposed Fe–Cr–Co Flake Composite. *M. Yamaguchi*[1], Y. Miyazawa[1], S. Sugimoto[2], S. Ashida[3], K. Watanabe[4], R. Sakai[3], H. Uehara[3], M. Nagata[3] and S. Tanaka[3] *1. New Industry Creation Hatchery Center, Tohoku University, Sendai, Japan; 2. Department of Materials Science, Tohoku University, Sendai, Japan; 3. Graduate School of Science, Technology and Innovation, Kobe University, Kobe, Japan; 4. Radio Research Institute, National Institute of Information and Communications Technology, Koganei, Japan*

This paper demonstrates the performance of electromagnetic noise suppressor embedded inbetween flip-chip mounted IC chip and interposer to countermeasure high-order harmonics of digital switching noise generated from IC chips in 26-30 GHz range. The use of this frequency range will deploy further progress of 5G and future communication system for ultra-reliable and low latency communication (URLLC) schemes [1], where electromagnetic noise problems need to be mitigated. Prior to this work, we have; (1) Found the existance of 'conductive (in circuit)' digital switching noise that should degrades telecommunication sensitivity in 22-30 GHz band in [2], in spite of the general understanding in the EMC community that the 'radiation' noise is dominant in this frequency range. (2)Developed a new technology to embed magnetic composite paste in-between IC chip die and its interposer (small printed circuit board) to countermeasure (1), as shown in Fig. 1, effective up to 14 GHz because of materials limitation [3]. (3)Extended the measurable frequency range of harmonic resonace cavity pertervation method to evaluate complex permeability up to 37 GHz [4]. Nevertheless, magnetic material for 26-30 GHz range was lacking. Recently it was reported that (4)Resin composites of spinodally decomposed Fe–Cr–Co flakes exhibit excellent noise suppression performance in 15-40 GHz on a microstrip line but not on any applied circuits or devices[5-7]. In this work, all of (1)-(4) were put together. The Fe-Cr-Co flakes were mixted together with epoxy resin and pasted on the interposer to 30-60 μm thick. The IC chip was flip-chip mounted on it using a commertially available mounting process. Resulting magneteic composite thickess is 37-38 μm, with estimated magnetic volume ratio between 15-40 %. Number of test IC chip was 3. Each chip was measured the noise twice and its average is shown in Fig. 2. The even harmonics of digital switching noise generated from IC chip operatng at 500 MHz clock signal was sucessfully suppresed in 26-30 GHz range up to 8.5 dB.

[1]P. Popovski et al., "5G Wireless Network Slicing for eMBB, URLLC, and mMTC: A Communication-Theoretic View," in IEEE Access, vol. 6, pp. 55765-55779, 2018, doi: 10.1109/ACCESS.2018.2872781. [2] K. Watanabe, T. Wadatsumi M. Nagata et al, EMCCompo 2021, DOI: 10.1109/EMCCompo52133.2022.9758594 (2022). [3] M. Yamaguchi, et al, EMC Sappro & APEMC 2019, MonPM2C.6 (2019). [4] M. Yamaguchi, Y. Miyazawa, T. Miura, IEEE Trans. Magn., DOI 10.1109/TMAG.2023.3287928 (2023). [5] S. Ajia, H. Asa, S. Sugimoto et al, J. Alloys and Compounds, 903, 163920-1~9 (2022) DOI: 10.1016/j.jallcom.2022.163920 [6] S. Ajia, H. Asa, S. Sugimoto, et al, JMMM, 564, Part2, 170200-1~11 (2022) DOI: 10.1016/j.jmmm.2022.170200 [7] M. Sato, S Ajia, M. Ikeda, et al, Collected Abstracts of 2023 Spring Annual Meeting of the Japan Institute of Metals and Materials, 233, (2023) in Japanese.

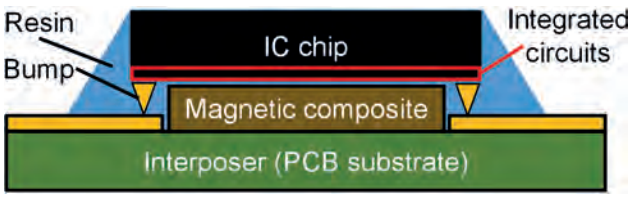

Fig. 1 Magnetic noise suppressor embedded inbetween flip-chip mounted IC chip and interposer

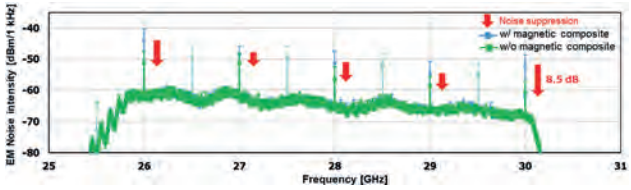

Fig. 2 Magnetic near field noise generated from an IC chip in 26-30 GHz range

EG-11. Development of sensing carbon fiber composites with continuous ferromagnetic microwires. V. Zhukova[2,3], R. Garcia- Etxabe[1], J. Malm[4], C. Johansson[4], F. Vallejo[5], P. Olaskoaga[5], M. Ipatov[2,3] and *A. Zhukov*[2,3]
1. GAIKER Technology Centre, Basque Research and Technology Alliance (BRTA), Spain, Zamudio, Spain; 2. Dept. Advanced Polymers and Materials, University of Basque Country, UPV/EHU, San Sebastian, Spain; 3. Dept. Appl. Phys., University of Basque Country, UPV/EHU, San Sebastian, Spain; 4. Digital Systems, RISE Research Institutes of Sweden, Göteborg, Sweden; 5. IDEKO Technology Center, Basque Research and Technology Alliance (BRTA), Elgoibar, Spain

One of the common problems in early damage detection in composite materials is wireless monitoring of stresses or temperature. Non-destructive techniques (NDT) are expensive and labor-intensive [1] and employed sensors are not wireless or require for instance attached electrodes for supplying electrical field, occupying a significant space [2]. One of the recently proposed solutions for composites monitoring is a new sensing method involving free space microwave spectroscopy using inclusions of ferromagnetic microwires presenting high frequency magnetoimpedance, MI, with high sensitivity to applied stress, temperature and magnetic field [3]. Amorphous glass-coated microwires present superior mechanical and corrosive properties, together with excellent magnetic softness and high MI effect and, therefore, are suitable for the wireless monitoring of stresses and temperature of composites [4]. The integration of such microwires into composite materials significantly modify the effective microwave response, making it possible to obtain a new tunable and self-sensing composite material [2]. However, the conductive carbon fibers interfere with the microwave signal generated by the ferromagnetic microwires, making it difficult to be measured. We present new experimental results on wireless monitoring of composites containing both carbon fibers and glass-coated microwires. Using Taylor-Ulitovsky technique we prepared Co-rich microwires with nearly-zero magnetostriction coefficients, extremely low coercivity (of about 5 A/m) and MI ratio up to 570%. The composites with parallel oriented long microwire inclusions separated by 3 mm have been successfully prepared. The reflection (R) and transmission (T) coefficients were measured in free-space. The experimental set-up consists of a pair of broadband horn antennas (1-17 GHz) and a vector network analyzer [3]. In spite of the influence of the conductive carbon fibers, application of an external low frequency modulated magnetic field allows to sensitive and stable extraction of the response signal (R and T coefficients) from the ferromagnetic microwires inclusions.

1. Güemes A., Fernandez-Lopez A., Renato Pozo A. and Sierra-Pérez J. J. Compos. Sci. 2020, 4(1), 13 2. Nelson, L. J., Mat. Sci. and Tech., vol. 18, 1245-1256, 2002 3. Makhnovskiy, D., Zhukov, A., Zhukova, V. and Gonzalez, J. Advances in Science and Technology, Vol. 54, 201–210, 2008. 4.Zhukov, A., Corte-Leon, P., Gonzalez-Legarreta, L., Ipatov, M., Blanco, J.M., Gonzalez, A., Zhukova, V. J. Phys. D: Appl. Phys., vol. 55, 253003, 2022.

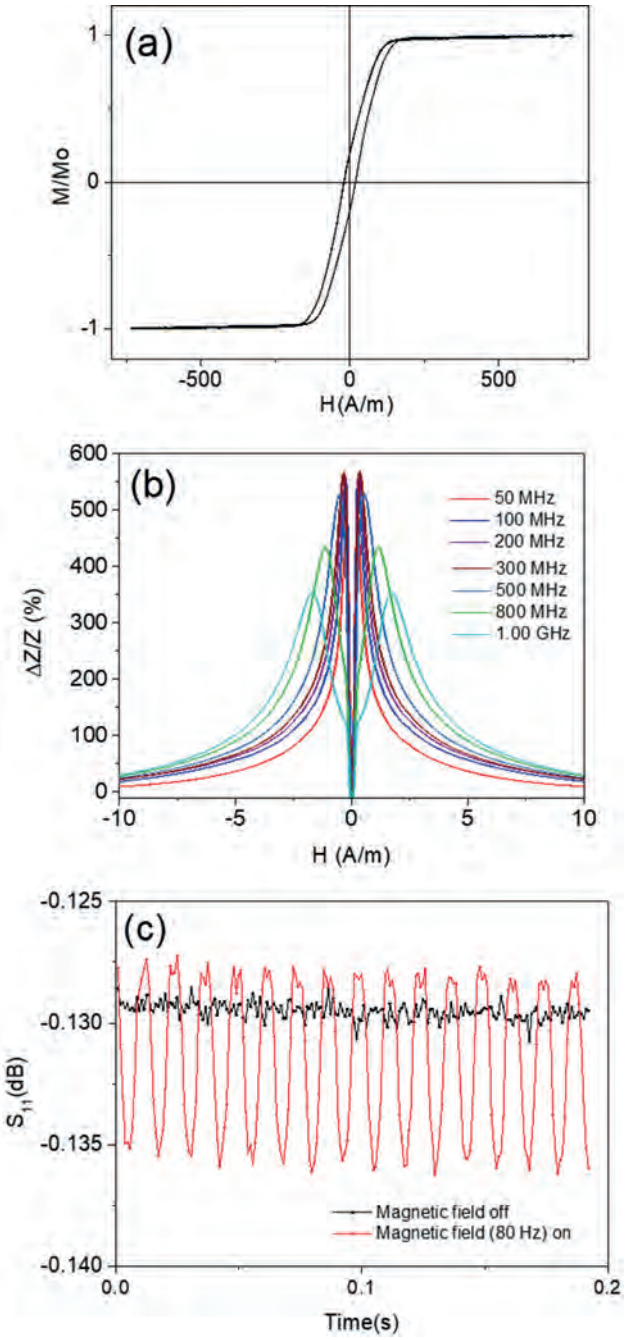

Hysteresis loops (a), GMI ratio at 1 GHz (b) and S_{11} parameter with on/off of a modulation magnetic field (c).

Session EP
MAGNETIC TUNNEL JUNCTIONS AND DEVICES
(Poster Session)

Minori Goto, Chair
Osaka University, Toyonaka, Japan

EP-01. The role of capping layers on tunneling magnetoresistance and microstructure in CoFeB/MgO/CoFeB magnetic tunnel junctions upon annealing. *G. Kim*[1], S. Lee[1], B. Park[1], M. Lee[2] and Y. Kim[2] *1. KAIST, Daejeon, The Republic of Korea; 2. Korea University, Seoul, The Republic of Korea*

This study investigates the annealing effects on tunnel magnetoresistance (TMR) ratio in CoFeB/MgO/CoFeB-based magnetic tunnel junctions (MTJs) with different capping layers and correlates them with microstructural changes. It is found that the capping layer plays an important role in determining the maximum TMR ratio and the corresponding annealing temperature (T_a). For a Pt capping layer, the TMR reaches ~95% at a T_a of 350 °C, then decreases upon a further increase in T_a. A microstructural analysis reveals that the low TMR is due to severe intermixing in the Pt/CoFeB layers. On the other hand, when introducing a Ta capping layer that exhibits negligible diffusion into the CoFeB layer, the TMR continues to increase with T_a up to 400 °C, reaching ~250%. Our findings indicate that the proper selection of a capping layer can increase the annealing temperature of MTJs such that it becomes compatible with the complementary-metal-oxide-semiconductor backend process.

[1] J.-G. Zhu, C. Park, Magnetic tunnel junctions, Materials Today, 9 (2006) 36-45. [2] S.S.P. Parkin, C. Kaiser, A. Panchula, P.M. Rice, B. Hughes, M. Samant, S.-H. Yang, Giant tunnelling magnetoresistance at room temperature with MgO (100) tunnel barriers, Nat. Mater. 3 (2004) 862-867. [3] S. Yuasa, T. Nagahama, A. Fukushima, Y. Suzuki, K. Ando, Giant room-temperature magnetoresistance in single-crystal Fe/MgO/Fe magnetic tunnel junctions, Nat. Mater. 3 (2004) 868-71. [4] S. Ikeda, J. Hayakawa, Y. Ashizawa, Y.M Lee, K. Miura, H. Hasegawa, M. Tsunoda, F. Matsukura, H. Ohno, Tunnel magnetoresistance of 604% at 300K by suppression of Ta diffusion in CoFeB/MgO/CoFeB pseudo-spin-valves annealed at high temperature, Appl. Phys. Lett. 93 (2008) 082508.

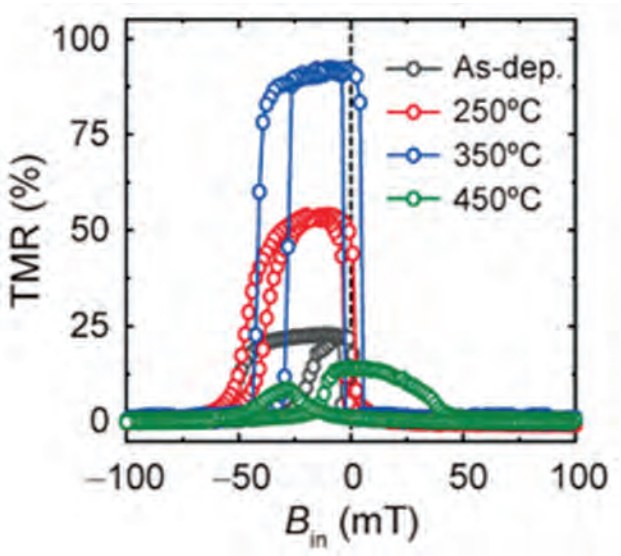

TMR graph of Pt-capped MTJs

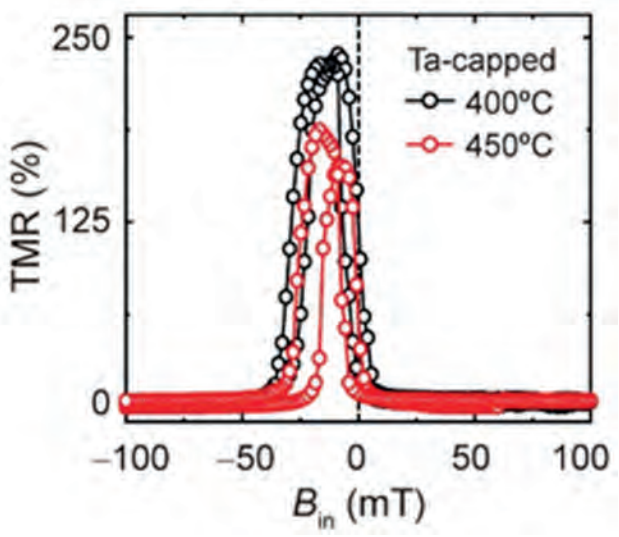

TMR graph of Ta-capped MTJs

EP-03. Temperature Dependence of 1/*f* Noise in MTJs with Various Thickness of MgO Barrier Layers. *Y. Wang*[3], M. Al-Mahdawi[1], Z. Jin[2] and M. Oogane[3,1] *1. CSIS, Tohoku University, Sendai, Japan; 2. State Key Laboratory of Transducer Technology, Aerospace Information Research Institute (AIR), Chinese Academy of Sciences, Beijing, China; 3. Department of Applied Physics, Tohoku University, Sendai, Japan*

The investigations on noise characteristics in magnetic tunnel junctions (MTJs) holds significant importance for magneto-resistance (TMR) sensors based on MTJs. For the application of bio-magnetic field sensors, 1/*f* noise serves as a performance-limiting factor in the low-frequency range. The exact cause of 1/*f* noise is generally believed to be associated with the quality of the MTJ films and disturbances in the magnetization and magnetic domain walls. The thickness of the MgO barrier layer in the MTJs may potentially impact the electron tunneling process. Temperature is primarily considered as one of the influencing factors for white noise. Therefore, this study aims to investigate the low-frequency noise characteristics of MTJs under various temperature conditions by varying the thickness of the MgO barrier layer. The MgO barrier thicknesses (t_{MgO}) of MTJs were set to 1.2 nm, 1.4 nm, and 1.6 nm, respectively. Figure 1(a) illustrates the temperature dependence of resistance in the samples under parallel state. As shown in the figure, samples with t_{MgO} =1.2 nm and t_{MgO} =1.4 nm exhibit an increasing trend in resistance with increasing temperature. However, the sample with t_{MgO} =1.6 nm shows the opposite trend, suggesting the presence of an alternative electron transport mechanism different from electron tunneling in samples. In Figure 1(b), it is observed that the samples with t_{MgO} =1.4 nm and t_{MgO} =1.6 nm exhibit similar high TMR ratios. Figure 1(c) illustrates the voltage-normalized noise power density of samples with different t_{MgO} at 10 Hz. It can be observed that the samples with t_{MgO} =1.2 nm and t_{MgO} =1.4 nm exhibit lower noise levels. Additionally, all three samples show a slight increasing trend in noise with increasing temperature. The potential causes of variations in the noise level could be attributed to changes in tunneling barrier

quality resulting from the variation in t_{MgO}. These variations may include the presence of lattice defects or pinholes, leading to metallic transport processes other than the Δ_1 electron tunneling.[1)]

1) VENTURA *et al*., PHYSICAL REVIEW B 78, 024403 (2008).

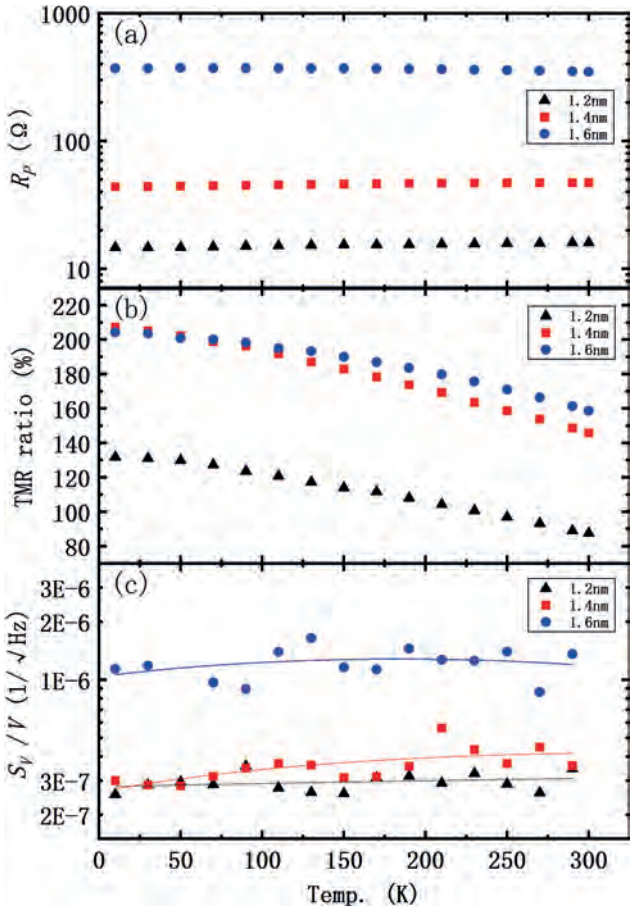

Fig. 1 Temperature dependence of (a) Resistance in the parallel state (R_P), (b) TMR ratio and (c) Normalized noise power density by the voltage (S_V /V) at 10 Hz.

EP-04. $L1_0$ FePd-Based Perpendicular Magnetic Tunnel Junctions with 65% Tunnel Magnetoresistance and Ultralow Switching Current Density. *D. Lyu*[1], J.E. Shoup[2], A.T. Habiboglu[3], Q. Jia[1], P. Khanal[3], B.R. Zink[1], Y. Lv[1], B. Zhou[3], D.B. Gopman[2], W. Wang[3] and J. Wang[1]
1. University of Minnesota, Minneapolis, MN, United States; 2. National Institute of Standards and Technology, Gaithersburg, MD, United States; 3. University of Arizona, Tucson, AZ, United States

Magnetic tunnel junctions (MTJs) and their energy-efficient switching are core research topics for the spintronics community due to their broad prospects in both applied and fundamental sciences. To lower the MTJ switching energy, $L1_0$ FePd with strong bulk perpendicular magnetic anisotropy and low damping has been studied as an appealing free layer material in recent years [1-4]. In this study, we fabricated $L1_0$ FePd-based perpendicular MTJs (Fig. 1) and surprisingly obtained high tunnel magnetoresistance (TMR) up to 65% with an ultralow switching current density of J_{SW}≈1.4×10^5 A/cm^2, which is about one order of magnitude lower than that of typical spin-transfer torque (STT) MTJs. An ultrathin Ru/Mo bilayer spacer is used to suppress the diffusion of Pd and thus enhance the TMR. The switching behaviors are sensitive to external magnetic fields (Fig. 2) so the resistive switching mechanism could be ruled out. Considering the devices' stack structure, we proposed two possible theories to describe their switching process: 1. Mediated by the ultrathin Ru/Mo bilayer spacer, the strength and sign of the interlayer exchange coupling between the bottom CoFeB and $L1_0$ FePd are voltage-dependent, which features the voltage-controlled exchange coupling (VCEC) switching mechanism we previously reported [5-7]. This possibility is supported by the small J_{SW} and high resistance-area (RA) product exceeding 630 Ω μm^2 because they should limit the contribution of STT. 2. The bottom CoFeB and $L1_0$ FePd tightly couple together and form a composite free layer, as indicated by vibrating-sample magnetometry and the direction of switching current. In this case, the switching is still driven by STT, though it might be weak. These results are encouraging, worth further exploration, and may advance the development of low-energy spintronic devices.

[1] H. Naganuma, *et al.*, Nano Lett., Vol. 15, p.623–628 (2015) [2] D.-L. Zhang, *et al.*, Appl. Phys. Lett., Vol. 112, 152401 (2018) [3] D.-L. Zhang, *et al.*, Phys. Rev. Appl., Vol. 9, 044028 (2018) [4] D. Lyu, *et al.*, Adv. Funct. Mater., Vol. 33, 2214201 (2023) [5] B. R. Zink, *et al.*, Adv. Electron. Mater., Vol. 8, 2200382 (2022) [6] D. Zhang, *et al.*, Nano Lett., Vol. 22, p.622–629 (2022) [7] D. Lyu, *et al.*, Appl. Phys. Lett., Vol. 120, 012404 (2022)

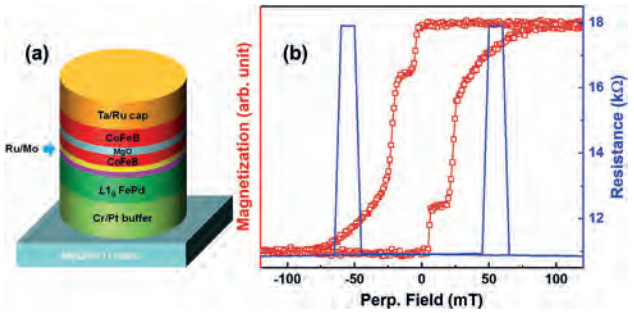

Fig. 1 (a) The stack structure of the $L1_0$ FePd-based perpendicular MTJ. (b) Red squares and curves: the magnetization-field (*M-H*) loop measured from a blanket film. Blue curves: the room-temperature major loop collected from a 300 nm device.

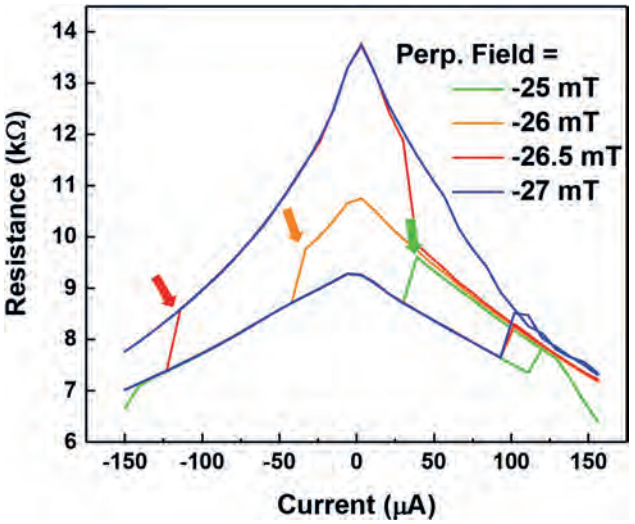

Fig. 2 The resistance-current (*R-I*) loops under different magnetic fields. Arrows indicate the antiparallel→parallel switching points.

EP-05. Withdrawn

EP-06. Improved Robustness against Magnetic Field in Spin-Orbit-Torque-Based Physical Unclonable Functions through Write-Back Operation. *D. Koh*[1], J. Kang[1], T. Kim[3], J. Lee[2], J. Kwon[2], S. Lee[1], J. Park[3] and B. Park[1] *1. KAIST, Daejeon, The Republic of Korea; 2. Hyundai Motor Company, Hwaseong, The Republic of Korea; 3. Korea University, Seoul, The Republic of Korea*

Physical unclonable functions (PUFs), which exploit uncontrollable and unpredictable randomness of materials or devices, have been investigated as a hardware-based security primitive owing to their robustness against adversarial attacks. Spin–orbit torque (SOT) switching is one of the promising techniques for PUF applications because it can provide randomness by the stochastic switching distribution of perpendicular magnetization. In this study, the improvement in the reliability of SOT-based PUFs against external magnetic fields with write-back operation (WBO) is demonstrated. A PUF consisting of 8 × 4 array Hall-bar devices with a Ta/CoFeB/MgO structure is fabricated, where the random distribution of the SOT switching current serves as an entropy source. However, the information stored in the PUF is easily modified by the application of an external magnetic field. To improve the robustness against magnetic fields, a WBO is introduced that applies an additional current to saturate the magnetization in either the upward or downward direction depending on the magnetic state. As a result, the SOT-based PUF maintains an entropy value close to unity under a magnetic field of up to the coercive field of the CoFeB layer.

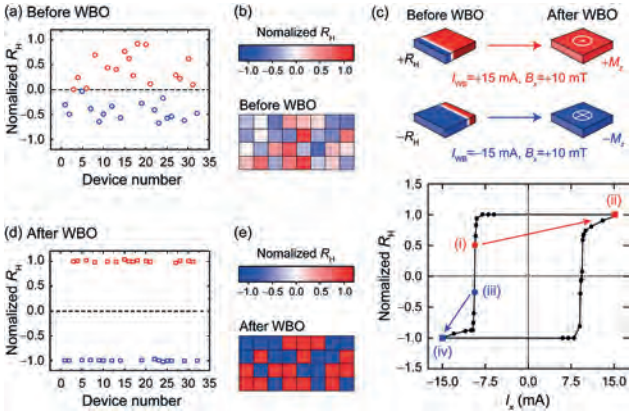

Fig. 1 SOT-based PUF construction with a write-back operation (WBO). a) Normalized R_H of the 32 Hall-bar devices after applying an $I_{challenge}$ of –8.8 mA. b) The spatial distribution of R_H's in the SOT-based PUF. c) Schematic description of the WBO for two devices with positive and negative R_H. The top figures illustrate the magnetization configuration of the CoFeB before and after the WBO. The bottom switching loop shows the R_H change during WBO. d,e) Normalized R_H and their spatial distribution of the 32 Hall-bar devices after WBO

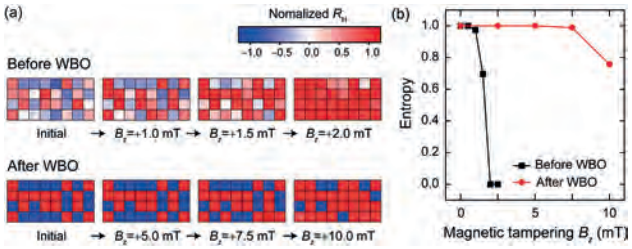

Fig. 2 Reliability against external magnetic fields. a) Distribution of R_H after being exposed to different out-of-plane magnetic fields (B_z) for 2 s. The upper (lower) panel represents the PUF patterns before (after) the write-back operation (WBO). The amplitude of the normalized R_H is denoted by colors. b) The entropy value E of the SOT-based PUF device versus magnetic tampering B_z.

EP-12. Modulation of binary stochastic switching behavior in an imperfect perpendicularly magnetized magnetic tunnel junction. *J. Kwon*[1], S. Karki[1], C. Cui[1], H. Jin[1], S. Liu[1], S.G. Cardwell[2], C.D. Schuman[3], J. Smith[2], S. Misra[2], J.B. Aimone[2] and J.C. Incorvia[1] *1. Electrical and Computer Engineering, University of Texas at Austin, Austin, TX, United States; 2. Sandia National Laboratories, Albuquerque, NM, United States; 3. Electrical Engineering and Computer Science, University of Tennessee, Knoxville, TN, United States*

Probabilistic computing relies on random number generators (RNGs) to create bit streams (BSs) to efficiently process naturally probabilistic algorithms.[1] Magnetic tunnel junction (MTJ) is being studied as a candidate to produce probabilistic bits (p-bits): by lowering the anisotropy, free layer magnetization fluctuates at room temp, and it can be sampled in time to produce a BS of 0's and 1's, in a stochastic read process.[2] The MTJ not only can act as a 50/50 coin, but the weight of the coin can be dynamically tuned, making it attractive for creating device-inherent probabilistic algorithms. To-date, this has been experimentally studied in in-plane MTJs[3,4], as well as preliminary studies of perpendicular MTJs (p-MTJs) with weight modulated with voltage.[5] Here, we fabricate p-MTJs with 200 nm diameter, shown in Fig. 1a inset. Fig. 1a shows the field loop using 5 μA sensing current. Then, 1 V is applied across the MTJ, close to but lower than the breakdown voltage of 1.5 V, to lower the energy barrier. Subsequently, the field loop is again measured in Fig. 1b with 5 μA. The magnetization has become stochastic, and monitoring the voltage across a MTJ shows fluctuation between the two resistance states. Fig. 1c shows the measured random BS vs. DC field amplitude for 3 μA, with a sampling rate of 400 per min., around 9 bits per 2 min. As the field ramps up from 369 Oe towards the coercive field of 550 Oe, MTJ starts stably in LRS (high voltage in 1c), and as higher field is applied, stochastically fluctuates to high resistance state (HRS). An approximately 50/50 coin is achieved at 500-520 Oe. After 530 Oe, MTJ switches to be relatively stable to a HRS. The probability of achieving a 0 vs. 1 (σ) vs. field amplitude is extracted, showing tunability between 1 and 0.4. Results show p-MTJ RNGs can be tuned with a DC field bias, which could be substituted for other methods as well to lower the energy barrier between the magnetization directions. Sandia National Laboratory is managed and operated by NTESS under DOE NNSA contract DE-NA0003525

[1] S. Misra, L. C. Bland, S. G. Cardwell, J. A. C. Incorvia, C. D. James, A. D. Kent, et al., Adv. Mater., e2204569 (2022) [2] K. Y. Camsari, B. M. Sutton and S. Datta, Appl. Phys. Rev. 6, 1 (2019). [3] K. Hayakawa, S. Kanai, T. Funatsu, J. Igarashi, B. Jinnai, W. A. Borders, et al., Phys. Rev. Lett. 126, 117202 (2021) [4] K. Kobayashi, W. A. Borders, S. Kanai, K. Hayakawa, H. Ohno and S. Fukami, Appl. Phys. Lett. 119, 13 (2021) [5] Y. Shao, S. L. Sinaga, I. O. Sunmola, A. S. Borland, et al., I. IEEE Magnetics Lett. 12: 1-5 (2021)

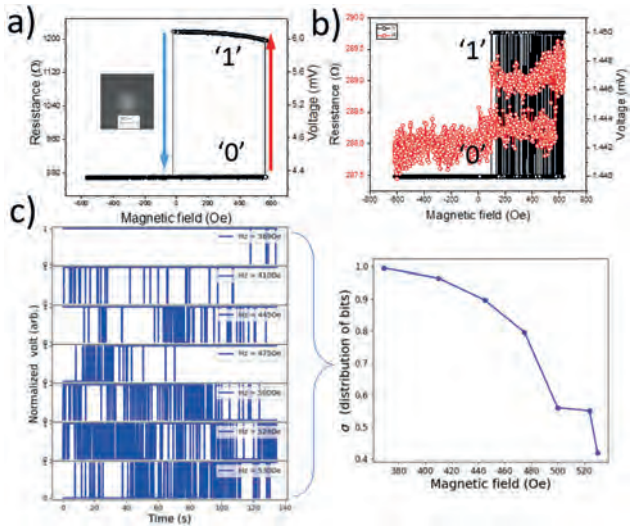

Fig. 1: a) Out-of-plane (OOP) field-dependent R. b) MTJ minor loop with weakened anisotropy as a function of OOP magnetic field. c) Creation of tunable RNGs based on ramping up field.

EP-13. Laser induced ultrafast magnetization reversal of Tb/Co-based Magnetic Tunnel Junctions. D. Salomoni[1], *E.A. Tremsina*[2,1], Y. Peng[3], L. Farcis[1], S. Auffret[1], M. Hehn[3], G. Malinowski[3], S. Mangin[3], B. Dieny[1], L.D. Buda-Prejbeanu[1], R. Sousa[1] and I. Prejbeanu[1] *1. Univ. Grenoble Alpes/CNRS/CEA, SPINTEC, Grenoble, France; 2. Department of Electrical Engineering and Computer Science, Massachusetts Institute of Technology, Cambridge, MA, United States; 3. Institut Jean Lamour, UMR CNRS 7198, Université de Lorraine, Nancy, France*

Magnetic tunnel junctions which can be operated through the mechanism of all optical switching (AOS) provide a promising avenue for developing fast and reliable magnetic recording devices[1-3]. In particular, this switching process is up to two orders of magnitude faster than the commonly used electrical approaches based on spin transfer or spin orbit torques. In this work successful field-free 50fs single-laser-pulse-driven switching of a [Tb/Co] storage layer in a perpendicular magnetic tunnel junction (MTJ) was demonstrated [4]. Experimental studies of the reversal processes in continuous films of this material composition show peculiar concentric rings with opposite magnetic directions [4-5]. These rings are shown to correspond to switching probability as a function of the applied laser fluence in the patterned devices. The magnetization reversal is independent of the pulse duration, suggesting that the key reversal dynamics occur at longer timescales. The main features of the [Tb/Co] multilayer system could be correctly predicted by a macrospin two-temperature model considering two key features: i) fast in-plane reorientation of the magnetization with increasing temperature and ii) tilt of the uniaxial anisotropy axis with respect to the out-of-plane direction. These aspects are of great interest both for the physical understanding of the switching phenomenon and their consequences for all-optical-switching memory devices, since they allow for a large fluence operation window with high resilience to pulse length variability.

1. A. Olivier *et al.,* Nanotechnology 31, 425302 (2020) 2. L. Avilés-Félix *et al.,* Scientific Reports 10, 1 (2020). 3. K. MISHRA *et al.,* Physical Review Research, vol5. B, 023163 (2023). 4. D. Salomoni *et al.,* arXiv: 2305.15135 (2023). 5. Y. Peng *et al.,* arXiv preprint arXiv:2212.13279 (2022).

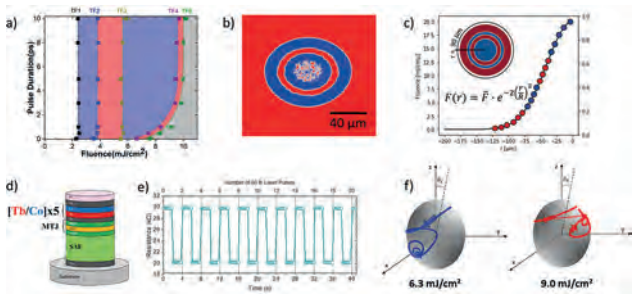

Figure 1. a) Experimental state diagram of the magnetization reversal upon varying the pulse duration and fluence[5], b) Background-subtracted images after each single pulse, c) Calculation of the expected magnetization pattern given by a 50 fs Gaussian-shaped laser pulse, blue (red) dots represent the final magnetization direction, which is reversed (not reversed), d) AOS-MTJ stack illustration, e) TMR measurement of AOS field-free toggle switching between parallel and anti-parallel states[4], f) Magnetization dynamics 3D view as predicted by macrospin model [4].

EP-14. Structural and Magnetic Properties of RuFe. S. Myrtle[1], J. Besler[1], *M. Rojas*[1], D.H. Ryan[2], R. Hübner[3], P. Omelchenko[1], Z.R. Nunn[1] and E. Girt[1] *1. Physics, Simon Fraser University, Burnaby, BC, Canada; 2. Physics, Mcgill University, Montreal, QC, Canada; 3. Structural Analysis Electron Microscopy Laboratory, Institute of Ion Beam Physics and Materials Research, Dresden, Germany*

Iron is a highly abundant material with the largest magnetic moment of all elements above room temperature. For this reason, it is widely used for the fabrication of magnetic devices. This study investigates how the structural and magnetic properties of iron are affected by the addition of ruthenium in $Ru_{100-x}Fe_x(d)$ films ($x \geq 50$ and $d \geq 20$ nm). X-ray diffraction and transmission electron microscopy demonstrate that for $x < 80$, the alloy has hexagonal close-packed (hcp) structure, while for $x \geq 93$ the alloy has body-centered cubic (bcc) crystal structure. For $80 \leq x < 93$, both hcp and bcc structures are present in the alloy. The vibrating sample magnetometry and Mössbauer spectroscopy measurements show that the hcp RuFe phase is paramagnetic while bcc RuFe phase is magnetic. The dependence of the remanence, M_r, saturation magnetization, M_s, and their ratio M_r/M_s of $Ru_{100-x}Fe_x$ alloy as a function of x is shown in Fig. 1. From Fig. 1 it is evident that the M_r/M_s ratio for pure Fe films is 0.93, while for $Ru_{100-x}Fe_x$ and $x \leq 93$, the M_r/M_s ratio is below 0.5. Furthermore, the external magnetic fields required to saturate the magnetization in $Ru_{100-x}Fe_x$ ($x \leq 96$) are over 5 T, as shown in Fig. 2. Since magnetic domains are removed in much smaller external magnetic fields, the large saturation fields indicate a noncollinear magnetic alignment in bcc RuFe alloys. The noncollinear magnetic structure of bcc RuFe alloys is modelled with micromagnetic calculations. This finding is important since for most applications it is desired that Fe have a noncollinear magnetic alignment.

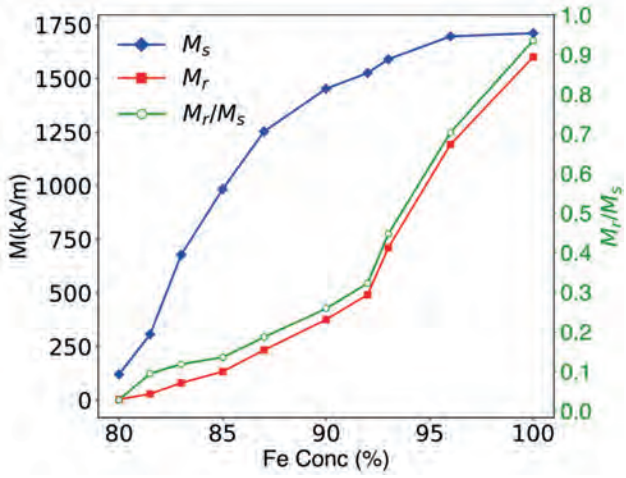

Fig. 1: Dependence of the saturation magnetization M_s, the remanence M_r, and M_r/M_s on x in $Ru_{100-x}Fe_x$(d) alloys (d ≥ 20 nm)

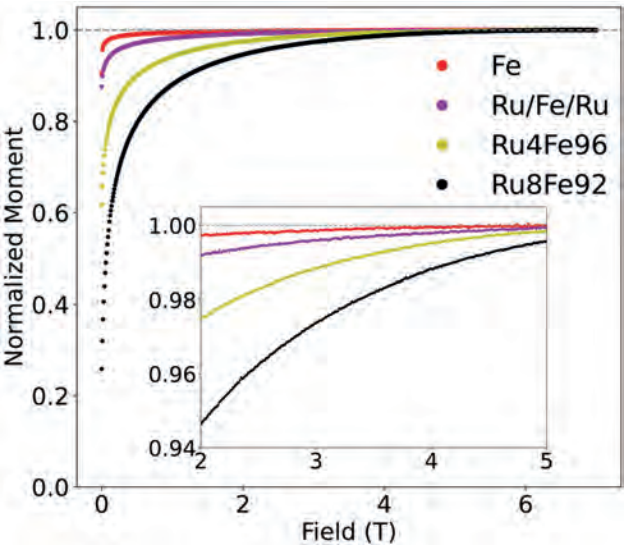

Fig. 2: Normalized M(H)/M_s curves of pure Fe, Ru/Fe/Ru, and Ru/$Ru_{100-x}Fe_x$/Ru where x = 96, and x = 92. Both Fe and $Ru_{100-x}Fe_x$ films are 100 nm thick. M(H)/M_s plots close to saturation (normalized moment between 0.94 and 1) and in external fields from 2 to 5 T are shown in the insert.

EP-15. Chirality-Dependent Magnetoresistance through Highly Distorted 2D Chiral Hybrid Perovskites at Room Temperature.

I. Hwang[1], M. Kang[1] and B. Park[1] *1. Department of Materials Science & Engineering, KAIST, Daejeon, The Republic of Korea*

Chirality-induced spin selectivity (CISS) effect has received attention because spin current can be induced without a magnetic field through passing chiral materials. (1) Nevertheless, chiral material-based spintronic devices have been rarely reported due to the absence of proper materials which have chirality and process suitability. These days, many studies show that chirality can be successfully transferred to inorganic materials from organic molecules. (2) Perovskite has structural flexibility which can easily induce chirality and large spin-orbit coupling. Based on these outstanding properties, various chiral perovskites have been synthesized and they exhibit intense chirality and CISS effect. (3) However, studies on the correlation between the CISS effect and the structure of chiral perovskites have not been conducted. Also, chiral perovskite-based spintronic devices are rarely reported. In this study, we synthesized two types of chiral perovskites by using different organic cations, methyl benzylamine (MBA) and naphthyl ethylamine (NEA). $(NEA)_2PbI_4$ has stronger chirality because NEA has two benzene rings that connect each perovskite layer and this connection enhanced the distortion of chiral perovskites. Finally, we fabricated chiral perovskite-based spin-valve devices having one ferromagnet and one chiral perovskite layer. Both $(MBA)_2PbI_4$ and $(NEA)_2PbI_4$ -based spin-valve devices showed magnetoresistance(MR) even at room temperature and $(NEA)_2PbI_4$ -based spin-valve device showed higher MR value. These results demonstrate that spin current induced by the CISS effect is related to the degree of chirality which can be controlled by the structure of chiral perovskites and chiral perovskites are proper materials for chiral spintronic devices. Finally, our results suggest that chiral perovskite is a promising material that replaces the complex fixed layer in the spin valve and advanced MR can be achieved with further study.

(1) R. Naaman, Y. Paltiel and D.H. Waldeck, Nature Reviews Chemistry., 3, 250-260 (2019) (2) J. Liu, L. Yang and Z. Huang, Advanced Materials., 33, 2005506 (2021) (3) H. Lu, C. Xiao, and M.C. Beard, Journal of the American Chemical Society., 142, 13030-13040 (2020)

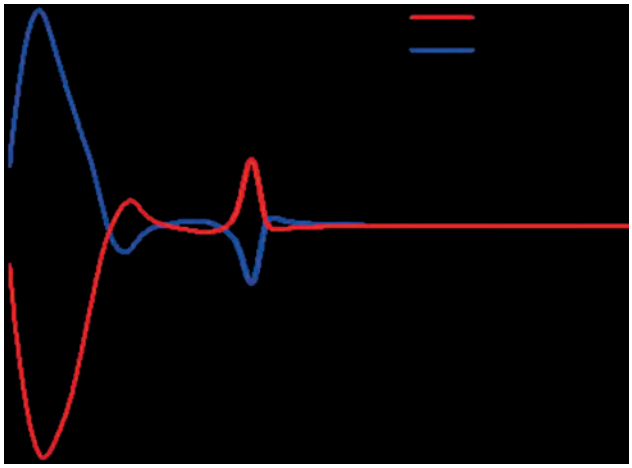

Circular Dichroism of NEA based chiral perovskite

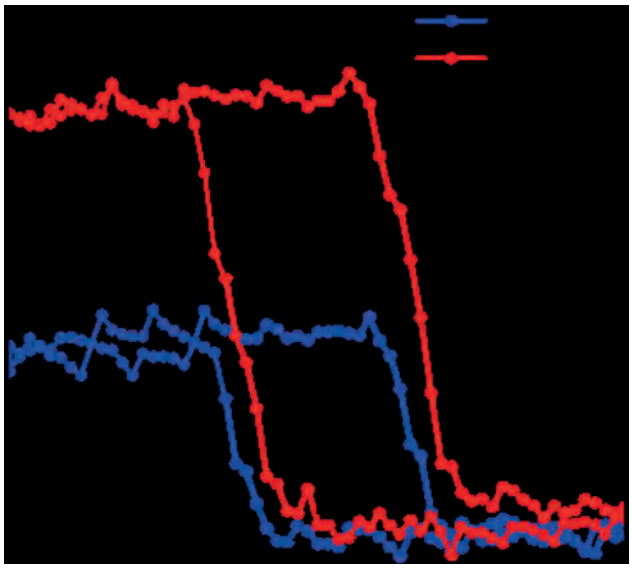

Magnetoresistance of $(MBA)_2PbI_4$ and $(NEA)_2PbI_4$ based spin-valve devices

EP-16. Strong perpendicular magnetic anisotropy at Ta/CoFeB/MgO-based MTJs via microwave annealing. *L. Chang*[1], Y. Ho[1,2], Y. Cheng[1] and S. Lee[3] *1. Mechanical and Mechatronics Systems Research Labs, Industrial Technology Research Institute (ITRI), Hsinchu County, Taiwan; 2. Department of Power Mechanical Engineering, National Tsing Hua University, Hsinchu, Taiwan; 3. Institute of Physics, Academia Sinica, Taipei, Taiwan*

In this study, we demonstrate for the first time that rapid low-temperature microwave annealing (MWA) method [1] forms perpendicular magnetic anisotropy (PMA) in Ta/CoFeB/MgO-based MTJs at atmospheric pressure and zero magnetic field. Conventional thermal annealing takes tens of minutes and a high temperature of up to 300 in a vacuum environment [2]. In contrast, we found that the MWA method achieves sufficiently high perpendicular anisotropy energy density to satisfy thermal stability K=3.7X10^{5}J/m^3, lower current-induced magnetization switching, and high tunnel magnetoresistance (TMR) ratio 110% within a few minutes at an annealing temperature of about 55 degree C. As shown in Figure 1(a), samples were grown in multilayer stacks on thermally oxidized Si substrates by DC/RF magnetron sputtering system. The structure of the MTJs is Si substrate/SiO_2(100)/Pt(8)/[Co/Pt](9.2)/Ru(0.75)/[Co/Pt](4.6)/CoFeB(1.9)/MgO(1.6)/CoFeB(1.2)/Ta(5) (numbers in parenthesis are layer thickness in nanometers and brackets represent multilayers). Figure 1(b) shows the experimentally setup, MWA was performed in a modified commercial microwave oven (NE-1853 Panasonic, Japan) at frequency 2.45GHz with maximum output power 3000W. Figure 2 shows magnetic hysteresis loops measured along the out-of-plane and in-plane directions for microwave annealed single ferromagnetic layer sample Ta(5)/CoFeB(1.2)/MgO(1.6) at a power of 2000W for 5 minutes. Inset is the Kerr image of remanence magnetic domain. The sample shows a clear perpendicular easy axis and large saturation field is needed along the in-plane direction, exhibiting PMA behaviors. The origin of the MWA effects on Ta/CoFeB/MgO-based MTJs with perpendicular magnetic anisotropy as well as possible means to further enhance tunneling magnetoresistance will be discussed.

[1] Chun-Hsiung Tsai, Chandrashekhar P. Savant, Mohammad Javad Asadi, Appl. Phys. Lett. 121, 052103 (2022). [2] S. Ikeda, K. Miura, H. Yamamoto, Nature Materials 9, 721–724 (2010).

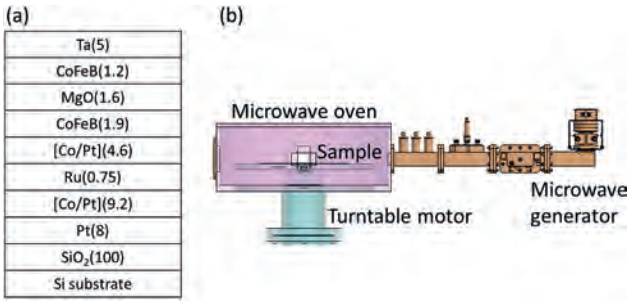

Fig. 1 (a) Ta/CoFeB/MgO-based MTJ stack. (b) Schematic of the MWA setup.

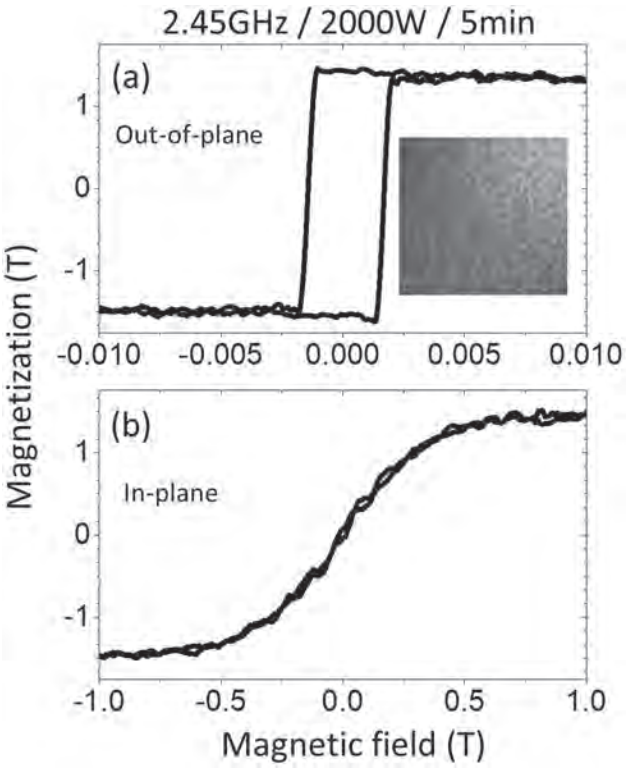

Fig. 2 M-H loops of Ta(5)/CoFeB(1.2)/MgO(1.6) after MWA at 2000W/5 minutes (a) out-of-plane and (b) in-plane external field. Inset is the Kerr image of remanence magnetic domain.

Session EQ
THIN FILMS, MULTILAYERS AND INTERFACE EFFECTS II (Poster Session)

Dustin Allen Gilbert, Chair
University of Tennessee, Gaithersburg, MD, United States

EQ-01. Optimization of Electromagnetic Microwave Absorption Performance for $Fe_{50}Co_{50}$/C-aerogel Composites. *C. Zhao*[1], S. Lv[1], L. Song[1], J. He[1] and D. Zhao[1] *1. Central Iron and Steel Research Institute, Beijing, China*

In this study, $Fe_{50}Co_{50}$-cluster-films/C-aerogel ($Fe_{50}Co_{50}$/C-aerogel) composites were successfully synthesized by the combination of nanobeam composite deposition technique and sol-gel method. By optimizing the auxiliary electric field, an absorber with excellent microwave absorption performance was obtained, and its microstructure composition and absorbing mechanism were investigated. A reflection loss (RL) below -10 dB is obtained in the wide frequency range of 2.3-18 GHz of $Fe_{50}Co_{50}$/C-aerogel composites, when an appropriate absorber thickness from 1.4 to 6 mm is chosen, suggesting that it has excellent broadband absorption characteristics (S-Ku band). Furthermore, carbon aerogel compounded by multilayer $Fe_{50}Co_{50}$ cluster films exhibits an optimal RL value of -52.57 dB at 9.16 GHz (corresponding to X-band) with a thickness of only 1.9 mm. The prepared composites show superior wave-absorbing performance, which is mainly attributed to the introduction of more polarization centers and dielectric that triggering multiple polarization effects, which further improves dielectric loss. It is notable that, the magnetic cluster films play a decisive role in the magnetic loss and multiple scattering and reflection processes, which is conducive to obtaining better impedance matching to achieve microwave absorption and dissipation. Compared with other carbon-based electromagnetic wave absorbing materials such as core-shell FeCo@C[1], FeCo/C nanocages[2] and FeCo/C hybrid nanofibers[3], $Fe_{50}Co_{50}$/C-aerogel not only actualize the characteristics of light weight and temperature resistance, but also bring about a quite small absorption layer thickness (the minimum RL thickness is less than -10 dB), which imply that $Fe_{50}Co_{50}$/C-aerogel have broad development space and potential application value.

[1] S. S. S. Afghahi and A. Shokuhfar, *J. Magn. Magn. Mater.*, vol. 370, p. 37–44 (2014) [2] Y. Xiong, L. Xu, and C. Yang, *J. Mater. Chem. A*, vol. 8, no. 36, p. 18863–18871 (2020) [3] J. Xiang, X. Zhang and Q. Ye, *Mater. Res. Bull.*, vol. 60, p. 589–595 (2014)

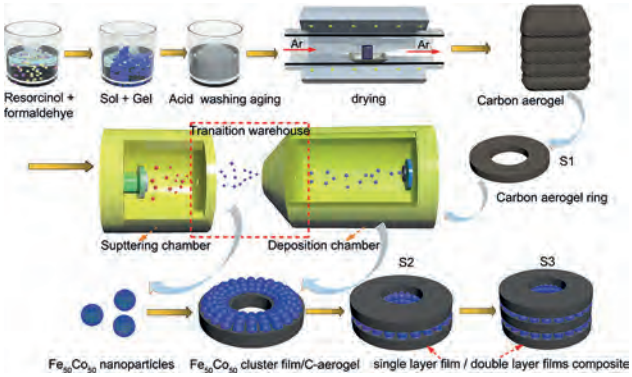

Fig.1 $Fe_{50}Co_{50}$/C-aerogel composites synthesized by combination of nanobeam composite deposition technology and sol-gel method

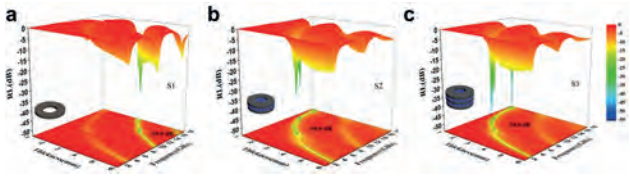

Fig.2 Three-dimensional plots of RL of the C-aerogel (S1) and $Fe_{50}Co_{50}$/C-aerogel composites (S2,S3) (a)-(c) present S1 to S3 with the thickness from 1mm to 6mm in the 1-18GHz range. (The black dotted line represents RL≤-10dB)

EQ-02. Temperature Dependence of the Ferromagnetic Resonance Linewidth in a Weyl Semimetal Co_2MnGa Thin Film. *N. Alzahrani*[1,2], N. Schulz[1], A. Chanda[1], M. Phan[1], H. Srikanth[1], D. Arena[1], A. Markou[3] and C. Felser[4] *1. Physics, University of South Florida, Tampa, FL, United States; 2. Physics, University of Jeddah, Jeddah, Saudi Arabia; 3. Physics, University of Ioannina, Ioannina, Greece; 4. Max Planck Institute for Chemical Physics of Solids, Dresden, Germany*

Co_2MnGa, a Heusler compound with Weyl fermion lines and topological surface states, has attracted significant attention due to its large intrinsic Berry curvature driven remarkably high anomalous Nernst thermopower [1], large negative magnetoresistance [2], high spin polarization, and low magnetic damping [3,4]. However, a deeper understanding of its magnetic properties remains limited, especially in thin films. To effectively utilize Co_2MnGa in spintronics and magnetic memory devices, it is crucial to comprehend its dynamic magnetic properties. Here, we investigated the temperature dependence of ferromagnetic resonance (FMR) in an 80nm thick Co_2MnGa film grown on MgO substrate with the applied field parallel to [110]. Our findings revealed a double peak structure in the FMR resonance (Fig.1a). Analyzing the linewidth as a function of temperature; we observed increased inhomogeneous broadening as the temperature decreased (Fig.1b). Furthermore, the ratio between the secondary and main peaks amplitudes exhibited a consistently increasing trend with decreasing temperature (Fig.1c). This provides valuable insights into the temperature-dependent dynamics of the FMR in Co_2MnGa. The origin of the secondary resonance and the underlying mechanisms will be discussed in detail. This examination will provide a deeper understanding of the dynamic magnetic properties of the Co_2MnGa thin films for tunable spintronic applications.

[1] S. Guerin, S.A.M. Tofail, and D. Thompson, NPG Asia Mater 11, 10 (2019). [2] T. Sato, S. Kokado, S. Kosaka, T. Ishikawa, T. Ogawa, M. Tsunoda, Appl. Phys. Lett. 113, 112407 (2018). [3] C. Guillemard, S. Petit-Watelot, L. Pasquier, D. Pierre, J. Ghanbaja, J. Rojas-Sánchez, A. Bataille, J. Rault, P. Fèvre, F. Bertran, and S. Andrieu, Phys. Rev. Applied 11, 064009 (2019). [4] P. Swekis, A. S. Sukhanov, Y. C. Chen, A. Gloskovskii, G. H. Fecher, I. Panagiotopoulos, J. Sichelschmidt, V. Ukleev, A. Devishvili, A. Vorobiev, D. S. Inosov, S. T. B. Goennenwein, C. Felser, and A. Markou, Nanomaterials 11(1), 251 (2021).

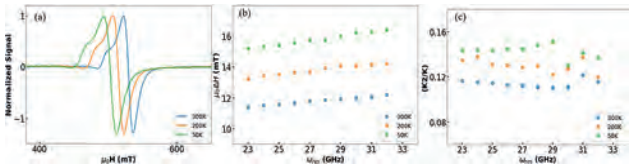

Fig. 1: (a) Temperature dependence of FMR signals (27 GHz) in 80nm Co_2MnGa film with the applied field parallel to the Co_2MnGa [110] direction. A secondary resonance can be observed in all spectra; (b) FMR linewidth *vs.* frequency at three select temperatures; (c) Ratio of the amplitude of the secondary peak to the main peak (K2 / K) at select temperatures.

EQ-03. Effect of MgO thickness on CoFe/MgO and CoFe/MgO/CoFe interfaces. *S. Ahn[1] 1. Pohang University of Science and Technology, Pohang, The Republic of Korea*

To investigate CoFe/MgO and CoFe/MgO/CoFe to possess a volume uniaxial magnetic anisotropy (UMA) like coercivity (H_C) and unidirectional magnetic anisotropy (H_E) like exchange field [1, 2] with respect to MgO thickness, Ta/$Co_{80}Fe_{20}$ (CoFe)/MgO [SET1] and Ta/CoFe/MgO/CoFe [SET2] for MgO thickness spanning 1.8 to 4.5 nm has been studied. Figure 1 shows in SET1, with increasing MgO thickness, coercivity (H_C) of 4-nm CoFe is linearly increased but in SET2, H_C at 1.8-nm MgO is larger than that at 2.7-nm MgO, which means H_C tendency at SET1 is different from that at SET2. To effectively understand the difference, the hysteresis loops of SET2 annealed at 150 and 250 deg. C, respectively, are shown in fig. 2(a). At 2.7-nm MgO, its loop appears to be shrunken compared to others. Based on grazing incidence x-ray diffraction study as shown in fig. 2(b), formation of CoO in uncompensated surface with the [111] direction(f, g), compensated surfaces with the [110] directions(b, c), and $CoFe_2O_4$ with Fe_3O_4(e) were found at annealed CoFe/MgO interfaces [3], which indicates they act as antiferromagnetic sources giving rise to H_E in the exchange-coupled antiferromagnetic/ferromagnetic interface [4]. Furthermore, as annealing temperature increased up to 200 deg. C, FCC peaks of MgO and CoFe at 150 deg. C were changed to be BCC peaks, which means locally bcc-like structure results in strong volume UMA [1].

[1] A. T. Hindmarch et al., Phys. Rev. B 83, 212404 (2011). [2] T. Ambrose et al., Phys. Rev. B 56, 83 (1997). [3] S. Grytsyuk et al., Eur. Phys. J. B. 85, 254. (2012). [4] J. Spray et al., J. Phys. D: Appl. Phys. 39, 4536 (2006).

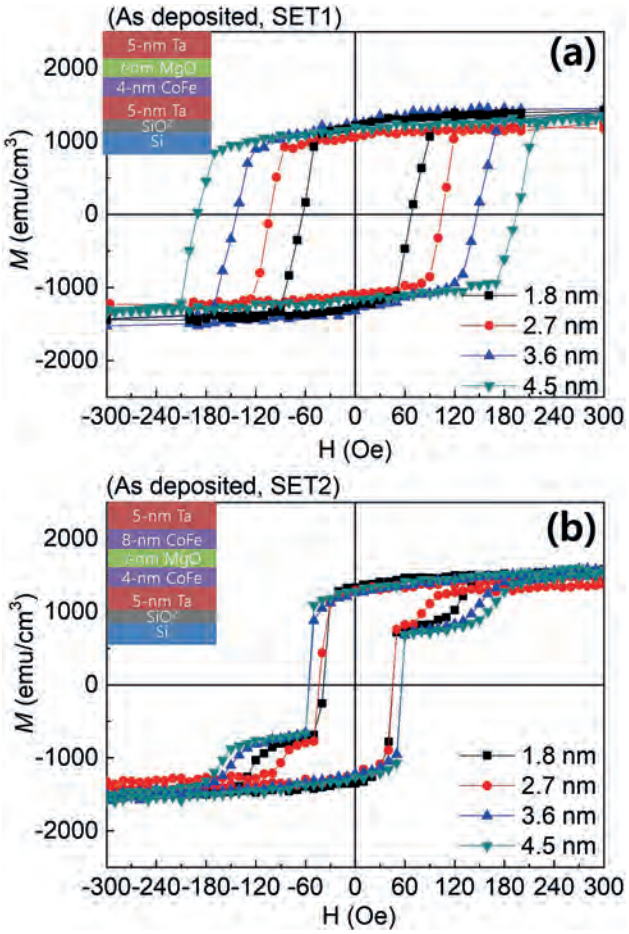

Fig. 1 Magnetic hysteresis loops of as-deposited (a) Ta/CoFe/MgO (SET1) and (b) Ta/CoFe/MgO/CoFe (SET2) films for MgO thickness spanning 1.8 to 4.5 nm. Inset: stacking schematics of SET1 and SET2, respectively.

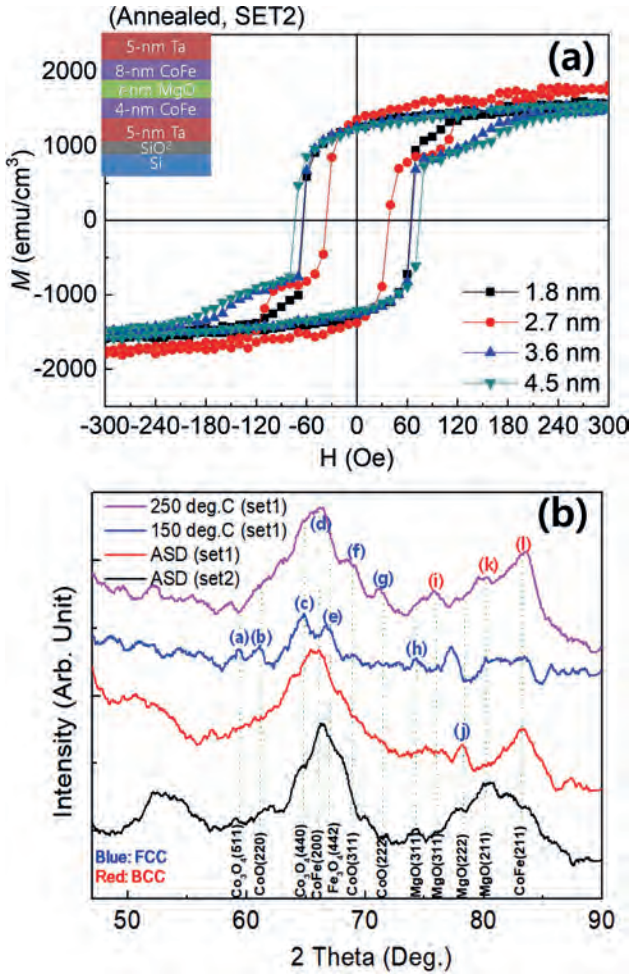

Fig. 2 (a) Magnetic hysteresis loop of (annealed, SET2) (b) Grazing-incidence X-ray diffraction (GIXD) patterns of SET1 at as-deposited (ASD), SET2 at ASD, and annealed (ANN) at 150 and 250 deg. C for 1 hour, respectively.

EQ-04. Magnetic properties of Er film obtained by pulsed laser deposition. E. Rohde[1,2], T.J. Del Rose[2] and *Y. Mudryk*[2] *1. Department of Materials Science and Engineering, Iowa State University, Ames, IA, United States; 2. Ames National Laboratory of US DOE, Iowa State University, Ames, IA, United States*

Pulsed laser deposition (PLD) is a well-developed technique,[1] routinely employed to obtain two-dimensional specimens of magnetic inorganic compounds and heterostructures. The vacuum achieved in a deposition chamber is generally near 10^{-6}-10^{-7} Torr, sufficient to deposit most inorganic materials, including oxides, nitrides, and transition metal compounds. However, rare earth elements have a high affinity to oxygen and usually form oxides when PLD is performed under standard conditions. Thus, the first step in creating novel films and heterostructures of magnetic rare earth metallic materials using PLD is to ensure that there is not enough oxygen in the atmosphere to affect the properties of the deposited compound. To test this hypothesis, we performed PLD of Er metallic film in UHV conditions (10^{-9} Torr) using excimer KrF laser with 248 nm wavelength. The Er films with ≤900 nm thickness were obtained and characterized by electron microscopy and profilometry. The SEM/EDX data confirmed uniform deposition of Er on the Si substrate with only a minor presence of oxygen and carbon impurities. The magnetic properties of the thickest film were measured using Quantum Design SQUID magnetometer and were found to agree with the magnetic properties of the bulk Er metal.[2] Thus, our results prove that high-quality rare earth metallic films can be obtained by PLD and used to study intrinsic magnetic properties of two-dimensional samples and heterostructures. This work was performed at Ames National Laboratory and supported by the Division of Materials Science and Engineering of the Office of Basic Energy Sciences, Office of Science of the U.S. Department of Energy (DOE). Ames National Laboratory is operated for the U.S. DOE by Iowa State University of Science and Technology under Contract No. DE-AC02-07CH11358. The authors would like to pay our gratitude and respects to our longstanding mentor, late Prof. Vitalij K. Pecharsky, without whom this work would have not been possible.

[1] Chrisey, D. B. and Hubler, G. K. Pulsed Laser Deposition of Thin Films. John Wiley & Sons, New York (1994). [2] Elliott, J. F., Legvold, S., and Spedding, F. H. Magnetic properties of erbium metal. Phys. Rev., Vol. 100, p. 1595 (1955).

EQ-05. GdFe-based nanostructured thin films with large perpendicular magnetic anisotropy for Spintronic applications. M. Salaheldeen[1,2], *V. Zhukova*[1,3], M. Ipatov[1,3] and A. Zhukov[1,3] *1. Department of Polymers and Advanced Materials, University of the Basque Country, UPV/EHU, San Sebastian, Spain; 2. Physics, Sohag University, Sohag, Egypt; 3. Department of Applied Physics I, EIG, University of Basque Country, UPV/EHU, San Sebastian, Spain*

Magnetic thin films with perpendicular magnetic anisotropy (PMA) have accelerated the progress of magnetic and magneto-optic (MO) recording technologies [1]. Presently the industry is moving towards high density patterned media with heat-assisted magnetic recording which facilitates the demand for thermal stability as well as switching of the highly anisotropic magnetic bits within the limited field of the present write-heads [2]. To meet the pace of the technological advancement, the role of external perturbations has been investigated to modify the magnetic properties. The inclusion of artificial defects in the bilayers thin film has been demonstrated as a powerful approach to engineer their magnetic properties in multiple ways. In particular, the antidot arrays nanostructured thin films represent nowadays an important tool for modifying the static and dynamic magnetic properties of host material by changing its geometrical parameters [3-5]. In this regard, it has been recently found that the magnetic anisotropy can be reoriented from in-plane (INP) to out-of-plane by only modifying the hole size for a single layer of ferromagnetic materials. The ability to control the strength and orientation of magnetic anisotropy becomes essential in advanced applications such as innovative electronic devices, spintronic devices, or perpendicular bit pattern magnetic recording media, especially for improving the thermal stability and switching reliability of magnetic bits [2]. By analysing the INP and OOP loops we can estimate the effective magnetic anisotropy coefficient, K_{eff} -which represents an important parameter in spintronic application- as a function of the size of holes diameter variation. The effective magnetic anisotropy is determined from the difference between the areas of the INP and OOP hysteresis loops and can be calculated by the given expression [5]: $K_{eff} = K_{(OOP)} - K_{(INP)}$

[1] Hirohata A., Sukegawa H., Yanagihara H., Zutic I., Seki T., Mizukami S., Swaminathan R. Roadmap for Emerging Materials for Spintronic Device Applications. *IEEE Trans. Magn.* 2015;51:0800511. doi: 10.1109/TMAG.2015.2457393. [2] Zhang X., Cai W., Wang M., Pan B., Cao K., Guo M., Zhang T., Cheng H., Li S., Zhu D., et al. Spin-Torque Memristors Based on Perpendicular Magnetic Tunnel Junctions for Neuromorphic Computing. *Adv. Sci.* 2021;8:2004645. doi: 10.1002/advs.202004645. [3] Salaheldeen, M.; Mendez, M.; Vega, V.; Fernández, A.; Prida, V.M. Tuning Nanohole Sizes in Ni Hexagonal Antidot Arrays: Large Perpendicular Magnetic Anisotropy for Spintronic Applications. *ACS Appl. Nano Mater.* 2019, *2*, 1866–1875. [4] Salaheldeen, M.; Vega, V.; Ibabe, A.; Jaafar, M.; Asenjo, A.; Fernandez, A.; Prida, V.M. Tailoring of Perpendicular Magnetic Anisotropy in $Dy_{13}Fe_{87}$ Thin Films with Hexagonal Antidot Lattice Nanostructure. *Nanomaterials* 2018, *8*, 227. [5] Salaheldeen, M.; Goyeneche, M.L.M.; Alvarez-Alonso, P.; Fernandez, A. Enhancement the perpendicular magnetic anisotropy of nanopatterned hard/soft bilayer magnetic antidot arrays for spintronic application. *Nanotechnology* 2020, *31*, 485708.

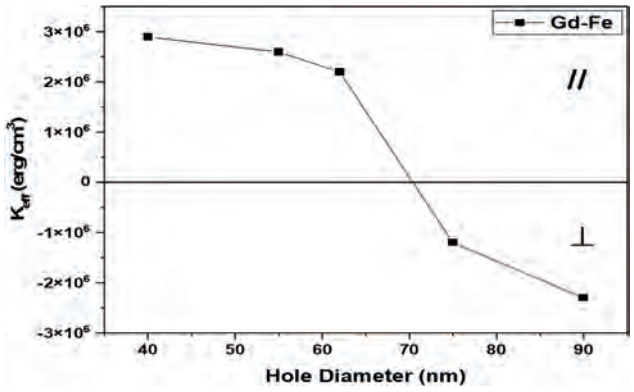

Effective anisotropy, K_{eff}, as a function of antidot hole diameter for Gd-Fe antidot thin films. Negative values of K_{eff} correspond to antidot samples with perpendicular (OOP) effective anisotropy.

EQ-07. Temperature dependence of interlayer exchange fields in permalloy based synthetic antiferromagnets. J. Sklenar[1], K. Deng[2], B. Flebus[2] and *M. Subedi*[1] *1. Wayne State University, Detroit, MI, United States; 2. Boston College, Chestnut Hill, MA, United States*

Synthetic antiferromagnets are magnetic heterostructures composed of consecutive ferromagnetic layers separated by non-magnetic spacers of appropriate thickness. This arrangement induces antiferromagnetic coupling through the Ruderman-Kittel-Kasuya-Yosida (RKKY) interaction. Measurement of the antiferromagnetic exchange field between the layers is a crucial parameter to extract upon synthesis of these magnetic multilayers. In this study, we synthesized and characterized synthetic antiferromagnets comprised of both an even and odd number of permalloy layers separated by ruthenium spacer layers. Specifically, we investigated bilayer, trilayer, and tetralayer structures. Through magnetometry measurements, we were able to determine the interlayer exchange interaction for these different structures. We observed a consistent enhancement in the interlayer exchange field across all structures and permalloy thicknesses examined, as the temperature decreased from 300 K to 150 K. In this work we report the temperature-dependent values of interlayer exchange interaction for bilayers, trilayers, and tetralayers, where the permalloy layers range from 2 to 15 nm in thickness.

EQ-08. Static and Dynamic Magnetic Properties of Iron Oxide Nanoparticles in Colloid and Embedded in Polymer Nanocomposites. *E. Correa*[1], F.M. Abel[1], C. Gruettner[2], J.E. Seppala[1] and C. Dennis[1] *1. National Institute of Standards and Technology, Gaithersburg, MD, United States; 2. Micromod Partikeltechnologie, Rostock, Germany*

Magnetic nanoparticles (MNPs) have been the subject of intense study for many decades, due, in part, to their many applications such as water/gas purification to data storage to drug delivery. While it is well-known that the physical properties of MNPs, such as composition, size and size distribution, crystallinity, shape, etc. determine the magnetic properties, it is not as widely discussed what impact the MNP environment has on the measured properties. For example, MNPs can physically move in a liquid under the influence of an external magnetic field, forming structures like rings and chains [1]. When dispersed in a solid matrix, or nanocomposites, their physical movement can be significantly restricted, if not eliminated, leaving only magnetic (Neel) rotations. Here, we compared colloidal dispersions of iron oxide MNPs in water and toluene with nanocomposites of the iron oxide MNPs made by dispersion of the MNPs in polymer followed by either UV polymerization (water-based) or rapid precipitation (toluene-based). Measurement of magnetization as a function of applied field show two distinct behaviors: the nanocomposite virgin curve is centered in the first quadrant major loop before merging with the falling major loop, in stark contrast with the MNPs in liquid which track the rising side of the major loop (Fig. 1). Furthermore, in the nanocomposites, there is a peak in the imaginary AC susceptibility component based on the magnetic properties of the individual MNPs. In liquid, the peak in the imaginary component shifts out of range based on the magnetic properties of a chain. (Fig. 2) The changing structures possible in liquid (which are restricted in nanocomposites) also modify the interactions, resulting in a dynamic magnetic anisotropy [2]. This has profound implications for magnetic applications, especially as many of these use AC magnetic fields where the magnetic anisotropy is crucial to their detailed response.

1. Abel et.al. ACS Applied Materials and Interfaces, 2023 2. Dennis, et al, Nanotechnology 2018.

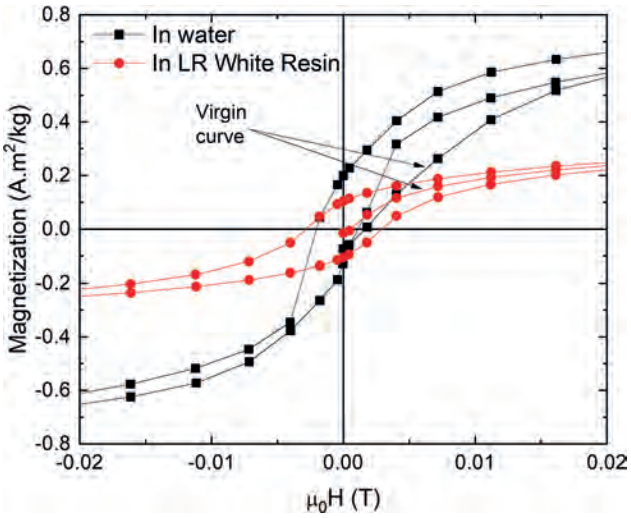

Fig. 1 – 300K Hysteresis of MNPs in water and in a nanocomposite

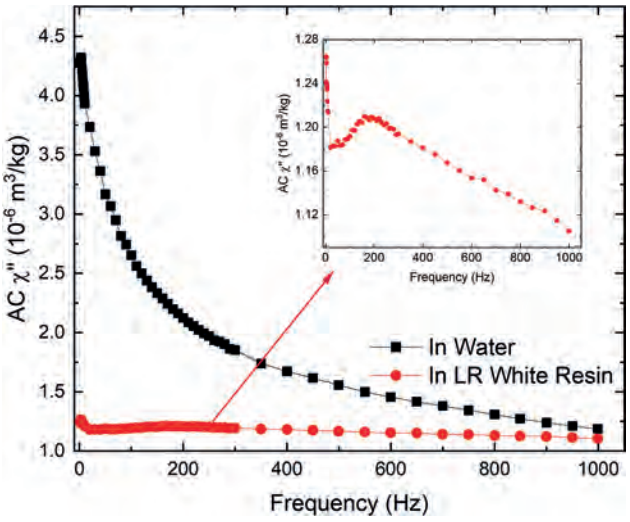

Fig. 2 – Imaginary AC susceptibility component for MNPs in water and in a nanocomposite.

EQ-09. Epitaxial Ru-Mo(0001) Thin Films with Nano-Scale Resistivity Gradient for Charge-Spin Conversion. *K. Tang*[1,2], C. He[1], Z. Wen[1], H. Sukegawa[1], T. Ohkubo[1], Y. Nozaki[3] and S. Mitani[1,2] *1. Research Center for Magnetic and Spintronic Materials, National Institute for Materials Science, Tsukuba, Japan; 2. Graduate School of Science and Technology, University of Tsukuba, Tsukuba, Japan; 3. Department of Physics, Keio University, Yokohama, Japan*

Nonmagnetic thin films with well-controlled interfaces and nano-scale multi-layered structures have shown great potential for charge-spin conversion to achieve energy-efficient spintronic devices [1]. Several mechanisms of the conversion in such structures are discussed, such as the interface Rashba effect [2], the spin-vorticity coupling (SVC) [3], and the orbit Hall effect [4]. Among them, the SVC is drawing increasing attention, where the spin

currents are generated when a thin film has a nano-scale gradient in the resistivity. In this study, we focused on a Ru-Mo alloy to create well-controlled nano-resistivity gradients. Since Ru and Mo are materials with small spin Hall interactions, the Ru-Mo gradient may give us a suitable platform to demonstrate the SVC-generated spin currents. The $Ru_{1-x}Mo_x$ thin films with x from 0 to 0.5 were epitaxially grown on c-plane sapphire substrates by co-sputtering using Ru and Mo targets. Structural analyses show the RuMo films have a single hcp structure with an epitaxial relationship of RuMo(0001)[11-20] // Al_2O_3(0001)[10-10] in all the compositions. In accordance with the Nordheim's rule, the resistivity of the films continuously increases from 7 to 53 μΩ cm with increasing x from 0 to 0.5, indicating the resistivity gradient can be obtained by tuning compositions to the thickness direction using our epitaxial technique. We fabricated a $Ru_{1-x}Mo_x$ (7.7 nm)/CoFeB(0-10 nm) structure, as shown in Fig. 1, where the $Ru_{1-x}Mo_x$ layer has a gradient composition starting from x = 0.5 (bottom side) to 0% (top side). The measurements of the spin-torque ferromagnetic resonance (ST-FMR) were performed to characterize the spin-transport properties. As shown in Fig. 2, a voltage signal consisting of antisymmetric and symmetric line shapes was observed. The damping-like torque efficiency ξ_{DL} of the gradient $Ru_{1-x}Mo_x$ film was evaluated to be ~1.6%. In contrast, ξ_{DL} of a reference sample with a constant composition $Ru_{50}Mo_{50}$/CoFeB structure was estimated to be only ~0.4%, indicating the enhanced ξ_{DL} by the gradient. Further investigations, including nanostructural analysis, are expected to provide insights into the origin of the enhancement.

[1] J. Song, et al., Nanotechnology 34, 365704 (2023). [2] T. Gao, et al., Phys. Rev. Lett. 121, 017202 (2018). [3] G. Okano, et al., Phys. Rev. Lett. 122, 217701 (2019). [4] D. Go et al., Phys. Rev. B 103, L121113 (2021).

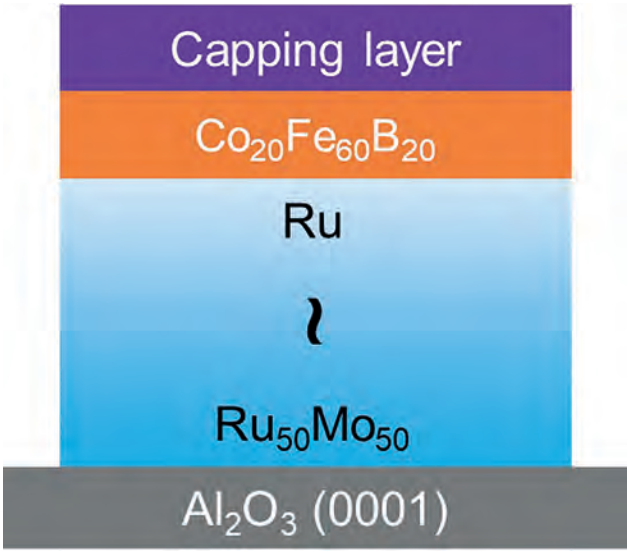

Fig. 1. Sample structure.

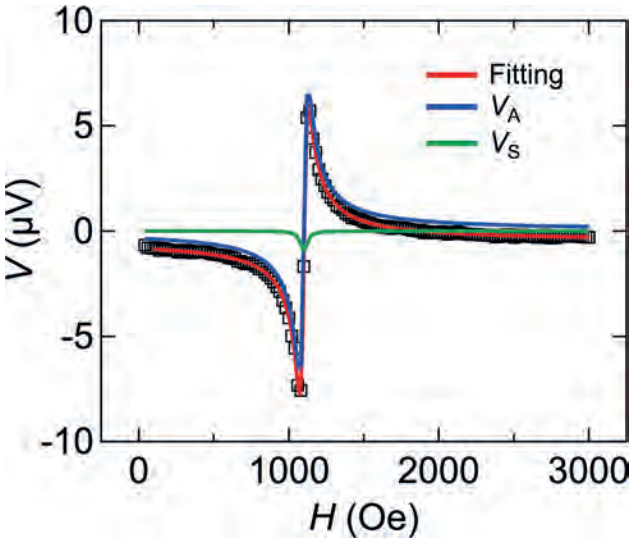

Fig. 2. ST-FMR signals.

EQ-10. Withdrawn

EQ-11. Compositionally magnetostrictive effect of Ta/CoFe(B)/MgO films with perpendicular magnetic anisotropy. *S. Ahn*[1] *1. Pohang University of Science and Technology, Pohang, The Republic of Korea*

The mechanical difference of nanometer or sub-nanometer layers making up magnetic tunnel junctions (MTJs) generates a high compressive strain in the MTJ and results in a detrimental magnetostrictive effect related to its magnetic response [1]. Ta/CoFe(B)/MgO is fundamental elements consisting of the MTJ, so understanding of its magnetostrictive effect is critical to optimize the MTJ [1]. For this work, the magnetostrictive effect in Ta/Co_xFe_{100-x}(B)[CoFe(B)]/MgO for alloy compositions spanning Fe-rich (x=20) to Co-rich (x=80) films has been studied in order to investigate the relation between the magnetostrictive effect and the onset of perpendicular magnetic anisotropy (PMA) at the Ta/CoFe(B)/MgO interfaces. Figure 1 shows K_u*t versus t for x=20, 50, 60, and 80, and dependences of crossover thicknesses (t_{cro})—CoFe(B) thickness for K_u*t =0 of Ta/CoFe(B)/MgO films—on the Co composition indicating dependences of t_{cro} and magnetostriction constant (λ_s) of 0.8-nm CoFe/MgO films on Co composition [2]. By considering the CoFe(B)/MgO interface with in-plane (ip) and out-of-plane (op) orbital magnetizations, the relative ratio of ip to op orbital magnetization consisting of the interface is found to be closely related to λ_s [3]. It is clearly seen that the composition dependence of ip and op orbital magnetization at the CoFe/MgO interface caused by the relative population of op (ip) orbital moment ($m_{orb}^{op(ip)}$) [4], plays an important role in controlling the PMA ($H_d^{eff} < 0$) and magnetostrictive effect at the metal/oxide interface as shown in Fig. 2 [5].

[1] K. Sankaran et al., doi: 10.1109/IEDM.2018.8614627 (2018). [2] C. Kuhrt and L. Schultz, J. Appl. Phys. 71, 1896 (1992). [3] A.T. Hindmarch et al., Phys. Rev. B 83, 212404 (2011). [4] P. Bruno, Phys. Rev. B 39, 865 (1989). [5] S.-M. Ahn, G. S. D. Beach, J. Appl. Phys. 113, 17C112 (2013).

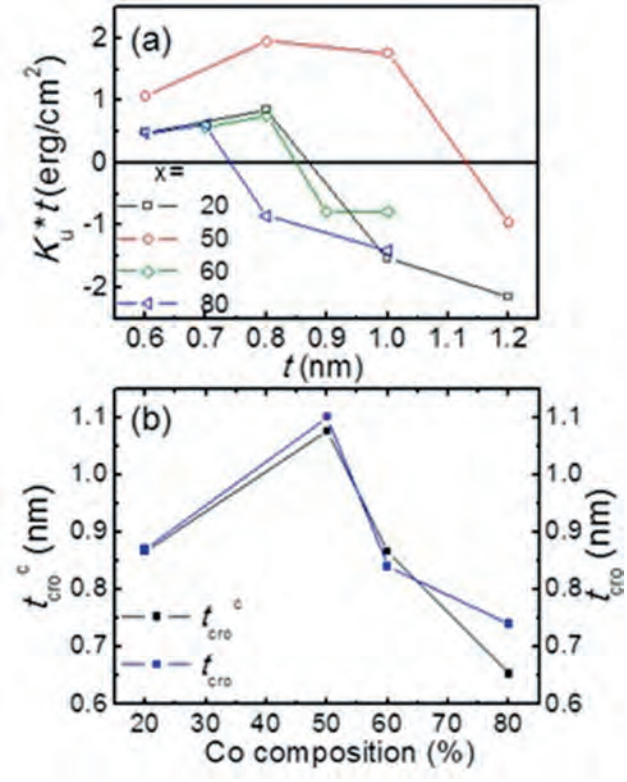

Fig. 1 (a) Magnetic anisotropy energy (K_u) times the CoFe(B) thickness (t) versus t for CoFe(B)/MgO films with several Co compositions. (b) Dependences of crossover thicknesses of CoFe(B)/MgO films on the Co composition.

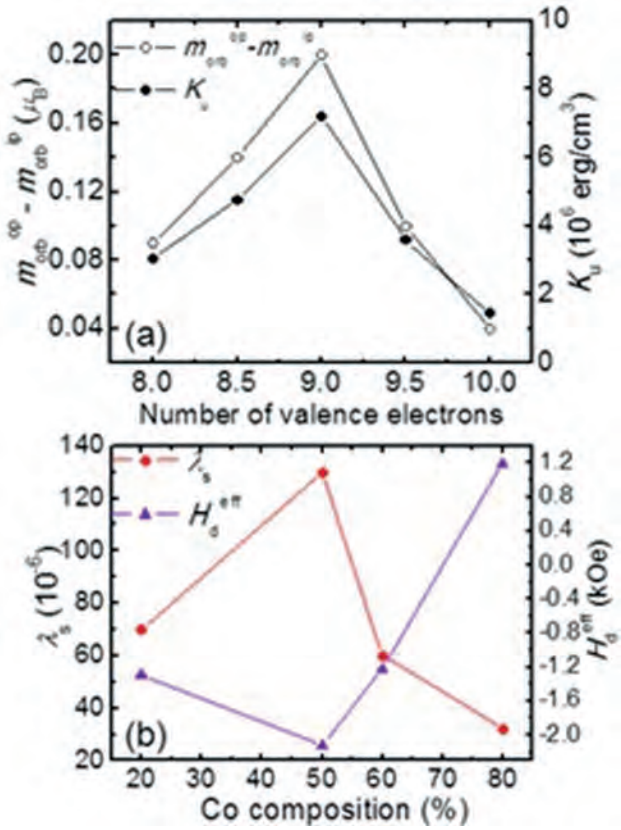

Fig. 2 Dependences of (a) difference between op orbital moment (m_{orb}^{op}) and ip orbital moment (m_{orb}^{ip}) and estimated magnetic anisotropy energy on the number of valence electrons and (b) dependence of λ_s and effective demagnetization field H_d^{eff} on Co composition.

EQ-12. Characterization of Magnetic Properties in $(FeCo)_{1-x}Gd_x$ Ferrimagnetic Thin Films: Magnetometry and Spectroscopic Studies.

N. Alzahrani[1,2], S. Saha[4,3], R. Knut[3], C. Luo[5], F. Radu[5] and D. Arena[1]
1. Department of Physics, University of South Florida, Tampa, FL, United States; 2. Department of Physics, University of Jeddah, Jeddah, Saudi Arabia; 3. Department of Physics and Astronomy, Uppsala University, Uppsala, Sweden; 4. Department of Physics, Ashoka University, Sonepat, India; 5. Helmholz-Zentrum Berlin fur Materialien und Energie, Berlin, Germany

Rare-earth/transition metal (RE/TM) ferrimagnetic amorphous alloys have gained attention for spintronic applications. These alloys allow tunability of magnetic properties (e.g., magnetization, anisotropy, spin polarization) by adjusting composition, film thickness, temperature, and capping materials [1,2]. They also exhibit magnetic compensation, where the temperature-dependent magnetization profiles of TM (Fe & Co) and RE (Gd) nearly cancel each other [3]. This study investigates the magnetic properties of $(FeCo)_{1-x}Gd_x$ ferrimagnetic thin films using magnetometry, x-ray magnetic circular dichroism (XMCD), and ferromagnetic resonance (FMR) across the magnetic compensation temperature. The Gd content (x) is systematically varied to modify the compensation temperature. The FeCoGd films are prepared via DC magnetron sputtering onto Si substrate and x-ray transparent SiN membranes. The hysteresis loops and M vs. T curves were measured using vibrating sample magnetometry (VSM) and magneto-optical Kerr effect (MOKE) to characterize the magnetic properties of the films. The M vs. T curves exhibit a compensation temperature, which varies according to Gd concentration changes (Fig. 1a). The orientation of the FeCo sublattice magnetization was determined by using MOKE, which confirmed the transitions observed in the M vs. T data. To gain deeper insights into the magnetic behavior, XMCD spectra were acquired in a perpendicular geometry from 14 K up to 300 K, with the external magnetic field saturating parallel to

the x-ray beam. The obtained XMCD spectra at the transition metal (TM L-edge) and (Gd M-edge) validate the antiferromagnetic alignment of the transition metal and Gd moments. Element-specific hysteresis loops (Fig.1b) also confirm the antiferromagnetic alignment. Through the analysis of the XMCD spectra, we investigate the evolution of the elemental moments with changing temperatures.

[1] S. K. Kim, G. S. Beach, et al., Nature Materials, 21(1), 24-34, (2022). [2] B. Hebler, A. Hassdenteufel, P. Reinhardt, et al., Frontiers in Materials, 3, 8, (2016). [3] A. Chanda, J. E. Shoup, N. Schulz, et al., Physical Review B, 104(9), 094404, (2021).

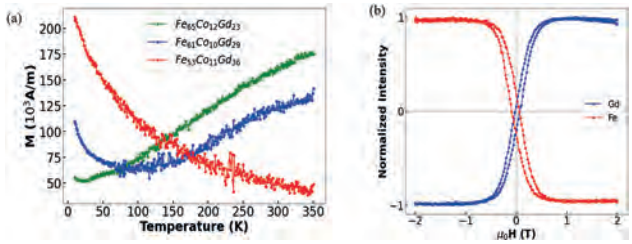

Fig.1:(a) M vs. T data for $(FeCo)_{1-x}Gd_x$ thin films with different concentrations of Gd show different compensation temperatures. (b) Element-specific hysteresis loops at Gd M and Fe L edges confirmed the anti-ferromagnetic alignment of TM and RE moments at 14K.

EQ-13. Antiferromagnetic Coupling in Co/RuY/Co (Y = Co and Fe).

Z.R. Nunn[1], J. Besler[1], *K.D. Winther*[1], S. Arapan[2], D. Legut[2], F. Schulz[3], E. Goering[3], T. Mckinnon[1], S. Myrtle[1] and E. Girt[1] *1. Physics, Simon Fraser University, Burnaby, BC, Canada; 2. IT4Innovations, VSB Technical University of Ostrava, Ostrava, Czechia; 3. Modern Magnetic Systems, Max-Planck-Institute for Intelligent Systems, Stuttgart, Germany*

Since its discovery in 1986, interlayer exchange coupling in metallic multilayer structures between two ferromagnetic layers across a nonmagnetic spacer layer (FM/NM/FM) has been widely researched for its usage in spintronic devices. Modern device deposition techniques, such as magnetron sputtering, can cause interlayer mixing between the ferromagnetic layers and the spacer layers, which affects the exchange coupling strength. This has not been researched in depth until now. In this work, the strength of antiferromagnetic coupling in Co/RuY/Co (Y = Co and Fe) was studied as a function of RuY composition and thickness. It was found that antiferromagnetic coupling can be achieved across RuY spacer layers with maximum concentrations of 60 at.% for Co and 79 at.% for Fe. Additionally, it was found that the bilinear coupling constant, J_1, in Co/Ru(d)/Co structures oscillates as the spacer layer thickness, d, increases. These oscillations persist with the addition of Fe to the spacer layer but are damped following a $1/d^2$ dependence with the addition of Co as seen in Fig. 1 (a) and (b). In Fig. 1 (c) for Co(2)|$Ru_{100-x}Y_x$(d)|Co(2) structures where d is fixed to a thickness of two atomic layers (d = *0.4 nm*), J_1 strongly increases with the addition of Fe to a maximum of 7.4 mJ/m^2. This is the largest antiferromagnetic interlayer exchange coupling ever observed in sputtered multilayers. It was also found that the addition of Co to the Ru spacer layer causes J_1 to decrease monotonically. Electronic structure calculations of Co(2)|$Ru_{100-x}Y_x$(d)|Co(2) structures performed with the Vienna Ab initio Simulation Package (VASP) depicted in Fig 1. (c), show direct agreement with experimental results. To further investigate the reasoning for the high values of J_1 when Fe is introduced to the spacer layer, X-ray Magnetic Circular Dichroism measurements were performed and found that the Fe in the spacer has a large magnetic moment directly impacting the coupling strength.

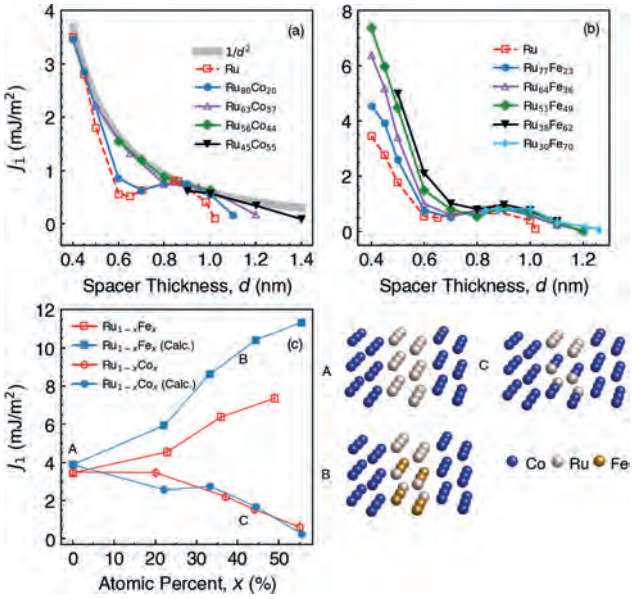

Fig.1: J_1 as a function of the spacer layer thickness, d, of Co(2)|$Ru_{100-x}Y_x$(d)|Co(2) for (a) Y = Co and (b) Y = Fe. (c) Experimental measurements and theoretical calculations of J_1 for Co(2)|$Ru_{100-x}Y_x$(0.4 nm)|Co(2) with structures depicted on the right.

EQ-15. Influence of Gd substitution on the structure and magnetic properties of pulsed laser deposited Sr M-type hexaferrite thin films.

K.A. Murphy[1], O. Fitchorova[4,2], W. Liang[3] and V.G. Harris[1] *1. Center for Microwave Magnetic Materials and Integrated Circuits, Department of Electrical and Computer Engineering, Northeastern University, Boston, MA, United States; 2. Department of Electrical and Computer Engineering, Northeastern University, Boston, MA, United States; 3. Kostas Advanced Nano-Characterization Facility, Innovation Campus at Burlington MA, Northeastern University, Burlington, MA, United States; 4. KRI at Northeastern University, LLC, Burlington, MA, United States*

M-type hexaferrites are useful materials as substrates in components in transmit and receive modules such as low loss isolators and circulators. Decreasing the size of these devices is vital since these devices are commonly part of an ever-crowded array. Because of this, film-based processing has become attractive in device fabrication. Formerly, Barium M-type hexaferrite (BaM) films were grown on sapphire (0001) using pulsed laser deposition (PLD). [1] These films demonstrated high out-of-plane crystal texturing, with the alignment of the c-axis perpendicular to the substrate surface. Magnetic properties consisted of saturation magnetization of 4.36 kG and coercivity of 920 Oe. Other work included BaM films grown on and due to the strain induced by the amorphous template a much higher coercivity of 2148 Oe resulted. [2] Here, the effects of Gadolinium (Gd) doping were explored as a means to increase coercivity and loop squareness. To this end, Gd-doped Strontium M-type hexaferrite (i.e., Sr(Gd)M) thin films were grown on c-plane sapphire (0001) substrates by PLD to evaluate the influence of Gd on the composition, structure and magnetic properties. A 248 nm KrF Excimer laser was employed and Gd was doped for Sr at concentrations of x= 0.1, 0.2, 0.3. As the Gd concentration increased saturation magnetization (as $4\pi M_s$) decreased from 4246 G to 1387 G and loop squareness (as M_r/M_s) increased from 0.48 to 0.54 (see Fig. 1). Coercivity increased to a maximum value of 3129 Oe in films deposited with a Gd level x=0.2. XRD confirmed phase purity (see Fig. 2(a)) and a high degree of c-axis alignment normal to the sample surface for compositions doped at x=0.1 and 0.2. These results clearly demonstrate the strong influence of Gd doping on SrM PLD-grown hexaferrite thin films and provide guidance for creating submicron (~850 nm) thin films with high levels of coercivity for use as hard magnet RF device substrates.

[1] C. Yu, A. Sokolov, P. Kulik and V. G. Harris, *Journal of Alloys and Compounds,* Vol. 814, p. 152301 (2020) [2] P. Kulik, C. Yu, A. Sokolov, W. Liang and V. G. Harris, *Scripta Materialia,* Vol. 188, p. 190-194 (2020)

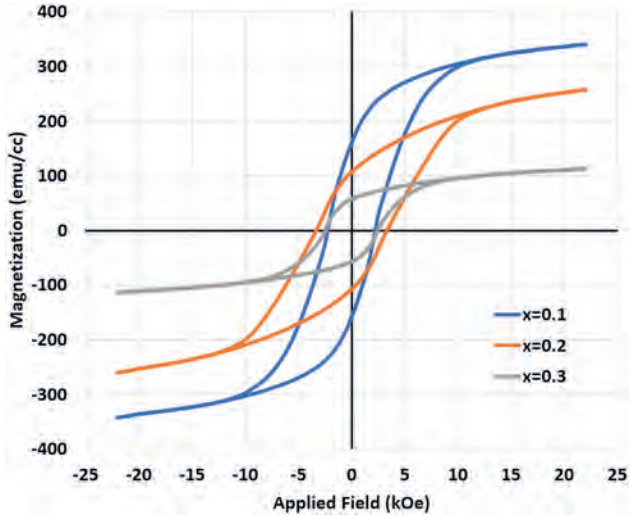

Fig 1. Room temperature M-H out-of-plane loops for $Sr_{1-x}Gd_xFe_{12}O_{19}$, x= 0.1, 0.2, 0.3.

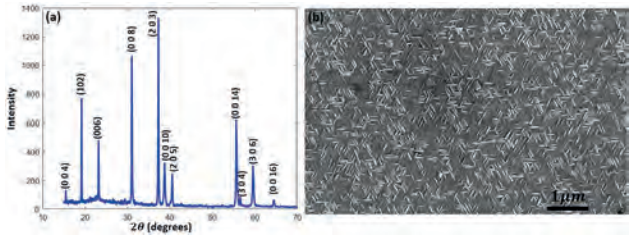

Fig 2. (a) XRD pattern and (b) SEM image of $Sr_{0.8}Gd_{0.2}Fe_{12}O_{19}$ film.

Session ER
MAGNETOELECTRIC MATERIALS
(Poster Session)

Markus Goessler, Chair
Chemnitz University of Technology, Chemnitz, Germany

ER-01. FeGaB Alloys for Magnetoelastic Coupling at Microwave Frequencies. *Z. Zhang*[1] and A. Hoffmann[1] *1. Department of Materials Science and Engineering, University of Illinois Urbana-Champaign, Urbana, IL, United States*

Magnetoelastic coupling is an efficient approach to manipulate magnetization in magnetic materials and has great potential for magnetoelectrical applications, such as surface acoustic wave devices. Towards this end, $Fe_{80}Ga_{20}$ is a well-studied material due to its high magnetoelastic response. In order to achieve a high magnetoelastic response, the disordered A2 phase is crucial. It has already been demonstrated that it is possible to stabilize the disordered A2 phase via epitaxy [1]. Here, we chose a different approach, incorporating boron dopants into magnetron sputtered $Fe_{80}Ga_{20}$ films and studied the influence of boron doping on the structure, damping and magnetostriction using X-ray diffraction (XRD), ferromagnetic resonance (FMR) and magnetoelastic measurements. FeGaB thin films with varying B concentration from 2% to 18% and fixed Fe to Ga concentration of 80:20 were synthesized by simultaneously sputtering from three targets. Precise control on boron, iron, and gallium compositions was achieved by tuning individual gun power and the compositions were later characterized with X-ray photoemission spectroscopy (XPS) and Rutherford backscattering (RBS). XRD reveals a gradual reduction in the Fe (100) peak with increasing B concentration from 2% to 8%, and vanishing peak at 10% B concentration, which is consistent with the films transitioning from crystalline to amorphous structures. Concomitantly, the coercivity obtained from magnetization hysteresis loops decreased rapidly from 150 Oe with 2% B to 25 Oe with 18% B, with a sudden change around 8% B associated with the structural transition, see Fig. 1. For utilizing magnetostriction at microwave frequencies, low damping is also required. We have measured a low damping around 3×10^{-3} with a 12 % B doped FeGa films, see Fig. 2, indicating that these films are well suited for applications at microwave frequencies.

[1] P. Meisenheimer, R. Steinhardt, S. Sung, *Nature Communications 12,* 2757 (2021).

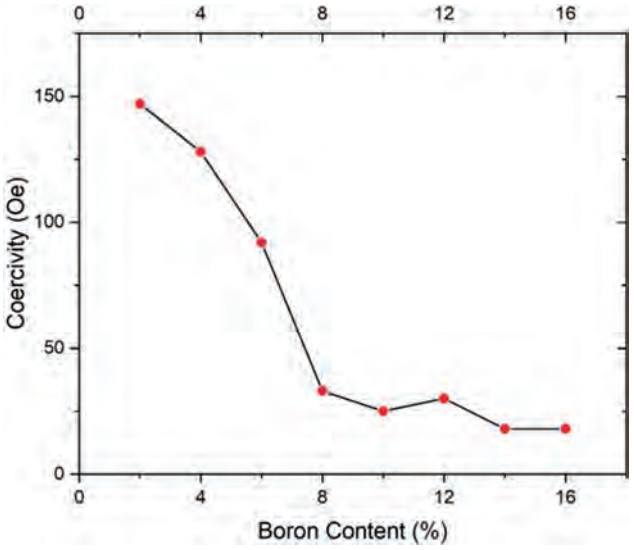

Fig. 1: Coercivity vs. B concentration for $(Fe_{80}Ga_{20})_{1-x}B_x(80)$, with a sudden transition beyond 8% B.

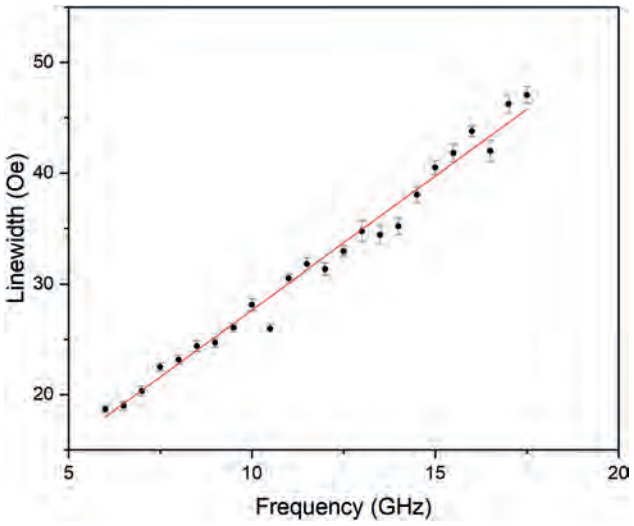

Fig. 2: Linewidth vs. frequency for $(Fe_{80}Ga_{20})_{88}B_{12}(20)$/MgO(3)/Ta(3). The extracted damping is 3.38×10^{-3}.

ER-02. Doping effect on magnetic properties of high-temperature multiferroic compound $YBaCuFeO_5$. *Y. Yasui*[1], S. Kihara[1], K. Ikeda[1] and T. Banshodani[1] *1. Physics, Meiji University, Kawasaki, Japan*

In spin systems with geometrical frustration or with competing exchange interactions, non-trivial magnetic structure often induces a ferroelectricity, which is called "multiferroic". If we have multiferroics above room temperature, we may be able to control their ferroelectricity by external magnetic field or their magnetization by external electric field at ambient conditions.

We adopt an oxygen-deficiency ordered perovskite $YBaCuFeO_5$ to study high temperature multiferroics. The multiferroic transition at T_{N2} (~ 210 K) for $YBaCuFeO_5$ was first reported by Ref. [1]. After that, our group reported the results of magnetic susceptibilities, pyrocurrents, and neutron magnetic reflection intensities of $YBaCuFeO_5$ [2]. $YBaCuFeO_5$ exhibits an antiferromagnetic magnetic transition with collinear structure at T_{N1}. The magnetic structure changes at T_{N2} from the collinear to a spiral one accompanied with a ferroelectricity and multiferroic phenomena. Other group reported that T_{N2} of $YBaCuFeO_5$ can be increased above 310 K through a controlled manipulation of the Cu/Fe chemical disorder [3]. They also reported that increase of T_{N2} value and stabilization of spiral magnetic structure are caused by increasing Cu/Fe chemical disorder. This result is surprising, because the magnetic transition is usually disturbed by disorder of atomic configuration. In this work, we have investigated the magnetic properties and magnetic transitions of $YBaCu_{1-x}M_xFeO_5$ (M= Mn, Ni, and Zn), because the M-doping to Cu/Fe site is expected to induce the Cu/Fe chemical disorder. We synthesized the polycrystalline samples of $YBaCu_{1-x}M_xFeO_5$ (M=Mn, Ni, and Zn), and carried out measurements of magnetic susceptibility up to 650K. From anomalies of the magnetic susceptibility – temperature curves, x - dependences of T_{N1} and T_{N2} were determined. We found that T_{N2} raise by Mn-doping above 360 K at x_c=0.05, Ni-doping above 370 K at x_c=0.03, and Zn-doping above 340 K at x_c=0.07. However, it was found that x - dependences of T_{N1} and T_{N2} in the region of $x > x_c$ differs depending on the type of doping ions. We discuss the doping effect on magnetic properties of high-temperature multiferroic compound $YBaCuFeO_5$.

[1] B. Kundys *et al.*: Appl. Phys. Lett. 94, 072506 (2009). [2] Y. Kawamura *et al.*: J. Phys. Soc. Jpn. 79, 073705 (2010). [3] M. Morin *et al.*: Nature Comm. 7, 1 (2016).

ER-03. Enhanced Tunneling Electroresistance in Multiferroic Tunnel Junctions Through the Barrier Insulating-Metallic Transition. *B. Chi*[1], L. Jiang[1] and X. Han[1] *1. Institute of Physics CAS, Beijing, China*

Tunneling electroresistance (TER) ratio is an important device merit of ferroelectric tunnel junction (FTJ) and multiferroic tunnel junction (MFTJ) devices. Here we propose an efficient way to achieve a sizable TER effect through the interface engineering in both $SrRuO_3/PbTiO_3$/FeO/Fe and $SrRuO_3/PbTiO_3$/CoO/Co MFTJs. It is found that the interfacial FeO or CoO layer can significantly modify the band alignment between $PbTiO_3$ barrier and electrodes through its large depolarization field, causing the insulating–metallic transition of $PbTiO_3$ barrier upon polarization reversal. As a result, the tunneling resistance changes significantly, leading to a giant TER effect of 10^5 %. Our results suggest a practical way to enhance the TER effect in MFTJs.

E. Y. Tsymbal and H. Kohlstedt, Science, 313, 181-183 (2006) D. Pantel and M. Alexe, Nat. Mater., 11,289-293 (2012) Yong Wang and E. Y. Tsymbal, Phys. Rev. Lett.,109, 247601 (2012) Xiaohui Liu and E. Y. Tsymbal, Phys. Rev. B, 88,165139 (2013) Qiong Yang, E. Y. Tsymbal and Vitaly Alexandrov, Nano Lett., 19, 7385-7393 (2019) Rui Guo, E. Y. Tsymbal and Jingsheng Chen, Sci. Adv., 7, 1033 (2021) Jing Su, Xiaohui Liu and E. Y. Tsymbal, Phys. Rev. B, 104, L060101 (2021) Jing Su and Xiaohui Liu, npj comput. Mater., 8, 54 (2022)

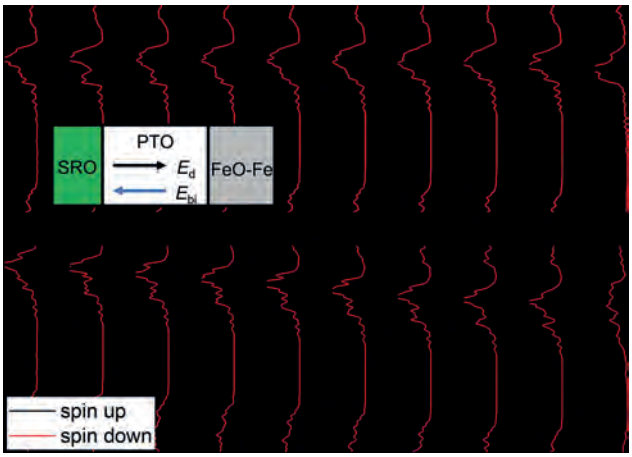

Spin- and layer-resolved local density of states projected onto the TiO_2 layers in the $SrRuO_3/PbTiO_3$/FeO/Fe MFTJ with (a) left polarization and (b) right polarization states. Spin-up and spin-down are represented by black and red curves, respectively. The horizontal dashed line indicates the position of Fermi energy.

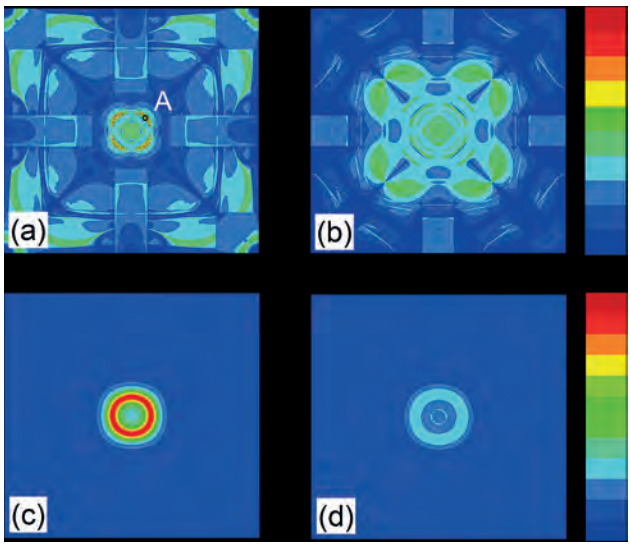

The k‖-resolved transmission coefficient distributions in the 2DBZ at the Fermi energy in the $SrRuO_3/PbTiO_3$/FeO/Fe MFTJs for (a) left-polarized state and (b) right-polarized state. The k‖-resolved total LDOS of $PbTiO_3$ barriers for (c) left-polarized state and (d) right-polarized state.

ER-04. Withdrawn

ER-05. Converse magnetoelectric response and tunable inductance in $BaTiO_3$:$BaFe_{12}O_{19}$ composites. P. Mola II[2], S.C. Mills[3], T.R. Mion[1] and *M. Staruch*[3] *1. NOVA Research, Alexandria, VA, United States; 2. NREIP Intern, U.S. Naval Research Laboratory, Washington, DC, United States; 3. U.S. Naval Research Laboratory, Washington, DC, United States*

Magnetoelectric composites have garnered much interest over the past several decades, creating new functionalities utilizing the coupling between magnetism and the dielectric/ferroelectric response. While the magnetodielectric response and the direct magnetoelectric are often well understood, there is relatively little focus on the tuning of the magnetic properties and functionalities with a voltage. In this work, ceramic composites of well-known ferroelectric $BaTiO_3$ and high-frequency magnetic material $BaFe_{12}O_{19}$ (80/20, 60/40, 50/50, 40/60, and 20/80 wt% samples) were fabricated and studied. The dielectric and magnetodielectric response is established with

low dielectric losses and ferroelectric behavior observed for all samples. A tunability of the inductance was observed for all samples but maximized in the 60:40 composite with a 14% change, stemming from a strain-induced change in the relative permeability of the magnetic phase. Lastly, a converse magnetoelectric (CME) effect was seen in the magnetization measurements with electric field for samples with over 40% $BaTiO_3$, with sufficient strain developed to the hexaferrite to produce a measurable CME response.

ER-06. Electronic Transport in Structural Domains of Multiferroic $SrMnO_3$. J. van Rijn[1], *I. Bhaduri*[1] and T. Banerjee[1] *1. Zernike Institute for Advanced Materials, University of Groningen, Groningen, Netherlands*

Multiferroic materials exhibiting strong magnetoelectric coupling between different ferroic orders have generated considerable interest in recent times. This stems from the possibility of integrating them into low-power spintronic devices where the magnetization is manipulated using energy-efficient electric fields instead of magnetic fields. We study both the magnetic and ferroelectric order in thin films of perovskite $SrMnO_3$, a complex oxide with correlated electrical, magnetic and structural properties. Thin films of $SrMnO_3$, when strained, show different antiferromagnetic-ferroelectric phases that persist up to room temperature as discussed in recent works [1, 2]. Both the superexchange-mediated magnetic order and ion-displacement-driven ferroelectric order are expected to arise from the body-centered Mn cation, leading to strong magnetoelectric coupling. Thin films of $SrMnO_3$ were grown on doped $SrTiO_3$ substrates using pulsed laser deposition. The substrate imposed a tensile strain of 2.63% which was confirmed using different structural characterization techniques. Our earlier work on probing the magnetic order in such strained films, using spin Hall magnetoresistance studies, shows antiferromagnetic exchange interaction [3]. In this present work, we show how electronic conductivity varies across differently sized structural domains in strained $SrMnO_3$ films as studied using conductive atomic force microscopy. We study the temporal evolution of these structural domains and their electrical conduction and model the potential landscape incorporating both the tip/film and the substrate/film Schottky interface. A remarkable observation is that over time, the structural domain walls morph into cracks, as confirmed by extended high-angle annular dark field (HAADF) and differential phase contrast (iDPC) images obtained using scanning transmission electron microscopy. Our work is a comprehensive study on combining the influence of structural domains on magnetization and electrical conduction in strained $SrMnO_3$ thin films and is crucial for the understanding of the ferroelectric order in $SrMnO_3$.

[1] A. Edström and C. Ederer, Phys. Rev. Lett., Vol. 124, no. 16 (2020) [2] J. H. Lee and K. M. Rabe," Phys. Rev. Lett., Vol. 104, no. 20, p. 207204 (2010) [3] J. J. L. van Rijn, D. Wang, B. Sanyal and T. Banerjee, Phys. Rev. B., Vol. 106, no. 21 (2022)

ER-07. Withdrawn

ER-08. Withdrawn

ER-09. Interfacial band structure of $BaTiO_3/La_{0.8}Sr_{0.2}MnO_3$ multiferroic heterostructures probed with angle resolved photoemission spectroscopy. F. Stramaglia[1], M. Husanu[2], V.N. Strocov[1], F. Alarab[1], F. Nolting[1] and *C.A. Vaz*[1] *1. Swiss Light Source, Paul Scherrer Institut, Villigen PSI, Switzerland; 2. National Institute of Materials Physics, Magurele, Romania*

We have studied the interfacial band structure of $BaTiO_3/La_{0.8}Sr_{0.2}MnO_3$ multiferroic heterostructures for the two states of the $BaTiO_3$ ferroelectric polarization by using angle resolved photoemission spectroscopy to probe the occupancy of the electron-derived z_2-r_2 and the hole-derived x_2-y_2 bands for the depletion and accumulation states at the interface. Our results show a change in the charge carrier density consistent with the accumulation/depletion of hole carriers at the interface of the $La_{0.8}Sr_{0.2}MnO_3$ layer that is responsible for the interfacial magnetic spin reconstruction observed in this system.

ER-10. Voltage-Controlled Easy-Cone States for Energy Efficient Spintronic Devices. *Y. Park*[1], J. Jeong[1], Y. Jang[3], M. Kang[1], S. Lee[1], J. Kang[1], J. Park[3], K. Lee[2] and B. Park[1] *1. Material Science and Engineering, KAIST, Daejeon, The Republic of Korea; 2. KAIST, Daejeon, The Republic of Korea; 3. Korea University, Seoul, The Republic of Korea*

Spin-orbit torque(SOT) is a promising way to control the direction of magnetization in spintronic devices such as Magnetic random-access memory(MRAM). However, to fully utilize a benefit of SOT, the switching current density should be reduced[1]. In this respect, Voltage-Controlled Magnetic Anisotropy (VCMA) is one of the feasible candidates to reduce the SOT switching current density[1]. It has been reported that SOT switching current density can be reduced by controlling the magnetic anisotropy field in perpendicular magnetic anisotropy (PMA) system[2]. In addition, it is theoretically predicted that the SOT switching current density could be further reduced by controlling the magnetic easy-cone states which has not yet been experimentally demonstrated[3]. In this work, we experimentally demonstrate the reduction of the SOT switching current density by modulating the magnetic easy-cone states through the VCMA. We effectively control the first-(second-) order magnetic anisotropy field and related magnetic easy-cone states by the gate voltages in Ta/CoFeB/Pt/MgO structures. By varying the magnetic easy-cone angle from 0 to 58 degrees through gate voltages, we observe a significant reduction of up to 50% in the SOT switching current density. In addition, we demonstrate the multilevel characteristics based on VCMA and SOT switching. Utilizing the easy-cone multilevel device, We simulate artificial neural networks of convolutional neural network (CNN) and spiking neural network (SNN) to perform pattern recognition. The proposed VCMA-based MTJ array reaches a recognition accuracy near the baseline accuracy while the energy consumption is significantly reduced compared to the current-driven binary spintronic device.

[1] Y. Yan, C. Wan, C. Song, Adv. Electron. Mater. Vol. 2, 1600219 (2016) [2] I. M. Miron, K. Garello, P. Gambardella, Nature. Vol. 476, p.189–193 (2011) [3] K.-W. Park, J.-Y. Park, B.-G. Park, Appl. Phys. Lett. Vol. 109, 012405 (2016)

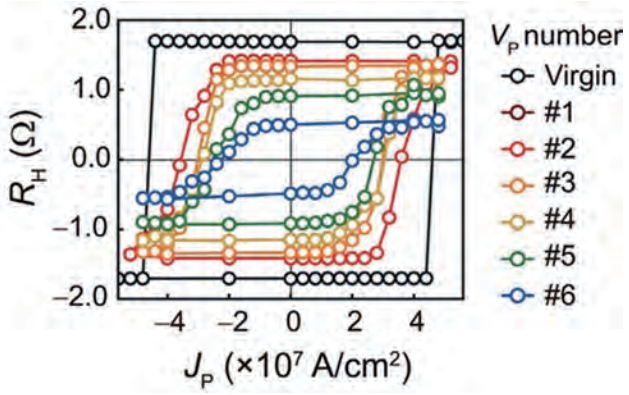

SOT switching loops for sequential numbers of V_Ps

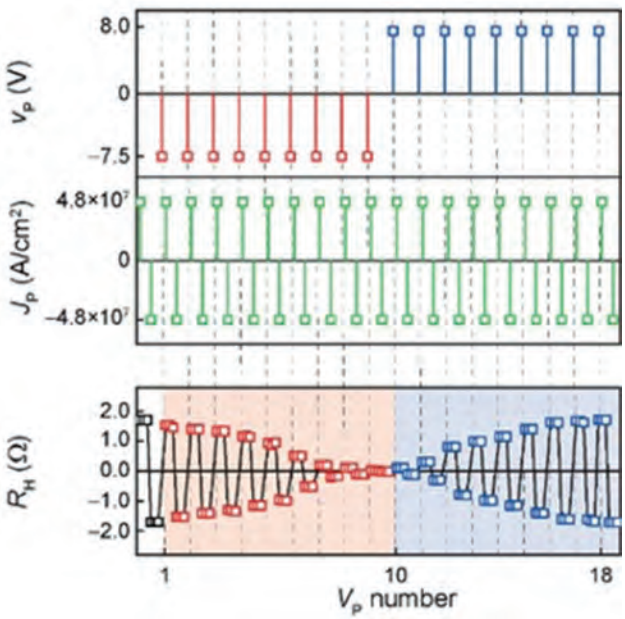

Multi-level operation of the PMA structure sample. Variation of R_H by the sequential V_P and J_P

ER-11. Reversible controlling of perpendicular magnetic anisotropy in Co/Pd multilayers via gateless hydrogen absorption/desorption.

R. Shen[2], C. Chen[3], Y. Tang[3], W. Lin[4] and *J. Hong*[1] *1. Department of Physics, Tamkang University, New Taipei City, Taiwan; 2. Bachelor's Program in Advance Materials Science, Tamkang University, New Taipei City, Taiwan; 3. Department of Physics, National Central University, Taoyuan City, Taiwan; 4. Department of Physics, National Taiwan Normal University, Taipei City, Taiwan*

Hydrogenation induced magneto-ionic controlling of magnetic properties has been studied extensively in Pd-based alloys and multilayers.[1-3] Understanding the mechanism by which hydrogen affects magnetic anisotropy in representative ferromagnetic/nonmagnetic metal layers addressed intensive attention.[4] In this study, we take Co/Pd multilayers as a model system which has been widely studied in spintronics. The anisotropic magnetoresistance (AMR), planar Hall effect (PHE) and anomalous Hall effect (AHE) of Co/Pd multilayers with various hydrogen pressure are investigated to understand its underlying mechanism. Here we demonstrate a reversible and non-destructive magneto-ionic controlling of magnetic anisotropy of Co/Pd multilayers at room temperature, showing that perpendicular magnetic anisotropy could be enhanced by a gateless hydrogen absorption.

[1] Po-Chun Chang et al., *J. Alloys Compd.* 710, 37 (2017). [2] Aik Jun Tan et al., *Nat. Mater.* 18, 35 (2019). [3] Stuart Watt et al., Phys. Rev. B 101, 174422 (2020). [4] K. Klyukin et al., *Phys. Rev. Materials* 4, 104416 (2020).

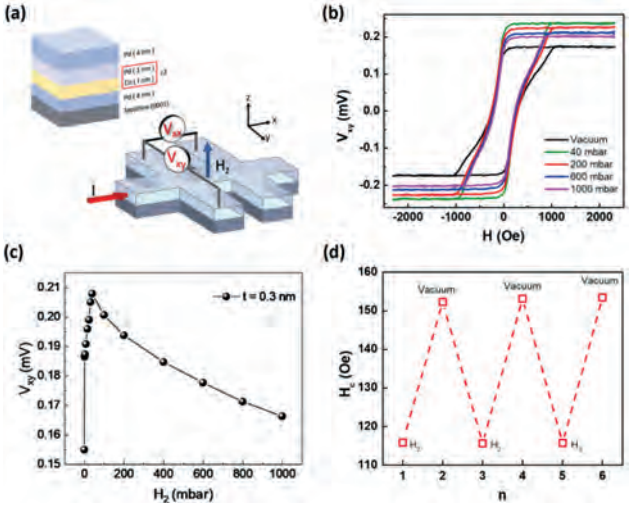

Fig 1. (a) Schematic illustration of layer sequence and Hall bar structure. (b) AHE hysteresis loop measured at various hydrogen pressure. (c) Hydrogen pressure dependent of AHE voltage. (d) Variation of coercivity of Co/Pd multilayers in vacuum and 1000 mbar H_2. Note that n represents the experimental steps.

Session ES
MAGNETICS FOR POWER ELECTRONICS AND CONTROL
(Poster Session)

Changgeng Zhang, Chair
Hebei University of Technology, Tianjin, China

ES-01. Vibration Analysis of a Permanent Magnet Synchronous Generator Considering Electromagnetic Vibration Sources Under AC and DC Load Conditions. *W. Jung*[1], H. Lee[1], J. Yang[1], K. Shin[2] and J. Choi[1] *1. Chungnam National University, Daejeon, The Republic of Korea; 2. Chonnam National University, Yeosu, The Republic of Korea*

A permanent magnet synchronous generator (PMSG) has a simple magnetic circuit design, fast response, linear torque–current and speed–voltage characteristics, and is suitable for constant speed operation. However, as with all rotating machines, noise is generated by electromagnetic, mechanical, and aerodynamic phenomena. This study investigated vibrations generated by the magnetic field between the stator and the magnet of the rotor during generator operation. First, considering AC and DC load conditions, the electromagnetic characteristics of a 4-pole 24-slot model were analyzed, which included the back electromotive force (back-EMF), cogging torque, torque ripple, and unbalanced magnetic force (UMF). Next, the noise, vibration, and harshness (NVH) characteristics were investigated using electromagnetic analysis. Thus, we confirmed the effects of electromagnetic characteristics on the vibration of the generator. Fig. 1 shows the experimental equipment and the fabricated model. The load resistance was set to 6 and 4.5 Ω under DC and AC load conditions, respectively. Fig. 2(a) and (b) show the unbalanced electromagnetic force and fast Fourier transform (FFT) results, respectively, under AC and DC load conditions. The maximum value of the unbalanced electromagnetic force in the x and y directions was 43 Nm, and, when the FFT results were checked, harmonics of the order 4n were generated. Moreover, the harmonics of the unbalance magnetic force under the DC load condition were larger than those under the AC load condition. Fig. 2(c) and (d) show the NVH characteristics under AC and DC load conditions, respectively. Both results confirmed that the largest vibration occurred in the 4n-order harmonic component, which is the frequency of the unbalanced electromagnetic force. More detailed electromagnetic analysis, NVH results, and discussions will be provided in full papers.

[1] J. Zou, H. Lan, Y. Xu, and B. Zhao, IEEE Trans. Energy Convers., vol. 32, no. 4, pp. 1523–1532, (2017). [2] D. Torregrossa, F. Peyraut, B. Fahimi, J. MBoua, and A. Miraoui, IEEE Trans. Energy Convers., vol. 26, no. 2, pp. 490–500, (2011). [3] H. Yang and Y. Chen, IEEE Trans. Energy Convers., vol. 29, no. 1, pp. 38–45, (2014). [4] P. Beccue, J. Neely, S. Pekarek, and D. Stutts, IEEE Trans. Power Electron., vol. 20, no. 1, pp. 182–191, (2005). [5] Z. Q. Zhu, Y. Liu, and D. Howe, IEEE Trans. Magn., vol. 42, no. 10, pp. 3512–3514, (2006).

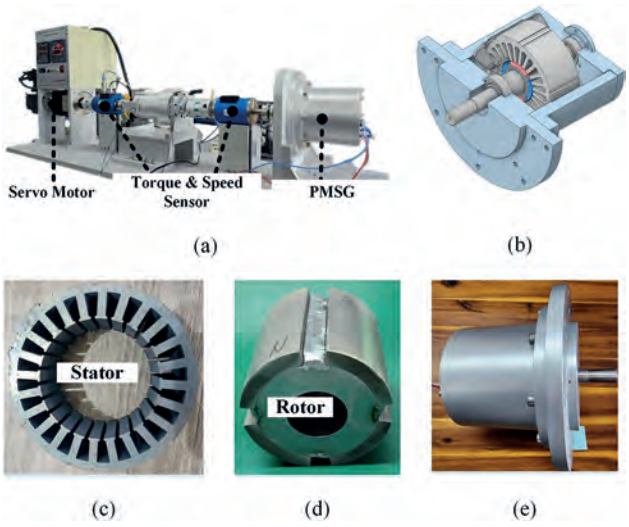

Fig. 1. (a) Experimental setup, (b) 3D_Model (c) stator, (d) rotor and (e) prototype.

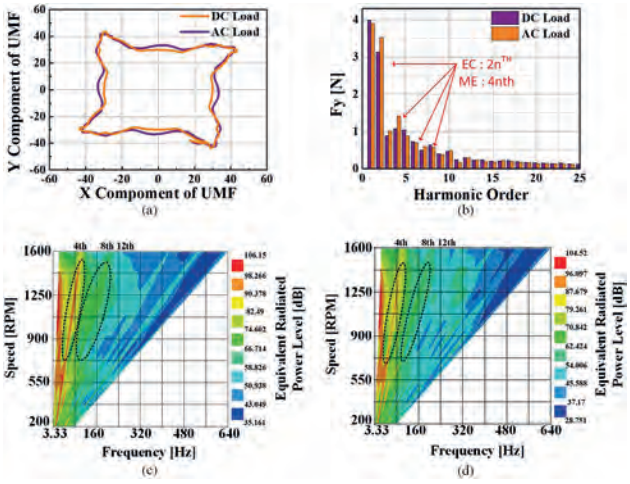

Fig. 2. Results of characteristic analysis: (a) UMF, (b) UMF FFT, (c) NVH characteristic of DC Load, and (d) NVH characteristic of AC Load.

ES-02. Optimization Design and Analysis of Axial Flux Permanent Magnet Motor with Halbach Array PM rotor Based on 3D Analytical Method. *M. Koo*[1], H. Shin[2] and K. Shin[3] *1. Automotive Materials & Components R&D Group, Korea Institute of Industrial Technology, Gwangju, The Republic of Korea; 2. Smart Agricultural Machinery R&D Group, Korea Institute of Industrial Technology, Gimje, The Republic of Korea; 3. Power System Engineering, Chonnam National University, Yeosu, The Republic of Korea*

An axial flux permanent magnet motor (AFPM) has been widely used in various industrial applications such as industries, in-wheel motor, drone propulsion motor, and related studies are being actively pursued [1]. Owing to its structural features and leakage flux in air-gap, the AFPM requires three-dimensional (3D) analysis methods. Various approaches for electromagnetic field analysis were addressed in previous studies including [2] and [3]. The finite element method (FEM) is a numerical method with high reliability, while its long analysis time is a drawback when 3D analysis is performed. In this paper, we propose an analytical approach that can consider the 3D effect of the AFPM. In particular, it is a method capable of considering a magnet segment ratio of a dual rotor of a split arrangement. Fig. 1(a) shows the 3D analysis model, which has a coreless stator and Halbach array PM rotor. In general, with this type of winding, the AFPM has a relatively larger magnetic air-gap; consequently, its electromagnetic characteristics in the radial direction are strongly influenced by end effects, resulting in fringing and leakage flux. To consider the tangential direction, the analysis model can be simplified as shown in Fig. 1(b). Fig. 1(c) shows the electromagnetic field analysis in the radial direction. Using Figs. 1(b) and (c), it is assumed that the r-θ plane is infinite for our initial analysis. Fig. 2(a) shows the magnetic flux density in air-gap using the proposed 3D analytical approach at full AFPM model. Fig. 2(b) and (c) are the magnetic field according to r-direction and no-load voltage performance obtained using the proposed method were compared with those obtained using the 3D FEM. As Fig. 2 cannot be easily obtained using 3D FEM, the proposed method is very effective because of its high reliability. The analytical approach, analysis, and discussions of AFPM with Halbach array PM will be explained in more detail in the full paper.

[1] J. F. Gieras, R, -J, Wang, and M. J. Kamper, *Axial Flux Permanent Magnet Brushless Machines*. Dordrecht, The Netherlands: Kluwer, 2004. [2] O. de la Barriere, S. Hlioui, H. Ben Ahmed, M. Gabsi, and M. LoBue, "3-D Formal Resolution of Maxwell Equations for the Computation of the No-Load Flux in an Axial Flux Permanent-Magnet Synchronous Machie," *IEEE Trans. Magn*., vol. 48, no. 1, pp. 128-136, Jan. 2012. [1] Y. Huang, B. Ge, J. Dong, H. Lin, J. Zhu, and Y. Guo, "3-D Analytical Modeling of No-Load Magnetic Field of Ironless Axial Flux Permanent Magnet Machine," *IEEE Trans. Magn*., vol. 48, no. 11, pp. 2929-2932, Nov. 2012.

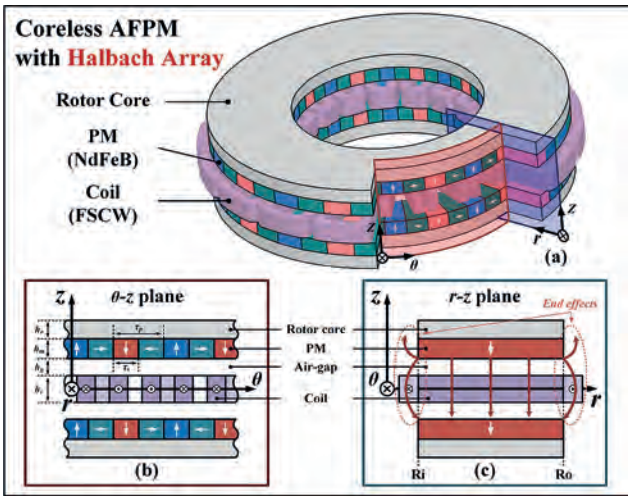

Fig. 1. (a) Analysis model, (b) end effects with overhang in θ-z plane, and (c) simplified magnetic field analysis model in r-z plane.

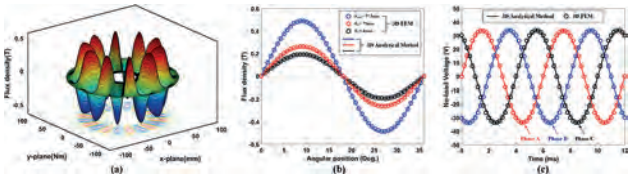

Fig. 2. (a) Axial flux density in air-gap, (b) comparison of axial flux density according to r-direction, comparison of back-EMF at 1000-rpm.

ES-03. Analytical Study and Experimental Verification for Electromagnetic Characteristics of Surface Mounted Permanent Magnet Synchronous Machine considering Semi-Closed Slot. *J. Yang*[1], H. Lee[1], M. Nguyen[1], T. Kim[1], K. Shin[2], Y. Kim[3] and J. Choi[1] *1. Electrical Engineering, Chungnam National University, Daejeon, The Republic of Korea; 2. Power System Engineering, Chonnam National University, Chonnam, The Republic of Korea; 3. Biosystems Machinery Engineering, Chungnam National University, Daejeon, The Republic of Korea*

Permanent magnet machines are widely used in modern electric-driven industries that require high power and efficiency, such as the robotic, aerospace, electric vehicle, and telecommunications industries. Therefore, designing technologies for permanent magnet machines is important and their electromagnetic characteristics should be quickly obtained. Analytical methods require short analysis periods and can be used to derive analytical solutions based on assumptions of geometry and material properties to easily understand electromagnetic phenomena. This study presents an analysis method for a surface-mounted permanent magnet synchronous motor with semi-closed slots. Figures 1 (a) and (b) show a model of a 6-pole, 27-slot surface-mounted permanent magnet synchronous motor and simplified model for employing the analytical method, respectively. The set used for the experiment and the shape of the stator are shown in Figures 1 (c) and (d), respectively. First, modeling based on the magnetization direction of the magnet and modeling of the current of the winding according to the pole slot combination were obtained using the Fourier series. The models were divided into each domain using the governing equations. Additionally, the circumferential and radial magnetic flux densities within the air gap were derived using boundary conditions. Figures 2 (a) and (b) show the magnetic flux density within the air gap derived using the analytical method and finite element method (FEM), and results of the fast Fourier transform (FFT) analysis, respectively. Moreover, back electromotive force (EMF) was derived using the magnetic vector potential. Figure 2 (c) shows the results of the EMF compared to FEM and experimental data. Additionally, the FFT analysis of the back EMF is shown in Figure 2 (d). More detailed equations and discussions are presented in the full paper.

[1] S. -M. Jang, H. -I. Park, and J. -Y. Choi, *IEEE Trans. on Magn*., vol. 47, p. 3586-3589 (2011) [2] C. He and T. Wu, *CES trans. electr. mach. syst.*, vol. 3, p.94-100 (2019) [3] V. Simón-Sempere, M. Burgos-Payán and J. -R. Cerquides-Bueno, *IEEE Trans. on Magn*., vol. 51, p. 1-10 (2015) [4] B. L. J. Gysen, K. J. Meessen, and J. J. H. Paulides, *IEEE Trans. on Magn*., vol. 46, p. 39-52 (2010)

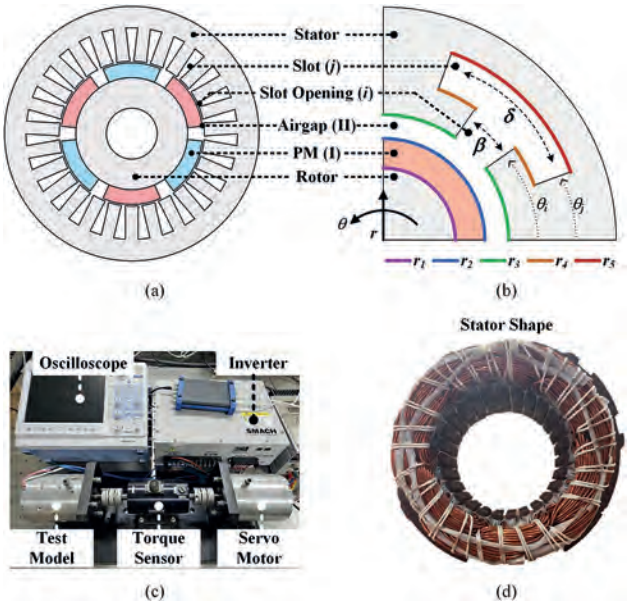

Fig. 1. (a) 6-pole 27-slot SPMSM model, (b) simplified analytical model, (c) experimental set, and (d) stator

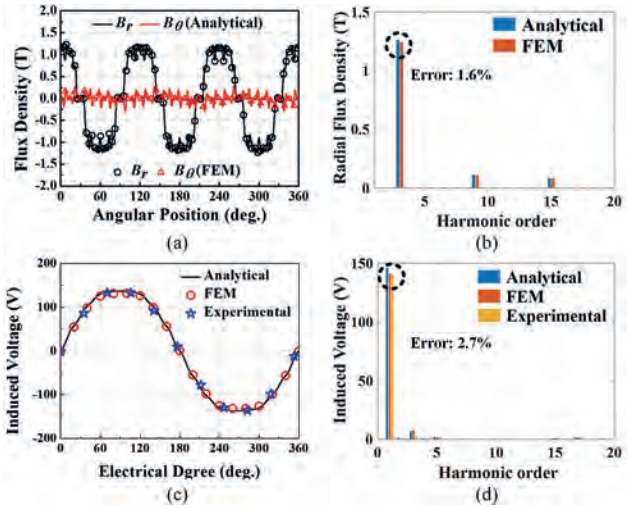

Fig. 2. Analysis results for the analysis model: (a) air gap magnetic flux density, (b) harmonic component of air gap magnetic flux density, (c) induced voltage, and (d) harmonic component of induced voltage

ES-04. Comparative Study on Heteropolar/Homopolar Magnetic Bearings for High-Speed Rotating Applications. *S. Noh*[1], J. Park[1], K. Shin[2] and H. Cho[3] *1. Department of Convergence System Engineering, Chungnam National University, Daejeon, The Republic of Korea; 2. Department of Power System Engineering, Chonnam National University, Yeosu, The Republic of Korea; 3. Department of Electric, Electronic and Communication Engineering Education, Chungnam National University, Daejeon, The Republic of Korea*

Non-contact magnetic bearings (MB) are increasingly important for high-speed and high-precision rotating machinery. This paper presents the design and evaluation of five types of magnetic bearings, incorporating electromagnets and permanent magnets to enhance power efficiency. Figure 1 illustrates various bearing configurations: an 8-pole conventional heteropolar MB (a), a pork-type heteropolar MB (b), and a hybrid pork-type MB with both permanent magnets and electromagnets (c). Additionally, there are homopolar magnetic bearing utilizing solely electromagnets (d) or a combination of electromagnets and permanent magnets (e). In order to enable a rigorous quantitative evaluation, the mechanical parameters were carefully standardized, including equal application of coil volume and current. Heteropolar bearings used laminated 35PN440 steel plates for stacking, while pure iron was employed for homopolar bearings due to stacking limitations. The bias current was determined considering the respective material properties. Control coefficients, such as position and current stiffness coefficients, were determined using analytical formulas. Using Ansys Electronics 2022 R2 program facilitated electromagnetic force analysis by varying displacement (±0.2mm in 0.1mm increments) along the x-axis and current (±2A in 1A increments). Linear control regions were determined through exhaustive analysis of the interdependencies between electromagnetic force, current, and displacement. Magnetic flux density was assessed at maximum control current, alongside loss characteristics evaluation at 30,000 rpm. Fig. 2(a) presents the current and position stiffness coefficients for each bearing type, while Fig. 2(b) illustrates the losses. Notably, for mechanically identical sizes and coil amounts, type (d) exhibited a 649% higher current stiffness coefficient compared to the smallest model, while type (b) demonstrated a 167% higher position stiffness coefficient.

Shilei Xu and Jinji Sun, IEEE Trans. On Magnetics, Vol. 50, pp.1-8 (2014)
Alexei Filatov, Larry Hawkins and Patrick McMullen, MDPI, pp.1-25 (2014)

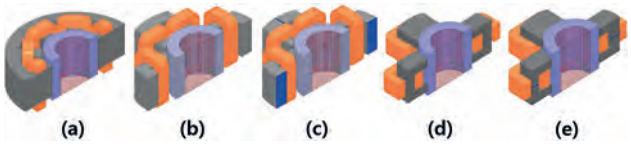

Fig. 1. (a) Conventional heteropolar MB (b) Pork-type heteropolar MB (c) Pork-type PM-biased heteropolar MB (d) Homopolar MB (e) PM-biased homopolar MB

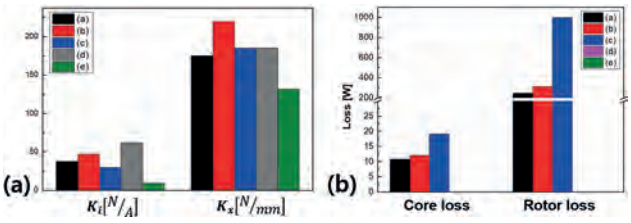

Fig. 2 Comparison between heteropolar, homopolar MB's (a) Ki, Kx (b) Core loss and rotor loss

ES-05. Experimental Verification and Electromagnetic Analysis of Axial Flux Permanent Magnet Motor Using the Subdomain Method. *J. Yang*[1], H. Lee[1], S. Kim[1], W. Jung[1], K. Shin[2], Y. Kim[3] and J. Choi[1] *1. Electrical Engineering, Chungnam National University, Daejeon, The Republic of Korea; 2. Power System Engineering, Chonnam National University, Chonnam, The Republic of Korea; 3. Biosystems Machinery Engineering, Chungnam National University, Daejeon, The Republic of Korea*

Axial flux permanent magnet motors (AFPMs) are used as in-wheel and compressor of electric vehicle because they can generate high torque density within a limited axial length. Additionally, AFPMs cannot be interpreted in 2D owing to their structure, and 3D analysis is required. However, 3D analysis entails a significant amount of time to confirm the analysis results based on the design variables employed, and it is difficult to determine the direct physical relationships between design variables. The subdomain method has exhibited reliable analysis results and entails a short analysis time. Therefore, it is suitable for AFPM design and analysis, whose initial design and optimization are challenging owing to the requirement of 3D analysis. Therefore, this study presents a method of deriving the electromagnetic characteristics of AFPM using the subdomain method. Figure 1 (a) shows the analysis model, whereas Figure 1 (b) shows a simplified model obtained through z-theta coordinates using the subdomain method. Figures 1 (c) and (d) show the experimental set and the actual manufactured rotor and stator, respectively. The governing equation was derived using the magnetic

vector potential. Thereafter, the solution of the governing equation for each region was obtained, and the flux density was derived by calculating the undetermined coefficient using boundary conditions. Figure 2 (a) shows the magnetic flux densities obtained in an air gap using the subdomain and finite element methods, and (b) shows the induced voltage. The back electromotive force values measured during the experiment are presented in Figure 2 (c), whereas (d) shows the result of comparing the analysis of the electromagnetic torque values with the experimental data. More details are provided in the full paper.

[1] W. Zhao, T. A. Lipo, and B. -I. Kwon, *IEEE Trans. on Magn*., vol. 50, p. 1-4 (2014) [2] Z. J. Liu, J. T. Li, and Q. Jiang, J. *Appl. Phys*., vol. 103, 07F135 (2008) [3] T. Lubin, S. Mezani, and A. Rezzoug, *IEEE Trans. on Magn*., vol. 47, p. 479-492 (2011) [4] Jikai Si, Tianxiang Zhang, and Rui Nie, *IEEE Trans. Energy Convers*., vol. 70, p.1216-1228 (2023)

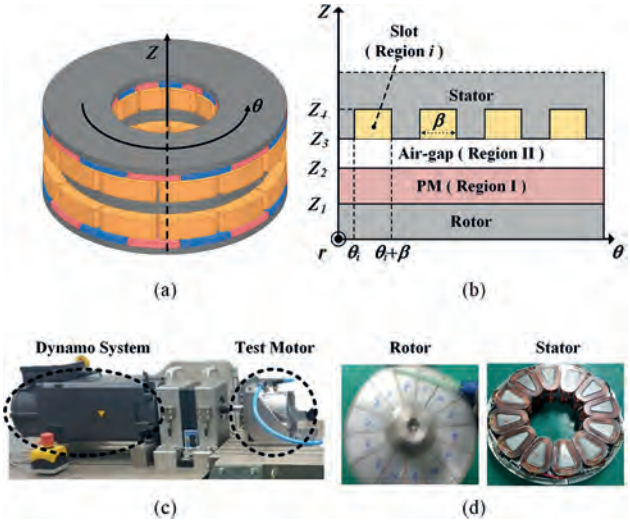

Fig. 1. Axial flux permanent magnet motor: (a) analysis model, (b) simplified analytical model, (c) experimental set, and (d) actual manufactured rotor and stator

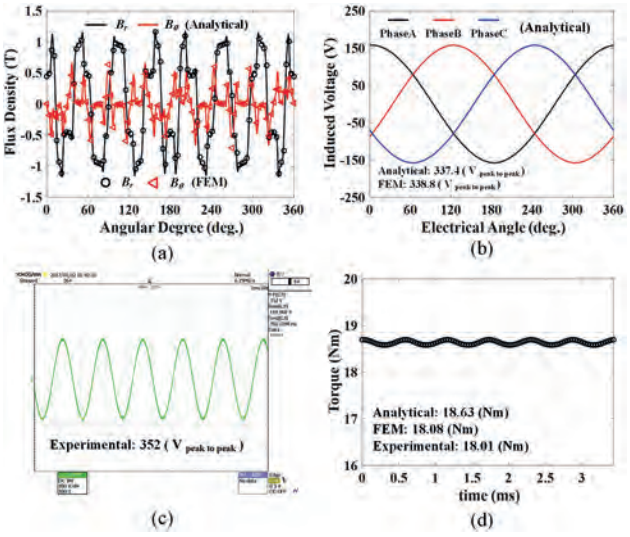

Fig. 2. Analysis results of analysis model ((a) magnetic flux density and (b) induced voltage), (c) measured back EMF, and (d) comparison of analytical, FE and measured results for electromagnetic torque

ES-06. Characteristics Analysis and Experimental Study on Vibration from Electromagnetic Excitation Source of Permanent Magnet Synchronous Generator using Subdomain Method. *K. Shin*[1], J. Choi[2], K. Kim[3] and H. Cho[2] *1. Chonnam National University, Yeosu, The Republic of Korea; 2. Chungnam National University, Daejeon, The Republic of Korea; 3. Korea Research Institute of Ships and Ocean Engineering, Daejeon, The Republic of Korea*

Permanent magnet synchronous generators (PMSGs) have the drawback of vibration caused by the interaction between the stator teeth and the rotor magnets, significantly affecting the machine's performance [1]. The electromagnetic excitation source is the dominating one in low- to medium-power rated machines. Cogging torque, torque ripple, and unbalanced magnetic forces are the major electromagnetic vibration sources. Therefore, it is desirable to account for these electromagnetic sources at the design stage. In this paper, an analytical solution based on Fourier analysis is proposed to compute the cogging torque, torque ripple, and unbalanced magnetic forces in PMSGs, as shown in Figs. 1(a) and 1(b). The magnetic field solutions are obtained using a magnetic vector potential and a boundary condition [2]. Based on these solutions, the electromagnetic torque and force are determined analytically. Figs. 1(c) and 2(d) show the results of the electromagnetic source analysis according to pole arc to pole pitch ratio. To verify the analytical results of the proposed method, an experimental system was implemented on a servomotor with a torque sensor and a gap sensor, as shown in Fig. 2(a). The forced vibration analysis was performed by mapping the electromagnetic force with the air gap, which converted the harmonic orders generated by electromagnetic analysis using ANSYS EM and WORKBENCH, as shown in Fig. 2(b). Fig. 2(c) shows the results of the loci graph for the displacement of the rotor in the x and y direction under the rated condition. Therefore, the proposed analysis method could be very useful in the initial design and optimization process of PMSGs for improving electromagnetic vibration. The detailed analysis results, discussions, and measurements of the PMSMs will be presented in the full paper.

[1] V. Simon-Sempere, M. Burgos-Payan, J.-R. Cerquides-Bueno, *IEEE Trans. Magn.*, Vol. 51, Art. no. 8105910, (2015). [2] B. L. J. Gysen, K. J. Meessen, J. J. H. Paulides, E. A. Lomonova, *IEEE Trans. Magn.*, Vol. 46, pp. 39-52, (2010).

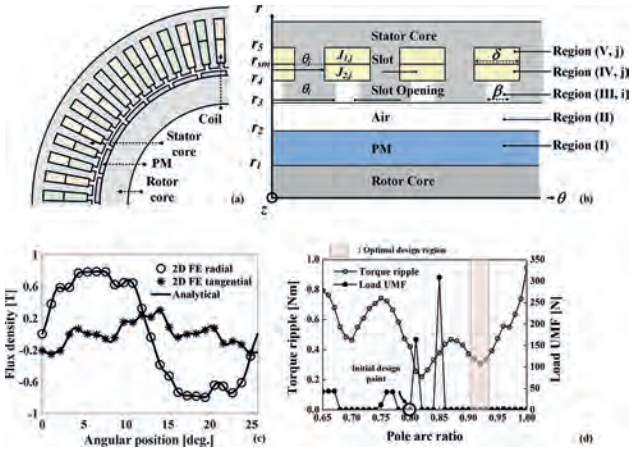

Fig. 1. (a) Analysis model of PMSG, (b) analytical model, (c) magnetic flux density from analytical and FEM results, and (d) electromagnetic vibration source analysis according to pole arc ratio.

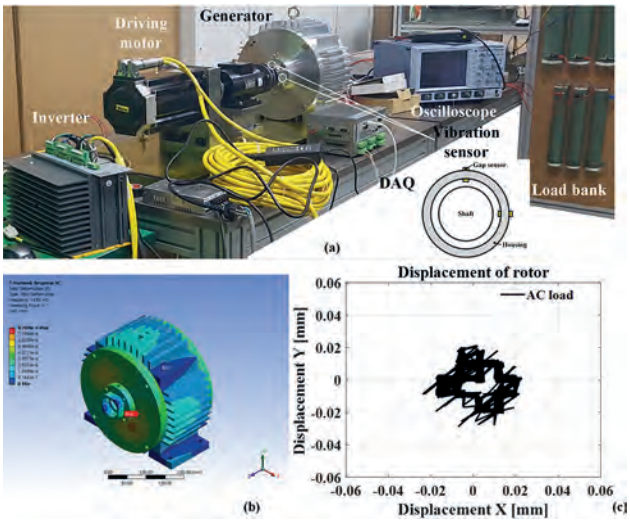

Fig. 2. (a) Experimental setup for force and torque measurement, (b) analysis on harmonic response, and (c) displacement of the rotor under AC load conditions.

ES-07. Characteristic Analysis of Bearingless Motor Considering 3D Leakage Flux Using Equivalent Multilayer Method. *M. Koo*[1], H. Shin[2] and K. Shin[3] *1. Automotive Materials & Components R&D Group, Korea Institute of Industrial Technology, Gwangju, The Republic of Korea; 2. Smart Agricultural Machinery R&D Group, Korea Institute of Industrial Technology, Gimje, The Republic of Korea; 3. Power System Engineering, Chonnam National University, Yeosu, The Republic of Korea*

A bearingless motor can be seen as a motor type in which a magnetic bearing and a motor are integrated into one. Therefore, it possesses the advantages of compact size, simplified structure, and reduction cost in comparison to a magnetic bearing and motor system [1]. We electromagnetic analyze a bearingless motor with slice stator, taking in to consideration leakage flux of 3D effects. Fig. 1(a) shows the structure and components of the slice-type bearingless motor. In particular, the structure of the stator is deformed in an axial direction, and as shown in Fig. 1(b), a large leakage occurs in a magnetic flux path due to distortion and saturation of a magnetic field during a full-load condition, and thus a 3-D analysis is essentially required. Fig. 1(c) shows the structural specificity and the density of magnetic flux leaking into the air region at full-load conditions due to magnetic flux saturation. However, although the performance of computers and analysis tools has recently improved, the design and interpretation of the bearingless motor based on 3D analysis may be a high burden, and interpretation may be limited according to parameter changes. Therefore, there is a need for an analysis technique capable of considering leakage effects in the air region as shown in Fig. 1(d). Thus, in this study, a method of generalizing the permittivity of slots by dividing them into multilayers was proposed [2]. Fig. 2(a) shows the magnetic flux path of the load of the existing 2D model and the proposed method applied. As shown in the Fig. 2(a), it can be seen that a leakage effect occurs in the slot in the proposed method. In addition, Fig. 2(b) shows the torque analysis results under the full-load condition, and it can be confirmed that the proposed 2D analysis method almost matches the 3D FEM result considering the leakage effects and have high reliability. In the complete manuscript, we will present the physical phenomenon used to aid the related research and industrial applications.

[1] A. Chiba, T. Fukao, O. Ichikawa, M. Oshima, M. Takemoto, and D. G. Dorrell, *Magnetic Bearings and Bearingless Drives*. Amsterdam, The Netherlands" Elsevier, Mar. 2005. [2] J. Y. Jung, H. I. Park, J. P. Hong, and B. H. Lee, "A Novel Approach for 2-D electromagnetic Field Analysis of Surface Mounted Permanent Magnet Synchronous Motor Taking Into Account Axial End Leakage Flux," *IEEE Trans. Magn*., vol. 53, no. 11, Jan. 2012, Art. No. 8208104.

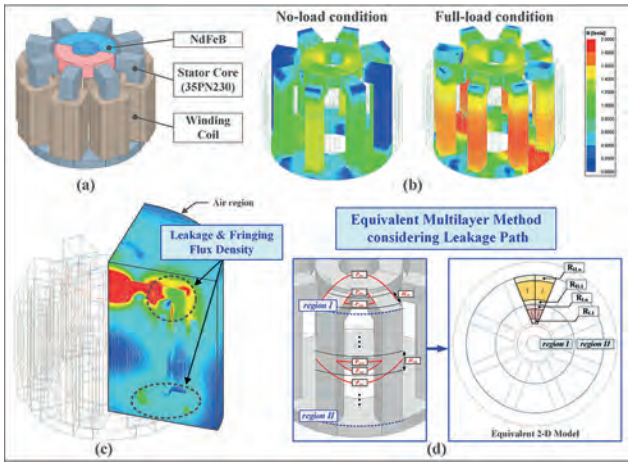

Fig. 1. (a) Analysis model, (b) 3-D flux density, (c) Leakage flux density, and (d) Equivalent 2-D coupled model.

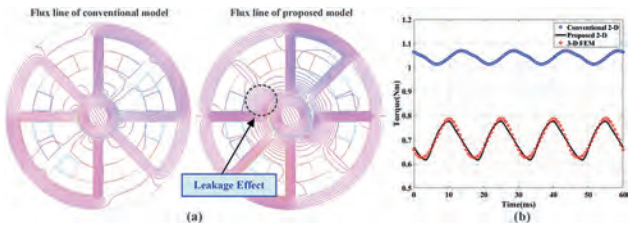

Fig. 2. (a) Comparative leakage flux line, (b) Electromagnetic torque according to analysis methods.

ES-08. Characteristic analysis for Improving Detent Force of Linear Oscillatory Generator with Spring Permanent Magnet for Stirling Engines Based on Subdomain Method. *K. Shin*[1], J. Choi[2], H. Cho[2], M. Koo[3], K. Lee[3] and S. Lee[3] *1. Chonnam National University, Yeosu, The Republic of Korea; 2. Chungnam National University, Daejeon, The Republic of Korea; 3. Korea Institute of Industrial Technology, Gwangju, The Republic of Korea*

A single-phase linear oscillatory generator (LOG) is widely used in direct-drive systems such as the Stirling engine system due to its advantages such as high transmission efficiency and simple structure as shown in Fig. 1 [1], [2]. However, one of their drawbacks is the generation of detent force caused by the attraction between the permanent magnet (PM) and the iron core. A large detent force causes thrust ripples and noise, which results in poor positioning accuracy [3]. Therefore, the characteristic analysis and improvement of the detent force is a key factor to be considered in the design of the LOG with spring PM. To solve these problems, this study proposes an electromagnetic analysis using an analytical method to optimize the detent force by applying spring PM to the PM mover [1]. This paper derives analytical solutions in terms of magnetic vector potential based on the subdomain model as shown in Figs 1 (b) and (c). From the analytical solution, the electromagnetic force is derived using the Maxwell stress tensor. The validity of the proposed method is verified through comparison with the results of finite element (FE) analysis as shown in Figs. 2 (a) and (b). Fig. 2 (c) shows the analysis result of the detent force according to the width of the spring PM at a minimum position of the stroke. Therefore, positive values of the detent force are generated to use restoring force. Fig. 2 (d) shows the comparison between the detent force with and without spring PM. It is observed that the direction of the detent force changes in the spring PM model and the force is hardly generated in the stroke region. The analytical technique, analysis results, discussions, and measurements of the LOG will be presented in more detail in the full paper.

[1] J.-M. Kim, J.-Y. Choi, K.-S. Lee, and S.-H. Lee, *AIP Adv.*, Vol. 7, Art. no. 056667 (2017). [2] J. Sjölund, M. Leijon, S. Eriksson, *AIP Adv.*, Vol. 10, Art. no. 035312 (2020). [3] K. H. Shin, K. H. Kim, K. Hong, J. Y. Choi, *IEEE Trans. Magn.*, Vol. 53, Art. no. 810450 (2017).

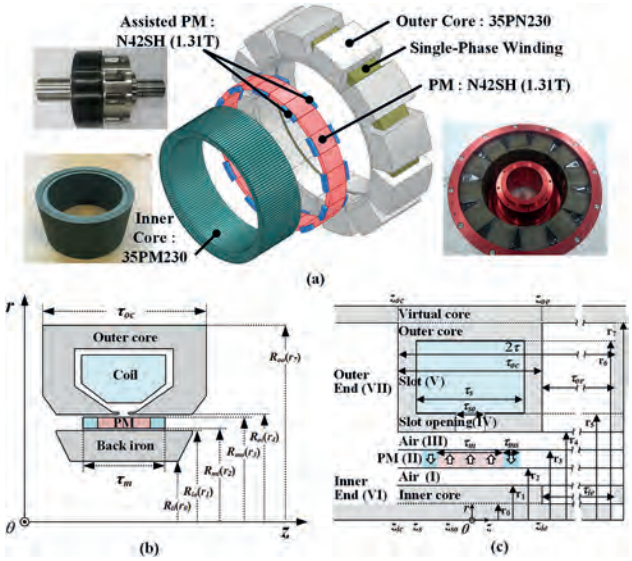

Fig. 1. Structure of single-phase LOG with spring PM: (a) prototype, (b) analysis, and (c) analytical model.

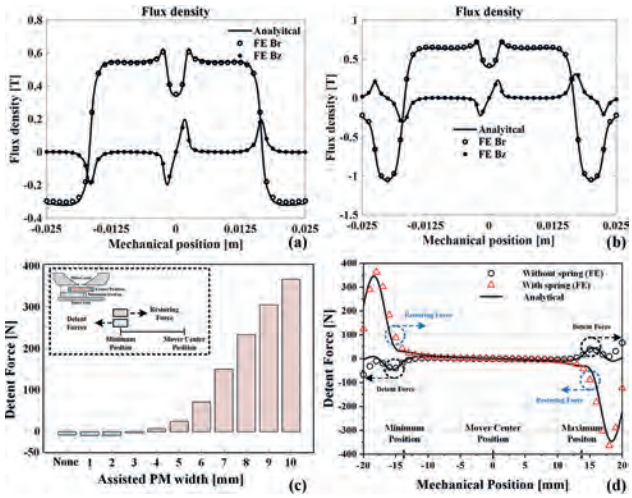

Fig. 2. Comparison between analytical and FE results: flux density without (a) spring PM and (b) with spring PM, (c) detent force according to the width of spring PM, and (d) detent force with and without spring PM.

ES-09. Electromagnetic Analysis and Experimental Study of Permanent Magnet Synchronous Machine with Segmented Phase Modular Stator.

J. Lee[1], K. Yu[1], H. Ban[1], J. Choi[2], K. Kim[3], H. Cho[2] and K. Shin[1] *1. Chonnam National University, Yeosu, The Republic of Korea; 2. Chungnam National University, Daejeon, The Republic of Korea; 3. Korea Research Institute of Ships and Ocean Engineering, Daejeon, The Republic of Korea*

To improve the electromagnetic performance and ease the manufacturing process, particularly stator winding, it is often able to employ a modular stator, e.g., individual stator tooth/back-iron segments, or separate stator tooth segments and back-iron segments [1, 2]. Among them, stator tooth segmentation and back-iron segmentation are the key solutions to ease the process of manufacturing PMSM. However, due to the limitations in the manufacturing process and the tolerances between stator segments, there are additional air gaps. In practice, such air gaps are likely to be non-uniform due to manufacturing tolerances. In this study, a PMSM with a segmented modular stator with concentrated winding is proposed and the performance analysis results are presented. The proposed model is a structure that can be usefully utilized not only for the increase in power density and specific power but also for maintenance when a failure occurs in each phase. As shown in Figs. 1(a) and 1(b), based on the 'Star of Slots' theory, a pole slot combination that enables phase concentrated winding is presented. Considering the tolerances that may occur during the manufacturing process, the electromagnetic analysis based on finite element analysis are performed as shown in Figs. 1(c) and 1(d). To confirm the reliability of the analysis results, a prototype and test set are constructed as shown in Fig. 2(a). As shown in Figs. 2(b) and 2(c), the error analysis and causes between the experimental results and the analysis results are presented. The electromagnetic modeling, analysis results, performance rating, and discussion of PMSM with segmented phase modular stator will be presented in the full paper.

[1] Z. Q. Zhu, Z. Azar, and G. Ombach, IEEE Trans. Magn., Vol. 48, pp. 2049–2055 (2012). [2] N. J. Baker, D. J. B. Smith, M. C. Kulan, and S. Turvey, IEEE Trans. Energy Convers., Vol. 33, pp. 40–48, (2018).

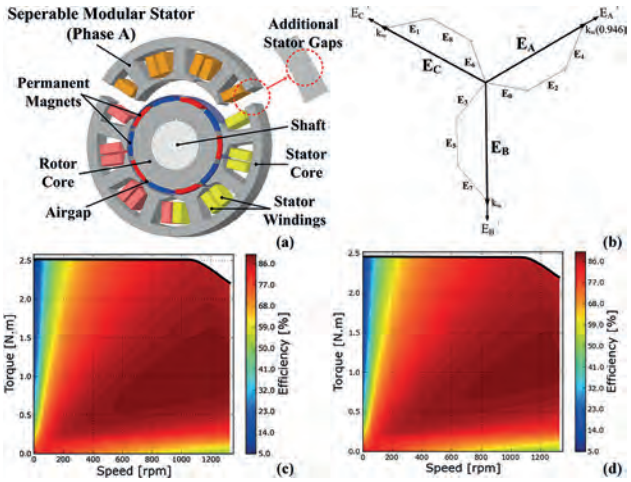

Fig. 1. (a) Schematics of PMSM with segmented modular stators, (b) EMF phasor diagram for 10-pole and 9-slot PMSM, Efficiency map considering the additional air gaps between stator core modules: (c) 0.0mm and (d) 0.2mm.

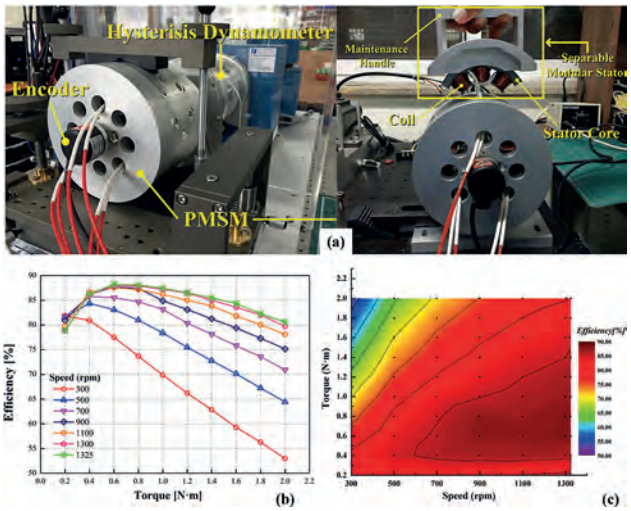

Fig. 2. Experimental setup and results: (a) experimental system, (b) efficiency curve according to defined torque and speed, and (c) efficiency map with the experimental results at each test point.

ES-10. Electromagnetic Analysis of Wound Rotor Synchronous Machine using Improved Subdomain Technique considering Finite Permeability of Core. *K. Yu*[1], H. Ban[1], J. Lee[1], K. Shin[1], J. Choi[2], S. Sung[3] and J. Park[3] *1. Chonnam National University, Yeosu, The Republic of Korea; 2. Chungnam National University, Daejeon, The Republic of Korea; 3. Korea Research Institute of Ships and Ocean Engineering, Daejeon, The Republic of Korea*

Brushless WRSM are designed to work in harsh environment conditions such as high temperature and high humidity [1], [2]. Therefore, brushless WRSM is an alternative to permanent magnet synchronous machine (PMSM), which has problems of weaponization of resources and environmental destruction. Since brushless WRSM can be applied to various applications, development of WRSM design and analysis methods is required. In this paper, an electromagnetic field analysis of WRSM using an improved analytical method considering the permeability of core is proposed. As shown in Fig. 1, simplified analytical model considering the magnetic permeability of each region is presented. The governing equations of each region are derived from Maxwell's equations and electromagnetic field theories [3], and a two-dimensional general solution is derived by considering components in the radial and circumferential directions using mathematical techniques. The analytical solution of all domains is derived by calculating the boundary conditions. To verify the validity of the proposed analytical method, the radial and circumferential magnetic flux density results were compared with finite element analysis (FEA) results, as shown in Figs. 1(c) and 1(d). In addition, electromagnetic performance results such as flux linkage, back-EMF, and torque were presented using electromagnetic theories. In particular, as shown in Fig. 2, magnetic saturation of soft magnetic material is caused by field current, and the superiority of the proposed method was demonstrated by comparing the improved analytical method considering the global saturation of each region with the nonlinear FEA result considering the local saturation. The analytical technique, analysis results, discussions, and measurements of the WRSM will be presented in more detail in the full paper.

[1] G. Jawad, Q. Ali, T. A. Lipo, and B.-I. Kwon, IEEE Trans. Magn., Vol. 52, Art. no. 8106104, (2016). [2] A. Di Gioia et al., IEEE Trans. Ind. Appl., Vol. 54, pp. 1390–1403, (2018). [3] L. Roubache, K. Boughrara, F. Dubas, and R. Ibtiouen, IEEE Trans. Magn., Vol. 54, Art. no. 8103315, (2018).

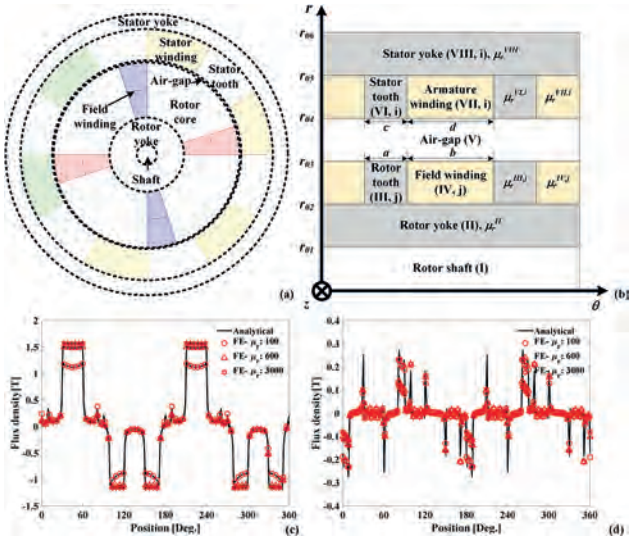

Fig. 1. Analysis model and results of WRSM: (a) 2D FE model, (b) simplified analytical model, (c) radial flux density, (d) tangential flux density.

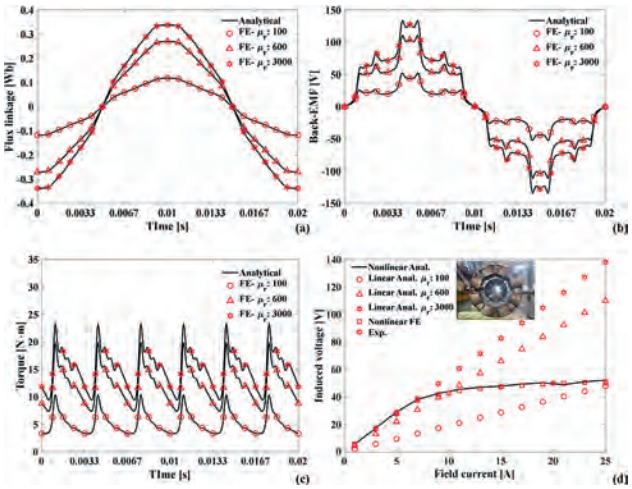

Fig. 2. Comparison of electromagnetic performances according to permeability of soft magnetic material based on analytical, FEA, and experimental results: (a) flux linkage, (b) back-EMF, (c) electromagnetic torque, and (d) back-EMF according to field current.

ES-11. Improved Design and Analysis for Electromagnetic Performance of Magnetic Geared Permanent Magnet Machine According to Pole/Slot Combination. *K. Yu*[1], H. Ban[1], J. Lee[1], K. Shin[1], J. Choi[2], S. Sung[3] and J. Park[3] *1. Chonnam National University, Yeosu, The Republic of Korea; 2. Chungnam National University, Daejeon, The Republic of Korea; 3. Korea Research Institute of Ships and Ocean Engineering, Daejeon, The Republic of Korea*

Magnetic-geared permanent-magnet (MGPM) machines are known for their high-torque density and high efficiency [1]. The major challenges of MGPMMs include high manufacturing cost, complex control, increased maintenance cost, and high-frequency noise [2]. In particular, the increase in vibration and the decrease in efficiency and power factor of the MGPMMs are problems to be solved because they are related to the decrease in system performance. Therefore, this paper presented a comprehensive electromagnetic analysis and performance improvement according to pole-slot combinations and gear ratios. As shown in Fig. 1, a MGPMM typically consists of a rotor with permanent magnets and a stator with windings. The complicated structure and non-linear operating conditions of MGPM machines effectively prohibit the use of analytical modeling techniques. Therefore, this study relies on two- and three-dimensional (2D and 3D) finite-element analysis (FEA) to deal with the detailed calculation of the considered loss mechanisms. Four typical configurations are considered for the stator: 12, 24, 36, and 48 slots as shown in Fig. 2(a). To compare the different designs, the same stator dimensions, number of windings turns to satisfy the same induced voltage, and winding factor are assumed throughout the analysis. The calculation of MGPM machine losses considers the existence of three loss sources: copper loss, rotor eddy current loss, and core loss. Fig. 2(b) shows the core losses distribution for the considered stator configurations. To evaluate eddy current losses, magnet segmentation must be considered in the 3D FEA. The reduction in resistive losses for different magnet segmentation levels is shown in Fig 2(c). The design, analysis, and discussion of MGPM machines will be presented in more detail in the final paper, along with the analysis results.

[1] L. Jing, W. Tang, T. Wang, T. Ben, and R. Qu, IEEE Trans. Transp. Electrific., Vol. 8, pp. 2874–2883, (2022). [2] K. Atallah, J. Rens, S.Mezani, and D. Howe, IEEE Trans. Magn., Vol. 44, pp. 4349–4352, (2008).

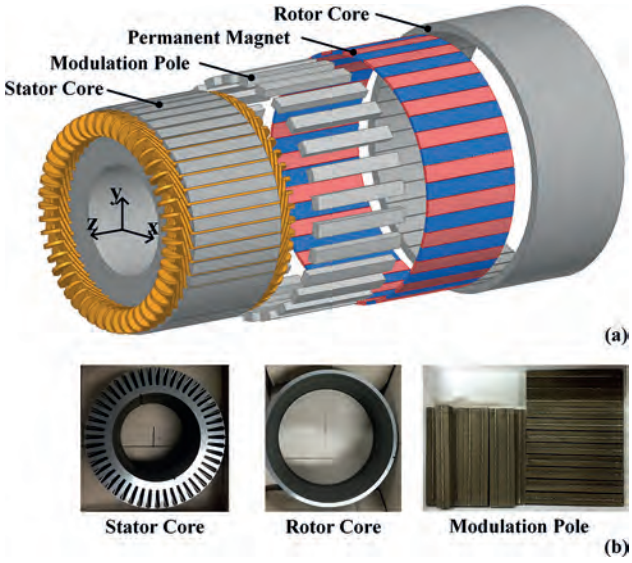

Fig. 1. Structure of the MGPM machine: (a) analysis model and (b) parts for prototype.

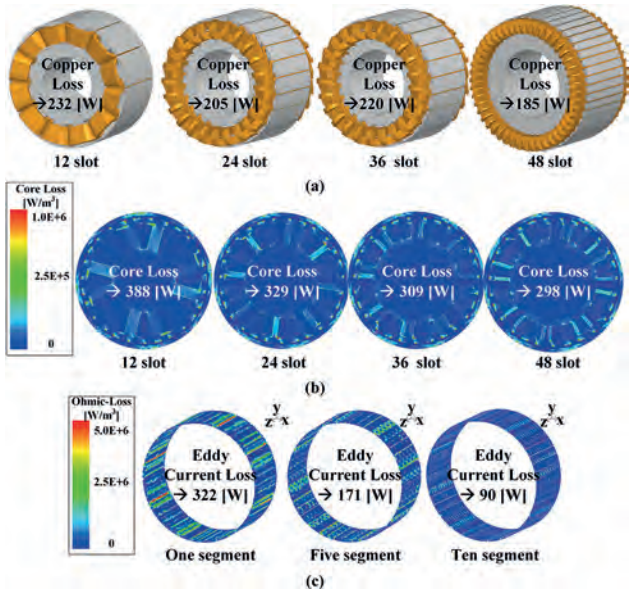

Fig. 2. Electromagnetic losses under rated condition: (a) four stator configurations with copper loss, (b) core loss distribution with stator configurations, and (c) eddy current losses in PM for different numbers of PM segments.

ES-12. A Study on Motor Characteristics Based on Pole-Slot Combinations. *S. Kim[1] 1. Korea Electronics Technology Institute, Gangju Metropolitan City, The Republic of Korea*

Motors, electrical devices with a century-long history, are the largest consumers of electricity worldwide. According to statistics, motors account for approximately 45% of global electricity usage. They have been extensively employed in various applications such as factories, households, automobiles, and ships, where mechanical power is required. Therefore, I believe that developing high-efficiency motors can naturally contribute to the global effort of reducing carbon emissions. One of the primary aspects in motor development is determining the combination of pole numbers and slot numbers. This crucial decision is essential for creating efficient motors that align with specific objectives. The selection of pole numbers and slot numbers varies depending on the application, manufacturing costs, and the utilization of divided cores. Consequently, the determination of the combination of pole numbers and slot numbers holds significant importance. In this paper, I aim to analyze the characteristics of widely used structures, namely the 8-pole 12-slot, 6-pole 9-slot, and 8-pole 9-slot combinations, to examine which application benefits the most from each configuration. Additionally, I propose a solution to address the structural limitations and electromagnetic shocks associated with the 8-pole 9-slot design. My proposed method involves increasing the combination of pole numbers and slot numbers in multiples, such as the 16-pole 18-slot, 24-pole 27-slot, and 32-pole 36-slot configurations. I have validated these methods through numerical analysis using simulations. Furthermore, I have complemented the simulation results by fabricating a motor with a 24-pole 27-slot configuration.

[1] Ming-Shi Huang; Kuan-Cheng Chen; Tse-Kai Chen; Yu-Chiang Liang; Guan-You Pan, "An Innovative Constant Voltage Control Method of PMSM-Type ISG Under Wide Engine Speed Range for Scooter With Idling Stop," vol. 7, pp. 20723–20733 [2] G. Friedrich and A. Girardin, "Integrated starter generator," IEEE Ind.Appl. Mag., vol. 15, no. 4, pp. 2634, Jul. 2009. [3] Jae-Woo Jung; Sang-Ho Lee; Geun-Ho Lee, "Reduction Design of Vibration and Noise in IPMSM Type Integrated Starter and Generator for HEV," in Magnetism, vol. 46, pp. 2454–2457. [4] Natural Resources Canada. (2018). Learn the Facts: Idle Stop-Start Technology and Its Effect on Fuel Consumption. [Online]. Available: nhttp://www.nrcan.gc.ca/energy/efciency/transportation/cars-lighttrucks/ buying/16757 [5] HONDA. (2018). What is the Idling Stop System. [Online]. Available: http://world.honda.com/motorcycle-picturebook/idling-top/index.html

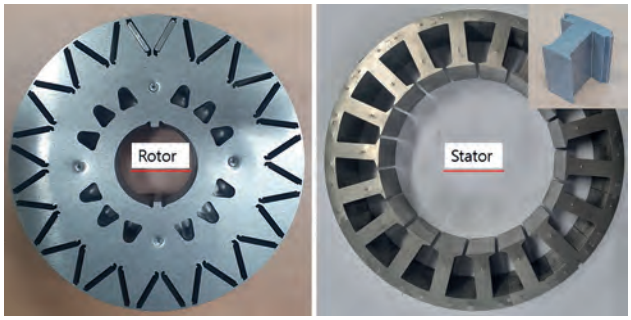

Fabricated core shape of 16 poles and 18 slots

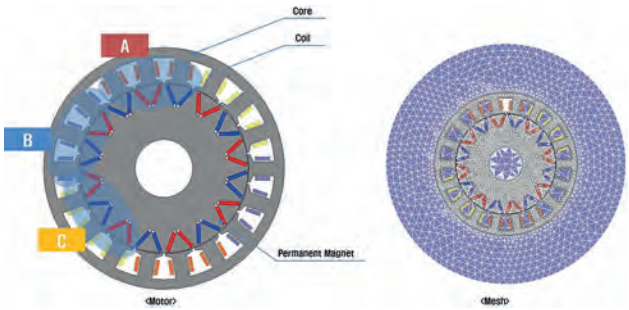

Simulation modeling of 16 poles and 18 slots

ES-15. Design of Continuous Repeater Power Transmission Coil for Wireless Power Transfer System for EVs with Consideration of Vehicle Deviation. *A. Saito[1], Y. Oishi[1], S. Miyahara[3], F. Sato[1] and H. Matsuki[2] 1. Graduate School of Engineering, Tohoku Gakuin University, Sendai, Japan; 2. New Industry Creation Hatchery Center (NICHe), Tohoku University, Sendai, Japan; 3. Tohoku Gakuin University, Sendai, Japan*

In recent years, EVs have become increasingly popular around the world, and research on wireless power supply technology for EV driving has been acting accordingly. In order to realize this wireless power transfer system for EVs on a real scale, it is necessary to lengthen the power supply section per power supply unit and to secure a sufficient power supply section with

a small number of power supply units as a whole. A single coil method that extends a single coil has been proposed as a solution to this problem. However, since the resistance loss increases as the coil length increases, resulting in a decrease in efficiency, it is necessary to propose a method that can extend the feeding section while keeping the coil length constant to some extent. We propose a repeater coil method. This method extends the feed section by inserting a booster repeater coil between each transmission coil, which acts as a bridge between the two coils. This allows the use of a minimum length of coils, reducing efficiency loss due to resistance loss. It is necessary to consider transient phenomena in this in-transit power-feeding system when the EV to be fed deviates from the feeding lane. For this reason, we have proposed a new repeater coil configuration for the transmission side that assumes no-load conditions. In this study, a new repeater coil system combining rectangular coils and orthogonal coils is proposed, which enables stable feeding of power to EVs by rectangular coils and response to transient phenomena. A comparison was also made with the single coil method that has been studied previously. Schematic diagrams of each method used in the comparison experiments and the experimental results are shown in Fig. 1 and 2. In this study, a spiral coil is assumed to be used as the receiving coil on the EV side. The result, the newly proposed repeater coil system, which repeats the current from the transmitter coil to which the power supply is connected, narrowed the range where the power supply efficiency drops significantly. It was also confirmed that a stable power supply was possible.

[1] ABE Hideaki: "Non-Contact Energy Transfer Equipment for Home Appliances", The journal of the Institute of Electrical Engineers of Japan 128(12), 808-811, (2008) [2] Dukju Ahn, Songcheol Hong: "A Study on Magnetic Field Repeater in Wireless Power Transfer", IEEE Trans, Vol 60, No.1, pp.1373-1382 (2013) [3] MISAWA: "Relationship between Feeding Coil Size and Transmission Efficiency of Contactless Power Transmission for Moving Electric Vehicle", IEICE Technical Report WPT2012-33, (2012) [4] N. Aruga et al.: "A Study on a Contactless Charging System for Moving Electric Vehicles with a Full-Scale Model", Journal of the Magnetics Society of Japan, Vol. 39, No. 3, pp. 121-125 (2015) [5] H. Abe, "Resonant Voltage Transient Phenomenon Analysis and Design Precautions for Magnetic Coupled Wireless Power Transfer," IEICE Technical Report, WPT2020-28,(2020)

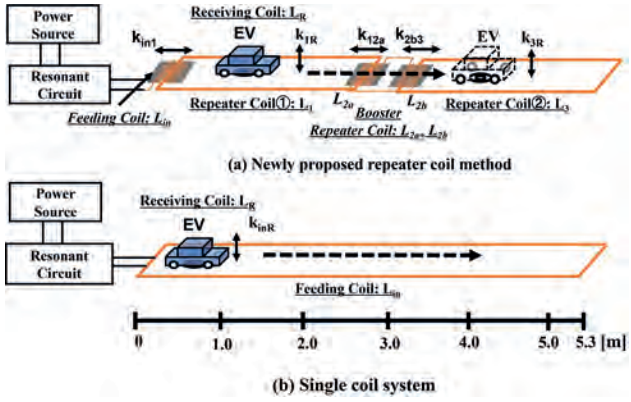

Schematic diagram of the system used in the experiment

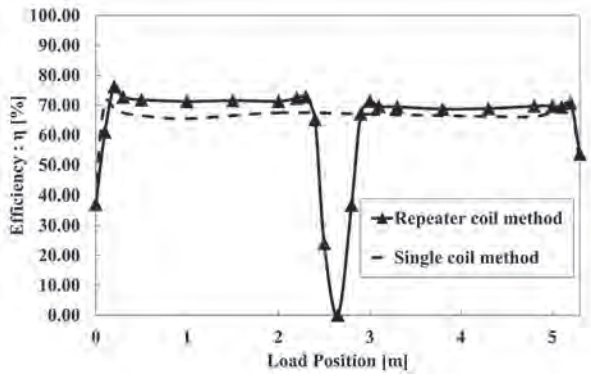

Experimental results

ES-16. Trade-off Between Torque Ripple and Vibration in a IPMSM by Examining the Temporal and Spatial Harmonics of Flux Density.

S. Lee[1], G. Yun[1], G.F. Lukman[1] and C. Lee[1] *1. Electrical Engineering, Pusan National University, Busan, The Republic of Korea*

Interior permanent magnet synchronous motors (IPMSMs) are widely used in various applications due to their high efficiency, high power density, and excellent control characteristics. However, the use of permanent magnet inside the lamination stack of a rotor presents two challenges, and one is torque ripple caused by rotor core saliency. In many cases, the other challenge is electromagnetic vibration leading to noise, and this physical impact causes the deterioration of overall performance in IPMSMs [1-2]. Despite the continuous effort of previous studies on torque ripple minimization, vibration is not significantly improved in a logical manner without identifying the relationship between those two performances. The reason for this lack of coherence is that torque is dependent only on tangential force, but vibration is proportional to radial force. In other words, trade-off between torque ripple and vibration is not straightforward at all. In this paper, the relationship between torque ripple and vibration in IPMSMs is investigated by examining air-gap flux density in the radial and tangential direction. The analysis of temporal and spatial harmonics in flux density is conducted in a 6-pole/9-slot IPMSM as a reference pole/slot combination. In Fig. 1, the height of two tips on a stator pole shoe (SH1 and SH2) is chosen as a design parameter. In my previous study [3], it is noted that the height of the tips is critical to reduce torque ripple. However, as shown in Fig. 2, this result does not match the case of vibration with respect to the height of SH1 and SH2. As mentioned above, this discrepancy between torque ripple and vibration is reasonable since their governing equations are totally different each other. In Fig. 2, twelve combinations regarding SH1 and SH2 are compared in terms of torque ripple as depicted in lines and vibration given by a bar graph. In my full paper, it is expected that trade-off between the two key characteristics in an IPMSM gives peer engineers and researchers some insights into a multi-physical design.

[1] C. Peng, D. Wang, B. Wang, IEEE Transactions on Magnetics, vol. 58, no. 9, pp. 1-5 (2022) [2] Zamani Faradonbeh, V., Taghipour Boroujeni, S., Takorabet, N, Electr Eng, Vol. 102, 1117–1127 (2020) [3] Sangjin Lee, Changhwan Kim, Yongha Choo, *AIP Advances,* Vol.13, no.2, pp. 025313 (2023)

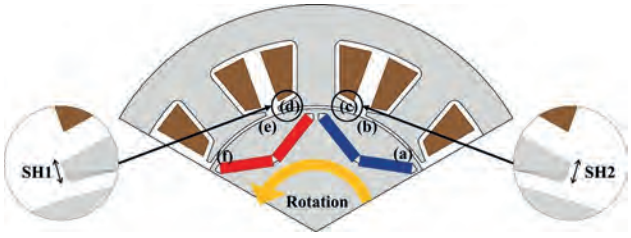

Modification of stator pole tips.

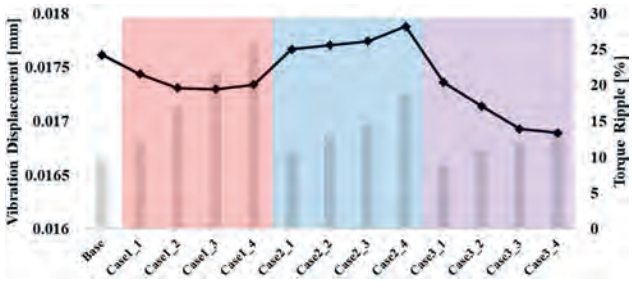

Vibration displacement (bar graph) and torque ripple (line) in twelve cases compared to base.

Session FA
IMAGING MAGNETIC TEXTURES AT THE NANOSCALE

Jack C Gartside, Chair
Imperial College London, London, United Kingdom

INVITED PAPERS

FA-01. Tailoring Ferromagnetic and Antiferromagnetic Spin Textures in Nanostructured Complex Oxides. *Y. Takamura*[1], D.Y. Sasaki[1], M. Lee[1], R.V. Chopdekar[2], A. Scholl[2], S.T. Retterer[3], P.S. Rickhaus[4] and J. Lenz[4] *1. Materials Science and Engineering, University of California, Davis, Davis, CA, United States; 2. Advanced Light Source, Lawrence Berkeley National Laboratory, Berkeley, CA, United States; 3. Center for Nanophase Materials Sciences, Oak Ridge National Laboratory, Oak Ridge, TN, United States; 4. QNami, Muttenz, Switzerland*

The development of spintronic devices based on the patterning of antiferromagnetic (AFM) materials or coupled ferromagnetic (FM)/AFM systems has received significant interest in recent years due to promising characteristics including fast operating speeds, nanoscalability, and stability against stray magnetic fields. However, challenges remain in terms of the control and detection of AFM spin textures, particularly in nanoscale geometries needed for device implementation. Complex oxide heterostructures such as the FM/AFM $La_{0.7}Sr_{0.3}MnO_3$ (LSMO)/$La_{1-x}Sr_xFeO_3$ (LSFO) system provide a unique opportunity to control the orientation of the AFM Néel vector through interfacial spin-flop coupling where the FM and AFM layers maintain a perpendicular orientation relative to one another and can be reoriented with modest applied magnetic field values (~0.1 T).[1] Furthermore, micro- and nanoscale patterning provides an intriguing means to tailor both the FM and AFM spin textures in the coupled LSMO/LSFO systems. In this work, an ion implantation-based patterning process was used to define magnetic islands embedded within a non-magnetic matrix.[2] The combination of x-ray photoemission electron microscopy and scanning N-V magnetometry was used to image the resulting spin textures and these images demonstrate that an intricate interplay exists between shape and magnetocrystalline anisotropy energies as well as exchange interactions.[3] When patterned into extended arrays of artificial spin ice structures (ASIs), the competition between intra- and inter-island interactions can result in the formation of complex spin textures rather than Ising states for certain nanoisland geometries (width and interisland spacing).[4] The magnetic stray fields associated with these complex spin textures provide additional means to tune interisland interactions in new and existing ASI structures. Together these studies demonstrate that complex oxide heterostructures provide a unique platform for engineering spin textures applications such as AFM spintronics and neuromorphic computing.

[1] E. Arenholz, Y. Takamura *et al., APL,* 94, 072503 (2009) [2] Y. Takamura *et al., Nano Letters,* 6 1287 (2006) [3] Y. Takamura *et al., PRL,* 111, 107201 (2013), M.S. Lee, Y. Takamura *et al., ACS Nano,* 10, 8545 (2016); M.S. Lee, Y. Takamura *et al., JAP,* 127, 204901 (2020) [4] D. Sasaki, Y. Takamura, *et al., PR Applied,* 17, 064057 (2022)

FA-02. Direct imaging of electrical control of the magnetic texture in a multiferroic oxide. *P. Meisenheimer*[1], S. Zhou[2], H. Zhang[1], L.M. Caretta[2], P. Stevenson[3] and R. Ramesh[1,4] *1. University of California, Berkeley, Berkeley, CA, United States; 2. Brown University, Providence, RI, United States; 3. Northeastern University, Boston, MA, United States; 4. Rice University, Houston, TX, United States*

Materials for antiferromagnetic spintronics are becoming a popular topic due to their potential applications in next generation technologies. A primary advantage lies in their stability with external magnetic fields and potentially ultrafast spin dynamics, making them promising candidates for high-speed data storage and processing. A key challenge in this field, however, is the control of the antiferromagnetic order parameter on the nanometer scales applicable to solid state technologies. Bismuth ferrite is a multiferroic material that exhibits both ferroelectric and antiferromagnetic properties at room temperature, making it a unique candidate in the development of electrically controllable magnetic devices. In this material, the magnetic moments are arranged into a long-range spin cycloid, resulting in a unique set of magnetic properties that are intimately tied to the ferroelectric order parameter. Here we show that the propagation axis of this spin cycloid can be deterministically controlled with careful tuning of the ferroelectric order. Through precise application of electric fields, we show reversable, deterministic control of the spin texture in $BiFeO_3$ thin films and study the influence of ferroelectric domain walls on magnetic properties.

FA-03. Tracking 3D Magnetic Topological Nanodefects with X-rays. *M. Di Pietro Martínez*[1] *1. MPI-CPfS, Dresden, Germany*

In recent years, there has been a surge of interest in expanding from two to three dimensional (3D) magnetic systems [1,2]. This extra dimension brings new magnetic textures [3-5], which promise applications in information storage and processing [6,7]. The detection and 3D visualization of these nanometric magnetic textures has been made possible by the development of magnetic tomography [8]. We have recently extended magnetic tomography to soft X-ray holography, allowing for the high spatial resolution imaging of textures within thick samples [9]. Secondly, we have combined 3D X-ray magnetic imaging with the application of in situ magnetic fields, allowing for the tracking of the field-driven motion of topological magnetic defects, such as Bloch points, merons and vortices [10]. These advances establish necessary capabilities for the study of the behavior of topological textures in 3D, opening the door to insights into three dimensional magnetic textures.

[1] Streubel et al., J. Phys. D 49, 363001 (2016); [2] Fernández-Pacheco et al., Nat. Commun. 8, 15756 (2017); [3] Hierro-Rodriguez et al., Nat. Commun. 11, 6382 (2020); [4] Donnelly et al., Nature Physics 17, 316–321 (2021); [5] Kent et al., Nat. Commun. 12, 1562 (2021); [6] Meng et al., Micromachines 12, 859 (2021); [7] Göbel et al., Physics Reports 895 (2021); [8] Donnelly et al., Nature 547, 328 (2017); [9] Di Pietro Martínez et al., PRB 107, 094425 (2023); [10] Di Pietro Martínez et al., In preparation.

FA-04. Strain- and Strain-gradient-induced Phenomena in Cr_2O_3. *O. Pylypovskyi*[1,2] *1. Helmholtz-Zentrum Dresden-Rossendorf, Dresden, Germany; 2. Kyiv Academic University, Kyiv, Ukraine*

Cr_2O_3 is a rare example of room-temperature magnetoelectric uniaxial antiferromagnets, which renders it to be a perspective material for low-energy-consuming electronics [1]. We study the behavior of domain walls and a possibility of tuning magnetic responses relying on strain and defect nanostructure of Cr_2O_3 thin films. Complex defects at grain boundaries act as effective pinning sites for domain wall, favoring the appearance of maze-like domains in polycrystalline films with out-of-plane easy axis [2]. Measuring characteristic scales of these domains by Nitrogen vacancy (NV) magnetometry provides a possibility to estimate inter-grain coupling parameters.

Combining statistical analysis of domain size with quantification of the fractal dimension of the domain pattern, we determine the effective strength of the exchange coupling between neighboring grains. To reproduce the domain pattern measured by NV magnetometry, it is crucial to have a small amount of ferromagnetic bonds, which in the case of Cr_2O_3 can be satisfied by local change of ion valence. The statistically quantified material parameters are in agreement with the estimation using machine learning approach [3]. In films epitaxially grown on sapphire, crystal defects relax strain stemming from the substrate and allow obtaining a sizable strain gradient. Cr_2O_3 films with thickness of 30-50 nm initially grow pseudomorphically to sapphire, and compressive in-plane strain leads to the enhancement of the Neel temperature locally. Dislocations as strain-relaxing sites propagate into the film from the top surface. The latter induces distribution of the Neel temperature along the film thickness and enables irreversible out-of-plane magnetization of flexomagnetic origin. We found the reversible part of flexomagnetism-induced magnetization is determined by the direction of the Neel vector and quantified it via combined magnetotransport and NV magnetometry measurements [4].

[1] Y. Shiratsuchi, K. Toyoki, R. Nakatani, J. Phys. Cond. Mat. Vol. 33, p. 243001 (2021); J. Han, R. Cheng, L. Liu et al., Nat. Mater. Vol. 22, p. 684 (2023) [2] I. Veremchuk, M. O. Liedke, P. Makushko et al., Small, Vol. 18, p. 2201228 (2022) [3] O. Pylypovskyi, N. Hedrich, A. Tomilo et. al., Phys. Rev. Applied, in press (2023) [4] P. Makushko, T. Kosub, O. Pylypovskyi et al., Nat. Comm., Vol. 13, p. 6745 (2022)

FA-05. Scanning Nitrogen-Vacancy Magnetometry of 2D Magnets.

M. Tschudin[1], D. Broadway[1], P. Reiser[1], C. Schrader[1] and P. Maletinsky[1]
1. University of Basel, Basel, Switzerland

The recent discovery of two-dimensional (2D) magnetic materials [1] has sparked wide interest in the scientific community due to their potential for a novel atomic-scale platform hosting exotic spin-textures and exhibiting different magnetic phases [2]. Future advances of these materials and their applications, however, rely on quantitative understanding of their magnetic properties at the nanoscale. Here we present our results on nanoscale magnetic imaging of van der Waals (vdW) materials using scanning Nitrogen-Vacancy (NV) magnetometry. We report on quantitative studies of magnetism in the vdW magnet chromium triiodide (CrI_3) [3], where we investigate the interlayer exchange coupling in this material and shine light on the correlation between structural order and magnetization of the material. We then describe our most recent efforts of imaging layered, antiferromagnetic 2D magnets, where we study spin textures down to the monolayer limit. With our experiments we gain insight into different magnetic phases, domain formation and magnetic anisotropies in these systems. Our studies provide a solid basis for future fundamental experiments on low-dimensional magnetism and open the path for studying more exotic phenomena, such as magnetic excitations (magnons) in 2D magnets.

[1] Huang et al., Nature 546, 270 (2017); C. Gong et al., Nature 546, 265 (2017) [2] Gibertini et al., Nature Nano. 14, 408 (2019) [3] Thiel et al., Science 364, 973 (2019)

Session FB
ANTIFERROMAGNETS: NON-COLLINEAR SPIN STRUCTURES AND DYNAMICS

Dominik Kriegner, Chair
Czech Academy of Science, Prague, Czechia

CONTRIBUTED PAPERS

FB-01. Spin Polarized Tunneling in Antiferromagnet/Insulator/ Ferromagnet Tunnel Junctions. *C. Chou*[1,2], B.C. McGoldrick[2], T. Nguyen[3], S. Ghosh[4], A. Mkhoyan[4], M. Li[3] and L. Liu[2] *1. Department of Physics, Massachusetts Institute of Technology, Cambridge, MA, United States; 2. Department of Electrical Engineering and Computer Science, Massachusetts Institute of Technology, Cambridge, MA, United States; 3. Department of Nuclear Science and Engineering, Massachusetts Institute of Technology, Cambridge, MA, United States; 4. Department of Chemical Engineering and Materials Science, University of Minnesota, Minneapolis, MN, United States*

Achieving a high tunneling magnetoresistance (TMR) in junctions with antiferromagnetic (AFM) electrodes has been an enthusiastically pursued goal in spintronics, with the prospect of employing AFMs as next-generation memory and spin logic devices. Traditionally, a finite TMR is believed to be forbidden in AFM tunnel junctions due to the translation-time reversal symmetry in most collinear AFMs. Recently a high TMR has been theoretically predicted in non-collinear AFM tunnel junctions [1] and verified experimentally [2, 3]. However, the underlying mechanism for the TMR and the relation between TMR and AFM ordering are still not fully understood, and the TMR ratios need to be further increased. The study of spin polarized tunneling from a ferromagnet (FM) to an AFM in asymmetric tunnel junctions is also lacking. In this work, we study Mn_3Sn/MgO/CoFeB asymmetric tunnel junctions where AFM Mn_3Sn and FM CoFeB serve as fixed layer and free layer, respectively. Large TMR ratios up to 49% are observed in these junctions and are comparable to that in conventional FM tunnel junctions. The large TMR suggests the effective spin polarization in non-collinear AFMs can be as large as that in FMs when proper tunneling barrier and counter electrode are selected. Furthermore, opposed to previous beliefs, the TMR cannot be toggled by reorienting the AFM ordering in the bulk Mn_3Sn and remains stable under a few Tesla magnetic fields. We systematically demonstrate that this unexpected field resilience of TMR is because the interfacial region of AFM behaves differently from the bulk. The interface-bulk decoupling has not been shown in conventional FM tunnel junctions and is a unique feature of AFMs. The new physical mechanisms revealed by our results are critical for understanding spin polarized tunneling in AFM tunnel junctions and improving their performance, including increasing the TMR ratio and enhancing the field robustness.

[1] J. Dong, X. Li, and G. Gurung, *Phys. Rev. Lett.* 128, 197201 (2022) [2] P. Qin, H. Yan, and X. Wang, *Nature* 613, 485–489 (2023) [3] X. Chen, T. Higo, and K. Tanaka, *Nature* 613, 490–495 (2023)

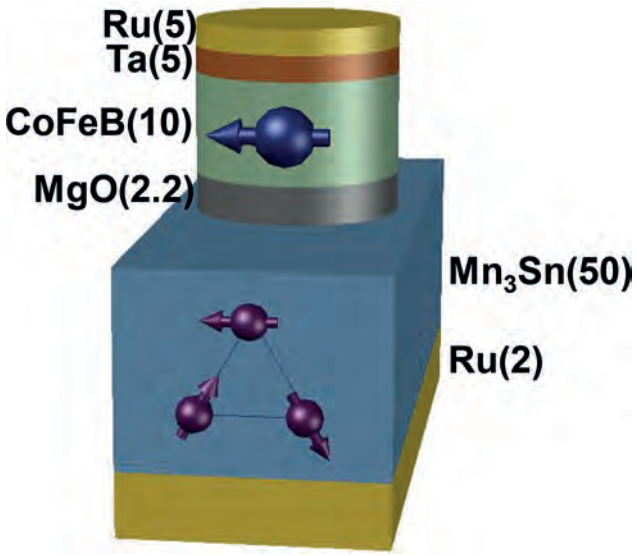

Fig. 1 Schematic of the Mn_3Sn/MgO/CoFeB stack for antiferromagnetic tunnel junctions (unit in nm). Purple arrows represent magnetic moments of individual Mn atoms, and the blue arrow represents CoFeB moment.

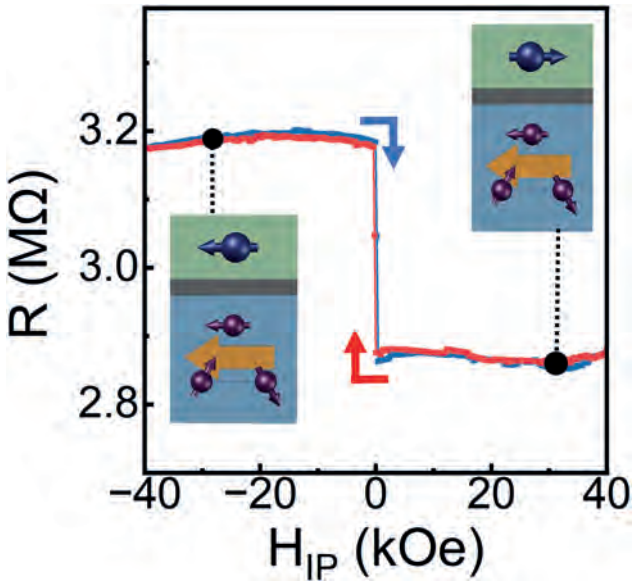

Fig. 2 Tunneling magnetoresistance of the antiferromagnetic tunnel junction measured at 10 K.

FB-02. Extraordinary Tunneling Magnetoresistance in Antiferromagnetic Tunnel Junctions with Antiperovskite Electrodes.

G. Gurung[1,2], D. Shao[3] and E. Tsymbal[1] *1. Department of Physics and Astronomy, University of Nebraska-Lincoln, Lincoln, NE, United States; 2. Trinity College, University of Oxford, Oxford, United Kingdom; 3. Key Laboratory of Materials Physics, Institute of Solid-State Physics, HFIPS, Chinese Academy of Sciences, Hefei, China*

Antiferromagnetic (AFM) spintronics offers a new paradigm for information technologies where the AFM Néel vector serves as a state variable. Efficient electric detection and control of the Néel vector is an important prerequisite for these applications. Recent theoretical predictions [1,2] and experimental demonstrations [3,4] of tunneling magnetoresistance (TMR) in AFM tunnel junctions (AFMTJs) may provide such prerequisite. A large TMR is important for the applications, and, in this regard, it is critical to find promising electrode-barrier material combinations to realize high-performance AFMTJs. Here, we predict an extraordinary TMR (ETMR) effect in AFMTJs utilizing noncollinear AFM antiperovskite $GaNMn_3$ electrodes (Fig. 1a) and perovskite oxide $SrTiO_3$ tunneling barrier (Fig. 1b). The ETMR effect stems from the perfectly spin-polarized electronic states in $GaNMn_3$ (Fig. 1c) that can efficiently tunnel through the low-decay-rate evanescent states of $SrTiO_3$ (Fig. 1d) while preserving their spin state. By performing quantum-transport calculations for an $GaNMn_3$/$SrTiO_3$/$GaNMn_3$ (001) AFMTJ (Fig. 2a), we demonstrate a TMR ratio exceeding 10^4% (Fig. 2b) and originating from the ETMR effect [5]. This TMR value is gigantic, significantly larger than the values known for conventional MTJs and reminiscent to an infinitely large TMR expected for MTJs based on ideal half-metallic electrodes. The predicted ETMR effect is expected to be widely supported in other antiperovskite/perovskite/antiperovskite AFMTJs. Our results are promising for the efficient detection and control of the Néel vector in AFM spintronics, and thus we encourage experimentalists working in this field to verify our predictions.

[1] D.-F. Shao et al., Nat. Commun., Vol. 12, p. 7061 (2021). [2] J. Dong et al., Phys. Rev. Lett., Vol. 128, p. 197201 (2022). [3] P. Qin et al., Nature, Vol. 613, p. 485 (2023). [4] X. Chen et al., Nature, Vol. 613, p. 490 (2023). [5] G. Gurung, D.-F. Shao, and E. Y. Tsymbal, arXiv:2306.03026 (2023).

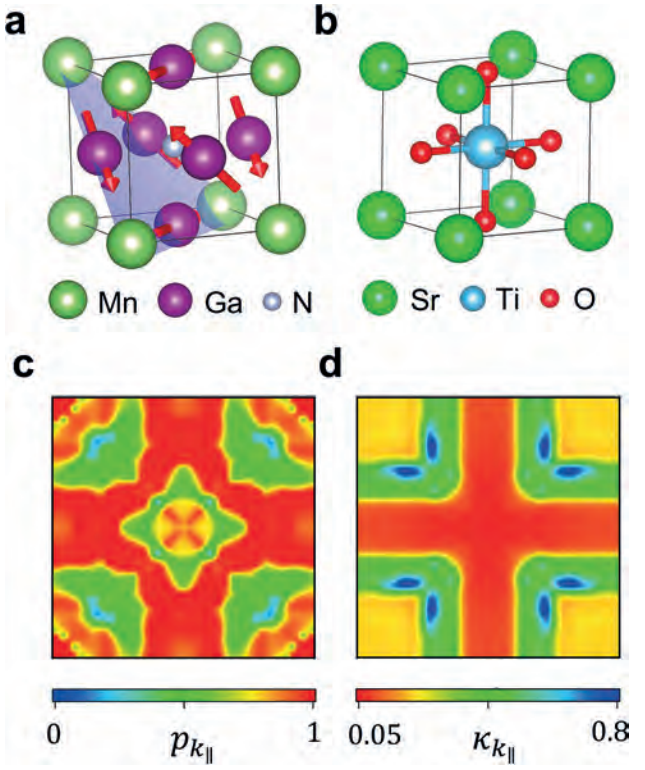

FIG. 1 (a,b) Atomic and magnetic structure of antiperovskite $GaNMn_3$ (a) and perovskite $SrTiO_3$ (b). (c) $k_\parallel$-resolved effective spin polarization of $GaNMn_3$ (001). (d) $k_\parallel$-resolved lowest decay rate of the evanescent states of $SrTiO_3$ (001).

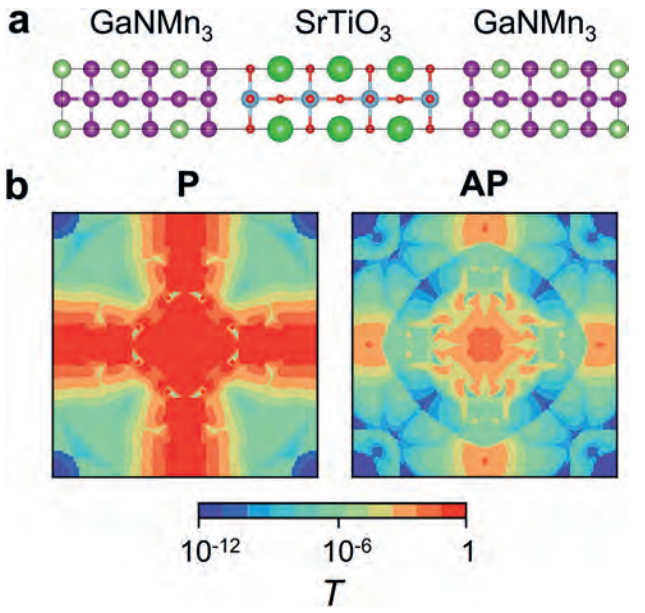

FIG. 2 (a) Atomic structure of $GaNMn_3$/$SrTiO_3$/$GaNMn_3$ (001) AFMTJ. (c) Calculated $k_\parallel$-resolved transmission across for parallel (P, left) and antiparallel (AP, right) alignment of the Néel vector in the $GaNMn_3$ electrodes. The corresponding TMR ratio is 10^4%.

FB-03. Comprehensive study of crystalline structure, magnetic and magnetotransport properties of Mn_3Sn thin films with various thicknesses. *S. Wakabayashi*[4,3], J. Yoon[4,3], K. Gas[1,5], Y. Takeuchi[6], Y. Yamane[4,2], T. Uchimura[4,3], Y. Sato[4,3], K. Kishi[4,3], S. Kanai[4,1], M. Sawicki[5], H. Ohno[4,1] and S. Fukami[4,1] *1. CSIS, Tohoku University, Sendai, Japan; 2. FRIS, Tohoku University, Sendai, Japan; 3. Graduate School of Engineering, Tohoku University, Sendai, Japan; 4. Laboratory for Nanoelectronics and Spintronics, RIEC, Tohoku University, Sendai, Japan; 5. Institute of Physics, Polish Academy of Sciences, Aleja Lotnikow, Poland; 6. WPI-AIMR, Tohoku University, Sendai, Japan*

Non-collinear antiferromagnet $D0_{19}$-Mn_3Sn has attracted much attention owing to its unique physical properties [1,2] and functionalities [3,4]. For further exploration, comprehensive characterization of crystalline structure and magnetic/magnetotransport properties is of great importance. Here, we systematically investigate these fundamental properties of Mn_3Sn thin film as a function of thickness and discuss the correlation between each parameter. For the sample preparation, we deposit stacks consisting of W (2 nm)/Ta (3 nm)/Mn_3Sn (t)/MgO (1.3 nm)/Ru (1 nm) on MgO substrate by DC/RF magnetron sputtering with various Mn_3Sn thicknesses t ranging in 10-100 nm, followed by annealing at 500 °C for an hour. X-ray diffraction reveals that the oriented epitaxial structure is formed in 20-40 nm, where the lattice parameter a approaches the bulk value as t increases [Fig. 1(a)], and polycrystalline structure is formed above 50 nm. Magnetization measurement reveals that the Mn_3Sn layer has a spontaneous magnetization M_s of 4.5±1.0 mT with a magnetically inactive thickness of about 7 nm [Fig. 1(b)]. Magnetic anisotropy evaluated from a transport measurement reveals a dominant contribution of two-fold anisotropy λ_2, which decreases with t in the range of 20-40 nm [Fig. 1(c)]. The saturated Hall conductivity $\sigma_{H,sat}$ rapidly increases from 15 to 20 nm and, above 20 nm, it saturates at ~20 Scm^{-1} [Fig. 1(d)], which is close to the one reported for a bulk sample [1]. From the obtained results, we infer that λ_2 is correlated with a through the strain as pointed out in a previous report [5] and $\sigma_{H,sat}$ is affected by a formation of $D0_{19}$ structure. This work is an important step towards developing functional devices based on non-collinear antiferromagnetic thin films. This work was partly supported by JSPS Kakenhi (Nos. 19H05622, 21J23061, and 22K14558), Casio foundation (No. 40-4), and RIEC Cooperative Research Projects.

[1] S. Nakatsuji *et al.*, Nature 527, 212 (2015). [2] T. Higo *et al.*, Nat. Photon. 12, 73 (2018). [3] H. Tsai *et al.*, Nature 580, 608 (2020). [4] Y. Takeuchi *et al.*, Nat. Mater. 20, 1364 (2021). [5] T. Higo, *et al.*, Nature, 607, 474 (2022).

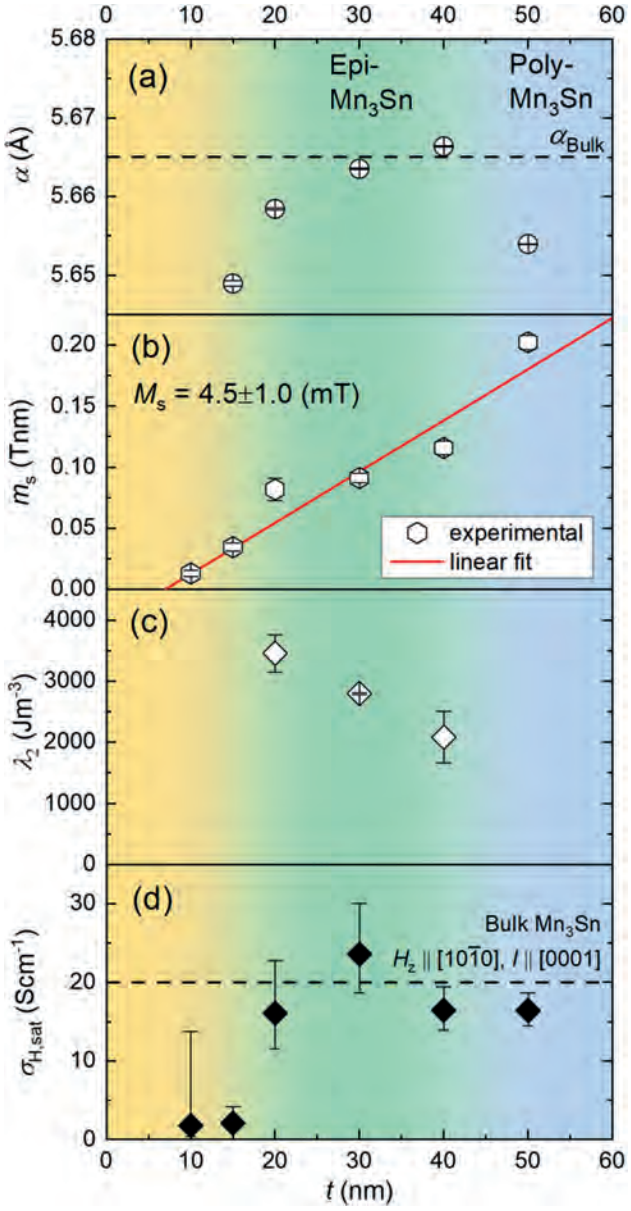

Fig. 1. t dependence of (a) lattice parameter a, (b) spontaneous magnetic moment m_s, (c) two-fold anisotropy λ_2 and (d) saturated Hall conductivity $\sigma_{H,sat}$.

FB-04. Interfacial Dzyaloshinskii-Moriya interaction in a non-collinear antiferromagnet/heavy metal heterostructure. *T. Uchimura*[1,2], Y. Yamane[1,3], T. Dohi[1], J. Han[1], J. Yoon[1,2], Y. Sato[1,2], S. Wakabayashi[1,2], Y. Takeuchi[4], S. Kanai[1,5], J. Ieda[6], H. Ohno[1,5] and S. Fukami[1,5] *1. RIEC, Tohoku University, Sendai, Japan; 2. Grad. Sch. Eng., Tohoku University, Sendai, Japan; 3. FRIS, Tohoku University, Sendai, Japan; 4. WPI-AIMR, Tohoku University, Sendai, Japan; 5. CSIS, Tohoku University, Sendai, Japan; 6. ASRC, JAEA, Ibaraki, Japan*

The interfacial Dzyaloshinskii-Moriya interaction (DMI) gives rise to exotic spin textures such as chiral Néel domain wall (DW) in ferromagnet/heavy metal (HM) heterostructures [1,2]. While recent studies suggested an existence of the interfacial DMI in antiferromagnet (AFM)/HM heterostructures [3], systematic investigation of the interfacial DMI for AFM remains to be addressed. In this work, we show the evidence of the interfacial DMI in a non-collinear AFM Mn_3Sn/HM heterostructure. We deposit stacks consisting of W (2)/Ta (3)/Mn_3Sn (15)/MgO (1.3)/Ru (1) (in nm)

on MgO(110) substrate by DC/RF sputtering followed by annealing at 500 °C for an hour. This stack and process condition allow for a growth of (1-100)-oriented Mn_3Sn thin films [4]. We first measure the effective field H_{eff} acting on the Néel DW by hysteresis loop shifts in the presence of in-plane magnetic field H_x and currents I (Fig. 1). Note that this scheme assumes that the switching is mediated by DW motion assisted by the spin-orbit torque (SOT). Figure 2 shows the hysteresis loops of Hall resistance R_H where the H_x and I are applied parallel to the Néel DW. Finite shift is clearly observed and the shift direction (the sign of H_{eff}) reverses with respect to the current direction, proving a formation of chiral DWs that are stabilized by the DMI and are driven by the SOT. In contrast, for the Bloch DW configuration, no appreciable shifts are observed, which can be attributed to the ineffective action of SOT on the chiral spins [5]. We next measure the DMI effective field as a function of the Mn_3Sn thickness. We find that the DMI effective field is inversely proportional to the Mn_3Sn thickness, indicating an interfacial origin of the DMI. Our findings provide a new foundation of non-collinear antiferromagnetic spintronics with topological properties harnessing the interfacial DMI. This work is supported by the JSPS Kakenhi (Nos. 19H05622, 21J23061, 22K14558, 22KK0072, and 23K13655), JST TI-FRIS, Casio Science and Technology Foundation.

[1] M. Bode *et al*., Nature 447, 190 (2007). [2] S. Emori *et al*., Nat. Mater. 12, 611 (2013). [3] Y. Cheng *et al*., Phys. Rev. Lett. 123, 237206 (2019). [4] J.-Y. Yoon *et al*., Appl. Phys. Express 13, 013001 (2019). [5] Y. Takeuchi *et al*., Nat. Mater. 20, 1364 (2021).

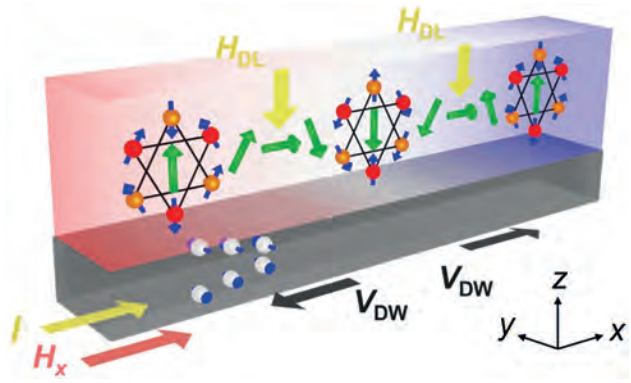

Fig. 1. Schematic of current-induced hysteresis loop shift for the Néel DW configuration.

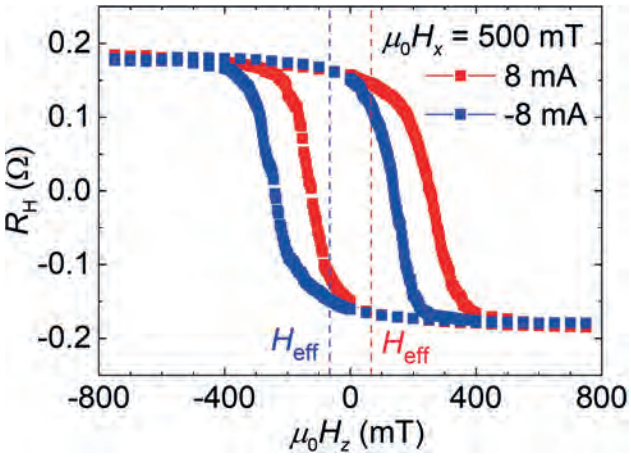

Fig. 2. Results of current-induced hysteresis loop shift, proving the existence of interfacial DMI in Mn_3Sn-based heterostructure.

FB-05. Large Anomalous Hall Effect at Room Temperature in a Fermi-Level-Tuned Kagome Antiferromagnet Mn_3Ga. L. Song[1], F. Zhou[2], H. Li[2], X. Xi[1], *Y. Lau*[1,3] and W. Wang[2] *1. Chinese Academy of Sciences, Institute of Physics, Beijing, China; 2. Tiangong University, Tianjin, China; 3. University of Chinese Academy of Sciences, Beijing, China*

Antiferromagnets are promising materials for future magnetic memory and logic applications in spintronics. Of particular interest are the non-collinear kagome antiferromagnets Mn_3X (Sn, Ge, Ga) that surprisingly show large anomalous Hall [1,2], anomalous Nernst [3] and spin Hall effects [4] despite the vanishing net moment. *Ab initio* electronic band structure calculations [5] attribute these unconventional transverse transport phenomena to the nonzero Berry curvature generated by the antiferromagnetic Weyl nodes near the Fermi energy. So far, extensive studies have only focused on Mn_3Sn and Mn_3Ge single crystals [1-4]. By contrast, there are only scarce studies on polycrystalline hexagonal Mn_3Ga [6] and no report on Mn_3Ga single crystal, possibly due to the complicated Mn-Ga binary phase diagram [7] that hinders the growth of stoichiometric hexagonal Mn_3Ga in equilibrium. Here, we report the first experimental realization of Ga-rich hexagonal Mn_3Ga single crystals that exhibit relatively large and highly anisotropic anomalous Hall conductivity σ_H at 300 K. Figure 1 compares the magnetic and transport properties of Mn_3Ga single crystals and those of polycrystalline ribbons stabilized by melt-spinning process. Interestingly, with a tiny net moment of only 0.025 μ_B/f.u., we found a large spontaneous σ_H in Mn_3Ga single crystal with applied current I and orthogonal magnetic field H both in the kagome plane. This is reminiscent of the magnetic and transport properties for Mn_3Sn, albeit the off stoichiometry in our sample. Combining transmission electron microscopy and nuclear magnetic resonance techniques, we conclude that the excess Ga atoms mostly form antisite defects by substituting Mn atoms. *Ab initio* calculations suggest such atomic arrangement promote a shift of the Fermi level, leading to enhanced anomalous Hall effect compared to the stoichiometric Mn_3Ga [5]. This work found the last member of the kagome antiferromagnetic Mn_3X family and demonstrated efficient Fermi level engineering via off-stoichiometric substitutional alloying.

[1] S. Nakatsuji, N. Kiyohara, T. Higo, Nature, Vol.527, p.212-215 (2015). [2] A.K. Nayak, J.E. Fischer, Y. Sun, et al. Sci. Adv., Vol.2, p.e1501870 (2016). [3] M. Ikhlas, T. Tomita, T. Koretsune, et al. Nature Physics, Vol.13, p.1085-1090 (2017). [4] M. Kimata, H. Chen, K. Kondou, et al. Nature, Vol.565, p.627-630 (2019). [5] Y. Zhang, Y. Sun, H. Yang, et al. Phys. Rev. B., Vol.95, p.075128 (2017). [6] L.X. Song, B. Ding, H. Li, et al. Appl. Phys. Lett., Vol.119, p.152405 (2021). [7] K. Minakuchi, R.Y. Umetsu, K. Ishida, et al. J. Alloy. Compd. Vol.537, p.332-337 (2012).

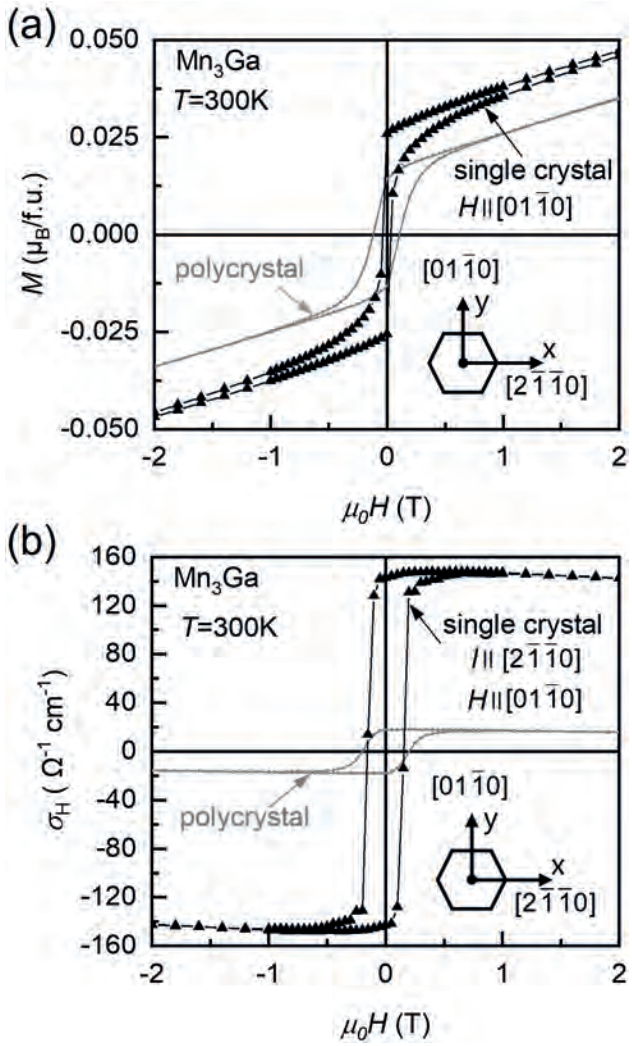

Figure1. Comparison of (a) magnetization and (b) anomalous Hall conductivity loops for Ga-rich Mn_3Ga polycrystalline ribbon and single crystal at 300K.

FB-07. Withdrawn

FB-08. THz magnetism of antiferromagnetic CoF_2 and NiO/Pt in the non-collinear phase. *T.W. Metzger*[1], K. Grishunin[1], P. Fischer[2], C. Reinhoffer[3], R. Dubrovin[4], A. Arshad[5], I. Ilyakov[5], T.A. de Oliveira[5], A. Ponomaryov[5], J. Deinert[5], S. Kovalev[5], T. Kikkawa[6], E. Saitoh[6], R.V. Pisarev[4], M.I. Katsnelson[1], B.A. Ivanov[1], P.H. van Loosdrecht[3], A.V. Kimel[1], D. Bossini[2] and E.A. Mashkovich[3] *1. Radboud University, Nijmegen, Netherlands; 2. University of Konstanz, Konstanz, Germany; 3. University of Cologne, Cologne, Germany; 4. Ioffe Institute, St. Petersburg, Russian Federation; 5. Helmholtz-Zentrum Dresden-Rossendorf, Dresden, Germany; 6. The University of Tokyo, Tokyo, Japan*

The booming fields of antiferromagnetic spintronics and THz magnonics urge to understand the ultrafast dynamics triggered in antiferromagnets by ultrashort (sub-100 ps) stimuli. The interest in the ultrafast magnetism of antiferromagnets has led to new and vastly counter-intuitive findings in experimental and theoretical research [1-2]. However, the majority of the studies was dedicated to antiferromagnets in their ground state. Here, we report on ultrafast dynamics in the poorly explored, non-collinear phase of NiO and CoF_2 antiferromagnets, in which the spins of the sublattices are canted by high magnetic fields up to 7 T. We show that tuning the spin canting by an external magnetic field, one can create conditions for the impulsive magnon-phonon Fermi resonance between otherwise non-interacting modes in CoF_2, see Fig. 1 (a). In particular, if the frequencies of the magnon f_m and the phonon mode f_{ph} obey the condition of the Fermi resonance [3] $f_{ph}=2f_m$ selective pumping of the magnon results in an excitation of the phonon via a nonlinear mechanism [4]. Measuring THz-induced rotation of the probe polarization in magnetic fields up to 7 T, we reveal these two distinct modes in the time domain data (Fig. 1 b). By supporting our findings with numerical calculations following the sigma-model, we reveal that a large amplitude of lattice vibrations is not necessarily a requirement for initiating the nonlinear excitation of phononic modes and thus nourishes new ways for coherent control of magnon-phonon energy exchange [5]. Inspired by the recent discoveries of ultrafast spin currents in NiO/Pt heterostructures [6-7], we performed THz emission spectroscopy experiments on ultrathin (<50 nm) heterostructures in high magnetic fields, see Fig. 2 (a). Our measurements as a function of temperature, sample rotation θ, pump polarization α, magnetic field μH_{ext} and polarization of the emitted THz waves reveal that the magnetic field initiates a new and unprecedented source of THz emission and spin current in this material [8], see Fig. 2 (b-c).

[1] P. Němec, M. Fiebig, T. Kampfrath et al., Nature Phys 14, 229–241 (2018) [2] A. Kimel, B. Ivanov, R. Pisarev et al., Nature Phys 5, 727–731 (2009). [3] E. Fermi, Zeitschrift fuer Physik 71(3-4), 250–259 (1931) [4] E. Mashkovich et al., Science 374,1608-1611 (2021) [5] T.W.J. Metzger, K.A. Grishunin, C. Reinhoffer, R.M. Dubrovin, A. Arshad, I. Ilyakov, T.A.G. de Oliveira, A. Ponomaryov, JD. Deinert, S. Kovalev, R.V. Pisarev, M.I. Katsnelson, B.A. Ivanov, P.H.M. van Loosdrecht, A.V. Kimel, and E.A. Mashkovich (submitted to Nature Physics in 2023) [6] E. Rongione, O. Gueckstock, M. Mattern et al., Nature Communications, 14, 1818 (2023) [7] H. Qiu, L. Zhou, C. Zhang et al., Nature Physics, 17, 388–394 (2021) [8] T.W.J. Metzger, P. Fischer, T. Kikkawa, E. Saitoh, A.V. Kimel, and D. Bossini (in preparation)

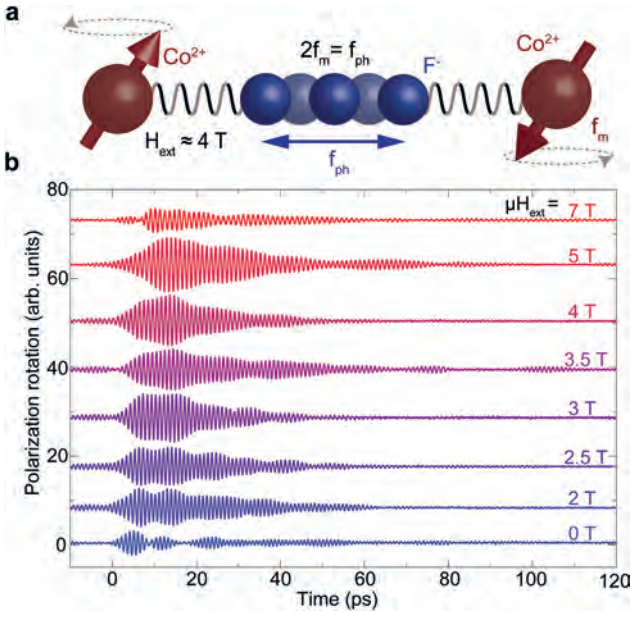

Fig. 1 Impulsive Fermi magnon-phonon resonance of CoF_2 (a) Sketch (b) Time-domain transients

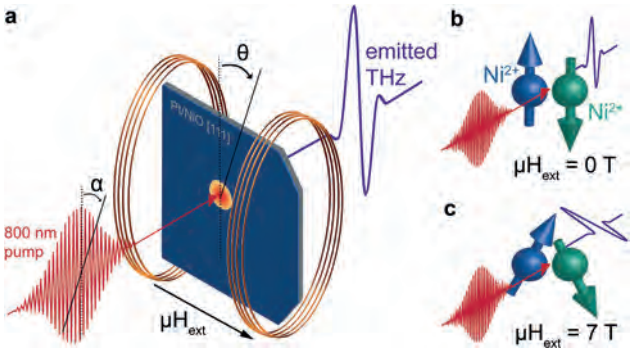

Fig. 2 THz Emission spectroscopy of NiO (a) setup (b) ground state (c) canted state

FB-10. Magnetism, Spin Dynamics and Spin Transport in 2D van der Waals Antiferromagnet $CrPS_4$. C. Freeman[1,2], Z. Xue[2], S. Khan[2], O. Kazakova[1], H. Kurebayashi[2] and *M. Cubukcu*[1,2] *1. National Physical Laboratory, Teddington, United Kingdom; 2. University College London, London, United Kingdom*

The ability to generate, transport and manipulate spin currents in 2D materials suggests that they could provide a suitable platform to build beyond-CMOS spintronic devices [1, 2]. Antiferromagnets have attracted attention due to their absence of stray fields, high intrinsic precession frequency (~THz) and high stability under magnetic fields [3]. We present a detailed study of the 2D van der Waals antiferromagnet chromium thiophosphate ($CrPS_4$), a material with layer dependent magnetic properties [4], through vibrating-sample magnetometer (VSM), ferromagnetic resonance (FMR) and magneto transport of a Pt/$CrPS_4$/h-BN device. We report on the evolution of the FMR measurements across temperatures below the Neel transition along the three crystallographic axes. We demonstrate the opening of a zero-field gap in the easy axis orientation (z-axis) and discuss its origin from Dzyaloshinskii-Moriya interaction, "residual anisotropy" and the biaxial nature of the material as can be seen in Fig. 1. Furthermore, we report on the magnetic properties and spin dynamic parameters across the temperature range. Finally, we present magneto-transport measurements in a Pt(3nm)/$CrPS_4$(18nm)/h-BN device and show spin Hall magnetoresistance (SMR), demonstrating the potential to exfoliate $CrPS_4$ into thin layers and manipulate the magnetization through spin currents in such devices (Fig. 2). This result combined with the biaxial nature of the device paves the way for neuromorphic devices based on 2D antiferromagnetic materials making use of the biaxial switching [5].

[1] X. Lin *et al.,* Nat. Electronics. 2, 274-283 (2019) [2] H. Kurebayashi *et al.,* Nat. Rev. Phys. 4, 150-166 (2022) [3] T. Jungwirth *et al.,* Nat. Nanotechnol. 11, 231 (2016) [4] J. Son *et al.,* ACS Nano 15 (10), 16904-16912 (2021) [5] K. Olejnik *et al.,* Nat. Comm. 8, 15434 (2017)

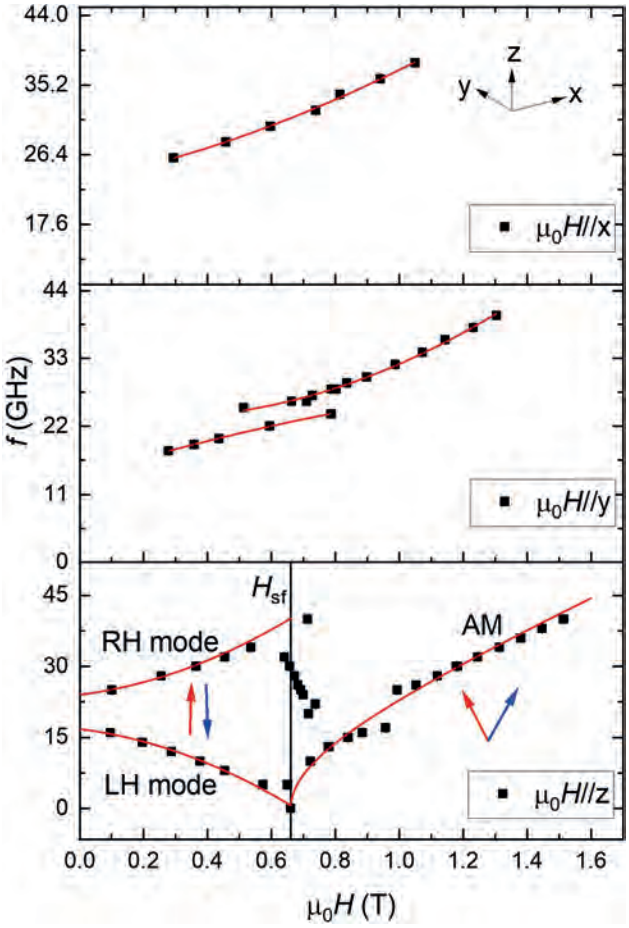

Fig. 1. The frequency dependent FMR results taken at 20 K, where the magnetic field applied along the three crystallographic axes (black square) and the guideline fitting (red line). H_{sf} is the spin-flop transition. RH, LH, AM are right-hand, left-hand, and acoustic mode respectively.

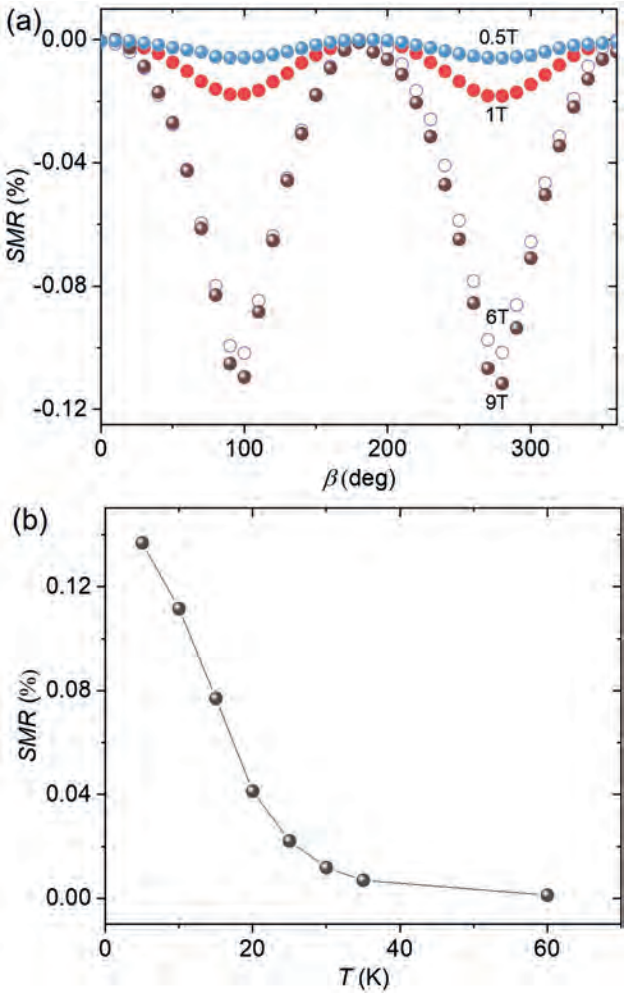

Fig. 2. (a) SMR signal observed when rotating the sample in the zy plane under a range of applied fields up to 9T. The magnetization is always perpendicular to current in this rotation plane. (b) SMR as a function of temperature for the Pt/$CrPS_4$/h-BN device where we see a sharp increase in amplitude at and below the Neel transition at 37K. The applied magnetic field is 9T.

FB-11. Picosecond-scale Encoding of Laser Pulses in Analog Antiferromagnetic Memory. *M. Surýnek*[1], J. Zubáč[2,1], K. Olejník[2], F. Krizek[2], A. Farkaš[2,1], L. Nadvornik[1], P. Kubaščík[1], F. Trojánek[1], V. Novák[2], T. Jungwirth[2,3] and P. Němec[1] *1. Faculty of Mathematics and Physics, Charles University, Prague, Czechia; 2. Institute of Physics, Czech Academy of Sciences, Prague, Czechia; 3. School of Physics and Astronomy, University of Nottingham, Nottingham, United Kingdom*

Antiferromagnetic materials are gaining attention due to their potential in constructing next-generation memory devices [1]. With the prospect of achieving both ultrafast (THz) and, simultaneously, low-dissipative (meV) operation [2], they promise significant advancements in digital memory technology. In addition, compensated magnets offer a route towards ultra-scalable energy-efficient analog devices with neuromorphic functionalities [3]. However, this analog route has been virtually unexplored at the ultrafast (sub)ps time scales. In this work, we demonstrate at room temperature switching by an individual sub-ps laser pulse in an analog opto-electronic memory. The device is microfabricated from a thin-film CuMnAs antiferromagnet into an elementary-resistor geometry. Electrical readout of the incident laser pulse, encoded by pulse intensity into the variable resistance, is demonstrated after the pulse at times up to 10^{10} larger than the pulse length. Using a sequence of two laser pulses, we demonstrate an encoding of a time-delay between the consecutive pulses into the memory's variable resistance for delays on scales from ~ ps to ~ ns. Our results pave the way towards ultrafast low-energy implementations of spiking neuron and synapse functionalities [4] using a thin-film resistive analog memory.

[1] Němec, P. *et al*. *Nature Physics* 14, 229–241 (2018) [2] Schlauderer, S. *et al. Nature* 569, 383–387 (2019) [3] Kašpar, Z. *et al*. *Nature Electronics* 4, 30–37 (2021) [4] Kurenkov, A. *et al*. *Advanced Materials* 31, 1900636 (2019)

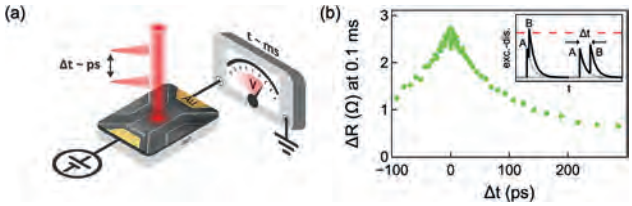

Fig. 1: Encoding of laser pulses in variable resistance of an analog CuMnAs memory. (a) Schematic illustration of the experiment using two Δ*t* time-delayed sub-ps laser pulses. (b) Δ*t*-dependence of resistive signal Δ*R* measured ~ ms after the incidence of the pulse-pair.

FB-12. Anomalous Hall transport in sputtered antiferromagnetic Mn_3Ga epitaxial thin films. *M. Raju*[1], T. Higo[2,3], D. Hamane[4], C. Broholm[1] and S. Nakatsuji[2,1] *1. Institute for Quantum Matter, Physics and Astronomy, Johns Hopkins University, Baltimore, MD, United States; 2. Department of Physics, University of Tokyo, Tokyo, Japan; 3. CREST, Japan Science and Technology Agency, Kawaguchi, Japan; 4. Institute for Solid State Physics, University of Tokyo, Kashiwa, Japan*

Mn_3X(X=Sn, Ga, Ge) antiferromagnetic (AFM) Weyl semimetals have attracted significant research efforts due to their large Berry phase effects and potential for applications[1-2]. Fabrication of the thin film form of Mn_3Sn is shown to be straightforward compared to Mn_3Ge and Mn_3Ga, leading to many reports on Mn_3Sn [3]. Within this class of materials, Mn_3Ga is expected to have the largest Néel temperature (T_N≈480K) and spin Hall conductivity [4], but this remains unexplored. Here, we present the epitaxial growth of Mn_3Ga thin films by using magnetron sputtering. Our structural investigations using X-ray diffraction and cross-sectional high-resolution transmission electron microscopy establish the control over crystal growth variation accessing vertical and in-plane kagome spin structure of the Mn_3Ga films. Our magnetotransport investigations between 10-400K temperature range show, for the magnetic field applied along the kagome planes, a large spontaneous AHE up to ≈30 $[\Omega cm]^{-1}$, which vanishes for the magnetic field applied along the normal direction to the kagome planes. In summary, we have established the epitaxial growth of antiferromagnetic hexagonal Mn_3Ga thin films, a promising material for AFM spintronics.

1. Satoru Nakatsuji and Ryotaro Arita, Topological Magnets: Functions Based on Berry Phase and Multipoles. *Annu. Rev. Condens. Matter Phys. 13, 119 (2022)* 2. Šmejkal, L., MacDonald, A.H., Sinova, J. et al. Anomalous Hall antiferromagnets. *Nat. Rev. Mater. 7, 482–496 (2022)* 3. Tomoya Higo and Satoru Nakatsuji, Thin film properties of the non-collinear Weyl antiferromagnet Mn_3Sn. *JMMM 564, 170176 (2022)* 4. Yang Zhang, Yan Sun, Hao Yang, Jakub Zelezny, et.al. Strong anisotropic anomalous Hall effect and spin Hall effect in the chiral antiferromagnetic compounds Mn_3X (X=Ge, Sn, Ga, Ir, Rh, and Pt). *Phys. Rev. B 95, 075128 (2017)*

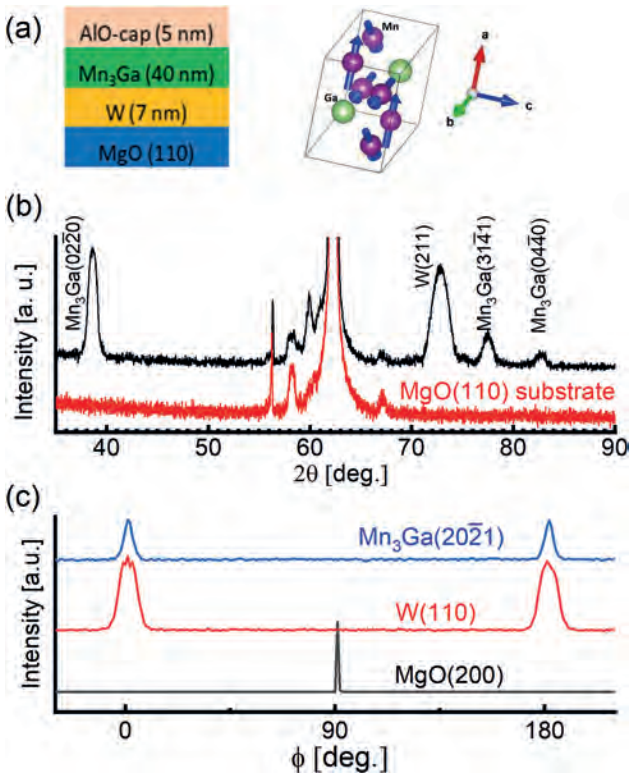

X-ray diffraction of Mn_3Ga (40 nm) thin film. (a) Schematic thin film stack structure MgO(110)/W/Mn_3Ga/AlO-cap used for crystal orientation resulting in kagome plane standing normal to the film surface. (b) Out-of-plane X-ray diffraction and (c) in-plane Φ-scans establishing the epitaxial nature of the films.

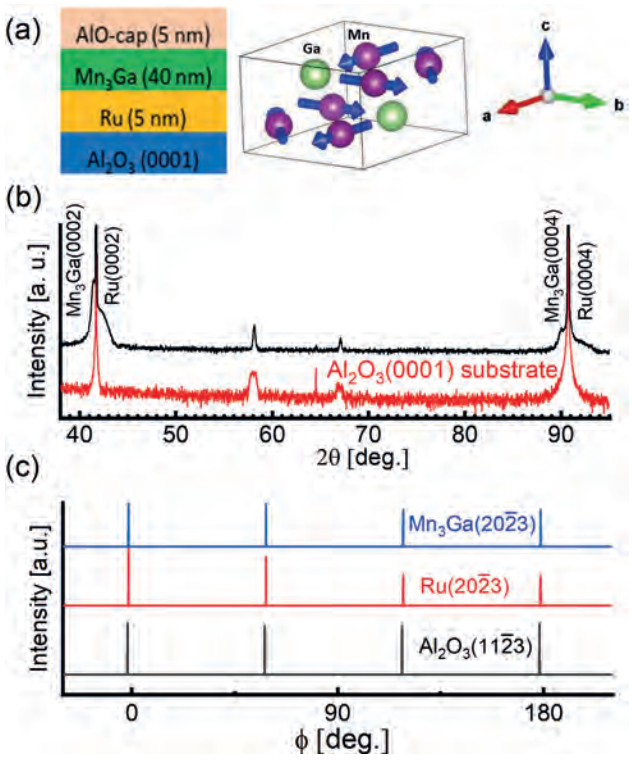

X-ray diffraction of Mn_3Ga (40 nm) thin film. (a) Schematic thin film stack structure Al_2O_3(0001)/Ru/Mn_3Ga/AlO-cap used for crystal orientation resulting in kagome plane parallel to the film surface. (b) Out-of-plane X-ray diffraction and (c) in-plane Φ-scans establishing the epitaxial nature of the films.

INVITED PAPER

FB-13. Manipulating chiral-spin transport with ferroelectric polarization. *X. Chen*[1] and R. Ramesh[1] *1. University of California, Berkeley, Berkeley, CA, United States*

A collective excitation of the spin structure in a magnetic insulator can transmit spin-angular momentum with negligible dissipation. This quantum of a spin wave, introduced more than nine decades ago, has always been manipulated through magnetic dipoles, (i.e., timereversal symmetry). Here, we report the experimental observation of chiral-spin transport in multiferroic $BiFeO_3$, where the spin transport is controlled by reversing the ferroelectric polarization (i.e., spatial inversion symmetry). The ferroelectrically controlled magnons produce an unprecedented ratio of up to 18% rectification at room temperature. The spin torque that the magnons in $BiFeO_3$ carry can be used to efficiently switch the magnetization of adja-cent magnets, with a spin-torque efficiency being comparable to the spin Hall effect in heavy metals. Utilizing such a controllable magnon generation and transmission in $BiFeO_3$, an alloxide, energy-scalable logic is demonstrated composed of spin-orbit injection, detection, and magnetoelectric control. This observation opens a new chapter of multiferroic magnons and paves an alternative pathway towards low-dissipation nanoelectronics[1-3].

[1] X. Chen, T. Higo and S. Nakatsuji, Nature, 613, 490 (2023) [2] X. Chen, C. Song, Nature Materials, 20, 800 (2021) [3] X. Huang, X. Chen and R. Ramesh, arXiv:2306.02185 (2023)

Session FC
SOFT MAGNETIC MATERIALS III: CRYSTALLINE ALLOYS

Arcady Zhukov, Chair
University of Basque Country and Ikerbasque, San Sebastian, Spain

INVITED PAPER

FC-01. Designing strong and ductile soft-magnetic multicomponent alloys for harsh environment. *L. Han*[1], O. Gutfleisch[2], Z. Li[3] and D. Raabe[1] *1. Max-Planck-Institut für Eisenforschung, Düsseldorf, Germany; 2. Technische Universität Darmstadt, Darmstadt, Germany; 3. Central South University, Changsha, China*

Soft magnetic materials (SMMs) are indispensable components in electrified applications, allowing instant variations to high frequency changes of the applied magnetic field. The global trend towards electrification leads to a massive increase in energy consumption due to hysteresis losses. Therefore, minimizing coercivity, which scales the losses, is crucial. Yet, meeting this target alone is not enough: SMMs used in advanced electrical motors and engines must withstand severe and complex profiles under harsh environments. The practically infinite compositional space of multicomponent alloys (MCAs) renders plenty of opportunities for achieving good combinations of soft magnetic and mechanical properties over a wide temperature range. This provides a new paradigm for crucial applications of advanced SMMs under severe mechanical loads where conventional SMMs cannot serve the needs. It is always challenging and almost impossible to overcome the multiple trade-offs of mechanical, magnetic and electrical resistance in one alloy, even for advanced MCAs. Therefore, MCAs should not pretend that they can achieve all the property corners but target achieving several of the property corners where most dilute alloys are hard to overcome based on the compositional space. This is because the limited compositional space further restricts the tunable microstructural features as well as the intrinsic and extrinsic properties. We designed a system of Fe-Co-Ni-Ta-Al multicomponent alloys with excellent combination of mechanical and magnetic properties outperforming other multicomponent alloys and conventional SMMs by tuning the intrinsic features down to near-atomic scale [1]. Through a further modification, the precipitates enhancing strength and ductility and create an interaction volume below the magnetic domain wall width, leading to minimal domain wall pinning [2]. The new alloy design approach allows for tailoring SMMs for magnetic parts exposed to severe mechanical loads, be it from manufacturing and/or during service, for which conventional SMMs are mechanically too soft or too brittle.

[1] Han, L et al. *Advanced Materials* 33 (2021) 2102139. [2] Han, L et al. *Nature* 608 (2022) 310–316.

CONTRIBUTED PAPERS

FC-02. Design of materials with low magnetic hysteresis: the unexpected role of magnetostriction. *A. Singh*[1], G. Grekas[1,2] and R. James[1] *1. Aerospace Engineering and Mechanics, University of Minnesota, Minneapolis, MN, United States; 2. Institute of Applied and Computational Mathematics, Foundation for Research and Technology, Heraklion, Greece*

Numerous studies in the 1950-1970s based on linear stability analysis of the single domain state on the shoulder of the hysteresis loop show that this method fails to predict the width of the loop, a conclusion referred to as the "coercivity paradox". In this talk we argue that the basic idea of using micromagnetics to predict coercivity is reasonable, but the fault lies with linear stability analysis; one needs to account for large but localized disturbances arising from potent defects. To investigate the prediction of coercivity in this context, we develop an implementation of micromagnetics using magnetization and vector potential as basic unknowns using the recent work of Di Fratta et al. (SIAM J. Math. Anal. 52, (2020), 10.1137/19M12613652020), and we borrow ideas from the strategy of Balakrishna et al. (npj Computational Materials 8, (2022), 10.1038/s41524-021-00682-7). We find that small values of magnetostriction have an important effect on coercivity. The introduction of magnetostriction(magneto-elastic energy) affects the nucleation barrier, which forces the magnetization to take an alternative path consistent with strain compatibility that in turn affects the coercivity of the material. The predictions are in a form that can be used for alloy development of soft magnetic materials.

[1] Di Fratta, G., Muratov, C. B., Rybakov, F. N., & Slastikov, V. V. (2020). Variational principles of micromagnetics revisited. *SIAM Journal on Mathematical Analysis*, *52*(4), 3580-3599. [2] Balakrishna, A. R., & James, R. D. (2021). A tool to predict coercivity in magnetic materials. *Acta Materialia*, *208*, 116697. [3] Renuka Balakrishna, A., & James, R. D. (2021). A solution to the permalloy problem—A micromagnetic analysis with magnetostriction. A*pplied Physics Letters*, *118*(21), 212404. [4] Renuka Balakrishna, A., & James, R. D. (2022). Design of soft magnetic materials. *npj Computational Materials*, *8*(1), 4.

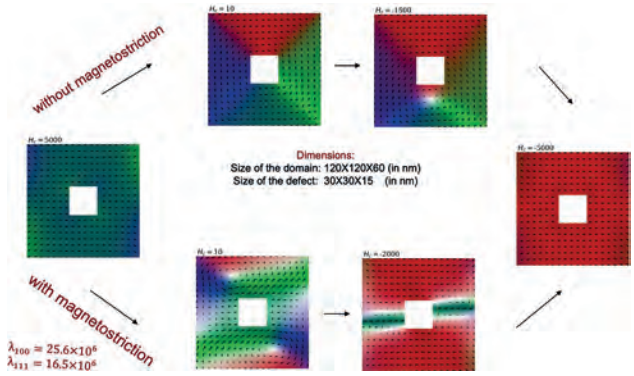

Fig.1 Effects of magnetostriction on domain pattern with the reducing applied field in FeNi alloy

FC-03. Microstructure and magnetic properties evolution of $CoFeMn_xAl_yTi_z$ alloys. J. Gu[1,2], J. Bai[3,2], Z. Leong[2] and *N. Morley*[2] *1. State Key Laboratory of Metastable Materials Science and Technology, Yanshan University, Qinhuangdao, China; 2. Materials Science and Engineering, University of Sheffield, Sheffield, United Kingdom; 3. School of Materials Science and Engineering, Northeastern University, Shenyang, China*

Soft magnetic materials are used in a wide range of high frequency applications, but are often limited by their cost and functional properties. High Entropy alloys (HEAs) offer an opportunity to investigate new soft magnetic materials within a very large compositional space. By incorporating the non-magnetic elements of Mn, Al, and Ti, into conventional CoFe soft magnetic materials, high entropy alloys were synthesized via arc-melting. The influence of these elements on the microstructure and magnetic

performance of the $CoFeMn_xAl_yTi_z$ HEAs were investigated. Key findings indicate that the alloys primarily consist of a body-centred cubic (BCC) phase when the Mn content (x) ranges from 0.2 to 0.6, Al content (y) ranges from 0.2 to 0.8, and the Ti content (z) is between 0 and 0.4. However, when the Mn content exceeds 0.5 and the Al-to-Ti ratio approaches 1.7, spinodal decomposition BCC phases are formed. All investigated CoFeMnAlTi alloys exhibit excellent soft magnetic properties. Notably, the $CoFeMn_{0.2}Al_{0.2}Ti_{0.2}$ alloy demonstrates the highest saturation magnetization value of 181 Am^2/kg, maintaining stability within a temperature range of 5 K to 300 K. The coercive field for the alloy series is deemed acceptable, measuring approximately 2 kA/m. These findings suggest that the multicomponent CoFeMnAlTi alloys present a promising alternative for soft magnetic material applications.

FC-04. Magnetic, structural, and transport properties of Heusler alloy Cr_2FeSn. *G. Karthik*[1], M. Muthuvel[2], K. Pradeep[3], S.P. Nagappan Nair[4] and K. Ravichandran[1] *1. Department of Nuclear Physics, University of Madras, Chennai, India; 2. Defense Metallurgical Research Laboratory, Defence Research and Development Organisation, Hyderabad, India; 3. Department of Metallurgical and Materials Engineering, Indian Institute of Technology Madras, Chennai, India; 4. Department of Physics, Indian Institute Of Technology, Chennai, India*

The study of magnetic properties of Heusler alloys have attracted immense attention in recent times due to their fascinating properties such as high spin polarization, half metallicity, crystalline ordering and low damping constant which makes them potential applicants in ultralow power spintronic devices [1,2]. In this study, we have explored how the structural disorderness of Heusler alloy Cr_2FeSn (CFS) influences its physical transport characteristics. The full Heusler alloy was synthesized by vacuum arc melting followed by vacuum annealing. In order to investigate the structure and composition of the prepared CFS sample, X-ray diffraction and electron microscopy analysis has been carried out. We infer that the sample has a disordered phase of the $L2_1$ type, with secondary phases of $FeSn_2$ and Sn. Further, local electrode atom probe (LEAP) analysis was performed and we see that the elements are homogeneously distributed in the FH phase. Magnetic measurements performed using SQUID suggest that the alloy is soft ferromagnetic in nature having low coercive field values with a saturation magnetization of 1.5 μ_B/f.u. (at 4K) and a Curie temperature of 375K. The intrinsic structural disorder dramatically affects the thermal and electrical transport in the sample. At the high-Sn end, strange thermal transport behavior with unusually low thermal conductivity ~7.6 W/mK at 8K is observed for CFS. By analyzing transport properties of CFS, we observe that the linear magnetoresistance obtained is mainly dominated by the high-mobility bulk electron carriers present in the sample. Also, we notice that the secondary phase of non-cubic $FeSn_2$ intermetallic is highly anisotropic in behaviour at low temperatures. We further predict that the reduced electrical conductivity can be correlated with the microstructure of the sample. We believe that these findings are useful for further investigation towards the design of potential bulk materials for magnetic Heusler alloy applications and also allow us to comprehend the effect of the kind and degree of disorder on its functional properties.

Zhang, Xiaoqian, et al. "Direct observation of high spin polarization in Co2FeAl thin films." *Scientific Reports* 8.1 (2018): 8074. Feng, Yu, et al. "Ultrahigh spin transport performance in Ti2CoGe based magnetic tunnel junction." *Journal of Magnetism and Magnetic Materials* 492 (2019): 165669. Karati, Anirudha, et al. "Ti2NiCoSnSb-a new half-Heusler type high-entropy alloy showing simultaneous increase in Seebeck coefficient and electrical conductivity for thermoelectric applications." *Scientific reports* 9.1 (2019): 1-12.

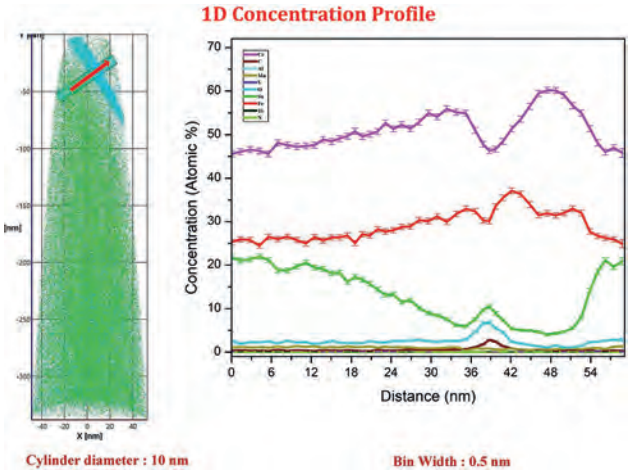

Fig.1 APT study showing composition profile of Cr_2FeSn alloy.

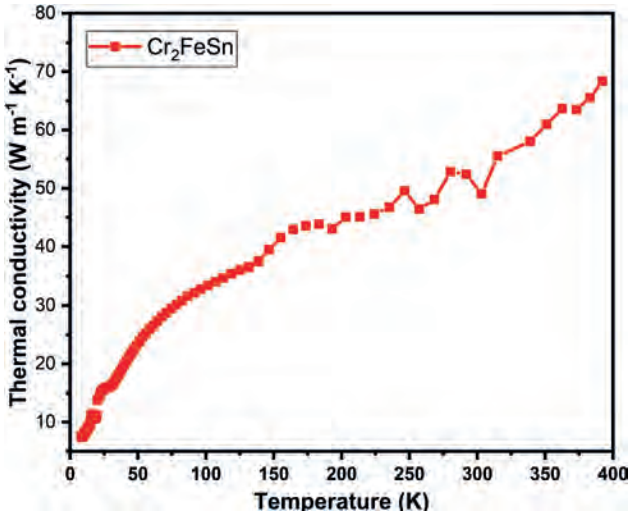

Fig.2 Thermal conductivity of Cr_2FeSn alloy.

INVITED PAPER

FC-05. A little bit of Information: Spin-Crossover and Magnetic Molecules for Information Science. *A. N'Diaye*[1] *1. Advanced Light Source, Lawrence Berkeley National Lab, Berkeley, CA, United States*

The physics of organic molecule thin films has opened up the field of molecular spintronics research. Organic molecules are coveted as the active ingredients for novel spintronic and electronic devices due to their versatility and energy efficiency, but also for their inexpensive ingredients and much reduced processing cost compared to conventional circuitry. Bi-stable spin-crossover molecules are promising candidates for memory and logic devices [1], while at the same time a number of fascinating fundamental questions regarding their switching mechanism remain to be explored [2,3]. I will present our recent work on spin-crossover and valence-tautomeric molecules. We investigated a number of ways to change the energetics of the transition between the spin states, primarily by choosing and manipulating the interface of a molecular thin film with its support. Figure 1 shows how spin state occupations change with the polarization of a ferroelectric interface using the spin states' fingerprints in x-ray absorption spectroscop. We will lay out a path to using this effect to propose spin-crossover molecule based devices [4].

[1] T. K. Ekanayaka *et al.*, "Nonvolatile Voltage Controlled Molecular Spin-State Switching for Memory Applications," *Magnetochemistry*, vol. 7, no. 3, p. 37, Mar. 2021, doi: 10.3390/magnetochemistry7030037. [2] G. Hao *et al.*, "Intermolecular interaction and cooperativity in an Fe(II) spin crossover molecular thin film system," *J. Phys.-Condes. Matter*, vol. 34, no. 29, p. 295201, Jul. 2022, doi: 10.1088/1361-648X/ac6cbc. [3] A. Mosey, A. S. Dale, G. Hao, A. T. N'Diaye, P. A. Dowben, and R. Cheng, "Quantitative Study of the Energy Changes in Voltage-Controlled Spin Crossover Molecular Thin Films," *J. Phys. Chem. Lett.*, vol. 11, no. 19, pp. 8231, Oct. 2020, doi: 10.1021/acs.jpclett.0c02209. [4] A. Dhingra *et al.*, "Molecular transistors as substitutes for quantum information applications," *J. Phys.-Condes. Matter*, vol. 34, no. 44, p. 441501, Nov. 2022, doi: 10.1088/1361-648X/ac8c11.

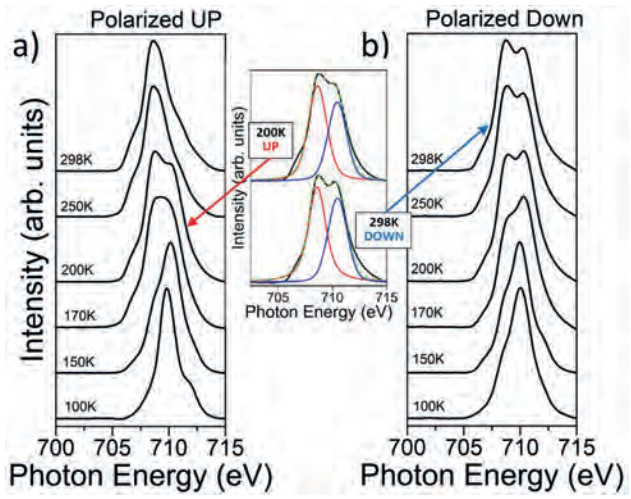

X-ray absorption spectra of [Fe{$H_2B(pz)_2$}$_2$(bipy)] on PVDF-HFP ferroelectric substrate. As the substate is polarized towards the molecular film (panel a), the film prefers the high spin state up to higher temperatures compared to the situation where the ferroelectric is poled away from the film (panel b).

CONTRIBUTED PAPERS

FC-06. $L1_0$-FePd(001) and epitaxial FePd|Ir|FePd (001) Synthetic Antiferromagnets on Si/SiO_2 Wafers. D. Lyu[2], J.E. Shoup[1], D. Huang[3], X. Wang[3], J. Wang[2] and *D.B. Gopman[1] 1. Materials Science and Engineering Division, National Institute of Standards and Technology, Gaitherburg, MD, United States; 2. Electrical and Computer Engineering, University of Minnesota, Minneapolis, MN, United States; 3. Mechanical Engineering, University of Minnesota, Minneapolis, MN, United States*

We present a more practical growth method for high-quality $L1_0$-FePd films on thermally-oxidized Si wafers, critical for energy-efficient magnetic tunnel junctions (MTJs). Owing to the advantageous <001> MgO film growth on amorphous surfaces (<001> is the highest density, electrically neutral planes in rock salt solids), we employ radio-frequency (*rf*) magnetron sputtering to deposit a 5 nm, fiber-textured MgO seed layer on thermal oxide to replace bulk MgO ($SrTiO_3$ or (001) alternatives) [1]. Subsequent layers inherit this (001) texture, contributing to high perpendicular magnetic anisotropy (PMA) and low Gilbert damping in the FePd (8 nm) layer. This technique was further refined for a fiber-textured synthetic antiferromagnet (SAF), achieved by a (001) FePd (6 nm) | Ir (0.45 nm) | FePd (3 nm) trilayer, displaying substantial PMA and interlayer exchange coupling (IEC). Sample stacks were fabricated through direct current magnetron sputtering, consisting of a Cr (30 nm) / Pt (4 nm) bilayer buffer, the FePd (8 nm) layer, and capping Ru (2 nm) / Ta (3 nm) layers. Microstructure was analyzed using X-ray diffraction and high-resolution transmission electron microscopy (HRTEM). Magnetic properties were characterized using vibrating-sample magnetometry (VSM) and time-resolved magneto-optical Kerr effect (TR-MOKE) spectroscopy. Magnetic property measurements reveal that even on an amorphous SiO_2 surface, the FePd layer exhibited strong PMA. HRTEM (see Fig. 1) confirms strong crystallinity and grain-on-grain growth from the MgO buffer, essential for the observed functional properties. We also show that by adjusting the thickness of the spacer in the SAFs, the strength of the IEC can be tuned. The largest IEC strength obtained in this study is 3.48 mJ m^{-2}, 35% larger than previous results (see Fig. 2). Fiber-texture FePd SAFs can exhibit large PMA, low damping and large PMA without the need for bulk epitaxial wafers, bringing the application of FePd into magnetic and spintronic devices on industry-ready Si/SiO2 wafers closer to practical realization [2].

[1] L. Zepeda-Ruiz and D. Srolovitz, Effects of ion beams on the early stages of MgO growth. *Journal of Applied Physics* 91, 10169–10180 (2002) [2] D. Lyu, *et al*., Sputtered $L1_0$-FePd and its Synthetic Antiferromagnet on Si/SiO_2 Wafers for Scalable Spintronics. *Advanced Functional Materials* 33, 2214201 (2023)

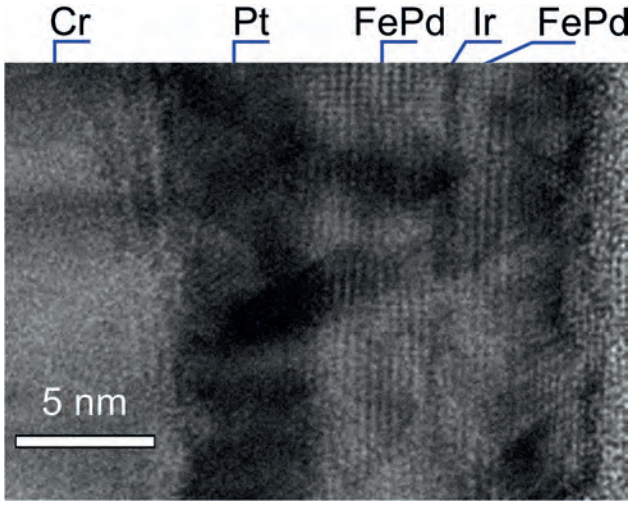

HR-TEM of <001> FePd|Ir|FePd pSAF

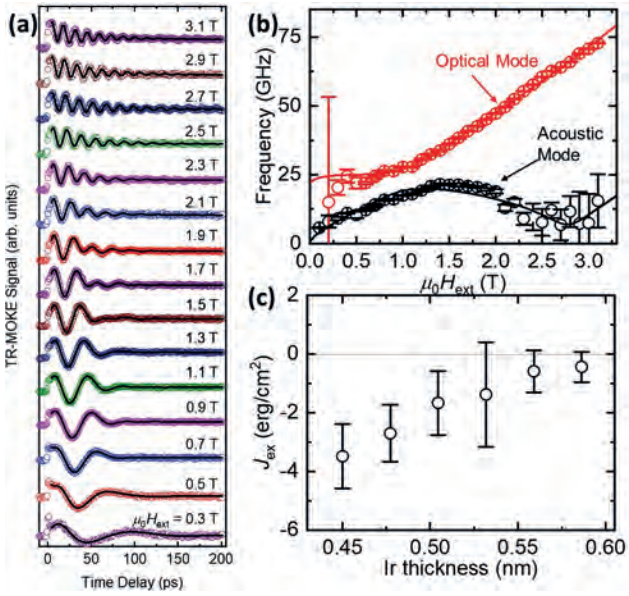

(a) TR-MOKE of FePd|Ir(0.45 nm)|FePd SAF; (b) Frequency vs field spectra; and (c) interlayer exchange coupling strength versus Ir thickness.

FC-07. Study of α″-phase $Fe_{16}X_{2-n}Y_n$ (X,Y=N, C) Alloys by Molecular Dynamics Modeling. *J. Zhu*[1], J. Wang[1] and G. Guo[1] *1. Electrical and Computer Engineering, University of Minnesota - Twin Cities, Minneapolis, MN, United States*

Research and development of soft magnetic materials without critical elements has gained a great deal of attention recently. Minnealloy, α″-phase $Fe_{16}(N_xC_{1-x})_2$, is one of promising candidates along this direction [1,2,3]. Theoretical calculation for this composition and its crystalline structure and lattice has been highly desirable to further advance the experimental effort. In fact, the level of 3d-orbital hybridization has strong dependence of inter-atomic distance between different Wycoff Fe positions (4d, 4e and 8h) to N atoms in α″-$Fe_{16}N_2$ [4]. Most of the DFT simulations commonly use the experimentally obtained $Fe_{16}N_2$ lattice structure as the starting point for study of $Fe_{16}X_2$ when X is non-N element. This may introduce inaccuracy as the starting lattice may not represent a global minimum state of the lattice to be studied. In this paper, we investigated crystal structures of α″-phase $Fe_{16}N_2$, $Fe_{16}C_2$ and the ternary alloy $Fe_{16}X_{2-n}Y_n$ (X, Y=N, C) using the energy minimization method based on the Molecular Dynamics (MD) modeling package. With a set of hybrid Fe-C and Fe-N Modified-Embedded Atom Method (MEAM) interatomic potentials and a designed structure energy minimization process, where the possible local energy minimum states were searched and evaluated to find the global lowest energy state, the mechanical-relaxed crystal lattices for these compositions were obtained and decided. Further atomic-level energy analysis on the minimum state lattice shows the relationship of atomic potential vs. their spatial locations with regards to X and Y atoms.

[1] Md Mehedi et al., "Minnealloy: a new magnetic material with high saturation flux density and low magnetic anisotropy," J. Phys. D: Appl. Phys. 50., 37LT01 (2017) [2] X.W. Zhang and J. P. Wang, "High saturation magnetization and low magnetic anisotropy Fe-CN martensite thin film", Appl. Phys. Lett. 114, 152401 (2019). [3] G. Guo, J. Liu, and J. P. Wang, "Carbon and Microstructure Effects on the Magnetic Properties of Fe–CN Soft Magnetic Materials (Minnealloy)", TMS 2020 149th Annual Meeting & Exhibition Supplemental Proceedings. The Minerals, Metals & Materials Series. Springer, Cham. pp 1841–1852. [4] N. Ji, X. Liu, and J.-P. Wang, "Cluster + Atom model: Theory of giant saturation magnetization in α″-$Fe_{16}N_2$: role of partial localization in ferromagnetism of 3d transition metals," N. J. Phys., 12 063032 (2010).

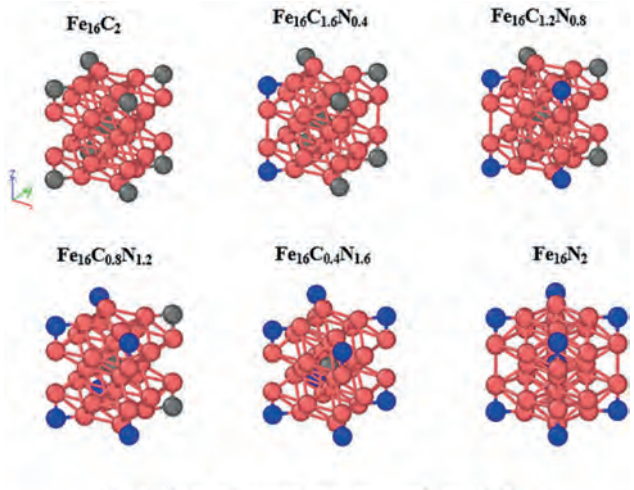

Fig.1. Unit cell crystal structures of $Fe_{16}(C_xN_{2-x})$

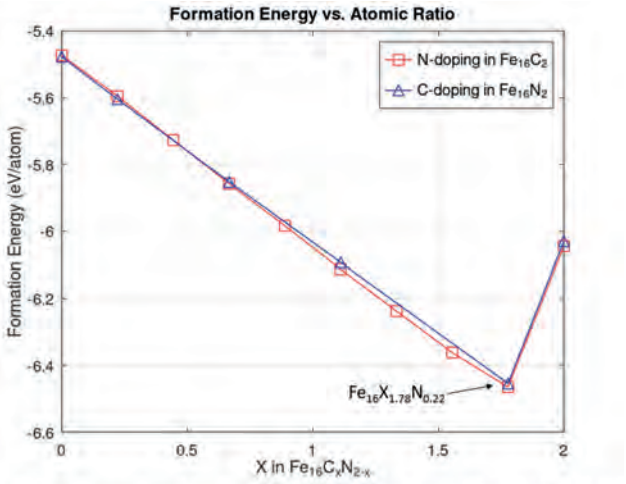

Fig.2. Calculated formation energy for various atomic composition in $Fe_{16}(C_xN_{2-x})$

FC-08. Chemical Anisotropy for Magnetic Anisotropy in Anti-Perovskites. *S. O'Donnell*[1], R.W. Smaha[2], S. Mahatara[2], S. Lany[2], S. Bauers[2] and J.R. Neilson[1] *1. Chemistry, Colorado State University, Fort Collins, CO, United States; 2. National Renewable Energy Lab, Golden, CO, United States*

The current energy transition to renewable sources will also see the demand for permanent magnets drastically increase. The current paradigm for designing hard permanent magnets is based on alloys of transition metals combined with rare-earth elements. However, there is a desire to reduce or eliminate the use of rare-earth elements due to their relative scarcity and geopolitical factors. Transition-metal rich nitride compounds are intriguing alternative, rare-earth free, permanent magnets. For example, $Fe_{16}N_2$, which forms as a vacancy-ordered anti-perovskite, is a promising rare-earth free alternative. Therefore, continued investigation of transition metal rich anti-perovskite nitrides is needed to further understand this interesting class of compounds. We present the investigation of Mn-based anti-perovskites with the general formula Mn_3AN. We discuss the synthesis and magnetism of these anti-perovskites, which are found to be antiferromagnetic with the unique exception of Mn_3AlN which is ferromagnetic with a T_C ~800 K. Further, we demonstrate the controlled removal of N from these phases to yield Mn_3AN_{1-x} ($0 < x \leq 1$) and discuss the role of N with respect to the structural and magnetic properties.

Session FD
NEXT-GENERATION MRAM TECHNOLOGY

Jonathan Z Sun, Chair
IBM T. J. Watson Research Center, Yorktown Heights, NY, United States

INVITED PAPER

FD-01. High performance spintronic devices for microwave technology and computing. *G. Finocchio*[1] *1. University of Messina, Messina, Italy*

In this talk, I will present recent advances achieved in the development of spintronic microwave technology. In particular, I will focus on detectors, oscillators and a new class of devices spintronic amplifiers based on magnetic tunnel junctions (MTJs)[1]. In fact, only a few concepts for spintronic amplifiers have been proposed, typically requiring complex device configurations or material stacks. Here, I will present a spintronic amplifier with a record gain of 2 for input power on the order of nW (< - 40 dBm) based on two-terminal magnetic tunnel junctions (MTJs). It is produced with CMOS-compatible material stacks that have already been used for spin-transfer torque memories. The latter part of the talk will focus on probabilistic computing which is one direction to implement Ising Machines. Probabilistic computing is a computational paradigm using probabilistic bits (p-bits), unit in the middle between standard bit and q-bits. I will show how to map hard combinatorial optimization problems (Max-Sat, Max-Cut, etc) into Ising machine and how to implement those in spintronic technology. I will also compare different annealing processes including simulated annealing, simulated quantum annealing and parallel tempering. This work was supported under the project number 101070287 — SWAN-on-chip — HORIZON-CL4-2021-DIGITAL-EMERGING-01, the project PRIN 2020LWPKH7 funded by the Italian Ministry of University and Research., and by the PETASPIN association (www.petaspin.com). This work has been also partially funded by European Union (NextGeneration EU), through the MUR-PNRR project SAMOTHRACE (ECS00000022).

[1] Zhu, K. *et al.* Nonlinear amplification of microwave signals in spin-torque oscillators. *Nat. Commun. 2023 141* 14, 1–9 (2023).

CONTRIBUTED PAPERS

FD-02. Thermal Stability Factor of $L1_0$-MnAl nanodot for STT-MRAM Applications. *T. Shinoda*[1,4], Y. Takeuchi[3], B. Jinnai[3], J. Igarashi[1], Y. Sato[1,4], S. Fukami[1,2] and H. Ohno[1,2] *1. Tohoku Univ., RIEC, Sendai, Japan; 2. Tohoku Univ., CSIS, Sendai, Japan; 3. Tohoku Univ., WPI-AIMR, Sendai, Japan; 4. Tohoku Univ., Graduate School of Engineering, Sendai, Japan*

As the commercialization of spin-transfer torque magnetoresistive random access memories (STT-MRAMs) with perpendicular-easy-axis magnetic tunnel junctions (MTJs) [1] progresses, material development for MTJs has become increasingly significant for advanced generations. In recent years, Mn-based ferromagnetic alloys have been intensively investigated due to their favorable switching and data-retention properties for STT-MRAMs. In particular, $L1_0$-ordered MnAl is a prime candidate because it has high spin polarization, low magnetization, low Gilbert damping constant, and large magnetocrystalline anisotropy [2-5]. Recently, epitaxial growth of nanometer-thin $L1_0$-MnAl film with $B2$-CoAl layer was demonstrated [5]. To utilize $L1_0$-MnAl in MTJs, it is necessary to investigate the data-retention performance of MnAl. In this study, we measure the thermal stability of MnAl nanodots with various thicknesses. $L1_0$-MnAl thin films are prepared using the same way as in the previous study [5] with various MnAl thicknesses (t). The stacks are annealed at 400 °C for an hour and are processed into dot devices with various diameters (D) using electron beam lithography, reactive ion etching, and Ar ion milling. Figure 1 shows the scanning electron microscopy (SEM) image of the MnAl nanodot formed on a Hall cross. We evaluate the thermal stability factor $\Delta(\equiv E/k_Bt)$ of the MnAl nanodot through the measurement of switching probability versus amplitude of pulse magnetic fields H. Figure 2 shows an example of obtained results for D = 72 nm and t = 5 nm. The thermal stability factor Δ of 231.3 and coercivity of 840 mT, much larger than the conventional CoFeB/MgO systems, are obtained. We investigate the MnAl thickness dependence of Δ and find that samples with thicker MnAl tend to show larger Δ, indicating that one can tune the retention performance depending on the application by varying the thickness of the MnAl.

[1] S. Ikeda *et al.*, Nature Mater. 9, 721 (2010). [2] M. Hosoda *et al*., J. Appl. Phys. 11, 07A324 (2012). [3] X. Zhang *et al*., Appl. Phys. Lett. 110, 252403 (2017). [4] D. Ozaki *et al*., IEEE Trans. Magn. 53, 1300604 (2017). [5] Y. Takeuchi *et al*., Appl. Phys. Lett. 120, 052404 (2022).

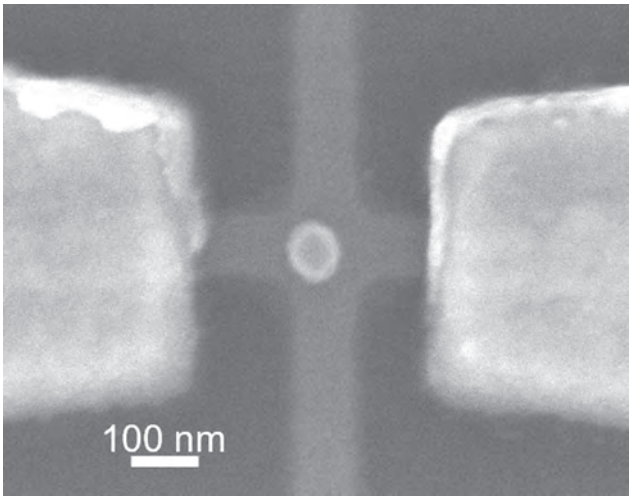

Fig. 1. SEM image of the nanodot. The MnAl thickness and the dot diameter are 5 nm and 72 nm, respectively.

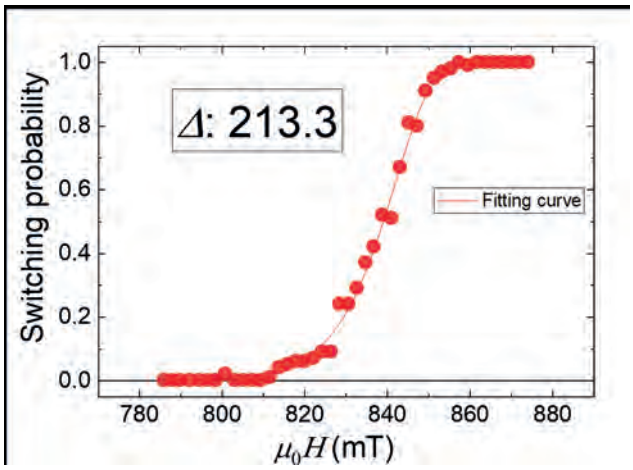

Fig. 2. Switching probability as a function of *H* for the device shown in Fig. 1.

FD-03. Impacts of Bottom Ferromagnetic Layer's Microstructure on Switching and Memristivity Performance in a Tri-layer SOT Device. *Y. Huang*[1], Y. Lin[1], C. Cheng[1], Y. Wu[1], W. Chang[2] and Y. Tseng[1]
1. National Yang Ming Chiao Tung University, Hsinchu, Taiwan;
2. Powerchip Semiconductor Manufacturing Corporation, Hsinchu, Taiwan

Spin-orbit torque (SOT) in a ferromagnet metal/nonmagnetic metal/ferromagnet metal (FM/NM/FM) tri-layer system attracts research interests as SOT switching driven by spin current from FM metal can be as efficient as classic heavy metal (HM)/FM system, and unconventional spin current, such as z-polarized spin current, enables novel device functionalities [1,2]. Thus, the second FM layer properties, such as anisotropy and microstructure, determine the effects of the above two merits of the tri-layer SOT device. We investigate the SOT switching and memristivity of a buffer/CoPt (5nm)/Cu (2nm)/Pt (2nm)/Co (0.8nm)/Pt (2nm) system, where the bottom CoPt (in-plane anisotropy) assists in the switching of top Pt/Co/Pt layer with perpendicular anisotropy. Ta and Cu were chosen as the buffer layer to control the CoPt microstructure. We find that the bottom CoPt is with an A1-disorder phase originally. The Ta and Cu buffers resulted in (111) texture and non-textured structures on the CoPt layer, respectively, despite close resistivity (~55μΩ.cm) and saturation magnetization (~550emu/cc). The non-textured Cu-CoPt exhibits a 10% reduction of critical current compared to the Ta-CoPt. Due to the nature of the tri-layer structure, both devices possess stable pulse-dependent intermediate states and exhibit potential memristor behaviors. The non-textured Cu-CoPt is more promising than the textured Ta-CoPt regarding the multi-state stability versus current-dependent performance.

[1] S. C. Baek et al. *Nature Mater* 17, 509 (2018). [2] J. Ryu et al., *Nature Elec.* 5, 217 (2022).

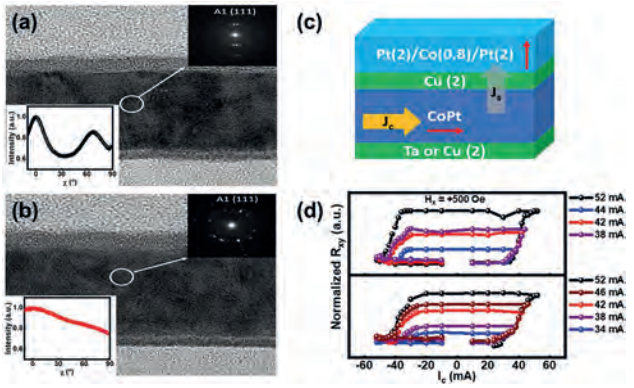

Fig. 1: HRTEM images of (a)Ta-CoPt and (b)Cu-CoPt devices with a CoPt layer of 20nm. Upper insets are the nanobeam electron diffractions of circled regions of the TEM images. XRD χ scans, particularly converted from the (111) diffraction rims, are shown in lower insets. (b) schematic of the tri-layer stacking; upper Pt/Co/Pt stack promises a perpendicular anisotropy, but the bottom CoPt has an in-plane anisotropy. Jc and Js represent charge and spin currents, respectively. (d) Memristor performance of Ta-CoPt (upper) and Cu-CoPt (lower) with pulse current dependence.

FD-04. Ultrafast SOT-induced magnetization switching in 75°-canted MTJ. *T. Nguyen*[1,2], H. Naganuma[2,1], H. Honjo[2], S. Ikeda[2,1] and T. Endoh[2,1]
1. Center for Science and Innovation in Spintronics, Tohoku University, Sendai, Japan; 2. Center for Innovative Integrated Electronic Systems, Tohoku University, Sendai, Japan

Spin-orbit torque (SOT)-induced magnetization switching has been widely investigated for high-performance MRAMs. So far, we have demonstrated the 0.35 ns field-free switching in canted SOT devices with 88 x 315 nm^2 MTJ integrated under a CMOS back-end-of-line fully compatible process [1-4]. For the SRAM replacement, a faster switching time and a lower switching current in a smaller MTJ are required for low power consumption and high-density MRAM. For this purpose, in addition to the experimental investigation, a thoughtful simulation is necessary to efficiently support the experimental results. Herein, we investigate the change in SOT-induced magnetization switching in a 75°-canted MTJ against a channel line by using micro-magnetic simulations under the influence of the field-like torque (T_FL), the Slonczewski-like torque (T_SL), and the damping constant (α). 10 x 30 nm^2 elliptic MTJ device was designed so that the current was applied in a direction that was 75°-canted along the long axis of the MTJ. The free layer has an in-plane easy axis with an out-of-plane magnetic anisotropy field of $\mu_0 H_k^{OP}$ = 0.01 T, excluding the demagnetization field. Using micro-magnetic simulations, the evolution of the magnetization can be described under the change in the ratio between T_FL and T_SL, i.e., the FL coefficient (β), and α. The switching time (τ), evaluated from the time evolution of the magnetization curve, is defined as the time at which the magnetization of the free layer is switched from the P state to the AP state. Fig. 1 (a), (b) show the dependence of τ on β and a, respectively. τ decreases with the increase of β and τ could be reduced from 200 ns to 30 ps by increasing β from 0 to around 1. As β > 1, τ did not change much. The decrease of τ was related to the increase in the value of the transverse component of the total spin torque in the device. In addition, τ increases with the increase of α, and the sub-nanosecond switching could be maintained as α increases up to 0.14, above which τ increases to a few nanoseconds. The results suggested that T_FL would enable the ultrafast field-free SOT switching down to a few tens pico-second time scale in a few tens nanometer MTJ.

[1] H. Honjo *et al.*, IEDM Technical Digest 28.5, (2019). [2] M. Natsui *et al.*, JSSC 56, 1116 (2020). [3] S. Fukami *et al.*, Nat. Nanotechnology 11, 621 (2016). [4] S. Fukami *et al.*, VLSI Tech., T61 (2016).

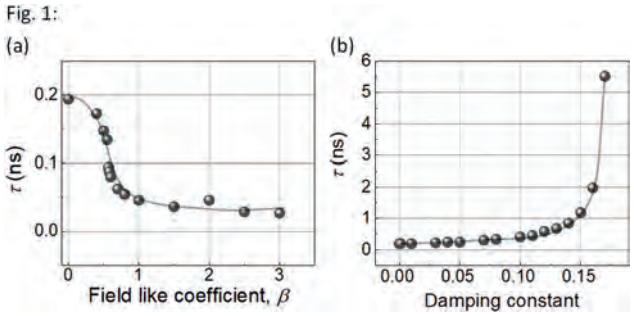

Dependence of τ on (a) β and (b) α.

FD-05. Using Transient Dynamics to Improve Switching Efficiency in In-Plane SOT-MRAM. *S. Nallan*[1] and J. Zhu[1] *1. Data Storage Systems Center, Carnegie Mellon University, Pittsburgh, PA, United States*

In this work, we present a series of strategies for reducing the underlayer current required to change state in spin orbit torque magnetic random access memory (SOT-MRAM) devices stabilized by an in-plane axis of anisotropy. We begin by studying the transient dynamics of the SOT-MRAM switching process through time-resolved simulations of the Landau-Lifshitz-Gilbert equation, with particular reference to the dependence of the critical switching current on the duration, magnitude, and injection angle of the in-plane charge current pulse. We demonstrate that this switching behavior is anisotropic and complex in nature, featuring significant nonlinearities and regions of stochasticity that can be manipulated to alter the boundary between failed and successful switching. We then present theoretical justification for a series of methods to achieve these alterations, including: imposing an in-plane magnetocrystalline hard axis through epitaxial lattice-matching; introducing a small amount of out-of-plane spin Hall current through geometric symmetry breaking; and creating effective bias fields through exchange coupling with other magnetic layers. We employ a series of numerical simulations to quantify the effective parameter range and relative improvements in switching current associated with each of these alternative switching strategies. Finally, we discuss methods to create the proposed crystal structures and device architectures in the lab to enable experimental validation of these simulation results.

FD-06. Ultra-highly Efficient SOT-writing in strained MTJs. *H. Yoda*[1], Y. Ohsawa[1], T. Kishi[1], Y. Yamazaki[1], T. Yoda[1] and T. Yoda[1] *1. YODA-S, Inc., Tsukuba, Japan*

STT-MRAMs using MTJs with perpendicular magnetic anisotropy (PMA-MTJs) have been commercialized mainly as embedded Flash-memory replacement where nonvolatility matters. However, the inherent trade-off relationships between critical switching-voltage (V_{csw}) or critical switching-current (I_{csw}) and nonvolatility have been obstacles to be broadly applied as cache-memories where active power consumption matters. In order to break the trade-off relationships, MTJs with strain-induced magnetic anisotropy (SIMA-MTJs) were proposed for SOT-writing [1]. In this study, MTJ size dependencies of write-efficiencies were studied. Since the power consumption across MTJs is roughly proportional to the product of write-voltage (V_w) and Write-current (I_w), new metrics for write-efficiency of retention energy (ΔE_r) over V_{csw} was introduced in addition to the conventional metrics of ΔE_r over I_{csw} and studied experimentally. The ΔE_r was estimated by switching probability due to magnetic field application. The material and the structure were the same as those of conventional MTJs with in-plane magnetic anisotropy. CoFeB with magneto-striction constant of 4E-5 was used in the MTJs. Sputter-deposited stack was etched by ion-beam into MTJs with aspect-ratio of 1 to 2. Anisotropic strain was produced in the MTJs by the same concept reported before [1]. The V_{csw} and the I_{csw} had almost no dependence on ΔE_r. The trade-off relationships were resolved. Fig.1 shows the MTJ length dependencies of the write-efficiencies in comparison with those of STT-writing in PMA-MTJs. The efficiencies of 1550 k_BT/V and 3.9 k_BT/microampere were obtained for the smallest MTJ with about 70nm by 80nm in size. The product of the two efficiencies is $6045(k_BT)^2$/(V×microampere) which is 13 times larger than $450(k_BT)^2$/(V×microampere) for STT-writing in PMA-MTJs with diameter of 25nm. Fig.1 also suggests that further shrinking the size will improve the efficiency. In summary, SOT-writing in SIMA-MTJs proved to have very high write-efficiencies and is thought to be a promising candidate for nonvolatile cache-memories.

[1] H. Yoda, K. Yakushiji, and A. Fukushima, Digests of VLSI-TSA 2022.

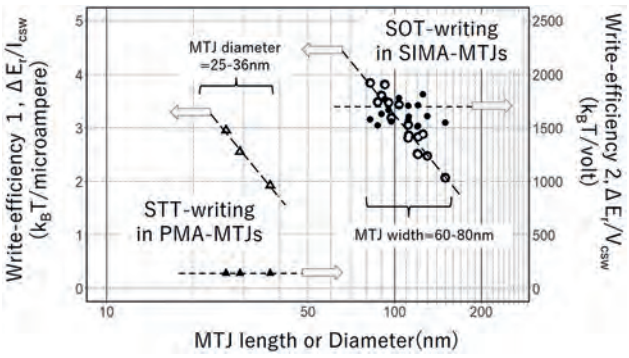

Fig.1 Comparison of write-efficiencies with 10nsec. pulse-width of SOT-writing in SIMA-MTJs with STT-writing in PMA-MTJs

FD-07. Competing Contributions from Spin-Transfer Torque, Voltage-Controlled Magnetic Anisotropy, and Joule Heating to Magnetic Properties in SOT-MRAM Devices. *K. Fan*[1,2], K. Cai[1], S. Van Beek[1], G. Talmelli[1], J. De Boeck[1,2], B. Soree[1,2], S. Rao[1], K. Wostyn[1] and S. Couet[1] *1. IMEC, Leuven, Belgium; 2. Department of Electrical Engineering (ESAT), KU Leuven, Leuven, Belgium*

Spin-orbit torque magnetoresistive random access memory (SOT-MRAM) is an emergent technology due to its non-volatile, sub-ns speed, and CMOS process compatibility [1], which garnered significant research attention. Especially, hybrid SOT switching with assisted voltage or current has been demonstrated for lower energy consumption, higher integration density, and field-free switching [2,3]. For those scenarios, either an additional current or voltage is required on the magnetic tunnel junction (MTJ), where contributions from spin-transfer torque (STT), voltage-controlled magnetic anisotropy (VCMA) and Joule heating are competing [4]. It is important to clarify these contributions and underlying physics. Our top-pinned three-terminal SOT-MRAM devices are deposited and integrated with the IMEC 300 mm platform with varying resistance area (RA) products. In this study, we analyzed the competing contributions by investigating the influence of three effects on the magnetic property. Figure 1(a) illustrates the switching fields of the free layer extracted from hysteresis loops by sweeping the external magnetic field. To separate different contributions, we performed a global fitting of the paired parameters of switching fields and quantified them as effective fields, respectively, as shown in Figure 1(b). In devices with RA 110, the B_{sw} correlates with a parabolic contribution because the contribution of heating is comparable with that of STT and VCMA. Additionally, the dependencies of effective fields on RA and CD size are displayed in Figure 2. High RA devices exhibit lower effective fields from STT and Joule heating, while all effects demonstrate limited correlations with the CD size, consistent with our model. Our study may contribute to RA and CD optimization of SOT-MRAM aiming at various functionalities. This work was supported by IMEC's industrial affiliation program on MRAM device and the European Union's Horizon 2020 research and innovation programme under the Marie Sklodowska-Curie (grant No. 955671).

1. K. Garello *et al.*, 2018 IEEE Symposium on VLSI Circuits, pp. 81-82 (2018) 2. K. Cai *et al.*, 2022 IEEE Symposium on VLSI Technology and Circuits, pp. 375-376 (2022) 3. W. Cai *et al.*, IEEE Electron Device Letters, Vol. 42, No. 5, pp. 704-707 (2021) 4. G. Mihajlović *et al.*, Physical Review Applied, 13, 024004 (2020)

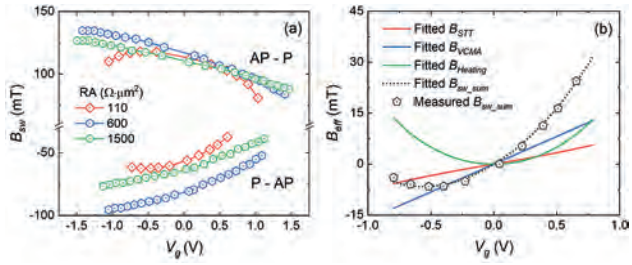

Fig.1 Gate voltage dependence of (a) switching fields; (b) fitted effective fields and the measured sum.

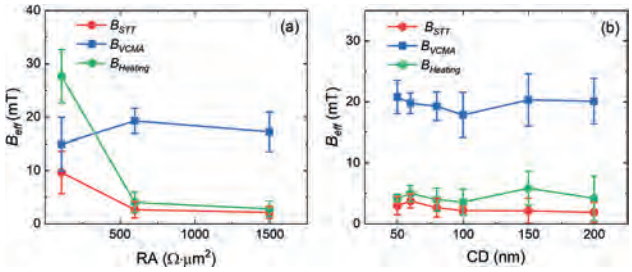

Fig. 2 Dependences of effective fields when V_g = 1V (a) RA dependence; (b) CD dependence.

FD-08. Electric field manipulation of tunnel magnetoresistance through localized strain. *S. Karki*[1], J. Kwon[1], J.E. Davies[2], R. Fabiha[3], T. Leonard[1], S. Bandyopadhyay[3] and J.C. Incorvia[1] *1. Electrical and Computer Engineering, The University of Texas at Austin, Austin, TX, United States; 2. NVE Corporation, Eden Prairie, MN, United States; 3. Electrical and Computer Engineering, Virginia Commonwealth University, Richmond, VA, United States*

Strain provides an additional means of controlling the magnetization of the free layer in magnetic tunnel junctions (MTJs) for energy-efficient computing. By using electric field-induced strain, the MTJ free layer can be switched with 1000 times lower energy compared to standard spin-transfer torque switching[1]. In previous works, an electric field of approximately 8 kV/cm, equivalent to 400 V, is required for magnetization rotation through induced strain, when voltage is applied across a Pb $(Mg_{1/3}Nb_{2/3})_{0.7}Ti_{0.3}O_3$ (PMN-PT) [011] substrate of thickness 0.5 mm[2,3]. Another previous study used a local gate on PMN-PT [001] and reported an operating voltage of around 100 V for micron-sized devices[4]. In this work, we demonstrate that by applying voltage through a local gate technique and using a piezoelectric substrate interfaced with the free layer, we can control and tune the switching field and tunnel magnetoresistance of nanoscale MTJs with record-low voltage. Figure 1 shows a top-down image of the 480 nm 520 nm elliptical in-plane MTJ on a PMN-PT [001] substrate, with voltage pads for local strain positioned 48 um apart. Figure 2 shows the in-plane field loop along the long axis of the ellipse at gate voltages of 5 V, 15 V and 20 V, showing the change in resistance ΔR (resistance in antiparallel alignment [R_{AP}]- resistance in parallel alignment [R_P]). The results show that when 20 V is applied to the PMN-PT substrate, which is equivalent to an electric field of 4.17 kV/cm, there is an 86% increase in leading to enhancement, and when voltage as low as 5 V is applied to the PMN-PT, which is equivalent to electric field of 1.04 kV/cm, there is 20% increase in leading to enhancement. The enhancement is attributed to strain-induced improvement in alignment of the magnetization between the free and fixed layers of the MTJ, as well as strain-induced modification of the crystalline lattice of the MgO barrier[4,5]. These results are important next steps in achieving energy-efficient straintronic devices based on MTJs.

(1) Barangi, M.; Mazumder, P. Straintronics: A leap toward ultimate energy efficiency of magnetic random access memories. *IEEE Nanotechnol. Mag.* 2015, *9* (3), 15-24. https://doi.org/10.1109/MNANO.2015.2441106. (2) Liu, M.; Lou, J.; Li, S.; Sun, N. X. E-field control of exchange bias and deterministic magnetization switching in AFM/FM/FE multiferroic heterostructures. *Adv. Funct. Mater.* 2011, *21* (13), 2593-2598. https://doi.org/10.1002/adfm.201002485. (3) Chen, Y.; Fitchorov, T.; Vittoria, C.; Harris, V. G. Electrically controlled magnetization switching in a multiferroic heterostructure. *Appl. Phys. Lett.* 2010, *97* (5). https://doi.org/10.1063/1.3475417. (4) Zhao, Z.; Jamali, M.; D'Souza, N.; Zhang, D.; Bandyopadhyay, S.; Atulasimha, J.; Wang, J. P. Giant voltage manipulation of MgO-based magnetic tunnel junctions via localized anisotropic strain: A potential pathway to ultra-energy-efficient memory technology. *Appl. Phys. Lett.* 2016, *109* (9). https://doi.org/10.1063/1.4961670. (5) Loong, L. M.; Qiu, X.; Neo, Z. P.; Deorani, P.; Wu, Y.; Bhatia, C. S.; Saeys, M.; Yang, H. Strain-enhanced tunneling magnetoresistance in MgO magnetic tunnel junctions. *Sci. Rep.* 2014, *4*, 1-7. https://doi.org/10.1038/srep06505.

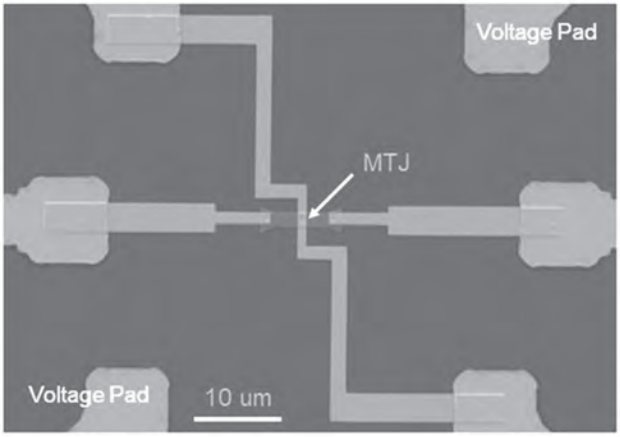

Figure 1: Top-down scanning electron microscope image of the 480 nm 520 nm MTJ.

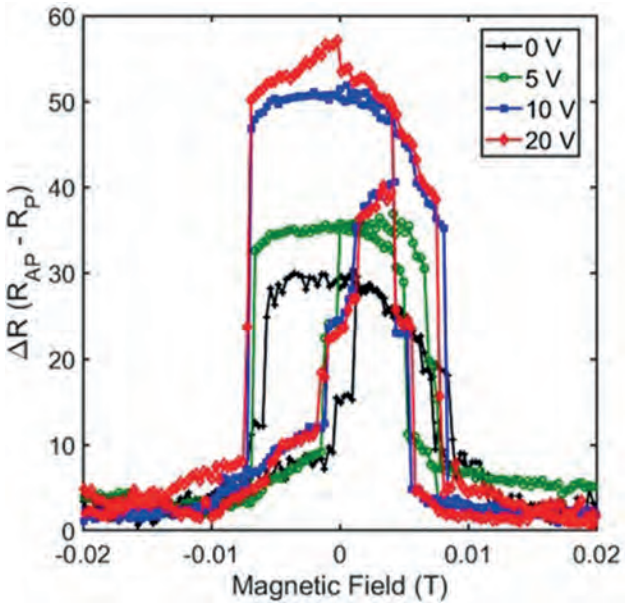

Figure 2: Field loop (H vs ΔR) for 480 nm 520 nm elliptical MTJ at various applied voltages.

FD-09. Physically Unclonable Functions using Voltage-Controlled Magnetic Anisotropy Effect in Magnetic Tunnel Junctions. Y. Tanaka[1], *M. Goto*[1,4], A.K. Shukla[1], K. Yoshikawa[1], H. Nomura[1,3], S. Miwa[1], S. Tomishima[2] and Y. Suzuki[1,3] *1. Osaka University, Toyonaka, Japan; 2. Intel Labs, Hillsboro, OR, United States; 3. CSRN-Osaka, OTRI-Osaka, Toyonaka, Japan; 4. University of Fukui, Fukui, Japan*

Physically unclonable functions (PUFs) exploit variations in device properties caused by device imperfections such as lattice defects to generate irreproducible bit strings. PUFs have potential applications in hardware security and can be used for device authentication, private key generators, and IoT security. In recent years, various types of his PUF have been proposed [1-3], however, these PUFs have a large footprint due to the large number of elements in the memory cell. On the other hand, PUF based on a magnetic tunnel junction (MTJ) results in a smaller footprint. Therefore, PUFs using current-driven MTJs have been proposed [4]. However, it has the disadvantage that it is susceptible to thermal disturbance due to Joule heat. We implemented MTJ-PUF using the voltage-controlled magnetic anisotropy (VCMA) effect [5-6] which is less Joule heat. We deposited V (30 nm)/Fe (0.3 nm)/Co (0.14 nm)/MgO (1.4 nm)/Fe (10 nm)/Au (5 nm) on MgO substrate using a molecular beam epitaxy. Forty independent MTJ samples were microfabricated by photolithography, Ar ion milling, magnetron sputtering, and a vacuum evaporation system. By measuring the magnetoresistance, VCMA effect was observed as shown in Fig 1. Figure 2 shows the process for controlling the magnetization potential of the MTJs. $\mu_0 H_{\mathrm{eff}}$ is the effective magnetic field in the free layer, which varies for every MTJ depending on the manufacturing variation. Once voltage of -1000 mV is applied and turned off, the magnetization randomly directs left or right depending on $\mu_0 H_{\mathrm{eff}}$. We evaluated the PUF fundamental parameters: uniqueness, reliability, and uniformity as 57.5%, 87.1%, and 45.0%, respectively. These results indicate that voltage-controlled MTJs function as PUFs. This research was supported by the JST CREST Grant Number JPMJCR20C1, JSPS KAKENHI Grant Number JP20H05666, and JP23H01838, Research Grants from the University of Fukui (FY 2023).

[1] D. P. Sahoo, et al., IEEE Trans. Comput., 2018. [2] L. Lu, et al., IEEE International Symposium on Circuits and Systems, ISCAS, 2019. [3] S. Khan et al., Analog Integr. Circuits Signal Process, 2020. [4] T. Marukame, et al., IEEE Trans. Magn., 2014. [5] M. Weishiet et al., Science, 2007. [6] T. Maruyama et al., Nat. Nanotechnol., 2009.

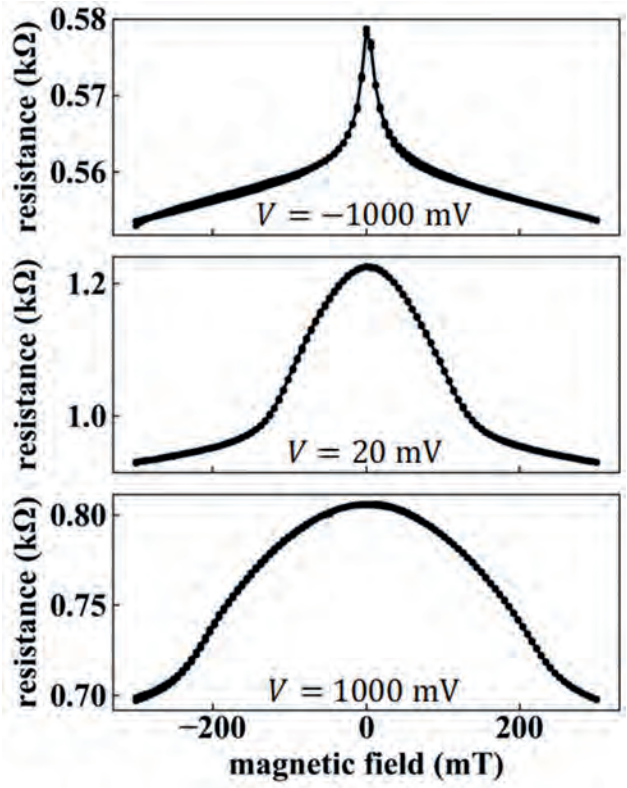

Fig. 1 Dependence of resistance on the perpendicular magnetic field for applied voltage V.

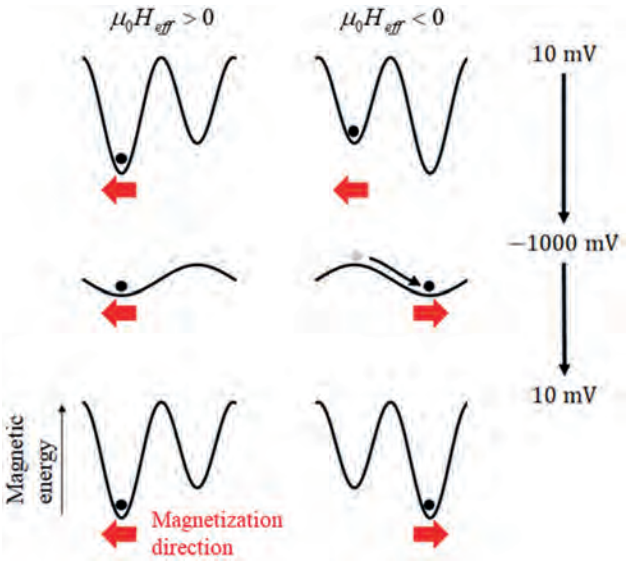

Fig. 2 Process for controlling the magnetization potential in the free layer of MTJs. The vertical and horizontal axes show the magnetization potential and direction, respectively. The red arrow is the magnetization direction.

FD-10. Giant spin-valve-like behavior induced by magnetic-field-controlled resistive switching in an Fe/MgO/Ge-based two-terminal device.
M. Kaneda[1], S. Tsuruoka[1], T. Endo[1], T. Takeda[1], Y. Tadano[1], T. Fukushima[2,3], H. Shinya[1,4], A. Masago[2,5], M. Tanaka[1,4], H. Katayama-Yoshida[2,4] and S. Ohya[1,4] *1. Department of Electrical Engineering and Information Systems, The University of Tokyo, Bunkyo-ku, Japan; 2. Center for Spintronics Research Network, Graduate School of Engineering Science, Osaka University, Toyonaka, Japan; 3. Institute for Solid State Physics, The University of Tokyo, Kashiwa, Japan; 4. Center for Spintronics Research Network, Graduate School of Engineering, The University of Tokyo, Bunkyo-ku, Japan; 5. Research Institute for Value-Added-Information Generation, Japan Agency for Marine-Earth Science and Technology, Yokohama, Japan*

Resistive switching (RS) has attracted considerable attention for its potential use in next-generation nonvolatile memory and neuromorphic computing [1,2]. Although the electric-field control of RS has been intensively studied, it is not widely known that RS devices also have unexplored multi-functionalities [3-5]. In particular, oxide materials, which are typically used for RS devices, sometimes exhibit d° ferromagnetism, a type of ferromagnetic behavior without d orbitals. There have been no reports of utilizing this intriguing feature in RS devices. Our previous study has revealed anomalous and colossal magneto-resistive switching (CMRS) in Fe/MgO/Ge heterostructure-based two-terminal devices, which can be attributed to the d°-ferromagnetic-filament formation via Mg vacancies in MgO [6]. Here, we present, for the first time, an unusual CMRS that exhibits spin-valve-like behavior with a large magnetoresistance (MR) ratio of up to 33,400% when applying appropriate bias voltages to the two-terminal device. Our findings imply that RS can be applied to spintronics devices, such as magnetic sensors and nonvolatile magnetic memory. We prepared a lateral two-terminal device composed of Co (5 nm) / Fe (17 nm) / MgO (1 nm) / Ge:B (17 nm, B concentration: 1×10^{18} cm^{-3}) epitaxially grown on a Ge (001) substrate. At the gap region with a width of 3 μm between the electrodes, carriers conduct through the Ge substrate. In our device, the *I–V* curve displays electric- and magnetic-field-controllable RS, as demonstrated by the hysteresis loop with a significant dependence on the magnetic field *H* (Fig. 1). The threshold voltage, at which the current abruptly increases, increases with increasing |*H*|. Using this hysteretic behavior about *H*, we obtained spin-valve-like MR curves with an MR ratio of 33,400 % (Fig. 2). The inset of Fig. 2 presents a distinct minor loop, indicating the nonvolatility of our device when applying appropriate voltages. This work was partly supported by Grants-in-Aid Scientific Research, JST CREST, JST ERATO, and the Spintronics Research Network of Japan.

[1] T. Shi *et al.*, Small Struct. 2, 2000109 (2021). [2] J. Zhu *et al.*, Appl. Phys. Rev. 7, 011312 (2020). [3] D. Sahu *et al.,* Sci. Rep. 7, 17224 (2017). [4] A. Kalitsov *et al.*, AIP Adv. 1, 42158 (2011). [5] S. Das *et al.*, Phys. Chem. C 114, 6671 (2010). [6] S. Ohya, M. Kaneda *et al.*, submitted.

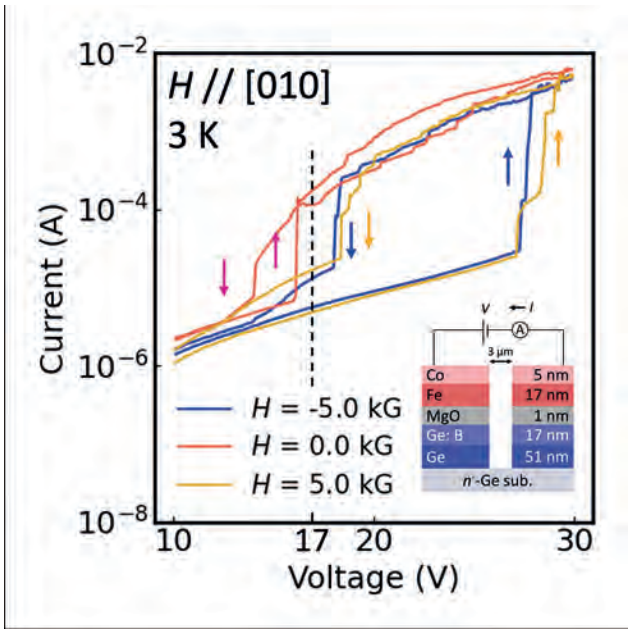

Fig. 1 *I–V* hysteresis loops at 3 K under different magnetic fields.

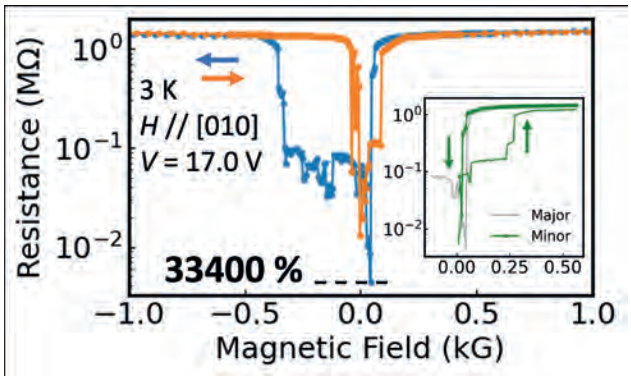

Fig. 2 Magnetoresistance at 17.0 V at 3 K. The minor loop is shown in the inset.

FD-11. Reconfigurable physically unclonable functions based on nanoscale voltage-controlled magnetic tunnel junctions.
Y. Shao[1], N. Melendez[2], F. Ebrahimi[3], J. Katine[2], G. Finocchio[4] and P. Khalili Amiri[1] *1. Department of Electrical and Computer Engineering, Northwestern University, Evanston, IL, United States; 2. Western Digital Corporation, San Jose, CA, United States; 3. Fe Research Inc, Los Angeles, CA, United States; 4. Department of Mathematical and Computer Sciences, Physical Sciences and Earth Sciences, University of Messina, Messina, Italy*

With the fast growth of the number of electronic devices in the internet of things (IoT), hardware-based security primitives such as physically unclonable functions (PUFs) have emerged to overcome the shortcomings of conventional software-based cryptographic technology[1, 2]. A PUF is an "electronic fingerprint" that provides certain outputs (known as responses) with respect to certain inputs (known as challenges), where the challenge-response pairs (CRPs) are unpredictable and unique to each particular device. Existing PUFs mainly exploit manufacturing process variations in a semiconductor foundry technology, which results in a static challenge-response behavior, and can present a long-term security risk. Spintronic devices provide a promising solution due to their abundant entropy, electrical reconfigurability, nonvolatility, and reliable magneto-resistive (MR) readout. Previously proposed PUF designs based on spin-transfer torque magnetic random-access memory (STT-MRAM) were still primarily dependent on

manufacturing variations[3-21], and thus were not reconfigurable. In addition, they suffered from the well-known read-disturb challenge of resistive memories[22-25], which reduces the CRP reliability if frequently used. Here we show a reconfigurable PUF based on nanoscale magnetic tunnel junction (MTJ) arrays that uses stochastic dynamics induced by voltage-controlled magnetic anisotropy (VCMA) for true random bit generation. A total of 100 PUF instances were implemented using 10 ns voltage pulses on a single chip with a 10×10 MTJ array. The unipolar nature of the VCMA mechanism was exploited to stabilize the MTJ state and eliminate bit errors during readout. All PUF instances showed entropy close to 1, inter-Hamming distance close to 50%, and no bit errors in 10^4 repeated readout measurements, the results are shown in Fig 1.

[1] R. Pappu, B. Recht, J. Taylor, and N. Gershenfeld, "Physical one-way functions," *Science,* vol. 297, no. 5589, pp. 2026-2030, 2002. [2] M. Tehranipoor and C. Wang, *Introduction to hardware security and trust*. Springer Science & Business Media, 2011. [3] L. Zhang, X. Fong, C.-H. Chang, Z. H. Kong, and K. Roy, "Highly reliable memory-based physical unclonable function using spin-transfer torque MRAM," in *2014 IEEE International Symposium on Circuits and Systems (ISCAS)*, 2014: IEEE, pp. 2169-2172. [4] L. Zhang, X. Fong, C.-H. Chang, Z. H. Kong, and K. Roy, "Highly reliable spin-transfer torque magnetic RAM-based physical unclonable function with multi-response-bits per cell," *IEEE Transactions on Information Forensics and Security,* vol. 10, no. 8, pp. 1630-1642, 2015. [5] E. I. Vatajelu, G. Di Natale, M. Indaco, and P. Prinetto, "Stt mram-based pufs," in *2015 Design, Automation & Test in Europe Conference & Exhibition (DATE)*, 2015: IEEE, pp. 872-875. [6] E. I. Vatajelu, G. Di Natale, and P. Prinetto, "Security primitives (puf and trng) with stt-mram," in *2016 IEEE 34th VLSI Test Symposium (VTS)*, 2016: IEEE, pp. 1-4. [7] E. I. Vatajelu, G. D. Natale, M. Barbareschi, L. Torres, M. Indaco, and P. Prinetto, "STT-MRAM-based PUF architecture exploiting magnetic tunnel junction fabrication-induced variability," *ACM Journal on Emerging Technologies in Computing Systems (JETC),* vol. 13, no. 1, pp. 1-21, 2016. [8] S. Khaleghi, P. Vinella, S. Banerjee, and W. Rao, "An stt-mram based strong puf," in *2016 IEEE/ACM International Symposium on Nanoscale Architectures (NANOARCH)*, 2016: IEEE, pp. 129-134. [9] S. B. Dodo, R. Bishnoi, S. M. Nair, and M. B. Tahoori, "A spintronics memory PUF for resilience against cloning counterfeit," *IEEE Transactions on Very Large Scale Integration (VLSI) Systems,* vol. 27, no. 11, pp. 2511-2522, 2019. [10] S. Lim, B. Song, and S.-O. Jung, "Highly independent MTJ-based PUF system using diode-connected transistor and two-step postprocessing for improved response stability," *IEEE Transactions on Information Forensics and Security,* vol. 15, pp. 2798-2807, 2020. [11] B.Song,S.Lim,S.H.Kang,andS.-O.Jung,"Environmental-Variation-Tolerant magnetic tunnel junction-based physical unclonable function cell with auto write-back technique," *IEEE Transactions on Information Forensics and Security,* vol. 16, pp. 2843-2853, 2021. [12] Z. Kahleifeh, H. Thapliyal, and S. M. Alam, "Adiabatic/MTJ based Physically Unclonable Function for Consumer Electronics Security," *IEEE Transactions on Consumer Electronics,* 2022. [13] X. Zhang *et al.*, "A novel PUF based on cell error rate distribution of STT-RAM," in *2016 21st Asia and South Pacific Design Automation Conference (ASP-DAC)*, 2016: IEEE, pp. 342-347. [14] L. Zhang, X. Fong, C.-H. Chang, Z. H. Kong, and K. Roy, "Feasibility study of emerging non-volatilememory based physical unclonable functions," in *2014 IEEE 6th International memory Workshop (IMW)*, 2014: IEEE, pp. 1-4. [15] L. Zhang, X. Fong, C.-H. Chang, Z. H. Kong, and K. Roy, "Optimizating emerging nonvolatile memories for dual-mode applications: Data storage and key generator," *IEEE Transactions on Computer-Aided Design of Integrated Circuits and Systems,* vol. 34, no. 7, pp. 1176-1187, 2015. [16] S. Ghosh, "Spintronics and security: Prospects, vulnerabilities, attack models, and preventions," *Proceedings of the IEEE,* vol. 104, no. 10, pp. 1864-1893, 2016. [17] A. Iyengar, S. Ghosh, K. Ramclam, J.-W. Jang, and C.-W. Lin, "Spintronic PUFs for security, trust, and authentication," *ACM Journal on Emerging Technologies in Computing Systems (JETC),* vol. 13, no. 1, pp. 1-15, 2016. [18] J. Das, K. Scott, S. Rajaram, D. Burgett, and S. Bhanja, "MRAM PUF: A novel geometry based magnetic PUF with integrated CMOS," *IEEE Transactions on Nanotechnology,* vol. 14, no. 3, pp. 436-443, 2015. [19] H. Chen *et al.*, "Highly secure physically unclonable cryptographic primitives based on interfacial magnetic anisotropy," *Nano letters,* vol. 18, no. 11, pp. 7211-7216, 2018. [20] Y. Tanaka *et al.*, "Physically Unclonable Functions With Voltage-Controlled Magnetic Tunnel Junctions," *IEEE Transactions on Magnetics,* vol. 57, no. 2, pp. 1-6, 2020. [21] T. Marukame, T. Tanamoto, and Y. Mitani, "Extracting physically unclonable function from spin transfer switching characteristics in magnetic tunnel junctions," *IEEE Transactions on Magnetics,* vol. 50, no. 11, pp. 1-4, 2014. [22] R. Bishnoi, M. Ebrahimi, F. Oboril, and M. B. Tahoori, "Read disturb fault detection in STT-MRAM," in *2014 International Test Conference*, 2014: IEEE, pp. 1-7. [23] W. Zhao, T. Devolder, Y. Lakys, J.-O. Klein, C. Chappert, and P. Mazoyer, "Design considerations and strategies for high-reliable STT-MRAM," *Microelectronics Reliability,* vol. 51, no. 9-11, pp. 1454-1458, 2011. [24] H. Naeimi, C. Augustine, A. Raychowdhury, S.-L. Lu, and J. Tschanz, "STTRAM SCALING AND RETENTION FAILURE," *intel technology journal,* vol. 17, no. 1, 2013. [25] T. Na, S. H. Kang, and S.-O. Jung, "STT-MRAM sensing: a review," *IEEE Transactions on Circuits and Systems II: Express Briefs,* vol. 68, no. 1, pp. 12-18, 2020.

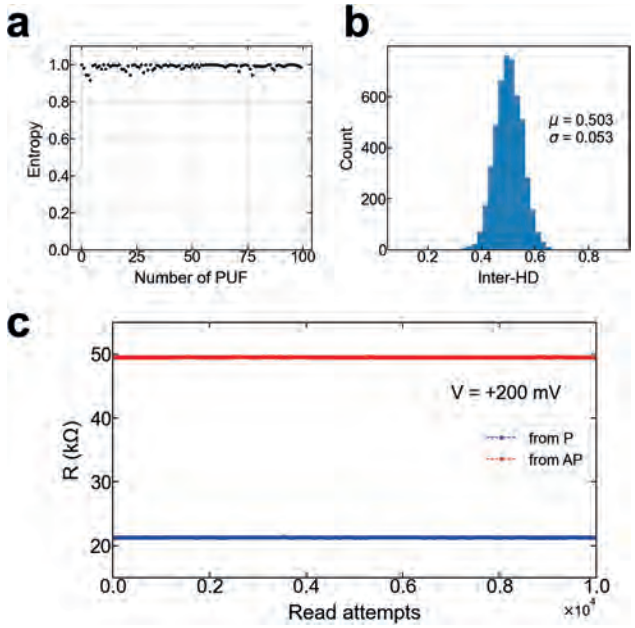

Fig. 1. PUF uniqueness characterization. a Entropy of 100 PUF instances implemented on the same 10×10 MTJ array. c Inter Hamming distance between the 100 reconfigured PUFs. c Results of 10^4 consecutive readout attempts with 200 mV read voltage. Red and blue represent starting from anti-parallel and parallel states, respectively. No bit errors are observed.

FD-12. Hybrid Hardware Security Systems with Strain-Modulated Magnetic Anisotropy. *A.N. Chin*[1], J.D. Arzate[1], Y. Makris[1], N. Hassan[1], A.J. Edwards[1] and J.S. Friedman[1] *1. Electrical and Computer Engineering, The University of Texas at Dallas, Richardson, TX, United States*

By obfuscating chip functionality behind a programmable key stored in on-chip non-volatile memory, logic locking aims to prevent the reverse-engineering and counterfeiting of integrated circuits [1-2]. After fabrication, the locked chip is activated and the security of the key in the open market determines the security of the design. Recently, researchers were able to directly reveal the obfuscation key by electrical imaging [3], thus posing a severe challenge for logic locking based on electron charge. We have therefore proposed using electron spin to circumvent this challenge, with a logic locking approach based on nanomagnetic logic (NML) [4]. As summarized in Fig. 1, a strain-inducing capping layer preserving perpendicular magnetic anisotropy along with the inherent polymorphism and non-volatility of NML enable storage of key bits. Without any electrical signatures of the key bits'

transportation or use, electrical imaging attacks are rendered useless, and the tamper-proof capping layer thwarts physical attacks. To mitigate the performance and reliability impacts from NML, we further proposed hybrid CMOS/NML logic systems that increase speed and reliability while inheriting the physical security benefits of NML by storing the key bits in secure NML islands (Fig. 2) [5]. We have evaluated the algorithmic security of the hybrid logic system, demonstrating strong resilience against a conventional algorithmic attack model and a physically-enhanced attack model where the attacker has illicit visibility of the activity of the CMOS portion of the chip. This highlights the capacity of these hybrid NML/CMOS logic systems to comprehensively offer physical and algorithmic security, while incurring minimal overhead costs from NML.

[1] J. A. Roy, F. Koushanfar, and I. L. Markov, "EPIC: Ending piracy of integrated circuits," in Proc. DATE, 2008, pp. 1069–1074. [2] P. Subramanyan, S. Ray, and S. Malik, "Evaluating the security of logic encryption algorithms," in Proc. IEEE HOST, 2015, pp. 137–143. [3] M. T. Rahman, S. Tajik, M. S. Rahman, M. Tehranipoor, and N. Asadizanjani, "The key is left under the mat: On the inappropriate security assumption of logic locking schemes." in Proc. HOST, 2020, pp. 262–272. [4] N. Hassan, A. J. Edwards, D. Bhattacharya, M. M. Shihab, V. Venkat, P. Zhou, X. Hu, S. Kundu, A. P. Kuruvila, K. Basu, J. Atulasimha, Y. Makris, and J. S. Friedman, "Secure logic locking with strain- protected nanomagnet logic," in Proc. DAC, 2021. [5] A. J. Edwards, N. Hassan, D. Bhattacharya, M. M. Shihab, P. Zhou, X. Hu, J. Atulasimha, Y. Makris, and J. S. Friedman, "Physically and algorithmically secure logic locking with hybrid cmos/nanomagnet logic circuits," in Proc. DATE, 2022, (invited).

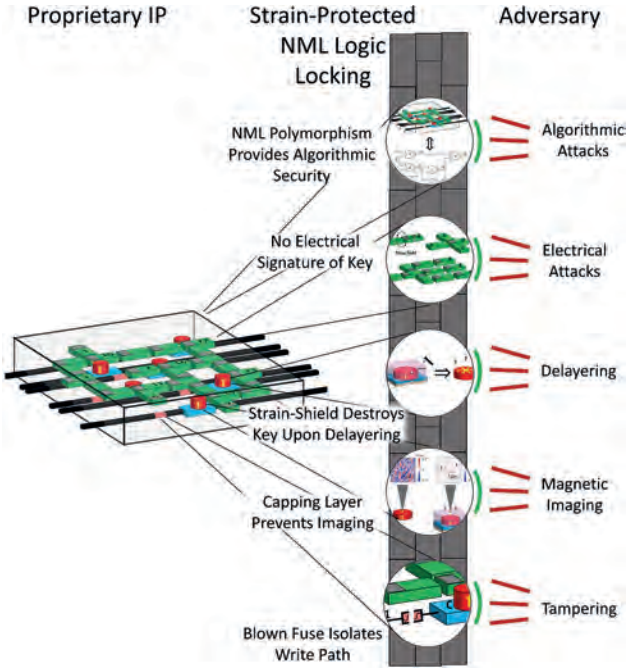

Security of strain-protected NML. As we demonstrated in [4], NML protected with an opaque strain-inducing shield is secure against all known physical and algorithmic attacks against logic locking.

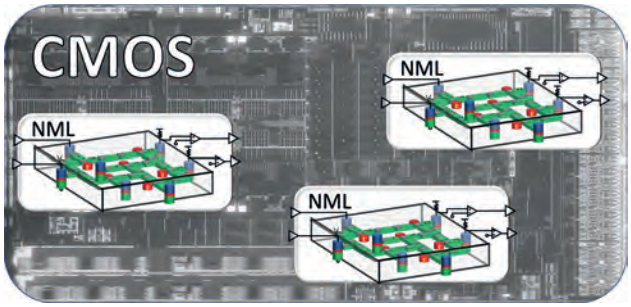

To reduce the NML overhead, hybrid CMOS/NML systems are proposed in which islands of NML work in tandem to secure a CMOS chip. The secret obfuscation key is stored in the physically secure NML islands, and the attacker cannot reveal the key even with complete knowledge of the CMOS portion of the logic.

Session FE
THIN FILMS, MULTILAYERS AND INTERFACE EFFECTS I

Markus Goessler, Chair
Chemnitz University of Technology, Chemnitz, Germany

INVITED PAPER

FE-01. Generation of Highly Anisotropic Physical Properties in Ferromagnetic Thin films Controlled by their Differently Oriented Nano-sheets. *C. Favieres*[1,2], J. Vergara[1,2], C. Magén[3,4], M. Ibarra[3,4] and V. Madurga[1] *1. Laboratorio de Magnetismo. Departamento de Ciencias. Física, Universidad Pública de Navarra (UPNA), Pamplona, Spain; 2. Instituto de Materiales Avanzados y Matemáticas, Universidad Pública de Navarra (UPNA), Pamplona, Spain; 3. Instituto de Nanociencia y de Materiales de Aragón (INMA), CSIC-Universidad de Zaragoza, Zaragoza, Spain; 4. Departamento de Física de la Materia Condensada, Universidad de Zaragoza, Zaragoza, Spain*

The generation and control of magnetic anisotropy in thin films at the nano-scale is a key question for addressing applications in many different fields, including sensors, actuators, permanent magnets, magneto-electronics, information processing or storage devices. For the first time we successfully fabricated and studied pulsed laser deposited ferromagnetic nano-crystalline thin films constituted by nano-sheets with a controlled slant. Films of Fe, Co, Co–Fe and Co-rich Co–MT (MT= V, Cr, Cu, Zn, Cd, Hf) were grown. The visualization of these nano-sheets by Scanning Tunneling Microscopy (STM) and High-Resolution Transmission Electron Microscopy (HRTEM) showed typically tilt angles ≈ 56° with respect to the substrate plane, and nano-sheets ≈ 3.0–4.0 nm thick, ≈ 30–100 nm wide, and ≈ 200–300 nm long, with an inter-sheet distance of ≈ 0.9–1.2 nm, depending on their constitutive elements. Induced by this special nano-morphology, all these films exhibited a large uniaxial magnetic anisotropy in the plane of the films, the easy direction of magnetization being parallel to the longitudinal direction of the nano-sheets and the hard direction being perpendicular to the nano-sheets. In the as-deposited films, typical values of the anisotropy field were measured between H_k = 600 and 1400 Oe (≈ 48 and 112 kA/m) depending on composition. The deduced effective shape anisotropy constant associated to the nano-sheets was, in some cases, similar or even higher than the magnetocrystalline anisotropy constant. The magnetic domains configuration of these thin films was also studied through the observation of charged domain walls. In addition to this magnetic anisotropy, we also found large uniaxial anisotropy in other physical properties of the films, such as transport, light reflection, mechanical and magneto-mechanical properties. The discovery of the nano-sheets allowed us to elucidate the origin of all these anisotropies. The changes in the nano-morphology of these films caused by thermal treatments, and hence in their anisotropic properties, were also studied. HRTEM, including chemical analysis at the nano-scale, allowed seeing these morphological and chemical changes. The nature and the activation energy spectra of the corresponding atomic relaxation processes developed were stablished when the dependence of the anisotropic resistance on temperature was simultaneously monitored. Remarkably interesting, some films retained their nano-sheet morphology, at least up to 500 °C, and retained and even increased their anisotropies by up to three times, with anisotropy fields H_k≈ 3000-3500 Oe (≈240-280 kA/m). For example, the thermal treatments produced crystallization processes and the growth of CoV magnetic phases maintaining the nano-sheets morphology. Similar and useful behavior has recently been found in some Co-Fe films with these nano-sheets. In contrast, other annealed films, CoZn, CoCu, CoCd… lost their nano-sheet-morphology. This work opens a new path of study for these new magnetically anisotropic materials, particularly with respect to the nano-morphological and structural changes related to the increase in magnetic anisotropy. A method for generating anisotropies by controlling the nano-sheet morphology of films, including oriented crystallization processes at the nano-scale, has been established in this work.

[1] V. Madurga, J. Vergara, C. Favieres. J. Magn. Magn. Mater. 272–276, 1681 (2004) [2] V. Madurga, C. Favieres, J. Vergara. Nanotechnology 21, 095702 (2010) [3] V. Madurga, J. Vergara, C. Favieres. Nanoscale Research Letters 6, 325 (2011) [4] J. Vergara, C. Favieres, V. Madurga. J. Phys. D: Appl. Phys. 48, 435003 (2015) [5] C. Favieres, J. Vergara, C. Magén, M. R. Ibarra, V. Madurga. J. Alloy. Compd. 664, 695 (2016) [6] J. Vergara, C. Favieres, C. Magén, J.M. De Teresa, M. R. Ibarra, V. Madurga. Materials 10, 1390 (2017) [7] C. Favieres, J. Vergara, C. Magén, M. R. Ibarra, V. Madurga. J. Alloy. Compd. 911, 164950 (2022) [8] C. Favieres, J. Vergara, V. Madurga. J. Appl. Phys. 133, 124301 (2023)

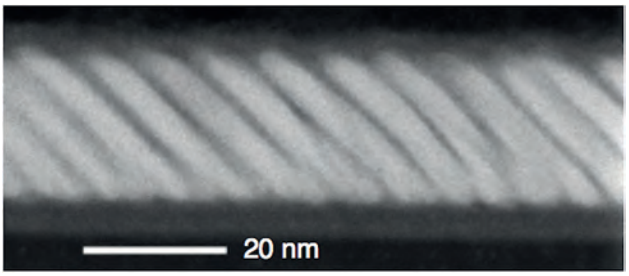

Fig. 1: Cross-section of a Co–Zn film, showing the corresponding internal cross section of the nano-sheets formed during the growth of the films. STEM HAADF was used to obtain the image [7].

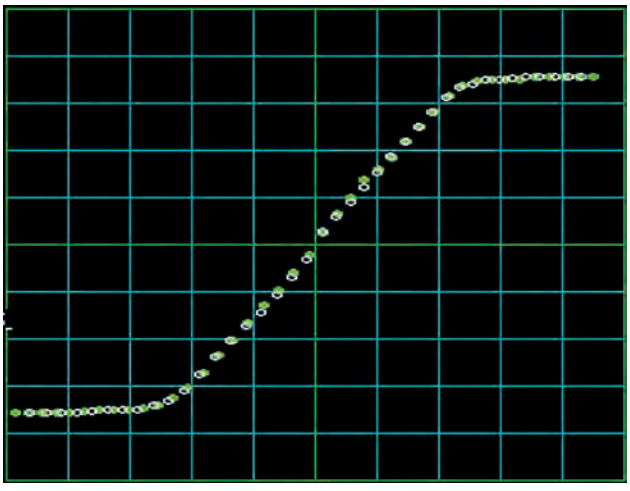

Fig. 2: In-plane non-hysteretic loop, magnetic moment *versus* applied magnetic field, *m–H*, measured in the hard direction corresponding to an as-grown Co(35%)-Fe(65%) film (≈ 40 nm thick, 7 mm in diameter) with uniaxial anisotropy. The film is constituted by inclined nano-sheets, similar to the nano-sheets whose cross section is shown in Fig. 1. The maximum applied magnetic field is 2300 Oe. The maximum value of the magnetic moment is 2.1 memu.

CONTRIBUTED PAPERS

FE-02. Fabrication and characterization of $Co_{25}Fe_{75}$/Hf multilayer thin films to decrease the magnetic damping coefficient. *S.C. Mills*[1], S.A. Mathews[1], K. Bussmann[1] and M. Staruch[1] *1. Material Science and Technology, U.S. Naval Research Laboratory, Washington, DC, United States*

In magnonic and spintronic devices, a low magnitude magnetic damping is desired for efficient operation via the long-range propagation of spin waves [1]. However, thin magnetic ferrite films (low damping but insulating) may not suffice if a charge current is needed [2]. Thin films of the conducting binary alloy of cobalt and iron ($Co_{25}Fe_{75}$) have exhibited low damping (~10^{-3}) [3]. To further decrease the damping of this system, a multilayer film consisting of ten 10 nm layers of $Co_{25}Fe_{75}$ alternated with 2 nm layers of hafnium (Hf) is proposed to prevent eddy current losses as well as simultaneously decreasing coercivity via smaller crystallite size [4,5]. Single phase (10 and 100 nm) and multilayer films were deposited via DC magnetron and RF sputtering. The ferromagnetic resonance (FMR) of the films showed as thickness increases, at a constant frequency (18 GHz shown), the FMR field decreases and linewidth increases, while the multilayered film achieves a lower linewidth and FMR field when compared to the 10 nm film (Fig. 1). The damping parameter (α) of the 10 nm $Co_{25}Fe_{75}$ and multilayer film was calculated, showing that the damping of the multilayered film (~$3x10^{-3}$) is lower than the 10 nm $Co_{25}Fe_{75}$ film (~$9x10^{-3}$) (Table 1). The total damping can have a variety of contributions; the contribution from eddy current generation is investigated to determine if the Hf interlayers are suppressing eddy current generation, lowering the overall damping. The multilayer structure shows the ability to tune the FMR and damping, demonstrating that these and other similar heterostructures are promising avenues for optimizing high frequency materials. Future development could include the use of an insulating interlayer or other magnetic materials.

[1] H. Glowinski, F. Lisiecki, P. Kuswik, J. Dubowik, and F. Stobiecki, *J. Alloys Compd.*, 785, 891-896 (2019). [2] E. Edwards, H. Nembach, and J. Shaw, *Phys. Rev. Appl.*, 11, 054036 (2019). [3] R. Weber, D. Han, I. Boventer, S. Jaiswal, R. Lebrun, *J. Phys. D: Appl. Phys.*, 52, 325001 (2019) [4] S. Balaji and M. Kostylev, *J. Appl. Phys.*, 121, 123906 (2017). [5] L. Garten, M. Staruch, K. Bussmann, J. Wollmershauser, and P. Finkel, *ACS Appl. Mater. Interfaces*, 14, 25701-25709 (2022).

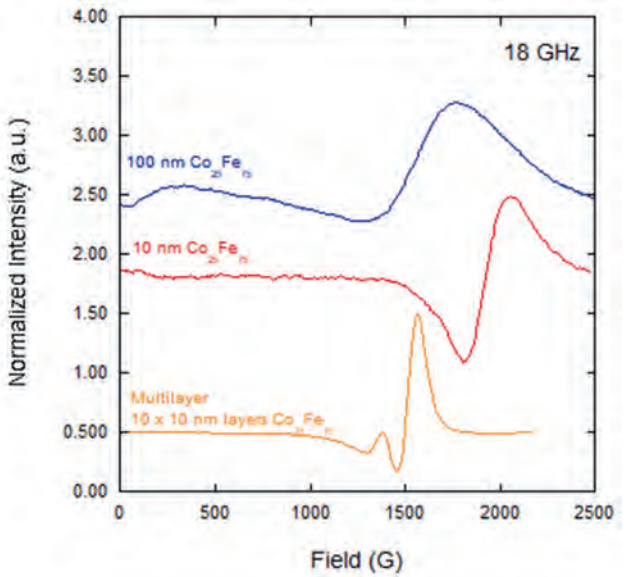

FMR measurements of $Co_{25}Fe_{75}$ films at 18 GHz, showing a decrease in FMR field and increase in linewidth as thickness increases, and the multilayer film with a lower linewidth and FMR field than the 10 nm film.

Sample	M_s (T)	H_c (Oe)	γ	Linewidth (G)					Resonance Field (G)					α
				Frequency (GHz)					Frequency (GHz)					
				14	15	16	17	18	14	15	16	17	18	
10 nm	1.21	97	237	136	147	149	158	164	1185	1342	1512	1688	1872	**0.0096**
100 nm	1.80	130	206											
Multilayer	1.55	30	189	73	78	79	77	84	1065	1207	1363	1529	1694	**0.0030**

Measured and calculated magnetic and FMR values for the 10 and 100 nm $Co_{25}Fe_{75}$ and multilayered films, used to ultimately calculate the damping (α). Linewidth and resonance field values (and therefore α) could not be measured due to limits in the curve fitting algorithm.

FE-03. Withdrawn

FE-04. Tuning the blocking temperature distribution of the antiferromagnetic grains by organic molecules. L. Gnoli[1], A. Riminucci[1], R.K. Rakshit[1], M. Singh[1], A. Mezzi[2], K. Lin[3], S. Achilli[4], E. Molteni[4], G. Fratesi[4], V.A. Dediu[1] and *I. Bergenti*[1] *1. CNR-ISMN, Bologna, Italy; 2. CNR-ISMN, Monterotondo Scalo, Italy; 3. Department of Materials Science and Engineering, NCHU, Taichung City, Taiwan; 4. University of Milan, Milan, Italy*

The interface between organic molecules and a magnetic layer has been designated as the key element in defining the the spin functionality of hybrid molecular spintronic devices. The origin of such effects is related to the formation of the so-called "Spinterface" that can affect the spin properties of both interface components as for example the generation of a spin polarization in the molecular layer or a change of the magnetic behaviour of the ferromagnetic layer (FM)[1]. Hybridization effects have been widely investigated both theoretically and experimentally considering FM layers[2] while the adsorption and coupling of molecules on surfaces with Antiferromagnetic (AFM) order has not a clear clue. In this view, because of the insensitivity of AFM to the external magnetic fields, with the aim of evidencing the effect of coupling between AFM and organics, we have considered the AFM layer also coupled to a FM featuring thus exchange bias effect. We deposited polycrystalline thin films of Co and we formed a bilayer with a single interface between Co and CoO by exposing the sample to a controlled oxygen atmosphere (10^4L), generating an oxide thickness of 2.5 nm. On the top of CoO a thick molecular layer (MOL 25nm) (C60 -buckminsterfullerene or Gaq3- Gallium tri(8-quinolinolate)) was deposited. The magnetic properties of the Co/CoO/MOL stacks were determined with a MOKE apparatus. Temperature dependent of Co hysteresis loops of the samples were acquired after cooling down to 80 K after appropriate training. The presence of the molecular layer onto CoO determines a hardening of the Co layer and an increase of the blocking temperature related to the exchange bias effect. We interpret our data considering that the hybridization with molecular layer generates an imbalance of Energy barrier for AFM reversal in CoO[3]. DFT calculations on model Co/Co/C60 slab support the experimental findings indicating a more stable eneregetic landscape for flipping AFM spins when the molecule is adsorbed on the surface.

[1] I. Bergenti and V. Dediu, V, Nanomaterials science 1 (2019) 149. [2] M. Cinchetti, V. Dediu, L.E. Hueso, Nat. Mater., 16 (2017) 507 [3]K. O'Grady et al., J. Magn. Magn. Mater., 322 (2010) 883

FE-05. Investigation of the Spin Rotation in a Ferrimagnetic Insulator with Easy Plane Anisotropy. *Y. Song*[1], T. Nguyen[2], K. Lasinger[1,3], G. Beach[1] and C.A. Ross[1] *1. Materials Science and Engineering, Massachusetts Institute of Technology, Cambridge, MA, United States; 2. Nuclear Science and Engineering, Massachusetts Institute of Technology, Cambridge, MA, United States; 3. Materials, ETH Zurich, Zurich, Switzerland*

An easy plane anisotropy 90° tilted from the film plane is critical for the specific spin current injection geometry to experimentally demonstrate novel phenomena of spin super-fluidity and terahertz signal generation. Both phenomena rely on a coherent magnetization rotation within the easy plane. Here, we demonstrate a thin film ferrimagnetic insulator, 13 nm thick (110)-oriented europium iron garnet ($Eu_3Fe_5O_{12}$, EuIG), in which we engineer an easy plane perpendicular to the film plane, Fig. 1a, b. To establish this unusual anisotropy landscape, we measure the temperature-dependence of the anisotropy by probing the equilibrium magnetization direction in a Pt/EuIG heterostructure under an applied magnetic field through spin-Hall magnetoresistance (SMR), Fig. 1c, d. With an in-plane field swept along the principal anisotropy axes ([1-10] and [001]), we characterize the anisotropy energies along these two in-plane axes. With an out-of-plane field along [110], we zoom in on the SMR signature. We identify a temperature range over which the easy-plane transition occurs, where the anisotropy energies along in-plane [1-10] and out-of-plane [110] axes balance each other giving the desired (001) easy plane perpendicular to the film plane. We observe a broad transition range instead of a sharp spin-reorientation transition because a weak cubic symmetric magnetocrystalline anisotropy modifies the ideally easy plane anisotropy landscape, creating energy barriers for spin-reorientation. We will discuss the implications of an easy plane anisotropy landscape in rare-earth iron garnet thin film systems on the investigation of spin orbit torques, switching and exchange driven ferrimagnetic dynamics.

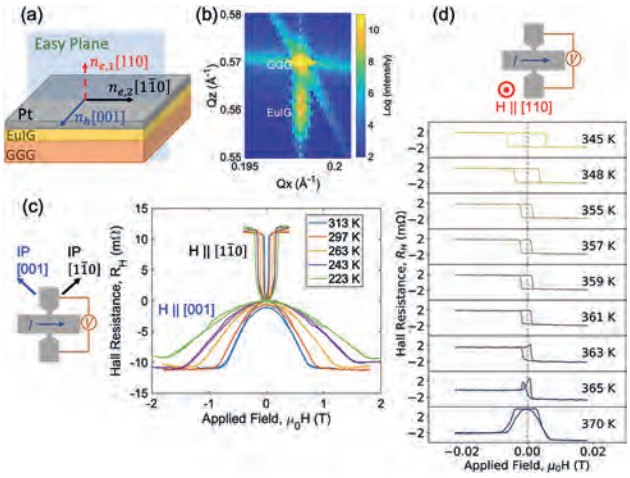

Fig. 1(a) Schematics of the heterostructure Pt(4nm)/EuIG(13nm)/GGG(110). The easy plane is characterized by a hard axis along [001] and two easy axes along [110] and [1-10]. (b) Reciprocal space map of EuIG(13nm)/GGG(110), showing EuIG is fully strained to GGG. (c) Left: SMR in-plane measurement geometry. Right: temperature dependence of the anisotropy energies along [1-10] and [001]. (d) Top: SMR out-of-plane measurement geometry. Bottom: SMR signature as temperature increases across the easy-plane transition.

FE-06. Growth-induced Changes in the Magnetic Properties of Co/Gd-based Synthetic Ferrimagnets for Magneto-Photonic Integration. *T. Kools*[1], J. Hintermayr[1], B. Koopmans[1] and R. Lavrijsen[1] *1. Department of Applied Physics, Eindhoven University of Technology, Eindhoven, Netherlands*

Recent work has demonstrated Co/Gd (double) bilayers to combine all-optical switching of the magnetization with efficient current-driven manipulation of the magnetic order in one material system [1]. This makes them interesting candidates for bridging the gap between spintronics and photonics [2]. Therefore, we systematically study the simplest Co/Gd-based synthetic ferrimagnet with PMA, the Pt/Co/Gd system [3]. Experimentally, we perform polar MOKE measurements on double wedge samples (Fig. 1) to investigate the transition of the net moment from Co- (red) to Gd-dominated (dark blue), and between non-magnetic, out-of-plane, and in-plane magnetization. For high Gd thickness (~ >3 nm) we would expect that the magnetic properties do not change anymore as the Gd is only magnetized close to the Co interface [3]. Strikingly, we observe the opposite, where the magnetic properties keep on changing monotonically up to at least 6 nm of Gd. We hypothesize that sputter-induced intermixing plays a role here. To test this we grow the films with different working gas pressures, changing the kinetics of the sputtered atoms, and indeed a large dependence is observed as shown in Fig 2. To corroborate this observation, we performed numerical simulations of the intermixing process of the Pt/Co/Gd system. We simulate our DC sputtering process in Tridyn [4], and use the extracted atomic profiles in conjunction with a layered Weiss model [5] to calculate the net moment and effective anisotropy. We find that key features in the experimental phase diagram (Fig. 1) can be reproduced, further suggesting that sputter-induced intermixing between Co and Gd in these systems cannot be neglected when describing their magnetic properties. In conclusion, our work provides highly relevant insight on the impact sputtering has on fundamental magnetic properties of Co/Gd bilayers and paves the way towards a better understanding of synthetic ferrimagnetic systems for spintronics.

[1]: Li, P., Kools, T. J., *et al.* (2023), *Adv. Electron. Mater.* 9, 2200613. [2]: Lalieu, M.L.M., *et al.,* (2019). *Nat Commun* 10, 110 [3]: Lalieu, M. L. M., *et al.* (2017). Phys. Rev. B, 96, 220411. [4]: Möller, W., & Eckstein, W. (1984). Nuclear Instruments and Methods in Physics Research Section B: Beam Interactions with Materials and Atoms, 2(1), 814–818. [5]: Beens, M., *et al.,* (2019). *Physical Review B*, *100*(22), 220409.

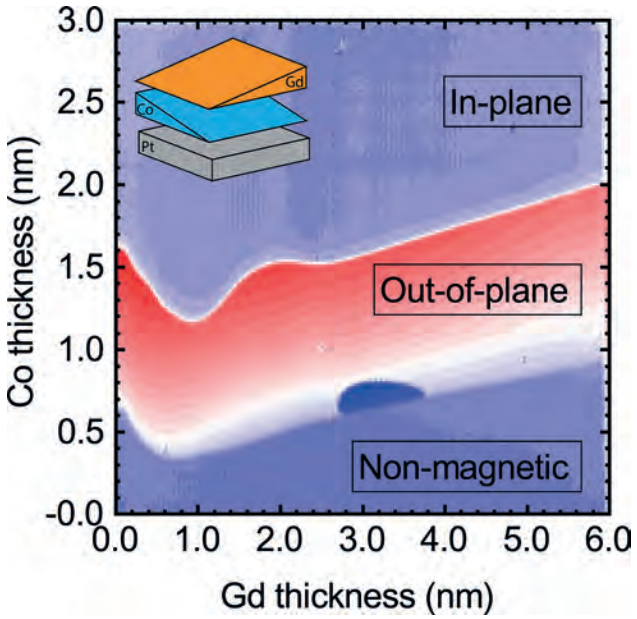

Fig. 1: Polar MOKE scan of the remanence of a Pt/Co(y-axis)/Gd(x-axis) synthetic ferrimagnetic bilayer sample.

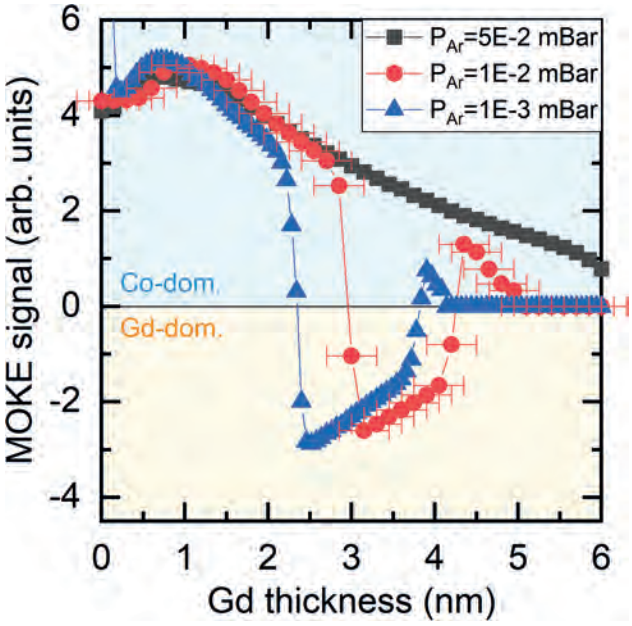

Fig 2.: Polar MOKE remanence for a Pt/Co(0.7)/Gd(x-axis) sample for different Ar gas pressures during the deposition process of the Gd.

FE-07. Combinatorial thin film plasma processing for investigation of magnetic antiperovskite nitrides. *S. Bauers[1] 1. Materials Science, National Renewable Energy Laboratory, Golden, CO, United States*

Metal nitrides are recognized as highly functional materials, including for magnetic applications. One family of magnetic nitrides is materials in the antiperovskite (or derived) crystal structure, with striking examples such as the strong ferromagnet $Fe_{16}N_2$ and negative thermal expansion in Mn_3AN, where *A* can be one of many main group or transition metals or alloys. However, the stability of the N_2 molecule makes reliable metal nitride synthesis difficult. Nitrides can often form with significant off-stoichiometry and quantitative composition characterization is difficult, leading to under-reporting of baseline chemical (and crystallographic) details, which has stymied the functionalization of many predicted and promising magnetic nitrides. Our group has synthesized several new thin film nitride materials using nitrogen plasma to create N* radicals, which are far more reactive than N_2,[1-3] while carefully measuring nitrogen composition using both Rutherford backscattering (RBS) and electron probe microanalysis (EPMA). We have recently adopted these approaches to the synthesis of magnetic materials.[4] This talk will discuss our work using combinatorial reactive co-sputtering for the rapid exploration of materials in Mn-(Ge, Si, Al)-N chemical spaces using spatially graded films to rapidly survey hundreds of unique synthesis conditions with only a few growths. We find that the use of a nitrogen plasma source directly influences the phases formed, for example controlling whether $MnGeN_2$ + MnN_x vs. phase pure Mn_3GeN forms in the germanium ternaries. We will also discuss our topotactic denitridation of the films to Mn_3AN_{1-x}, achieved by annealing under vacuum. The magnetic order in these antiperovskites is sensitive to nitrogen concentration and baseline stoichiometric Mn_3AlN is a soft ferromagnet while Mn_3GeN is antiferromagnetic. Thus, the alloyed systems provide several controls to systematically explore transitions in magnetic and electronic transport properties as a function of growth and post-processing conditions.

1 - *Proc. Natl. Acad. Sci. USA.* 2019, 116, 30, 14829-14834 2 - *Nat. Mater.* 2019, 18, 7, 732–739 3 - *Chem. Mater.* 2022, 34, 4, 1418–1438 4 - *Chem. Mater.* 2023, 35, 7, 2936–2946

FE-09. Annealing Induced Anomalous Phase Transformation in Mn-Ni-Sn Heusler Alloy Thin Films Grown by RF Magnetron Sputtering. *A. Verma*[1,2], K. Bhatt[1,2], P.K. Siwach[1,2], P. Kushwaha[1,2], J. Dev[1,2], J.S. Tawale[1], G.D. Varma[3], N. Singh[1,2] and H.K. Singh[1,2]
1. CSIR-National Physical Laboratory, New Delhi, India; 2. Academy of Scientific and Innovative Research (AcSIR), CSIR-HRDC Campus, Kamla Nehru Nagar, Ghaziabad, India; 3. Department of Physics, IIT Roorkee, Roorkee, India

Among Heusler alloys, Mn-Ni-Sn are noticeable due to their multifunctional properties. Here we are reporting about Mn-Ni-Sn based thin films which are important for various applications and offer an opportunity to tune the physical properties through the application of strain and epitaxy. In the present study we have grown the films by UHV RF magnetron sputtering of a target of composition $Mn_2Ni_{1.6}Sn_{0.4}$ on STO (100) substrates. The films were deposited at 500°C, 600°C, 700°C, and 800°C and annealed for 6h at deposition temperature. The XRR yielded the thickness of the films to be ~40nm. XRD (fig.1) shows a cubic structure and the presence of (200), (220) and (400) peaks suggest the B2-type symmetry. The films annealed up to 700°C are nearly single-phase but have spatial inhomogeneity. In film annealed at 800°C, the majority phase (lattice constant ~0.6nm) is still a cubic one but shows the formation of Sn-free unknown phases with an excess of Ni. The composition of thin film annealed at 500°C was found to be $Mn_{2.2}Ni_{1.5}Sn_{0.3}$. At higher temperatures the continuous layer was found to have the composition of ~ $Mn_{2.1}Ni_{1.6}Sn_{0.3,}$ while the granules at 600°C and 700°C are Ni-rich and Sn-deficient. In the film at 800°C, all the regions were Ni-rich and Mn-deficient, with the average composition of $Mn_{0.2}Ni_{3.1}Sn_{0.7}$. The evolution of the magnetization as a function of annealing temperature is depicted in Fig.2. The 500°C film shows a magnetic moment of ~21 emu/cm^3 which increases to ~28 emu/cm^3 and ~80 emu/cm^3 at 600°C and 700°C, respectively but magnetization drops to the lowest value ~16 emu/cm^3 at 800°C. The increase in the magnetic moment is accompanied by a decrease in the ZFC-FCW bifurcation and an increase in the T_C up to 700°C. The Ni-rich phase formed at 800°C has a smaller ZFC-FCW bifurcation. It also shows a transition from a low moment to a higher moment phase around ~270 K. The observed evolution of the magnetic and transport properties has been explained in terms of the structural and microstructural features of the films.

K. Elphick, W. Frost, M. Samiepour et al., Science and Technology of Advanced Materials, 22 (2021) 235 J. Dubowik, K. Zaleski, I. Goscianska et al., Appl. Phys. Lett. 100 (2012) 162403 B. Borgohain, P.K. Siwach, N. Singh et al., J. of Supercond. and Novel Magnet. 32 (2019) 3295 P. Pal, A.K. Majumdar, A.K. Nigam et al., J. of Magn. and Magnetic Materials 341 (2013) 65

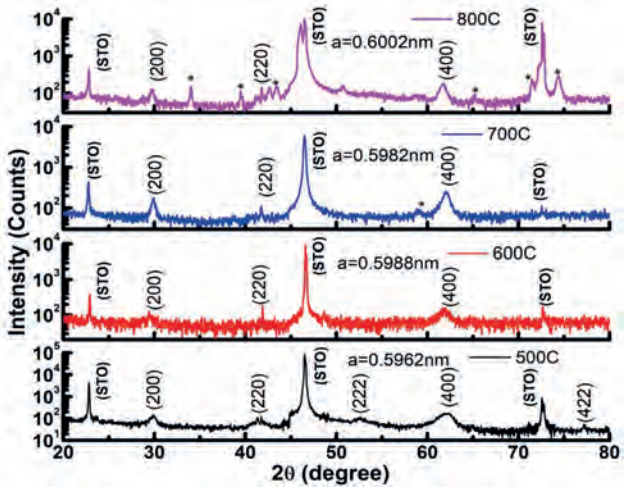

XRD pattern on the Mn-Ni-Sn films. The impurity peaks are indicated by asterisk

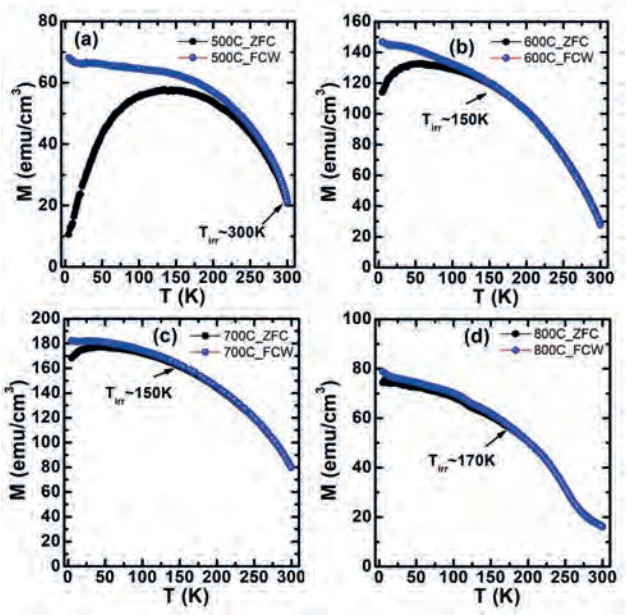

Temperature-dependent ZFC and FCW magnetization curves measured at H=100 Oe applied parallel to the film plane

FE-10. Tuning of the out of plane component of the magnetization in electrodeposited NiFe thin films. N. Coton[1], M. Jaafar[3], J. Andrés González[2], A. Begue[1] and *R. Ranchal*[1] *1. Materials Physics, Universidad Complutense de Madrid, Madrid, Spain; 2. Universidad Castilla-La Mancha, Ciudad Real, Spain; 3. Condensed Matter Physics, Universidad Autonoma de Madrid, Madrid, Spain*

Stripe domains are among the spin textures capable to promote reproducible spin waves generation [1-2]. In systems with moderate perpendicular magnetic anisotropy they appear above a critical thickness $t_{cr}= 2\pi(A_{ex}/K_U)^{1/2}$ where A_{ex} is the exchange energy per unit length and K_U the perpendicular magnetic anisotropy constant. Here we present how to exploit the electrodeposition technique to achieve a higher control of stripe domains formation. Firstly we have investigated the influence of the magnetic stirring during growth of $Ni_{90}Fe_{10}$ thin films deposited on glass substrates capped with a Au capping layer of 50 nm. Stripes can be clearly observed when electrolyte is not stirred but their presence is avoided when it is stirred (Fig. 1). This abscence of stripes has been measured even for a layer thickness above 1 μm which opens the possibility of using these layers in applications in which thick stripe domains-free permalloy layers are needed such as giant magnetoimpedance sensors. When stripes domains are present, an applied magnetic field of 100 Oe perpendicular to the sample plane has no effect on the hysteresis loop (Fig. 1). The quality of these samples from the magnetic point of view has been confirmed even when deposited on curved flexible substrates in which it has been measured a magnetostriction constant (λ) of -22 ppm, pretty close to the theoretical value [3]. We have also analyzed whether it is possible to promote the formation of stripe domains by means of an applied magnetic field perpendicular to the sample plane in the thickness range in which stripes are not observed in magnetic force microscopy but the IP hysteresis loops exhibit the transcritical shape. Finally, we have also investigated the growth of $Ni_{80}Fe_{20}$ thin films to check a potential effect of magnetostriction on the formation of stripe domains since this alloy, $Ni80Fe_{20}$, has a null λ.

[1] C. Liu, S. Wu, J. Zhang, J. Chen, J. Ding, J. Ma, Y. Zhang, Y. Sun, S. Tu, H. Wang, P. Liu, C. Li, Y. Jiang, P. Gao, D. Yu, J. Xiao, R. Duine, M. Wu, C.-W. Nan, J. Zhang, H. Yu, Nature Nanotech. 14 (2019) 691. [2] J. Ben Youssef, N. Vukadinovic, D. Billet, M. Labrune, Phys. Rev. B 69 (2004), 174402. [3] N. Coton, J.P. Andres, E. Molina, M. Jaafar, R. Ranchal. J. Magn.Magn. Mater. 565 (2023) 170246.

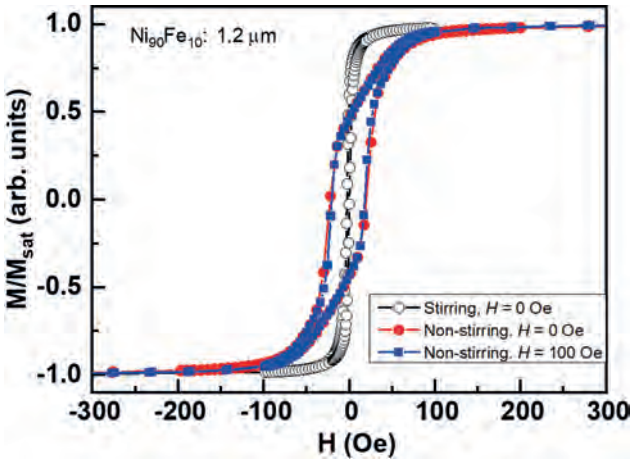

Fig. IP hysteresis loops for 1.2 μm thick-$Ni_{90}Fe_{10}$ layers deposited in different conditions: (○) stirring and H = 0, (●) non-stirring and H = 0 Oe, (■) non-stirring and H = 100 Oe.

FE-11. Molecular-Chemisorption-Induced Strong Modifications of the Magnetic Properties in Thin Polycrystalline Co Films. M. Benini[1], G. Allodi[2], A. Shumilin[3], R.K. Rakshit[1], M. Singh[1], A. Riminucci[1], P. Graziosi[1], V. Kabanov[3], T. Mertelj[3], I. Bergenti[1] and *V.A. Dediu*[1] *1. CNR-ISMN, Bologna, Italy; 2. Department of Mathematical, Physical and Informatics sciences, University of Parma, Parma, Italy; 3. Jozef Stefan Institute, Ljubljana, Slovenia*

The formation of hybrid *p-d* chemical bonds at the interface between thin ferromagnetic (FM) films with molecular (MOL) layers has proved to heavily modify key magnetic properties in the FM, such as magnetic anisotropy, interfacial magnetic moments and others. [1-4] This represents a versatile way to tailor device-relevant parameters in magnetic and spintronics devices. In this work we present the results obtained by interfacing thin polycrystalline Co layers (thicknesses 3-7 nm) with C_{60} and Gaq_3 molecules. Several characterization techniques were employed, allowing to investigate the magnetic state dynamics at various timescales (nanoseconds to minutes) and to study how the interface-located modifications on the magnetic anisotropy can influence the magnetic response of the whole FM layer. MOKE magnetometry and AMR measurements showed a molecule-dependent increase of the in-plane coercivity already present at room temperature (RT) that nevertheless is enormously enhanced at low temperatures (see Fig.1a). We also performed minor loops measurements at 150 K which showed a critical deviation (see Fig.1b) from the universal power law behaviour derived for coercive fields from Rayleigh law [5]. The magnetic stiffness of the Co/Molecule systems in the MHz range by ^{59}Co Zero-Field NMR characterization, observing an increase of the magnetic stiffness of the whole FM layer: This demonstrates the possibility to modify the bulk FM properties (up to several nm) by exploiting interfacial modifications of the magnetic anisotropy [6]. All the observed molecule-induced effects indicate the establishment of a conceptually new magnetization dynamics that is reasonably well explained by a new phenomenological model based on a correlated random anisotropy approach.

[1] M. Cinchetti, V. A. Dediu, L. Hueso, Nat. Mater. 16, 507 (2017) [2] K. V. Raman, A. M. Kamerbeek, Arup Mukherjee *et al*., Nature, 493, 509 (2013) [3] K. Bairagi, A. Bellec, V. Repain *et al.*, Phys. Rev. Lett. 114, 5 (2015) [4] T. Moorsom, M. Wheeler, Taukeer Mohd Khan *et al*., Phys Rev. Lett. B 90, 6 (2014) [5] Takahashi S, Kobayashi S. Philosophical Magazine. 2011, 91(17) 2216-26. [6] M. Benini, G. Allodi, A. Surpi *et al.*, Adv. Mater. Interfaces 2022, 9, 220

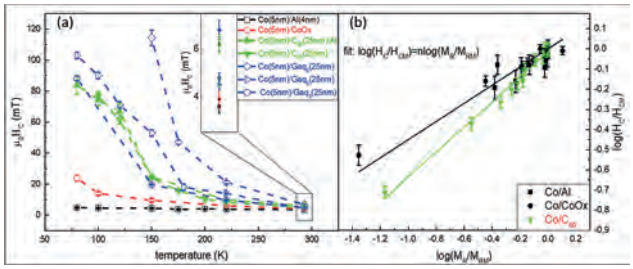

Figure 1 (a) Temperature dependence of the in-plane coercive fields for Co/Gaq$_3$ and Co/C$_{60}$ systems, compared with reference Co/Al and Co/CoOx bilayers, showing a coercivity that is colossally enhancementt low temperatures. Inset: values obtained at RT. (b) Logarithmic coercive field ratio (minor loops divided by saturated loop) vs remanence anisotropy ratio, showing a clear change in the slope between reference samples (black points) and Co/C$_{60}$ (green points).

Session FF
MAGNETO-CALORIC MATERIALS AND DEVICES

Andrei Rogalev, Chair
ESRF, Grenoble, France

INVITED PAPER

FF-01. Can Magnetocaloric High-Entropy Alloys Go Far? *J. Law*[1], Á. Díaz-García[1], L.M. Moreno-Ramírez[1] and V. Franco[1] *1. University of Seville, Seville, Spain*

High-entropy alloys (HEAs), which are made up of multiple principal elements, have been hailed as a paradigm shift in alloy design that now extends to ceramics and intermetallics. They have been discovered to have excellent mechanical properties in the central region of the multiprincipal elements phase diagram, but it is still unclear whether they could be used in functional applications. By clarifying this, we can move one step closer to realizing our objective of developing functional materials with the best possible mechanical properties. This is essential for magnetic or magnetocaloric materials because many of them trade off brittleness and short lifespan for high performance. We recently reviewed how HEA compositions are sought and how remaining in the center of the multiprincipal elements phase diagram leads to subpar performance in the magnetocaloric effect (MCE) [1,2]. The underlying cause is the dilution of the overall magnetic moment caused by the multi-principal elemental composition, which is similar to the saying "Too many cooks spoil the soup". We recently found $FeMnNiGe_xSi_{1-x}$ HEAs in a strategic search in the vast HEA space [3,4], exhibiting the largest MCE reported among magnetocaloric HEAs (Figure 1). In this talk, we review the impact of this breakthrough on the community′s work and present our recent findings on the new MCE benchmark of magnetocaloric HEAs: up to ~145% improvement via microstructural management (Figure 1). We present their competitive MCE magnitude in Figure 2 in comparison with notable conventional magnetocaloric materials of high performance [5]. These findings could open new research avenues, where we could use the HEA game-changer to discover and study functional materials with unusual combinations of properties, ultimately benefiting industries. Supported by PID2019-105720RB-I00/AEI/10.13039/501100011033, Air Force Office of Scientific Research (FA8655-21-1-7044) and the European Union within the project CoCoMag (Grant no. 101099736). J.Y.L. acknowledges EMERGIA 2021 fellowship from Junta de la Andalucía (ref. EMC21_00418).

[1] J.Y. Law, V. Franco, "Review on magnetocaloric high entropy alloys: Design and Analysis Methods", Journal of Materials Research 38, 37-51 (2023). [2] J.Y. Law, V. Franco, "Pushing the limits of magnetocaloric high entropy alloys", APL Materials 9, 080702 (2021). [3] J.Y. Law, et al., Acta Materialia 212, 116931 (2021). [4] J.Y. Law, et al., Journal of Alloys and Compounds 855, 157424 (2021). [5] Á. Díaz-García, J.Y. Law, L.M. Moreno-Ramírez, R. Schäfer, V. Franco, to be submitted (2023). [6] J.Y. Law, et al., Journal of Applied Physics 133, 040903 (2023).

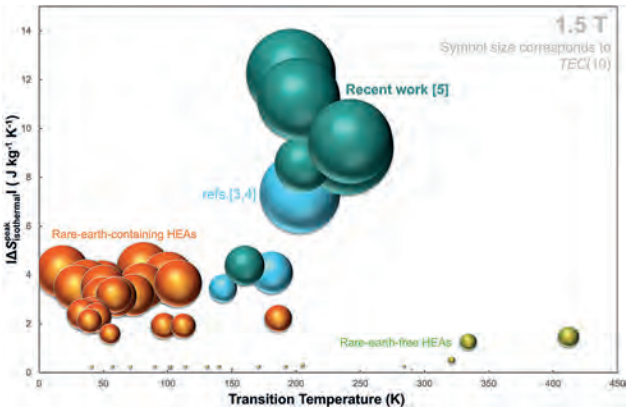

Fig 1. Our recent work finds a new benchmark for magnetocaloric HEAs. Each data point represents a single material with a diameter proportional to its temperature averaged entropy change (*TEC*) over the span of 10K.

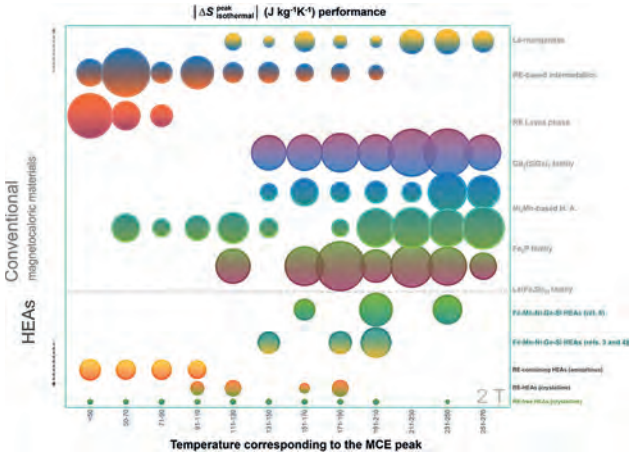

Fig 2. MCE performance matrix (adapted from ref. [6]) shows the competitive MCE of the new results in FeMnNiGeSi HEAs vs conventional magnetocaloric materials. Symbol size corresponds to the magnitude of the MCE.

CONTRIBUTED PAPERS

FF-02. Effective Evaluations of Magnetocaloric Properties by Direct Measurement Methods. *J. Kim*[1], K. Kang[1], A. Lee[1] and K. Chung[1] *1. Korea Institute of Materials Science, Changwon, The Republic of Korea*

Magnetic cooling systems using magnetocaloric materials has been focused for its zero-carbon emission features, and the possibility of the replacement the gas compression cooling systems. The efficiency of magnetic cooling system is significantly dependent on the magnetocaloric properties of the magnetocaloric materials, i.e. magnetic coolants, therefore to find high performance magnetocaloric materials is a recent matter of research. Among the magnetic

coolant candidates, Gadolinium (Gd) received a huge attention for its remarkable magnetocaloric properties, but it has various problems in commercialization. In order to study materials that can replace Gd in the magnetic cooling system, *the real cooling performance* that can only be realized when the material is placed into the cooling system should be compared [1, 2], but most studies have been conducted through indirect property evaluations, for instance, magnetic entropy change via Maxwell relations. In addition, because the magnetic cooling system is operated repeatedly, i.e. cycle process, maintaining the magnetocaloric properties during the cycle process becomes significant related to the system efficiency. In this presentation, the direct measurement methods of magnetocaloric properties of Mn-Fe-P-Si and $La(Fe,Si)_{13}$ *in cyclic process* will be discussed as an effective evaluation method. For the direct measurement method, *home-made equipment* that can measure magnetic cooling performance in cycle condition was constructed. Through this evaluation method, the recent measurement results on whether the magnetocaloric material can actually have better magnetic cooling performance compared to other candidates in the magnetic cooling system applications also will be shown in detail.

[1] L. Griffith, V. Pecharsky, Energy Conversion and Management, Vol. 199, p. 111948 (2019) [2] K. Kang, E. Kim, J. Kim, J. Appl. Phys., Vol. 128, p. 223903 (2020)

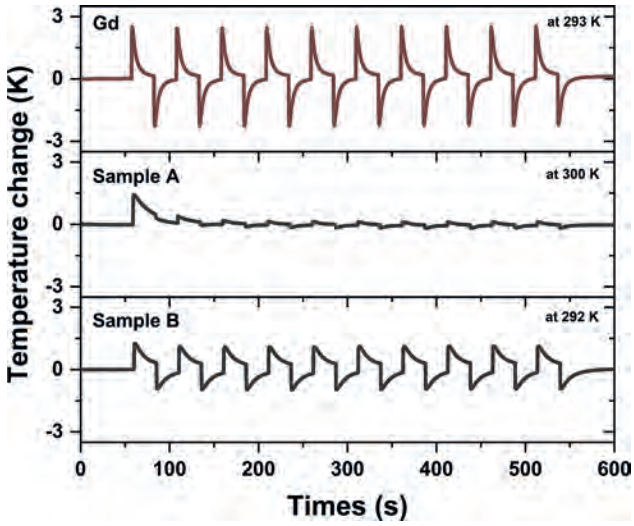

Fig.1 The comparison of the temperature change variations in cycle process with the applied magnetic field of ΔH=0.9T.

FF-03. Contribution of rare earth sublattice to total entropy change at the phase transition in magnetocaloric $DyCo_2$. *J. Lill*[1], B. Eggert[1], J. Zhao[2], D. Koch[3], B. Beckmann[3], B. Lavina[2,4], A. Karpenkov[3], M.Y. Hu[2], K.P. Skokov[3], T. Toellner[2], E.E. Alp[2], K. Ollefs[1], O. Gutfleisch[3] and H. Wende[1] *1. University of Duisburg-Essen, Duisburg, Germany; 2. Advanced Photon Source, Argonne National Laboratory, Lemont, IL, United States; 3. Technical University of Darmstadt, Darmstadt, Germany; 4. Center for Advanced Radiation Sources, The University of Chicago, Chicago, IL, United States*

Energy efficient cooling technologies are essential to keep energy consumption as low as possible. Magnetocaloric cooling technologies are promising, but one drawback is the reduced entropy change (respective applicable magnetocaloric effect) of first-order phase transitions after the first magnetic field application due to hysteresis. To keep the entropy change at a high value, applying external stimuli during cycling is an approach to circumvent hysteresis losses. The total entropy change has contributions of electronic, magnetic and lattice subsystem [1], and while the electronic contribution is very small, both, lattice and magnetic contributions are sizeable. As magnetocaloric cooling is driven by magnetic fields, the external stimuli are used to trigger the lattice subsystem. For the $DyCo_2$ Laves phase, a candidate for hydrogen liquefication [2], the lattice contribution is investigated here by nuclear resonant inelastic X-ray scattering experiments. The ^{161}Dy-partial vibrational density of states (VDOS) is deduced [3] and shown in Figure 1), and the corresponding vibrational entropy at the respective temperatures is calculated [4]. In Figure 2) it is shown that we were able to resolve a sizeable sublattice contribution in the order of 3 $Jkg^{-1}K^{-1}$ to the overall entropy change. Therefore, we can state that for $DyCo_2$ it is feasible to apply external simuli to circumvent hysteresis losses. Furthermore, changes in electronic and magnetic properties within the low-temperature high-magnetization phase can be correlated to changes in the ^{161}Dy-partial VDOS but are not responsible for changes in the vibrational entropy. At higher temperatures, changes of other features in the ^{161}Dy-partial VDOS can be correlated to the modifications in the vibrational entropy at the first-order phase transition. We acknowledge financial support from DFG through CRC/TRR 270 HoMMage.

[1] F. Scheibel et al., Energy Technology 6, 1397-1428 (2018) [2] W. Liu et al., Applied Materials Today 29, 101624 (2022) [3] W. Sturhahn et al., Physical Review Letters 74, 3832 (1995) [4] M. Y. Hu et al., Physical Review B 87, 064301 (2013)

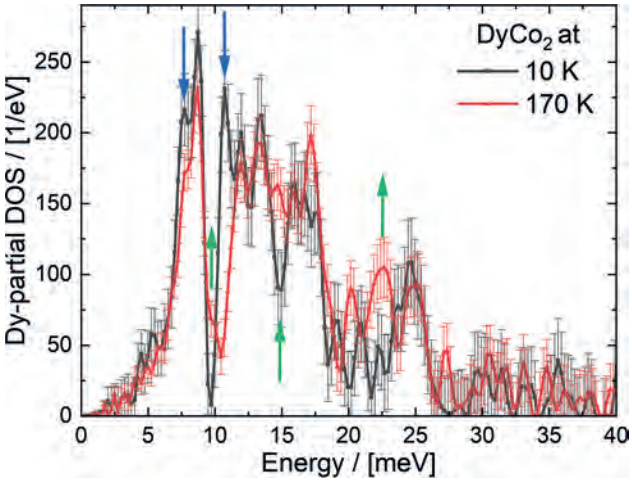

Fig. 1: ^{161}Dy-partial VDOS in both magnetic states, differences are indicated via arrows.

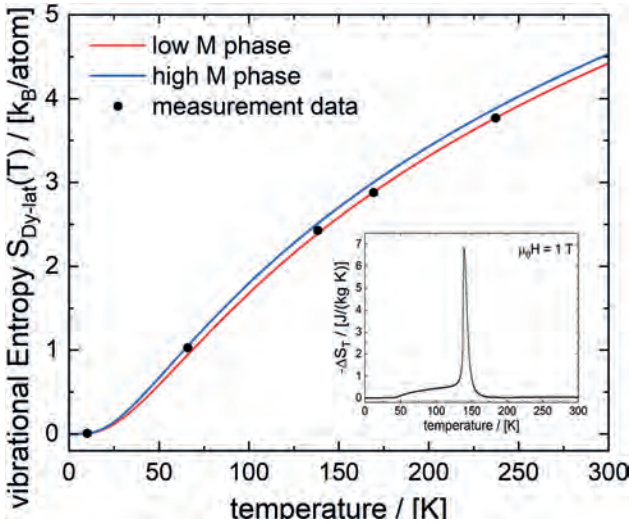

Fig. 2: To Fig. 1) corresponding vibrational entropy vs. temperature. As an inset, total entropy change is shown.

FF-04. Magnetocaloric effect and critical behavior of the novel $Nd_xGd_{3-x}CoNi$ intermetallic compounds. A. Oleaga[1], A. Erkoreka[1], *A. Herrero Hernandez*[1], A. Provino[2], D. Peddis[2,3] and P. Manfrinetti[2,4]
1. Department of Applied Physics, University of the Basque Country, Bilbao, Spain; 2. Department of Chemistry and Industrial Chemistry, University of Genova, Genova, Italy; 3. Institute of Structure of Matter (ISM) – CNR, nM2-Lab, Rome, Italy; 4. Institute SPIN-CNR, Genova, Italy

Crystallographic, magnetic and magnetocaloric properties have been investigated for the $Nd_xGd_{3-x}CoNi$ series with x = 0.15, 0.5, 1.0, 1.5. All compounds crystallize with the monoclinic Dy_3Ni_2-type (*mS*20, *C*2/*m*, No. 12) structure. Each composition presents a paramagnetic to ferromagnetic (PM-FM) second order phase transition with decreasing Curie temperature (171 K, 150 K, 120 K and 96 K, respectively) whereas there is a spin reorientation transition at a lower temperature (see Fig. 1) to a complex magnetic state, which has been found to show antiferromagnetic components. The shape of the hysteresis loops at 2K, together with the appearance of a growing coercive field as Nd doping is increased, indicate that Nd introduces magnetocrystalline anisotropies due to the spin-orbit coupling. A critical behaviour study has been undertaken for the PM-FM transition, extracting the critical exponents (β, γ, δ). For x = 0.15, 0.5, 1.5, γ ≈ 1 indicating long-range magnetic interactions while β values deviate from the 3D-Heisenberg universality class. For x =1, β is close to the Mean Field model while γ is close to the uniaxial 3D-Ising one. Regarding magnetocaloric properties, the magnetic entropy change ranges from 4.1 to 7.9 J/(kgK), see Fig. 2, while the refrigerant capacity ranges between 129-458 J/kg (for $\mu_0\Delta H$ = 5 T). These compounds therefore present interesting properties for cryogenic applications, which are accompanied by extremely good values of the thermal diffusivity (in the range 1.5-3 mm^2/s).

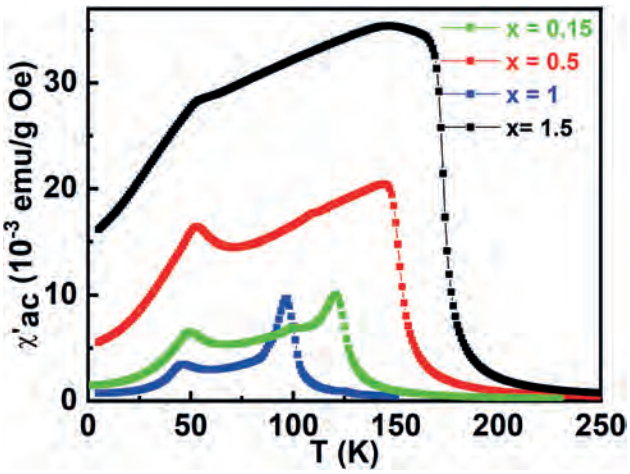

Fig. 1. Real part of *ac* susceptibility.

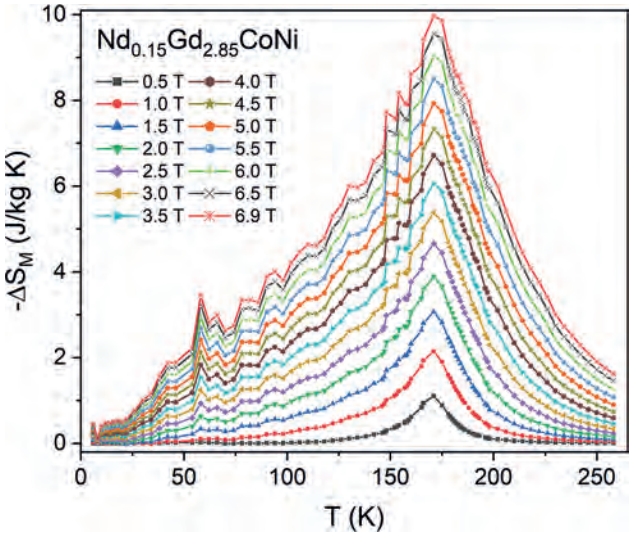

Fig. 2. Magnetic entropy change for $Nd_{0.15}$ $Gd_{2.85}CoNi$

FF-05. Towards Additive Manufacturing of Thin-walled "Magnetocaloric Structures". *V. Sharma*[1], R.L. Hadimani[1,2], H. Zhao[1] and R. Barua[1] *1. Mechanical and Nuclear Engineering, Virginia Commonwealth University, Glen Allen, VA, United States; 2. Department of Biomedical Engineering, Virginia Commonwealth University, Richmond, VA, United States*

Magnetic refrigeration is an energy-efficient, environmentally friendly alternative to conventional vapor-compression cooling technology. A key challenge in manufacturing magnetocaloric devices is the lack of fabrication methods for shaping the brittle caloric alloys into thin-walled channeled structures with optimized heat transfer characteristics, while preserving the functional response of the working material. To this end, a Direct-Ink-Writing (DIW) extrusion-based additive manufacturing (AM) method has been developed to 3D print porous magnetocaloric structures with complex architecture.[1,2] In DIW, the liquid-phase "ink" is dispensed out of small nozzles under controlled flow rates and deposited along digitally defined paths to fabricate 3D structures layer by layer. The novelty of our research effort lies in the initial material feedstock that consists of magnetocaloric powders (up to ~ 90 wt%) and a sacrificial polymer binder dispersed in a multi-solvent system.[1] While the solvents control the ink rheology, the polymers bind the magnetic particles, enabling the retention of the regenerator architecture. A two-step sintering process removes the binder and, subsequently, promotes grain growth and densification of the final finished part. Key fundamental questions about the AM process development will be discussed, particularly the thermofluidic mechanism governing the deposition of the ink and the sintering mechanism for the development of the microstructure. The effect of various process parameters (e.g. powder morphology, viscosity of printing ink, deposition speed, sintering conditions) on the functional response and mechanical strength of the printed part will be deliberated upon. Overall, this study provides strategies for realizing low-cost magnetocaloric heat exchange structures (Fig 1), thus potentially eliminating one of the main barriers to commercialization of magnetic cooling technology.

[1] Sharma, V., Balderson, L...& Barua, R. Room-temperature polymer-assisted additive manufacturing of microchanneled magnetocaloric structures. Journal of Alloys and Compounds, 920, 165891. DOI.org/10.1016/j.jallcom.2022.165891. (2022) [2] H. Zhao, R. Barua and R. Hadimani, "3D Printed Magnetocaloric Devices with Controlled Micro-channels and Magnetic Anisotropy and Methods of Making the Same", Application (#69/928, 002)

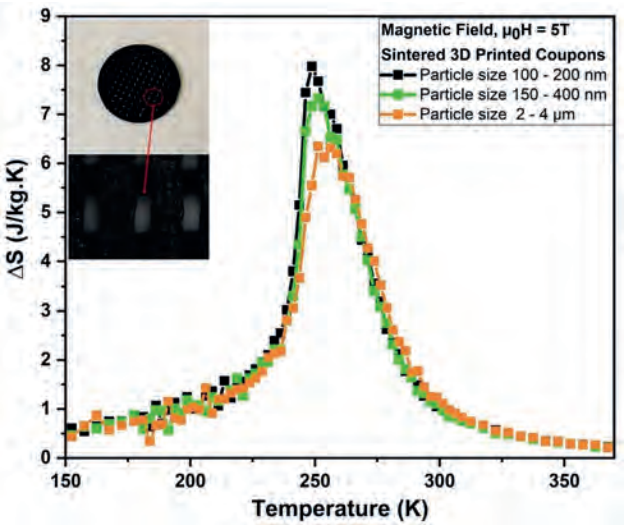

Fig 1. Magnetic entropy change curves of 3D printed test coupons fabricated using $La_{0.6}Ca_{0.4}MnO_3$ magnetocaloric powders of dimensions ranging from 100 nm to 2 µm. Inset shows image of a sintered part with ~150 µm spatial resolution.

FF-06. Laser Synthesis of FeRh Microstructures for Enhanced Magnetocaloric Refrigeration. *S. Tahir*[1], C. Doñate Buendía[1], D. Koch[2], J. Landers[3], S. Salamon[3] and B. Gökce[1] *1. Chair of Materials Science and Additive Manufaturing, University of Wuppertal, Wuppertal, Germany; 2. Institute of Materials Science, Technical University of Darmstadt, Darmstadt, Germany; 3. Faculty of Physics and Center for Nanointegration Duisburg-Essen (CENIDE), University of Duisburg-Essen, Duisburg, Germany*

Magnetocaloric refrigeration is a promising alternative to gas-based cooling systems, providing enhanced energy efficiency and reduced environmental impact. FeRh is a standout magnetocaloric material with the largest magnetocaloric effect due to the AFM-FM phase transition. The desired magnetocaloric response in FeRh structures depends on the composition and processing conditions.[1] In this contribution we present a comprehensive pathway for creating FeRh magnetocaloric microstructures by laser processing (Fig. 1). γ-FeRh nanoparticles with reduced oxidation are synthesized via picosecond pulsed laser ablation in ethanol (Fig. 1a).[2] These nanoparticles are employed to create 1 wt.% ethanol-FeRh ink which is then dispersed on PVP-coated glass substrates and subsequently patterned using a continuous wave laser (Fig. 1b and c). Laser-based direct writing facilitates sintering into custom structures (Fig. 2a) and partially induces the γ-FeRh to B2-FeRh phase transition.[3,4] A 52% partial phase transformation can be achieved, resulting in a significant magnetization increase of ca. 35 Am^2/kg during the field-induced AFM-FM transition (Fig. 2b). Notably, laser sintering demonstrates a remarkable sixfold enhancement of the achieved magnetization compared to furnace annealed FeRh ink which measured ca. 6Am^2/kg. This study presents a robust and efficient approach to generate magnetocaloric structures. Laser synthesis and sintering enable the production of diverse FeRh-based microstructures with high spatial resolution, in-situ annealing, and design flexibility (Fig. 2a). These advancements hold promise for the development of miniaturized devices like magnetic microcoolers, thermal sensors, and magnetic micropumps, leveraging pronounced magnetocaloric effects at a small scale.

[1] S.Nikitin, G.Myalikgulyev, A.Tishin, Physics Letters A 148, 363–366 (1990) [2] R. Nadarajah, S.Tahir and J. Landers, Nanomaterials., 10 (12), 2362 (2020). [3] R. Nadarajah, J.Landers, S.Salamon, B.Gökce, Scientific Reports., 11 (1), 13719 (2021). [4] S.Tahir, J.Landers, S.Salamon, Advanced Engineering Materials, 2300245 (2023)

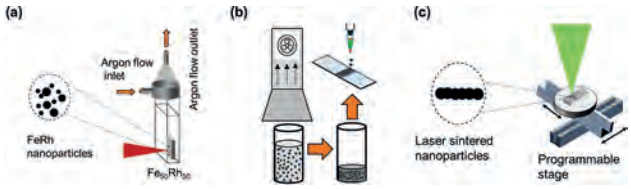

Fig. 1: Step-by-step pathway for producing magnetocaloric microstructure by a) Synthesis of FeRh nanoparticles then b) ink formulation and dispersion on glass substrate, and c) Sintering of FeRh dispersed ink.

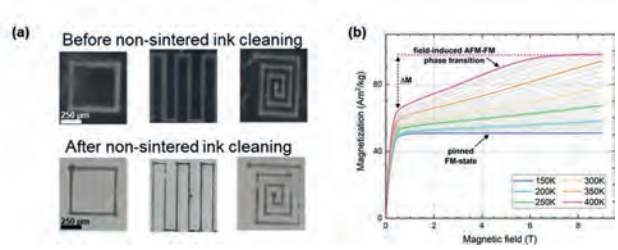

Fig. 2: (a) Custom microstructures before and after the cleaning of dispersed ink, (b) Field-driven AFM-FM phase transition at different temperatures.

FF-07. Magnetoelastic Coupling and Wide-Temperature Range Transition Behavior in $(Mn,Ni,Fe)_2(P,Si)$ Alloys. *K. Kang*[1], A. Lee[1] and J. Kim[1] *1. Korea Institute of Materials Science, Changwon, The Republic of Korea*

In magnetic cooling devices, which are likely to be used as replacing gas compression cooling devices, magnetocaloric materials (MCMs) used as coolants are the most important factor in the devices. Since the possibility of a magnetic cooling device using gadolinium (Gd), many materials have been studied to replace rare earth Gd for commercialization of the magnetic cooling device. Among the MCMs, $(Mn,Fe)_2(P,Si)$ alloys which have excellent magnetocaloric property are one of the most promising alternative materials. In this work, we investigated the alloys with compositional approach, and observed the *magnetoelastic coupling* phenomenon in which magnetic phase transition occurs according to lattice variation in the alloys (Fig.1). With the composition variations, a significant influence of transition metal doping on the lattice structure and the formation of characteristic temperature groups were revealed. Through this compositional approach, the magnetic entropy change is recorded as high as >15 J/kg K at 2T in the room temperature range (Fig.2), remarkably comparable to other giant MCMs. Furthermore, a temperature separation of the magnetic transition was observed in compositions where the ratio of the non-metal element P/Si exceeded 1.5. This characteristic exhibited a *table-top* shape magnetic entropy change curve, and was confirmed as a phenomenon resulting from the formation of *multi-phase transition* in the Fe_2P-type hexagonal structure. The phase transition over a wide temperature range can offer distinct advantage as it can be effectively utilized as coolants in devices such as active magnetic regeneration (AMR) system. In this presentation, the compositional approach in magnetocaloric material design for magnetic cooling devices will be discussed in detail.

K. Kang, A. Lee and J. Kim, Journal of Alloys and Compounds, Vol. 927, p 167008 (2022)

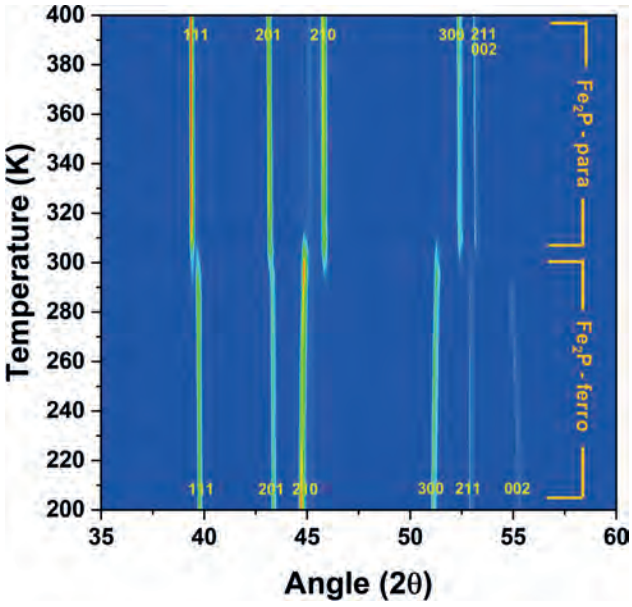

Fig.1 Contour plot of temperature dependent XRD data of $MnFe_{0.91}Ni_{0.04}P_{0.5}Si_{0.5}$

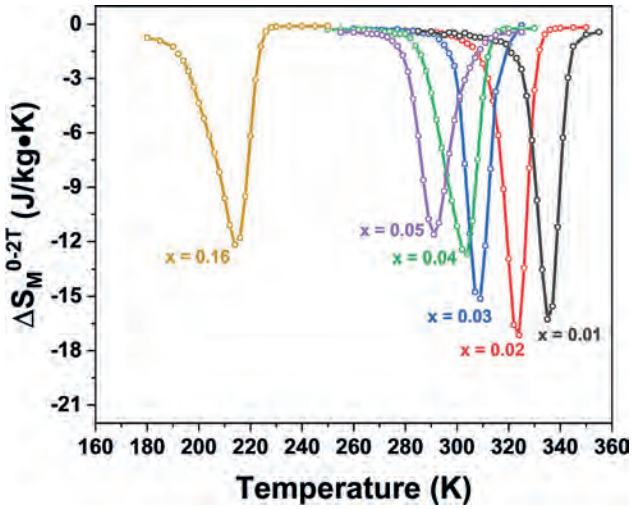

Fig.2 ΔS_M - T curve as a function of $MnFe_{0.95-x}Ni_xP_{0.50}Si_{0.50}$ composition with applied magnetic field 2 T

FF-08. Magnetocaloric Effect and Magnetic, Electrical Properties in One-dimensional Spin Chain Antiferromagnet $Eu_4Ga_8Ge_{16}$ Compound.

S. Cha[1], J. Kim[1], J. Yun[1] and J. Rhyee[1] *1. Physics, Kyung Hee University, Yongin-si, The Republic of Korea*

The $Eu_4Ga_8Ge_{16}$ is a homologous structure compound comparable with a cage-structured clathrate $Eu_8Ga_{16}Ge_{30}$ which investigated in respect of magnetocaloric effect (MCE). The $Eu_4Ga_8Ge_{16}$ has an orthorhombic structure (Cmcm) with the charge-balancing Ga/Ge framework encompasses the Eu^{2+} (J=S=7/2) atomic chains, resulting in the one-dimensional caged spin chain structure. It is distinctive because due to the RKKY exchange interaction, spins of Eu^{2+} ferromagnetically align along a-axis intrachain during interchain (in-plane of a-axis) orders antiferromagnetically. It shows metamagnetic transition from antiferromagnetic state by low magnetic field and this behavior is thought to be beneficial to MCE because there are several reported giant magnetocaloric materials with such property. So, we examined the magnetic and electrical properties of single and polycrystalline $Eu_4Ga_8Ge_{16}$. Then, we evaluated its MCE and compared with $Eu_8Ga_{16}Ge_{30}$ clathrates to elucidate the effect of magnetic interaction to MCE. We found its unique properties that may come from its one-dimensional spin chain structure such as an unconventional inverse magnetic hysteresis at T = 2 K e.g. appearance of rapid spin saturation for increasing magnetic field and spin disordering for decreasing magnetic field at intermediate magnetic field ranges. We also observed non-normal behaviors in resistivity, which led us to suggest possible explanations such as the Kondo-like effect, strong electron-phonon coupling. The magnetic entropy change (ΔS_M) and adiabatic temperature difference (ΔT_{ad}) are $-\Delta S_M$ = 14.6 J kg^{-1} K^{-1} and ΔT_{ad} = 7.8 K at T_N along the a-aixs, which are superior values than those of previously reported type-I clathrate $Eu_8Ga_{16}Ge_{30}$ compound. Therefore, the high magnetocaloric materials are not restricted to materials showing the first-order ferromagnetic ordering but also can be extendable to materials with an antiferromagnetic ground state with low-magnetic field metamagnetic transition. Also, we suggest that unique properties of $Eu_4Ga_8Ge_{16}$ are worthy of further magnetic and electrical investigations.

J. D. Bryan, H. Trill, H. Birkedal, Phys. Rev. B, Vol. 68, p. 174429 (2003) M. H. Phan, G. T. Woods, A. Chaturvedi, Appl. Phys. Lett., Vol. 93, p. 252505 (2008) L. Liu, W. Zhang, P. Liu, Metall. Mater. Trans. A, Vol. 52, p. 284–292 (2021)

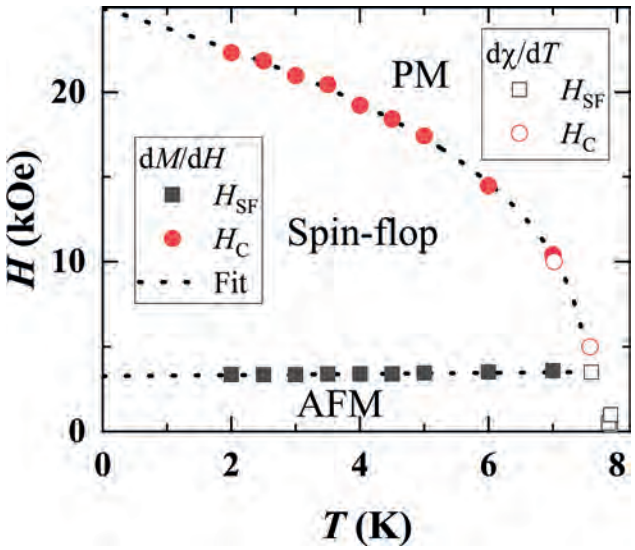

Fig. 1

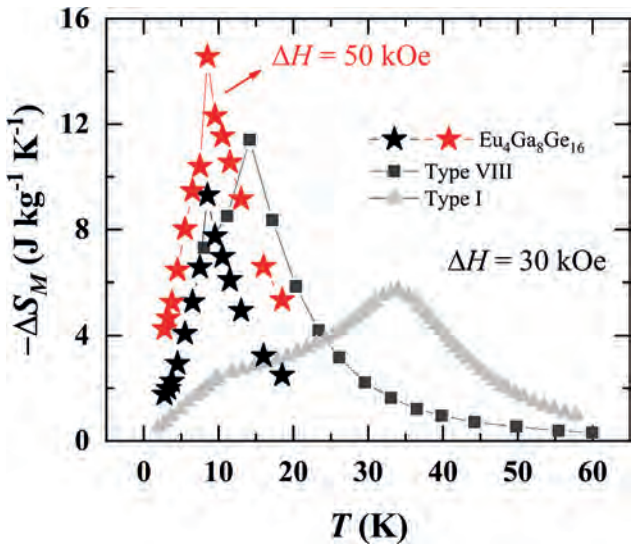

Fig. 2

FF-09. Withdrawn

FF-10. Effect of quenching and post-annealing on magnetic, magnetocaloric, and crystallographic properties in giant magnetocaloric materials $ErCo_2$ and $HoAl_2$. *A.T. Saito*[1], T.D. Yamamoto[2], H. Takeya[1], K. Terashima[1], Y. Takano[1] and T. Numazawa[1] *1. National Institute for Materials Science, Tsukuba, Japan; 2. Dept. of Materials Science and Technology, Tokyo University of Science, Katsushika-ku, Japan*

Magnetic materials with a large magnetocaloric effect (MCE) have attracted attention owing to their potential application to highly efficient and environmentally friendly magnetic refrigeration. Because Laves compounds RT_2 (R = Gd-Yb, T = Al, Ni, Co) exhibit large MCEs associated with a magnetic transition occurring in the temperature range between the two liquefaction temperatures of hydrogen and nitrogen [1,2], which are expected to be used in magnetic refrigeration to liquefy hydrogen [3]. Processing magnetocaloric bulk materials into magnetic refrigerant particles is an essential for developing magnetic refrigerators. However, the effect of the quenching during particle fabrication on the material properties has not been investigated in detail. In this work, the effect of the quenching process and post-annealing on the magnetic, magnetocaloric and crystallographic properties in gas-atomized particles of the $ErCo_2$ and $HoAl_2$ was investigated. The results demonstrate that the physical properties of $ErCo_2$ are significantly changed by quenching process and post-annealing. Changing the annealing conditions of the quenched $ErCo_2$ particles can change the magnetic transition temperature, and the order of the magnetic phase transition from a second-order to a first-order (Fig. 1). Moreover, a strong correlation is observed between the Curie temperature and the lattice constant, suggesting the importance of the magneto-structural coupling. As the particles anneal progress, they develop a giant magnetic entropy change due to the change from a second-order to a first-order transition (Fig. 2). In $HoAl_2$ compound, no significant changes in magnetic and magnetocaloric properties between the quenched particle and annealed one were observed (not shown), even though $ErCo_2$ and $HoAl_2$ are the same Laves compounds. In this presentation, we will show the differences of the detailed properties between the $ErCo_2$ and $HoAl_2$ compounds and discuss possible mechanism. This work was supported by JST-Mirai Program Grant Number JPMJMI18A3, Japan.

[1] T. D. Yamamoto, A. T. Saito et al., J. Alloy. and Compd. 935, 168040 (2023). [2] T. D. Yamamoto, H. Takeya, A. T. Saito et al., J. Magn. Magn. Mater. 547, 168906 (2022). [3] K. Kamiya, K. Matsumoto, T. Numazawa et al., Appl. Phys. Express 15 053001 (2022).

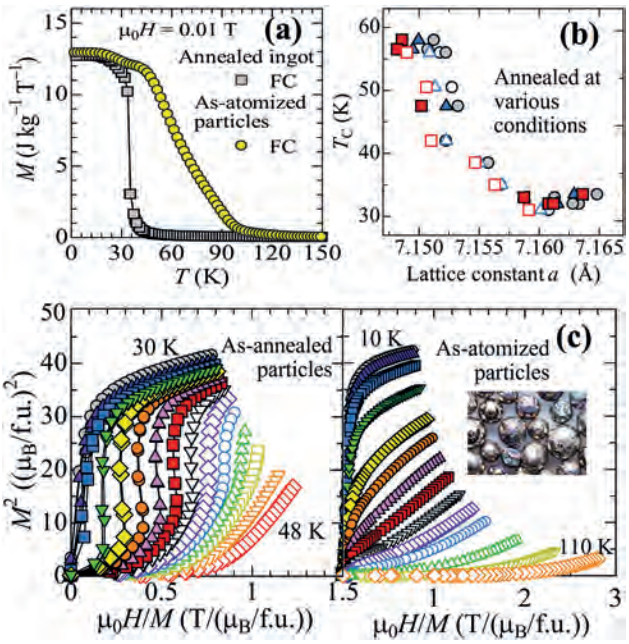

Fig. 1 (a) M-T curves (b) Curie temperature vs. lattice constants, and (c) Arott-plots for $ErCo_2$ particles.

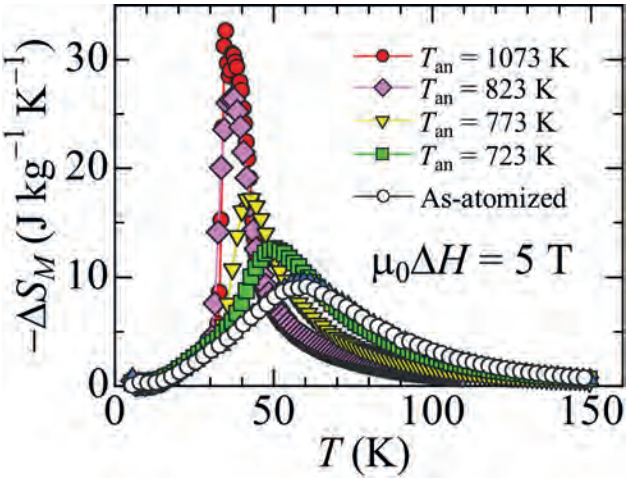

Fig. 2 Temperature dependances of magnetic entropy change of $ErCo_2$ particles.

FF-11. Magnon Diffusion Length and Longitudinal Spin Seebeck Effect in Vanadium Tetracyanoethylene ($V[TCNE]_x$, $x \sim 2$). *D.R. Candido*[1], S.W. Kurfman[3], B. Wooten[2], Y. Zheng[2], M. Newburger[3], S. Cheng[3], R.K. Kawakami[3], J. Heremans[2,3], M.E. Flatté[1] and E. Johnston-Halperin[3] *1. Department of Physics and Astronomy, University of Iowa, Iowa City, IA, United States; 2. Department of Materials Science and Engineering, The Ohio State University, Columbus, OH, United States; 3. Department of Physics, The Ohio State University, Columbus, OH, United States*

The field of spin caloritronics deals with the fundamental interactions, interconversion, and applications of charge, heat, and spin currents. In magnetic insulators, the spin Seebeck effect produces spin currents from thermal gradients that can be detected in adjacent heavy metal layers through spin-to-charge conversion via the inverse spin Hall effect. Here, we build on existing models of the spin Seebeck effect to include variations of the magnon scattering rates to provide a comprehensive picture of predicted functionality [1]. Specifically, our work accurately describes [1] previously unexplained experimental results and identifies a regime of low-Ms, low-loss, and

low-bandwidth magnonic excitations to produce efficient thermally-driven spin pumping. We validate this regime by observing a large spin Seebeck response in the low-Ms, low-loss organic-molecule-based ferrimagnet $V[TCNE]_x$. Accordingly, the excellent agreement between theory and experiment in this material reveal a magnon diffusion length in $V[TCNE]_x$ exceeding 1μm at room temperature and magnon-life time 1-10μs, longer than YIG. These results establish the foundation of next-generation efficient spin-injection devices utilizing organic-based materials and highlight the importance of expanding the materials used in spin caloritronic applications.

[1] S. W. Kurfman*, D. R Candido*, B. Wooten, Y. Zheng, M. J. Newburger, S. Cheng, R. K. Kawakami, J. P. Heremans, M. E Flatté, E. Johnston-Halperin, arXiv preprint arXiv:2308.09752

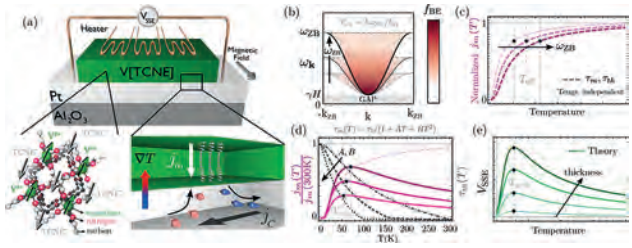

Fig. 1 (a) Schematic of the conventional setup for measuring the longitudinal SSE voltage VSSE in the V[TCNE]x/Pt/Al2O3 sample. (b) V[TCNE] acoustic magnon energies vs. wavevector for three different values of ω_{ZB}. (c)-(e) Normalized SEE spin current and voltage as a function of temperature for temperature dependent and independent parameters.

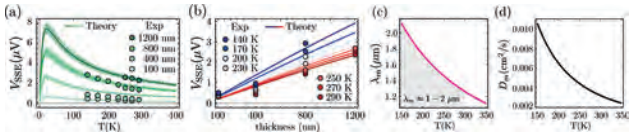

Fig. 2 (a) VSSE vs temperature for different V[TCNE] thickness values = 100, 400, 800 and 1200 nm. Green circles represent the experimental data while solid lines represent the plot of the theoretical modeling using Eq. (2). The dashed solid lines accounts for a ±10% error on the thickness values. (b) VSSE vs thickness size for different temperature. (c) Plot of extracted magnon diffusion length of V[TCNE]x as a function of temperature. (d) Plot of the extracted magnon diffusion coefficient for V[TCNE]x as a function of temperature.

FF-12. Role of Debye temperature in achieving large adiabatic temperature change: case study on Pr_2In. *W. Liu*[1], F. Scheibel[1], T. Gottschall[2], I. Dirba[1], N. Fortunato[1], H. Zhang[1], K.P. Skokov[1] and O. Gutfleisch[1] *1. Materials Science, TU Darmstadt, Darmstadt, Germany; 2. Helmholtz-Zentrum Dresden-Rossendorf, Dresden, Germany*

The discovery of Pr_2In exhibiting a significant magnetic entropy change (ΔS_T) resulting from its first-order phase transition [1] breaks the stereotype that light rare-earth-based alloys demonstrate smaller ΔS_T compared to their heavy rare-earth counterparts [2]. As shown in Fig. 1, ΔS_T of Pr_2In at around 60 K in magnetic fields of 5 T reaches about 20 J kg^{-1} K^{-1} [1], surpassing the heavy rare-earth based alloy Er_2In [2]. The noteworthy ΔS_T of Pr_2In within the temperature range of 20 ~ 77 K makes it an intriguing candidate for magnetocaloric hydrogen liquefaction. However, as an equally important parameter, the adiabatic temperature change (ΔT_{ad}) of Pr_2In has yet to be reported. In this study, we construct the total entropy curves S(T, H) through heat capacity measurements to determine ΔT_{ad}. Fig. 2 demonstrates that ΔT_{ad} of Pr_2In reaches approximately 4.2 K under a 5 T magnetic field, which is not as impressive as its large ΔS_T, considering that $DyAl_2$ has a smaller ΔS_T but a nearly twice larger ΔT_{ad} than Pr_2In [2]. A closer analysis of the heat capacity measurements reveals that the Debye temperature (T_D) of Pr_2In is relatively low, approximately 110 K. In contrast, $DyAl_2$ possesses a T_D of around 374 K [2]. To explore the correlation between T_D and ΔT_{ad}, we adopt a mean-field approach in this study. Our findings indicate that materials with higher T_D tend to exhibit larger ΔT_{ad}. This study serves as a valuable tool for comprehending the magnetocaloric effect at cryogenic temperatures and guiding the search and design of materials exhibiting both large ΔS_T and ΔT_{ad}. This work is supported by the project HyLICAL (Grant No. 101101461).

[1] Biswas et al., Phys. Rev. B 101, 224402 (2020) [2] Liu et al., Appl. Mater. Today 29, 101624 (2022) [3] Biswas et al., Phys. Rev. Mater. 6, 114406 (2022) [4] Liu et al., J. Phys: Energy 5, 034001 (2023)

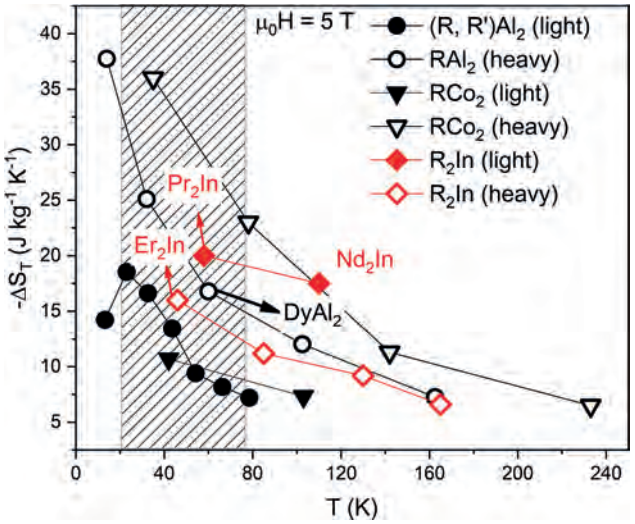

Fig.1 ΔS_T vs. T for R_2In [1, 3], RCo_2 [2], RAl_2 [2, 4] (R: light rare-earth elements (Pr and Nd) and heavy rare-earth elements (Gd, Tb, Dy, Ho, and Er)) material systems.

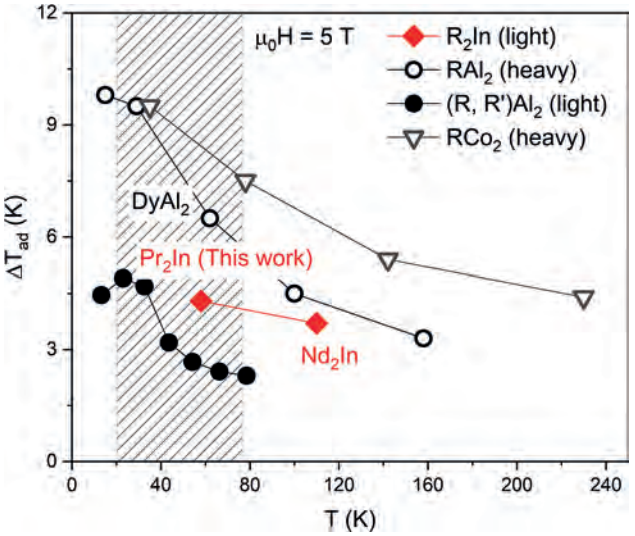

Fig.2 ΔT_{ad} vs. T for R_2In [3], RCo_2 [2], and RAl_2 [2, 4]. ΔT_{ad} of Pr_2In is from this work.

Session FG
NEW MATERIALS AND INTERFACES FOR MAGNETIC JUNCTIONS

Thomas Scheike, Co-Chair
National Institute for Materials Science (NIMS), Tsukuba, Japan
Van Dai Nguyen, Co-Chair
IMEC, Leuven, Belgium

CONTRIBUTED PAPERS

FG-01. Electronic, magnetic, and structural properties of CoVMnSb: ab initio study. *P. Lukashev*[1], A. Ramker[1], B. Schmidt[1], P. Shand[1], P. Kharel[2], V. Mkhitaryan[3], Z. Ning[3] and L. Ke[3] *1. Physics, University of Northern Iowa, Cedar Falls, IA, United States; 2. Physics, South Dakota State University, Brookings, SD, United States; 3. Ames National Laboratory, Ames, IA, United States*

We present computational results on electronic, magnetic, and structural properties of CoVMnSb, a quaternary Heusler alloy. Our calculations indicate that this material may crystallize in two energetically close structural phases: inverted and regular cubic. The inverted cubic phase is the ground state, with ferromagnetic alignment, and around 80% spin polarization. Despite having a relatively large band gap in the minority-spin channel close to the Fermi level, this phase does not undergo a half-metallic transition under pressure. This is explained by the "pinning" of the Fermi level at the minority-spin states at Γ point. At the same time, the regular cubic phase is half-metallic, and retains its perfect spin polarization under a wide range of mechanical strain. Transition to regular cubic phase may be attained by applying uniform pressure (but not biaxial strain). In practice, this pressure may be realized by atomic substitution of non-magnetic atom (Sb) with another non-magnetic atom (Si) of smaller radius. Our calculations indicate that 25% substitution of Sb with Si results in half-metallic regular cubic phase being the ground state. In addition, $CoVMnSb_{0.5}Si_{0.5}$ retains its half-metallic properties under a considerable range of mechanical pressure, thus making it attractive for potential spintronic applications. We hope that the presented results will stimulate experimental efforts to synthesize this compound. This research is supported by the *US Department of Energy* (DOE) Visiting Faculty Program (VFP) at the Ames National Laboratory, and by the *National Science Foundation* (NSF) under Grant Numbers 2003828 and 2003856 via DMR and EPSCoR.

FG-02. Multi-state memory devices and mechanism for flat bands from chiral domain wall superlattices in magnetic Weyl semimetals. *V.C. Rogers*[1], S. Chaudhary[2,3], R. Nguyen[1] and J.C. Incorvia[1] *1. Chandra Dept. of Electrical and Computer Engineering, The University of Texas at Austin, Austin, TX, United States; 2. Dept. of Physics, Northeastern University, Boston, MA, United States; 3. Dept. of Physics, The University of Texas at Austin, Austin, TX, United States*

In this work based on[1], we propose an analog memory device utilizing the gigantic magnetic Weyl semimetal (MWSM) domain wall (DW) magnetoresistance. Previous works have predicted the emergence of large magnetoresistances at DWs[2] or in magnetic tunnel junctions (MTJs) constructed from MWSMs[3], and one experimental work has shown an elevated DW resistance of ~7%[4]. Additionally, highly-efficient current-driven topological hall torques (THTs) have been observed in MWSM thin films[5], thus permitting a platform for both read and write in MWSM DW racetrack devices. Using NEGF quantum transport, we predict that the nucleation of domain walls between contacts will strongly modulate the conductance and allow for multiple memory states, which has been long sought-after for use in magnetic random access memories (MRAM) or memristive neuromorphic computing platforms. Analysis of the helically-magnetized MWSM Hamiltonian shows the generation of Axial Landau levels and provides insight into the observed bulk flat bands for both Neel and Bloch-type domain walls. Additionally, we show that chirality-polarized currents can be generated via filtering through Bloch DW lattices, allowing for the potential use of chirality as a degree of freedom in spintronics.

[1] V. Rogers, S Chaudhary, R. Nguyen, J.A.C. Incorvia, arXiv:2303.16918v1 [cond-mat.mes-hall] (2023) [2] K. Kobayashi, Y. Ominato, and K. Nomura, Journal of the Physical Society of Japan 87, p.7 (2018) [3] D. J. P. de Sousa, C. O. Ascencio, and T. Low, Physical Review B 104, p.4 (2021) [4] J. Shiogai, J. Ikeda, and A. Tsukazaki, Phys. Rev. Mater. 6, p.114203 (2022). [5] M. Yamanouchi, Y. Araki, J. Ieda, Science Advances 8, p.15 (2022)

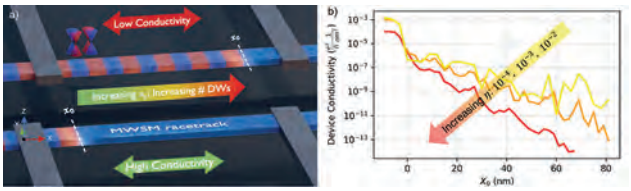

Figure 1. Diagram of DW lattice MWSM device. x_0 represents the start position of a series of chiral DWs in a ferromagnetic DW racetrack (red and blue domains depicted). In the bottom device, few MWSM DWs are present between nonmagnetic electrodes. In the top device, x_0 is increased, injecting DWs into the active region, increasing resistance between the grey, nonmagnetic contacts b) An increase of x_0, and thus injection of chiral DWs, provides a mechanism to decrease conductivity by orders of magnitude. Additionally, stairsteps in conductance corresponding to the nucleation of individual magnetic DWs form for an increasing scattering energy η (or decreasing mean-free-path). From Rogers [1].

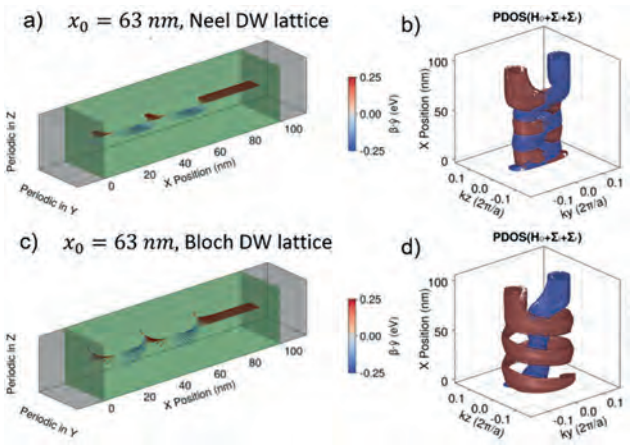

Figure 2. At left, we show magnetization profiles for Neel (a) and Bloch (c) – type domain wall lattices. At right, their corresponding mixed-space Fermi surfaces (b,c) show the twisted Weyl nodes resulting from the helical magnetic texture.

FG-03. Observation and enhancement of room temperature bilinear magnetoelectric resistance in sputtered topological semimetal Pt_3Sn. *Y. Fan*[1], Z. Cresswell[1], Y. Yang[1], W. Jiang[1], Y. Lv[1], T. Peterson[1], D. Zhang[1], J. Liu[1], T. Low[1] and J. Wang[1] *1. Electrical and Computer Engineering, University of Minnesota, Minneapolis, MN, United States*

Topological semimetal materials have become a research hotspot due to their intrinsic strong spin-orbit coupling which leads to large charge-to-spin conversion efficiency and novel transport behaviors. In this work, we have observed a bilinear magnetoelectric resistance (BMER) of up to 0.0067 $nm^2A^{-1}Oe^{-1}$ in a single layer of sputtered semimetal Pt_3Sn at room temperature. Different from previous observations, the value of BMER in sputtered Pt_3Sn does not change out-of-plane due to the polycrystalline nature of Pt_3Sn. The observation of BMER provides strong evidence of the existence of spin-momentum locking in the sputtered polycrystalline Pt_3Sn. By adding an adjacent CoFeB magnetic layer, the BMER value of this bilayer system is doubled compared to the single Pt3Sn layer. This work broadens the material system in BMER study, which paves the way for the characterization of topological states and applications for spin memory and logic devices.

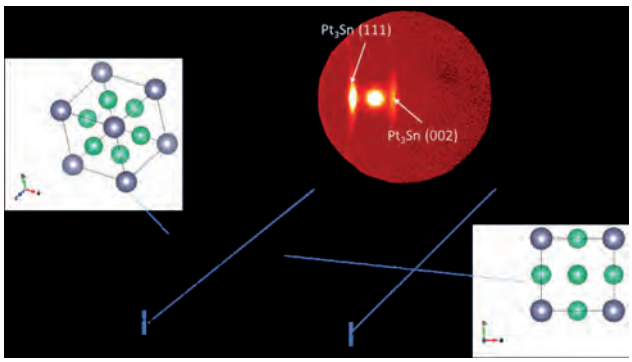

XRD data of the (001)MgO/Pt_3Sn(15)/capping sample. The inset shows the original 2D detector image in the range of 2θ containing the [111] and [002] Pt_3Sn peaks. The inner set figures show the crystalline structure of Pt_3Sn along [111] and [002], respectively, which reveals a polycrystalline textured nature.

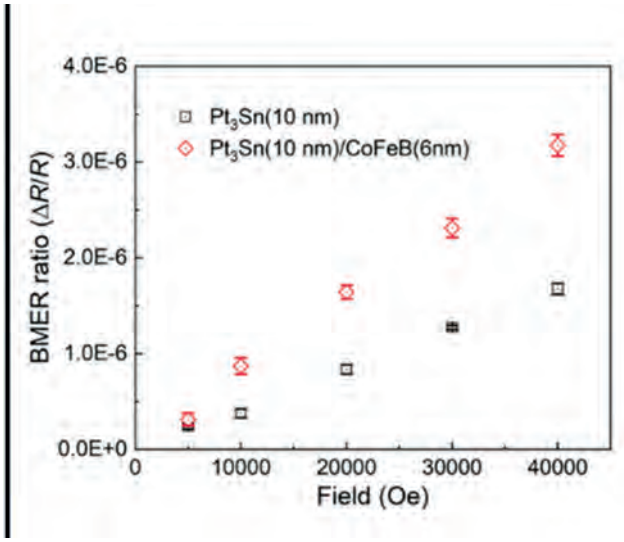

Observation and enhancement of BMER value in Pt_3Sn.

FG-04. Inverse tunnel magnetoresistance driven by interfacial resonance states in a (001)-oriented FeRh/MgO/FeCo junction. *Z. Wen*[1], T. Scheike[1], C. He[1], K. Masuda[1], H. Sukegawa[1], T. Ohkubo[1] and S. Mitani[1] *1. National Institute for Materials Science (NIMS), Tsukuba, Japan*

The magnetic tunnel junction (MTJ) [1-3] consists of two ferromagnetic layers separated by a thin insulating layer and the relative change in MTJ resistance is called tunnel magnetoresistance (TMR). The MTJs with large TMR are indispensable for spintronic applications, such as magnetic field sensors and magnetic random access memories. The TMR effect conventionally originates from the spin polarization of ferromagnetic layers and the coherent tunneling through the MgO(001) barrier. Recently, Masuda et al. reported interfacial resonance effect can contribute to a giant tunnel magnetoresistance in (111)-oriented MTJs. [4] Engineering materials and interfaces of MTJs exhibiting large and unique TMR properties are of particular importance for broadening the applications of MTJs. In this study, we report an inverse TMR effect in an epitaxial MTJ with a core structure of FeRh/MgO/FeCo MTJs originating from the interfacial resonance effect. All the films were deposited on MgO(001) substrates by magnetron sputtering. Microstructure analyses indicate a fully epitaxial growth with (001) orientation in the MTJ stack. It is found that the TMR is inversed with changing the applied voltage from positive to negative. When the applied voltage is -0.6V, the value of TMR is about -20%; and when the voltage becomes 0.6V, the value of TMR becomes about 20%. The positive voltage indicates that the current flows from FeCo to FeRh. We further performed first-principles calculations to figure out the mechanism of the TMR property. The electronic band structures show that minority electrons with Δ_2 and Δ_5 symmetries are half-metallic at the Fermi level of the FeRh electrode. It is confirmed that the TMR characteristics arise from the interfacial resonance states, which can be found from the $k_{//}$ dependence of transmittance and the energy dependence of spin-resolved local density of states of interfacial atoms of FeRh and FeCo electrodes. The inverse TMR effect may open up a new avenue for the application of MTJs. This work was partially supported by the KAKENHI (Nos. 20K04569, 20K14782, 21H01750, 22H04966, and 23K03933) from the Japan Society for the Promotion of Science (JSPS).

[1] S. Parkin et al. Nat Mater 3, 862–867 (2004). [2] S. Yuasa et al. Nat Mater 3, 868–871 (2004). [3] T. Scheike, Z. Wen, H. Sukegawa, and S. Mitani, Appl. Phys. Lett. 122, 112404 (2023). [4] K. Masuda, H. Itoh, and Y Miura, Phys. Rev. B 101, 144404 (2020).

FG-05. Interfacial Improvement by Introducing a Pulsed Current in a Magnetic Tunnel Junction. T. Dale[1], L. Soumah[2], R. Sousa[2], P. Talatchian[2], L. Prejbeanu[2], W.J. Frost[1] and *A. Hirohata*[1,3] *1. University of York, York, United Kingdom; 2. Spintec, Grenoble, France; 3. Tohoku University, Sendai, Japan*

Post-Moore processing unit, a series of new computation architectures has been proposed and demonstrated. Among them, neuromorphic computing to mimic a brain operation, where a neuron only sends a signal when a spike input to the neuron exceeds a threshold, is advantageous over the others due to the energy efficiency for example [1]. In spintronics, an increasing number of device concepts have been reported. Bio-inspired computing leverages voltage-controllable resistance in a magnetic tunnel junction (MTJ), to emuluate an array of hardware nano-neurons to solve cognitive tasks such as vowel recognition [2]. Recently, current-induced crystallisation of a ferromagnetic Heusler-alloy film used in a giant magnetoresistive (GMR) junction has been demonstrated [3],[4], which can be used as data-logging and potentiation functionality into the neuromorphic computation. In this study, we fabricated MTJs consisting of Ta buffer (15)/(Co/Pt) based synthetic antiferromagnet/FeCoB (0.9)/MgO (1.2)/FeCoB (1.2)/W (2) (thickness in nm). The MgO layer was naturally oxidised for 30 s. These MTJs were measured using a non-magnetic probe station (HiSOL, HMP-400 SMS) with a Keithley 2400 sourcemeter and a Keithley 2182A nanovoltmeter in a similar manner as reported previously [3],[4]. The initial TMR behaviour was measured by measuring a current-voltage curve under an application of a magnetic field of ±1 kOe and a sensing current of 50 μA flowing perpendicular to the pillar. The nanopillar was then exposed to current pulses of 30 μA for 200 μs. We observed a resistance change of up to ~0.1%, which is much larger than the previously reported changes detected in GMR junctions [3],[4]. These results indicate the introduction of pulsed current can induce Joule heating and promote atomic diffusion in the vicinity of the FeCoB/MgO interfaces. This results in the improvement of the interfacial smoothness and sharpness. This project was partially supported by EPSRC (EP/V007211/1) and JST CREST (No. JPMJCR17J5).

[1] B. V. Benjamin *et al.*, *Proc. IEEE* 102, 699 (2014). [2] M. Romera *et al.*, *Nature* 563, 230 (2018). [3] W. Frost *et al.*, *Sci. Rep.* 11, 17382 (2021). [4] Z. Zhou *et al.*, *J. Magn. Magn. Mater.* 571, 170575 (2023).

FG-06. Influence of Edge Roughness and elastic dephasing on performance parameters of MTJs. *R.R. Pandey*[1] and A. Tulapurkar[1] *1. Electrical engineering, Indian Institute of Technology Bombay, Mumbai, India*

We conducted a study to examine how phenomena like edge roughness and elastic dephasing impact the electrical transport properties of magnetic tunnel junctions. The NEGF (nonequilibrium Green's function) method was applied to address the fundamental physics within a magnetic tunnel junction[1,2]. To account for the edge roughness, we incorporated a random fluctuation in the cross-sectional profile of the magnetic tunnel junction[3]. The stochastic variation in the junction's shape and size affected the transverse energy mode profile, consequently leading to fluctuations in both the resistance and switching voltage of the magnetic tunnel junction(Fig. 1). To incorporate dephasing within the NEGF framework, we selected a self-energy function based on the momentum-relaxing dephasing model, so as to closely resemble the scattering and randomization of momentum of practical MTJs.[4] We observed that the variations due to edge roughness were more pronounced as the size of the magnetic tunnel junction decreased, primarily due to the quantum confinement effect. Additionally, it was noted that as the intensity of dephasing is increased, the fluctuations in switching voltage reduce while they escalate for the resistance-area (RA) product. We proposed a model that approximates the cross-sectional geometry to a circle with an equivalent cross-sectional area. We compared the variations obtained from the 3 techniques, a.k.a, numerically solving the Schrodinger equation (labeled as detailed calculation in Fig 2), approximation by a perfect circle (equivalent circle), and third by estimating variance using a function(estimated from eqn.) [5] for validation. The knowledge obtained from our research has tangible implications for the design of dependable spin transfer torque-magnetic random access memory (STT-MRAM) that employs ultra-small magnetic tunnel junctions. By comprehending and addressing these effects, we can elevate the performance and reliability of these memory devices to a higher level.

[1] S. Datta, Quantum Transport: Atom to Transistor. Cambridge, U.K.:-Cambridge Univ. Press, 2005. [2] D. Datta, B. Behin-Aein, S. Datta, and S. Salahuddin, "Voltage asymmetry of spin-transfer torques," IEEE Trans. Nanotechnol., vol. 11, no. 2, pp. 261–272, Mar. 2012, doi: 10.1109/TNANO.2011.2163147 [3] Y. Ban, Y. Ma, H. J. Levinson, Y. Deng, J. Kye, and D. Z. Pan, "Modeling and characterization of contact-edge roughness for minimizing design and manufacturing variations in 32-nm node standard cell," in Design for Manufacturability Through Design-Process Integration IV, vol. 7641, M. L. Rieger and J. Thiele, Eds. Bellingham, WA, USA: SPIE, 2010, Art. no. 76410D, doi: 10.1117/12. 846654 [4] D. Das, A. Tulapurkar and B. Muralidharan, "Effects of Elastic Dephasing on Scaling of Ultra-Small Magnetic Tunnel Junctions," in IEEE Transactions on Magnetics, vol. 55, no. 2, pp. 1-4, Feb. 2019, Art no. 1400404, doi: 10.1109/TMAG.2018.2868562. [5] R. R. Pandey, S. Dutta, H. A. Mendonca and A. A. Tulapurkar, "Effect of Edge Roughness on Resistance and Switching Voltage of Magnetic Tunnel Junctions," in *IEEE Electron Device Letters*, vol. 44, no. 5, pp. 745-748, May 2023, doi: 10.1109/LED.2023.3254811.

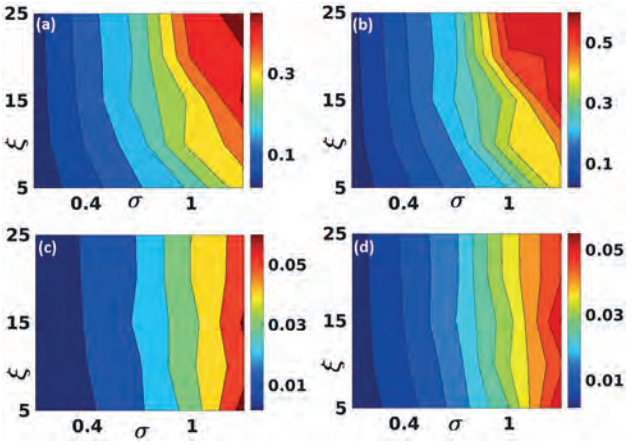

Fig. 1 Coefficient of Variation plots for: (a) Resistance (P) (b) Resistance (AP) (c) |Vc(P)| (d) Vc(AP)

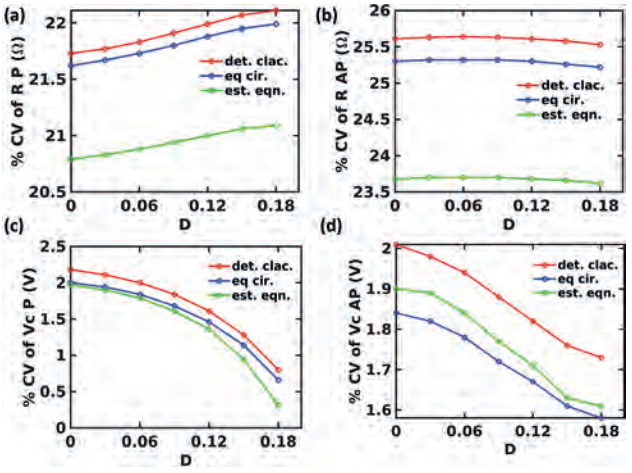

Fig.2 Coefficient of Variation vs dephasing strength plots for: (a) Resistance (P) (b) Resistance (AP) (c) |Vc(P)| (d) Vc(AP)

INVITED PAPER

FG-07. Giant oscillatory tunnel magnetoresistance: an unsolved spin dependent tunneling puzzle. *T. Scheike*[1], C. He[1], Z. Wen[1], H. Sukegawa[1] and S. Mitani[1] *1. National Institute for Materials Science, Tsukuba, Japan*

Magnetic tunnel junctions (MTJs) in principle consist of an insulator sandwiched between two magnetic layers. The relative alignment of the magnetic layers moments in a parallel (P) or antiparallel (AP) state results in a low or high resistance state, respectively; the tunnel magnetoresistance (TMR) ratio. With the experimental demonstrations of the coherent tunneling mechanism using a crystalline MgO barrier in 2004 [1,2], MTJs found their way into various applications, i.e., sensors and magnetic random-access memory (MRAM). Interestingly, one of the reports observed oscillation of the TMR ratio as a function of the barrier thickness with an oscillation period of 0.32 nm in Fe/MgO/Fe(001) [2]. Since then, oscillations with similar periods have been reported in other systems with different materials. However, compared to the total number of publications on TMR, MTJs with TMR oscillation are rarely observed. Additionally, theoretical calculations satisfactorily explaining the observed behavior are lacking making them a longstanding puzzle. We recently showed that the room temperature (RT)-TMR ratio of a single-crystal Fe/barrier/Fe(001) (barrier = MgO [3] or $MgAlO_x$ (MAO) [4]) can be doubled from the commonly reported 200% to over 400% by careful engineering of each layer of the stack. The TMR ratio can be further enhanced by thin CoFe insertion layers at the Fe/MgO interfaces resulting in a >630% RT-TMR ratio [5]. We observed strong TMR oscillations as a function of the barrier thickness exceeding the amplitude of previous reports by several times. In this presentation, we will highlight our experimental observations of the details of the giant TMR demonstration with additional information on the TMR oscillations. Multilayer stacks were fabricated using an ultrahigh magnetron sputtering system: MgO(001) substrate// Cr (60)/Fe (50)/CoFe (0 or 2.24)/Mg (0.5~0.6)/wedged barrier ($d_{barrier}$)/CoFe (0 or 0.56)/Fe (5)/IrMn (10)/Ru (12) (units in nm). MgO or MAO (target composition: $MgO:Al_2O_3$ = 8:1) were used as barrier materials using electron beam evaporation from a sintered pellet and a linear motion shutter. The bottom-Cr, bottom-Fe, barrier, and top-Fe were annealed at 600°C, 300°C, 250°C, and 400°C, respectively. The stacks were patterned using photolithography and ion etching. The MTJs were measured at RT using a 4-probe measurement system. Figure 1 (a) shows the RT-TMR ratio vs. barrier thickness for three optimized MTJs: Fe/MgO/Fe, Fe/MAO/Fe, and Fe/CoFe/MgO/CoFe/Fe with maximum RT-TMR ratios of 417%, 429%, and 632%, respectively. Here, a TMR ratio is defined by $(R_{AP}/R_P - 1)100\%$, with $R_{P(AP)}$ is the tunneling resistance in the P (AP) state. Strong TMR oscillations with barrier thickness are observed which become stronger with increase of the maximum TMR ratio. Interestingly, the oscillation shape changes for the MTJ with a MAO barrier leading to a saw-tooth like pattern showing the influence of Al doping. Oscillations can also be observed in R_P vs barrier thickness plots after removing the exponential background as shown in Fig. 1 (b). The R_P oscillations of the Fe/MgO/Fe and Fe/CoFe/MgO/CoFe/Fe MTJ show similar amplitudes and oscillation periods. The MTJ with the MAO barrier shows a spike-like oscillation of the corrected *RA* strongly deviating from the ones with a MgO barrier. We find a similar behavior of *RA* in the AP state. Structural characterization using scanning transmission electron microscopy gave no explanation for the observed behavior. In this presentation we will further discuss other key behaviors of the TMR oscillation, e.g., the bias voltage and temperature dependence. The work was partly supported by JSPS KAKENHI Grant Nos. 16H06332, 21H01750, 21H01397, and 22H04966 and is partly based on results obtained from a project, JPNP16007, commissioned by the New Energy and Industrial Technology Development Organization (NEDO).

[1] Parkin *et al.*, Nat. Mater. 3 862 (2004) [2] Yuasa *et al.*, Nat. Mater. 3, 868 (2004). [3] Scheike *et al.*, Appl. Phys. Lett. 118, 042411 (2021). [4] Scheike *et al.*, Appl. Phys. Lett. 120, 032404 (2022). [5] Scheike *et al.*, Appl. Phys. Lett. 122, 112404 (2023).

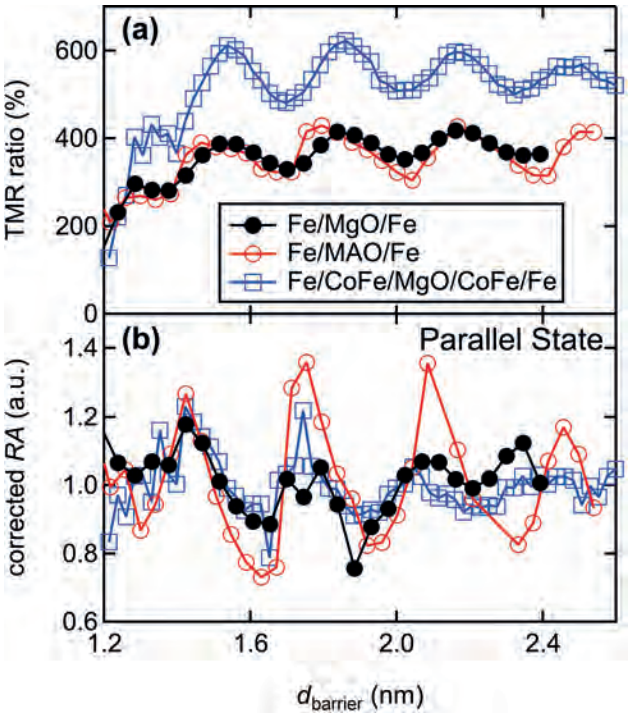

RT-TMR ratio (a) and corrected *RA* in P state (b) vs barrier thickness for different MTJs.

CONTRIBUTED PAPER

FG-08. Analysis of Ferro- and Antiferromagnetic Memory Bits by Scanning NV Magnetometry. *P.S. Rickhaus*[1], V. Borras[1], R. Carpenter[2], S. Couet[2], L. Zaper[3,1], S. Rao[2], A. Stark[1], M. Munsch[1], H. Zhong[1], C. Adelmann[2], P. van der Heide[2], A. Finco[4], V. Jacques[4], V. Garcia[5] and P. Maletinsky[3,1] *1. Qnami, Basel, Switzerland; 2. IMEC, Leuven, Belgium; 3. University of Basel, Basel, Switzerland; 4. University of Montpellier, Montpellier, France; 5. CNRS-Thales, Palaiseau, France*

Storing information in magnetic bits requires excellent control over their nanoscale magnetic properties. A prime example of this challenge are STT-MRAM (spin transfer torque magnetic random access memory) devices - which have rather high failure rates. In order to investigate the sources of potential failure, a technique that can resolve small magnetic fields with high spatial resolution is required. The request is even more urgent for next-generation magnetic memory materials, such as antiferromagnets, which generate even smaller magnetic signals. Scanning NV magnetometry (SNVM) is an emerging quantum sensing technique that offers the required sensitivity. Here, we will look at the local magnetic properties of bits in state-of-the-art STT-MRAM devices using scanning-NV magnetometry [1]. Furthermore, we will demonstrate magnetic images of a few hot candidate materials for future magnetic memory devices including antiferromagnetic chromia, BFO [2] and ultra-scaled CoFeB nanowires [3]. We will reveal magnetic textures that are undetectable with more standard characterization techniques and discuss implications on device fabrication.

[1] P. Rickhaus et.al., https://arxiv.org/abs/2306.15502 [2] H. Zhong et al, Phys. Rev. Applied 17, 044051 (2022) [3] U. Celano et al, Nano Lett. 21, 24, 10409–10415 (2021)

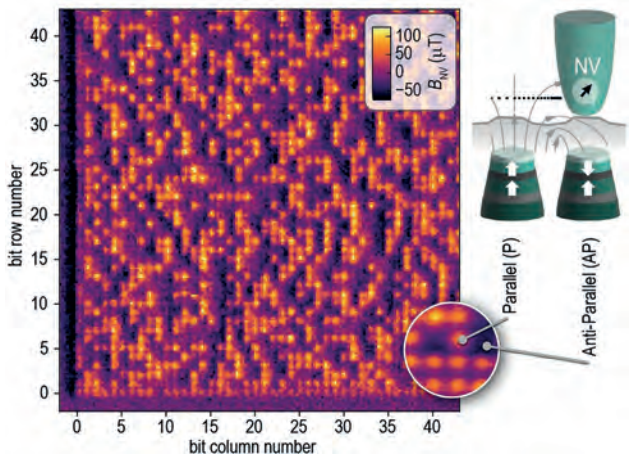

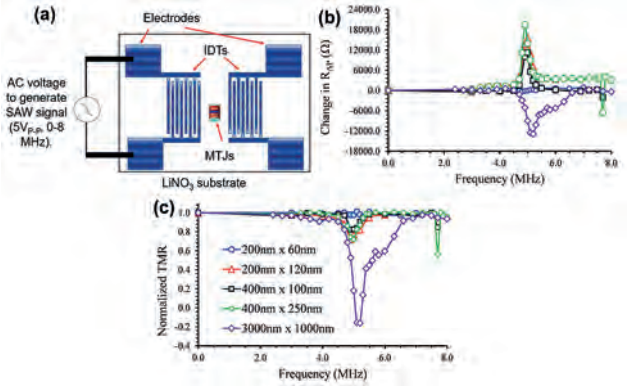

Fig. 1. (a) Experiment set-up of in-plane MTJs fabricated on a $LiNO_3$ substrate between two IDTs used to generate the SAW signal. Change in (b) AP-state resistance and (c) normalized TMR ratio with respect to SAW signal frequency.

INVITED PAPER

FG-09. Influence of surface acoustic wave (SAW) on nano-sized in-plane magnetic tunnel junctions. *B.R. Zink*[1], B. Ma[1], D. Zhang[1], D. Bhattacharya[2], M. Abeed[2], S. Bandyopadhyay[2], J. Atulasimha[2] and J. Wang[1] *1. Electrical and Computer Engineering, University of Minnesota, Minneapolis, MN, United States; 2. Mechanical Engineering Department, Virginia Commonwealth University, Richmond, VA, United States*

Switching magnetic tunnel junctions (MTJs) with voltage generated strain is a promising solution for reducing switching energy in MRAM [1-2]. However, large voltages are required to induce enough strain to switch, which hinders reduction of the switching energy. One way to overcome this is to employ time-varying (instead of static) strain via a surface acoustic wave (SAW) [3]. Previous studies on micron scale structures showed that the tunneling magnetoresistance (TMR) ratio and the anti-parallel (AP) and parallel (P) state resistances all decrease at a SAW frequency around 5 MHz [3]. In this study, we fabricated in-plane MTJs on $LiNbO_3$ substrates and generated the SAW signal using interdigitated transducers (IDTs), as shown in Fig. 1(a). We analyzed the effect of the SAW signal on both nanometer and micrometer size MTJs and found their behaviors to be very different. The MTJs were patterned into elliptical nano-pillars via electron beam lithography with long and short axis dimensions varying between 200 nm/60 nm to 3000 nm/1000 nm. Figures 1(b) and 1(c) show the changes in R_{AP} and the TMR ratio, respectively, which peaked (reached a maximum or minimum) at a SAW signal frequency around 5.1 MHz. Figure 1(b) shows that the SAW signal causes R_{AP} to increase in nanometer sized devices but decrease in micrometer sized devices. Figure 1(c) shows that the SAW signal causes the TMR ratio to decrease for all devices; however, this effect is much more pronounced in micrometer sized devices. Most surprisingly, the SAW signal causes the TMR ratio to drop below zero for the micrometer size MTJ, meaning that R_{AP} is temporarily less than R_P under SAW excitation. Our results provide insight into the dynamic behavior of MTJs under periodic strain and the dependence of this behavior on the device dimensions as they are scaled down below micrometer sizes.

[1] D. Bhattacharya *et al*, *Multifunct. Mater.* 2, 032001 (2019). [2] Z. Zhao *et al*, *Appl. Phys. Lett*. 109, 092403 (2016). [3] D. Bhattacharya *et al*, *J. Appl. Phys.* 130, 033901 (2021).

CONTRIBUTED PAPERS

FG-10. Proximity-mediated Magnetotransport in Ferromagnetic/ Helimagnetic Fe/MnP Bilayers. *N.W. Mudiyanselage*[1], C. Hung[1], D. Detellem[1], A. Chanda[1], J.E. Shoup[1], N. Alzahrani[1], A. Duong[2], J. Frisch[3,4], M. Bär[3,4], D. Arena[1], H. Srikanth[1], S. Witanachchi[1] and M. Phan[1] *1. Physics, University of South Florida, Tampa, FL, United States; 2. Phenikaa University, Hanoi, Vietnam; 3. Department of Interface Design, Helmholtz-Zentrum Berlin für Materialien und Energie GmbH (HZB), Berlin, Germany; 4. Energy Materials In-situ Laboratory Berlin (EMIL), Helmholtz-Zentrum Berlin für Materialien und Energie GmbH (HZB), Berlin, Germany*

In the past few years, extensive research on magnetic multilayers like spin valves and magnetic tunnel junctions has yielded significant discoveries in spin electronics [1]. Among these heterostructures, ferromagnetic (FM)/ collinear antiferromagnetic (AFM) bilayers have gained immense attention for such applications. The significant interest in collinear AFMs arises from their fast spin dynamics and the absence of stray fields [2]. However, the influence of a thin FM layer on the helical state of a non-collinear AFM remains largely unexplored. Motivated by our recent findings that demonstrate the enhanced magnetic properties of Ta (2 nm)/ Fe(5nm)/manganese phosphide (MnP)(100nm) films due to the magnetic proximity effect (MPE), in this work, we explore the MPE on the magneto-transport properties of this FM/helimagnetic (HM) heterostructure. Like MnP [3], we find a metallic behavior for Ta/Fe/MnP over a temperature range of 10-300 K from temperature-dependent resistivity measurements. The bipolar field scan of the field-dependent magnetoresistance (MR) of both MnP and Ta/ Fe/MnP films exhibits a distinct butterfly-like hysteresis loop with a low-field negative peak throughout the same temperature range. Additionally, two broader high-field positive peaks are observed below 58 K in the MR loops. The absolute value of MR for both films increases upon decreasing temperature from 300 K and exhibits a sharp maximum at the HM transition temperature (~110 K) and approaches zero with further lowering temperature. Interestingly, the sign of MR for both MnP and Ta/Fe/MnP films changes from positive to negative when lowering temperature below 58 K. While the absolute value of MR is much lower in Ta/Fe/MnP compared to MnP above 58 K, the value of MR for both films is nearly equal below 58 K. Notably, the maximum value of MR at 110 K is ~52% for Ta/Fe/MnP which is much lower than that for MnP (~90%). These observations indicate the important role of MPE in mediating the magneto-transport properties of the Ta/Fe/MnP heterostructure, which will pave the way for tunable magnetism and spin transport properties of FM/noncollinear AFM systems for efficient spintronic device applications.

[1] K. Lenz, S. Zander, and W. Kuch, *Magnetic Proximity Effects in Antiferromagnet/Ferromagnet Bilayers: The Impact on the Néel Temperature*, Phys Rev Lett 98, 237201 (2007). [2] J. H. Kim, H. J. Shin, M. K. Kim, J. M. Hong, K. W. Jeong, J. S. Kim, K. Moon, N. Lee, and Y. J. Choi, *Sign-Tunable Anisotropic Magnetoresistance and Electrically Detectable Dual Magnetic Phases in a Helical Antiferromagnet*, NPG Asia Mater 14, (2022). [3] B. Muchharla, R. P. Madhogaria, D. Detellem, C. M. Hung, A. Chanda, N. W. Y. A. Y. Mudiyanselage, A. T. Duong, M. T. Trinh, S. Witanachchi, and M. H. Phan, *Intergranular Spin Dependent Tunneling Dominated Magnetoresistance in Helimagnetic Manganese Phosphide Thin Films*, Nanomaterials 13, (2023).

FG-11. Spintronics with Black Phosphorus. *H. Wei*[1], M. Galbiati[1], J. Peiro[1], S.M. Dubois[2], F. Brunnett[1], V. Zatko[1], R. Galceran[1], P. Brus[3], F. Godel[1], D. Perconte[1], F. Bouamrane[1], E. Gaufres[4], A. Loiseau[4], O. Bezencenet[3], B. Servet[3], F. Petroff[1], J. Charlier[2], M. Martin[1], B. Dlubak[1] and P. Seneor[1] *1. Unité Mixte de Physique CNRS/Thales, Université Paris-Saclay, Palaiseau, France; 2. Institute of Condensed Matter and Nanosciences, Université Catholique de Louvain, Louvain-la- Neuve, Belgium; 3. Thales Research and Technology, Palaiseau, France; 4. Laboratoire d'Étude des Microstructures, CNRS, ONERA, Université Paris-Saclay, Châtillon, France*

Spintronics is a paradigm focusing on spin as the information vector in fast and ultra-low-power that aims at providing more complex architectures for beyond-CMOS solutions from storage to quantum information. 2D materials opened novel exciting opportunities in terms of functionalities and performances for spintronics devices[1-3]. In this direction, graphene has been shown to provide both highly efficient spin information transport properties [4,5] and potential for strong spin filtering in 2D-MTJs[1-3]. However it lacks a gap and its semiconducting sibling has remained elusive. Black phosphorus (BP) possesses major properties (high mobilities, high on/off ratios in transistors) and has attracted explosive interest since 2014. Additionally, its bandgap is predicted to be widely tunable in relation to the number of stacked layers and remains direct from the bulk to the monolayer. Thanks to the natural low spin-orbit coupling, BP is expected to present highly efficient spin information transport, similar to graphene [4,5] but with the addition of a band gap. This difference with graphene is fundamental for the implementation of spin manipulation schemes and the experimental realization of a spin gate. Here we present the first results of large MR in efficient BP spin valve devices. We will first present a recently developed in-situ approach to circumvent the main issue of degradation under atmospheric conditions [6,7,8]. By passivating the BP without exposing it to air we achieve protection down to the monolayer. We will further show that this passivation even can play the role of the tunnel barrier required for efficient spin injection [4,5,7,8] and provide a high potential path for spintronics applications from vertical to lateral devices. We will finally demonstrate the BP integration into Co/BP/Co spin valves showing large spin signals (up to 500% MR). We will explain those results, developing a novel selective spin-splitted transport mechanism supported by first-principle theoretical investigation. Overall, this illustrates the potential of BP for spin injection/detection, strongly supporting BP's vision as an outstanding platform for spintronics.

[1] V. Zatko, M. Galbiati, S. M.-M. Dubois et al., ACS Nano., Vol.13, p.14468 (2019), [2] M. Piquemal-Banci, R. Galceran, S. M.-M. Dubois et al., Nat Commun., Vol.11, p.5670 (2020), [3] M. Piquemal-Banci, R. Galceran, M.-B. Martin et al., J.Phys.D., Vol.50, p.203002 (2017) [4] B. Dlubak, M.-B. Martin, C. Deranlot et al., Nature Phys, Vol.8, p.557 (2012), [5] P. Seneor, B. Dlubak, M.-B. Martin et al., MRS Bulletin, Vol.37, p.1245 (2012) [6] A. Favron, E. Gaufrès, F. Fossard et al., Nature Mat, Vol.14, p.826 (2015) [7] R. Galceran, E. Gaufres, A. Loiseau et al., APL., Vol.111, p.243101 (2017), [8] L.-M. Kern, R. Galceran, V. Zatko et al., APL., Vol.114, p.053107 (2019)

Session FP
NEUROMORPHIC COMPUTING III
(Poster Session)

Yusuke Imai, Chair
The University of Tokyo, Bunkyo, Japan

FP-01. Probabilistic Computing with Magnetic Tunnel Junctions.
E. Raimondo[1], Y. Shao[2], A. Grimaldi[1], A. Giordano[1], M. Carpentieri[3], P. Khalili Amiri[2] and G. Finocchio[1] *1. University of Messina, Messina, Italy; 2. Northwestern University, Evanston, IL, United States; 3. Politecnico of Bari, Bari, Italy*

Physics-inspired unconventional computing paradigms [1-2] are a topic of great scientific interest due to their high compatibility with scalable hardware implementations for the solution of hard combinatorial optimization problems. Among these, Ising machines (IMs) are a promising class of heuristic solvers [3] due to the flexibility of their energy minimization schedule and to their general graph topology. Probabilistic computing is a general approach based on the concept of IMs [2,3,4], known for its high compatibility with spintronics. In this work we propose a probabilistic bit (p-bit) implementation with three-terminal magnetic tunnel junctions (MTJs), envisioning a hardware probabilistic Ising machine (pIM). The perpendicular MTJ is designed so that the energy landscape of the free layer (FL) magnetization has two stable minima along the z-axis. By applying a spin-orbit torque current (SOT), the FL magnetization is brought to a metastable state aligned along the direction of the spin-current (y-axis). When the SOT is switched off, the FL magnetization relaxes, with equal probability, towards one of the two z-axis directions. The switching probability is tuned with a spin-transfer torque current applied to the third terminal, resulting in a sigmoidal curve when averaging the FL magnetization after the SOT pulse across many events, as shown in Fig. 1. A hardware implementation of a pIM involves considering the geometrical and physical device-to-device variations. To study this, we consider an instance of a maximum satisfiability problem (MAX-SAT) and attempt to reach the optimal while randomly changing the slope of the sigmoidal curve of each p-bit. The variations are sampled from a normal distribution with unit mean and several values of standard deviation σ. The results in Fig. 2 show that the probability of obtaining the optimal solution is only slightly affected for σ less than 0.3. See Ref. [5] for founding statement.

[1] G. Finocchio, J. Magn. Magn. 521, 167506 (2021). [2] A. Grimaldi, Phys. Rev. Appl. 17, 024052 (2022). [3] N. Mohseni, Nat. Rev. Phys. 4, 363 (2022). [4] K. Y. Camsari, Phys. Rev. X 7, 031014 (2017). [5] This work was supported under the project number 101070287 - SWAN-on-chip - HORIZONCL4-2021-DIGITAL-EMERGING-01, the project PRIN 2020LWPKH7 "The Italian factory of micromagnetic modelling and spintronics" funded by the Italian Ministry of University and Research (MUR), and by the PETASPIN association (www.petaspin.com). The work at Northwestern University was supported by the National Science Foundation (NSF) grant numbers 1919109 and 2106562.

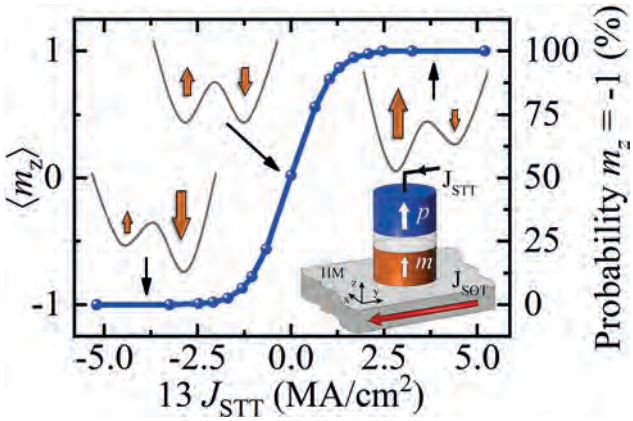

Figure 1: Sigmoidal behaviour of the average FL magnetization tuned by an STT current

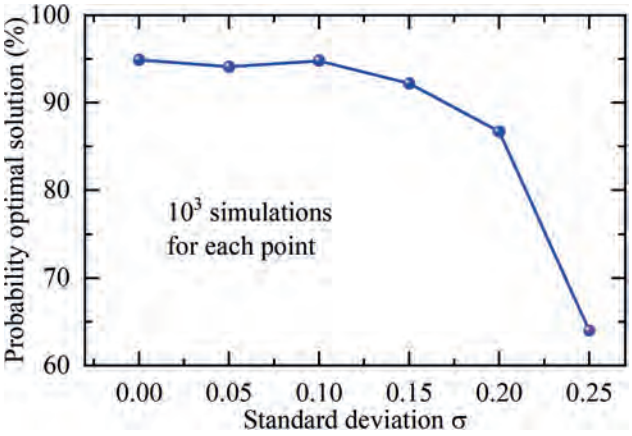

Figure 2: Probability of obtaining the optimal solution as a function of the standard deviation σ of the normal distribution used to sample the slope of each p-bit's sigmoidal curve.

FP-02. Probability-Distribution-Configurable True Random Number Generators Based on Spin-Orbit Torque Magnetic Tunnel Junctions.
R. Zhang[1], X. Li[1], M. Zhao[1], C. Wan[1], X. Luo[1], S. Liu[1], Y. Zhang[1], Y. Wang[1], G. Yu[1] and X. Han[1] *1. State Key Laboratory of Magnetism, Institute of Physics, Chinese Academy of Sciences, Beijing, China*

The incorporation of randomness into stochastic computing can provide ample opportunities for applications such as simulated annealing, non-polynomial hard problem solving, and Bayesian neuron networks. In these cases, a considerable number of random numbers with an accurate and configurable probability distribution function (PDF) are indispensable. Preferably, these random numbers are provided at the hardware level to improve speed, efficiency, and parallelism. In this work, we demonstrate how spin-orbit torque magnetic tunnel junctions (SOT-MTJs) with high barriers are suitable candidates for the desired true random number generators. Not only do these SOT-MTJs perform excellently in speed and endurance, but their

randomness can also be conveniently and precisely controlled by a writing voltage, which makes them a well-performed Bernoulli bit. By utilizing these SOT-MTJ-based Bernoulli bits, we can realize any PDF, including Gaussian, uniform, exponential, Chi-square, and even arbitrarily defined distributions. These PDF-configurable true random number generators can then promise to advance the development of stochastic computing and broaden the applications of the SOT-MTJs.

S. Misra, L. Bland and J. Aimone, *Advanced Materials*, n/a, 2204569(2022) K. Y. Camsari, H. Ohno, and S. Datta, *Nature* 573, 390 (2019) M. Zhao, R. Zhang and X. F. Han, *Applied Physics Letters* 120, 182405 (2022) K. Y. Camsari, R. Faria and S. Datta, *Phys. Rev. X* 7, 19, 031014 (2017) J. Grollier, D. Querlioz and K. Y. Camsari, *Nat. Electron.* 3, 360 (2020) T. Dalgaty, N. Castellani and C. Turck, *Nat. Electron.* 4, 151 (2021) B. Zhang, Y. Liu and T. Gao, in *2021 IEEE IEDM*, pp. 27.6.1(2021) P. Debashis, H. Li and D. Nikonov, *IEEE Magnetics Letters* 13, 1 (2022)

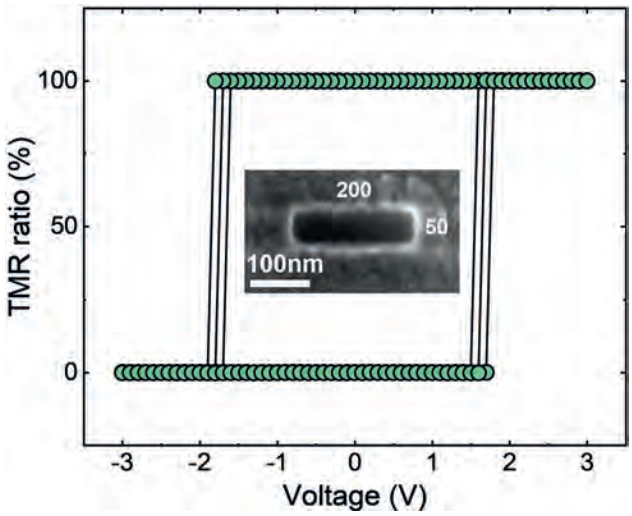

Characterization of the performance of current-driven field-free switching of the SOT-MTJ. Field-free magnetization switching driven by 6ns pulse currents. The current-induced switching degree is 100%, compared with the field-induced switching. Inset is the top view of the scanning electron microscope (SEM) image of an MTJ showing that the MTJs have been well-defined as 50 nm × 200 nm rectangles.

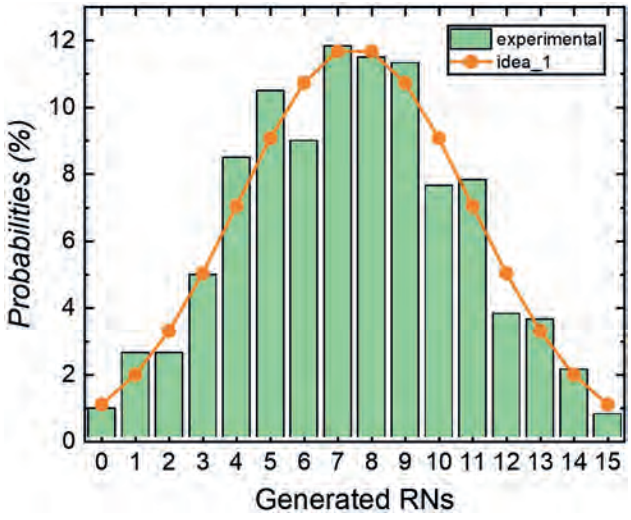

Results of the PDF-configurable TRNGs based on SOT-MTJs. The Gaussian PDF has been realized. In order to generalize the Bernoulli bits to a continuous TRNG with a desired PDF, we consider a Bayesian network. In a continuous five-step operation, the transistors are turned on in sequence, and remain off at all other time. For the 2nd-4th MTJs, the write voltage of each MTJ is influenced by the state of all previous MTJs.

FP-03. Modelling of Reservoir Computing in Out-of-Plane Artificial Spin Ice. *J. Maes*[1], A. Kurenkov[2] and B. Van Waeyenberge[1] *1. Solid State Sciences, Ghent University, Ghent, Belgium; 2. Mesoscopic Systems, ETH Zürich, Zürich, Switzerland*

In *Reservoir Computing* (RC), a temporal input signal is applied to a nonlinear dynamical system (the 'reservoir') [1,2]. Its response becomes a nonlinear transformation of the input, upon which a single readout layer can be trained for machine learning purposes. [1,3] Interestingly, many physical systems are highly nonlinear with fading memory, so they can directly be used as a reservoir without further abstraction. [4] RC has already been demonstrated numerically in various in-plane artificial spin ices (ASI). [1,5,6] Here, we study *out-of-plane (OOP)* ASI as the reservoir, because efficient physical mechanisms for input and readout are expected to be available in such systems. To this end, the *software tool "Hotspice"* was developed: it simulates thermally active ASI using an Ising approximation with an energy barrier between states. An effective Zeeman energy is used to model an external stimulus that provides input data. Either Néel relaxation theory or Glauber dynamics can be used for time evolution. [7] RC metrics can then be calculated for a given combination of input, ASI, and readout, which can be used to identify suitable input procedures and optimize system parameters. [8] In OOP ASI, neighboring spins prefer anti-parallel alignment, giving rise to two degenerate ground states with net zero magnetization. An external field can not meaningfully distinguish between them, so a more intricate input scheme was needed for RC. We devised an input scheme which moves the domain walls in the system by only a few lattice units per input value, as shown in Figure 1. This procedure creates memory by avoiding avalanches, as evidenced by Figure 2. Currently, work is underway to get RC in *thermally active* OOP ASI. Such systems could be better suited for RC by using their dynamics to our advantage.

[1] J. H. Jensen and G. Tufte, *Artificial Life Conference Proceedings*, p.376-383 (2020) [2] D. Verstraeten, B. Schrauwen, M. D'Haene et al., *Neural Networks*, Vol. 20, p.391-403 (2007) [3] W. Maass, T. Natschläger and H. Markram, *Neural Computation*, Vol. 14, p.2531-2560 (2002) [4] G. Tanaka, T. Yamane, J. B. Héroux et al., *Neural Networks*, Vol. 115, p.100-123 (2019) [5] J. H. Jensen, E. Folven and G. Tufte, *Artificial Life Conference Proceedings*, p.15-22 (2018) [6] K. Hon, Y. Kuwabiraki, M. Goto et al., *Applied Physics Express*, Vol. 14, p.033001 (2021) [7] P. A. Flinn and G. M. McManus, *Physical Review*, Vol. 124, p.54 (1961) [8] J. Love, J. Mulkers, R. Msiska et al., *arXiv preprint*, arXiv:2108.01512 (2021)

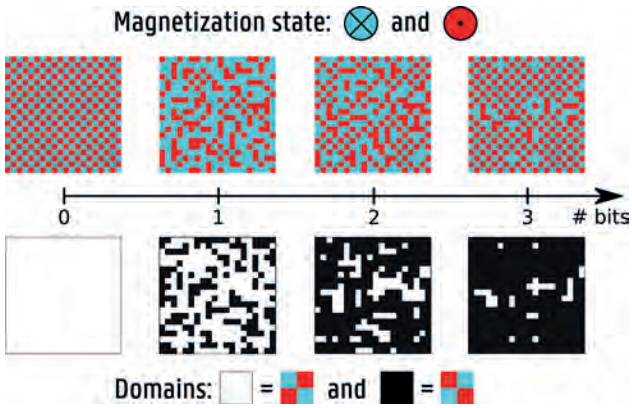

Fig. 1: Time evolution upon applying the same bit multiple times. *Top* – magnetization of individual magnets. *Bottom* – alternative view showing the 2 domain types, to illustrate their stepwise growth.

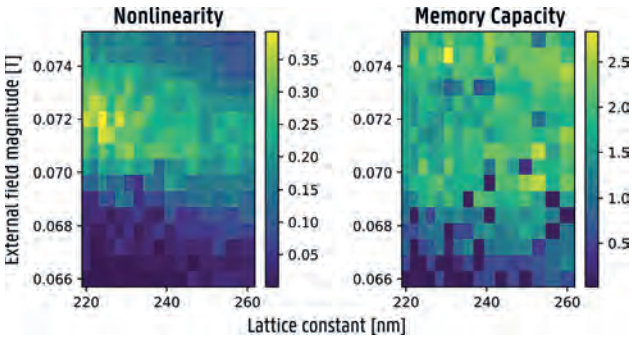

Fig. 2: RC metrics for the stepwise input scheme in 20×20 OOP Square ASI (with 10×10 readout), as a function of nearest-neighbor spacing and input magnitude.

FP-05. SHE-MTJ based ReLU-max pooling functions for on-chip training of Neural Networks. *V. Vadde*[1], B. Muralidharan[1] and A. Sharma[2] *1. Department of Electrical Engineering, Indian Institute of Technology Bombay, Mumbai, India; 2. Department of Electrical Engineering, Indian Institute of Technology Ropar, Rupnagar, India*

Hardware realization of neuromorphic computing based on spintronic devices results in an energy-efficient design [1]. Spin Hall effect-based magnetic manipulation has recently become a popular route toward low-power consumption devices [2]. This study examines the influence of various Spin Hall Effect (SHE) layers and their corresponding input resistances on the power consumption of the rectified linear activation (ReLU)-max pooling functions. The design for ReLU-max pooling relies on the continuous rotation of magnetization, which is accomplished by applying orthogonal spin current to the free-FM layer. We also demonstrate the non-trivial power-resistance relation, where the power consumption decreases with an increase in SHE resistance. We utilize the hybrid spintronic-CMOS simulation platform that combines Keldysh non-equilibrium Green's function (NEGF) with Landau-Lifshitz-Gilbert-Slonzewski (LLGS) equations and the HSPICE circuit simulator to evaluate our network [1,3]. We also validate the continuous magnetization change of free FM through micromagnetic simulations. To validate the efficiency of our design, we implement a convolutional neural network that classifies the MNIST datasets. This implementation illustrates that the classification accuracies achieved are comparable to those attained using the ideal software ReLU-max pooling functions.

[1]. Vadde, V., Muralidharan, B., & Sharma, A. IEEE Transactions on Electron Devices (2023). [2]. Grollier, J., Querlioz, D., Camsari, K. Y., Everschor-Sitte, K., Fukami, S., & Stiles, M. D. 3(7), 360-370(2020). [3]. Vadde, V., Muralidharan, B., & Sharma, A. Journal of Physics D: Applied Physics (2023).

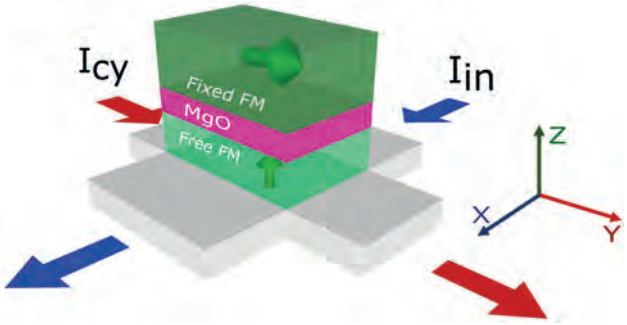

Fig. 1. MTJ on top of the SHE layer. The charge currents I_{in} and I_{cy} are injected into the SHE layer in the x- and y- directions, resulting in y- and x-polarized spin current injection to the free-FM layer, respectively.

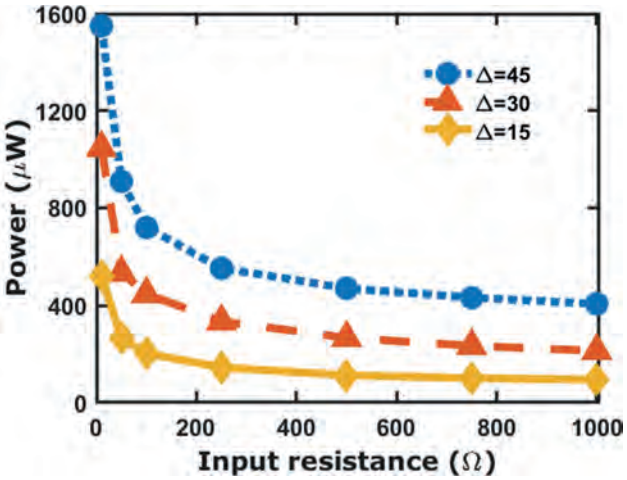

Fig. 2. The power consumption of the 9-input ReLU-max pooling network averaged over 50 Monte-Carlo simulations with respect to the input resistance of the SHE layer for different thermal stability factors with $Au_{0.25}Pt_{0.75}$ as heavy metal.

FP-06. Weight transfer method of a Hardware Neural Network constructed by Magnetic Tunnel Junction neurons using Telegraphic Switching Phenomenon. *J. Jang*[1] and W. Park[1] *1. Hanyang University, Seoul, The Republic of Korea*

This paper shows a weight transfer scheme in a hardware artificial neural network (H-ANN), using rate coding enabled by magnetic tunnel junctions(MTJ). In order for H-ANN to perform classification tasks, synaptic weights obtained from software training should be transferred to the hardware system. We use telegraphic switching of the MTJ to produce rated voltage signals to transfer weights and program the memristor synapse array. Telegraphic switching is constant magnetization direction switching of the MTJ. [1] An in-plane MTJ with MgO barrier is used. Constant resistance switching occurs under certain conditions; STT current biasing from -50μA to 50μA results signals with different state composition ratio. MTJ neurons were constructed by using a sensing amplifier along with the telegraphic MTJ. For the synaptic element, a standard TiO_2 memristor model [2] is used, synaptic weights of the network are stored as a form of conductance in the memristor. The MTJ H-ANN array consists of 784 pre-neurons for each pixel inputs, and 10 post-neurons for each classification label. 7840 memristor synapses are arranged in each cross-point. We have trained a neural network with the same configuration by software gradient descent algorithm. Weights obtained by software learning should be transferred to the H-ANN to perform classification task. We proposed a rate coding scheme, where the software weights were normalized, and quantized into

16 levels. Then, a program signal activates each row of the H-ANN for weight transfer; different STT current biases according to the quantized synaptic levels were induced to the program neurons, creating rated neural signals. For instance, a neural signal with spiking rate 0.1 will be used to transfer the lowest level of synaptic weight; whereas a signal with rate 0.9 is used to transfer the highest level of synaptic weight. The voltage of program neuron signals (3V) is higher than the memristor synapse threshold (2.5V), enabling weight modification of the synapse. Weights are transferred row-by-row, programming all 7840 synapses within the H-ANN array.

[1] M.R. Pufall, *et al*, "Large-angle, gigahertz-rate random telegraph switching induced by spin-momentum transfer.", Physical Review B, 2004, 69(21), 214409. [2] D.B. Strukov *et al*., "The missing memristor found." *Nature,* 2008, 453, 7191, pp 80-83.

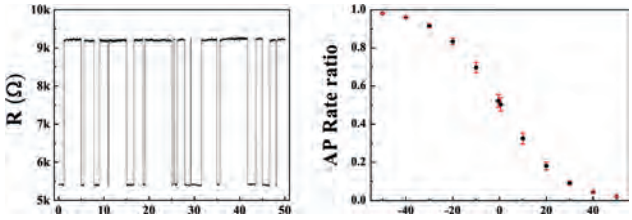

Telegraphic switching observed in the proposed MTJ; different AP rates depending on the STT current bias

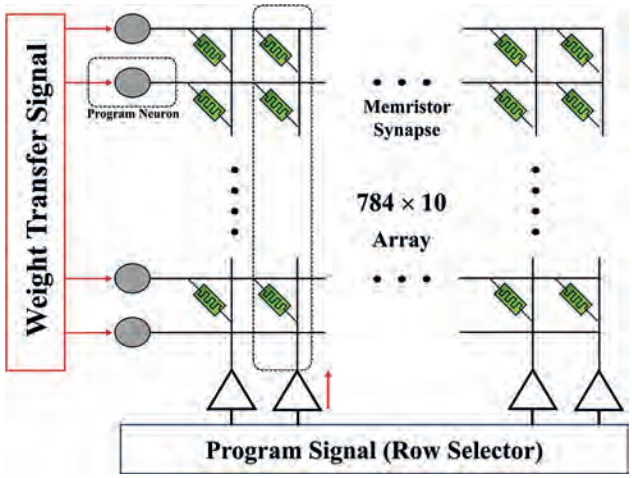

Proposed weight transfer scheme of H-ANN

FP-07. Generation of multiple resistive state using superconductivity-controlled magnetism. *B. Dutta*[1] and A. Pal[1] *1. Metallurgical Engineering & Materials Science, Indian Institute of Technology Bombay, Mumbai, India*

Ferromagnetism's ability to govern superconducting events is well known and well established, but research on the opposite effect has lagged. The first theoretical prediction of superconductivity induced change of micromagnetic arrangement or crypto ferromagnetic was made by P. W. ANDERSON AND H, SUHL [1]. A perfect and imperfect switching phenomenon of a GdN(5nm)/Nb(x)/GdN(3nm) spin valve, where GdN is a ferromagnetic insulator, has been demonstrated in this work. FIG.a shows the typical magnetoresistance behavior of the spin valve (x = 8.5 nm) at 2.8 K. The perfect switching phenomena between the superconducting state and the normal state (shown in FIG.b) is happening because of the field cycling event shown by red arrow in FIG.a, this phenomenon can only be explained by superconducting exchange coupling (SEC [2]) between two ferromagnets via the superconductor. The spin valve device exhibits non-volatile states between its completely on and off states (shown in FIG.c), and it has been shown at constant temperature (below the superconducting transition temperature) these non-volatile states can be accurately replicated by carefully cycling the magnetic field (represented by the blue dotted arrow in FIG.a). The SEC between various micromagnetic structures leads to these diverse nonvolatile states. These states can be utilized to create an entirely novel kind of superconductor-based cryogenic neuromorphic system [3].

[1]. P.W. Anderson, H. Suhl, *Phys. Rev.*, *116*, 898 (1959). [2]. Y. Zhu, A. Pal, M. G. Blamire, Z. H. Barber, *Nat. Mater.*, *16*, 195 (2017). [3] Kim, H., Mahmoodi, M.R., Nili, H. et al., *Nat Commun* 12, 5198 (2021).

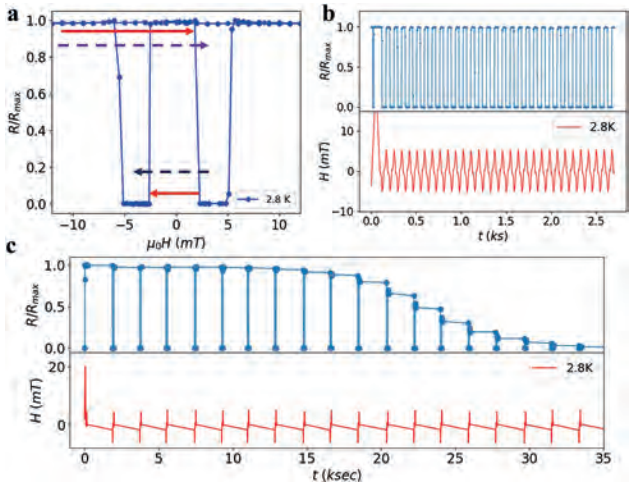

FP-08. Echo State Network with Spin-Transfer Nano Oscillators. *S. Qian*[1] and S. Rakheja[1] *1. Micro and Nanotechnology Laboratory, University of Illinois Urbana-Champaign, Champaign, IL, United States*

The Echo State Network (ESN), a Recurrent Neural Network (RNN) variant, handles time-series data using straightforward ridge regression for training, thereby reducing computational demand. We employ a Spin-Transfer Nano Oscillator (STNO) [1] as the recurrently connected neurons in our reservoir in the ESN model. Using numerical simulations, we gauge the performance of the STNO-based ESN while performing time-series predictions (Fig. 1). The STNO, a multilayer structure with ferromagnetic electrodes, has an out-of-plane oriented polarizer and an in-plane free layer. The free layer's z-component of magnetization, which responds to input current's amplitude and duration, creates the STNO's output via tunneling magnetoresistance and serves as the reservoir's signal. Our simulations indicate that the relaxation time of the STNO plays a pivotal role in the network's prediction accuracy. When the STNOs initialize from their equilibrium state at each time step, the performance of the network considerably surpasses that without a relaxation time, as depicted in Fig. 2(a). This figure portrays the Root-Mean-Square Error (RMSE) of the Mackey-Glass (MG) series prediction task as a function of the reservoir size. The performance of the ESN is also contingent upon the interplay between the input-to-signal conversion coefficient ($\gamma = J(t)/x(t)$) and the pulse width (t_{pw}). Figure 2(b) illustrates the relationship between RMSE and reservoir size for various (γ,t_{pw}) combinations. When contrasted with the commonly used *tanh* as the activation function, the STNO-based ESN delivers more accurate predictions. The network's Short-Term Memory (STM) capacity is evaluated using simulated random data to assess its data retention ability. With an adequately extensive relaxation time, the maximum STM capacity significantly surpasses that of other spintronics-based ESNs [2,3].

[1] Ebels, U., et al. *Physical Review B* 78.2 (2008): 024436. [2] Kanao, Taro, et al. *Physical Review Applied* 12.2 (2019): 024052. [3] Furuta T, Fujii K, Nakajima K, et al. Physical Review Applied, 2018, 10(3): 034063.

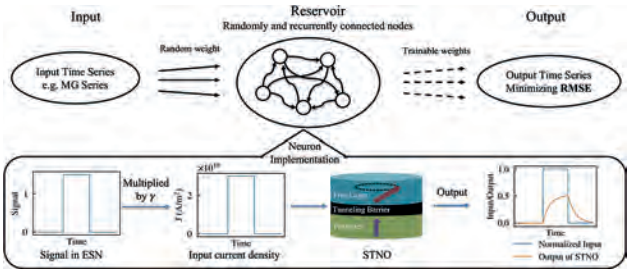

The flowchart of the ESN implementation and the process of converting the ESN signal into a current, inputting it into the STNO, and obtaining the output.

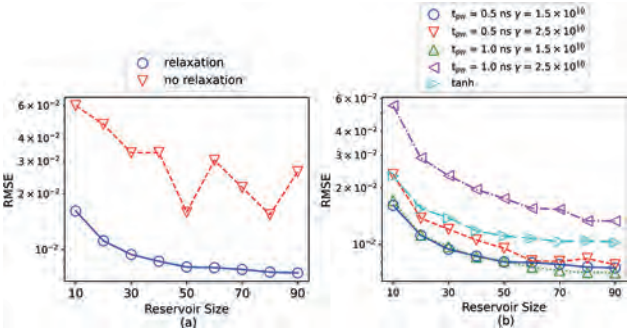

(a) ESN performance with and without relaxation time. (b) ESN performance across various (γ,tpw) pairs and the tanh activation function.

FP-09. Volatile Resistive Switching Induced by Competing Magnetic Phases in $La_{0.67}Sr_{0.33}MnO_3$ Thin Films for Neuromorphic Computing.
A. Jaman[1,2], A. Goossens[1,2], J. van Rijn[2] and T. Banerjee[1,2] *1. Groningen Cognitive System and Material Centre, University of Groningen, Groningen, Netherlands; 2. Zernike Institute for Advanced Materials, University of Groningen, Groningen, Netherlands*

The development of non-von Neumann computing depends on the realization of new devices that can be integrated into traditional circuitry. In this context, volatile memristive devices that exploits the rich phase space intrinsic to complex oxides and where the magneto transport characteristics can be controllably changed by external stimuli, constitutes key hardware components, mimicking certain human brain functionalities exhibited by neurons and synapses. Manganites are a class of strongly correlated oxides materials that exhibit versatile physical properties due to the coupling between charge, spin, orbital, and lattice degrees of freedom. The rich phase diagram intrinsic to these materials has been exploited in this work to stabilize competing magnetic states in divalently doped $La_{0.67}Sr_{0.33}MnO_3$ thin films [1]. Here we report on how an electric current-induced Joule heating triggers differences in conductivity across a textured substrate of $LaAlO_3$. This arises due to local differences in the magnetic phases in the current pathway and manifested as sharp onsets correlating with magnetic transitions from a ferromagnetic to a paramagnetic state, due to the coupled phase transition in manganite thin films. Crucial to the observed differences in the resistive switching pattern along the different directions, is the non-homogeneous strain induced in the $La_{0.67}Sr_{0.33}MnO_3$ thin films and the presence of twin domains in the substrate. This changes the hopping probability between the Mn atoms, leading to a spatial distribution of competing and coexisting magnetic phases throughout the 10 nm thick film. Our findings indicate that the phases are strongly coupled down to the nanometer scale and can be tuned locally at the microscale by the choice of a textured substrate. This demonstration of voltage driven volatile resistive switching in such manganite thin films is a new route for designing spintronic devices for neuromorphic computing.

A. Jaman, A.S. Goossens, and T. Banerjee, *Frontiers in Nanotechnology* 5, 1121492 (2023)

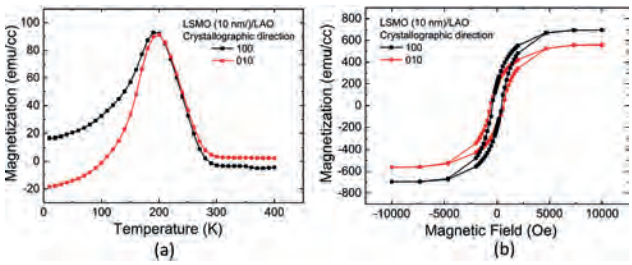

Fig 1. (a) M-T, (b) M-H shows anisotropic distributions of coexisting magnetic phase in the entire film.

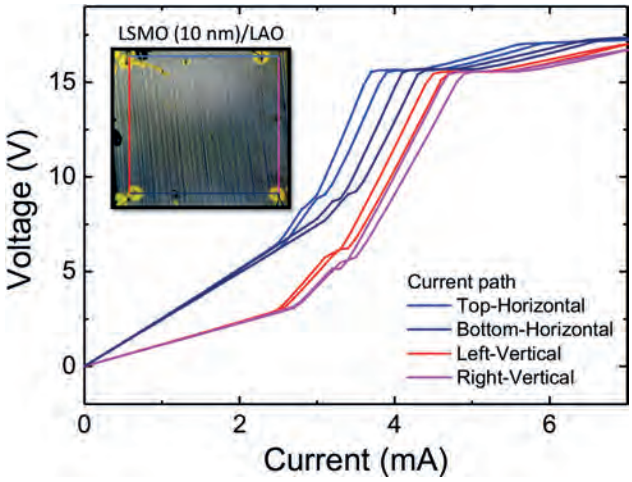

Fig 2. Current-controlled hysteretic resistive switching in twinned LSMO/LAO measured in four directions.

Session FQ
MAGNETICS FOR POWER ELECTRONICS AND TRANSFORMERS (Poster Session)

Marco Trapanese, Chair
Palermo University, Palermo, Italy

FQ-02. Analysis of Variable Inductor Employing Vegetable-Based Transformer Oil with Magnetic Nanoparticles. *M. Baek*[2] and H. Lee[1]
1. Changshin University, Changwon-si, The Republic of Korea; 2. Korea Electrotechnology Research Institute, Changwon-si, The Republic of Korea

In this study, a multi-physics CAE analysis method is applied to a variable inductor with vegetable oil-based magnetic nanofluid embedded in the ferrite core, and the heat transfer characteristics are analyzed numerically and verified by experiments applied to a simplified test model. Recently, variable inductors using magnetic fluids driven by high-frequency pulsed voltage sources have been developed [1]-[2]. Temperature rise is an important issue for inductors operating at high frequency, and engineers want to predict the thermal characteristics of the circuit during operation. Core losses in variable inductors are the main cause of temperature rise in magnetic materials such as ferrite cores and magnetic nanofluids for power electronics applications. For ferrites, the loss mechanism is well understood and loss data can be obtained relatively easily from manufacturers; however, for magnetic nanofluids, such information is not readily available in the literature [3]. To analyze the losses in the magnetic nanofluid, the B-H curve was measured experimentally and used as physical information in the multiphysics CAE analysis. Finally, the inductance and temperature rise with average operating current were measured and analyzed, as shown in Figure 1. The temperature predictions of the variable inductor are shown to be in good agreement with experimental data, and the developed analytical technique of magnetic-thermal hydrodynamics can be used to design variable inductors with high-frequency voltage sources.

[1] D. W. Kim, H. N. Cha and D. H. Kim, IEEE Trans. on Magnetics, Vol. 49, p. 1901, (2013) [2] H. Y. Lee, I. M. Kang and S. H. Lee, J. Appl. Phys. Vol. 117, p. 17D508 (2015) [3] R. E. Rosensweig, J. Magn. Magn. Mater. Vol. 252, p. 370 (2002)

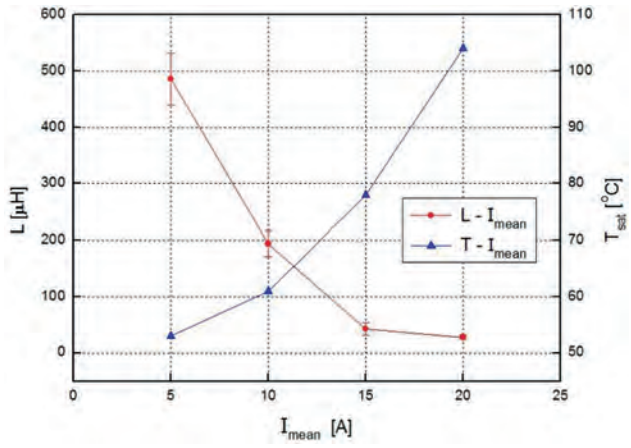

The change of inductance and temperature driven by the average operating current in the variable inductor employing magnetic nanofluids.

FQ-03. Magnetic properties of Fe-Ni powder core for high frequency device applications. *M. Nguyen*[1], S. Yoshida[2], S. Okamoto[2,3], T. Miyazaki[4] and Y. Endo[1,5] *1. Department of Electrical Enginering, Graduate School of Engineering, Tohoku University, Sendai, Japan; 2. Institute of Multidisciplinary Research for Advanced Materials, Tohoku University, Sendai, Japan; 3. National Institute for Material Science (NIMS), Sendai, Japan; 4. Faculty of Engineering, Tohoku University, Sendai, Japan; 5. Center for Science and Innovation in Spintronics, Tohoku University, Sendai, Japan*

Compared to the performance of gapped ferrite or iron powder core at a similar size, a higher energy capability and more effective permeability in Fe-50 at. % Ni were well-known to be shown due to the high saturation magnetization of 1.5 T. In addition, a low core loss and excellent DC bias characteristics offer a good magnetic property as well as reduction in size and number of windings. Therefore, Fe-Ni cores are one of the excellent candidates for switching regulator inductors, transformers, reactors and in-line noise filters. However, contrary to the industrial importance in powder core due to high saturation magnetization with magnetic softness, the academic researches to reduce the core loss is very few. In this study, dependence of binder content and compacting pressure on magnetic properties as well as core loss of Fe-Ni powder core is investigated. The Fe-Ni powder cores were prepared as follows: at first, the 10 μm size Fe-Ni powder with 50 % in weight percentage of Ni was mixed with different phenol contents as binder and insulator. Next, a ring core was done by compacting process at various pressures from 980 to 1960 MPa. Finally, the powder cores were annealed at 400 °C to remove the stress due to the compacting process at room temperature and improve the magnetic properties. These increases in density and higher permeability were obtained when the compacting pressure increased. That is, the density increased from 6.54 to 7.43 g/cm^3 as the resin content was decreased from 3 to 0.3 %. The maximum value of real part relative permeability (μ') was approximately 51.3 in the core with 1 % of resin content. The spectrum of real and imaginary parts of relative permeability (μ' and μ'') showed the stable values and zero up to 1 MHz, respectively, suggesting that the eddy current loss suppresses. This result means that Fe-Ni powder core can be used for high frequency region. Additionally, saturation magnetization (M_s) was higher in case of both lower resin content and higher compacting pressure. Therefore, these results demonstrate that the optimum core loss with high (M_s) can be obtained by proper binder content and compacting pressure condition for high frequency applications.

4mp.pdf (pacificsowa.co.jp) Acknowledgement This work was supported in part by MEXT Program for Creation of Innovative Core Technology for Power Electronics Grant Number JPJ009777 and Data Creation and Utilization-Type Material Research and Development Project (Digital Transformation Initiative Center for Magnetic Materials) Grant Number JPMXP1122715503. This work was supported in part by CSIS, CSRN, and CIES, Tohoku University.

FQ-04. Analysis of electric streamer discharge current using the generalized energy method in vegetable-based transformer oil with magnetic nanoparticles and experimental validation. *H. Lee*[1], H. Kang[1] and M. Baek[2] *1. Changshin University, Changwon-si, The Republic of Korea; 2. Korea Electrotechnology Research Institute, Changwon-si, The Republic of Korea*

In this paper, the electrical streamer discharge current was numerically and experimentally investigated in vegetable-based transformer oil with magnetic nanoparticles. The numerical calculation of the discharge current induced by the motion of charged particles was compared with the expanded Sato's equation, the integral Ohm's law and generalized energy method. To verify the results of the calculated current through analysis, a streamer discharge experiment with tip-plate electrode was constructed. The plate electrode to evaluate the discharge current was designed as a multi-port system by dividing it into a conductive ring electrode, and it was tried for the first time in the experimental study of a streamer in a vegetable-based transformer oil with magnetic nanoparticles.

[1] Morrow. R and Sato. N, Appl. Physics. Technology. 32, 5 (1999) [2] Zahn. M, Tsang. C. F and Pao. S. C, Appl. Physics. Technology. 45, 6 (1974) [3] H. Y. Lee and S. H. Lee, IEEE Tans. Magn., Vol. 6, p. 7006204 (2014)

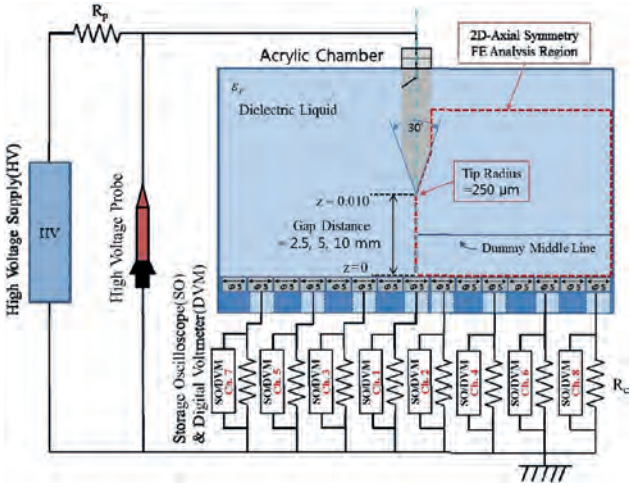

Schematic diagram of the set-up for experimental and numerical validation with the tip-plates model

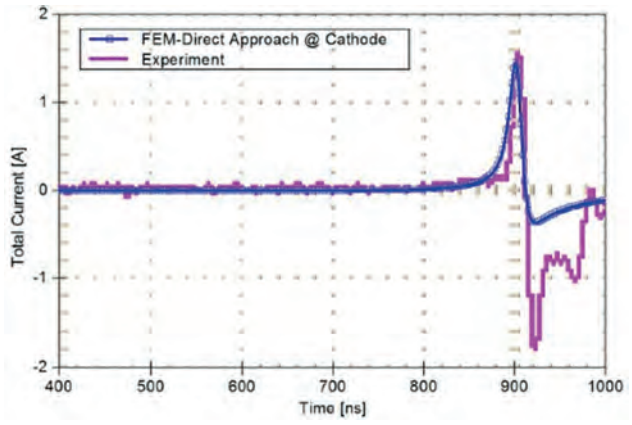

Comparison of a discharge current in dielectric liquid

FQ-05. Investigation of Electromagnetic Noise in an Induction Cooktop by examining circular membrane vibration modes in terms of their harmonics. *G. Yun*[1], S. Lee[1], G.F. Lukman[1] and C. Lee[1] *1. Electrical Engineering, Pusan National University, Busan, The Republic of Korea*

This study aims to identify the mechanism of noise generation in an induction cooktop (IC) due to its electromagnetic vibration. Fig. 1 shows the key components of an IC, and they are a glass cover, coils, and ferrites along with a pot on the cooktop. Through the electromagnetic induction of an IC among its components, heat is generated directly by eddy current flowing inside the surface of a pot. The main fucus of recent research on ICs is the improvement of output power and/or efficiency by modifying their hardware topologies and/or software controls [1-2]. During this modification, however, it has been reported that undesirable sound known as humming or buzzing was recognized as discomfort to users. In this paper, it is suggested that the analysis of noise and vibration commonly used in an electric motor [3] is extended to ICs in a similar way. During the energy conversion of an IC, electromagnetic force is generated in the z-axis direction from the surface of its cooktop, and the air-gap force is numerically analyzed as the main source of noise. As shown in Fig. 2, the mode of vibration is defined in terms of its shape as a circular membrane, and the harmonics of vibration are decomposed into their spatial and temporal components by the three-dimensional Fast Fourier Transform (FFT). In particular, the spatial harmonics are separated by a variable of either radius or angle, which is represented in rho or phi, respectively. Considering the different materials of a pot such as SUS403, SUS409, and SUS440 as the load of an IC, their vibration patterns are compared by means of a circular membrane mode analysis. A dominant circular membrane is distinguished with respect to its spatial harmonics in rho and phi at the same time, and hence, the correlation of vibration with noise has been verified through the proposed numerical technique. As a result, it is claimed that the improvement of noise in an IC is feasible by analyzing vibration in terms of its harmonics.

[1] O. Lucia et al., IEEE Access, vol. 7, p. 181668-181677 (2019) [2] Villa, Jorge, et al., IEEE Transactions on Industrial Electronics, vol 68.8, p. 6762-6772 (2020) [3] Song, Zaixin, et al., IEEE Transactions on Magnetics, vol 54.11, p. 1-5 (2018)

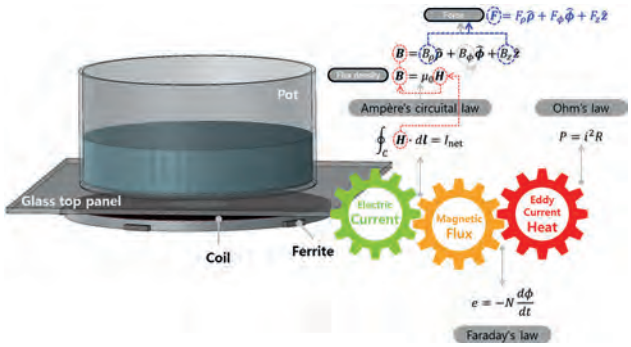

Configuration of an induction cooktop

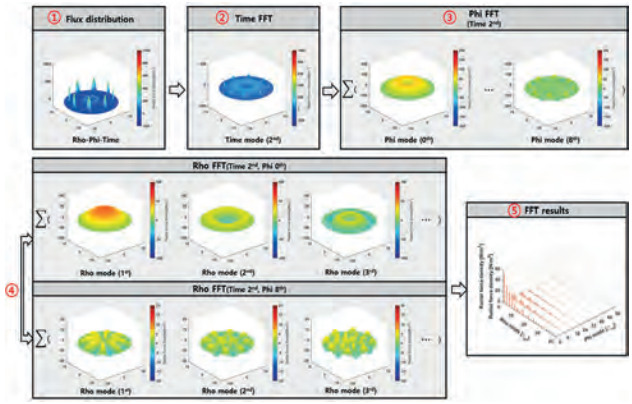

Three-dimensional FFT of an IC by means of circular membrane analysis

FQ-06. Improved Calculation of Core Losses of High-Speed Motors with Two Different Permanent Magnets Considering Higher order current harmonics. *S. Kim*[1], J. Woo[1], K. Shin[2] and J. Choi[1] *1. Electrical Engineering, Chungnam National University, Daejeon, The Republic of Korea; 2. Power System Engineering, Chonnam National University, Yeosu, The Republic of Korea*

In high-speed permanent magnet synchronous motor (PMSM) drives, the carrier frequency of the inverter causes time harmonics in the current, which affects the iron losses, a component of electromagnetic losses. According to Steinmetz's equation, iron losses are proportional to the frequency and flux density and each component is influenced by the current harmonics. Therefore, the influence of harmonics needs to be considered to accurately predict iron losses [1]. In this study, the prediction of current harmonics and its impact on iron losses are analyzed by comparing two models with different permanent magnet materials but the same output. The iron losses are significantly influenced by the harmonic content of the current and magnetic behavior, making the analysis of harmonic components and magnetic behavior essential. Thus, the stator core was divided to examine the magnetic behavior according to current harmonics in each region and perform a final analysis of iron losses accordingly [2, 3]. Fig. 1 shows the models used in this study and the 3D-FEM shape of the segmented stators along with the applied current. Fig. 2(a) illustrates the variation in magnetic behavior due to current harmonics, while Fig. 2(b) represents the harmonic components of losses caused by current harmonics. The analysis results indicate that harmonic components of iron losses occur at higher orders, around the 30th order, similar to the current harmonics. Finally, Fig. 2(c) demonstrates the losses and output at different speeds for each model. Furthermore, detailed comparisons and experimental results of the two models will be presented in the complete paper.

[1] Carlos A.Hernandez-Aramburo, Tim C.Green and Alexander C.Smith, IEEE Trans. Magn., Vol. 39, p. 3527-3533 (2003) [2] J. H. Lee, J. Y. Choi and K. H. Shin, MDPI Energies., Vol. 15, Art. no. 9213 (2022) [3] J. H. Woo, T. K. Bang and J. Y. Choi, IEEE Trans. Magn., Vol. 57, p. 1-5 (2020)

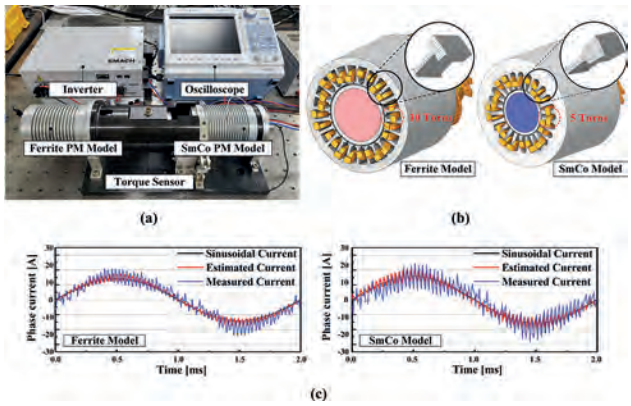

Fig. 1 (a) Experimental setup, (b) 3D-FEM structure of the split stator, (c) current waveforms according to the magnetic material.

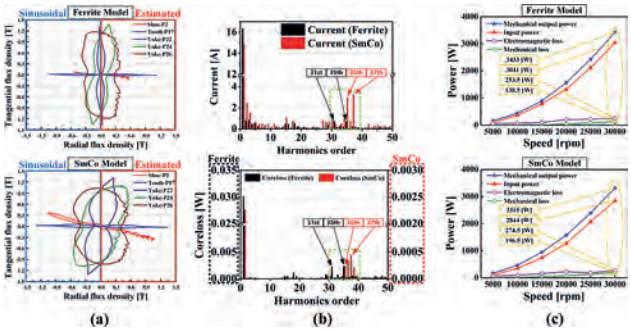

Fig. 2 Comparison according to current harmonics (a) magnetic field behavior, (b) current harmonics orders and their corresponding impact in the core loss, (c) measured power and loss according to rotor speed.

FQ-07. Demagnetization Analysis of Outer Rotor Type BLDC Motors Considering Permanent Magnet Overhang Structure. *T. Kim*[1], H. Shin[1], J. Yang[1], K. Shin[2], Y. Kim[1] and J. Choi[1] *1. Chungnam National University, Daejeon, The Republic of Korea; 2. Chonnam National University, Yeosu, The Republic of Korea*

Fan motors usually use outer-rotor-type brushless DC (BLDC) motors due to their high torque density and inertia [1]. Generally, a BLDC motor has a permanent magnet (PM) overhang that increases the effective flux linkage, as shown in Fig. 1.(a). Fig. 1.(b) shows the housing rotor and PM of the manufactured model. Since 3D analysis to consider these structure is time consuming, a 2D equivalent analysis method is useful [2]. Fig. 1.(c) shows a 2D equivalent model derived by converting the operating point of the PM and calculating the thickness of the rotor yoke by considering the housing rotor. Fig. 1.(d) shows that the no-load EMF of the experiment and 2D equivalent analysis are similar with an error rate of 1.02%. Moreover, BLDC motors generally use ferrite PMs, which exhibit low-temperature demagnetization characteristics [3]. Therefore, in this study, demagnetization analysis is carried out at low temperature by applying a 2D equivalent model, and the results are compared with the 3D analysis results. The demagnetization analysis method is carried out by comparing the change due to the supply of overcurrent through EMF and the magnetic flux density distribution. Fig. 2.(a), (b), show that demagnetization increases as the temperature decreases or when more current is supplied. Fig. 2.(c) shows that the error rate of EMF of the 2D equivalent model and 3D model after demagnetization is 2.17%, which is highly similar. Moreover, Fig. 2.(d) shows that the changes in the magnetic flux density distribution of both models show a similar tendency. These results confirm that the demagnetization analysis method using the 2D equivalent model instead of the conventional model is more accurate. In the full paper, more detailed results will be presented.

[1] T. Y. Lee, M. K. Seo, Y. J. Kim and S. Y. Jung, IEEE Trans. Appl. Supercond., Vol. 26, Art. no. 5205506 (2016). [2] H. S. Shin, K. H. Shin, G. H. Jang, S. K. Cho, K. H. Jung and J. Y. Choi, IEEE Trans. Appl. Supercond., Vol. 30, Art. no. 5201805 (2020). [3] N. Duan, W. Xu, S. Wang, J. Zhu, R. Qu and S. Jia, IEEE Trans. Magn., Vol. 53, Art. no. 2001304 (2017).

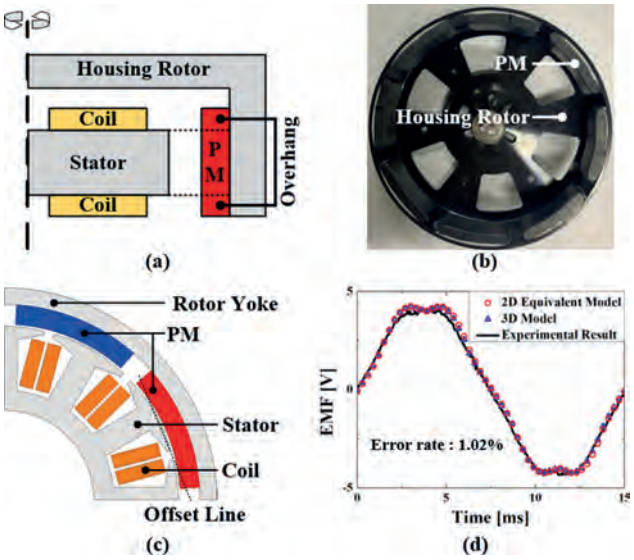

Fig. 1.(a) 3D structure of outer rotor type BLDC motor (b) Rotor of manufactured model (c) 2D equivalent model (d) EMF results of 3D, 2D equivalent analysis and experiment.

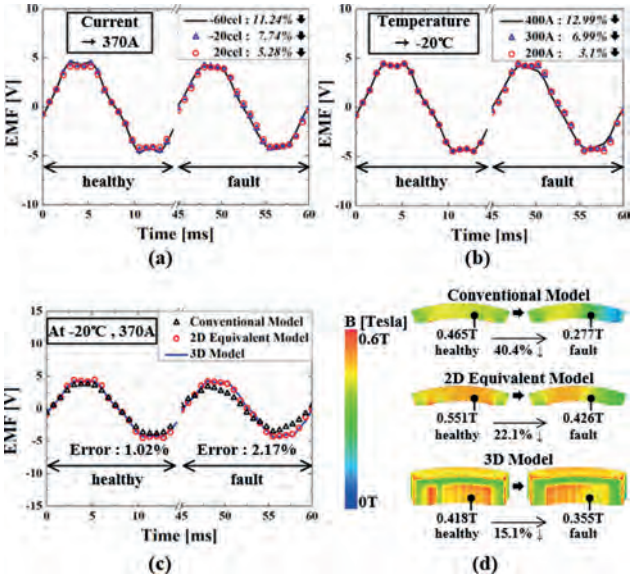

Fig. 2. EMF variation results of 2D equivalent model according to (a) temperature at a fixed current 370A (b) current at a fixed temperature -20C, (c) 2D and 3D EMF variation results and (d) 2D and 3D magnetic flux distribution according to imposing of demagnetization current at a fixed temperature (-20C).

FQ-08. Comparative Study on Design and Analysis of Interior Permanent Magnet Synchronous Motors with Different Rotor Structures based on Magnetic Equivalent Circuit Method and Finite Element Method. *J. Lee*[1], K. Yu[1], H. Ban[1], J. Choi[2], S. Sung[3], J. Park[3], C. Kim[4] and K. Shin[1] *1. Chonnam National University, Yeosu, The Republic of Korea; 2. Chungnam National University, Daejeon, The Republic of Korea; 3. Korea Research Institute of Ships and Ocean Engineering, Daejeon, The Republic of Korea; 4. Chungnam State University, Cheongyang, The Republic of Korea*

The interior permanent magnet synchronous motor (IPMSM) offers several advantages such as high-power density, high torque capability, and improved efficiency, making it an ideal choice for traction applications [1]. The rotor structure of an IPMSM significantly influences its electromagnetic performance, efficiency, and torque characteristics [2]. Therefore, understanding and optimizing the rotor structure is crucial to further improve the efficiency and power density of IPMSMs. In this study, the initial design of bar-type and V-type IPMSMs using the magnetic equivalent circuit (MEC) method and detailed analysis and comparison by finite element analysis (FEA) and experimental study are carried out. First, the design and analysis of the flux linkage and inductance of the IPMSM according to the rotor structure are carried out using MEC. The derived models are analyzed in detail for electromagnetic characteristics such as electromagnetic losses and torque by FEA. Finally, experimental studies are conducted to compare the driving characteristics and performance evaluation results. Based on the requirements and constraints of the system, the structures of the bar-type and V-type IPMSMs are shown in Fig. 1(a). As shown in Figs. 1(b) and 1(c), design models satisfying the requirements can be derived from MEC for calculating the magnetic flux linkage and d-q axis inductance according to the design flow and rotor structure. The composition of the prototypes and the experiment set is shown in Fig. 2(a). Fig. 2(b) shows the performance characteristics of each model and compares the results at the rated operating point. Figs. 2(c) and (d) show the efficiency maps with the main, rated, and maximum speed operating points for each model. The detailed design, analysis results, discussions, and measurements of the IPMSMs will be presented in the full paper.

[1] Y. Hu, S. Zhu, C. Liu, and K. Wang, "Electromagnetic performance analysis of interior PM machines for electric vehicle applications," *IEEE Trans. Energy Convers.*, vol. 33, no. 1, pp. 199-208, 2017. [2] A. Wang, Y. Jia, and W. Soong, "Comparison of five topologies for an interior permanent-magnet machine for a hybrid electric vehicle," *IEEE Trans. Magn.*, vol. 47, no. 10, pp. 3606-3609, 2011.

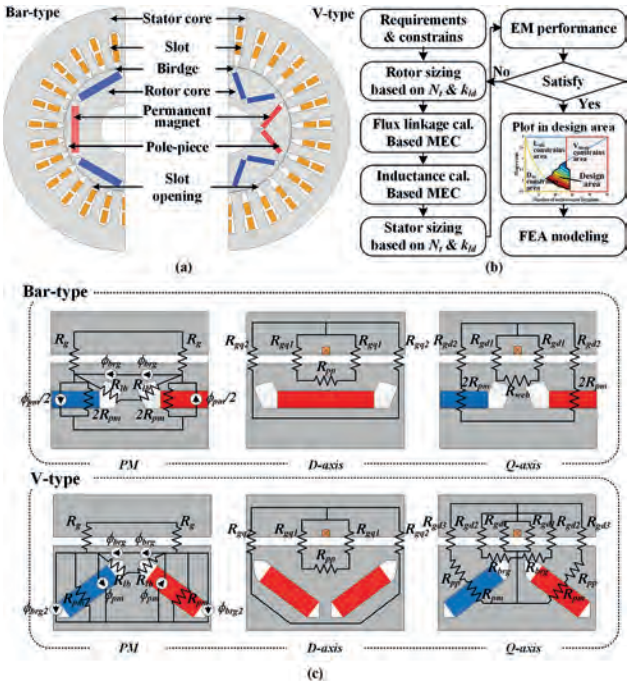

Fig. 1. (a) Analysis models of IPMSM, (b) flow chart of initial design with MEC, (c) MEC model with bar-type and V-type IPMSM.

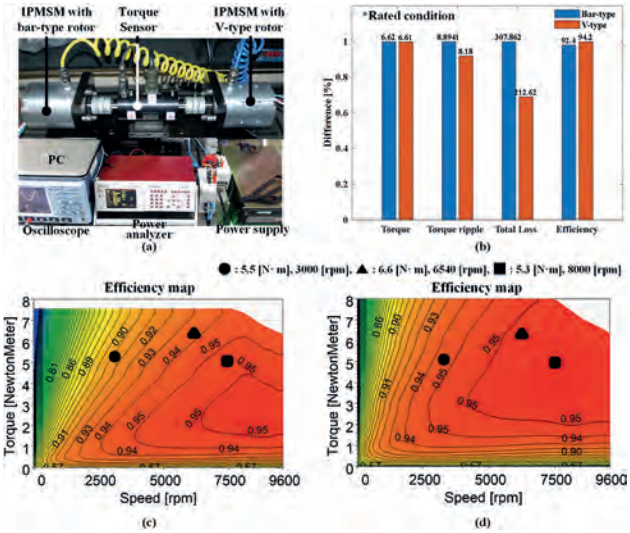

Fig. 2. (a) Experimental setup (b) electromagnetic analysis under rated conditions, efficiency map from (c) bar-type IPMSM and (d) V-type IPMSM.

FQ-09. Electromagnetic analysis of permanent magnet-assisted synchronous reluctance motor based on magnetic equivalent circuit.

S. Kim[1], T. Kim[1], W. Jung[1], M. Nguyen[1], K. Shin[3], Y. Kim[2] and J. Choi[1]

1. Electrical Engineering, Chungnam National University, Daejeon, The Republic of Korea; 2. Bio-systems and Mechanical Engineering, Chungnam National University, Daejeon, The Republic of Korea; 3. Power System Engineering, Chonnam National University, Yeosu, The Republic of Korea

Permanent magnet synchronous motors (PMSMs) are designed to achieve high performance and high efficiency by using rare earth permanent magnets. However, the production of these magnets causes environmental pollution, and a high unit price results in an economic disadvantage. Therefore, non-rare earth PMSMs are being researched to reduce dependence on rare earth permanent magnets[1]. Fig.1(a) shows a permanent-magnet-assisted synchronous reluctance motor (PMa-SynRM) using non-rare earth permanent magnets. Incorporating non-rare earth permanent magnets in the rotor's multi-layer structure improves the power factor and power of the synchronous reluctance motor. However, the geometry of these rotors complicates the design process and makes electromagnetic analysis time-consuming[2]. Generally, electromagnetic analysis methods include the finite element method (FEM) and magnetic equivalent circuit (MEC) method. The FEM provides accurate analysis results in the nonlinear region but requires a long analysis time for geometrically complex structures such as the PMa-SynRM. By contrast, the MEC cannot accurately analyze nonlinear regions, but it can quickly analyze geometrically complex shapes using a simplified equivalent circuit[3]. This study investigated the electromagnetic analysis of a non-rare earth PMa-SynRM using MECs. Fig.1(b) shows the MEC of the rotor's permanent magnet. Fig.1(c) and (d) show MECs of the d-axis and q-axis of the stator winding. Through these MECs, the air gap flux densities of the rotor's permanent magnet and the d-axis and q-axis field windings were derived Fig.2(a)–(c)[4]. Subsequently, the flux linkage was obtained Fig.2(d). Additionally, the MEC method was verified through a comparison with the electromagnetic analysis results of the FEM.

[1] Thanh-Anh Huynh, Po-Hsun Chen, Min-Fu Hsieh, IEEE Trans. Veh. Technol, Vol. 71, NO. 6, p.5727-5742 (June 2022) [2] Thanh Anh Huynh, Min-Fu Hsieh, IEEE Trans. Ind. Appl, Vol. 54, NO. 6, p.5856-5868 (July 2018) [3] Sascha Neusüs, Andreas Binder, IEMDC, p.1464-1471 (August 2019) [4] Meimei Xu, Guohai Liu, Qian Chen, IEEE Trans. Ind. Electron., Vol. 7, NO. 1, p.202-213 (July 2020)

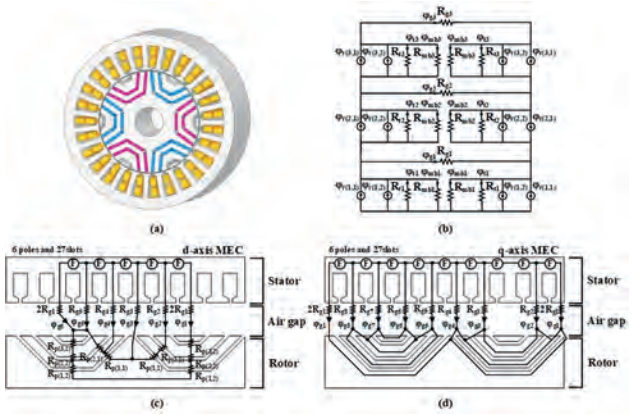

Fig.1 MEC of PMa-SynRM: (a) Analysis model, (b) MEC of magnet, (c) MEC of d-axis current, (d) MEC of q-axis current

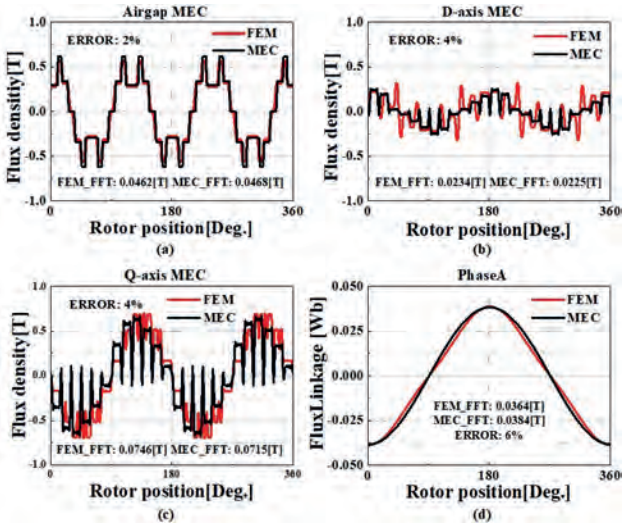

Fig.2 Electromagnetic Analysis with MEC: (a) Flux density of magnet, (b) Flux density of d-axis current, (c) Flux density of q-axis current, (d) Flux linkage of phase A

FQ-10. Analytical and Experimental Study of Electromagnetic Loss and Temperature Rise in Induction Machine. *H. Ban*[1], K. Yu[1], J. Lee[1], J. Choi[2], S. Sung[3], J. Park[3] and K. Shin[1] *1. Chonnam National University, Yeosu, The Republic of Korea; 2. Chungnam National University, Daejeon, The Republic of Korea; 3. Korea Research Institute of Ships and Ocean Engineering, Daejeon, The Republic of Korea*

The temperature rise in an induction machine critically affects the failure rate and service life. In particular, the temperature rises of the stator and rotor resulting from a significant stator core loss, copper loss, or rotor loss, as caused by variations in the current, could adversely affect the torque characteristics and durability [1]. Moreover, the temperature rise affects the fabrication quality and cutting error in ultra-precision rotational machine tools. To reduce the fabrication and cutting errors caused by thermal strain in a machine tool spindle, the power loss and thermal behavior of an induction motor should be calculated over a wide range of loads. In this paper, an analytical prediction of electromagnetic losses and temperature rise of induction machines is presented. Fig. 1(a) and 1(b) show the manufactured model and the proposed analytical model considers stator and rotor slotting effect. The proposed method is based on the subdomain method, by using the Fourier's series and the method of separation variables. Fig. 1(c) shows the results of electromagnetic loss analysis for each load using the analytical solution [2], [3]. The analytical results were verified by comparing with the finite element (FE) results. To verify the proposed method, a thermal measurement system was constructed as shown in Fig. 1 (d). As shown in fig. 2(a) and 2(b), the transient thermal characteristics of the induction motor are calculated by applying the equivalent thermal resistance model from Motor-CAD software (Motor Design Ltd.). Fig. 2(c) and 2(d) compare the temperature results obtained from the proposed method with the FE and experimental results. The proposed method can be verified from the comparison results. The analytical modeling, analysis results, discussions, and measurements of the induction machine will be presented in more detail in the final paper.

[1] P. Zhang, Y. Du, T. G. Habetler, and B. Lu, IEEE Ind. Electron., Vol. 58, pp. 1479–1489, (2011). [2] K. H. Shin, K. Hong, H. W. Cho, and J. Y. Choi, IEEE Trans. Appl. Supercond., Vol. 28, Art. no. 5205005, (2018). [3] K. Boughrara, N. Takorabet, R. Ibtiouen, O. Touhami, and F. Dubas, IEEE Trans. Magn., Vol. 51, Art. no. 8200317, (2015).

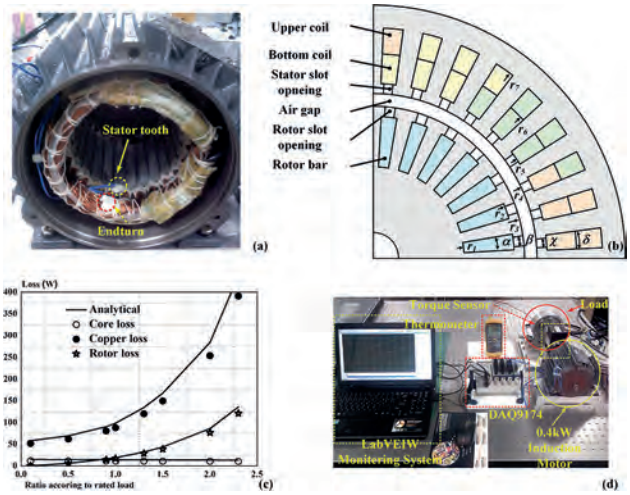

Fig. 1. Induction machine: (a) Prototype, (b) analytical model, (c) electromagnetic analysis results, and (d) experimental setup.

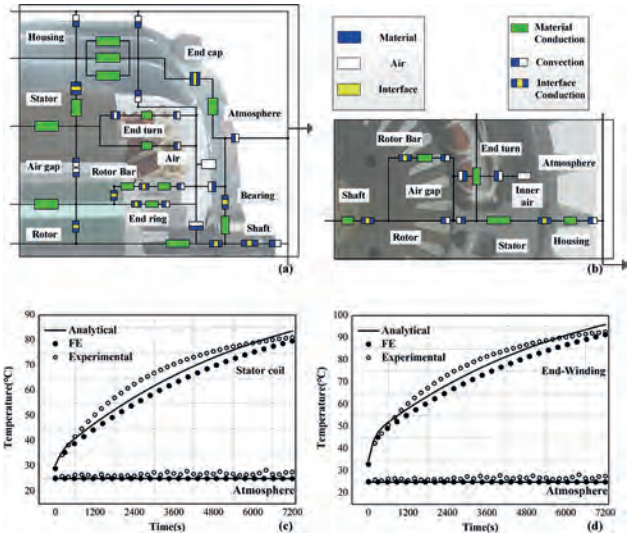

Fig. 2. Modeling and results of thermal equivalent circuit: (a) axial direction modeling, (b) radial direction, (c) temperature results in end-turn, and (d) temperature results in stator core.

FQ-11. Comparison of Electromagnetic Performance in MW class Superconducting Machines according to Shielding and Structures Based on Analytical Method. *H. Ban*[1], K. Yu[1], J. Lee[1], J. Choi[2], K. Kim[3], H. Cho[2] and K. Shin[1] *1. Chonnam National University, Yeosu, The Republic of Korea; 2. Chungnam National University, Daejeon, The Republic of Korea; 3. Korea Research Institute of Ships and Ocean Engineering, Daejeon, The Republic of Korea*

In this paper, a study on the electromagnetic design of the MW class superconducting (SC) machine according to electromagnetic structure was carried out [1], [2]. The structure of a partially SC machine has a three-phase copper coil on the inner rotor and a shield coil or magnetic core in the outermost structure for magnetic shielding. To improve the power density, the weight of the system, and the shielding capability, the electromagnetic field analysis of SC machine is very important in the design stage [3], [4]. To establish the design process of the SC machine, an analytical method considering shielding conditions and type of armature core was proposed. The proposed analytical method is to calculate the analytical solution by deriving the governing equation and general solution for each domain based on Maxwell's equation and electromagnetic field theory and applying appropriate boundary conditions. The magnetic permeability of the air core is the same as that of the vacuum,

and the magnetic permeability of the electrical steel core can be calculated using the iteration method based on magnetic field analysis. In addition, the active shield and the passive shield were selected to have the same magnetic field at the outermost shell. As shown in Fig. 2, the electromagnetic performances obtained using the analytical method were compared with those obtained using finite element (FE) analysis, and the validity of the analytical method presented in this paper was verified through comparison of the analysis results. The analytical modeling, analysis results, performance rating, and discussion according to the core type and shielding conditions of SC machines will be presented in the full paper.

[1] K. S. Haran, T. O. Deppen, and L. Zheng, IEEE Trans. Appl. Supercond., Vol. 26, Art. no. 5202508 (2016). [2] Y. Terao, W. Kong, H. Ohsaki, H. Oyori, and N. Morioka, IEEE Trans. Appl. Supercond., Vol. 28, Art. no. 5208005 (2018). [3] P. N. Barnes, M. D. Sumption, and G. L. Rhoads, Cryogenics, Vol. 45, pp. 670–686 (2005). [4] F. Lin, R. Qu, D. Li, Y. Cheng, and J. Sun, IEEE Trans. Appl. Supercond., Vol. 28, Art. no. 5205905 (2018).

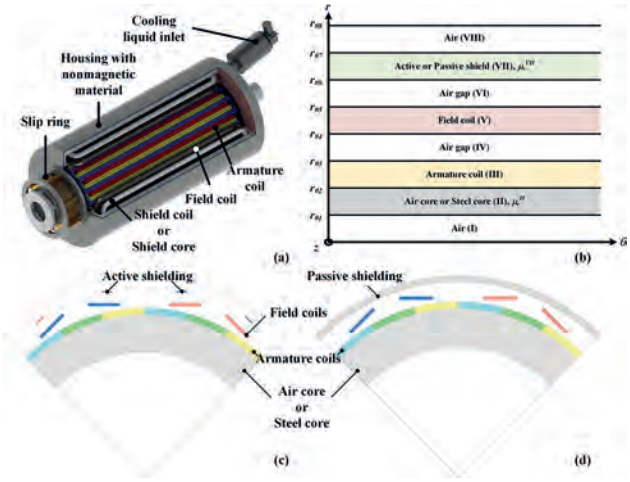

Fig. 1. Structure of SC machine: (a) structure, (b) analytical model, (c) actively shielded SC machine, and (d) passively shielded SC machine according to core materials.

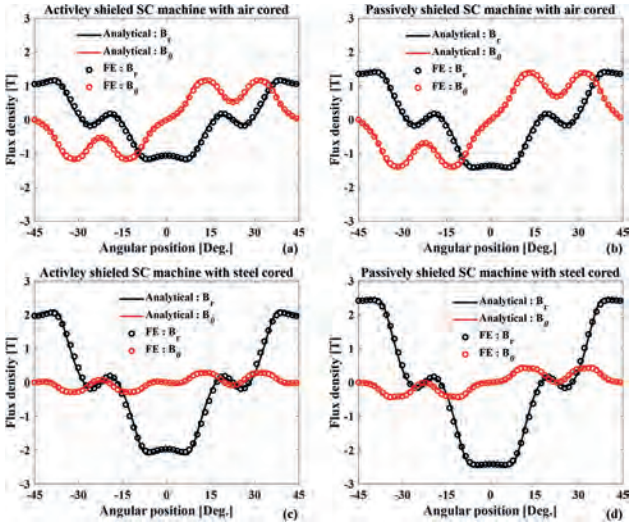

Fig. 2. Comparison of the flux density at the center of the armature coil by analytical and FE analysis.

FQ-12. Maximizing the Output Power of Magnetically Geared Generator in Low-Speed Applications Using Analytical Method and Particle Swarm Optimization. *M. Nguyen*[1], S. Kim[1], H. Shin[1], K. Shin[2], A. Phung[3] and J. Choi[1] *1. Chungnam National University, Daejeon, The Republic of Korea; 2. Chonnam National University, Yeosu, The Republic of Korea; 3. Hanoi University of Science and Technology, Hanoi, Vietnam*

The electrical machine industry faces a challenge in addressing high-torque, low-speed applications, with the two existing approaches presenting drawbacks. The first approach combines physical gear with a small-pole machine. In contrast, the second approach uses a large pole number machine, leading to a complicated winding organization and a higher manufacturing cost. To overcome these challenges, magnetically geared machines (MGMs) have gained popularity by integrating permanent magnet synchronous machines (PMSMs) and magnetic gears (MGs) into one structure. MGMs offer several advantages over traditional mechanical gear systems, including improved efficiency, reliability, reduced noise and vibration, and reduced wear and maintenance requirements [1-2]. The finite element method (FEM) is widely recognized as a reliable solution for electrical machine analysis but has a significant running time in calculating electromagnetic problems. The analytical method, on the other hand, offers faster computation times and results that agree well with FEM simulations, making it a promising solution for MGM design and optimization [3]. This approach is favored in the preliminary design process, as it saves time and improves performance. In this paper, the authors present a fully analytical approach obtained by solving differential equations, then integrated into a MATLAB program to derive a maximum output power using particle swarm optimization. The results are compared with FEM simulations to demonstrate the superiority of the proposed method. Fig.1(a) shows a simplified model employing the analytical method and optimization variables definition. Fig.1 (b-c) presents a fluctuation of variables and objective function respectively. Fig.2 compares an optimal model with the initial model in terms of structure, efficiency, and output power.

1. Qingsong Wang, Xing Zhao, and Shuangxia Niu, “Flux-Modulated Permanent Magnet Machines: Challenges and Opportunities” *World Electr. Veh. J.* 12, 13, Jan. 2021. 2. L. L. Wang, J. X. Shen, P. C. K. Luk, W. Z. Fei, C. F. Wang, and H., “Development of a Magnetic-Geared Permanent-Magnet Brushless Motor” *IEEE Trans. Magn.,* vol. 45, no. 10, Oct. 2009. 3. L. J. Wu, Z. Q. Zhu, D. Staton, M. Popescu, and D. Hawkins, “An Improved Subdomain Model for Predicting Magnetic Field of Surface-Mounted Permanent Magnet Machines Accounting for Tooth-Tips,” *IEEE Trans. Magn*, vol. 47, no. 6, pp. 1693-1704, June 2011.

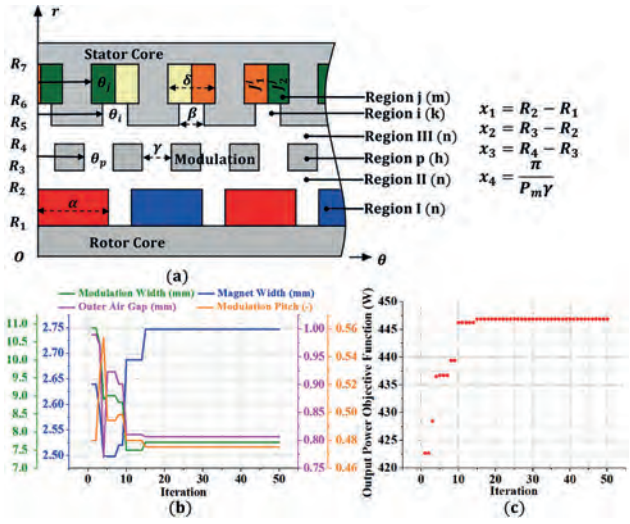

(a) Simplified model of MGM and optimal variables definition; (b) the optimal variables and (c) objective function according to the iteration.

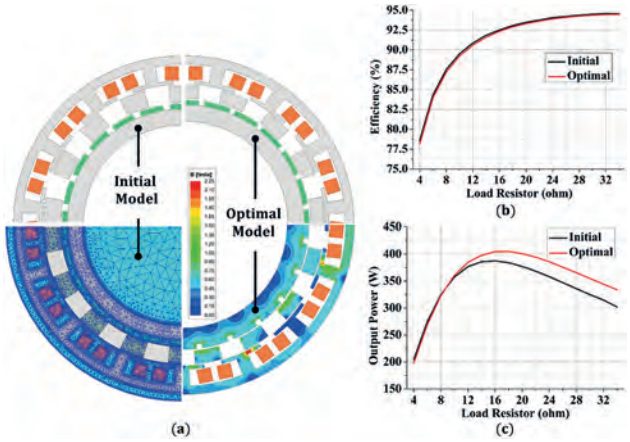

(a) Dimension comparison between the initial with the optimal model, meshes implement (97 960 elements), and flux density distribution; (b) efficiency and (c) output power comparison according to load resistors

FQ-13. Magnetic Force Calculation in PM Assembly Process of Direct-Drive Permanent Magnet Synchronous Generators based on Analytical Method. *H. Shin*[1], K. Shin[2] and J. Choi[1] *1. Chungnam National University, Daejeon, The Republic of Korea; 2. Chonnam National University, Yeosu, The Republic of Korea*

Direct-drive (DD) permanent magnet synchronous generators (PMSGs) have garnered increasing interest for wind power due to no mechanical gearbox and low maintenance[1]. However, the size of the generator increases due to low speed, and PM assembly is difficult because of the magnetic force. Therefore, PM assembly equipment is required to decrease the magnetic force, and the analytical method can be useful in the initial design of equipment as the process requires calculating the magnetic force according to changes in design variables. Figure 1. (a) shows a PMSG analysis model, and figure 1. (b) show a the analysis model of PM assembly equipment. A steel plate and non-magnetic material are adjoined with the PM, and the steel plate cancels out the magnetic force. Figure 1. (c) shows the simplified model of PM assembly equipment for analytical calculation. To ignore magnetic saturation, the permeability of the rotor yoke and steel plate is assumed to be infinite[2]. Figure 1. (d) shows the waveform of the magnetization. Since flux is spread out by the fringing effect as shown in figure 2. (a), the range of the flux density is wider than the magnetization. The flux density obtained by the analytical solution and finite element method (FEM) considering the fringing effect are as shown in figure 2. (b), and the results are almost same. The magnetic force is calculated by the Maxwell stress tensor (MST) using the flux density[3]. Figure 2. (c) depicts the PM assembly equipment zig in down scale, and the load cells measure the magnetic force. The magnetic force results of the analytical solution, FEM, and experiment are presented in figure 2. (d), and the analytical solution has a high reliability compared with other results. Since the analytical solution yields accurate and immediate results, it is useful in the initial design of PM assembly equipment. More detailed results and discussions will be presented in the final paper.

[1] N. Bhuiyan and A. McDonald, "Optimization of Offshore Direct Drive Wind Turbine Generators with Consideration of Permanent Magnet Grade and Temperature," *IEEE Trans. Energy. Convers.,* vol. 34, no. 2, pp. 1105-1114 (2019). [2] Z. Zhu, D. Howe, and E. Bolte, "Instantaneous Magnetic Field Distribution in Brushless Permanent Magnet DC Motors: I. Open-Circuit Field," *IEEE Trans. on Magn.*, vol. 29, no. 1, pp. 124-138 (1993). [3] K. Meessen, J. Paulides, and E. Lomonova, "Force Calculation in 3D Cylindrical Structures using Fourier Analysis and the Maxwell Stress Tensor," *IEEE Trans. Magn.,* vo1. 49, no. 1, pp. 536-545 (2012).

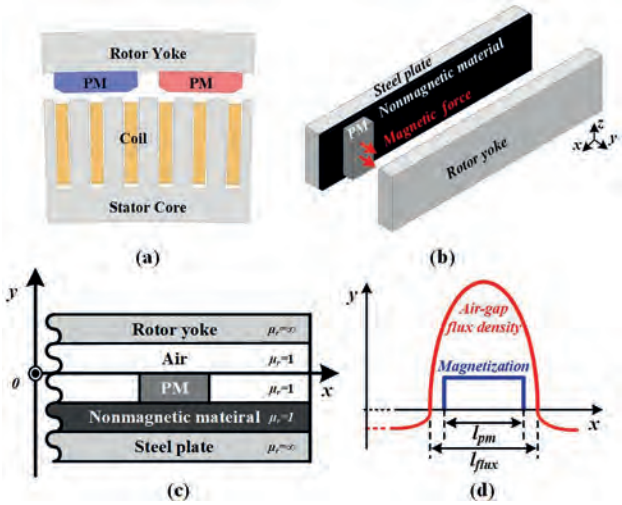

(a) Analysis model of PMSG (b) Analysis model of PM assembly equipment (c) Simplified model of PM assembly equipment (d) Waveform of the magnetization and flux density

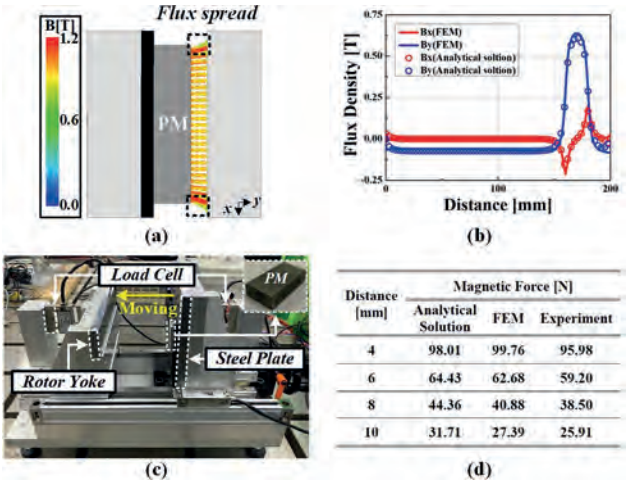

Distance [mm]	Magnetic Force [N]		
	Analytical Solution	FEM	Experiment
4	98.01	99.76	95.98
6	64.43	62.68	59.20
8	44.36	40.88	38.50
10	31.71	27.39	25.91

(d)

(a) Fringing effect of flux (b) Air-gap flux density (c) PM assembly equipment zig (d) Magnetic force results

FQ-14. Volume Optimization of High-speed Surface-mounted Permanent Magnet Synchronous Motor Based on Sequential Quadratic Programming Technique and Analytical Solution. *D. Hoang*[1], M. Nguyen[1], J. Woo[1], H. Shin[1], K. Shin[2], A. Phung[3] and J. Choi[1] *1. Chungnam National University, Daejeon, The Republic of Korea; 2. Chonnam National University, Yeosu, The Republic of Korea; 3. Hanoi University of Science and Technology, Hanoi, Vietnam*

Reducing the motor volume while maintaining optimal performance characteristics enables compact and efficient motor designs. It results in space-saving installations and improved overall system efficiency in various applications, especially air compressors and air blowers [1]. However, achieving such volume reduction without compromising the performance is a challenging task. This paper proposes an innovative approach that integrates the subdomain method [2] with sequential quadratic programming (SQP) to optimize the volume of a high-speed surface-mounted permanent magnet synchronous motor in an air compressor operating at 110000 rpm. Unlike conventional optimization tools that often rely on finite element analysis (FEA) software, by leveraging the subdomain method for electromagnetic modeling, we obtain an analytical solution that accurately represents the behaviors of the motor. Subsequently, the SQP technique is applied to iteratively adjust the geometric parameters and optimize the

volume of the model while satisfying design constraints. Fig.1(a) and (b) illustrate the 2D FEA model and the analytical model of the actual motor whose individual parts are shown in Fig. 1(c), (d), (e), (f). Fig.2a and Fig.2b demonstrate a significant reduction of the volume (28.1%) while Fig.2c shows that not only the volume is effectively reduced but also the torque capability is preserved, even having a slight improvement in efficiency in Fig 2d. This is due to the core loss being a majority component in the high-speed motor type which is reduced significantly in the optimized model.

[1] Z. Huang and J. Fang, "Multiphysics Design and Optimization of High-Speed Permanent-Magnet Electrical Machines for Air Blower Applications," *IEEE Trans. Ind. Electron*. vol. 63, no. 5, pp. 2766-2774, 2016. [2] K. -H. Shin, H. -I. Park, H. -W. Cho and J. -Y. Choi, "Analytical Calculation and Experimental Verification of Cogging Torque and Optimal Point in Permanent Magnet Synchronous Motors," *IEEE Trans. Magn.* vol. 53, no. 6, pp. 1-4, 2017.

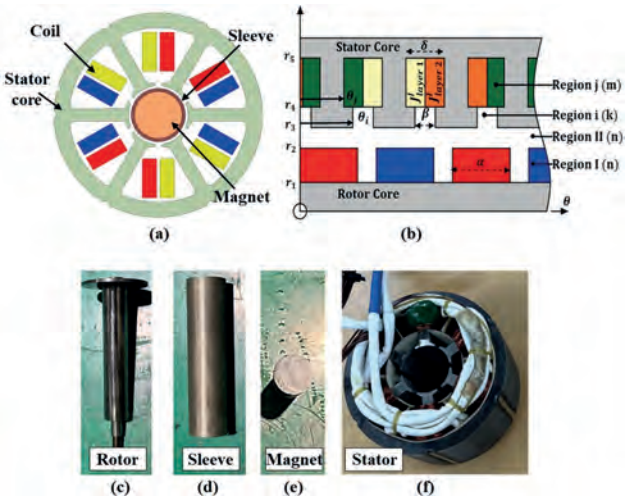

(a) 2D FEA model, (b) analytical model (c), (d), (e), (f) individual parts of the actual motor

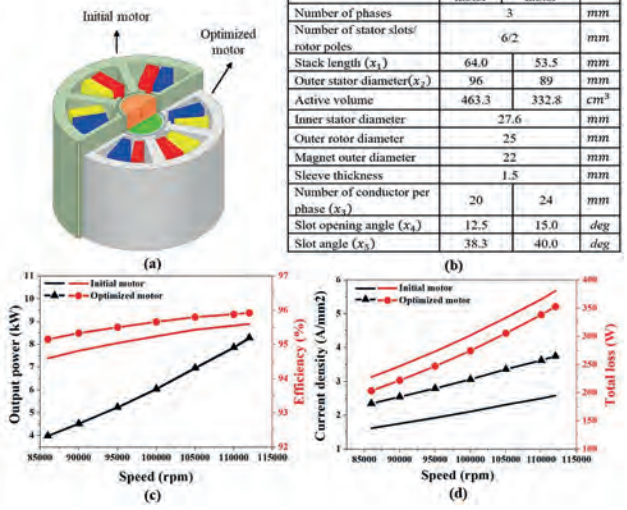

Parameter	Value		Unit
	Initial motor	Optimized motor	
Number of phases	3		*mm*
Number of stator slots/ rotor poles	6/2		*mm*
Stack length (x_1)	64.0	53.5	*mm*
Outer stator diameter(x_2)	96	89	*mm*
Active volume	463.3	332.8	cm^3
Inner stator diameter	27.6		*mm*
Outer rotor diameter	25		*mm*
Magnet outer diameter	22		*mm*
Sleeve thickness	1.5		*mm*
Number of conductor per phase (x_3)	20	24	*mm*
Slot opening angle (x_4)	12.5	15.0	*deg*
Slot angle (x_5)	38.3	40.0	*deg*

Initial and optimized model comparisons of (a) Shape (b) Parameters (c) Output power and efficiency (d) Current density and total loss

FQ-15. Inductance Derivation and Experimental Verification According to Operating Range of Interior Permanent Magnet Synchronous Motor. *K. Kwak*[1], J. Woo[1], Y. Kim[1], K. Shin[2] and J. Choi[1]
1. Chungnam National University, Daejeon, The Republic of Korea;
2. Chonnam National University, Yeosu, The Republic of Korea

Recently, electric machine systems require technology to efficiently utilize limited energy. Therefore, the application of various current vector control techniques is necessary to improve the efficiency at high speeds. Since inductance is a critical parameter in these current vector control techniques, it is crucial to derive accurate inductance values during characterization analysis. In most motor characteristic analyses, the inductance values are calculated using the apparent inductance calculation method. However, for motors that utilize permanent magnets and operate at high levels of core saturation, it is necessary to derive inductance values by considering the influence of core saturation on the relationship between current and magnetic flux. Therefore, in this study, the incremental inductance calculation method is used to derive inductance values in all operating regions. Fig. 1(a) shows the 3D structure of the analyzed model, and Fig. 1(b) and (c) show the stator and rotor of the actual manufactured model, respectively. Fig. 1(d), (e) and (f) show the cross section of flux density distributions at various load condition. Fig. 2(a) and (b) show the d-axis and q-axis inductances obtained using the apparent inductance calculation method and incremental inductance calculation method, respectively. Fig. 2(c) show the torque-speed performances at load condition with experiment result. Based on the analysis results, it is confirmed that calculating the inductance using the incremental inductance calculation method yields more accurate results in a specific operating range. These results indicate the importance of accurately determining the inductance in the analysis of electric motors. Detailed calculation process, comparative analysis and experimental results will be presented in the complete paper.

[1] K. H. Shin, J. Y. Choi and H. W. Cho, IEEE Trans. on Applied Superconductivity, Vol. 26, pp. 1-4, (2016). [2] B. Stumberger, G. Stumberger, D. Dolinar, A. Hamler and M. Trlep, IEEE Trans. on Industry Applications, Vol. 39, pp. 1264-1271, (2003).

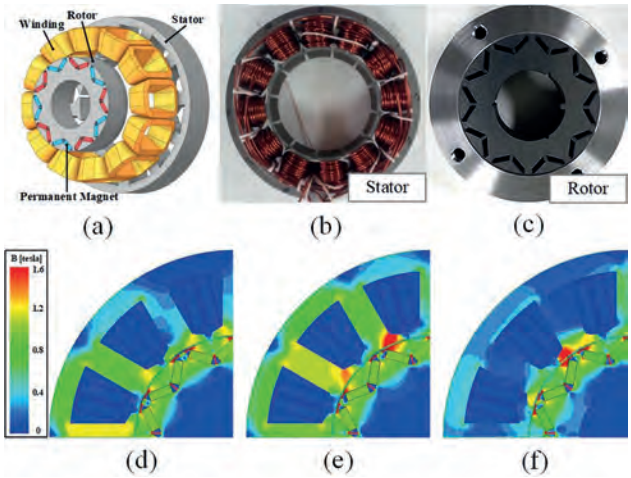

Fig. 1. (a) 3D structure of IPMSM, (b) manufactured model stator and (c) rotor, cross section of flux density distributions at (d) no-load operation (e) load condition (I_a: 8 [A], β: 40 [Deg.]) and (f) load condition (I_a: 15 [A], β: 80 [Deg.])

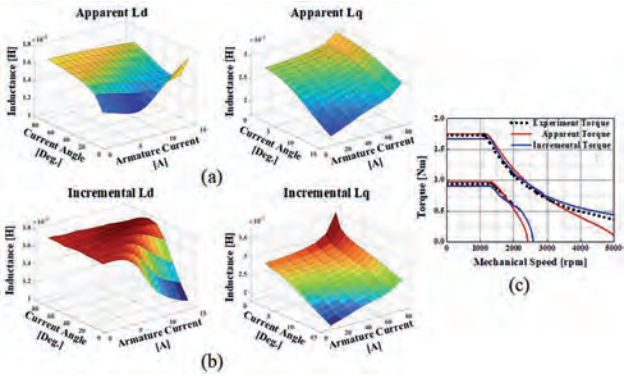

Fig. 2. Calculation of (a) apparent d, q-axis inductance and (b) incremental d, q-axis inductance, (c) torque-speed performances at load condition with experiment result

Session FR
BIOMEDICAL APPLICATIONS II
(Poster Session)

Hendrik Ohldag, Chair
Lawrence Berkeley National Laboratory, Berkeley, CA, United States

FR-01. Temperature-Induced Dispersion of Magnetic Nanoparticles: Insights from ESR Experiments and Simulations. *B. Cheng*[1], J. Sakurai[1], S. Hata[1] and C. Oka[1] *1. Micro-Nano Mechanical Science and Engineering, Nagoya University, Nagoya, Japan*

The agglomeration behavior of magnetic particles in thermotherapy affects heat production. We consider two simulations to explain the nonlinear variation of peak width *Hpp* in electron spin resonance (ESR) experiments using iron oxide nanoparticles dispersed in liquid paraffin at variable temperatures (250 K-470 K) caused by agglomeration to the dispersion of the particles. Such heat-driven behavior can be expected in the application of thermotherapy. A 3D Metropolis simulation is considered on Brownian mechanism; randomly distributed particles at different temperatures update the rotation angle and distance of the particles in each iteration step to change relaxes energy barrier ΔE which contains dipole interaction, Zeeman energy, Brownian energy and Electrostatic energy. The Boltzmann distribution judges the acceptance of the change. Calculated ΔE and R are substituted into the equation of *Hpp* reported by A.L. Tronconi et al. [1] Simulation results fitted by the equation shown,like the experimental results, *Hpp* changes at high temperatures appear saturated.[Fig.1] Another magnetic simulation is considered on Néel mechanism; two different particle distributions form are set up for agglomeration and Dispersion, respectively. They are both fixed, and magnetic moment is driven by the *LLG* equations, where the effective field contains spin wave interactions, thermal perturbations, magnetocrystalline anisotropy, and external magnetic fields to simulate ESR in different temperatures. An apparent resonance phenomenon is observed, and the magnetization before and after the resonance is fitted to obtain relaxation times (*A/D_Left/Right_Hpp*) corresponding to the left and right width (*Left/Right_Hpp*) in ESR. Results show that the saturated line width variation in ESR is consistent with the dispersed form, and the linear decrease is consistent with the agglomerated form. [Fig.2] By simulating two mechanisms of magnetic moment and comparing them with the experimental results, we verified that agglomerates can be destroyed at high temperatures.

[1] A.L. Tronconi et al., J. Magn. Magn. Mater., Vol. 122, p. 90 (1993)

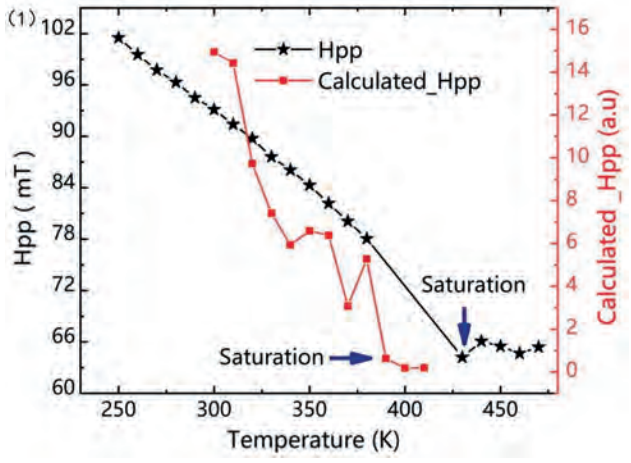

Fig.1 Peak widths of ESR and Peak widths of Metropolis simulation versus temperature

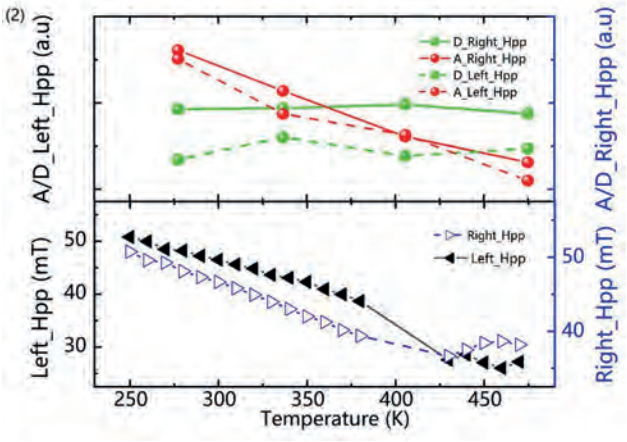

Fig.2 Left/right peak widths of ESR and left/right peak widths of LLG simulation versus temperature

FR-02. Differential Magnetization Dynamics of Superparamagnetic Iron Oxide Nanoparticles: Implications for Biomedical Applications and Magnetic Particle Imaging. *S.A. Shah*[1] *1. Physics, Forman Christian College (University), Lahore, Pakistan*

This study explores the differential magnetization dynamics of superparamagnetic iron oxide nanoparticles (SPIOs) in both liquid and frozen states. Our study has uncovered that these nanoparticles exhibit distinct rotational dynamics in different states, which cannot be solely attributed to temperature changes. In the liquid state, we observed a combination of Brownian alignment and Néel rotation of the nanoparticles' magnetic moments. This behavior was modeled using stochastic differential equations, assuming log-normal distributions and partial Brownian alignment of an effective anisotropy axis. Our findings contradict the prior belief that nanoparticles would reorient their magnetic moment internally via the Néel mechanism, regardless of the local environment. Additionally, our findings suggest that the large shift in dynamics could be due to the presence of small chain formations or local reorientation of the nanoparticles themselves. This comprehensive analysis of nanoparticle behavior in different states, combined with the use of Langevin equation simulations, underscore the need for precise particle-specific characterization in predicting solution dynamics and optimizing their use in biomedical technologies, including Magnetic Particle Imaging (MPI).

[1] K. M. Krishnan, Biomedical nanomagnetics: A spin through possibilities in imaging, diagnostics, and therapy, IEEE Trans. Magn. 46, 2523 (2010). [2] B. Gleich and J. Weizenecker, Tomographic imaging using the nonlinear response of magnetic particles, Nature (London) 435, 1214 (2005). [3] S. A. Shah, R. M. Ferguson, and K. M. Krishnan, Slewrate dependence of tracer magnetization response in magnetic particle imaging, J. Appl. Phys. 116, 163910 (2014). [4] R. Ferguson, A. Khandhar, E. Saritas, L. Croft, P. Goodwill, A. Halkola, J. Borgert, J. Rahmer, S. Conolly, and K. Krishnan, Magnetic particle imaging with tailored iron oxide nanoparticle tracers, IEEE Trans. Med. Imaging 34, 1077 (2015).

FR-03. Tissue Distribution Analysis of Anti-CD3 Conjugated Magnetic Nanoparticles (Fe_3O_4) Using In vivo Imaging System. *M. Hasan*[1,2], J. Choi[1] and S. Lee[1] *1. Department of Digital Healthcare Engineering, Sangji University, Wonju, The Republic of Korea; 2. Department of Biochemistry and Molecular Biology, Bangabandhu Sheikh Mujibur Rahman Science and Technology University, Gopalganj, Bangladesh*

Drug distribution is a vital parameter for depicting the pharmacokinetic properties of therapeutic agents[1]. MNP conjugated with anti-CD3 (Ab-MNP) is a promising immunotherapeutic agent. The distribution of MNPs is routinely analyzed by measuring Fe levels using inductively coupled mass spectrometry (ICP-MS) or ICP-OES[2,3]. However, the ICP based-methods measure the total iron content, including endogenous iron. We used an efficient approach that measured Ab-MNP distribution after intravenous administration using an in vivo imaging system. The fluorescent-labeled anti-CD3 are conjugated with dextran-coated magnetic nanoparticles (50 nm diameter) by the glutaraldehyde conjugation method. Ab-MNP was intravenously administered to BALB/c mice for 0, 1 hr, and 24 hrs. The fluorescence intensity in live animal and organs were analyzed. Buffer exchanges were performed by using a low-gradient permanent magnet[4]. The fluorescence analysis results validated the conjugation of antibodies and MNPs. Imaging reveals the concomitant reduction of unconjugated antibodies. Conversely, the fluorescence in the MNP solution indicated the presence of fluorescent-tagged Ab conjugated with MNP (Fig. 1). The organ imaging revealed the deposition of MNP-Ab primarily in the liver after 1 hr of administration. After 24 hrs, the fluorescence intensity increased in the liver. At the same time, the trapped fluorescence in the kidneys increased (Fig. 2). The size-dependent distribution patterns of nanoparticles have been identified recently. The nanoparticles less than 10 nm are quickly eliminated from the body by renal clearance, whereas the spleen efficiently traps higher than 100 nm[5]. Our results indicated the distribution of antibody-conjugated MNP of a specific diameter. Further, extended time-dependent administration efficiently revealed the compartmentalization of antibody-conjugated MNP.

[1] L. Di, B. Feng, and T. C. Goosen, Drug metabolism and disposition: the biological fate of chemicals 41, 1975-1993 (2013) [2] D. Clases and R. Gonzalez de Vega, Analytical and bioanalytical chemistry 414, 7337-7361 (2022) [3] M. Hasan, J.-G. Choi, and S.-S. Lee, AIP Advances 13, 025135 (2023) [4] J.-G. Choi, M. Hasan, and S.-S. Lee, Current Applied Physics 48, 79-83 (2023) [5] A. K. Gupta and M. Gupta, Biomaterials 26, 3995-4021 (2005)

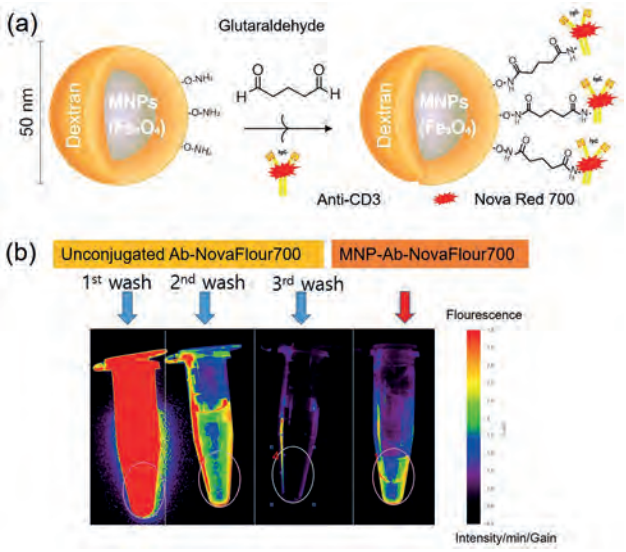

Fig 1: A) The two-step conjugation of MNP and Novaflour700-tagged anti-CD3 antibody. B) The fluorescence intensities were measured in three washouts and conjugated MNP-Ab solution.

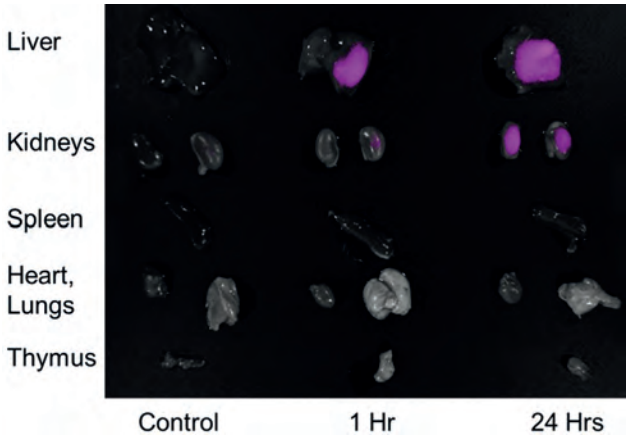

Fig 2: Organ distribution of MNP-Ab. Representative merged images from control, 1 Hr, and 24 Hrs mice organs show MNP-Ab distribution.

FR-04. Dumbbell-like Au–Fe_3O_4 Nanoparticles for Magnetic Hyperthermia. *L. Tonthat*[1], T. Ogawa[1] and S. Yabukami[1] *1. Tohoku University, Sendai, Japan*

Dumbbell-like gold and iron oxide hybrid nanoparticles (Au-Fe_3O_4 NPs) have emerged as promising candidates for magnetic hyperthermia-based cancer treatment [1]. However, conventional synthesis for these NPs involves using toxic and volatile iron pentacarbonyl ($Fe(CO)_5$), which raises safety concerns. Addressing this research gap, we present a novel alternative method utilizing triiron dodecacarbonyl ($Fe_3(CO)_{12}$), a relatively stable and less sensitive compound to air and moisture, ensuring safer handling. Herein, we describe a simplified synthesis process involving the reduction of gold(III) chloride trihydrate using tert-butylamine-borane complex at room temperature, forming Au NPs. Subsequently, the Au NPs were mixed with a solution of 1-octadecene, oleylamine, oleic acid, and $Fe_3(CO)_{12}$, followed by heating at 300°C for 1h to obtain the desired dumbbell-like Au-Fe_3O_4 NPs. To validate their dumbbell-like morphology, the EDS elemental mapping analysis in Fig.1(a) demonstrates distinct contrast between the Au and Fe_3O_4 NPs, attributed to the higher atomic number of Au. The average sizes of Au and Fe_3O_4 NPs are determined to be 5 nm and 15 nm, respectively. Furthermore, we evaluate the heating efficiency of hydrophilic-treated Au-Fe_3O_4 NPs (M_S=49.5 emu/g at 3T, 300K) under various field strengths (8.6-30.0 kA/m) and a fixed frequency of 270 kHz. Fig. 1(b) shows the temperature rise increases with higher field strengths, surpassing the therapeutic threshold of 45°C (ΔT=8°C), highlighting the potential for effective cancer treatment. Additionally, the heating efficiency was quantitatively evaluated through specific absorption rate (SAR in W/g) and intrinsic loss power (ILP=SAR/(fH^2) in nHm^2kg^{-1}). The results demonstrate superior performance with SAR=60.0 W/g, ILP=0.25 nHm^2kg^{-1} at maximum field strength, which is much higher than our previously developed Au-coated Fe_3O_4 [2-4]), and comparative with clinically-used Fe_3O_4 NPs (Resovist®) (SAR=57.5 W/g, ILP=0.18 nHm^2kg^{-1}), emphasizing high potential for magnetic hyperthermia applications.

(1) C. Wang, H. Yin, S. Dai, and S. Sun, "A general approach to noble metal-metal oxide dumbbell nanoparticles and their catalytic application for CO oxidation", Chemistry of Materials, 22(10), pp.3277-3282, 2010. (2) L. Tonthat, M. Kimura, T. Ogawa, et al: "Development of gold-coated magnetic nanoparticles as a theranostic agent for magnetic hyperthermia and CT imaging applications," AIP Advances, 13(2), 2023. (3) L. Tonthat, T. Ogawa and S. Yabukami: "Ultrasmall Fe_3O_4@Au Composite Nanoparticles with Different Sizes of Fe_3O_4 for Magnetic Hyperthermia," IEEE Transactions on Magnetics, doi: 10.1109/TMAG.2023.3287505 (early access). (4) L. Tonthat, A. Kuwahata, T. Ogawa and S. Yabukami, "Ultrafast Heating Rate of Ultrasmall Gold-coated Iron Oxide Magnetic Nanoparticles by Ferromagnetic Resonance," IEEE Transactions on Magnetics, doi: 10.1109/TMAG.2023.3287550 (early access).

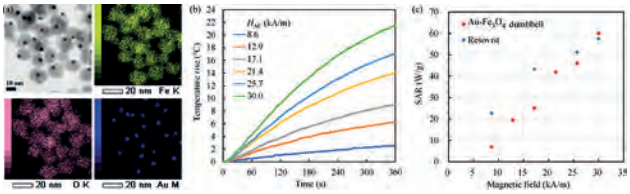

Fig. 1 (a) EDS elemental mapping of dumbbell-like Au-Fe_3O_4 NPs (b) their temperature rise under applied magnetic fields, and (c) their SAR values compared to commercial Fe_3O_4 NPs.

FR-05. Optimizing A Deep Learning Model for the Prediction of Electric Field Induced by Transcranial Magnetic Stimulation for Mild to Moderate Traumatic Brain Injury Patients. Y.R. Saxena[1,2], C.J. Lewis[3], J.V. Lee[1], L.M. Franke[4,5], M. Alam[1], M. Tashli[1], J. Atulasimha[1] and *R.L. Hadimani*[1,6] *1. Mechanical and Nuclear Engineering, Virginia Commonwealth University, Richmond, VA, United States; 2. Maggie L Walker Governor's School, Richmond, VA, United States; 3. Biomedical Engineering, Virginia Commonwealth University, Richmond, VA, United States; 4. Physical Medicine and Rehabilitation, Virginia Commonwealth University, Richmond, VA, United States; 5. Hunter Holmes McGuire Veterans Affairs Medical Center, Richmond, VA, United States; 6. Psychiatry, Harvard University, Boston, MA, United States*

Transcranial magnetic stimulation (TMS) is a non-invasive method for treating neurological and psychiatric disorders [1]. It is being tested as an experimental treatment for patients with traumatic brain injuries (TBI) [2]. Due to the complex, heterogeneous composition of the brain, it is difficult to determine if targeted brain regions receive the correct amount of the electric field induced by the TMS coil. The electric field distribution can be calculated by running a time-consuming simulation of TMS on a magnetic resonance imaging (MRI) derived patient head model. Another method using machine learning can predict the induced electric field in real-time. Our prior work [3] used a Deep Convolutional Neural Network (DCNN) to predict the induced electric field in healthy patients. This study applies the same DCNN model to TBI patients and investigates how model depth and color space of the induced electric field image affect model performance. Segmented head models were created using the SimNIBS pipeline from patient MRI. Sim4Life, a finite element analysis software, was used to run simulations of TMS on head models to generate the induced electric field. The anatomical and electric field slices for each head model at the coronal slice with the highest electric field value were captured and used to train the DCNNs. 9 DCNNs were created using combinations of 3, 4, or 5 encoders and decoders in tandem with the color spaces RGB, LAB, and YCbCr. As model depth increased, training and testing peak signal-to-noise ratios (PNSR) increased and spikes in validation loss decreased. Also, over the course of training for each model depth models with LAB and YCbCr were able to achieve lower testing loss than RGB. Additionally, the depth 5 YCbCr model had the highest training and testing PSNRs. Compared to the model in our prior work [3], the depth 5 models had a higher testing PSNR and, except for RGB, higher training PSNRs. Also, alternative color space DCNNs at depth 5, while losing some information through color space conversions, better represented color information in the pixels than RGB, resulting in higher PSNRs.

[1] B. R. Mishra, S. Sarkar, and S. K. Praharaj, Annals of Indian Academy of Neurology, Vol 14(4), p. 245-251 (2011) [2] L. M. Franke, G. T. Gitchel, and R. A. Perera, Taylor and Francis Online, Vol. 36(5), p. 683-692 (2022) [3] M. Tashli, M. S. Alam, and J. Gong, bioRxiv (2022)

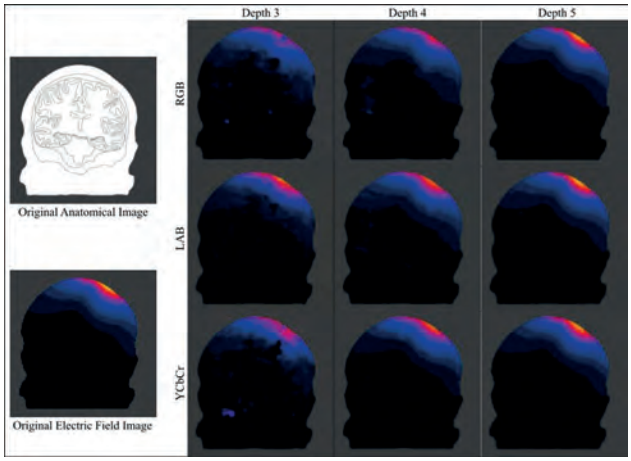

Fig 1. Induced electric field images predicted by each model

Training PSNRs				Testing PSNRs			
	Color Space				Color Space		
Depth	RGB	LAB	YCbCr	Depth	RGB	LAB	YCbCr
3	25.84	26.86	25.79	3	24.51	25.26	24.59
4	31.27	29.69	29.53	4	28.07	27.82	27.72
5	32.77	33.48	34.77	5	28.9	29.05	29.08

Fig 2. Training and Testing PSNRs for each model

FR-06. Quantification of Cellular States through Magnetic Labeling Single-Cell Analysis Techniques. *C. Tsou*[1], T. Ger[1], J. Huang[1] and H.A. Li[2] *1. Department of Biomedical Engineering, Chung Yuan Christian University, Taoyuan, Taiwan; 2. ARVIN Bio-Medical Devices Co., Hsinchu, Taiwan*

Magnetic nanoparticles (MNPs), which possess excellent biocompatibility and stable physicochemical properties, are widely applied in the field of biomedical engineering. Regardless of whether magnetic nanoparticles are used as drugs or reagents, cell testing is essential. However, the use of magnetic materials often leads to cell aggregation, making it difficult to perform single-cell quantification and verification. In this research, magnetic-labeled cells were used for single-cell analysis to enable cell quantification. Magnetic labeling cell was achieved by the process of endocytosis. Through the combination of a magnetic field control system and a microscopic image capture system, cells are manipulated using magnetic fields. Cellular images were be subjected to object detection and image recognition using deep learning techniques, followed by further calculation of cell magnetic content. It was measured the magnetic content of each individual cell wthin the field of view of the microscopic imaging capture system. The obtained cell magnetic content is finally validated against the standard instrument ICP-MS. The results demonstrate that the method used in this research aligns with the trends observed in ICP-MS results. In the future, this technology can be utilized for cellular analysis in various fields, including drug development, drug screening, cell diagnostics, and therapy. It enables the analysis of individual cells without need to disrupt cell samples, thereby assisting in advancement and detection of cell research related to magnetic materials.

[1] J. Kolosnjaj-Tabi, C. Wilhelm, and F. Gazeau et al., Journal of nanobiotechnology, vol. 11, no. 1, pp. 1-19 (2013) [2] O. L. F. d. Carvalho et al., Remote Sensing, vol. 13, no. 1, p. 39 (2021)

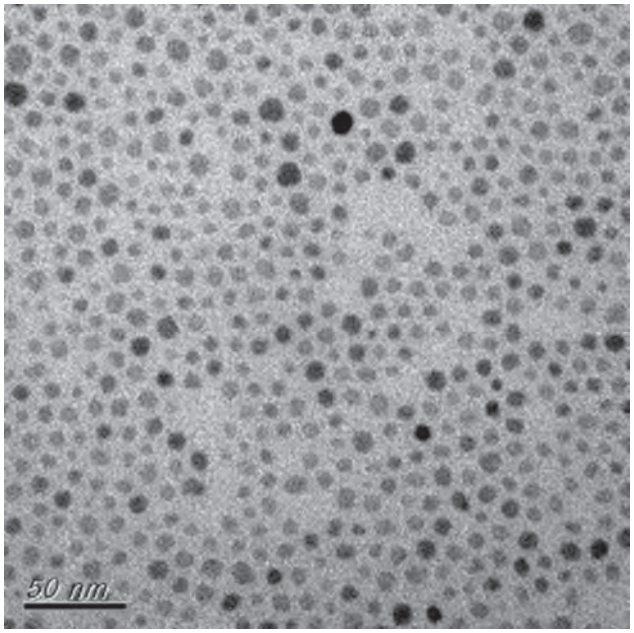

Fig. SEM of magnetic nanoparticles.

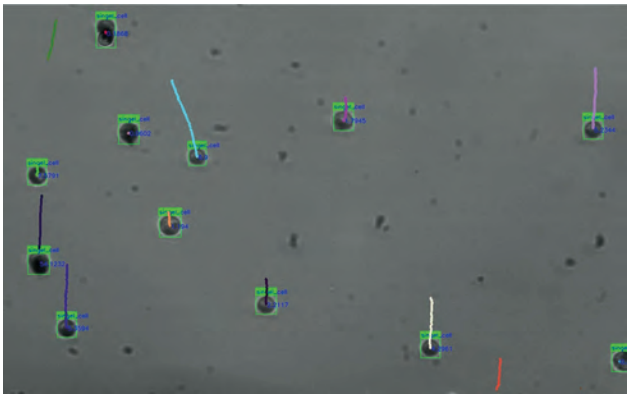

Fig 2. Magnetic labeling single-cell analysis results.

FR-07. Skin Permeability and Magnetic Susceptibility Analysis of Hyaluronic Acid-Based Magnetized Microneedles Containing Iron Oxide Nanoparticles. *J. Choi*[1], M. Hasan[1,2] and S. Lee[1] *1. Department of Digital Healthcare Engineering, Sangji University, Wonju, The Republic of Korea; 2. Department of Biochemistry and Molecular Biology, Bangabandhu Sheikh Mujibur Rahman Sci. and Tech. University, Gopalganj, Bangladesh*

Microneedles comprise arrays of micron-sized needles that offer a pain-free method of delivering actives across the skin[1]. Iron oxide magnetic nanoparticles (MNPs) have been used as the subject of many studies on drug delivery systems due to their excellent magnetic properties and biocompatibility in response to external magnetic fields[2]. In this study, hyaluronic acid-based magnetized microneedles (HA-MMNs) containing MNPs were prepared with bio-sodium hyaluronic acid as matrix materials[3]. Mechanical properties were confirmed by measuring the permeability to an artificial polymer membrane and porcine back skin (Fig. 1). The magnetic properties of the microneedles were monitored using the hysteresis analysis. The manufactured HA-MMNs, having MNPs of 1 mg/ml, and HA-MMNs patch-treated porcine back skin were separately analyzed for their magnetization properties. The change in magnetic susceptibility was confirmed according to the ratio containing MNPs. It was confirmed that the hysteresis curve of the MNPs did not change the magnetic characteristics even after the HA-MMNs were manufactured, and the M-H curves were shown the same magnetic properties having a coercivity of H_c = 60 Oe and a susceptibility of $c = 4\times10^{-6}$ emu/gOe. We confirmed the magnetization properties were retained after MMNs were fabricated and stamped on the porcine back skin (Fig. 2). In conclusion, it was found that HA-MMNs are stable materials in vivo because their magnetic properties are not deformed during the manufacturing process, and their superparamagnetic properties are maintained. It will also be used as valuable data for determining the mixing ratio of iron oxide and hyaluronic acid in evaluating the efficacy of HA-MMNs and developing the formulation process of products. Therefore, HA-MMNs can be applied in vivo, contributing to simultaneous molecular imaging and therapy.

[1] J. Pan, W. Ruan, and M. Qin, *Scientific reports*, 8, 1117 (2018) [2] J. F. Liu, B. Jang, and D. Issadore, *Wiley interdisciplinary reviews. Nanomedicine and nanobiotechnology*, 11, e1571 (2019) [3] J. A. Kim, S. C. Park, and S.-J. Lee, *Cellulose*, 29, 9881-9897 (2022)

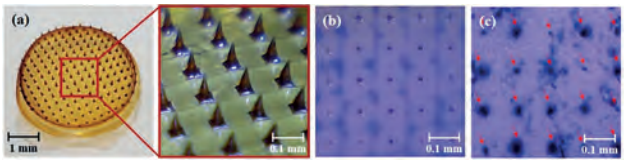

Fig 1. (a) Image of MMNs containing MNPs and its magnified view. Optical microscope images of (b) polymer membrane permeability of MMNs and (c) porcine back skin permeability of MMNs in stained with trypan blue.

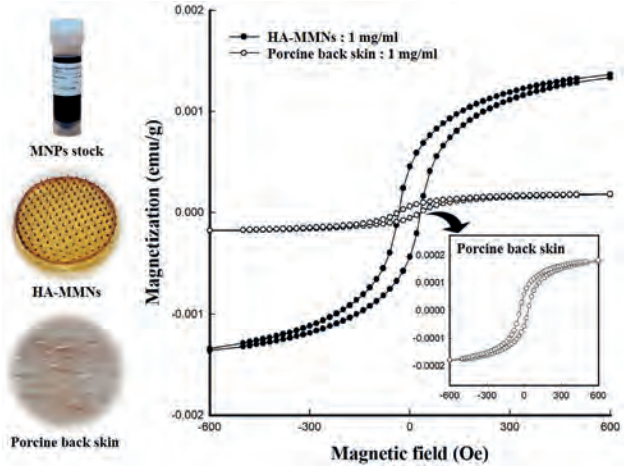

Fig 2. The M-H curves of MNPs in the HA-MMNs patch and in porcine back skin with HA-MNPs.

FR-08. Tuning the structural and magnetic properties of iron oxide nanoparticles. *X. Sun*[1], J. Zhang[1], O. Petracic[2] and A. Tayal[1] *1. Deutsches Elektronen-Synchrotron DESY, Hamburg, Germany; 2. Jülich Centre for Neutron Science JCNS and Peter Grünberg Institut PGI, JARA-FIT, Forschungszentrum Jülich, Jülich, Germany*

Magnetic iron oxide nanoparticles (NPs) have gained significant attention in biomedical applications such as targeted drug delivery and hyperthermia therapy. This is due to their magnetic properties and non-toxic nature. Combining magnetic iron oxide NPs with plasmonic gold NPs, novel multifunctional nanomaterials can be produced. Depending on their oxidation states, iron may form various crystal structures, thus showing different magnetic properties. However, their magnetic properties in nanoscale may differ from the bulk behavior due to the finite size effect. Moreover, the synthesis of single-phase oxide NPs is challenging, often resulting in the presence of an oxidized layer at the surface. We observe a shift in the center of the hysteresis loops of iron oxide NPs. This is due to the exchange interaction between the magnetite core and a shell with disordered/oxidized surface spins. By comparing hysteresis loops cooled at different magnetic fields, a hardening effect is observed, i.e. the squareness and hardness of hysteresis loops is significantly enhanced with increasing magnetic cooling

field. This indicates that an anisotropy axis is induced due to the exchange bias effect. To synthesize nanomaterials with tunable magnetic properties, it is important to understand how the crystallographic structure or the phase composition inside the NPs influences their magnetic properties. In this work, we performed systematic investigations on single iron oxide NPs as well as Au@FeO_x multifunctional NPs with various sizes and shapes. The crystallographic structure and the magnetic properties of the samples were tuned by oxidation or reduction via different annealing procedures. From the X-ray absorptions spectroscopy results, one obtained the ratio of different iron oxide phases existing inside the particles. Anomalous small-angle X-ray scattering provides us with information about the size and thickness of core/shell structures. Combining these X-ray techniques with magnetometry, one can better understand the relationship between structural and magnetic properties. Furthermore, we studied the influence of a thin Au shell or a small Au NP attaching to the surface of the iron oxide NPs on their magnetic properties.

FR-09. Feasibility Study on On-board Magnetoencephalography with Optically Pumped Magnetometers. *X. Cao*[1], M. Fushimi[1], S. Chikaki[1] and M. Sekino[1] *1. Department of Electrical Engineering and Information Systems, The University of Tokyo, Bunkyo-ku, Japan*

With advancements in measurement technology, there is a growing potential to transcend the limitations of closed laboratory environments and study brain function in real-world settings [1], [2]. On-board measurement, as a potential application scenario for assessing brain function in the real world, has attracted significant attention worldwide [3], [4]. This study explores the theoretical feasibility of utilizing optically pumped magnetometers (OPMs) for on-board magnetoencephalography (MEG) measurements. Simulations were conducted to generate steady-state visually evoked response (SSVER) signals incorporating vehicle noise, and a noise reduction strategy specifically designed for on-board applications was proposed. Upon engine activation, the magnetic field vibration of a conventional gasoline vehicle measured in an urban environment was found to be approximately 7 times greater in the vertical direction compared to the horizontal direction, as shown in Figure 1. The movement of the internal combustion engine's pistons and the engine fan were identified as the primary contributors to magnetic field noise in the vehicle [5]. The maximum signal-to-noise ratio of SSVER in an automotive environment was simulated to be -110 dB, as shown in Figure 2. A 350 mm side-length, 20-turn active compensation coil can achieve an attenuation rate of approximately 28 dB at the target frequency of 24 Hz for measurements inside the vehicle cabin. Hence, increasing the number of coil turns would result in a higher attenuation rate. Further attenuation of noise to the level inside a magnetic shielding room requires approximately 80 dB.

[1] E. Boto, N. Holmes, J. Leggett, et al., Nature., Vol. 555(7698), p. 657-661 (2018) [2] G. Roberts, N. Holmes, N. Alexander, et al., NeuroImage., Vol. 199, p. 408-417 (2019) [3] A. Fort, R. Martin, A. Jacquet-Andrieu, et al., Brain Research., Vol. 1363, p. 117–127 (2010) [4] K. Sakihara, M. Hirata, K. Ebe, et al., Frontiers in Human Neuroscience., Vol. 8, p. 975 (2014) [5] A. Vassilev, A. Ferber, C. Wehrmann, et al., IEEE Transactions on Electromagnetic Compatibility., Vol. 57(1), p. 35–43 (2015)

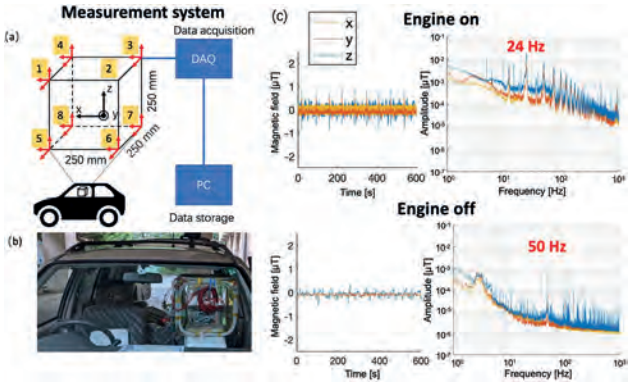

Figure 1. (a) Schematic diagram and (b) photograph of the measurement system. 24 magnetoresistive sensors are positioned at the 8 corners of a 250 mm side-length frame to measure the AC magnetic field in 3 vertical directions inside the vehicle. (c) AC magnetic field inside the vehicle and its FFT plot. The most prominent frequency components are highlighted in red text.

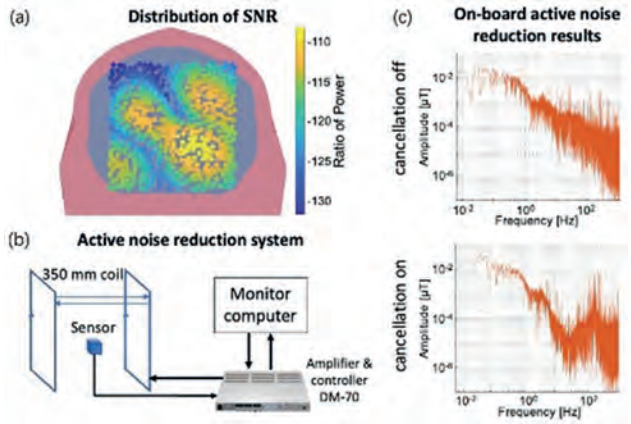

Figure 2. (a) The signal-to-noise ratio of each virtual sensor in the simulation. (b)The on-board active noise reduction system and (c) the reduction results. Note the attenuation in the signal's FFT at the target frequency of 24 Hz.

FR-10. A study on the scalability of the self-assembled magnetic millirobot for minimally invasive medicine. *Y. Lee*[1], S. Seo[1], J. Lee[1] and S. Jeon[1] *1. Mechanical and Automotive Engineering, Kongju National University, Cheonan, The Republic of Korea*

Small-scale magnetic robots that can access the internal organs of the human body in a minimally invasive manner, such as through medical syringes or natural openings, have been extensively investigated for various biomedical applications [1-4]. In previous work, we proposed a self-assembled magnetic millirobot (SAMM) capable of multimodal locomotion actuated by external magnetic fields [4]. The SAMM consists of serially connected multiple magnetic modules, and it can self-assemble into a circular chain from a linear chain due to the magnetic interactions among the modules. Thus, the SAMM can be inserted into a target area via a minimally invasive medical syringe. The self-assembled SAMM inside the area can then perform specific tasks, including cargo delivery and material removal (Fig. 1), actuated by external magnetic fields. After that, it can also be retrieved outside by the medical syringe. Generally, the desirable size and function of the SAMM may vary with respect to different target areas, such as the human body's ocular, vascular, and gastrointestinal regions. In this study, we proposed a design methodology that can yield proper SAMM geometric and magnetic properties for various applications. We investigated the geometric and magnetic scalability of the SAMM, taking into account various design variables, such as the allowable size of the invasion, the number of the SAMM's modules,

the SAMM's self-assembling strength, the strength of the magnets used for the modules, the size of the cargo the SAMM will deliver, the range of the magnetic field that an external electromagnetic coil system can generate, etc. As a result, we established various dimensionless variables of the SAMM that can be used to determine the SAMM's geometric and magnetic properties straightforwardly, considering different target applications. We also constructed prototype SAMMs with different geometric and magnetic design parameters and demonstrated various controlled motions of the SAMM in a mockup of a gastrointestinal organ (Fig. 2).

[1] M. Sitti, H. Ceylan, W. Hu, J. Giltinan, M. Turan, S. Yim, and E. Diller, "Biomedical Applications of Untethered Mobile Milli/Microrobots," *Proc. IEEE*, vol. 103, no. 2, pp. 205-224, 2015. [2] S. Yim and M. Sitti, "Soft-Cubes: Stretchable and self-assembling three-dimensional soft modular matter," *Int. J. Rob. Res.*, vol. 33, no. 8, pp. 1083–1097, 2014. [3] H. Lee and S. Jeon, "An intravascular helical magnetic millirobot with a gripper mechanism performing object delivery and collecting motions actuated by precession rotating magnetic fields," *AIP Adv.*, vol. 11, pp. 025236, 2021. [4] S. Lee and S. Jeon, "A Study on the Self-Assembly and Disassembly Abilities of a Multi-Modular Magnetic Millirobot," *J. Instit. Cont., Rob. Sys.*," vol. 25, no. 3, pp. 235-240, 2019.

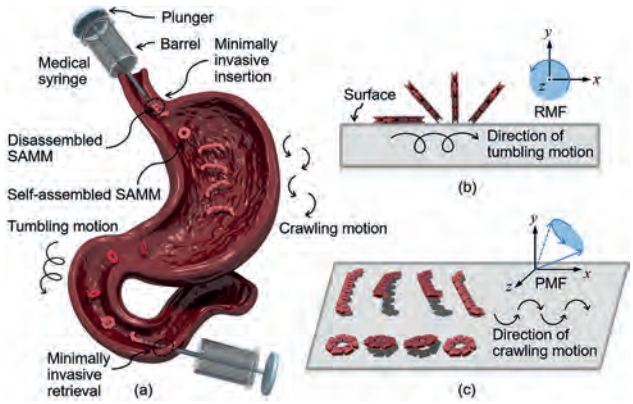

Fig. 1. Schematic view of (a) the SAMM in a gastrointestinal organ. (b) Tumbling and (c) crawling motions of the SAMM.

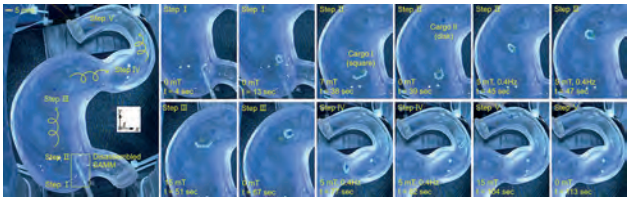

Fig. 2. Multi-modal locomotion of the prototype SAMM in a gastrointestinal mockup.

FR-11. Cancer cell death induced by magneto-mechanical actuation of Fe-Cr-Nb-B magnetic particles loaded with chemotherapeutic drugs, carried by Stem cells to the cancer cell area. H. Chiriac[1], C. Stavila[1,2], A.E. Minuti[1,2], D. Herea[1] and *N. Lupu*[1] *1. National Institute of Research and Development for Technical Physics, Iasi, Romania; 2. Faculty of Physics, Alexandru Ioan Cuza University, Iasi, Romania*

We have recently presented the effect of Fe-Cr-Nb-B magnetic nanoparticles (MPs), prepared by wet milling superferromagnetic precursor glassy ribbons, on cancer treatment by magneto-mechanical actuation (MMA) [1]. The shape anisotropy and high saturation magnetization of MNPs generate an improved torque in a rotating magnetic field, producing important damages on the cellular viability of cancer cells through MMA. The purpose of this work is to combine the magneto-mechanical effect with the effect of adsorbed and controlled release of anticancer drugs through magneto-mechanical actuation. We studied the possibility of transporting the magnetic particles loaded with anticancer drugs in the area of cancer cells with the help of adipose derived stem cells (ADSC) and their release through MMA. Using spectrophotometric methods, we found that $Fe_{68.2}Cr_{11.5}Nb_{0.3}B_{20}$ MPs can be loaded with doxorubicin (DOX) or mitoxantrone (MTX) (up to 6.6% for DOX and 5.7% for MTX). MPs are releasing 20–24% from the loaded chemotherapeutic drug in controlled time, enough to destroy the cancer cells such as human osteosarcoma (HOS) cells. The particles, either loaded or non-loaded, are added onto the culture cells, co-incubated for 24 h and magneto-mechanically actuated. Fig. 1 shows the viability of HOS cells after magneto-mechanical actuation, for particles without drugs and for particles covered with DOX / MTX. The results were obtained by performing MTT tests. The presence of drugs on the surface of the particles further reduces the viability compared to the magneto-mechanical effect only. The MMA of MPs in contact with the cancer cells damages the cells membrane through the rotation of MPs located on it, as shown by HR-SEM, and destroys the cells from inside by actuation of internalized MPs, a process that can induce cellular apoptosis, an effect observed through caspase assays. *Financial support from UEFISCDI Contract # PCE20/2021 (PN-III-P4-ID-PCE-2020-2381) and NUCLEU Programme Contract # 18N/01.01.2023 (PN 23 11 01 01) is highly acknowledged.*

[1] H. Chiriac, E. Radu, M. Tibu, G. Stoian, G. Ababei, L. Labusca, D.D. Herea, N. Lupu, Sci. Rep. 8(1) (2018) 11538.

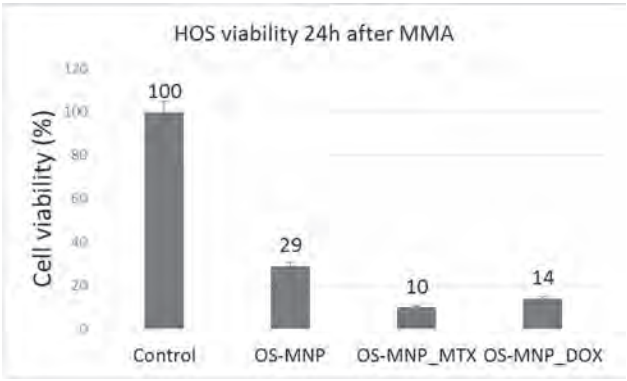

Fig. 1. Human osteosarcoma cell viability 24h after magneto-mechanical actuation of MPs with or without chemotherapeutic agents adsorbed on their surface.

FR-12. Multidimensional Imaging of Phantoms with a Single-Sided Magnetic Particle Imaging Scanner. *C. McDonough*[1], J. Mattern[1], J. Chrisekos[1] and A. Tonyushkin[1] *1. Oakland University, Rochester, MI, United States*

Magnetic Particle Imaging (MPI) is an emerging medical imaging modality with great potential for diagnostics and biopsy of cancer [1,2]. Compared to conventional closed bore scanners, our single-sided device offers an open imaging volume, making it suitable for imaging larger subjects such as humans. Previously, we showed 1D [3] and basic 2D imaging [4] in a single plane with a manual rotation of rod phantoms. In this work we demonstrate 2D imaging of various phantoms in two orthogonal planes using two imaging methods: filtered backprojection (FBP) in the xy plane and the projection imaging in the xz plane. This new functionality of our scanner comes from the implementation of a custom built electronic rotation and height adjustment table (Fig. 1). For 2D projection imaging in the xz plane we utilized phantoms consisting of glass rods with a length of 30 mm and a diameter of 1 mm filled with SynomagD SPIO. The rods are orientated parallel with the FFL, and are inserted into different positions of a 3D printed holder in the xz plane (see Fig. 2(a,b)). The magnetic field gradient of our scanner is 0.84 T/m at the center of the FOV. For xy plane imaging we used an anatomical 3D-printed mouse kidney phantom (Fig. 2(d)), filled with SynomagD SPIO. By dynamically scanning the FFL along arc trajectories across the sample, we achieved image encoding. The image (Fig. 2(c)) is reconstructed using projections acquired at 21 angles by FBP image reconstruction [5] with a deconvolution from the simulated point spread function. In this study we

presented the improved FBP imaging of an anatomical 3D-printed mouse phantom and introduced a novel feature of the FFL scanner of 2D projection imaging by imaging 2D rod phantoms aligned with the FFL. Our results demonstrate spatial resolutions of 3 mm and 6 mm in the xz and xy planes, respectively. Using the demonstrated imaging methods will allow for multislice imaging of subjects in this open geometry, which offers compactness and robustness compared standard MPI scanners.

[1] B. Gleich, and J. Weizenecker, Nature, vol. 435, p.1214-1217 (2005). [2] T. F. Sattel, T. Knopp, and S. Biederer, J. of Phys. D: Applied Physics, vol. 42, p.022001 (2009). [3] C. McDonough, D. Newey, and A. Tonyushkin, IEEE Trans. on Magnetics, vol. 58(8), p.6501105 (2022). [4] C. McDonough, A. Tonyushkin, Int J Magn Part Imaging. vol. 9(1): Suppl 1, p.2303028 (2023). [5] C. Chinchilla, C. McDonough, and A. Tonyushkin, Int J Magn Part Imaging. vol. 7, p.2104001 (2021).

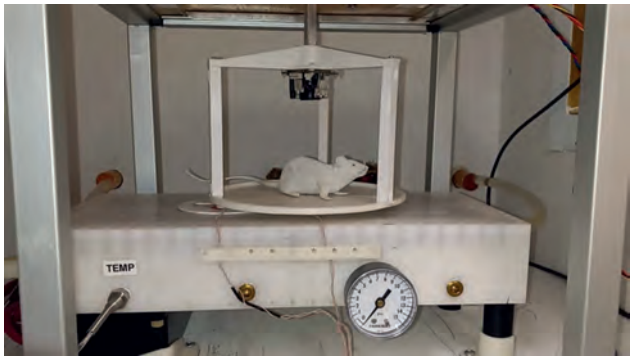

Single-sided field free line MPI scanner with rotational table assembly

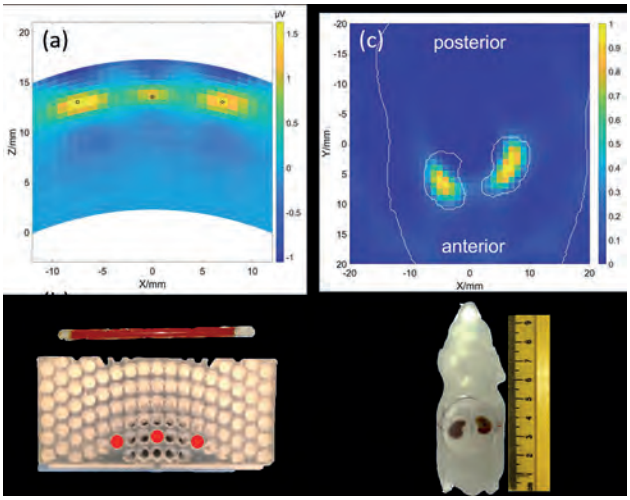

Reconstructed images of phantoms in two orthogonal planes: (a) xz plane and (c) xy plane with the respective phantoms: rods (b) and mouse (d).

FR-13. Systematic Analysis of Parameters Affecting Colorization Performance for Magnetic Particle Spectroscopy Applications.

V.K. Chugh[1], S. Liang[2], V.D. Krishna[3], P. Yari[4], M.C. Cheeran[3], K. Wu[4] and J. Wang[1,2] *1. Electrical and Computer Engineering, University of Minnesota, Minneapolis, MN, United States; 2. Chemical Engineering and Materials Science, University of Minnesota, Minneapolis, MN, United States; 3. Veterinary Population Medicine, University of Minnesota, St. Paul, MN, United States; 4. Electrical and Computer Engineering, Texas Tech University, Lubbock, TX, United States*

Colorization of magnetic nanoparticles (MNPs) has been of key interest for multiplexed biosensing and targeting applications in magnetic particle spectroscopy (MPS)[1–5]. Herein, we present a systematic analysis of different parameters in play affecting the colorization performance for such practical applications. Three commercially available multicore MNPs DSPIO, SPG0050, and SC0102 were used for the colorization experiments utilizing a single-frequency MPS system. Firstly, experiments were conducted to investigate the dependence of colorization error on the excitation frequency and field amplitude as presented in Fig. 1. It was observed that MPS operation at larger excitation frequency/ field amplitude resulted in better colorization predictions which could be attributed to SNR improvement. Thereafter, experiments were also carried out investigating the effects of utilizing single harmonic information at varying excitation conditions (3rd harmonic information recorded for varying excitation frequency or field amplitude) vs using multiple harmonic information obtained for a single excitation condition (3rd and 5th harmonic information recorded for a fixed excitation frequency of 5 kHz and field amplitude of 200 Oe) for the colorization application. It was found that best colorization predictions were achieved by utilizing the 3rd harmonic information alone collected for varying excitation frequencies as noted in Fig. 2. These observations provide valuable insights for the future design and applications of magnetic colorization in biosensing applications.

[1] V.K. Chugh, S. Liang, P. Yari, K. Wu, and J.-P. Wang, "A method for multiplexed and volumetric-based magnetic particle spectroscopy bioassay: mathematical study," J. Phys. Appl. Phys. 56(31), 315001 (2023). [2] T. Viereck, S. Draack, M. Schilling, and F. Ludwig, "Multi-spectral Magnetic Particle Spectroscopy for the investigation of particle mixtures," J. Magn. Magn. Mater. 475, 647–651 (2019). [3] A.V. Orlov, S.L. Znoyko, V.R. Cherkasov, M.P. Nikitin, and P.I. Nikitin, "Multiplex Biosensing Based on Highly Sensitive Magnetic Nanolabel Quantification: Rapid Detection of Botulinum Neurotoxins A, B, and E in Liquids," Anal. Chem. 88(21), 10419–10426 (2016). [4] S. Achtsnicht, A.M. Pourshahidi, A. Offenhäusser, and H.-J. Krause, "Multiplex Detection of Different Magnetic Beads Using Frequency Scanning in Magnetic Frequency Mixing Technique," Sensors 19(11), 2599 (2019). [5] A.M. Rauwerdink, A.J. Giustini, and J.B. Weaver, "Simultaneous quantification of multiple magnetic nanoparticles," Nanotechnology 21(45), 455101 (2010).

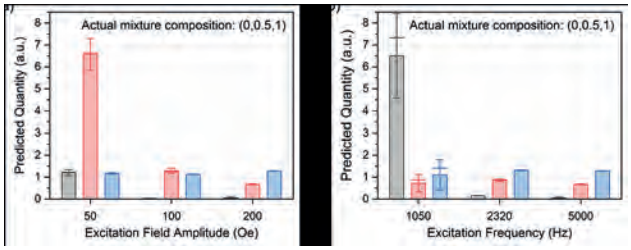

Dependence of colorization prediction on the excitation frequency and amplitude have been presented in (a) and (b) respectively for a mixture of 3 MNPs. Use of a higher excitation frequency or field amplitude results in better prediction.

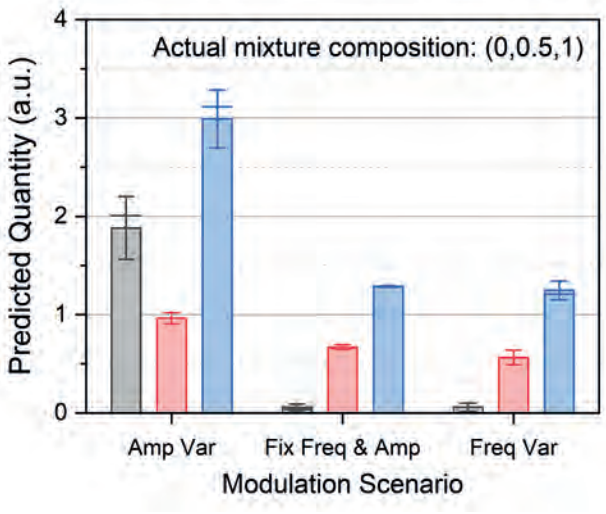

Colorization prediction utilizing three scenarios (1) using 3rd harmonic information at 50 Oe, 100 Oe, and 200 Oe for a fixed excitation frequency of 5kHz; (2) utilizing 3rd and 5th harmonic components for the excitation frequency of 5kHz and field amplitude of 200 Oe; (3) using 3rd harmonic components at varying excitation frequencies of 1.05 kHz, 2.32 kHz, and 5 kHz, whilst maintaining a constant field amplitude of 200 Oe.

FR-14. Characteristics of Spatial Pulse Wave Velocity and Peripheral Blood Flow Velocity Measured Using Magnetoplethysmography and Photoplethysmography Devices. *S. Lee*[1], R. Choi[1], W. Kim[1], M. Shin[1], J. Choi[1], M. Hasan[1,2] and B. Jung[3] *1. Department of Digital Healthcare Engineering, Sangji University, Wonju, The Republic of Korea; 2. Department of Biochemistry and Molecular Biology, Bangabandhu Sk. Mujibur Rahman Sci. and Tech. University, Gopalganj, Bangladesh; 3. School of Biomedical Engineering, Yonsei University, Wonju, The Republic of Korea*

The Hall element and optical sensor, which can detect the magnetic field change caused by the minute fluctuations of the permanent magnet according to the periodic movement of the radial artery and the light absorption and reflection intensity according to the change in wrist blood flow, respectively, are used as key elements in digital healthcare devices. The pulse waves of the radial artery in the inside of the wrist were measured and analyzed using MPG (magnetoplethysmography), a clip-type pulsimeter[1]. A permanent magnet is placed at the center of the radial artery, and the role of the Hall element is to convert the magnetic field strength, which varies with the low and high positions of the pulsation, into a voltage signal which has a sensitivity of 10 mV/Oe[2]. The SpO_2 pulse wave, which is the change in blood flow obtained by PPG (photoplethysmography), was measured on the dorsal side of the wrist at the same time with MPG (Fig. 1a). SPWV (spatial pulse wave velocity) can be defined as L_H(hand length)/$\Delta\tau$. $\Delta\tau$ represents the time difference between the MPG pulse wave peak and the PPG pulse wave peak. PBFV(peripheral blood flow velocity) is several tens of cm/s as $2L_H$ devided by $2\Delta T$ which is the time difference between the first peak of MPG waveform and the third peak of PPG waveform (Fig. 1b). Table 1 shows the comparison of the measured SPWV and PBFV for 4 male subjects in their 20s with an average values of SPWV=2.5 m/s and PBFV=0.28 m/s. In the future, a smart band-type MPG equipped with a PPG is used as a data-based digital healthcare smart PBFV medical device[3]. Furthermore, it is possible to develop an AI (artificial intelligence) algorithm for diagnosing and predicting peripheral vascular disease to be applied to personal health management.

[1] S. S. Lee, S. D. Choi and M. C. Ahn, Pulsimeter Sensor Using Hall Device, Patent US 8,632,471 B2 (2014) [2] I. H. Son, K. H. Kim and J. G. Choi, IEEE Transactions on Magnetics., Vol. 47, p.3063 (2011) [3] R. G. Choi, W. T. Kim and S. S. Lee, Journal of the Korean Magneitcs Society., Vol. 33, p.69 (2023)

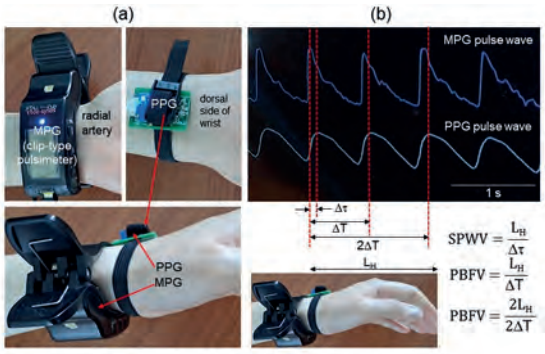

Fig. 1

(a) MPG as clip-type pulsimeter worn on the wrist according to the pulsation position of the radial artery and PPG on the dorsal side of the wrist. (b) Radial artery and SpO_2 pulse waveforms simultaneously measured for 10 s by MPG and PPG with equations of SPWV and PBFV.

Subject (male, 20s)				SPWV	PBFV
No.	SBP	DBP**	BMI***		
#1	120 mmHg	83 mmHg	19.5 kg/m²	3.2 m/s	0.38 m/s
#2	123 mmHg	82 mmHg	20.3 kg/m²	2.4 m/s	0.27 m/s
#3	118 mmHg	75 mmHg	22.4 kg/m²	2.3 m/s	0.25 m/s
#4	121 mmHg	76 mmHg	23.5 kg/m²	2.1 m/s	0.22 m/s
Average				2.5 m/s	0.28 m/s

*systolic blood pressure, **diastolic blood pressure, ***body mass index

Table 1

SPWV and PBFV values measured by MPG and PPG for four subjects (male, 20s)

FR-15. Electrically Conductive and Anatomically Accurate Physical Rat Brain Phantoms for Experimental Validation of Transcranial Magnetic Stimulation. *W.H. Lohr*[1] and R.L. Hadimani[2,3] *1. Biomedical Engineering, Virginia Commonwealth University, Richmond, VA, United States; 2. Mechanical and Nuclear Engineering, Virginia Commonwealth University, Richmond, VA, United States; 3. Martino's Center for Biomedical Engineering, Harvard University, Boston, MA, United States*

Transcranial magnetic stimulation (TMS) has been found effective in the treatment of neurological and psychiatric conditions and is approved by the FDA to treat depression, OCD, and smoking cessation [1]. Although this technology is by and large noninvasive, trials on live subjects are not always appropriate, which lead to the development of human phantoms that mimic the electrical properties and anatomical features of the human brain [2]. These phantoms are individualized by computationally processing MRI and utilizing 3d printing technology. Yet there are no reported animal phantoms of similar design. An individualized brain phantom for rats is needed to accelerate the study of neuromodulation techniques, especially for making repetitive measurement of induced electric fields and voltages in the same brain regions when stimulated by a time-varying magnetic field. The main objective of this paper is to develop an individualized rat brain model that mimics the anatomical features and electrical properties of a rat for TMS research. We initially obtained MRIs from public databases to create anatomically accurate models. The images were segmented with SPM using the SIGMA brain atlases. Each section of the rat's head; the skin, the skull, the gray matter, and the white matter; were imported into SolidWorks to create 3D-printed molds and parts. The gray and white matter are made into hollow molds by creating a part in SolidWorks that is the inverse of the brain

volume. A composite material of carbon nanotubes and polydimethylsiloxane is used to mimic the electrical properties of the brain. This composite is mixed, injected into the molds, and left to cure in a vacuum chamber to form the brain. Currently the anatomical accuracy, conductivity and induced brain voltage due to the magnetic field have been characterized. The induced voltage in the brain phantom is assessed using a Magstim coil with a maximum output of 5000 amps at a frequency of 2500 Hz. An oscilloscope is connected through embedded electrodes in the phantom and the induced voltage is measured at different distances from the TMS coil and different stimulation intensities.

REFERENCES [1] E. M. Wassermann and S. H. Lisanby, "Therapeutic application of repetitive transcranial magnetic stimulation: a review," Clin. Neurophysiol. Off. J. Int. Fed. Clin. Neurophysiol., vol. 112, no. 8, pp. 1367–1377, Aug. 2001, doi: 10.1016/s1388-2457(01)00585-5. [2] H. Magsood, C. H. A. Serrate, A. A. El-Gendy, and M. L. R. Hadimani, "Anatomically accurate brain phantoms and methods for making and using the same," US20190057623A1, Feb. 21, 2019 Accessed: Oct. 28, 2022. [Online]. Available: https://patents.google.com/patent/US20190057623A1/e n

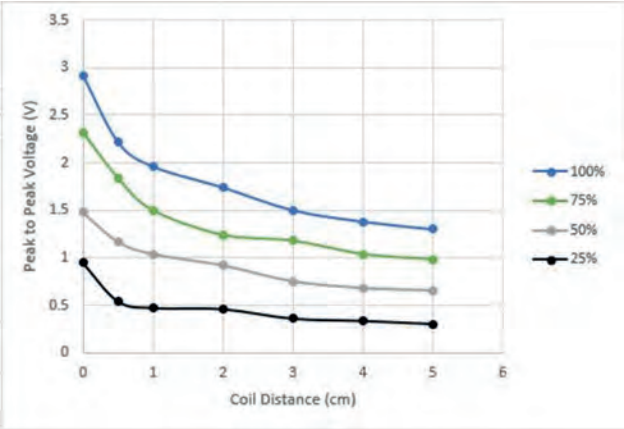

voltages at different distances and intensities

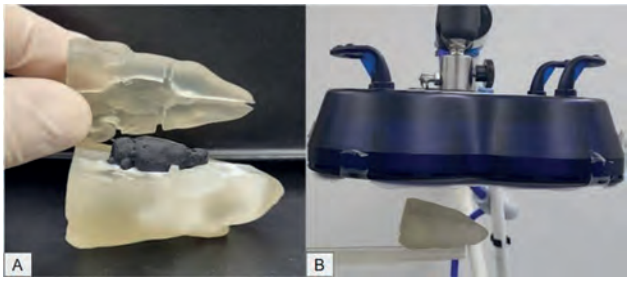

Rat phantom and stimulator

FR-16. On Trajectory Control of Magnetized Spherical Solids Driven by Magnetic Force Through Soft Medium. *Y. Malkova*[2,1], A. Guez[1] and G. Friedman[1] *1. Electrical and Computer Engineering, Drexel University, Philadelphia, PA, United States; 2. Electrical and Computer Engineering, Exponent, New York, NY, United States*

The application of untethered millimeter-sized devices, referred to as bots, for manipulation inside the human body holds immense potential in the field of medicine[1]. Many future medical procedures involve operating within soft tissues, where the behavior of bots differs significantly from their motion in fluids[2], where magnetically driven transport of untethered devices has been extensively explored[3]. By contrast, trajectory control of small untethered solid bots in soft media has not been reported in the literature. Soft media environment presents new challenges associated with movement history dependence and non-linear effects absent in most fluids. This work formulates, simulates, and experimentally tests a method of control and manipulation of millimeter-sized magnetized solid spherical bots in soft media environments that mimic soft tissues. Spherical bot shapes offer the flexibility of permitting abrupt changes in motion direction. The primary challenge, however, lies in the nonlinear and history-dependent soft medium reaction forces resulting from irreversible modifications to the medium. This work discusses magnetically actuated motion control method for spherical bots in soft media along elementary trajectories consisting of circular and straight segments, which can be combined to generate more complex paths. The proposed control approach is based on a phenomenological model that captures the response forces exhibited by soft media[2] using control method illustrated roughly in Fig. 1. Numerical implementation of the suggested trajectory control for circular paths demonstrates excellent agreement with experimental results as evidenced by the examples in Fig. 2, indicating achievable accuracy at the scale of the bot's radius for trajectories with radii of curvature on the order of 10 times the bot's radius.

[1] B. J. Nelson, I. K. Kaliakatsos, and J. J. Abbott, *Annu. Rev. Biomed. Eng.*, vol. 12, no. 1, p. 55 (2010) [2] Y. Malkova, S. Ran, G. Friedman, J. *Mech. Behav. Biomed. Mater.*, vol. 126, p.105040 (2022) [3] B. J. Nelson, S. Gervasoni, P. W. Y. Chiu, L. Zhang, and A. Zemmar, Proc. *IEEE*, p. 1 (2022)

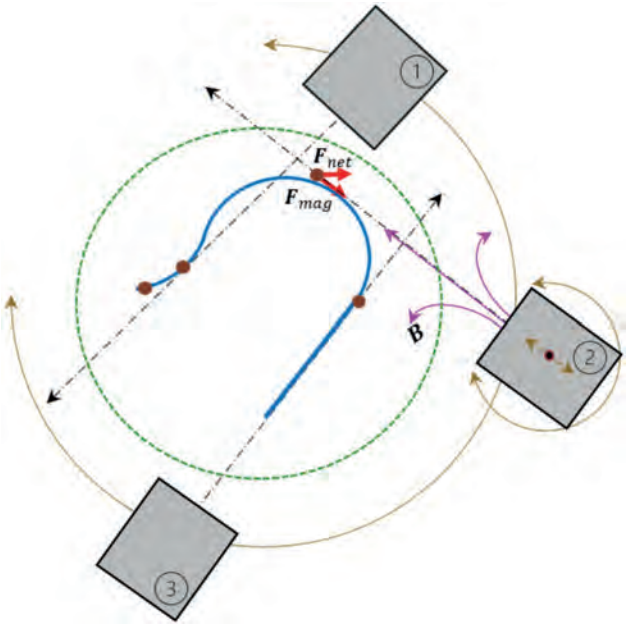

Illustration of the magnetic field-driven trajectory control methodology and setup. When the bot is close to its desired trajectory, the magnet is positioned to have its axis being nearly tangential to the trajectory at the bot's position.

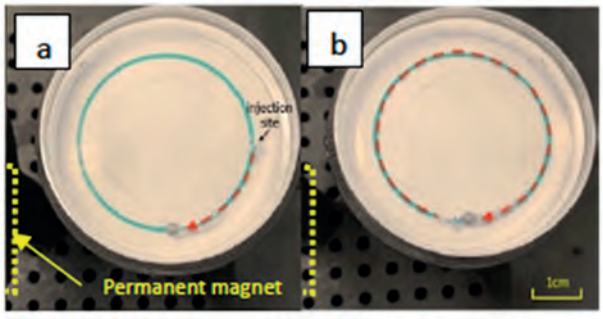

Demonstration of trajectory control for a permanent magnet (NdFeB) spherical bot using sliding-mode control in 0.6% agarose gel.

Session GA
MAGNETIZATION DYNAMICS IN TWO-DIMENSIONAL VAN DER WAALS MAGNETS

Axel Hoffmann, Chair
University of Illinois at Urbana-Champaign, Urbana, IL, United States

INVITED PAPERS

GA-01. Probing spin dynamics of nm-thick $Cr_2Ge_2Te_6$ by superconducting resonators and time-resolved beam-scanning Kerr microscopy. C. Zollitsch[1], S. Khan[1], M. Dabrowski[2], I. Verzhbitskiy[3], P.S. Keatley[2], G. Eda[3], R. Hicken[2] and *H. Kurebayashi*[1] *1. University College London, London, United Kingdom; 2. University of Exeter, Exeter, United Kingdom; 3. National University of Singapore, Singapore*

Due to their mechanical exfoliation nature as well as low crystalline symmetry, van der Waals layered magnets have been intensively studied for exploring a novel design/control of magnetism, spin dynamics as well as spin transport phenomena [1-2]. Typical dimensions of a few-monolayer vdW exfoliated flake are several μm in lateral directions and a few nm in thickness. Electrical and optical probes for exfoliated flakes can be relatively readily achieved by conventional lithographic techniques as well as visible focused laser to access to the small objects, respectively. On the other hand, an efficient coupling of the vdW flakes to microwave is not trivial. The sensitivity of such microwave detection schemes is mainly determined by the spatial matching between the microwave and magnetic modes. This means that we have to employ a small-mode-volume microwave probe, in order to efficiently excite spin dynamics of exfoliated vdW magnets to study the fundamental nature of spin dynamics at the few-monolayer level. We use on-chip superconducting (SC) microwave resonators for this application [3]. High-quality-factor superconducting lumped element resonators, with a small mode volume, allow a sizable coupling between its microwave photons to excited magnons in nm-thick/μm-sized exfoliated CGT flakes. We performed microwave spectroscopy at low temperatures and observed modification of SC resonator mode spectra by the hybridization with magnons. We applied a coupled harmonic oscillator model to the hybridized spectra to extract magnetic properties (magnetic anisotropy and relaxation) of the CGT flakes. Using the linewidth for the thinnest CGT flake investigated (11 nm), we determined an upper limit of the Gilbert damping parameter of 0.02 and the spin-dynamics detection of the monolayer CGT flake using this scheme will also be discussed. In the last part of this talk, we introduce our latest work of time-resolved beam-scanning Kerr microscopy performed on SiO2/CGT/hBN with various CGT flakes, with sub-micron spatial resolution and sub-picosecond temporal resolution [4]. We show that CGT undergoes a two-step demagnetization process, and that the total magnetization quenching can be achieved at the time delay of around 300 ps. We will show and discuss the remagnetization process in CGT for different thicknesses.

[1] C. Tang et al., arXiv:2301.09822 [2] H. Kurebayashi et al., Nat. Rev. Phys. 4 150 (2022). [3] C. W. Zollitsch et al., Nat. Comm. 14, 2619 (2023). [4] M. Dabrowski et al., in-preparation.

GA-02. Probing Intrinsic Magnon Bandgap in Layered Perovskite Antiferromagnet by a Superconducting Resonator. Y. Li[1,2], T. Draher[1,2], A. Comstock[3], Y. Xiong[4], M. Haque[5], E. Easy[6], J. Qian[7], T. Polakovic[8], J. Pearson[1], R. Divan[9], J. Zuo[7], X. Zhang[6], U. Welp[1], W. Kwok[1], A. Hoffmann[7], J. Luther[5], M. Beard[5], D. Sun[3], W. Zhang[4] and *V. Novosad*[1,8] *1. Materials Science Division, Argonne National Laboratory, Lemont, IL, United States; 2. Department of Physics, Northern Illinois University, Dekalb, IL, United States; 3. Department of Physics and Organic and Carbon Electronics Laboratory, North Carolina State University, Raleigh, NC, United States; 4. Department of Physics & Astronomy, University of North Carolina, Chapel Hill, IL, United States; 5. Chemistry & Nanoscience Center, National Renewable Energy Laboratory, Golden, CO, United States; 6. Department of Mechanical Engineering, Stevens Institute of Technology, Stevens Institute of Technology, Hoboken, NJ, United States; 7. Department of Materials Science and Engineering, University of Illinois Urbana-Champaign, Urbana, IL, United States; 8. Physics Division, Argonne National Laboratory, Lemont, IL, United States; 9. Center for Nanoscale Materials, Argonne National Laboratory, Lemont, IL, United States*

The controllability of coupling between fundamental solid-state excitations is an important prerequisite for expanding their functionality in hybrid quantum systems. In hybrid magnonics, the dipolar interaction between magnon and photon usually persists and cannot be switched off. On the other hand, the recent two-dimensional (2D) organic layered magnets offer distinct advantages in their structure-enabled topological chirality and symmetry breaking [1]. One interesting class of materials is 2D magnetic hybrid organic-inorganic perovskites (HOIPs), possessing both superior structural versatility and long-range magnetic order. They usually exhibit an interlayer antiferromagnetic (AFM) coupling, inducing the acoustic and optical magnon modes in the gigahertz (GHz) frequency range. In addition, the structural symmetry breaking leads to a bulk Dzyaloshinskii-Moriya interaction (DMI), causing a finite spin canting and creating an intrinsic magnon band gap where the acoustic and optic modes intersect. This is fundamentally different from the dipole-induced magnon band gap in that the DMI-induced magnon band gap is intrinsic, regardless of magnetization orientation, and can be sensitively tuned with small temperature changes, thus leading to new opportunities for modulating coherent magnonic coupling. In this work, we report a hybrid magnonic system consisting of 2D HOIPs, $(CH_3CH_2NH_3)_2CuCl_4$ (Cu-EA) [2], coupled to a superconducting resonator. The high sensitivity of the superconducting resonator [3-4] enables strong magnon-photon coupling and avoided crossing with a small Cu-EA flake. By changing the temperature of the sample, the location of the DMI-induced magnon band gap can be adjusted so that the resonator photon mode completely falls into the gap and cancels the mode hybridization. At the non-hybridized state, the magnetic interaction with the resonator causes the resonator linewidth to broaden. Using our developed analytical model, the narrow-band linewidth broadening measurements can be used to extract the magnon band gap, which quantitatively agrees with the broad-band FMR measurements. Our results highlight the opportunity of manipulating coherent mode hybridization with new quantum materials and probing their complex magnonic dispersion with narrow-band microwave characterizations. Work at National Renewable Energy Laboratory was supported through the Center for Hybrid Organic-Inorganic Semiconductors for Energy (CHOISE), an Energy Frontier Research Center funded by the Office of Basic Energy Sciences, Office

of Science within the U.S. Department of Energy. This work was authored in part by the National Renewable Energy Laboratory (NREL), operated by Alliance for Sustainable Energy LLC, for the U.S. Department of Energy (DOE) under contract no. DE-AC36-08GO28308. Works at Argonne National Laboratory and University of Illinois Urbana-Champaign, including the superconducting resonator fabrication, design, ICP chemical analysis, and hybrid magnonics characterization, were supported by the U.S. DOE, Office of Science, Basic Energy Sciences, Materials Sciences, and Engineering Division under contract No. DE-SC0022060.

[1] Q. H. Wang *et al.*, The Magnetic genome of two-dimensional van der Waals materials, ACS Nano 16, 6960 (2022). [2] A. H. Comstock, *et al.*, Hybrid magnonics in hybrid perovskite antiferromagnets, Nature Comm. 14, 1834 (2023). [3] Y. Li *et al.*, Strong coupling between magnons and microwave photons in on-chip ferromagnet-superconductor thin-film devices, Phys. Rev. Lett. 123, 107701 (2019) [4] C. W. Zollitsch *et al.* Probing spin dynamics of ultra-thin van der Waals magnets via photon-magnon coupling, Nature Commun. 14, 2619 (2023)

GA-03. Magnon-magnon interactions in layered antiferromagnets.

J. Sklenar[1], M. Subedi[1], K. Deng[2], Y. Xiong[5], J. Mongeon[2], M. Hossain[3], P. Meisenheimer[4], E. Zhou[1], J. Heron[4], B. Jungfleisch[3], W. Zhang[5] and B. Flebus[2] *1. Wayne State University, Detroit, MI, United States; 2. Boston College, Chestnut Hill, MA, United States; 3. University of Delaware, Newark, DE, United States; 4. University of Michigan, Ann Arbor, MI, United States; 5. University of North Carolina, Chapel Hill, NC, United States*

Van der Waals (vdW) antiferromagnets and synthetic antiferromagnets have emerged as significant material systems for exploring the impact of magnon-magnon interactions on the antiferromagnetic resonance spectrum. These materials exhibit a modest interlayer exchange interaction, allowing the excitation of acoustic and optical magnons at GHz frequencies. The presence of interactions can be detected through characteristic avoided energy level crossings in the spectrum between optical and acoustic modes. Manipulating and controlling these interactions is crucial for utilizing antiferromagnets as building blocks for hybrid quantum systems[1]. In easy-plane layered antiferromagnets, a common method to modify the antiferromagnetic magnon spectrum with a magnon-magnon interaction is by applying an external field oblique to the easy plane[2,3]. Strategies such as dynamic dipolar fields[4] and interlayer DMI interactions[5] offer alternative means to manipulate the magnon spectrum. In this study, we investigate the emergence of new opportunities for controlling magnon-magnon interactions by modifying the structure of layered antiferromagnets to include a finite number of layers greater than two[6]. Using micromagnetic simulations and a macrospin formalism, we analyze how the magnon energy spectrum is affected in tetralayers, hexalayers, and octalayers consisting of four, six, and eight coupled layers. Unlike bilayers or vdW materials with many layers that can be deconstructed into two magnetic sub-lattices, these layered systems exhibit multiple optical and acoustic magnon branches. For instance, a tetralayer possesses two optical magnon modes that predominantly reside on the surface and interior layers, respectively. In the antiferromagnetic resonance spectrum, there are regions in the field-frequency space where these two magnon excitations approach and avoid each other due to dynamic interlayer exchange fields. Our micromagnetic simulations demonstrate the potential for electrical control of such magnon-magnon interactions. By applying damping-like torques on the surface layers, avoided energy crossings can be continuously opened and closed through all-electrical means. To confirm the existence of these interactions in layered antiferromagnetic materials with more than two layers, our experimental focus has been on permalloy-ruthenium based synthetic antiferromagnets. To verify the applicability of the relevant macrospin models and micromagnetic simulations, we synthesized bilayers, trilayers, and tetralayers with various permalloy thicknesses (2-15 nm) and a fixed ruthenium spacer layer that promotes an antiferromagnetic interaction between permalloy layers. Magnetometry measurements confirm that our materials are well-described by the macrospin picture, allowing for the extraction of the interlayer exchange field. When measuring the antiferromagnetic resonance spectra of these materials, we observe avoided energy level crossings between pairs of acoustic magnons that align with our initial model. However, we also observe unexpected additional avoided energy level crossings between optical and acoustic magnons, which cannot be accounted for by models considering only dynamic interlayer exchange interactions. By modifying the macrospin equations of motion to incorporate interlayer spin pumping in a non-collinear magnetization configuration, we find that field-like torques arising from interlayer spin pumping generate a new magnon-magnon interaction responsible for the experimentally observed avoided energy level crossings[7].

[1] D.D. Awschalom, C.R. Du, R. He, et al. IEEE Transactions on Quantum Engineering. 2, 1-36 (2021) [2] D. MacNeill, J.T. Hou, D.R. Klein, et al. Phys. Rev. Lett. 123, 047204 (2019). [3] A. Sud, C.W. Zollitsch, A. Kamimaki, et al. Phys. Rev. B 102, 100403(R) (2020). [4] Y. Shiota, T. Taniguchi, M. Ishibashi, et al. Phys. Rev. Lett. 125, 017203 (2020). [5] A.H. Comstock, C.-T. Chou, Z. Wang, et al. Nat. Comm. 14, 1834 (2023). [6] J. Sklenar and W. Zhang, Phys. Rev. Appl. 15, 044008 (2021). [7] M.M. Subedi, K. Deng, Y. Xiong, et al. arXiv:2301.07311 (2023).

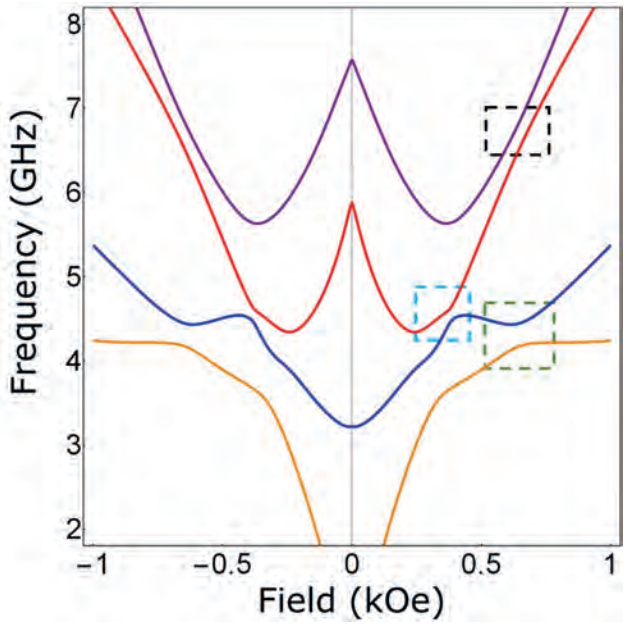

Theoretical field-frequency relationship of the acoustic and optical magnon branches in a tetralayer. Dashed boxes indicate where interlayer spin pumping generates avoidance between the energy levels.

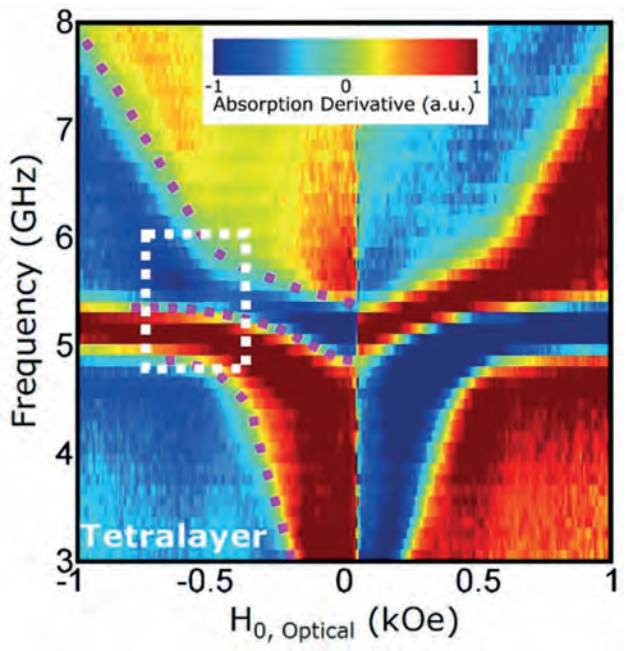

Experimental magnetic resonance spectrum in the tetralayer. Green contours highlighted with dashed lines indicate where the modes are excited. Note the mutual avoidance between the three experimentally observed modes.

GA-04. Quantum Sensing and Imaging of Two-Dimensional van der Waals Magnets. *C. Du*[1] *1. Physics, Georgia Institute of Technology, Atlanta, GA, United States*

Two-dimensional (2D) van der Waals crystals with emergent magnetic and electrical properties have been a rising topic of modern magnetism and spintronics research over the past years. Currently, there is ongoing intense activity to develop and understand this new family of magnetic materials, as well as to create new ones. The success of these efforts relies simultaneously on advances in theory, material synthesis, and development of new, sensitive metrology tools capable of evaluating the key material properties at the nanoscale. Nitrogen-vacancy (NV) centers, optically active atomic spin defects in diamond, are naturally relevant in this context due to their excellent quantum coherence, highly competitive spatial and field sensitivity, and remarkable functionalities over broad experimental conditions. In this talk, I will present our recent work on using NV centers to perform quantum sensing and imaging measurements of 2D van der Waals magnets. Specifically, we utilized NV centers to visualize the exotic spin properties of layered, topological antiferromagnetic materials and twisted van der Waals magnet based heterostructures, revealing the rich physics of low-dimensional magnetism at the nanoscale. If time permits, I will also briefly discuss our ongoing efforts on exploring 2D quantum sensing technologies using color centers beyond NVs.

GA-05. Probing spin dynamics with spin defects embedded in 3D and 2D systems. *S. Singh*[1] and C. Hammel[2] *1. Department of Physics, Carnegie Mellon University, Pittsburgh, PA, United States; 2. Department of Physics, The Ohio State University, Columbus, OH, United States*

Layered quantum materials host a broad range of phenomena ranging from emergent magnetism to spin-defects for quantum technologies including quantum sensing. In this talk, we will present our recent studies that are aimed at utilizing spin defects embedded in 3D and 2D systems to probe magnetization dynamics in 3D and 2D magnets. First, we will talk about the case of the newly discovered boron vacancy (BV−) atomic defect in hexagonal boron nitride (h-BN) and its utility as a probe of magnetic dynamics in a magnetic insulator, i.e., yttrium iron garnet (YIG, $Y_3Fe_5O_{12}$). We present a straightforward process for creating BV− centers in h-BN and demonstrate their efficacy as a sensor for probing spin dynamics. Optically detected ferromagnetic resonance of the YIG uniform mode dispersion was measured using an ensemble of BV− centers placed in a close proximity to the YIG thin film. Secondly, we will talk about the optical detection of antiferromagnetic resonance (AFMR) in a 2D antiferromagnet, i.e., $CrCl_3$. Magnetism in 2D materials has been a focus of much recent interest due to their unique and useful properties in spintronic devices. To understand and control the spin states of 2D magnets, sensitive measurements of the spin dynamics are essential. We will present first optical detection of AFMR in $CrCl_3$ using nitrogen-vacancy (NV−) centers in diamond. Field, frequency, and temperature dependence of the AFMR are measured and material parameters are extracted which are consistent with estimates based on other methods.

Session GB
MICROSCOPY & CHARACTERIZATION III: SPIN TEXTURES, MAGNETIC INTERACTIONS, NANOPARTICLE DYNAMICS AND X-RAY METHODS

Sophie A Morley, Chair
Lawrence Berkeley National Laboratory, Berkeley, CA, United States

INVITED PAPER

GB-01. Imaging Stripes, Skyrmions and Higher-order Spin Textures in 2D Magnets. *M. Birch*[1], L. Powalla[2], K. Litzius[3], S. Wintz[4], F. Schulz[5], F.S. Yasin[1], M. Weigand[4], D. Mayoh[6], G. Balakrishnan[6], L. Turnbull[8], X. Yu[1], O. Hovorka[7], M. Burghard[2] and G. Schütz[5] *1. RIKEN Center for Emergent Matter Science, Wako, Japan; 2. Max Planck Institute for Solid State Physics, Stuttgart, Germany; 3. University of Augsberg, Augsberg, Germany; 4. Helmholtz Zentrum Berlin, Berlin, Germany; 5. Max Planck Institute for Intelligent Systems, Stuttgart, Germany; 6. Warwick University, Coventry, United Kingdom; 7. University of Southampton, Southampton, United Kingdom; 8. Durham University, Durham, United Kingdom*

Two-dimensional (2D) magnets have recently emerged as an exciting new platform for the design of spintronic devices [1]. While significant work has been performed on the transport properties of these systems, including some prototype heterostructure designs [2,3], detailed understanding of the basic magnetic behaviour is incomplete. In this talk, I will discuss our wide-ranging x-ray microscopy imaging results on a selection of exfoliated flakes of 2D magnets, focusing primarily on $Fe_{3-x}GeTe_2$, showing observations of stripes, skyrmions and higher-order composite skyrmions. The results reveal the level of control of the magnetic spin textures which can be achieved by varying the flake thickness and structural composition of these systems, attained via manipulation of the out-of-plane anisotropy [4,5]. Furthermore, I will detail our attempts at employing manipulation of the hosted spin textures, including current pulse-induced including skyrmion nucleation and motion [6,7]. Finally, I will explain our observations of the composite skyrmions with higher-order topology, and their implications on the concept of topological protection [8].

[1] K. S. Burch, D. Mandrus & J.-G. Park, *Nature* 563, 47 (2018). [2] Z. Wang, et al. *Nano Lett.* 18, 4303 (2018). [3] S. Albarakati, et al. *Sci. Adv.* 5, eaaw0409 (2019). [4] M. T. Birch, L. Powalla, et al. *Nat. Commun.* 13, 3035 (2022). [5] M. T. Birch, L. Powalla, et al. *Under Review* (2023). [6] L. Powalla, M. T. Birch, et al. *Nano Lett.* 22, 9236-9243 (2022). [7] K. Litzius, et al. *In Preparation* (2023). [8] L. Powalla, M. T. Birch, et al. *Adv. Mater.* 35, 2208930 (2023).

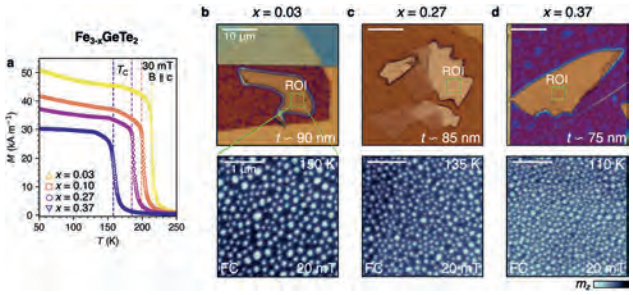

Compositional dependence of $Fe_{3-x}GeTe_2$ flakes. a) Magnetometry measurements reveal the Curie temperature dependence of the bulk FGT crystals. b-d) Optical micrographs of the exfoliated FGT flakes, stamped on Si_3N_4 membranes, and capped with hBN flakes. Below, x-ray micrscopy images of disordered arrays of skyrmions in each FGT flake are shown. The colourmap indicates the out-of-plane magnetic contrast, *mz*.

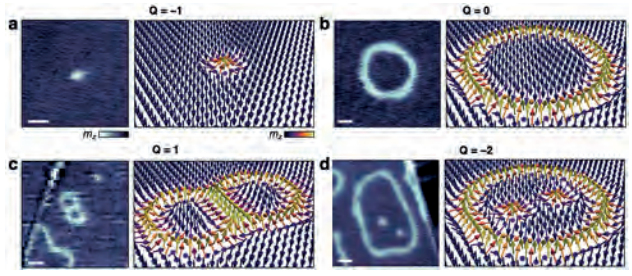

Real-space observations and visualizations of composite skyrmion states in the 2D magnet $Fe_{3-x}GeTe_2$ (FGT). a–d) Scanning transmission X-ray micrographs and schematic visualizations of composite skyrmion objects observed in the exfoliated FGT flakes, including skyrmion (a), skyrmionium (b), skyrmion bag (c), and skyrmion sack (d) states. In each case, the total topological charge *Q* is labeled. Images a-c are of the *x* = 0.27 flake, image d is of the *x* = 0.03 flake. The color map is proportional to the out-of-plane magnetization component, m_z. The scalebar is 250 nm. The schematic illustrations are mathematical constructions of the expected vector field demonstrating each spin configuration.

CONTRIBUTED PAPERS

GB-02. Radial dependent stray field signature of chiral magnetic skyrmions. *C.W. Barton*[1], A. Fernandez-Scarioni[2], B. Sakar[2], S. Sievers[2], F. Garcia-Sanchez[3], P. Thompson[4], F. Ajejas[5], W. Legrand[5], N. Reyren[5], T. Thomson[4], V. Cros[5], H. Schumacher[2] and O. Kazakova[1] *1. National Physical Laboratory, Teddington, United Kingdom; 2. Physikalisch-Technische Bundesanstalt, Braunschweig, Germany; 3. Universidad de Salamanca, Salamanca, Spain; 4. University of Manchester, Manchester, United Kingdom; 5. Unité Mixte de Physique, CNRS, Thales, Palaiseau, France*

Magnetic skyrmions are topological spin structures that arise in chiral magnetic systems which exhibit broken inversion symmetry [1,2] and high spin-orbit coupling resulting in a sizable Dzyaloshinskii–Moriya interaction. Following a decade of intense research several promising applications have been identified. Of these, skyrmion based neuromorphic spintronic computing is gaining significant traction with examples of skyrmion synaptic devices and reservoir computing being recently reported [3]. Understanding the local spin texture of skyrmions is a vital metrological step in the development of skyrmionic technologies required for novel logic or storage devices in addition to providing fundamental insight into the nanoscale chiral interactions inherent to these systems. In this talk will discuss a hitherto unreported [4], radially dependent stray field signature that emanates from magnetic skyrmions, figure 1 (a). To demonstrate this, we have used quantitative magnetic force microscopy [5,6] (qMFM), figure 1 (b) to experimentally explore this stray field signature. To corroborate the experimental observations a semi-analytical model is developed which is validated against micromagnetic simulations. This novel approach provides a route to understand the unique radially dependent field signature from skyrmions, which allows an understanding of the underlying local magnetisation profile to be obtained. From a practical standpoint, our results provide a rapid approach to validate outputs from numerical or micromagnetic simulations. Our approach could be employed to optimise the complex matrix of magnetic parameters required for fabricating and modelling skyrmionic systems, in-turn accelerating the technology readiness level of skyrmionic based devices. Fig. 1. (a) Experimentally observed radial dependant stray field by qMFM: data points are experimental data; and solid lines are modelled data for different skyrmion chiralities (b) qMFM micrographs of the skyrmions used for analysis in this study. Inset is the current pulse used to nucleate sckyrmions in this work.

[1] A. Bogdanov, and D. A. Yablonskii, Thermodynamically stable vortices in magnetically ordered crystals. The mixed state of magnets. Sov. Phys. JETP., 68, 101–103 (1989). [2] A. Fert, N. Reyren, and V. Cros, Advances in the physics of magnetic skyrmions and perspective for technology, Nat. Rev., 2, 17031 (2017). [3] K. Raab, M. A. Brems, G. Beneke, T. Dohi, J. Rothörl, F. Kammerbauer, J. H. Mentink & M. Kläui, Brownian reservoir computing realized using geometrically confined skyrmion dynamics, Nat. Commun., 13, 6982 (2022). [4] C. Barton, A. Fernández Scarioni, B. Sakar, S. Sievers, F. Garcia-Sanchez, P. Thompson, F. Ajejas, W. Legrand, N. Reyren, T. Thomson, V. Cros, H. W. Schumacher and O. Kazakova, Radial dependent stray field signature of chiral magnetic skyrmions, Phys Rev B, (2023) Accepted. [5] H. J. Hug, B. Stiefel, P. J. A. van Schendel, A. Moser, R. Hofer, S. Martin, and H.-J. Güntherodt, Steffen Porthun, L. Abelmann, and J. C. Lodder, G.Bochi and R. C. O'Handley, Quantitative magnetic force microscopy on perpendicularly magnetized samples, J. Appl. Phys., 83, 5609 (1998). [6] O. Kazakova, R. Puttock, C. Barton, H. Corte-León, M. Jaafar, V. Neu, and A. Asenjo, Frontiers of magnetic force microscopy, J. Appl. Phys., 125, 060901 (2019).

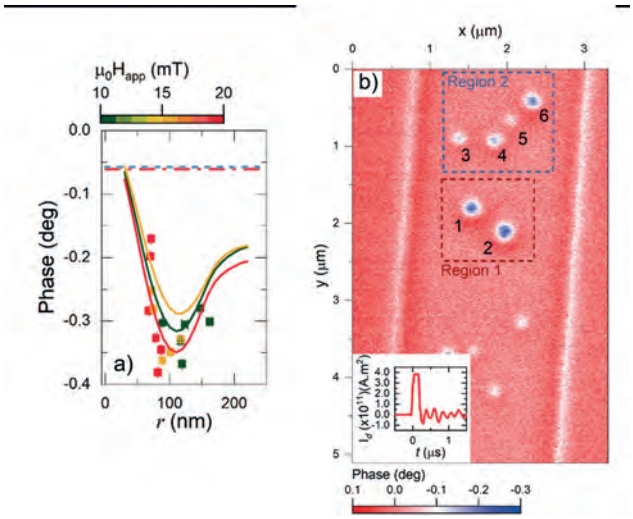

GB-03. Quantifying the topology of a skyrmion in 3D with soft x-ray laminography. *D.W. Raftrey*[1,2], S. Finizio[4], R.V. Chopdekar[3], T. Bayaraa[2], S.M. Griffin[2], T. Santos[3] and P. Fischer[1,2] *1. Physics, University of California Santa Cruz, Santa Cruz, CA, United States; 2. Material Sciences Division, Lawrence Berkeley National Lab, Berkeley, CA, United States; 3. Western Digital Corporation, San Jose, CA, United States; 4. Paul Scherrer Institute, Villigen, Switzerland*

The push into three dimensions is of growing interest in basic nanomagnetism research with high relevance for future spintronics devices. A spin texture is a three dimensional vector-valued structure which is the result of competition between fundamental energetic interactions and defines the emergent properties of the system including real-space topology (Skyrmion number) and transport behavior responsible for device functionality. A complete description of this microstate requires knowledge of the three components of the magnetization vector covering the volume of the sample in three spatial dimensions. Soft x-ray laminography using magnetic circular dichroism (XMCD) as a contrast mechanism is a three-dimensional imaging technique for magnetic systems which can resolve this information at the nanoscale. The physical information contained in such a [Mx(x, y, z), My(x, y, z), Mz(x, y, z)] dataset categorically surpasses what it is possible to quantify with typical Mz(x,y) image data. In this study a magnetic 30×[Ir/Co/Pt] DMI 800 nm diameter nanodisk is imaged with x-ray laminography at the Pollux end station of the Swiss Light Source. From this data we quantitatively measure the topological profile of a skyrmion and its chirality over the full 90 nm thickness of the sample. From the vector data the relative energy densities of the different micromagnetic energies are derived. The skyrmion topological profile and energetic densities are found to vary across the thickness of the disk demonstrating that the structure of magnetic skyrmions in repeating multilayer systems is more complex that what can be accommodated in a simple two-dimensional framework. Our results provide the foundation for nanoscale magnetic metrology for future tailored spintronics devices using topology as a design parameter, and have the potential to reverse-engineer a spin Hamiltonian from macroscopic data, tying theory more closely to experiment.

This work was supported by the U.S. Department of Energy, Office of Science, Office of Basic Energy Sciences, Materials Sciences and Engineering Division under Contract No. DE-AC02-05-CH11231 within the Non-equilibrium Magnetic Materials Program.

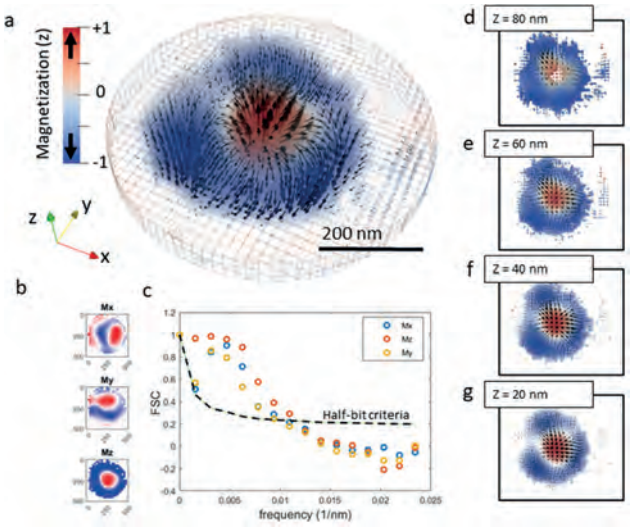

a) A rendering of the 3D reconstruction. b) Z-axis projections of individual cartesian magnetization components. c) Fourier shell correlation analysis establishing the resolution. d-g) Individual 20nm resolved slices along z-axis.

GB-04. Unveiling unusual magnetic domain configurations in NiFe microbar ensembles by high-resolution soft X-ray ptychography.

T. Feggeler[1,2], A. Levitan[3,2], O. Brunn[4,5], J. Sadilek[4,6], *H. Ohldag*[2,7], D.A. Shapiro[2], R.W. Falcone[1], K. Ollefs[8] and N. Rougemaille[9] *1. Department of Physics, University of California, Berkeley, Berkeley, CA, United States; 2. Advanced Light Source, Lawrence Berkeley National Laboratory, Berkeley, CA, United States; 3. Department of Physics, Massachusetts Institute of Technology, Cambridge, MA, United States; 4. Institute of Scientific Instruments, Czech Academy of Sciences, Brno, Czechia; 5. Institute of Physical Engineering, Brno University of Technology, Brno, Czechia; 6. Department of Microelectronics, Brno University of Technology, Brno, Czechia; 7. Department of Material Sciences and Engineering, Stanford University, Stanford, CA, United States; 8. Faculty of Physics, University of Duisburg-Essen, Duisburg, Germany; 9. Institut Néel, Grenoble INP, Université Grenoble Alpes, CNRS, Grenoble, France*

Magnetic domains originate from multiple in part competing interactions in magnetic materials ranging from magnetic dipolar and exchange coupling to magnetic anisotropies. Understanding and visualizing domain configurations, their formation, and the respective separating domain walls in magnetic micro- and nano-ensembles is a crucial part in understanding the connection between the aforementioned fundamental magnetic properties and macroscopic properties like the magnetization, a necessity in understanding and design of spin-based devices. Here we present X-ray Magnetic Circular Dichroism (XMCD) Ptychography on NiFe microbars with different lateral aspect ratios and edge curvatures arranged in 3x3 bar ensembles. The bars share a thickness of 80 nm and are deposited on an Si_3N_4 membrane with 30 nm thickness. The lateral dimensions range in length from 0.5 to 6.25 μm with widths ranging from 0.2 to 2.5 μm, with edge curvature radii ranging from r = 1/2 to 1/4 in relation to the width. High resolution XMCD ptychography was performed in remanence at the Fe L_3 edge under a 45 degree incidence angle. As a result of competing magnetic anisotropies, a plethora of domain configurations is observed in an interplay from classical Landau patterns, over domain walls with magnetic discontinuities to bipolar vortices and combinations of respective patterns. Complementary micromagnetic simulations are presented in support of the experimental observations. T.F. and R.W.F. acknowledge support from STROBE: A National Science Foundation Science & Technology Center, under Grant No. DMR–1548924. A.L. acknowledges support from the U.S. Department of Energy, Office of Science Office of Science Graduate Student Research (SCGSR) program, managed by ORAU under contract number DE–SC0014664. K.J.O acknowledges support from the Deutsche German Research Foundation (DFG) Project-ID 405553726 TRR 270. The Czech Academy of Sciences (Project No. RVO:68081731) is acknowledged for funding of research infrastructure. This research used resources of the Advanced Light Source, a U.S. DOE Office of Science User Facility under contract no. DE-AC02- 05CH11231.

INVITED PAPER

GB-05. Emerging Image Interpretation Paradigm for Advanced Material Design with an Extended Landau Free Energy Model.

K. Masato[1] *1. Tokyo University of Science, Tokyo, Japan*

In recent years, the quest for advanced material design, crucial for low-power, high-speed next-generation electronic devices and high-efficiency electric vehicle motors, has intensified. Microscopic image data, direct evidence of device operation, forms a critical source of information for this design process. However, the interpretation of such data, especially for nanoscale magnetic bodies exhibiting complex nanostructures and interactions, has been a challenging task. Until now, image data interpretation has been largely qualitative and subjective, leading to a significant issue in functional design: an insufficient understanding of the underlying mechanisms, hindering device performance improvement. To address these challenges, we developed the "Extended Landau Free Energy Model," a unique blend of topology, information science, and free energy, enabling automated interpretation of image data (Figure 1) [1-6]. Traditionally, the Landau Free Energy Model, a tool to explain magnetization reversal phenomena based on magnetization and magnetic fields, was only applicable to single crystals, making it inadequate for real materials with nanostructures. We overcame this limitation by incorporating topology and data science into the model, creating a framework capable of analyzing real materials. Our approach employed Persistent Homology, a concept of topology, to extract complex magnetic domain structures as features. We then applied interpretable machine learning to draw a new energy landscape in the information space, constructing the Extended Landau Free Energy Model. Characterized by the use of physics-based features for analyzing the magnetization reversal process, our model establishes a relationship between magnetic domain structure changes and energy barriers through simple variable transformation and differentiation. It facilitates a bidirectional connection between micro magnetic domain structures and macro magnetization reversal phenomena across hierarchies (Figure 2), further allowing for the quantitative analysis of underlying physical interactions. Applying our model to the analysis of the information recording process of nanomagnetic bodies revealed the dominance of the demagnetization field effect. It also succeeded in visualizing the spatial concentration of energy barriers impeding the change in magnetic domain structure. This visualization indicates an improved understanding of mechanisms previously challenging to analyze visually and the ability to highlight subtle changes in microscopic images. The model potentially transforms overlooked microscopic data into a "goldmine" of information. Moreover, based on our model, we successfully proposed nanostructures with lower energy consumption, suggesting potential applications in the reverse design of devices. Applicable to various materials driven by complex mechanisms, our model promises wide-ranging contributions to the fabrication of diverse products, including quantum information technologies, electric vehicle motors, and autonomous distributed systems.

1) S. Kunii, K. Masuzawa, A. L. Fogiatto, C. Mitsumata & M. Kotsugi, Sci. Rep. 12, 19892 (2022) 2) A. L. Foggiatto, S. Kunii, C. Mitsumata & M. Kotsugi, Communications Physics 5, 277 (2022) 3) S. Kunii, A. L. Foggiatto, C. Mitsumata & M. Kotsugi, Sci. Tech. and Adv. Mater. Methods, 2 445-459 (2022) 4) C. Mitsumata, M. Kotsugi, J. Magn. Soc. Jpn, 46, (2022) pp. 90-96 5) K. Masuzawa, S. Kunii, A. Foggiatto, C. Mitsumata, M. Kotsugi, T. Magn. Soc. Japan. 6 (2022), 1-9. 6) T. Nishio, M. Yamamoto, T. Ohkochi, D. Nanasawa, A. Foggiatto, M. Kotsugi, Sci. Tech. and Adv. Mater. Methods, 2, pp 345-354, (2022)

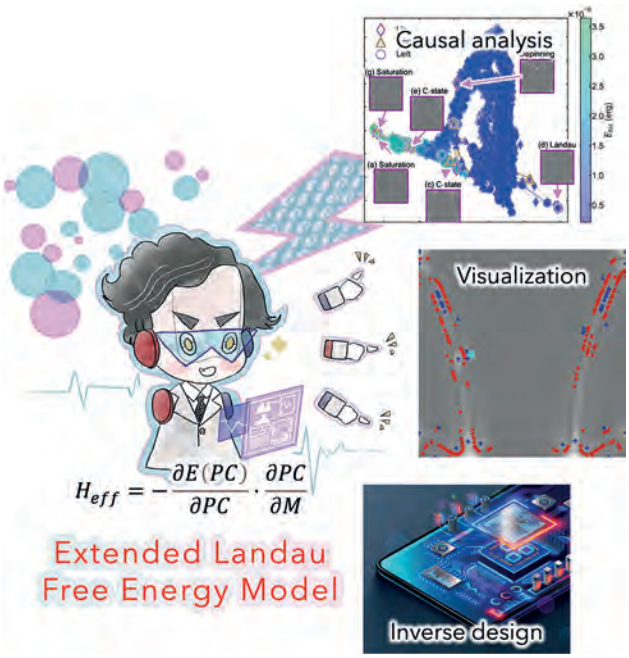

Figure 1

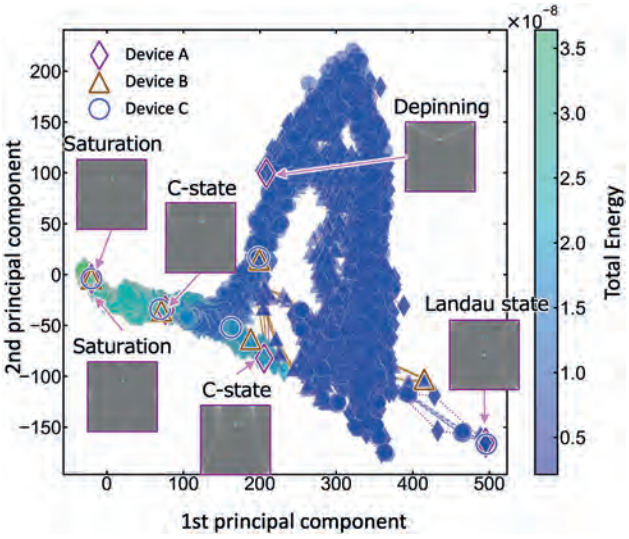

Figure 2

CONTRIBUTED PAPERS

GB-06. Magneto-optical detection of spin-orbit torque vector with first-order Kerr effects. *C.A. Gonzalez*[1], M. Abellan[2] and S. Oyarzun[1]
1. Physics, Universidad de Santiago, Santiago, Chile; 2. Physics, Universidad Tecnica Federico Santa Maria, Valparaiso, Chile

When spin-polarized currents diffuse into a ferromagnetic (FM) material, they induce spin-orbit torques (SOTs): a powerful mechanism for magnetic order manipulation with applications in magnetic recording, logic devices, and neuro-morphing computing [1]. To date, detection SOTs have relied almost exclusively on measuring electrical voltages arising from the device under excitation. In this line, techniques such as second harmonic generation, spin transfer torque ferromagnetic resonance (STT-FMR), and spin pumping have dominated the scene. In these techniques, signals are often contaminated by unwanted thermo-electric voltages. Also, the sensitivity depends critically on magneto-electric coefficients showing large variations even for typical 3d ferromagnetic materials [2]. This work presents a powerful new method for detecting SOTs based on Magneto-Optical Kerr Effect (MOKE). We can quantify the damping-like and field-like SOT effective fields (h_{DL} and h_{FL}, respectively) of SOTs, employing a simple and low-cost set-up that has already been widely employed in MOKE magnetometry (Fig. 1). We tested our method in NiFe/Pt, NiFe/Pd, and Ta/CoFeB bilayers, obtaining a damping-like SOT efficiency (ζ_{DL}) equal to 0.08 ± 0.01, 0.034 ± 0.004 and -0.15 ± 0.01 respectively. On the other side, we obtained $h_{FL}\backslash h_{DL}$ ratios equal to 0.24 ± 0.03 and 0.11 ± 0.03 in the samples with 4 nm thick NiFe and CoFeB, respectively. The results for ζ_{DL} are close to the most accepted values reported in the literature for the studied materials. The $h_{FL}\backslash h_{DL}$ ratios fit well inside the diffusive model of spin accumulation in the ferromagnetic layer [3], with a finite spin dephasing length. This effect has often been disregarded in STT-FMR works.

[1] A. Hiroata *et al.*, J. Magn. Magn. Mater. 509, 166711 (2017). [2] M.-H. Nguyen and C.-F. Pai, APL Materials 9, 030902 (2021). [3] S. Zhang, P. M. Levy, and A. Fert, Phys. Rev. Lett. 88, 236601 (2002).

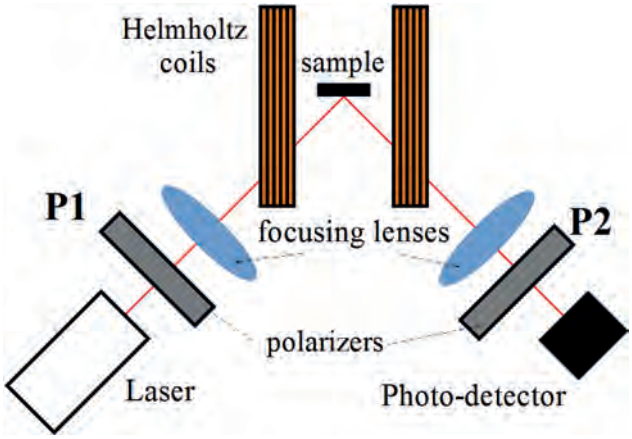

Schematic diagram of the set-up employed for magneto-optical detection of SOTs

GB-07. A Sensitive Magneto-Optic Kerr Effect and Optical Hall Effect Technique. *N. Am-Shalom*[1], M. Korcia[1], N. Bernstein[1] and A. Capua[1]
1. Applied Physics, The Hebrew University of Jerusalem, Jerusalem, Israel

We present an ultrasensitive magneto-optical Kerr effect (MOKE) technique that is based on a large-amplitude modulation of the externally applied magnetic field. The large amplitude modulation turns out to enhance the sensitivity to the Kerr signal by two orders of magnitude such that the optical Hall effect (OHE) becomes measurable for non-magnetic metals at optical wavelengths. The technique was inspired by the analogies between the optical and electrical Hall measurements (Fig.1 (a)). We find good agreement with previously measured responses in Au, Cu and Py, and derive a model that builds on the Lorentz-Drude model that accounts for the electromagnetic skin effect. The technique is then applied to thin films of Pt and Ta for which the conduction band electrons have effective masses of opposite sign, and on Bi_2Te_3 which is a topological insulator at room temperature. The measurements of the OHE for Pt, Ta, and Bi_2Te_3 as presented in Fig 1(b), illustrates a linear dependence of the optical response on the applied magnetic field as predicted theoretically. The reported technique and results, pave the way to novel characterization methods for studies of solid-state physics and novel imaging techniques that can provide additional information beyond the morphological structure.

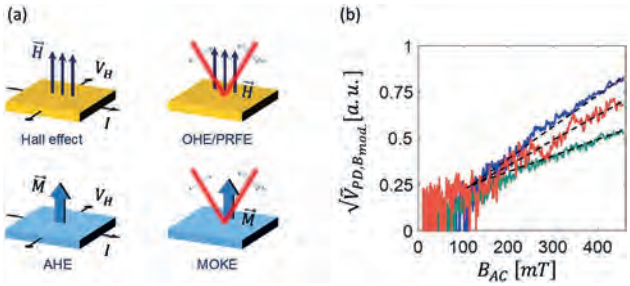

(a) Analogy between the electrical and optical Hall measurements. (b) OHE measurements for Pt, Ta and Bi_2Te_3.

GB-08. The Ferris ferromagnetic resonance technique: principles and applications. A. Rothschild[1], B.J. Assouline[1], N. Am-Shalom[1], N. Bernstein[1], G. Daniel[1], G. Cohen[1] and *A. Capua*[1] *1. The Hebrew University, Jerusalem, Israel*

Measurements of ferromagnetic resonance (FMR) are pivotal to modern magnetism and spintronics. Recently, we reported on the *Ferris FMR* technique [1], which relies on large-amplitude modulation of the externally applied magnetic field. It was shown to benefit from high sensitivity while being broadband. The Ferris FMR also expanded the resonance linewidth such that the sensitivity to spin currents was enhanced as well. Eventually, the spin Hall angle () was measurable even in wafer-level measurements that require low current densities to reduce the Joule heating. Despite the various advantages, analysis of the Ferris FMR response is limited to numerical modeling where the linewidth depends on multiple factors such as the field modulation profile and the magnetization saturation. Here [2], we describe in detail the basic principles of operation of the Ferris FMR and discuss its applicability and engineering considerations. We demonstrated these principles in a measurement of the orbital Hall effect taking place in Cu, using an Au layer as the orbital to spin current converter. This illustrates the potential of the Ferris FMR for the future development of spintronics technology.

[1] A. Rothschild, N. Am-Shalom, N. Bernstein, M. y. Meron, T. David, B. Assouline, E. Frohlich, J. Xiao, B. Yan, and A. Capua, "Generation of spin currents by the orbital Hall effect in Cu and Al and their measurement by a Ferris-wheel ferromagnetic resonance technique at the wafer level", Physical Review B 106, 144415 (2022). [2] A. Rothschild, B. Assouline N. Am-Shalom, N. Bernstein, G. Daniel, G. Cohen, and A. Capua, The Ferris ferromagnetic resonance technique: Principles and applications, AIP Advances 13, 065319 (2023).

GB-09. The combined study of Valence band structure and magnetization behaviour of Cr-VO_2 thin films using the synchrotron-based spectroscopic technique. *A. Kumari*[1] and V. Singh[1] *1. Department of Physics, Central University of South Bihar, Gaya, India*

In a rapidly evolving scientific discipline of spintronics, there is currently much interest to hunt for dilute magnetic semiconductors with high Tc, with an emphasis on the investigation of various semiconductor hosts. The electronic structure of the oxide material is thought to be altered by altering the matrix of host oxide via defect engineering or magnetic ions doping. We present the studies on the crystal, magnetic, and electronic structures of Cr-doped VO_2 thin films, i.e., $V_{1-x}Cr_xO_2$ (VCO), where x = 0, 0.05, and 0.10. These VCO films were produced by pulsed laser deposition on an r-sapphire substrate. Studies using X-ray diffraction and Raman spectroscopy demonstrate that the films are formed mostly along the a-axis and have a single monoclinic (M1) phase in VO_2 and a triclinic (T) phase in the Cr-doped VO_2 sample. The VCO films showed ferromagnetism and magnetic hysteresis when tested with Vibrating sample magnetometer (VSM) at RT. These films display a distinct hysteresis curve with a coercivity of 0.03 T, saturation magnetic field of 0.6 T, and saturation magnetic field of 0.7 T. Magnetization (Ms) ranges from 0.1 μ_B/u. c to 0.4 μ_B/u. c for x = 0 and 0.05, respectively. The measured Ms is significantly less than the calculated Cr^{3+} spin magnetic moment (3.87 μ_B/u. c). This shows that such magnetic behaviour is not only caused by Cr ions. It is crucial to understand the potential causes of such a decrease in magnetism. Valence band spectroscopy and Resonant photoemission spectroscopic measurements have been made in order to better understand the variance in the electronic structure of VCO thin films. X-ray photoelectron spectroscopy negates the possibility of Cr metal clusters in VCO films by revealing the electronic states of the Cr ion in the VO_2 matrix and their interactions with the cations. While the film's valence band spectra show that they are mostly composed of O 2*p* and Cr 3*d* derived states in VCO samples, the resonant photoemission spectra show that Cr 3*d* states and V^{5+} defect states have strongly hybridized.

GB-10. New Versatile Tool Combining Element-specific and Macroscopic Measurements. A. Aubert[1], G. Gomez[2,3], K.P. Skokov[1], F. Wilhelm[2], H. Wende[3], *A. Rogalev*[2], O. Gutfleisch[1] and K. Ollefs[3] *1. Functional Materials, Technische Universität Darmstadt, Darmstadt, Germany; 2. ESRF, Grenoble, France; 3. Faculty of Physics, University of Duisburg-Essen, Duisburg, Germany*

X-ray Magnetic Circular Dichroism (XMCD), featuring element and orbital selectivity, ability to probe very small sample volumes and extreme sensitivity, combined with the unique possibility to determine spin and orbital magnetic moments separately has developed into a workhorse technique in modern magnetism research. However, a large number of outstanding XMCD results are difficult to compare with macroscopic data, often obtained on different samples and under different experimental conditions. To address this challenge, we have initiated a project dubbed "ULMAG – ULtimate MAGnetic characterisation" aiming at development of an experimental tool by combining synchrotron- and laboratory-based techniques. The first instrument was built around the high-field XMCD end-station at the ESRF beamline ID12 [1]. It makes possible to measure under strictly the same experimental conditions the XMCD signals together with the sample magnetization; the parallel and perpendicular magnetostriction; magnetotransport and caloric properties of a bulk magnetic material as a function of magnetic field (up to 17 T) and temperature (5–325 K). The performance of this instrument is illustrated with a study of a nearly equiatomic FeRh alloy across the first-order magnetostructural transition. It was built as a prototype of a more advanced and fully dedicated setup based on a 7 Tesla split-coil superconducting magnet that offers a possibility to accommodate a 2D detector for X-ray diffraction measurements. To illustrate the potential and features of the new ULMAG setup we present a thorough study of the metamagnetic transition in $HoCo_2$ associated with large structural changes. Field induced tetragonal distortion is shown to be fully correlated with the element-specific and macroscopic magnetic properties of this crystal. The ULMAG setup is now open to all ESRF users and will serve as a unique and versatile tool to study magnetic materials in which the interplay between the magnetic, structural, and electronic subsystems is essential. This work was supported in part by the ESRF under long-term project MA-4551, and in part by the German Federal Ministry of Education and Research (BMBF) under Grant BMBF-Projekt05K2019

[1] A. Aubert et al., "Simultaneous Multi-Property Probing During Magneto-Structural Phase Transitions: An Element-Specific and Macroscopic Hysteresis Characterization at ID12 of the ESRF," in IEEE Transactions on Instrumentation and Measurement, vol. 71, pp. 1-9, 2022, Art no. 6002409

GB-11. Withdrawn

Session GC
SOFT MAGNETIC MATERIALS IV: FERRITES AND GARNETS

Liuliu Han, Chair
Max-Planck-Institut für Eisenforschung, Düsseldorf, Germany

INVITED PAPER

GC-01. Magnetic hysteresis mechanism in $Lu_{0.90}Sr_{0.10}Cr_{0.50}Fe_{0.50}O_3$ studied by Monte Carlo simulations. *F. Lurgo*[1], R. Sanchez[1], R. Carbonio[2] and O. Billoni[3] *1. Magnetic Resonance Laboratory, INN-CNEA-CONICET, San Carlos de Bariloche, Argentina; 2. INFIQC-UNC-CONICET, Córdoba, Argentina; 3. IFEG-UNC-CONICET, Córdoba, Argentina*

In this work we report magnetic properties of the orthorhombic perovskite $Lu_{0.90}Sr_{0.10}Cr_{0.50}Fe_{0.50}O_3$ synthesized by a wet chemical method [1]. As in $LuCr_{0.5}Fe_{0.5}O_3$ the compound with Sr shows the magnetization reversal phenomenon, but the magnetic order occurs at high temperatures and the temperature of compensation increases. Interestingly, in M vs H curves a hysteresis loop is observed when Cr^{4+} and Cr^{3+} ions coexist in B sites of the perovskite with Sr. To explain this behavior, we performed a numerical simulation in a magnetic model of $Lu_{1-x}Sr_xCr_{0.5}Fe_{0.5}O_3$ perovskites with x=0 and x=0.1 using a cubic lattice (see Fig. 1). We found that the ferromagnetic coupling of Fe^{3+} and Cr^{4+} through double exchange interactions increases the magnetization at high fields and that the hysteretic behavior found in simulations might be due to the coupling of the Cr^{4+} magnetic moments with the applied field, which induces a reorientation of the spins of the B lattice [2,3].

[1] F. Lurgo, S. Limandri, R. Carbonio and G. Tirao, Journal of Physics and Chemistry of Solids 157, 110200 (2021) https://doi.org/10.1016/j.jpcs.2021.110200. [2] F. Lurgo, O. Billoni, V. Pomjakushiin, J. Bolletta, C. Martin, A. Maignan and R. Carbonio, Physical Review B 103,014447 (2021) DOI: 10.1103/PhysRevB.103.014447 [3] F. Lurgo, R. Carbonio, R. Sánchez and O. Billoni. Manuscript sent to PRB.

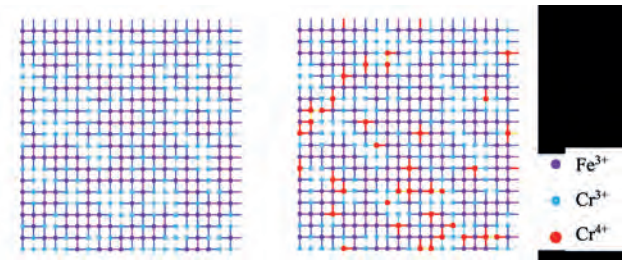

Fig. 1. Two-dimensional view of ions and magnetic interactions of the B sites in the cubic lattice. The lines of three different colors indicate the three different magnetic interactions Left: Fe^{3+} (magenta circles) and Cr^{3+} (cyan circles) ions corresponding to a system with x=0. For instance, the magenta line corresponds to Fe^{3+}-O-Fe^{3+} AFM interaction. Right: Fe^{3+} (magenta circles), Cr^{3+} (cyan circles) and Cr^{4+} (red circles) ions corresponding to a system with x= 0.1. In particular, red lines indicate Fe^{3+}-O-Cr^{4+} FM interactions, which are characteristic of this system. Notice that red circles correspond to Cr^{4+} ions which amount a ~10% of the B sites.

CONTRIBUTED PAPERS

GC-02. Wet Chemistry-Synthesized Fe/Mixed Ferrite Soft Magnetic Composites for High-Frequency Power Conversion. *W. Burgess*[1,2], J. Devkota[1,2] and B. Howard[1] *1. National Energy Technology Laboratory, Pittsburgh, PA, United States; 2. NETL Support Contractor, Pittsburgh, PA, United States*

State-of-the-art soft magnetic (SM) alloy systems such as electrical steels and permalloys exhibit large eddy current losses at high frequency (kHz range and above), limiting their application in fast switching devices. Eddy current losses can be reduced for metallic alloys through a decrease in characteristic length scale or embedding them in an insulation layer. This work proposes the development of fine-scale core materials consisting of metallic SM nano/microparticles with inorganic insulation layers having magnetic phases and their synthesis using a wet chemistry-based scalable method for high-frequency and high-power applications. More specifically, a magnetic ferrite coating ($Ni_{0.5-x}Mn_xZn_{0.5}Fe_2O_4$, x = 0.0 – 0.5) was applied via either (1) deposition of ferrite powder produced using a "wet chemistry-based" co-precipitation method, or (2) by means of a chemical reaction to a commercially available Fe-based microparticle substrate. Powder cores were synthesized by compaction of the synthesized composites. Relative magnetic permeability and core loss were measured at excitation frequencies up to 200 kHz. A core loss of 305 kW/m^3 was measured at an excitation frequency of 100 kHz and magnetization of 0.02 T. This value is similar to the value of 199.3 kW/m^3 reported in literature [1] at the same excitation conditions for a compact formed from $Ni_{0.5}Zn_{0.5}Fe_2O_4$-coated Fe microparticles (Figure 1). Scanning electron microscopy (SEM) was used to observe the microstructure of the core cross section, and X-ray diffraction (XRD) was employed to determine the effect of temperature on the integrity of the insulative ferrite layer. The effect of relative density and grain size on the core loss and relative magnetic permeability properties was also examined. The effect of ferrite coating techniques and post-processing by microwave annealing on core loss and relative magnetic permeability are being examined to potentially improve the loss properties.

[1] Y. Peng, Y. Yi, L. Li, H. Ai, X. Wang and L. Chen. Fe-based Soft Magnetic Composites Coated with NiZn Ferrite Prepared by a Co-precipitation Method. *J. Magn. Magn. Mater.*, Vol. 428, pp. 148-153 (2017).

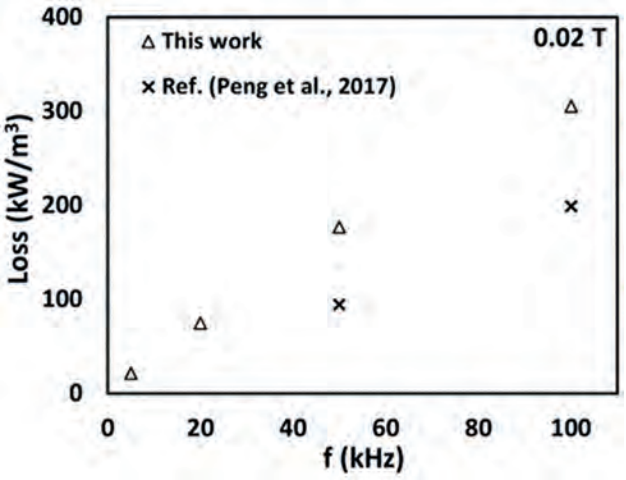

Figure 1. Core loss as a function of frequency at B = 0.02 T. Loss reported by Peng et al. [1] has also been plotted for reference.

GC-03. Influence of Controlled Dipolar Interaction for Polymer Coated Gd Doped Magnetite Nanoparticles towards Magnetic Hyperthermia Application. *K. Hazarika*[1] *1. Physics, NIT Nagaland, Dimapur, India*

To maximize heat release from immobilized nanoparticles (NPs), a detailed understanding of controlled dipolar interaction is essential for challenging magnetic hyperthermia (MH) therapies. To design optimal MH experiments, it is necessary to precisely determine magnetic states impacted by the inevitable concurrence of magnetic interactions under a common experimental form. In this work, we describe how the presence of dipolar interaction significantly alters the heating mechanism of host materials when NPs are embedded in it for MH applications. The concentration of nanoparticles and the intensity of their interaction can profoundly impact the amplitude and shape of the heating curves of the host material. The heating capability of interacting nanoparticles might be enhanced or diminished depending on their concentration within the host material. We propose a chitosan and dextran-coated Gd-doped Fe_3O_4 NPs directing dipole interactions effective for the linear regime to enlighten the pragmatic trends. The outcomes of our study may have substantial implications for cancer therapy and could inspire novel approaches for maximizing the effectiveness of magnetic hyperthermia.

[1.] Slimani, Y. et al. Impact of Sm^{3+} and Er^{3+} Cations on the Structural, Optical, and Magnetic Traits of Spinel Cobalt Ferrite Nanoparticles: Comparison Investigation. ACS Omega vol. 7 6292–6301 (2022). [2.] Hazarika, K. P.; Borah, J. P. RSC Advances Role of Site Preferred Substitution, Tuning the Magnetic Parameters, and Self Heating in Magnetic Hyperthermia Application: Eu-doped Magnetite Nanoparticles. RSC Adv. 2023, 13 (2023), 5045–5057. https://doi.org/10.1039/D2RA07924K [3.] Hazarika, K.P.; Borah, J. P. Biocompatible Tb Doped Fe_3O_4 Nanoparticles with Enhanced Heating Efficiency for Magnetic Hyperthermia Application. J. Magn. Magn. Mater. 2022, 560 (2022), 251–256. https://doi.org/10.1016/j.jmmm.2022.169597 [4.] Hazarika, K.P; Fopase, R.; Pandey, L. M.; Borah, J. P. Physica B: Physics of Condensed Matter Influence of Gd-Doping on Structural, Magnetic, and Self-Heating Properties of Fe_3O_4 Nanoparticles towards Magnetic Hyperthermia Applications. Phys. B Phys. Condens. Matter 2022, 645 (July), 414237. https://doi.org/10.1016/j.physb.2022.414237

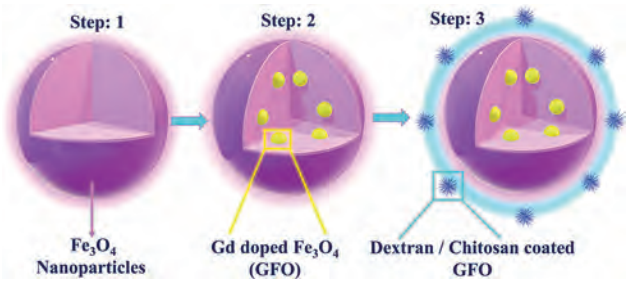

GC-04. All-around electromagnetic wave absorber based on Ni-Zn ferrite. *D. Mandal*[1], B. Bhandari[1], S.V. Mullurkara[1] and P. Ohodnicki[1]
1. Mechanical Engineering and Material Sciences, University of Pittsburgh, Pittsburgh, PA, United States

Exploring a convenient, scalable yet broadband effective electromagnetic wave absorber (EMA) is of high interest today to quench its expanding demand [1]. Herein, we investigated EM wave attenuation properties of $Ni_{0.5}Zn_{0.5}Fe_2O_4$ (NZF) samples substituting Mn^{2+} in place of Fe^{3+} ($Ni_{0.5}Zn_{0.5}Fe_{2-x}Mn_xO_4$) as well as Mn^{2+} in Zn^{2+} site ($Ni_{0.5}Zn_{0.5-x}Mn_xFe_2O_4$) within a widely used frequency range of 0.1 GHz – 9 GHz. Among the sample sets, the optimized sample shows excellent microwave absorption with a maximum reflection loss (*RL*) of -50.2 dB, wide bandwidth (*BW*) (*RL* < −10 dB, i.e., attenuation >90%) of 6.8 GHz at thickness (*t*) of only 6 mm (presented in Fig. 1). Moreover, attenuation constant (α) is found to exhibit a significant increment from ~217 Np/m to 301 Np/m with Mn-doping in NZF. The key contribution arises from magnetic-dielectric properties synergy along with enhanced dielectric and magnetic losses due to the cation rearrangement in spinel NZF. In addition, porosity is induced to the system with a controlled two-step heat treatment that promotes the total loss with multiple internal scattering of the EM wave [2]. Besides the thickness dependent study, *RL* is simulated considering transmission line theory by varying incident EM wave angles for the optimized sample displaying its angle insensitiveness up to 50 degrees. Hence, this study demonstrates Mn-substitution in NZF as an effective strategy and the porosity induced optimum NZF sample as a futuristic wave absorber suitable for practical high-frequency applications.

[1] L. Wang, X. Li, X. Shi, M. Huang, X. Li, Q. Zeng, R. Che, Recent progress of microwave absorption microspheres by magnetic-dielectric synergy, Nanoscale. 13 (2021) 2136–2156. https://doi.org/10.1039/d0nr06267g. [2] D. Mandal, K. Mandal, Enhancement of electromagnetic wave absorption in $MnFe_2O_4$ nano-hollow spheres, J. Appl. Phys. 129 (2021). https://doi.org/10.1063/5.0039560.

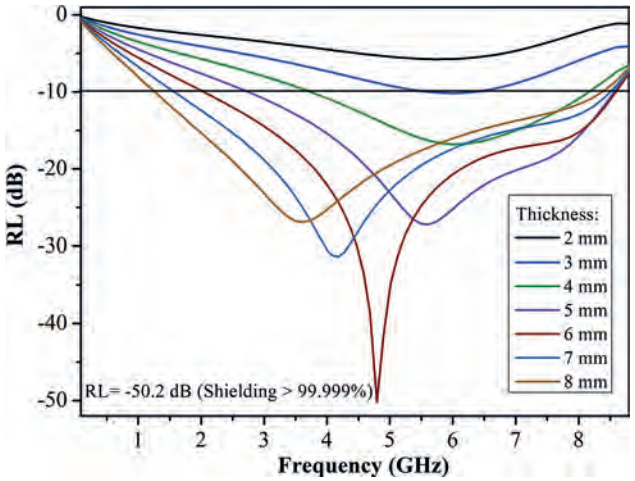

Fig. 1: Thickness dependent reflection loss vs. frequency study showing maximum *RL* for the optimized Mn-doped NZF core.

GC-05. First-principles Study on Electronic Properties of Rare-earth Iron Garnet Mixed Crystals. *Y. Yahagi*[1], Y. Omori[1] and M. Ishida[1]
1. NEC Corporation, Tsukuba, Japan

We study the electronic properties of rare-earth iron garnet (RIG) mixed crystals with special attention to their composition dependence. Magnetic insulators in RIG, $R_3Fe_5O_{12}$ (where R is a rare-earth ion, e.g., Y), are at the heart of fundamentals and applications of magnonic devices due to their notably low Gilbert damping [1]. Although research on RIG is extensive, most of it has focused on only a few areas of composition and remains insufficiently systematic. Composition optimization under systematic exploration is desirable to satisfy the required performance at a level of practical use. In this study, we perform systematic first-principles calculations for (Y_x, Lu_1-x)IG mixed crystals based on a Kohn-Sham density functional theory (DFT) in a plane wave pseudo-potential approach [2]. We use full relativistic ultrasoft pseudo-potential in this work. We apply PBE-GGA functional with Hubbard-U for Fe d states. Instead of taking configurational average on mixed structures, we apply the virtual crystal approximation (VCA) [3]. Figure is a calculation result of lattice constant optimized by fitting with the Birch--Murnaghan equation of state, indicating a systematic decrease from the expectation of Vegard's law. Moreover, the Y-rich region shows a remarkable deviation with approximately 0.5% change of the lattice constant. Therefore, tuning x of (Y_x, Lu_1-x)IG in the range of 0.8 to 1.0 is effective in optimizing lattice constants and thus improving film quality. Further results in other compositions of RIG will be presented at the conference. This work was supported by JST-CREST (JPMJCR20C1)

[1] L. J. Cornelissen, *et al.*, Nature Physics 11, 1022-1026 (2015). [2] P. Giannozzi, *et al.*, J.Phys.: Condens. Matter 21, 395502 (2009). [3] L. Bellaiche, and D. Vanderbilt, Phys. Rev. B 61, 7877 (2000).

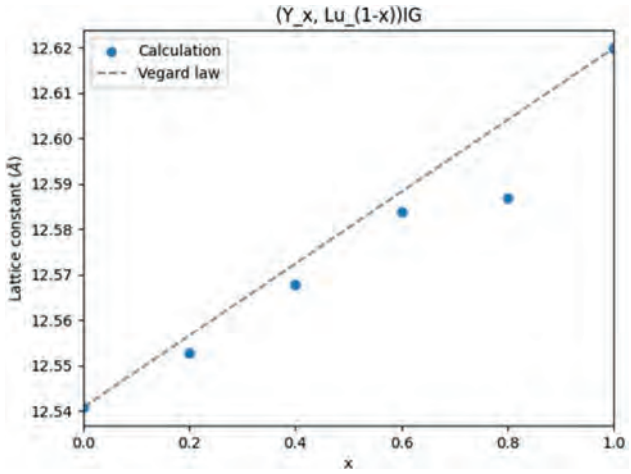

Calculation results of lattice constants of (Y, Lu)IG for each composition.

GC-06. Combinatorial FMR and MOKE measurement on magnetic garnet dots. *Y. Omori*[1], H. Someya[1] and M. Ishida[1] *1. NEC, Tokyo, Japan*

Magnetic Garnets (MGs) such as Yttrium Iron Garnet (YIG: $Y_3Fe_5O_{12}$) are recently attractive type of magnets for the use of application and also for the stage of research of physical phenomena. Especially the small gilbert damping and strong magneto-optic effects are the important features for the magnetic devices [1]. For instance, it is pointed that YIG dots have potential to be used for probabilistic bit operation [2]. It will be beneficial to find MGs with both small gilbert damping and strong magneto-optic effects. There has been numerous studies on MG films, however, the exploration space are vast when considering mixed crystal systems, and the development of fabrication processes requires significant effort. Systematic experimental study are necessary for MGs. In this study, we performed combinatorial experiments for MGs. First, we performed combinatorial magnetron sputtering to obtain widely different composition ratio in a single substrate. For instance, $(Y_xLu_yBi_{1-x-y})$IGs were sputtered as shown in Fig.1. The films were fabricated to the dot shapes. By using the Vector Network Analyzer and the semi-auto prober system, the Ferromagnetic Resonance (FMR) properties of the hundreds samples of different conditions were measured in a few hours. Also, the Magneto-Optic Kerr Effects (MOKEs) were measured for these dots. We observed the FMR and the MOKE can be more significant in mixed crystal region. The more detailed effect of the composition ratio, doped elements and the processes will be discussed at the presentation. This work was supported by JST-CREST (JPMJCR20C1).

[1] Y Yang, et al., "Recent advances in development of magnetic garnet thin films for application in spintronics and photonics", Journal of alloys and Compounds 860 158235 (2021). [2] T. Makiuchi, et al., "Parametron on magnetic dot: Stable and stochastic operation", Appl. Phys. Lett. 118, 022402 (2021).

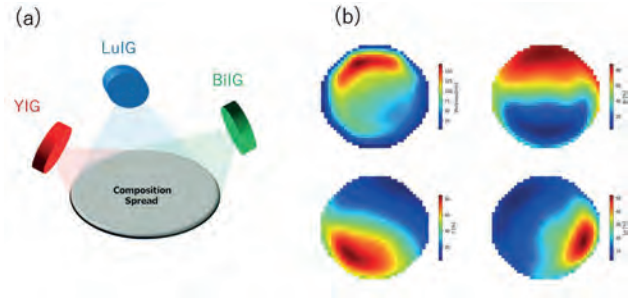

Fig. 1: (a) Schematic of combinatorial sputtering technique. Different garnets or oxides were co-sputtered to a substrate and we obtained a composition-spread film. (b) The composition ratios and the thickness were mapped.

GC-07. Withdrawn

GC-08. Magnetic interactions and reversal mechanisms of spinodally decomposed cobalt ferrites as a function of temperature using first order reversal curves (FORC). *S.V. Mullurkara*[1], R. Egli[2], B.C. Dodrill[3], C. Radu[3], S. Tan[4] and P. Ohodnicki[1] *1. MEMS, University of Pittsburgh, Pittsburgh, PA, United States; 2. Zentralanstalt für Meteorologie und Geodynamik (ZAMG), Vienna, Austria; 3. Lake Shore Cryotronics, Westerville, OH, United States; 4. Electrical and Computer Engineering, University of Pittsburgh, Pittsburgh, PA, United States*

Cobalt ferrites are cubic spinel ferrites given by the chemical formula AB_2O_4 with A and B being divalent and trivalent cations. Cobalt ferrites have been shown to undergo spinodal decomposition to form periodic microstructures with nanometer characteristic length scales. Resultant changes in magnetic properties have been shown to be dependent on the periodicity and degree of decomposition which can be controlled by selection of relevant thermal processing parameters. Previous investigations have shown the periodic variation in composition results in spatial variations of intrinsic magnetic properties and magnetic interactions to yield wasp-waisted major hysteresis loops indicative of multiple magnetization reversal events. Moreover, large coercive fields have been measured at lower temperatures with enhanced wasp-waisting. Detailed analysis requires advanced magnetometry techniques to disentangle reversible, irreversible, and viscous magnetization processes and their dependence on the previous magnetic history. In this work, cobalt ferrite samples have been synthesized using standard powder processing techniques. Different aging treatments have been achieved by varying the annealing time from 24 to 120hrs and at 500 & 700 °C within the coherent spinodal range. TEM and XRD has been used to determine periodicity, degree of decomposition, lattice parameters, lattice mismatch and coherency strains between decomposed phases at the nm length scale. Magnetization processes occurring in these materials have been investigated through vibrating sample magnetometry using major M-H loops and

temperature-dependent magnetization. These measurements have been complemented with both saturating and non-saturating high-resolution first order reversal curve (FORC) diagrams, the latter obtained with different pre-conditioning fields, in order to explore magnetic states inaccessible from the major loops. These measurements were also repeated at cryogenic temperatures to disentangle the various switching events and magnetic interactions occurring in the material. Finally, the corresponding features observed in the FORC diagrams have been identified and correlated with microstructural observations.

Suraj V. Mullurkara, Ramon Egli, B. C. Dodrill, Susheng Tan, P. R. Ohodnicki; Understanding magnetic interactions and reversal mechanisms in a spinodally decomposed cobalt ferrite using first order reversal curves. *AIP Advances* 1 February 2023; 13 (2): 025328. https://doi.org/10.1063/9.0000562

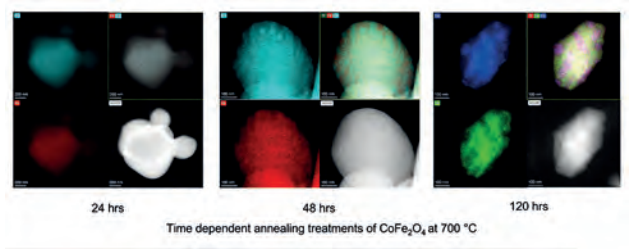

Figure 1. EDS of $Co_{1.8}Fe_{1.2}O_4$ aged at 700°C

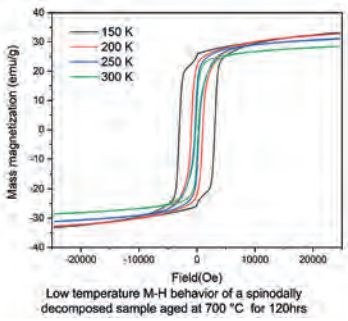

Figure 2.

Session GD
SPIN INJECTION AND SPIN TORQUE DEVICES

Ryo Ohshima, Chair
Kyoto University, Kyoto, Japan

INVITED PAPER

GD-01. Topological spintronics in epitaxial Dirac and Weyl semimetal heterostructures. *N. Samarth*[1], W. Yanez[1] and Y. Ou[1] *1. Physics, Penn State University, University Park, PA, United States*

The notion of 'topological spintronics' began with the intuition that spin-momentum correlation in the helical Dirac states of topological insulators might be efficiently exploited for efficient spin-charge interconversion [1]. In this talk, we describe the extension of this idea into the realm of topological semimetals wherein we probe spin-charge conversion via bulk states with Dirac dispersion. We first describe the molecular beam epitaxy (MBE) and characterization of thin films of Dirac semimetals (Cd_3As_2, $ZrTe_2$, TaAs, NbAs), showing that the Dirac nature of the band structure can be verified using *in vacuo* angle resolved spectroscopy measurements in the first two materials [2,3]. After interfacing these films with $Ni_{0.8}Fe_{0.2}$, we use spin torque ferromagnetic resonance (ST-FMR) to measure spin-charge interconversion at room temperature and find reasonable agreement with theoretical calculations of the spin Hall conductivity. We also demonstrate the clean epitaxial growth of ferromagnetic $CrTe_2$ on $ZrTe_2$, allowing the demonstration of current driven spin-orbit torque switching of a 2D ferromagnet by a Dirac semimetal in a wafer-scale van der Waals platform [3]. We next discuss the synthesis by MBE of Weyl semimetal thin films (TaAs, NbAs) [4,5] and the systematic measurement of ST-FMR in heterostructures that interface these films with $Ni_{0.8}Fe_{0.2}$ [4]. Finally, we discuss the serendipitous (and currently unexplained) finding that an oxidized interface may enhance the spin-charge conversion efficiency in some of these heterostructures and can reverse the sign of the spin Hall conductivity. This work was sponsored in part by SMART, a funded center of nCORE, a Semiconductor Research Corporation (SRC) program sponsored by NIST, the Institute for Quantum Matter under DOE EFRC grant DE-SC0019331, and the Penn State Two-Dimensional Crystal Consortium-Materials Innovation Platform (2DCC-MIP) under NSF Grant No. DMR- 2039351.

1. A. R. Mellnik, *et al.*, "Spin-transfer torque generated by a topological insulator," *Nature* 511, 449 (2014). 2. W. Yanez *et al*., "Spin and charge interconversion in Dirac semimetal thin films," *Physical Review Applied* 16, 054031 (2021). 3. Y. Ou *et al*., "$ZrTe_2/CrTe_2$: an epitaxial van der Waals platform for spintronics," *Nature Communications* 13, 2972 (2022). 4. W. Yanez *et al*., "Giant dampinglike-torque efficiency in naturally oxidized polycrystalline TaAs thin films," *Physical Review Applied* 18, 054004 (2022). 5. W. Yanez *et al*., "Thin film growth of the Weyl semimetal, NbAs," arXiv:2304.13959

CONTRIBUTED PAPERS

GD-02. Efficient Spin-Orbit Torque Switching with Large Damping-Like Torque in Bi_2Se_3/Fe_3GeTe_2 van der Waals Heterostructures. M. Lohmann[1], D. Wickramaratne[1], J. Moon[1], M. Noyan[1], H. Chuang[1], B.T. Jonker[1] and *C.H. Li*[1] *1. Naval Research Lab, Washington, DC, United States*

Topological insulators (TIs) have shown promise as a spin-generating layer to switch the magnetization state of ferromagnets via the spin-orbit torque (SOT) effect due to efficient charge-to-spin conversion efficiency of the TI surface states that arises from spin-momentum locking. However, when TIs are interfaced with conventional bulk ferromagnetic metals, the combination of charge transfer and hybridization can potentially destroy the spin texture and hampers the possibility of accessing the TI surface states. Here we fabricate an all van der Waals (vdW) heterostructure consisting of molecular beam epitaxy grown bulk-insulating Bi_2Se_3 and 2D metallic ferromagnet Fe_3GeTe_2 (FGT). By detecting the magnetization state of the FGT via the anomalous Hall effect and magneto-optical Kerr effect measurements, we determine the critical switching current density for magnetization switching to be $1.2x10^6$ A/cm2, the lowest reported for the switching of a perpendicular anisotropy ferromagnet using Bi_2Se_3. From second harmonic Hall measurements, we further determine the SOT efficiency to be comparable to the highest values reported for Bi_2Se_3. Through first-principles calculations, we attribute these results to the weak interlayer interaction at the Bi_2Se_3/FGT interface, which leads to low or no proximity-induced magnetism and the preservation of the in-plane nature of the spin texture associated with the spin-generating Bi_2Se_3 states at the Fermi level. Our results highlight the clear advantage of all-vdW heterostructures with weak interlayer interactions that can enhance SOT efficiency and minimize critical current density, an important step towards realizing next generation low-power non-volatile memory and spintronic devices.

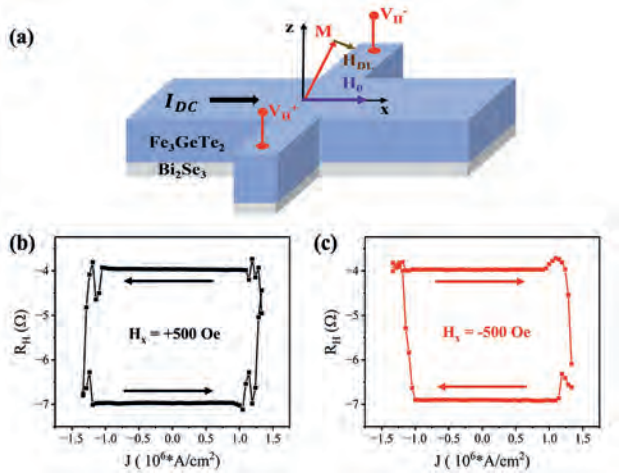

Pulsed current magnetization switching in Bi_2Se_3/FGT van der Waals heterostructure. (a) Schematic diagram of the damping-like effective field responsible for magnetization switching. (b,c) Hall resistance measured at T = 50 K following the application of each 50 μs current pulse with fixed in-plane bias field (b) H_x = 500 Oe and (c) H_x = -500 Oe. The reversal of loop chirality when bias field is reversed indicate the SOT from the Bi_2Se_3 is the source of observed magnetization reversal.

GD-03. Current-induced magnetization switching by two-dimensional van der Waals material $ZrSe_3$. L. Cao[1], Q. Chen[1], Y. Zhu[1], K. Tong[2], J. Ma[2], *Z. Huang*[1], J. Wu[2] and Y. Zhai[1] *1. Key Laboratory of Quantum Materials and Devices of Ministry of Education, School of Physics, Southeast University, Nanjing, China; 2. Department of Physics, Engineering and Technology, University of York, York, United Kingdom*

Two-dimensional van der Waals (2D vdW) materials are widely used in spin-orbit torque (SOT) devices. Compared with other 2D semiconductors such as WS_2 and MoS_2, 2D vdW $ZrSe_3$ shows a lower resistivity and the broken crystal symmetry, which are beneficial for SOT devices with low power consumption [1]. Here, we study SOTs and current-induced magnetization switching in $ZrSe_3$ (10nm)/Py ($Ni_{80}Fe_{20}$,10nm) and $ZrSe_3$ (10nm)/Cu (1nm)/Py (10nm) heterostructures. SOT efficiencies of samples are detected by the spin-torque ferromagnetic resonance (ST-FMR) and an out-of-plane damping-like torque () is observed. decreases from 0.175 to 0.138 when insert 1 nm Cu at the interface, indicating that Cu intercalation inhibits the component of SOT. However, the SOT efficiency is increased from 3.05 to 3.23, which may be attribute to the spin absorb of $ZrSe_3$ and Cu intercalation is beneficial to improve the interface between Py and $ZrSe_3$. [2,3]. Furthermore, MOKE microscopy is employed to verify the current-driven magnetization switching in these structures. Compared with $ZrSe_3$/Py bilayer, the critical current of $ZrSe_3$/Cu/Py is reduced when insert 1nm Cu as shown in Fig.1, demonstrating the higher SOT efficiency and lower power consumption in $ZrSe_3$/Cu/ Py structures. This work is support by National Natural Science Foundation of China (Nos. 52071079, 12274071,12104484).

[1] Y. Zhu et al., J Alloy. Comp. 2022, 918, 165579. [2] P. Debashis et. al., npj 2D Mater. Appl., 2020, 4,18. [3] Q. Xiu et al., Adv. Mater. 2019, 31, 1900776.

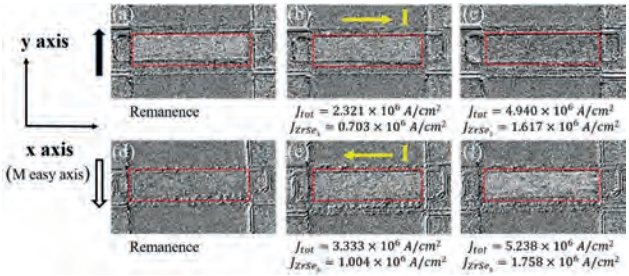

Fig. 1. MOKE images of the current induced magnetization switching in $ZrSe_3$/Cu/Py structure at zero magnetic field. The dark (light) arrow represents the initial magnetization direction along +y (-y).

GD-04. Anomalous Hall effect in heavy metal/ ferrimagnetic Mn_4N epitaxial bilayers. *W. Mi*[1] *1. Department of Applied Physics, Tianjin University, Tianjin, China*

Spin-orbit torque has attracted much attention due to the potential applications in memory and logic devices [1]. The perpendicular magnetic anisotropy and low saturation magnetization make rare-earth-free Mn_4N a promising candidate for spin-orbit torque applications [2]. Here, the anomalous Hall effect of the facing-target sputtered Pt/Mn_4N bilayers on MgO (001) substrates have been investigated systematically. Fig. 1(a) shows XRD θ-2θ patterns of Pt/Mn_4N bilayer, Mn_4N film and MgO (001) substrate. The diffraction peaks from Mn_4N and Pt layer are observed, which suggests the Mn_4N and Pt layer grow with a preferred (001) and (111) orientation, respectively. Fig. 1(c) diplays the TEM image of the Pt(36 nm)/Mn_4N(60 nm) bilayer, which shows that Mn_4N/MgO and Pt/Mn_4N interfaces are sharp. As is shown in Fig. 1(c), temperature-dependent sign reversal of anomalous Hall resistivity appears in Pt/Mn_4N bilayers, which is dominated by the competition between the magnetic proximity and spin Hall effects. Fig. 1(d) indicates that the magnitude of anomalous Hall resistivity can be manipulated by applied current density. This work was supported by the National Natural Science Foundation of China (52271185).

[1] A. Brataas and K. M. D. Hals, Spin-orbit torques in action, Nat. Nanotechnol. 9, 86 (2014). [2] Y. Yasutomi, K. Ito, T. Sanai, K. Toko, and T. Suemasu, Perpendicular magnetic anisotropy of Mn_4N films on MgO (001) and $SrTiO_3$ (001) substrates, J. Appl. Phys. 115, 17A935 (2014).

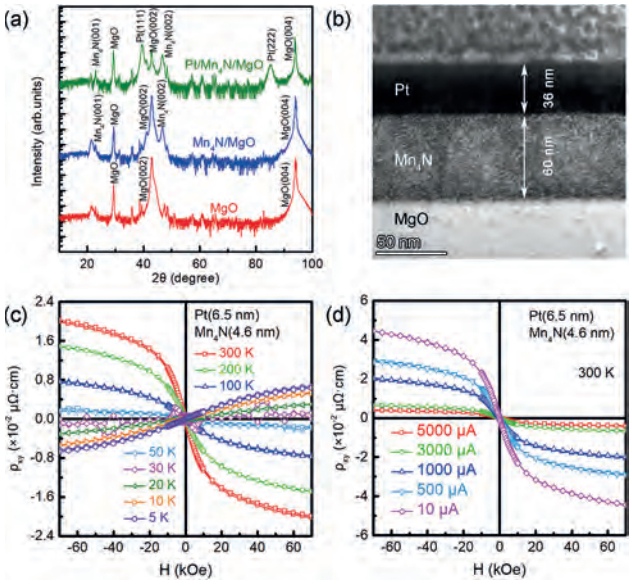

Fig. 1. (a) XRD θ-2θ patterns and (b) TEM image of Pt/Mn_4N bilayer. ρ_{xy}-*H* curves of Pt/Mn_4N bilayers measured with (c) different temperatures and (d) different applied current densities.

GD-05. Ultra-fast spin transfer torque switching in ferrimagnetic tunneling junctions. *P. Khanal*[1], B. Zhou[1], A. Enriquez[1], K. Warrilow[1], A.T. Habiboglu[1], J. O'Brien[1] and W. Wang[1] *1. Physics, University of Arizona, Tucson, AZ, United States*

The spin transfer torque (STT) switching of ferrimagnetic tunneling junctions is of great interest due to the potential fast dynamics compared to conventional magnetic tunneling junctions (MTJs) with ferromagnetic free layers. Perpendicular MTJs with GdCoFe free layers have been investigated, however the sub-ns STT switching in this system has not been thoroughly explored. One of the reasons is the low tunneling magnetoresistance (TMR) exhibited by this system. By employing a unique approach, we successfully achieved TMR ratios exceeding 45% in pMTJs with GdCoFe free layers. The room temperature transport measurements have been done to study the magnetoresistance of ferrimagnetic tunneling junctions. Fig. 1 (a) illustrates the TMR as a function of Gd concentration whereas, the inset shows the dependance of coercive field (H_C) on Gd concentration. The H_C first increases, reaches its maximum value, and decreases again, which is a typical signature of magnetization compensation. Fig. 1 (b) and (c) represent the TMR curves for the CoFe and Gd dominating regions respectively. STT switching experiments were carried out to study the switching dynamics of ferrimagnetic tunneling junctions down to 100ps. The switching probability (P) as a function of pulse duration (τ) is shown in Fig. 2, where blue (black) curve represents the results of pMTJs with ferromagnetic (ferrimagnetic) free layers. An obvious increase of switching speed has been observed in pMTJs with ferrimagnets, suggesting ferrimagnetic tunneling junctions are great candidates for high-speed, energy-efficient applications. This work is supported by the National Science Foundation.

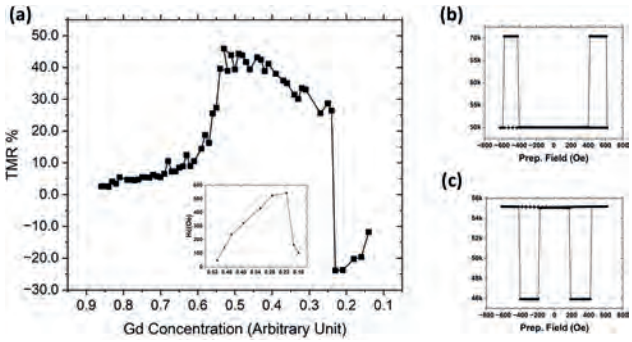

Fig. 1. (a) Gd concentration dependence of TMR in the ferrimagnetic tunneling junctions. Inset represents the coercive field (H_C) as a function of Gd concentration. (b) and (c), representative TMR curves of the ferrimagnetic tunneling junctions in the CoFe-rich and Gd-rich regions, respectively.

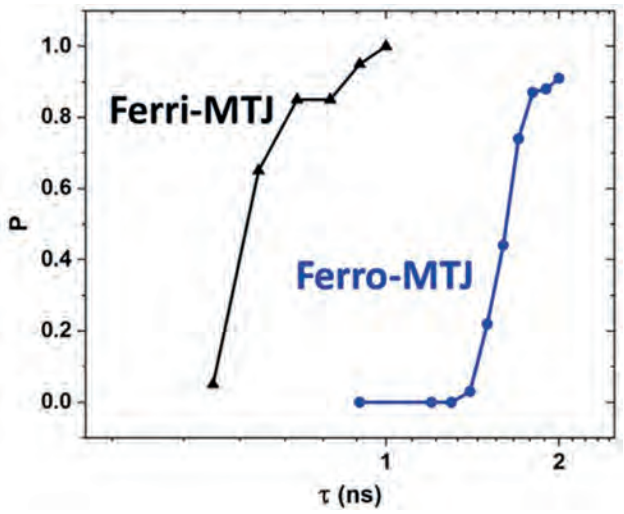

Fig. 2. Switching probability (P) as a function of pulse duration (τ) in pMTJs with ferrimagnetic and ferromagnetic free layers.

GD-06. Spin Polarization and Magnetoresistance in a Si-based Spin MOSFET. *S. Sato*[1,2], M. Tanaka[1,2] and R. Nakane[1,3] *1. Dept. of Electrical Eng. and Information Systems, Graduate School of Engineering, The University of Tokyo, Tokyo, Japan; 2. Center for Spintronics Research Network (CSRN), Graduate School of Engineering, The University of Tokyo, Tokyo, Japan; 3. System Design Lab (d.lab), Graduate School of Engineering, The University of Tokyo, Tokyo, Japan*

Si-based spin MOSFETs [1-4] have been actively studied owing to their potential applications to low-power electronics leveraging nonvolatility. A significant challenge currently faced for practical applications is insufficient magnetoresistance (MR) ratio (<0.2% [2-4]). To address this issue, Fe/Mg/MgO/SiOx/n^+-Si junctions are promising as they can generate a high spin polarization P_S (~42%) of electrons in n^+-Si substrates [5]. Our previous study revealed that the P_S value decreases with increasing the junction voltage drop V_J. Considering that the junction resistance R_J decreases with increasing V_J, it is important to clarify how the MR ratio is enhanced when this junction structure is used for a spin MOSFET by characterizing both P_S value and MR ratio with various V_J values. Figure 1 shows our spin MOSFET structure that has Fe(3 nm)/Mg(1 nm)/MgO(1.2 nm)/SiO$_x$(0.2 nm)/n^+-Si for the source (S) and drain (D) junctions, a p-type 8-nm-thick Si for the inversion channel, and a buried SiO_2 layer for the gate dielectric. First, the spin-valve signal ΔV_{SV} was estimated from the change in V_{DS} with a constant current I_{SD} (= –4 ~ 4 mA) and a gate voltage V_{GS} = 40 V, and a sweeping in-plane magnetic field $H_{//}$. Then, P_S was estimated from ΔV_{SV} using the same method as shown in our previous papers [3,4]. Other parameters were calculated as follows: $V_J = [V_{DS} - I_{SD}\times(\text{channel resistance})]/2$ and the MR ratio = $\Delta V_{SV}/V_{DS}$. Figure 2 shows P_S (blue dots, left axis) and MR ratio (red dots, right axis) plotted as a function of V_J, in which P_S has a positive peak at $|V_J|$ = ~0.3 V. A distinctive feature is that a high P_S value of ~48% is achieved in the spin MOSFET. On the other hand, the MR ratio has a positive peak of 0.35% at $|V_J|$ = ~0.8 V and the peak position is higher than that for P_S. From detailed analyses we found that the MR ratio is limited by the large parasitic resistance of R_J when $|V_J|$ = ~0.3 V, despite the high P_S value. Therefore, a matching of these two peaks at the same V_J value is required to further enhance the MR ratio.

[1] S. Sugahara and M. Tanaka, Appl. Phys. Lett. 84, 2307 (2004). [2] T. Tahara et al., APEX 8 113004 (2015). [3] S. Sato et al., Phys. Rev. B. 99, 165301 (2019). [4] S. Sato et al., Phys. Rev. Appl. 18, 064071 (2022). [5] R. Nakane et al., Phys. Rev. Mater. 3, 024411 (2019). [6] Baisen Yu et al., JSAP Spring Meeting, 23p-E205-9 (2022). This work was partially supported by CREST of JST (No. JPMJCR1777), Spintronics Research Network of Japan, and Grants-in-Aid for Scientific Research (Grant 23H00177).

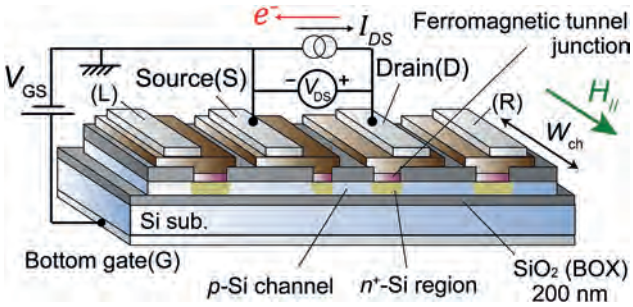

Fig.1 Schematic illustration of our spin MOSFET structure and measurement setup.

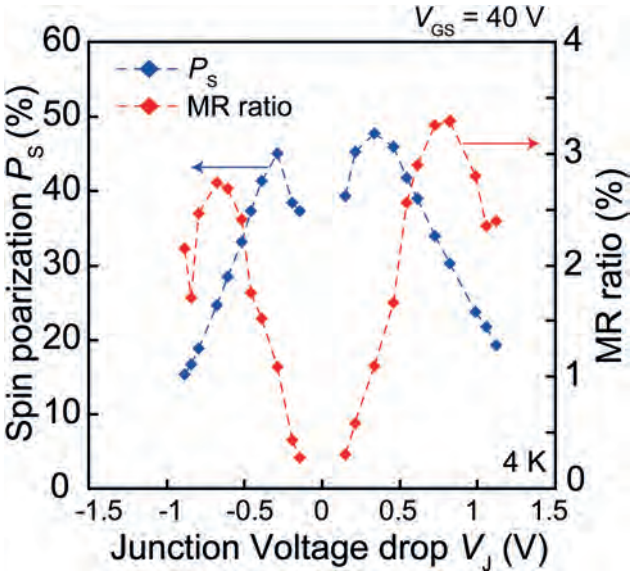

Fig.2 Spin polarization P_S (left axis) and the MR ratio (right axis) as a function of the junction voltage drop V_J.

GD-07. Spin Signal Optimization in Metallic Non-Local Spin Valves via Tuned Interface Resistance. *B. Kaiser*[1], J. Ramberger[1], M. Norum[1], J.E. Dewey[1] and C. Leighton[1] *1. Chemical Engineering and Material Science, University of Minnesota - Twin Cities, Minneapolis, MN, United States*

Hard disk readers based on magnetic tunnel junctions have enjoyed great success. However, they now face challenges due to high resistance-area products (*RA*), which limit signal-to-noise ratios due to impedance mismatch [1]. There is thus interest in exploring all-metal spintronic devices, particularly spin accumulation sensors based on non-local spin valves (NLSVs) [2]. Enhancing spin signal in metallic NLSVs is highly desirable both for applications and fundamentals. One approach to significant signal gains is incorporating "tunnel" contacts that mitigate back-diffusion of injected spins [3-6]. However, the relationships between spin signal, interfacial *RA*, and tunneling spin polarization are poorly understood. Here, we tune *RA* in highly-spin-polarized Al/$Co_{75}Fe_{25}$ NLSVs (Fig. 1b, inset) [7], from the tunneling limit (10^6 Ω μm^2) to transparent interfaces (10^{-3} Ω μm^2) by controlled oxidation of ~10-nm-thick Al. Ultrahigh-vacuum multi-angle evaporation into electron-beam-lithographic masks is used. As shown in Fig. 1, over a wide *RA* range, both conductance-voltage and *RA*-temperature dependencies suggest tunneling transport. Notably, Al oxidation in 1 mTorr of O_2, to an *RA* of only 0.4 Ω μm^2, already induces 2-order-of-magnitude increases in spin signal relative to transparent interfaces (Fig. 2a). Full analysis reveals that this increase is only partly due to enhanced polarization, but also, surprisingly, an unanticipated enhancement of spin diffusion length (Fig. 2b). This leads to the remarkable conclusion, supported by additional experiments, that controlled oxidation of Al channels leads to larger spin diffusion length than natural oxidation, of high interest for applications. Work supported by the National Science Foundation and Advanced Storage Research Consortium.

[1] T. Nakatani, Z. Gao, and K. Hono, MRS Bull. 43, 106 (2018) [2] H. Takagishi, K. Yamada, and H. Iwasaki, IEEE Trans. Mag. 46, 2086 (2010) [3] S. Takahashi, and S. Maekawa, Phys. Rev. B 67, 052409 (2003) [4] F.J. Jedema, H.B. Heersche, J. J. A. Baselmans, Nature 416, 713 (2002). [5] S.O. Valenzuela, and M. Tinkham, Appl. Phys. Lett. 85, 5914 (2004). [6] A. Vogel, J. Wulfhorst, and G. Meier, Appl. Phys. Lett. 94, 122510 (2009). [7] B. Kaiser, J. Ramberger J.D. Watts, APL Materials 11, 051108 (2023).

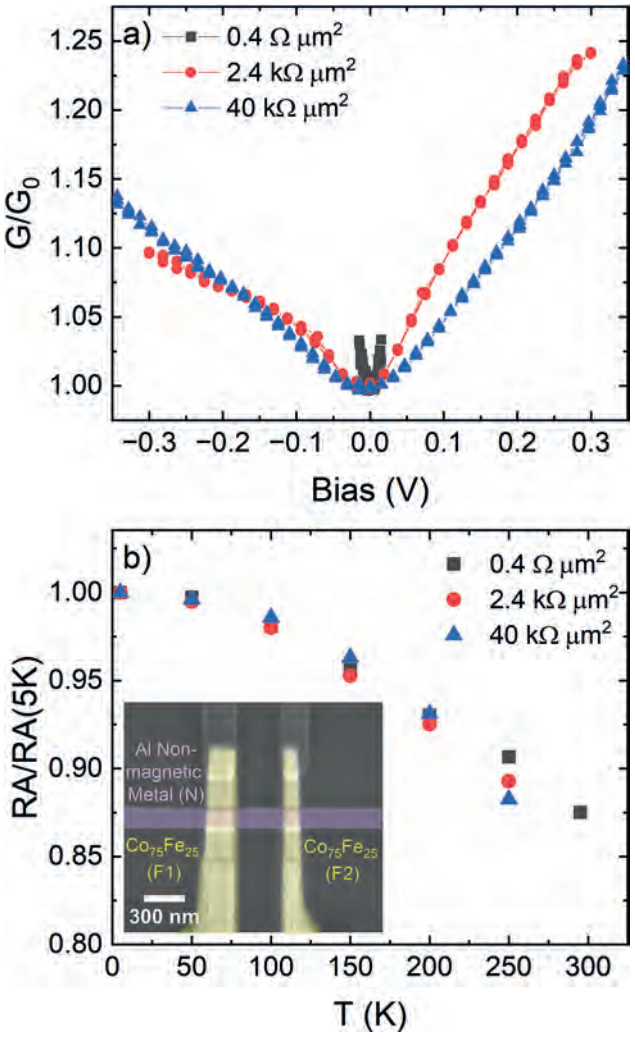

Fig. 1: a) Normalized conductance of Al/AlO_x/$Co_{75}Fe_{25}$ interfaces *vs.* bias for three oxidation conditions with three *RA*. b) Temperature dependence of *RA* for each device in (a). Inset: Scanning electron micrograph of an NLSV.

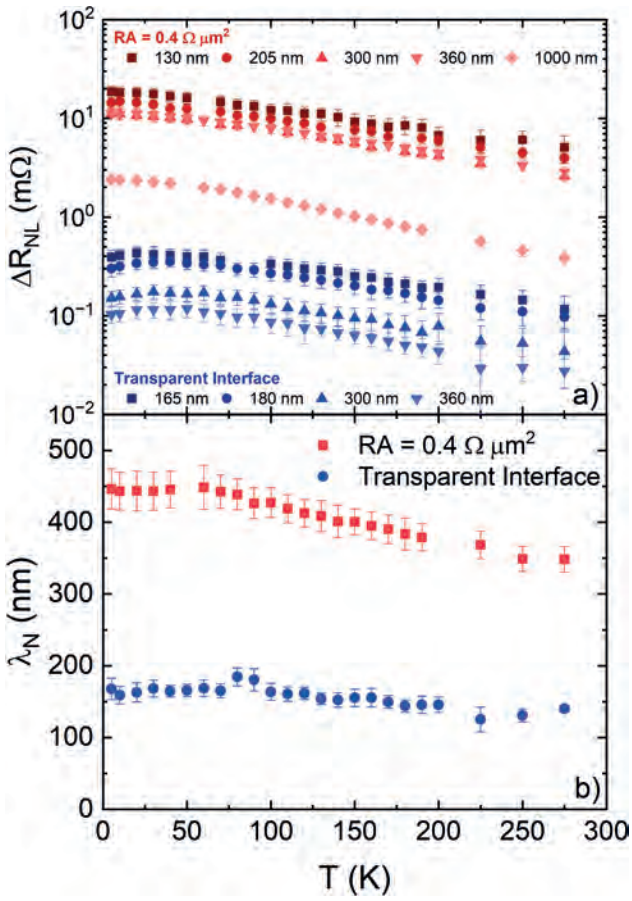

Fig. 2: a) Temperature dependence of the spin signal in Al/$Co_{75}Fe_{25}$ NLSVs with transparent interfaces (blue), and with Al oxidized in 1 m Torr of O_2 for 20 min (red). b) Corresponding spin diffusion length (l_N).

GD-08. Influence of exchange coupling torque in hybrid spin transfer torque and spin-orbit torque switching of synthetic antiferromagnets. *V. Kateel*[1,2], T. Vantilt[1], S. Van Beek[1], M.G. Monteiro[1], G. Talmelli[1], B. Soree[1,2], J. De Boeck[1,2], S. Couet[1] and S. Rao[1] *1. IMEC, Leuven, Belgium; 2. KU Leuven, Leuven, Belgium*

Full electrical control of perpendicular magnetic tunnel junction (pMTJ) has made magneto-resistive random-access memory (MRAM) technology an attractive option to replace existing charge-based memories due to its non-volatility, high endurance, and high density [1]. Traditionally, the reversal of a single free layer (FL) in pMTJs can either be achieved by the spin transfer torque (STT) effect caused by a current flowing through the pMTJ stack or by the spin-orbit torque (SOT) effect induced due to the current through a SOT layer beneath the pMTJ. Though both effects are promising, they face challenges – high switching current in STT-MRAM, while SOT MRAM needs a field for deterministic switching. Combining both torque effects is an exciting method to overcome the drawbacks of individual technologies [2,3]. However, a single FL is unsuitable for applications because of low retention and large stray fields from the reference layer. Incorporating a hybrid FL design (Fig. 1a) with a Co-based synthetic antiferromagnet (SAF) coupled ferromagnetically with a CoFeB (SAF-HFL) has been demonstrated to overcome former challenges [1,4]. In this work, we perform micromagnetic simulations to understand the dynamics of hybrid STT+SOT switching on SAF-HFL. We study 80 nm-sized SAF-HFL with STT acting on CoFeB and SOT acting on the Co-I. In the absence of an in-plane field, we observe switching with the assistance of an STT current (Fig. 1b). STT+SOT switching causes a loss of SAF coupling during reversal, indicating there is competition between the current-induced torques and exchange coupling torques. Furthermore, we observe an incubation delay and a significant transition time during the reversal. In this talk, we will explain the role of individual torque by varying the currents, field-like torque, and Dzyaloshinskii–Moriya interaction. Finally, the importance of exchange coupling strength on the required switching energy and magnetization dynamics is also investigated. These insights will help in developing an energy-efficient MRAM with SAF-HFL design.

[1] S. Couet *et al*., "BEOL compatible high retention perpendicular SOT-MRAM device for SRAM replacement and machine learning," *2021 Symposium on VLSI Technology*, 2021, pp. 1-2. [2] M. Wang, *et al.* Field-free switching of a perpendicular magnetic tunnel junction through the interplay of spin–orbit and spin-transfer torques. *Nat Electron* 1, 582–588 (2018). [3] W. Cai *et al*., "Sub-ns Field-Free Switching in Perpendicular Magnetic Tunnel Junctions by the Interplay of Spin Transfer and Orbit Torques," in *IEEE Electron Device Letters*, vol. 42, no. 5, pp. 704-707, May 2021. [4] E. Raymenants, *et al.* Nanoscale domain wall devices with magnetic tunnel junction read and write. *Nat Electron* 4, 392–398 (2021).

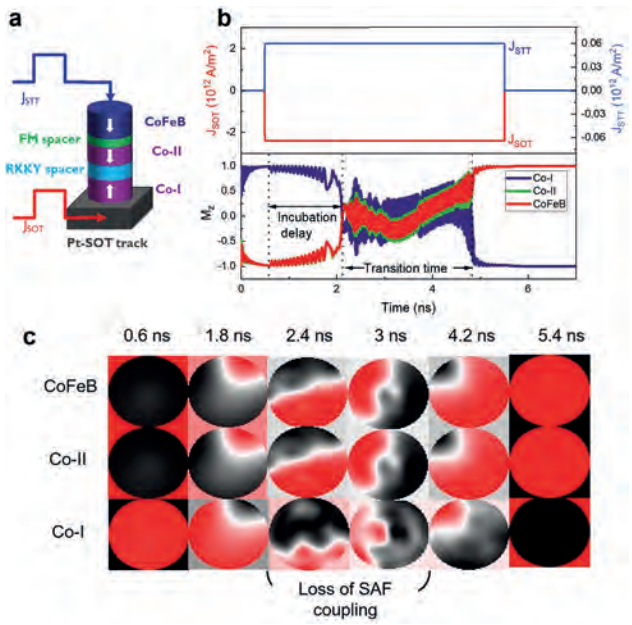

Fig. 1: a) Schematic of hybrid switching in SAF-HFL. (b & c) Micromagnetic simulation for hybrid switching in SAF-HFL with a 5 ns pulse b) Normalized M_z trace c) M_z Snapshot.

GD-09. Exotic Spin-Orbit Torques in Chiral Tellurium. *S. Li*[1], C. Niu[2], A. Hoffmann[1] and P. Ye[2] *1. University of Illinois at Urbana-Champaign, Urbana, IL, United States; 2. Purdue University, West Lafayette, IN, United States*

Tellurium has a chiral helical structure, which breaks the inversion symmetry and results in a momentum-dependent radial spin texture at the Fermi level. With a charge current applied along the chirality direction, the Fermi level will be shifted and spins of electrons will be polarized either parallel or anti-parallel to the current (or chirality) direction depending on the handedness of the Te chirality [1]. We are studying this chirality-induced spin polarizations by using spin-torque ferromagnetic resonance (ST-FMR) to observe the spin-orbit torques generated from single-crystalline Te flakes. In order to integrate exfoliated Te samples into devices, we first deposited a 10-nm Permalloy (Py; $Ni_{80}Fe_{20}$) layer and used ion-milling and lithography to integrate Te/Py heterostructure into a coplanar waveguide for radio frequency (rf) measurements. We applied GHz rf currents through Te/Py devices and collect a dc mixing voltage (V_{mix}) due to the mixing of anisotropic magnetoresistance of Py and rf current [2]. We define the current direction to be along x direction and out-of-plane direction to be z. The characteristics of spin-orbit torque components generated by Te flakes can be obtained by studying the dependence of V_{mix} as a function of applied

magnetic field direction. As shown in Fig.1, the asymmetric component of V_{mix} from our measurements reveals that indeed the current in Te results in spin polarizations that are collinear with the current direction, which is a direct consequence of the chiral structure of Te. At the same time, from the symmetric component, we also found substantial in-plane damping-like torques (τ_y) due to spins with polarizations along y direction, which originate from the spin Hall effect of the Te with large spin-orbit couplings [3]. We further calculated the spin-orbit torque efficiencies of chirality-induced torques τ_x and SHE-induced torques τ_y, and found them to be around 1.61 and 1.88 respectively.

[1] T. Furukawa, et al., Observation of current-induced bulk magnetization in elemental tellurium Nature Communications 8, 954 (2017) [2] L. Liu, et al., Spin-Torque Ferromagnetic Resonance Induced by the Spin Hall Effect, Phys. Rev. Lett. 106, 036601 (2011) [3] C. Niu, et al., Gate-tunable strong spin-orbit interaction in two-dimensional tellurium probed by weak antilocalization, Physical Rev. B 101, 205414 (2020)

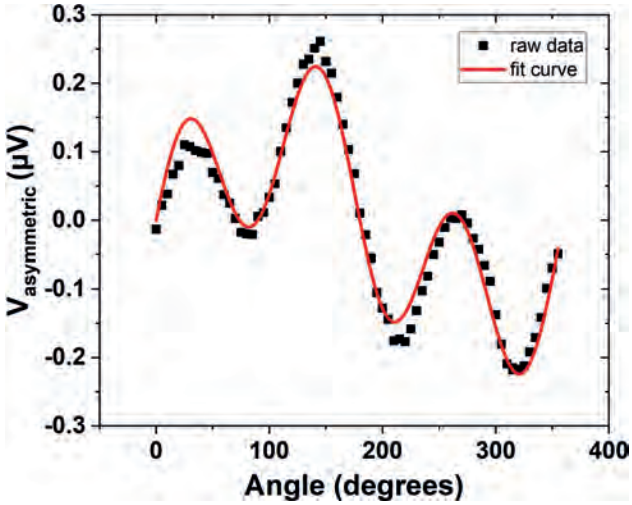

Fig. 1 Asymmetric component extracted from V_{mix} as a function of the angle between the applied rf current and the mangetic field. By fitting, we found the sizes of chirality-induced torque τx = -0.07 and Oesterd torque τy = 0.238.

GD-10. Spin injection through a Si-based ferromagnetic tunnel junction: a band diagram model. *B. Yu*[1], S. Sato[1,2], M. Tanaka[1,2] and R. Nakane[1,3]
1. Dept. of Electrical Eng. and Information Systems, School of Engineering, The University of Tokyo, Tokyo, Japan; 2. Center for Spintronics Research Network (CSRN), School of Engineering, The University of Tokyo, Tokyo, Japan; 3. System Design Lab (d.lab), School of Engineering, The University of Tokyo, Tokyo, Japan

Si-based spin transport devices are promising for next-generation electronics with low-power consumption [1]. For practical applications, it is a key metric to achieve a high spin-valve signal that is proportional to the product $P_{inj}P_{det}$, where P_{inj} and P_{det} represent the efficiency of spin injection and that of spin detection obtained by measuring a spin-originated voltage drop, respectively. Hence, maximizing $P_{inj}P_{det}$ is of critical significance. Nevertheless, the physical origins of P_{inj} and P_{det} have not yet been well explained despite many attempts (e.g. spin-filter based tunneling model) [2]. Here we pioneer a unique model by combining the tunneling theory with the realistic band diagram in a magnetic tunnel junction (MTJ) consisting of Fe/Mg/amorphous-MgO/SiO_x/n^+-Si(001). Fig. 1 shows a schematic band alignment of the MTJ under a spin extraction bias, where V_J is the MTJ voltage drop that corresponds to the Fermi-level difference between Fe and Si ($E_{F,Fe} - E_{F,Si}$). Here the s-like Fe band is assumed since the heavier d-band electrons contribute little to the tunneling current [3]. The total current $J(V_J)$ is determined by integrating the tunneling current per energy level, which depends on the product of the tunneling possibility as well as the densities of initial and final electron states [4]. Finally, $P_{det}(V_J)$ is calculated from $J(V_J)$ [5]. Fig. 2 shows our theoretical $P_{det}(V_J) - V_J$ curve. To experimentally examine how P_{det} changes with V_J, we measured a set of data points for $P_{inj}P_{det}(V_J)$ under a constant P_{inj} value by using a multi-terminal device and a setup similar to that described in ref. [2]. In Fig. 2, the feature of $P_{inj}P_{det}(V_J)$ agrees well with our theoretical $P_{det}(V_J)$-V_J curve. In addition, when $P_{inj}(V_J)P_{det}$ was experimentally examined in a similar manner, its feature also agrees well with our theoretical $P_{inj}(V_J)$-V_J curve (not shown). These results indicate that our model is effective to understand and analyze both P_{inj} and P_{det} in a wide range of V_J. Thus, we find that the band diagram of the MTJ can well explain the physical origins of P_{inj} and P_{det}.

[1] S. Sugahara and M. Tanaka, Appl. Phys. Lett. 84, 2307 (2004). [2] R. Jansen, et al., Phys. Rev. Appl. 10, 064050 (2018). [3] S. Valenzuela et al., Phys. Rev. Lett. 94, 196601 (2005). [4] J. Simmons, J. Appl. Phys. 34, 1793 (1963). [5] A. Fert and H. Jaffres, Phys. Rev. B 64, 184420 (2001).
This work was partially supported by CREST of JST (No. JPMJCR1777), Spintronics Research Network of Japan, and Grants-in-Aid for Scientific Research (23H00177).

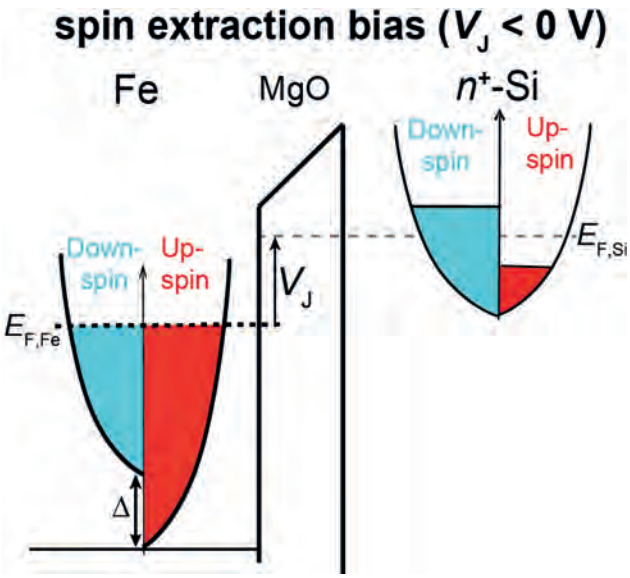

Fig. 1 Schematic band alignment of the MTJ.

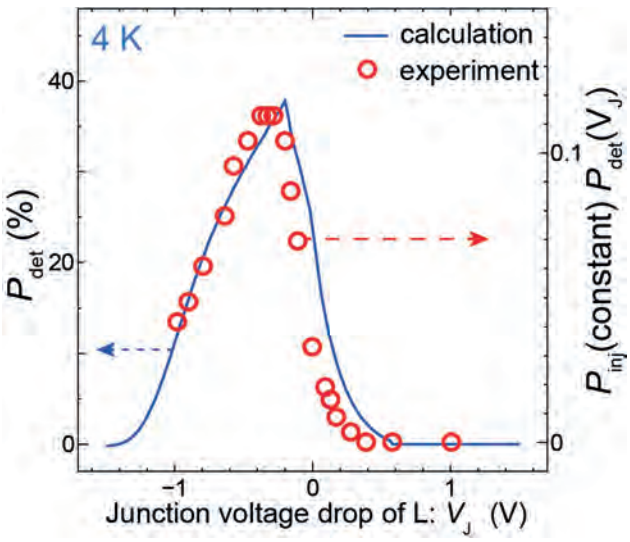

Fig. 2 Experimental $P_{inj}P_{det}(V_J)$ (the right axis) and theoretical $P_{det} - V_J$ curve (the left axis).

GD-11. Unconventional Spin-Orbit Torque in $CrPt_3$. *R. Klause*[1], Y. Xiao[4], J. Gibbons[3], A. Hoffmann[1] and E. Fullerton[2] *1. University of Illinois Urbana-Champaign, Urbana, IL, United States; 2. University of California San Diego, San Diego, CA, United States; 3. Western Digital, San Jose, CA, United States; 4. TDK, Milpitas, CA, United States*

The topological semimetal $CrPt_3$ has potential for generating exotic spin-torques due to its ferrimagnetic ordering, topological band structure and high anomalous Hall conductivity. As $CrPt_3$ exhibits ferrimagnetic behavior only in its chemically ordered phase while it is paramagnetic in its chemically disordered phase, comparing spin-torque generation in the two phases we can investigate whether unconventional torques originate from the magnetic or crystal structure. We have studied spin-torques generated in epitaxial $CrPt_3$(110) films in $CrPt_3$/Cu/$Fe_{80}Ni_{20}$ structures. By controlling the growth and annealing temperatures epitaxial films of both chemically ordered and disordered phases of $CrPt_3$ are achieved. We use angle dependent spin-torque ferromagnetic-resonance (STFMR) measurements with currents applied along specific directions with respect to the magnetic and crystal order to reveal an unconventional in-plane field-like spin-torque in both chemically ordered and disordered $CrPt_3$ thin films. Because this exotic torque is present in both ordered and disordered films as shown in the two figures, we conclude that it does not originate from the magnetic, but rather the crystal order. In the device orientations where an unconventional torque is measured the current flows along the <1-1-1> (+35.3° device) and <1-11> (-35.3° device) directions, which are lacking a mirror plane and thus allow an unconventional torque to be generated. This work was supported as part of Quantum Materials for Energy Efficient Neuromorphic Computing (Q-MEEN-C), an Energy Frontier Research Center funded by the US Department of Energy, Office of Science, Basic Energy Sciences under Award No. DE-SC0019273.

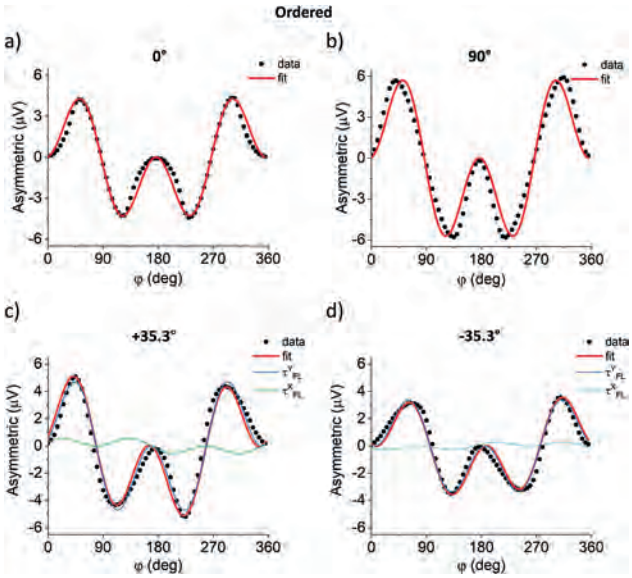

STFMR measurements of chemically ordered $CrPt_3$ in devices oriented at an angle of 0°, 90°, +35.3°, and -35.3° with respect to the in-plane <1-10> direction. The +35.3° and -35.3° devices show opposite unconventional torque components.

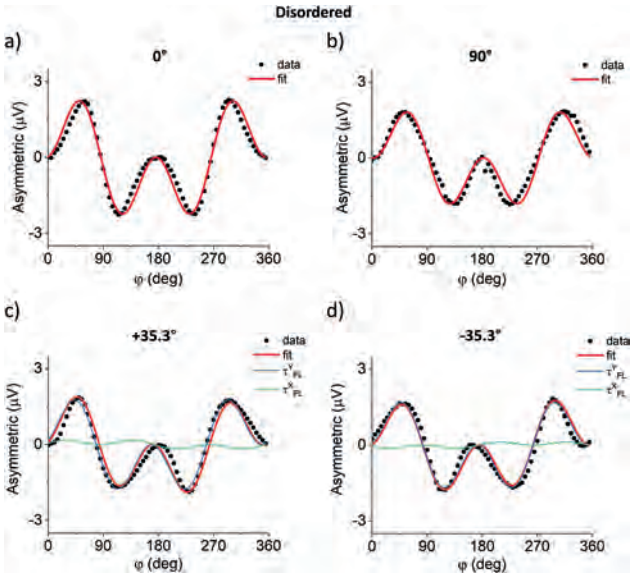

STFMR measurements of chemically disordered $CrPt_3$ in devices oriented at an angle of 0°, 90°, +35.3°, and -35.3° with respect to the in-plane <1-10> direction. The +35.3° and -35.3° devices show opposite unconventional torque components.

Session GE
HALF-METALLIC MATERIALS, MAGNETIC SEMICONDUCTORS AND OTHER ADVANCED MATERIALS FOR SPINTRONICS

Kenji Nawa, Chair
Mie University, Tsu, Japan

INVITED PAPER

GE-01. Controlled Spin Structure and Magnetic Anisotropy for Efficient Spintronics Applications. *J. Hong*[1], J. Ha[1], H. Kim[2], W. Choi[1], S. Yoon[1], B. Tran[1] and T. Kim[1] *1. DGIST, Daegu, The Republic of Korea; 2. KRISS, Daejeon, The Republic of Korea*

Magnetic material is usually classified based on the alignment states of magnetic moments or atomic spins over the crystalline lattice structure. Ferromagnetism is based on the parallel couplings of spins while antiferromagnetism assumes antiparallel spin alignments. With the development of spintronics technology enabling efficient manipulations of spin direction, modification of conventional parallel or antiparallel spin structure has become possible, and various spin structures based on noncollinear spin structure could be realized in diverse magnetic materials. It is expected that the diversification of spin structures in engineering materials would guide the development of novel spin properties for emerging spintronics. In the thin film systems, coupling of FM and AFM layers has long been utilized to modify the simple ferromagnetic spin structure. Antiparallel couplings such as oxygen mediated super-exchange or ferrimagnetic couplings between heterogeneous atoms can be combined with conventional ferromagnetic parallel exchange couplings to form a spin structure of atomic spins that is beyond the simple parallel alignments to realize noncollinear spin structures. Our results show examples of spin structure modifications from simple ferromagnetism and the resulting magnetic properties which is not achievable with conventional FM materials. Firstly, it is noted that magnetic domain wall naturally includes noncollinear spin alignments, hence the dynamics of domain wall motion is not symmetric with respect to the exchange coupling state. Domain wall propagation along the patterned path made of exchange biased magnetic thin film was observed with tilted wall front and its asymmetry was understood with the consideration of noncollinear spin structure and the effective field from the neighboring AFM.[1] Noncollinear spin alignments can also be established by combination of in-plane magnetic anisotropy (IMA) and perpendicular magnetic anisotropy (PMA) in the $(Gd/Co)_N$ multilayers. Broken symmetry due to the presence of IMA could successfully utilized for the deterministic field-free SOT switching of perpendicular magnetization.[2] Stronger modification to the parallel FM spin alignments were also applied by double exchange bias couplings on both sides of FM thin film layer. Spin alignment directions in the AFM can be locally controlled by spin Hall effect, hence the exchange couplings can be applied in different directions on the single FM layer. Depending on the relative directions of exchange couplings, helimagnetic spin structure can be established with desired chiral sense. Further disturbing the symmetries of spin alignments, spin glass behaviors begin to appear as seen in the $Co_{0.7}Ni_{0.3}O_{1-x}$-Pt system, which is also useful in device operations. With these examples, it is recognized that diverse spin structures in the functional magnetic materials can enrich the spintronics device technology.

[1] H. J. Kim, S. G. Je, K. W. Moon, et al., Advanced Science, Vol. 8, 2100908 (2021) [2] H. J. Kim, K. W. Moon, B. X. Tran, et al., Advanced Functional Materials, Vol. 32, 2112561 (2022)

CONTRIBUTED PAPERS

GE-02. Combinatorially Sputtered $Co_2Mn_xFe_{1-x}Ge$ ($0 \le x \le 1$) Heusler Thin Films for High-Throughput Analysis of Magnetoresistance and Spin-Transfer Torque. *V. Barwal*[1], H. Suto[1], R. Toyama[1] and Y. Sakuraba[1] *1. Research Center for Magnetic and Spintronics Materials, National Institute for Materials Science, Tsukuba, Japan*

Heusler alloys with high spin polarization(P), high Curie temperature and low Gilbert damping are recently being studied for their potential applications in spintronics [1–3]. Composition variation is known to be promising for tuning magnetic properties in Heusler systems. Combinatorial sputtering allows for compositional variation over a wide range on a substrate thereby facilitating systematic and efficient analysis of composition-dependent properties. We studied the composition dependence of MR and STT in CPP GMR devices containing composition gradient $Co_2Mn_xFe_{1-x}Ge$ ($0 \le x \le 1$). Figure(a) shows the composition gradient thin film deposition process. Two types of structure were prepared, as shown in Fig (b): in type-A, both magnetic layers consist of $Co_2Mn_xFe_{1-x}Ge$, where MR ratio was measured, and in type-B, magnetic layers consist of $Co_2Mn_xFe_{1-x}Ge$ and NiFe, where magnetization reversal of the NiFe layer was induced to evaluate STT efficiency[4]. We observed $L2_1$ ordering in 300°C annealed type-A sample from XRD measurements [Figure(c) and (d)]. Figure(e) shows the change in MR % with Mn content at different annealing temperature (T_a) for the type-A sample. We observed enhancement in MR% with increasing T_a, and the maximum MR%(ΔRA) reaching to ~35 % (~6 mΩμm^2) at T_a =300°C. On the other hand, the scattering in MR% is smaller at T_a =200 °C, and we observe composition dependence with the maximum around 28 % at Mn content 0.8. Figure(f) shows the change in STT efficiency parameter and out-of-plane and in-plane MR% with Mn content for the type-B sample. STT efficiency and the MR decreased near the Mn-side. The experiment is novel in terms of design and implementation and helps elucidating the composition dependent MR and STT response of the CPP-GMR devices.

[1] T. Nakatani, Z. Gao, and K. Hono, MRS Bull. 43, 106 (2018). [2] T. Kubota, Z. Wen, and K. Takanashi, J. Magn. Magn. Mater. 492, 165667 (2019). [3] M. R. Page, T. M. Nakatani, D. A. Stewart, B. R. York, J. C. Read, Y.-S. Choi, and J. R. Childress, J. Appl. Phys. 119, 153903 (2016). [4] H. Suto, T. Nakatani, N. Asam, H. Iwasaki, and Y. Sakuraba, Appl. Phys. Express 16, (2023).

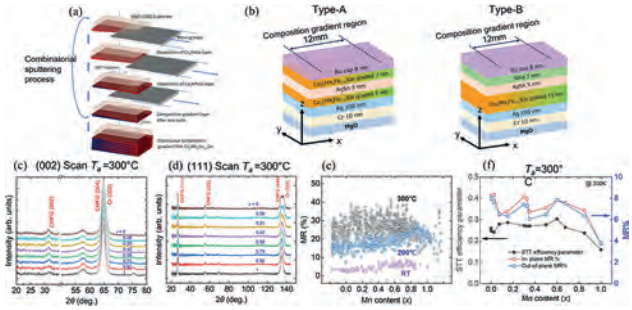

(a) Combinaorial sputtering process, (b) stack configuration for the type-A and type-B sample, θ-2θ XRD profiles for the T_a = 300 °C sample along (c) (002) and (d) (111) direction for the type-A sample, (e) change in MR% with Mn content at different T_a. for type-A sample, (e) change in STT efficiency and MR% (at 300K) with Mn content for the T_a = 300 °C type-B sample.

GE-03. Intrinsic Berry curvature driven anomalous Nernst thermopower in the semimetallic quaternary Heusler alloy CoFeVSb. A. Chanda[1], J. Nag[2], A. Alam[2], K. Suresh[2], M. Phan[1] and *H. Srikanth*[1]
1. Physics, University of South Florida, Tampa, FL, United States;
2. Physics, Indian Institute of Technology Bombay, Bombay, India

Understanding of spin-heat coupling mechanisms and transverse magneto-thermoelectric phenomena, including the anomalous Nernst effect (ANE), in emergent quaternary Heusler alloys is of practical importance for applications in thermal management and energy efficient spincaloritronic devices [1,2]. Among the Heusler systems of current interest, CoFeVSb possesses a very high ordering temperature (850 K) and a large saturation magnetization at room temperature [3]. This quaternary Heusler alloy shows asymmetric magnetoresistance at room temperature, indicative of the spin-valve like nature of the material in its bulk form [3]. Furthermore, this sample possesses a very high thermoelectric power factor of at room temperature, making it a promising thermoelectric material. The coexistence of these striking physical properties in a single phase of CoFeVSb prompted us to investigate its spin-caloritronic properties. Here, we demonstrate an intrinsic Berry curvature mediated ANE in CoFeVSb. We show that the electron-electron elastic and electron-magnon inelastic scatterings dominate longitudinal electrical transport at low temperatures (below 50K), whereas the electron-phonon and electron-magnon scatterings govern it at high temperatures. The longitudinal thermopower is resulted mainly from the diffusive contribution, with a very large longitudinal Seebeck coefficient (42μV/K at 395 K). The value of the anomalous Nernst coefficient (0.039 μV/K) for CoFeVSb at room temperature is which is higher than the compressively strained $SrRuO_3$ film (0.03 μV/K) as well as the spin gapless semiconductor CoFeCrGa (0.018 μV/K). On lowering temperatures, both the ordinary Nernst coefficient and carrier mobility increase but an opposite trend is found for. Our *ab-initio* simulations reveal the topological semimetallic nature of CoFeVSb with a pair of Weyl points. These Weyl crossings result in a significant contribution to the Berry curvature, leading to an intrinsic anomalous Hall conductivity of 85 S/cm, which matches well with experiment (77 S/cm at 2 K). Our experimental findings and *ab-initio* calculations support the dominance of the intrinsic Berry curvature in the observed ANE.

[1] S. N. Guin et al., *Anomalous Nernst Effect beyond the Magnetization Scaling Relation in the Ferromagnetic Heusler Compound Co_2MnGa*, NPG Asia Mater. 11, 1 (2019). [2] A. Sakai et al., *Giant Anomalous Nernst Effect and Quantum-Critical Scaling in a Ferromagnetic Semimetal*, Nat. Phys. 14, 1119 (2018). [3] J. Nag et al., *CoFeVSb: A Promising Candidate for Spin Valve and Thermoelectric Applications*, Phys. Rev. B 105, 144409 (2022).

GE-04. Spin-Gapless Semiconducting Heusler-Alloy Films. W. Li[1,2], T. Sarfo[1], K. Wang[1,3], W. Kong[1,3] and *A. Hirohata*[1,4] *1. University of York, York, United Kingdom; 2. Yanshan University, Yanshan, China; 3. City University of Hong Kong, Hong Kong; 4. Tohoku University, Sendai, Japan*

Ternary Heusler alloys has demonstrated half-metallic ferromagnetic, antiferromagnetic and ferrimagnetic natures as well as topological insulating properties by selecting relevant compositions out of over 2,500 combinations [1],[2]. In this study, we used conventional sputtering for the deposition of Heusler-alloy film, which has theoretically predicted to become a spin-gapless semiconductor [3], which is also predicted to show a large spin Hall angle. 20-nm-thick polycrystalline Heusler-alloy thin films of FeCrTiAl, CoFeMnSi and CoCrFeAl were deposited on a thermally-oxidised Si substrate using a sputtering system. The base pressure was about 3×10^{-6} mbar and the Ar pressure during the deposition was 10×10^{-3} mbar. The films were typically grown at the rate of 0.1~0.4nm/s. The Heusler-alloy films were post-annealed at elevating temperatures between 300 and 500°C for up to two hours in a tube furnace for their crystallisation. The films were then structurally and magnetically characterised by X-ray diffraction and vibrating sample magnetometer, respectively, for optimisation. The optimised film capped with a 2-nm-thick Pt or W layer was patterned into a Hall bar with the wire width of 1 mm for spin Hall measurements with a conventional direct-current four-terminal method with a sensing current of 50 μA. This project was partially supported by EPSRC (EP/V007211/1) and JST CREST (No. JPMJCR17J5).

[1] C. Felser and A. Hirohata (Eds.), "Heusler Alloys," Springer, Berlin, Germany, Nov. 2015. [2] K. Elphick *et al.*, *Sci. Technol. Adv. Mater.* 22 (2020) 235. [3] X. Wang *et al.*, *Phys. Rep.* 888 (2020) 1.

GE-05. Low-temperature antiferromagnetism in quaternary $Mn_2FeSi_{0.5}Al_{0.5}$ alloys. *O. Zivotsky*[1], L. Gembalova[1], K. Skotnicova[2], I. Szurman[2], T. Cegan[2], J. Jurica[2], O. Malina[3] and J. Cizek[4] *1. VSB - Technical University of Ostrava, Faculty of Electrical Engineering and Computer Science, Ostrava, Czechia; 2. VSB - Technical University of Ostrava, Faculty of Materials Science and Technology, Ostrava, Czechia; 3. Regional Centre of Advanced Technologies and Materials, Czech Advanced Technology and Research Institute, Olomouc, Czechia; 4. Charles University Prague, Faculty of Mathematics and Physics, Prague, Czechia*

Manganese-based full- and half-Heusler alloys are often studied because of their interesting antiferromagnetic properties. Currently, the complex physical characterization of ternary Mn_2FeSi and Mn_2FeAl alloys revealed not only antiferromagnetism at low temperatures, but also complicated microstructure affecting their potential applications in spintronics [1]. Mn_2FeSi exhibits crystalline $L2_1$ or XA Heusler structure pointing to the half-metallicity behavior, while Mn_2FeAl crystallizes in geometrically frustrated cubic β-Mn structure having metallic character of density of electronic states [2]. In this work, the quaternary $Mn_2FeSi_{0.5}Al_{0.5}$ alloys are prepared for the first time in the form of ingots by traditional induction melting technique followed by homogenization annealing for 100 h at 773 K. Their microstructural and magnetic properties are analyzed in detail and compared to the Mn_2FeSi and Mn_2FeAl alloys. The scanning electron microscopy supplemented by the energy dispersive X-ray (EDX) spectroscopy confirmed uniform distribution of elements and the composition slightly deviated from the nominal one (about 48.5 at.% Mn, 24.6 at.% Fe, 13.9 at.% Si, and 13.0 at.% Al). The results of X-ray diffraction (see Figure 1) revealed the existence of cubic β-Mn structure with the lattice constant 0.6274 nm being slightly lower than that of Mn_2FeAl sample (0.6339 nm). The magnetic properties studied in wide temperature range from 5 K to 573 K indicate paramagnetic behaviour at room and elevated temperatures. The transition to antiferromagnetic state occurred at a Néel temperature of 34 K (see Figure 2) and also other magnetic parameters like negative Curie temperature (≈ -700 K) or temperature of irreversibility (≈ 43 K) are comparable to Mn_2FeAl ingot. The strong antiferromagnetic spin fluctuation of $Mn_2FeSi_{0.5}Al_{0.5}$ system is caused by the geometric frustration of β-Mn structure (frustration parameter $f \approx 20$).

[1] O. Zivotsky et al., J. Alloys Comp., Vol. 947, p. 169672 (2023) [2] S. Dash et al., J. Magn. Magn. Mater., Vol. 513, p. 167205 (2020)

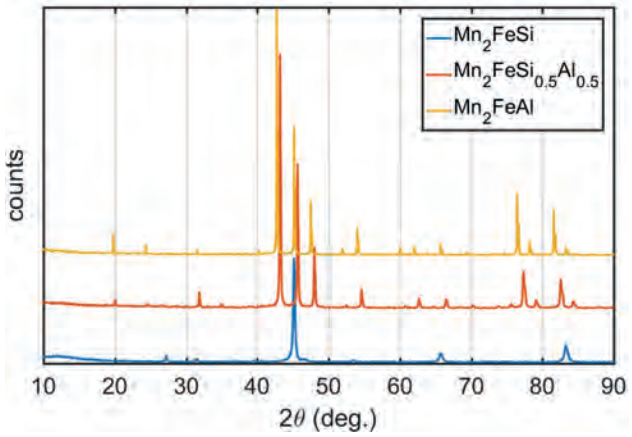

Fig. 1 X-ray diffraction patterns showing Mn_2FeSi Heusler structure and primitive cubic β-Mn structures of Mn_2FeAl and $Mn_2FeSi_{0.5}Al_{0.5}$ ingots.

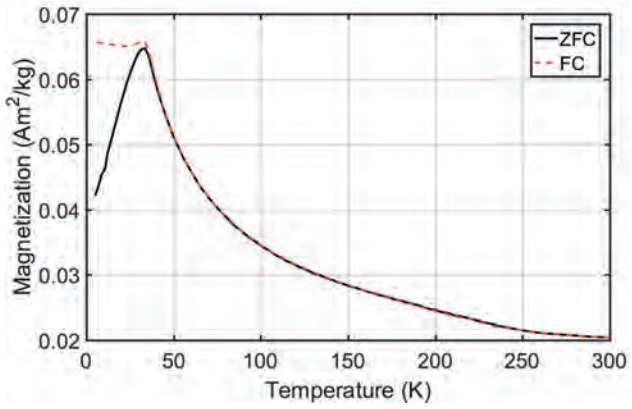

Fig. 2 Zero field-cooled and field-cooled (ZFC/FC) curves of $Mn_2FeSi_{0.5}Al_{0.5}$ ingot measured at a constant magnetic field of 8 kA/m.

GE-06. Tailoring properties of Heusler alloys by elemental substitution: $(Co_{2-\alpha}Mn_\alpha)FeGe$, $Co_2(Fe_{1-\beta}Mn_\beta)Ge$, and $(Co_{2-\alpha}Fe_\alpha)MnGe$. *P.R. LeClair*[1], R. Mahat[1], J. Law[2], V. Franco[2], W.H. Butler[1] and A. Gupta[1] *1. Physics and Astronomy, The University of Alabama, Tuscaloosa, AL, United States; 2. Fisica de la Materia Condensada, Universidad de Sevilla, Sevilla, Spain*

Rational material design by elemental substitution is useful in tailoring novel functional materials with desired properties. We consider three non-equivalent substitutional series based on Co_2FeGe, viz; $(Co_{2-\alpha}Mn_\alpha)FeGe$, $Co_2(Fe_{1-\beta}Mn_\beta)Ge$, $(Co_{2-\alpha}Fe_\alpha)MnGe$ ($0\leq\alpha\leq2$, $0\leq\beta\leq1$), and study how material properties evolve with the interchange of Mn, Fe, and Co in Co_2FeGe. The study of $(Co_{2-\alpha}Mn_\alpha)FeGe$ suggests that single-phase compounds can be obtained across a wide substitution range (i.e., $0.125\leq\alpha\leq1.375$). For the $Co_2(Fe_{1-\beta}Mn_\beta)Ge$ and $(Co_{2-\alpha}Fe_\alpha)MnGe$ substitutional series single-phase compounds can be stabilised over a wide substitution range ($0\leq\beta\leq1$, and $0\leq\alpha\leq1.5$). All the single-phase compounds crystallise in an fcc structure with chemical ordering that is consistent with the Burch rule. The single-phase alloys are soft ferromagnets and exhibit very high saturation magnetisations that match closely with the expected Slater-Pauling moment. Extremely high Curie temperatures (~1000K for lower Mn concentrations) are also obtained. Based on first-principles calculations and backed by experimental results, what we propose to be the most stable atomic configurations are consistent with the Burch rule. Further, the electronic structure calculations reveal alloys with half-metallic character with Fermi level locating in the middle of the gap, a condition necessary for robust half-metallicity. Upon comparing the results of the three series, it is found that the alloy properties such as phase-stability, structural, magnetic, and electronic depend primarily on the number of valence electrons far more than on the substitution scheme employed.

Session GF
MULTI-FUNCTIONAL MAGNETIC MATERIALS AND APPLICATIONS II

Harshida G Parmar, Chair
Ames Laboratory, Ames, IA, United States

INVITED PAPERS

GF-01. Use of Nanoscale Perpendicular Spin Transfer Torque Magnetic Tunnel Junctions as Magnetic Sensors. *R. Sousa*[1], H. Nicolas[2], A. Mora-Hernandez[1], H. Karaoui[1], I. Prejbeanu[1], L. Hebrard[3], J. Kammerer[3] and J. Pascal[2] *1. Univ. Grenoble Alpes/CNRS/CEA, SPINTEC, Grenoble, France; 2. School of Life Sciences, University of Applied Sciences Northwestern Switzerland, Muttenz, Switzerland; 3. ICube, University of Strasbourg, Strasbourg, France*

Spin transfer torque in perpendicular anisotropy magnetic tunnel junctions is the foundation of current STT MRAM technology that has achieved mass production at some foundries. In perpendicular configuration, the critical currents to switch between parallel and anti-parallel alignment between a storage or sensing layer and the reference layer magnetization depend linearly on the value of an applied field, applied along the perpendicular direction. This has been confirmed first in perpendicular anisotropy spin-valves [1] and later in magnetic tunnel junctions, where the in-plane STT term can be shown to dominate over the perpendicular torque contribution [2]. The effect of an applied field on the switching current is most easily seen in pulse phase diagrams that minimize non-linearities induced by possible Joule heating in DC current diagrams. The linear dependence of the switching voltage is clearly observed in the p-MTJ bi-stable field region, in either field sweep or voltage sweep measurements. The field sensitivity has typical values in the range of 0.1-1mV/Oe, representing the change in critical switching voltage under an applied perpendicular field. Resistance changes between parallel and anti-parallel configurations are used to create a pulse width modulation (PWM) signal whose duty cycle is changing according to the external magnetic field. The resulting PWM signal is then averaged through a low pass filter generating an analog output voltage whose average value is proportional to the applied magnetic field. Based on the above principle, a magnetic tunnel junction sensing element of 50 nm in diameter was demonstrated to detect perpendicular magnetic field with a sensitivity of 1.28 V/T and a dynamic range of 80 mT using an associated signal processing electronics [3]. The advantages of the proposed sensor are its small size, hence low power consumption, and reduced packaging electronics footprint. The detection range can be wider than typical magneto-resistive sensors, as there is no longer a trade-off between resistance change detection and field range. The sensor is also insensitive to the intense fields sometimes causing irreversible damage to magnetoresistive sensors. Experimental results are detailed and compared to state-of-the-art commercially available integrated magnetic sensors.

1. S. Mangin, Y. Henry, D. Ravelosona, J. A. Katine, and E. E. Fullerton, Applied Physics Letters, vol. 94, p. 012502 (2009) 2. A. A. Timopheev, R. Sousa, M. Chshiev, L. D. Buda-Prejbeanu, and B. Dieny, Phys. Rev. B, vol. 92, p. 104430 (2015) 3. H. Nicolas, R.C. Sousa, A. Mora-Hernández, I.-L. Prejbeanu, L. Hebrard, J.-B. Kammerer, J. Pascal, IEEE Sensors Journal, p. 1–1 (2023)

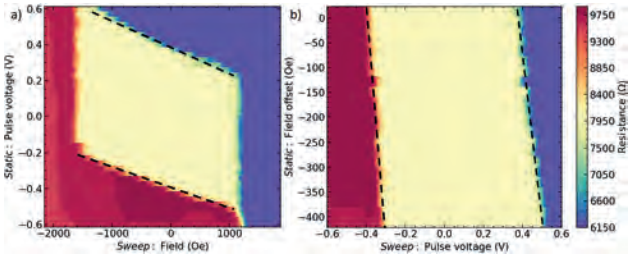

Pulse phase diagrams of perpendicular magnetic tunnel junction under a) applied current pulses at each field sweep and b) under applied static field for each pulse voltage sweeps. Dashed lines highlight the linear critical voltage dependence. Current pulses are 100ns long and field is applied perpendicularly.

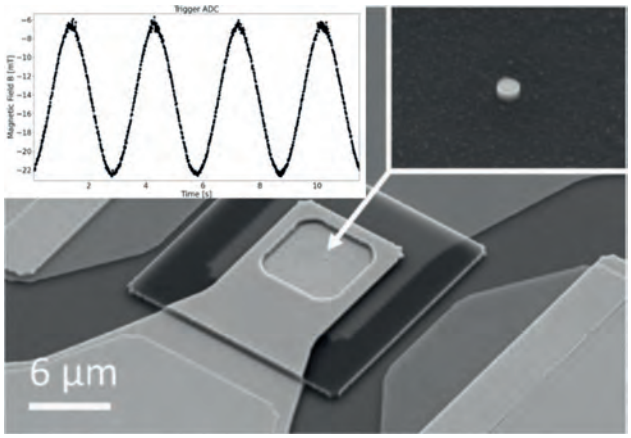

Top view of 50nm diameter junction, showing a demonstration of detected magnetic field applied at 300 mHz.

GF-02. Strain-induced hardening of ferromagnetic Ni evidenced by off-axis electron microscopy and micromagnetic simulations. D. Kong[2,3], A. Kovacs[2], *M. Charilaou*[1], F. Zheng[2,4], L. Wang[5], X. Han[5] and R.E. Dunin-Borkowski[2] *1. Department of Physics, University of Louisiana at Lafayette, Lafayette, LA, United States; 2. Ernst Ruska-Centre for Microscopy and Spectroscopy with Electrons, Forschungszentrum Jülich, Jülich, Germany; 3. Department of Physics and Optoelectronics, Beijing University of Technology, Beijing, China; 4. School of Physics and Optoelectronics, South China University of Technology, Guangzhou, China; 5. Institute of Microstructure and Properties of Advanced Materials, Beijing University of Technology, Beijing, China*

The intricate mechanisms via which magnetic states change due to mechanical strain, i.e., magnetoelasticity, or the inverse phenomenon, magnetostriction, remain poorly understood. Bulk measurements have provided important insight to these phenomena, but a deeper understanding of how strain, i.e., the modification of inter-atomic distances, changes the magnetic state remains elusive. In this contribution, we provide direct nanoscale

observations of how tensile strain modifies the magnetic domains in a ferromagnetic Ni thin plate using *in situ* Lorentz transmission electron microscopy and off-axis electron holography [1]. We will present high-resolution images of magnetic domains and we will show how tensile strain transforms the domain-wall structure to a periodic pattern of 180 degree domain walls perpendicular to the strain axis, as shown in the figure here. Additionally, we will show that the magnetization transformation exhibits stress-determined directional sensitivity and is reversible and tunable through the size of the nanostructure. By comparing experimental data with micromagnetic simulations and analyzing the structure of domain walls in the absence and presence of strain, we attribute the observed magnetic changes to strain-induced anisotropy and hardening. Given these observations, we propose that this phenomenon may have potential applications in directional mechanical strain sensing.

[1] D. Kong, A. Kovács, M. Charilaou, F. Zheng, L. Wang, X. Han and R. E. Dunin-Borkowski: Direct observation of tensile-strain-induced nanoscale magnetic hardening. Nature Communications (accepted for publication, 2023)

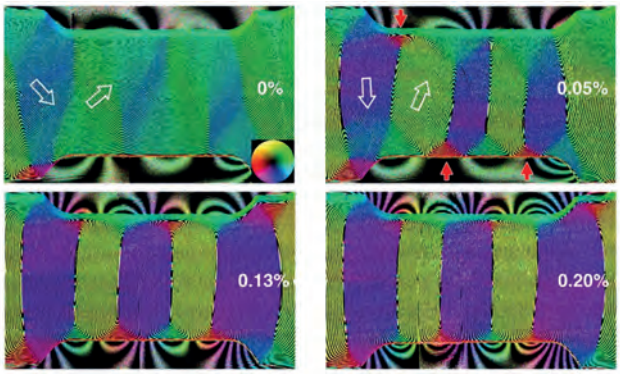

Fig. 1: Off-axis electron holography images of a Ni ferromagnetic film under tensile strain, as indicated in each panel. The domain walls form a periodic pattern perpendicular to the strain axis. Taken from [1].

CONTRIBUTED PAPERS

GF-03. Simultaneous magnetization reversal in a magnetoelastic bilayer structure. N. Coton[1], J. Andrés González[3], M. Maicas[2] and *R. Ranchal*[1] *1. Universidad Complutense de Madrid, Madrid, Spain; 2. Universidad Politecnica de Madrid, Madrid, Spain; 3. Universidad Castilla-La Mancha, Ciudad Real, Spain*

One of the most active investigation field is the development of innovative multilayers exploiting interfacial interactions. The exchange stiffness and the magnetic anisotropy are fundamental parameters to tune the critical thickness to avoid the presence of uncoupled regions. For example, in spring magnets in which soft and hard materials are coupled, it is in general considered that the dimension of the soft phase needs to be smaller than twice the thickness of a Bloch domain wall of the hard one in order to achieve a coherent magnetization reversal in the hysteresis loop [1-2]. Due to the magnetostriction effect a magnetic material changes its dimensions when it is magnetized. In this work we show how in a magnetostrictive bilayer structure comprised of two materials with magnetostriction constants of opposite sign, $Fe_{70}Ga_{30}$ and $Ni_{90}Fe_{10}$, the magnetic switching is affected by the magnetoelastic coupling. We have studied a bilayer system grown by electrodeposition in which the thickness of both layers exceeds that of their respective Bloch domain wall. Whereas the layer with positive magnetostriction tries to elongate in the direction of the applied magnetic field, the layer with negative magnetostriction tries to contract (Fig. 1). Since magnetoelasticity is not an interfacial interaction, the mechanical strain promoted by the applied magnetic field affects the layers as a whole. The net effect is a coherent reversal of the magnetization of the two layers regardless of their thickness (Fig. 2). These results demonstrate the possibility of using this physical mechanism to beat the critical limit thickness imposed by interfacial interactions in magnetically coupled multilayers in such a way that the magnetization reversal is made coherently regardless of the layer thickness [3].

[1] R. Coehoorn, D.B. de Mooij, and C. de Waard, J. Magn. Magn. Mat. 80, 101 (1989). [2] E. F. Kneller, and R. Hawig, IEEE Trans. Magn. 27, 3588 (1991). [3] N. Coton, J. P. Andres, A. Cabrera, M. Maicas and R. Ranchal. Submitted.

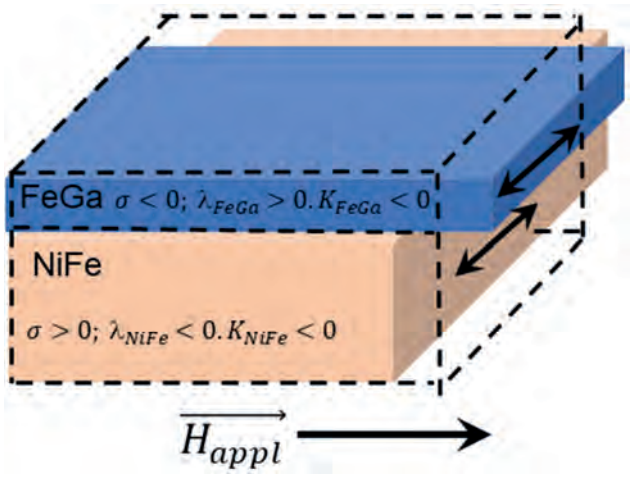

Fig. 1. Schematic view of a NiFe/FeGa bilayer showing the expected mechanical deformation due to the magnetization process promoted by the applied magnetic field

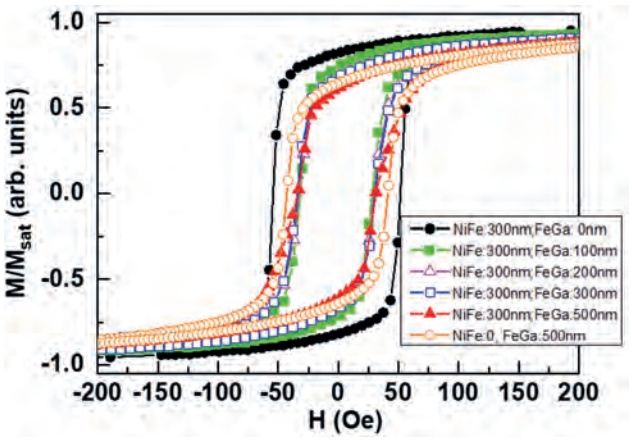

Fig. 2. Hysteresis loops for $Ni_{90}Fe_{10}$ and $Fe_{70}Ga_{30}$ single layers with a thickness of 300 nm and 500 nm, respectively, together with the IP hysteresis loops of different $Ni_{90}Fe_{10}/Fe_{70}Ga_{30}$ bilayers in which the $Ni_{90}Fe_{10}$ is 300 nm and $Fe_{70}Ga_{30}$ varies from 100 nm to 500 nm.

GF-04. Mechanical and Magnetostrictive Properties of Additively Manufactured $Fe_{81}Al_{19}$ rods. *N.J. Jones*[1], J.H. Yoo[1], B.G. Kessel[2], T.R. Mion[3], E.F. Holcombe[1,4] and P.K. Lambert[5] *1. Physical Metallurgy and Fire Performance Branch, Naval Surface Warfare Center, Carderock Division, Bethesda, MD, United States; 2. Additive Manufacturing Project Branch, Naval Surface Warfare Center, Carderock Division, Bethesda, MD, United States; 3. Naval Research Laboratory, Washington, DC, United States; 4. Materials Science and Engineering Department, Johns Hopkins University, Baltimore, MD, United States; 5. Johns Hopkins University Applied Physics Laboratory, Laurel, MD, United States*

Solid rods of $Fe_{81}Al_{19}$ were additively manufactured on a Direct Metal Laser Sintering 3D printer (ProX 200, 3D systems) using 200 W laser power and laser scan speeds of 1 and 1.5 m/s. Pre-alloyed atomized powder with a spherical morphology and sizes between 40 and 125 μm was used for the build; the build was completed with a 1:1 compaction ratio to conserve powder. Rods were machined to a 6 mm diameter and 50 mm long. Magnetic and magnetostrictive properties were measured as a function of applied magnetic field under various applied compressive stresses. Solid rod performance was compared to similar rods fabricated with an internal lattice structure, printed horizontally at 200 W laser power and 1 m/s laser scan speed. Lattice rod magnetostriction was measured using laser Doppler vibrometry. The measured magnetostriction of the solid rods was low, $3/2\,\lambda_s = 36.5$ ppm, compared to the expected polycrystalline value of 77 ppm, however both the solid and lattice rods exhibited approximately the same magnetostriction values (lattices showed $3/2\,\lambda_s = 34.3$ ppm). While the crystallographic texture is not yet aligned for maximum magnetostriction, material can be conserved by printing a more hollow structure, if allowed by the application. The measured saturation magnetization for the solid rods was also lower than anticipated (~1.2 T). Sample microstructure was analyzed to understand the impact of crystallography on performance, and thermal annealing, field annealing and stress annealing were performed to understand the ability to induce anisotropy into 3D printed samples and to remove any internal stresses due to printing. The mechanical properties of the rods were also evaluated. Both the elastic modulus and the yield stress of the rods was highly dependent upon the laser parameters used, exhibiting worse properties with the higher laser scan speed of 1.5 m/s. Young's modulus increased by a factor of 1.6 (from 53 to 85 GPa), and the yield stress increased by a factor of 1.7 (from 148 to 248 MPa) by decreasing the laser speed. The yield stress was still lower than for a bulk sample, mainly due to internal porosity, indicated by the rather pebbly fracture surface.

GF-05. U-shape Magnetostrictive Harvester: Design and Experimental Validation. *D. Gandia*[1,2], E. Garayo[1,2], J.J. Beato-López[1,2], I. Royo[1,2] and C. Gomez-Polo[1,2] *1. Departamento de Ciencias, UPNA, Pamplona, Spain; 2. Institute for Advanced Materials and Mathematics INAMAT2, Upba, Pamplona, Spain*

An energy harvester is a device that transforms ambient energy (light, temperature, vibration, motion, or RF radiation) into electrical energy to power small autonomous devices [1]. Among the range of available sources, vibrational harvesters stand out due to the wide presence of vibrations in the environment. In this scenario, electromagnetic harvesters, specifically based on magnetostrictive materials, have demonstrated higher conversion efficiency [2] and simpler setup, assuring a longer lifetime [3]. In this study, a procedure for the optimization of the performance of a U-shape energy harvester [4] (Fig. 1) is presented. The device is composed of a Fe-based ferromagnetic frame, a NdFeB permanent magnet, and a magnetostrictive Fe-Ga (Galfenol) strip (0.5x4x20 mm). Changes in the magnetic flux linked to the magnetoelastic coupling of the strip, enable the conversion of the mechanical energy into electrical energy (i.e. use of a pick-up coil). A 3D Finite Element (FE) model was employed to analyze and optimize the harvester's design. Fig. 2 shows the agreement between the experimental tip deflections of the frame (laser position sensor) and the simulated deflections employing a Rayleigh mechanical damping model (α=1 s, β=8x10^{-5} s^{-1}). The fitting of the mechanical damping enabled the estimation of the stresses generated by the resonance modes of the structure, on the magnetostrictive strip (~2 MPa). This outcome allows the optimization of the energy conversion through suitable control of the Galfenol magnetoelastic coupling conditions which are determined by the material magnetoelastic response at the working bias magnetic field. The results show the possibility to increase the amplitude of the tip deflection, providing an enhancement in the associated stresses, through the reduction of the frame width (from 0.5 to 0.1 mm) or by making the top section thinner than the bottom (4 to 8 mm). In both cases, we have confirmed that the resonance frequency decreases while the effective stresses increase, indicating potential improvements in the energy conversion efficiency. Acknowledgments: This work has been developed by the project TED2021-130884B-I00 funded by MCIN/AEI/10.13039/501100011033 and European Union "Next Generation EU"/PRTR.

1. Narita, F. & Fox, M. A Review on Piezoelectric, Magnetostrictive, and Magnetoelectric Materials and Device Technologies for Energy Harvesting Applications. *Adv. Eng. Mater.* 20, 1–22 (2018). 2. Zhao, X. & Lord, D. G. Application of the Villari effect to electric power harvesting. *J. Appl. Phys.* 99, 8–11 (2006). 3. Ueno, T. Magnetostrictive low-cost high-performance vibration power generator. *J. Phys. Conf. Ser.* 1052, (2018). 4. Wahi, S. K., Kumar, M., Santapuri, S. & Dapino, M. J. Computationally efficient locally linearized constitutive model for magnetostrictive materials. *J. Appl. Phys.* 125, (2019).

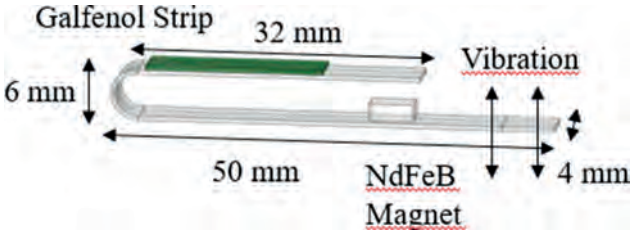

Schematic design of the vibration energy harvesting device.

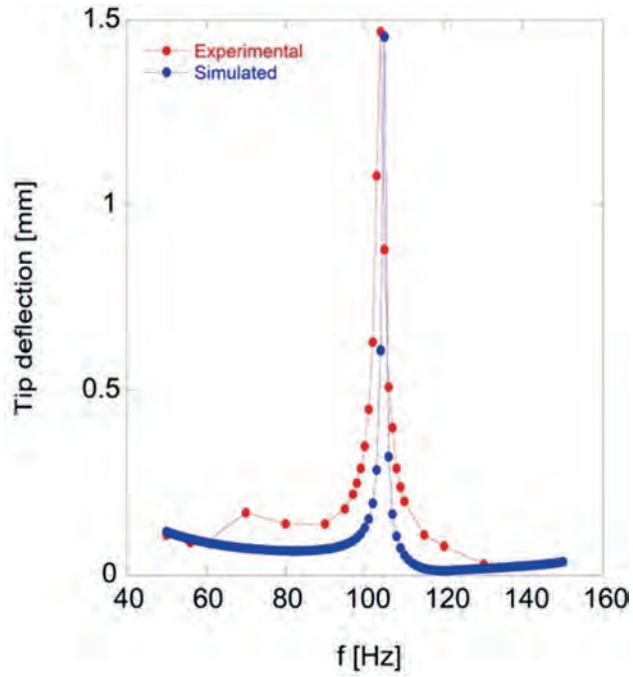

Tip deflection of the harvester at 9.8 m/s^2: experimental *vs* simulated results

GF-06. Giant Magnetovolume Effects Including Negative Thermal Expansion in Thin Film Antiperovskite Manganese Nitrides.
S.K. Patel[1,2], S.B. Hrkac[2], J. Brock[1], N. Hua[2], H. Wen[3], D. Walko[3], O.G. Shpyrko[2] and E. Fullerton[1] *1. Center for Memory and Recording Research, University of California San Diego, La Jolla, CA, United States; 2. Department of Physics, University of California San Diego, La Jolla, CA, United States; 3. Advanced Photon Source, Argonne National Laboratory, Argonne, IL, United States*

Antiperovskite manganese nitrides Mn_3AN (where A is a metal or semiconducting element) are a class of materials of interest for a wide range of physical phenomena including giant magnetoresistance, piezoelectric effects, anomalous Nernst effect, and magnetostructural effects. Studies in bulk of some of these compounds have shown giant magnetovolume effects [1, 2] including negative thermal expansion [2, 3] tied to transitions between ferrimagnetic, antiferromagnetic, and paramagnetic phases which can be tuned by composition [4]. Here, we demonstrate successful growth of thin films of Mn_3AN (001) on MgO (001) substrates which exhibit these magnetovolume effects. Films with composition $Mn_3Cu_{1-x}Ge_xN$ with x = 0.1 to 0.6 demonstrate negative thermal expansion during Néel transitions with out-of-plane thermal expansion coefficients ranging from –58 ± 2 (10^{-6}/K) to near zero with a total out-of-plane lattice contraction of 0.3-0.8%. Films with composition $Mn_3Cu_{0.9}Ni_{0.1}N$ demonstrate a low temperature hysteretic magnetostructural phase transition with a 1.3% out-of-plane lattice expansion and a higher temperature Néel transition exhibiting negative thermal expansion with an over 0.5% out-of-plane lattice contraction. Time-resolved x-ray diffraction measurements following photoexcitation with an optical laser pulse within and through the magnetic phases conducted at the Advanced Photon Source are presented, demonstrating both positive and negative thermal expansion dynamically. Work at UCSD was supported by the U.S. Department of Energy (DOE), Office of Science, Office of Basic Energy Sciences, under Contracts No. DE-SC0018237 and DE-SC0001805. This research used resources of the Advanced Photon Source, a DOE Office of Science user facility operated for the DOE Office of Science by Argonne National Laboratory under Contract No. DE-AC02-06CH11357.

[1] Kim, Chi, Kim, *et al.*, *Phys. Rev. B*, Vol. 68, p. 172402 (2003). [2] Hamada and Takenaka, *J. Appl. Phys.*, vol. 111, p. 07A904 (2012). [3] Sun, Wang, Wen, *et al.*, *Appl. Phys. Lett.*, vol. 91, p. 231913 (2007). [4] Takenaka and Takagi. *Appl. Phys. Lett.*, Vol. 87, p. 261902 (2005).

GF-07. Plastic deformation and damage detection using magnetostrictive Alfenol powder-epoxy composite patches.
S. Na[1], J.H. Yoo[1], B. Yoo[2], D.J. Pines[2] and N.J. Jones[1] *1. Physical Metallurgy and Fire Performance Branch, Naval Surface Warfare Center Carderock Division, West Bethesda, MD, United States; 2. Aerospace Engineering, University of Maryland, College Park, MD, United States*

Many structural health monitoring (SHM) solutions observe only single points of strain or require processing of an acoustic signal to understand what is happening in the structure beneath. It is particularly challenging to apply SHM to ship/aircraft and the supporting structure, however, due to their large and varied physical size and geometry, extreme operational and environmental conditions, and limited sensing technologies available for SHM. Multifunctional materials could provide various SHM solutions as a surface coating composed of functional powders inside of an epoxy matrix. The powder properties, functional interactions, and powder-matrix interactions provide many challenges for adapting such solid state solutions to a large-scale, coating problem. The static and dynamic magneto-elastic sensing properties of Fe-Al alloy (Alfenol) powder-epoxy composites were previously determined in the elastic range of stress/strain [1]. In this work, polymer-matrix composites with magnetostrictive Alfenol particles are evaluated for plastic deformation and damage detection in the composite patches attached to an aluminum substrate. Figure 1(a-c) shows magnetic permeability changes in the magnetostrictive composite patch (MCP) with spherical and flake-type powders. Magnetization and permeability were monitored while tensile stress/strain was applied to the composite patch bonded on the aluminum dog-bone until fracture. Flakes show higher sensitivity and a greater level of magneto-elastic coupling than spheres, exhibiting a 13% change in permeability and a linear response as strain increases up to ~0.5% strain. In addition, aluminum dog-bone specimens with fabricated defects will be discussed, which were instrumented with PZT actuators and an MCP patch to monitor fatigue cycling (Fig. 1d), and the method of monitoring crack propagation and defect evolution by identifying the reflection signals from the MCP at frequencies of ~120 kHz using ultrasonic guided wave techniques.

[1] S.-M. Na *et al.*, *Magnetism* 2, 105-116 (2022).

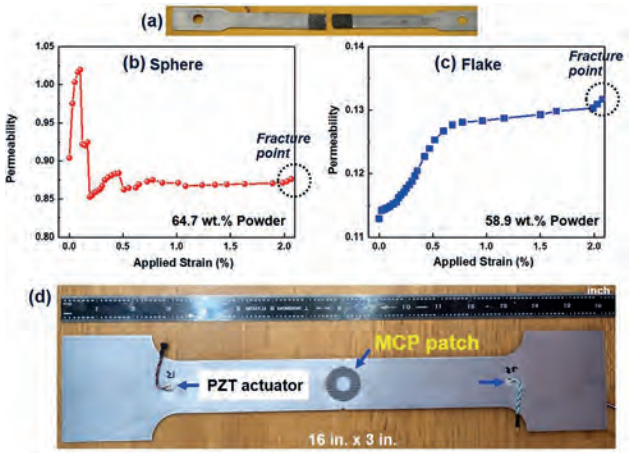

Magnetic permeability changes in the magnetostrictive composite patch embedded on aluminum dog-bone tensile samples for damage detection in static (a) and dynamic (d) conditions.

GF-08. Low-power On-chip Optical Devices Based on the Integration of Tunable Magnetic Nanomaterials.
M. Martí-Carrascosa[1,2], J. Navarro-Arenas[1,4], R. Torres-Cavanillas[3,2], A. García-Regueiro[2], A. Forment-Aliaga[2], J. Parra[1], T. Mengual[1], P. Sanchis[1] and *E. Pinilla-Cienfuegos*[1] *1. Nanophotonics Technology Center, Universitat Politècnica de València, Valencia, Spain; 2. Instituto de Ciencia Molecular (ICMOL), Universitat de València, Paterna, Spain; 3. Department of Materials, University of Oxford, Oxford, United Kingdom; 4. Institute of Materials Science (ICMUV), Universitat de València, Paterna, Spain*

Electro-optical bistability is a functionality which can be crucial for a wide range of applications as it can enable non-volatile and ultra-low power switching performance [1]. In this work an advance in nanophotonics is presented with a new approach for the development of low-power on-chip optical switching devices. This new approach is based on the integration of a tunable magnetic molecular nanomaterial that presents bistable Spin Crossover (SCO) phenomenon near room temperature in the Si platform [2]. SCO is a spin-state switching phenomenon present in some molecular compounds such as the coordination complexes of transition-metal ions in which, under certain external stimuli (variation of temperature, pressure, electric field, or light irradiation), the electronic configuration can be switched between two molecular spin states, Low Spin (LS) and High Spin (HS) states [3]. Furthermore, the spin state change is accompanied by a change in the structural, magnetic, and optical properties, as well as in the electrical conductivity and color. These properties vary as a function of the external stimulus following a hysteretic response, recognized as one of the most promising aspects of the system since hysteresis confers bistability and thus a memory effect (Figure 1). Finally, the SCO material can be synthetized as nanoparticles so that it can be easily integrated in the silicon platform and have the potential to allow optical switching at room temperature.

[1] A. H. Atabaki *et al.*, Nature, 556, no. 7701, 349–354 (2018). [2] M. Giménez-Marqués *et al.* J. Mater. Chem. C, 3, no. 30, 7946–7953 (2015). [3] O. Kahn and C. Jay Martinez, Science, 279, no. 5347, 44–48 (1998).

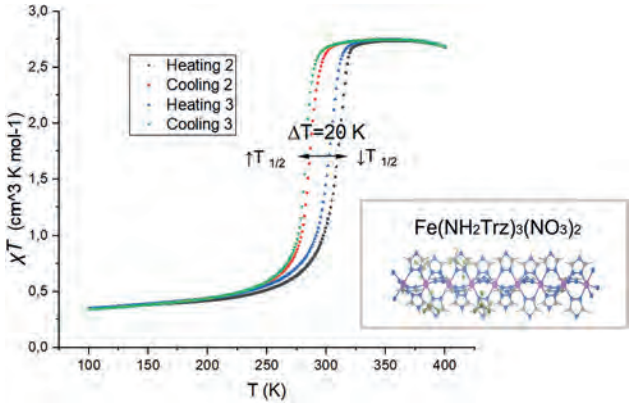

Fig. 1: Temperature dependence of χT of $Fe(NH_2Trz)_3(NO_3)_2$ in the cooling and heating modes. The insert shows the room temperature crystal structure of the corresponding compound.

GF-09. Integrating plasmonic entities into shape controlled magnetic nanomaterials. *H. Khurshid*[1], R. Yoosuf[1], D. Anjum[2] and H. Srikanth[3] *1. University of Sharjah, Sharjah, United Arab Emirates; 2. Khalifa University, Abu Dabhi, United Arab Emirates; 3. University of South Florida, Tampa, FL, United States*

Over the years, magnetic nanomaterials have attracted growing attention due to their potential applications in biomedicine, storage devices, micro and nano-electromechanical systems and magneto-resistive sensors. Particular attention has recently been drawn to the multisegmented hybrid magneto-optic materials because of their multifunctionality and ability of individual tuning of the magnetic and optical segments [1]. On the other hand combining core/shell morphology with shape anisotropy, the multilayered core/shell structured exhibit much higher surface area and interface than segmented ones. In this work we present a novel synthesis approach of tuning the growth pattern of multisegmented nanorods into core/shell structured by utilizing electrochemical deposition method. Fe-Au multisegmented nanorods and the fabrication process was modified to obtain core/shell structured Fe/Au and inverted Au/Fe nanorods. It is demonstrated that with a precise control of deposition parameters, a brick-stacked wire like growth led to the formation of hollow nanotubes that was further tuned to multilayered hollow nanotubes and core/shell structured nanorods [2]. TEM imaging and STEMEELS technique were used to explore the morphology, microstructure and the distribution of Au and Fe in the nanorods. The easy magnetization direction was found to be perpendicular to the nanorods' growth direction in the segmented nanorods. On the other hand, core/shell nanorods exhibited isotropic behavior. Our findings provide deeper insights into the fabrication of hybrid nanorods and the opportunity to tune the fabrication method to vary their morphology accordingly. Our study provides deeper insights into the formation mechanisms of hybrid multisegmented solid nanorods versus hollow nanotubes and core/shell nanorods and hence tunning specific morphologies and physical properties by tunning fabrication conditions. That is an important aspect when designing one dimensional material for sensing, spintronics and other potential biomedical and technological applications.

L. Piraux, Appl. Sci. 10, 1832 (2020). H. Khurshid et al, Nanotech. 34, 185602 (2023).

GF-10. Template-Assisted Growth of Co-$BaTiO_3$ Vertically Aligned Nanocomposite Thin Films with Strong Magneto-optical Coupling Effect. *Z. Hu*[1], J. Lu[2], H. Dou[2], J. Shen[2], J. Barnard[2], J. Liu[2], X. Zhang[2] and H. Wang[1,2] *1. Electrical and Computer Engineering, Purdue University, West Lafayette, IN, United States; 2. Materials Engineering, Purdue University, West Lafayette, IN, United States*

Hybrid oxide-metal metamaterials have attracted tremendous interest in the past decades for the tunable physical properties and multifunctionalities toward emerging technologies [1-4]. For example, self-assembled epitaxial Au-$BaTiO_3$ (BTO) hybrid nanostructures have been shown to have tailorable Au pillar morphology, density, and tunable optical and ferroelectric properties [1,3,5-7]. In this work, a unique Anodic Aluminum Oxide (AAO) template was used to grow a thin Co seed layer and the following self-assembled metal-oxide (Co-$BaTiO_3$) vertically aligned nanocomposite thin film layer. The AAO template allows the uniform growth of Co-seeds and successful deposition of highly ordered Co pillars (with diameter < 5 nm and the interval between pillars < 10 nm) inside the oxide matrix. Significant magnetic anisotropy and strong magneto-optical coupling properties have been observed. A thin Au-$BaTiO_3$ template was also later introduced for further enhanced nucleation and ordered growth of the Co-nanopillars. Taking advantage of such a unique nanostructure, a large out-of-plane (OP) coercive field (H_c) of ~5000 Oe has been achieved, making the nanocomposite an ideal candidate for high-density perpendicular magnetic tunneling junction (p-MTJ). A strong Polar magneto-optical Kerr effect (MOKE) has also been observed which inspires a novel optical-based reading of the MTJ states.

[1] L. Li, L. Sun, J. S. Gomez-Diaz *et al.*, Nano Letters 16, 3936 (2016) [2] J. Huang, T. Jin, S. Misra, H. Wang *et al.*, Advanced Optical Materials 6, 1800510 (2018) [3] M. Kalaswad, D. Zhang, X. Gao *et al.*, ACS Applied Materials & Interfaces 11, 45199 (2019) [4] S. Misra, L. Li, D. Zhang *et al.*, Advanced Materials 31, 1806529 (2019) [5] D. Zhang, Z. Qi, J. Jian *et al.*, ACS Applied Nano Materials 3, 1431 (2020) [6] J. Liu, X. Wang, X. Gao *et al.*, Applied Materials Today 21, 100856 (2020) [7] D. Zhang and H. Wang, Advanced Photonics Research 2, 2000174 (2021)

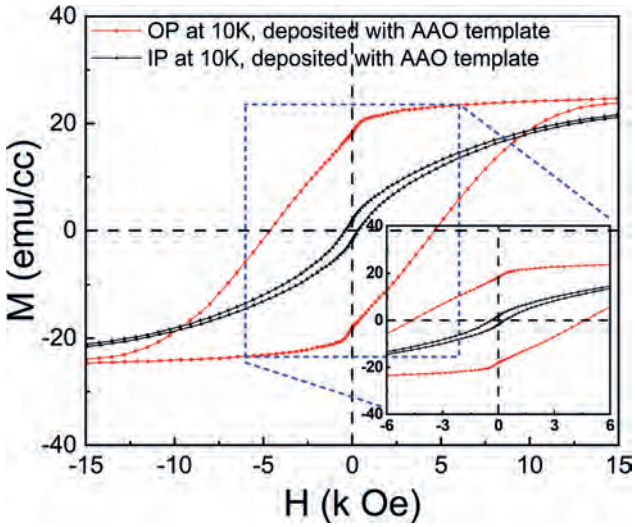

Fig.1 Hysteresis loops of Co-$BaTiO_3$ VAN thin film deposited with AAO template at 10 K for both out-of-plane (red solid line with squares) and in-plane (black solid line with triangles), the inset represents the hysteresis loop under lower external magnetic field.

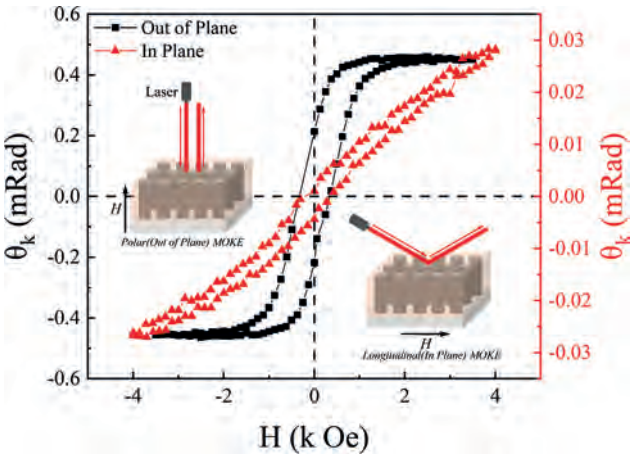

Fig.2 MOKE results for Co-$BaTiO_3$ VAN thin film deposited with AAO template. The black solid line with squares represents the polar (Out-of-plane) MOKE results while the red solid line with triangles represents the longitudinal (In-plane) MOKE results. The insets show the measurement set-up for both cases, respectively.

Session GG
MAGNETIC RECORDING
Simon Greaves, Chair
Tohoku University, Sendai, Japan

CONTRIBUTED PAPERS

GG-01. Study of Grain-Patterned Highly-Ordered $L1_0$-FePt HAMR Media Using Reactive Molecular Dynamics Method. *J. Zhu*[1] and J. Wang[1] *1. Electrical and Computer Engineering, University of Minnesota - Twin Cities, Minneapolis, MN, United States*

Embedded Hard-mask Patterning (EMP) has been proposed as a cost-effective fabrication method to be capable of patterning sub 5-nm grain sizes on highly-ordered $L1_0$-FePt media for Heat-Assisted Magnetic Recording (HAMR) [1]. Understanding the etching patterning mechanism of FePt is critical to maintain the highly-ordered $L1_0$ structure and low damage to the magnetic grains. In this research, Reactive Molecular Dynamics (MD) modeling is developed to study methanol (MeOH) plasma etch on highly-ordered continuous $L1_0$-FePt media film. Reactive interactions between the main plasma product etchant CO/H_2 molecules and Fe/Pt atoms are studied using a modified embedded atom method (MEAM) interatomic potential and a bond-order based ReaxFF force field with atomic charge equilibration. As in $L1_0$-FePt thin film, Fe and Pt atoms are sitting in alternating layers in <001> directions, these interaction mechanisms are studied on Fe and Pt terminated surface respectively. It shows upon the dissociation of the CO ligand deposited at low energy (<10 eV) strong Fe-C interactions lead to Fe_n-C cluster formation as volatile product on the Fe-terminated surface. On the Pt-terminated surface, however, C-Pt interaction does not form any form of cluster volatile product. Dissociated C atoms also interact with Fe atoms under the Pt-layer and therefore can create crystal structure defects. The chemical yield without any physical ion sputtering is 4-5X higher on the Fe-terminated surface than on the Pt-terminated surface. The before and after etched media film is also analyzed with virtual XRD method to show the chemical ordering change from the plasma treatment. This study uncovered not only the etching mechanism of high methanol etch rate on Fe-based magnetic materials but also the magnetic material damage mechanism.

[1] H. Wang et al., Appl. Phys. Lett. 102, 052406 (2013). [2] J. Zhu et al., IEEE Trans. Magn. Vol 52, No.7 (2016).

GG-02. Comparison of *h*BN and graphene nanosheet grain boundary materials for granular FePt-$L1_0$ thin films. *V. Bollapragada*[1], C. Xu[1], B.L. Reese[1], D.E. Laughlin[1] and J. Zhu[1] *1. ECE, Carnegie Mellon University, Pittsburgh, PA, United States*

Highly ordered FePt-$L1_0$ granular media has been the choice for the recording medium for heat-assisted magnetic recording (HAMR). Narrow grain size distribution and high grain aspect ratio are two critical characteristics of film microstructures for enabling recording area density capability (ADC). It is the grain boundary materials that play a key role in achieving these two important aspects. Our recent investigation using a bias sputtering technique has demonstrated the formation of crystalline boron nitride (h-BN) grain boundaries with honeycomb monolayers conforming to FePt grain boundaries. Not only do the *h*-BN nanosheets completely encircle the FePt grains, but they also facilitate columnar growth of the FePt grains which in turn enables a grain aspect ratio as high as h/D = 2.5 [1]. In this paper, we present a systematic study to achieve graphene sheets as grain boundary material for FePt granular media. To realize desired graphene sheets in the granular media by co-sputtering of FePt and Carbon we need proper reverse bias and a high deposition temperature. Figure 1 shows the plane view of transmission electron microscopy (TEM) images for FePt-*h*BN (a) and FePt-C (b), both samples were sputtered at high temperatures with substrate reverse bias. Fig. 1(b) clearly shows the formation of graphene nanosheets conforming to FePt grain boundaries and encircling FePt grains, like that of FePt-*h*BN. The cross-sectional TEM image of FePt-C shows the graphene nanosheets growing vertically along the grain boundary surface of the FePt grains. However, they do not seem to facilitate the columnar growth and the grain aspect ratio is only unity. Further optimization is required to realize the columnar grain growth with graphene nano sheets.

1) "Bias sputtering of granular L10-FePt films with hexagonal boron nitride grain boundaries" Chengchao Xu, B. S. D. Ch. S. Varaprasad, David E. Laughlin, and Jian-Gang (Jimmy) Zhu. https://doi.org/10.48550/arXiv.2303.11411

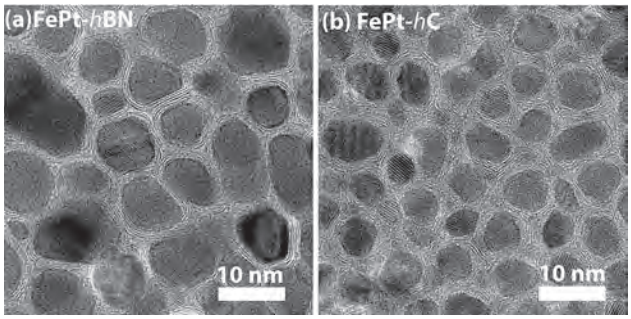

Fig 1. In-plane HRTEM of FePt-*h*BN and FePt-*h*C granular films deposited at 650°C

GG-03. Spin Torque Assist for HAMR Media. *A. Ghoreyshi*[1], A. Venugopal[1], Y. Fan[1], C. Chow[1], J. Gadbois[1], P. Czoschke[1] and S. Hernandez[1] *1. Seagate Technology LLC, Bloomington, MN, United States*

Track pitch scaling is the primary mechanism to increase areal density capability (ADC) in Heat-Assisted Magnetic Recording (HAMR) [1-2], as linear density capability improvement becomes more difficult, particularly for ADC > 3Tbpis. In this study, we propose that spin current injection at elevated temperature near the Curie temperature can significantly improve switching probability (Fig. 1a) and enhance linear density capability of FePt recording media. We study the magnetization dynamics of single grain FePt during the writing process using atomistic simulations. We calculate switching probabilities after cooling down from different peak temperatures to room temperature while an applied field opposes the initial magnetization direction. During this process, spin current is injected at the bottom interface layer with polarization along the -z direction. According to Fig. 1b, the number of high-frequency magnons increases as $T \rightarrow T_c$. Near T_c, spin current can enhance temporal oscillation of the population of the in-plane magnon. These oscillations lead to higher reversal probability. As depicted in Fig. 1a, J=1e13 A/m^2 injecting greatly reduces both writing temperature (by ~100K) and transition sigma, which will improve transition SNR and jitter. At the device level, different mechanisms for spin generation such as the spin Seebeck effect and spin transfer torque (head to media tunneling) will be explored.

1. Rea, Chris, et al. "Areal-density limits for heat-assisted magnetic recording and perpendicular magnetic recording." *IEEE Transactions on Magnetics* 52.7 (2016): 1-4. 2. Hernandez, Stephanie, et al. "Geometrical scaling limits of heat-assisted magnetic recording." *IEEE Transactions on Magnetics* 57.3 (2020): 1-5.

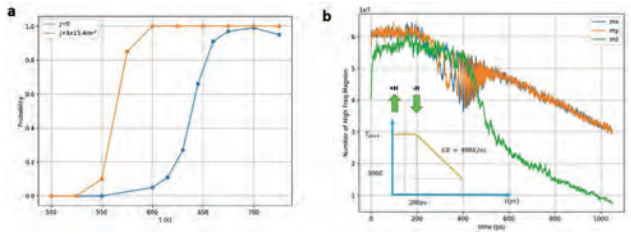

a) Switching probability for 6nm × 6nm × 12nm FePt grain b) number of high frequncy magnons

GG-04. Recording Medium Configurations for Double-Layer Bit-Patterned Magnetic Recording. C. Buajong[1] and *C. Warisarn*[1]
1. King Mongkut's Institute of Technology Ladkrabang, Bangkok, Thailand

With the tremendous increase in the demand for larger storage capacity, new recording technologies are essential to support this ever-increasing demand. One of the promising technologies is bit-patterned magnetic recording (BPMR) [1]. Recently, ideas of increasing an areal density (AD) by stacking multiple recording mediums upward have been explored on a conventional medium [2]-[3]. To further maximize the storage capacity, BPMR system with a stack of two recording layers each of which is a bit-patterned medium has been investigated [4]-[5]. Since the lower layer is further from the read/write head, difficulty in the retrieval signal and processing of data from the lower layer is expected. In this work, we examine two distinct configurations of recording medium in BPMR system with double recording layers as shown in Fig. 1. Recording medium in the first configuration employs two layers containing rectangular close-packed arrays of circular islands. In contrast, hexagonally packed arrays of islands are considered in the second configuration. In both configurations, the centers of individual islands on the lower layer are positioned under the gaps between magnetic islands on the upper layer. Such an arrangement potentially mitigates inter-layer interference that may occur during the superposition of signals from the upper and lower layers in the readback waveforms as shown in Fig. 2. By utilizing oversampling, we simply achieve the separation of the individual layer signals since the centers of islands on both layers are not aligned with one another. This also allows the simultaneous processing of data from both layers during one-dimensional equalization and detection. In the early stages, simulation results indicate that the proposed configurations can deeply improve the bit error rate (BER) performance compared with the single-layer BPMR system, considering a total AD of 4 Tb/in^2 and a perfect writing condition.

[1] B.D. Terriset et al., Microsyst. 13(2), 189–196 (2006). [2] K. S. Chanet et al., IEEE Trans. Magn. 55(12), 1–16 (2019). [3] Y. Nakamura et al., IEEE Trans. Magn. 58(8), 1–4 (2022). [4] N. Rueangnetr et al., AIP Adv. 13 (3), 035104 (2023). [5] H. Saito, IEEE Trans. Magn, 59(3), 3000810 (2023).

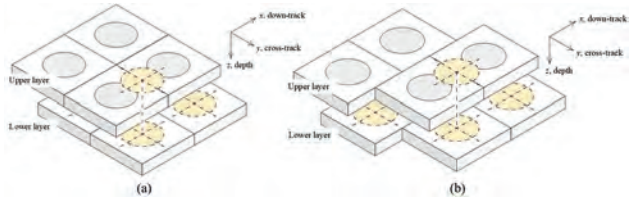

Fig. 1 The double-layer BPMR system with two configurations.

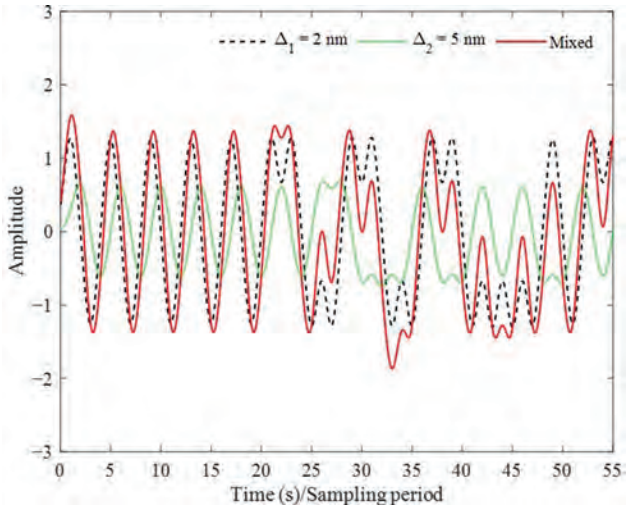

Fig. 2: Readback waveform without noise retrieved from the proposed double-layer BPMR system. The separation between the read/write head and the upper- and lower-layers are Δ_1 and Δ_2, respectively. "Mixed" represents the superposition of signals.

GG-05. Reducing Transition Jitters in Composite Media for Magnetic Recording. *Y. Liu*[1] and R.H. Victora[2,1] *1. School of Physics and Astronomy, University of Minnesota, Minneapolis, MN, United States; 2. Department of Electrical and Computer Engineering, University of Minnesota, Minneapolis, MN, United States*

In order to minimize the thermal effect of T_c variation of the media in heat-assisted magnetic recording (HAMR), we investigate a three-layer thermally exchange coupled composite (ECC) media with reduced Tc = 500 K for FePt. Compared to the two-layer ECC media [1], our work, as shown in Table I, demonstrates a 20K reduction in writing temperature (T_{write}), ~8% reduction in FWHM of the switching probability distribution (SPD) curve and ~13% reduction in transition jitter for the three-layer ECC media subject to grain pitch (5.5nm), 3% Tc and 15% Ku variation of each layer. The original two-layer ECC structure was first proposed in [2] to mitigate the issues of thermal fluctuation, consisting of a superparamagnetic writing layer and a storage layer (FePt). Our three-layer structure is achieved by inserting a middle layer that separates the superparamagnetic layer and storage layer (FePt) and each layer is set to be 3nm thick as shown in Fig.1. The optimized parameters for the superparamagnetic layer are Ms = 1300 emu/cm^3, $K_u = 0.5 \times 10^7$ erg/cm^3 at 300 K and Tc = 600K. M_s = 600 emu/cm^3, $K_u = 3.2 \times 10^7$ erg/cm^3 at 300 K and Tc = 515K are for the middle layer. Magnetic simulations are conducted with 1.5nm renormalized cells based on renormalization group theory [3]. Compared to the previous two-layer ECC structure [1], we found that a new set of parameters for the superparamagnetic layer and the introduction of reasonable interlayer exchange coupling between the middle layer and the storage layer are responsible for the improvement of switching and recording performance. Our results can potentially promote the commercialization of HAMR technology by further suppressing the thermal noise and hence improving the areal density.

[1] N. A. Natekar, W. Tipcharoen, and R. H. Victora, "Composite media with reduced write temperature for heat assisted magnetic recording," J. Magn. Magn. Mater., vol. 486, Sep. 2019, Art. no. 165253. [2] Z. Liu and R. H. Victora, "Composite structure with superparamagnetic writing layer for heat-assisted magnetic recording," IEEE Trans. Magn., vol. 52, no. 7, Jul. 2016, Art. no. 3201104, [3] R. H. Victora and P.-W. Huang, "Simulation of heat-assisted magnetic recording using renormalized media cells," IEEE Trans. Magn., vol. 49, no. 2, pp. 751–757, Feb. 2013.

	FWHM of SPD (K)	T_{write} (K)	SNR(dB)	Jitter(nm)
2-layer	53.6	492	16.0	1.29
3-layer	49.8	472	16.1	1.13

Table I: Comparison between the proposed two-layer and three-layer ECC structure.

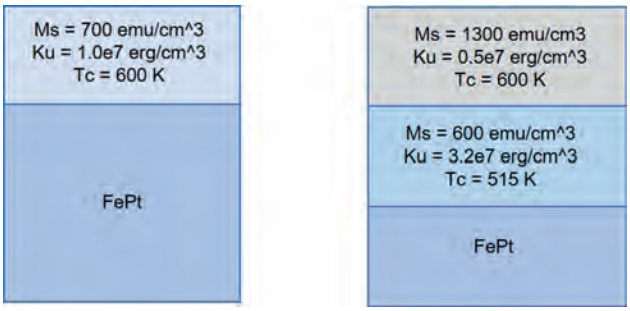

Fig1. Left: proposed two-layer structure with 3nm top layer and 6nm storage layer. Right: proposed three-layer structure and each layer is 3nm thick.

GG-06. Bit-Island Arrangement and Signal Processing in Double-Layer Magnetic Recording Technology. V. Sawangarom[1], C. Buajong[1], *K. Kankhunthod*[1] and C. Warisarn[1] *1. King Mongkut's Institute of Technology Ladkrabang, Bangkok, Thailand*

To overcome the superparamagnetic limitation [1]-[2] that is the barrier to increasing the areal density (AD) of perpendicular magnetic recording technology, bit-patterned magnetic recording (BPMR) has been presented and applied together with the double layer magnetic recording (DLMR) [3]-[5]. Those works reveal the possibility and potential of DLMR to continuously increase AD. In this work; therefore, we first propose a DLMR structure that is designed based on bit-patterned media as shown in Fig. 1. The bit islands are aligned with a rectangular grid but the relative positions of each layer were shifted at the along- and cross-track directions by $T_x/2$ and $T_z/2$, respectively. On the top view, we have staggered-like recording media [6]. Then, we also present the use of an array reader that consists of three readheads in reading process, the way to retrieve all three readback signals will be described. The first (H_1) and third (H_3) readheads are positioned at the center of the *l*-th and *l*+2-th tracks (upper layer), respectively. The second readhead (H_2) is positioned over the middle of the *l*+1-th track (lower layer). To evaluate the BER performance between our proposed media design under equivalent AD of 4.0 Tb/in^2 (2.0+2.0 Tb/in^2) denoted by "Prop. System" with the conventional single-layer bit-patterned media under AD of 4.0 Tb/in^2 denoted by "Conv. System" as shown in Fig. 2. BER performances of the 1st, 2nd, and 3rd tracks are denoted by "Prop. System. H1 (UL)", "Prop. System. H2 (LL)," and "Prop. System. H3 (UL), respectively. The average BER of three data tracks is denoted by "Prop. System. Avg." The BER performances of the 1st and 3rd tracks are great because of lower ITI interference. On the other hand, the performance of the 2nd track is degraded by ILI effect. It implies that the proposed media structure based on a double-layer magnetic recording can enhance performance. Moreover, in this work, the optimal diameter of bit islands for each layer and the coding schemes will be also examined for avoiding ISI, ITI, and ILI effects.

[1] C. Ross, Annual Review of Materials Research, 31(1). pp. 203-235 (2001) [2] R. L. White et al., IEEE Trans. Magn., pp. 990-995 (1997) [3] Y. Nakamura et al., 2021 IEEE INTERMAG, LYON, France, pp. 1-5 (2021) [4] H. Saito, IEEE Trans. Magn., 59(3), 3000810 (2023) [5] Y. Nakamura et al., IEEE Trans. Magn., 58, pp. 1-5 (2022) [6] Y. Ng et al., IEEE Trans. Magn. 48(6), pp. 1976-1983 (2012)

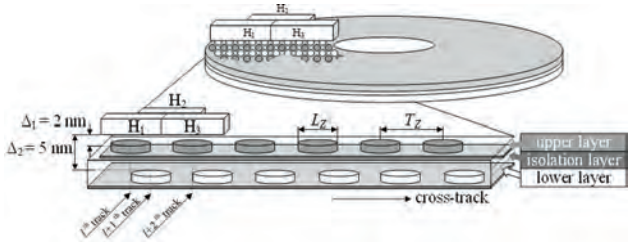

Fig. 1 Media structure and readhead positions of proposed double-layer BPMR systems.

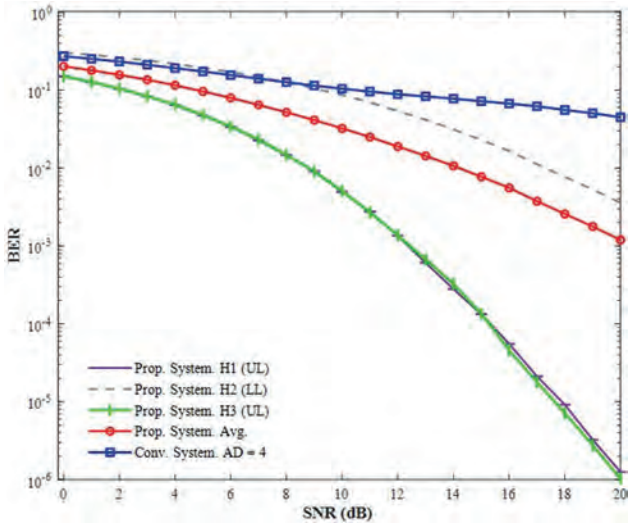

Fig. 2 Performance comparison in terms of BER between the proposed and conventional systems.

GG-07. Capacitive Plasmonic Near Field Transducer with Tapering Design. *T. Du*[1], D.E. Laughlin[1] and J. Zhu[1,2] *1. Materials Science and Engineering, Carnegie Mellon University, Pittsburgh, PA, United States; 2. Electrical and Computer Engineering, Carnegie Mellon University, Pittsburgh, PA, United States*

A near field transducer (NFT) is a key component in heat assisted magnetic recording (HAMR). [1][2] In this work, we present a novel NFT design through the capacitive coupling. Fig 1 shows the geometry of our design, tapered metal bars separated by thin dielectric materials with gap distance G are used to create the plasmonic resonance and focus the electromagnetic field. The motivation for the design is that the segmentation by more thermally stable dielectric material between the metal bars should significantly enhance the stability of the plasmonic metal. Using COMSOL software, the performance of this capacitive-coupled NFT is systematically modeled. Fig 2 shows the simulation result of $|E|^2$ intensity inside the dielectric gaps with a resonant free wavelength of 1180 nm, matching one of the resonance modes determined by the length of the NFT and the number of dielectric gaps. The focusing effect is evidently pronounced due to the tapering towards the air bearing surface (ABS). The inset of the figure shows the peak intensity profile of the electric field for three different peg widths (at the ABS). In addition, this design also results in efficient coupling of the laser light. In conclusion, this capacitive-coupled NFT with dielectric separation gaps and tapering yields relative high efficiency similar to that of the lollipop NFT design with the potential for significantly enhanced material thermal stability.

[1] W.A. Challener, et al, Nature Photonics, 3 (4), 220-224 (2009) [2] K. Shimazawa, W. Xu, K. Fujil, US11,315,591B1, Headway Technologies, (2022)

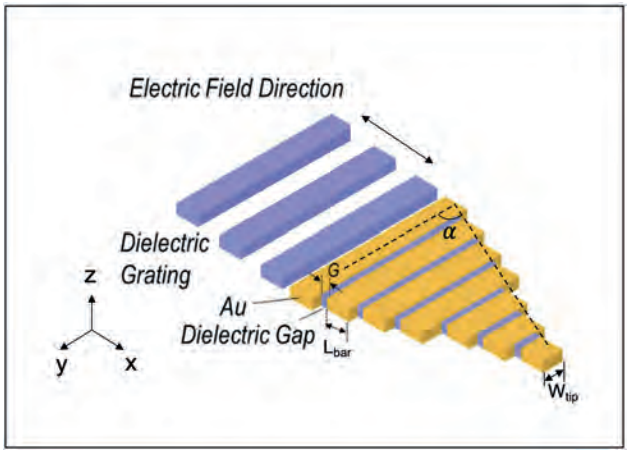

Fig 1: Schematic view of the designed capacitive plasmonic NFT.

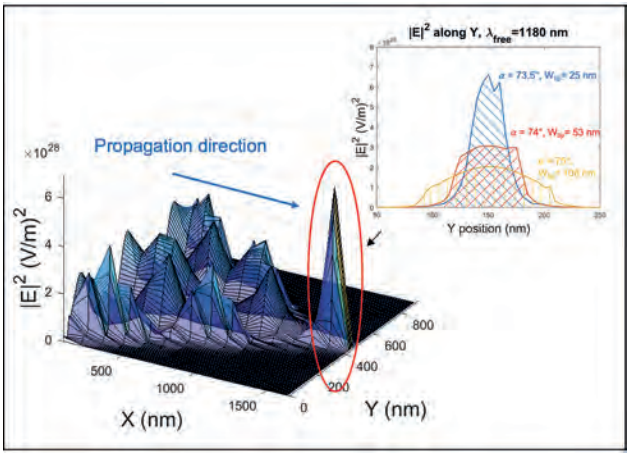

Fig 2: The propagation of the electromagnetic wave inside the tapered structure at a free wavelength of 1180 nm with peg width 25 nm. The insert shows the $|E|^2$ profile along the Y direction for different NFT tapering angle and tip size.

GG-08. Magnetic Read Sensor Design using a Lateral Spin Valve.
R. Hao[1] and R. Victora[1] *1. Department of Electrical and Computer Engineering, University of Minnesota, Minneapolis, MN, United States*

We propose a magnetic read sensor design based on a lateral spin valve (LSV) structure as shown in Fig. 1(a). Compared to other LSV read sensor designs, like in [1], our design is different in that: (1) we place the left spin injection part near the recording medium and the right spin detection part away from the medium. (2) For spin detection, we form a magnetic tunnel junction below the Al channel for tunneling magnetoresistance (TMR) measurement [2] as the reading signal. Spin-polarized electrons from Al can enter the ferromagnet FM2 and change its magnetization, while unpolarized electrons will not alter the TMR ratio so their shot noise influence is reduced, and the signal-to-noise ratio (SNR) of reading can be enhanced. (3) The applied voltage across the spin detection part also helps suppress electrons diffusing reversely from the pinned layer into FM2, thus further reducing shot noise. Next, we propose to replace the single layer FM2 by a synthetic antiferromagnetic (SAF) structure, see Fig. 1(b), since the Ruderman-Kittel-Kasuya-Yosida (RKKY) interaction in SAF free layer (SAF-FL) may help spin-transfer torque (STT) driven magnetization switching [3] [4]. Macrospin magnetic simulation results show that at room temperature, a 4-nm-thick FM2 can follow a GHz current signal only with saturation magnetization M_S below 150 emu/cm^3, while a SAF-FL with each component ferromagnetic layer 2 nm thick can work with M_S = 520 emu/cm^3. Using a pseudorandom binary sequence 4 for current spin polarization direction, with 40 iterations of 100 ns operations, the influence of field-like STT amplitude on the SNR of SAF-FL is shown in Fig. 2. It shows that field-like STT can play an important role in STT switching in SAF-FL.

[1] M. Yamada, D. Sato, N. Yoshida, *et al*., in *IEEE Transactions on Magnetics*, Vol. 49, p. 713 (2013). [2] T. Valet and A. Fert, *Phys. Rev. B*, Vol. 48, p. 7099 (1993). [3] T. Ochiai, Y. Jiang, A. Hirohata, *et al*., *Appl. Phys. Lett.*, Vol. 86, p. 242506 (2005). [4] M. Ichimura, T. Hamada, H. Imamura, *et al*., *J. Appl. Phys.*, Vol. 109, p. 07C906 (2011).

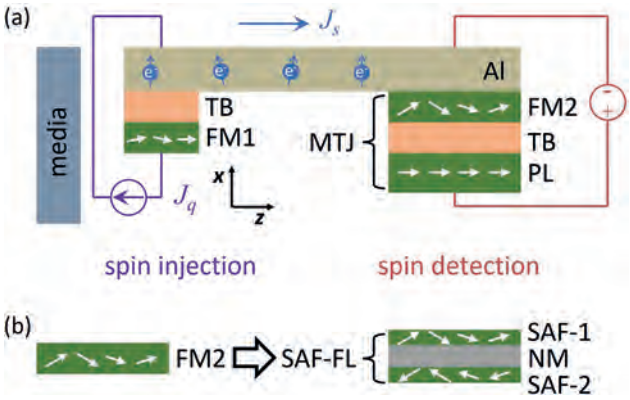

Fig. 1. (a) Our magnetic read sensor design based on a lateral spin valve structure. TB: nonmagnetic tunnel barrier. PL: ferromagnetic pinned layer. (b) Proposal of replacing single layer FM2 by a synthetic antiferromagnetic structure as the free layer. NM: nonmagnetic layer like Ru.

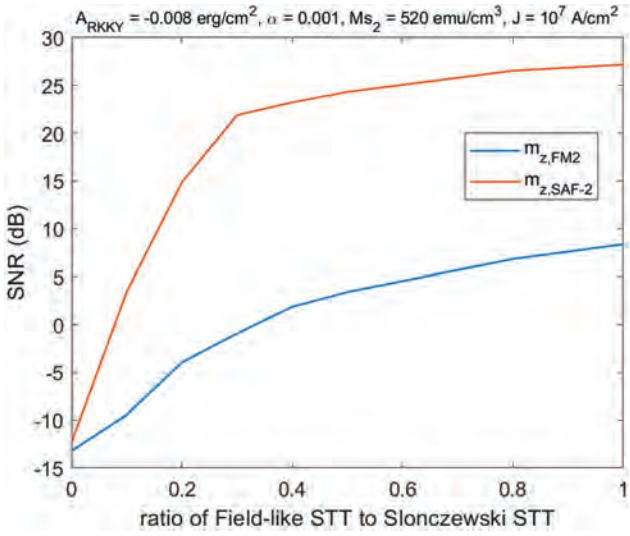

Fig. 2 Macrospin simulation of spin-transfer torque switching in SAF-FL. The applied current density is 10^7 A/cm^2, the damping constant is 0.001, and the RKKY interaction strength is -0.008 erg/cm^2.

GG-09. Multilayer Perceptron-Based Array Reader Optimization for Ultra-High Density Magnetic Recording.
N. Rueangnetr[1] and *C. Warisarn*[1] *1. King Mongkut's Institute of Technology Ladkrabang, Bangkok, Thailand*

To support the exponential growth of data storage demand, bit-patterned magnetic recording (BPMR) [1] has been presented as a new alternated recording technology using the patterned isolated magnetic islands in place of granular media. The signal-to-noise ratio can be gained, so an areal

density (AD) can be also increased up to 4.0 Tb/in^2. To reach the expected AD; however, the distance between bit-island must be shrunk closer to each neighboring island, which means two-dimensional (2D) interference and media noise will be also dramatically increased. Therefore, both 2D modulation encoding techniques [2-4] and deep neural networks [4-5] were wildly utilized to cope with those problems under the multi-reader systems [6]. we first propose to use the multilayer perceptron (MLP) for refining the soft information under the rate-5/6 2D modulation coded three-track/three-head BPMR systems as illustrated in Fig. 1, which has been continuously developed from prior soft-information flipper based on long-short term memory (LSTM) networks [4]. The data patterns and input numbers of the soft information are carefully investigated. Moreover, to cope with the codeword border effect, we also propose the MLP-based array reader optimization method. Among all three coded tracks, the upper- and lower-most tracks are still suffered from neighboring track interference; therefore, we present the suitable reader positions of three readers in three cases as shown in Fig. 1. The moving distance is considered in the percentage of the track pitch. Then, their readback signals are sent to the read channel for processing. As shown in Fig. 2, the proposed MLP soft information flipper can provide better recording performance in terms of bit-error rate (BER), which can gain 1.5 dB at BER = 10^{-4} over the LSTM soft information flipper [4]. Moreover, results also show that an appropriate position of an array reader can significantly yield better BER performance utilizing the MLP-based array reader optimization method.

[1] B. D. Terriset et al., Microsyst. 13(2), 189–196 (2006) [2] C. Warisarn, A. Arrayangkool, and P. Kovintavewat, IEICE Trans. Electron. E98.C, 528–533 (2015) [3] C. D. Nguyen and J. Lee, IEEE Trans. Magn. 53(3), 3101207 (2017) [4] N. Rueangnetr, L. M. Myint, and C. Warisarn1, AIP Advances 11, 015307 (2021) [5] A. Aboutaleb et al., Appl. Phys. Lett. 119, 010502 (2021) [6] G. Mathew et al., IEEE Trans. Magn., vol. 50, no. 3, pp. 155-161, (2014)

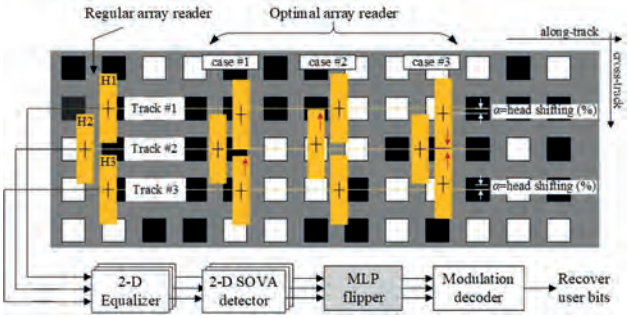

Fig. 1 Positions of three array readers that fly over the island and the proposed MLP soft information flipper.

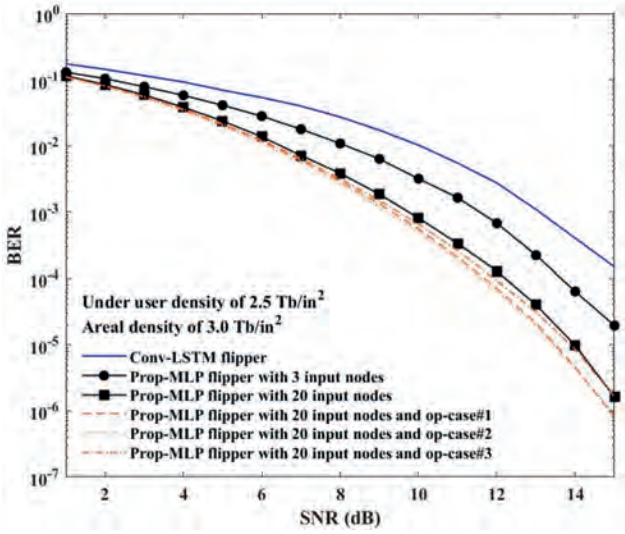

Fig. 2 BER performances of various recording systems with different reader configuration cases.

Session VP1
DOMAIN WALL, VORTEX, AND SKYRMION DYNAMICS AND DEVICES (VIRTUAL)
(Poster Virtual Session)

Susmita Saha, Chair
Ashoka University, Haryana, India

VP1-01. Current-induced domain wall motion in Pd/Co_2MnGa with perpendicular magnetic anisotropy. *T. Koyama*[1], Y. Nishioka[1], T. Uemura[1] and M. Yamanouchi[1] *1. Graduate School of Information Science and Technology, Hokkaido University, Sapporo City, Japan*

Reduction of current density required to move a domain wall (DW) is one of major issues for spintronics devices using current-induced DW motion. Perpendicularly magnetized Weyl ferromagnet is promising for such applications because efficient current-induced DW motion by Weyl electrons has been theoretically proposed [1] and demonstrated in a Weyl ferromagnet $SrRuO_3$ at low temperature [2]. Toward practical applications of Weyl ferromagnet, we study current-induced DW motion in a perpendicularly magnetized Co_2MnGa (CMG) because CMG is considered to be Weyl ferromagnet at room temperature [3]. Pd (2.5 nm) / CMG (1.6 nm) was deposited, from the surface side, on an MgO substrate, where the Pd layer was deposited to induce the perpendicular anisotropy in CMG [4]. The stack was processed into a Hall-bar structure with a 2-μm wide channel and a Au/Cr Oersted line. The transverse resistance showed a square hysteresis with respect to a perpendicular magnetic field, which indicates the CMG was perpendicularly magnetized. After preparing a DW in the channel by applying a current pulse to the Oersted line, successive current pulses with various amplitudes and 10 ms duration were applied to the channel under zero magnetic field at room temperature. When current density in Pd/CMG was higher than 2.9×10^7 A/cm^2, the DW was moved by current in the direction opposite to current. Considering that current density in the CMG layer was two orders of magnitude lower than that in Pd/CMG from resistivity measurements, the observed DW motion cannot be explained by the conventional spin transfer torque and field-like torque in CMG. We measured the propagation field of the DW under a DC current to elucidate the mechanism. The propagation field varied almost linearly with current, which indicates current acts as an effective magnetic field driving the DW. These results suggest that torque induced by Weyl electrons and/or spin orbit torque originating from spin Hall effect in the Pd layer play an important role in the observed current-induced DW motion. This work was supported in part by JSPS KAKENHI (22K18961), MEXT X-NICS (JPJ011438), MEXT ARIM (JPMXP1222HK0071), and JST CREST (JPMJCR22C2).

[1] Y. Araki and J. Ieda, Phys. Rev. Lett. 127, 277205 (2021). [2] M. Yamanouchi, *et al*., Sci. Adv. 8. 15 (2022). [3] Q. Wang, *et al*., Appl. Phys. Lett. 115, 252401 (2019). [4] B. M. Ludbrook *et al*., Appl. Phys. Lett. 110, 062408 (2017). [5] H. Jiajao *et al*., Appl. Phys. Lett. 119, 212409 (2021).

VP1-02. Dynamic Susceptibility of Dipolar Coupled Magnetic Vortices. T.G. Jales[1], S.M. Martins Jr[3], A. Carriço[4] and *A.L. Dantas*[1,2] *1. Department of Physics, State University of Rio Grande do Norte, Mossoró, Brazil; 2. Department of Science and Technology, State University of Rio Grande do Norte, NATAL, Brazil; 3. Department of Physics, State University of Maranhão, São Luís, Brazil; 4. Department of Physics, Federal University of Rio Grande do Norte, Natal, Brazil*

The ability to manipulate and control the motion of magnetic vortices offers new opportunities for developing high-density and low-power memory devices. We present a model calculation of the dynamic susceptibility of a pair of dipolar vortices coupled in two coaxial Py nanocylinders stacked along the z-axis. The nanocylinders have a height of h and are separated by a nonmagnetic layer with a thickness of t (Py(h)|NM(t)|Py(h)). We have found a bimodal spectrum for the in-plane susceptibility (χ_{xx}) for an oscillating magnetic field of 1.0 Oe, where the low-frequency mode is associated with the vortex core dynamics. Furthermore, we have found that the system dimensions may tune the susceptibility spectrum. For instance, the resonance frequency peaks of a vortex in an isolate Py(12 nm) nanocylinder with a 39 nm diameter are 1.6 and 11.5 GHz. While for a 63 nm diameter Py(12 nm) nanocylinder, the frequencies are 1.4 and 11.0 GHz. For a pair of Py(12 nm) nanocylinders, with 39 and 63 nm diameter, separated by a 1nm thick nonmagnetic layer, the vortex core's resonant frequencies increase to 1.7 and 2.1 GHz, respectively, while, in both cases, the second peak is at 10.5 GHz (see Fig.1). Fig.2 shows the vortex magnetization pattern in the bottom 63 nm diameter Py(12 nm) nanocylinder. The magnetization profile of the upper nanocylinder is the same. As seen in Fig.2, our results indicate that the low-frequency mode corresponds to vortex core excitations, while the higher-frequency mode originates from excitations away from the vortex core, located near the nanocylinder lateral surface.

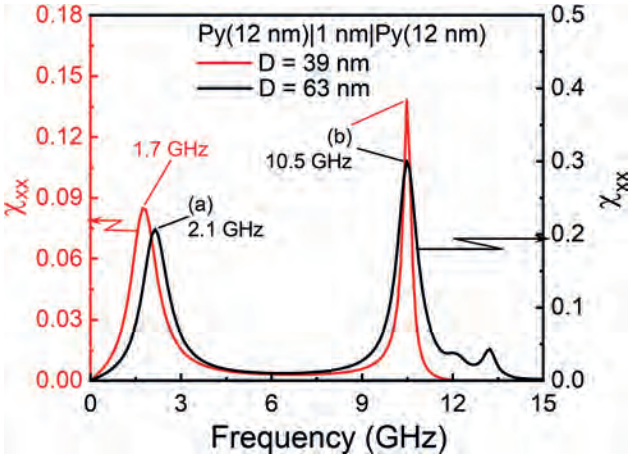

Dynamic susceptibility of a pair of Py(12 nm)|NM(1 nm)|Py(12 nm) nanocylinders with 39 and 63 nm diameters.

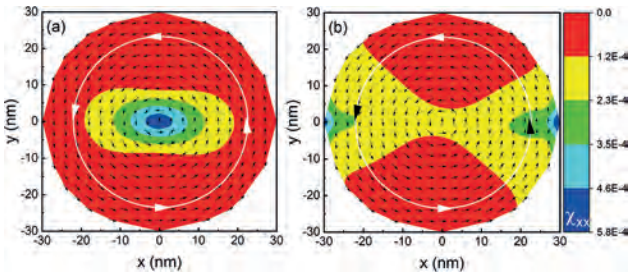

The panels show the magnetic profile of the bottom nanocylinder, and the color barcode indicates the local contributions for χ_{xx} in frequencies of (a) 2.1 GHz and (b) 10.5 GHz, pointed out in Fig.1. The white arrow lines are just a visual guide.

VP1-03. Domain Wall Excitation by Spin Polarized Current. F.V. Diniz[1], T.G. Jales[1], L.L. Oliveira[2], A. Carriço[3] and *A.L. Dantas*[1,2] *1. Department of Physics, State University of Rio Grande do Norte, Mossoro, Brazil; 2. Department of Science and Technology, State University of Rio Grande do Norte, NATAL, Brazil; 3. Department of Physics, Federal University of Rio Grande do Norte, Natal, Brazil*

We presently report a theoretical discussion of the spectra of interface pinned domain walls (DW), in Py stripes subjected to spin-polarized currents and exchange coupled to two-sublattices vicinal antiferromagnetic (AFM) substrates. The DW are pinned at the edges between terraces, with length L_x, holding magnetic moments from opposite substrate sublattices [1]. The terraces exhibit alternate effective interface exchange field ($\pm H_{int}$), and the terrace length (L_x) sets the distance between consecutive DW (See Fig.1). We consider the spin-transfer torque of a weak spin current density ($J=10^7$ A/m^2) along the x-axis and perpendicular to the interface steps edges. Owing to the magnetization gradients along the stripe, we investigated the effect of the Zhang-Li torques on the magnetic domain wall dynamics. Fig.1 shows the equilibrium configuration of a domain wall sequence in a Py micrometer stripe on a vicinal AFM substrate with 250 nm terraces, 50 nm width, and 20 nm thick subjected to an alternate interface field of 200 Oe. The time oscillation of the x-component of the magnetization is shown in the inset of Fig.2. As in the magnetic domain region (see Fig.1), the magnetization x-component is saturated, then the time oscillations of M_x are exclusively from the domain walls region. Therefore, from the oscillatory function of M_x, we calculate the fast Fourier transform and obtain the resonant frequencies of the domain walls. Our results indicate that the magnetic domain resonance is proportional to the interface exchange field—accordingly, the effect of the interface is inversely proportional to the thickness of the stripe. So, as shown in Fig. 2, the domain wall resonance decreases with Py stripe thickness. For the Py/AFM stripe with dimensions of 1μm x 50 nm, with 10, 15, and 20 nm thicknesses, the domain wall frequency mode are 1.41 GHz, 606, and 505 MHz, respectively.

[1] F. A. L. Andrade et al, AIP Advances, 12, 035252 (2022)

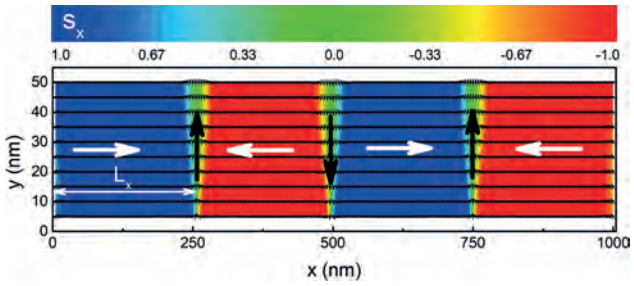

Magnetization pattern of a Py stripe with dimensions of 1μm x 50 nm x 20 nm on a vicinal AFM substrate, with 250 nm wide terraces.

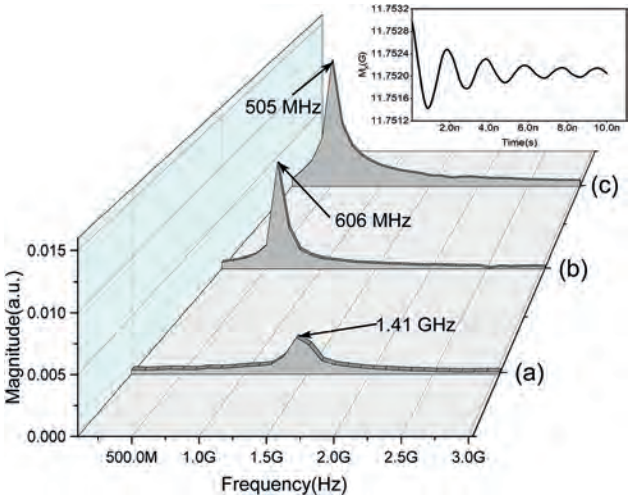

Domain wall spectrum of Py/AFM stripe with dimensions of 1μm x 50 nm and thickness of (a) t = 10 nm, (b) t = 15 nm, and (c) t = 20 nm. The inset shows the x-component magnetization with time.

VP1-04. Realization of zero-field skyrmions in a magnetic tunnel junction. *B. He*[1,2], Y. Hu[3] and G. Yu[1,2] *1. Institute of Physice, Chinese Academy Sciences, Beijing, China; 2. University of Chinese Academy of Sciences, Beijing, China; 3. Lanzhou university, Lanzhou, China*

The stability of skyrmions in zero external magnetic field is significant for promoting fundamental studies and device applications. Here, we develop a zero-field exchange-biased skyrmion material and integrate it into an MTJ device. An Ir layer is inserted between the antiferromagnetic and ferromagnetic layers, which plays a key role in prohibiting interlayer diffusion under thermal annealing, resulting in simultaneous enhancement of exchange bias and thermal stability. The zero-field skyrmion material is then integrated into a perpendicularly-magnetized MTJ, leading to the first demonstration of zero-field skyrmions in an MTJ, which is an important step toward developing skyrmion-based spintronic devices

[1] B. He, Y. Hu, G. Q. Yu, Adv. Electron. Mater., Vol 9. p. 2201240 (2023)
[2] A. Fert, V. Cros, J. Sampaio, Nat. Nanotechnol., Vol 8. p.152168 (2013)
[3] N. Nagaosa., Y. Tokura, Nat. Nanotechnol., Vol 8. p. 899911 (2013) [4] X. Ma., G. Yu., S. A. Razavi., Phys Rev Lett, Vol.119, p. 027272 (2017)

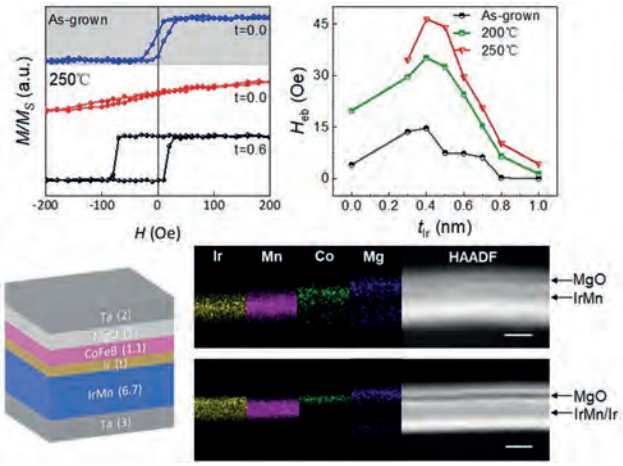

Enhanced exchange bias and thermal stability

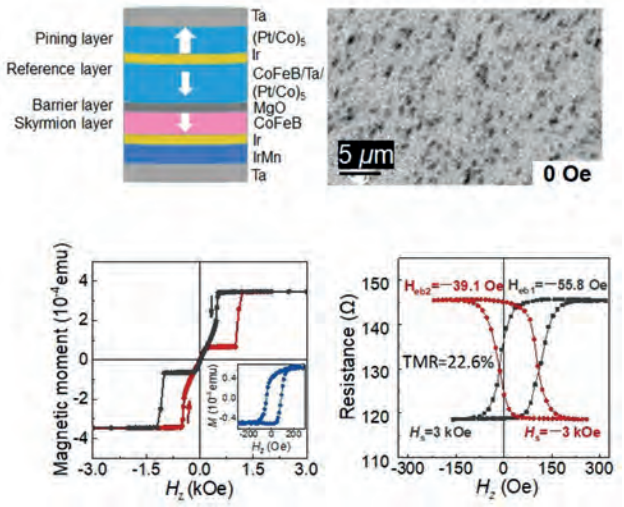

Zero-field skyrmions in an MTJ

VP1-05. Current Induced Conversion of Neel Stripe Domain to Pairs of Bimeron – Antibimeron in Square Nanodot. *B. Priyanka*[1], S. Syamlal[1], H. Perumal[1] and J. Sinha[1] *1. Department of Physics and Nanotechnology, SRM Institute of Science and Technology, Chennai, India*

In depth understanding of the stabilization mechanism of magnetic bimeron, also known as analogues of skyrmion in in-plane magnetized systems, is crucial in building future spintronic based memory and logic technologies [1, 2]. Here, using micromagnetic simulation mumax³[3], we investigate the dynamics of Neel stripe domain under the continuous application of Zhang-Li type spin transfer torque in a ferromagnetic square nanodot (side length – 512 nm, thickness – 4nm). We consider in-plane magnetic anisotropy and select the material parameters corresponding to Pt/Co with interfacial Dzyaloshinskii-Moriya interaction. For such parameters, initially a Neel stripe domain is stabilized in the square nanodot and subsequently, it is subjected to an in plane current density of 100 MA/cm^2 along – x direction. Our results show that the domain starts to deform its shape from the lower boundary of the nanodot due to the instabilities caused by the competing terms such as STT, DMI and exchange interactions. As a consequence of this instability, we observe the transformation of the Neel type stripe domain (Q = 0) into pairs of bimeron (Q = +1) and antibimeron (Q = -1) (cf. Fig. 1). The temporal evolution of total energy plot exhibits distinct characteristics during this conversion process as shown in Fig. 1 (b). By analysing the spin configurations at specific time stamps in the total energy plot, we infer that it is energetically favourable for the stripe domain to completely transform into the pairs of bimerons – antibimerons (cf. Fig. 1(a)). We report that the number of bimerons and antibimerons stabilized in the nanodot can be controlled by properly choosing the strength of current density that drives the stripe domain [4]. We believe, these results provide important insight into the controlled conversion and dynamics of bimeron that may have technological applications.

[1] K.W. Moon *et al*. Phys. Rev. Appl Vol.12, p. 064054 (2019) [2] Börge Göbel *et al*. Tretiakov. Phys. Rev. *B*, Vol. 99, p. 060407 (2019) [3] M. Beg, M. Lang, H. Fangohr, IEEE Trans. Magn. Vol. 58, p. 1-5 (2021) [4] B. Priyanka, P. Hari Prasanth, S.K. Syamlal, J. Sinha, Manuscript under preparation.

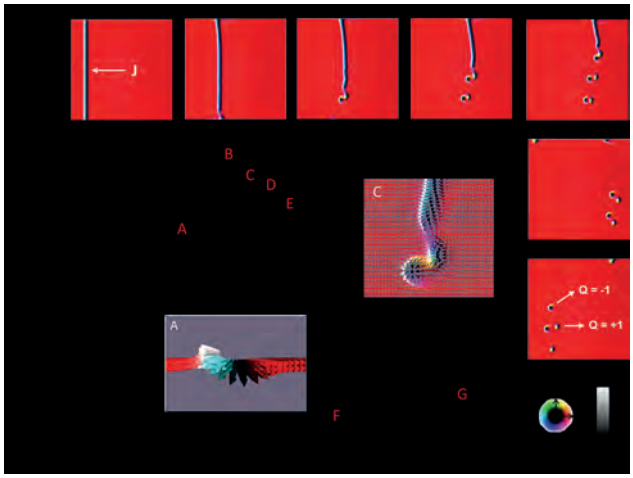

Fig 1: (a) Top view snapshots of the spin configuration describing the dynamical conversion process from a Neel stripe domain to pairs of bimeron-antibimeron in the presence of steady current density, j = -100 MA/cm^2 and α = 0.1, = 0.2. (b) Plot of total energy density as a function of time. Inset snapshots a zoomed in view of A and C.

VP1-06. Stochastic Skyrmion Dynamics in Chambers and Application as Spike-Timing-Dependent Plasticity (STDP) Synapses. *Z. Khodzhaev*[1], E. Turgut[2] and J.C. Incorvia[1] *1. Electrical and Computer Engineering, The University of Texas at Austin, Austin, TX, United States; 2. Physics, Oklahoma State University, Stillwater, OK, United States*

Skyrmions are being examined in chambers for potential computing applications, including reservoir computing and random bitstream generation at the chamber's output [1, 2]. A detailed analysis of skyrmion stochasticity in these chambers is required to understand how skyrmions respond to changes in temperature, grain sizes, and current densities, specifically with regard to their motion and pinning effects. This research presents a comprehensive investigation into the stochastic behavior of skyrmion shuffling chambers (Fig. 1), considering realistic material variations and temperature effects for potential neuromorphic computing applications. The simulations based on MuMax3 reveal that the skyrmion's diameter influences stochasticity and that the skyrmion's trajectory can be altered without changing its diameter through local temperature control. This ability to dynamically adjust the skyrmion shuffling chamber's input/output properties and stochasticity using temperature offers an additional level of control for neuromorphic computing applications. Moreover, the observed behavior of the shuffling device aligns with the integrate and fire neuron model. Based on this simulation platform, the skyrmion chamber shows new dynamic behaviors when operational parameters are changed, e.g., induced stochastic skyrmion motion within a single chamber and alterations in the longevity of the skyrmion path [3]. We then expand the simulation platform to include three side-by-side chambers which shows a novel function for the skyrmion chamber. It can act as an artificial synapse with spike-timing-dependent plasticity (STDP) response, where the synapse weight correlates with the number of skyrmions in the center chamber (Fig. 2). The device allows for varying rates of weight updates based on skyrmion dynamics and applied currents, enabling the device to mimic different forms of synaptic plasticities, such as Hebbian and dendritic location-based plasticity. This work explores neuromorphic systems, focusing on creating efficient and adaptable non-volatile devices for machine learning and spiking neural networks, while also developing tunable probabilistic computing devices and artificial synapses utilizing magnetic skyrmions.

[1] Zázvorka et al. Nature nanotechnology, 14, 658 (2019). [2] Pinna, D. et al. Phys. Rev. Appl., 9 (2018). [3] Khodzhaev, Z., Turgut, E., & Incorvia, J. A. C. IEEE Magnetics Letters, 14, pp.1-5 (2023).

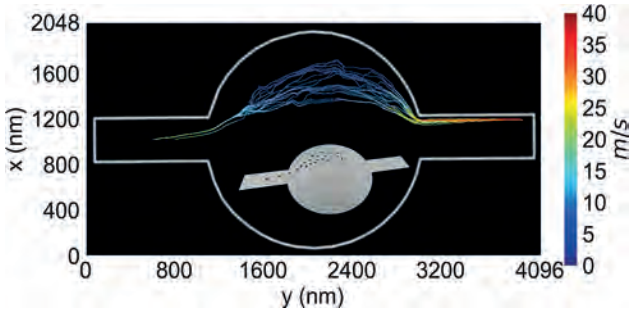

Figure 1.

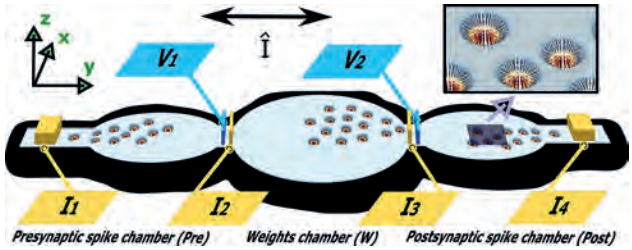

Figure 2.

Session VP2
FUNDAMENTAL PROPERTIES AND COOPERATIVE PHENOMENA (VIRTUAL)
(Poster Virtual Session)

Cheng Song, Chair
Tsinghua University, Beijing, China

VP2-01. Numerical analysis of write-error-rate in magnetic-topological-insulator-based devices with voltage-controlled magnetization switching. *T. Komine*[1] and T. Chiba[2] *1. Ibaraki University, Ibaraki, Japan; 2. Frontier Research Institute for Interdisciplinary Sciences, Tohoku University, Miyagi, Japan*

Electrical control of magnetization has attracted much attention for next generation spintronic devices such as non-volatile magnetic memory, high-speed logic, and low-power data transmission. Voltage-controlled magnetization anisotropy (VCMA) is a promising way to drive magnetization switching with high energy efficiency. Recently, we proposed the magnetic topological-insulator(MTI)-based device with field-effect-transistor (FET)-like structrure[1]. It was reported clear magnetization switching by combining adequate source-drain voltage and gate pulse with low writing energy of less-than 0.1fJ/bit. Although the gate pulse shape and the signal-to-noise ratio affect the write-error-rate(WER) by peripheral electrical circuits in the practical application, WER in the MTI device has not been discussed yet. In this study, we demonstrate magnetization switching in the MTI devices under external disturbance such as electrical circuit noise and thermal fluctuation by the micromagnetic simulation. Figure 1 illustrates a MTI-based device involving a MTI film as in which the top of the surface of MTI is a conduction-channel layer. This device realizes magnetization switching via spin-orbit torque (SOT) and voltage-controlled magnetic anisotropy (VCMA) which originate from 2D-Dirac electronic structure without external bias. From the numerical calculation, we reveal that the device operation is extremely robust against circuit delay and signal-to-noise ratio. Figure 2 shows WER as a function of temperature *T*. The device size *L* of 100 nm was used. We demonstrate that the WER on the order of approximately 10^{-4} or below is achieved around room temperature due to steep change in VCMA. Also, we show that the larger SOT improves thermal stability factor. This study provides a new perspective for developing voltage-driven spintronic devices with ultra-low power consumption.

[1] T. Chiba and T. Komine, *Phys. Rev. Appl.* 14, 034031 (2020).

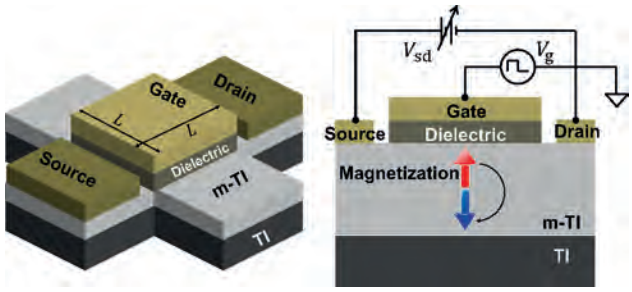

Fig.1 Schematic illustration of a MTI-based device with a FET-like structure consisting of magnetic-TI (MTI) and TI film.

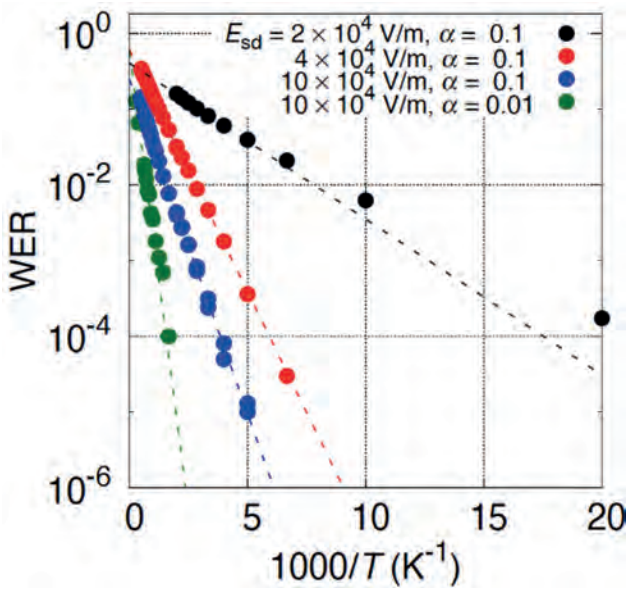

Fig.2 Write-error-rate (WER) as a function of temperature *T*. The device size *L* of 100 nm was used.

VP2-02. Signature of non-Fermi liquid behaviour in itinerant Ni-Nb alloys. *D. Patra*[1], S. Vishvakarma[1] and S. Veeturi[1] *1. Physics, Indian Institute of Technology Madras, Chennai, India*

Recent studies on ground state properties of Ni-based alloys with varying external magnetic field or stoichiometry have attracted considerable attention and offer new challenges to theory and experiments [1, 2]. From the electronic band structure calculations Kobayashi et al., have shown that the average moment of $Ni_{100-x}Nb_x$ alloy drops to zero value at x=11 [3]. Jesser et al., have probed magnetic properties in the range $0<x<6.3$ and suggested that ferromagnetism is close to the localized limit of itinerant-electron ferromagnetism [4]. However, no experimental attempts were made to validate the predictions of the critical concentration and to investigate the nature of transition. In this work, we attempt to determine the critical concentration to validate the predictions on $Ni_{100-x}Nb_x$ alloys and to understand the electronic properties near critical concentration. The $Ni_{100-x}Nb_x$ polycrystalline alloys of different concentration were synthesised by arc melting method and annealed at 1000°C for 3 days. The low temperature specific heat (C_p) and resistivity (ρ) measurements were carried out on structurally and chemically well characterized samples. It is observed that Curie temperature vanishes at x_{cr}=11.5, which corroborates well with Kobayashi et al., predictions. Specific heat measurements show the enhancement of Sommerfeld constant (γ) value at x_{cr}, while the low temperature upturn in $C_p(T)/T$ fits well when spin fluctuation component is added. It is also observed that low temperature variation of C_p and ρ deviate from conventional Fermi liquid (FL) behaviour. The inset of Fig.1 shows suppression of C_p/T curvature and inset of Fig.2 shows low temperature linear behavior of ρ with magnetic field suggesting a transition from non-Fermi liquid to FL behavior. Further to understand the electron correlation in the system, the Kadowaki-Woods ratio is calculated for all the samples. Results based on detailed analysis of the data will be presented.

1. A. Schroeder, S. Ubaid-Kassis and T. Vojta, J. Phys.: Condens. Matter 23, 094205 (2011). 2. S. Vishvakarma and V. Srinivas, J. Appl. Phys. 129, 143901 (2021). 3. M. Kobayashi, T. Kai, N. Takano et al., J. Magn. Magn. Mater. 166, 329 (1997). 4. R. Jesser, R. Clad and G. Schmerber, J. Magn. Magn. Mater. 124, 151 (1993).

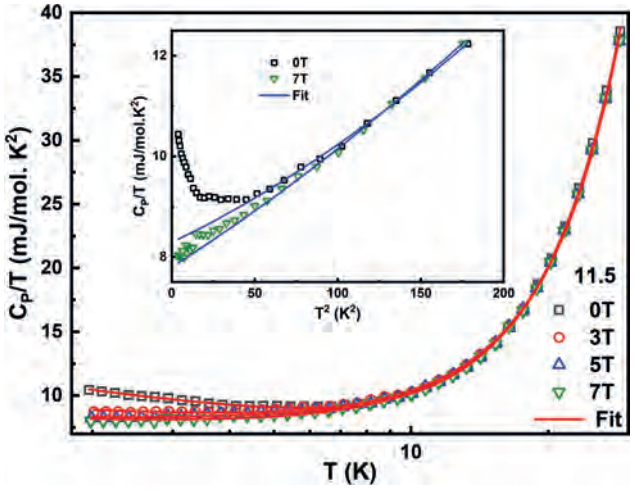

Fig.1. Specific heat of $Ni_{88.5}Nb_{11.5}$ fitted to $C_P(T)/T = \gamma + \beta T^2 + \delta T^4 + \kappa \log(T_{SF}/T)$ (solid line) and $C_P(T)/T$ vs T^2 plots with FL fitting (inset).

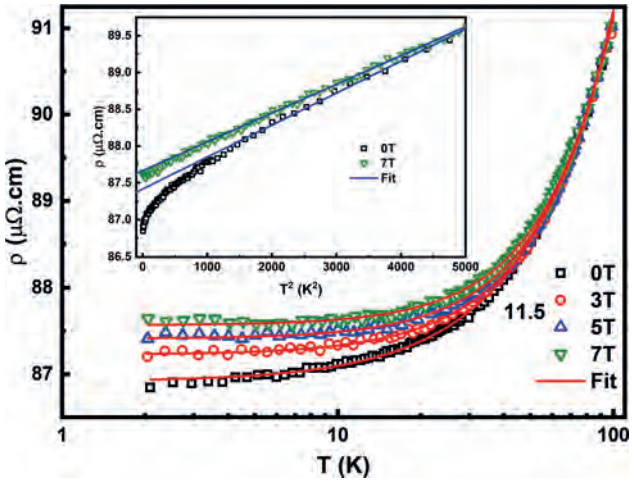

Fig.2. Resistivity of $Ni_{88.5}Nb_{11.5}$ fitted to $\rho(T) = \rho_0 + AT^n$ (solid line). Inset: $\rho(T)$ vs T^2 plots and solid lines are linear fit.

VP2-03. Magnetization Process of Antiferromagnetic Quantum Spin Chains with the Biquadratic Exchange Interaction. *T. Sakai[1,2] 1. School of Science, University of Hyogo, Kamigori, Japan; 2. SPring-8, National Institutes for Quantum Science and Technology, Sayo, Japan*

The quantum spin chains exhibit various interesting phenomena in the magnetization process, for exmaple, the magnetization jump, plateau, and spin nematic liquid etc. The density matrix renormalization group analysis of the S=1 antiferromagnetic chain with the biquadratic exchange interaction indicated that the spin nematic liquid phase appears in the magnetization process[1]. It was also supported by the numerical diagonalization and the conformal field theory analysis[2,3]. In the present work, the magnetization processes of the S=3/2 and S=2 antiferromagnetic chains with the biquadratic exchange interaction are investigated using the numerical diagonalization of finite-size clusters. It is found that the magnetization jump appears just before the saturation magnetization, as well as the classical spin system. This behavior is different from the S=1 chain. In addition it is indicated that the magnetization process where each magnetization step is 2S appears for sufficiently large biquadratic interaction. Namely the three-magnon and four-magnon bound states are realized for the S=3/2 and S=2 chains, respectively. In the case of the S=1 chain, the spin nematic liquid phase appears in the two-magnon bound state. Thus in general it can be predicted that the 2S-magnon bound state would be induced by the biquadratic exchange interaction in the magnetization process of the spin-S antiferromagnetic chain. The phase diagrams with respect to the biquadratic interaction and the magnetization are also presented for S=3/2 and S=2 antiferromagnetic chains.

[1]S. R. Manmana, A. M. Lauchli, F. H. L. Essler and F. Mila, Phys. Rev. B 83, 184433 (2011). [2]T. Sakai, AIP Advances 11, 015306 (2021). [3] T. Sakai, H. Nakano, R. Furuchi and K. Okamoto, J. Phys.: Conf. Ser. 2164, 012030 (2020).

VP2-04. Spin dynamics of room temperature van der Waals (vdW) ferromagnets and their usage in microwave devices. P. Kumar[1], S. Patnaik[1] and *B.K. Kuanr[2] 1. School of Physical Science, Jawaharlal Nehru University, New Delhi, India; 2. Special Centre for Nano Science, Jawaharlal Nehru University, New Delhi, India*

Quasi-two-dimensional van der Waals (vdW) materials with long-range ferromagnetic ordering near room temperature (RT) have emerged as significant research field to explore fundamental condensed matter physics due to their intriguing physical properties. These vdW materials enable a futuristic platform for implementing novel spintronic devices. Here, we study aspects of spin dynamics of polycrystalline Fe_5GeTe_2 (S1) and $Fe_{4.8}Co_{0.2}GeTe_2$ (S2) vdW materials using ferromagnetic resonance (FMR) spectroscopy. FMR measurement reveals that the effective magnetization of S1 is ~0.66kOe and S2 is 0.58kOe at RT which are consistent with reported VSM data in the literature [1]. S1 and S2 exhibit broad linewidths 0.69kOe and 0.75kOe respectively which can be due to inhomogeneous line broadening. Furthermore, obtained effective Gilbert damping constant (α) ~ 0.05 for S1 and 0.053 for S2 at RT. These are comparable to soft 3D transition metals. Besides intrinsic contribution to linewidth it is also affected by extrinsic Gilbert damping which is influenced by conflicting intra-band and inter-band electronic transitions according to Modified Kambersky's theory [2, 3]. In addition, we designed microwave signal processing devices with these materials and tested as microwave band-reject filter and phase shifter. The stop-band response can cover from 5 to 30 GHz with an applied magnetic field up to 6kOe. For these flip-chip based devices, attenuation is -5dB/cm for Fe_5GeTe_2 based filter and -3dB/cm on sample S2 at 6 kOe. Same microstrip filter can also be used as tunable phase shifter at the off-resonance region. Optimal differential phase shift studied for S1 and S2 based phase shifter in high frequency region (18GHz) is 10°/cm and 12.6°/cm respectively at 6kOe. These devices can be integrated into numerous applications like in phased-array antenna and wireless communication systems.

[1] L. Alahmed, B. Nepal and J. Macy, 2D Mater. 8 045030 (2021) [2] T. Qu, and R. H. Victora, Journal of Applied Physics 115, 17C506 (2014) [3] V. Kamberský, Physical Review B 76, 134416 (2007)

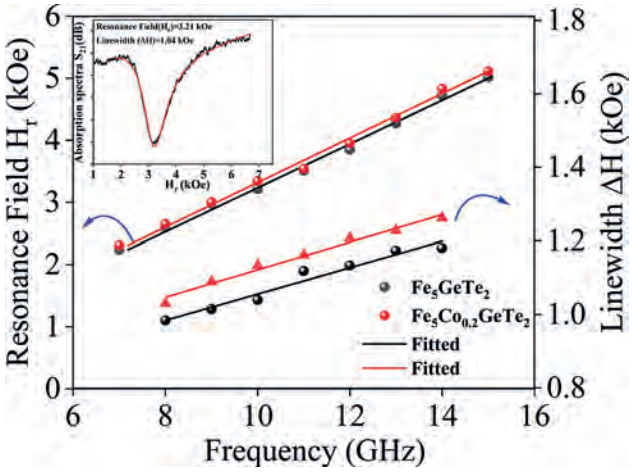

Fig.1 Resonance field and line-width as function of f (GHz) for S1 and S2. Inset shows absorption spectrum of S1 at 10GHz

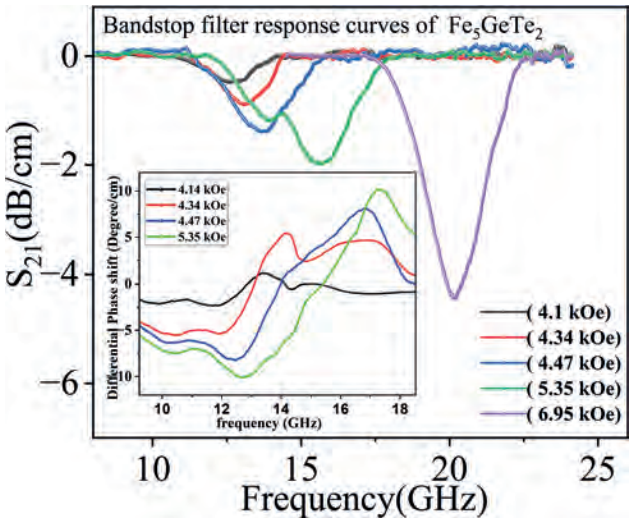

Fig.2 shows Band-stop filter response of Fe_5GeTe_2. Inset shows transmitted phase (S_{21}) of Fe_5GeTe_2 coated CPW device as a function of f (GHz).

VP2-05. Effect of Vacancies on the Electronic and Magnetic Properties of Heusler Compound Mn_2CoAl. *Z.W. Muthui*[1] *1. Physical Sciences, Chuka University, Nakuru, Kenya*

Investigation of the effect of vacancies occurring within the crystal structure of Heusler compound Mn_2CoAl, reveal the emergence of half-metallicity or a metallic electronic structure, depending on the site where the vacancy occurs. The Density Functional Theory (DFT) method, as implemented in the Vienna Ab Initio Simulation package (VASP) has been used. The site specific vacancies reveal that for a Mn vacancy occurring at the tetrahedral site and for a Co vacancy, an increased intersection of states with the Fermi level in one spin channel occurs, with the emergence of a half metallic gap in the minority and majority spin channels respectively. The resultant spin polarizations are 68% and 37% respectively, with magnetic moments of 1.989 and 2.028 μ_B/formula unit for the systems with Mn and Co vacancies respectively. These values are close to the 2 μ_B/formula unit predicted by the Slater Pauling rule for this system. An octahedral Mn void as well as simultaneous Mn and Co vacancies result in a metallic electronic structure. In both of these cases, there is a marked deviation from the Slater Pauling rule, with magnetic moments of 1.356 and 1.168 μ_B/formula unit respectively. The Mn magnetic moments couple ferrimagnetically and the magnetic order is preserved in all cases, except in the case of the simultaneous Co and Mn vacancies.

[1] Özdoğan, K., Sasioğlu, E., Galanakis, I. Vacancy-induced minority-spin states in half-metallic Heusler alloys. *phys. stat. sol. (RRL).* 1862-6254. (2007). [2] Wei, M.-S., Cui, Z., Ruan, X., Zhou, Q.-W., Fu, X.-Y., Liu, Z.-Y., Ma, Q.-Y., and Feng, Y. Interface Characterization of Current-Perpendicular-to-Plane Spin Valves Based on Spin Gapless Semiconductor Mn_2CoAl. *Appl. Sci.* (2018). [3] Galanakis, I., Özdoğan, K., Sasioğlu, E., and Blügel, S. Conditions for spin-gapless semiconducting behavior in Mn_2CoAl inverse Heusler compound. *J. Appl. Phys.* 115, 93908. (2014) [4] Chen, X.-R., Zhong, M.-M., Feng, Y., Zhou, Y., Yuan, H.-K., and Chen, H. Structural, electronic, elastic, and thermodynamic properties of the spin-gapless semiconducting Mn_2CoAl inverse Heusler alloy under pressure. *Phys. Status Solidi B* 252, 2830–2839. (2015)

VP2-06. Magnetism and magnetic anisotropy of a single rare-earth atom on transition metal dichalcogenides: A first-principles prediction. *B. Narangerel*[1], T. Ochirkhuyag[1], O. Bayarsaikhan[2], G. Munkhsaikhan[2] and D. Odkhuu[1,3] *1. Department of Physics, Incheon National University, Incheon, The Republic of Korea; 2. School of Applied Sciences, Mongolian University of Science and Technology, Ulaanbaatar, Mongolia; 3. Institute of Physics and Technology, Mongolian Academy of Sciences, Ulaanbaatar, Mongolia*

Exploring magnetism in otherwise nonmagnetic two-dimensional materials, such as graphene and transition metal dichalcogenides (TMDs), is at the heart of spintronics research. Employing systematic density-functional theory and Monte Carlo simulations, we have studied the energetics and magnetism of a series of rare-earth (RE) atoms on WSe_2 and $MoSe_2$ monolayers with various possible natural defects. In this talk, we will emphasize on significantly large perpendicular magnetocrystalline anisotropy (PMA) up to an order of 10 meV predicted in WSe_2 with Nd and Sm substitutions for the W site. Numerical results of PMA are elucidated in terms of an energy level change in the large spin-orbit coupled RE 4*f* – W 5*d* orbital states that are hybridized with the Se 4*p* orbital states in the low-spin bipyramidal crystal field. The present argument is also applicable for $MoSe_2$. The RE concentration and strain dependences of magnetic moment and PMA, and its underlying mechanism will also be discussed. The research is funded by Office of Naval Research and Office of Naval Research Global of the US Department of Defense Grant N62909-23-1-2035.

VP2-07. Adjusting Magnetic Coercivity of Magnetic Filament via Current Compliance. *F. Tan*[1], C.X. Lee[1], T. Jin[1], S. Li[1] and W. Lew[1] *1. School of Physical and Mathematical Sciences, Nanyang Technological University, Singapore, Singapore*

The utilization of spintronic devices has experienced tremendous growth in the past decade, ranging from usage in satellites to diverse fields to neuromorphic computing. However, the scalability of these devices at the nanoscale is hindered by the thermal stability of magnetic materials, which primarily depends on the magnetic volume. This study investigates on the nanoscale magnetic filament formation in a Pt(3)/Co(1.2)/Ta(1)/CoFeB(1.2)/MgO(2)/TaO(9)/Co(30)/Ta(3) heterostructure, where the numbers in parentheses represent the layer thickness in nanometre. The proposed heterostructure as shown in Fig. 1 facilitates the formation of a vertical magnetic filament, enabling the retention of a large magnetic volume while overcoming scalability issues in the planar direction. In its pristine state, without the filament formed, the device exhibits insignificant resistance change in a magnetic field sweep. However, with the application of a voltage sweep enables the formation of magnetic conductive filament, a significant drop in resistance is observed accompanied by the manifestation of tunnelling magnetoresistance as shown in Fig. 2. The hysteresis loop indicates the perpendicular magnetic anisotropy of the filament, attributed to its shape. Through vibrating sample magnetometer measurement on the unpatterned thin film, it is verified that Pt/Co/Ta/CoFeB/MgO layer exhibits perpendicular anisotropy from the Pt/Co and CoFeB/MgO interfaces and is magnetically coupled, while the 30 nm thick Co layer shows in-plane anisotropy. This suggests that the magnetic filament consist of Co from the top electrode. By adjusting the compliance current in a subsequent voltage sweep, the magnetic coercivity of the Co

filament can be finely tuned from 59 Oe to 14 Oe. This post fabrication fine tuning of coercivity offers enhanced control over the trade-off between energy efficiency and thermal stability of the device.

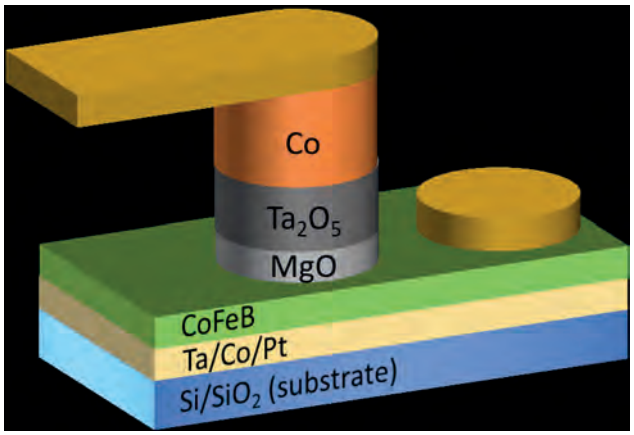

Fig. 1. Schematic diagram of fabricated device

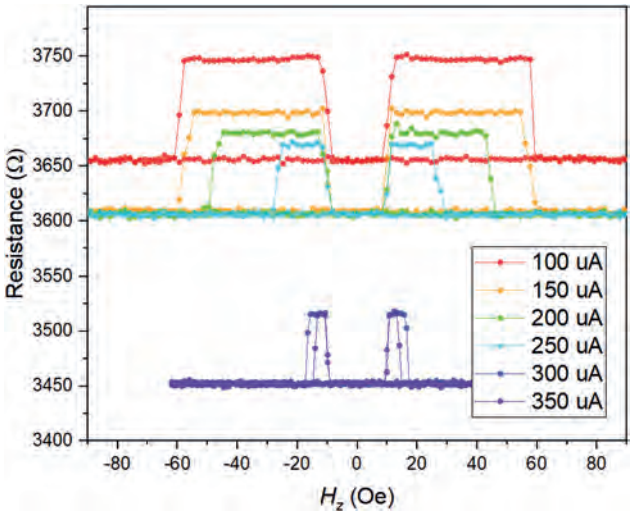

Fig. 2. Tunnelling magnetoresistance loops measured after application of increasing compliance current

Session VP3
HARD MAGNETIC MATERIALS (VIRTUAL)
(Poster Virtual Session)

Tetsuji Saito, Chair
Chiba Institute of Technology, Narashino, Japan

VP3-01. Solid-liquid phase separation diffused Nd-Fe-B sintered magnets by using DyH_3 nano powder realize high-efficiency coercivity improvement and overcome thickness limit. *H. Wu*[1], W. Liu[1], Z. Wang[1], M. Yue[1] and D. Zhang[1] *1. Beijing University of Technology, Beijing, China*

Novel solid-liquid phase separation diffused (SepD) Nd-Fe-B sintered magnets were successfully prepared by using TbH_3 nanopowder [1]. In this study, SepD and solid-liquid phase simultaneous diffusion (SimD) are used to create grain boundary diffusion (GBD) Nd-Fe-B sintered magnets by using DyH_3 nanopowder. The magnetic properties and microstructure of sintered Nd-Fe-B magnets of varying thicknesses are thoroughly investigated. The magnetic properties of SepD magnets are higher than SimD magnets when the weight increase ratio is 0.25 wt.% as shown in Fig. 1. When the magnet is 8 mm thick, SepD magnets have a coercivity of 18.10 kOe, which is higher than SimD magnets (17.00 kOe). It is determined that this new GBD mode can manufacture thick magnets with excellent coercivity. The diffusion depth of the Dy element in SepD magnets is deeper than that in SimD magnets. The core-shell structure is formed on the surface of the SepD magnet with a wider shell, while there forms an anti-core-shell structure that is unfavorable to magnetic properties on the surface of the SimD magnet as shown in Fig. 2. More continuous core-shell structure created by the deeper diffusion depth of the Dy element is the fundamental cause of the enhanced coercivity of the SepD magnet.

[1] Z. J. Wang, M. Yue, W. Q Liu, Tuning the distribution of Tb in Nd-Fe-B sintered magnet to overcome the magnetic properties trade-off, Scripta Materialia 217 (2022)

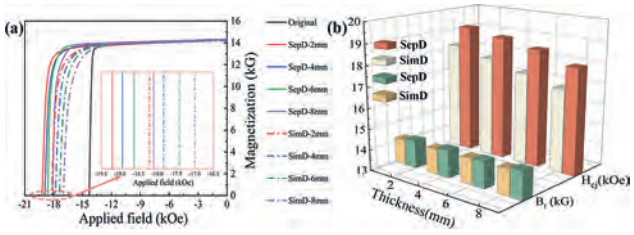

Demagnetization curve (a), coercive and remanence (b) of SepD and SimD magnets with different thicknesses

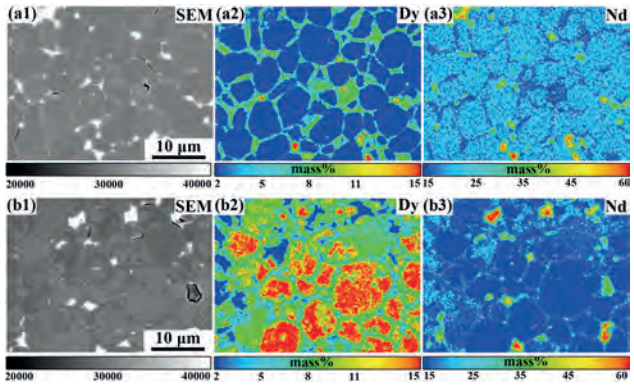

BSE images and distribution of Dy and Nd elements on the surface of SepD (a1-a3) and SimD magnets (b1-b3)

VP3-02. The effect of powder shape on the magnetic anisotropy in NdFeB bonded magnets. *Z. Qu*[1], Q. Wu[1], M. Zhang[1], Z. Wang[1], M. Yue[1] and W. Liu[1] *1. Beijing University of Technology, Beijing, China*

Bonded magnets consisting of magnetic powders and polymer binders have gained significant attention owing to their near-net shape characteristics and their capability to be shaped into intricate forms, thus finding widespread applications in fields such as electric motors, automobiles, and electronic communications [1,2]. In this paper, the effect of powder shape on the degree of alignment (DOA) for NdFeB bonded magnets fabricated via calendaring molding was investigated. The magnetic measurement results that the magnetic properties perpendicular to the rolling direction were considerably greater than those parallel to the rolling direction, indicating anisotropy in MQA bonded magnets. In contrast, both magnetic properties perpendicular and parallel to the rolling direction were found to be comparable in HDDR bonded magnets, indicating isotropy. In addition, the magnetic properties of MQA bonded magnet were significantly greater than that of HDDR bonded magnet [Fig. 1(b)], despite both powders having comparable magnetic properties [Fig. 1(a)]. Microstructural analysis revealed that partially parallel aligned platelet-shaped particles induced by mechanical stress were present in MQA bonded magnets [Fig. 2(a)], whereas sphere-like particles exhibited a random distribution in HDDR bonded magnets [Fig. 2(b)]. In summary, platelet-shaped particles present a superior magnetic performance in bonded magnets prepared via calendaring molding than that sphere-like particles.

[1] K. Gandha, I.C. Nlebedim and V. Kunc, Scr. Mater., 183, 91-95(2020)
[2] J.J. Tian, S.G. Zhang, and X.H. Qu, Mater. Lett., 68, 212-214(2012)

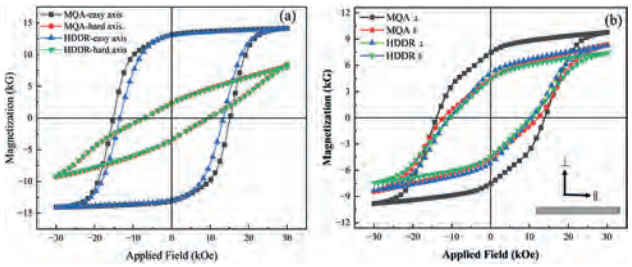

Fig.1. (a)The magnetic hysteresis loop of MQA and HDDR powders, (b) magnetic properties of MQA and HDDR bonded magnets perpendicular (⊥) and parallel (∥) to the rolling direction.

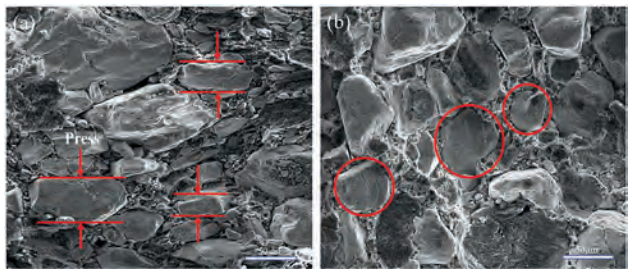

Fig.2. The cross-sectional morphology of MQA(a) and HDDR (b) bonded magnets.

VP3-03. Magnetic properties and microstructure of nanocrystalline $(Sm,Zr)(Fe,Co,Ti)_{12}$ magnets. L. Liu[1], Y. Li[1], *X. Zhang*[1] and M. Yue[1]
1. Beijing University of Technology, Beijing, China

In recent years, Sm-Zr-Fe-Co-Ti ternary alloys with $ThMn_{12}$ structure have been reported to have ultra-high intrinsic magnetic properties[1], which have the potential to be developed into new rare earth permanent magnet materials, thus attracting widespread attention. In this study, we attempts to prepare nanocrystalline $(Sm,Zr)(Fe,Co,Ti)_{12}$ magnets through methods such as melt-spun, annealing, and hot pressing, thereby, the magnetic properties and microstructure of the magnets are study. Revealed by XRD and SEM, the ingots with a composition of $Sm_{1.1}Zr_{0.2}Fe_{9.2}Co_{2.3}Ti_{0.5}$ are consist of two main-phase ($TbCu_7$ and $ThMn_{12}$, i.e., 1:7 and 1:12 phase) and a small amount of α- Fe phase and Zr-rich phase. After rapid quenching, single main phase, $ThMn_{12}$ phase, can be obtained. By adjusting the quenching rate, at 30 m/s, the rapidly-quenched ribbons have a high saturation magnetization, but the remanence and coercivity are low. Subsequently, the ribbons (30m/s) were annealed at 850 centigrade for different time. As the annealing time increases, the remanence and coercivity improved. The remanence of 86.1 emu/g is achieved when annealing at 850 centigrade for 45 minutes. Corresponding XRD patterns revealed the presence of a small amount of α- Fe phase coexisting with the main phase of $ThMn_{12}$ phase. In addition, the bulk $Sm_{1.1}Zr_{0.2}Fe_{9.2}Co_{2.3}Ti_{0.5}$ hot-pressed magnet was prepared under the condition of 650 centigrade and 500MPa. After hot pressing, a small portion of $ThMn_{12}$ phases in the magnet decompose into Sm-rich phases and α- Fe. The TEM results revealed that the grains in the $Sm_{1.1}Zr_{0.2}Fe_{9.2}Co_{2.3}Ti_{0.5}$ ribbons are uneven and there are also some amorphous, which are not conducive to achieve magnetic hardening, that is, to obtain high coercivity. But after annealing and hot-pressing process, the presence of soft magnetic phases α- Fe is still against to obtain high coercivity. In summary, to prepare high-performance $(Sm,Zr)(Fe,Co,Ti)_{12}$ magnets, the comprehensive coordination of high intrinsic magnetic properties and high phase stability remains the primary issue that needs to be addressed.

[1] Tozman P, Sepehri-Amin H, Takahashi Y K, et al. Acta Materialia, 2018,153:354-363.

VP3-04. The effect of Nd content on the elemental interdiffusion mechanism of Nd-Dy-Fe-B magnets. *Y. Qin*[1], W. Liu[1], Z. Wang[1], R. Du[1] and M. Yue[1] *1. Faculty of Materials and Manufacturing, Key Laboratory of Advanced Functional Materials, Ministry of Education of China, Beijing University of Technology, Beijing, China*

At present, the most effective way to improve the coercivity of sintered Nd-Fe-B magnets is to directly add HRE elements Dy/Tb [1]. However, excessive Dy/Tb additions can lead to significant reductions in remanence and magnetic energy product [2]. Therefore, achieving a balance in the composition-structure-property relationship has become a central research objective. This investigation explores the influence of grain boundary continuity on the magnetic properties, microstructure, and interdiffusion mechanism of Nd/Dy elements in Nd-Dy-Fe-B magnets. Two types of magnets were prepared using the dual alloy method: $Nd_{29+x}Fe_{69.27-x}M_{0.79}B_{0.94}$ (X=0, 0.5, M=Cu, Co, Zr, Al) and $Dy_{42.06}Fe_{57.06}B_{0.88}$, in a 9:1 ratio, denoted as magnets A and B. The X-ray diffraction (XRD) results showed that as the Nd content increased, the main phase inside the magnet did not change and remained as the 2:14:1 phase, but the peak shifted to the right [Fig. 1(a)], indicating that more (Nd, Dy)-Fe-B was formed in magnet B [Fig. 1(c)]. The coercivity of the magnet increased, but the remanence and magnetic energy product decreased [Fig. 1(b)]. During the demagnetization process, a higher magnetic field was required for the irreversible part of magnet B, while the reversible part gradually decreased. This indicates that with the increase of Nd content, a relatively uniform and continuous layer of RE-rich phase formed inside the magnet, which had a good magnetic isolation effect. This helps to increase the high coercivity of the magnet [Fig. 1(d)]. This paper elucidated the influence of the Nd content on the interdiffusion mechanism of Nd-Dy-Fe-B magnets, which has important guiding significance for the preparation of high-performance Nd-Dy-Fe-B magnets.

[1] X.L. Liu, M.J. Pan and P. Zhang. J. Rare Earths., Vol. 39, p.558-564 (2021). [2] K.H. Bae, T.H. Kim and S.R. Lee. J. Alloys Compd., Vol. 612, p. 183-188 (2014).

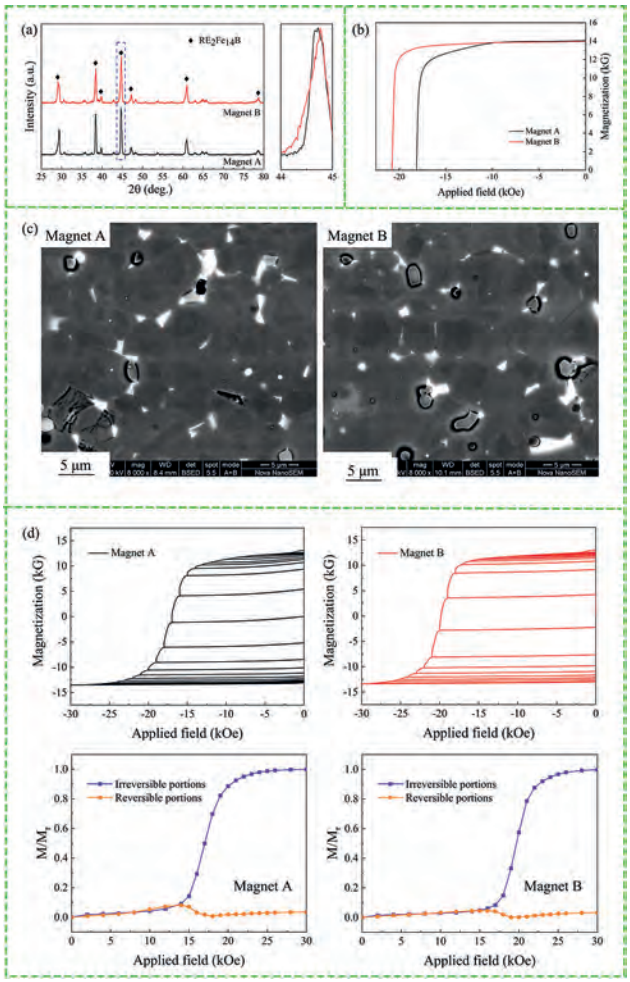

Fig.1 XRD pattern (a), Demagnetization curve (b), Microscopic morphology (c), Recovery curve, reversible and irreversible portions during the magnetization reversal process (d)

VP3-06. Effects of Lithium Addition on Structural and Magnetic Properties of M-type Strontium Hexaferrite. *S. Yoon*[1] *1. Department of Physics, Gunsan National University, Gunsan, The Republic of Korea*

Effects of lithium addition on structural and magnetic properties of M-type strontium hexaferrite have been studied by using crystallographic and magnetic measurements. First, high purity $SrCO_3$ and Fe_2O_3 were mixed to get $SrFe_{12}O_{19}$ powder. After dividing it into several parts, 0, 2, 4, 8, 15 and 30 % mol of Li_2CO_3 were subsequently added per 1 mol of $SrFe_{12}O_{19}$ powder. Then the fine mixtures were pressed into pellets and processed by the conventional solid state reaction method thru repeated sintering at 1250 °C for 24 hours. XRD patterns showed that all the samples were M-type hexaferrite with the space group of P63/mmc. Lattice parameters deduced from the GSAS refinement show that both *a* and *c* have no noticeable variation with increasing lithium content (Table 1), which indicates that the lithium addition did not cause any significant substitution of Fe sites by lithium. Variations of the magnetization and the coercivity *Hc* with lithium content was checked by room temperature VSM measurement. Since the magnetizations did not show any trend of saturation, we calculated the saturation magnetization *Ms* and the magnetic anisotropy constant *K* from the high field region of the *M-H* curve using the law of approach to saturation method. Whereas the *Ms* decreases slightly, the decrease in *Hc* with the

lithium addition is remarkable. Magnetic anisotropy constants *K* also shows slight decrease with increasing lithium content as shown in Table 1. Mössbauer spectra show that their mossbauer parameters are almost invariant with the lithium addition up to as high as 30% mol (Fig. 1 left). This means most of lithium ions do not participate in a competition to occupy the crystallographic sites. Rather, it is very likely that the lithium reside mainly on the grain boundary. FE-SEM images (Fig. 1 right) show that the lithium addition resulted in a better degree of grain separation between layers. It seems that the lithium acts as a kind of flux that suppresses the degree of coalescence of particles and affects significantly on the morphology, finally resulting in the decrease of *Hc* with the lithium addition. This suggests that Li^+ could also play the same role of process-salt with Na^+ or K^+ in the molten salt synthesis.

Table 1.

x (%)	*a* (Å)	*c* (Å)	*Ms* (emu/g)	*Hc* (Oe)	*K* (J/m³)
0	5.8792	23.0684	58.0	2117	3.16×10^5
2	5.8789	23.0606	57.9	1403	3.07×10^5
4	5.8790	23.0558	56.2	1099	2.94×10^5
8	5.8797	22.0609	54.5	918	2.66×10^5
15	5.8793	23.0566	53.4	778	2.54×10^5
30	5.8801	23.0520	52.6	845	2.61×10^5

Table 1

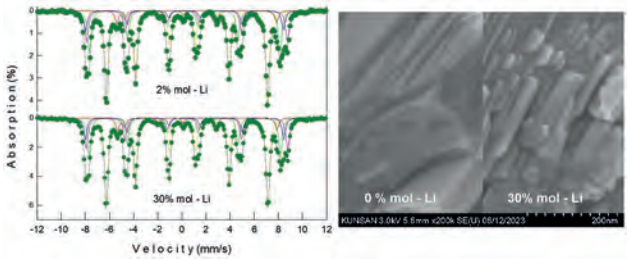

Figure 1

VP3-07. Structure and Magnetic Properties of Nanocrystalline $SmCo_5$ and $SmCo_3Cu_2$ Prepared by High Pressure Torsion. *F. Wang*[1], P. Si[1], Q. Wu[1], H. Ge[1], J. Park[2] and C. Choi[2] *1. College of Materials Science and Chemistry, China Jiliang University, Hangzhou, China; 2. Korea Institute of Materials Science, Changwon, The Republic of Korea*

Sm-Co magnets have been widely used in high temperature environments for their high Curie temperature and extra-large magnetocrystalline anisotropy. The rare earth-transition metal-based bulk magnets are usually produced by using the powder-metallurgical sintering route in which the magnetic powders are aligned and then sintered. The grain size and aligned texture have substantial effect on the magnetic performance of a magnet. Recently, textured nanocrystalline $SmCo_5$-Cu/Fe magnets were produced by high-pressure torsion (HPT) of powder blends consisting of $SmCo_5$ and Cu or Fe powder [1, 2]. HPT is a severe plastic deformation technique where a sample is subjected to torsional shear straining under a high hydrostatic pressure [3]. HPT of magnetic materials has attracted increasing research interests for its high efficiency in producing ultra-fine grain size, which has substantial effect on the magnetic properties. Moreover, $SmCo_5$ was found to be capable of forming amorphous shear bands to induce dislocation-free plastic deformation at large strains[4]. In this work, the effect of high pressure torsion on the structure and magnetic properties of $SmCo_5$ and $SmCo_3Cu_2$ alloys prepared by induction melting are investigated systematically by using XRD, SEM and magnetic measurements. The grain size of $SmCo_5$ and $SmCo_3Cu_2$ alloys has been refined significantly by HPT. The coercivity of both $SmCo_5$ and $SmCo_3Cu_2$ increases with increasing rotation turns of HPT, as shown in Fig. 1. After ten tuns of rotation, the nanocrystalline $SmCo_5$ and $SmCo_3Cu_2$ show a coercivity of 0.5 T and 1.64 T, respectively. A lamellar texture was observed in the $SmCo_3Cu_2$ after HPT, as shown in the inset of Fig. 1. This work demonstrates an alternative approach for the generation of textured nanocrystalline hard magnets.

[1] F. Staab, E. Bruder, L. Schäfer, et al., Acta Materialia, Vol. 246, p.118709 (2023) [2] L. Weissitsch, M. Stückler, S. Wurster, Crystals, Vol. 10, p.1026 (2020) [3] K. Edalati, Z. Horita, Materials Science and Engineering: A, Vol. 652, p.325 (2016) [4] H. Luo, H. Sheng, H. Zhang, et al., Nature Communications, Vol. 10, p. 3587 (2019)

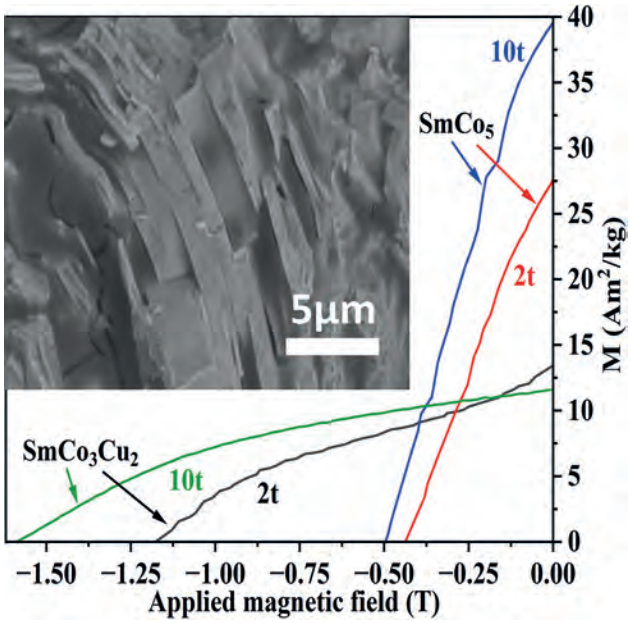

Fig. 1. The room temperature demagnetization curves of $SmCo_5$ and $SmCo_3Cu_2$ alloys processed by HPT for 2 and 10 turns, respectively. The inset shows the lamellar texture of $SmCo_3Cu_2$ alloys processed by HPT for 2 turns.

VP3-08. Effect of chloride ion in plating baths on coercivity of electroplated Fe-Pt film magnets. *D. Fukushima*[1], A. Yamashita[1], T. Yanai[1], M. Nakano[1] and H. Fukunaga[1] *1. Graduate School of Engineering, Nagasaki University, Nagasaki, Japan*

Owing to high crystalline magnetic anisotropy and excellent corrosion resistance, Platinum-based magnets are expected to be used in medical applications. Recently, we reported Fe-Pt thick films electroplated from plating baths containing different concentrations of NaCl and pointed out the possibility of coercivity enhancement by Na ions [1,2]. In this study, we focused on Cl ions and evaluated the effect of Cl ions on the coercivity of electroplated Fe-Pt film magnets. We employed an electroplating method using a dc current source. The bath composition and the plating conditions were almost the same as those in the previous study. The as-plated films on Cu substrates were annealed at 700°C for 5 min in a vacuum to obtain the fct structure. Figure 1 shows the hysteresis loops when the Cl ion concentration in the plating baths was changed from 0 to 0.86 mol/L using the NH_4Cl reagent. As shown in Fig.1, the coercivity decreased with increasing Cl ion concentration. In this case, as NH_4 ion concentration was also changed, we employed another method to change the Cl ion concentration. Cl_2 gases are generated from the anode in our experiment ($2Cl^- \rightarrow Cl_2 + 2e^-$). Therefore, we repleted the electroplating using the same plating bath. Figure 2 shows the coercivity of the annealed films as a function of the pre-electroplated time t_{pre}. $t_{pre} = 0$ min indicates the fresh baths, and $t_{pre} \neq 0$ min means the used baths. The plating times were set at 5 or 15 min. As shown in Fig.2, the coercivity increased with increasing the pre-electroplating time. The difference in the coercivity at $t_{pre} = 0$ min is attributable to the thickness. The thickness of the films plated for 5 min is thinner than that for 15 min. The magnetic properties of thin films tend to deteriorate by diffusion of Cu from the substrate [3]. Although the magnitude of the coercivity between the results of 5 min and 15 min, we obtained the same tendency of the coercivity increasing. As mentioned above, the pre-electroplating reduces the Cl ion concentration; we, therefore, found that the Cl ions decrease the coercivity of the electroplated Fe-Pt films.

[1]T. Yanai, J. Honda, R. Hamamura et al., "Effect of Na ions in plating baths on coercivity of electroplated Fe-Pt film-magnets", *J of Alloys Compounds*, 752, (2018) 133. [2]T.Yanai, J. Honda, R. Hamamura et al., "Effect of Na and Cl Ions on Coercivity of Electroplated Fe-Pt Film-Magnets" *J. Electron. Mater*, 48, (2019) 1412. [3]T. Yanai, Y. Omagari, S. Furutani et al., "High-temperature properties of Fe-Pt film-magnets prepared by electroplating method", *AIP Advances*, 10, (2020) 015149.

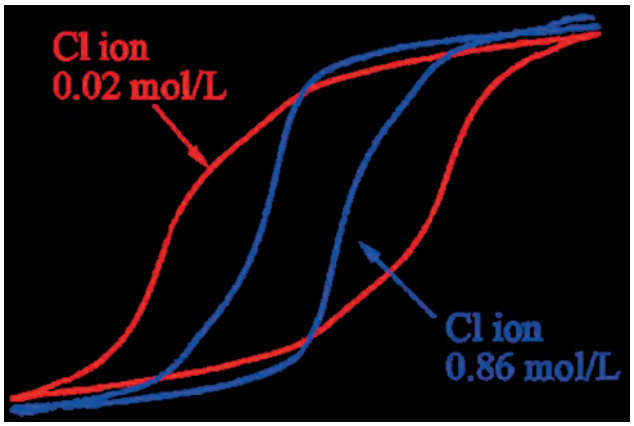

Figure 1

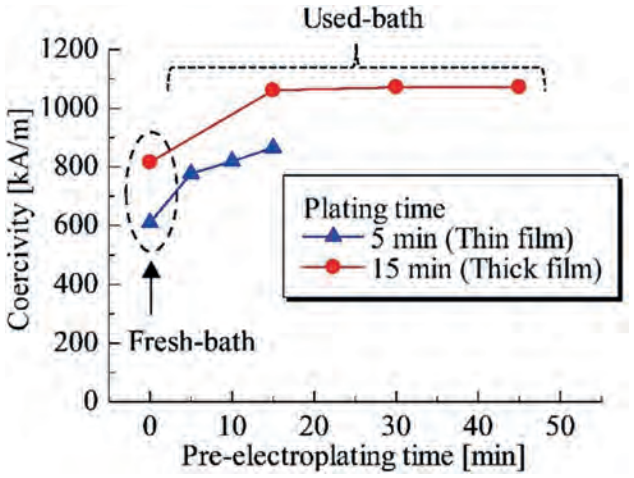

Figure 2

VP3-09. Structural and Magnetic Properties of Hexagonal Ferrite composites with Planar and Perpendicular Anisotropy. *S. Singh*[1], P. Sharma[1] and B. Chudasama[1,2] *1. School of Physics & Material Sciences, Thapar Institute of Engineering & Technology, Patiala, India; 2. TIET-VT Centre for Excellence in Emerging Materials, Thapar Institute of Engineering & Technology, Patiala, India*

M-type ferrite possess c-axis anisotropy with high magnetocrystalline anisotropy and moderate permittivity making them suitable for microwave applications in W-band. Z-type and Y-type ferrites have basal plane anisotropy with low coercivity and hence their applications are limited to few GHz only. M-type and Y-type ferrites are plausible candidates due to their ease of processing and wide difference in magnetic properties. Their composite represents Z-type ferrite, which is a superposition of M-type ($SrFe_{12}O_{19}$) and Y-type ($Ba_2Co_2Fe_{12}O_{22}$) structural units. Compared to M and Y-type, Z-type ferrites shows complex phase formation with high sintering temperature. One type of hexaferrite has limited frequency range; therefore, focus has been shifted on development of composite ferrites with contrast magnetic and microwave properties. Such composite provides wider compositional flexibility with tunable properties and can be realized in technological applications such as antenna substrates, EMI shielding and for nonreciprocal devices. In the present work, composites of $(x)SrFe_{12}O_{19}(SrM)/(1\text{-}x)Ba_2Co_2Fe_{12}O_{22}(Co_2Y)$ [where x= 0.1,0.2,0.3,0.4] were prepared by solid-state reaction. Effect of exchange coupling on structural, morphological, and magnetic properties have been investigated. XRD patterns confirmed the co-existence of SrM and Co_2Y phases. It is interesting to note that with increase in x=0.1 to 0.4 the intensity of diffraction lines along (*00l*) planes increases dramatically indicating preferential growth. Smooth hysteresis loops without any kink confirmed that SrM/Co_2Y phases in composites are exchange-coupled. This signifies that there is cooperative magnetic switching among M-Y spins. Linear increase in magnetization was observed with increasing M content. On the other hand decrease in coercivity was observed due to strong intervening coupling between the phases. Switching of Y-phase magnetic spins at low nucleation field drives away the hard M-phase spins. Single peak in switching field distribution curve (SFD) in composites confirms strong coupling between M and Y phases.

1. V.G. Harris, A.S. Sokolov, J. Supercond. Nov. Magn. 32 97–108(2019).
2. E.F. Kneller, R. Hawig, IEEE Trans. Magn. 27 3588–3600 (1991).

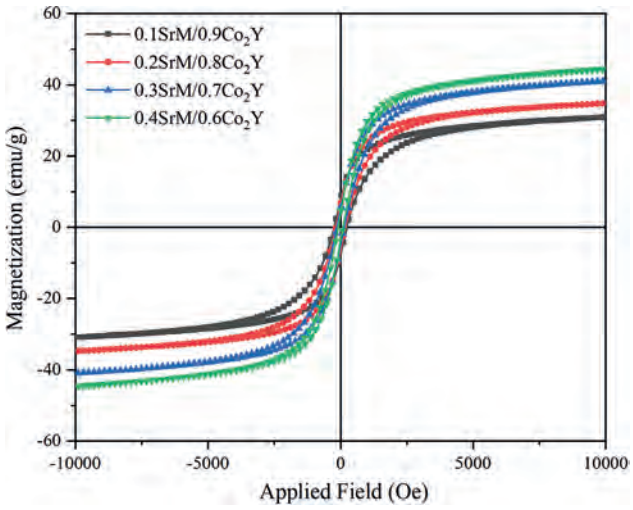

Fig.1 Comparative M-H loops of (x)SrM/(1-x)Co_2Y composite ferrites.

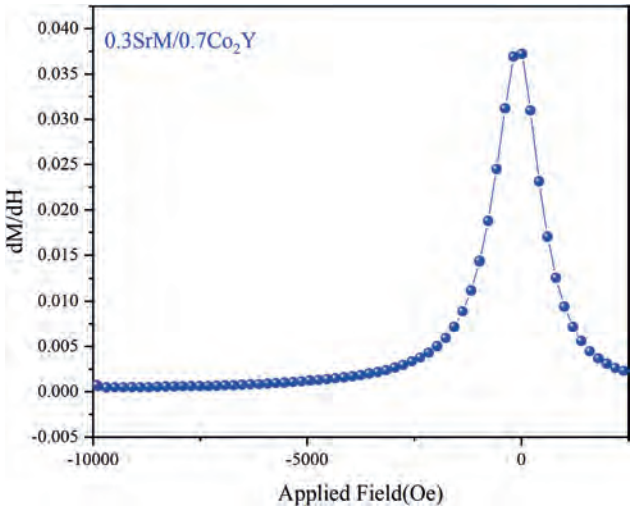

Fig.2 dM/dH vs applied field curve of SrM/Co_2Y exchange coupled composite

VP3-10. Optimization of microstructure in grain boundary diffusion processed sintered Nd-Fe-B magnets via Zr addition. *Z. Gao*[1], K. Zhong[1,2], C. Wang[3], M. Wu[1] and D. Shi[1] *1. Institute of Rare Earth Magnetic Materials, Xiamen Tungsten Co. Ltd., Xiamen, China; 2. Powder Metallurgy Research Institute, Central South University, Changsha, China; 3. College of Materials Science and Engineering, Fuzhou University, Fuzhou, China*

Due to its excellent magnetic properties, endless effort has been paid to the exploration of high performance Nd-Fe-B permanent magnets since its discovery [1]. Experimental maximum energy product [(BH)max] has reached 59.5 MGOe, which is approximately 93% of the theoretical value. Heavy rare earth (HRE) elements addition is inevitable in order to meet the requirements of high temperature working stability in motors. There is still a significant gap between the coercivity reported and the calculated value in HRE free magnets, which seriously limits the further applications of the sintered Nd-Fe-B permanent magnets [2, 3]. Grain boundary diffusion (GBD) process can enhance coercivity of the magnets effectively with limited HRE usage [4]. However, it should be noted that applicable thickness limitation on the GBD magnets is prominent because of relatively low diffusion depth and diffusion efficiency. In this work, we report a study on the microstructure and magnetic properties of the Zr-doped Nd-Fe-B magnet with GBD treatment. R(Nd,Pr,)-T(Fe,Co,Cu,Al,Ga,Zr)-B sintered magnets with different Zr addition (0.1 wt%, 0.2 wt%, 0.4 wt%) were prepared by typical powder metallurgy method. $Tb_{70}Cu_{15}Ga_{15}$ powders with an average particle size of ~8 μm were used as the HRE diffusion source here. Increment of coercivity varies greatly between 6 kOe and 11 kOe in magnets with different Zr addition. A greater abundance of ZrB_2 precipitates were found to be presented at the GBs in the magnet with high Zr addition, which strongly influence the microstructure of GB phases and diffusion process of HRE elements in the magnets. HRE-rich shell and diffusion depth can be significantly improved with appropriate Zr addition after GBD treatment. Present study provides new insights into the manufacture of the magnets with high coercivity and low HRE content.

[1] M. Sagawa et al., *J. Appl. Phys.,* 55, 2083-2087 (1984). [2] X. D. Xu et al., *Acta Mater.,* 156, 146-157 (2018). [3] K. Niitsu et al., *J. Alloys Compd.,* 752, 220-230 (2018). [4] H. Nakamura et al., *IEEE Trans. Magn.,* 41, 3844-3846 (2005).

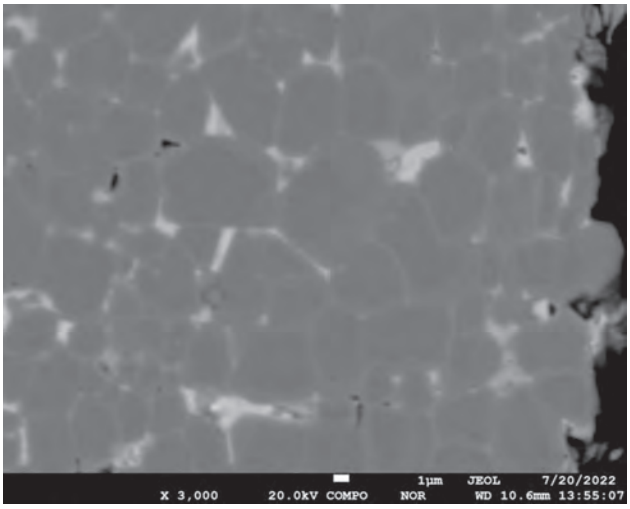

Back-scattered electron SEM picture of the GBD processed magnet with appropriate Zr addition

VP3-11. Study on the Structural and Magnetic Properties of τ-phase MnAl Prepared by Cryo Milling. D. Liang[1], T. Zhu[1], Z. Shao[1], Z. Luo[1], S. Liu[1], J. Han[1], H. Du[1], Q. Xu[1], C. Wang[1], W. Yang[1] and *J. Yang*[1] *1. Peking University, Beijing, China*

The unique characteristics, such as high magnetic moment, high Curie temperature, large magnetic crystalline anisotropy constant, and low cost [1-5], make the τ-phase MnAl a promising candidate as the market alternatives which could fill the gap between the rare earth magnets and ferrite magnets [6]. Due to the importance of microstructure to magnetism, several processes have been reported for manufacturing the τ-phase MnAl and the cryo milling has been proved to be an advanced method for preparing high-performance powder samples [7, 8]. At low temperatures, the alloys become brittle and the cryo milling allows the alloy samples to be broken quickly and introduce as few crystal defects as possible. In this study, the cryo milling was used to grind the τ-phase MnAl, and the relationship between the structure and magnetic properties were investigated. It was found that powder agglomeration can be dramatically suppressed by the cryo milling, and the larger particles tend to be broken down into smaller ones rather than being agglomerated to larger thin layers by the room-temperature milling. The powders after cryo milling have a particle size distribution of 1-10 μm and the morphology of cryo-milled powders is granular (Fig. 1), dramatically different from the room-temperature ball-milled powders with thin layer structures (Fig. 2). With increasing the cryo milling time, the grain size *D* reduced continuously from 145 nm to 36 nm, while the strain gradually accumulated and reached a maximum of 2.24%, and then decreased. The coercivity increased with increasing the cryo milling time, while the saturation magnetization decreased. The maximum coercivity of 4.9 kOe was obtained by cryo milling for 100 minutes. By the neutron diffraction analysis, it was confirmed that the decrease of the saturation magnetization is mainly due to the migration of Mn atoms from 1a site to the 1d site and the decrease of Mn atomic magnetic moment.

[1] O. Moze, L. Pareti and A.E. Ermakov, J. Appl. Phys., 63, 4616 (1988). [2] P.B. Braun and J.A. Goedkoop, Acta Cryst., 16, 737 (1963). [3] J. Konstantinović, D. Popov and N.B. Nešković et al., Solid State Commun., 25, 337 (1978). [4] Y.C. Yang, W.W. Ho and C. Lin et al., J. Appl. Phys., 55, 2053 (1984). [5] L. Pareti, F. Bolzoni and F. Leccabue et al., J. Appl. Phys., 59, 3824, (1986). [6] J.M.D. Coey, Script. Mater., 67, 524 (2012). [7] H.L. Fang, J. Cedervall and D. Hedlund et al., Sci. Rep., 8, 2525 (2018). [8] L.G. Marshall, I.J. McDonald and L.H. Lewis, J. Magn. Magn. Mater., 404, 215 (2016).

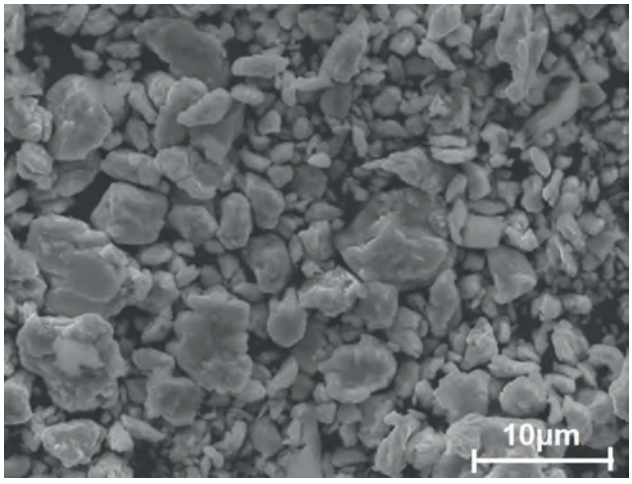

Fig. 1 SEM image of the cryo-milled MnAl for 60 min.

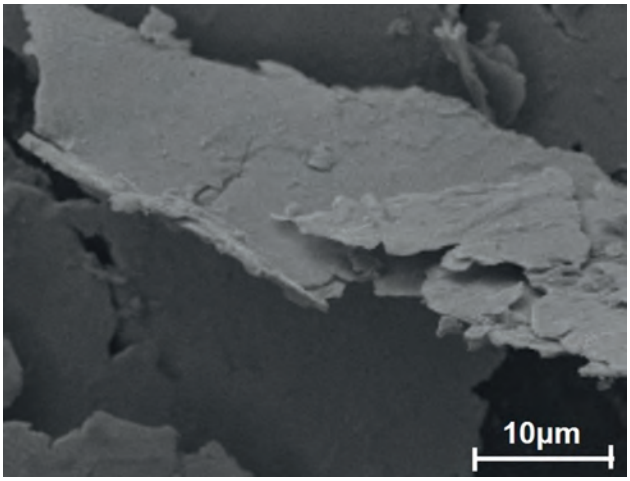

Fig. 2 SEM image of the room-temperature ball-milled MnAl for 120 min.

VP3-12. Optimizing Sintering Conditions for Enhanced Magnetic Performance in LCCSFO Ferrite Permanent Magnets. *H. Muhammad*[1], H. Zhang[1], Y. Li[1], G. Zhaowen[2] and M. Yue[1] *1. College of Material Science and Engineering, Beijing University of Technology, Beijing, China; 2. Central South University, State Key Lab Powder Met, Beijing, China*

The effectiveness of employing La-Ca-Co co-doing has been demonstrated as the optimal approach for enhancing the magnetic performance of strontium ferrite [1-2]. However, limited studies have explored the evolution of the magnetoplumbite phase and its correlation with the two-step sintering temperature for La-Ca-Co doped strontium ferrite (LCCSFO). In our research, we show the progression of the M-phase and determine the ideal temperature for attaining the maximum magnetic performance of LCCSFO. LCCSFO permanent magnets were fabricated using a conventional ceramic process and a two-step sintering technique. In the initial phase, the powder, which was wet mixed and pelletized, underwent calcination at 1260 °C followed by a second step of sintering at varying temperatures between 1175 °C and 1205 °C. XRD results in Fig.1 (a) validated the presence of the hexagonal ($P6_3/mmc$) $SrFe_{12}O_{19}$ phase in the doped samples. After sintering at different temperatures, all the samples possess proper c-axis orientation, as shown in Fig.1 (b). When the sintering temperature was raised from 1175 °C to 1205 °C, there was an upward trend observed in the remanence B_r, as shown in Fig.2 (a), increasing from 0.430 T to 0.439 T. The coercivity H_{cj} exhibited an increase from 380 kA/m and reached its peak at 397 kA/m at 1185 °C. Although the B_r value remained favorable, the coercivity experienced substantial deterioration, reaching its lowest point at 303 kA/m at 1205 °C. Under ideal circumstances, the optimal magnetic performance was achieved, with B_r measuring 0.439 T, H_{cj} at 379 kA/m, H_{cb} at 318 kA/m, and $(BH)_{max}$ at 35.5 kJm^{-3} at a sintering temperature of 1195 °C. Keywords: Strontium ferrite, magnetoplumbite phase, coercivity

De Julian Fernandez, C., et al. Progress and prospects of hard hexaferrites for permanent magnet applications. *Journal of Physics D: Applied Physics* 54.15 (2021): 153001. Kobayashi, Yoshinori, et al. Magnetic properties and composition of Ca-La-Co M-type ferrites. *Funtai Oyobi Funmatsuyakin* 55.7 (2008): 541-546.

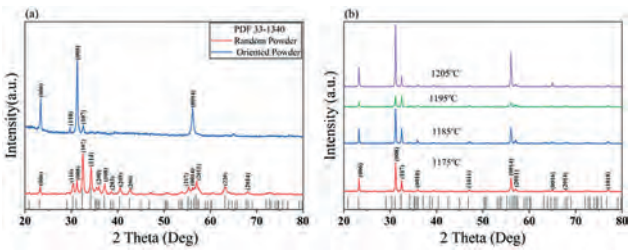

Fig.1 XRD patterns of the calcined powder and sintered magnets

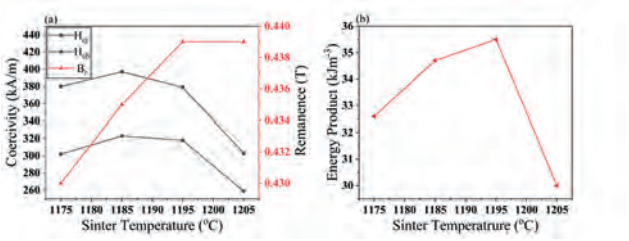

Fig. 2 The variation of coercivity, remanence and the energy product value for the magnets sintered at 1175 °C, 1185 °C, 1195 °C and 1205 °C.

VP3-13. Mechanochemical Synthesis of MnBi/Fe_3C@C Exchange Coupled Hard Magnetic Nanocomposites. *S. Namuduri*[1], S. Shaw[1], C. Upadhyay[2] and N. Prasad[1] *1. Department of Metallurgical Engineering, IIT(BHU), Varanasi, India; 2. School of Materials Science and Technology, IIT(BHU), Varanasi, India*

Permanent magnets have become indispensable components of several renewable energy technologies, like electric vehicles and wind turbines. Price constraints on rare-earth elements led to the search for viable rare-earth-free, permanent magnetic materials. With a theoretical energy product of 18 MGOe, low-temperature phase (LTP) MnBi appears to be a probable "gap magnet" (with an energy product >5 and <30 MGOe) without rare-earth elements. However, due to their low magnetization values, practical energy products greater than 10 MGOe could not be achieved in bulk MnBi magnets. In this study, nanocomposites of $Mn_{55}Bi_{45}/Fe_3C$@C with improved magnetic properties have been prepared by cryogenic ball milling. Further, the viability of utilizing Fe_3C@C as a soft phase in composites of hard and soft magnets was also evaluated. Fe_3C@C nanoparticles with an exceptional saturation magnetization of 150 emu/g have been synthesized by solvothermal route followed by calcination. These nanoparticles were added in different proportions (0, 5, 10, 15, and 20 wt%) to $Mn_{55}Bi_{45}$ powder to cryo-mill. It was found that a 10 weight percent addition provided the most enhanced magnetic properties with H_C of 6.6 kOe, M_S ~ 57 emu/g and M_r ~35 emu/g, improving M_S and M_r values by 37% and 58%, respectively (Figure1). The XRD, TEM, and magnetic analyses corroborate the exchange-coupled nanocomposites. This finding not only opens up the opportunity to use Fe_3C@C as a soft phase, a comparatively less oxidation-prone soft phase, in other hard magnetic systems but also paves the way for improving the energy product of the MnBi system.

1. Coey J M D Permanent magnets: Plugging the gap *Scr. Mater.* 67 524–9(2012). 2. Cui J, Kramer M, Zhou L, *Acta Mater.* 158 118–37 (2018). 3. Zhang D T, Cao S, Yue M, *J. Appl. Phys.* 109 07A722 (2011).

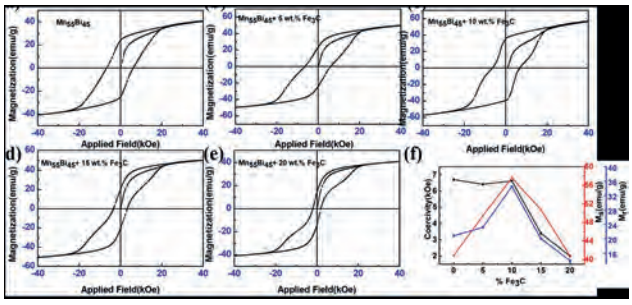

Figure 1. M *vs.* H hysteresis loops of cryo-milled powders of (a) $Mn_{55}Bi_{45}$ with (b) 5, (c) 10, (d) 15 and (e) 20 wt. % of Fe_3C@C (f) Variation of magnetic properties of cryo-milled nanocomposites with varying Fe_3C@C addition to $Mn_{55}Bi_{45}$.

VP3-14. Theoretical Study of Thermal Stability of α″–$Fe_{16}N_2$ Against Other Iron Nitrides. *P. Stoeckl*[1], P.W. Swatek[2] and J. Wang[2,1] *1. Physics, University of Minnesota, Minneapolis, MN, United States; 2. Electrical and Computer Engineering, University of Minnesota, Minneapolis, MN, United States*

α″–$Fe_{16}N_2$ has been investigated as one of promising candidates for environment friendly magnets.[1] While giant saturation magnetization has previously been experimentally observed in α″–$Fe_{16}N_2$, its magnetic anisotropy and structural stability leave room for improvement. Recent theoretical studies have considered alloying $Fe_{16}N_2$ with various elements to improve the magnetic properties and/or stability against decomposition.[2] However, estimates of stability in particular are typically restricted to simple ground-state-energy comparisons, *i.e.* effectively taken at 0 K. For a more practical measure of stability, we therefore extend ground-state energies, obtained with the plane-wave density-functional theory (DFT) code Quantum ESPRESSO, with appropriate empirical and/or statistical corrections to obtain free energies at arbitrary temperature. We then compare the stability of $Fe_{16}N_2$ against the neighboring phases in the Fe-N binary system, to estimate the range of temperatures at which it is stable. We compare against experimental observations of the Fe-N phase diagram.[3]

[1] J.-P. Wang, *J. Magn. and Magn. Mat*. 497, 165962 (2020). [2] P. Stoeckl, P. W. Swatek, & J.-P. Wang, *AIP Advances* 11(1), 015039 (2021). [3] Cf. e.g. M. Hillert & M. Jarl, *Metall. Transac. A* 6A 553–9 (1975).

VIRTUAL PLATFORM ONLY

Session VP4
INTERDISCIPLINARY AND EMERGING TOPICS: BIOMEDICAL APPLICATIONS; MAGNETIC FLUIDS AND SEPARATIONS; NEW APPLICATIONS AND OTHER EMERGING TOPICS (VIRTUAL) (Poster Virtual Session)

Thomas Feggeler, Chair
Lawrence Berkeley National Laboratory, Berkeley, CA, United States

VP4-01. Magnetic Flux Density Distribution and Stimulus Resolution on the Figure-Eight Coil During Transcranial Magnetic Stimulation.

T. Torii[1,2] and A. Sato[1] *1. Department of Human Information Engineering, Tokai University, Kumamoto, Japan; 2. Graduate School of Science and Technology, Tokai University, Kumamoto, Japan*

Transcranial magnetic stimulation (TMS) is a non-invasive method of stimulating the human brain; it uses a magnetic field to induce eddy currents in the cerebral cortex. TMS can provide local stimulation via a figure-eight coil, with applications for brain and nerve disease treatments and research into brain function. However, the detailed energy dynamics of TMS on the cerebral cortex remain unclear. The present study focused on magnetic energy distribution and stimulation resolution via magnetic flux density, which was measured using a simple instrument consisting of a probe, integrator, and buffer amplifier. A Rapid2 stimulator and figure-eight coil were used to apply magnetic stimulation to a brain model. For magnetic induction by TMS, stimulus pulses (pulse width 320 μs, intensity 75%) were used. The brain model was based on a subject with a motor threshold of approximately 62% and a scalp-to-primary-motor-cortex distance (i.e., distance from the scalp to the center of the sensor coil) of 15 mm. Magnetic flux density was measured within a range of ±50 mm from the center of the *x*- or *y*-axis on the figure-eight coil. In the current study, the highest magnetic flux density was approximately 270 mT at the center of the stimulus coil. The flux density near the center of the circle of the figure-eight coil (approximately ±40 mm) is theoretically zero. Background noise was therefore estimated using the magnetic flux density with the probe at –40 mm (approximately 80 mT, minimum). The central part of the figure-eight coil had the highest magnetic flux density (approximately 190 mT), and the TMS resolution was approximately 4 mm on both the *x*- and *y*-axes. The stimulus area was therefore estimated as approximately 13 mm^2. Moreover, the stimulation area in which the magnetic flux density decreased by less than 1% compared with the highest magnetic flux density was approximately 28 mm^2, and that in which the magnetic flux density decreased by less than 5% was approximately 174 mm^2. Together, these findings suggest that the distribution of magnetic stimulation energy delivered to a target cortex may be evaluated using a simple measurement device and brain model.

[1] M. Hallett, *Neuron*, vol. 55(2), pp. 187-199 (2007) [2] S. Ueno, T. Matsuda et al., *J Appl. Phys*., vol. 67(9), pp. 5838-5840 (1990)

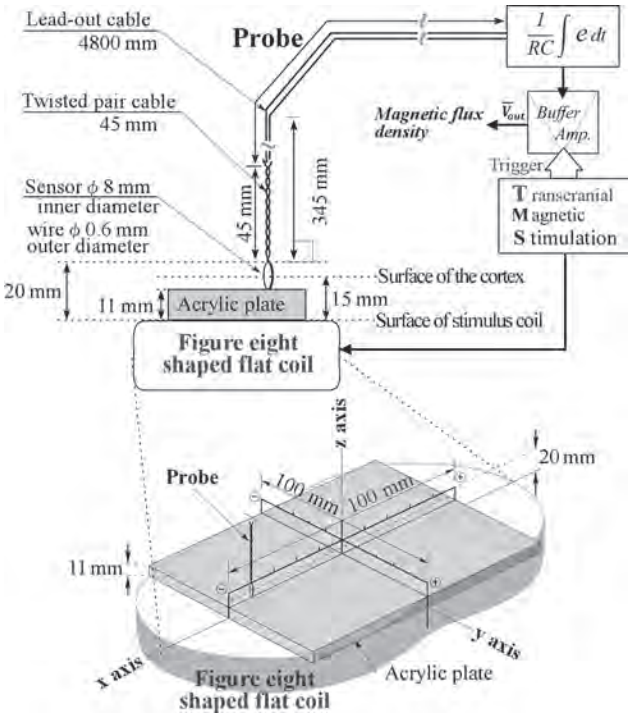

Fig.1 Experimental system

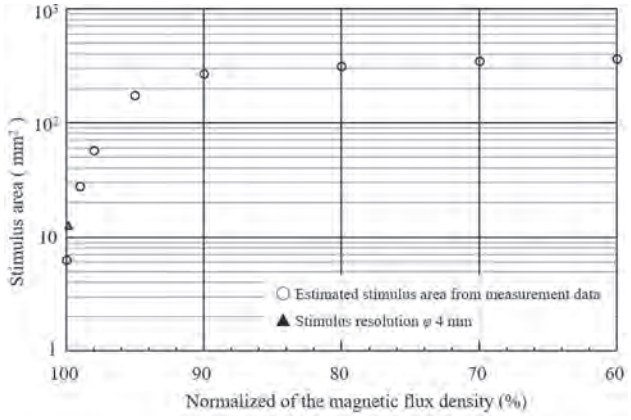

Fig.2 Normalized stimulation area.

VP4-02. Detection of blood coagulation in an extracorporeal circuit using magnetic and absorbance properties. *H. Sakamoto*[1], N. Hibino[1], Y. Mizukuchi[2], A. Sato[3] and T. Torii[3] *1. Department of Clinical Engineering, Komatsu University, Komatsu, Japan; 2. Department of Clinical Engineering Center, Tonami General Hospital, Tonami, Japan; 3. Department of Human Information Engineering, Tokai University, Kumamoto, Japan*

In extracorporeal circulation, intra-circuit blood coagulation can lead to serious problems. However, intra-circuit coagulation cannot be monitored in real-time and is only intermittently monitored by measuring the activated clotting time (ACT). Changes in blood coagulation can be detected using devices with optical sensors because the absorbance is likely to change as blood coagulates. However, the absorbance may also increase when oxygen partial pressure is altered by artificial lungs. Thus, there is a need for a device that is not affected by blood oxygenation. We used a magnet and a flux meter to assess changes in the magnetic force with blood coagulation. The absorbance was first measured with a spectrophotometer to identify characteristic changes with blood coagulation. The absorbance of uncoagulated blood was measured. Calcium chloride was then added to the blood to promote coagulation. The blood was left for 1 day to completely coagulate before the absorbance was measured. The results confirmed that the absorbance increased as the blood coagulated. As magnetism is unaffected by changes in the fraction of inspired oxygen and oxygen flow rate, we measured changes in the magnetic flux density during coagulation. As blood cells aggregate due to coagulation, the flux meter measurement will change when the blood circuit passes between the magnet and flux meter (Figure 1). Blood (100 ml) was stored in a beaker. Calcium chloride (0.2 ml) was then added to the beaker to promote coagulation. Blood from the beaker was drawn into a syringe and set in the magnetic flux measurement fixture, and a magnet was fixed on top of the syringe for 40 minutes. The ACT of the blood in the beaker undergoing accelerated coagulation was measured at 2-minute intervals. The flux meter readings in decreased as the blood coagulated (Figure 2). The results suggest that it is possible to capture magnetic flux density changes during the process of blood coagulation. These results may lead to the development of a device that monitors coagulation in extracorporeal circuits in real time by monitoring two aspects of the coagulation process: absorbance and magnetic flux density.

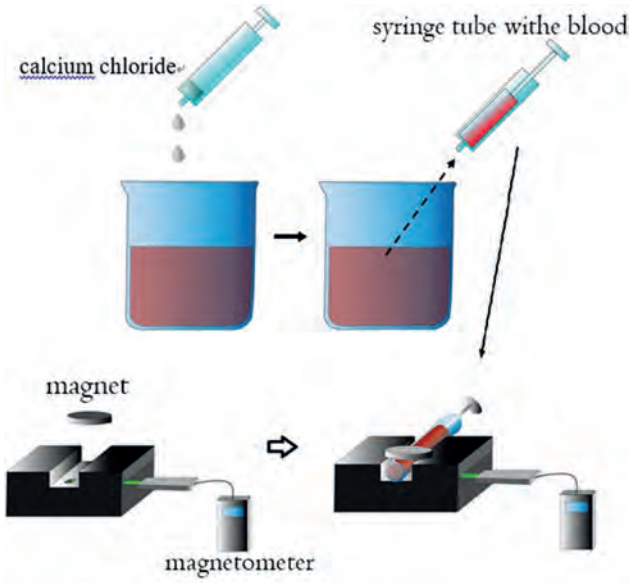

figure 1. Measurement Model

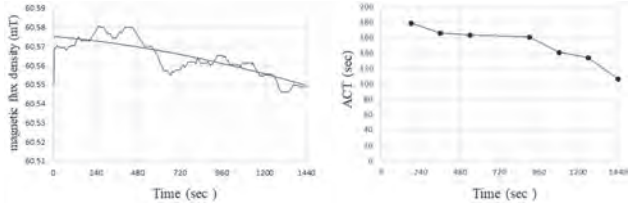

figure 2. experimental results

VP4-03. Multi-core Superparamagnetic Nanoparticles for MPI and High-efficiency Drug Delivery. S. Bai[1], *X. Zhang*[1], G. Hou[1], X. Wang[1], Y. Lin[1] and K. Li[1] *1. Shenyang University of Technology, Shenyang, China*

Magnetic drug delivery is a novel drug targeting modality in which drugs or proteins were bound to nano-sized magnetic carries, and has important application prospects in the treatment of cancer and other major diseases. However, there is an important challenge that the larger magnetic nanoparticle (MNP) shows larger attractive power due to the larger magnetic moment *m*, while the superparamagnetism and rapid relaxation time were necessary in MPI which were presented only in small MNP (usually under 30nm). In this paper, we proposed a novel MNP solution for magnetic drug delivery. In the new MNP, the magnetic core (Fe_3O_4 or γ-Fe_2O_3) was designed as multi-small particles (around 10nm) and formed a total magnetic core size of approximately 25 nm. The structure showed a rapid Neel relaxation time due to the small particles with a relatively large total superparamagnetic magnetic moment *m*. The non-magnetic shell composed of dextran was designed to a very large hydrodynamic size (more than 200nm) to avoid magnetic dipole interactions between particles, and larger aggregation effect in the physiological state. Thus, larger space occupation between magnetic cores was designed in this study. A series of nanoparticles were synthesized with difference in core size, hydrodynamic size, and production process. All synthesized MNPs and some classical commercial superparamagnetic MNPs were characterized utilizing X-ray diffraction (XRD), X-ray photoelectron spectra (XPS), scanning electron microscopy (SEM), high-resolution transmission electron microscope (HRTEM), vibrating sample magnetometer (VSM), home-made magnetic particle spectroscopy (MPS, same to one-dimension MPI) and home-made drug delivery device. Experimental results show that the synthesized samples exhibit superparamagnetic properties that meet the requirements of both MPI and high-efficiency drug delivery. The new MNP design and synthetization method was suitable as a solution to the competition between MNP drug delivery and dynamic imaging.

[1] Stefan, L., Raminder, S., Rainer, T., Christoph, A.: Magnetic nanoparticles for magnetic drug targeting. Biomedical Engineering/Biomedizinische Technik. 60(5), 465–475 (2015). [2] Fattahi, H., Laurent, S., Liu, F., Arsalani, N., Vander Elst, L., Muller, R.N.: Magnetoliposomes as multimodal contrast agents for molecular imaging and cancer nanotheragnostics. Nanomedicine. 6(3), 529–544 (2011). [3] Slimani, Y., Almessiere, M.A., Shirsath, S.E., Hannachi, E., Yasin, G., Baykal, A., Ozçelik, B., Ercan, I.: Investigation of structural, morphological, optical, magnetic and dielectric properties of $(1–x)BaTiO_3/xSr_{0.92}Ca_{0.04}Mg_{0.04}Fe_{12}O_{19}$ composites. J. Magn. Magn. Mater. 510, 166933 (2020). [4] Kudr, J., Haddad, Y., Richtera, L., Heger, Z., Cernak, M., Adam, V., Zitka, O.: Magnetic nanoparticles: from design and synthesis to real world applications. Nanomaterials (Basel). 7(9), 243(2017). [5] Katz, E.: Synthesis, Properties and applications of magnetic nanoparticles and nanowires—a brief introduction. Magnetochemistry. 5, 61 (2019). [6] Antone, A.J., Sun, Z., Bao, Y.: Preparation and application of iron oxide nanoclusters. Magnetochemistry. 5, 45 (2019).

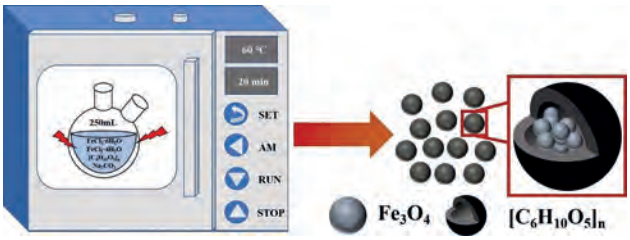

Fig. 1 MNP synthesis and structure diagram

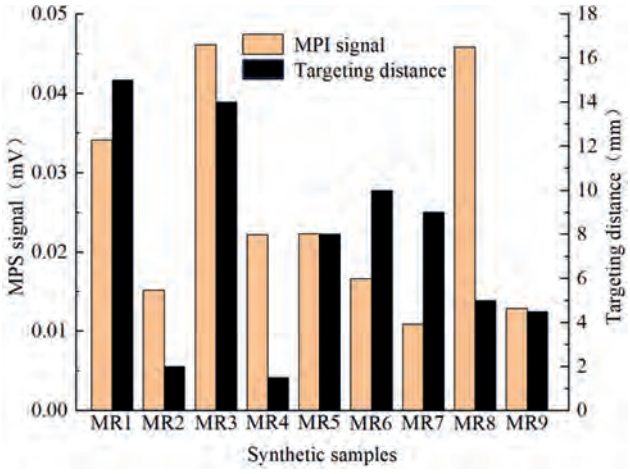

Fig. 2 Synthetic samples test results(targeting distance is the movement distance of the sample after 1s targeting with the home-made drug delivery device)

VP4-04. A new Insight into Anti-viral/microbial Activity: Validation of ClO_2-Deriving Radical Chain Reactions under Exposure to Static Magnetic Field. K. Saito[1], *H. Nakagawa*[2], M. Fujimoto[3], R. Miyauchi[1] and S. Ebihara[4] *1. Aqueous Chlorine Dioxide Council, Tokyo, Japan; 2. Tokyo Denki University, Tokyo, Japan; 3. University of Human Arts and Sciences, Tokyo, Japan; 4. Chiyoda Paramedical Care Clinic, Tokyo, Japan*

Recent *in vivo* experimental studies using chlorine-based disinfectants have shown new scientific discoveries about their capabilities for sterilizing power [1]–[3] and inhalation safety/toxicity [4], [5]. In this study, we used aqueous chlorine dioxide (aqCD) as a radical pair-forming agent to investigate whether magnetic fields can control a viral membranous autoxidation through differences in the physical properties of biomembranes. A prepared dry thin film was hydrated by vortexing with 2 mL of 50 mM Tris-HCl buffer (pH 7.4) or D_2O, according to the previous method [6]. The dispersion (10 mM) was transferred to a Mini-Extrudor (Avanti Polar Lipids, Inc.) to produce artificial biomembranous nanoparticles. Exposure to a static magnetic field of 0.25 T was performed using a pair of commercially availablepermanent magnets (*W*215 x *D*138 x *H*15 mm). Irradiations of the nanoparticles were performed using an original air-cooled UV-LED irradiation system. To begin with, we analyzed the structural and physicochemical properties of an oxidized viral membranes induced by the peroxyl radical generation after photo-induced degradation of aqCD in the biomembrane. We secondary compared the release rates of aqCD with magnetic field effects on the photochemical reactions developing in the model membrane systems. According to the overall results, the aqCD-radical releases with the field effects obtained using a static field of 0.25 T were more extensive than those obtained at geomagnetic fields. Among other thing, we found the possibility that a static magnetic field influences the pair mechanism in the process of membrane peroxidations induced by excited singlet oxygen ($^1O_2$), etc. This innovative methodology must be one of the most adaptable techniques, which may be able to evaluate a detailed reaction scheme in many viral outer membranes equipped with possible magnetic controls, and/or analogize the ultrastructural state of molecular nanoenvironments swiftly and easily. Consequently, further detailed studies on the reaction field-dependent radical pair model with inhalation safety *in vivo* are now under investigation.

1) M. Jutte et al., Water Res. 231, 119626 (2023). 2) T. Li et al., Sci. Total Environ. 838, 156193 (2022). 3) N. Parveen et al., Environ. Sci. Pollut. Res. Int. 29, 85742 (2022). 4) B. Murashevych et al., Environ. Inhal. Toxicol. 34, 1 (2020). 5) T. Zellner and F. Eyer, Toxicol. Lett. 320, 73 (2020). 6) H. Nakagawa, AIP Advances 10, 025019 (2020).

VP4-05. Study on Wireless Power Transmission System for Real-Time Telemetry of Mouse Activity and Body Temperature. *T. Omori*[1], F. Sato[1], F. Yoshiki[2] and S. Sasaki[2] *1. Graduate School of Engineering, Tohoku Gakuin University, Sendai, Japan; 2. Hikaridenshi Co.,Ltd, Osaki, Japan*

Animal experimentation involves recording changes in biological information such as body temperature, heart rate, blood pressure, and activity level during the experiment using specialized equipment. To take the recording of activity levels as an example, there are methods to analyze videos taken by infrared cameras[1], to refer to the number of revolutions of a spinning wheel[2], and so on. However, for experiments that require accurate biometric information, the use of an implantable biometric device, rather than the above devices, is one of the most suitable options. Implantable biometric acquisition devices often rely on batteries for their means of power supply[3],[4],[5],[6]. However, when a battery is implanted with the device, it must be small and lightweight so that the weight of the battery does not become a burden on the animal experimentation, and its capacity cannot be ensured. Therefore, it is impossible to conduct long-term experiments or to monitor biological information in real time. For this reason, a method has been proposed in which, instead of batteries, a power receiving coil is implanted in the animal experimentation, and power is supplied by a power transmitting coil installed around the rearing cage. Since this method can constantly send electric power, the acquired data can be transferred to an external recording terminal such as a PC in a very short cycle, enabling real-time monitoring of biological information. However, in prior research, it has been suggested that the power supply may become unstable due to the heat generated in the receiving coil from the power consumption and the position and posture of the animal experimentation[7]. To solve these problems and ensure stable power supply, we worked on the creation of a power transmission coil that generates a uniform magnetic field and conducted demonstration experiments. Figure 1 shows a model diagram of the created power transmission coil. Figure 2 shows the measured and graphed magnetic field distribution at a height of 0 mm from the top of the power transmission coil, indicating that the magnetic field is uniform.

[1] K. Kobayashi, N. Shimizu, S. Matsushita and T. Murata, "The assessment of mouse spontaneous locomotor activity using motion picture," in *Journal of Pharmacological Science*, vol. 143, issue 2, pp. 83-88 (2020) [2] D. M. Edgar et al., "Influence of running wheel activity on free-running sleep/wake and drinking circadian rhythms in mice," in *Physiology & Behavior*, vol. 50, issue 2, pp. 373-378 (1991) [3] H. Mei, K. A. Thackston, R. A. Bercich, J. G. R. Jefferys and P. P. Irazoqui, "Cavity Resonator Wireless Power Transfer System for Freely Moving Animal Experiments," in *IEEE Transactions on Biomedical Engineering*, vol. 64, no. 4, pp. 775-785 (2017) [4] S. T. Lee, P. A. Williams, C. E. Braine, D. -T. Lin, S. W. M. John and P. P. Irazoqui, "A Miniature, Fiber-Coupled, Wireless, Deep-Brain Optogenetic Stimulator," in *IEEE Transactions on Neural Systems and Rehabilitation Engineering*, vol. 23, no. 4, pp. 655-664 (2015) [5] T. A. Szuts et al., "A wireless multi-channel neural amplifier for freely moving animals," in *Nature Neuroscience*, vol. 14, no. 2, pp. 263-269 (2011) [6] Fan D, Rich D, Holtzman T, Ruther P, Dalley JW, Lopez A, Rossi MA, Barter JW, Salas-Meza D, Herwik S, Holzhammer T, Morizio J, Yin HH. "A wireless multi-channel recording system for freely behaving mice and rats," in *PLOS ONE* 6(7). [7] S. T. Warren, F. Lev, A. Daniel, "Rotating Field Inductive Data Telemetry and power Transfer in an Implantable Medical Device System," U.S. Patent 2009069869-A1 (2007)

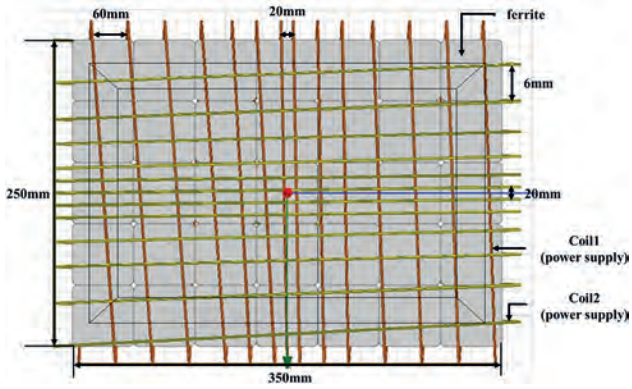

Fig. 1 Exterior of power transmission coil

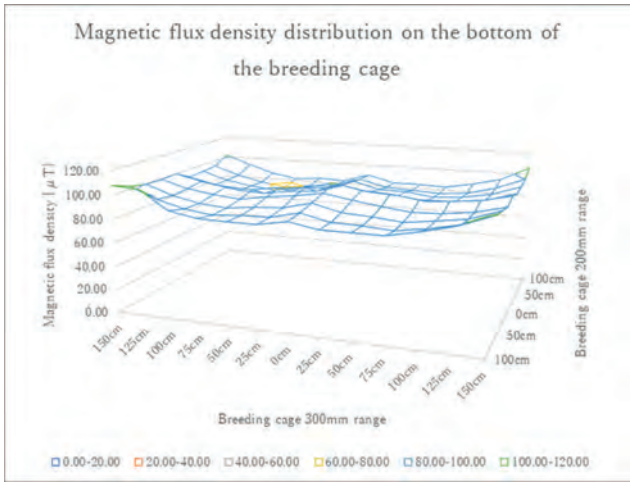

Fig. 2 Magnetic field distribution on the power transmission coil

VP4-07. Anti-inflammatory effects of pulsed magnetic field on the immune system. *S. Kim*[1] and H. Lee[1] *1. Sangji University, Wonju, The Republic of Korea*

When an inflammatory response occurs in the body, primary immune cells, such as macrophages, phagocytize and present antigens, and secondary immune cells, such as T cells, produce antibodies against the presented antigens to prevent infection in the body.[1] Excessive inflammation releases pro-inflammatory cytokines such as TNF-α and IL-6, which damage normal tissues and cells in the body, leading to rheumatoid arthritis and sepsis.[2] This study has tried to confirm the change in inflammatory activity across innate immunity and acquired immunity and investigate the effects of pulsed magnetic field (PMF) on the immune system in regulating excessive inflammation. Raw 264.7 and EL4 cells were co-cultured in a DMEM medium using insert well. Inflammation was induced using LPS. Our PMF stimulator has the maximum intensity of 4700G at a transition time of 136 μs with pulse intervals of 1Hz. In order to confirm changes in inflammatory activity between the two cells and the anti-inflammatory effects of PMF, the level of IL-6 and mitochondrial activity (MA) were measured using ELISA and MTT assay, respectively. The concentration of IL-6 increased in macrophages and T cells after inflammation was induced, and decreased after PMF stimulation. MA also increased under inflammation. When PMF was applied after inflammation induction, MA decreased in both cells, suggesting that PMF has an anti-inflammatory effect on the immune system. From the results of both experiments, it was confirmed that macrophages respond more rapidly than T cells to PMF stimulation with a decrease in cellular activity and a decrease in IL-6, which indicates inflammation relief. Our results show that macrophages, the primary immune cells, are first involved in the inflammatory response and recovery and influence T cells, the secondary immune cells. Therefore PMF stimulus is thought to affect the immune system of the human body by balancing the activation and suppression of immune cells and improve anti-inflammation. For clinical use, non-invasive PMF can be developed as a medical devices modulating immune system with optimizing the PMF conditions such as pulse shape, duration, or repetition rate.

[1] M. U. David, B. Michael, J. Exp. Med., Vol. 190, p.1909-1914(1999) [2] M. Edward, Autoimmunity, vol.7, pp. 305-308(2008)

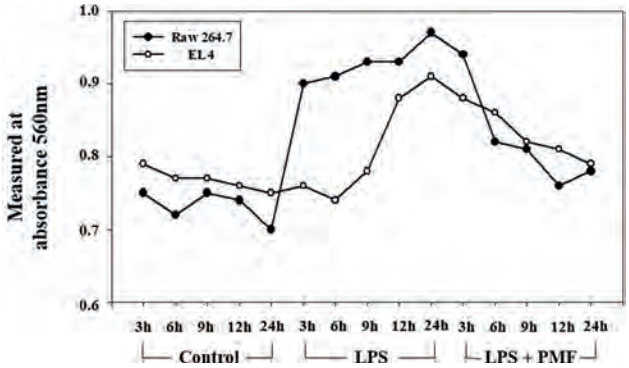

Mitochondrial activity of macrophages and T cells

VP4-09. Withdrawn

VP4-10. Withdrawn

VP4-11. Sedimentation Evaluation of High-Viscosity Linear Polysiloxane-Based Magnetorheological Fluids Using Automated Vertical Axis Inductance Monitoring System. *Y. Choi*[1], P. Sztein[2], G. Hiemenz[2] and N.M. Wereley[1] *1. Department of Aerospace Engineering, University of Maryland, College Park, MD, United States; 2. Innovital Systems Inc., Calverton, MD, United States*

The sedimentation of magnetorheological fluids (MRFs) has been an obstacle to achieving successful commercial MRF-based applications. To mitigate such sedimentation issues, high-viscosity linear polysiloxane-based MRFs (HVLP MRFs) have been recently developed. These HVLP MRFs utilize highly viscous carrier fluid for stabilizing MRFs because the settling velocity of particles is inversely proportional to the viscosity of carrier fluid. Thus, in this study, the long-term sedimentation stability of HVLP MRFs is experimentally investigated by using an automated vertical axis inductance monitoring system (AVAIMS). In our previous studies [1, 2], the mudline of HVLP MRFs with lower particle loadings up to 32 vol% was tracked by using a nonautomated VAIMS. But, these previous studies focused on the particle descending only from the fluid top of the HVLP MRFs' columns. The sedimentation zones of the HVLP MRFs below mudline such as original concentration, variable concentration, and sediment were not identified in the previous studies. Thus, in this study, the long-term sedimentation stability of the HVLP MRFs with high particle loadings up to 45 vol% was tracked for 204 days by using AVAIMS, and the four different sedimentation zones were identified. To this end, the automated identification method to determine the sedimentation zone boundaries of highly stable MRFs was proposed. The testing setup for the AVAIMS used in this study was presented in Fig. 1. The inductance sensor was vertically movable by the linear vertical motion mechanism with the step motor. Using this inductance sensor and LCR meter, the inductances of the HVLP MRF in the testing tube were measured almost every week. The measured inductances were converted into the particle concentration by using the calibration function. The measured particle concentration profiles of the HVLP MRFs tested in this study were presented in Fig. 2. Based on these measured particle concentration profiles, the sedimentation zones were determined by the automated identification method proposed in this study.

[1] L. Xie et al. “Characterization of stratification for an opaque highly stable magnetorheological fluid using vertical axis inductance monitoring system”. In: Journal of Applied Physics 117 (2015), 17C754, (4pp).
[2] L. Xie et al. “Long term stability of magnetorheological fluids using high viscosity linear polysiloxane carrier fluids”. In: Smart Mater. Struct. 25 (2016), 065006, (11pp)

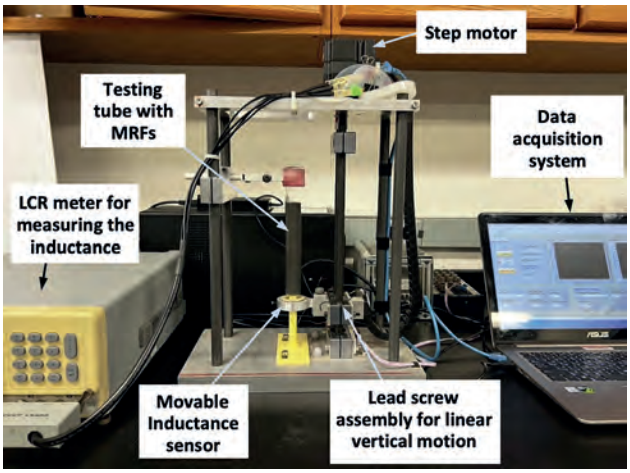

Fig.1 Testing setup to track the particle concentration of an HVLP MRF column by using the AVAIMS

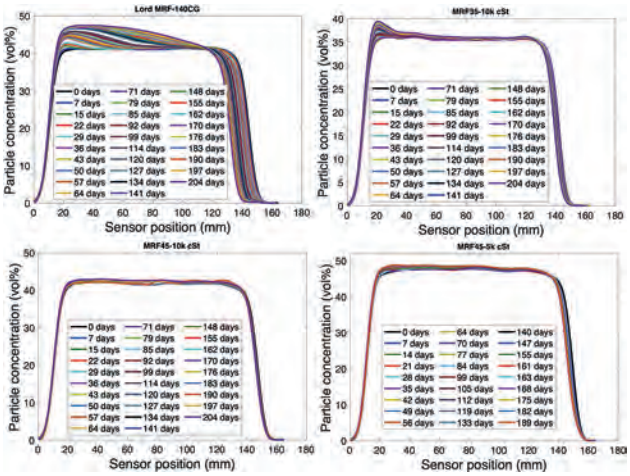

Fig.2 Particle concentration profiles of the HLVP MRFs for 204 days

VP4-12. A method for detecting and locating multiple weak magnetic target signals under the interference of strong magnetic sources.

S. Zhang[1], J. Qiu[1], H. Song[1], H. Sun[1] and S. Huang[1] *1. College of Optoelectronic Engineering, Chongqing University, Chongqing, China*

Due to the high-speed attenuation characteristics of the magnetic field generated by the magnetic source, it is extremely difficult to locate the weak magnetic sources with multiple targets at different depths and positions, which means weak magnetic sources signals are often covered. This paper propose an multi-objective positioning method combining the optimized Euler deconvolution positioning algorithm and the Moth-flame optimization algorithm[1] to solve the problem of weak magnetic sources in strong magnetic environments. According to the normalized source strength (NSS) is only affected by the magnetization[2], for the NSS of the measured magnetic field, two signal processing methods, stochastic resonance signal enhancement (SR) and automatic multiscale-based peak detection (AMPD) algorithm[3], are used to enhance the weak magnetic field and suppress environmental noise, and estimate the number and potential area of the measured targets, the Magnetic Gradient Tensor (MGT) contains more abundant position and magnetic moment information, using MGT as a magnetic measurement and using differential means to improve the inherent defects of traditional magnetic positioning methods that are susceptible to geomagnetic interference [4]. Using the preliminary single-point positioning data to propose an optimization scheme for the initial population and iteration process of the Moth-Flame optimization algorithm, which improves the stability of the algorithm and improves the shortcoming that the algorithm is easy to fall into a local optimal solution, further eliminate the mutual interference and influence between the magnetic sources to be measured to improve the positioning accuracy of multiple covered positioning targets, the simulation results prove that this method can achieve effective multi-target positioning in the case of strong magnetic source interference, and compared with the traditional Euler deconvolution positioning method, and the positioning accuracy is improved by more than 15% before.

[1] Seyedali Mirjalili. Moth-flame optimization algorithm: A novel nature-inspired heuristic paradigm[J]. Knowledge-Based Systems, 2015,89.
[2] Beiki M, Clark D, Austin J, et al. Normalized Source Strength and it Application to Estimate Magnetic Source Location In the Presence of Remanent Magnetization[C]//Seg Technical Program Expanded.2012. DOI:10.1190/segam2012-0993.1. [3] Scholkmann F, Boss J, Wolf M. An Efficient Algorithm for Automatic Peak Detection in Noisy Periodic and Quasi-Periodic Signals[J].Multidisciplinary Digital Publishing Institute, 2012(4). DOI:10.3390/A5040588. [4] G. Yin, Y.T. Zhang, H.B Fan, Z.N. Li, Magnetic dipole localization based on magnetic gradient tensor data at a single point, J. Appl. Remote Sens. 8, 2014(8).

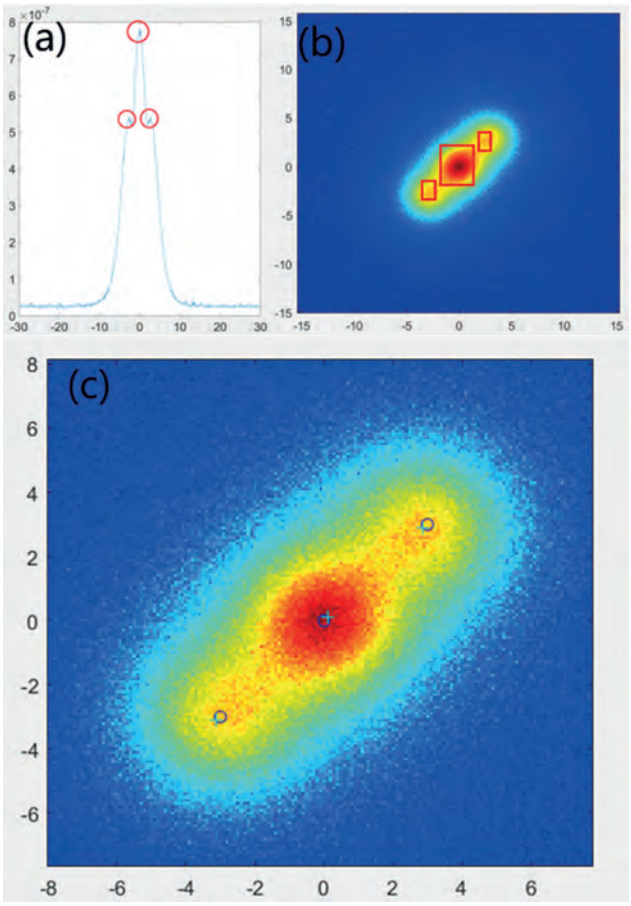

Fig.1 (a) Weak magnetic source signal detection of NSS magnetic anomaly curve; (b) Identify potential areas of interest; (c) Simulation results of multi-target

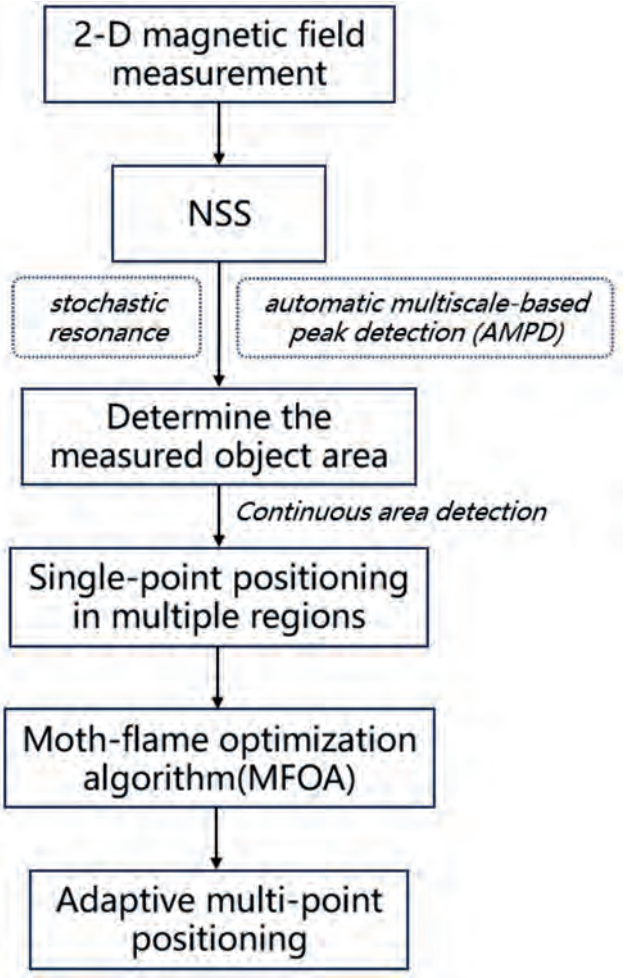

Fig. 2 Technical route of multi-target magnetic positioning

VP4-13. Repulsive Magnetic Levitation-based Electromagnetic Energy Harvesting of a Low-frequency Ocean Wave. *J. Park*[1], R. Pillai[1], N.M. Wereley[1] and A. Flatau[1] *1. Aerospace Engineering, University of Maryland, College Park, MD, United States*

The global demand for energy is steadily rising, leading to a range of environmental problems such as global warming, primarily attributed to the consumption of fossil fuels for power generation. Numerous technologies have been developed for harvesting ocean waves[1]. However, proper maintenance of wave energy converters in the harsh marine environment is key from a business perspective. One of the issues is friction, which can cause wear and degradation of key moving components, increasing maintenance costs. Magnetic levitation, due to its friction-free nature, has been utilized for implementing low-maintenance electromagnetic energy harvesting[2, 3, 4]. In this research, ocean wave energy is harvested using repulsive magnetic levitation. The energy generated by the waves, which have frequencies of 0.25–1.0 Hz, is captured by an absorber, such as a buoy. A buoy is used to transfer a movable magnet toward the bottom, where it encounters a fixed permanent magnet. These magnets are positioned facing each other with identical polarities. As the buoy brings the magnet closer to the bottom, it experiences a powerful repulsive force, which activates a release mechanism. This mechanism propels the movable magnet to accelerate upward [Figure 1]. Consequently, as the magnet passes through the coil, it induces electricity. Due to gravity, the magnet descends again, generating electricity once more. A sine wave of 0.1 Hz was used to simulate ocean waves using a hydraulic actuator [Figure 2(a)]. Figure 2(b) demonstrates that peaks with an output voltage of approximately 2 volts appear at 10-second intervals. Additionally, a peak of 0.5 volts was observed after 5 seconds, suggesting that the magnet is successfully connected to the transferring magnets. Figure 2(c) shows a ringdown waveform of the output voltage in a wave cycle due to gravity and magnetic repulsion. This result demonstrates the feasible use of repulsive magnetic levitation in low-frequency wave energy harvesting.

[1.] K. Veerabhadrappa, B. Suhas, C. K. Mangrulkar, R. S. Kumar, V. Mudakappanavar, K. Seetharamu et al., "Power generation using ocean waves: a review," Global Transitions Proceedings, 2022. [2.] D. J. Apo and S. Priya, "High power density levitation-induced vibration energy harvester," Energy Harvesting and Systems, vol. 1, no. 1-2, pp. 79–88, 2014. [3.] M. P. Soares dos Santos, J. A. Ferreira, J. A. Simoes, R. Pascoal, J. Torrao, X. Xue, and E. P. Furlani, "Magnetic levitation-based electromagnetic energy harvesting: a semi-analytical non-linear model for energy transduction," Scientific reports, vol. 6, no. 1, p. 18579, 2016. [4.] B. Drew, A. R. Plummer, and M. N. Sahinkaya, "A review of wave energy converter technology," 2009.

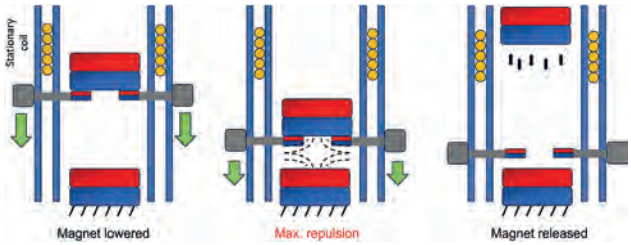

Schematic illustrations of repulsive magnetic levitation-based electromagnetic energy harvesting.

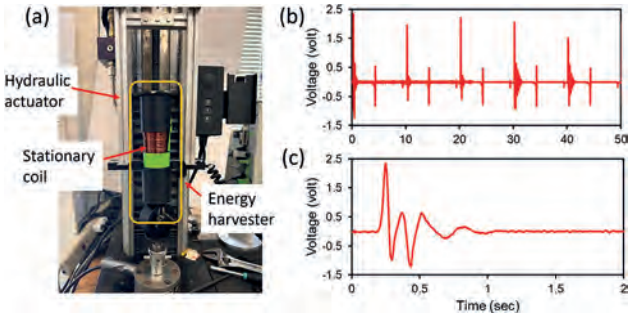

a) Experimental setup (b) voltage acquired with 0.1 Hz sine wave (c) voltage acquired in a single wave cycle.

VP4-14. 3D Inversion of Magnetic Gradient Data Based on Equivalent Source Weighting Method. S. Huang[1], *J. Qiu*[1], H. Sun[1] and S. Zhang[1] *1. Chongqing University, Chongqing, China*

The three-dimensional inversion of magnetic data is a crucial technology for detecting and recognizing magnetic objects such as sunken ships, unexploded ordnance, and pipelines [1]. Due to the non-uniqueness of inversion, different norm regularization methods will result in different inversion results. The L_2 norm is a common choice of the model norm, mainly because L_2 norm optimization is equivalent to solving linear simultaneous equations, which is simple and stable. However, the solution obtained by the L_2 norm regularization method is usually smooth and continuous [2]. L_1 norm regularization has also been widely used to generate solutions with sharp boundaries. Without an appropriate upper limit of magnetic susceptibility, the L1 norm will lead to an over-concentrated solution [3]. To solve the problem caused by norm regularization, we propose a three-dimensional inversion method for magnetic gradient data based on equivalent source weighting. Firstly, we use the correlation imaging method of magnetic gradient tensors to estimate the center positions of magnetic models. Then an equivalent source weighting function is constructed using the obtained center positions. To make the magnetic sources with the same magnetic anomaly signal but different volumes have an equal model objective function, this function reasonably adjusts the weight of each grid in the inversion space according to the distance from the grid to the center of the magnetic models. Here we

use European distance and Chebyshev distance for comparison. Finally, we add the equivalent source weighting function to the total objective function and find the solution by the Conjugate gradient method. The results of the simulation model experiment (Figure 1) show that our proposed method can avoid generating overly smooth or concentrated results. The structural similarity of Fig. 1(b-d) is 0.7444, 0.9082, and 0.9056, respectively, indicating equivalent source weighting can improve the inversion accuracy.

[1] Z. Cai, Z. Li and H. Fan, Micromachines., Vol. 13, p.1813 (2022) [2] W. Du, L. Cheng and Y. Li, Applied Sciences., Vol. 11, p.1072 (2021) [3] U. Mitsuru, Geophysical Journal International., Vol. 228, p.510-537 (2022)

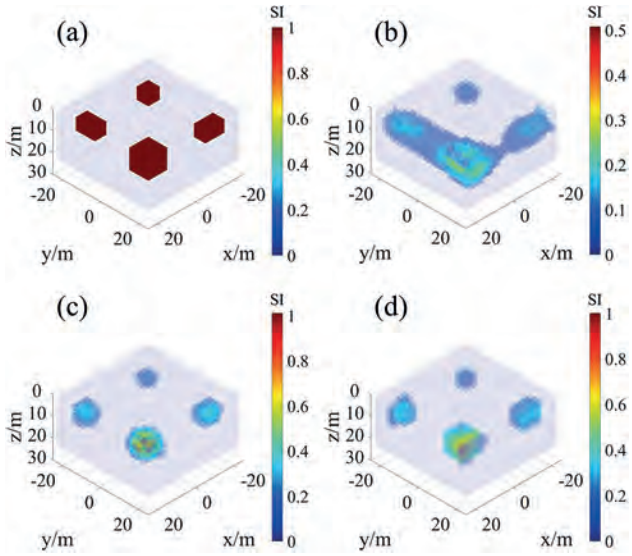

Fig. 1 Simulation models (a) and inversion results (b-d). (b) Traditional L_2 norm regularization method; (c) equivalent source weighting method using Euclidean distance; (d) equivalent source weighting method using Chebyshev distance.

VP4-15. Withdrawn

Session VP5
MAGNETIC RECORDING (VIRTUAL)
(Poster Virtual Session)

Varaprasad Bollapragada, Chair
Carnegie Mellon University, Pittsburgh, PA, United States

VP5-01. Effect of Ta buffer layer on the structural and magnetic properties of stoichiometric intermetallic FeAl alloy. S. Bhardwaj[1], *P. Kumar*[2], R. Ghosh[3] and B.K. Kuanr[1] *1. Special Centre for Nanoscience, Jawaharlal Nehru University, New Delhi, India; 2. Department of Electronic Science, University of Delhi, South Campus, New Delhi, India; 3. Department of Electronics & Communication Engineering, Indraprastha Institute of Information Technology, New Delhi, India*

Using density functional theory, we study chemically ordered paramagnetic (B2) and disordered ferromagnetic (FM) (A2) phases of $Fe_{50}Al_{50}$ alloy for applications in phase-change magnetic memory devices. To explore A2 phase, we employ three distinct atomic configurations in a 2×2×2 supercell. The simulated results averaged over three configurations indicate that A2 phase exhibits high magnetic moment (2.2 μ_B/Fe-atom), substantial magnetocrystalline anisotropy (-0.04 meV/f.u.), and low intrinsic Gilbert damping (α) (8×10^{-4}) than B2 phase. The onset of ferromagnetism and high magnetic moment in A2 phase is due to an increase in number of Fe-Fe nearest neighbors which provides large overlap of d-orbitals leading to long-range FM order [1]. Low α in A2 phase is possibly due to its lower density of states at Fermi level which results in less availability of states for electrons to scatter into. Therefore, we experimentally study A2 phase of 50 nm $Fe_{50}Al_{50}$ film deposited on Al_2O_3 substrate with and without Ta buffer layer. A2 phase is confirmed with appearance of peak in X-ray diffraction in Al_2O_3/Ta(5 nm)/$Fe_{50}Al_{50}$(50 nm) (S1) film and no peak in as-grown Al_2O_3/$Fe_{50}Al_{50}$(50 nm) (S2) film [2]. For S2, it might be due to large lattice mismatch between FeAl (a= 0.29 nm) film and Al_2O_3 (0.48 nm) substrate. The hysteresis curves reveal high saturation magnetization (M_s) (848 emu/cc) in S1 as compared to 576 emu/cc in S2. The rise in M_s is attributed to structural improvement of FeAl layer on Ta. However, presence of Ta layer increases surface roughness (ρ) from 0.41 nm to 0.56 nm shown by atomic force microscopy. It may be associated with possible reaction between FeAl film and thin Ta layer at interface. Magnetization dynamics study using ferromagnetic resonance shows enhancement in α from 4.35×10^{-3} in S2 to 4.94×10^{-3} in S1 due to extrinsic contributions induced by surface inhomogeneities [3]. Large inhomogeneous broadening in S1 (81 Oe) is due to its high ρ which further results in large α as compared to S2 (63 Oe).

[1] Polushkin, N. I., Oliveira, V., Vilar, R., et al. Physical Review Applied 10.2 (2018): 024023. [2] Vahaplar, K., Tari, S., Tokuç, H., et al. Journal of Vacuum Science & Technology B: Microelectronics and Nanometer Structures Processing, Measurement, and Phenomena 27.5 (2009): 2112-2116. [3] Smith, D. A., Rai, A., Lim, Y., et al. Physical Review Applied 14.3 (2020): 034042.

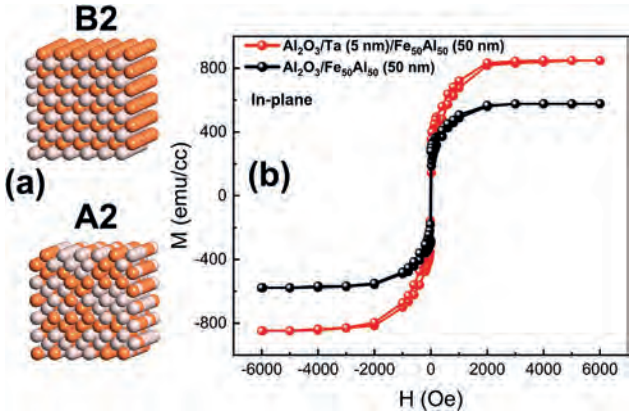

Fig.1a) Ordered (B2) and disordered (A2) phase in $Fe_{50}Al_{50}$ b) M-H loop of S1 and S2 films.

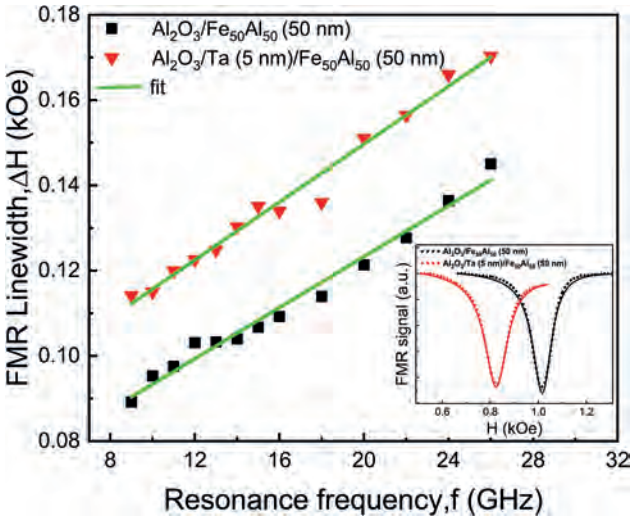

Fig.2 Ferromagnetic resonance (FMR) linewidth Vs frequency plot and inset shows FMR spectra at 10 GHz of S1 and S2 films.

VP5-02. Magnetic printing characteristics of burst signals by using double magnet mater media. *T. Komine*[1] *1. Ibaraki University, Ibaraki, Japan*

Magnetic printing technique is a strong candidate for servo track writing with extremely high speed and low cost. Recently, the double magnet master (DMM) was proposed for energy-assisted magnetic recording media with high coercivity[1]. The previous work showed that DMM printing can achieve superior characteristics for periodical line/space, dot, and checkerboard patterns[2, 3]. However, the servo-signals include servo-burst and address part with Gray code address which are non-periodic patterns. In this study, as the more realistic servo signals, the printing characteristics of burst signals can be demonstrate by utilizing micromagnetic simulation. Figure 1 shows the calculation model for master media and recording layer. The A/B burst is assumed in the simulation. The servo information typically includes

track centering information and quadrature reference information providing position error signal (PES). The DMM media consists of two magnetic materials with different magnetic properties. One magnet is $L1_0$-FePt which has a coercivity higher than the coercivity of recording layer, while the other magnet is FeCo alloy with a lower coercivity. Two magnetic materials have no exchange interaction between these materials by insertion of non-magnetic separation layer. In order to calculate the printed magnetization distributions, the micromagnetic simulation has been carried out. Figure 2 shows the printed magnetization distributions onto the recording layer with the coercivity of about 10 kOe. The track width is 50 nm. During the printing process, the recording field difference generated by DMM media is about 15 kOe for burst pattern which is much larger than that of conventional master. As a result, the DMM can clearly print burst pattern and the clear PES is expected, especially even if in off-center region the clear magnetization distribution can be achieved. This study provides the feasibility of DMM printing for realistic servo writing technique.

[1] T. Komine, *IEEE Trans. Magn.* 58, 3200105 (2021). [2] T. Komine, *IEEE Trans. Magn.* 58, 3200905 (2022). [3] T. Komine, *AIP Advances* 13, 025310 (2023).

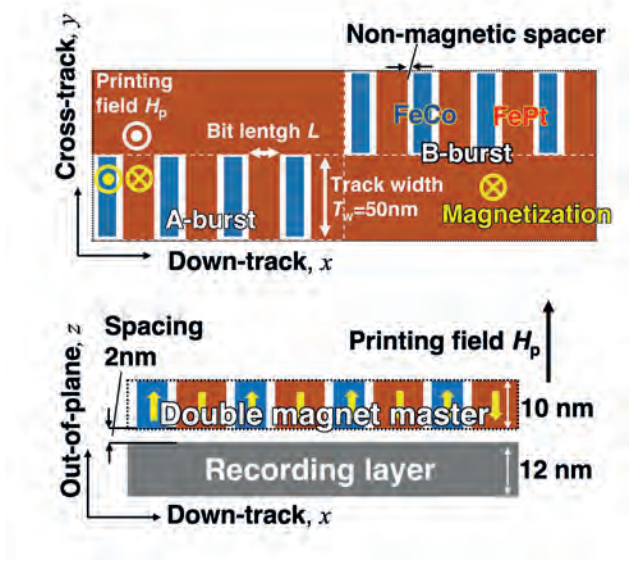

Fig. 1 Schematic illustrations of conventional master and double magnet master media for servo burst.

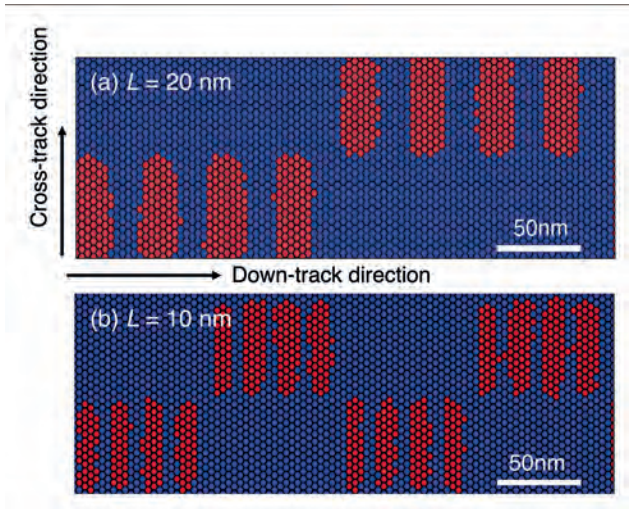

Fig. 2 Printed magnetization distributions for burst signals with bit length of (a) 20 nm and (b) 10 nm. The printing field *Hp* is 8.5 kOe.

VP5-03. Impact of thermal spin-transfer torque on all-optical switching in $L1_0$-ordered FePt thin films. *J. Wang*[1], Z. Wen[2], Y. Sasaki[2], Y. Takahashi[2], K. Uchida[2], K. Takagi[1] and K. Ozaki[1] *1. National Institute of Advanced Industrial Science and Technology, Nagoya, Japan; 2. National Institute for Materials Science, Tsukuba, Japan*

The promising technology of FePt nanogranular film-based heat-assisted magnetic recording (HAMR) utilizes laser heating during writing to increase storage density in hard disk drives[1]. Besides the heating effect, circularly polarized lasers can induce helicity-dependent magnetization reversal, known as all-optical switching (AOS)[2]. Integrating AOS into HAMR, specifically achieving laser-induced deterministic (100%) magnetization switching in FePt nanogranular film, is of great interest. However, thus far, deterministic AOS has only been observed in soft magnetic materials like GdFeCo or [Co/Pt]n films[3]. In this study, we demonstrated a thermal spin-transfer torque (STT) assisted AOS in nanogranular FePt films on ferrimagnetic yttrium iron garnet (YIG) substrates. By exposing the sample to circularly polarized lasers (σ+/σ−), a thermal gradient (∇T) is generated in the YIG/FePt bilayer film, creating a pure spin current through the spin Seebeck effect (SSE). This spin current, in turn, applies a torque on the magnetic moment of FePt film, aiding the magnetization reversal associated with AOS (Fig. 1). FePt-C nanogranular films were deposited on both YIG and GGG substrates by magnetron sputtering. YIG and GGG substrates allowed a valid comparison due to their close lattice constants but distinct spin Seebeck coefficients, enabling the extraction of the potential contribution of thermal STT on AOS in FePt films. The study investigated the AOS in all samples by analyzing the dependence on laser helicity and laser fluence. The MOKE measurements revealed an enhanced helicity-dependent AOS in the YIG/FePt-C bilayer compared to the GGG/FePt-C bilayer film. Additionally, the AOS effect showed a positive correlation with laser fluence in the YIG/FePt-C bilayer film but remained nearly unchanged in the GGG/FePt-C bilayer sample. The presentation will provide a detailed discussion of the potential contribution of thermal STT on AOS in FePt nanogranular films, based on experimental results. This work was supported by Early-Career Scientists (21K14521) from JSPS KAKENHI, Japan.

[1] D. Weller, *et al.*, *J. Vac. Sci. Technol. B* 34, 060801 (2016). [2] Y. K. Takahashi, *et al.*, *Phys. Rev. Appl.* 6, 054004 (2016). [3] S. Mangin, *et al.*, *Nat. Mater.* 13, 286 (2014).

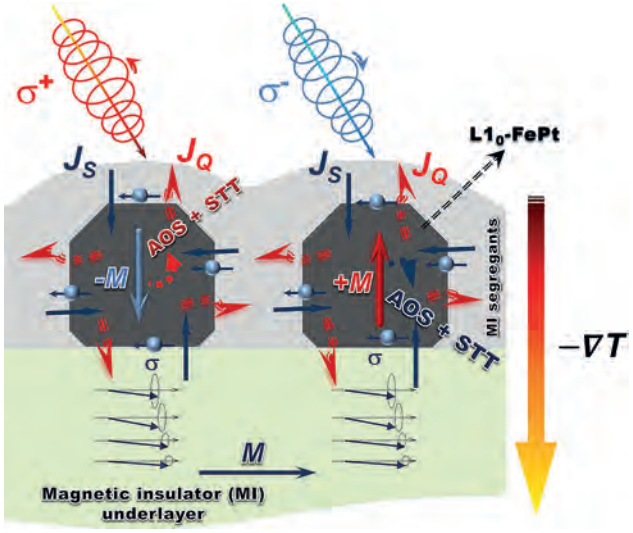

Fig. 1. Conceptual diagram of the laser-induced thermal spin-transfer torque for assisting magnetization reversal in FePt nanogranular media.

VP5-04. Withdrawn

VP5-05. A Study on Acceleration of SP Decoder Using Reliability of Recording Sequence by Neural Network Based on Parity Check Result in SMR System. *M. Nishikawa*[1], Y. Nakamura[1], Y. Kanai[2] and Y. Okamoto[1] *1. Graduate School of Science and Engineering, Ehime University, Matsuyama, Japan; 2. Department of Engineering, Niigata Institute of Technology, Kashiwazaki, Japan*

We study low-density parity-check (LDPC) coding and iterative decoding using a neural network (NN) in the shingled magnetic recording (SMR) system. The read/write (R/W) channel consists of the granular media shown in [1], [2]. In addition, the system noise defined by the signal-to-noise ratio (SNR_S) generates at the reading point, where the SNR_S = 21.5dB. Here, i_{sp} and i_{global} stand for the maximum number of iterations in the sum-product (SP) decoder and turbo equalization, respectively. In the conventional SP decoder with the NN, we updated the reliable γ_n, and the update parameters were TH_γ = 0.9 and W_γ = 1.34 [1]. The γ_n means the transition probability from the previous point to the current point on the trellis diagram for the nth (n = 1 to 3) sub-matrix. The NN outputs the reliability of the recording sequence using s for 3 sub-matrices. When the NN output is greater than TH_γ or smaller than (1 – TH_γ), we assume that the decoding result is "1" or "0", respectively. Also, W_γ means the weight to be multiplied by γ_n. In the proposed SP decoder with the NN, in order to update more reliable γ_ns, we set TH_γ and W_γ according to the NN input type, respectively, and realize more effective iterative decoding in the SP decoder. Using the parity check matrix, the NN input type is obtained by modulo 2 addition operation to the hard decision results for the NN input in the row direction and adding the rows determined to be incorrect by the parity check in the column direction [3]. Therefore, we set TH_γ = 0.6, 0.8, 0.9, and 0.9, respectively, such that the update accuracy for NN input types 0, 1, 2, and 3 is about 0.98. Also, we set W_γ = 1.37, 1.34, 1.34, and 1.34, respectively, such that the bit error rate (BER) shows good performance. Figure 1 shows the number of correct updates for i_{global}. Here, we set i_{sp} = 6. From the figure, for any i_{global}, the number of correct updates is larger for the proposed SP decoder with NN. Figure 2 shows the BER performances for i_{global}, where the simulation parameters are the same as those in the previous figure. From the figure, the proposed SP decoder with NN achieves no errors, but the others go into the error floor.

[1] M. Nishikawa, Y. Nakamura, Y. Kanai, and Y. Okamoto, "A study on accelerating SP decoding by neural network in SMR system," *IEEE Trans. Magn.*, 2023 (to be published). [2] M. Yamashita, Y. Okamoto, Y. Nakamura, H. Osawa, S. J. Greaves, and H. Muraoka, "Performance evaluation of neuro-ITI canceller using a modified writing process for TDMR," *IEICE Trans. Electron.*, vol. E96-C, no. 12, pp. 1504–1507, Dec. 2013. [3] M. Nishikawa, Y. Nakamura, Y. Okamoto, H. Osawa, Y. Kanai, and H. Muraoka, "A study on iterative decoding with LLR modulator by parity check information in SMR system," *IEEE Trans. Magn.*, vol. 54, no. 11, 3001304, Nov. 2018.

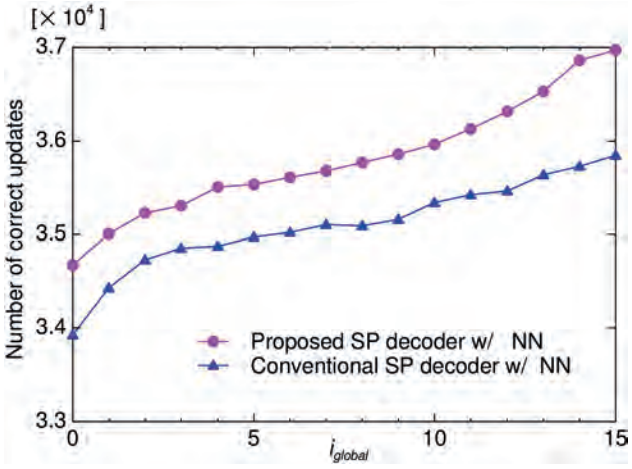

Number of correct updates

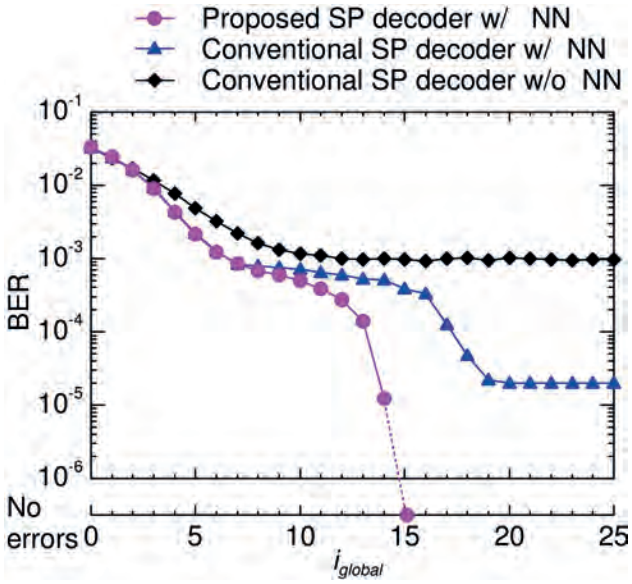

BER performances

VIRTUAL PLATFORM ONLY

Session VP6
MAGNETIC SENSORS AND HIGH FREQUENCY DEVICES (VIRTUAL)
(Poster Virtual Session)

Tian-Yue Chen, Chair
New York University, New York, NY, United States

VP6-01. Magnetic Tunnel Junction Micropillar with Magnetic Flux Concentrators for High-Sensitivity Magnetometers. *D. Tonini*[1], O. Benally[1], Y. Chen[1], B.R. Zink[1], S. Liang[2], V.K. Chugh[1], Q. Jia[1], R. Saha[1], J. Chen[1], K. Wu[3] and J. Wang[1] *1. Electrical and Computer Engineering, University of Minnesota, Minneapolis, MN, United States; 2. Chemical Engineering and Materials Science, University of Minnesota, Minneapolis, MN, United States; 3. Electrical and Computer Engineering, Texas Tech University, Lubbock, TX, United States*

This study focuses on characterizing the properties of circular magnetic tunnel junction (MTJ) micropillars. These micropillars were subjected to various current densities and external magnetic flux concentrators (MFCs) to determine the optimal sensitivity under a DC bias field, as represented in Fig. 1(a). The MTJ stacks in this study consist of: Ru (5)/Ta (5)/CoFeB (3)/MgO (2.5)/CoFeB (3)/Ru (0.85)/CoFe (2.5)/IrMn (10)/NiFe (5)/Ta (5)/Ru (10)/Ta (5). Numbers in parentheses are nominal thickness of the individual layers, in nanometer (nm). For individual circular micropillars with a diameter of approximately 9.3 μm, we achieved a tunneling magnetoresistance (TMR) ratio of 183% (R_{min}~6.4 kΩ, R_{max}~18.2 kΩ), a maximum sensitivity of 300-350 %/Oe around 0 Oe bias field suitable for high-sensitivity magnetometers, as shown in Fig. 1(b). This was accomplished using 0.1-0.15 mm thick external MFCs made of soft magnetic alloy $Co_{69}Fe_4Mo_4Nb_1Si_{16}B_7$, placed 300 μm from the micropillar, as illustrated in Fig. 1(c)-(i). The MTJs represented in Fig. 1(c)-(ii) were annealed at 325 Celsius under a magnetic field of 0.5 T for 2 hours to fix the pinned layer (CoFe). In the future, we will investigate the impact of the relative orientation of the MFCs to the external magnetic field direction. The $Co_{69}Fe_4Mo_4Nb_1Si_{16}B_7$ for MFCs is replaced with MuMetal in an aim to achieve a higher TMR ratio and sensitivity. To assess the TMR behavior of the assembled devices combined with MFCs, the hysteresis loops are collected under an external field of -100 Oe to 100 Oe. The devices are wirebonded with gold microwires to a PCB for testing purposes, as shown in Fig. 1(c)-(iii). Furthermore, we will study the RH responses of MTJ devices under different current densities and compare the results with existing literature [1,2].

[1] G. He, Y. Zhang, L. Qian, G. Xiao, Q. Zhang, J.C. Santamarina, T.W. Patzek, and X. Zhang, "PicoTesla magnetic tunneling junction sensors integrated with double staged magnetic flux concentrators," Appl. Phys. Lett. 113(24), 242401 (2018). [2] M. Oogane, K. Fujiwara, A. Kanno, T. Nakano, H. Wagatsuma, T. Arimoto, S. Mizukami, S. Kumagai, H. Matsuzaki, N. Nakasato, and Y. Ando, "Sub-pT magnetic field detection by tunnel magneto-resistive sensors," Appl. Phys. Express 14(12), 123002 (2021).

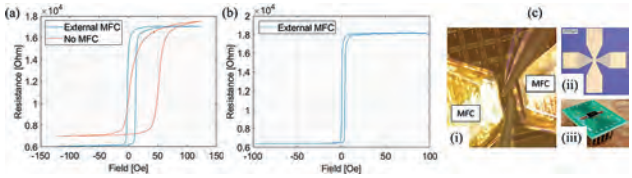

(a) Hysteresis loops of MTJ micropillar with and without external MFCs. (b) MTJ micropillar show a sensitivity of 300-350 %/Oe. (c)-(i) Microscopic representation of the MTJ device; (ii) External MFCs; (iii) Device wirebonded on a PCB.

VP6-02. Design of Fe-based Amorphous Alloy Thin Sensor with Tunable Compensation Magnetic Resonance System. *C. Hsu*[1] *1. Mechanical Engineering, Asia Eastern University of Science and Technology, Banqiao District, Taiwan*

This study introduces the design and analytical measurement of Fe-based amorphous alloy thin sensors, in which the thin amorphous materials used in the study include SA1, HB1-M and other different materials, which are fabricated into magnetic sensors. During the manufacturing process, due to its iron-based characteristics, the sensor characteristics will produce magnetic drift with temperature changes. The magnetic characteristics of the magnetic sensor are shown in Figure 1. In order to test the performance of the magnetic sensor, the configuration design of the soft magnetic core structure is carried out on the circuit, mainly to study the sensing mode of the magnetic field and current. Figure 2 shows the wiring diagram of the magnetic field and current sensing modes, and the design diagram is for measuring the magnetic field connection sensing terminal voltage signal. Therefore, a uniform test field (B) produces magnetic sensitivity as shown in Figure 2. The excitation field is anti-parallel to the polarity of the induced electromotive force (EMF) in the induction coil, followed by current measurement by connecting the core terminals, sensitive to the inhomogeneous magnetic field induced by the test current on straight wires passing through two fluxgates and analyse. Therefore, this study designs an improved magnetic circuit to compensate and reduce the temperature coefficient of the magnetic sensor. Magnetic circuits are used in place of static DC bias currents in a DC bias inversion method. The study uses different input signals including square wave and triangular wave and different switching signals to adjust the current bias. In the experiment, the switching frequency is adjusted between 100Hz and 1kHz to observe the compensation of the bias to reduce the temperature coefficient of the magnetic sensor, as a verification of the measurement sensitivity of different amorphous sensors in the frequency domain.

[1] X. Shen, Y. Teng, and X. Hu, "Design of a low-cost small-size fluxgate sensor," Sensors, vol. 21, no. 19, p. 6598, Oct. 2021. [2] M. Dressler, M. Janosek, and M. Butta, "Reduction of magnetic noise limits of orthogonal fluxgate sensor," AIP Adv., vol. 11, 2021, Art. no. 015347.

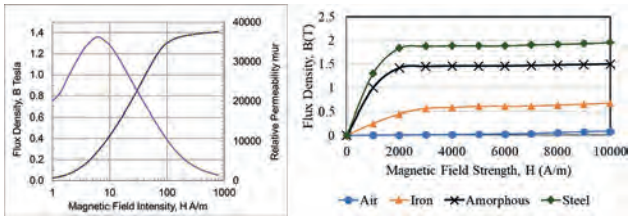

Fig. 1 Magnetic characteristics of magnetic sensor: (a) magnetic permeability, (b) hysteresis loop characteristics

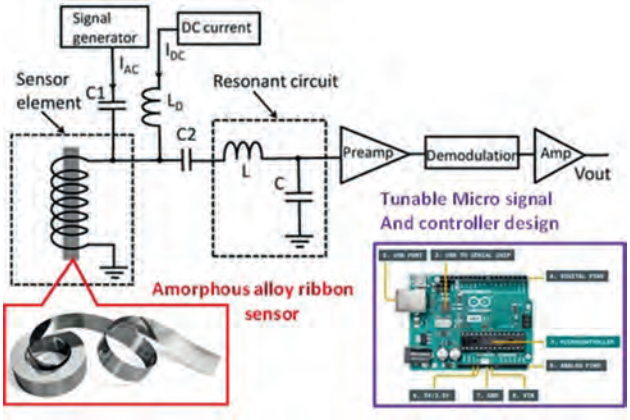

Figure 2 Magnetic sensor and its circuit design structure

VP6-03. A Metal Object Detection System for Electric Vehicle Wireless Charging based on LC Oscillating Circuit and Reverse-Winding-Incorporated Detection Coils. *Y. Zheng*[1], R. Xie[1], C. Liu[1], X. Chen[1] and Y. Zhang[1] *1. Fuzhou University, College of Electrical Engineering and Automation, Fuzhou, China*

In the magnetic-coupled wireless charging system of electric vehicles, the ingress of metal objects into the charging system is a common occurrence. During such instances, the strong magnetic field between the receiver and the transmitter induces an eddy current effect in the metal object, resulting in the generation of substantial heat. This heat accumulation poses significant risks, including the potential for fire incidents. Current commercial metal detection technology used in this context suffers from issues such as severe interference from charging systems and detection blind spots. To address these challenges, this paper presents a novel metal object detection system specifically designed for wireless charging of electric vehicles. This system designs a reverse-winding-incorporated detection coil, which consists of an external forward winding and an internal reverse winding in series. The arrangement enables effective decoupling from the receiver and transmitter, while simultaneously eliminating adverse effects on the wireless charging system. Metal object detection is achieved through the utilization of an LC oscillator based on transformer feedback, complemented by an appropriate detection circuit. Finally, a metal detection experimental platform for wireless charging of electric vehicles was constructed to validate the proposed system. Through testing, it has been demonstrated that the system can promptly and accurately detect the presence of metal objects. This research holds significant implications for enhancing the safety and efficiency of wireless charging systems in electric vehicles.

[1] J. Lu, G. Zhu and C. C. Mi, "Foreign Object Detection in Wireless Power Transfer Systems," in IEEE Transactions on Industry Applications, vol. 58, no. 1, pp. 1340-1354, Jan.-Feb. 2022. [2] Y. Sun, K. Song, T. Zhou, G. Wei, Z. Cheng and C. Zhu, "A Shared Method of Metal Object Detection and Living Object Detection Based on the Quality Factor of Detection Coils for Electric Vehicle Wireless Charging," in IEEE Transactions on Instrumentation and Measurement, vol. 72, pp. 1-17, 2023. [3] H. Chen, C. Liu, Y. Zhang, S. Liu, J. Wu and X. He, "Metal Object and Vehicle Position Detections Integrated With Near-Field Communication for Wireless EV Charging," in IEEE Transactions on Vehicular Technology, vol. 71, no. 7, pp. 7134-7146, July 2022. [4] S. Niu, S. Niu, C. Zhang and L. Jian, "Blind-Zone-Free Metal Object Detection for Wireless EV Chargers Employing DD Coils by Passive Electromagnetic Sensing," in IEEE Transactions on Industrial Electronics, vol. 70, no. 1, pp. 965-974, Jan. 2023. [5] C. Zhang, S. Niu and L. Jian, "Vehicle Position Measurement and Misalignment-Effect-Eliminated Metal Object Detection for Wireless EV Charging System: A Dual-Purpose Design of Sensing Coils," 2020 IEEE 4th Conference on Energy Internet and Energy System Integration (EI2), Wuhan, China, 2020, pp. 591-596. [6] J. Xiao, X. Guo, H. Shi, P. Bai, W. Gong and C. Tang, "Method of Non-blind-zone Foreign Object Detection in Wireless Power Transfer System," 2022 IEEE 9th International Conference on Power Electronics Systems and Applications (PESA), Hong Kong, Hong Kong, 2022, pp. 1-6. [7] S. Y. Jeong, V. X. Thai, J. H. Park and C. T. Rim, "Self-Inductance-Based Metal Object Detection With Mistuned Resonant Circuits and Nullifying Induced Voltage for Wireless EV Chargers," in IEEE Transactions on Power Electronics, vol. 34, no. 1, pp. 748-758, Jan. 2019. [8] S. Y. Chu, X. Zan and A. -T. Avestruz, "Electromagnetic Model-Based Foreign Object Detection for Wireless Power Transfer," in IEEE Transactions on Power Electronics, vol. 37, no. 1, pp. 100-113, Jan. 2022.

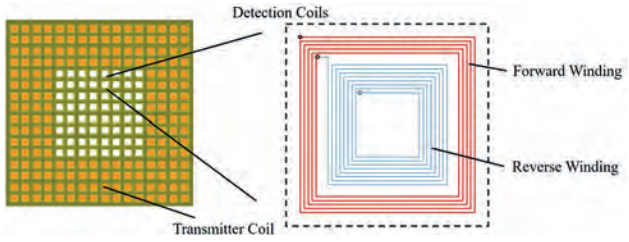

Fig. 1 Internal structure of the detection coil

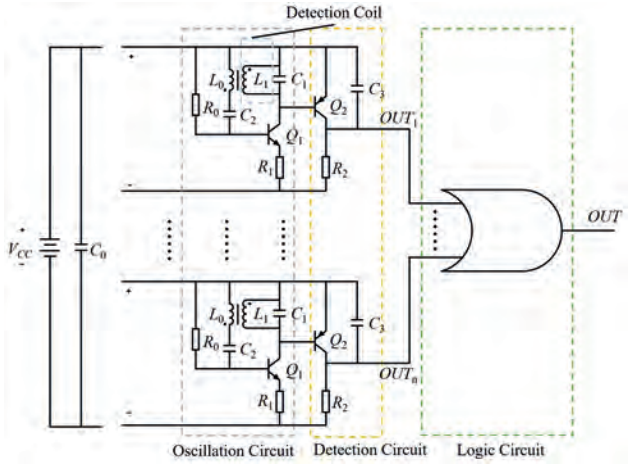

Fig. 2 Detection system circuit topology diagram

VP6-04. Magnetic Tunnel Junction Molecular Spintronics-based chemical sensing device. P. Tyagi[1] and *P. Suh*[1] *1. Mechanical Engineering, University of the District of Columbia, Washington, DC, United States*

The Magnetic Tunnel Junction (MTJ) was first successfully fabricated and tested in the 90s. it consists of a Tri-layer of two ferromagnets, sandwiching a 2nm ultra-thin layer of dielectric or insulator called the tunneling barrier. If a voltage is applied to the ferromagnets, electrons can tunnel across the barrier in a process called quantum mechanical tunneling. The tunneling current in this case is maximum if the direction of magnetization of the two electrodes are parallel to each, and minimum when the two electrodes are anti-parallel to the direction of magnetization. The tunneling current and resistance of this device will therefore change in response to changes in the magnetic orientation of the two ferromagnetic electrodes. The Magnetic Tunnel Junction Molecular spintronic device (MTJMSD) can transform ferromagnetic materials and produce intriguing spin transport characteristics with high sensitivity, low power consumption, very small in size, and less expensive. This disclosure is directed toward a new MTJ-based spintronics device for converting chemical absorption into a change in magnetoresistance. Due to its high sensitivity, excellent scalability, and low power consumption, MTJMSD-based sensors can be widely implemented in different applications. In our investigation, we tested some commonly used chemicals in the lab on our device, both at the excited state (with light) and at the ground state (in the dark) We tested Acetone (CH_3COCH_3), Ethyl Alcohol (CH_2CHOH) and Dichloromethane (CH_2C_{l2}) and studied the trend. The IV measurements were conducted before and after molecular attachment. There was no clear

distinction in the detectivity between the measurement done under the light and in the dark, however, a general observation before and after molecular attachment showed a significant increase in the current. In the present work, we fabricated a metal/insulator/semiconductor MTJ as a testbed for our MTJMSD-based chemical sensing device. This paper is part of an ongoing investigation with the aim of fabricating an MTJMSD-based sensor for the detection of dopamine concentration and other chemicals.

[1] H. Chen et al., "Spintronics-based biosensors for biomedical applications," Biomedical Microdevices, vol. 19, no. 3, pp. 58, 2017. [2] M. Alper and E. Demir, "Molecular spintronics-based biosensors: A review," Journal of Molecular Liquids, vol. 256, pp. 329-334, 2018. [3] X. Wang et al., "Magnetic tunnel junction-based biosensors for detection of biomolecules," Biosensors and Bioelectronics, vol. 135, pp. 94-102, 2019. [4] A. Ghosh, et al., "Molecular Spintronics: From Organic Semiconductors to Self-Assembled Monolayers and Single-Molecule Junctions," Chemical Reviews, vol. 119, no. 1, pp. 1081-1134, 2019. [5] R. Naaman, and D. H. Waldeck, "Spintronics and Chirality: Spin-Selective Transport of Chiral Molecules with Magnetic Nanostructures," Annual Review of Physical Chemistry, vol. 66, no. 1, pp. 263-281, 2015.

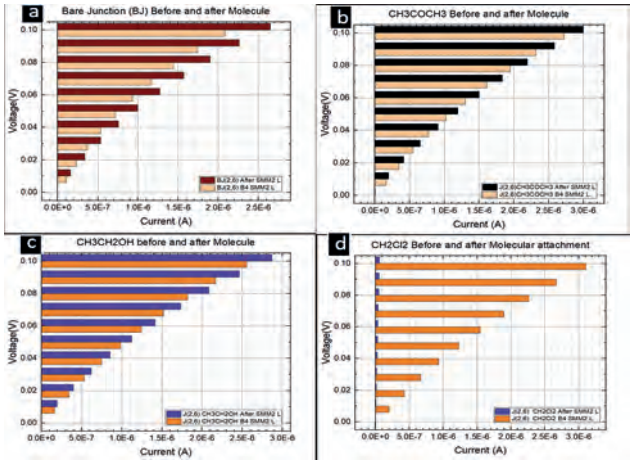

Figure 1

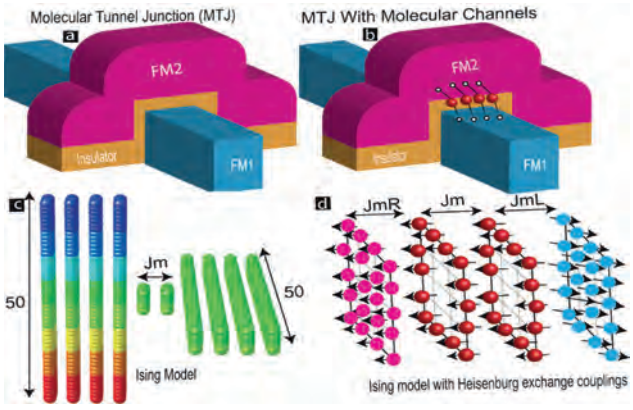

Figure 2

VP6-05. Fabrication of compact circular ring antenna loaded with Gd-YIG ferrites: Photon - Magnon Interaction. S. Yadav[1], *M. Sharma*[2,1] and B.K. Kuanr[1] *1. Special Centre For Nanoscience, Jawaharlal Nehru University, Southwest Delhi, India; 2. Department of Physics, Deshbandhu College, University of Delhi, Delhi, India*

In telecommunication technology, transmitting and receiving signal is not possible without integrating antenna [1]. Miniaturized tunable multi-band microwave devices can be realized by incorporating ferromagnetic materials that exhibit both low loss and high permeability at gigahertz frequencies. A circular ring antenna with a compact size of 25 x 25 mm^2, fed by a microstrip line is proposed at 12 GHz. The antenna is composed of a circular-ring resonator and Gd(x)-doped YIG thin disks (x= 0.0, 0.1, 0.2, 0.3) placed over the ring. It provides tunable operation over tri-band (C to Ku) due to the photon-magnon coupling which enables coherent qubit information transmission from an electromagnetic (EM) carrier to the magnetostatic spin oscillations (magnons) of a magnetic material [2]. The proposed antenna is validated using HFSS simulation. To characterize the frequency tunability of the designed antenna, we measured the return loss (S_{11}) as a function of dc magnetic field. Different concentration Gd-doped YIG ferrites have been loaded on ring antenna to observe strong anti-crossing phenomena with the application of external magnetic field (Fig. 1) for $Gd_{0.2}$-YIG sample (inset: schematic of antenna). The designed antenna has a tunability of around 300% for an applied magnetic field up to 3.7 kOe. The maximum gain of dual resonance antenna is 1.4 for higher magnetic field. Fig. 2 represents the measured normal mode splitting spectrum as a function of bias magnetic field that gives the coupling distance of 1.29 for $Gd_{0.2}$-YIG sample. The inset of Fig 2 shows the efficiency and bandwidth % as a function of Gd concentration. It is apparent that they are maximum for $Gd_{0.3}$-YIG. The radiation patterns of the antenna with all the samples indicated exhibit omnidirectional characteristic, which suggested that the signal could be received by this antenna in various positions. Such antenna are suitable candidates for use in multi-band applications.

[1] Hasan, I. H., Hamidon, M. N., Ismail, A., et al. *IEEE Access*, *6*, 32601, 2018. [2] Bhoi, B., Cliff, T., Maksymov, et al. *Journal of Applied Physics*, *116*(24), 243906, (2014).

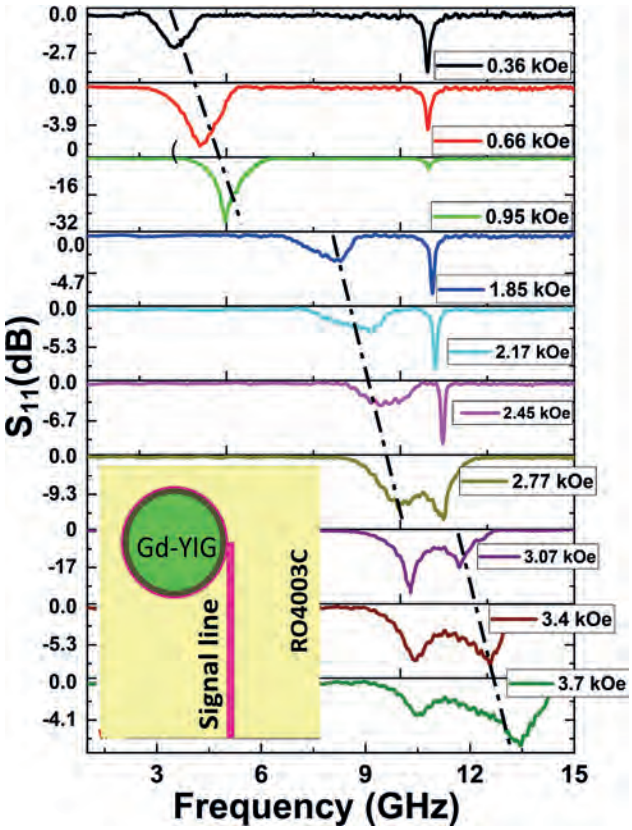

Fig. 1 Return loss of $Gd_{0.2}$-YIG loaded ring antenna for different applied magnetic fields (inset: schematic diagram).

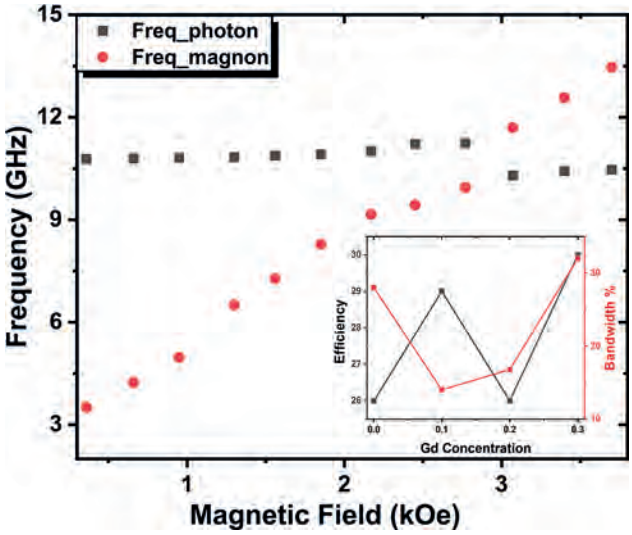

Fig. 2 Measured normal mode splitting spectrum vs bias magnetic field for $Gd_{0.2}$-YIG sample (inset: efficiency and bandwidth% as a function of Gd concentration).

VP6-06. Ultra-Sensitive Magnetic Current Sensor for Smart Grid Applications. *G. Wang*[1], X. Liang[1], H. Huang[1], D. Ju[1] and J. Guo[1] *1. State Grid Smart Grid Research Institute Co., LTD., Beijing, China*

An ultra-sensitive magnetic current sensor in a smart grid is a device used to measure and monitor electric currents with high precision and sensitivity. It is an essential component in the power grid infrastructure, enabling accurate current measurement and monitoring. The sensor utilizes the principle of magnetic field sensing to measure electric currents. Its core is composed of magnetoelectric stress-coupled magnetic field sensors, with a strong coupling coefficient and excellent frequency selection performance [1,2]. When an electric current flows through a conductor, it generates a magnetic field around it. The magnetic current sensor detects and measures this magnetic field to determine the magnitude and direction of the current. The ultra-sensitivity of these sensors allows them to detect extremely small current levels, typically in the range of mA to μA accurately [3,4]. This level of sensitivity is crucial in smart grid applications where precise current measurement is required, especially in situations involving partial discharge monitoring, fault detection, and topology identification. Fig. 1 shows the schematic diagram of the application of ultra-sensitive magneto-sensitive current sensors in grounding fault detection. By injecting characteristic small current signals of different frequencies, a path is formed between the injection point and the grounding point, the sensors can effectively identify the characteristic current signal for fault detection. The sensitivity of the sensor is very important to the process of ground fault discrimination. We have achieved a high-sensitivity linear measurement of 20μA-200mA, as shown in Table 1. And it already has the ability to identify the characteristic frequency current in the complex background current situation, which will play an important role in early fault detection.

[1] Xiao N, Wang Y, Chen L, et al. Theoretical analyses of magnetoelectric effects for magnetostrictive/radial mode piezoelectric transformer composite under dual ac stress and magnetic field modulation[J]. Smart Materials and Structures, 2021, 30(7): 075018. [2] Zaeimbashi M, Nasrollahpour M, Khalifa A, et al. Ultra-compact dual-band smart NEMS magnetoelectric antennas for simultaneous wireless energy harvesting and magnetic field sensing[J]. Nature communications, 2021, 12(1): 3141. [3]Reis S, Castro N, Silva M P, et al. Fabrication and characterization of high-performance polymer-based magnetoelectric DC magnetic field sensors devices[J]. IEEE Transactions on Industrial Electronics, 2017, 64(6): 4928-4934. [4]Wang Z, Hu J, Ouyang Y, et al. A self-sustained current sensor for smart grid application[J]. IEEE Transactions on Industrial Electronics, 2020, 68(12): 12810-12820.

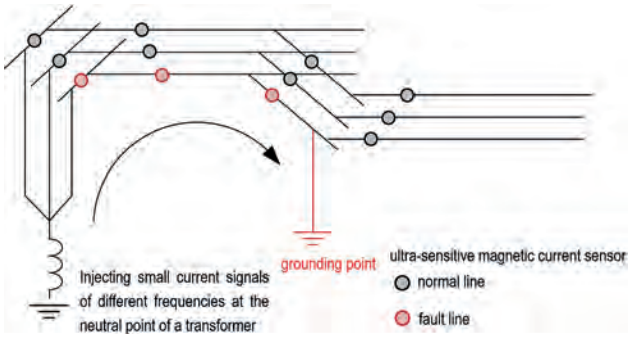

Fig. 1 Schematic diagram of ultra-sensitive magnetic current sensors for grounding fault detection.

Power frequency	I (mA)	V_{out} (dBm)
229 Hz	0	-63.5
	0.01	-63.6
	0.03	-61.8
	0.04	-59.8
	0.05	-57.8
	0.075	-54.5
	0.1	-52.9
	0.2	-47.2
	0.3	-43.1
	0.4	-40.75
	0.5	-38.85
	1	-32.85
	2	-26.37
	3	-22.84
	4	-20.32
	5	-18.43
	10	-12.37
	50	1.59
	100	7.6

Table. 1 The amplitude measurement of the ultra-sensitive magnetic current sensor.

VP6-07. Low-frequency Resonant Magnetoelectric Sensors for Topology Identification of Power Distribution Network. *X. Liang*[1], G. Wang[1], H. Huang[1], Y. Lu[1], D. Ju[1] and J. Guo[1] *1. State Grid Smart Grid Research Institute Co., LTD., Beijing, China*

Accurate topology data is an important foundation for the optimization of distribution network operation mode, fault handling, line loss calculation and other applications [1]. The active injection method of characteristic current is an effective technique used in power systems for topology and fault detection [2,3]. This method provides accurate fault location information, which aids in the quick troubleshooting, reduction of downtime, and improvement of power system reliability. However, detecting the frequency and amplitude of the characteristic current signal imposes strict requirements. On one hand, the frequency of characteristic current should not be too high or too low. High-frequency signals attenuate rapidly, while low-frequency signals are susceptible to the interference from power frequency harmonics. On the other hand, injecting large current signals can easily interfere with power frequency signals, while extremely weak current signals are limited by the sensitivity of existing current sensors, leading to a decrease in identification accuracy. The Micro-Electro-Mechanical Systems (MEMS) magnetoelectric(ME) sensors offer advantages such as high sensitivity, excellent frequency selectivity, and low power consumption, enabling effective measurement of weak current [4, 5]. In order to improve the accuracy and reliability of distribution network topology identification, we proposed a new recognition strategy based on low-frequency resonant ME sensors. Fig. 1 displays the topology identification diagram of power distribution network. In this work, we designed, fabricated, and tested the ME sensor that operates at 229Hz and has a current limit of detection (LoD) of 20 uA, as shown in

Fig. 2. We also measured the mixed signal of 50Hz power frequency current and 229Hz characteristic current, in which the weak characteristic signal of 1mA has the same output voltage as that of the power frequency current of 1A. This means the low-frequency resonant ME sensors are a promising candidate for topology identification of power distribution network.

[1] Fan, J., & Borlase, S. IEEE Power and Energy magazine, 7(2), 63-68 (2009). [2] Wang, B., Geng, J., & Dong, X. (2016). IEEE Transactions on Smart Grid, 9(4), 3783-3791 (2016). [3] Lai, X., Cao, M., ... & Sun, C. In 2021 6th Asia Conference on Power and Electrical Engineering (ACPEE) (pp. 1233-1238). IEEE (2021). [4] Liang, X., Chen, H., & Sun, N. X. APL Materials, 9(4), 041114 (2021). [5] Dong, C., Liang, X., ... & Sun, N. X. Advanced Electronic Materials, 8(6), 2200013 (2022).

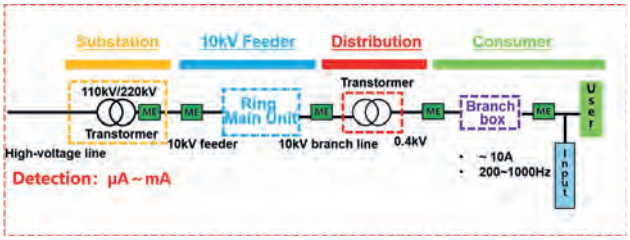

Fig. 1 Topology identification diagram of power distribution network.

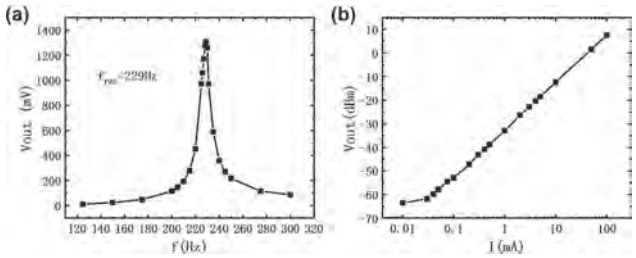

Fig. 2 Freuqncy and amplitude measurement of the ME sensor.

VP6-08. Two-dimensional Synchronous Motion Modulation MEMS Structure with High Modulation Efficiency. *Q. Jiao*[1] and J. Chen[1]
1. State Key Laboratory of Transducer Technology, Aerospace Information Research Institute, Chinese Academy of Sciences, Beijing, China

In recent years, high-resolution magnetic field sensors (within the pT range) have been widely used in the fields of transportation, medical, and aviation[1], Compared with traditional magnetic field sensors, magnetoresistance (MR) sensors have advantages such as small size, low power consumption and good linearity, making them highly competitive in the field of miniaturized high-performance magnetic field sensors. However, the MR sensor is greatly affected by 1/*f* noise interference, and the resolution of the sensor in the low frequency range is significantly lower than that in the high frequency range. Due to the fact that the frequency of the magnetic field that people are interested in is often less than 10 Hz, reducing the interference of 1/*f* noise is currently a scientific challenge that urgently needs to be solved in the application of MR sensors. In the past, some research groups proposed the introduction of MEMS modulation structures to reduce low-frequency 1/*f* noise[2-5], but most devices have low modulation efficiency. In order to improve the modulation efficiency of MR-MEMS sensors and optimize the resolution of MR components in low-frequency magnetic fields, this paper proposes a two-dimensional synchronous motion modulation (TDSMM) method based on comb-driven resonators. The model of a MR sensor based on TDSMM structure is shown in Figure 1. The magnetic flux concentrator deposited above the transverse resonator amplifies the spatial magnetic field. The MR element is located at the end of the longitudinal resonator, and in order to achieve electrical isolation between the MR element and the longitudinal resonator, a layer of SiO_2 is deposited between them. Finite element simulation was conducted on TDSMM model, and the result showed that the modulation efficiency of TDSMM was as high as 127% (the modulated magnetic field is shown in Figure 2), which is currently the highest value among MR-MEMS sensors. In the future, integrating TDSMM MEMS structure with MR components is expected to further improve the detectivity rate of MR components for low-frequency magnetic fields.

[1] J. Lenz and S. Edelstein, *IEEE Sensors Journal*. 6, 3, 2006. [2] A. Guedes *et al*, *IEEE Transactions on Magnetics*. 44, 11 (2008). [3] A. Guedes *et al*, *Journal of Applied Physics*. 103, 07E924 (2008). [4] A. Guedes *et al*, *IEEE Transactions on Magnetic*. 48, 11 (2012). [5] Q. Du *et al*., *IEEE Electron Device Letters*. 40, 11 (2019).

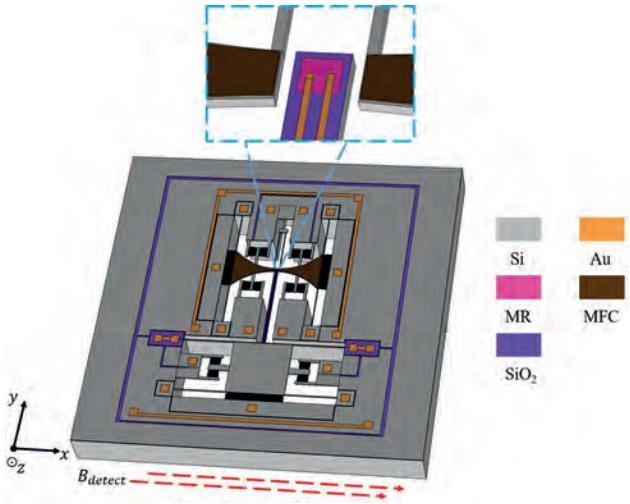

Fig.1. Schematic diagram of MR sensor based on TDSMM MEMS structure

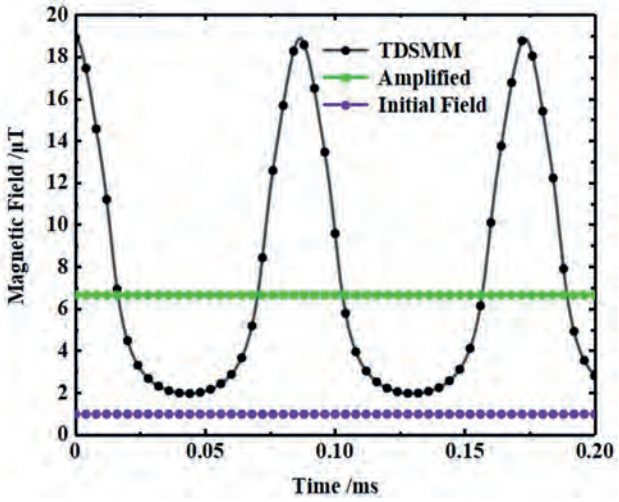

Fig.2. Modulation magnetic field of TDSMM

Session VP7
MAGNETIZATION DYNAMICS AND SWITCHING (VIRTUAL)
(Poster Virtual Session)

Alpha N'Diaye, Chair
Lawrence Berkeley National Laboratory, Berkeley, CA, United States

VP7-01. Size dependence of domain wall mediated switching dynamics of perpendicular magnetic tunnel junctions in the presence of reference layer stray field. *A. Nisar*[1], B. Kaushik[1] and T. Pramanik[1] *1. Electronics & Communication Engineering, Indian Institute of Technology Roorkee, Roorkee, India*

Recent investigations employing time domain measurements and micromagnetic simulations of spin-transfer-torque-induced switching dynamics of perpendicular magnetic tunnel junction (p-MTJ) have explained many experimental observations of switching anomalies [1-3]. Here we report the influence of reference-layer (RL) stray field on the domain wall mediated switching of the free-layer for varying MTJ diameters, studied via finite temperature micromagnetic simulations, utilizing the simulation parameters from [3]. For the larger MTJ diameters (~80–120nm), presence of unoptimized stray field from RL gives rise to persistent back-and-forth oscillation of the domain wall delaying the switching process and causing increased write errors. Such oscillations involve a DW containing a "Bloch line" like configuration [2]. Fig. 1 shows a similar trajectory produced from zero-temperature simulations for better clarity. While such oscillations are suppressed in relatively shorter diameter MTJs (~60–70nm), another interesting mode emerges where a bubble-like feature is observed to evolve during the switching process (Fig. 2). These paths are observed to originate from DWs partly in Bloch and partly in Neel configuration. We note that at the intermediate ranges of device size, the stray field becomes stronger for a given RL configuration [4] and the energy difference between the Neel and Bloch configurations is also lowered. Hence, a stronger stray field presumably distorts the moving domains, leading to complex magnetization behavior. Finally, quasi-uniform switching dominates at much shorter MTJ diameters (~ 30nm). Our findings present further insights into the non-idealities of DW-mediated switching modes in p-MTJ structures.

[1] T. Devolder *et al*., Phys. Rev. B 93, 224432 (2016) [2] P. Bouquin *et al*., Rev. Appl. 15, 024037 (2021) [3] A. Nisar *et al*., Phys. Rev. App. 19 (2), 024016 (2023) [4] T. Devolder *et al*., J. Phys. D: Appl. Phys. 52 274001 (2019)

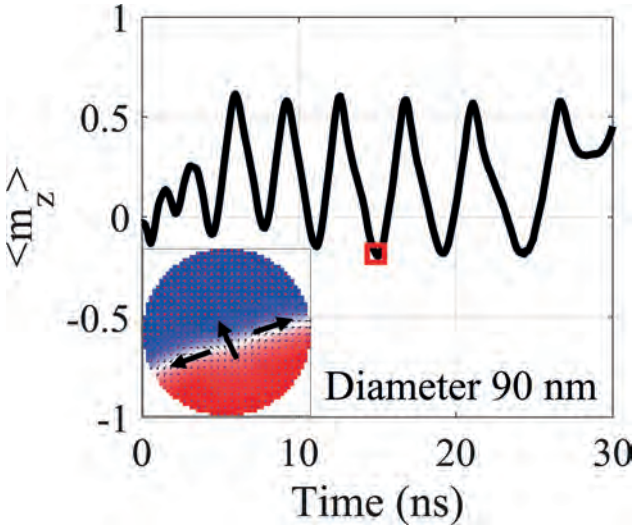

Fig. 1: Typical oscillatory switching trajectory of average out-of-plane magnetization (m_z) vs. time of larger diameter MTJs at 0K. The inset shows the domain wall structure (Blue = -z and Red = +z magnetized state, with black arrows indicating the magnetization direction in the wall).

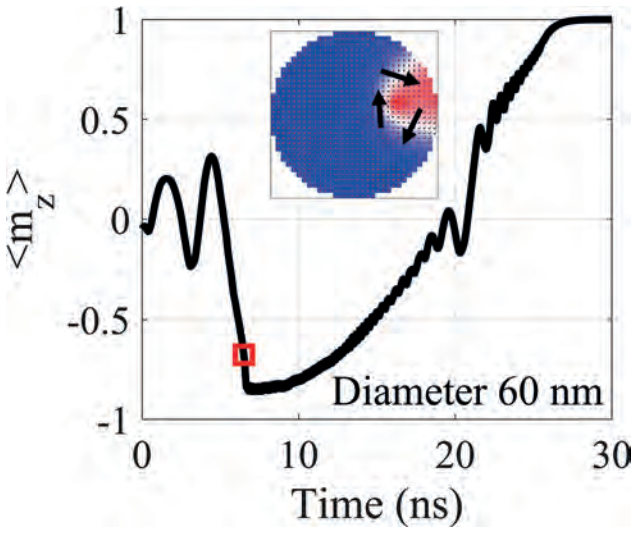

Fig. 2: A switching trajectory of average out-of-plane magnetization (m_z) vs. time of intermediate sized MTJs at 0K showing the formation of a bubble (inset) and its annihilation. The color scale is the same as in Fig. 1.

VP7-02. Dynamic Stress-dependent Magnetostriction Model of Silicon Steel Based on Simplified Multi-scale and Jiles-Atherton Theory.

T. Ben[1], N. An[1], L. Chen[1], X. Zhang[2] and Y. Kong[1] *1. College of Electrical Engineering and New Energy, China Three Gorges University, Yichang, China; 2. State Key Laboratory of Reliability and Intelligence of Electrical Equipment, Hebei University of Technology, Tianjin, China*

Introduction To obtain the vibration property of silicon steel core with clamping applied under an alternating magnetic field, a dynamic stress-dependent magnetostriction model of silicon steel must be constructed. Multiscale modeling can describe the domain behavior of a single crystal with respect to the localized magnetic field and stresses. And one single crystal will be extended for polycrystalline material by using homogenization laws[1]. But it is computationally expensive, and the hysteresis effect is not considered in magnetostriction loops. Based on an improved quadratic domain rotation model[2], this paper proposed a dynamic stress-dependent magnetostriction model combining the simplified multiscale model with JA model. Method and Discussion Based on the simplified multiscale model, the stress-dependent expression of the anhysteretic magnetization M_{an} is coupled with the JA model to simulate the effect of stress on magnetic properties, as shown in Fig.1. The correction factors v and γ_k are introduced to improve the calculation accuracy of the inner symmetrical static hysteresis loops. And the eddy current field and excess loss field are introduced to realize the dynamic expansion of the model. Then, an improved quadratic domain rotation magnetostriction model is constructed by expanding the irreversible magnetization component. And combined with the improved magnetic hysteresis model above, the dynamic stress-dependent magnetostriction model for silicon steel under stress is proposed. The parameters of the model are identified based on the measurement data at the peak magnetic density B_p= 0.1T, 0.4T, 0.7T, 1.0T, 1.3T to find out the variation pattern of parameters with B_p, which will pre-simulate the magnetic properties at other B_p. Finally, based on the proposed model, the magnetostriction loops were simulated under varying stresses and magnetic flux densities, as shown in Fig.2. Conclusion The measured and simulated results show that the magnetostriction strain decreases with the increase of stress when the stress is between 1.2MPa to 2.4MPa.

[1] L. Daniel, The European Physical Journal Applied Physics., Vol. 83, 30904(2018) [2] Y. Li, J. Zhu and L. Zhu, Journal of Magnetism and Magnetic Materials., Vol. 529, 167854 (2021)

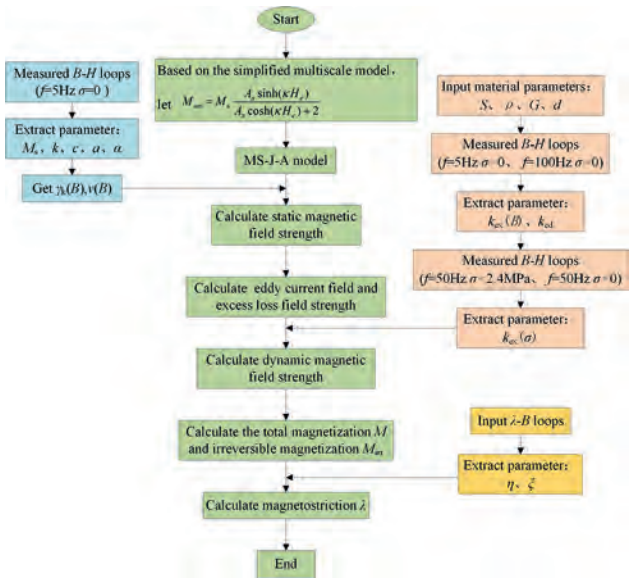

Fig.1 Flow chart of modeling magnetostriction property

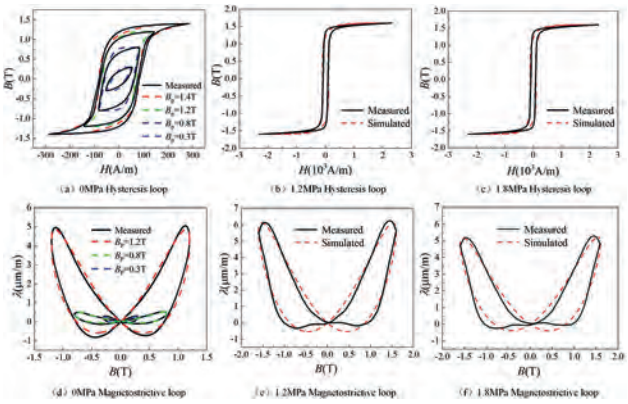

Fig.2 The hysteresis loops and magnetostrictive loops under different magnetic flux densities and stresses

VP7-03. Study on the Loss Characteristics of Nanocrystals at Wideband Frequency Based on Improved Loss Separation Model.

J. Zhou[1,2] and Y. Li[1,2] *1. Hebei University of Technology, Tianjin, China; 2. State Key Laboratory of Reliability and Intelligence of Electrical Equipment, Tianjin, China*

Core loss is an important reason for the increase in the operating temperature of high-frequency transformers, which also directly determines the performance of high-power power electronic equipment [1-2]. So the construction of an accurate and reliable loss model with physical significance is of guiding significance for the design of high-frequency transformers. In several traditional core loss calculation methods, the loss separation model divides the total loss into hysteresis loss, eddy current loss and excess loss, and the physical meaning is relatively clear, but the traditional loss separation model is only suitable for cases that do not consider the skin effect, and the calculation results will have obvious errors as the frequency increases [3]. In this paper, the three types of losses will be analyzed separately, and a more physically meaningful loss model will be constructed by further improving the loss separation formula. By observing the magnetic domain of the quasi-static magnetization process of nanocrystals, as shown in Fig.1. It can be observed that the magnetization process is mainly the magnetization rotation of the magnetic domains, which is manifested as the displacement of the domain wall. A more detailed analysis of magnetic domains is described in full text. In an alternating magnetic field, the magnetic material is repeatedly magnetized, and the power dissipated by the rotational friction of the magnetic domain is the hysteresis loss. Since the traditional loss separation model does not take into account the skin effect, the calculation of eddy current loss can be made more accurate and has more clear physical significance by introducing complex magnetic permeability. In order to obtain the excess loss with more physical significance, six aspects were analyzed, including domain wall bending and non-uniform and non-repetitive domain wall motion etc. Then an excess loss expression is proposed for calculation. Some of the results are shown in Fig.2. A more detailed analysis is described in full text.

[1] Z. Guo, R. Yu, W. Xu, X. Feng, and A. Q. Huang, “Design and optimization of a 200-kW medium-frequency transformer for medium-voltage SiC PV inverters,” IEEE Trans. Power Electron., vol. 36, no. 9, pp. 10548–10560, Sep. 2021. [2] M. Mogorovic and D. Dujic, “100 kW, 10 kHz mediumfrequency transformer design optimization and experimental verification,” IEEE Trans. Power Electron., vol. 34, no. 2, pp. 1696–1708, Feb. 2019. [3] D. Eggers, S. Steentjes, and K. Hameyer, “Advanced iron-loss estimation for nonlinear material behavior,” IEEE Trans. Magn., vol. 48, no. 11, pp. 3021–3024, Nov. 2012.

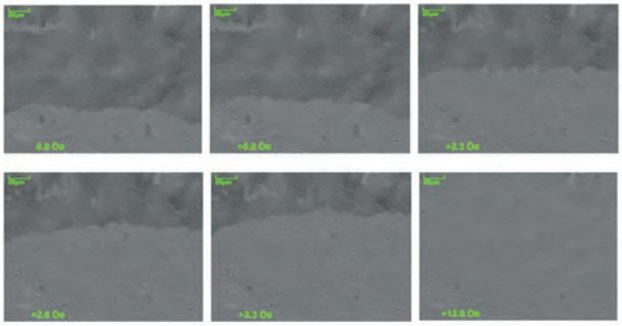

Fig.1 Quasi-static observation of nanocrystals

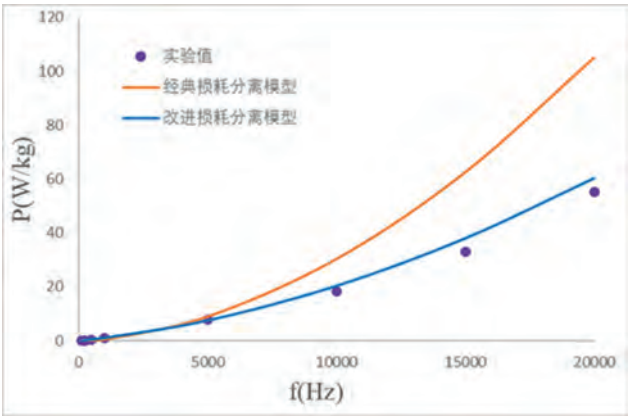

Fig.2 Calculated and measured loss of Nanocrystalline(B_m=0.9T)

VP7-04. Effect of Fe to Ti ratio on the resonant microwave power absorption in $Co_2Fe_{0.5}Ti_{0.5}Si$ (CFTS) quaternary Heusler alloy thin films. *M. Rahaman*[1], L.A. Longchar[1], P. Pardeep[2], G. Basheed[2], M. Muthuvel[3], S. Kaul[1] and S. Srinath[1] *1. School of Physics, University of Hyderabad, Hyderabad, India; 2. CSIR-National Physical Laboratory (NPL), Dr. K. S. Krishnan Marg, India; 3. Advanced Magnetics Group, Defence Metallurgical Research Laboratory, Hyderabad, India*

Cobalt-based Heusler alloys, Co_2YZ, where Y and Z are transition metals and p-block elements, stand out due to their low Gilbert damping constant (α), high T_c, large magnetic moment and half-metallicity with 100% spin polarization [1-7]. 50 nm thin $Co_2Fe_{0.5}Ti_{0.5}Si$ (CFTS) films, with two different Fe to Ti concentration ratios, termed CFTS-1 and CFTS-2, were deposited on Si (100)/ SiO_2 substrate at 500 °C substrate temperature (T_S) by ultrahigh vacuum dc magnetron sputtering. Cobalt-rich Co_2FeSi and Ti targets were connected to DC and RF power supplies for co-sputtering. The GIXRD confirms the fundamental reflections (220), (400) and (422) and the (222) even superlattice reflection validates the presence of B2 order in both films. The composition of the films was found to be $Co_{2.05}Fe_{0.57}Ti_{0.32}Si_{1.06}$ (CFTS-1) and $Co_{1.94}Fe_{0.58}Ti_{0.61}Si_{0.88}$ (CFTS-2). To investigate the magnetization relaxation processes and magnetic anisotropy present in the films, broad-band (4- 40 GHz) FMR at a fixed azimuthal field angle and X-band (9.5 GHz) FMR at different polar field angles, in the 'in-plane' (IP) and 'out-of-plane' (OP) sample configurations, are employed. Resonance fields (H_{res}) and linewidth (ΔH) are extracted from the recorded FMR spectra and plotted against the microwave frequencies (f) (Fig. 1) and the polar field angles (θ_H) (Fig. 2). Based on the elaborate analysis of the FMR data, the following conclusions can be drawn. (I) With increasing Fe to Ti ratio, ΔH increases indicating the inhomogeneity in magnetization and angular spread of crystalline misorientation increase (II) Regardless of composition, both the films show OP uniaxial anisotropy, confirmed from the angular variation of H_{res} (Fig.2). (III) Frequency-dependent H_{res} follows the IP Kittel resonance condition [8] (Fig.1). The CFTS-1 film has maximum M_S = 773 G, the least values for H_k(62 Oe) and α = 0.0089. These optimum values of M_S and α at RT, are conducive for spintronics applications.

[1] H. Atsufumi and T. Koki, J. Phys. D: Appl. Phys. 47(19) 193001 (2014). [2] H.C. Kandpal, G.H. Fecher, C. Felser, J. Phys. D. Appl. Phys. 40 1507 (2007). [3] M. Belmeguenai, H. Tuzcuoglu, M. Gabor, et al., J. Magn. Magn. Mater 373 140–143 (2015). [4] B. K. Hazra, S. N. Kaul, S. Srinath, et al., J. Phys. D: Appl. Phys. 52 325002 (2019). [5] Y. Miura, M. Shirai and K. Nagao, J. Appl. Phys. 99 08J112 (2006). [6] Y. Jin, J. Waybright, P. Kharel, et al., AIP Advances 7 055812 (2017). [7] J. Chen, Y. Sakuraba, K. Masuda, et al., Appl. Phys. Lett. 110 242401 (2017). [8] C. Kittel, Phys. Rev.73 155 (1948).

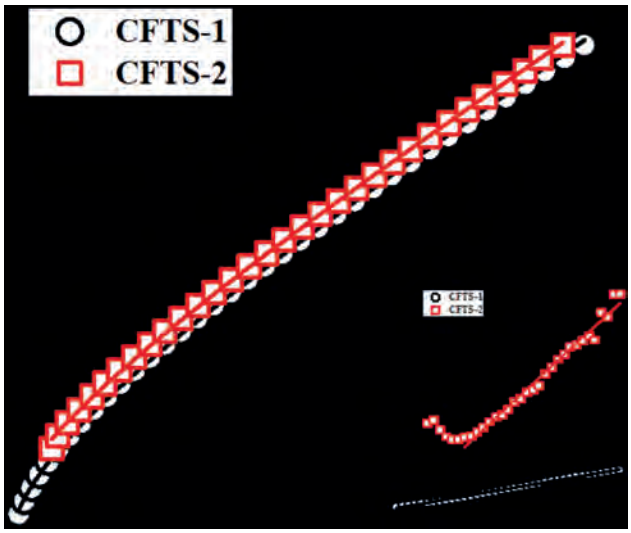

Fig 1. Frequency dependent resonance field, f (H_{res}) in IP configuration. Inset: Linear variation of the ΔH with f in the higher frequency range.

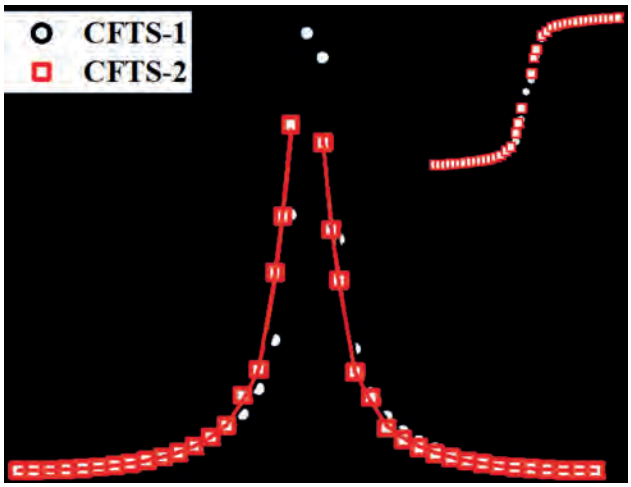

Fig 2. H_{res} (θ_H) data (symbols) and theoretical fit (continuous lines). Inset: θ_M, as a function of θ_H.

VP7-05. Transition States for Thermally Activated Switching of Perpendicular Magnetic Nanopillars in Transverse Fields. C.C. Capriata[1,3], B.G. Malm[1], *G.D. Chaves-O'Flynn*[2] and A.D. Kent[3] *1. Division of Electronics and Embedded Systems, KTH - Royal Institute of Technology, Stockholm, Sweden; 2. Thin Films, Institute of Molecular Physics, Polish Academy of Sciences, Poznan, Poland; 3. Center for Quantum Phenomena, Department of Physics, New York University, New York, NY, United States*

Perpendicular Magnetic Tunnel Junctions (pMTJs) are good candidates in future approaches for stochastic computing since they provide two equally probable states separated by an energy barrier which can be reduced with in-plane fields. Thermally activated swiching between these states can be

used to generate a random stream of bits. Here, we report on numerical and analytical studies of activation barriers for thermally activated switching of the free layer of a pMTJ with circular shape. In a fashion that mimicks previous results of thermal activation transition states [1], we identify two reversal modes for thermal activation that dominate at different points of our parameter state. For small disks, the thermally activated switching occurs via a uniformly magnetized state (Macrospin model) and has been known for a long time [2]. For large disks, the sadlle state is not uniform but a domain wall with a sigmoidal profile that depends on diameter and applied field [Fig 1] (Domain Wall mediated model). We have compared our analytical predictions with numerical studies as follows: the macrospin model is compared with overdamped micromagnetic simulations in OOMMF, the Domain Wall mediated model is compared to results from String Method calculations [3]. For small samples the macrospin model is the preferred reversal mode and the energy barrier values overlap into a single curve after a shape dependent correction is taken into account. For large samples, the Wall Mediated reversal is the preferred transition mode and the analytical model approximates very well results from String Method calculations [Fig. 2].

[1] Martens et al., "Magnetic reversal in nanoscopic ferromagnetic rings", PRB 73, 054413 [2] Garanin et al., "Thermally activated escape rates of uniaxial spin systems with transverse field:Uniaxial crossovers," PRE 60, 6499 (1999). [3] E,etal., "Simplified and improved string method for computing the minimum energy paths in barrier-crossing events" PRB 66, 052301 (2002) This research is supported in part by: National Science Centre Poland under OPUS funding grant No. 2019/33/B/ST5/02013 Polish National Science Center, project no. UMO-2018/30/Q/ST3/00416; the Swedish Research Council (VR), project Fundamental Fluctuations in Spintronics, 2017-04196. The research at NYU was supported by the DOE Office of Science (ASCR /BES) for our Microelectronics Co- Design project COINLFIPS. Any subjective views or opinions that might be expressed in the paper do not necessarily represent the views of the U.S. DOE or the United States Government.

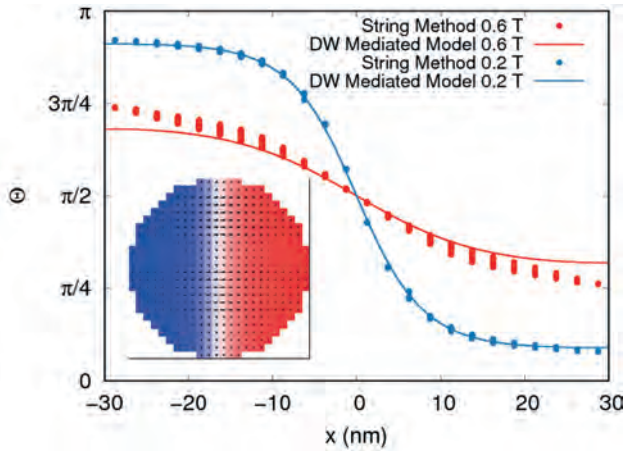

Profiles of the saddle points for two different fields. Points correspond to orientations of the discretization cells in the OOMMF based implementation of the String Method. The continuous line shows the prediction from the analytical model. The inset shows a top view of the magnetization configuration at the saddle point.

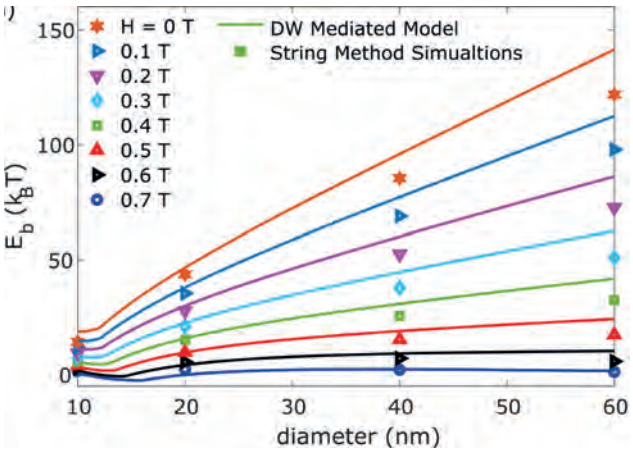

Comparison of energy barriers obtained from String Method calculations (points) to those from analytical predictions (continuous lines) for a variety of fields and sizes. The curves' kinks at small diameters occurs in the transition from macrospin switching to a wall mediated reversal.

VP7-06. Full Quantum Theory for Magnon Transport in Two-sublattice Magnetic Insulators and Magnon Junctions. *T. Zhang*[1] and X. Han[1]
1. Institute of Physics, Chinese Academy of Science, Beijing, China

Magnon, as elementary excitation in magnetic systems, can carry and transfer angular momentum. Due to the absence of Joule heat during magnon transport, researches on magnon transport have gained considerable interests over the past decade. Recently, a full quantum theory has been employed to investigate magnon transport in ferromagnetic insulators (FMIs). However, the most commonly used magnetic insulating material in experiments, yttrium iron garnet (YIG), is a ferrimagnetic insulator (FIMI). Therefore, a full quantum theory for magnon transport in FIMI needs to be established. Here, we propose a Green's function formalism to compute the bulk and interface magnon current in both FIMIs and antiferromagnetic insulators (AFMIs). We investigate the spatial distribution and temperature dependence of magnon current in FIMIs and AFMIs generated by temperature or spin chemical potential step. In AFMIs, magnon currents generated by temperature step in the two sublattices cancel each other out. Subsequently, we numerically simulate the magnon junction effect using the Green's function formalism, and result shows near 100% magnon junction ratio. This study demonstrates the potential for investigating magnon transport in specific magnonic devices using a full quantum theory.

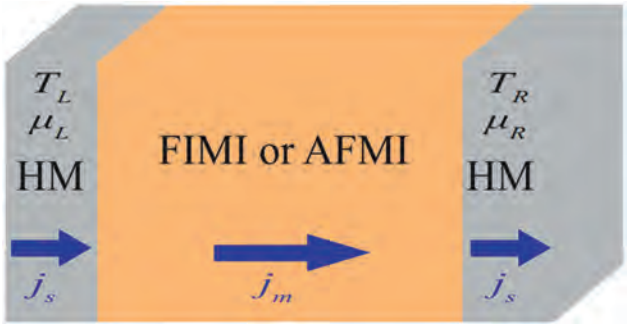

Schematic diagram that illustrates the transport of magnon current through FIMI or AFMI driven by temperature or spin chemical potential difference.

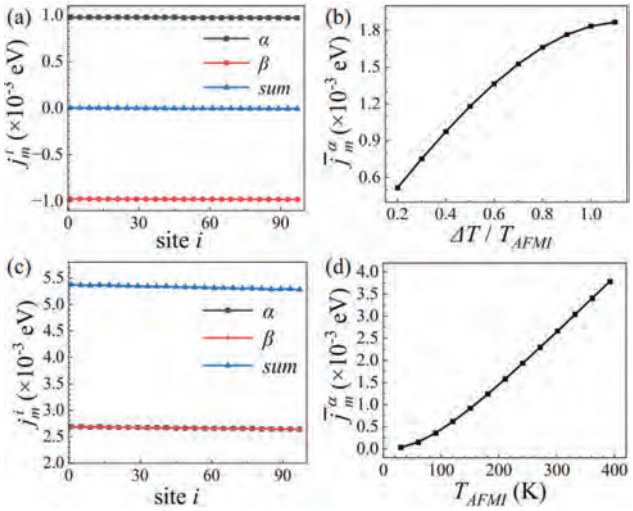

Spatial distribution and temperature dependence of magnon currents generated by SSE (a, b) and SHE (c, d) in AFMI.

VP7-07. Ultrastrong to Nearly Deep Strong Magnon-magnon Coupling in Synthetic Antiferromagnets with Intrinsic Symmetry Breaking.

Y. Wang[1], Y. Zhang[2], J. Wei[1], Z. Yan[1], W. Yang[2], B. He[1], X. Luo[1], W. He[1], H. Xu[1], J. Dong[1], F. Ma[2], P. Yan[3], C. Wan[1], X. Han[1] and G. Yu[1] *1. Institute of Physics, Chinese Academy of Sciences, Beijing, China; 2. School of Physics and Technology, Nanjing Normal University, Nanjing, China; 3. School of Electronic Science and Engineering and State Key Laboratory of Electronic Thin Films and Integrated Devices, University of Electronic Science and Technology of China, Chengdu, China*

Ultrastrong coupling and deep strong coupling are two novel coupling regimes with abundant intriguing physical phenomena. In the past decade, hybrid magnonic systems emerge as candidates for further exploration of these regimes due to their unique advantages in quantum engineering. However, due to the relatively weak coupling between magnons and other quasi-particles in hybrid magnonic systems, the few reports of ultrastrong coupling realization generally require cryogenic temperature, while deep strong coupling has not been realized yet. In our work, we realize room-temperature magnon-magnon ultrastrong coupling in synthetic antiferromagnets with magnetic anisotropic asymmetry. The coupling strength can be continuously tuned to be nearly equal to the bare frequency as high as $g/\omega_0 \sim 0.972$, which is the largest value reported experimentally in hybrid magnonic systems so far, indicating that deep strong coupling regime is almost achieved. Moreover, unlike most ultrastrong coupling systems where the counter-rotating coupling strength g_2 is bound to the co-rotating coupling strength g_1, g_2 in our systems has an extremely high degree of freedom, which can lead to highly adjustable quantum phenomena. Our results indicate that synthetic antiferromagnets are ideal platforms for exploring ultrastrong coupling regime or even deep strong coupling regime.

[1] J. Bourhill, N. Kostylev and M. Goryachev, Phys. Rev. B, Vol. 93, p.144420 (2016) [2] G. Flower, M. Goryachev and J. Bourhill, New J. Phys., Vol. 21, p.095004 (2019) [3] I. A. Golovchanskiy, N. N. Abramov and V. S. Stolyarov, Sci. Adv., Vol. 7, p.eabe8638 (2021) [4] I. A. Golovchanskiy, N. N. Abramov and V. S. Stolyarov, Phys. Rev. Appl., Vol. 16, p.034029 (2021) [5] L. Liensberger, A. Kamra and M. Weiler, Phys. Rev. Lett., Vol. 123, p.117204 (2019) [6] T. Makihara, S. Cao and M. Bamba, Nat. Commun., Vol. 12, p.3115 (2021)

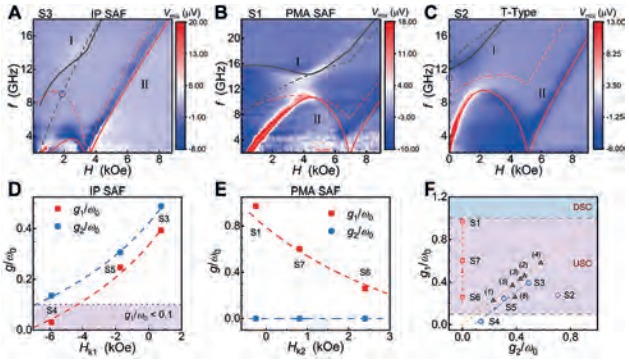

Fig. 1. (A to C) Color plots of the mixing voltages V_{mix} as a function of H and f for the IP SAF sample S3 (A), the PMA SAF sample S1 (B) and the T-Type sample S2 (C). From (A) to (C), the co-rotating normalized coupling strengths g_1/ω_0 are determined to be 0.393, 0.972, 0.278, respectively, while the counter-rotating normalized coupling strengths g_2/ω_0 are determined to be 0.489, 0, 0.706, respectively. (D and E) Extracted g_1/ω_0 (red squares) and g_2/ω_0 (blue dots) of the three IP SAF samples S3, S4 and S5 (D) and the three PMA SAF samples S1, S6 and S7 (E). (F) Comparison of g_1/ω_0 and g_2/ω_0 in our PMA SAF samples (squares), IP SAF samples (circles), T-Type sample (diamond) and other works (triangles). The numbers in parentheses represent reference numbers.

VP7-08. Interlayer Dzyaloshinskii-Moriya Interaction Induced Ultrastrong Magnon-magnon Coupling in Synthetic Antiferromagnets.

Y. Wang[1], J. Xia[1], C. Wan[1], X. Han[1] and G. Yu[1] *1. Institute of Physics, Chinese Academy of Sciences, Beijing, China*

Magnon-magnon hybrid systems have attracted great attention recently due to their potential in quantum engineering. To increase the efficiency of quantum information processing, it is vital to realize strong coupling or even ultrastrong coupling (USC). While the strong coupling has been widely reported in magnon-magnon hybrid systems, the USC is seldom reported. To explore more possible mechanisms to realize the magnon-magnon USC is the focus of current research. Here, we point out that interlayer Dzyaloshinskii-Moriya interaction (DMI) can break the rotation-symmetry in SAFs when the DMI vector D is nonorthogonal to the external dc magnetic field. Therefore, magnon-magnon coupling can be induced by the interlayer DMI, which is verified by both macrospin model and micromagnetic simulations. We point out that the strength of magnon-magnon coupling can be greatly tuned by tuning prameters. More interestingly, in the region where the total magnetic anisotropy field approaches zero, a sudden sharp increase in the coupling strength occurs. We point out that in this region, the coupling properties are very sensitive to anisotropy, and even an extremely small interlayer DMI intensity can induce USC. The maximum normalized coupling strength is also realized in this region, which is over 0.5, much larger than the 0.1 required by the USC, indicating the system is deep into the USC regime. Our study indicates that SAFs with interlayer DMI are great platforms to study magnon-magnon USC, which contributes to this emerging area.

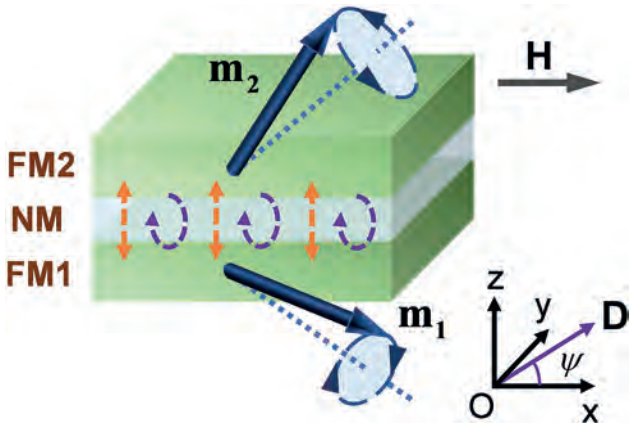

Fig. 1. Schematic of resonance in a SAF structure with interlayer DMI.

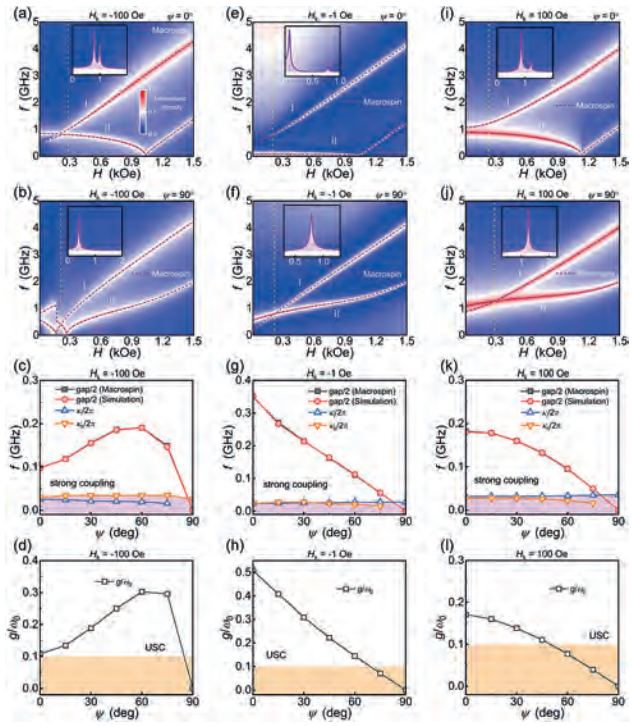

Fig. 2. (a) to (d) Calculated and simulated coupling properties of the case where H_k = -100 Oe, H_{ex} = -0.5 kOe, and H_D = 0.2 kOe. Similarly, (e) to (h) show the coupling properties of the case where H_k = -1 Oe, H_{ex} = -0.5 kOe, and H_D = 0.2 kOe, and (i) to (l) show the coupling properties of the case where H_k = 100 Oe, H_{ex} = -0.5 kOe, and H_D = 0.2 kOe.

VP7-09. Efficient spin–orbit torque magnetization switching with the two-pulse scheme. T. Jin[1], *F. Tan*[1], S. Li[1] and W. Lew[1] *1. Nanyang Technological University, Singapore, Singapore*

Spin-orbit torque (SOT) induced magnetization switching occurs via either coherent switching or domain nucleation followed by domain wall (DW) propagation. This study reveals that the energy required in domain nucleation is up to five times higher than DW propagation to achieve magnetization switching. Hence, the minimization of the domain nucleation energy is critical to the optimization of energy efficiency. To capitalize on the energy difference between domain nucleation and DW propagation, we propose a two-pulse scheme that utilizes a brief high-power pulse to initiate domain nucleation followed by a longer low-power pulse for DW propagation. The two-pulse scheme can achieve energy savings of up to 72 % compared to using a single-pulse scheme. In the two pulse schemes, we conducted further investigations on the effects of various parameters on magnetization switching, including nucleation pulse width τ_{nu}, propagation pulse width $\tau_{p,}$ and the interval $\Delta\tau$ between two pulses. Figure 1(a) provides the illustration of τ_{nu} on switching. To ensure complete switching, τ_p was set to an excessive value of 2 ns. Figure 1(b) demonstrates a clear minimum value of τ_{nu} required for achieving full switching, as well as a rapid decrease and saturation of switching time with increasing τ_{nu}. The influence of τ_p on switching is illustrated in Fig. 1(c). Here, we observe a straightforward relationship where the minimum value of τ_p required for achieving full switching is considered optimal. Figure 1(d) showcases the increasing degree of switching with increasing τ_p. When τ_p is insufficient, an oscillatory behavior in perpendicular magnetization is observed, which corresponds to the back hopping of the DW. Figure 1(e) provides an illustration of the influence of $\Delta\tau$ on switching. We observe a maximum threshold value of $\Delta\tau$ = 0.10 ns, above which full switching cannot be achieved. Additionally, we observe a decrease in switching time below this threshold, as depicted in Fig. 1(f).

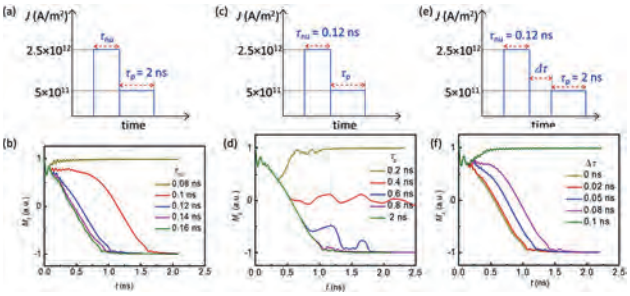

Fig. 1. Schematic of two-pulse current with various (a) τ_{nu}, (c) τ_p and (e) $\Delta\tau$. (b), (d) and (f) magnetization evolution with simulation time *t*.

Session VP8
MAGNETOELECTRIC MATERIALS (VIRTUAL)
(Poster Virtual Session)

Julius de Rojas, Chair
Oklahoma State University, Stillwater, OK, United States

VP8-01. Realistic Spin Model for Multiferroic NiI_2: Importance of Kitaev Interaction. X. Li[1], *C. Xu*[1], B. Liu[1], X. Li[1], L. Bellaiche[2] and H. Xiang[1] *1. Fudan University, Shanghai, China; 2. University of Arkansas at Fayetteville, Fayetteville, AR, United States*

A realistic first-principle-based spin Hamiltonian is constructed for the type-II multiferroic NiI_2, using a symmetry-adapted cluster expansion method. Besides single ion anisotropy and isotropic Heisenberg terms, this model further includes the Kitaev interaction and a biquadratic term, and can well reproduce striking features of the experimental helical ground state, that are, e.g., a proper screw state, canting of rotation plane, propagation direction and period. Using this model to build a phase diagram, it is demonstrated that, (i) the in-plane propagation direction of <1-10> is determined by the Kitaev interaction, instead of the long-believed exchange frustrations; and (ii) the canting of rotation plane is also dominantly determined by Kitaev interaction, rather than interlayer couplings. Furthermore, additional Monte Carlo simulations reveal three equivalent domains and different topological defects. Since the ferroelectricity is induced by spins in type-II multiferroics, our work also implies that Kitaev interaction is closely related to the multiferroicity of NiI_2.

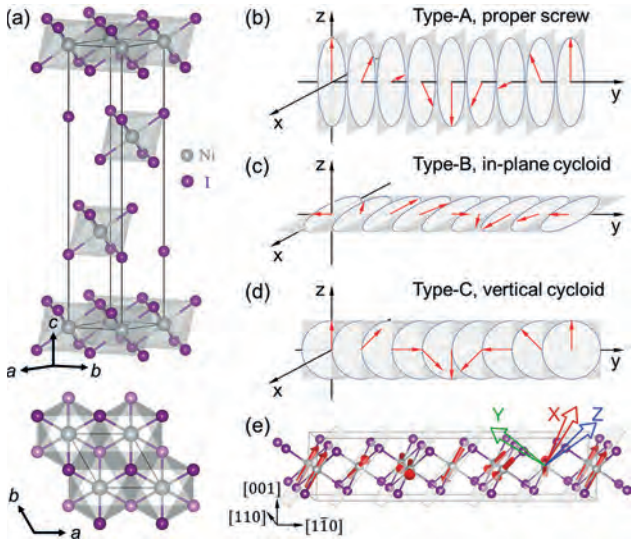

Schematics of (a) NiI_2 crystal structure and common helical spin structures, (b) proper screw, (c) in-plane cycloid and (d) vertical cycloid. Panel (e) displays the $PS^{1\text{-}10}_{cant}$ state of NiI_2, where spins rotate in a canted plane that is spanned by the Ni_2I_2 clusters. The hollow red, green and blue arrows denote the Kitaev basis {XYZ}.

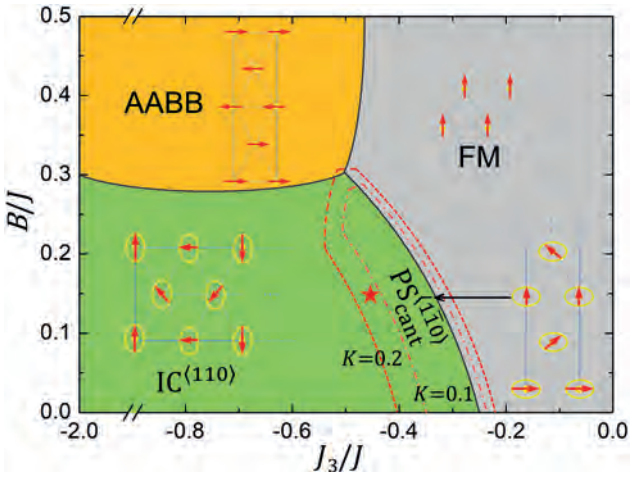

Phase diagram for the studied triangular lattice. J=-1 meV is fixed in these calculations, J_3 and B can vary in magnitude but not in sign. The red dashed (respectively, dot-dashed) line indicates that the ground state becomes $PS^{1\text{-}10}_{cant}$ state when K/J=-0.2 (respectively, K/J=-0.1). The red star denotes the model-predicted position in this phase diagram for NiI_2.

VP8-02. Multilevel Magnetic Synapses Based on Voltage-Controlled Ion Migration for Neuromorphic Application. *M. Peda*[1], Z. Ma[1], E. Pellicer[1], E. Menéndez[1] and J. Sort[1,2] *1. Universitat Autònoma de Barcelona, Barcelona, Spain; 2. Institució Catalana de Recerca i Estudis Avançats (ICREA), Barcelona, Spain*

Synaptic devices with synchronized memory and processor are considered the core elements of Neuromorphic computing (NC) for low-power artificial intelligence (AI). So far, most synaptic devices are based on resistive memories, where the device resistance is tuned with applied voltage or current. However, the use of electric current in such resistive devices causes significant power dissipation by Joule heating. Higher energy efficiency has been reported in materials exhibiting voltage control of magnetism (VCM).[1] In particular, voltage-driven ion motion to modulate magnetism (magneto-ionics) is an emerging VCM mechanism that could offer new prospects for low-power implementation of NC.[2,3] In the present work, we exploit the voltage-controlled motion of different ions (such as N^{3-} and O^{2-}) in transition metal nitrides and oxides (i.e., magneto-ionics) to emulate biological synapses, where synaptic weight (presented by sample magnetization) is tuned with pulsed voltage application. In the proposed devices, by carrying out room-temperature magnetometry measurements while electrolyte gating the nitride and oxide thin films, we have realized multilevel non-volatile and reversible magnetic states for analogue computing and high-density storage (see Fig. 1). Moreover, representative synaptic functionalities illustrating both short and long-term plasticity have been successfully emulated. Furthermore, the devices exhibit high dynamic range, excellent retention and remarkable endurance for real-life hardware implementation of NC. This research provides insight into the great potential of magneto-ionics-based synaptic devices for spin-based neuromorphic computing.

[1] M. Nichterwitz, S. Honnali and K. Leistner, *APL Mater.,* 9, 030903 (2021). [2] S. Martins, J. De Rojas and J. Sort, *Nanoscale,* 14, 842 (2022). [3] R. Mishra, D. Kumar, H. Yang, *Phys. Rev. Appl.,* 11, 054065 (2019).

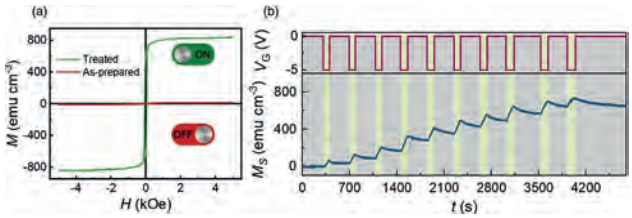

Fig.1 (a) The room-temperature M-H hysteresis loop of the CoFeN thin film showing a paramagnetic (OFF) to ferromagnetic (ON) switching with voltage treatment of –12 V for 20 min. (b) Multilevel non-volatile magnetic states were obtained by applying ten consecutive gate voltage pulses (V_G = –5 V, t_P = 90 s) spaced apart by 300 s.

VP8-03. Withdrawn

VP8-04. Giant Magnetoimpedance effect and Spin Accumulation in Conjugated Polymeric Networks with Inhomogeneity. *S. Singh*[1,2], M. Rampur[1], A. Chetty[1] and R. Joshi[1] *1. Physics, Central University of Karnataka, Kalaburagi, India; 2. Physics, Parishkar College of Global Excellence, Autonomous, Jaipur, India*

INTRODUCTION Magnetocapacitance (MC) is the property of any dielectric or heterostructure that shows change in the value of capacitance when magnetic field is applied externally. It can be an intrinsic property of the solid or extrinsic as well due to interface effects [1]. The intrinsic MC effect is found in multiferroic compounds and composites with the magnetoelectric coupling [2] and extrinsic effect relates to the contribution of magnetoresistance (MR) effect, spin accumulation at the interface [3],[4]. In the present work, we study effect of inhomogeneity on spin accumulation reflected using MC in the conjugated polymers. The conjugated polymers are expected to have rich electron path networks formed out of coiling or reticulation. These are electrically inhomogeneous and form scattering sites. For this study we choosed PANI, which is one of the important electronic materials. ABSTRACT The magnetoimpedance effect allows us to estimate the extent of spin dependent scattering in disordered solids. The change in impedance with respect to applied magnetic field manifests through local change in permeability on the surface and it amplifies at defect sites. The local electrical inhomogeneities are expected to aid this effect through spin dependent scattering. The conjugated electrical networks provide a significant scope for producing spin dependent scattering mediated by path defects and protonic charge accumulations. This hypothesis is investigated in the present work taking polyaniline as a prototype network. The electrical inhomogeneities in the network were controlled by selective oxidation and aging in polyaniline. The Giant Magnetoimpedance (GMI) was observed in these networks with the change of the order of 50-60% for lower frequencies with prominent capacitive coupling and colossal change of the order of 200% at higher frequencies with prominent inductive coupling. However, the no spin accumulation was observed in the insulating network units. This study is expected to a serve as a tool to develop frequency selective spin accumulation based magnetic field sensors and oscillator networks.

[1]. T Kimura, S Kawamoto, I Yamada, M Azuma, M Takano, and Y Tokura. Magnetocapacitance effect in multiferroic $BiMnO_3$. Physical Review B, 67(18):180401, 2003. [2] Donald A Neamen. Semiconductor physics and devices: basic principles. McGraw-Hill, New York, N.Y, 2012. [3] G Catalan. Magnetocapacitance without magnetoelectric coupling. Applied Physics Letters, 88(10):102902, 2006. [4] Yao-Hui Zhu, Xiao-Xue Zhang, Jian Liu, and Pei-Song He. Spin-accumulation capacitance and its application to magnetoimpedance. Journal of Applied Physics, 122(4): 043902, 2017.

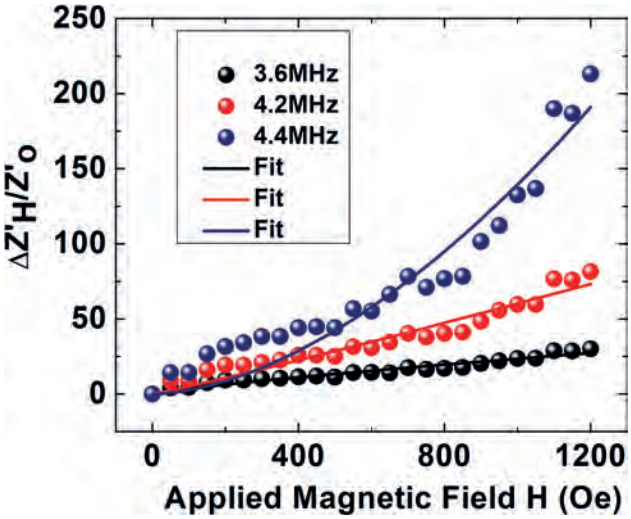

Change in the Impedance with respect to applied magnetic field.

Session VP9
MAGNETORESISTANCE AND ASSOCIATED EFFECTS (VIRTUAL)
(Poster Virtual Session)

Shunsuke Fukami, Chair
Tohoku University, Sendai, Japan

VP9-01. Revisiting the anisotropic magnetoresistance of reactively sputtered magnetite epitaxial films. *X. Liu*[1] and W. Mi[2] *1. College of Science, Civil Aviation University of China, Tianjin, China; 2. Department of Applied Physics, Tianjin University, Tianjin, China*

Anisotropic magnetoresistance (AMR) was considered as the result of anisotropic scattering of *s-d* electrons. Recent investigations reveal the dependence of AMR on the different electronic structures tuned by magnetization directions in epitaxial Co_xFe_{1-x} and $L1_0$-FePt alloys [1,2]. Fe_3O_4 is a typical strongly correlated material showing Verwey transition at ~120 K (T_V). Our previous investigations have determined the symmetry of AMR in epitaxial Fe_3O_4 films at different temperatures and magnetic fields (Fig. 1). Below T_V, the evolution of AMR symmetry depends on the distribution of trimeron, which exhibits uniaxial magnetic anisotropy. The dependence of trimeron and AMR may result from the changes of electronic structures as well. Further investigations focusing on the electronic structure may not only give the intrinsic mechanism of AMR in Fe_3O_4, but also extend the mechanism of AMR to strongly correlated electronic systems. This work was supported by Scientific Research Project of Tianjin Education Commission (2022KJ068) and Fundamental Research Funds for the Central Universities (3122021071).

[1] F. L. Zeng, Z. Y. Ren, Y. Li, et al., Intrinsic mechanism for anisotropic magnetoresistance and experimental confirmation in Co_xFe_{1-x} single-crystal films. Phys. Rev. Lett. 125, 097201 (2020). [2] Y. Dai, Y. W. Zhao, L. Ma, et al., Fourfold anisotropic magnetoresistance of $L1_0$ FePt due to relaxation time anisotropy. Phys. Rev. Lett. 128, 247202 (2022).

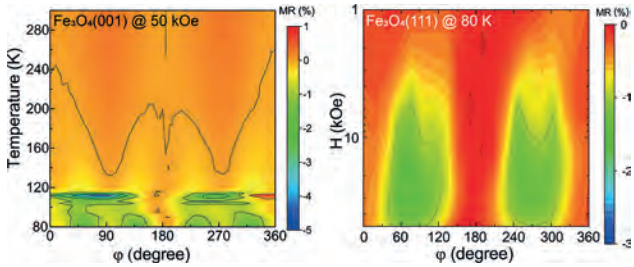

Fig. 1. The AMR in Fe_3O_4(001) and (111) films.

VP9-02. Spin Hall magnetoresistance in antiferromagnetic LSMO/Pt heterostructures. *R. Li*[1] and C. Jin[1] *1. Tianjin Key Laboratory of Low Dimensional Materials Physics and Processing Technology, School of Science, Tianjin University, Tianjin, China*

Antiferromagnetic materials are expected to replace ferromagnets for the future spintronic applications due to the advantages such as zero stray field, large magnetotransport effects and ultrafast dynamics. However, detecting the antiferromagnetic order usually requires synchrotron radiation, neutron diffraction and other large equipment, making the research inconvenient. Therefore, magnetotransport measurements have been developed as effective probes for detecting the antiferromagnetic order, such as anisotropic magnetoresistance (AMR) [1] and spin Hall magnetoresistance (SMR) [2]. $La_{0.35}Sr_{0.65}MnO_3$ (LSMO) is at the phase boundary with an antiferromagnetic ground state. Changes in temperature and strain make it exhibits abundant magnetic phase transitions and orbital occupancy states. Herein, the AMR of LSMO and the SMR of Pt/LSMO bilayers on (001) $SrTiO_3$ (STO) have been investigated systematically. Fig. 1(a) shows the AMR of LSMO (20 nm)/STO and Fig. 1(b) shows the SMR of Pt/LSMO (20 nm)/STO at 50 K, in which both the magnetic field (H=5 T) rotates in the film plane. There is a 90° phase shift between the AMR and SMR, indicating the presence of interface effect. The positive SMR indicates that the ferromagnetic state dominates at the interface of Pt/LSMO. Our results provide an idea for studying the magnetic phase transition and spin order of antiferromagnetic manganites. This work was supported by the National Natural Science Foundation of China (11774254).

[1] X. Marti, I. Fina, C. Frontera, J. Liu, P. Wadley, Q. He, R. J. Paull, J. D. Clarkson, J. Kudrnovsky, I. Turek, J. Kuneš, D. Yi, J-H. Chu, C. T. Nelson, L. You, E. Arenholz, S. Salahuddin, J. Fontcuberta, T. Jungwirth and R. Ramesh. Room-temperature antiferromagnetic memory resistor, Nat. Mater. 13, 367 (2014). [2] Y. Ji, J. Miao, Y. M. Zhu, K. K Meng, X. G. Xu, J. K. Chen, Y. Wu, and Y. Jiang. Negative spin Hall magnetoresistance in antiferromagnetic Cr_2O_3/Ta bilayer at low temperature region, Appl. Phys. Lett, 112, 232404 (2018).

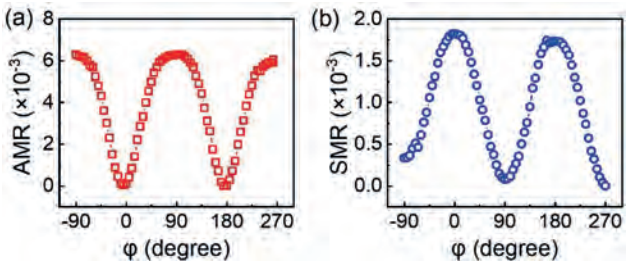

Fig. 1. (a) The AMR of LSMO/STO and (b) The SMR of Pt/LSMO/STO at 50 K under 5 T magnetic field rotating in the film plane.

VP9-03. Optimization of the 3D Multi-level SOT-MRAMs. *H. Lin*[1] and Y. Jiang[1] *1. Jiangnan University, Wuxi, China*

With the development of electronic technology, semiconductor memory is gradually shifting towards smaller area and power consumption. Spin orbit torque magnetic random-access memory (SOT-MRAM) is one of the competitive substitutes for DRAM and SRAM due to its superior endurance and switching speed[1][2]. In contrast to spin-transfer torque magnetic random-access memory (STT-MRAM), the separation of read and write routes allows SOT-MRAM with lower error rate. However, it density is still too high to be accepted. In recent years, vertical integrated circuits have relied on TSV to complete 3D stacking to ease the pressure of Moore's Law on scaling circuits[3]. SOT-MRAM can take advantage of 3D stacking to reduce power and latency and more importantly to compensate for the loss of density. The implementation of multi-level cells (MLC) can also be effective in increasing integration density and reducing cost per bit, a technology that is applicable to other types of memory such as FLASH[4]. As a simulator, DESTINY includes TSV model to NVSIM to evaluate the performance of MRAM 3D structures[5]. However, the structure in DESTINY is simpler, using a bus layer and interconnect structure between layers, and does not add MLC SOT-MRAM. 3D structures require more complex interconnect structures to truly meet the high density requirements, especially for

multi-level SOT-MRAMs. For this reason, a 3D model of unit interconnection using TSV is presented in the paper. Compared to the conventional 2D SOT-MRAM, the area of this structure is reduced by 15%. In addition, the read energy is reduced by 23% because of the structural adjustment. Memory has several components, of which the memory array is the one with the largest area share. This paper explores the spatial structure of the array and proposes a new model which allows more complex interconnect structures to be accomplished on the same area. This corresponds to no change in area, but an increase in the number of interconnected basic units. Since the number of TSVs has been increased, a TSV model is proposed that applies to this structure. Figure 1 shows a schematic representation of this structure. Figure 2 shows the TSV model adapted to this 3D model.

[1] K. Garello, F. Yasin, and G. S. Kar, 2019 IEEE 11th International Memory Workshop (IMW), p.1-4(2019). [2] M. Baumgartner, K. Garello, J. Mendil, Nature Nanotechnology, Vol.12, p.980-986(2017). [3] W. R. Davis, J. Wilson, S. Mick, IEEE Design & Test of Computers, Vol.22, p.498-510(2005). [4] Y. Jang and J. Park, IEEE Transactions on Circuits and Systems II: Express Briefs, Vol.69, p.1622-1626(2022). [5] M. Poremba, S. Mittal, D. Li, 2015 Design, Automation & Test in Europe Conference & Exhibition (DATE), p.1543-1546(2015).

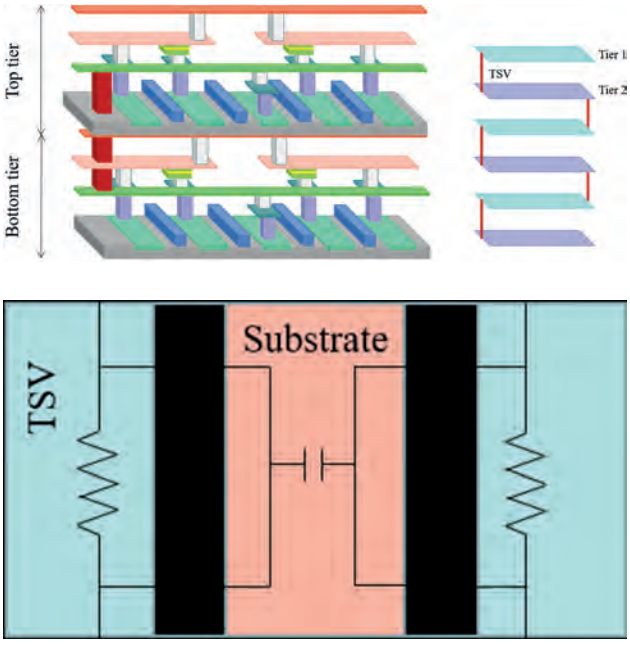

VP9-04. Photo Voltaic effect on Metal/Insulator/Semiconductor (MIS) based Magnetic Tunnel Junction-Based Molecular Spintronics Devices (MTJMSD). P. Tyagi[1] and *P. Suh*[1] *1. Mechanical Engineering, University of The District of Columbia, Washington, DC, United States*

The photovoltaic effect, which involves the generation of electric current or voltage when a solar cell system is exposed to light of a suitable wavelength, holds promise for the advancement of photovoltaic systems utilizing common materials like Nickel Iron (NiFe), Aluminum Oxide (AlOx), and Silicon (Si). This study focuses on investigating the photovoltaic effect in a Magnetic Tunnel Junction Molecular Spintronics Device (MTJMSD). The incorporation of Metal/Insulator/Semiconductor (MIS); NiFe/AlOx/Si structure, within the Magnetic Tunnel Junction (MTJ) enables the exploration of the interplay between photovoltaic effects and spintronics, facilitated by a molecule bridging the two electrodes. The presence of the molecule leads to increased exchange coupling and a heightened photovoltaic effect [1]. The primary emphasis of this paper lies in understanding the photovoltaic effect. By comparing experiments with and without the attached molecule, it is observed that the photovoltaic effect occurs specifically when the molecule is present on the device. The experiments were conducted under various lighting conditions (white light, and in darkness) and utilizing a solar simulator to modulate light intensity. The photovoltaic effect exhibited a significant enhancement under lighting conditions compared to darkness, with a more pronounced increase as the light intensity from the solar simulator was amplified. To comprehend the underlying mechanisms responsible for the observed photovoltaic effect, it is important to delve into the principles of photovoltaic energy conversion. When photons, which are discrete packets of electromagnetic radiation, interact with the photovoltaic cell, they transfer energy to the electrons in the semiconductor layer [2]. This energy absorption propels the electrons to higher energy states, generating electron-hole pairs and facilitating the movement of charge carriers. This paper establishes a foundation for further investigations into the photovoltaic effect, exploring diverse combinations of MTJs and magnetic molecules. These explorations hold the potential for the large-scale production of affordable spin photovoltaic devices.

[1] Lu, L., Zheng, X., & Yan, W. (2015). Low-cost high-efficiency inorganic nanostructures for solar photovoltaics. Journal of Materials Chemistry A, 3(36), 18653-18686. [2] Green, M. A., Emery, K., Hishikawa, Y., Warta, W., & Dunlop, E. D. (2019). Solar cell efficiency tables (version 53). Progress in Photovoltaics: Research and Applications, 27(7), 565-575 [3] Wolf, S. A., Awschalom, D. D., Buhrman, R. A., Daughton, J. M., von Molnár, S., Roukes, M. L., ... & Treger, D. M. (2001). Spintronics: A spin [4] Tsymbal, E. Y., & Gruverman, A. (Eds.). (2012). Tunneling phenomena in solids: Spintronics. CRC Press.

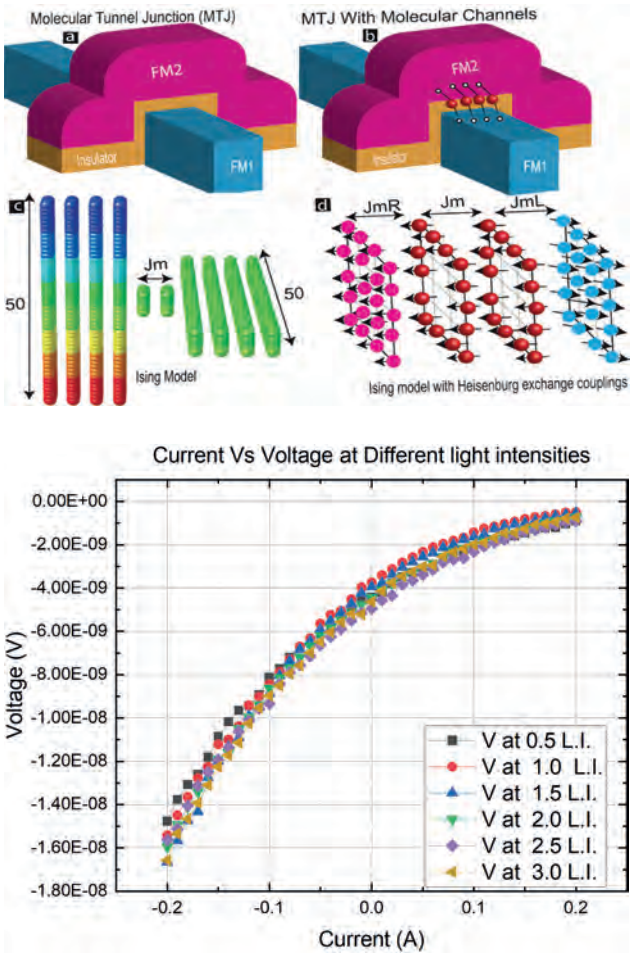

VP9-05. A novel non-destructive self-reference reading scheme for MTJ storage unit. *X. Jia*[1] and Y. Jiang[1] *1. Jiangnan University, Wuxi, China*

Spin transfer torque magnetic random access memory (STT-MRAM) has been extensively investigated with its merits of nonvolatility, high density, and good dependability versus other traditional memory. However, the continuous shrinkage of the feature size in modern circuits and systems leads

to worse bit-to-bit process variation. In addition, Spin orbit torque magnetic random access memory (SOT-MRAM) has also received a lot of attention, has many similarities with STT-MRAM, and is faster to read out. Whether it is STT-MRAM or SOT-MRAM, both are composed of similar devices. In a single memory cell, the data is stored in magnetic tunneling junction (MTJ) as a resistive state (low resistance state RL or high resistance state RH). The parameters of the device can inevitably fluctuate with the fabrication process. The traditional data reading scheme is generally obtained by comparing the storage and reference units. However, as the process size continues to shrink, the MTJ process fluctuation will become larger, resulting in the yield of the memory array is still low even when the external detection circuit is completely ideal. The design of data-cell-variation-tolerant (DCVT) can achieve high yield. The self-reference nondestructive scheme is a kind of DCVT, which uses the nonlinear characteristics of MTJ in the high resistance state to identify the stored data. The NSRS scheme is the beginning, but it is difficult to achieve a high yield under the current process, and the main research direction of the self-reference scheme is to improve the sensing margin as much as possible without increasing too much power consumption. VDRS, as well as time-domain reading schemes, are attempts at such breakthroughs, but they add too much power consumption and circuit complexity. This paper presents a multi-sensing reading scheme with a new type of voltage adder. It belongs to the category of self-reference non-destructive reading schemes. Compared with other schemes, it has more ideal and comprehensive performance in power consumption, sensing margin, and circuit complexity.

[1] T. Na, S. H. Kang, and S. O. Jung, "STT-MRAM" sensing: A review," Circuits and Systems II: Express Briefs, IEEE Transactions on, vol. PP, no. 99, pp. 1–1, 2020. [2] L. Jing, H. Liu, S. Salahuddin, and K. Roy, "Variation-tolerant spintorque transfer (stt) mram array for yield enhancement," in Custom Integrated Circuits Conference, 2008 [3] Y. Jang et al., "Stochastic SOT device based SNN architecture for onchip unsupervised STDP learning," IEEE Trans. Comput., early access, Oct. 14, 2021 [4] S. Motaman, S. Ghosh, and J. P. Kulkarni, "A novel slope detection technique for robust sttram sensing," in IEEE/ACM International Symposium on Low Power Electronics & Design, 2015.

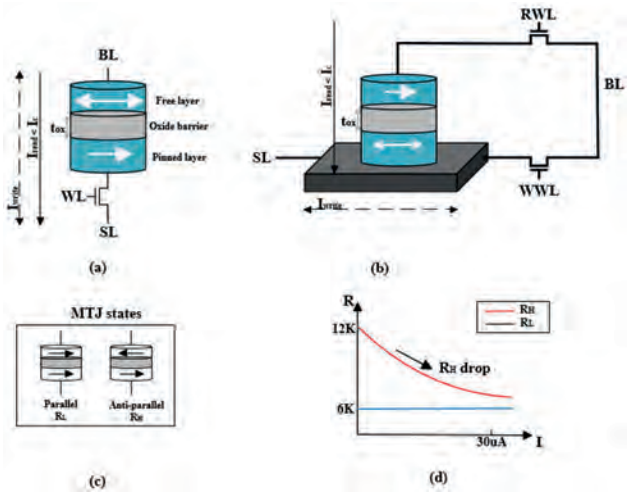

(a) Schematic diagram of STT-MRAM storage unit (b) Schematic diagram of SOT-MRAM storage unit (c) Two states of MTJ (d) The nonlinearity of RH

VP9-06. Improving the Performance of the Magnetic Tunnel Junction by Optimizing the CoFeB/MgO/CoFeB Stack. *C. Ghemes*[1], M. Tibu[1], O. Dragos-Pinzaru[1], N. Lupu[1] and H. Chiriac[1] *1. National Institute of Research and Development for Technical Physics, Iasi, Romania*

In this work, we focused on improving the magnetoresistance ratio (MR) in the magnetic tunnel junction (MTJ) structure by investigating the influence of the deposition rate, the thickness of the junction layer, i.e., MgO, and the thickness of the ferromagnetic layers in the CoFeB/MgO/CoFeB stack. Among magnetoresistive devices, MTJ structures exhibit higher magnetoresistance at room temperature [1], making them good candidates for a wide range of applications [2,3]. High performance sensors based on the tunnel magnetoresistance (TMR) effect must have defect-free and smooth junction - the biggest challenge in the fabrication process. Except for the MgO layer obtained by electron beam evaporation, all the other component layers of the MTJ structure were deposited by magnetron sputtering on Si/SiO_2 wafers as follows: Ta(5 nm)/Ru(20 nm)/Ta(5 nm)/CoFe(2.5 nm)/IrMn(20 nm)/CoFe(2.5 nm)/Ru(0.85 nm)/CoFeB(y nm)/MgO(x nm)/CoFeB(y nm)/Ta (10 nm), where the thicknesses of MgO and CoFeB were varied (x=1, 1.5, 1.8, 2 and y=1.5, 2, 3, 3.5 nm). Transmission electron microscope (TEM) analysis and atomic force microscope (AFM) measurements of the MgO surface deposited at different rates (0.1, 0.2, and 0.3 Å/s) and different thicknesses, showed that the 1.5 nm MgO deposited at a rate of 0.1 Å/s was smoother and had fewer defects as compared to those deposited in other conditions. Of particular importance for the MTJ structure is the thickness of the ferromagnetic CoFeB layers. For different CoFeB thicknesses, the magnetoresistance curves were obtained by measuring the electrical resistance of the samples as a function of the applied magnetic field. A significant difference was found between the MR ratio of the MTJ structure with a CoFeB layer thickness of 3 nm (MR=44%) and the other thicknesses: 10% at 1.5 nm, 15% at 2 nm, and 32% at 3.5 nm. This proves that the optimization of the deposition conditions and the thickness of the thin films in the CoFeB/MgO/CoFeB stack improve the MR ratio of the MTJ structure. Acknowledgements This work was supported by a grant of the Ministry of Research, Innovation and Digitization, CCCDI - UEFISCDI, project number PN-III-P2-2.1-PED-2021-2739, within PNCDI III.

[1] Y. Nagamine, H. Maehara and K. Tsunekawa, Appl. Phys. Lett. Vol. 89, p.162507 (2006) [2] N. Maciel, E. Marques and L. Naviner, Sensors, Vol. 20(1), p.121 (2020) [3] Z. Q. Lei, L. Li, G. J. Li and C. W. Leung, J. Appl. Phys. Vol. 111, p.07E505 (2012)

VP9-08. Study on the Performance of MTJ Array with Shielding Layer. *J. Xiong*[1,2], F. Jin[1,2], L. Liu[1,2], K. Dong[1,2], J. Song[1,2] and W. Mo[1,2] *1. School of Automation, China University of Geosciences, Wuhan, China; 2. Hubei key Laboratory of Advanced Control and Intelligent Automation for Complex Systems, Wuhan, China*

In STT-MRAM, data is stored in a magnetic tunnel structure (MTJ) containing multiple ferromagnetic layers. Each ferromagnetic layer generates a stray field, which affects the critical overturning current, overturning time, thermal stability and the density of the MTJ cell array directly affects the performance and storage capacity of STT-MRAM. Previously, we have studied that hexagonal MTJ arrays can improve the storage density, but this increases the intra-cell and inter-cell stray fields, affecting the device performance[1]. This paper expects to reduce the inter-cell stray field by covering each MTJ unit with a soft magnetic shielding layer and the performance of the MTJ array with a shielding layer is studied. The simulation model of a single MTJ is built by using the simulation software COMSOL. The schematic diagram of the MTJ is shown in Fig.1(a). The model and the observation line are shown in Fig.1(b)-(c). The magnetic field distribution along the observation line is depicted in Fig. 1(d)-(f) under varying parameters. Based on modeling MTJ elements, we have established square and hexagonal MTJ arrays as shown in Fig2(a)-(b). We quote the inter-cell magnetic coupling coefficient(Ψ) and define Ψ=2% as the threshold, below which the inter-cell magnetic coupling can be considered negligible[2]. Fig.2(c) and (d) show the Ψ under different parameters, respectively. The results show that the soft magnetic shielding layer can effectively shield the stray field, thereby reducing its impact on MTJ performance. Specifically, a thicker shielding layer with higher magnetic permeability provides better shielding efficacy. And after magnetic shielding, the stray field between cells of a hexagonal array is larger.

[1]L. Liu, F. Jin and L. Yang, IEEE Transactions on Magnetics., Vol. 59, p.1-5 (2023) [2]L. Wu, S. Rao and M. Taouil, Design, Automation & Test in Europe Conference & Exhibition (DATE)., p.1211-1216 (2020)

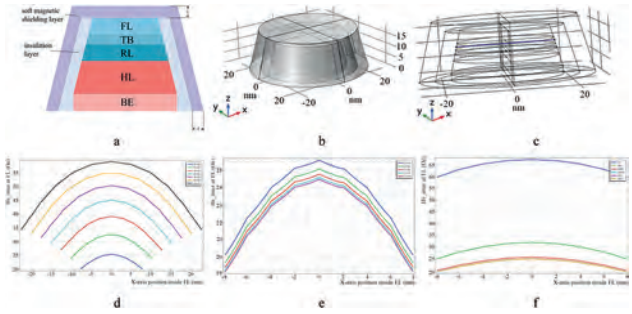

Fig.1 (a) Schematic diagram of MTJ unit. (b) MTJ simulation model. (c) Main observation lines. (d)-(f) The magnetic field distribution on the observation line when changing the dimensions of the MTJ unit eCD, the thickness of the magnetic shield, and the permeability of the magnetic shield.

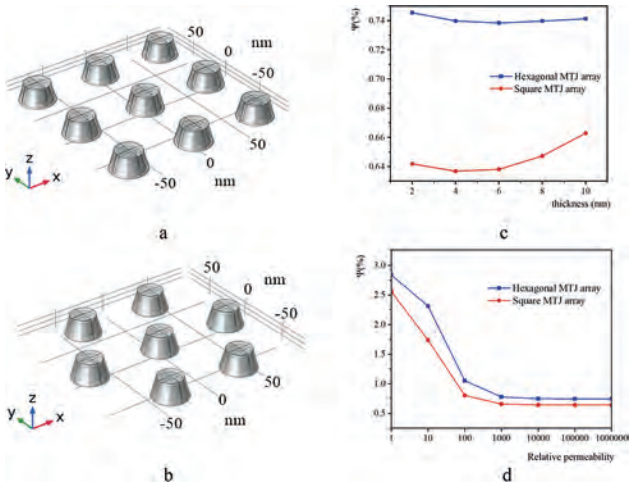

Fig.2 (a) Square MTJ array model. (b) Hexagonal MTJ array model. (c) Relationship between Ψ and the thickness of the shielding layer. (d) Relationship between Ψ and the relative permeability of the shielding material.

VP9-09. Advanced Hybrid MRAM based Novel GPU Cache System for Graphic Processing with High Efficiency. *S. Han*[1] and Y. Jiang[1]
1. Department of Electrical Engineering, School of Internet of Things (IoTs), Jiangnan University, Wuxi, China

Magnetic random access memory (MRAM) technology is being vastly explored in recent years as a viable alternative to static random access memory (SRAM) in Last Level Cache (LLC), L2 cache and even L1 cache [1, 2], with the excellent advantages of non-volatility, low leakage power, high security, high density and scalability [3]. The application of MRAM-based CPU cache systems is increasingly reaching maturity at present. The option of applying MRAM cache to more cutting-edge computing and data processing units is being actively considered. With the rapid development of portable computing devices and users' demand for high-quality graphics rendering, embedded GPU systems for graphics processing are increasingly turning into a key component of computer architecture to enhance computility. The reinforcement of main memory processing speed is far from catching up with the computational power of GPU [4]. In this way, the cache, located between the GPU computing unit and the main memory, serves a crucial role in data transfer. In this paper, spin transfer torque (STT)-MRAM [5] and spin orbit torque (SOT)-MRAM [6] are utilized in L1 and L2 caches to construct a novel GPU system for highly efficient graphics processing. As shown in Fig.1, a novel architecture for GPU cache systems is proposed, including the equipment of prefetching modules in L2 cache assumed by STT-MRAM to raise cache hit rate and hit latency. A controller design scheme for dynamically configuring the cache capacity is adopted in the L1 cache borne by SOT-MRAM. Meanwhile optimized cache coherency protocols are put forward and applied for better productive graphics processing and bandwidth output. Finally the MRAM-based CPU and GPU fusion design scheme is proposed to provide novel ideas for the future design of computer processing units undertaken by non-volatile magnetic memory. Simulation results demonstrated that the GPU cache system proposed in this paper has significant power savings and processing efficiency. As illustrated in Fig.2, the total power consumed by GPU cache system equipped with MRAM (GPU3) can be economized by up to 47.68%.

[1] R. Saha, Y. P. Pundir, and P. Kumar Pal, Journal of Magnetism and Magnetic Materials, vol. 551, p. 169161 (2022). [2] F. Oboril, R. Bishnoi and M. Ebrahimi et al., IEEE Trans. Comput.-Aided Des. Integr. Circuits Syst., vol. 34, p. 367–380 (2015). [3] R. Rajaei, M. Fazeli, and M. Tabandeh, IEEE Trans. Magn., vol. 51, p. 1–14 (2015). [4] P. Hijma, S. Heldens and A. Sclocco, et al., ACM Comput. Surv., vol. 55, p. 1–81 (2023). [5] A. Khvalkovskiy, D. Apalkov and S. Watts et al., Journal of Physics D: Applied Physics, vol. 46, p. 074001 (2013). [6] G. Prenat, K. Jabeur and P. Vanhauwaert et al., IEEE Transactions on Multi-Scale Computing Systems, vol. 2, p. 49-60 (2015).

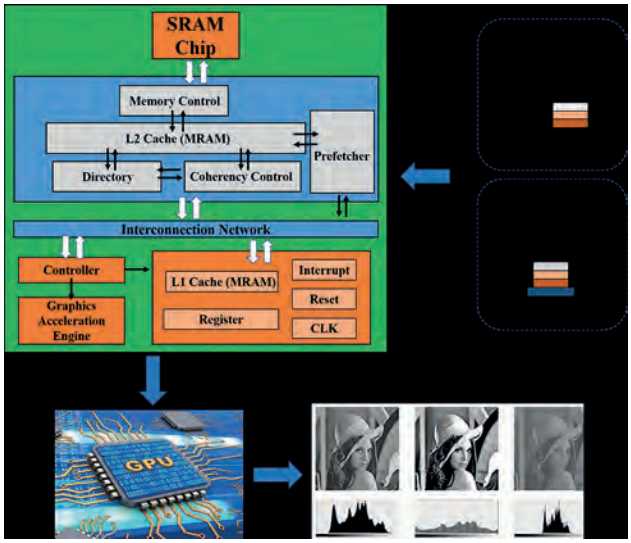

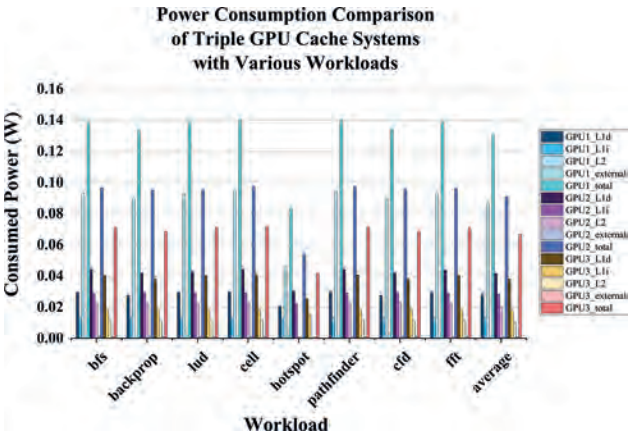

VP9-10. The Novel CPU Cache Architecture of MTJ based on Two-Dimensional Ferromagnetic Crystal. *S. Han*[1] and Y. Jiang[1]
1. Department of Electrical Engineering, School of Internet of Things (IoTs), Jiangnan University, Wuxi, China

Two-dimensional van der Waals ferromagnets have excellent controllable ferromagnetism and scalability for non-volatile information memory based on spintronics. In recent years, the exploration of advanced two-dimensional

materials such as MoS_2 and Fe_3GeTe_2 (FGT) has contributed a novel platform for the realization of spintronics storage [1-3]. FGT based on van der Waals layered structure exhibits excellent electromagnetic physical properties such as two-dimensional intrinsic ferromagnetism, large magnetic anisotropy, high-quality surfaces, large coercivity, and high Curie temperature. It is widely probed for information processing and storage computing [4]. The FGT-based Magnetic Tunnel Junction (MTJ) device has a huge TMR value [5], which is promising to mitigate the read/write interference and enhance the sensing margin in the magnetic random access memory (MRAM) cell circuit. Therefore it is of paramount significance for storage applications. In this paper, a novel Spin-Orbit Transfer (SOT)-MRAM composed of FGT is employed as a storage medium in the computer architecture, as shown in Fig.1. It forms a hybrid storage (L1, L2, Last Level Cache) with conventional SOT-MRAM and Spin Transfer Torque (STT)-MRAM, replacing the original static random access memory (SRAM) in the novel triple-level CPU cache architecture. This can override the increasing leakage problem of SRAM, while opening up the application of non-volatile storage technology in computer systems to the L1 cache level, as shown in Fig. 2. Traditional MRAM suffers from various problems such as poor integration and low flip rate at the L1cache. FGT addresses these deficiencies. Meanwhile, this paper proposes various cache optimization schemes for magnetic memory to better match the performance of FGT-SOT-MRAM to CPU. As shown in Fig.2, the simulation results demonstrate that the FGT-based MRAM can achieve up to 54.41% energy optimization in the CPU cache system compared to the conventional MRAM.

[1] Kim. T.H., Han. S.H. and Cho. B.K., Commun. Phys, vol. 2, p. 41 (2019). [2] Zhao. M., Zhao. Y. and Xi. Y. et al., Nano Lett., vol. 21, p. 9233–9239 (2021). [3] Xu. C., Li. X. and Chen. P. et al., Adv. Mater, vol. 34, p. 2107779 (2022). [4] May. A.F., Ovchinnikov. D. and Zheng. Q. et al., ACS Nano, vol. 13, p. 4436–4442 (2019). [5] Jiang. M., Asahara. H. and Sato. S. et al., Nat. Electron, vol. 3, p. 751–756 (2020).

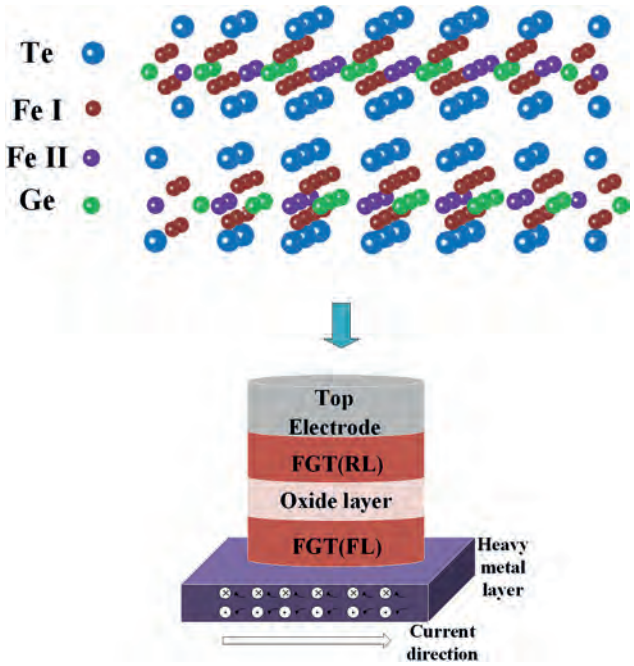

Figure 1

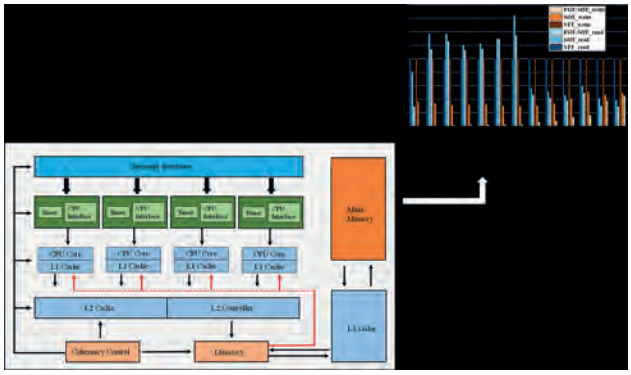

Figure 2

VP9-11. Modulation of Spin-orbit Torque and Large Enhancement of Perpendicular Magnetic Anisotropy in W/$Co_{20}Fe_{60}B_{20}$/MgO by Ir Insertion Layer. *X. Luo*[1], X. Han[1] and G. Yu[1] *1. Institute of Physics, Chinese Academy of Sciences, Beijing, China*

Iridium (Ir) is a 5d heavy metal with strong spin-orbit coupling (SOC), which introduces various intriguing phenomena when interacting with a ferromagnetic layer. In this study, we utilize Ir as an insertion layer in the W/Ir (t_{Ir})/$Co_{20}Fe_{60}B_{20}$/MgO heterostructures to tune SOC and study its influence on the spin-orbit torque (SOT), perpendicular magnetic anisotropy (PMA), and Dzyaloshinskii-Moriya interaction (DMI). The SOT efficiency decreases first and then increases with the increase of Ir insertion layer thickness because of the opposite spin Hall angle between W and Ir, and the sigh changes when the thickness of Ir is 1.5 nm, which is closed into the spin diffusion length of Ir 1.35 nm. Importantly, the 0.25 nm-thick Ir layer enhances the effective PMA largely by 140%-350% under different annealing temperatures than that of the sample without insertion. Meanwhile, the DMI constant is also enhanced. The enhancement of PMA and DMI is likely due to the enhancement of interfacial SOC when Ir diffuses into $Co_{20}Fe_{60}B_{20}$ and leads to the formation $Fe_{1-x}Ir_x$. These results provide an effective method to tune SOC by inducing a dusting layer with strong SOC to meet different requirements in spintronic devices like smaller magnetic tunnel junctions (MTJs).

[1] Xuming luo, Xiufeng Han, Guoqiang Yu, Phys.Rev. Appl. 19, 034043 (2023).

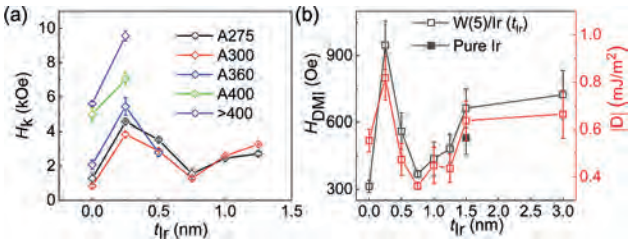

(a) The effective perpendicular magnetic anisotropy field H_k under different thicknesses of Ir insertion layers t_{Ir}. The annealing temperatures are 275°C, 300°C, 360°C, 400°C, and >400°C. (b) The effective field of DMI H_{DMI} and DMI exchange constant |D| with different thicknesses of Ir insertion layers t_{Ir} under 275°C annealing. The solid black square is the H_{DMI} of Ir/CoFeB/MgO.

VP9-12. Field-free SOT switching driven by spin current in a T-type ferromagnetic trilayer. *S. Liu*[1], C. Wan[1], G. Yu[1] and X. Han[1] *1. Institute of Physics, Chinese Academy of Sciences, Beijing, China*

Recently, we have developed the SOT-MTJ-compatible $Co_{20}Fe_{60}B_{20}$/W/$Co_{20}Fe_{60}B_{20}$ "T-type" magnetic trilayers, where the upper CoFeB layer has perpendicular magnetic anisotropy (PMA) and the bottom CoFeB has in-plane magnetic anisotropy (IMA). We can realize field-free switching

in a series of samples whose interlayer coupling field can be tuned from 20 Oe to 255 Oe through changing the thicknesses of W interlayer, a sizeable value for assisting SOT switching of PMA materials. The anisotropic field H_k of this "T-type" system is about 13.9 kOe, which is well suited for magnetic storage and scaling down devices. Meanwhile, this system verifies the possibility of SOT switching using ferromagnetic metals as a spin source and the spin hall angle of this system is: $|\theta_{SH}| = 0.149$, considerable for write efficiency. Finally, we tested the SOT-switching probability of this PMA system and we found that it can implement the function of probability-adjustable true random number generator (TRNG) in principle. We think this "T-type" system will play an important role in the future of low-power, non-volatile, multifunctional logic integrated circuits.

[1] Ma, Tianyi, Wan, Caihua, Dong, Jing, Physical Review B 101(13): 134417(2020) [2] Yang, Yumeng, Xie, Hang, Xu, Yanjun, Physical Review Applied 13, 034072 (2020) [3] Grimaldi, E., Krizakova, V., Sala, G., Nat Nanotechnol 15(2): 111-117 ((2020)) [4] Kim, J., Sinha, J., Hayashi, M., Nat Mater 12(3): 240-245 (2013) [5] Lau, Y. C., Betto, D., Rode, K., Nat Nanotechnol 11(9): 758-762 (2016) [6] Fukami, S., Anekawa, T., Zhang, C., Nanotechnol 11(7): 621-625 (2016) [7] Yang, W. L., Yan, Z. R., Xing, Y. W., Applied Physics Letters 120(12) (2022) [8] Li, X. H., Zhao, M. K., Zhang, R., arXiv:2306.02780 (2023)

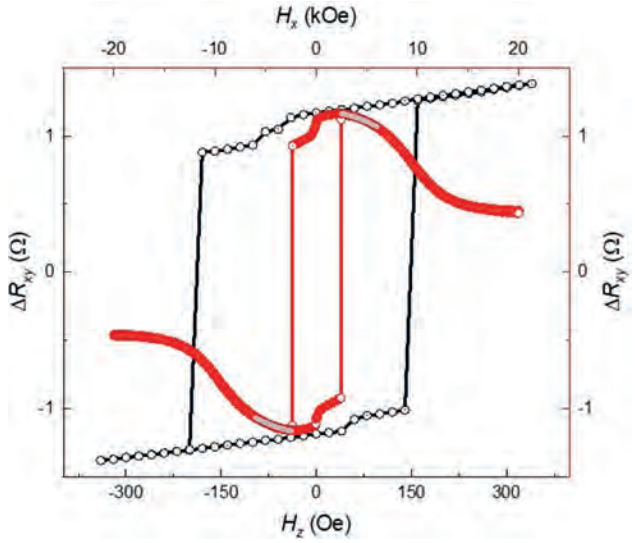

Fig.1 The anomalous Hall resistance ΔR_{xy} changes with H_z field (black line) and large H_x field (red line). The gray line is the plot line that fits the formula of H_k

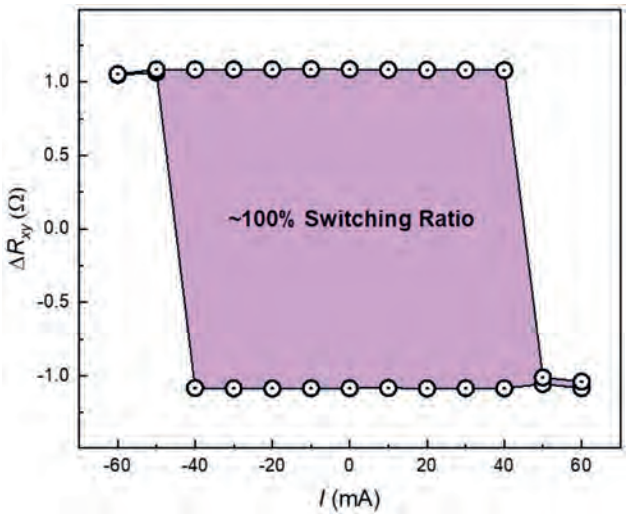

Fig.2 Free field SOT switching of nearly 100% switching ratio while the current width is 10 μs.

VP9-13. Giant Tunneling Magnetoresistance in Spin-Filter Magnetic Tunnel Junctions Based on van der Waals A-Type Antiferromagnet CrSBr. *G. Lan*[1], X. Han[1] and G. Yu[1] *1. Beijing National Laboratory for Condensed Matter Physics, Institute of Physics, University of Chinese Academy of Sciences, Chinese Academy of Sciences, Beijing 100190, China, Beijing, China*

Two-dimensional (2D) van der Waals (vdW) magnetic materials have demonstrated a great potential for new generation high performance and versatile spintronic devices. Among them, magnetic tunnel junctions (MTJs) based on A-type antiferromagnets, such as CrI_3, possess record-high magnetic tunnel magnetoresistance (TMR) because of the spin filter effect of each insulating ferromagnetic unite layers. However, the relatively low working temperature and the instability of the chromium halides hinder the applications of this system. Using a different technical scheme, we fabricated the MTJs based on an air-stable A-type antiferromagnet, CrSBr, and observed a giant TMR of up to 47,000% at 5 K. Meanwhile, because of a relatively high Néel temperature (T_N) of CrSBr, a sizable TMR of about 50% was observed at 130 K, which makes a big step towards the spintronic devices at room temperature. Our results reveal the potential of realizing magnetic information storage in CrSBr-based spin-filter MTJs (sf-MTJs).

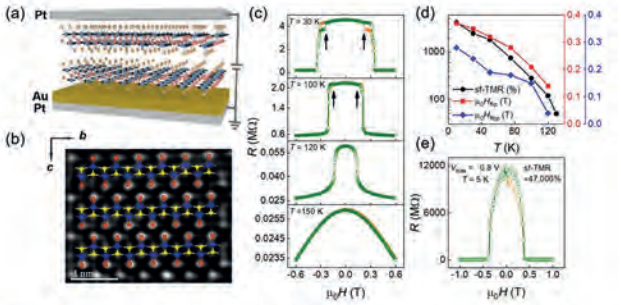

Figure 1: (a) Schematic of the device for the sf-MTJ, with A-type antiferromagnet CrSBr as the spin-filter layer between Pt/Au and Pt electrodes. (b) The cross-sectional STEM images. (c-d) Tunneling magnetoresistance for the sf-MTJs based on CrSBr with different temperature.

VP9-14. Symmetrical Voltage-Controlled Stochasticity of Perpendicular Synthetic Antiferromagnetic Magnetic Tunnel Junctions. *Y. Lv*[1], B.R. Zink[1], D. Zhang[1] and J. Wang[1] *1. Department of Electrical and Computer Engineering, University of Minnesota, Minneapolis, MN, United States*

For practical applications, such as random number generation[1], and for novel computing, such as stochastic computing[2], stochastic neuromorphic computing[3], and the recently-proposed probabilistic computing[4], the stochasticity of magnetic tunnel junctions (MTJs) is the key element of the proposed systems. Furthermore, often the possibility of electrical control or tunability of the stochastic behavior is desired for robust, efficient, flexible, reconfigurable system designs with even additional functionalities. For example, the biasing on MTJ can tune the rate and mean of the stochastic fluctuation MTJ[5] to compensate for device-device variations, improve speed[6], or enable system throttling. On the other hand, the recent development of advanced MTJ involving implementing perpendicular synthetic antiferromagnetic (SAF) layer structures[7], which aims at significantly improving the performance for memory applications, also opens up new possibilities for MTJ-based stochastic signal generations for novel computing. Here, we report an experimental observation of an unusual voltage-controlled spontaneous telegraphic switching. Unlike what one would expect for the voltage-controlled magnetic anisotropy (VCMA) effect, the observed spontaneous telegraphic switching occurs at the electrical biases that are symmetrical on both positive and negative side. The MTJ stack structure is substrate/seed layers/FePd/Ru/FePd/Ta/CoFeB/MgO/CoFeB/Ta/$[Pd/Co]_8$/Pd. Fig. 1 shows the tunneling magnetoresistance (TMR) vs. current bias. The bistability only appears around +-30 nA bias current. Fig. 2 shows that under +-30 nA electrical bias, the MTJ exhibits spontaneous telegraphic switching. We believe that this phenomenon is linked to the well-compensated SAF MTJ structures and the effect of both VCMA and the voltage modulation of interlayer exchange coupling[8]. We believe that such unique voltage-controlled stochastic behavior of perpendicular SAF MTJ could bring new opportunities for novel computing scenarios.

[1] W. H. Choi *et al.*, in *2014 International Electron Devices Meeting (IEDM)*, pp. 12.5.1-12.5.4 (2014) [2] Y. Lv and J.-P. Wang, in *2017 IEEE International Electron Devices Meeting (IEDM)*, pp. 36.2.1-36.2.4 (2017) [3] A. Sengupta, P. Panda, P. Wijesinghe *et al.*, *Scientific Reports*, vol. 6, no. 1, pp. 1–8, (2016) [4] K. Y. Camsari, B. M. Sutton, and S. Datta, *Applied Physics Reviews*, vol. 6, no. 1., p. 011305 (2019) [5] B. R. Zink, Y. Lv, and J.-P. Wang, *IEEE Trans. Electron Devices*, vol. 66, no. 12, pp. 5353–5359 (2019) [6] Y. Lv, R. P. Bloom, and J. P. Wang, *IEEE Magn. Lett.*, vol. 10, pp.1-5 (2019) [7] D. Zhang *et al.*, https://arxiv.org/abs/1912.10289v1 (2019). [8] D. J. P. De Sousa, P. M. Haney, D. L. Zhang *et al.*, *Phys. Rev. B*, vol. 101, no. 8, p. 081404 (2020)

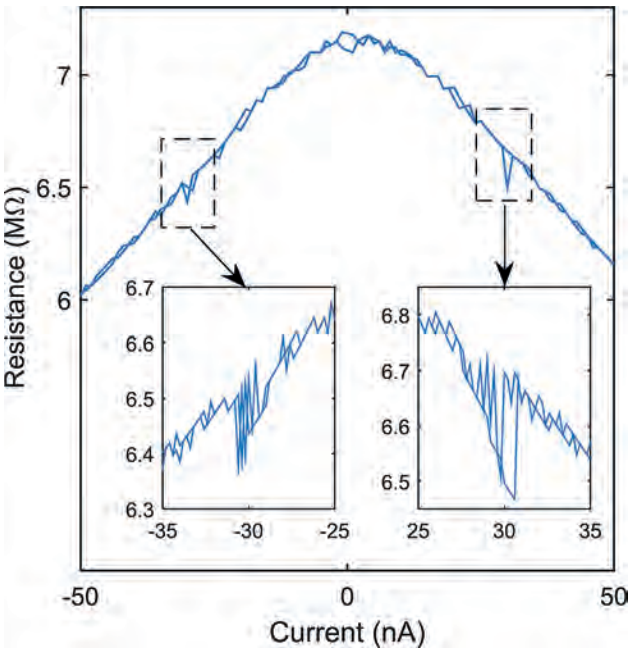

Fig. 1. Tunneling magnetoresistance (TMR) vs. current bias.

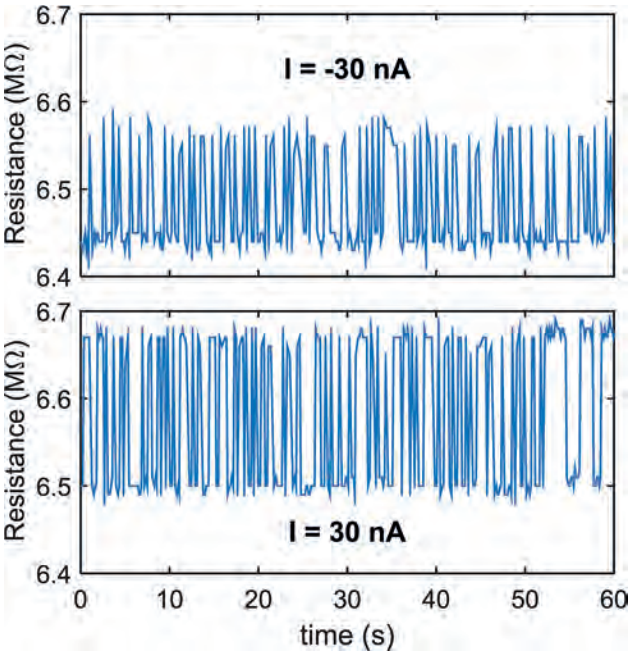

Fig. 2. TMR vs. time with bias of +/-30 nA.

VP9-15. Stochastic p-Bits Based on Spin-Orbit Torque Magnetic Tunnel Junctions. *X. Li*[1], M. Zhao[1], X. Han[1] and C. Wan[1] *1. Beijing National Laboratory for Condensed Matter Physics, Institute of Physics, University of Chinese Academy of Sciences, Chinese Academy of Sciences, Beijing, China*

Stochastic p-Bit devices play a crucial role in addressing NP-hard problems, neural network computing, and hardware accelerators for algorithms such as simulated annealing. In this study, our focus is on Stochastic p-Bits based on high-barrier magnetic tunnel junctions (HB-MTJs) with identical stack structure and cell geometry, but utilizing different spin-orbit torque (SOT) switching schemes. We conducted a comparative analysis of their switching probability, considering the pulse amplitude and width of the applied voltage. Through a combination of experimental and theoretical

investigations, we have observed that the Y-type SOT-MTJs exhibit the most moderate dependence of the switching probability on the external voltage. This characteristic indicates superior tunability in randomness and enhanced resilience against external disturbances when Y-type SOT-MTJs are employed as stochastic p-Bits. Moreover, the random numbers generated by these Y-type SOT-MTJs, following XOR pretreatment, have successfully passed the National Institute of Standards and Technology (NIST) SP800-22 test. This comprehensive study demonstrates the high performance and immense potential of Y-type SOT-MTJs for the implementation of stochastic p-Bits.

[1] Borders, W. A., Pervaiz, *Nature*, 573 (7774), 390-393 (2019) [2] X. Li, M. Zhao and X. Han, *arXiv* preprint arXiv:2306.02780 (2023)

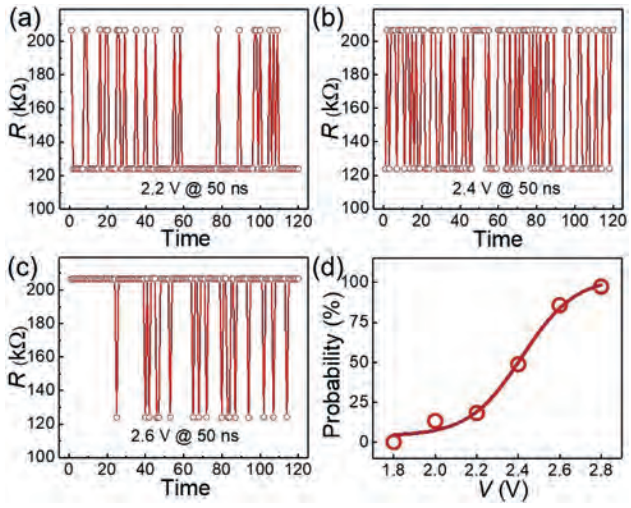

A stochastic p-Bit device demonstration using the Y-type SOT-MTJ. Resistance of the Y-type SOT-MTJ at V_{in}=2.2 V (a), 2.4 V (b) and 2.6 V (c) after 120 writing pulses. (d) Switching probability as a function of V_{in} with a well-matched sigmoid curve.

VP9-16. Non-Uniform Superlattice Minimalistic Magnetic Tunnel Junction. S. Chakraborti[1] and *A. Sharma*[1] *1. Electrical Engineering, Indian Institute of Technology, Ropar, Rupnagar, India*

Tri-layer magnetic tunnel junction(MTJ) has emerged as a building block for engineering propitious integrated circuits with meager energy consumption (Fig. 1(a)). High switching energy(≈50 fJ) and low TMR(≈ 200%) [1,2] are the bottlenecks that hinder its possibility of becoming a superior alternative for static and dynamic random access memory. In this work, we introduce a device featuring a minimalistic non-uniform superlattice (Fig. 1(b)) instead of the oxide layer in a conventional MTJ premised on the self-consistent coupling of the Non-Eqilibrium-Green's Function and the Landau-Liftshitz-Gilbert-Slonczewski equation. We find the presence of electronic Bloch states in the neighborhood of resonant peaks in the proposed non-uniform superlattice(Nu-SL) gives rise to a highly spin-selective box car-shaped transmission. This adaptation enables a high TMR(%) in the order of 3×10^{4}%(Fig.2(f)) and a significant reduction(Fig.2(h)) in the spin transfer torque switching bias (88%). As a result of the high opposite spin transmission, the spin filtering capability of an MTJ suffers a decline while failing to generate a large spin current($I_S = I_{up} - I_{down}$). This gives rise to a high switching bias resulting in higher switching energy. Comparative studies divulge that the proposed Nu-SL-based tunnel junction(Nu-SLTJ) is capable of rendering far superior spin-selectivity via broadband tunneling and thus may lay the bedrock for exploring the horizon of heterostructure-based spintronic devices in the near future.

[1] Sabarna Chakraborti and Abhishek Sharma 2023 Nanotechnology 34 185206 [2] Abhishek Sharma, Ashwin. A. Tulapurkar, and Bhaskaran Muralidharan Appl. Phys. Lett. 112, 192404 (2018) [3] Pankaj Priyadarshi et al 2018 J. Phys. D: Appl. Phys. 51 185301

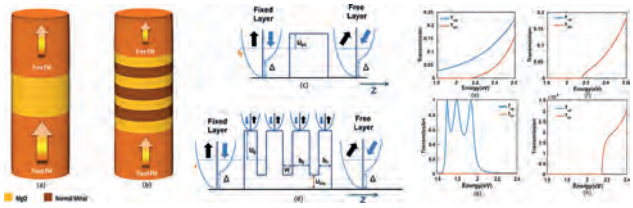

Fig.1 Device schematic of the (a) MTJ and the (b) Nu-SLTJ. Band diagram of the (c) MTJ and the (d) Nu-SLTJ. Transmission of the MTJ in the (e) parallel configuration(PC) and the (f) anti-parallel configuration(APC). Transmission of the Nu-SLTJ ins the (g) PC and the (h) APC.

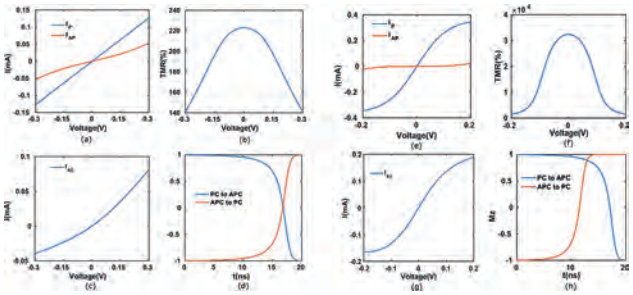

(a) I–V characteristics of the MTJ in the PC(IP) and the APC (IAP). (b) Variation of TMR(%) and (c) Is‖ with the applied voltage. (d) STT-based switching of the free layer from the PC to APC (V = –74 mV) and the APC to PC (V = 60 mV). (e) I–V characteristics of the LRW-SLTJ in the PC(IP) and APC(IAP). (f) Variation of TMR(%), (g) Is‖ with the applied voltage. (h) STT-based switching of the free layer from the PC to APC (V = –7.8 mV) and the APC to PC (V = 7.8 mV).

Session VP10
MICROSCOPY & CHARACTERIZATION (VIRTUAL)
(Poster Virtual Session)

Kotsugi Masato, Chair
Tokyo University of Science, Tokyo, Japan

VP10-01. Characterization of carbon coated core-shell iron nanoparticles annealed by oxygen and nitrogen. *C. Reynaga Gonzalez*[1], J. Baughman[1], J. Shallenberger[2], F.M. Iglesias[1], A. Khodagulyan[1], O. Bernal[1] and A.N. Kocharian[1] *1. Physics and Astronomy, California State University, Los Angeles, CA, United States; 2. Material Research Institute, Pennsylvania State University, Road University Park, PA, United States*

The carbon microspheres consisting of few layer graphene nanostructures can be produced by solid phase pyrolysis using a metal-free porphyrin and phthalocyanine[1] as organic precursors. The morphology, structure and size of multilayered graphene nanostructures are investigated using XRD, XPS, SEM and HR TEM microscopy images, and PPMS magnetic measurements. We investigate structural and magnetic properties of synthesized by pyrolysis of iron phthalocyanine (FePc) and iron porphyrin (FePr) nanoparticles of "core-shell" architecture with the high magnetic moment of core (such as a pure Fe), and the shell consisting of carbide encapsulated in carbon matrix. Using the two step of pyrolysis by annealing we synthesized also Fe-Fe_3O_4 nanoparticles having "core-shell" architecture dispersed in biocompatable carbon matrix that can significantly influence magnetic properties as compared with those of pyrolysis of iron-based porphyrin and phthalocyanine. We conducted investigations of structural and magnetic properties of biocompatable Fe-Fe_3O_4@C nanoparticles annealed by oxigen at different temperatures and different oxygen content using XRD, measurements of XPS spectra, high resolution SEM/STEM images, and magnetometry PPMS measurements. The oxygen and nitrogen content and structures are directly achieved from the XPS and also from XRD data analysis using the VESTA program. The measured zero field cooling (ZFC) magnetization M versus magnetic field H shown in Figure at T=10 K with the corresponding data provided in the Table display high specific absorption rate (SAR) because of a large area of hysteresis loop that are of special interest. Under external alternative electromagnetic field, the magnetic heating of these materials shows unique properties because of high M_r/M_s ratio controlled by composition and annealing temperature. These annealed nanoparticles can be considered promising for magnetic hyperthermia treatment of cancer cells. Further research into optimization of the annealing temperatures as well as changing the composition, time and temperature of pyrolysis, can provide more interesting magnetic features,.

[1] A. Manukyan, H. Gyulasaryan, A. Kocharian, P. Oyala, R. Chumakov, M. Avramenko, C. Sanchez, O. O. Bernal, L. Bugaev, and E. Sharoyan, J. Phys. Chem. C 126, 493–504 2022, *This research at CSULA is supported by the National Science Foundation-Partnerships for Research and Education in Materials under Grant DMR-1523588

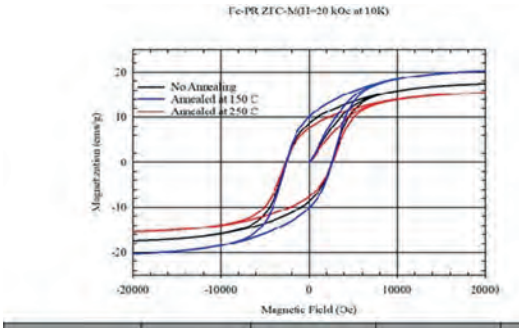

Fe-PR Samples	M_S (emu/g)	M_R (emu/g)	H_C (Oe)	M_R/M_S
No Anneal	17.4	8.6	2500	0.49
Annealed at 150 C	20.3	10.1	2600	0.49
Annealed at 250 C	15.4	7.6	2650	0.49

Magnetization M versus field H at 10 K and at different annaeling temperatures by oxygen

VP10-02. Shape Effects on Magnetic Behaviors of Sr-substituted BaM Ferrite Substrates Applied for Self-biased Circulators. *X. Jiang*[1], Y. Gong[1], Q. Su[1], K. Sun[1], C. Wu[1], Q. Li[1], Z. Yu[1] and Z. Lan[1] *1. School of Materials and Energy, University of Electronic Science and Technology of China, Chengdu, China*

For ferrite substrate of self-biased circulators[1], high coercivity is beneficial to inhibit irreversible demagnetization[2], which can enhance the remanence ($4\pi M_r$) and its stability. Now, some researches have focused on the field. V. Laur *et al.* [3] have proposed the $(La\text{-}Co)_x$-SrM hexaferrite pucks applied in the self-biased Y-junction rectangular waveguide circulators. Xu Zuo *et al*. [4] have demonstrated a self-biased microstripline circulator/isolator using SrM ferrite, in which the hexaferrite disk was embedded in the alumina substrate. Considering that magnetic behaviors have closed relationship with the shape of the ferrite substrate. We present the shape effect on the magnetization behavior and mechanism of ferrite substrates. BaSrM ferrite were developed with magnetic pressing, with the composition of $Ba_{0.8-x}Sr_xLa_{0.2}Fe_{10.4}Cu_{0.2}O_{16.9}$ (where $0.2 \le x \le 0.8$). Two types of samples named sample 1 (S_1) and sample 2 (S_2) were prepared as shown in Fig.1. $4\pi M_s$ is determined via S_1, and magnetic properties of the ferrite substrate are determined via S_2 which are presented in Table 1. Phase formation and texture structure of the BaSrM were confirmed by XRD patterns and EBSD figures. HAADF pictures and mappings of the sample with x=0.4 exhibit the obvious textural orientation and the element distribution. Magnetic hysteresis loops of the substrates possess good anisotropy behaviors. Coercivity (H_c) reaches the maximum when x=0.4. Effects of substrate shape on the *M-H* curves were investigated, and the results show that saturation magnetization cannot be achieved if the aspect ratio (h/l) is less than 34.9% resulting from the strong demagnetizing field (H_d), though the magnetic field along z direction of the substrate is applied to 20 kOe. So the maximum magnetization is expressed as M_m. With the increase in aspect ratio, M_r/M_m is enhanced significantly. In addition, magnetic flux density versus the aspect ratio of the substrate was simulated by ANSYS Maxwell software, and the results reveal that enhancing the aspect ratio is a key method to enhance remanence of the textured hexaferrite in z direction.

[1] W. M. Gitzel, S. B. Rad, M. Heidenreich, et al. Integration concept for a self-biased Ka-band circulator[C]. 2020 23rd International Microwave and Radar Conference (MIKON). IEEE, 2020: 350-352. [2] Robert C. Pullar, Hexagonal ferrites: A review of the synthesis, properties and applications of hexaferrite ceramics, Progress in Materials Science, 57, 2012:1191-1334. [3] V. Laur, G. Vérissimo, P. Quéffélec, et al. Self-biased Y-junction circulators using lanthanum-and cobalt-substituted strontium hexaferrites. IEEE Transactions on Microwave Theory and Techniques, 63(2), 2015:4376-4381. [4] X. Zuo, H. How, S. Somu, et al. Self-biased circulator/isolator at millimeter wavelengths using magnetically oriented polycrystallline strontium M-type hexaferrtie. IEEE Transactions on Magnetics, 39(5), 2003:3160-3162.

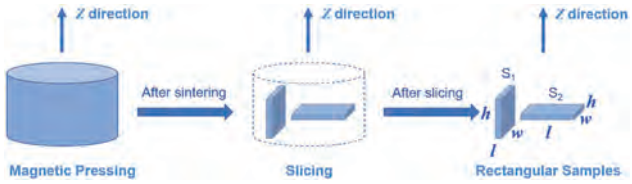

Diagram of samples preparation: pressing and slicing

Sample	*l*/mm	*w*/mm	*h*/mm	*h*/*l* (%)	N_z	$4\pi M_{is}$/G	$4\pi M_r$/G	M_r/M_{is}
$S_{2\text{-}1}$	4.69	4.69	0.76	16.2	0.732	3620	2527	0.70
$S_{2\text{-}2}$	4.18	4.18	0.76	18.2	0.712	3682	2575	0.70
$S_{2\text{-}3}$	3.68	3.68	0.76	20.7	0.689	3722	2639	0.71
$S_{2\text{-}4}$	3.13	3.13	0.76	24.3	0.657	3739	2685	0.72
$S_{2\text{-}5}$	2.68	2.68	0.76	28.4	0.625	4003	2919	0.73
$S_{2\text{-}6}$	2.18	2.18	0.76	34.9	0.580	4013	2982	0.74

Magnetic parameters of substrates with texture along *z* direction

VP10-03. The influence of hot-rolled densification on the properties of Nd–Fe–B magnets. *L. Qian*[1], Y. Li[1], L. Lingqi[1], W. Liu[1] and M. Yue[1]
1. Faculty of Materials and Manufacturing, Key Laboratory of Advanced Functional Materials, Ministry of Education of China, Beijing University of Technology, Beijing, China

In the past two decades, people have been exploring more effective ways to prepare Nd-Fe-B magnets. Nd-Fe-B magnets are usually densified by sintering or hot pressing followed by a process of hot deformation [1]. The first stage of hot deformation produces isotropic compact magnets [2]. Among the above methods, spark plasma sintering (SPS) has attracted great attention because pressure and electric field can be applied simultaneously to form densified sample during the SPS process [3]. At the same time, Gang et al. [4] studied the effect of heating rate on densification of electric field sintered Nd-Fe-B alloy. How to improve densification and enhance c-axis orientation are of great concern. The hot-rolled precursor Nd-Fe-B magnets with high c-axis crystal orientation and excellent magnetic properties can be prepared by controlling the reduction ratio. However, the research in this field is still scarce. Until now, no work has been reported on the microstructure and the associated magnetic properties of hot-rolled-densified Nd-Fe-B magnets. The initial materials used in the current job were industrial spun-melt Nd-Fe-B powder of Magnequench magnetic company [MQU-F, composition $Nd_{13.6}Fe_{73.6}Co_{6.6}Ga_{0.6}B_{5.6}$ (at%)] [Fig. 1 (a)]. One end of the steel sleeve mold was sealed, and the other end was filled with Nd-Fe-B powder under the condition of injecting argon gas, mainly to prevent oxidation of the sample in the hot-rolled process [Fig. 1 (b)]. The length of the steel sleeve was 30 mm, and the diameter of the steel sleeve was 30 mm. The sealed steel sleeve had been heated at 750 centigrade for 45 minutes, and the linear speed was 0.05 m/s [Fig. 1 (c)]. As a comparison experiment, the height of the hot-rolled steel sleeve decreased by 13 % in one sample and 18 % in the other sample. SPS was used to prepare hot-pressed samples, and the experimental parameters had been heated at 600 centigrade and held for 10 minutes. The sample with a reduction ratio of 13 % was named A. The sample with a reduction ratio of 18 % was named B. The hot-pressed sample was named C.

[1] Roberto, Orru, Roberta, et al. Materials Science & Engineering, 2009. [2] Kim H T, Kim Y B, Kim H S. Journal of Magnetism & Magnetic Materials, 2001, 224(2):173-179. [3] Yue M, Zhang J X, Liu W Q, et al. Journal of Magnetism & Magnetic Materials, 2004, 271(2-3):364-368. [4] Yang G, Yang Y, Lu D, et al. International Journal of Minerals Metallurgy & Materials, 2012, 19(011):1023-1028.

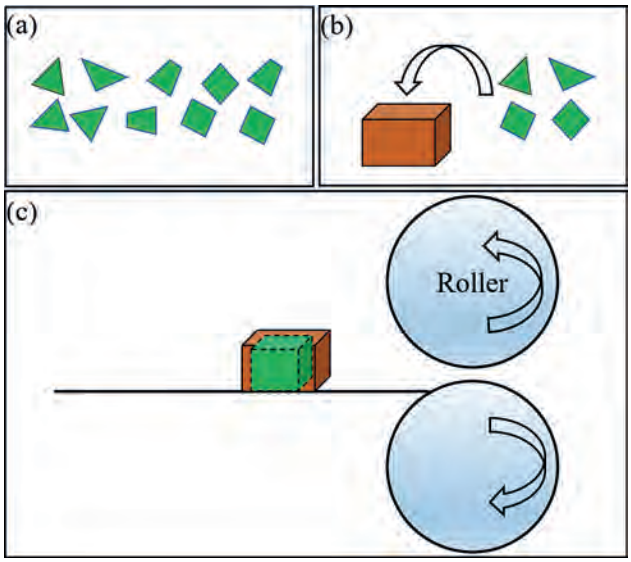

A schematic diagram of hot-rolled sample

VP10-04. A 2-D Magnetic Measuring System under the Co-loading of Temperature and Stress. *J. Gao*[2,1], Y. Li[2,1], Y. Dou[2,1] and S. Yue[2,1]
1. Hebei University of Technology, Tianjin, China; 2. State Key Laboratory of Reliability and Intelligence of Electrical Equipment, Tianjin, China

Temperature and stress are two influence factors of the magnetic properties of silicon steel, which means they affect the performance of electrical devices that use silicon steel sheets as cores. Accurate measurement and simulation of magnetic properties such as hysteresis and loss of magnetic materials under multiple working conditions are essential to their application in the design and improvement of new electromagnetic equipment. There are few devices that could measure the rotational magnetic properties under simultaneous loading of temperature and stress at present [1]. In order to obtain the magnetic properties of silicon steel sheets under a specific working condition, a 2-D magnetic measuring system that could apply temperature and stress at the same time is developed in this paper. The silicon steel sample is cut into a cross shape to fit the excitation structure consists of two orthogonal double-C yokes. An aluminum alloy plate with heating wires is used to locally heat the middle area of the sample. The uniformity and gradient changes of temperature loading were analyzed through simulation and experiment. Two stepper electrical cylinders are connected to the legs of the sample through stabilizers to apply stress. The magnetic flux density B and magnetic field intensity H in the middle area of the sample are measured by a combined B-H sensor which is able to withstand high temperatures above 200°C. The magnetic properties under different temperature and under different uniaxial stress of non-oriented silicon steels B25AV1300 are measured, which is under alternating magnetization. The hysteresis loop of magnetization along the rolling direction at different temperatures at a frequency of 400Hz and a magnetic flux density of 1T is shown in Fig. 1. Fig. 2 shows the power loss when different tensile and compress stress are applied along the rolling direction at different temperatures, at a frequency of 200Hz and a magnetic flux density of 1T. Results of rotational magnetic measurement will be presented in the full manuscript.

[1] D. Zhang, K. Shi, Z. Ren, et al. Measurement of Stress and Temperature Dependent Vector Magnetic Properties of Electrical Steel Sheet, *IEEE Transactions on Industrial Electronics*, vol. 69, no. 1, pp. 980-990 (2022)

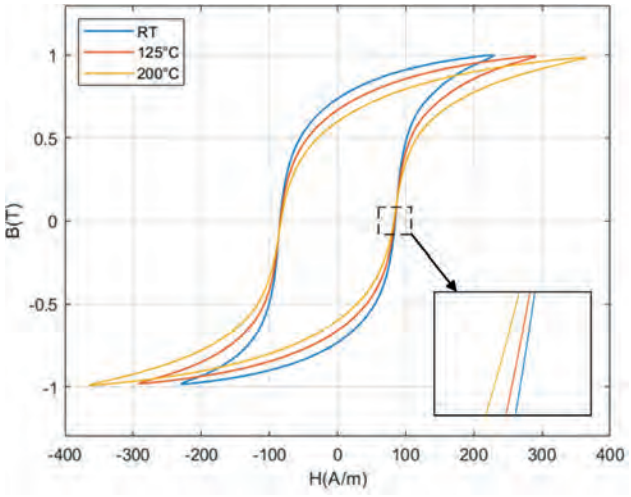

Fig. 1 B-H hysteresis loops at different temperatures

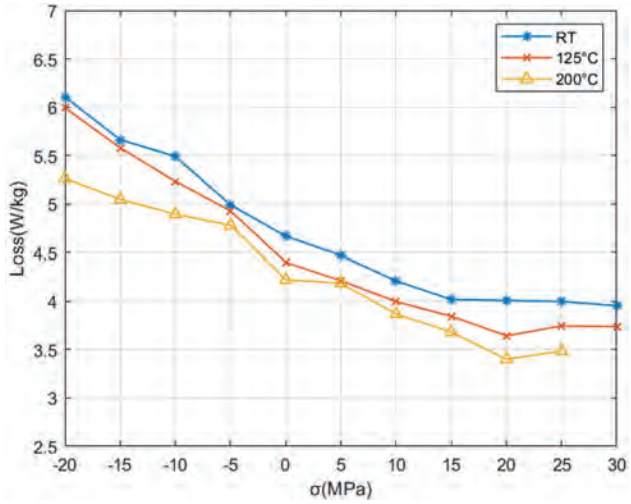

Fig. 2 Power loss at different temperatures and stress

VP10-05. Equalized Shape Feature Enhancement Method for Multiple Ferromagnetic Objects. H. Sun[1], *J. Qiu*[1], Z. Wang[1], S. Zhang[1] and S. Huang[1] *1. Key Laboratory of Optoelectronic Technology and System of Ministry of Education, College of Optoelectronic Engineering, Chongqing University, Chongqing, China*

When magnetic measuring instruments are used to measure the shape of ferromagnetic objects, the objects far away from the observation plane are likely to have blurred shape features because the magnetic field decays rapidly with distance[1]. A bigger challenge is to measure multiple objects at the same time. When the relative positions of multiple measured objects and the observation plane are inappropriate, it is easy to have problems that the shape features of the deeper measured objects are not obvious and the magnetic signals of multiple measured objects are aliased, which usually leads to shape feature measurement failed. To address this issue, we propose an equalized shape feature enhancement method for multiple ferromagnetic objects. The method enhances shape features by evaluating the trends of the total horizontal derivative[2] and vertical derivative[3] of the magnetic field within the measurement area using the standard deviation. Meanwhile, the method combines the theory of ratio equalization and normalization to improve the shape features convergence of deeper objects and balance the signal aliasing interference between objects of different depths. Experimental results (Fig.1) show that the shape feature measurement results of the proposed method(NFSD) are clear and in good agreement with the ideal model. The method can effectively balance the magnetic anomaly amplitudes of the measured objects with different depths, and improve the accuracy and stability of shape feature measurement. Furthermore, we compare and analyze the processing effects of the proposed method and the traditional NSTD method[4] (Fig. 2). It is calculated that the standard deviations of the results obtained by the proposed method and the NSTD method are 0.146 and 0.136, and the average peak-to-trough differences are 0.368 and 0.352, respectively. Therefore, the proposed method can better enhance the shape characteristics of ferromagnetic objects, and has more practical application value.

[1] J. Li, H. Fan and Y. Zhang, Journal of Military Engineering, Vol. 41, p.2033-2044 (2020) [2] G. Ma and L. Li, Computers & Geosciences, Vol. 41, p.83-87(2012) [3] Y. Zhu, W. Wang and C. G. Farquharson, Geophysics, Vol. 86, p.G23–G34 (2021) [4] G. Cooper and D. Cowan, Geophysics, Vol. 71, p.H1-H4 (2008)

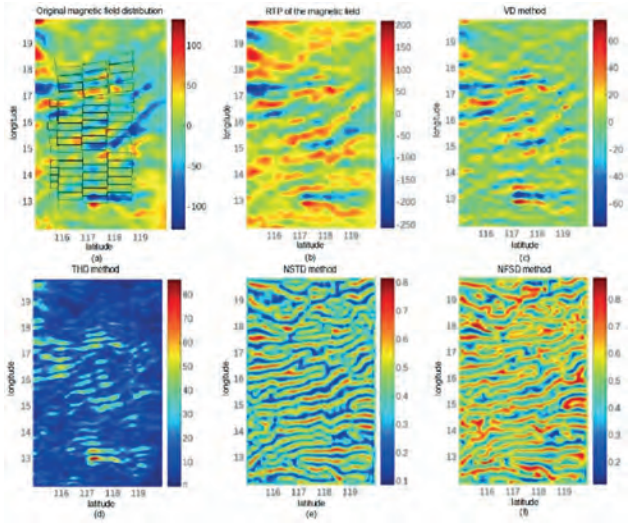

FIG.1 Original magnetic field distribution and the effect of shape features enhancement methods

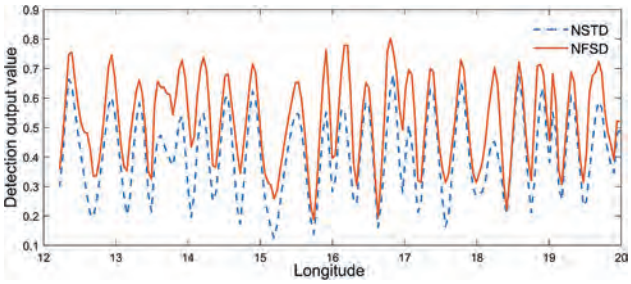

FIG.2 Detection output comparison of the NSTD method and the proposed method

VP10-06. Withdrawn

VIRTUAL PLATFORM ONLY

Session VP11
MULTI-FUNCTIONAL MAGNETIC MATERIALS AND APPLICATIONS (VIRTUAL)
(Poster Virtual Session)

Georgeta Salvan, Chair
Chemnitz University of Technology, Chemnitz, Germany

VP11-01. Barnett effect in ferrofluids. *M. Umeda*[1], H. Chudo[1], M. Imai[1], M. Matsuo[2], N. Sato[1], S. Maekawa[2,3] and E. Saitoh[1,4] *1. Japan Atomic Energy Agency, Advanced Science Research Center, Tokai, Japan; 2. Kavli Institute for Theoretical Sciences, University of Chinese Academy of Sciences, Beijing, China; 3. Center for Emergent Matter Science, RIKEN, Wako, Japan; 4. Department of Applied Physics, The University of Tokyo, Hongo, Japan*

Gyromagnetic effects can relate motions including rotation and vibration with the magnetic moment and currently gain renewed attention due to the potential applications in micro-electromechanical systems (MEMS). The Barnett effect is one of the gyromagnetic phenomena in which an object is magnetized when it is rotated [1]. We have investigated the Barnett effect using custom-made equipment with a gas rotation technique of the sample in a rotor and a fluxgate magnetic field sensor to detect small stray fields of the magnetized sample on the order of nT [2-5]. Precise measurement of the inertial field acting on an electron, i.e. Barnett field B_Ω, allows us to obtain not only the gyromagnetic properties of electron spin but also the angular velocity of the rotated samples in solid and liquid states. Here we present the first observation of the Barnett effect in ferrofluids. Ferrofluid is a novel kind of functional material with a stable colloidal suspension of fine particles in a liquid solvent that exhibits both magnetic and fluid properties. Magnetic measurement shows contained Fe_3O_4 fine particles are super-paramagnetic and have large magnetic susceptibility, whose properties are suitable for the measurement of the Barnett effect. By rotating the ferrofluid at high speed up to 1.8 kHz we found that B_Ω arises with almost twice larger the magnitude than that in a solid state as shown in Figure 1. The result at low temperatures suggests that the enhancement of B_Ω is due to the Brownian motion of the fine particles. We discuss the details of this enhancement in relation to fluid dynamics and an inertial force with additional results.

[1] S. J. Barnett, Phys. Rev. 6, 239 (1915). [2] M. Ono *et al*., Phys. Rev. B 92(17), 174424 (2015). [3] Y. Ogata *et al*., Appl. Phys. Lett. 110(7), 072409 (2017). [4] M. Imai *et al*., Appl. Phys. Lett. 113(5), 052402 (2018). [5] M. Umeda *et al*., Rev. Sci. Instrum. 94, 063906 (2023).

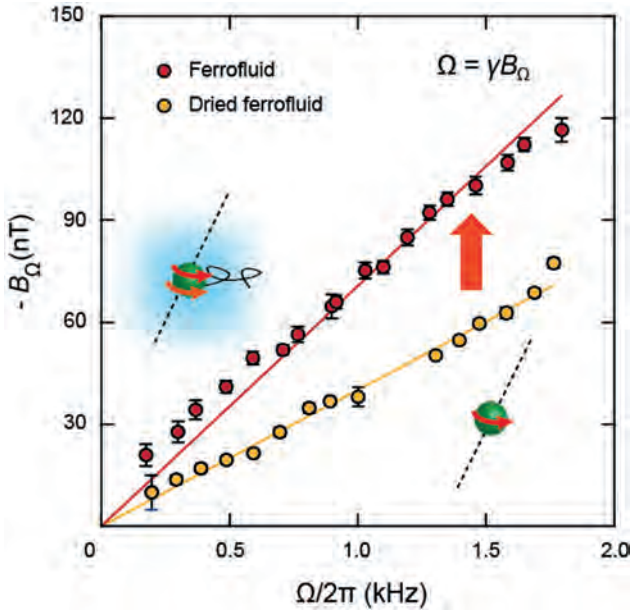

Fig.1 Rotational-frequency dependence of B_Ω. The solid lines show linear fits to the experimental data of the original ferrofluid (red-filled circles) and dried ferrofluid (yellow-filled circles) samples.

VP11-02. Withdrawn

VP11-03. Enhancement of magnetoelectric coupling in laminate composites of textured Galfenol and PZT. *J. Liu*[1], Z. He[1], C. Mi[1], Y. Sha[2], X. Zhu[1], L. Chen[1] and L. Zuo[2] *1. School of Materials Science and Engineering, Shenyang University of Technology, Shenyang, China; 2. Key Laboratory for Anisotropy and Texture of Materials (Ministry of Education), Northeastern University, Shenyang, China*

Multiferroic magnetoelectric (ME) coupling between the magnetostrictive and piezoelectric constituents has superior ME properties and shows promising potential for practical applications such as sensors, transducers, energy harvesters, etc [1-3]. More attention was focused on improving the ME coupling by utilizing different piezoelectric constituents with superior properties [3-4]. The ME coupling can also be enhanced by improving the magnetostrictive materials. Compared to the brittle of Terfenol-D, Galfenol (Fe-Ga) exhibits a combination of high mechanical strength and good ductility, allowing it to be used in harsh and shock-prone environments [5,6]. However, the larger ME output was limited by its low magnetostrictive coefficient. In this study, the laminate composites of the ME sandwich structure device were fabricated using a PZT piezoelectric ceramic plate polarized along the thickness direction sandwiched between two Fe-Ga thin sheets prepared by conventional rolling and annealing methods. Goss-oriented and random-textured Fe-Ga thin sheets were prepared to reveal the effect of texture and magnetostriction coefficient on the ME coupling. The ME laminate with Goss-oriented Fe-Ga sheet and magnetostrictive

coefficient of 244 ppm exhibits much higher ME coefficients (73.11 V/cm●Oe) than those of ME laminate (16.17 V/cm●Oe) with random-textured Fe-Ga sheet and magnetostrictive coefficient of 64 ppm. Meanwhile, higher ME coefficients can be obtained in a low resonance frequency (26.4 Hz) and excitation magnetic field (26 Gs).

[1]H. Liu, J. Wang and H. Wang, International Journal of Precision Engineering and Manufacturing., Vol. 18, p. 1605-1614 (2016). [2] H. Palneedi, S. Na and G. Hwang, Journal of Alloys and Compounds., Vol. 765, p. 764-770 (2018). [3]V. Annapureddy, S. Na and G. Hwang, Energy & Environmental Science., Vol. 11, p. 818-829 (2018). [4]F. Li, X. Zhang and T. Wu, Sensors and Actuators A: Physical., Vol. 349, p. 114020 (2023). [5] A. Clark, J. Restor and M. Wun-Fogle, IEEE Transactions on Magnetics., Vol. 36, p. 3238–3240 (2000). [6]J. Domann, C. Loeffler and B. Martin, Journal of Applied Physics., Vol. 118, p. 123904 (2018).

VP11-04. Investigation of Magnetic and Magnetocaloric Properties of Nanocrystalline $Pr_{0.6}Y_{0.1}Ba_{0.3}MnO_3$ Manganite. *G. Singh*[1], A. Gaur[1], P. Bisht[1] and R.N. Mahato[1] *1. School of Physical Sciences, Jawaharlal Nehru University, New Delhi, India*

Perovskite manganite has various applications in future technologies such as spintronics, magnetic sensors, storage media, colossal magneto-resistance, thermo-electric, and magnetic refrigerants [1]. Double exchange interaction and super-exchange interaction play a vital role in the afore-mentioned properties [2]. The magnetic and magnetocaloric properties of nanocrystalline $Pr_{0.6}Y_{0.1}Ba_{0.3}MnO_3$ (PYBMO) manganite synthesized via sol-gel wet chemical route have been investigated. X-ray diffraction pattern analysis has confirmed that our sample exhibits an orthorhombic crystal structure with a Pnma space group. [3] The Williamson-Hall strategy was used to compute the crystallite size and lattice strain, which came out to be ~ 25 nm and 0.00127 respectively. The transmission electron microscope (TEM) was performed to elaborate structural and morphological studies. The temperature-dependent magnetic measurements have been carried out within 2 K - 300 K at 0.05 T applied magnetic field, exhibiting a ferromagnetic to paramagnetic phase transition with a transition temperature (T_C) ~ 128 K. The paramagnetic Curie-Weiss temperature was found to be 164 K. The experimentally and theoretically calculated effective magnetic moment is ~ 5.9 μ_B/f.u. and ~ 5.38 μ_B/f.u. respectively. The M-H isotherms in a protocol of 0 T → 5 T → -5 T → 5 T indicate ferromagnetism at 2 K, although the linear hysteresis loop corresponds to the paramagnetic behavior at 300 K. The second-order magnetic phase transition was affirmed by the positive slopes of Arrott plots. The classical Maxwell theory was used to compute the magnetic entropy change, and hence further calculating the magnetic cooling capacity [4]. The collapsing behavior of Franco's curves presents the universality in magnetic entropy change, which corroborates the second-order phase transition in PYBMO, theoretically.

[1] M. Bourouina, A. Krichene, N. Chniba Boudjada, W. Boujelben, J. Alloys Compd. 680, 67–72 (2016). [2] A. Pal, A. Rao and D. Kekuda, J. Magn. Magn. Mater. 512, 167011 (2020) [3] M. Jeddi, H. Gharsallah, M. Bekri, E. Dhahri, E.K. Hlil, RSC Adv. 8, 28649–28659 (2018). [4] D. Mazumdar, K. Das, I. Das, J. Appl. Phys. 127, 0–13 (2020).

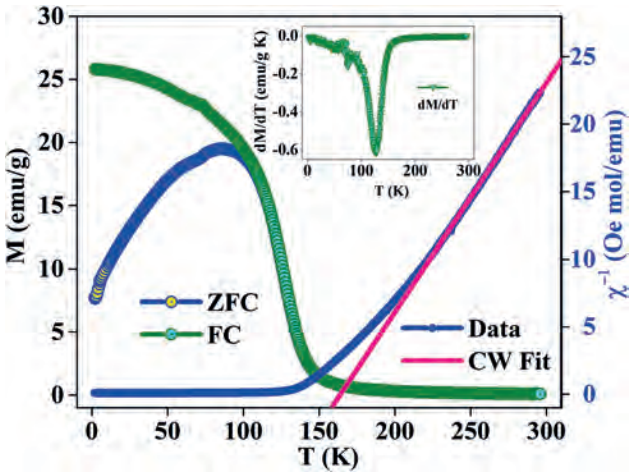

Fig.1 Temperature dependence of ZFC and FC magnetizations at 0.05 T magnetic field. The right side axis depicts the inverse susceptibility (χ^{-1}) vs T plot. The inset displays the dM/dT vs T plot.

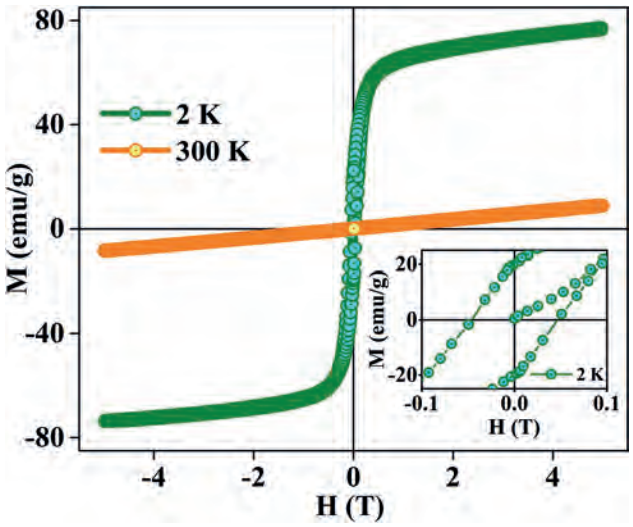

Fig.2 Magnetization vs magnetic field (H) plot at 2 K and 300 K temperature. Inset shows the magnified view of 2 K plot.

VP11-05. Magnetostructural transformation and magnetocaloric properties of $Ni_{37.5}Co_{12.5}Mn_{35}Ti_{15}B_x$ melt-spun ribbons (x= 0.00 and 0.04). *M. López Cruz*[1], J.L. Sanchez[1] and R. Varga[2] *1. División de Materiales Avanzados, Instituto Potosino de Investigación Científica y Tecnológica, San Luis Potosí, Mexico; 2. CPM-TIP, Universidad Pavol Jozef Šafárik, Kosice, Slovakia*

Melt-spun ribbons of the all-d-metal $Ni_{37.5}Co_{12.5}Mn_{35}Ti_{15}$ and $Ni_{37.5}Co_{12.5}Mn_{35}Ti_{15}B_{0.04}$ alloys were produced under similar synthesis conditions (i.e., at a linear wheel speed of 20 ms^{-1}) to get preliminary information on the effect of interstitial boron on the martensitic transformation (MT) and related first-order magnetocaloric effect. As-solidified ribbon samples were studied by X-ray diffraction, differential scanning calorimetry (DSC), scanning electron microscopy (SEM), and magnetization measurements. For both ribbon series, the MT occurs from a ferromagnetic B2-type austenite to an antiferromagnetic 5M martensite. However, DSC and $M(T)$ curves show a reduction of both the MT temperatures and Curie temperature of austenite (T_C^A) upon B addition (by about 47 K and from 334 K to 276 K, respectively); in addition, the magnetization change across the transition at 2 T has been reduced from 63 Am^2kg^{-1} to 53 Am^2kg^{-1}. SEM images show a partially grain-oriented microstructure consisting of columnar elongated grains whose main axis is aligned along the thermal gradient during

solidification, whereas with the addition of B the average grain size increased. For a magnetic field change of 2 T, undoped samples showed a maximum magnetic entropy change ΔS_M^{max} across the reverse (direct) MT of 13.8 (9.5) J kg^{-1} K^{-1}, whereas for the doped ones ΔS_M^{max} is reduced to 4.8 (4.7) J kg^{-1} K^{-1}. Acknowledgments. Work supported by SEP-CONAHCyT, Mexico (research project CF-2023-I-2143), and Laboratorio Nacional de Nanociencias y Nanotecnologia (LINAN, IPICyT). We acknowledge the technical assistance received from M.Sc. B.A. Rivera-Escoto, M.Sc. A.I. Peña Maldonado and Dr. I.G. Becerril-Juárez. M. López-Cruz is grateful to The National Scholarship Program of the Slovakia Republic for the scholarship granted, and to CONAHCYT for supporting his Ph.D. studies (fellowship No. 831827).

VP11-06. Magnetic and magnetocaloric properties of rare earth intermetallic compound $Gd_3Co_4Ge_{13}$. A.V. Morozkin[1], A.V. Garshev[1,3], V.O. Yapaskurt[4], S. Quezado[2], S.K. Malik[2] and *R. Nirmala[5] 1. Department of Chemistry, Moscow State University, Moscow, Russian Federation; 2. Universidade Federal do Rio Grande do Norte, Natal, Brazil; 3. Faculty of Materials Science, Moscow State University, Moscow, Russian Federation; 4. Department of Petrology, Moscow State University, Moscow, Russian Federation; 5. Department of Physics, Indian Institute of Technology Madras, Chennai, India*

Search for suitable magnetic material for use as refrigerant at low temperatures assumes immense importance for realization of magnetic refrigeration-based hydrogen and helium liquefaction [1]. In the present work, magnetic and magnetocaloric properties of polycrystalline $Gd_3Co_4Ge_{13}$ (Cubic $Yb_3Rh_4Sn_{13}$-type, space group *Pm*-3*n*, N 223, *cP*40) have been studied by dc magnetization measurements in fields up to 140 kOe. The compound $Gd_3Co_4Ge_{13}$ undergoes antiferromagnetic-like transition at 9 K (T_N) [Fig. 1a]. The antiferromagnetism appears to be weak and in applied magnetic fields larger than 40 kOe, ferromagnetic interactions become prevalent. This is evident via the field-induced cross-over from the antiferromagnetic to ferromagnetic state that is marked as a change from inverse to normal magnetocaloric effect in the isothermal magnetic entropy change vs temperature plot around the antiferromagnetic transition temperature. At 2 K, the sample shows S-type behaviour with a tendency towards saturation. A magnetic moment of 5.3 $\mu_{B/}$ per Gd^{3+} is obtained in 140 kOe field. The maximum isothermal magnetic entropy change at 8 K is -1.56 J/kg×K for a field change of 50 kOe and the corresponding relative cooling power is 34 J/kg. The isothermal magnetic entropy change shows a linear increase for magnetic field changes larger than 40 kOe [Fig. 1b].

[1.] Wei Liu, Eduard Bykov, Sergey Taskaev, Mikhail Bogush, Vladimir Khovaylo, Nuno Fortunato, Alex Aubert, Hongbin Zhang, Tino Gottschall, Jochen Wosnitza, Franziska Scheibel, Konstantin Skokov and Oliver Gutfleisch, "A study on rare-earth Laves phases for magnetocaloric liquefaction of hydrogen", *Appl. Mater. Today* vol. 29, pp. 101624(1) - 101624(13), 2022.

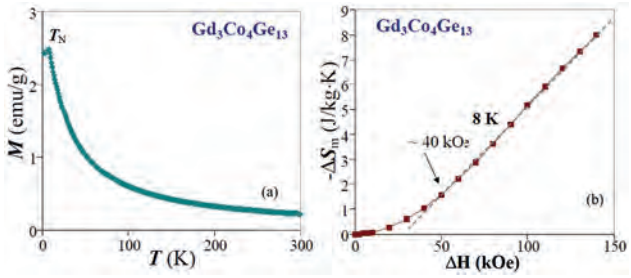

VP11-07. Enhanced magnetic and magnetocaloric effects driven by interfacial magnetic coupling of rare earth element doped LCMO-Mn_3O_4 nanocomposites. *M. Azim*[1], J. Mohapatra[2] and S. Mishra[1] *1. Physics and Material Science, University of Memphis, Memphis, TN, United States; 2. Physics, University of Texas at Arlington, Arlington, TX, United States*

Magnetic refrigeration technology, which works on the magnetocaloric effect (MCE) of magnetic materials, has attracted the interest of numerous research groups over traditional gas refrigeration. It has several advantages, including being highly energy-efficient, environmentally friendly, and cost-effective. The major effort is to improve the magnetic entropy change and the relative cooling power (RCP) of oxide magnetocaloric materials. This study reports the synthesis and magnetocaloric properties of the novel rare earth element doped LCMO composites. These tetragonal crystal structure-shaped compounds were synthesized with respect to AB_2O_7 type perovskite oxides with the *I4/mmm* group via the facile autocombustion technique. This rare earth europium element expanded the Curie temperatures from $La_{1.4}Ca_{1.6}Mn_2O_7$ ~ 182 K to $La_{1.3}Ca_{1.6}Eu_{0.1}Mn_2O_7$ of ~ 186 K, consequently enhancing the RCP value. Moreover, these composites were also prepared in the presence of 10 wt. % of Mn_3O_4 nanoparticles. The presence of Mn_3O_4 at the intervening grain boundaries between $La_{1.4}Ca_{1.6}Mn_2O_7$ and $La_{1.3}Ca_{1.6}Eu_{0.1}Mn_2O_7$ phases altered the double exchange interaction between Mn^{3+} and Mn^{4+} ions. The result does show that these interfacial disordered magnetic interactions of these nanocomposites further expanded the second-order paramagnetic-to-ferromagnetic phase transition temperature up to 257 K at the temperature-dependent field-cooled magnetization curve, which also led to enhance the change in magnitudes of magnetic entropy - (delta S) to 0.52 J/kg/k under an applied magnetic field of 5T. The fundamental key of this work is to demonstrate the potentiality of enhancing the magnetic phase transition temperature and magnetocaloric effect in the framework of interfacial coupling between Mn_3O_4 and LCMO nanocomposites.

[1] Mukherjee, D.; Bingham, N.; Phan, M.-H.; Srikanth, H.; Mukherjee, P.; Witanachchi, S.; Ziz-zag Interface and Strain-influenced Ferromagnetism in Epitaxial Mn3O4/La0.7Sr0.3MnO3 Thin Films Grown on SrTiO3 (100) Substrates. J. Appl. Phys. 2012, 111, 07D730. [2] E. Tasarkuyu, A. Coskun, A.E. Irmak, S. Aktürk, G. Ünlü, Y. Samancoğlu, A. Yücel, C. Sarkürkçü, S. Aksoy, M. Acet, J. Alloy. Compd. 509 (2011) 3717. [3] X. Zhao, W. Chen, Y. Zong, S.L. Diao, X.J. Yan, M.G. Zhu, J. Alloy. Compd. 469 (2009) 61–65. [4] H. Zhu, H. Song, Y.H. Zhang, Appl. Phys. Lett. 81 (2002) 3416.

VP11-08. Withdrawn

VP11-09. On the phase constitution of near equiatomic bulk FeRh alloys: X-ray versus neutron diffraction and magnetization measurements. *M. Arreguin Hernandez*[1], K. Padrón Alemán[2,3], P. Álvarez Alonso[2] and J.L. Sanchez[1] *1. Instituto Potosino de Investigación Científica y Tecnológica, San Luis Potosí, Mexico; 2. Departamento de Física, Universidad de Oviedo, Oviedo, Spain; 3. Diffraction Group, Institut Laue-Langevin, Grenoble, France*

The chemically ordered CsCl-type crystal structure (also called B2 structure) in near equiatomic FeRh alloys undergoes an isostructural first-order phase transition that changes the magnetic structure from antiferromagnetic to ferromagnetic; this change in the interatomic distances is accompanied by a drastic change in the saturation magnetization (120-140 Am^{2}kg^{-1}). Around 1% of the bcc B2-type unit cell volume changes during this magnetoelastic transition. It is well known that the B2-type structure is highly sensitive to stress and plastic deformation; this happens when it coexists with precipitates of the fcc gamma phase (A1, paramagnetic) [1], or when is plastically deformed fully transforming into this phase [2]. X-ray diffraction (XRD) is a basic and widely used tool for structural identification and phase analysis, but considering the abovementioned effects and the fact that bulk FeRh alloys are difficult to pulverize the only way to get structural information is

to prepare a flat polished surface to perform the analysis. Considering the limited penetration depth of the X-ray beam, the obtained XRD pattern will provide erroneous information about the volume sample constitution (this is, the phases that are identified are not representative of the sample volume and/or are contradictory to the achieved by other analysis techniques). In this work, we contrast the information obtained by XRD for the sample's surface with that provided by the neutron diffraction pattern (NDP) and the thermomagnetic analysis curves at 2 T for a slice cut from a bulk $Fe_{50}Rh_{50}$ alloy (prepared by induction melting followed by 48 hours of thermal annealing at 1273 K). Whereas NDP and $M(T)$ curves, directly and indirectly, confirm that the sample is a single phase possessing the CsCl-type crystal structure, a variety of phases, which modify upon polishing the surface or etching with a mixture of hydrochloric (HCl) and nitric acid (NHO_3) at a volume ratio of 90:10 (from 30 to 210 minutes) [3], are identified in XRD patterns.

[1] A. Chirkova, F. Bittner, K. Nenkov, N. V. Baranov, L. Schultz, K. Nielsch, T. G. Woodcock, Acta Materialia 131 (2017) 31. http://dx.doi.org/10.1016/j.actamat.2017.04.005. [2] J.M. Lommel, J.S. Kouvel, J. Appl. Phys. 38 (1967) 1263. http://dx.doi.org/10.1063/1.1709570. [3] Y. Danzaki, T. Ashino, Anal. Sci. 17 (2001) 1011. https://doi.org/10.2116/analsci.17.1011.

VP11-10. Optical and Magneto-optical Properties of Pulsed Laser Deposited Thulium Iron Garnet Thin Films. A. Sharma[1], O. Ciubotariu[2], P. Matthes[3], S. Okano[1], V. Zviagin[4], J. Kalbáčová[1,5], S. Gemming[1,6], C. Himcinschi[7], M. Grundmann[4], D. Zahn[1,6], M. Albrecht[2] and *G. Salvan*[1,6] *1. Semiconductor Physics, Chemnitz University of Technology, Chemnitz, Germany; 2. University of Augsburg, Augsburg, Germany; 3. Fraunhofer Institute for Electronic Nanosystems, Chemnitz, Germany; 4. Universität Leipzig, Leipzig, Germany; 5. HORIBA Jobin Yvon GmbH, Oberursel, Germany; 6. Center of Materials, Architectures and Integration of Nanomembranes, Chemnitz University of Technology, Chemnitz, Germany; 7. Institute of Theoretical Physics, TU Bergakademie Freiberg, Freiberg, Germany*

Garnets are complex orthosilicate minerals that have been used for several centuries as semi-precious gemstones. Among the vast family of garnets, magnetic garnets are of special interest due to their unique properties, such as ferromagnetic insulators [1], ultra-low magnetization damping [2], and high magneto-optical response [3], as well as strong and tunable magnetic anisotropy [4]. This work presents a combined optical and magneto-optical spectroscopic study of $Tm_3Fe_5O_{12}$ (TmIG) films on substituted gadolinium gallium garnet (sGGG) substrates, with a detailed analysis of the thickness-dependent properties. Spectroscopic ellipsometry, magneto-optical Kerr effect spectroscopy, and Raman spectroscopy results are presented for TmIG films with a thickness in the range from 20 nm to 300 nm grown on sGGG by pulsed laser deposition. The complex dielectric functions of TmIG and sGGG are determined for the first time. The magneto-optical Kerr effect (MOKE) spectra of the measured sample in the photon energy range from 1.5 eV to 5.0 eV clearly demonstrate the influence of strain in the thin films, which is induced by the lattice mismatch between the TmIG film and the sGGG substrate. The spectra reveal magneto-optical transitions between 2.5 eV and 3.5 eV which are marker spectral features for the stress in the thin films showing a blue shift with increasing film thickness. The corresponding magnetic hysteresis loops recorded using MOKE show an out-of-plane magnetic anisotropy for 50 nm and 70 nm thick films, while the 200 nm and 300 nm thick films exhibit an in-plane anisotropy. The increase in the coercive field with decreasing TmIG film thickness was associated with the stress-induced magnetoelastic anisotropy competing and eventually overcoming the shape anisotropy. In addition, spin-polarized density functional band structure calculations were performed to quantify the epitaxy-induced strain.

[1] N. Thiery et al., Phys Rev B 97, 1 (2018). [2] C. N. T. Wu et al., Sci Rep 8, 1 (2018). [3] M. Gomi et al., Jpn J Appl Phys 27, L1536 (1988). [4] S. Mokarian Zanjani et al. J Magn Magn Mater 499, 166108 (2020).

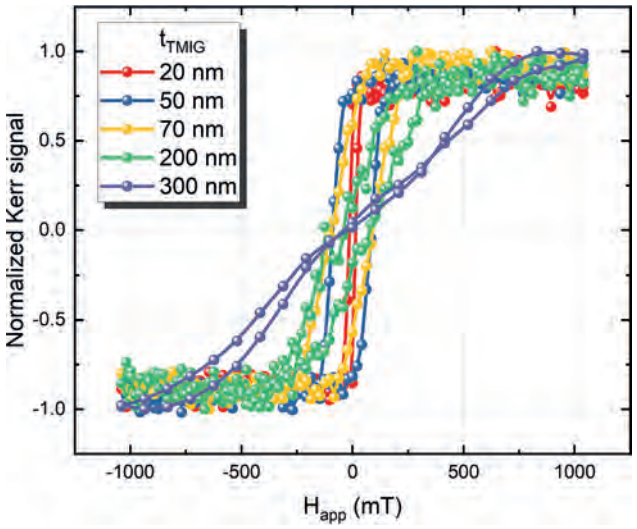

Normalized MOKE hysteresis loops measured with the magnetic field applied perpendicular to the sample surface for various thicknesses of the TmIG films, showing the transition from out-of-plane to in-plane anisotropy with the film thickness.

VP11-11. Magneto-Optic Interferometric System: exploring building blocks and subcircuits. *N. Bouda*[1], N. Prabhu Gaunkar[1], W. Theh[1] and M. Mina[1] *1. Iowa State Univeristy, Ames, IA, United States*

Recent developments in the standardization of magnetic field generators (MFG) have been considered for optical/electronic/optical industrial-scale applications. In this work, a strategy to identify all optical components that can be used to implement a broad range of functions for communications purposes. We propose a circuit design for a magneto-optic interferometric system (MOIS) based on building blocks and subcircuits consisting of an interferometer with magneto-optic phase shifters and a magnetic field generator. The paper shows the building blocks based on elementary 2x2 photonics coupling components. We demonstrate that such a design can be configured as a tunable system based on the phase shift experienced by the incoming signals from two input waveguides in their transitions The current state of the art for all-optical is very specialized devices carefully designed to implement certain functions. Each machine is designed to accomplish a specific function. They can have a high performance, such as low insertion loss and optimum power consumption, with flexibility in terms of cost. Designing for a particular part means engineering the optical device's geometry and simulation before prototyping(Fig. 2). The design cycle may take up to several months. Similar problems are also found in electronics [1-13]. Reconfigurability is a common theme in electronics systems (circuits and components). However, extending programmable systems to other systems is a question of the current time, especially to magneto-optic interferometric systems (MOIS) Fig.1 and photonics. This paper presents the key aspects of the magneto-optic interferometric system (MOIS). In the case of a single-mode system, we will show that complexity and tunability circuits for MOIS can be implemented using a set of standard building blocks, such as a resonator and transfer matrices. We briefly present the transfer matrices of the elementary building block, highlight technological issues, and revisit the critical functionalities achieved with these circuits

[1] G. Zhang, M. De Leenheer, A. Morea, and B. Mukherjee, "A survey onOFDM-based elastic core optical networking," IEEE Commun. Surveys Tuts., vol. 15, no. 1, pp. 65–87, 1st Quart., 2013 [2] N. Prabhu Gaunkar, J. Selvaraj, W.-S. Theh, R. Weber, and M. Mina, "Pulsed magnetic field generation suited for low-field unilateral nuclear magnetic resonance systems," AIP Advances, vol. 8, no. 5, p. 056814, 2018. [3] S. Kemmet, M. Mina, and R. J. Weber, "Magnetic pulse generation for high-speed magneto-optic switching," J. Appl. Phys., vol. 109, pp. 07E333–07E333-3, 201 [4] M. Acanski, J. Popovic-Gerber and J. A. Ferreira, "Comparison of Si and GaN power devices used in PV module integrated converters," *2011 IEEE Energy*

Conversion Congress and Exposition, Phoenix, AZ, 2011, pp. 1217-1223, doi: 10.1109/ECCE.2011.6063915. [5] K. Shah and K. Shenai, "Performance Evaluation of Point-of-Load Chip-Scale DC-DC Power Converters Using Silicon Power MOSFETs and GaN Power HEMTs," in 2011 IEEE Green Technologies Conference (IEEE-Green), 2011, pp. 1-5 [6] Yan, Jiabin, et al. "Complete active–passive photonic integration based on GaN-on-silicon platform." Advanced Photonics Nexus 2.4 (2023): 046003-046003. [7] C. R. Doerr, "Silicon photonic integration in telecommunications," Front. Phys. 3, 37 (2015*)* [8] Y. Ying, "Device Selection Criteria - Based on Loss Modeling and Figure of Merit", M.Sc. Thesis, Virginia Tech [9] N. Robert Bouda, N. Prabhu Gaunkar, W. Shen Theh, and M. Mina, "A typology for magnetic field generator technologies", AIP Advances 11, 015103 (2021) https://doi.org/10.1063/9.0000046 [10] J. W. Pritchard, M. Mina and R. J. Weber, "Improved Switching for Magneto-Optic Fiber-Based Technologies," in IEEE Transactions on Magnetics, vol. 48, no. 11, pp. 3772-3775, Nov. 2012, doi: 10.1109/TMAG.2012.2202275. [11] Toshiya Murai, Yuya Shoji, Nobuhiko Nishiyama, and Tetsuya Mizumoto, "Nonvolatile magneto-optical switches integrated with a magnet stripe array," Opt. Express 28, 31675-31685 (2020) [12] O. Solgaard, A. A. Godil, R. T. Howe, L. P. Lee, Y. Peter and H. Zappe, "Optical MEMS: From Micromirrors to Complex Systems," in *Journal of Microelectromechanical Systems*, vol. 23, no. 3, pp. 517-538, June 2014, doi: 10.1109/JMEMS.2014.2319266.

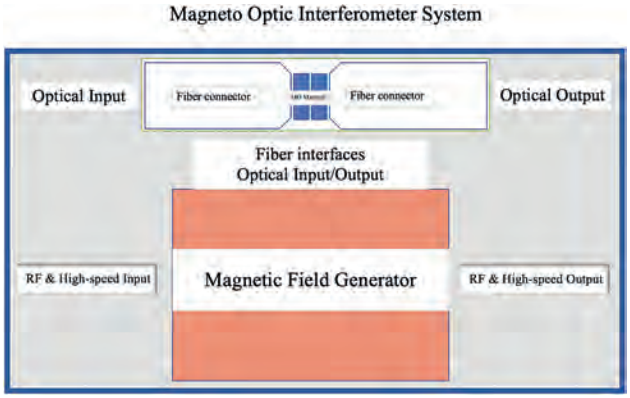

Fig.1 Magneto Optic Interferometer System (MOIS)

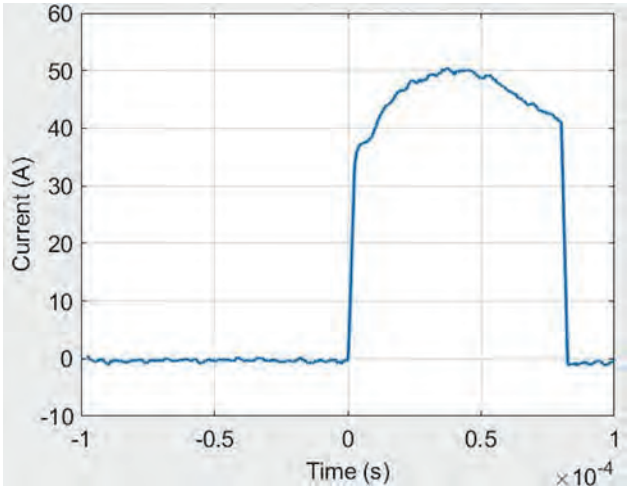

Fig. 2 Current of Magneto Optic Interferometer System (MOIS)

VP11-12. Withdrawn

VP11-13. Impact of nitrogen on large charge-to-spin conversion efficiency in a non-collinear antiperovskite Mn_3PtN antiferromagnet.

N. Tripathi[1], S. Mishra[1], *S. Isogami*[2] and Y. Takahashi[2] *1. School of Materials Science & Technology, Indian Institute of Technology (BHU), Varanasi, India; 2. Research Center for Magnetics and Spintronics Materials, National Institute of Materials Science, Tsukuba, Japan*

Elemental doping and/or alloying of light elements to ordinary metallic compounds have attracted attention in the field of recent spintronic materials.[1] For example, carbon greatly boosts the anomalous Hall conductivity of CoMn thin films[2], and boron modulates the spin structures and inter-band optical transitions of the host Mn_4N thin films[3] In order to explore the impact of nitrogen on charge-to-spin conversion efficiency, in this study we compared the spin-Hall angle (SHA) evaluated in the existing Mn_3Pt/CoFeB[4,5] and Mn_3PtN/CoFeB bilayer systems, which has not been reported to date. The Mn_3PtN compound is predicted to be one of the non-collinear antiferromagnets with Berry curvatures from Weyl points near the Fermi level,[6] promising large anomalous Hall conductivity. The multilayered samples with Mn_3PtN (t=5,7,10 nm)/CoFeB (3nm)/MgO (3nm) were deposited on MgO (001) substrates using the DC/RF magnetron sputtering systems. Figure 1 shows the V_{mix} line shape in the spin-orbit torque ferromagnetic resonance (ST-FMR) at fixed RF frequency 7 GHz, by scanning the in-plane dc external magnetic field H_{ext} at angle φ (typically 45°). Figure 2 significantly represents the thickness-dependent spin Hall angle, we observed a significant ten-fold higher SHA, which surpasses the performance of the controlled Mn_3Pt/CoFeB samples; therefore, the presence of N_2 would lead to higher efficient charge-to-spin conversion. While the strength of the damping-like field of the epitaxial samples is greater than that of the controlled Mn_3Pt/CoFeB samples, determined by the second harmonic Hall measurement provides qualitative support for the ST-FMR conclusion. One of the possible origins for the enhancement of SHA could be the electronic structures induced by the presence of nitrogen. In addition, the influences of crystal structures and surface morphologies on SHA will be discussed at the conference.

[1] Shinji Isogami and Yukiko K. Takahashi, Adv. Electron. Mater. 9, 2200515 (2023). [2] Shinji Isogami, Mitsuru Ohtake, Yukiko K. Takahashi, J. Appl. Phys. 131, 073904 (2022). [3] Jing Zhou, Xinyu Shu, Yaohua Liu, Phys. Rev. B 101, 184403 (2020). [4] H. Bai, X. F. Zhou, H. W. Zhang, Phys. Rev. B 104, 104401 (2021). [5] Yu-Xuan Wang, Wei-Chun Hung, Wei-Chieh Hung, Appl. Phys. Express 15, 033002 (2022). [6] Vu Thi Ngoc Huyen, Michi-To Suzuki, Kunihiko Yamauchi, Phys. Rev. B 100, 094426 (2019).

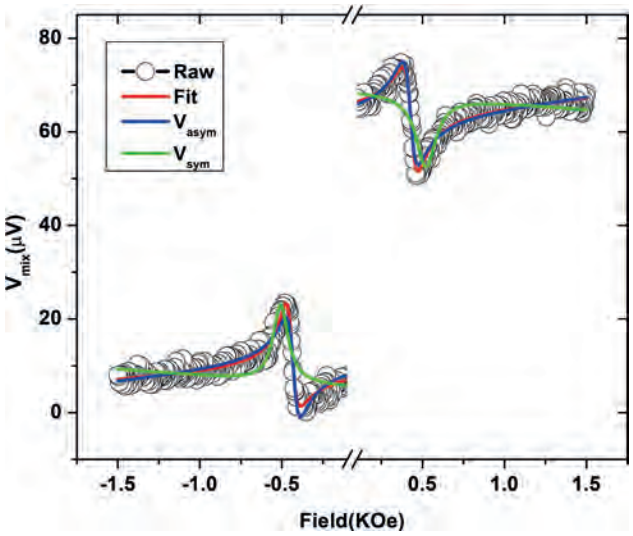

Fig. 1. Line shapes (V_{mix}) of the spin-orbit torque ferromagnetic resonance (ST-FMR) for the samples, Mn_3PtN (10)/CoFeB (3)/MgO (3) (in nm).

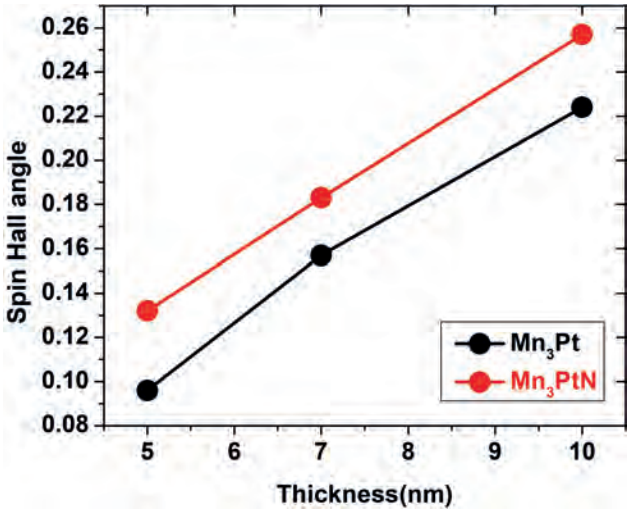

Fig. 2. Spin-Hall angle as a function of the thickness of Mn_3Pt and Mn_3PtN films.

VIRTUAL PLATFORM ONLY

Session VP12
SENSORS, HIGH FREQUENCY DEVICES, AND POWER DEVICES (VIRTUAL)
(Poster Virtual Session)

Sho Muroga, Co-Chair
Akita University, Akita, Japan
Connor Shane Smith, Co-Chair
U.S. Naval Academy, Annapolis, MD, United States

VP12-01. Measurement and Modeling of the Residual Flux in the Single-Phase Three-Limb Transformer. Y. Wang[1], *Y. Ren*[1] and C. Liu[1]
1. Hebei University of Technology, Tianjin, China

I Introduction Residual flux density (B_r) causes an inrush current when transformers are re-energized, leading to winding deformation, current imbalance and failure of the protection function [1]. The precise measurement of B_r is crucial to suppressing the generation of the inrush current. Existing measurement methods have rarely been studied for the widely used single-phase three-limb transformers. In this paper, a novel method for measuring and modeling the B_r of single-phase three-limb transformers is proposed, which can measure the distribution of the B_r in various parts of the transformer core. II Methodology and modeling The structure of the magnetic domains in the core varies with different B_r. When the same voltage excitation is applied to the transformer winding, the response current waveform will be influenced by the B_r in the transformer core. The response current waveform is shown in Fig. 1. Compared to the response current without B_r, the greater deviations in waveforms, the larger B_r in the core. Based on the difference between response current waveforms, the B_r can be determined by the Pearson correlation coefficient. The relationship between B_r and the response current is established by using the field-circuit coupling method. Unlike the core-type transformer, the single-phase three-limb transformer has two magnetic circuits. For the response current, the B_r in the core and the yoke are co-determinants. In order to improve the accuracy of simulating calculation, the local DC magnetization curve at the B_r is measured and adopted. The material properties of the core column and yoke are properly set according to the corresponding B_r. Then the fitted model for calculating B_r is obtained based on simulation results. III Conclusion The experiment is conducted on the 10 kV, 250 kVA single-phase three-limb power transformer, as shown in Fig. 2. The maximum measurement error does not exceed 6.02%, proving the validity and accuracy of the proposed method. The method is suitable for all single-phase transformers, providing valuable information for suppressing the inrush current.

[1]Y. Z. Gerdroodbari, M. Davarpanah, and S. Farhangi, "Remanent Flux Negative Effects on Transformer Diagnostic Test Results and a Novel Approach for Its Elimination," IEEE Transactions on Power Delivery., Vol. 33, no. 6, pp. 2938–2945 (2018)

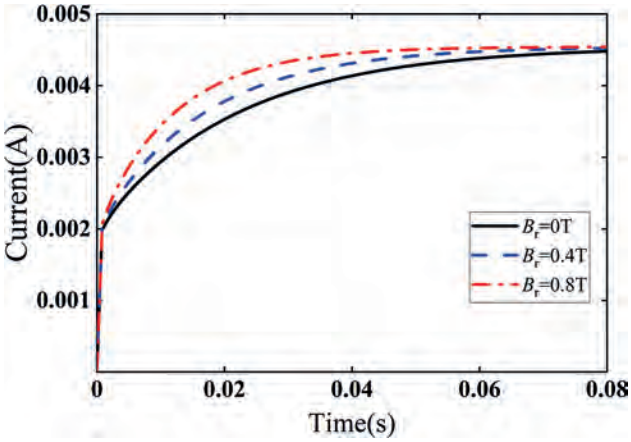

Fig. 1 The response current waveform under different residual flux density

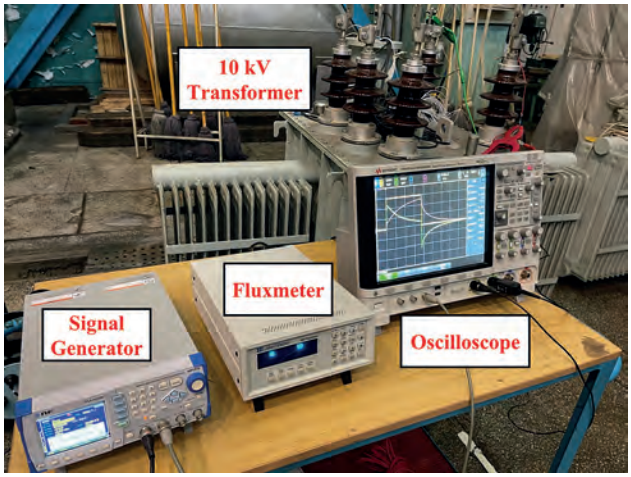

Fig. 2 The experimental platform on the 10 kV transformer

VP12-02. Research on the simulation accuracy of static hysteresis loops of non-oriented silicon steels using a simplified LLG equation. L. Chen[1], Y. Li[1], *T. Ben*[1], Z. Zhang[1] and L. Jing[1] *1. College of Electrical Engineering and New Energy, China Three Gorges University, Yichang, China*

Introduction Establishing an accurate hysteresis model is significant for predicting the loss of electrical equipment. Currently, most hysteresis models widely used are macroscopic phenomenological models, which lack research on the magnetization mechanism for the material[1]. Based on the micromagnetic Landau-Lifshitz-Gilbert (LLG) equation, a simplified meso-scale model for simulating the DC hysteresis characteristics of electrical steels is presented[2]. However, the simulation accuracy of this model is relatively poor for the hysteresis loops in the region of demagnetization

and low magnetic flux densities. To solve this problem, a modification of the simplified LLG equation model is proposed by introducing a hysteresis energy density function to improve the global hysteresis simulation ability of non-oriented(NO) electrical steel. Method and Discussion To improve the calculation accuracy for all flux density levels, a hysteresis energy density function is introduced, which considers the domain wall's movement, and the domain's volume fraction followed by the Boltzmann distribution, as shown in Fig.1(a). The total magnetization can be calculated as the sum of the hysteresis magnetization and the magnetization of the simplified LLG equation. To get the parameters of the modified model, five quasi-static hysteresis loops are measured by a one-dimensional measurement system based on the Epstein Frame, as shown in Fig.1(b). The trend of parameter changes with magnetic density is shown in Figure 2(a) to(d). To verify the validity of the improved model, the calculated results were compared with the experimental data. The simulation accuracy of the proposed model is better in the demagnetization region at high magnetic densities and low magnetic densities. Conclusion In this paper, a modification of the simplified LLG equation is proposed to simulate global static hysteresis properties of NO electrical steels. The obtained results show that the proposed model can accurately simulate the static hysteresis loops of NO electrical steels in high and low magnetic flux density regions.

[1] R. Zeinali, D. C. J. Krop, and E. A. Lomonova, IEEE Transactions on Magnetics, Vol. 56, no. 1, 6700904 (2020). [2] Y.Hane, K.Nakamura, and T.Ohinata, IEEE Transactions on Magnetics, Vol. 55, no. 7, 8401306 (2019).

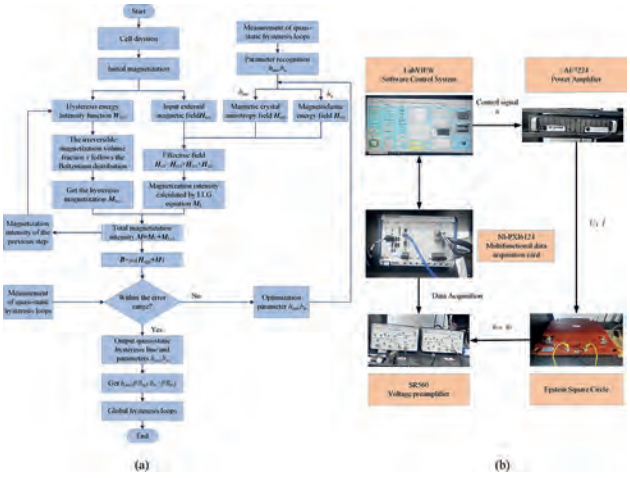

Fig.1. (a) Calculation process of the proposed model. (b) Measuring systems for NO electrical steels

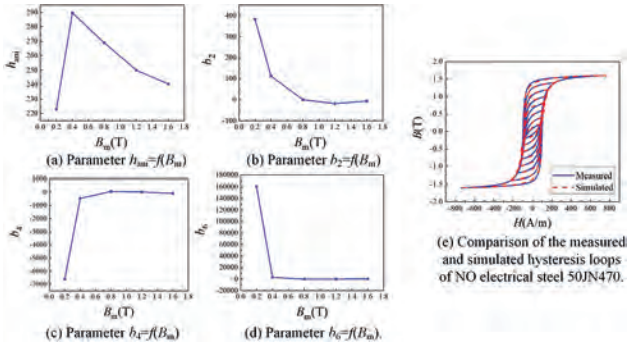

Fig.2. Calculation results of the model

VP12-03. Withdrawn

VP12-04. Residual Flux Density Estimation of the Three-Phase Transformer using BP Neural Network. Y. Wang[1], *Y. Ren*[1] and C. Liu[1]
1. Hebei University of Technology, Tianjin, China

I Introduction As crucial electrical equipment, the safe operation of transformers concerns the security of the power grid. The generation of inrush current during transformer re-energizing is a long-standing problem [1]. To weaken the adverse effects of inrush current, measuring the residual flux density (B_r) is necessary. The voltage integration method is a widely used B_r measurement method. However, the magnetic viscosity phenomenon proves that the magnetic domain structure changes irregularly with time [2]. Therefore, the test results are not reliable. Due to the limitations of existing research, there is an urgent need for an accurate method of measuring B_r in three-phase transformers. A novel approach is proposed in this paper to measure the B_r distribution of three-phase transformers accurately. II Measuring method The B_r measurement of a three-phase transformer is divided into two steps. First, the B_r direction in each core column can be measured by applying positive and negative DC voltage to different windings respectively. The B_r in each core column collectively affects the response current. According to the change rate of the response current waveform, the B_r direction of each phase can be determined. The next step is to assess the magnitude of the B_r. The implementation of the proposed measurement method is shown in Fig. 1. The three-phase transformer is first simulated using the finite element method (FEM), and BP neural network is trained based on FEM results. A positive DC voltage is then applied to each winding simultaneously. The response current of three-phase windings are measured and the eigenvalues are extracted. Measured current eigenvalues are inputted into the trained BP neural network, and the B_r of each phase is calculated. III Experimental results and conclusion The experiment was conducted on a three-phase transformer. The built measurement platform is shown in Fig. 2. The experiment results show that the proposed method can accurately measure B_r within an error of 5.2%, proving the validity and accuracy of the proposed method.

[1]F. de Leon, A. Farazmand, and S. Jazebi, "Elimination of Residual Flux in Transformers by the Application of an Alternating Polarity DC Voltage Source," IEEE Transactions on Power Delivery., Vol. 30, no. 4, pp. 1727–1734 (2015) [2]N. Abeywickrama, Y. V. Serdyuk, and S. M. Gubanski, "Effect of Core Magnetization on Frequency Response Analysis (FRA) of Power Transformers," IEEE Transactions on Power Delivery., Vol. 23, no. 3, pp. 1432–1438 (2008)

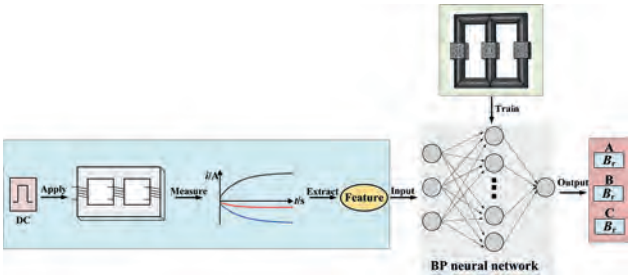

Fig. 1 The schematic diagram of measurement steps

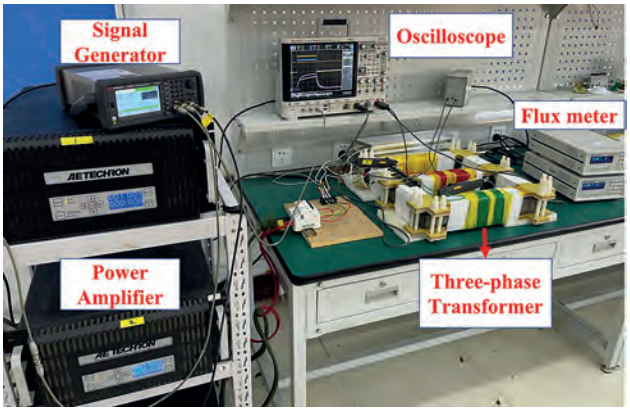

Fig. 2 The experimental platform of three-phase transformers

VP12-05. Investigation of the Over-Load Unintentional Remagnetization Effect in Series Hybrid Magnet Variable Flux Memory Machine. *R. Tu*[1], H. Yang[1], H. Zheng[2] and H. Lin[1] *1. Southeast University, Nanjing, China; 2. Huawei Technologies Company Ltd., Shanghai, China*

I. Introduction Variable flux memory machines (VFMMs) [1]-[4] using low coercive force (LCF) permanent magnets (PMs) have been extensively investigated. A series hybrid magnet VFMM (SHM-VFMM) with high coercive force (HCF) and LCF PMs is proposed in [2], featuring large flux regulation range and high efficiency. It is widely acknowledged that over-load currents may cause unintentional demagnetization. However, over-load unintentional remagnetization (UR) is also found in the SHM-VFMM. In this paper, the over-load UR effect and its mechanism are investigated. II. Investigation of Over-Load Unintentional Remagnetization Effect The machine topology is shown in Fig. 1 (a). To analyze the UR effect, the machine is initially set under the flux-weakened state, and then three periods including no-load, over-load and no-load operations are successively conducted. The back-EMF and LCF PM flux density are shown in Fig. 1 (b). The back-EMF has a 16% increase, and partial remagnetization happens in the LCF PMs, indicating that UR effect exists during over-load operation. The frozen permeability (FP) analysis [5] is applied to study the mechanism of this effect. Fig. 2 (a) shows the magnetic field with only over-load current. Due to the absence of HCF PMs, parts of the LCF PMs are demagnetized. Figs. 2 (b) shows the magnetic field of both over-load current and HCF PMs. The magnetic fields of the over-load current are pushed by the HCF PMs to the other parts of the LCF PMs, leading to UR effect. As shown in Figs. 2 (c), both PM flux linkages and LCF PM magnetization ratios increase with *q*-axis currents, indicating that magnetic cross-coupling [6] happens. III. Experimental Validation Fig. 2 (d) shows the SHM-VFMM prototype. The open-circuit back-EMFs under the flux-enhanced and -weakened states are shown in Fig. 2 (e). The test results agree well with the finite element (FE) results. The detailed UR mechanism, analyses and test results will be given in the full paper.

[1] V. Ostovic, "Memory motors," *IEEE Ind. Appl. Mag*., vol. 9, no. 1, pp. 52-61, Jan./Feb. 2003. [2] H. Yang, H. Zheng, H. Lin, Z. Q. Zhu and S. Lyu, "A novel variable flux dual-layer hybrid magnet memory machine with bypass airspace barriers," in 2019 *IEEE Int. Electric Machines & Drives Conf. (IEMDC)*, pp. 2259-2264. 2019. [3] Hui Yang, Xiaomin Chen, Heyun Lin, Z. Q. Zhu, and Shukang Lyu, "On-load demagnetization effect of high-coercive-force PMs in switched flux hybrid magnet memory machine", *AIP Advances*, vol. 9, no. 12, Article No. 125152, 2019. [4] R. Tsunata, M. Takemoto, S. Ogasawara and K. Orikawa, "Variable flux memory motor employing double-layer delta-type PM arrangement and large flux barrier for traction applications," *IEEE Trans. Ind. Appl*., vol. 57, no. 4, pp. 3545-3561, July-Aug. 2021. [5] W. Q. Chu and Z. Q. Zhu, "Average torque separation in permanent magnet synchronous machines using frozen permeability," *IEEE Trans. Magn*., vol. 49, no. 3, pp. 1202-1210, March 2013. [6] G. Qi, J. T. Chen, Z. Q. Zhu, D. Howe, L. B. Zhou and C. L. Gu, "Influence of skew and cross-coupling on d- and q-axis inductances and flux-weakening performance of PM brushless AC machines," in 2008 *Int. Conf. Electric. Machines & Syst. (ICEMS)*, Wuhan, China, 2008, pp. 2854-2859.

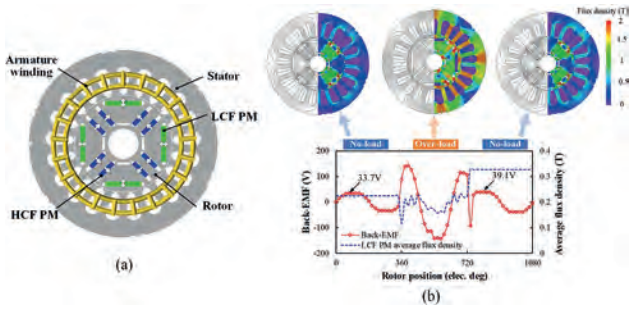

Fig. 1. (a) Topology. (b) Back-EMF and flux density.

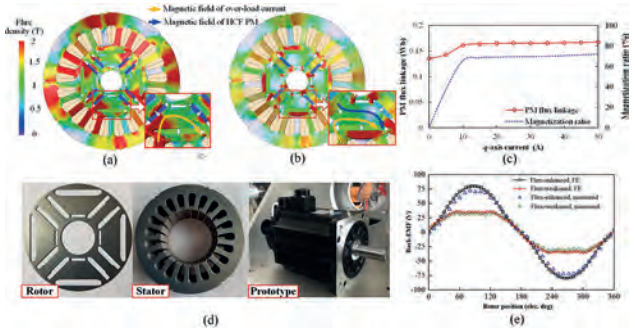

Fig. 2. (a) Magnetic field of over-load current. (b) Magnetic field of over-load current and HCF PMs. (c) PM flux linkages and magnetization ratios versus *q*-axis currents. (d) Prototype. (e) FE and tested back-EMFs.

VP12-06. Investigation on Sensorless Operation of Two New Fault-Tolerant Interior Permanent Magnet Motors from Perspective of Flux-Intensifying Effect. L. Zhang[1], *S. Deng*[1], X. Zhu[1] and Z. Xiang[1] *1. Jiangsu University, Zhen Jiang City, China*

Owing to the advantages of high-power density, high efficiency, and good fault tolerance, the fault-tolerant interior permanent magnet (FT-IPM) motor is favored for high-reliability applications [1]. To further improve the reliability of the motor system, sensorless control technologies were employed in the FT-IPM motor drive [2]. Most previous studies regarding FT-IPM motors aim to improve fault-tolerant capability but suffer the saliency characteristic problem, which is unfavorable for sensorless control. In [3], to improve the sensorless operation capability, the design idea of flux-intensifying effect was innovatively proposed. Typically, for FT-IPM motors, the fractional slot concentrated-windings (FSCWs) is applied to improve fault tolerance [4]. Yet, the use of FSCWs will increase the cross-axis magnetic circuit coupling, which results in a great challenge to achieving obvious inverse saliency. Thus, how to improve the sensorless operating capacity needs to be solved urgently under the premise of ensuring good fault-tolerant capacity. Inspired by this, two new five-phase FT-IPM motors are developed and compared from perspective of flux-intensifying effect. Fig. 1 shows the configuration of the two proposed motors. The cross-section of the partial rotors, with different rotor structures and slot-pole combinations, are presented in Fig. 2. Then, the proposed motors are compared comprehensively from the aspects of inductance characteristics, fault-tolerant performances, and back-EMF, respectively. Fig. 3 shows *d*- and *q*-axis inductance characteristics of two motors vary with *q*-axis current, showing the

flux-intensifying effect. To illustrate the fault-tolerant capacity, Fig. 4 illustrates the winding inductances of phase A. Fig. 5 compares the current responses of the two motors under phase-A short-circuit condition. Finally, Fig. 6 displays the experimental no-load back-EMF waveforms of both prototypes at rated speed, which verifies the effectiveness of the proposed FT-IPM motors with flux-intensifying effect design. More details about the fault-tolerance and sensorless operating performances of two motors with different features analyzed and experimental verification will be presented in the full paper.

[1] L. Zhang, X. Zhu, and L. Xu, *IEEE Trans. Ind. Electron.*, vol. 69, no. 7, pp. 6688-6699, (2022). [2] L. Zhang, Y. Fan, and C. Li, *IEEE Trans. Energy Convers.*, vol. 33, no. 1, pp. 87–95, (2018). [3] N. Limsuwan, Y. Shibukawa, and D. D. Reigosa, *IEEE Trans. Ind. Appl.*, vol. 47, no. 5, pp. 2004-2012 (2011). [4] Y. Fan, R. Cui, and A. Zhang, *IEEE Trans. Veh. Technol.*, vol. 69, no. 1, pp. 282-292, (2020).

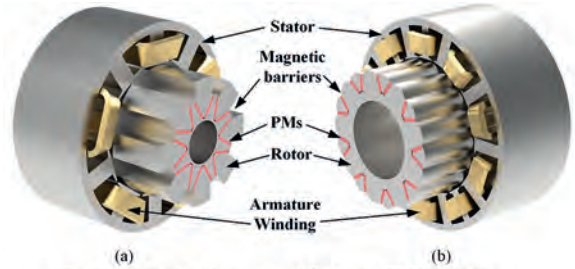

Fig. 1 Configuration of the proposed five-phase FT-IPM motors with flux-intensifying effect. (a) 10s-8p. (b)20s-18p.

Fig. 2. Cross section of partial rotor. (a) 10s-8p. (b)20s-18p.

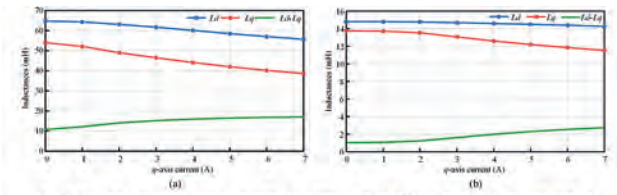

Fig. 3 *d*- and *q*-axis inductance characteristics vary with *q*-axis current. (a) 10s-8p FT-IPM motor with flux-intensifying effect. (b) 20s-18p FT-IPM motor with flux-intensifying effect.

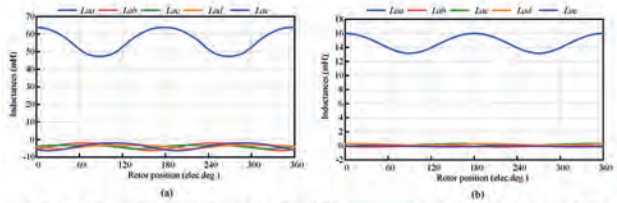

Fig. 4. No-load inductances of phase A. (a) 10s-8p FT-IPM motor with flux-intensifying effect. (b) 20s-18p FT-IPM motor with flux-intensifying effect.

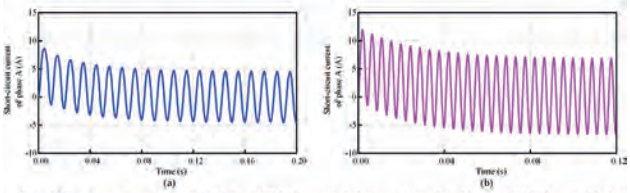

Fig. 5. Short-circuit current of phase A. (a) 10s-8p FT-IPM motor with flux-intensifying effect. (b) 20s-18p FT-IPM motor with flux-intensifying effect.

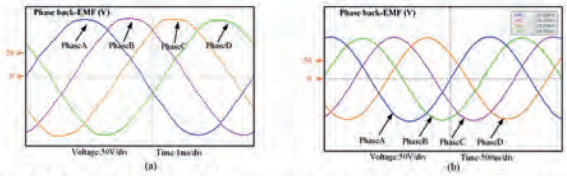

Fig. 6. Back EMFs. (a) 10s-8p FT-IPM motor with flux-intensifying effect. (b) 20s-18p FT-IPM motor with flux-intensifying effect.

VP12-07. A Saliency Ratio-Changeable Variable-Flux Permanent-Magnet Synchronous Machine for Performance Improvement in Overall Operating Region. *S. Zhang*[1], F. Wang[1], H. Zhao[1] and P. Zheng[2]
1. College of Marine Electrical Engineering, Dalian Maritime University, Dalian, China; 2. School of Electrical Engineering and Automation, Harbin Institute of Technology, Harbin, China

By partially substituting high-coercive-force (HCF) magnets in conventional permanent-magnet synchronous machines (PMSMs) with low-coercive-force (LCF) magnets, the controllable PM flux linkage can be obtained, known as variable-flux PMSMs (VF-PMSMs). By adjusting the magnetization state of the LCF magnet, the speed range of the VF-PMSM can be extended [1]. However, the reluctance torque is generated by negative *d*-axis current which exerting a demagnetizing MMF on the LCF magnet, and therefore the working point of the LCF magnets are not stable in heavy load condition. This paper presents a saliency ratio-changeable VF-PMSM (SRC-VF-PMSM) which is capable of changing the saliency ratio, and the machine can operate under most conditions by selecting magnetization state and suitable saliency type. The topology of the machine is shown in Fig.1. One V-type PM pole consists of a piece of HCF magnet and a piece of LCF magnet. In the positive saliency ratio state which implies that $L_q > L_d$, the magnetization directions of the HCF magnet and LCF magnet are shown in Fig. 1(a). The *d*-axis is the symmetry axis of the V-shape PM pole. When the LCF magnets are magnetized reversely, the rotor pole will be composed of the HCF magnet and the LCF magnet in the adjacent pole originally. Consequently, the *d*- and *q*-axis are interchanged with each other as shown in Fig. 1(b), and it can be found that $L_q < L_d$ in this case, namely negative saliency ratio state. The magnetic field distribution is shown in Fig. 2, it can be observed that positions of *d*- and *q*-axis are switched. The SRC-VF-PMSM can operate in negative saliency ratio state to produce reluctance torque with positive *d*-axis current and resist unintentional demagnetization. In high

speed operation, the SRC-VF-PMSM switches to positive saliency ratio state, which can further extend speed range with negative *d*-axis current. The re/demagnetization process and electromagnetic performance are investigated. The saliency types under different magnetization states are analyzed. The efficiency maps show that the SRC-VF-PMSM can operate over a wide speed range with high efficiency.

H. Yang, W. Liu, H. Zheng *et al.*, "A Novel Delta-Type Hybrid-Magnetic-Circuit Variable Flux Memory Machine for Electrified Vehicle Applications," *IEEE Trans. Transp. Electr.*, 8, 3512-3523 (2022).

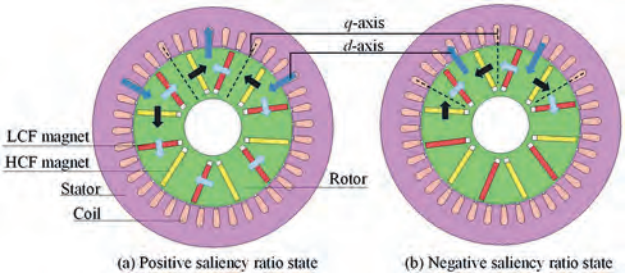

Fig. 1. The topology of the SRC-VF-PMSM

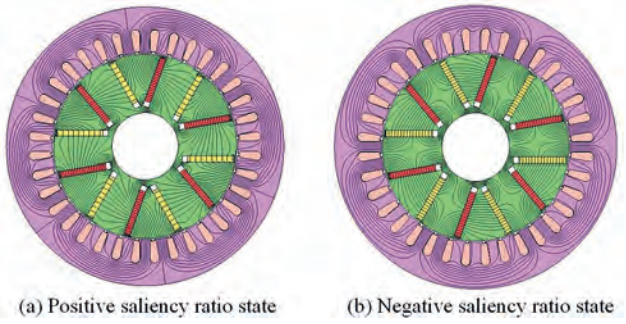

Fig. 2. The magnetic field distribution of the SRC-VF-PMSM

VP12-08. Design strategies for enhancing magnetic field generators for optical switching applications. *N. Bouda*[1], N. Prabhu Gaunkar[1], W. Theh[1] and M. Mina[1] *1. Iowa StateUniveristy, Ames, IA, United States*

Widespread adoption of Magnetic Field Generators (MFG) will require most electro-optical systems to incorporate high current devices, thereby demanding a decrease in power consumption due to loss reduction. Recent progress in magnetic field generator typologies has shown ways of reducing form factor while meeting better performance in terms of max current and magnetic field level based on selected transistor technologies. However, developments in the standardization of MFGs need to be considered for optoelectronic industrial-scale applications. This work describes a strategy for identifying the optimum condition for a high magnetic field, form factors contributing to power consumption, and the feasibility of such electro-optical systems. Magnetic Field Generator (MFG) devices have been in use for several years in various industries. [1-8]. In each industry, MFG aims to deliver a certain amount of current/power to the system (load) while minimizing system power consumption. Designing for maximum efficiency, means obtaining the highest output for a given input. One of the purposes of a MFG is the energy conversion. Considering a magneto optical interferometer where the phase shift caused an interference by magnetization of magneto optical material. The magnetic field generator (MFG) system based on MOSFET as switching device controls the magnetization of the magneto optic (MO) material. The magnetic field strength, conversion efficiency, non-linearity and/or linearity are the common characteristics, and they can be quantified. For a better understanding of the factors impacting efficiency and power loss, an analytical representation of the MFG is needed. The efficiency and power loss can be approximated based on an electronic analytical loss model. Power losses in MFGs consist of conduction loss and switching loss (Fig. 2). For an efficient MFG, it is critical to have devices with low switching and conduction losses. This paper describes the fundamental operation of an MFG and investigates the switching losses, energy losses and conduction losses in the various components of the system. The analysis is performed using an MFG systems (see Fig.1).

[1] G. Zhang, M. De Leenheer, A. Morea, and B. Mukherjee, "A survey onOFDM-based elastic core optical networking," IEEE Commun. Surveys Tuts., vol. 15, no. 1, pp. 65–87, 1st Quart., 2013 [2] N. Prabhu Gaunkar, J. Selvaraj, W.-S. Theh, R. Weber, and M. Mina, "Pulsed magnetic field generation suited for low-field unilateral nuclear magnetic resonance systems," AIP Advances, vol. 8, no. 5, p. 056814, 2018. [3] A. Lidow, "Is it the end of the road for silicon in power conversion?" 2010 6th International Conference on Integrated Power Electronics Systems, Nuremberg, 2010, pp. 1-8. [4] Taichi Goto, Ryohei Morimoto, John W. Pritchard, Mani Mina, Hiroyuki Takagi, Yuichi Nakamura, Pang Boey Lim, Takunori Taira, and M. Inoue, "Magneto-optical Q-switching using magnetic garnet film with micromagnetic domains," Opt. Express 24, 17635-17643 (2016). [5] M. Acanski, J. Popovic-Gerber and J. A. Ferreira, "Comparison of Si and GaN power devices used in PV module integrated converters," *2011 IEEE Energy Conversion Congress and Exposition*, Phoenix, AZ, 2011, pp. 1217-1223, doi: 10.1109/ECCE.2011.6063915. [6] Michael R. Watts, Jie Sun, Christopher DeRose, Douglas C. Trotter, Ralph W. Young, and Gregory N. Nielson, "Adiabatic thermo-optic Mach–Zehnder switch," Opt. Lett. 38, 733-735 (2013). [7] A. Ribeiro, A. Ruocco, L. Vanacker and W. Bogaerts, "Demonstration of a 4 × 4-port self-configuring universal linear optical component," 2016 Progress in Electromagnetic Research Symposium (PIERS), Shanghai, China, 2016, pp. 3372-3375, doi:10.1109/PIERS.2016.7735319. [8] N. Robert Bouda, N. Prabhu Gaunkar, W. Shen Theh, and M. Mina, "A typology for magnetic field generator technologies," AIP Advances 11, 015103 (2021) https://doi.org/10.1063/9.0000046.

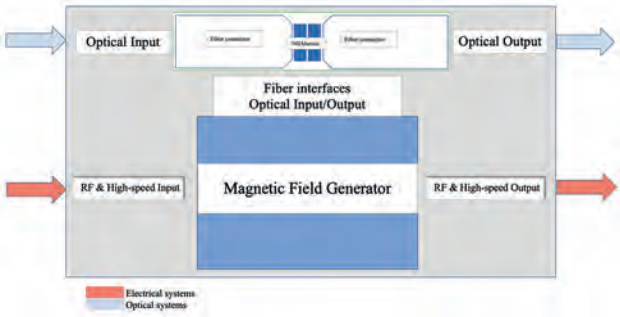

Fig. 1 Input and output Magnetic field generator

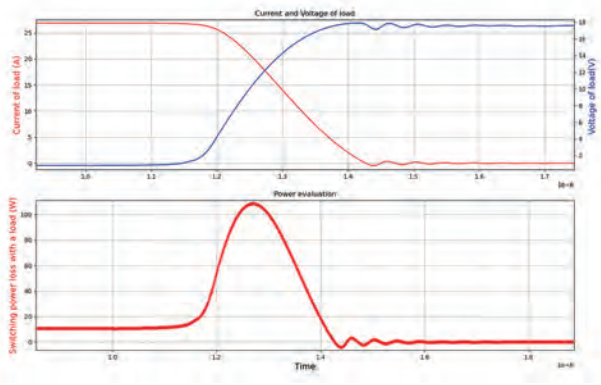

Fig. 2 Switching evaluation

VP12-09. Design and Investigation of Hybrid-Tooth Dual-Winding Vernier Permanent Magnet Motor with Improved Torque Performances. *D. Fan*[1], W. Shan[1] and X. Zhu[1] *1. School of electrical and information engineering, Jiangsu University, Zhenjiang, China*

Recently, split-tooth vernier permanent magnet (ST-VPM) motors have attracted considerable attention, due to their inherent advantages of high torque density [1]. In this kind of motors, owing to the split-tooth stator structure, motor end winding is reduced, so decreased motor loss and increased efficiency can be realized [2]. However, the split-tooth structure often results in unavoidable flux leakage and magnetic saturation, which limit further enhancement of torque performances. Thus, it has been a hot but challenging issue on how to further improve torque performances of ST-VPM motors. In this paper, a hybrid-tooth dual-winding vernier permanent magnet (HTDW-VPM) motor structure is proposed. The contribution of the proposed motor is presented as follows. Firstly, design principle of hybrid-tooth, which includes split-tooth and straight-tooth, is introduced, which reduces flux leakage and improves torque. In addition, with the assistance of the dual-winding configuration, flux harmonics of different pole pairs can be utilized to contribute to motor output torque. Furthermore, by the purposeful control of inner and outer windings, HTDW-VPM motor can operate during operation modes, which lays a foundation for multi-mode operation. Fig. 1(a) illustrates the structures of the proposed HTDW-VPM motor and the referenced ST-VPM motor. Fig. 1(b) compares the air gap magnetic density and corresponding harmonics distributions. It is observed that the amplitudes of key airgap flux harmonics of the proposed HTDW-VPM motor are higher than the referenced ST-VPM motor. To improve the torque performances of the HTDW-VPM motor, influences of the pole shoe width of both split-tooth and straight tooth are investigated based on the response surface method, as shown in Fig. 1(c). Fig. 2(a) presents flux density and magnetic density distributions of two motors. Fig. 2(b) demonstrates the electromagnetic performance of the two motors under both no-load and load conditions. It is indicated that motor torque is increased by 14.1% and torque ripple is reduced by 71.8% which verifies the reasonability of the proposed HTDW-VPM motor. More simulation and experimental results will be presented in the full paper.

[1] H. Qu and Z. Q. Zhu, "Analysis of Split-Tooth Stator Slot PM Machine," *IEEE Transactions on Industrial Electronics*, vol. 68, no. 11, pp. 10580-10591, Nov. 2021, doi: 10.1109/TIE.2020.3031535. [2] L. Fang, D. Li, X. Ren, and R. Qu, "A Novel Permanent Magnet Vernier Machine With Coding-Shaped Tooth," *IEEE Transactions on Industrial Electronics*, vol. 69, no. 6, pp. 6058-6068, June 2022, doi: 10.1109/TIE.2021.3088331.

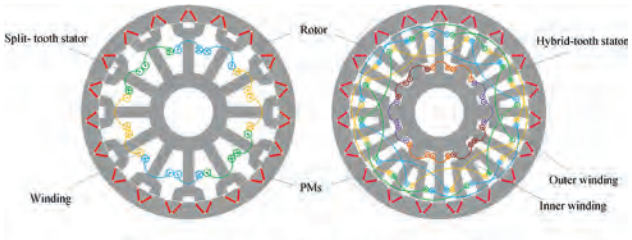

(a) The topological structure of the ST-VPM motor and the HTDW-VPM motor.

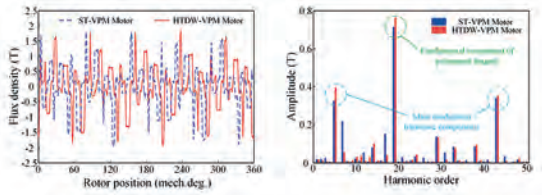

(b) Air gap magnetic density and harmonic analysis

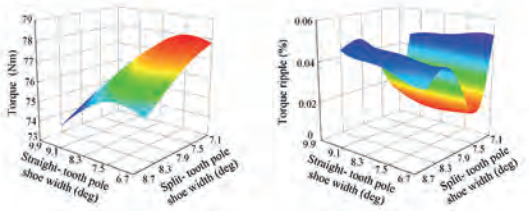

(c) The relationship between width of pole shoes and torque performance

Fig. 1. Motor structure, magnetic density analysis and the influence of parameters on torque performance.

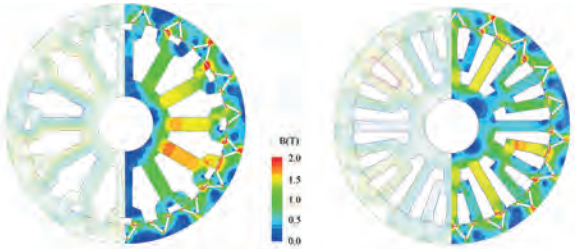

(a) Flux density and magnetic density clouds of ST-VPM motor and HTDW-VPM motor.

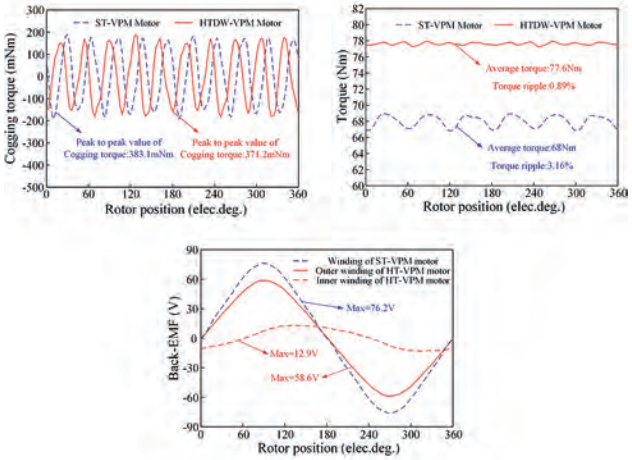

(b) Motor performance under no-load and load conditions.

Fig. 2. Comparison of electromagnetic performance of motors.

VP12-10. Comparison and Research on Load Characteristics of PM in Different Permanent Magnet Synchronous Machines. P. Zheng[1], *X. Liang*[1], M. Wang[1], J. Gao[1] and W. Li[1] *1. School of Electrical Engineering and Automation, Harbin Institute of Technology, Harbin, China*

The use of high-energy-product permanent magnets (PMs) in permanent magnet synchronous machine (PMSM) results in higher torque-density and power-density than other types of machines. However, PM have different load characteristics under different excitations, which can affect the performance of PMSM, especially with the issue of demagnetization. Many studies have been conducted to analyze the load characteristics of PM for the above issues [1]. Due to differences in the inductance and PM distribution, they are mainly divided into two categories: interior PM synchronous machine (IPMSM) and surface PM synchronous machine (SPMSM). Based on the differences of load characteristic between IPMSM and SPMSM, it is possible to design machines more efficiently according to different requirements. The load characteristics of PMSMs are the expression of the material properties of the PM in different structures of machine. The characteristics of NdFeB is shown in Fig. 1a. High-performance machines operate in high-temperature state commonly, so studying the load characteristics of PM to avoid demagnetization is necessary. The characteristics of demagnetization path in IPMSM and SPMSM are different under different magnetic fields of armature, as shown in Fig. 1b. The two types of 4P24S machines under different magnetic fields are shown in Fig. 2, and the electrical density(A/mm^2) is in parentheses. Under rated excitation(8), the PM demagnetization area of SPMSM is larger, while IPMSM only exhibits insignificant demagnetization in the middle of the V-shaped PM. Under high loads(14), the demagnetization area of SPMSM does not change much, but the PM of IPMSM is almost completely demagnetized. The different load characteristics depend on the different distributions of magnetic material such as PM, and armature magnetic field. By studying the above issues, the design of high-performance and high-stability machines can be completed more efficiently.

[1] H. Chen, R. Qu and J. Li, et al., "Demagnetization Performance of a 7 MW Interior Permanent Magnet Wind Generator With Fractional-Slot Concentrated Windings," IEEE Transactions on Magnetics., vol. 51, no. 11, pp. 1-4 (2015)

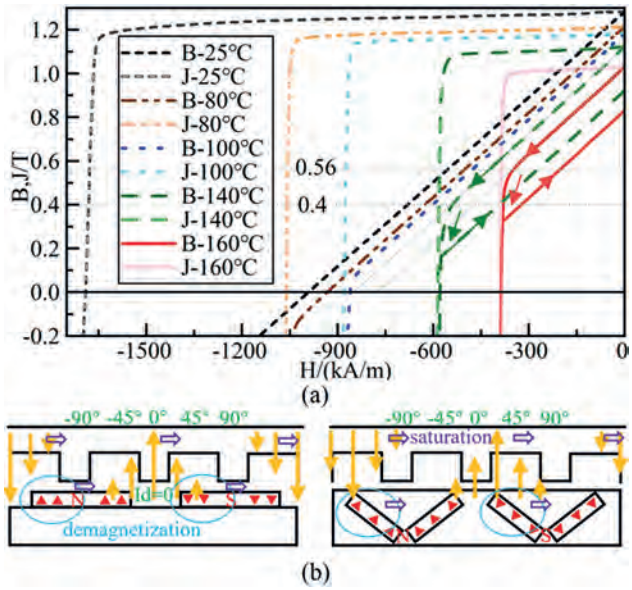

Fig.1. PM and Demagnetization.(a)Characteristic of N38SH,(b)PM on load in SPMSM and IPMSM.

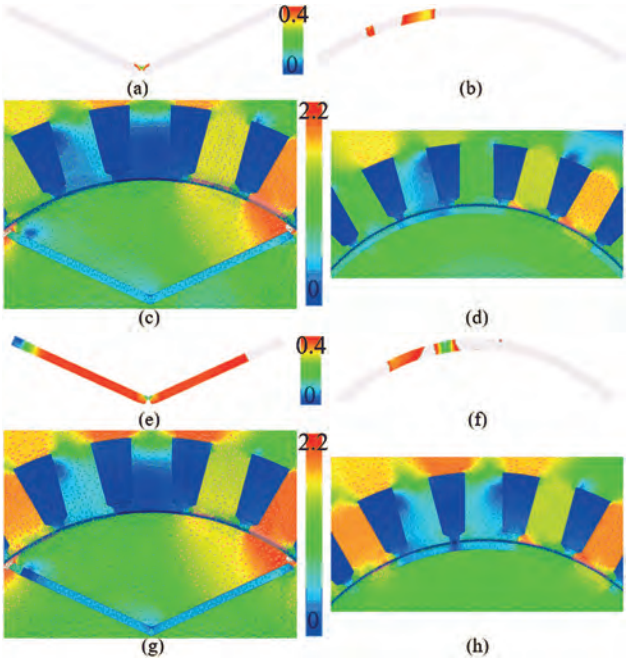

Fig. 2. PM Demagnetization.(a)IPMSM(8),(b)SPMSM(8),(c)Magnetic field of IPMSM(8),(d)Magnetic field of SPMSM(8),(e)IPMSM(14), (f)SPMSM(14),(g)Magnetic field of IPMSM(14),(h)Magnetic field of SPMSM(14).

VP12-11. Research on the Relationship between the Distribution of High-Permeability Materials of Rotors and Characteristics of Magnetic Field in Machines. *X. Liang*[1], M. Wang[1], P. Zheng[1], J. Gao[1] and W. Li[1] *1. School of Electrical Engineering and Automation, Harbin Institute of Technology, Harbin, China*

Synchronous reluctance machine (SRM) can achieve high torque-density and low torque ripple through reasonable design in reluctance machine. Compared with permanent magnet synchronous machine, SRM does not need expensive permanent magnet and has low cost. However, the rotor of SRM with many structural parameters is complex, and the design takes a long time. Many problems about the design and optimization of SRM have been studied and analyzed to improve the design efficiency and performance. [1] The magnetic barrier limits and guides the direction of the flux in machine. The width, start and end of magnetic barrier affect the modulation effect of the magnetic conductivity harmonic of rotor on the magnetomotive force of winding. The magnetic field harmonics, torque characteristics, loss, and other performances of machine will change as the rotor structure with above different parameters changes. Take conventional SRM as an example for analysis, as shown in Fig. 1. The energy conversion principle of machine with saliency can be obtained by using the energy method. Under the action of magnetic barrier with four shapes, the magnetic fields are shown in Fig. 2 (a), (b). The magnetic field distribution at d- and q-axis are basically consistent under magnetic barrier of different shapes. This indicates that when the load does not saturate the iron corn, the shape of the magnetic barrier does not affect the distribution and harmonic of the magnetic field, which is mainly related to the starting and ending positions of the magnetic barrier. Considering the influence of different loads, the design rules and constraints for the shape of magnetic barrier can be given. The influence and rules of magnetic barrier with different spatial distributions on harmonics of magnetic field is analyzed. As the number of magnetic barrier layers increases from 1 to 3, the growth rate of the maximum of difference between the d- and q-axis magnetic fields slows down, which can be quickly obtained by analyzing model. So, design efficiency and performance of SRM will be improved.

[1] Y. Bao, M. Degano and S. Wang, et al., "A Novel Concept of Ribless Synchronous Reluctance Motor for Enhanced Torque Capability," IEEE Trans. Ind. Electron., vol. 67, no. 4, pp. 2553-2563 (2019)

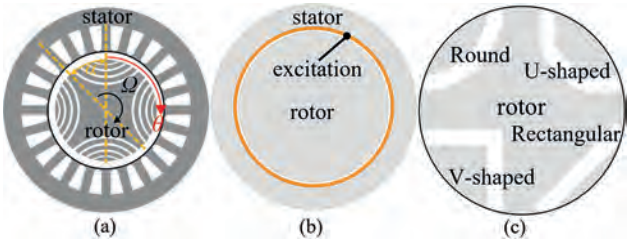

Fig. 1. SRM model. (a) analysis model, (b) schematic diagram, (c) Different magnetic barrier

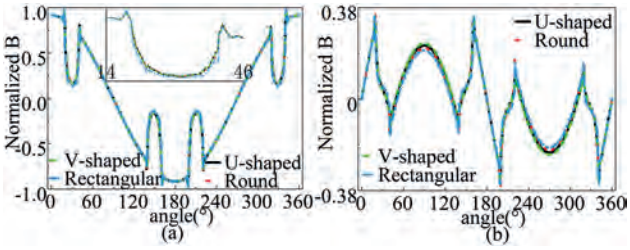

Fig. 2. Influence of magnetic barrier on magnetic field. (a) D-axis, (b) Q-axis

VP12-12. Torque Improvement of E-Core FSPM Motor using Double-Layer Distributed Armature Winding. *Y. Mao*[1], F. Xiao[1], Y. Du[1], X. Zhu[1], L. Quan[1] and C. Zhang[1] *1. Jiangsu University, Zhenjiang, China*

With the excellent achievement of permanent magnet (PM) materials, PM motors have attracted much attention for decades. Stator PM motor, in which the PMs and armature winding are located on the stator, can achieve simple rotor structure and favorable PM temperature management. Flux switching PM (FSPM) motor is one of the most popular stator PM motors due to the high torque density. This paper proposes a novel double-layer distributed armature winding configuration for 24/22-pole FSPM motor equipped with E-shaped stator iron core [1] so as to obtain a higher torque density. According to the air-gap flux modulation theory, the PM magnetic motive force of 24/22-pole E-core FSPM motors is modulated by the stator and rotor salient pole, generating the air-gap flux density with multiple excitation field harmonics. However, the excitation harmonics of the 24/22-pole E-core FSPM motor share different slot pitch angles, including 60 and 240 degrees. Therefore, when conventional winding design method based on the pole-pair number of armature winding (P_w=N_r-P_{PM}) is applied [2], only the excitation harmonics with the same slot pith angle as that of the harmonic of P_w pole-pair number are considered, leading to the underutilization of the main excitation field harmonics. In this paper, all of the main excitation field harmonics are analyzed to obtain the synthesis coil electromotive force, based on which a novel double-layer distributed winding configuration presented in Fig. 1 can be designed to fully utilize the main excitation field harmonics. Thus, the torque is improved efficiently. The electromagnetic performances of the proposed motor are investigated by finite element analysis. When compared with the conventional winding configuration with the pole-pair number of P_w, the output torque of the proposed scheme can be improved by 15.3% as shown in Fig. 2.

[1] Y. Mao, Y. Du, F. Xiao, X. Zhu, L. Quan and D. Zhou, "Design and optimization of a pole changing flux switching permanent magnet motor," *IEEE Tran. Ind. Electron.,* vol. 70, no. 12, pp. 12636-12647, Dec. 2023. [2] Y. Shi, L. Jian, J. Wei, Z. Shao, W. Li and C. C. Chan, "A new perspective on the operating principle of flux-switching permanent-magnet machines," *IEEE Tran. Ind. Electron.,* vol. 63, no. 3, pp. 1425-1437, Mar. 2016.

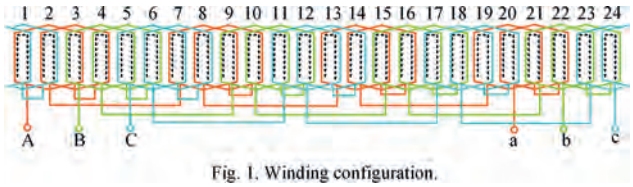

Fig. 1. Winding configuration.

Fig. 1

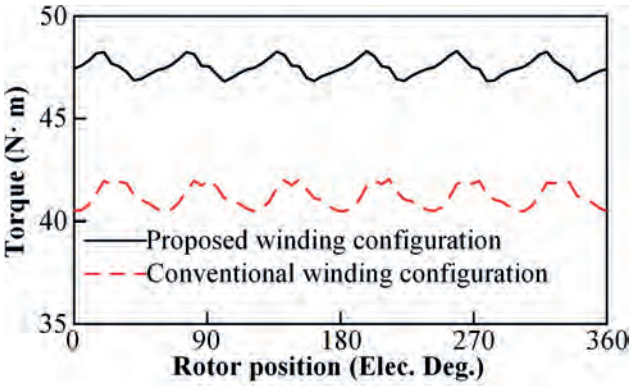

Fig. 2. Torque performance.

Fig. 2

VP12-13. A Pole-changing Double-side Flux Modulation Permanent Magnet Motor. Z. He[1], F. Xiao[1], Y. Du[1], X. Zhu[1] and *Y. Mao*[1] *1. Jiangsu University, Zhenjiang, China*

Permanent magnet (PM) flux modulation motors are well-known for high torque density compared with conventional PM motors. In this paper, a novel pole-changing double-side flux modulation permanent magnet motor (PC-DSFMM) is proposed based on a PC-PMVM adopting unevenly split modulation tooth structure [1]. The proposed PC-DSFMM is proven to own a considerably higher torque density than the PC-PMVM before and after PC operation due to the double-side flux modulation effect. The motor configuration of the PC-DSFMM is shown in Fig. 1. A PC-winding is installed in 12 stator slots, on which 18 modulation teeth are equipped, and the numbers of modulation teeth on adjacent stator teeth are 1 and 2, forming an unevenly split modulation tooth structure. 6 pieces of PMs are installed on the stator with the same magnetizing direction. Meanwhile, 17 PMs with the same direction of magnetization as rotor PM are half-embedded in the rotor. The original PC-PMVM and its prototype are also shown in Fig. 1 with surface-mounted PM of 17 pole-pairs equipped on the rotor. The two motors are both optimized and have the same assumption of PM. According to the air-gap field modulation theory [2], a fundamental air-gap PM harmonic component with 17 pole-pairs is generated by the PMs on the rotor in the PC-PMVM, which is modulated by the 18 modulation teeth to generate an air-gap PM harmonic of one pole-pair, working as the main source of torque. In the PC-DSFMM, a static air-gap PM harmonic with 18 pole-pairs can be generated by the 6 stator PMs, which interacts with the 17 rotor teeth to increase the amplitudes of the one pole-pair of flux density harmonic. Hence, the torque before and after the PC operation can be increased. The motor performances of the two motors are shown in Table I, where the Mode I and II refer to the motor operation modes before and after PC, respectively. The average torques of PC-DSFMM in Mode I and II are 16.8 and 7.0 Nm, respectively, which are 15.9% and 24.9% higher than those of the PC-PMVM benefitting from the double-side flux modulation effect. Meanwhile, the maximum efficiency, proportion and maximum speed of the high efficiency region (>80%) of PC-DSFMM are slightly smaller than the PC-PMVM.

[1] Y. Du, Z. He, X. Zhu, etc., A novel pole-changing permanent magnet vernier motor, *IEEE Trans. Ind. Electron.*, vol. 70, no. 6, pp. 6110-6120, (2023). [2] M. Cheng, P. Han, and W. Hua, General airgap field modulation theory for electrical machines, *IEEE Trans. Ind. Electron.*, vol. 64, no. 8, pp. 6063-6073, (2017).

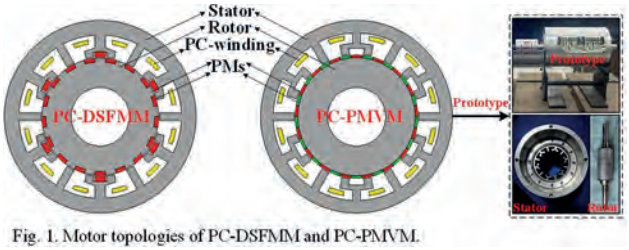

Fig. 1. Motor topologies of PC-DSFMM and PC-PMVM.

Fig. 1

TABLE I

MOTOR PERFORMANCES

Parameters	PC-PMVM (Mode I/II)	PC-DSFMM (Mode I/II)
Amplitude of phase back EMF @200 rpm, V	59.6/21.2	42.9/16.3
Average Torque, Nm	14.5/5.3	16.8/7.0
Max. eff.	88.2%/85.6%	89.5%/86.3%
Proportion of high eff. Region (>80%)	36.6%/22.3%	42.3%/25.8%
Max. speed of high eff. Region (>80%)	2100 rpm	1850 rpm

Tab. 1

VP12-14. A Flux Reversal Motor with Halbach Array Magnets Inserted into Stator Teeth. H. Chen[1], F. Xiao[1], Y. Du[1], X. Zhu[1] and *Y. Mao[1] 1. Jiangsu University, Zhenjiang, China*

Flux reversal motors (FRMs) have the merits of simple structure and easy heat dissipation [1]. In this paper, a novel FRM with Halbach array magnets inserted into the stator teeth is proposed. The topology of the proposed motor as well as its working principle is presented based on flux modulation theory. Meanwhile, the electromagnetic performances are comprehensively compared with the conventional surface-mounted permanent magnet (PM) FRMs. The results reveal that the proposed FRM has superior electromagnetic performances than the conventional one, which attributes to flux focusing effect of Halbach array magnets and the reduced equivalent airgap length. Fig. 1 shows two 12-slot/17-pole FRM topologies, both of which are consisted of doubly-salient laminations and three-phase concentrated windings, but the number, location and magnetized direction of PMs are different. For the conventional FRM (C-FRM), two radial magnetized PMs are surface-mounted on each stator tooth, and two PMs adjacent to a stator slot opening have opposite polarity. However, For the proposed FRM, a Halbach magnets array consisting of three magnets is inserted into each stator tooth, in which the middle PM is radial magnetized and PMs on the two sides are circumferentially magnetized in opposite directions. The proposed FRM is compared with the conventional FRM in terms of back electromotive force (EMF), self-inductance, average torque, overload capability and so on. It should be noted that two motors have been both optimized in conditions of the same stator outer diameter, stack length, airgap length, PMs usage, and copper loss. As shown in Fig. 2, the fundamental amplitude of back EMF (E_{m1}) and average torque (T_{av}) of the proposed FRM are 2 and 1.6 times those of the conventional FRM, respectively. Although the proposed FRM has a larger torque ripple (T_r) than its conventional counterpart, the difference is generally small. Moreover, other electromagnetic performance comparisons will be presented in the full paper.

[1] H. Hua, Z. Q. Zhu, *IEEE Trans. Energy Convers.*, vol. 37, no. 3, pp. 1815–1824 (2022).

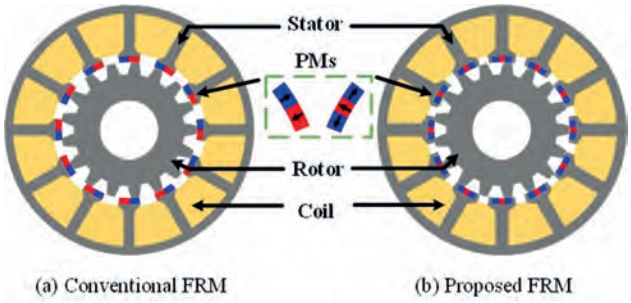

Fig. 1. FRM topologies.

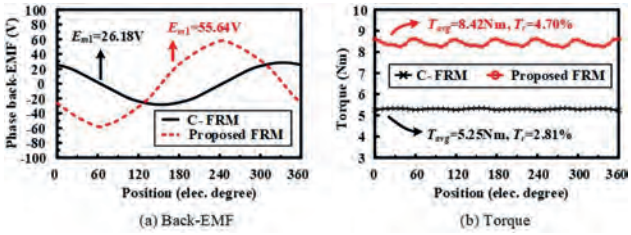

Fig. 2. Electromagnetic performance comparisons.

VP12-15. Comparative Analysis of Graphene-copper and Copper Material used in Electric Motor Winding. *S. Xu*[1], J. Li[1], D. Ma[1], Y. Li[1], X. Lu[1] and R. Pei[1] *1. Electrical Engineering, Shenyang University of Technology, Shenyang, China*

As a kind of new material, Graphene-copper combines the high conductivity, high thermal conductivity and excellent mechanical properties of Graphene and copper. Compared with the pure copper wire widely used in traditional motors, Graphene copper wire has more excellent conductivity and thermal conductivity, and its resistivity has more prominent advantages than traditional pure copper wire under high-frequency alternating current. In order to explore the improvement of mechanical performance and electrical performance of Graphene copper wire and traditional copper wire, as well as their performance changing trends at different temperatures, a set of experimental equipment that can simultaneously apply stress field and temperature field is specially built in this paper. The first part of the article mainly introduces the special preparation method of Graphene copper, and the special method used to process this new material into motor wires. In the second part, the mechanical properties of the two materials are compared and analyzed. Through the test results, it can be found that compared with traditional pure copper materials, Graphene copper materials have lower tensile strength and yield strength, but it has better toughness, which is more conducive to processing in the subsequent material application process. Finally, the electrical performance test results of the two materials are compared. Under DC, the conductivity of Graphene copper wire is 30% better than that of copper wire. Under AC condition, with the increase of frequency, the conductivity of Graphene copper wire is significantly improved, and its performance advantages become more prominent. This feature makes Graphene copper wire more advantageous in application scenarios such as high-speed motors with higher operating frequencies.

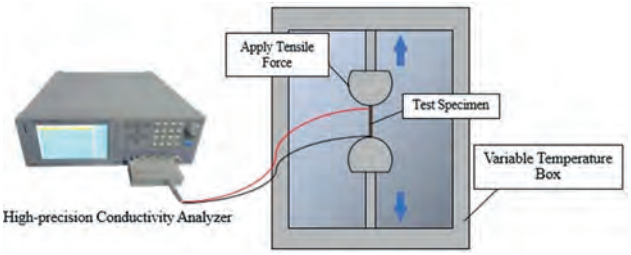

Fig. 1. Graphenen-copper and Copper material property test device

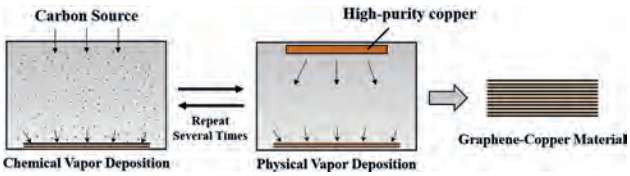

Fig. 2. Special perparation method for Graphene-copper material

VP12-16. Optimization Study on Local Anti-demagnetization Ability of Rotor Permanent Magnet of High-speed Motor. *W. Li*[1], Q. Fan[1], S. Xu[1], D. Ma[1] and R. Pei[1] *1. Electrical Engineering, Shenyang University of Technology, Shenyang, China*

Permanent magnet in High-speed motor rotor works in a harsh environment and is affected seriously by temperature, stress, reverse magnetic field and other multi-physical fields. Among them, temperature and reverse magnetic field have magnitude influence and are prone to local irreversible demagnetization under extreme operating conditions [1]. In the literature [2] [3], by analyzing the mixed structure of permanent magnets, the permanent magnets of different materials are mixed and spliced to reduce the amount of rare earths while achieving better performance, but the splicing method has high process requirements and the low performance magnets will affect the overall performance of the motor. Therefore, new paths and methods need to be further explored for the optimization of the local demagnetization resistance of magnets. In section II, a high-speed built-in PM motor model is established, as shown in Figure 1. The demagnetization distribution model of two structural magnets is given through finite element analysis (FEA), and the local anti-demagnetization optimization is carried out with this model as the target. Based on the principle of grain boundary diffusion, three optimization treatments are designed: I. Dy permeation in the demagnetization-prone region; II. Tb penetration in the demagnetization-prone region; III. Dy/Tb co-infiltration in the demagnetization-prone region. Multiple sets of experiments were conducted by varying the concentration, temperature and time to analyze the infiltration process from the material perspective. In section III, multi-physical field experiments are carried out. Comparative experiments close to the actual operating environment of the motor are designed to validate the local demagnetization resistance of the optimized permanent magnets. In section IV, in order to improve the local demagnetization performance, Dy infiltration, Tb infiltration and mixed co-infiltration are employed in the demagnetization-prone area of high-speed motor magnets, and the effectiveness of the proposed method is validated by multi-physics field experiments, which provides a reference for the subsequent research on rare-earth-less permanent magnets and their application in high-speed motors.

[1] M. Baranski, W. Szelag and W. Lyskawinski, “Experimental and Simulation Studies of Partial Demagnetization Process of Permanent Magnets in Electric Motors,” in IEEE Transactions on Energy Conversion, vol. 36, no. 4, pp. 3137-3145, 2021. [2] B. Poudel, E. Amiri, P. Rastgoufard and B. Mirafzal, “Toward Less Rare-Earth Permanent Magnet in Electric Machines: A Review,” in IEEE Transactions on Magnetics, vol. 57, no. 9, pp. 1-19, 2021. [3] Y. Zhang, Z. Xiang, X. Zhu, L. Quan and M. Jiang, “Anti-Demagnetization Capability Research of a Less-Rare-Earth Permanent-Magnet Synchronous Motor Based on the Modulation Principle,” in IEEE Transactions on Magnetics, vol. 57, no. 2, pp. 1-6, Feb. 2021.

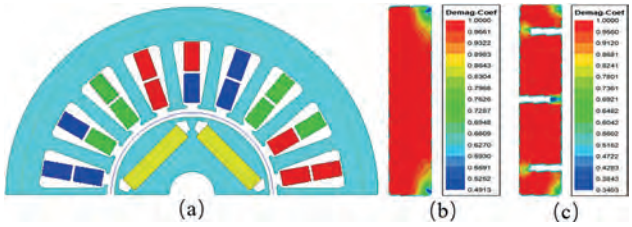

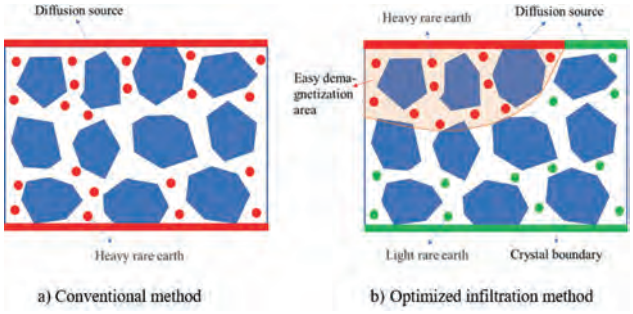

VP12-17. An Interoperable Wireless Power Transmitter for Unipolar and Bipolar Receiving Coils. *R. Xie*[1], W. Xu[1], C. Liu[1], Y. Zhuang[1] and Y. Zhang[1] *1. College of Electrical Engineering and Automation, Fuzhou University, Fuzhou, China*

Inductive power transfer (IPT) is a type of wireless power transfer (WPT) that utilizes the magnetic field as the power transmission medium. Various coil types are employed in IPT systems, such as unipolar and bipolar coils. They are decoupled from each other when aligned. If the transmitting and receiving coils are with different coil types, the interoperability issue would arise, which is crucial and should be solved. For interoperability, the transmitting coils should be designed in such a way that they can work with different receiving coils. But how to achieve interoperability presents researchers with considerable challenges. In order to solve the interoperability problem, an interoperable transmitter composed of two adjacently placed unipolar coils is proposed in this paper, which can be compatible with unipolar coils or bipolar coils through circuit configuration to achieve current direction alterations, and realize efficient wireless power transmission. When the switch S is on, the two unipolar coils are in parallel, and the current directions of the two unipolar coils are the same, forming a unipolar coil. When the switch S is off, the two unipolar coils are reversely connected in series, and the current directions of the two unipolar coils are opposite, equivalent to a bipolar coil. To charge different receiving coils, the proposed system can be reconfigured to be compatible with unipolar or bipolar receiving coils. The two different operating modes are studied, and the influence of different receiving coils on the maximum efficiency and power of the system is compared. An experimental prototype is established. The calculated and experimental results have revealed that the proposed IPT system can effectively improve interoperability and has great potential for development.

[1] Y. Zhang, C. Liu, M. Zhou, and X. Mao, “A Novel Asymmetrical Quadrupolar Coil for Interoperability of Unipolar, Bipolar, and Quadrupolar Coils in Electric Vehicle Wireless Charging Systems,” *IEEE Trans. Ind. Electron.*, pp. 1–4, 2023. [2] Y. Fan, Y. Sun, P. Deng, H. Hu, C. Jiang, and Y. Feng, “A Simultaneous Wireless Power and High-Rate Data Transfer System Based on Transient Responses Regulation,” *IEEE Trans. Power Electron.*, pp. 1–5, 2023. [3] L. Wang, U. K. Madawala, J. Zhang, and M.-C. Wong, “A New Bidirectional Wireless Power Transfer Topology,” *IEEE Trans. Ind. Appl.*, vol. 58, no. 1, pp. 1146–1156, Jan. 2022. [4] Z. Yan, L. Wu, and W. Baoyun, “High-Efficiency Coupling-Insensitive Wireless Power and Information Transmission Based on the Phase-Shifted Control,” *IEEE Trans. Power Electron.*, vol. 33, no. 9, pp. 7821–7831, Sep. 2018. [5] Y. Zhang, Y. Wu, W. Pan, Z. Shen, H. Wang, and X. Mao, “A multi-channel wireless charging system with constant-voltage outputs based on LCC-S topology and integrated magnetic design,” *Energy Rep.*, vol. 9, pp. 461–468, Apr. 2023. [6] Y. Jing, W. Feng, K. Qiao, L. Yang, S. Wang, and L. Lu, “Simultaneous Wireless Power and Data Transfer System With Full-Duplex Mode Based on LCC/CLC Resonant Network,” *IEEE Trans. Power Electron.*, vol. 38, no. 4, pp. 5549–5560, Apr. 2023. [7] Y. Jiang and B. Zhang, “A Fractional-Order Wireless Power Transfer System Insensitive to Resonant Frequency,” *IEEE Trans. Power Electron.*, vol. 35, no. 5, pp. 5496–5505, May 2020. [8] P. Mahure, R. K. Keshri, R. Abhyankar, and G. Buja, “Bidirectional Conductive Charging of Electric Vehicles for V2V Energy Exchange,” in *IECON 2020 The 46th Annual Conference of the IEEE Industrial Electronics Society*, Oct. 2020, pp. 2011–2016.

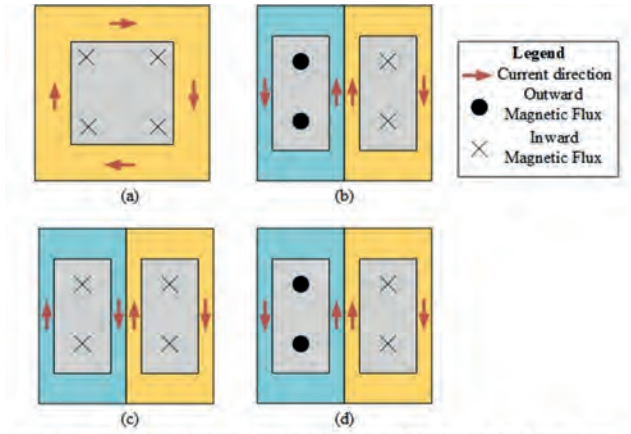

Fig. 1. Magnetic couplers and their flux. (a) Conventional unipolar coil. (b) Conventional bipolar coil. (c) Proposed transmitting coil forming a unipolar coil when S is off. (d) Proposed transmitting coil forming a bipolar coil when S is on.

Fig.1

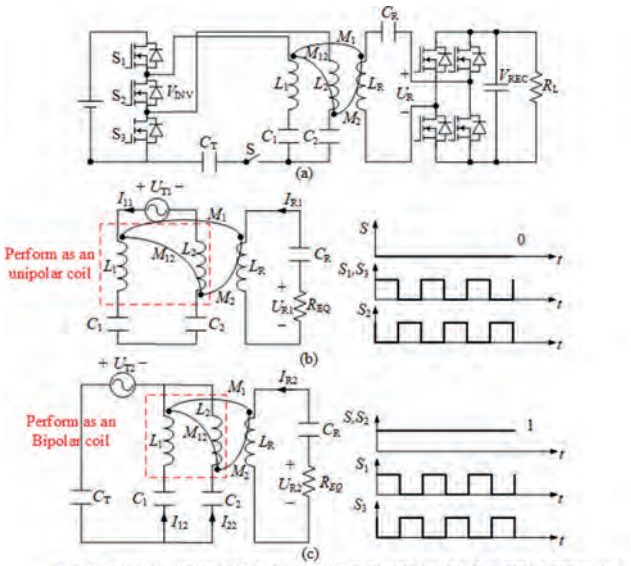

Fig. 2. Proposed system. (a) Topology. (b) Equivalent circuit and switching pattern as a unipolar coil when S is off. (c) Equivalent circuit and switching pattern as a bipolar coil when S is on.

Fig. 2

VP12-18. A reconfigurable bipolar coil for wireless charging systems with interoperability and misalignment tolerance characteristics.

C. Liu[1], R. Xie[1], X. Chen[1] and Y. Zhang[1] *1. College of Electrical Engineering and Automation, Fuzhou University, Fuzhou, China*

Electric vehicles (EVs), as an emerging means of transportation, can be charged via wireless power transfer (WPT) technology. There are many different coil types in EV wireless charging systems and each coil type may not be tolerant with the others, leading to the interoperability issue. Also, the misalignment between the transmitting and receiving coils can happen when parking. The issues of interoperability and misalignment tolerance for EV wireless charging need urgent care. To eliminate these problems, a reconfigurable bipolar coil structure with both interoperability and misalignment tolerance is proposed in this work. Based on the conventional bipolar coil and solenoid coil structures, a reconfigurable bipolar coil structure is built as shown in Fig. 1. The wires at different positions are shuttled up and down on the ferrite plate in a solenoid-like manner to form a bipolar coil-like structure. A longitudinal bipolar coil structure and a transverse bipolar coil structure can be formed by changing the current conduction and flow direction within the coils at different positions, as shown in Fig. 1(a) and (b), respectively.

In order to further verify the interoperability and anti-divergence characteristics of the coupling structure proposed in this study, an experimental prototype was built on the basis of the LCC-S topology, and the topology diagram used is shown in Fig. 1(c). Base on the above theoretical study and the superiority of LCC-S topology, an experimental prototype with a power of 500W is built to verify it. The designed coupling mechanism size of the prototype is 200mm×200mm, so that the experimental misalignment range is defined as [-140mm,140mm]. The structure of the simulation experiment is shown in Fig. 2, where Fig. 2(a) shows the effect of output power and transmission efficiency with offset corresponding to Fig. 1(a); Fig. 2(b) shows the effect of output power and transmission efficiency with offset corresponding to Fig. 1(b). The effectiveness of the proposed reconfigurable bipolar coil is finally verified through calculations, simulations and experiments.

[1] Y. Zhang, W. Pan, H. Wang, "Interoperability study of wireless charging system with unipolar and bipolar coils based on capacitor–inductor–capacitor–capacitor–series topology," *Energy Reports*, vol. 8, pp. 405-411, Aug. 2018. [2] K. Song, Y. Lan, R. Wei, G. Yang, F. Yang, W. Li, J. Jiang, C. Zhu, and Y. Li, "A control strategy for wireless EV charging system to improve weak coupling output based on variable inductor and capacitor," *IEEE Trans. Power Electron.,* vol. 37, no. 10, pp. 12853-12864, Oct. 2022. [3] Y. Zhang, S. Chen, X. Li, and Y. Tang, "Design methodology of free-positioning nonoverlapping wireless charging for consumer electronics based on antiparallel windings," *IEEE Trans. Ind. Electron.,* vol. 69, no. 1, pp. 825-834, Jan. 2022. [4] Y. Zhang, Y. Wu, Z. Shen, W. Pan, H. Wang, J. Dong, X. Mao, X. Liu, "Integration of onboard charger and wireless charging system for electric vehicles with shared coupler, compensation, and rectifier", IEEE Trans. Ind. Electron., vol. 70, no. 7, pp. 7511-7514, Jul. 2023. [5] G. Yang, K. Song, X. Huang, C. Wang, X. Huang, J. Li, C. Zhu, "Improved interoperability evaluation method for wireless charging systems based on interface impedance," IEEE Trans. Power Electron., vol. 36, no. 8, pp. 8588-8592, Aug. 2021. [6] Y. Chen, B. Yang, Z. Kou, Z. He, G. Cao and R. Mai, "Hybrid and Reconfigurable IPT Systems With High-Misalignment Tolerance for Constant-Current and Constant-Voltage Battery Charging," IEEE Trans. Power Electron., vol. 33, no. 10, pp. 8259-8269, Oct. 2018. [7] G. Yang, K. Song, Y. Sun, X. Huang, J. Li, Y. Guo, H. Zhang, Q. Zhang, R. Lu, C. Zhu, "Interoperability improvement for rectangular pad and DD pad of wireless electric vehicle charging system based on adaptive position adjustment," IEEE Trans. Ind. Appl., vol. 57, no. 3, pp. 2613-2624, Mar. 2021. [8] F. Grazian, T. B. Soeiro and P. Bauer, "Inductive power transfer based on variable compensation capacitance to achieve an EV charging profile with constant optimum load," *IEEE J. Emerg. Sel. Topics Power Electron.,* vol. 11, no. 1, pp. 1230-1244, Feb. 2023.

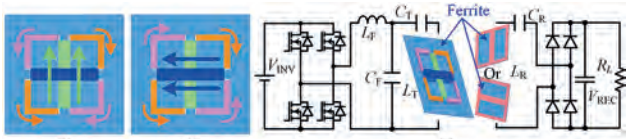

Fig. 1. Proposed reconfigurable bipolar coil structures and topology. (a) Vertical bipolar coil structure. (b) Horizontal bipolar coil structure. (c) Topology.

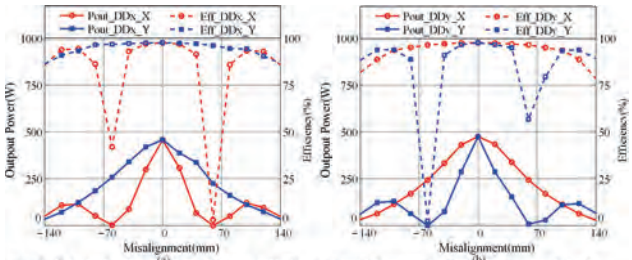

Fig. 2. Calculated output power and efficiency with offset in *X* and *Y* directions. (a) Transmitter is vertical bipolar coil structure. (b) Transmitter is horizontal bipolar coil structure.

VP12-19. Operation principle analysis of air-gap magnetic field modulation in flux-switching permanent-magnet double-rotor machine. *L. Mo[1] 1. Huaiyin Institute of Technology, Huai'an, China*

To achieve high torque density and little torque ripple, a flux-switching permanent-magnet double-rotor machine (FSPM-DRM) has been proposed [1]. In [2], based on the air-gap field modulation theory, the output torque of FSPM was analyzed and it shows that the stable electromagnetic torque is generated by the dominant harmonic instead of other order harmonics. More results show that some rotating harmonic components can induce the back EMF in the armature magnetic field, and then generate the torque. However, there are no more reports on the effect of different order harmonics to generate torque. In this paper, the FSPM-DRM airgap flux densities under various loads are calculated analytically, and the effective field harmonics, and the resulting electromagnetic torque, as well as their proportions, are derived theoretically and validated by simulation and experimental results. Fig.1 shows the configuration of the FSPM-DRM. Different from the traditional magnetic field modulation machine, the PMs in the inner rotor and the outer stator of the FSPM-DRM can be seen as the excitation source that produce the PM magnetomotive force (MMF). The double salient stator and rotor work as the modulator that modulate a series of MMF harmonics. The armature windings, as a filter, select the effective airgap field harmonics and induce the EMF and electromagnetic torque. In the FSPM-DRM, the inner (outer) airgap flux densities that produced by the inner (outer) PMs can be qualitatively and analytically calculated based on the equivalent magnetic circuit method. Table I lists the FSPM-DRM's effective harmonic orders of the airgap field modulation. It shows that the airgap harmonic orders 4,6,8 14,16,18,20 are effective, and is helpful to improve the electromagnetic torque, which is coincide with the simulation results. Further results follow that FSPM-DRM's output torques are mainly generated from the static working harmonic orders of 6, 18 and other dynamic rotating working harmonics. The working harmonics of the two machines both bring more than 97% of the total average torque. The experimental results on the 2kW prototype machine have verified the results.

[1] P. Zheng, R. Liu, P. Thelin, E. Nordlund, and C. Sadarangani, "Research on the cooling system of a 4QT prototype machine used for HEV," IEEE Transactions on Energy Conversion, vol. 23, no. 3, pp.61-67, 2008. [2] Shi Yujun,Jian Linni,Wei Jin,et al. "A new perspective on the operating principle of flux-switching permanent-magnet machines," IEEE Transactions on Industrial Electronics,2016,63(3): 1425-1437.

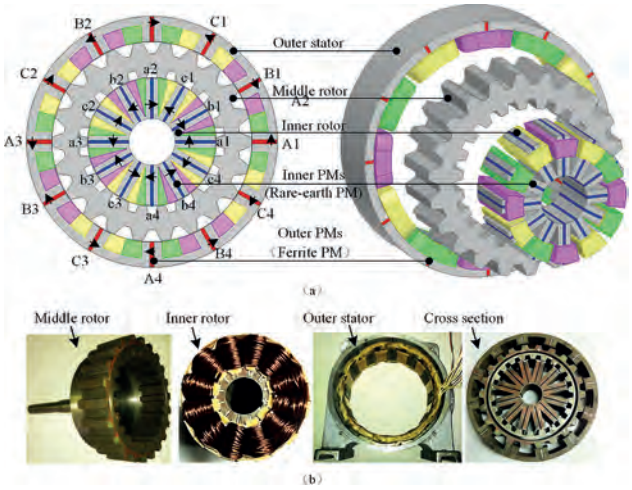

Fig.1 The porposed machine.

Harmonic order	$P^{so}_{(n,m)} = P^{wo}_{(k,v)}$	$\omega^{so}_{(n,m)}=\omega^{wo}_{(k,v)}$
4	$P^{so}_{(3,-1)} = P^{wo}_{(0,4)}$	$\omega^{so}_{(3,-1)}=\omega^{wo}_{(0,4)} = 5.5\omega$
6	$P^{so}_{(1,0)} = P^{wo}_{(-1,16)}$	$\omega^{so}_{(1,0)}=\omega^{wo}_{(-1,16)} = 0$
8	$P^{so}_{(5,-1)} = P^{wo}_{(-2,52)}$	$\omega^{so}_{(5,-1)} = \omega^{wo}_{(-2,52)} = -2.75\omega$
14	$P^{so}_{(5,-2)} = P^{wo}_{(-3,52)}$	$\omega^{so}_{(5,-2)} = \omega^{wo}_{(-3,52)} = 22\omega/7$
16	$P^{so}_{(1,-1)} = P^{wo}_{(0,16)}$	$\omega^{so}_{(1,-1)} = \omega^{wo}_{(0,16)} = 11\omega/8$
18	$P^{so}_{(3,0)} = P^{wo}_{(-1,4)}$	$\omega^{so}_{(3,0)} = \omega^{wo}_{(-1,4)} = 0$
20	$P^{so}_{(7,-1)} = P^{wo}_{(-2,64)}$	$\omega^{so}_{(7,-1)} = \omega^{wo}_{(-2,64)} = -1.1\omega$

Table I Effective harmonic orders

VP12-20. Performance Analysis of a Flux-Switching Double-Rotor PM Machine Considering PM demagnetization in Two Different PM Materials. *L. Mo[1] 1. Huaiyin Institute of Technology, Huai, China*

The flux-switching permanent-magnet double-rotor machine (FSPM-DRM) is favor for the HEV application for its compact structure and high torque density (Fig.1) [1]. In the FSPM-DRM, there are 12 inner rare-earth-PM and 12 outer ferrite-PM pieces. Two PM materials mean different B-H curves and temperature dependence features. The operation points of the PMs have certain influences on the magnetic field of the machine, especially when irreversible PM demagnetization is taken place [2]. Hence, to accurately evaluate FSPM-DRM's performance and make sure the safety operation of the system, the field distributions and the inductances considering the temperature rise are analyzed. The output performances accounting for PM temperature rise, as well as the PM operation points and PM irreversible demagnetization region, are also investigated. According to the preliminary studies on the thermal analysis, the temperatures of the inner PM, inner winding, outer PM, and the outer winding of the FSPM-DRM at rated load and hybrid driving mode are 96.9°C, 99.1°C, 90°C, and 91.5°C, respectively. Results show that the air-gap flux density, the back EMF and the average output torque of the outer machine nearly keep the same at different PM temperatures, while those of the inner machine decrease slightly with the temperature rise. It means that the temperature rise has greater influence on the inner machine. Further studies displays that the flux densities of the node A in ferrite-PM under two PM temperatures are both above the demagnetization limits of recoil lines under 20°C and 100°C PM temperatures. Whereas, the flux densities of node B in NdFeB-PM at 100°C are slightly deviated from the recoil line, and partial irreversible demagnetization is emerged(Fig.2). More results show the PM flux density distributions of the inner PMs and the outer PMs, in which the demagnetization region of the inner machine only accounts for ~1.15% of the total inner PM region. The machine's analytical and simulation analysis are verified by experimental results on a 1kW/1kW prototype machine of the FSPM-DRM.

[1] Chen Yunyun, Quan Li, Zhu Xiaoyong, Wei Hua, and Zheng Wang, "Electromagnetic Performance Analysis of Double-Rotor Stator Permanent Magnet Motor for Hybrid Electric Vehicle," IEEE Transactions on Magnetics, vol. 48, no. 11, pp. 4204-4207, 2012. [2] Silong Li, Yingjie Li, and Bulent Sarlioglu, "Partial Irreversible Demagnetization Assessment of Flux-Switching Permanent Magnet Machine Using Ferrite Permanent Magnet Material," IEEE Transaction on Magnetics, Vol. 51, No.7, 2015, Art. ID 8106209.

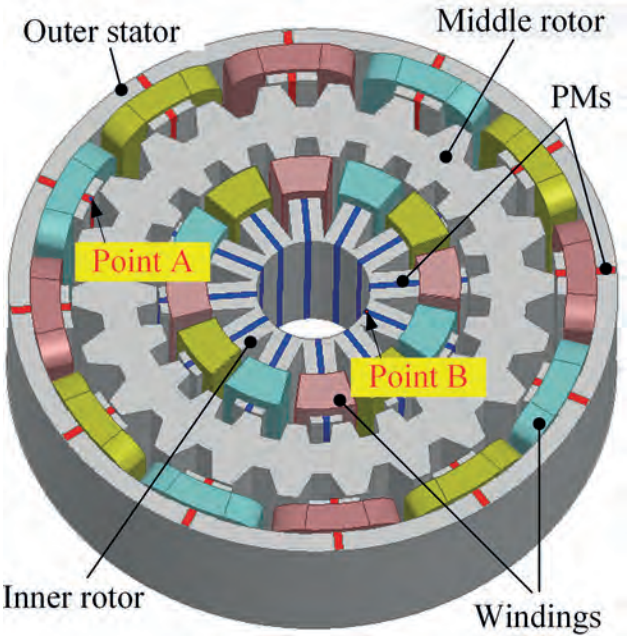

Fig.1. FSPM-DRM topology.

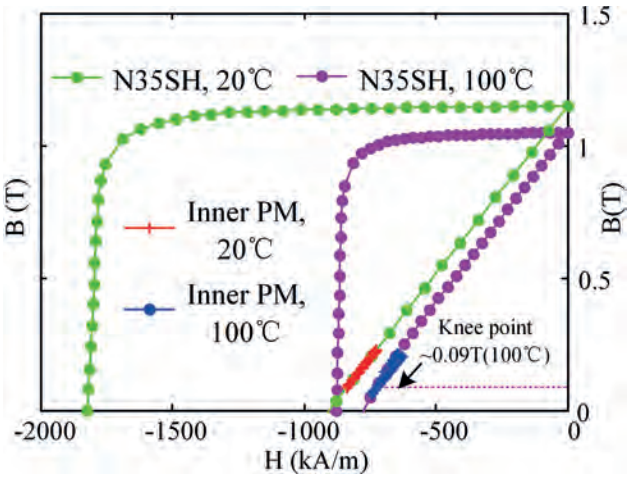

Fig.2. The operation points in inner PM

VP12-21. Investigation of the Excess Loss Behavior of the Grain-Oriented Steels in A High-Frequency Range Considering Skin Effect.

L. Chen[1], Z. Zhang[1], T. Ben[1], D. Yan[1] and X. Zhang[2] *1. College of Electrical Engineering and New Energy, China Three Gorges University, Yichang, China; 2. State Key Laboratory of Reliability and Intelligence of Electrical Equipment, Hebei University of Technology, Tianjin, China*

Introduction In the low-frequency range, the losses of the electrical steel can be calculated using the Statistical Theory of Loss (STL) [1]. However, with the increase of the frequency, the skin effect resulted in inaccurate results of the eddy current loss. Correspondingly, the excess loss cannot be properly determined. Assuming that the statistical parameter V_0 of the excess loss is a function of magnetizing frequency f and the flux density peak B_p, the total loss is in good agreement with the experimental results. However, the method in [2] is determined via parameter fitting and lacks a physical mechanism. In this paper, a 1-D lamination model is solved by considering the hysteresis field and the excess loss field in a wide frequency range. Then by comparing the total loss with the measuring results of GO silicon steel B30P105 up to 1 kHz. The relationship between the statistical parameter V_0 and f of is finally investigated. Method and Discussion To clarify the effect of magnetization frequency on the excess loss, the total loss considering the skin effect and the excess loss field is firstly calculated via a time domain 1-D model where the constitutive hysteresis relation is described by an inverse Preisach model, as shown in Fig.1. After solving the 1-D diffusion equations, the dynamic hysteresis loops formed by the average magnetic density B_{av} and the surface magnetic field H_{sur} can be calculated, which indicate that the eddy current and excess loss cannot be solved decoupled in high-frequency conditions as shown in Fig.2. Therefore, the skin effect of the eddy current field resulting a frequency dependence on the excess loss. Thus, the parameter V_0 is adjusted according to the computed results compared with the experimental results at different frequencies. Conclusion In this paper, the relationship between the excess loss statistical parameter V_0 and frequency f is studied by solving the 1D lamination model, considering. Obtained results show that the statistical parameter V_0 can be both a function of the peak magnetic flux density and the magnetizing frequency.

[1] S. E. Zirka, Y. I. Moroz and A. J. Moses, IEEE Transactions on Power Delivery., Vol. 26, p.2352-2362(2011) [2] X. Zhao, L. Yang and H. Xu, IEEE Transactions on Magnetics., Vol. 58, p.1-5(2022)

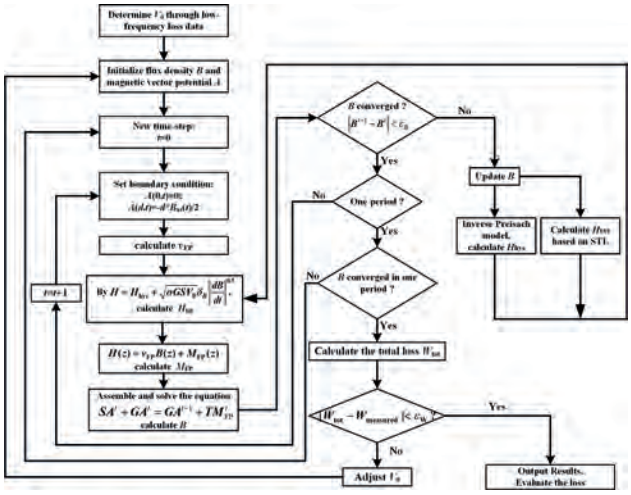

Fig. 1. Flow diagram for solving the dynamic loss by 1-D FEM

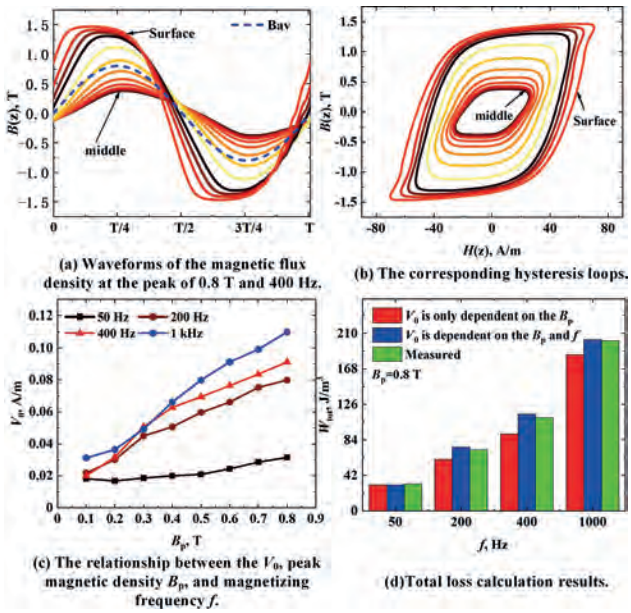

Fig. 2. Analysis and comparison of calculation results

VP12-22. Withdrawn

VP12-23. Research on Electromagnetic Transformation and Raising Knee Frequency of Hybrid Medium High Frequency Transformer.
C. Hsu[1] 1. Mechanical Engineering, Asia Eastern University of Science and Technology, Banqiao District, Taiwan

Transformer core material determines its operating frequency and magnetic flux saturation density due to its natural characteristics. This research proposes a design, simulation and experimental discussion of a composite miniature high-frequency transformer (HFT). In this paper, the artificial intelligence-like neural network algorithm is used to model the HFT transformer, and the calculation and evaluation are carried out from the aspects of core mathematical modeling, low core loss, high load power and operating efficiency, as shown in Figure 1. A medium-frequency high-power (MFHP) transformer is one of the most important components of a dc/dc converter, as shown in Figure 2. In the design application, consider the circulating current it has in the parallel secondary winding of the thin winding, and the primary series secondary parallel structure. Based on the asymmetrical mutual inductance phenomenon i.e. asymmetrical coupling between primary and secondary windings (primary-series secondary-parallel, PSSP) situation, this will not achieve an absolutely symmetrical result. There is an inflection point frequency for medium and high frequency operation of the transformer, and setting the operating frequency of the transformer at the inflection point frequency will result in an increase in the AC resistance. Therefore, this study uses the artificial intelligence algorithm to predict the position of the inflection point frequency caused by the asymmetric coupling of the winding. The neural network model analyzes the asymmetric coupling coefficient of the transformer, and compares the prediction with the calculation of the actual scaled transformer's corner frequency. Finally, based on the consideration of the inflection point frequency optimized by the experiment, it is used to construct the development and research of the miniature medium and high frequency transformer with PSSP structure.

[1] M. Mogorovic and D. Dujic, "100 kW, 10 kHz mediumfrequency transformer design optimization and experimental verification," IEEE Trans. Power Electron., vol. 34, no. 2, pp. 1696–1708, Feb. 2019. [2] B. Chen, X. Liang, and N. Wan, "Design methodology for inductorintegrated litz-wired high-power medium-frequency transformer with the nanocrystalline core material for isolated DC-link stage of solidstate transformer," IEEE Trans. Power Electron., vol. 35, no. 11, pp. 11557–11573, Nov. 2020. [3] Z. Guo, R. Yu, W. Xu, X. Feng, and A. Q. Huang, "Design and optimization of a 200-kW medium-frequency transformer for mediumvoltage SiC PV inverters," IEEE Trans. Power Electron., vol. 36, no. 9, pp. 10548–10560, Sep. 2021. [4] S. Somkun, T. Sato, V. Chunkag, A. Pannawan, P. Nunocha, and T. Suriwong, "Performance comparison of ferrite and nanocrystalline cores for medium-frequency transformer of dual active bridge DC–DC converter," Energies, vol. 14, no. 9, p. 2407, Apr. 2021.

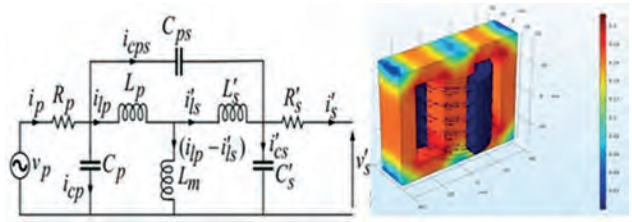

Figure 1 High frequency transformer: (a) equivalent circuit referred to primary and (b) FEA geometry.

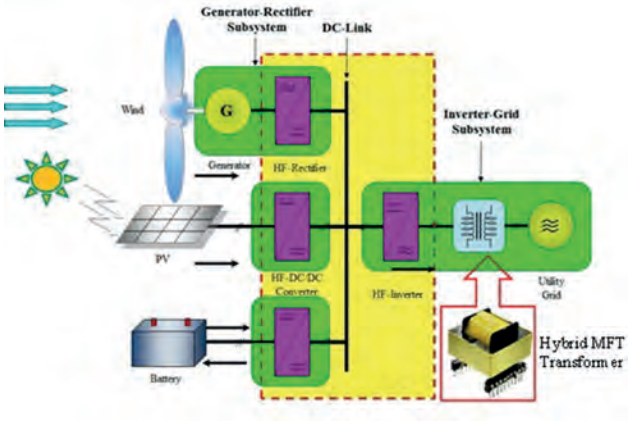

Figure 2 High frequency transformer structure under power electronic circuit.

VP12-24. Motor Vibration and Noise Dependence on Magnetostriction and Electromagnetic Power Variation Identify by AI Algorithm.
C. Hsu[1] 1. Mechanical Engineering, Asia Eastern University of Science and Technology, Banqiao District, Taiwan

The vibration measurement is mainly used natural frequency and resonance frequency to predict the magnetic device operation status [1,2]. This common feature is focused the electric motor device where is made by the electromagnetic silicon steel sheet. This study is used the magnetostrictive variation induced by the electromagnetic silicon steel sheet through the exciting power of the current and magnetic field which is to accelerate the vibration and noise variation. It is caused by the excitation of the core and coil. It can intercept the required characteristic signal, analyze the performance of dynamic magnetostrictive of ESS under DC bias and its complex dynamic anisotropy. The motors running under high-frequency conditions cause noise and vibration due to the interaction between magnetomotive forces (MMF). These MMFs are related to the fundamental wave current and switching harmonic current flowing into the motor. For experiment results and discussion, this article proposes the reference architecture of the IoT smart factory with neural network magnetic identification (NNMI). Regarding to the vibration frequency prediction as a multi-type classification problem, it uses the neural network features of deep learning to combine the input signal, as shown in Figure 1. That is classified into different categories [3, 4]. To use an optimized method with feedforward convolutional neural network, it can predict the frequency and analyze the AC and DC vibration frequency of the power motor and the non-fixed periodicity of the mechanical robot arm belong to different spectrum models. The sound pressure level is related to the sound intensity level (SIL). The conversion of voltage signal, current signal, and time domain and frequency domain FFT. As shown in Figure 2, to predict the vibration and sound module by using artificial intelligence method, it is verified the operating system through by measurement, numerical analysis and optimal calculation of NN method to identify the vibration and noise of the motor.

[1] Eshaan Ghosh, Aida Mollaeian, Seog Kim, Jimi Tjong, Narayan C. Kar, DNN-Based Predictive Magnetic Flux Reference for Harmonic Compensation Control in Magnetically Unbalanced Induction Motor, IEEE Transactions on Magnetics, Volume: 53, Issue: 11, 2017. [2] S. Nandi, H.A. Toliyat, X. Li, Condition Monitoring and Fault Diagnosis of Electrical Motors—A Review, IEEE Transactions on Energy Conversion, Volume: 20, Issue: 4, P. Paper, 1360, 2005. [3] Siliang Lu, Gang Qian;Qingbo He, Fang Liu, Yongbin Liu, Qunjing Wang, In Situ Motor Fault Diagnosis Using Enhanced Convolutional Neural Network in an Embedded System, IEEE Sensors Journal, Volume: 20, Issue: 15, 2020. [4] Jingsong Xie, Zhaoyang Li, Zitong Zhou, Scarlett Liu, A Novel Bearing Fault Classification Method Based on XGBoost: The Fusion of Deep Learning-Based Features and Empirical Features, IEEE Transactions on Instrumentation and Measurement, Volume: 70, 2021.

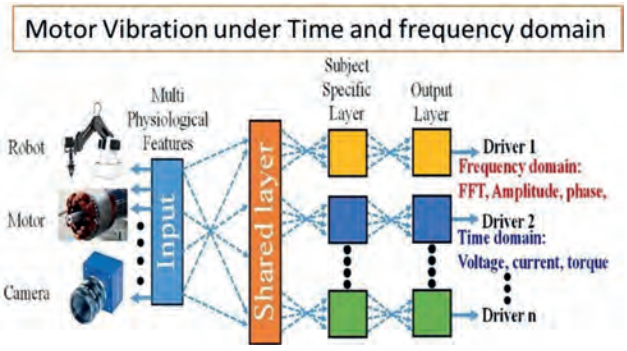

Figure 1 Motor vibration and noise recognition by NN method.

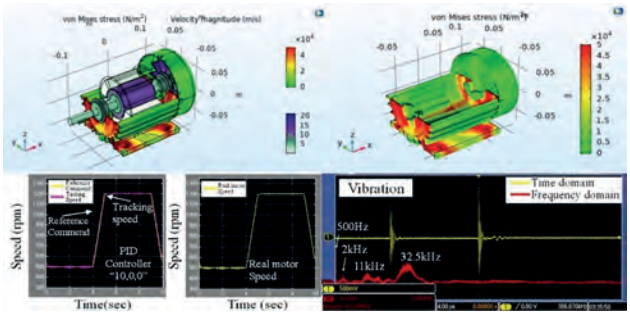

Figure 2 Motor Vibration and Noise: (a)-(b) FEA stress, (c) time domain and (d) frequency domain.

VP12-25. A Pole-Changing Flux Reversal Permanent Magnet Motor.
Y. Du[1], Z. Chen[1], F. Xiao[1], X. Zhu[1] and *Y. Mao*[1] *1. Jiangsu University, Zhenjiang, China*

Stator permanent magnet (PM) motors have the merits, such as ease of heat management and high torque density because the PMs and winding are located on the stator. So, stator PM motors become one of the potential candidates for electric vehicles. Flux reversal PM (FRPM) motor has the advantages of simple structure and high mechanical reliability. However, due to its constant excitation field, the speed regulation range is usually limited. Pole changing (PC) operation is a traditional method to expand the speed range for induction motors, which can be realized by changing the winding connection, as well as the pole number of armature and rotor fields. But the PC operation cannot be used directly for PM motors because of the unchangeable pole number of PMs. According to the field modulation theory, the PM magnetic field can be modulated into a series of harmonics with different pole numbers by a modulator [1], which provides a scheme for achieving PC PM motors. In this paper, a PC-FRPM motor is proposed. Fig. 1 shows the 12/7-pole PC-FRPM motor, in which the winding and the PMs are both located on the stator, and the rotor is composed of iron core with 7 salient teeth. The key difference is that only one PM magnetized in the radial direction mounts on the surface of each stator tooth, and the magnetization direction of PMs on each adjacent two stator teeth is opposite. So, the pole-pair number of the fundamental component of PM field is 3. Benefiting from this special PM arrangement, the interpole flux leakage can be reduced greatly. Furthermore, due to the modulation function of stator and rotor teeth, a series of harmonics with different pole pairs are generated [2], in which the pole-pair numbers of harmonics with relatively high amplitude are 2, 4, 10 and 16. And the slot pitch angles of 2- and 10-pole-pair components are 60°, and those of the others are 120°. So, two kinds of winding connection can be determined according to these two slot pitch angles to obtain two operation modes, namely Mode I and Mode II to perform the high speed and high torque operation, respectively. As shown in Fig. 2, the speed range can be expanded while maintaining a high torque output.

[1] M. Cheng, P. Han, and W. Hua, "General airgap field modulation theoryfor electrical machines," *IEEE Trans. Ind. Electron*., vol. 64, no. 8, pp. 6063-6073, Aug. 2017. [2] Y. Du, Z. He, X. Zhu, F. Xiao, C. Zhang, L. Xu, Y. Zuo, and L. Quan. "A novel pole-changing permanent magnet vernier motor," *IEEE Trans. Ind. Electron.* vol. 70, no. 6, pp. 6110-6120, June 2023.

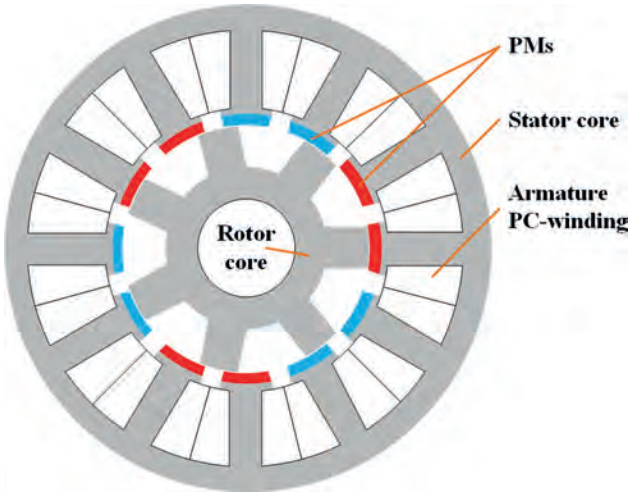

Fig. 1. PC-FRPM motor.

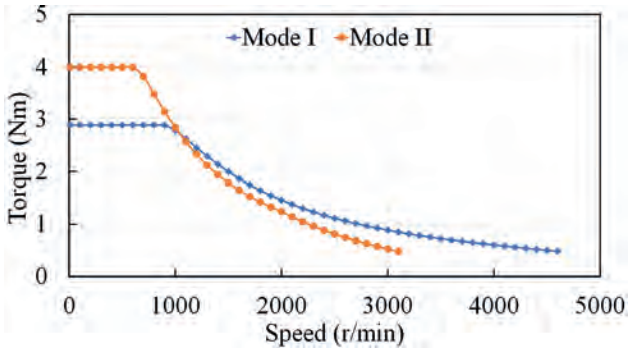

Fig. 2. T-n curves.

VP12-27. Design and analysis of a new series-parallel hybrid magnetic circuit permanent magnet synchronous motor.
S. Wang[1], L. Mo[1] and K. Zhang[1] *1. Huaiyin Institute of Technology, Huaian, China*

Traditional rare earth permanent magnet synchronous motor has the advantages of simple structure, small size, high efficiency and high power factor[1]. However, the local demagnetization or magnetic leakage flux of traditional rare earth permanent magnet synchronous motors is more serious, and due to the high magnetic flux density generated by permanent magnets, the structure has high torque density and large cogging torque, resulting in unfavorable torque ripple[2]. Therefore, this paper proposes a new series and parallel hybrid magnetic circuit permanent magnet synchronous motor, which uses series and parallel hybrid magnetic circuit to make the motor obtain higher magnetic convergence effect. More balanced and uniform Q-axis magnetic circuit. Parametric analysis results in minimal cogging torque and torque ripple. By finite element analysis, it is compared with the optimized conventional built-in V-type permanent magnet synchronous motor. This structure can well reduce the cogging torque and torque ripple of the motor. Figure 1 shows a schematic diagram of the motor of this structure. Figure 2 is a schematic diagram of the magnetic field lines of this structure.

[1] Salim Sazzad. Design and analysis of new magnetic shaft offset built-in permanent magnet motor for electric vehicles[D].Southeast University, 2020. [2] Li Shengnan. Research on direct torque control of three-phase permanent magnet synchronous motor[D].Southeast University, 2021.

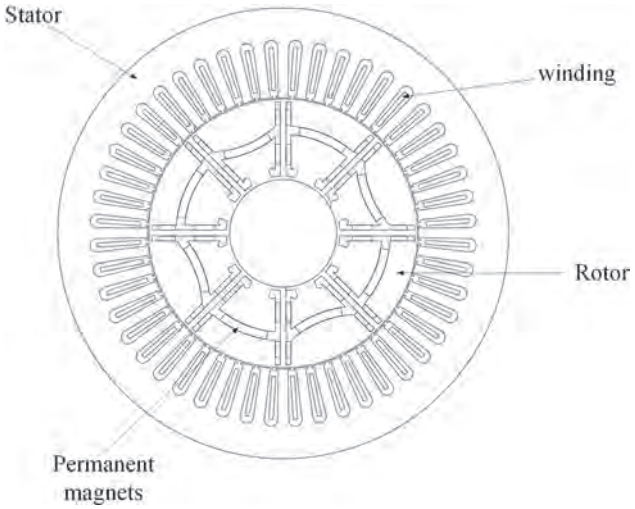

Fig.1 Schematic diagram of this structure motor.

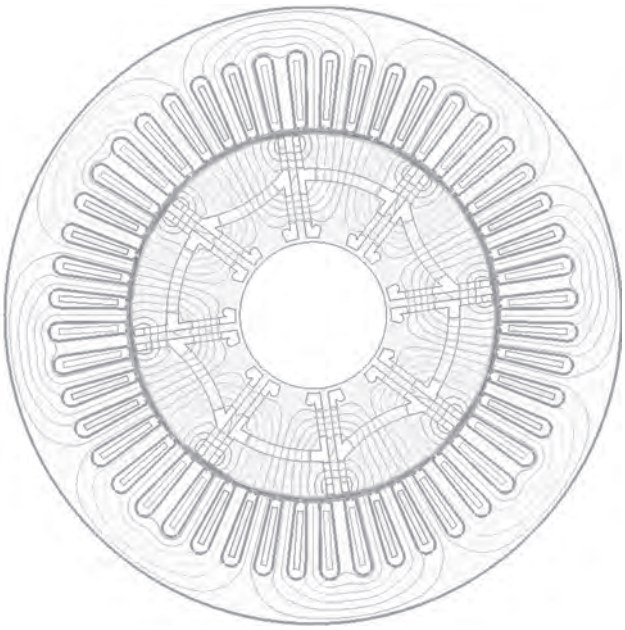

Fig.2 Schematic diagram of magnetic field lines.

VP12-28. Research on the method of cogging torque reduction of new built-in permanent magnet motor. *K. Zhang*[1] *1. Huaiyin Institute of Technology, Huaian, China*

Interior permanent magnet synchronous motors(IPMSMs) has strong overload capacity, high power density, wide speed regulation range, can effectively use magnetoresistive torque and easy to achieve weak magnetic speed expansion, which has become the development trend of drive motors for electric vehicles[1]. However, because the armature slotting inevitably produces the tooth groove torque, it affects the vibration and noise of the motor, speed fluctuation and reduces the control accuracy of the motor. For cogging torque, some methods have been studied, for example, by designing the shape of the rotor magnetic barrier and deflecting the wedge[2] and shifting the permanent magnet[3] to reduce torque ripple. This article describes a new type of built-in permanent magnet motor, as shown in Fig. 1. Optimize the cogging torque by combining the stator chute and rotor magnetic pole offset, as shown in Fig. 2. The optimization of the original structure, stator chute, rotor offset and stator chute plus magnetic pole offset are analyzed respectively. The results show that the cogging torque decreases from the initial 3.915N. to 0.965N.m of the stator chute and 0.727N.m of the pole shift, and finally the 0.259N.m of the stator chute plus pole offset combination is optimized. This method can reduce the vibration and noise of the new built-in permanent magnet motor and improve the control precision of the motor.

[1] Lin Y, Sun Y, Wang Y, "Radial electromagnetic force and vibration in synchronous reluctance motors with asymmetric rotor structures". J. IET Electric Power Applications. vol. 15, pp. 12080-120883, 2021. [2] Jang H, Kim H, Liu H C, "Investigation on the Torque Ripple Reduction Method of a Hybrid Electric Vehicle Motor". J. Energies. vol. 14, pp.1413-1415, 2021. [3] Mirzahosseini R, Darabi A, Assili M, "Magnet shifting for back EMF improvement and torque ripple reduction of a TORUS-type nonslotted axial flux permanent magnet machine". J. International Transactions on Electrical Energy Systems. vol. 30, pp. 12293-12295, 2019.

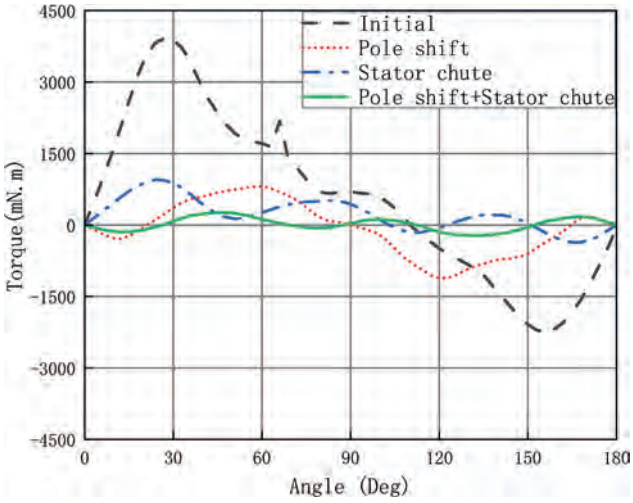

Fig. 2. Comparison of cogging torque.

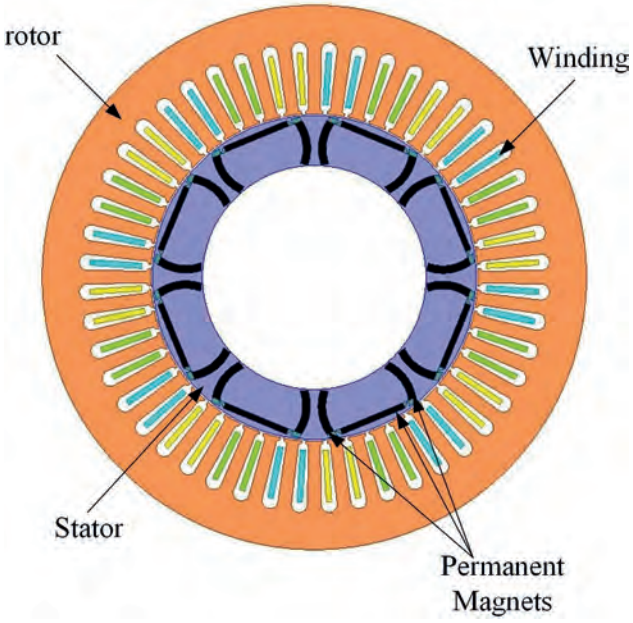

Fig. 1. Model of IPM motor.

VP12-29. Determination of matching capacitor for a distance variable wireless power transfer system. *S. Lee*[1], D. Kim[1], J. Cheon[1], H. Park[1] and D. Kim[1] *1. Department of Automotive Engineering, Yeungnam University, Gyeongsan, The Republic of Korea*

Recently, the wireless power transfer (WPT) system has been widely used as a practical application. Since the WPT system enables the wireless transfer of electrical energy, it eliminates the need for a physical connection between the power source and the load. Consequently, the WPT system exhibits significant potential in terms of interoperability. In general, to achieve high power transfer efficiency, compensation circuits comprising of Tx or Rx coils and matching capacitors are employed in both the transmitting and receiving parts. In this scenario, the value of the matching capacitor is determined based on the inductance of the Tx/Rx coils and the operating frequency [1]. However, due to variations in the dimensions of different applications, the air gap or distance between the transmitting coil and receiving coil can be deferred, as depicted in Fig. 1. In this condition, as the air gap affects the self-inductance of both the transmitting and receiving coils, the resonance frequency is varied, leading to an inevitable decrease in power transfer efficiency [2-4]. In this paper, we propose a method to determine the matching capacitor for achieving higher power transfer efficiency in a distance-variable WPT system. Through a theoretical approach, the matching capacitor is determined under the assumption that the Tx coil and Rx coil are at their farthest distance. Figure 2 illustrates the power transfer efficiency corresponding to the distance between the transmitting coil and receiving coil under various matching conditions. A comparison between the 2 mm and 8 mm matching conditions reveals that the 8 mm matching condition exhibits lower power transfer efficiency variation across the 2 mm to 8 mm air gap. The simulation results support the notion that the matching capacitance should be determined while considering the farthest distance condition of the WPT system in order to minimize power transfer efficiency variation.

[1] X. Mou, et al., "Survey on magnetic resonant coupling wireless power transfer technology for electric vehicle charging," IET Power Electronics, Vol. 12, No. 12, pp. 3005-3020, Sep., 2019. [2] T. P. Duong, and J.-W. Lee, "Experimental Results of High-Efficiency Resonant Coupling Wireless Power Transfer Using a Variable Coupling Method," IEEE Microwave and Wireless Components Letters, Vol. 21, No. 8, pp. 442-444, Aug., 2011. [3] J. Kim, and J. Jeong, "Range-Adaptive Wireless Power Transfer Using Multiloop and Tunable Matching Techniques," IEEE Transactions on Industrial Electronics, Vol. 62, No. 10, Oct., 2015. [4] J.-H. Cho, B.-H. Lee, and Y.-J. Kim, "Maximizing Transfer Efficiency with an Adaptive Wireless Power Transfer System for Variable Load Applications," Energies, Vol. 14, No. 5, p. 1417, Mar. 2021.

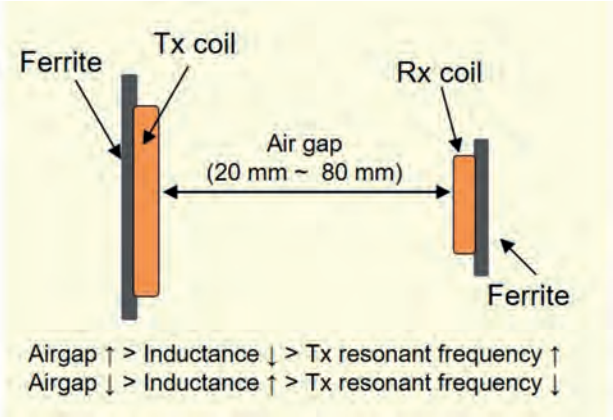

Fig. 1. Concept of variable distance wireless power transfer system

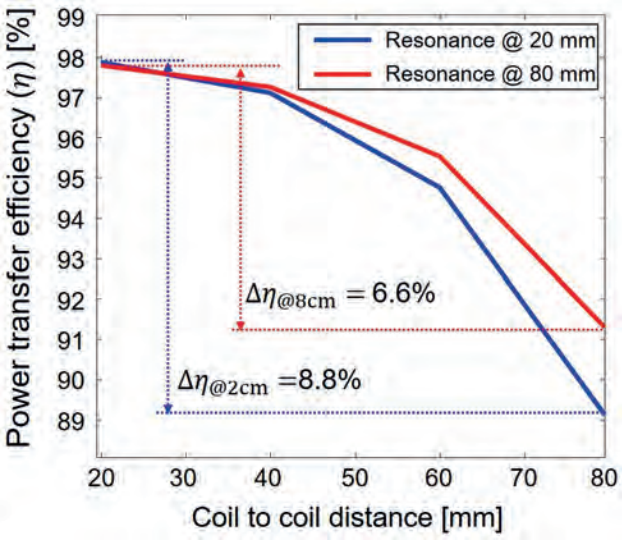

Fig. 2. The simulation results demonstrate the power transfer efficiency of a distance-variable wireless power transfer system.

VP12-30. Synthesis of $CoFe_2O_4$/Mesoporous Carbon hybrid Nanocomposite with Enhanced Microwave Absorption in K and Ka-band. P. Pantola[1,2], S. Kumar[2], D. Chaudhary[2], P. Agarwal[1] and *B.K. Kuanr*[2] *1. School of Basic Sciences, Galgotias University, Greater Noida, India; 2. Special Centre for Nanoscience, Jawaharlal Nehru University, New Delhi, India*

With the rapid development of 5G signals, autonomous vehicles, wireless communications devices, the electromagnetic (EM) radiation resulted in several adverse effects on environment and human body [1]. To reduce EM radiation, microwave absorption materials can effectively be used. Conventional microwave absorbing materials generally comprised of magnetic loss materials and dielectric loss materials. Carbonaceous materials as microwave absorbers have been investigated because of their high dielectric loss and environmental stability. To improve absorption capability in a wide frequency range, nanocomposites of carbon materials with various with magnetic materials are in a great demand [2-3]. Herein, $CoFe_2O_4$/Mesoporous carbon nanocomposite was fabricated via a facile hydrothermal method and demonstrates their microwave absorption properties in K and Ka-band frequencies. XRD results confirmed the pure phase formation of $CoFe_2O_4$ sample. Vibrating sample magnetometer (VSM) shows (Fig.1) decrease of magnetization value for $CoFe_2O_4$/Mesoporous carbon nanocomposites that can be ascribed to the increasing contents of non-magnetic mesoporous carbon. The reflection loss (RL) results demonstrate that minimum RL reached to -31 dB with a matching thickness of 2.5 mm (Fig.2). Effective absorption bandwidth (EAB) obtained is 4.4 GHz The enhanced microwave absorption properties derive from the synergistic effect between dielectric loss of mesoporous carbon, magnetic loss of ferrite and better impendence matching at the interface. The dielectric loss can be associated to the polarization relaxation and mesoporous carbon conductivity. Magnetic loss arises from the natural resonance of ferrite materials. The reflection loss and EAB results shows that $CoFe_2O_4$/Mesoporous carbon nanocomposite shows the admirable microwave absorption performances and can be a promising candidate for Stealth technology and in advanced communication system.

[1] L. Wang, Z. Du, L. Xiang, D. Hou, S. Zhu, J. Zhu, Y. Mai, R. Che, The ordered mesoporous carbon coated graphene as a high-performance broadband microwave absorbent, Carbon 179 (2021) 435-444. [2] Y. Liu, D. He, O. Dubrunfaut, A. Zhang, H. Zhang, L. Pichon, J. Bai, GO-CNTs hybrids reinforced epoxy composites with porous structure as microwave absorbers, Composites Science and Technology 200 (2020) 108450. [3] X. Zhang, L. Cai, Z. Xiang, W. Lu, Hollow CuS microflowers anchored porous carbon composites as lightweight and broadband microwave absorber with flame-retardant and thermal stealth functions, Carbon 184 (2021) 514-525.

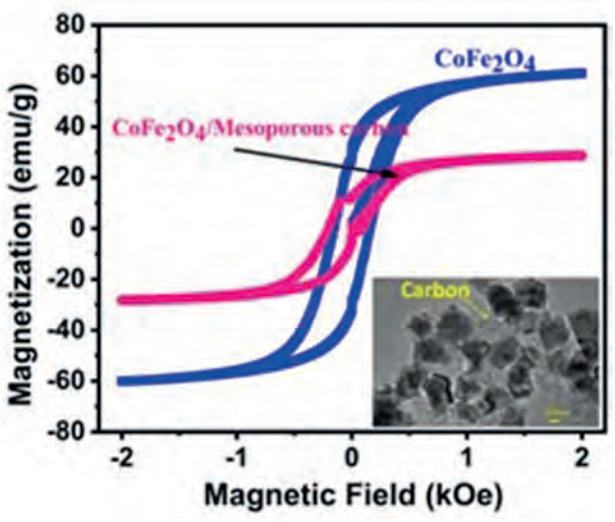

Fig. 1 VSM data of pure $CoFe_2O_4$ nanoparticles and $CoFe_2O_4$/Mesoporous carbon nanocomposite. Inset shows TEM image of the nanocomposite.

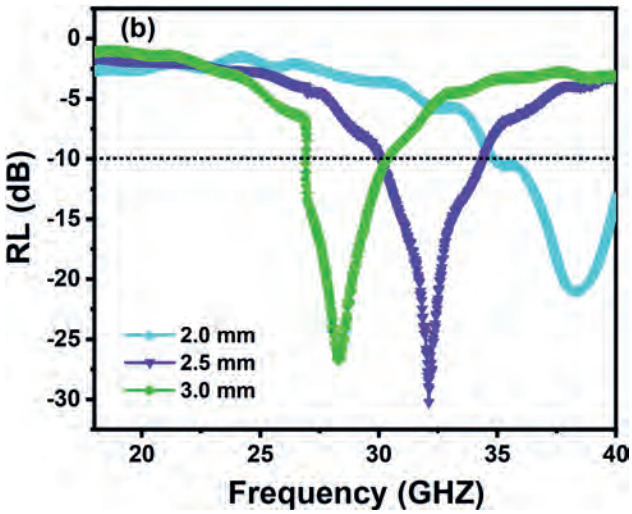

Fig. 2 RL plots for the $CoFe_2O_4$/Mesoporous carbon nanocomposite for different absorber thickness in the K and Ka-Band.

VP12-31. Design and analysis of sticker-built-in hybrid permanent magnet synchronous motor for flywheel energy storage. *T. Qin*[1]
1. Faculty of Automation, Huaiyin Institute of Technology, Huaian, China

The permanent magnet synchronous motor (PMSM) is widely utilized in flywheel energy storage systems due to its high efficiency and compact struture. However, the conventional built-in PMSM exhibits significant torque ripple. To address this issue, this paper proposes a hybrid rotor structure for the permanent magnet synchronous motor. The rotor structure integrates the benefits of surface mount and built-in rotor structures, while also exhibiting the drawback of a built-in air-gap magnetic density waveform. At the same time, it also shows that the air gap magnetic density waveform of the built-in permanent magnet synchronous motor is not sinusoidal. This article presents the sticker-built-in hybrid permanent magnet synchronous motor (SBH-PMSM) depicted in Figure 1. In rotor the mount and built-in hybrid PM structure is adopted design, The built-in PMs consist of the V-shape PM set and the spoke PM set. The series PM magnetic circuit allows for superposition of the PM magnetomotive force to enhance the main magnetic flux and improve torque density. The optimization of the surface mounted permanent magnet shape leads to an optimized sinusoidal magnetic density in the motor air gap. The finite element analysis results demonstrate that the proposed permanent magnet synchronous motor not only enhances torque density but also reduces torque ripple, while achieving a more sinusoidal air gap flux density.

[1]Bowen, Cui, Z.Jihua, and R. Zhang. "Modeling and simulation of permanent magnet synchronous motor drives." International Conference on Electrical Machines & Systems IEEE, 2001. [2]Honda, Y., et al. "Rotor design optimisation of a multi-layer interior permanent-magnet synchronous motor." IET electric power applications 2(1998):145. [3] Kato, Shingo. "Design Optimization of Interior Permanent Magnet Synchronous Motors for HEV and EV." SAE World Congress 2010.

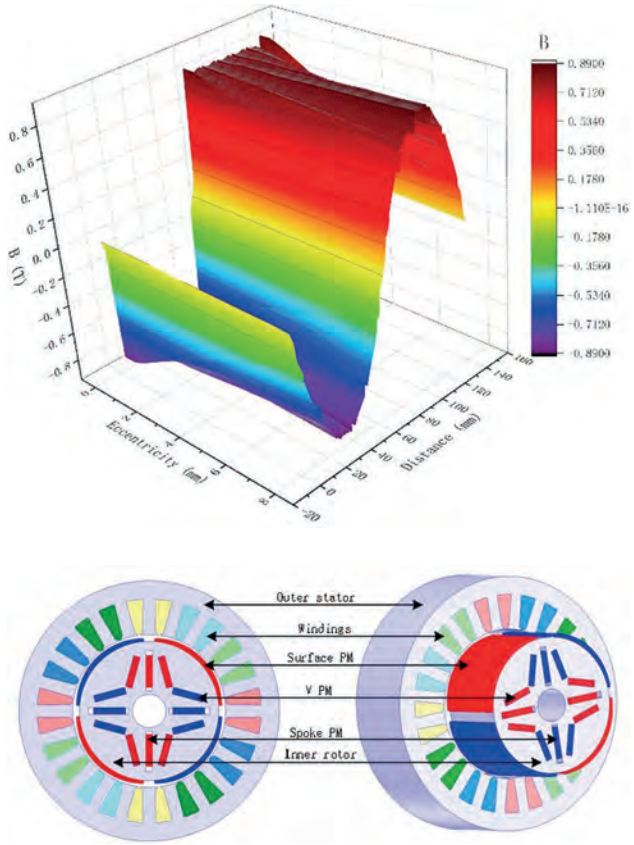

VP12-32. Design and analysis of flux switching motor for flywheel energy storage battery based on UPS. *Z. Zhao*[1] *1. Huaiyin Institute of Technology, Huaian, China*

With the rapid growth of social demand for electricity, flywheel energy storage batteries with high energy storage density, fast charging, non-pollution, and other characteristics gradually replace the traditional chemical batteries as the UPS energy storage unit. Currently, most motors used in flywheel batteries are reluctance motors, permanent magnet motors, etc. In contrast, flux-switching motors are relatively blank in flywheel energy storage applications. Among them, the outer rotor flux switching motor (OR-FSPM) has a higher air gap flux density due to the magnetization of the stator. It, therefore, has a more vital torque output capability, so it has a good application prospect in flywheel energy storage. However, its convex pole structure and higher air-gap flux density make the cogging torque and torque fluctuation larger, which needs further optimization research. In this paper, we mainly design and analyze a 12/22 OR-FSPM motor for a UPS flywheel battery (Fig.1), conduct electromagnetic performance analysis, mainly including data of magnetic field distribution, torque, air-gap magnetic density, etc., and analyze the contribution of different harmonics in the air-gap magnetic field of the FSPM motor to the output torque through the air-gap magnetic field modulation mechanism, to optimize the motor without affecting the output torque reducing the cogging torque. It also calculates copper losses, iron losses, permanent magnet eddy current losses, and various motor harmonics

losses. The simulation results of this article indicate that the 4th, 6th, 16th, 18th, 28th and 40th harmonics in the OR-FSPM motor designed in this article will provide the main torque, accounting for 86.76% of the output torque (Fig 2). Therefore, keeping the main harmonics constant and attenuating the other harmonics ensures that the motor has sufficient output capability and reduces torque pulsation.

[1] WANG Peixin, HUA Wei and HU Mingjin, Proceedings of the CSEE., Vol.42 No.22, p. 8372-8381 (2022) [2] ZHU Xiaofeng, HUA Wei, Proceedings of the CSEE., Vol.37 No.21, p. 6146-6157 (2017)

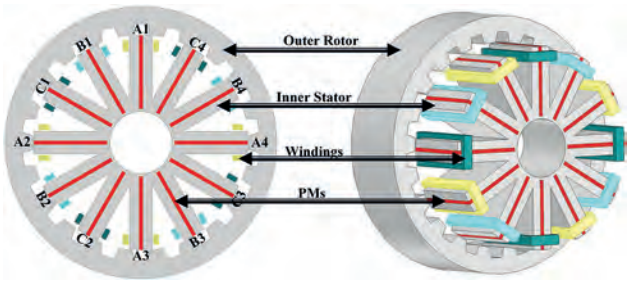

Fig. 1 Simulation model of 22/12 OR-FSPM motor

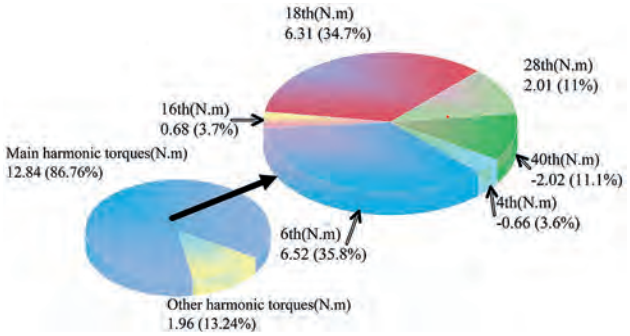

Fig. 2 Torque of the OR-FSPM machine

VP12-33. Comparison of flux-switching in-wheel PM machines with different PM configurations using magnetic gearing principle. *L. Mo*[1]
1. Huaiyin Institute of Technology, Huai'an, China

Stator permanent magnet (PM) machines, such as the flux-switching permanent-magnet (FSPM) machines, have attracted much attentions for its high torque density and simple rotor [1]. The purpose of this paper is to develop two kinds of Outer-Rotor-Permanent-Magnet Flux-Switching (ORPM-FS) machines and compare the differences on the airgap magnetic field and output torque. In Fig.1, 'Model 1' represents a 12s/22r ORPM-FS machine, and 'Model 2' shows a 12s/11r V-shape ORPM-FS machine. Fig.1(c) displays a 12s/22r stator-PM FSPM in-wheel machine, named as 'Model 3'. For the Model 1 and Model 2, the resulting output torque depends on the interaction of the airgap fields generated by the rotor-PMs and the stator-windings. The pole-pair numbers (PNN) of the armature windings are designed to equal to that of the PMs. And the speed of the rotational magnetic field yielded by armature currents is also equal to that of the rotor PMs. For the Model 3, the salient rotor poles can excite much field harmonics in the airgap. According to the magnetic gearing effect, the rotor pole number is the sum of the PPN of PMs and the PPN of armature windings [2]. The analytical and simulation results (Fig.2) show that the airgap harmonic orders 4,6,8 14,16,18,20 of the Model 3 are effective, and is helpful to improve the electromagnetic torque. And for the Model 1 and Model 2, there are only 11 and 22 as the effective harmonics. The results confirm that the electromagnetic torque is dominantly contributed by the fundamental component with PM pole-pairs for the rotor-PM machine, while the electromagnetic torque of the stator-PM machine is not only produced by the fundamental component, but also attributed by the modulation harmonics. Further research displays that the electromagnetic torques of Model 1 and Model 2 are mainly (>80%) contributed by the fundamental harmonic torque. While, the electromagnetic torque of Model 3 is mainly (>97%) contributed by the effective working harmonics (4th, 6th, 8th, 14th, 16th, 18th, 20th order). Three topologies have favorable torque-current characteristics, among which the Model 2 has the highest output capability.

[1]Ruiwu Cao, Chris Mi, and Ming Cheng, "Quantitative Comparison of Flux-Switching Permanent-Magnet Motors with Interior Permanent Magnet Motor for EV, HEV, and PHEV Applications," IEEE Transactions on Magnetics, 2012, 48(8):2374-2384. [2]Shi Yujun,Jian Linni, Wei Jin,et al. "A new perspective on the operating principle of flux-switching permanent-magnet machines," IEEE Transactions on Industrial Electronics, 2016,63(3): 1425-1437.

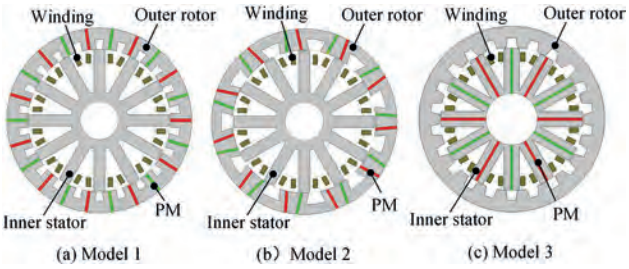

Fig. 1. Machine topologies

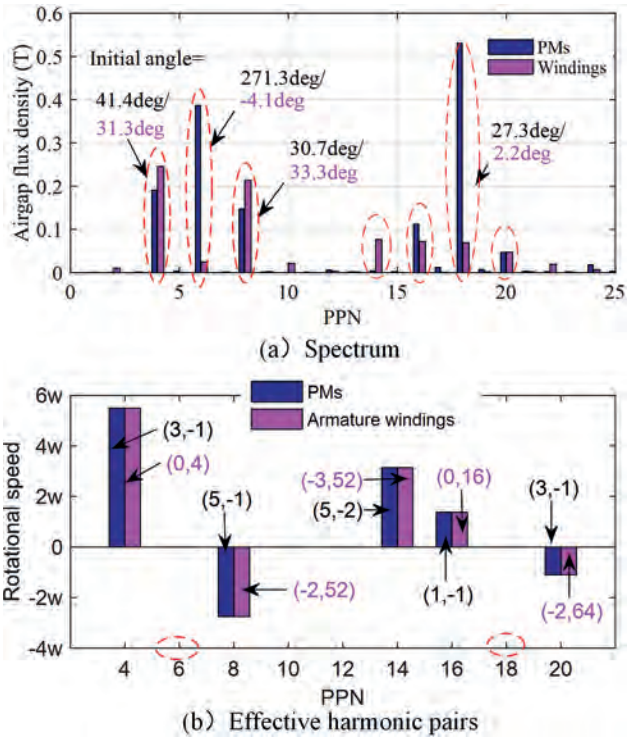

Fig. 2. Effective harmonic pairs of the Model 3

VP12-34. Analytical-Based Design Methodology and Performance Analysis of a Novel Alterable-Magnetic-Circuit Variable Flux Memory Machine. *S. Zhang*[1], F. Wang[1], Y. Nan[1] and P. Zheng[2] *1. College of Marine Electrical Engineering, Dalian Maritime University, Dalian, China; 2. School of Electrical Engineering and Automation, Harbin Institute of Technology, Harbin, China*

By regulating the magnetization level of the low-coercivity (low-*Hc*) magnet employed in variable flux memory machine (VFMM), the air-gap flux density of the VFMM can be flexibly adjusted to meet the operating condition requirement [1]. Low-*Hc* magnets and high-*Hc* magnets are simultaneously employed in recently developed VFMMs, in which the low-*Hc* magnets

offer the flux regulation capability while the high-*Hc* magnets assist to enhance the torque density of the machines. However, design tradeoff exists in current VFMMs, which results in the key performances in terms of torque production capability, flux regulation capability and resisting unintentional demagnetization capability not being optimized simultaneously. This paper proposes a novel alterable-magnetic-circuit variable flux memory machine (AMC-VFMM) as shown in Fig. 1(a). In the proposed AMC-VFMM the low-*Hc* magnets and high-*Hc* magnets constitute a quasi-series magnetic flux relationship and the flux regulation barrier provides a passive closed path for the high-*Hc* magnet's magnetic flux. As a result, the magnetization level of low-*Hc* magnets in the proposed machine are easier to regulate than in the existing VFMM topology and superior torque production capability can also be obtained. The no-load magnetic flux distribution of the AMC-VFMM are shown in Fig. 1(b) and (c). An analytical-based design methodology of the AMC-VFMM is proposed. Firstly, the analytical expression of the maximum *d*-axis MMF preventing the unintentional demagnetization and the required flux regulation MMF are derived. Secondly, the design methodology combined the analytical calculation and finite element analysis considering key performances of the AMC-VFMM are established, of which design flow chart is shown in Fig. 2. Thirdly, the key performances of the design scheme are calculated and analyzed. The results show that the flux linkage can be regulated from 3.4% to 100%, which indicates superior flux regulation capability of the proposed AMC-VFMM. Finally, the mechanical strength of the machine at 12000 r/min are verified to validate the rotor topology of the machine.

[1] S. Lyu, H. Yang, H. Lin *et al.*, "Improved MTPA Control for Variable-Flux Memory Machine with Operating Envelope Prediction-Based MS Manipulation," *IEEE Trans. Power Electron.*, 38(3), 3700-3710 (2023).

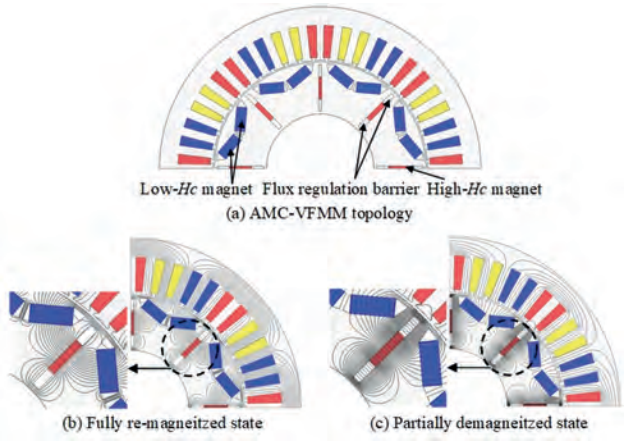

Fig. 1. Topology and no-load magneitc flux distribution of the AMC-VFMM

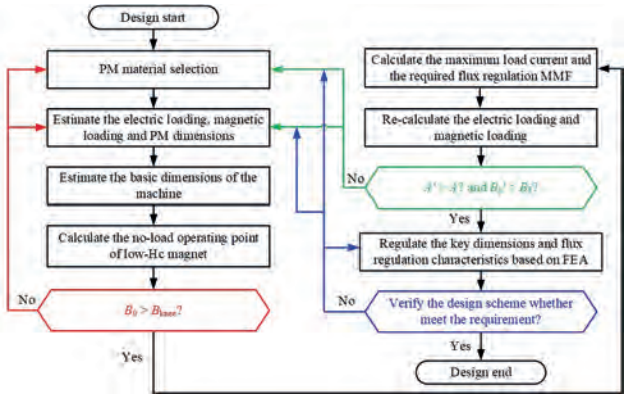

Fig. 2. Design methodology of the AMC-VFMM

VP12-35. Design and Analysis of a V-Shaped Leakage-Flux-Controllable PM Machine with Improved Torque Performances. *X. Cai*[1] and X. Zhu[1]
1. School of Electrical and Information Engineering, Jiangsu University, Zhenjiang, China

Permanent magnet (PM) motors have been widely applicable for electric vehicles due to their excellent power density and efficiency. Yet, due to the relatively constant airgap magnetic field, the motor always suffers from a limited speed range. So, the achievement of a wide speed range is one of the hot research orientations for PM motors. In recent years, a type of leakage-flux-controllable (LFC) motor has attracted some interest and attention of researchers, where the magnetic bridge and flux barrier are purposely designed in PM rotor for forming the controllable leakage flux[1]. Based on this, the LFC-PM motor possesses the potential advantages of speed regulation[2]. It is noted that to realize the condition of no leakage flux in motor drive process, a relatively strong armature field is usually required to be applied at this time, and, correspondingly, the magnetic saturation comes with that. It means that the torque capability of LFC PM motor is worthy of attention and full of challenge, especially on the drive requirements of low-speed large torque. In this study, a V-typed leakage-flux-controllable PM (VLFC-PM) motor with multiple functional magnetic flux barrier units is proposed, which can provide relatively high output torque and a wide speed range. The motor topology and magnetic barrier structure analysis are shown in Fig. 1. The magnetic field distributions under different operating conditions are shown in Fig. 2. At no load, the flux leakage barrier guides parts of PM flux into the flux leakage path and reduces the air gap effective flux. As the armature current increases, the flux focusing barrier guides the PM flux to pass through the air gap rather than flux leakage path, and the main flux is enhanced. And then, a response surface method is adopted to optimize the key parameters related to the magnetic flux barrier units in Fig. 3. After optimization, the torque performances of the motor are significantly improved both at different operating conditions as shown in Fig. 4. Finally, the torque characteristics of the motor are verified through experiments in Fig. 5. The experimental results are in good agreement with the simulation results, which verifies the effectiveness of the motor design.

[1] T. Kato, T. Matsuura, K. Sasaki, and T. Tanimoto, "Principle of variable leakage flux IPMSM using arc-shaped magnet considering variable motor parameter characteristics depending on load current," *in Proc. IEEE Energy Convers. Congr. Expo.*, 2017, pp. 5803–5810. [2] X. Zhou, X. Zhu, W. Wu, Z. Xiang, Y. Liu, and L. Quan, "Multi-objective optimization design of variable-saliency-ratio PM motor considering driving cycles," *IEEE Trans. Ind. Electron.*, vol. 68, no. 8, pp. 6516–6526, Aug. 2021.

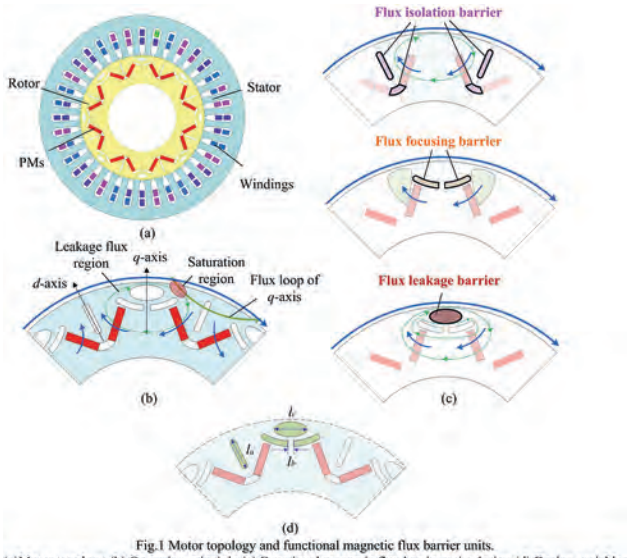

Fig.1 Motor topology and functional magnetic flux barrier units.
(a)Motor topology (b) Operating principle (c) Functional magnetic flux barrier units design (d) Design variables

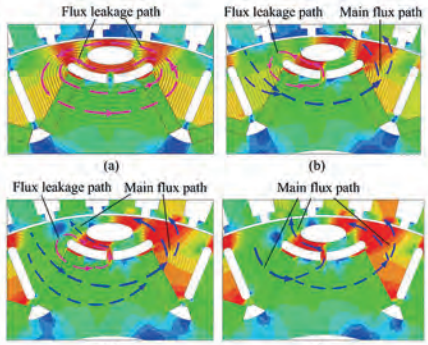

Fig. 2 Magnetic flux analysis under different operating conditions.
(a) i_q=0A (b) i_q=10A (c) i_q=20A (d) i_q=30A

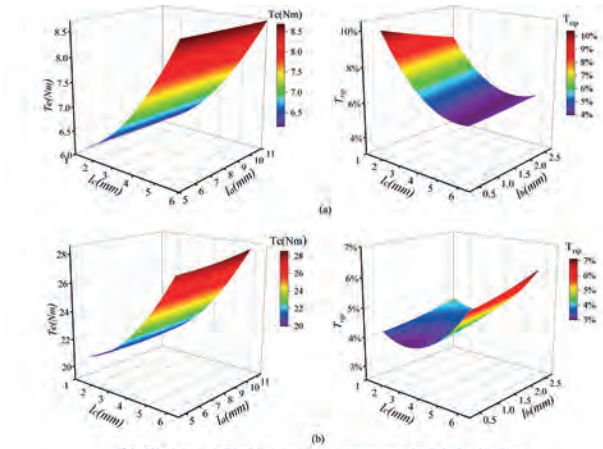

Fig. 3 The response surface of key magnetic barrier parameters and optimization objectives
(a) i_d=10A (b) i_q=30A

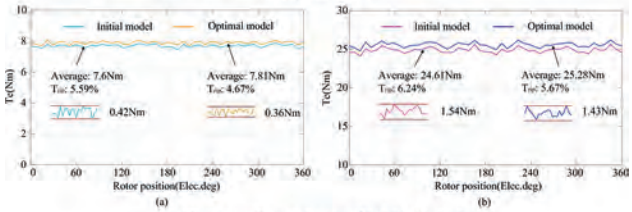

Fig. 4 Comparisons of torque performances of the initial and optimal motors
(a) i_d=10A (b) i_q=30A

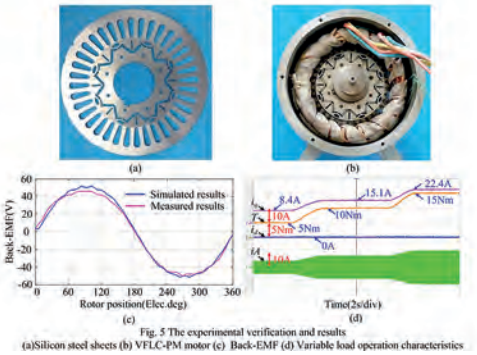

Fig. 5 The experimental verification and results
(a)Silicon steel sheets (b) VFLC-PM motor (c) Back-EMF (d) Variable load operation characteristics

VP12-36. *D-q*-axis Flux Design of Reverse-salient Multilayer Flux Barrier Motor with Wide Speed Range. *L. Ji*[1] and L. Quan[1] *1. School of Electrical and Information Engineering, Jiangsu University, Zhenjiang, China*

In recent years, PM-assisted synchronous reluctance motor has received extensive attention, due to the merits of high torque density and power density [1]. However, due to the existence of PMs and multi-layer flux barriers in the *d*-axis, the *d*-axis inductance is relatively low, which limits the further improvement of the speed range [2]. Therefore, a reverse-salient multilayer flux barrier (RS-MFB) motor is proposed in this paper. In the proposed motor, by the artful design of the *d-q*-axis flux path, so that d-axis inductance can be increased effectively. It means that the speed range is further improved, and the power output capacity in the high-speed region is enhanced. In addition, due to its reverse-salient characteristics, RS-MFB motor works in the flux-intensifying region under rated operation condition, which increases the PM operation point and reduce irreversible demagnetization risk. Fig. 1 shows the structure and the simplified *d*-axis flux circuit of RS-MFB motor. In order to demonstrate the advantages of the proposed motor, the referenced PMASR motor is also investigated and compared. Fig. 2 shows the comparison of electromagnetic performances of two motors, including magnetic distribution, torque-current angle characteristic, inductance characteristic and torque/power-speed characteristics. It is observed that the output torque of the two motors reaches the maximum value at current phase angle +55° and -21°, which verifies that the PMASR motor operates in the deep flux-weakening region, while the RS-MFB motor

operates in the flux-intensifying region. It is indicated that the PM operation point has been increased and irreversible demagnetization risk has been reduced. Furthermore, it is observed that the maximum output torque of the RS-MB is increased by 1.1Nm and torque ripple reduced from 24% to 10.3%,and the speed range widened by about 50%. In conclusion, it is noted that the proposed RS-MLF motor can realize improved output torque and widen speed range at the same time, which verify the assistance of *d*-*q*-axis design and he rationality of the RS-MLF motor design. More detailed analysis will be presented in the full paper.

[1] T. A. Huynh, and M. Hsieh, "Comparative study of PM-assisted SynRM and IPMSM on constant power speed range for EV applications," *IEEE Trans. Magn*., vol. 53, no. 11, Nov. 2017. Art. no. 8211006. [2] Y. Wang, G. Bacco, and N. Bianchi, "Geometry analysis and optimization of PM-assisted reluctance motors," *IEEE Trans. Ind. Appl.*, vol. 53, no. 5, pp. 4338-4346, Sep. 2017.

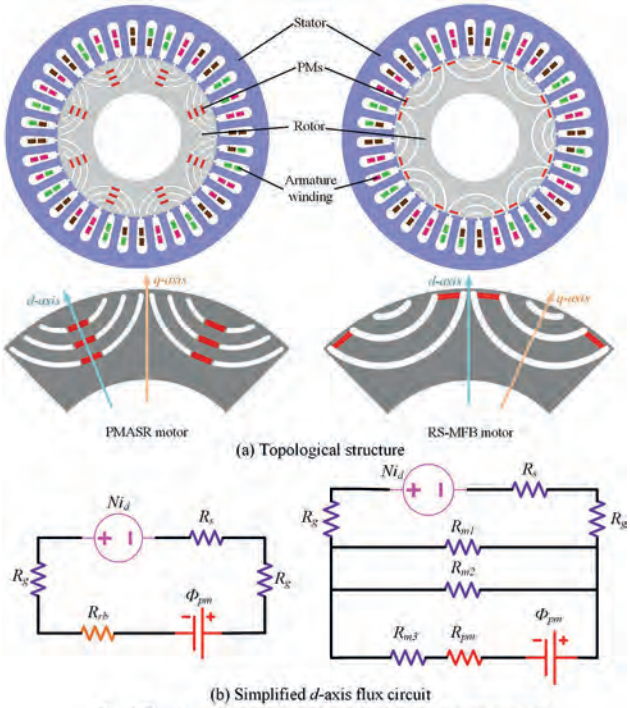

Fig. 1 Topological structure and simplified *d*-axis magnetic circuit

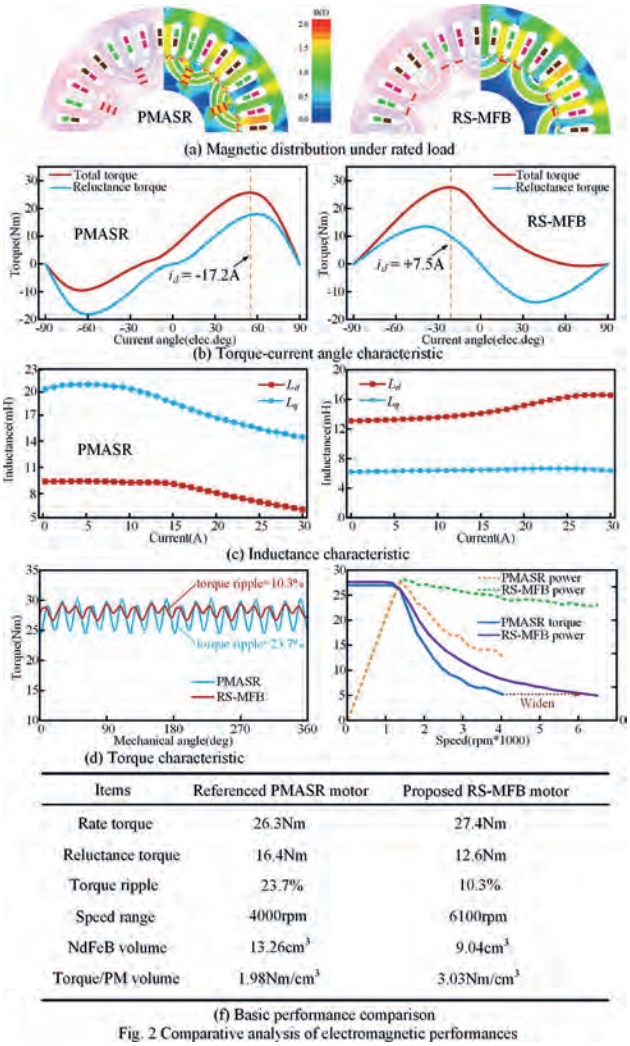

Items	Referenced PMASR motor	Proposed RS-MFB motor
Rate torque	26.3Nm	27.4Nm
Reluctance torque	16.4Nm	12.6Nm
Torque ripple	23.7%	10.3%
Speed range	4000rpm	6100rpm
NdFeB volume	13.26cm^3	9.04cm^3
Torque/PM volume	1.98Nm/cm^3	3.03Nm/cm^3

(f) Basic performance comparison

Fig. 2 Comparative analysis of electromagnetic performances

VP12-37. Torque Enhancement Design and Comparison of a Hybrid Permanent Magnet Variable Leakage Flux Motor. *M. Yang*[1] and L. Quan[1] *1. School of Electrical and Information Engineering, Jiangsu University, Zhenjiang, China*

Permanent magnet (PM) motors have been widely applied, due to high torque density and operating efficiency. However, since PM motors air gap magnetic field is difficult to adjust, its speed regulation range of constant power is relatively narrow. In recent years, variable leakage flux PM (VLF-PM) motor has been proposed [1]. By the targeted design of the magnetic barrier, bypass leakage flux can be controlled, so air-gap flux can be adjusted and corresponding motor speed range can be expanded. However, the magnetic leakage in the motor often leads to the reduction of torque output capability. Therefore, how to improve the torque output capability of the motor while ensuring its wide speed regulation capability has become a difficult research topic in the field of VLF-PM motors. To address this issue, this paper introduces a U-shaped variable leakage flux hybrid PM (VLF-HPM) motor. By incorporating ferrite magnets, the motor achieves the superposition of magnetic potential from the magnetic sources. Moreover, the ferrite magnets mitigates the end magnetic leakage of the NdFeB magnets, thereby improving the utilization rate of NdFeB magnets under heavy load conditions. Consequently, the increased torque output capacity and expanded speed range of VLF-HPM motor can be realized simultaneously. Fig. 1 shows the proposed VLF-PM and VLF-HPM motors and their flux leakage paths. Fig. 2(a) and Fig. 2(b) present the magnetic field lines and magnetic density distributions of the two motors under rated working condition. Fig. 2(c) shows that VLF-HPM motor not only improves the PM flux linkage

compared to the VLF-PM motor, but also increases the magnetic adjustment range from 24.5% to 35.5%. The total torque is also increased by 2Nm, as shown in Fig. 2(d). Due to the introduction of ferrite materials, the reluctance torque of VLF-HPM motor is increased by 5.5Nm in Fig. 2(e). Table 1 shows the cost and basic performance of the motor[2]. Fig. 2(f) shows the curves of torque-speed and power-speed of the two motors. In conclusion, the proposed VLF-HPM motor can not only realize the torque output capacity, but also expand the speed regulation range. More simulation and experimental results will be presented in the full paper.

[1] L. Xu et al., "Flux-Leakage Design Principle and Multiple-Operating Conditions Modeling of Flux Leakage Controllable PM Machine Considering Driving Cycles," in IEEE Transactions on Industrial Electronics, vol. 69, no. 9, pp. 8862-8874, Sept. 2022, doi: 10.1109/TIE.2021.3116588.
[2] Z. S. Du and T. A. Lipo, "Cost-Effective High Torque Density Bi-Magnet Machines Utilizing Rare Earth and Ferrite Permanent Magnets," in IEEE Transactions on Energy Conversion, vol. 35, no. 3, pp. 1577-1584, Sept. 2020, doi: 10.1109/TEC.2020.2978256.

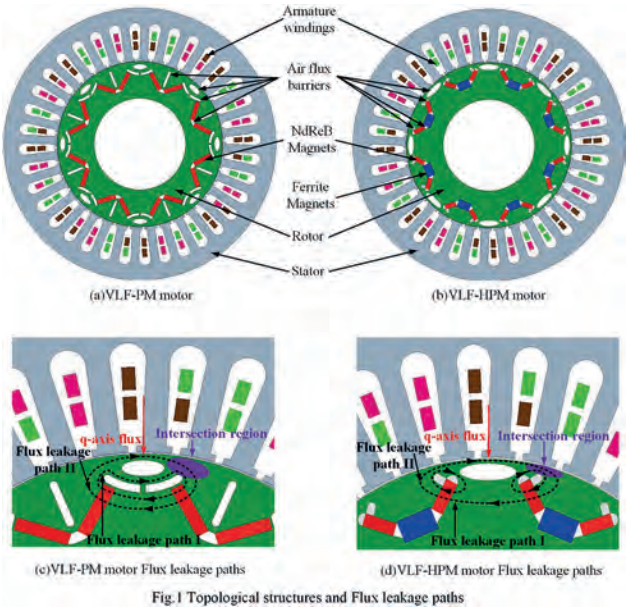

Fig.1 Topological structures and Flux leakage paths

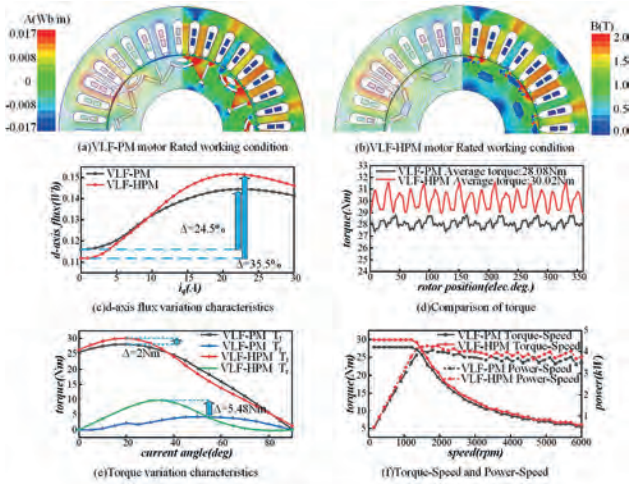

Table 1. Basic performance comparison

Items	VLF-PM motor	VLF-HPM motor
NdFeB PM volume	40560mm³	24960mm³
Ferrite PM volume	----	25272mm³
Rate torque	28.08Nm	30.02Nm
Reluctance torque	4.3Nm	9.8Nm
Adjustable d-axis flux range	24.5%	35.5%

Fig.2 Comparison of Electromagnetic Performance of VLF-PM and VLF-HPM motors

VP12-38. Phase Shift Investigation of Dual-Three Phase V-Shaped PMVM for Improved Torque and Power Factor. *D. Pang*[1] and X. Zhu[1]
1. School of Electrical and Information Engineering, Jiangsu University, Zhenjiang, China

In recent years, permanent magnet vernier machine (PMVM) has aroused extensive research, due to merits of high torque density [1]. However, because of the inevitable flux leakage and large number of airgap flux harmonics, PMVM suffers from the poor power factor, which limits the applications of PMVM [2]. Consequently, it has been a hot but challenging issue on how to realize high output torque and improved power factor simultaneously in the research field of PMVM. Therefore, this article proposes a dual three-phase (DTP) V-shaped PMVM (V-PMVM) with the phase shift angle. In the proposed machine, the influence of phase shift angle on machine torque and power factor is investigated in detail. Also, by the purposeful design of phase shift angle, magnetomotive force (MMF) harmonics are eliminated selectively and the phase winding self-inductance could be reduced, it can not only promote power factor but also increase torque and reduce loss, which lays foundation for the application of this kind of motors in electric vehicles. The topology of V-PMVM and the DTP drive control system are shown in Fig. 1 (a). The Fig. 1 (b) reveals the process of armature MMF harmonics elimination by the phase shift angle and the torque generation of V-PMVM. The machine electromagnetic performance is demonstrated in Fig. 2. As presented in Fig. 2 (a), the magnetic density of 30° phase shift reduces the magnetic density saturation most obviously under the condition of just the armature winding working. It is found that 30° phase shift eliminates more MMF harmonics in Fig. 2 (b). As shown in Fig. 2 (c), compared with 0° phase shift, the 30° phase shift average torque improves 6.5%. Stator core loss and rotor loss of 30° phase shift are lowered 13% and 8% than 0° phase shift. The power factor of 30° phase shift is promoted from 0.718 to 0.794 than 0° phase shift in Fig. 2 (d). In conclusion, the dual three-phase V-PMVM with 30° phase shift not only performs higher output torque and lower loss, but also has improved power factor which has a broad application prospect. More detailed analysis and verification will be presented in the full article.

[1] K. Du, L. Xu, W. Zhao and G. Liu, "Analysis and Design of a Fault-Tolerant Permanent Magnet Vernier Machine With Improved Power Factor," in IEEE Transactions on Industrial Electronics, vol. 69, no. 5, pp. 4353-4363, May 2022, doi: 10.1109/TIE.2021.3080206. [2] L. Guo, J. Xu, S. Wu, X. Xie and

H. Wang, "Analysis and Design of Dual Three-Phase Fractional-Slot Permanent Magnet Motor With Low Space Harmonic," in IEEE Transactions on Magnetics, vol. 58, no. 1, pp. 1-12, Jan. 2022, Art no. 8100112, doi: 10.1109/TMAG.2021.3111752.

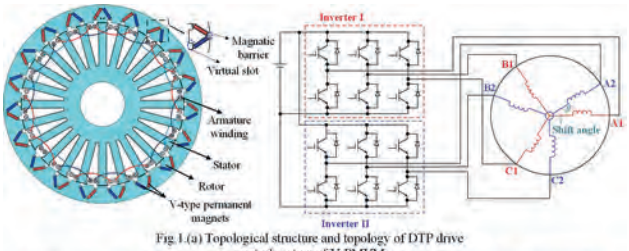

Fig.1.(a) Topological structure and topology of DTP drive control system of V-PMVM

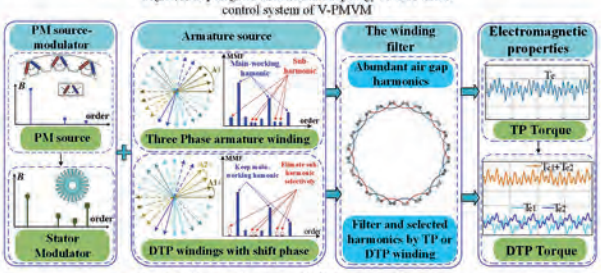

Fig.1.(b) Process of armature MMF harmonics elimination and torque generation of V-PMVM

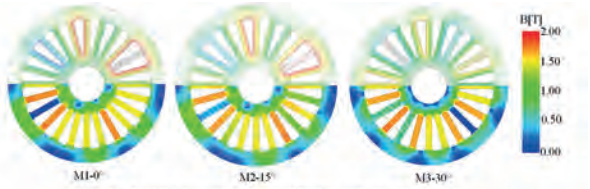

Fig.2.(a) Comparison of armature flux line and magnetic density without function of rotor modulator and PM

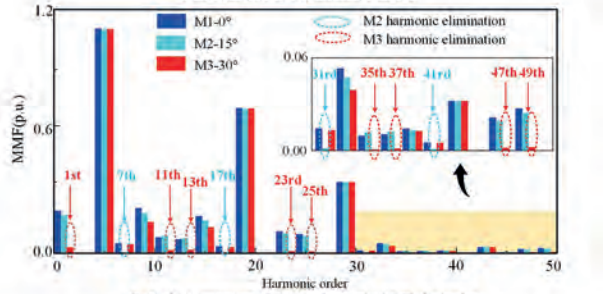

Fig.2.(b) Comparison of armature harmonics MMF elimination

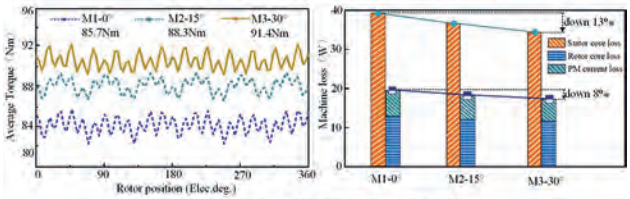

Fig.2.(c) Comparison of average torque and machine loss

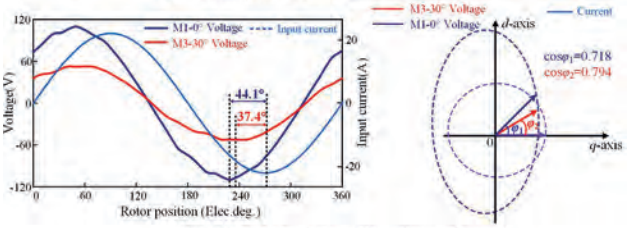

Fig.2.(d) Relationship between phase voltage and current of M1-0° and M3-30°

VP12-39. Design Consideration of Magnet Characteristics for Variable Flux Memory Machines: An Application of (Ce, Nd)-Fe-B Magnets.

S. Zhang[1], F. Wang[1], J. Zhu[1] and P. Zheng[2] *1. College of Marine Electrical Engineering, Dalian Maritime University, Dalian, China; 2. School of Electrical Engineering and Automation, Harbin Institute of Technology, Harbin, China*

The air-gap flux can be flexibly manipulated by regulating the magnetization state of the low-coercivity (low-*Hc*) magnet employed in variable flux memory machine (VFMM). And therefore, the VFMM can meet the operating requirement for both heavy load condition and extended-speed operating condition and obtain overall high efficiency [1]. The operating principle of VFMM is shown in Fig. 1. The VFMM can be demagnetized from P_0 to P_1 along the trajectory $P_0Q_1P_1$ and conversely be re-magnetized from P_1 to P_0 along the trajectory $P_1R_1S_0^+P_0$. Apparently, the coercivity *Hc*, the remanence *Br* and the slope of the demagnetization curve below the knee point μ′ of the low-*Hc* magnet have significant influence on magnetic flux regulation characteristics and torque performance of the VFMM. Dual-main-phase (Ce, Nd)-Fe-B magnet which substituting Ce element for partial Nd element is one kind of newly developed magnet material to reduce the consumption of heavy rare-earth element in conventional Nd-Fe-B magnet. The microstructure of (Ce, Nd)-Fe-B magnet is illustrated in Fig. 1(a). Samples of (Ce, Nd)-Fe-B magnets and corresponding magnetic characteristics are shown in Fig. 1(b). It can be found that *Hc* and *Br* of different grades of (Ce, Nd)-Fe-B magnets can be flexibly adjusted while another property can be kept constant. The feature of *Hc*- and *Br* degradation caused by the substitution of Ce element can be favorably utilized in VFMMs. The employment of (Ce, Nd)-Fe-B magnets makes it possible to design the VFMM with a desired flux regulation characteristic. That is, suitable design scheme can be obtained to meet various electromagnetic performance requirements for different power rating and application fields of VFMM. This paper investigates the influences of magnetic characteristics of (Ce, Nd)-Fe-B magnet on the electromagnetic performance of VFMM. Design consideration of selecting suitable magnetic characteristics for VFMMs to satisfy the design requirement is revealed. The flux regulation characteristics, torque performance and efficiency maps of VFMM with (Ce, Nd)-Fe-B magnet under different magnetization states are calculated and analyzed.

Y. Huang, H. Yang, H. Zheng *et al.*, "Analysis of flux barrier effect of LCF PM in series hybrid magnet variable flux memory machine," AIP Advances, 13(2), 025230 (2023).

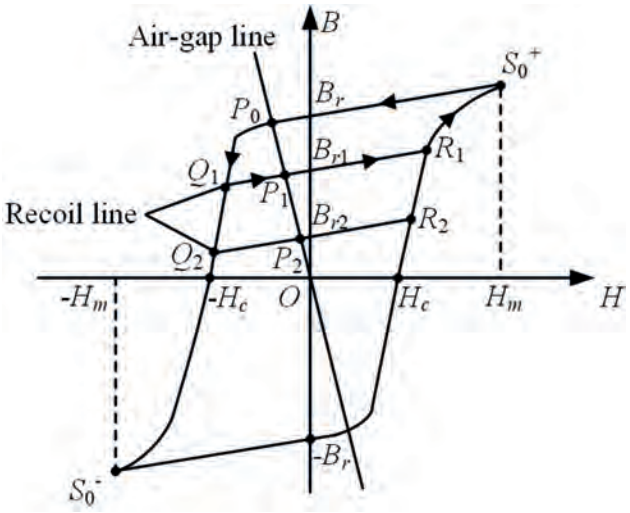

Fig. 1. Operating principle of VFMM

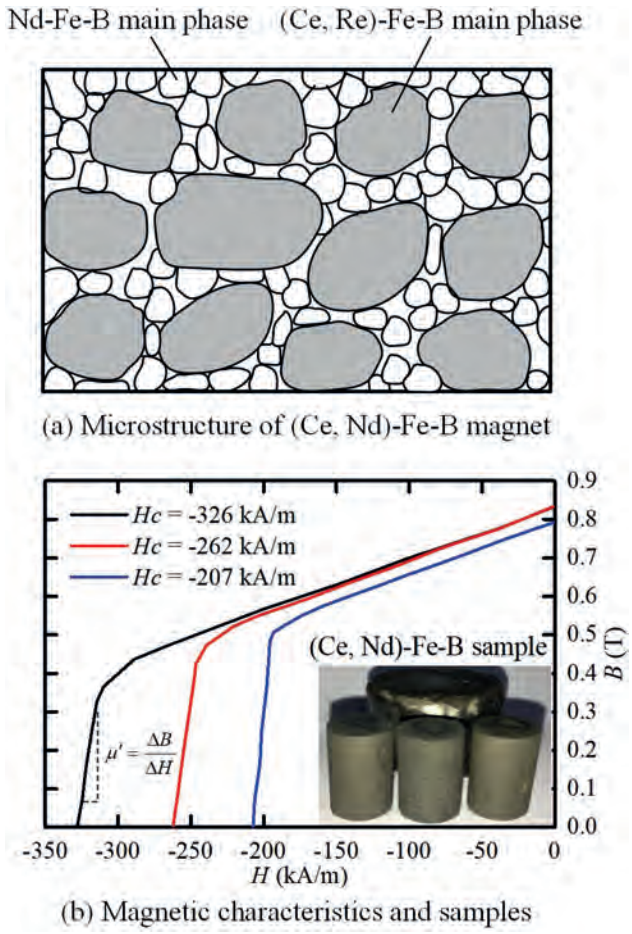

Fig. 2. Microstructure and magnetic characteristics

VP12-40. Electromagnetic performance improvement design method and characteristics analysis for conversion and use of synchronous condenser of coal-fired wound rotor synchronous generator. *G. Jang*[1]
1. Korea Electric Power Research Institute, Daejeon, The Republic of Korea

This paper dealt with the improvement electromagnetic design for converting an old wound rotor synchronous generator into a synchronous condenser, and the characteristics analysis based on finite element analysis. The purpose is to supply reactive power and inertia to the power grid system by using the synchronous condenser and increase system robustness. Globally, coal-fired power generation is decreasing due to carbon emission and environmental pollution problems, and renewable energy sources such as solar power, and wind power are continuously increasing. Renewable energy generation sources generally cannot supply the rotational inertia that conventional synchronous generators have supplied to the power system, and they have the disadvantage of not supplying enough reactive power necessary for system voltage stabilization [1-2]. One of the good solutions to solve these disadvantages is to install a synchronous condenser. However, compared to FACTS, ESS, etc., there is a disadvantage that it takes a long time to install and the cost is high. However, these disadvantages can be solved by converting synchronous generators into synchronous condensers. When used as a synchronous condenser that generates only reactive power, the operating range is different from that of a synchronous generator that generates active power. Therefore, it is necessary to improve the design of various components of the generator, including the rotor coil serving as an electromagnet [3]. Therefore, in this paper, various electromagnetic analyzes were performed for the currently installed generator as shown in Figure 1 and 2. Based on the analysis results, the improved design of the synchronous generator considering the electromagnetic performance and mechanical-thermal stability required for use as a synchronous condenser was performed and verified through finite element analysis. In future research, we plan to install an improved synchronous condenser and conduct a study to test its performance characteristics.

[1] S. S. Kalsi, D. Madura and G. Snitchler, IEEE *Transactions on Applied Superconductivity*, Vol. 17, p.2026 (2007) [2] Sajjad Hadavi, Dayan B. Rathnayake and Gamini Jayasinghe, IEEE *Transactions on Power Systems*, Vol. 37, p.1857 (2022) [3] Udochukwu B. Akuru, Mkhululi Mabhula and Maarten J. Kamper, IEEE *Transactions on Industry Applications*, Vol. 57, p.3687 (2021)

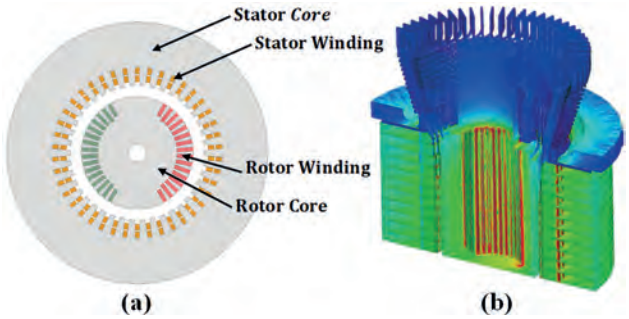

Fig 1. (a) Analysis model of wound rotor synchronous generator, (b) 3D magnetic field distribution analysis result.

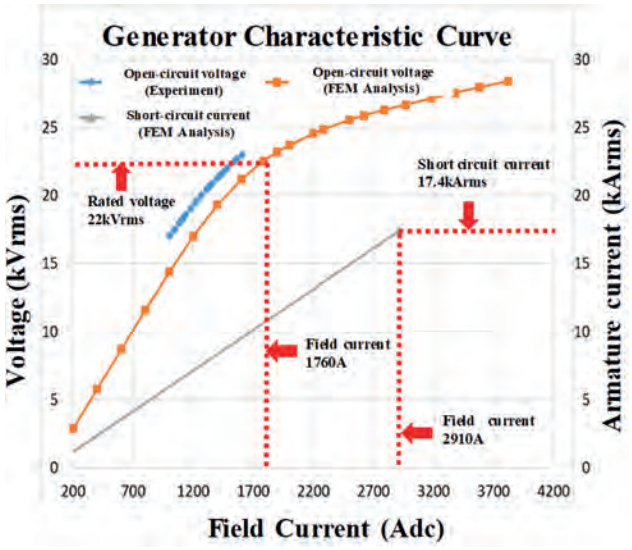

Fig 2. Open-circuit and short-circuit characteristics analysis results of wound rotor synchronous generator.

VP12-41. A study on axial motors to have a thin structure and high power density compared to radial motors. *M. Youn*[1], D. Nam[1], I. Yang[2], M. Hong[1] and W. Kim[1] *1. Department of Electrical Engineering, Gachon University, Seongnam, The Republic of Korea; 2. Hanyang University, Seoul, The Republic of Korea*

The EWP (Electric Water Pump) motor for automobiles is a very important element in the cooling system of automobiles. This is because it must have high output within a limited volume to circulate the cooling water and maintain a constant temperature. In the limited space of automobiles, the advantages of miniaturization and increase in power density are very great. In this paper, we propose an improved EWP motor for automobiles by reducing the axial size of the motor and increasing the radial size to take the form of a thin structure and increasing the power density to secure a spatial advantage. When replacing an existing radial permanent magnet motor with an axial flux motor, the torque density in the same volume is proportional to the cube of the motor diameter, resulting in higher electromagnetic torque and higher torque density. In the multi-pole multi-slot structure, the thickness of

the backyoke of the stator and rotor can be reduced. However, considering the volume of EWP motors, which are small motors, the number of winding turns decreases in the multi-slot structure, and the rate of leakage without linking magnetic flux to the stator increases in the multi-pole structure. In addition, if the number of poles increases, the yoke thickness can be reduced, but the mechanical strength can be lowered. Therefore, a 10-pole 12-slot structure was selected. As above, the design goal of Axial Flux Motor with small size and short axial length is that the backyoke core is saturated and performance has not deteriorated, and that as many windings as possible can be wound on the slot within a small size. Therefore, the rotor core thickness, slot width, and axial length were set as design variables. The proportional relationship between the output value according to the change of each design variable and the number of turns per tooth was confirmed, and even if the target output was satisfied, the model in which the core part was excessively saturated was excluded. Through this process, the optimal model was derived, and the volume increased by about 9% compared to the existing model, but the output increased by about 84%, confirming that the power density increased.

[1] A. Cavagnino, M. Lazzari, F. Profumo and A. Tenconi, "A comparison between the axial flux and the radial flux structures for PM synchronous motors," in IEEE Transactions on Industry Applications, vol. 38, no. 6, pp. 1517-1524, Nov.-Dec. 2002 [2] F. Profumo, Zheng Zhang and A. Tenconi, "Axial flux machines drives: a new viable solution for electric cars," in IEEE Transactions on Industrial Electronics, vol. 44, no. 1, pp. 39-45, Feb. 1997 [3] Sung Chul Oh and A. Emadi, "Test and simulation of axial flux-motor characteristics for hybrid electric vehicles," in IEEE Transactions on Vehicular Technology, vol. 53, no. 3, pp. 912-919, May 2004

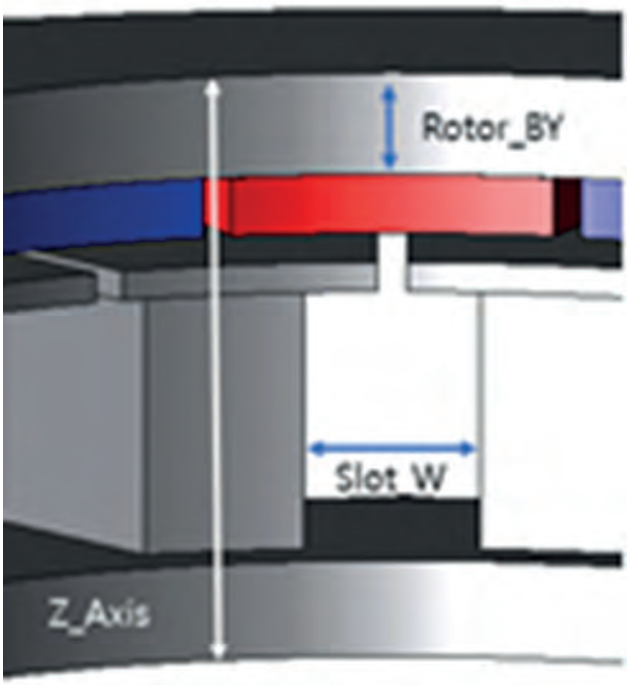

VP12-42. Electromagnetic Characteristic Analysis for Initial Design of Permanent Magnet Synchronous Generator Using Analytical Method.

H. Lee[1], J. Lee[2], W. Jung[1], J. Yang[1], K. Shin[3] and J. Choi[1] *1. Chungnam National University, Daejeon, The Republic of Korea; 2. Hyundai Transys, Suwon, The Republic of Korea; 3. Chonnam National University, Yeosu, The Republic of Korea*

Generally, permanent magnet synchronous generator (PMSG) have limited available space in various power generation system. Therefore, design and analysis should be performed using design constraints efficiently. In the design and analysis of PMSG, finite element method (FEM) are generally used to obtain accurate analysis results considering non-linear characteristics of materials. However, the FEM is difficult to understand the physical relationship between the design variables and performance of electrical machine. Therefore, it takes a lot of time to select the appropriate initial design point. Therefore, this study to deal with electromagnetic characteristic analysis for initial design of PMSG using analytical method. Fig. 1(a) shows the prototype model and experimental setup for verifying the proposed method. And then, a simplified analytical model of PMSG was presented in order to apply the analytical method as shown in Fig. 2(b). The governing equation and general solution for each analysis region were derived, and electromagnetic characteristics were derived based on electromagnetic theory. From this results, parametric analysis using analytical method was performed according to design variables for the initial design of PMSG under the design requirements. Fig. 2(b), (c), and (d) show the induced voltage, cogging torque, and THD of induced voltage according to design parameters, therefore, Initial design points were selected from analysis results. It can be confirmed that the analytical results agree well with FEM and experimental as shown in Fig. 2(b). More detailed results, discussions, and desired effects will presented in the full paper.

[1] W. Zhao, T. A. Lipo, B. -I. Kwon, "Comparative Study on Novel Dual Stator Radial Flux and Axial Flux Permanent Magnet Motors With Ferrite Magnets for Traction Application", *IEEE Trans. on Magn*., vol. 50 (11), pp. 1-4, November 2014. [2] Z. J. Liu, J. T. Li, and Q. Jiang, "An improved analytical solution for predicting magnetic forces in permanent magnet motors," J. *Appl. Phys*., vol. 103, no. 7, 2008. [3] T. Lubin, S. Mezani, A. Rezzoug, "2-D exact analytical model for surface-mounted permanent-magnet motors with semi-closed slots", *IEEE Trans*. Magn., vol. 47, no. 2, pp. 479-492, Feb. 2011. [4] Jikai Si, Tianxiang Zhang, Rui Nie, Chun Gan, Yihua Hu, "Comparative Study of Dual-Rotor Slotless Axial-Flux Permanent Magnet Machines With Equi-directional Toroidal and Conventional Concentrated Windings", *IEEE Trans. Ind*, vol.70, no.2, pp.1216-1228, 2023. [5] W. Geng and Z. Zhang, "Analysis and implementation of new ironless stator axial-flux permanent magnet machine with concentrated non overlapping windings," *IEEE Trans. Energy Convers*., vol. 33, no. 3, pp. 1274–1284, Sep. 2018.

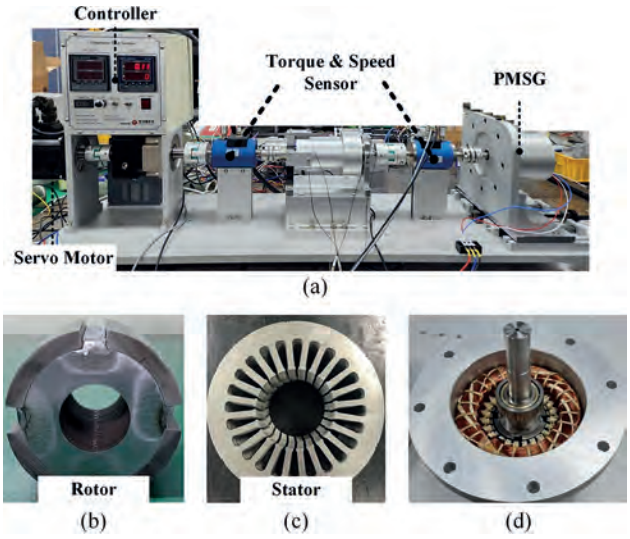

Fig. 1. Prototype for the designed PMSG: (a) experimental setup, (b) rotor, (c) stator, and (d) assembly of stator and rotor.

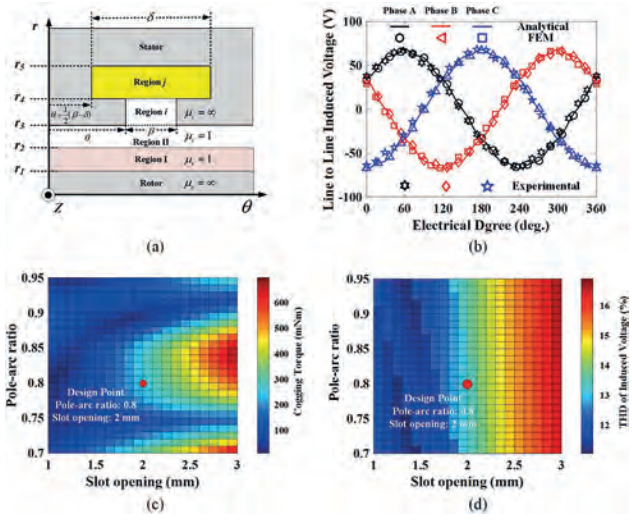

Fig. 2. Analysis model and results: (a) Simplified analytical model, (b) analysis result of the induced voltage of the analysis model, (c) analysis results of cogging torque according to pole-arc ratio and slot-opening, and (d) the THD of induced voltage according to pole-arc ratio and slot-opening.

VP12-43. A Core Loss Estimation Method Based on Improved Waveform Coefficient Steinmetz Equation for Asymmetric Triangular Flux Density Waveform. Y. Li[1], *K. Qin*[1], S. Mu[1] and J. Yin[1] *1. Hebei University of Technology, Tianjin, China*

Abstract: This paper proposes a waveform transformation principle, termed the equal derivative transformation (EDT), for piecewise linear flux density waveforms. Under the same maximum flux density, an asymmetric triangular flux density wave can be transformed into a symmetric one with a different frequency in terms of the calculation of core losses, hence the introduction of the improved waveform coefficient Steinmetz equation (iWcSE). The magnetic characteristics of three different toroidal samples (nanocrystalline alloy FT-3KL, amorphous alloy 1K101, ferrite N87) under square excitation at different duty ratios and certain frequencies are measured. Core losses predicted by the model are in good agreement with the measurement. Introduction: In a typical three-stage SST topology[2], the DC/DC stage usually adopts the dual-active-bridge (DAB) converter operated by the phase-shift pulsewidth modulation (PWM) scheme. Symmetric triangular and trapezoidal flux density waveforms are generated for the full-bridge configuration, while symmetric and asymmetric triangular flux density waveforms are generated for the half-bridge configuration[3]. Model Proposed: With the equivalent flux density derivative defined, the equal derivative transformation (EDT) is proposed as follows: *for piecewise linear flux density waveforms under the same peak flux density B_m, those with the same equivalent flux density derivative have equal core loss within one period.* Experimental Verification: The method adopted for the loss measurement is the classical B-H loop measurement, i.e., with the secondary winding open-circuited, the loss dissipated by the equivalent inductor is taken as the core loss. Fig. 1 displays the comparison of the core loss per period multiplied by a constant (20000) for the nanocrystalline alloy FT-3KL when the duty ratio varies from 0.1 to 0.4 under 20kHz, and when the duty ratio is exactly 0.5 yet the frequency changes. The relative errors are about 14% at most for the three different materials, which are demonstrated in Fig. 2.

[2] X. She, X. Yu, and F. Wang, "Design and demonstration of a 3.6-kV-120-V/10-kVA solid-state transformer for smart grid application," *IEEE Trans. Power Electron.,* vol. 29, pp. 3982-3996, 2014. [3] K. Kim, and H. Cha, "Split-Capacitor Dual-Active-Bridge Converter," *IEEE Trans. Ind. Electron.,* vol. 68, pp. 1445-1453, 2021.

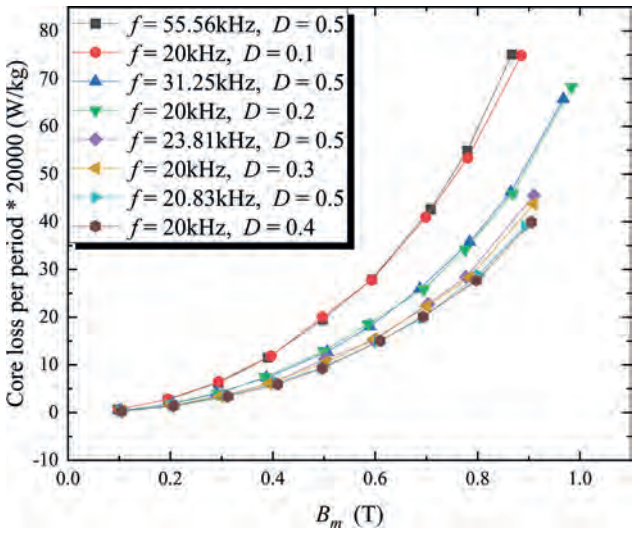

Fig. 1. The comparison of the core loss per period multiplied by a constant for FT-3KL under the two conditions.

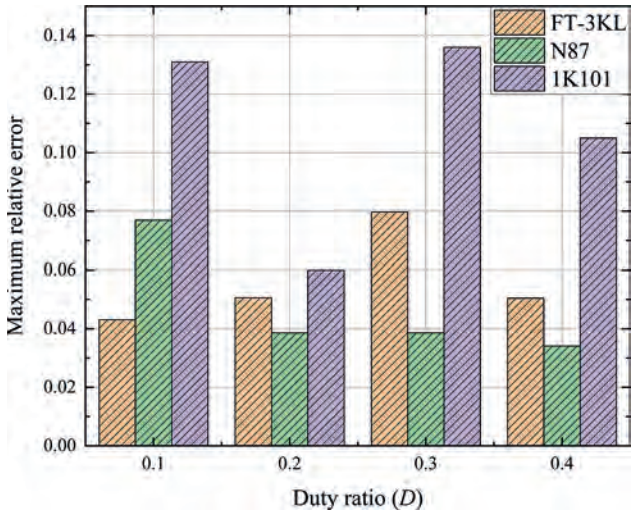

Fig. 2. Maximum relative errors for the three materials.

VP12-44. Simulation Analysis on Magnetic Core Loss Characteristic of Valve Reactor in UHVDC System. Y. Wang[1], J. Yuan[1], Z. Mo[1], *H. Zhou*[1] and Y. Zheng[1] *1. Wuhan University, Wuhan, China*

The valve reactor (VR) with multiple magnetic cores is an important electrical equipment in the UHVDC system. The large amplitude and fast changing pulse current during its operation can cause high temperature rise in the VR, threaten the thermal aging of the insulation, and even cause serious accidents such as combustion and explosion. Therefore, it is necessary to accurately quantify the loss characteristics of VR under different ferromagnetic materials. This article consists of the following three sections: 1. Theoretical Analysis The VR consists of several magnetic cores evenly distributed in the cooling-water winding, along with casing. The magnetic core is made of ultra-thin silicon steel sheets, and the casing is filled with Epoxy resin and Polyurethane, as shown in Figure 1. The current during operation is shown in the figure, and the heat source includes winding loss and magnetic core loss. 2. Finite Element Simulation Analysis of Electromagnetic Fields Simulations are conducted separately for single magnetic cores using GT100 and 30Q130 materials. The finite element simulation results of the magnetic field distribution and electromagnetic loss of a single magnetic core, as well as the temperature distribution of each magnetic core of the VR, are shown in Figure 2. 3.Conclusion This article establishes a VR 3D model of actual size and performs VR finite element simulation on

different materials,obtaining the following conclusions: 1) The distribution of magnetic flux density of the magnetic core is higher on the inner side compared to the outer side. 2) The average loss of a single magnetic core using GT100 is 109.6W, compared to 121.4W for 30Q130 Thinner silicon steel laminations result in lower losses. 3) The overall temperature distribution of VR is step-like temperature distribution with high in the middle and low on both sides, and the temperature of the magnetic core near the water inlet is lower than that far away from the water inlet.

[1] Wang Q, Liu P and Tian H, High Voltage., 7. 2, p.288-301 (2022) [2] Cao J, Davidson C and Moulson S, IET Science Measurement & Technology., 1. 3, p.138-144 (2007) [3] Yang W, Chen W and Zhou Y, High Voltage., 5.3, p.598-604 (2019) [4] Li X, Zha J and Wang S, IEEE Transactions on Dielectrics & Electrical Insulation., 24.6, p.3898-3905 (2018) [5] Cao J, Ji F and Liu J, IET Science Measurement & Technology., 10.2, p.77-83 (2016)

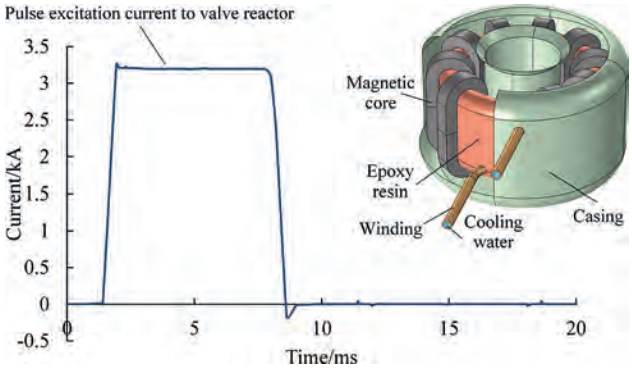

Fig. 1.

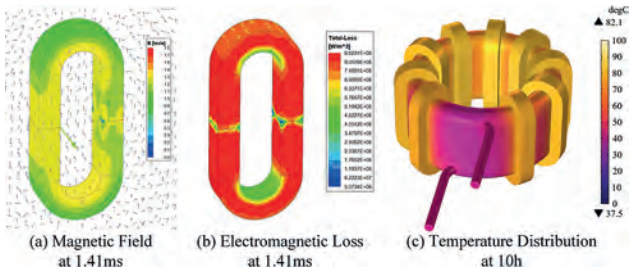

Fig. 2.

VIRTUAL PLATFORM ONLY

Session VP13
SOFT MAGNETIC MATERIALS (VIRTUAL)
(Poster Virtual Session)

Hee-Sung Han, Chair
Korea National University of Transportation, Chungju, The Republic of Korea

VP13-01. Study of High-Speed Motor Rotors Based on the Local Carburization Strengthening Mechanism of Non-Grain Oriented Silicon Steel. A. Wang[1], *Y. Li*[1], C. Zhao[2] and R. Pei[1] *1. Shenyang University of Technology, Shenyang, Liaoning, China; 2. Suzhou Yingci New Energy Technology Co., Ltd, Suzhou City, Jiangsu Province, China*

In order to meet the requirements of high speed, high power density and high efficiency of the drive motor of an energy vehicle, the core needs to be made of silicon steel with excellent magnetic properties. Currently, the usual strengthening methods to increase yield strength often deteriorates the magnetic properties of silicon steel. High strength silicon steel, as a typical silicon steel material, is gradually becoming the object of research by various automobile manufacturers and laboratories, but its iron loss value is higher than that of ordinary silicon steel of the same thickness. In this paper, based on the actual development needs of silicon steel for automotive drive motors, a local carburising strengthening method based on non-grain oriented (NGO) silicon steel is proposed to address the bottleneck problem of strength and magnetic properties of silicon steel materials for motors, and the characteristics of NGO silicon steel after carburising are investigated by building a silicon steel carburising device. In the first part of this paper, the current methods and research status of the industry to enhance the strength of motor rotors are summarized. This paper will briefly introduce the carburising process of NGO silicon steel in Part II and investigate the changes in magnetic properties and mechanical properties of a 0.35mm thick NGO silicon steel before and after carburising. The microstructural changes and hardness characteristics of the carburised samples before and after the tempering process are further investigated and the hardness analysis is shown in Figure 2. In the third part, the rotor structure is optimized based on the properties of the carburised material and compared with the conventional rotor design to analyze the changes in motor performance resulting from the partial optimization of the rotor flux barrier. The aim of this paper is to provide a more cost-effective measure to improve the strength of the rotor and to verify the feasibility and reasonableness of the solution through physical verification.

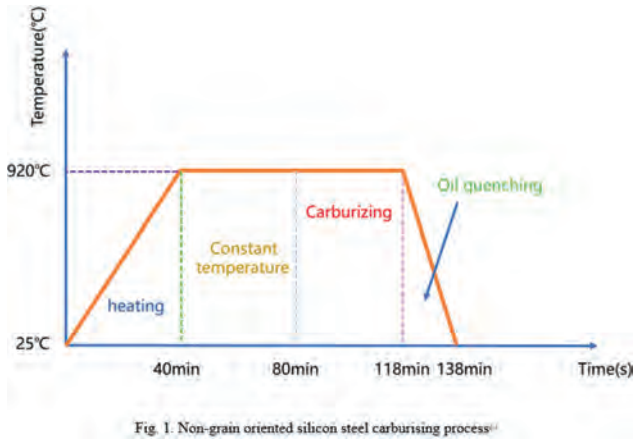

Fig. 1. Non-grain oriented silicon steel carburising process

Fig. 1. Non-grain oriented silicon steel carburising process

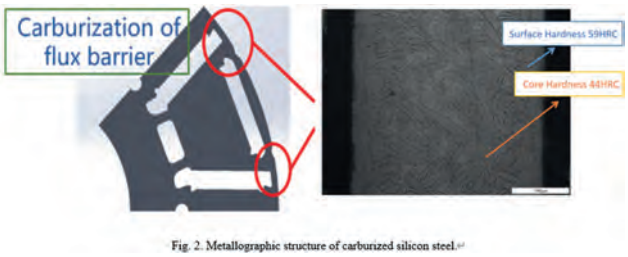

Fig. 2. Metallographic structure of carburized silicon steel.

Fig. 2. Metallographic structure of carburized silicon steel.

VP13-02. Magnetic first-order reversal curves for highly neutron-irradiated Fe-Cu alloys. *S. Kobayashi*[1], K. Yomogida[1] and E. Nomura[1] *1. Iwate University, Morioka, Japan*

Non-destructive evaluation (NDE) using a magnetic method has the potential for monitoring the level of irradiation hardening of reactor pressure vessel (RPV) steels. Recently, we have focused on a magnetic first-order reversal curve (FORC) method, because of a possibility for distinguishing magnetic regions with different magnetic hardness; magnetically hard region including nanoscale Cu precipitates and soft matrix. Previous FORC study for RPV steels revealed changes of FORC peaks after neutron irradiation; however, due to complex initial microstructures, information about irradiation-induced Cu precipitation was not fully extracted [1]. In this study, we have studied highly neutron-irradiated Fe-1wt%Cu alloys, which are simple simulated materials of irradiated RPV steels, to elucidate intrinsic FORC features due to Cu precipitation. To see the effect of Cu precipitation on initial microstructure, Fe-1wt%Cu alloys, which were cold-rolled with 0%, 10% and 20% reduction, were used. Figures 1(a) and 1(b) show a typical example of FORC diagrams before and after irradiation to fluence of 9.7×10^{19} n/cm^2 for 0% reduction. In Figs. 1(c) and 1(d), a half-width at half maximum (HWHM) of the FORC distribution peak along the coercivity (Hc) and interaction field (Hu) directions is given, respectively. For samples with 0% and 10% reduction the FORC peak along the Hc direction becomes broad in the initial stage of irradiation, whereas for 20% reduction the broadening appears in the later stage (Fig. 1(c)). This broadening reflects the evolution of nanoscale Cu precipitates, which increases microstructural inhomogeneity. On the other hand, the FORC peak along the Hu direction is significantly broadened after the irradiation for all the samples (Fig. 1(d)), implying the enhancement of magnetostatic interactions between magnetic region with nanoscale Cu precipitates and Fe matrix with lesser dissolved Cu atoms. These observations suggest that a FORC method is useful to monitor microstructural changes during neutron irradiation.

[1] S. Kobayashi, H. Murakami, T. Yamamoto, G.R. Odette, A. Horvath, A. Feoktystov, L. Almasy, J. Nucl. Mater. 552 (2021) 152973/1-7.

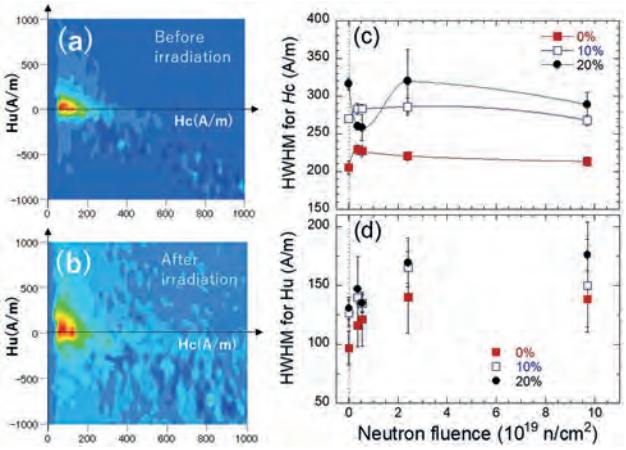

Fig. 1. FORC diagrams (a) before and (b) after neutron irradiation to a fluence of 9.7×10^{19} n/cm^2 for 0% rolling reduction. HWHM of FORC peak along (c) Hc and (d) Hu directions, as a function of neutron fluence.

VP13-03. A fabrication process of Fe-Ni films electroplated from gel electrolyte. *Y. Matsumoto*[1], R. Hosohata[1], Y. Yamaguchi[1], A. Yamashita[1], T. Yanai[1], M. Nakano[1] and H. Fukunaga[1] *1. Nagasaki Univercity, Nagasaki, Japan*

Typical-used electroplating electrolytes for magnetic films are aqueous solutions (liquid electrolytes), and we have already reported some electroplated Fe-Ni films using aqueous solutions [1-4]. Recently, environmental awareness has been raised, and we need to pay attention to environmental loads for the fabrication process. For electroplating, waste reduction is one of the actions to reduce environmental loads. In the present study, we proposed a fabrication process of electroplating soft magnetic films of Ni and Fe-Ni alloys using a gel electrolyte and investigated the magnetic properties of the films. Table 1 shows the bath conditions. We prepared a liquid electrolyte by stirring the water with the reagents at 50°C until the reagent was completely dissolved. After that, we added 23 g/L of gelatin to the liquid electrolyte and stirred for approximately 7 min at 60°C, and then the electrolyte was cooled for more than 60 min in a freezer. Figure 1 shows hysteresis loops of as-plated Fe-Ni films prepared from the gel electrolyte. The inset indicates a photograph of the cooled plating baths. As shown in Fig.1, saturation magnetization increased with the Fe content in the film. This result implies that Fe-Ni alloy films could be obtained. Gel electrolytes can be kept in their shapes without the beaker used as a vessel, indicating that electroplating flexibility is higher than liquid ones. Therefore, we concluded that electroplating Fe-Ni films using the gel electrolyte is an attractive fabrication process.

[1] H. L. Seet, X. P. Li, J. B. Yi, W. Y. Ooi, and K. S. Lee, "Effect of deposition methods on the magnetic properties of nanocrystalline permalloy," J. Alloys Compd., 449 (2008) 284. [2] B. Koo and B. Yoo, "Electrodeposition of low-stress NiFe thin films from a highly acidic electrolyte," *Surf. Coat. Technol.*, 205 (2010) 740. [3] J. L. McCrea, G. Palumbo, G. D. Hibbard, and U. Erb, "Properties and applications for electrodeposited nanocrystalline Fe-Ni alloys," *Rev.Adv. Sci.*, 5 (2003) 252. [4] T. Shimokawa, T. Yanai, K. Takahashi, M. Nakano, K. Suzuki, and H. Fukunaga, "Soft magnetic properties of electrodeposited Fe-Ni films prepared in citric acid based bath," IEEE Trans. Magn., 48, (2012) 2907.

Reagents	Concentration [g/L]
$NiSO_4\cdot6H_2O$	120
$FeSO_4\cdot7H_2O$	0 - 80
Glycine	15
NaCl	2
Sodium naphthalene trisulfonate	2

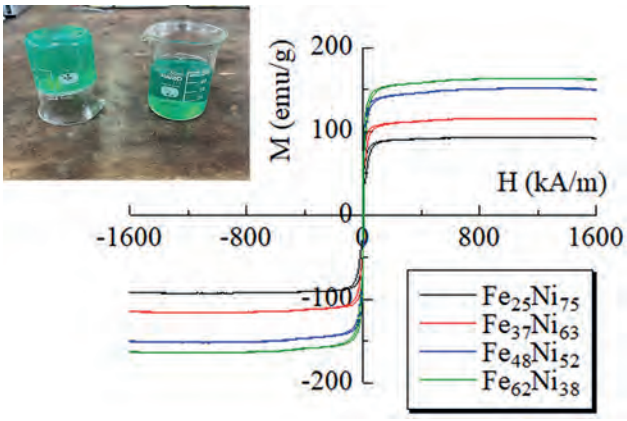

VP13-04. Withdrawn

VP13-05. The Role of Particle Size and Volume Fraction in Ferrite Microwave Absorbers. *A.S. Padgett*[1], S.R. Bishop[2], A.S. Peretti[2] and L.N. Robinett[1] *1. High Voltage Science and Experiment, Sandia National Laboratories, Albuquerque, NM, United States; 2. Electronic, Optical, and Nano Sciences, Sandia National Laboratories, Albuquerque, NM, United States*

As 5G technology becomes ubiquitous and the internet of things expands, sources of microwave EMI are rapidly increasing, and the threat of coupling EM energy into susceptible electronic circuits. Mitigating this threat requires compact, lightweight broadband absorbers to protect sensitive and high precision electronics. Magnetite, manganese zinc ferrite, and nickel zinc ferrite, alone and in conjunction, have previously been demonstrated to be magnetically and dielectrically lossy up to 18 GHz, and have the potential to meet the energy density and EM attenuation performance needs [1-3]. However, optimizing the absorption loss requires improved understanding of the role of particle size and volume fraction on the complex permittivity and permeability of these materials. This presentation discusses results, up to 20 GHz, from experimentally investigating the particle size, between 5 nm and 100 µm, and volume fraction, between 1 and 50 Vol%, on the absorption losses of these ferrites. Complex permeability and permittivity measurements were conducted to identify the absorption mechanisms. Diminishing returns in absorption were observed at loadings over 30 Vol%, while ferromagnetic resonance increased in frequency as particle size decreased. We present a possible explanation of these results in the context of Snoek's limit and the Landau-Lifshitz theory of permeability. This work was supported by the Laboratory Directed Research and Development program at Sandia National Laboratories, a multimission laboratory managed and operated by National Technology and Engineering Solutions of Sandia LLC, a wholly owned subsidiary of Honeywell International Inc. for the U.S. Department of Energy's National Nuclear Security Administration under contract DE-NA0003525.

[1] T. Tsutaoka, Journal of Applied Physics, Vol. 93, p. 2789 (2003) [2] R. Dosoudil, M. Usáková, J. Franek, IEEE Transactions on Magnetics, Vol. 46, p. 436 (2010) [3] Nan-Nan Jiang, Yang Yang, Yu-Xiang Zhang, Journal of Magnetism and Magnetic Materials, Vol. 401, p. 370 (2016)

VP13-07. Withdrawn

VP13-08. A Novel Hybrid Magnetic Material Based Three phase Saturated Core Fault Current Limiter. J. Yuan[1], Y. Sun[1] and *H. Zhou*[1]
1. School of Electrical Engineering and Automation, Wuhan University, Wuhan, China

1 Introduction Silicon steels, as one of the conventional soft magnetic materials, play a crucial role in the iron core of three-phase saturated core fault current limiters (TSFCLs). However, silicon steels have a high saturation point, requiring TSFCLs to use high DC excitation [1]. Additionally, the slope change rate of the B-H curve is small, resulting in a slow fault response speed. Moreover, the demagnetization permeability is also low, leading to poor current limiting performance. Nanocrystalline alloys [2] exhibit better performance in certain aspects but have weaker fault tolerance. Taking into account the characteristics of both materials, this paper proposes a novel hybrid magnetic material based TSFCL (HMTFCL). 2 Working Principle As shown in Fig.1, the magnetomotive force (MMF) generated by the DC coils aligns with the direction of the permanent magnets, leading to deep saturation of the six limbs. In each phase, the AC MMF and DC MMF have the same direction in one limb and opposite directions in another limb. Since the rated AC is small, neither limbs will experience demagnetization. So the equivalent inductance of the AC coils remains minimal and has negligible impact on system. During faults, the fault phase current surges, and the AC flux produced by the fault current counteracts the DC MMF. This causes alternating demagnetization of the two limbs within one cycle. At this stage, the unsaturated limb, along with the DC and AC coils placed on it, form a transformer. The inductance of the DC circuit restricts the fault current by coupling with the AC circuit. 3 Simulation Analysis In Fig.2, when an A phase ground fault occurs without FCL, the steady-state fault current reaches 9.8kA. With the installation of a TSFCL, the fault current can be reduced to 7.5kA. However, with the HMTFCL, the fault current is further limited to 5.8kA, which represents a 23% reduction compared to TSFCL. Moreover, the fault response time with HMTFCL is 2ms, which is only half of that achieved with TSFCL. Last, the required DC excitation current for TSFCL is 4000A, whereas it is lowered to 1500A for HMTFCL, resulting in a significant 62.5% reduction compared to TSFCL.

[1]J. Yuan, P. Gan, Z. Zhang, H. Zhou, IEEE Transactions on Power Delivery., Vol. 35, p. 1707-1715(2020). [2]H. Zhou, J. Yuan and F. Chen, IEEE Transactions on Industrial Electronics., Vol. 68, p. 11858-11869(2021).

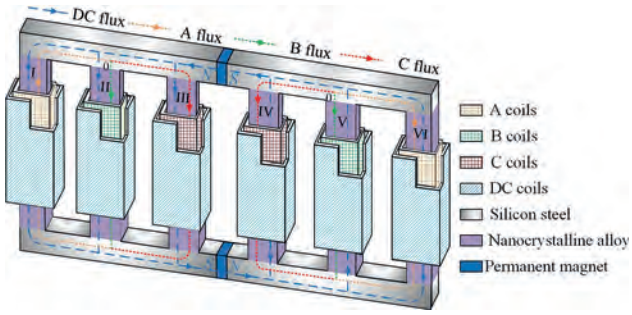

Fig.1 Configurations of HMTFCL

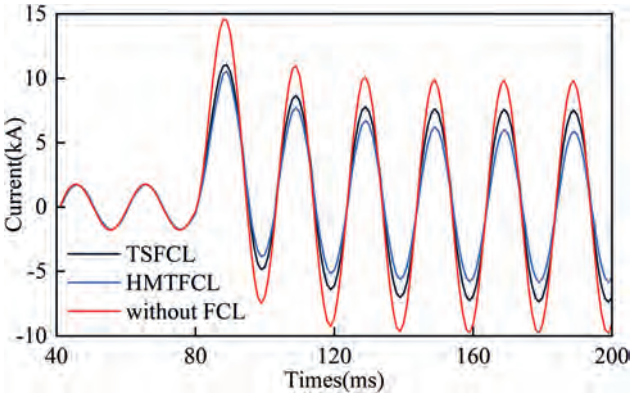

Fig.2 Comparison of currents

VP13-09. Withdrawn

VP13-10. Study of Magnetostrictive Properties of Electrical Steel with Different Silicon Content Considering the Effect of Stress. *D. Ma*[1], B. Tian[1], J. Li[1] and R. Pei[1] *1. Shenyang University of Technology, Shenyang, China*

Motor cores usually operate under stress loads, and the stresses can have an effect on their magnetostriction. When the Si content of electrical steel is 3.5%, the mechanical stress can cause magnetostriction saturation, resulting in increased motor vibration [1]. It has been reported that when the Si content of electrical steel reaches 6.5%, the magnetostriction effect is not obvious [2]. Therefore, it is particularly important to study the evolution of the magnetostrictive properties of electrical steels with different Si contents as influenced by stress. In the second part of this paper, the magnetostrictive properties of electrical steels with different Si contents (1.5%, 2.5%, 2.8%, 3.2%, 6.5%) were tested under variable stresses by using the magnetostrictive properties test method with loading stress along the rolling direction as shown in Fig. 1, and some experimental results are shown in Fig. 2, which reveal the hysteresis line and magnetostrictive properties of electrical steels with different Si contents under the influence of stress The third part extracts the magnetostriction The third part extracts the magnetostrictive strain, saturation wall shift magnetization strength and other key parameters based on the test results, and explains the reasons for the variation of magnetostrictive properties of electrical steels with different Si content under stress field from both macroscopic test data and microscopic mechanism of material magnetization behavior. In the fourth part, based on the above analysis, a finite element model of motor cores with different Si contents of electrical steel is established, and the noise analysis is carried out for the cores with and without considering the influence of stress to investigate the law that stress affects the core vibration noise by influencing the magnetostrictive properties of the material with different Si contents. Eventually, this paper will complete the test of magnetostriction characteristics of electrical steels with different Si content under variable stress and the analysis of the causes of microscale, which will be of great guidance to the design of low-noise motors.

[1] Sablik, M. J., & Jiles, D. C. (1993). Coupled magnetoelastic theory of magnetic and magnetostrictive hysteresis. IEEE transactions on magnetics, 29(4), 2113-2123. SABLIK MJ, JILESDC. Coupled magnetoelastic theory of magnetic and magnetostrictive hysteresis[J]. IEEE Transactions on Magnetics, 1993,29(4):2113-2123. [2] Phway, T. P., & Moses, A. J. (2008). Magnetostriction trend of non-oriented 6.5% Si–Fe. Journal of Magnetism and Magnetic Materials, 320(20), e611-e613.

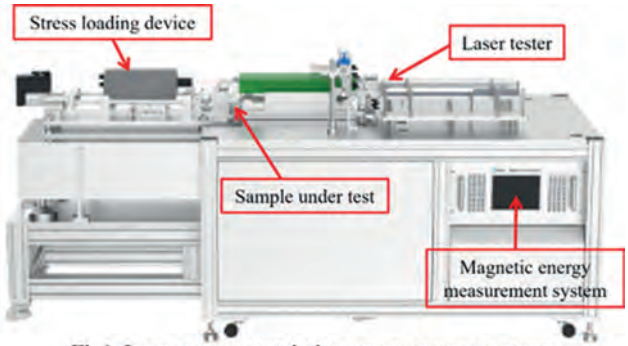

Fig1. Laser magnetostrictive measurement system

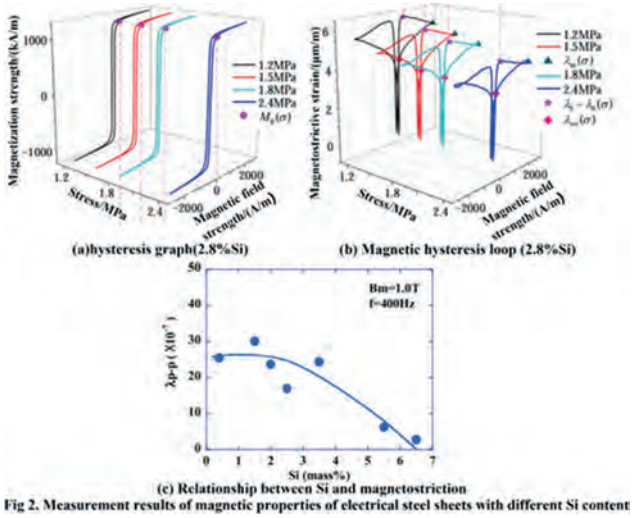

Fig 2. Measurement results of magnetic properties of electrical steel sheets with different Si content

VP13-11. Correction and Identification Method of Energetic Hysteresis Model Parameters under Variable Temperature Conditions. B. Chen[1], *Q. Zeng*[2], Y. Jia[3], L. Huang[1] and B. Tang[1] *1. Hubei Provincial Engineering Technology Research Center for Power Transmission Line, Yichang, China; 2. College of Electrical Engineering and New Energy China Three Gorges University, Yichang, China; 3. Sanmenxia Electric Company State Grid Henan Electric Power Company, Sanmenxia, China*

The hysteresis characteristics of ferromagnetic materials are temperature dependent, resulting in the performance of iron core equipment being affected by temperature. However, the existing Energetic hysteresis models can't effectively characterize the temperature, resulting in a significant error in the loss calculation. Therefore, the influence of each parameter of the Energetic hysteresis model on the shape of hysteresis loop are firstly studied in this paper. The magnetic properties and temperature dependence of the ferromagnetic material are analyzed. Then, on the basis of parameter identification by formula method, the shape eigenvalues of hysteresis loops at different temperatures are extracted. The Curie temperature and Critical exponent coefficients are introduced and the expressions of the shape eigenvalues with respect to temperature are proposed. The expression of eigenvalues are combined with the identification formulas of various model parameters. Then, the model parameter identification method considering temperature characteristics is proposed and a modified Energetic hysteresis model under variable temperature conditions is established. Finally, the hysteresis loop of the material at various temperatures was simulated and compared with multiple sets of measured values taking the measurement results of the ultimate hysteresis loop of a nanocrystalline alloy as an example, which verified the consistence and feasibility of the proposed model.

[1] Djekanovic N, Luo M and Dujic D, IEEE Transactions on Power Electronics, Vol.PP(99), p.1-1(2021). [2] Raghunathan A, Melikhov Y, Snyder J E, IEEE Transactions on Magnetics, Vol.45(10), p.3954-3957 (2009). [3] Xiang Y, Xu Q, Huang Y, IEEE Sensors Journal, Vol.18(4), p.1435-1441(2018).

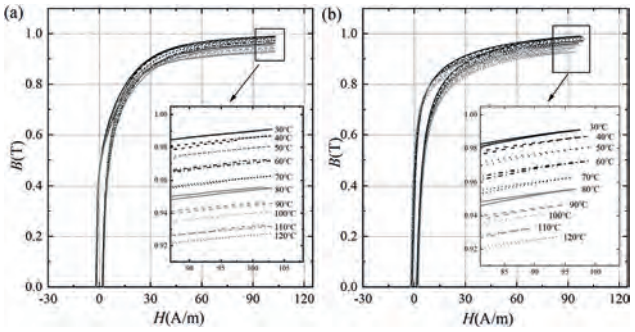

Fig.1 (a) Measured results of the limit hysteresis loops of nanocrystals at different temperatures (b) Simulation results of the limit hysteresis loops of nanocrystals at different temperatures

VP13-12. Measurement of magnetic properties of Grain-Oriented electrical steel considering Multi-Physics Factors influence. *L. Chen*[1], X. Liu[1], T. Ben[1], D. Yan[1] and X. Zhang[2] *1. College of Electrical Engineering and New Energy, China Three Gorges University, Yichang, China; 2. State Key Laboratory of Reliability and Intelligence of Electrical Equipment, Hebei University of Technology, Tianjin, China*

Introduction Grain-Oriented(GO) electrical steels are preferable to be processed into wound core structures in designing ultra-high-speed permanent magnet motors[1]. However, the presence of residual bending stresses of the wound core structure leads to the increase of the local losses. Meanwhile, motors often operate at high temperatures and under non-sinusoidal excitation, which leads to an abnormal increase in losses under serving conditions [2]. Thus, the loss behavior of the motor core material under the Multi-Physics Factors(MPF) influence needs to be fully investigated. Aiming at this problem, the complex magnetic properties of GO electrical steel are measured and discussed by developing a multi-physics magnetic measuring system considering the effect of bending stress, temperature loading, and non-sinusoidal magnetizing waveform. Method and Discussion To obtain different bending stresses, the single-sheet specimen was bent into different radii with the curvature of 100, 55,50, and 40 mm, and the bent specimen was heated and stabilized at the desired temperature using a thermostat. Using the measuring system described in Fig.1, the dynamic hysteresis loops and losses of the GO electrical steel B23P100 under different magnetizing conditions are measured and investigated. Partial loss measurement results of the GO electrical steel B23P100 under the MPF magnetizing conditions are shown in Fig.2. It can be found that with the bending stress increased, the magnetic permeability deteriorated severely, resulting in a noticeable loss increasement of the material. On the contrary, the temperature load would cause a slight loss decrease. These phenomena will become more apparent when adding the harmonic waveform to the excitation. Conclusion In this paper, the magnetic properties of GO electrical steels under MPF conditions were systematically measured. The loss shows a positive correlation with bending stress and the harmonic order while a negative correlation with temperature. The full paper will present more testing results and discuss this phenomena's physical mechanisms.

[1] Wang T, Liu C and Xu W, IEEE Transactions on Industrial Electronics., Vol. 64, p.1081-1091(2017) [2] Jiang Y, Wang D and Chen J, IEEE Transactions on Magnetics., Vol. 54, 8102705 (2018)

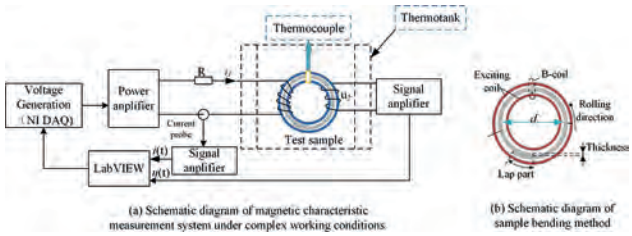

Fig. 1. Magnetic properties measurement system for electrical steel under MPF conditions

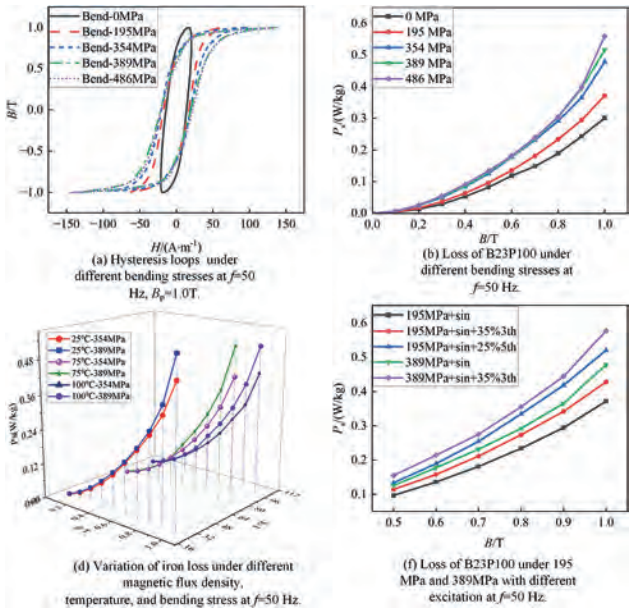

Fig. 2. Measurement results of B23P100 under MPF conditions

VP13-13. Analysis of Magnetostriction of Oriented Silicon Steel under Motor Magnetic Field. *Y. Li*[1], Z. Li[1], X. Lu[1] and R. Pei[1] *1. Shenyang University of Technology, Shenyang, China*

The performance requirements of motors are gradually increasing, and anisotropic soft magnetic materials have been applied in motors to improve performance. The magnetostriction of anisotropic soft magnetic materials is one of the main contributors in extensive research on anisotropic soft magnetic material transformers. Compared to transformers, the magnetic field in motors has more complex harmonic and multi-directional characteristics. In this paper, the air gap magnetic field of motors containing various harmonics is simulated to test the magnetostriction to research magnetostriction of anisotropic soft magnetic materials in motor magnetic field and predict the NVH performance of anisotropic soft magnetic material motors accurately. Furthermore, the magnetostriction in different magnetization angles is investigated for the multi-directional characteristics, and the result is explained from microscopic principles. This paper focuses on a splicing grain-oriented silicon steel (GOSS) motor. Under the coupling of magnetic field and motor structure, the magnetization angle of GOSS varying from 0° to 90°. Firstly, the equivalent formula of experiment current and armature and air gap magnetic field are obtained by analytic method. After that, the experiment magnetic field and simulated magnetic field is compared, and the magnetostriction of GOSS in different magnetization angle is measured. In the end, the variation character of magnetostriction of GOSS is summarized.

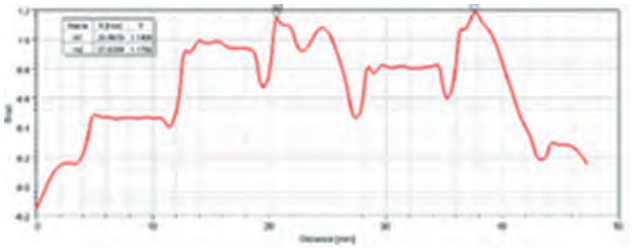

Fig.1 motor air gap magnetic field

Fig. 1. Motor air gap magnetic field

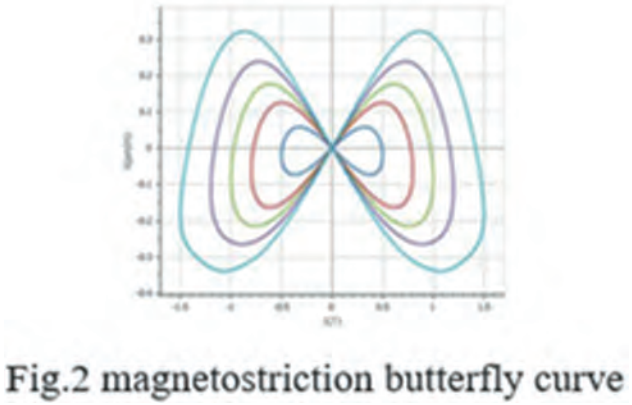

Fig.2 magnetostriction butterfly curve

Fig. 2. Magnetostriction butterfly curve

VP13-14. Influence of Tensile and Compressive Stresses on Magnetic Property of Amorphous Laminated Sheets. *X. Zhu*[1] and Y. Li[1] *1. State Key Laboratory of Reliability and Intelligence of Electrical Equipment, Hebei University of Technology, Tianjin, China*

Amorphous alloy exhibiting high permeability, high saturation flux density, and low coercivity have been widely investigated as cores of motors and high-frequency transformers. However, in comparison with silicon steel, its magnetic properties are sensitive to stress due to the rolling or stacking in manufacture. The causing additional power loss influences the performance of the equipment. Therefore, it is necessary to clarify the magnetic property of Fe-based amorphous alloys under stress. However, it is difficult to measure the magnetic property of amorphous alloys under stress because a single amorphous ribbon is thin and brittle and has poor ductility. Currently, the measurement of the magnetic properties of amorphous alloys is mostly performed using traditional standards and methods for electrical steel sheets [1]. Meanwhile, most of the existing studies have been carried out at low frequencies, which is not able to apply to high-frequency transformers [2]. In this paper, the magnetic properties of amorphous alloy laminates under stress are performed by using a custom-made single sheet tester device. To provide higher frequencies, the silicon steel core was replaced by a nanocrystalline core, and a servo motor was added to apply pressure to the specimen. The specimen size is W30 mm × t0.31 mm × L150 mm. The range of measurement frequency is from 1KHz to 10KHz, and the range of magnetic flux density is from 0.1T to 1.2 T. The hysteresis loops, maximum permeability, and power loss characteristics of the material loading uniaxial stress on are analyzed. The results show that the maximum strength of the magnetic field (Hm) decreases with tensile stress and increases with compressive stress. Meanwhile, the measured iron losses are analyzed based on statistical loss theory. The iron loss decreases with tensile stress and increases with compressive stress.

[1] Nakata T, Kawase Y and Nakano M, IEEE Transactions on Magnetics, 23.5,2596-2598(1987) [2] Mizuta, Takahiro, Yoshihiro Tani and Koji Fujiwara, IEEE Transactions on Magnetics, 54.11, 1-5 (2018).

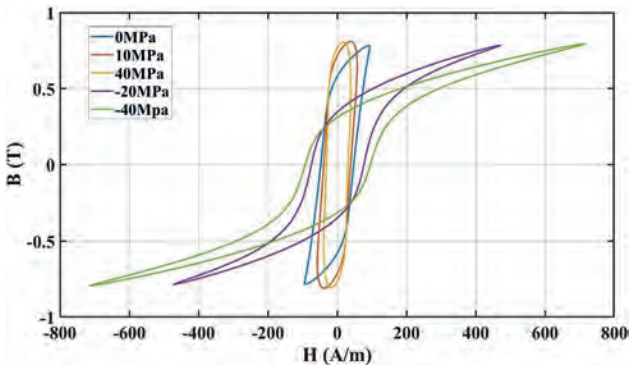

Fig. 1. Measured B-H loops under stress at 0.8 T,2k Hz

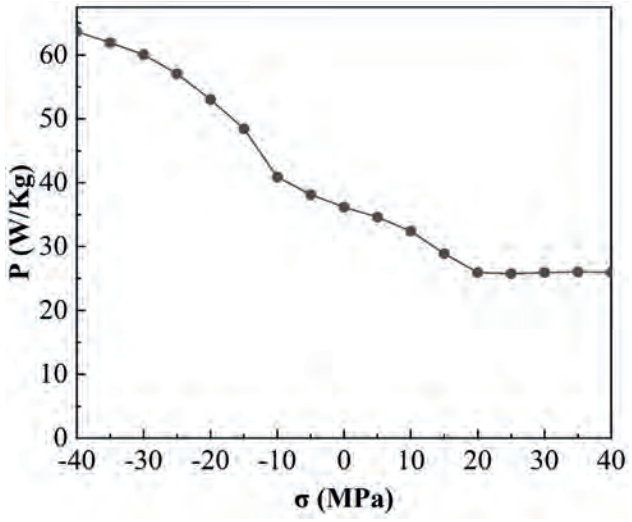

Fig. 2. Power loss depending on tress at f=2kHz,B_{max}=0.8T

VP13-15. Finite size effect on structural and static magnetic properties of $CoFe_2O_4$ nanoparticles. *P. Kumar*[1,2], S. Kumar[3], S. Pathak[4], A. Singh[5], K. Jain[2], R. Pant[2] and J. Partridge[1] *1. Applied Physics, RMIT University, Melbourne, ACT, Australia; 2. Indian Reference Materials Divisions, CSIR-National Physical Laboratory, Delhi, India; 3. Department of Physics, Hindu College, Sonepat, India; 4. Department of Materials Science and Engineering, Seoul National University, Seoul, The Republic of Korea; 5. Department of Physics, IIT Jammu, Jammu, India*

This study investigates the effect of particle size on the structural and static magnetic properties of $CoFe_2O_4$ magnetic nanoparticles (MNPs). A series of four $CoFe_2O_4$ MNPs samples with varying particle sizes were synthesized using the wet chemical co-precipitation method, and their structural and magnetic properties were measured. The results reveal a magnetic transition from superparamagnetic to ferromagnetic behavior with increasing particle size. The maximum exchange bias field (H_{EB}) was observed to be 1184 Oe for particles with a size of 17 nm, while the coercivity was found to be significantly higher (~10 kOe) for smaller particles (8 nm), decreasing with increasing particle size. Interestingly, a non-monotonic behavior in H_{EB} with increasing particle size was observed. Additionally, both negative and positive vertical magnetization shifts were observed in the smaller size particles. The dependence of the exchange bias and vertical shifts on particle size exhibited significant differences, which can be attributed to the presence of weakly and strongly pinned spins at the interface. It is proposed that the exchange bias is primarily influenced by the weakly pinned spins, whereas the vertical shift is affected by the strongly pinned spins. The synthesized $CoFe_2O_4$ MNPs hold great potential for applications in data storage and biomedical fields [1-2]. Keywords – MNPs, FM, XRD, VSM, Exchange bias.

[1.] Yuqiu Qu, Haibin Yang, Nan Yang, Materials Letters 60 (2006) 3548-3552.
[2.] P. Kumar, S. Pathak, A. Singh, Nanoscale Adv. (2020),2,19389-1948.

VIRTUAL PLATFORM ONLY

Session VP14
SPIN HALL AND RELATED EFFECTS (VIRTUAL)
(Poster Virtual Session)

Jingsheng Chen, Chair
National University of Singapore, Singapore

VP14-01. Electric Field Gated Magnon Transistor. *Y. Wang*[1], T. Zhang[1], C. Wan[1] and X. Han[1] *1. Instisute of Physics, Chinese Academy of Sciences, Beijing, China*

Magnons as the collective excitation of a magnetically ordered lattice possess both spin-angular momenta and phases but no charges, born an ideal information carrier for the Joule-heating-free electronics. Magnon transistors that can efficiently manipulate the magnon current are long desired as an elementary brick for magnonics. However, also due to their electric neutrality, magnons have no access to directly interact with an electric field and it is thus difficult to manipulate magnon transport by voltages straightforwardly. Predecessors have made outstanding contributions proposing the magnon transistor prototypes gated by magnetic field or bias current, however their difficulty in integrating or energy inefficiency will hinder theirs application. Inspired by the theoretical model established by Wei Chen *et. al* where the spin mixing conductance at a magnetic insulator/ normal metal interface relies sensitively on the interfacial *s-d* exchange coupling and thus conduction electron tunneling into the insulator. We theoretically and experimentally demonstrated a electric field gated magnon transistor based on the magnon mediated electric current drag effect (MECD) in an Pt/ $Y_3Fe_5O_{12}$(YIG)/ Pt sandwich. The gating electric field applied across the Pt/YIG interface bended the energy band of YIG then modulated the possibility of Pt conduction electron spin tunneled into YIG and consequently affect the spin-magnon conversion efficiency of the interface. The obtained efficiency (the change ratio between the MECD voltage at ±Vg) reached 10%/(MV/cm) at 300 K. This prototype of magnon transistor offers an effective scheme to control magnon transport by a gate voltage.

[1] C. Y. Guo, C. H. Wan, W. Q. He, *et. al*, "A nonlocal spin hall magnetoresistance in a platinum layer deposited on a magnon junction.", Nat. Electron. 3, 304 (2020). [2] L. J. Cornelissen, J. Liu, B. J. van Wees, and R. A. Duine, "Spin-current-controlled modulation of the magnon spin conductance in a three-terminal magnon transistor", Phys. Rev. Lett. 120, 097702 (2018). [3] W. Chen, M. Sigrist, J. Sinova, and D. Manske, "Minimal model of spin-transfer torque and spin pumping caused by the spin hall effect", Phys. Rev. Lett. 115, 217203 (2015). [4] S. S.-L. Zhang and S. Zhang, "Magnon mediated electric current drag across a ferromagnetic insulator layer", Phys. Rev. Lett. 109, 096603 (2012).

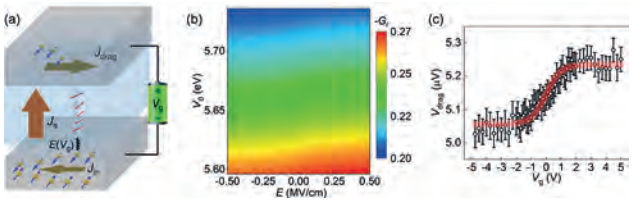

VP14-02. Unusual Spin-orbit Torque Switching in Perpendicular Synthetic Antiferromagnets with Strong Interlayer Exchange Coupling. *X. Luo*[1], Y. Wang[1], X. Han[1] and G. Yu[1] *1. Institute of Physics, Chinese Academy of Sciences, Beijing, China*

Synthetic antiferromagnet (SAF) is an outstanding system for controlling magnetic coupling via tuning the layer thickness and material composition. Here, we control the interlayer exchange coupling (IEC) in a perpendicularly magnetized SAF Pt/Co/Ir/CoFeB/MgO multilayer, which is tuned by varying the nonmagnetic layer Ir thickness and the magnetic layer Co thickness. And we study the spin-orbit torque (SOT) driven magnetization switching of the SAF. In the SAF with a weak IEC, the SOT-driven switching behavior is similar to that of a single ferromagnets system, which is dominated by the external magnetic field. In contrast, in the SAF with an ultra-strong IEC, the saturation magnetic field is large than 50 kOe, and the SOT-driven switching behavior is decided by the effective magnetic field. The effective field is correlated to the external magnetic field, the IEC field, magnetic moments of CoFeB and Co, and magnetic anisotropy. These results may advance the understanding of SOT switching of perpendicular SAFs and promote the applications of SAFs with low stray fields and lower power in spintronic devices.

[1] Xuming luo, Xiufeng Han, Guoqiang Yu, J. Phys.: Condens. Matter 35, 264004 (2023)

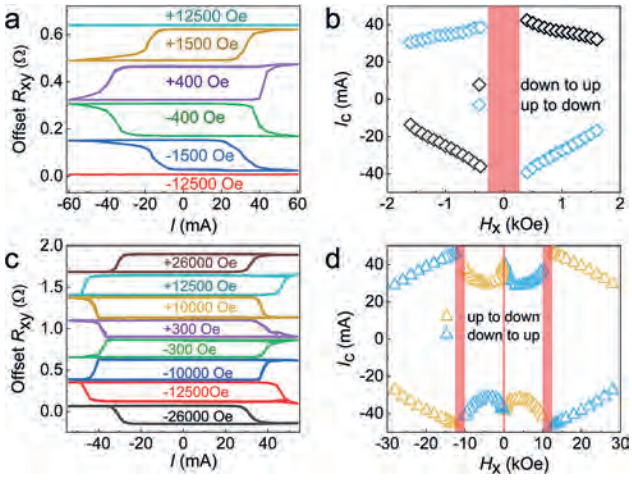

Fig. 1. (a) and (b) are results of the SAF Pt (4)/Co (1.2)/Ir (1.3)/CoFeB (1.3)/MgO (1.5) with weak IEC. (a) The SOT switching under various external filed H_x. (b) The dependence of critical switching current I_c on the external field H_x. (c) and (d) are results of the SAF Pt (4)/Co (1.2)/Ir (0.5)/CoFeB (1.4)/MgO (1.5) with strong IEC. (c) The SOT switching with various external filed H_x. (d) The dependency between critical switching current I_c and the external field H_x. The red area implies the SOT non-switching region

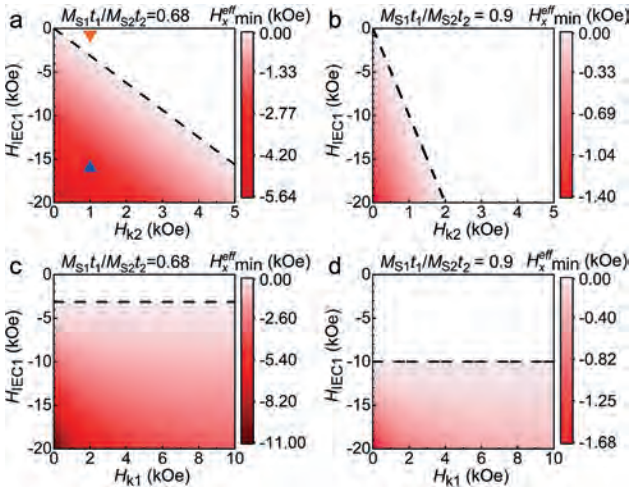

Fig. 2. The minimum external magnetic field as a function of H_{IEC1} and H_{k2} where $M_{S1}t_1/M_{S2}t_2$ is equal to 0.68 (a) and 0.9 (b). as a function of H_{IEC1} and H_{k1}, where $M_{S1}t_1/M_{S2}t_2$ is equal to 0.68 (c) and 0.9 (d). The orange inverted triangle corresponds to the parameters used in the weak IEC case and the blue triangle corresponds to the parameters used in the strong IEC case. The H_{k1} in (a) and (b) is 5 kOe, and the H_{k2} in (c) and (d) is 1 kOe. The dashed line indicates the boundary.

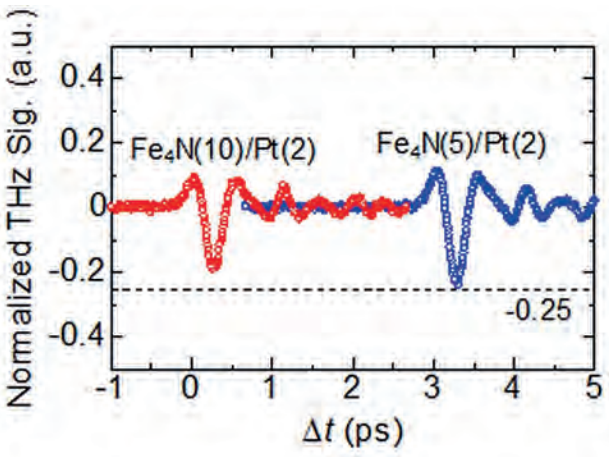

Fig. 1 Normalized amplitude of THz wave forms for the samples, MgOsub//Fe_4N (10 and 5)/Pt(2) (in nm). The wave for 5 nm is shown with horizontal shift.

VP14-03. Laser-induced terahertz emission in Fe_4N/Pt bilayers with negative spin polarization. *S. Isogami*[1], Y. Sasaki[1] and Y. Takahashi[1]
1. NIMS, Tsukuba, Japan

THz radiation has been observed in heavy metal/ferromagnetic bilayers as a result of the inverse spin Hall effect,[1)] and it has been revealed that the THz amplitude is dependent on not only the heavy metals but also the ferromagnetic layers.[2)3)] In contrast, the present study aims to elucidate the correlation between the sign of spin polarization at the Fermi level and the polarity of THz wave. The iron nitride (Fe_4N) has negative spin polarization judging from the theoretical calculation[4)] and the direct observation of band structures[5)], and the spin pumping has been studied in the Fe_4N/Pt bilayers.[6)7)] In recent years, transition metal nitrides/carbides/borides have attracted attention for next-generation spintronics;[8)] therefore, a Fe_4N/Pt bilayer systems were employed. The bilayer samples, MgO sub. / Fe_4N (d_{Fe4N}) / Pt (d_{Pt}) (in nm), were grown using DC magnetron sputtering. A Yb-doped KGW laser with a wavelength of 1028 nm, a frequency of 10 kHz, and a pulse width of 230 fs was used for excitation of THz radiation, and a magnetic field of about 0.5 kOe was applied to saturate the magnetization of the Fe_4N layer in-plane. The probe polarization, modulated in the THz detection crystal of CdTe(110), was detected using wollaston prism, photo diode, and lock-in amplifier. Figure 1(a) shows the THz waves for d_{Fe4N} = 10 nm (red) and 5 nm (blue). First, the polarity of the THz wave is in qualitative agreement with that of the Co_2MnSi Heusler alloy and CoFe alloy, indicating that the spin polarization of optically excited hot electrons is same as that for CoFe and Co_2MnSi. Next, an increase in amplitude is observed for the thinner d_{Fe4N}, which is similar to the previous study. The amplitude of about 0.25 for 5 nm was found to be slightly smaller than the values for the Co_2MnSi and CoFe with the same thickness. However, the value of d_{Fe4N} = 5 nm may not be the maximum, and further investigation of the ultra-thin film thickness is needed. In the talk, we will estimate the THz radiation efficiency and interpret the radiation properties in terms of electronic states.

[1] Xu *et al*., Adv. Mater. 29, 1703474 (2017). [2] Seifert *et al*., Nature Photonics 10, 483 (2016). [3] Sasaki *et al*., APEX. 13, 093003 (2020). [4] Kokado *et al*., JPSJ. 81, 024705 (2012). [5] Nakanishi *et al*., AP02, Intermag2023. [6] Isogami *et al*., APEX. 6, 063004 (2013). [7] Isogami *et al*., JJAP. 55, 043001 (2016). [8] Isogami *et al*., Adv. Electron. Mater. 9, 2200515 (2023).

Session VP15
SPIN ORBITRONICS (VIRTUAL)
(Poster Virtual Session)

Tai Kong, Chair
University of Arizona, Tucson, AZ, United States

VP15-01. Revisiting the Anomalous Hall Effects of Facing Target Sputtered Pt/Fe_4N/MgO Epitaxial Heterostructures. *X. Shi*[1] and W. Mi[2]
1. School of Physics and Electronic Engineering, Linyi University, Linyi, China; 2. Department of Applied Physics, Tianjin University, Tianjin, China

Noncollinear spin textures have attracted much attention due to their novel physical behaviors in heavy/ferromagnetic metal (HM/FM) systems[1]. The spin-dependent electronic transport anomaly appears as contrast humps in Hall resistivity curves, which may be the mark of noncollinear spin textures. In this work, the epitaxial Pt/Fe_4N/MgO heterostructures were fabricated by facing-target sputtering. Moreover, at 300 K, the magnetic bubble-like domains appear in Pt/Fe_4N/MgO heterostructures that just possess a 3-nm-thick ferromagnetic layer instead of $[HM/FM]_n$ or $[HM_1/FM/HM_2]_n$ multilayers. Additionally, the room-temperature transport anomalies with contrast humps in ρ_{xy}-H_z curves were observed in Pt(3 nm)/Fe_4N(t≤4 nm)/MgO heterostructures. The discovery of epitaxial Pt/Fe_4N/MgO heterostructures with noncollinear spin states is more crucial than polycrystalline or amorphous HM/FM systems for reducing ohmic heating, which provides a candidate for the noncollinear spintronic applications. This work is supported by National Natural Science Foundation of China (52271185 and 52201220).

[1] A. Fert, N. Reyren and V. Cros, Magnetic Skyrmions: Advances in Physics and Potential Applications. *Nat. Rev. Mater*. 2, 17031 (2017).

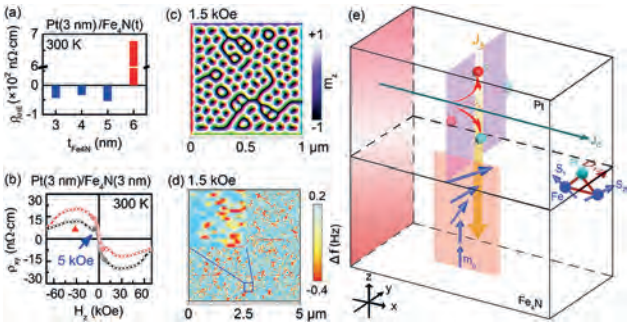

Fig. 1. (a) Fe_4N thickness-dependent anomalous Hall resistivity ρ_{AHE} of Pt(3 nm)/Fe_4N(t nm)/MgO heterostructures. (b) ρ_{xy}-H_z curves of Pt(3 nm)/Fe_4N(3 nm)/MgO at 300 K. (c) Micromagnetic simulation and (d) magnetic force microscopy image of Pt(3 nm)/Fe_4N(3 nm)/MgO at out-of-plane magnetic field of 1.5 kOe at 300 K. (e) Schematic diagram of the mechanism in Pt/Fe_4N/MgO heterostructures.

VP15-02. Threshold Current of Field-free Perpendicular Magnetization Switching Using Anomalous Spin-orbit Torque. *T. Zhang*[1], C. Wan[1] and X. Han[1] *1. Institute of Physics, Chinese Academy of Science, Beijing, China*

In this study, we derive the threshold current for field-free perpendicular magnetization switching using anomalous SOT and numerically calculate the magnetic moment trajectory in an FM free layer for currents smaller and greater than the threshold. We also investigate the dependence of switching time and energy consumption on applied current, finding that the minimum energy consumption decreases with an increasing out-of-plane torque proportion. Additionally, we explore the relationships between the threshold current and anisotropy strength, out-of-plane torque proportion, FM free layer thickness, and Gilbert damping constant. The results show a negative correlation between the threshold current and out-of-plane torque proportion, and positive correlations with the other three parameters. Finally, we demonstrate that even when the applied current is smaller than the threshold current, it can still add an effective exchange bias field H_{bias} on the FM free layer. The H_{bias} is proportional to the applied current J_{SOT}, facilitating the determination of anomalous SOT efficiency. Our findings provide insights into the design of spintronic devices that favor field-free switching of perpendicular magnetization using anomalous SOT and offer a means of adjusting the exchange bias field to control FM layer magnetization depinning.

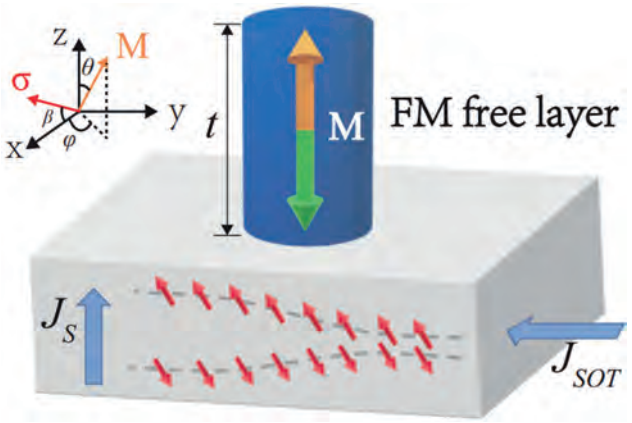

Fig. 1. A schematic diagram of the FM free layer magnetization switch driven by an anomalous SOT with both in-plane and out-of-plane components. The spin current diffuses into the FM free layer with the perpendicular magnetic anisotropy to drive its magnetization dynamics.

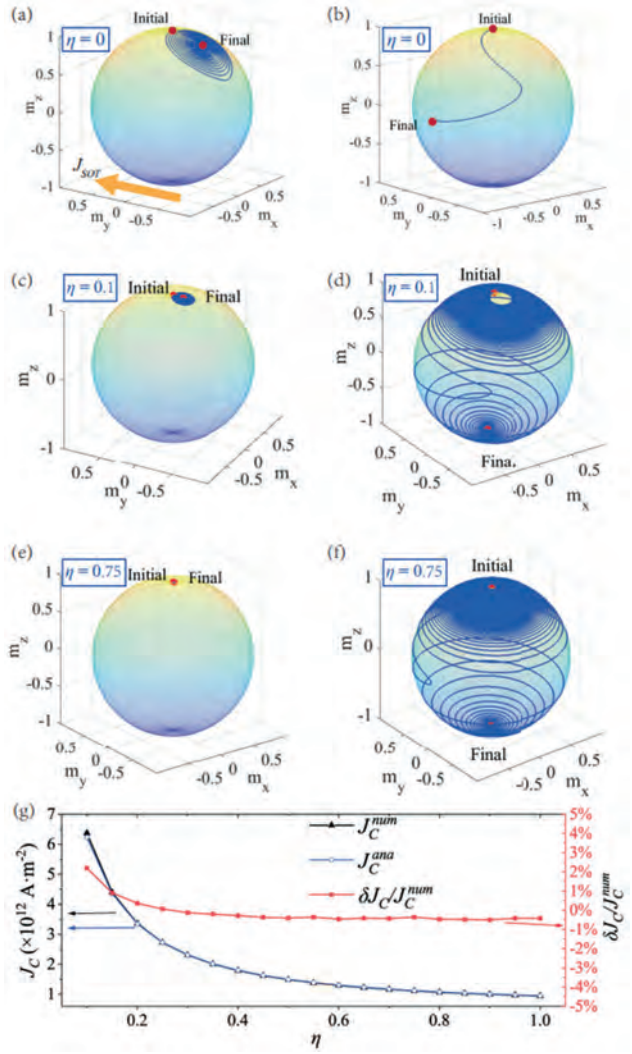

Fig. 2. (a)~(f) The magnetization trajectory with different η and J_{SOT}. The two parameters are shown as follows, η = 0, (a) $J_{SOT} = 1.8 \times 10^{13}$ Am^{-2} and (b) $J_{SOT} = 1.9 \times 10^{13}$ Am^{-2}; η = 0.1, with threshold current value $J_c = 6.23 \times 10^{12}$ Am^{-2}, (c) $J_{SOT} = 6.2 \times 10^{12}$ Am^{-2} and (d) $J_{SOT} = 6.37 \times 10^{12}$ Am^{-2}; η = 0.75, with threshold current value $J_c = 1.116 \times 10^{12}$ Am^{-2}, (e) $J_{SOT} = 1.1 \times 10^{12}$ Am^{-2} and (f) $J_{SOT} = 1.12 \times 10^{12}$ Am^{-2}. (g) The η - dependence of analytical threshold current J_C^{ana}, numerical threshold current JCnum and error $\delta J_C/J_C^{num} = (J_C^{num} - J_C^{ana})/J_C^{num}$.

VP15-03. Switching Model of Double Barrier Magnetic Tunnel Junction Based on Two-dimensional Materials. *Y. Yuan*[1] and Y. Jiang[1]
1. Jiangnan University, WuXi, China

Magnetic random access memory (MRAM) is a spintronic NVM, considered as a possible solution at all memory hierarchies. Most MRAM solutions are based on a perpendicular MTJ(PMTJ) with spin transfer torque(STT) [1].Spin-transfer torque magnetic RAMs(STT-MRAMS) have been gaining interests for high read capabilities[2]. However, STT-MRAM requires a high critical current density for switching, resulting in problems of aging and low durability [3]. In response to this situation, the researchers proposed the structure of the double magnetic tunnel junction (DMTJ). The DMTJ is actually manufactured in a vertical stack, with its area comparable to that of a single PMTJ. It can present four stable resistance states, respectively, expressed as '00,01,10,11'[4]. In this paper, a new structure of double magnetic tunnel junction is designed, using Fe_3GeTe_2 and WTe_2, two two-dimensional magnetic materials which have been widely concerned. The structure and physical model of the designed DMTJ device are presented and simulated. A hybrid CMOS/DMTJ read/write circuit based on DMTJ is introduced. Compared to SMTJ-based read/write units, the architecture based on DMTJ can improve write/read energy and latency by approximately 55%/61% and 64%/15%, respectively. These results are of great significance for the combination of 2D materials with MTJ and the application of MRAM based on DMTJ.

[1.] A. G. Qoutb and E. G. Friedman, Microelectronics Journal 131, 105635 (2023). [2.] E. Garzón, R. De Rose, F. Crupi, L. Trojman, A. Teman, and M. Lanuzza, Solid-State Electronics 194, 108315 (2022). [3.] E. Garzón, R. De Rose, F. Crupi, L. Trojman, G. Finocchio, M. Carpentieri, and M. Lanuzza, Integration 71, 56 (2020). [4.] T. Moposita, E. Garzón, F. Crupi, L. Trojman, A. Vladimirescu, and M. Lanuzza, IEEE Trans. Circuits Syst. II 70, 1254 (2023).

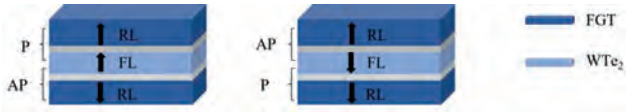

Fig 1. The magnetization direction of the free layer and the reference layer is different, representing the state "0" and state "1" respectively.

VP15-04. Field-free Spin-orbit Torque Switching of Magnetic Tunnel Junction Structure Based on Two-dimensional van der Waals WTe_2. *Y. Yuan*[1] and Y. Jiang[1] *1. Jiangnan University, WuXi, China*

In recent years, two-dimensional van der Waals (2D vdWs) heterostructures have attracted great research interest due to their great potential in fundamental physics research and spintronic devices (MTJS). Due to its excellent scalability, controllable magnetism and out-of-plane anisotropy, the compact nonvolatile memory controller (NV-MC) based on spintronics is expected to solve the memory bottle-neck problem [1]. At present, a series of in-depth studies have been conducted on advanced two-dimensional vdWs materials such as MoS_2, WSe_2,Fe_3GeTe_2(FGT)[2–4]. The results show that the two-dimensional vdWs materials have great TMR value and high SOT switching efficiency, both theoretically reported and experimentally verified. In this work, we propose a novel MTJ based on the WTe_2/MgO/WTe_2 heterostructure, which consists of two-dimensional WTe_2 with PMA. In the absence of an external magnetic field, the magnetization direction of the MTJ free layer can be reversed with certainty when the unipolar write current reaches about 5mA. Moreover, the TMR ratio of WTe_2 heterostructure reaches up to 250%, enabling the improvement of the reading reliability of SOT-MRAM in comparison with the traditional CoFeB-based MTJ's counterpart. In addition, the WTe_2 magnetized field-free SOT switch is robust over a wider temperature range from 150 K to more than 200 K, avoiding potential device damage due to the high current density required to implement the switch.

[1.] H. Lin, X. Luo, L. Liu, D. Wang, X. Zhao, Z. Wang, X. Xue, F. Zhang, and G. Xing, Micromachines 13, 319 (2022). [2.] H. Wang, Y. Liu, P. Wu, W. Hou, Y. Jiang, X. Li, C. Pandey, D. Chen, Q. Yang, H. Wang, D. Wei, N. Lei, W. Kang, L. Wen, T. Nie, W. Zhao, and K. L. Wang, ACS Nano 14, 10045 (2020). [3.] W. Li, Y. Zeng, Z. Zhao, B. Zhang, J. Xu, X. Huang, and Y. Hou, ACS Appl. Mater. Interfaces 13, 50591 (2021). [4.] M. Zhao, Y. Zhao, Y. Xi, H. Xu, H. Feng, X. Xu, W. Hao, S. Zhou, J. Zhao, S. X. Dou, and Y. Du, Nano Lett. 21, 9233 (2021). [5.] E. Garzón, R. De Rose, F. Crupi, L. Trojman, A. Teman, and M. Lanuzza, Solid-State Electronics 194, 108315 (2022).

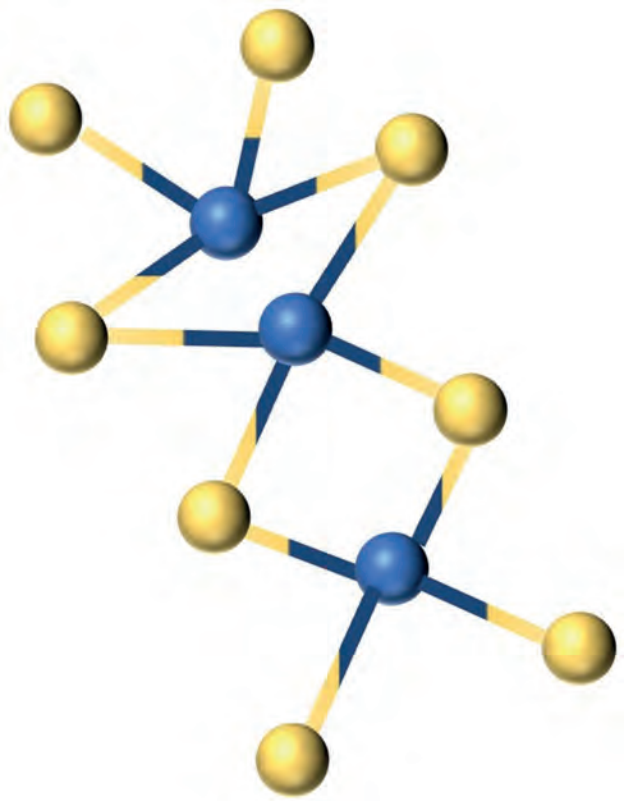

Fig. 1. The atomic crystal structure of WTe_2

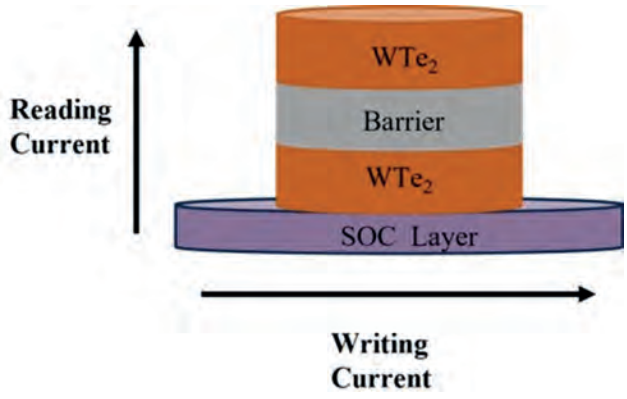

Fig. 2. The basic WTe_2 -MTJ structure.

VP15-05. Thickness dependent structural, morphological and magnetic properties of PLD grown CoFe thin film. *P. Kumar*[5,1], R. Kumar[2,1], V. Sharma[3], M.K. Khanna[4] and B.K. Kuanr[1] *1. Special Centre for Nanoscience, Jawaharlal Nehru University, New Delhi, India; 2. Shaheed Rajguru College of Applied Sciences for Women, New Delhi, India; 3. Department of Physics, Colorado State University, Fort Collins, CO, United States; 4. Ramjas College, New Delhi, India; 5. Department of Electronic Science, University of Delhi, South Campus, New Delhi, India*

Metallic ferromagnets consisting of transition elements are a great choice for developing a new material system for spin orbitronics and magnonic applications. While insulating ferromagnets such as YIG has the lowest Gilbert damping () in all the known ferromagnets but it lacks in electron-magnon coupling [1]. Heuslar compounds also show low but required high growth temperature which limits their use in spintronics. Therefore, a 3d transition metal ferromagnet alloy like CoFe is a promising material for spintronics. Good quality CoFe thin films can be grown at room temperature without further annealing which exhibit very low [2]. Here we report the growth of ultra-thin layers (5-30 nm) of CoFe by PLD technique on industrially relevant Si/SiO_2 substratewithout any buffer or seed layer. XRD peak at 44.5 shows the growth of CoFe along the (110) crystal plane. A nearly square M-H loop with high saturation magnetization (M_s) as shown in fig. 1 suggests good crystalline growth of CoFe. A high coercive field () as shown in Fig. 1 observed in the 5 nm film is due to several defects such as dislocations, and stacking faults that appear at very low thickness causing domain wall pinning and increasing. These defects gradually decrease with an increase in CoFe film thickness as evident in a decrease in the and an increase in M_s (Fig. 1). Fig.2 shows the obtained from the fitting of frequency-dependent FMR linewidth using the LLG equation. The is largest for the 5 nm film due to defects and magnetic homogeneity present in these thicknesses. Furthermore, two magnon scattering dominates and contributes extrinsically to the FMR linewidth at low film thickness [3]. The damping is reduced by an order of magnitude for a thin film which signifies a good quality film with fewer disorders present at a thickness greater than 7 nm. These results correlate thickness with structural, morphological, and magnetic properties of PLD-grown CoFe and are crucial for optimizing CoFe thickness for the spintronics device functionality.

[1] Serga, A. A., A. V. Chumak, and B. Hillebrands. "YIG magnonics." *Journal of Physics D: Applied Physics* 43, no. 26 (2010): 264002. [2] Sakai, S., M. Kawano, M. Ikawa, H. Sato, S. Yamada, and K. Hamaya. "Low-temperature growth of fully epitaxial CoFe/Ge/Fe3Si layers on Si for vertical-type semiconductor spintronic devices." *Semiconductor Science and Technology* 32, no. 9 (2017): 094005. [3]Arias, Rodrigo, and D. L. Mills. "Extrinsic contributions to the ferromagnetic resonance response of ultrathin films." *Physical review B* 60, no. 10 (1999): 7395.

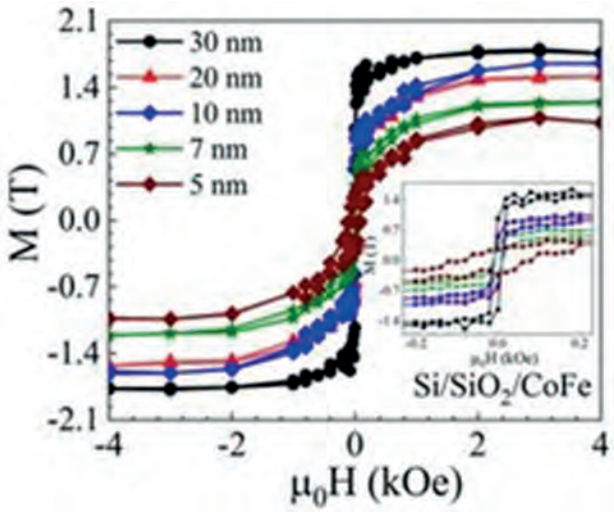

Fig. 1. M-H loop of CoFe film with varying thickness.

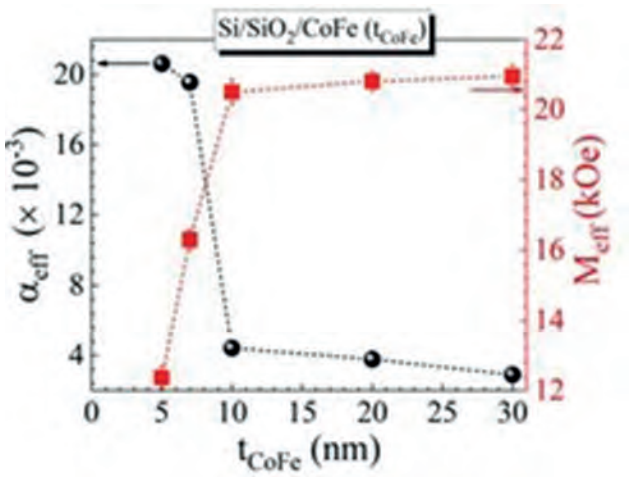

Fig. 2. Gilbert damping constant and effective magnetization vs. thickness of CoFe.

VP15-06. Spin–orbit Torque-induced Magnetization Switching in Ta/GdFeCo/Ta Structures. *H. Hu*[1], K. Wang[3], Y. Tao[2], L. Yang[2] and K. Dong[2] *1. School of Future Technology, China University of Geosciences, WuHan City, China; 2. School of Automation, China University of Geosciences, WuHan City, China; 3. School of Mechanical and Electronic Engineering, East China University of Technology, Nanchang City, China*

Spin-orbit torque (SOT) driven magnetization switching in ferrimagnets has attracted much attention due to its potential application in information storage devices. One particularly interesting material is ferromagnetic GdFeCo alloy, possessing the classic ferrimagnetic material systems with bulk perpendicular magnetic anisotropy. Importantly, it can significantly regulate the magnetization and angular momentum of alloys by changing the chemical composition or temperature. Hence, the purpose of this work is to explore the SOT effect in Ta(5nm)/GdFeCo(t)/Ta(5 nm) heterostructures, where t=20 nm, 30 nm, 40 nm. In order to study the perpendicular magnetic anisotropy of the sample, the magnetic field dependence of abnormal hall resistance curves with different thicknesses of GdFeCo were measured, as exhibited in Fig. 1(a). All samples showed excellent perpendicular anisotropy, especially for samples with t=20 nm, its coercivity is minimal (200 Oe). The current-induced switching experimental for GdFeCo(20 nm) sample is performed in Fig. 1(b). One can distinctly discover the hysteresis switching loops, except when H_x = 0 Oe. Meanwhile, the switching polarities (clockwise or counterclockwise) varies with the reversal of H_x. The switching ratio is up to 47.7% when the critical current density is 1.26Í10^7 A/cm^2. In addition, the changes in Hall resistance are tuned to programming consecutive pulse sequences, which can be simulated synaptic behavior, as demonstrated in Fig.1(c-d). The successive change in R_H reveals that when positive pulses are applied to the device, a gradual decrease in R_H appears, while negative pulses contribute to an augment in R_H, corresponding to synapse suppression and enhancement, respectively. This work confirms that GdFeCo materials have broad application prospects in neuromorphic computing.

VP15-07. Withdrawn

VP15-08. Field-free spin-orbit torque switching enabled by interlayer Dzyaloshinskii–Moriya interaction. *W. He*[1], C. Wan[1] and X. Han[1] *1. Institute of Physics, University of Chinese Academy of Sciences, Chinese Academy of Sciences, Beijing, China*

Perpendicularly magnetized structures that are switchable using a spin current under field-free conditions can potentially be applied in spin-orbit torque magnetic random-access memory (SOT-MRAM). Studies have shown that several methods, including wedge structures, exchange bias/coupling structures, gradient materials, single-crystal materials with low atomic or antiferromagnetic symmetries, can realize this purpose. However, among them, most methods are limited in their compatibility with MRAM technologies; thus, new symmetry-breaking physics and simpler MRAM-compatible structures for hosting field-free SOT-switching are still in demand. Herein, a typical structure in a perpendicular spin-transfer torque MRAM, the Pt/Co multilayer and its synthetic antiferromagnetic counterpart with perpendicular magnetic anisotropy, was observed to possess an intrinsic interlayer chiral interaction between neighboring magnetic layers, namely the interlayer Dzyaloshinskii–Moriya interaction (DMI) effect. Furthermore, using a current parallel to the eigenvector of the interlayer DMI, we switched the perpendicular magnetization of both structures without a magnetic field, owing to the additional symmetry-breaking introduced by the interlayer DMI. Compared with previous field-free switching of perpendicular magnetization with redundant functional layers or additional asymmetry designs, all the above factors make the Pt/Co multilayer system with the iDMI effect an ideal candidate to develop efficient and practical perpendicular SOT-MRAM devices. This SOT switching scheme realized in the Pt/Co multilayer and its synthetic antiferromagnet structure may open a new avenue toward practical perpendicular SOT-MRAM and other SOT devices.

[1] W.Q. He *et al.Nano Letters* 22,6857-6865(2022).

VP15-09. Withdrawn

VIRTUAL PLATFORM ONLY

Session VP16
STRUCTURED MATERIALS (VIRTUAL)
(Poster Virtual Session)

Takahiro Moriyama, Chair
Nagoya University, Nagoya, Japan

VP16-01. Enhanced heating efficiency for hollow Fe_3O_4 spherical submicron particles. *S. Kobayashi*[1] and T. Tsuji[1] *1. Iwate University, Morioka, Japan*

Recently, magnetic particles with a vortex structure have received much attention as useful biomedical materials, because of high saturation magnetization and wider tunability of a particle size from sub-100 nm to submicrometer scale. The vortex particles showed a high heating efficiency, which is comparable to that of superparamagnetic nanoparticles [1] and is enhanced with the number of vortices [2]. Moreover, recent studies revealed a better stability of a vortex structure for hollow particles [3]. Here, we report results of micromagnetic simulations for hollow Fe_3O_4 submicron particles with variable particle morphology to seek the possible application of a hollow particle for magnetic hyperthermia. Micromagnetic simulations were performed using OOMMF 2.0 for spherical particle with an outer diameter D_o of 100-700 nm, varying inner/outer diameter ratio of γ= 0-0.5. The typical magnetic parameters of Fe_3O_4 with <111> easy axes were used [3]. Alternating magnetic fields with an amplitude A up to 1.5 kOe and a frequency of 500 kHz were applied along the [100] axis. Fig. 1(a) shows M-H curves for A=1000 Oe for particles with γ = 0.5, but different D_o. Unlike the M-H curve for D_o =100 nm showing a high remanence, that for a larger D_o exhibits a double hysteresis loop with an extremely low remanence, reflecting a better vortex stability at low fields. Interestingly, a specific absorption rate (SAR), calculated from the loop area, maximizes at D_o~300 nm and attains 560 W/g for A=1000 Oe (inset of Fig. 1(a)). Moreover, the hysteresis loss (i.e. SAR) increases with increasing γ as shown in Fig. 1(b). This enhanced SAR for vortex particles with large γ was explained by strong irreversibility between vortex states with different orientation of the vortex axis, i.e. along the magnetic field and <111> easy axes (Fig.1(c)).

[1] N. A. Usov, et al., Sci. Rep. 8, 1224 (2018). [2] D. W. Wong, et al., Nanoscale Res. Lett. 14, 376 (2019). [3] N. Hirano, et al., Appl. Phys. Lett. 119, 132401 (2021).

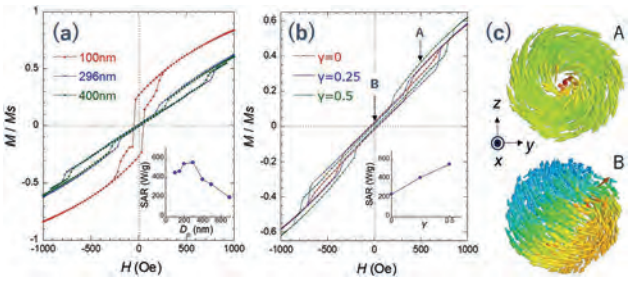

Fig. 1: M-H loops with A= 1000 Oe; (a) γ = 0.5 and D_o = 100, 296, 400 nm, (b) γ = 0, 0.25, 0.5 and D_o = 296 nm. Insets in (a) and (b) show SAR as a function of D_o and γ, respectively. (c) Spin configurations at H = 500 and 0 Oe (A and B in Fig. 1(b), respectively) on descending branch of M-H loop for D_o = 296 nm and γ = 0.5.

VP16-02. Stoichiometric effect on structural, morphological and magnetic properties of Co_2FeGa Nanowires. S. Singh[1], *M. Sharma*[2,1] and B.K. Kuanr[1] *1. Special Centre for Nanoscience, Jawaharlal Nehru University, New Delhi, India; 2. Department of Physics, Deshbandhu College, New Delhi, India*

Heusler alloys attracted extensive attention due to their novel properties like tunable composition and electronic structure which makes them suitable for applications in spintronics and superconductivity[1-2]. One-dimensional nanostructures are advantageous for rapid production, high performance and device miniaturization[3]. The present study uses an inexpensive electrodeposition technique at ambient temperature to fabricate Co_2FeGa Heusler alloy nanowires (HANWs) in anodic alumina templates (AAO). The influence of deposition parameter i.e. electrolyte solution's potential was optimized to achieve appropriate stoichiometry of HANWs. The structural, morphological, static and dynamic magnetic properties were investigated as a function of deposition potential for HANWs. The formation of Heusler alloy phase was confirmed by the X-ray diffraction pattern which indicates the B2 type crystal structure(Fig. 1). The most intense peak was observed for (220) reflection plane in the diffraction spectra for all samples. From morphological analysis, it was revealed that the nanowires were uniformly deposited in the AAO templates. The quantitative analysis using EDX confirmed the best stoichiometry for full Heusler alloy (X_2YZ) was obtained for –2V deposition potential. Fig.1 (inset) depicts the atomic percentage of HANWs for different deposition potentials. Magnetic properties derived from hysteresis loop of HANWs are saturation magnetization, remanence and coercivity. The dynamic properties were obtained using ferromagnetic resonance (FMR) measurements in flip-chip geometry in field-sweep mode. Fig.2 shows that the resonance field first decreases with the increase of deposition potential and then increases slightly with further increase in potential. Fig. 2 (inset) shows the resonance linewidth for all the deposition potentials. Various intrinsic parameters such as Gyromagnetic ratio, inhomogeneity and Gilbert damping constant were derived from the FMR data. It was observed that the Gilbert damping was minimum for appropriate stoichiometric Co_2FeGa NWs obtained at deposition potential of –2V.

[1] Elphick, K., Frost, W., Samiepour et al. *Science and technology of advanced materials*, *22*(1), 235-271, 2021 [2] Shigeta, I., Oku, S., Kubota, T. et al. *AIP Advances*, *13*(2), 2023 [3] Sharma, M., Das, A., Kuanr, B. K. *AIP Advances*, *9*(12), 125054, 2019

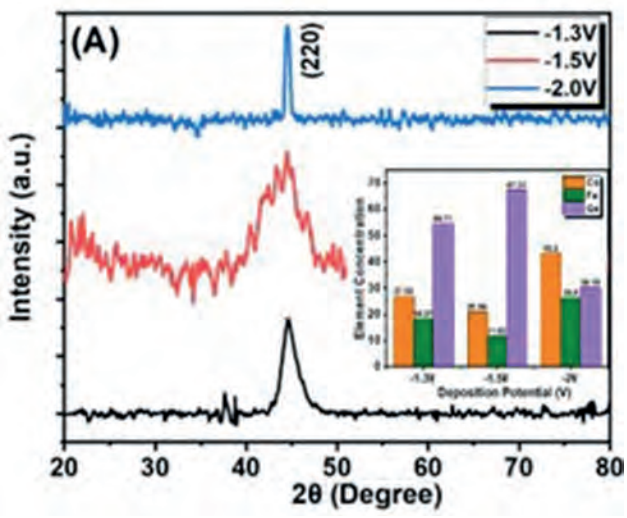

Fig. 1. Shows the XRD spectra (insert: Quantitative EDX analysis)

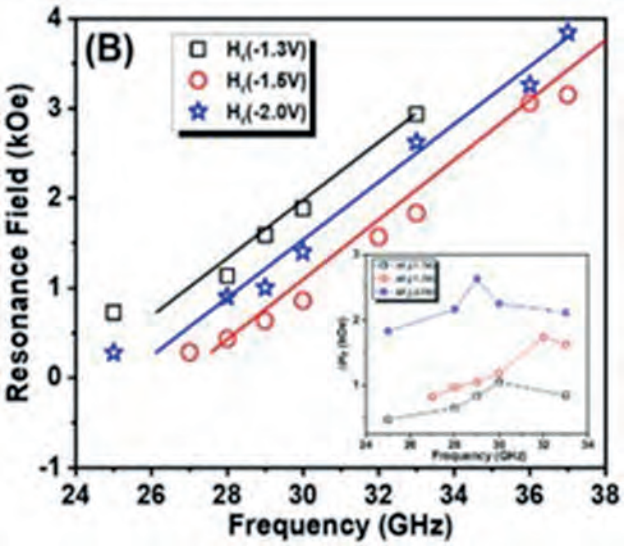

Fig. 2. H_r vs. f_r (inset: ΔH_r vs. f_r) for different deposition potential

VP16-03. Withdrawn

VIRTUAL PLATFORM ONLY

Session VP17
THIN FILMS, MULTILAYERS AND INTERFACE EFFECTS (VIRTUAL)
(Poster Virtual Session)

Nicolas Rougemaille, Chair
Centre National de la Recherche Scientifique/Thales, Grenoble, France

VP17-01. Nitrogen implantation induced α′-Fe_8N phase transition in α-Fe thin films and their stability. *G. d'Andrea*[1], S. Zhou[2], G. Gkouzia[1], M. Major[1] and L. Alff[1] *1. Institute of Materials Science, Technische Universität Darmstadt, Darmstadt, Germany; 2. Institute of Ion Beam Physics and Materials Research, Helmholtz-Zentrum Dresden-Rossendorf, Dresden, Germany*

In the pursuit of developing competitive rare-earth-free permanent magnets, α′-Fe_8N and α″-$Fe_{16}N_2$ metastable phases proved to be promising candidates due to the increased magnetic moment per Fe atom and induced magnetocrystalline anisotropy [1]. Ion implantation was established as a reliable method for producing these phases [2], enabling high solubilisation of nitrogen interstitials and volume ratios as high as 90% of the α′-phase or up to 70% of the ordered α″-phase [3,4]. A critical aspect hindering the application potential of this material is its low decomposition temperature. Upon obtaining the desired phase, significant decomposition is observed at temperatures as low as 200°C, given enough time [5]. It is reported that the heating rate and physical state of the material play a crucial role in determining its thermal stability [6,7]. Given the effectiveness of ion implantation in forming α′-Fe_8N and α″-$Fe_{16}N_2$ thin films, a thorough investigation into the thermal behaviour of the system when prepared under these conditions is essential. In our work, highly oriented Fe_8N films are produced at different fluences from 30 nm thin iron samples grown on MgO (100) substrates via molecular beam epitaxy (MBE). Small α′-Fe_8N crystallites are formed directly with the implantation process. Subsequent annealing induced relaxation in the structure allowing the c-lattice constant to increase, approaching literature values [8]. To investigate the thermal behaviour, the temperature dependence of the X-ray diffraction (XRD) patterns was studied using a Domed Hot Stage at low pressures ($< 10^{-2}$ mbar). Our samples exhibited stability for several hours at 250°C, as indicated by the maintained intensity of the Fe_8N 004 Bragg peak. This study aims at gaining insights on the favourable annealing conditions for maximising the volume ratio of metastable phases and investigate the role of the thin film model systems in the thermal stability of metastable materials. Additionally, higher annealing temperatures may help in the formation of the ordered phase without inducing material decomposition. Thus, a systematic study on samples prepared under various conditions may provide information on the most effective thermal treatment.

[1] T. Ogawa, Y. Ogata, R. Gallage et al., Appl. Phys. Express, 6, 073007 (2013) [2] T. Amarouche, L.-C. Garnier, M. Marangolo et al., J. Appl. Phys., 121, 243903 (2017) [3] H. Shinno, M. Uehara and K. Saito, J. Mater. Sci., 32, 2255 (1997) [4] K. Nakajima, T. Yamashita, M. Takata et al., J. Appl. Phys., 70, 6033, (1991) [5] S. Yamamoto, R. Gallage, Y. Ogata et al., Chem. Commun., 49, 7708 (2013) [6] M. Widenmeyer, T.C. Hansen, and R. Niewa, Z. Anorg. Allg. Chem., 639.15, 2851 (2013) [7] D. Gölden, E. Hildebrandt and L. Alff, J. Magn. Magn. Mater., 422, 407 (2017) [8] K. Toda, M. Honda, Y. Orihara et al., Key Eng. Mater., 181, 213 (2000)

VP17-02. Enhanced coercivity in $SmCo_4Cu$ thin films induced by chromium interlayer. *G. Gkouzia*[1], J. Soler Morala[2], A. Kovacs[3], D. Günzing[4], M. Major[1], R.E. Dunin-Borkowski[3], C. Navio[2], A. Bollero[2], K. Ollefs[4] and L. Alff[1] *1. Materials Science, Technical University of Darmstadt, Darmstadt, Germany; 2. IMDEA Nanoscience, Madrid, Spain; 3. Ernst Ruska-Centre for Microscopy and Spectroscopy with Electrons and Peter Grünberg Institute, Jülich, Germany; 4. Faculty of Physics and Center for Nanointegration (CENIDE), University of Duisburg-Essen, Duisburg, Germany*

$Sm(Co,Fe,Cu,Zr)_z$ alloys exhibit a characteristic microstructure comprising of $SmCo_5$ phase, Sm_2Co_{17} and Zr-rich platelets that intersect these phases. The unique microstructure of these alloys makes them superior high-temperature permanent magnets. However, owing to the intricate nature of the material, numerous questions remain unanswered, concerning the impact of individual phases on magnetic performance[1-2]. Research indicates that the thickness of the Z platelets play a critical role in determining the magnetic properties of the alloy. Specifically, increasing the thickness of the Z phase leads to a significant reduction in coercivity[3]. By exploring the impact of an antiferromagnetic interlayer between the Sm-Co layers in thin film model systems grown by molecular beam epitaxy (MBE), we have achieved to increase coercivity. Antiferromagnetic layers have been investigated in exchange bias systems, but have never been explored in connection with ultrahard magnetic materials and permanent magnetic properties. Expanding upon our understanding of Sm-Co thin films[4-5], we initiated our investigation by introducing Cr layers of varying thicknesses into a simplified system where Cr interlayers were sandwiched between layers of $SmCo_4Cu$. The films have been grown on Al_2O_3 substrates and have been characterized by X-ray diffraction (XRD) and superconducting quantum interference device (SQUID). Our findings provide clear evidence that the Cr layer within a specific thickness range can enhance coercivity. Cross-sectional high-angle annular dark field scanning transmission electron microscopy (HAADF-STEM) images provided visual evidence of sharp and coherent interface between the layers. Detailed chemical composition mapping of all elements, obtained through STEM/EDX, revealed a uniform distribution of chromium without any discernible diffusion into the Sm-Co layer. Our study offers new research opportunities in investigating the impact of functional layers, which are not conventionally part of the standard Sm-Co-Fe-Cu-Zr alloy composition. By widening the range of available phases in the development of future magnetic systems we can push the boundaries and unlock new possibilities for innovative magnetic materials.

[1] M. Duerrschnabel *et al.*, Nat. Commun. 8, 54 (2017) [2] O. Gutfleisch *et al.*, Acta Mat. 54, 997-1008 (2006) [3] L. Pierobon *et al.*, Sci. Rep. 10, 21209 (2020) [4] G. Gkouzia *et al.*, arXiv, 2304, 06457 (2023) [5] S. Sharma *et al.*, ACS Appl. Mater. Interfaces 13, 32415 (2021)

VP17-03. Low-temperature Manufacturable, Recyclable and Reconfigurable Liquid-metal/NdFeB Composites For Sensing and Robotic Applications. *R. Zhao*[1], H. Wang[1], Y. Shi[1], Z. Zhu[3,2] and B. Zhang[4]
1. Zhongyuan-Petersburg Aviation Colledge, Zhongyuan University of Technology, Zhengzhou, China; 2. Nanchang Institute of Technology, Nanchang, China; 3. Zhejiang Sci-Tech University, Hangzhou, China; 4. Henan University of Animal Husbandry and Economy, Zhengzhou, China

This paper presented a recyclable Liquid-metal/NdFeB magnet (LM magnet) with reconfigurable shape and polarity. Taking advantage of the low-temperature phase-transition characteristics of liquid-metal, we reshaped the magnetic mud and reorinted the NdFeB particles to produce complex magnetization profiles. The manufacturing process was realized at low temperature with the aid templates and paired permanent magnets. The microscopic morphology and element composition of LM magnet were analyzed by scanning electron microscopy (SEM) and energy dispersive sectroscopy (EDS). The influence of different particle size on the magnetic properties and phase transformation properties of the LM magnet was analyzed by vibrating sample magnetometer (VSM) and thermal difference analyzer (DSC). The experimental results verify that the LM magnet can be recycled, reconfigured, and welded. High-resolution (800 μm) magnetization profile design shows the ability of this technique to manufacture complex multipolar magnets(Fig.1). At last, three application cases show the application prospects of LM magnets in robots and sensors(as shown in Fig.2).

[1] N. Ebrahimi, C. Bi, D. J. Cappelleri, G. Ciuti, A. T. Conn, D. Faivre. Magnetic actuation methods in bio/soft robotics. Advanced Functional Materials, vol.31, no.11, pp.2005137, 2018. [2] C. Chi, X. Sun, X. Ning, L. Tong, C. Liu, "Recent Progress in Technologies for Tactile Sensors", Sensors, vol.18, no.4, pp.948, 2018. [3] Y.Kim, G. A. Parada, S.Liu, X. Zhao, "Ferromagnetic soft continuum robots", Science Robotics, *Sci. Robot.*, vol.4, pp.eaax7329, 2019. [4] R. Zhao, H. Dai, H. Yao, Y. Shi, G. Zhou, "Shape Programmable Mangetic Pixel Soft Robot", *Heliyon*, vol.8, pp.e21145, 2022. [5] W.Hu, G.Z. Lum, M. Mastrangeli, M. Sitti, "Small-scale soft-bodied robot with multimodal locomotion", Nature, vol.554, pp.18,2018. [6] S. Song, X. Qiu, W. Liu, M. Q.-H. Meng, "An Improved 6-D Pose Detection Method Based on Opposing-Magnet Pair System and Constraint Multiple Magnets Tracking Algorithm", *IEEE SENSORS JOURNAL*, vol.17, no. 20, pp.6752-6759, 2017. [7] J. Giltinan, M. Sitti, "Simultaneous Six-Degree-of-Freedom Control of a Single-Body Magnetic Microrobot," *IEEE Robotics and Automation Letters*, vol. 4, no. 2, pp. 508-514, 2019. [8] C. Becker, B. Bao, D.D. Karnaushenko, V.K. Bandari, B. Rivkin, Z. Li, M. Faghih, D. Karnaushenko, O. G. Schmidt, "A new dimension for magnetosensitive e-skins: active matrix integrated micro-origami sensor arrays", *Nat. Commun.*, vol.13, no.1, pp.2121, 2022. [9] Y.Yan, Z. Hu, Z. Yang, W. Yuan, C. Song, J. Pan, Y. Shen, "Soft magnetic skin for super-resolution tactile sensing with force self-decoupling", *Sci. Robot., vol.*6, pp.eabc8801, 2021. [10] Y. Kim, H. Yuk, R. Zhao, S. A. Chester, X. Zhao, "Printing ferromagnetic domains for untethered fast-transforming soft materials", *Nature*, vol.558, pp.274, 2018. [11] B. Sun, R. Jia, H.Yang, X. Chen, K. Tan, Q.Deng, J. Tang, "Magnetic Arthropod Millirobots Fabricated by 3D-Printed Hydrogels", *Adv. Intell. Syst.*, pp. 2100139,2021. [12] C. Zhang, X. Li, L. Jiang, D. Tang, H. Xu, P. Zhao, J. Fu, Q. Zhou, Y. Chen, "3D Printing of Functional Magnetic Materials: From Design to Applications", *Adv. Funct. Mater.*, pp.2102777, 2021. [13] Y. Alapan, A. C. Karacakol, S. N. Guzelhan, I. Isik, M. Sitti, "Reprogrammable shape morphing of magnetic soft machines", *Sci. Adv.*, vol.6, pp.eabc6414, 2020. [14] H. Deng, K.Sattari, Y. Xie, P. Liao, Z. Yan, J. Lin, "Laser reprogramming magnetic anisotropy in soft composites for reconfigurable 3D shaping", *Nature Commun.*, vol.11, pp.6325, 2020. [15] R. Zhao, H Dai, H. Yao, "Liquid-metal Magnetic Soft Robot With Reprogrammable Magnetization and Stiffness", *IEEE Robot. & Auto. Letter*, vol.4, pp., 2022.

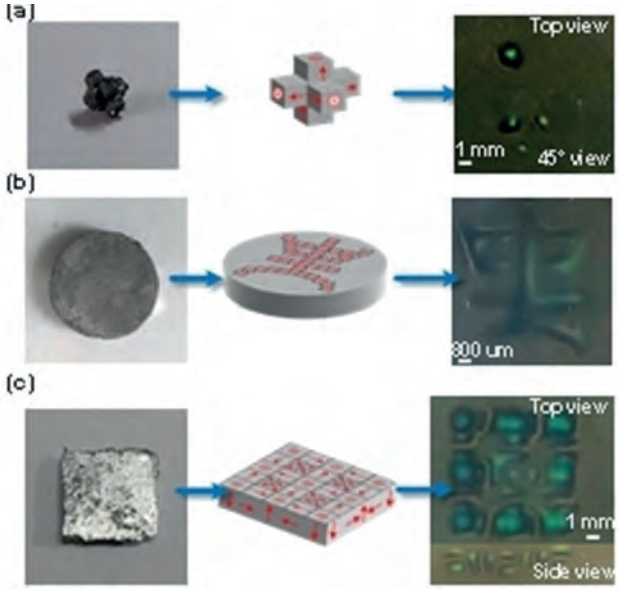

Fig. 1. Complex Multi-polarity magnets: (a) Asymmetric magnetic dipole,(b) School logo pattern, and (c) 2D Halbach array.

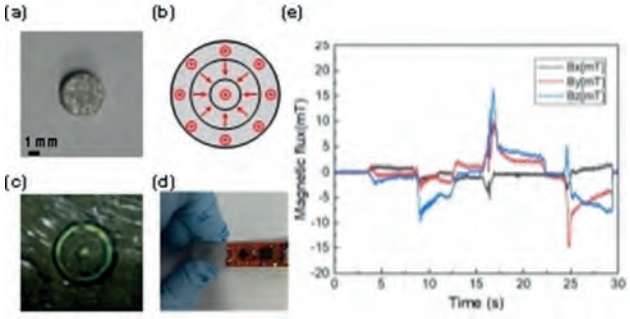

Fig. 2. The application cases: (a) ring-shape self-locking magnet for press closure of tissue, (b)One-sided magnetic field for 3D force/displacement sensing, and (c) Magnetic flux measured by 3D Hall.

VP17-04. Enhanced current-induced magnetization switching by forming ferrimagnetic interfacial alloy at Co/Ho heterojunction. *S. Li*[1,2], H. Poh[1], T. Jin[1], F. Tan[1], S. Wu[1], K. Shen[1], Y. Jiang[2] and W. Lew[1]
1. School of Physical and Mathematical Sciences, Nanyang Technological University, Singapore, Singapore; 2. Department of Electrical Engineering, Jiangnan University, Wuxi, China

Current-induced spin-orbit torque (SOT) allows effective control of magnetization switching in ferromagnetic (FM) system[1,2]. Recently, ferrimagnetic (FIM) materials with antiferromagnetic coupling have garnered numerous attentions due to ultrafast spin dynamics, demonstrating superiority over ferromagnetism[3-5]. However, the study on the mechanism of current-induced magnetization switching generated by SOT in interfacial ferrimagnetic materials is limited. In this work, we investigated the enhancement of current-induced magnetization switching in Ho/Co system, which formed an interfacial alloy with ferrimagnetic properties, as illustrated in Fig. 1. The exchange coupling field between FM and FIM is induced to improve SOT efficiency and reduce switching current density. The composition of Ho in the interfacial alloy increases with the thickness of Ho (t_{Ho}), which further enhances the exchange coupling field. The increased SOT efficiency up to 200% is achieved at t_{Ho} = 7 nm, with the critical switching current density of 2×10^{10} A/m^2, as presented in Fig. 2. The SOT efficiency decreased when Cu insertion was introduced at the Co/Ho interface to prevent the intermixing of Co and Ho atoms. This provides further verification that the enhancement of SOT efficiency is indeed induced by the exchange coupling occurring at the

FM/FIM interface. This interfacial alloy system with ferrimagnetic properties that we have demonstrated holds great promise for the development of low-power spintronic devices.

[1] Liu, L. *et al.* Current-induced self-switching of perpendicular magnetization in CoPt single layer. *Nat Commun* 13, 3539 (2022). [2] Isogami, S. *et al.* Spin-orbit torque driven magnetization switching in W/CoFeB/MgO-based type-Y three terminal magnetic tunnel junctions. *Sci Rep* 11, 16676 (2021). [3] Je, S.-G. *et al.* Spin-orbit torque-induced switching in ferrimagnetic alloys: Experiments and modeling. *Applied Physics Letters* 112 (2018). [4] Wu, Y. *et al.* Spin–orbit torque-induced magnetization switching in Pt/Co–Tb/Ta structures. *Applied Physics Letters* 118 (2021). [5] Sala, G. *et al.* Asynchronous current-induced switching of rare-earth and transition-metal sublattices in ferrimagnetic alloys. *Nat Mater* 21, 640-646 (2022).

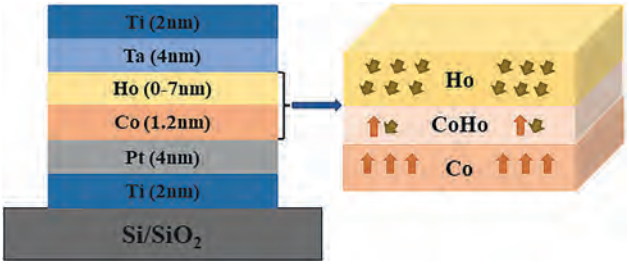

Figure 1. Schematic diagram of the multilayers (left) and the distribution of the magnetic moments of the interfacial alloy at Co/Ho heterojunction (right).

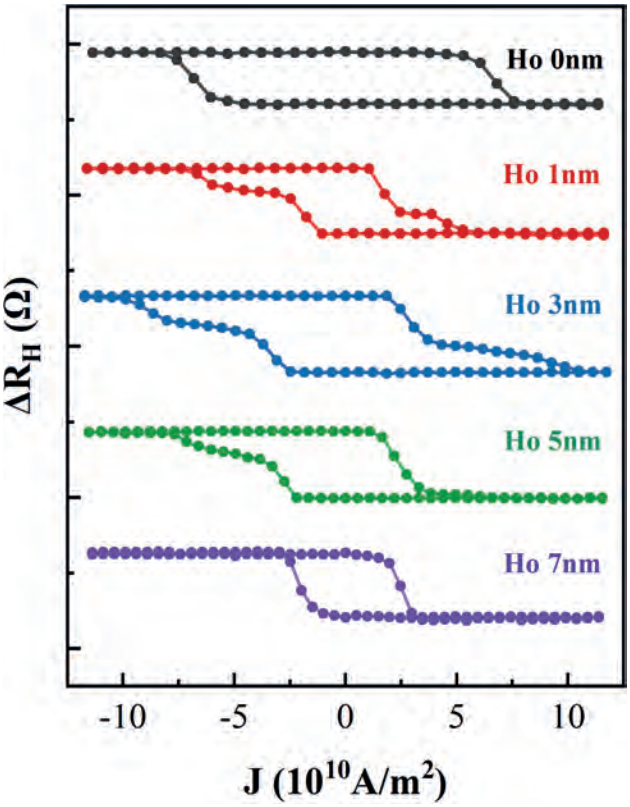

Figure 2. Current-induced magnetic switching curves under the in-plane bias field Hx = 1000 Oe with various Ho thickness

VP17-05. Understanding stability and behavior of Magnetic Tunnel Junction (MTJ) using Electron Spin Resonance (ESR). B.N. Mengesha[1], *J. Estevez Hernandez*[1], A. Feutmba[1], A. Grizzle[1], J. Martinez-Lillo[2] and P. Tyagi[1] *1. Mechanical Engineering, University of the District of Columbia, Washington DC, DC, United States; 2. Instituto de Ciencia Molecular, Universidad de Valencia, Valencia, Spain*

The unique attributes of magnetic tunnel junctions (MTJs), stemming from their sandwich-like structure, enable them to have promising applications across diverse fields. MTJs are composed of two ferromagnetic electrode layers separated by a thin insulator, such as aluminum oxide. MTJs properties could be tuned by carefully selecting and designing the materials used for the ferromagnetic electrodes and the thickness of the insulating layer. Thermal stability refers to the MTJ's ability to maintain magnetization despite thermal fluctuations. This study examines the thermal stability of a molecular spintronic device utilizing a magnetic tunnel junction (MTJMSD) with varying insulator thicknesses. The device fabrication involves photolithography, thin film sputtering, and a molecule attachment process. Single-molecule magnet (SMM) is used to create a channel connecting the top and bottom electrodes on the exposed side edge of the MTJ. To investigate the impact of increasing temperature on the device, the samples are subjected to a gradual heating process. The temperature is raised in 20°C increments, starting from room temperature until reaching 190°C. To explore the temperature-dependent variances, the magnetic resonance of the device is measured utilizing Electron Spin Resonance (ESR) technique. Initially, the ESR measurement is conducted at room temperature, serving as the baseline reference. Following this, the devices are exposed to heat, and subsequent ESR measurements are taken to examine any alterations in the magnetic resonance properties induced by the temperature changes. This approach allows for the investigation of temperature-dependent differences in the device's characteristics. The findings reveal that MTJMSD with thinner insulator thickness exhibits superior thermal stability compared to devices with thicker insulators. This observation correlates directly with the effect of the molecule, as the MTJMSD with a thinner insulator experiences a pronounced impact from the molecule, resulting in strong coupling and heightened thermal stability. This study sheds light on the creation of thermally stable MTJMSD, which is imperative for achieving reliable and consistent device performance.

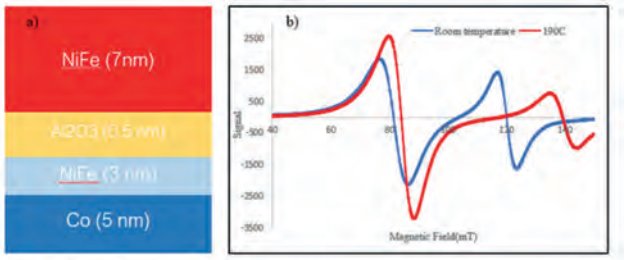

Figure 1a schematic of magnetic tunnel junction (MTJ) builds in experiment one which has a.5 nm insulator thickness, which contain a top ferromagnetic, insulator and bottom ferromagnetic layers. B) ESR spectra before heating the sample and after heating the sample.

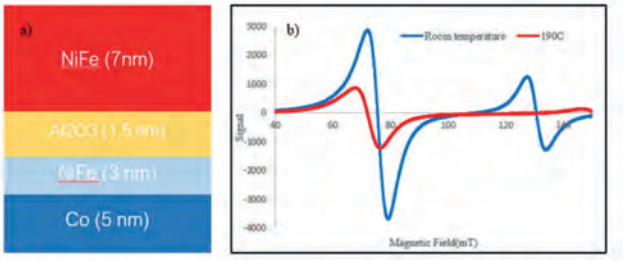

Figure 2a schematic of magnetic tunnel junction (MTJ) builds in experiment two which has 1.5 nm insulator thickness, which contain a top ferromagnetic, insulator and bottom ferromagnetic layers. B) ESR spectra before heating the sample and after heating the sample.

VP17-06. Studying Single-Molecule Magnet (SMM) induced coupling effect on Magnetic Tunnel Junction (MTJ) using Electron spin resonance (ESR). B.N. Mengesha[1], *J. Estevez Hernandez*[1], A. Feutmba[1], A. Grizzle[1], J. Martinez-Lillo[2] and P. Tyagi[1] *1. Mechanical Engineering, University of the District of Columbia, Washington DC, DC, United States; 2. Instituto de Ciencia Molecular, Universidad de Valencia, Valencia, Spain*

New types of metamaterials can be produced by enhancing the magnetic coupling between the two ferromagnetic layers of a magnetic tunnel junction (MTJ). One potential method to achieve strong coupling involves attaching molecules along the exposed side of the MTJ, acting as spin channels that connect the top and bottom ferromagnetic layers. This study focuses on examining the coupling effect of Single Molecule Magnetic (SMM) on MTJs with varying insulator thicknesses. The fabrication process of the MTJ involves coating a silicon wafer with photoresist through spin coating, creating patterns via photolithography, depositing thin films through sputtering, and finally removing the unwanted material through liftoff. After fabrication, the top and bottom electrodes are covalently connected on the exposed side edges using SMMs to establish a strong magnetic coupling. Through multiple experiments, it has been observed that strong coupling, facilitated by SMM channels, alters the magnetic properties of both ferromagnetic metals. Electron spin resonance (ESR) is a valuable technique utilized to characterize the magnetic properties, interactions, and dynamics of the individual layers within the structure of a magnetic tunnel junction (MTJ). In this study, an ESR investigation was conducted both before and after the treatment of the MTJ with the SMM to assess the impact of the molecules. The ESR results displayed a discernible shift in the acoustic and optical modes of the MTJ subsequent to the introduction of the SMM. This shift observed in the ESR spectra indicates that the SMM has a significant effect on the properties of the ferromagnetic electrodes within the MTJ. To understand the SMM impact, the ESR response of the heated MTJs was compared. It was found that the shift induced by the SMM on the MTJ was of a similar magnitude to the shift observed on a heated sample. Examining the influence of SMM coupling in magnetic tunnel junctions (MTJs) is of utmost importance, as MTJs based on molecular components open up novel possibilities for nanoscale electronics, quantum information processing, and advanced sensor technologies.

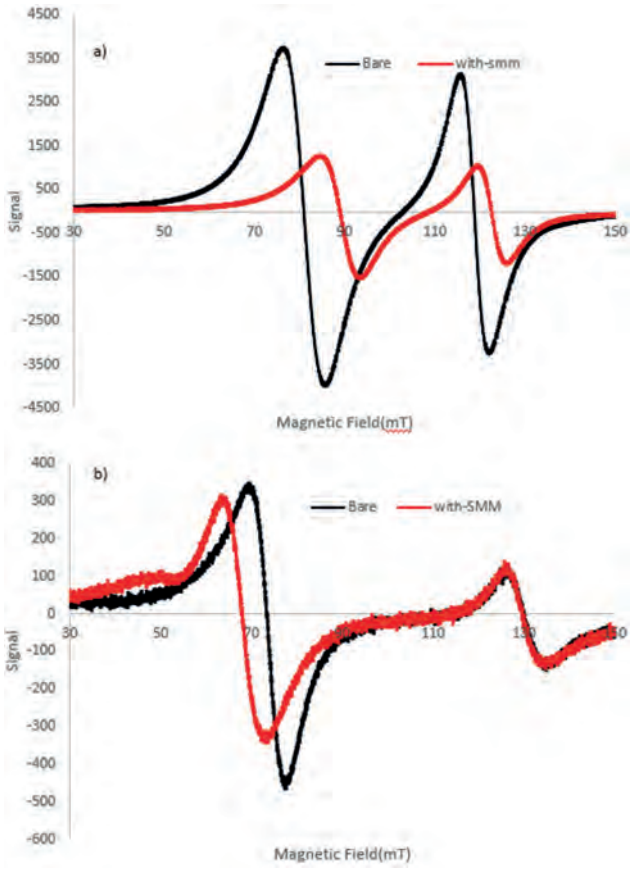

Fig. 1. ESR spectra before and after SMM, a) 0.5 nm insulator thickness, b) 1.5 nm insulator thickness.

- A -

- B -

*Best student presentation award finalist

*Best student presentation award finalist

- C -

*Best student presentation award finalist

- D -

*Best student presentation award finalist

- E -

- F -

*Best student presentation award finalist

- G -

- H -

*Best student presentation award finalist

*Best student presentation award finalist

- I -

- J -

*Best student presentation award finalist

- K -

*Best student presentation award finalist

*Best student presentation award finalist

- L -

*Best student presentation award finalist

- M -

*Best student presentation award finalist

*Best student presentation award finalist

- N -

*Best student presentation award finalist

- O -

- P -

*Best student presentation award finalist

- Q -

- R -

*Best student presentation award finalist

- S -

*Best student presentation award finalist

*Best student presentation award finalist

- T -

*Best student presentation award finalist

- U -

- V -

*Best student presentation award finalist

- W -

*Best student presentation award finalist

- X -

- Y -

*Best student presentation award finalist

- Z -

*Best student presentation award finalist

*Best student presentation award finalist